SYNTHESIS AND REACTIVITY OF TRANSITION METAL STABILIZED POLYPNICTOGEN CATIONS

DISSERTATION

zur Erlangung des
Doktorgrades der Naturwissenschaften

DR. RER. NAT.

am Institut für Anorganische Chemie
der Fakultät für Chemie und Pharmazie
der Universität Regensburg

vorgelegt von

CHRISTOPH RIESINGER

aus Passau

im Jahr 2023

Das Promotionsgesuch wurde eingereicht am: 16.10.2023

Tag der mündlichen Prüfung: 30.11.2023

Vorsitzender:	Apl. Prof. Dr. Rainer Müller
Prüfungsausschuss:	Prof. Dr. Manfred Scheer
	Prof. Dr. Nikolaus Korber
	Prof. Dr. Frank-Michael Matysik

Diese Arbeit wurde angeleitet von: Prof. Dr. Manfred Scheer.

Universität Regensburg

Eidesstattliche Erklärung

Ich erkläre hiermit an Eides statt, dass ich die vorliegende Arbeit ohne unzulässige Hilfe Dritter und ohne Benutzung anderer als der angegebenen Hilfsmittel angefertigt habe; die aus anderen Quellen direkt oder indirekt übernommenen Daten und Konzepte sind unter Angabe des Literaturzitats gekennzeichnet. Die Arbeit wurde bisher weder im In- noch im Ausland in gleicher oder ähnlicher Form einer anderen Prüfungsbehörde vorgelegt.

Christoph Riesinger

This thesis was elaborated within the period from January 2020 until October 2023 in the Institute of Inorganic Chemistry at the University of Regensburg under the supervision of Prof. Dr. Manfred Scheer.

The following is a chronological list of all peer reviewed publications the author of this thesis contributed to, including chapters 3 – 10 of this thesis (marked with ⬥), which already have been published. † marks equal contributions.

List of Publications:

(⬥) C. Riesinger, L. Dütsch, G. Bálazs, M. Bodensteiner, M. Scheer
"*Cationic Functionalization by Phosphenium Ion Insertion*"
Chem. Eur J. **2020**, *26*, 17165–17170.

(⬥) C. Riesinger, G. Bálazs, M. Bodensteiner, M. Scheer
"*Stabilization of Pentaphospholes as η^5-coordinating Ligands*"
Angew, Chem. Int. Ed. **2020**, *59*, 23879–23884.

L. Dütsch, C. Riesinger, G. Balázs, M. Scheer
"*Synthesis of Tetrahedranes Containing the Unique Bridging Hetero-Dipnictogen Ligand EE´ (E ≠ E´ = P, As, Sb, Bi)*"
Chem. Eur. J. **2021**, *27*, 8804–8810.

M. Piesch, S. Reichl, C. Riesinger, M. Seidl, G. Balazs, M. Scheer
"*Redox Chemistry of Heterobimetallic Polypnictogen Triple-Decker Complexes – Rearrangement, Fragmentation and Transfer*"
Chem. Eur. J. **2021**, 27, 9129–9140.

(⬥) C. Riesinger, G. Balázs, M. Seidl, M. Scheer
"*Substituted aromatic pentaphosphole ligands – a journey across the p-block*"
Chem. Sci. **2021**, *12*, 13037–13044.

L. Dütsch, C. Riesinger, G. Balázs, M. Seidl, M. Scheer
"*Structural Diversity of Mixed Polypnictogen Complexes: Dicationic $E_2E'_2$ (E, E' = P, As, Sb, Bi) Chains, Cycles and Cages Stabilized by Transition Metals*"
Chem. Sci. **2021**, *12*, 14531–14539.

(⬥) C. Riesinger,† L. Dütsch,† M. Scheer
"*Synthesis and Redox Chemistry of a Homoleptic Iron Arsenic Prismane Cluster*"
Z. anorg. allg. Chem. **2022**, *648*, e202200102.

(⬥) C. Riesinger, F. Dielmann, R. Szlosek, A. V. Virovets, M. Scheer
"*Synthesis and Reactivity of a Cyclo-Octatetraene-Like Polyphosphorus Ligand Complex [Cyclo-P_8]*"
Angew. Chem. Int. Ed. **2023**, *135*, e202218828.

(⬥) C. Riesinger, D. Röhner, I. Krossing, M. Scheer

"*Teaching old tricks to new dogs – rational synthesis of multi-decker complexes featuring cyclo-P_5 decks*"

Chem. Commun. **2023**, *59*, 4495–4498.

M. Haimerl, C. Schwarzmaier, C. Riesinger, A. Y. Timoshkin, M. Melaimi, G. Bertrand, M. Scheer

"*Reactivity of Yellow Arsenic towards Cyclic (Alkyl)(Amino) Carbenes (CAACs)*"

Chem. Eur. J. **2023**, *29*, e202300280.

(⬥) C. Riesinger,† L. Zimmermann,† M. Scheer

"*Redox Chemistry of an End-Deck cyclo-As_3 Nickel Complex*"

Organometallics **2023**, *42*, 2065–2069.

M. Elsayed Moussa, E.-M. Rummel, G. Balázs, C. Riesinger, A. Noor, R. Kempe, M. Scheer

"*Unusual coordination mode for 1,3-diphosphete ligands towards a Cr–Cr quintuple bond complex*"

Chem. Commun. **2023**, *59*, 8588–8591.

(⬥) C. Riesinger, A. Erhard, M. Scheer

"*Ring expansion vs. addition – reactivity of a cyclo-P4 complex towards pnictogenium cations*"

Chem. Commun. **2023**, *59*, 10117–10120.

L. Zimmermann, C. Riesinger, G. Balázs, M. Scheer

"*Synthesis and Reactivity of Hetero-Pnictogen Diazonium Analogs Stabilized by Transition Metal Units*"

Chem. Eur. J. **2023**, e202301974.

S. Reichl, C. Riesinger, M. Scheer

"*Nucleophilic Attack at Pentaarsaferrocene [Cp*Fe(η^5-As_5)]-The Way to Larger Polyarsenide Ligands*"

Angew. Chem. Int. Ed. **2023**, *62*, e202307696.

To my Family

Preface

This thesis deals with the synthesis of transition metal stabilized polyphosphorus (chapters 3 – 8) and polyarsenic (chapters 9 and 10) cations. Furthermore, it explores the reactivity of selected transition metal stabilized polyphosphorus cations towards nucleophilic functionalization (chapters 11 and 12).

Most of the presented work (chapters 3 – 10) has already been published during the preparation of this thesis and the corresponding publications are listed above.

Every chapter includes a separate preface with a list of authors and their respective contributions to the chapter. Moreover, if any of the presented results have previously been reported within other theses, it is stated in the beginning of the respective chapter.

To ensure uniform design of this work, all chapters are divided into the sections ‘Abstract’ ‘Introduction’, ‘Results and Discussion’, ‘Conclusion’, ‘Supporting Information’ and ‘References’. With minor exceptions all published work has been adapted to fit uniform text settings, language and font. Numeration of compounds, figures, schemes and tables begins anew in each chapter. Generally, starting materials are labelled with capital letters, while products are labelled with Arabic numerals, except for chapters 3, 5 and 6, in which the starting materials are included into the Arabic numerals. Deviation from this uniform design in e. g. figures or within the supporting information is due to different publication requirements of the journals/publishers and the article types the respective results have previously been published in.

The general introduction in the beginning of this thesis puts the presented results into a greater context and the conclusion at the end summarizes them comprehensively.

Table of Contents

1. Introduction

1.1. The Pnictogens

The elements of group 15 – the so called pnictogens (Pn) – consist of nitrogen (N, number 7), phosphorus (P, 15), arsenic (As, 33), antimony (Sb, 51) and bismuth (Bi, 83) and occupy the center of the p-block in the periodic table of elements.[1] Only recently even the synthesis of element number 115, named moscovium (Mc), could be achieved, which constitutes the heaviest known group 15 element known to date.[2] The name “pnictogen” arises from the greek word pniktos (choked) and points towards the suffocating properties of pure elemental nitrogen.[3] Occasionally, these elements are also regarded as the pentels which is associated with their position as the fifth main group of elements. Within group 15 the electronegativity (Pauling) of the elements decreases from 3.0 (N) to 1.9 (Bi) while the metallic character increases in the same order.[4]

Nitrogen is the lightest of the pnictogens and yet comprises 0.017 % (w/w) of the earth’s crust making it the second most abundant of the group 15 elements. However, most of the nitrogen on earth is found in the atmosphere, where it occurs as highly inert dinitrogen (N_2). It was independently discovered and identified as part of the air we breathe by Carl Scheele, Henry Cavandish, Joseph Priestley and Daniel Rutherford, in 1772.[5] The synthetic utilization of N_2 for the production of ammonia played a crucial role at the beginning of the 20th century, as traditional farming and conventionally manufactured fertilizers failed to meet the nutritional demands of an ever growing global population. This challenge could only be circumvented by the efficient reduction of widely abundant N_2 to ammonia (NH_3), as the latter is a feedstock chemical for the production of fertilizers, drugs and food additives.[6] The solution to this problem was provided within the Haber-Bosch-Process, which allows the catalytic (Fe catalyst) hydrogenation of N_2 under elevated pressures and temperatures.[7] Both Fritz Haber (1918)[8] as well as Carl Bosch (1931)[9] were awarded the Nobel Prize in Chemistry for this achievement.[10] Besides ammonia, nitrogen is a crucial element for numerous biologically relevant molecules and together with carbon, oxygen and hydrogen constitutes the elemental foundation of organic chemistry. For example, the complex molecular structures of proteins or the DNA (desoxyribonucleic acid) would be unimaginable without the presence of nitrogen in amino acids or nucleobases.[1]

Phosphorus is the most abundant of the pnictogens at 0.1% (w/w) in the earth´s crust. However, it does not occur in its elemental form due to its high oxophilicity and is rather found within phosphates, such as apatite $Ca_5(PO_4)_3(OH, F, Cl)$. Famously, phosphorus was discovered by Hennig Brand in 1669, who observed a glowing substance upon heating human urine.[5,11] Although not occurring naturally, phosphorus has several solid elemental modifications (Scheme 1). White phosphorus, consisting of molecular P_4 tetrahedra,[12] is the modification obtained during its highly energy intensive synthesis. While this is the synthetically most useful modification of phosphorus due to its high reactivity and solubility in organic solvents, it is self-igniting in air ad furthermore extremely toxic. Both attributes create vast

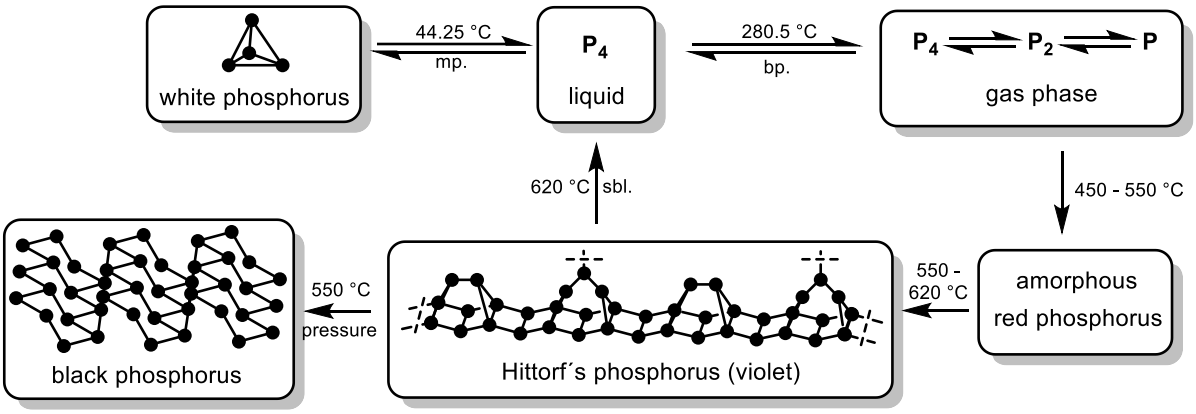

Scheme 1: Elemental modifications of phosphorus and their transformation into each other.

amounts of safety issues with the handling, storage and transport of white phosphorus. While P_4 can also be melted, gaseous phosphorus exists in an equilibrium of P_4 the P_2 molecule and P atoms dependent on the respective temperature and pressure. The less reactive modifications of phosphorus, violet (Hittorf´s) phosphorus and several amorphous modifications (red phosphorus) can be obtained by exposing white phosphorus to heat or light. Both consist of interconnected strains of alternating P_8 and P_9 cages, although final statement about the connectivity of red phosphorus is difficult due to its amorphous character. Black phosphorus can be obtained from Hittorf´s phosphorus under elevated pressures and consists of phosphorene sheets, which themselves are built from interconnected six membered phosphorus rings.[1,13] Notably, single layer phosphorene itself constitutes a phosphorus based 2D material, which has experienced rising interest due to its intriguing properties for its use in semiconductor applications.[14] Finally, phosphorus nanorods could recently be obtained by coordination to copper halides.[15]

Similar to nitrogen, the biological relevance of phosphorus cannot be overstated, as phosphate groups are found within the backbone of our DNA as well as the universal energy carrier ATP (adenosine triphosphate) and even within our skeletal bones.[16] Besides, phosphorus is also

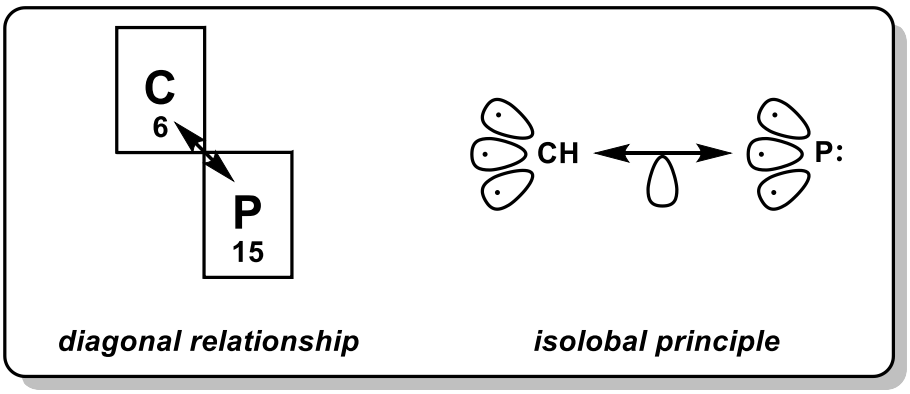

Scheme 2: Fundamental relationships between phosphorus and carbon: Diagonal relationship in the periodic table (left) and the isolobal principle applied to the relation of the phosphorus atom to the ubiquitous CH fragment, which is commonly found in aromatic organic compounds (right).

an important part of modern fertilizers. However, one of the most important applications of phosphorus emerging over the past century, have been organo-phosphines as ligands in transition metal (TM) chemistry. While seminal TM complexes, such as Wilkinson´s[17] or Grubb´s[18] catalysts employed simple triorgano-phosphine ligands, development of ever more complex phosphines as ligands is a thriving field of chemical research. In fact, the endeavor to access these highly sought-after species in rational and more importantly efficient ways also constitutes a part of the academic motivation of this thesis. Lastly, phosphorus shares a diagonal relation to carbon within the periodic table and the P atom is additionally related to the ubiquitous (in organic chemistry) CH fragment by the isolobal principle (Scheme 2).[19] Both of these observations predict a rich structural chemistry for phosphorus bordering that of carbon and keep inspiring research on ever more complex molecular architectures in the context of phospha-organic chemistry.[20]

The heavier pnictogens, arsenic, antimony and bismuth are much rarer compared to their lighter homologs and thus are found only in 1.7 ppm (w/w, As), 0.2 ppm (w/w, Sb) and 0.2 ppm (w/w, Bi) of the earth´s crust, respectively. While elemental bismuth is known since ancient times, the discovery of arsenic and antimony is ascribed to Albertus Magnus (ca. 1250) and Basilius Valentinus (1492), respectively. All three elements occur as sulfidic minerals or even their elemental form in nature, with arsenic and antimony classifying as metalloids and bismuth expressing significant metallic character. Several elemental modifications are known for all three of them, but only arsenic shows a molecular modification, namely yellow arsenic (As_4), which is isostructural to white phosphorus.[21] As yellow arsenic is extremely light sensitive and autocatalytically transforms into grey arsenic, elaborate ways for its storage have been developed to simplify its synthetic utilization.[22] Furthermore, antimony and especially arsenic compounds are known for their high toxicity and must be handled with great care. Yet, these elements find important application e. g. in semiconductors or dopants in certain alloys. The heavier bismuth and its compounds are regarded as non-toxic. Its large scale industrial applications are more limited, but it is used in alloy manufacturing and even pharmaceutical chemistry.[23] An interesting, yet for now primarily academic, application is the use of bismuth complexes in radical[24] and even redox catalysis.[25] Both reactivity patterns have long been postulated to be reserved to TM only.

1.2. Organic and Main Group Pnictogen Compounds

(Poly-)pnictogen compounds play a crucial role in numerous applications, such as semiconductors, ligands in TM catalysis, organocatalysis, fertilizers or food additives (*vide supra*). Many of the employed pnictogen species are purely inorganic solid state compounds and thus not covered within the scope of this thesis. However, the developments on molecular (poly-)pictogen systems over the past decades furnished a multitude of fascinating and extremely useful compounds, which are discussed in the following. This overview aims towards providing the background for the significance of developing TM stabilized polypnictogen cations and the investigation of their reactivity. While a comprehensive summary of molecular

(poly-)pictogen chemistry would by far exceed the scope of this thesis, this overview highlights recent developments within (poly-)pnictogen chemistry and sets them into perspective with seminal work in the field.

1.2.1. Mononuclear Pnictogen Species

Although the focus of this thesis is on the synthesis of compounds featuring polypnictogen frameworks, significant achievements in the preparation of highly reactive species involving only one pnictogen center have been made over the past decades. While some of them simply display milestones in this field of chemistry, others also bear implications on the synthesis of polypnictogen compounds (*vide infra*). One of the main goals within this field is the isolation of low valent pnictogen species (e. g. Pn(I)) with the goal of exploring the reactivity of these still exotic species. For comparison, stable singlet carbenes, are a staple in nearly all disciplines of chemistry since their discovery more than 30 years ago.[26] In contrast, the corresponding first stable pnictinidene, namely the singlet nitrene **I** (Scheme 3) was only synthesized in 2012.[27] The stable singlet phosphinidene **II** was reported four years later requiring a sterically super bulky phosphino substituent for its isolation.[28] Earlier an isolable phosphinidene transfer reagent based on anthracene was introduced by the group of *Cummins*,[29] a platform which could also be used to transiently generate the exotic P_2 molecule.[30] While a stable triplet bismuthinidene (**III**) was isolated in the beginning of this year,[31] singly substituted species of arsenic and antimony remain unknown. However, additional dative stabilization allowed the isolation of singlet stibinidenes and bismuthinidenes.[32] Notably, the carbene adducts (**IVa**, Scheme 4) of phosphinidenes,[33] arsinidenes,[34] stibinidenes[35] as well as bismuthinidenes[36] have been synthesized over the past decade. However, these compounds owe most of their stability to the resonance forms **IVb** (imidazolium-pnictide) and **IVc** (pnictaolefin). The nitrogen analogs to these species are imines, a common functionality in organic molecules featuring a C=N double bond. When a third carbon nitrogen bond is introduced, one arrives at nitriles, which again are ubiquitous organic molecules. In contrast, the heavier homologs, so called phospha-[37] and arsaalkynes,[38] have first been synthesized in 1990 and 1994, respectively. They owe their name to the closer resemblance of e. g. their reactivity to alkynes rather than nitriles. While the corresponding antimony and bismuth compounds remain unknown the C≡P triple bond can also be found in the cyaphide anion $[C{\equiv}P]^-$,[39] which was first described as a bridging ligand in a platinum complex.[40] The recent isolation of a transfer reagent[41] of this

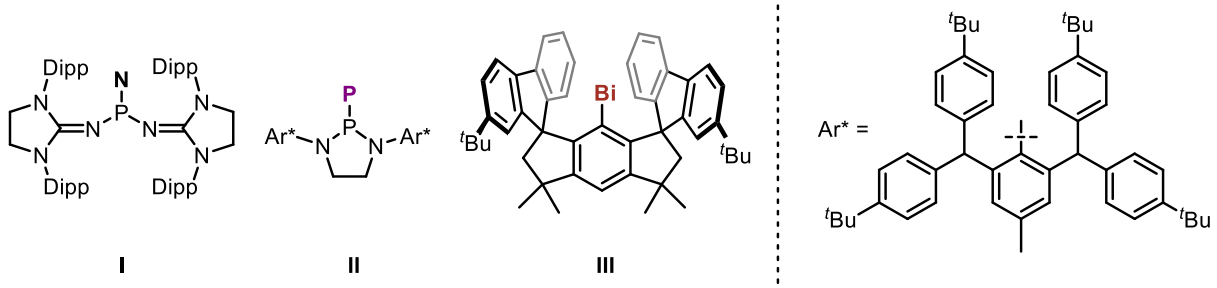

*Scheme 3: Isolated singly substituted pnictogen compounds, namely the singlet nitrene (**I**), phosphinidene (**II**) and triplet bismuthinidene (**III**); the ^{t}Bu groups in **III** pointing back are omitted for clarity, Dipp = 2,6-diisopropylphenyl.*

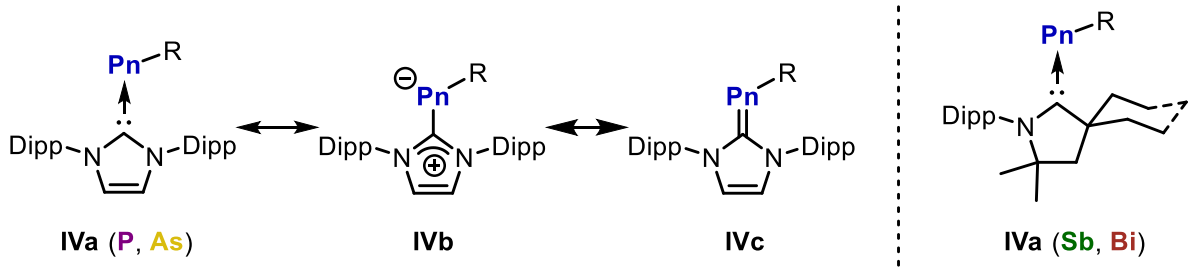

*Scheme 4: Resonance forms of isolated carbene adducts of pnictinidenes **IVa** – **c**; R = H, Ph, Cl; Dipp = 2,6-diisopropylphenyl.*

exotic analog of simple cyanide sparked renewed interest in its coordination[42] and oligomerization reactivity.[43] Similarly, the chemistry of phosphinines has recently gained momentum,[44] although the first isolation of triphenylphosphinine dates back to 1966.[45] Besides these multiply bonded species, the group of *Scheer* was able to isolate several representatives of Lewis base stabilized parent pnictogenyltrielanes.[46] These mixed group 13/15 compounds represent isolobal analogs of prototypical ethylene.

The rise of carbenes as stabilizing ligands in main group chemistry[26] also furnished numerous ionic and neutral radical species of group 15 elements.[47] However, carbenes have also been employed to stabilize exotic Pn(I) cations (**V**, Scheme 5),[48] which could otherwise only be obtained for P(I) and As(I) as bis-phosphine complexes.[49] Recently, a series of Pn(I) cations could also be stabilized by a novel bis-silylene ligand.[50] One of the most important classes of pnictogen based cations are pnictogenium cations, which bear two substituents at the pnictogen center in addition to their positive charge. Thus, these highly reactive species are isolobal analogs to the aforementioned widely applied carbenes and significant effort has been put into their investigation. Salts of donor-stabilized phosphenium ions have first been isolated 50 years ago.[51] Interestingly, their lighter homologs, nitrenium ions, could only be synthesized more than 20 years later and reveal intriguing ligand properties.[52] While the bisferrocenyl-phosphenium cation was initially claimed to be the first donor-free pnictogenium cation, it was later shown that its central P atom experiences significant Fe-P interaction.[53] Thus, donor-free pictogenium cations (**VI**) were isolated only recently in 2018 (for Sb and Bi)[54] and 2021 (for P and As)[55] employing bulky terphenyl or hydrindacen substituents. Introduction of an even higher charge of +2 at the pnictogen center was possible using the electronically flexible Cp*

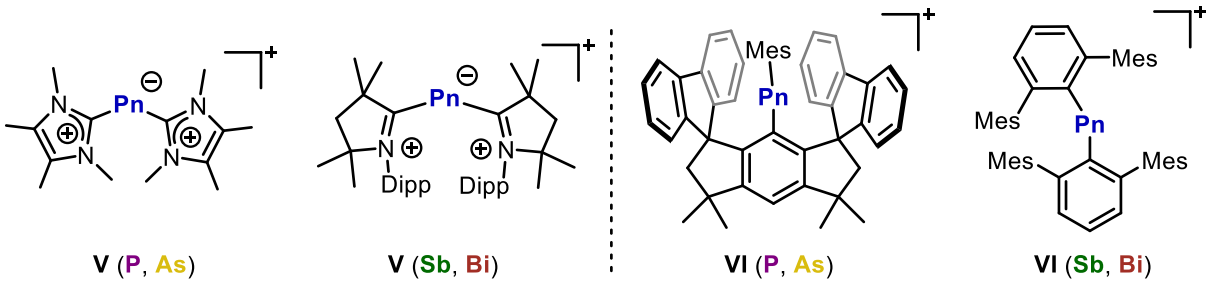

*Scheme 5: Carbene stabilized formal pnictogen(I) cations (**V**) depicted in their charge separated mesomeric form, and donor-free pnictogenium cations **VI**; Dipp = 2,6-diisopropylphenyl, Mes = 2,4,6-trimethylphenyl.*

(pentamethylcyclopentadienyl, C_5Me_5) substituent. Thus, salts of $[Cp^*Pn]^{2+}$ (Pn = P, As, Sb, Bi) could be identified.[56] Besides their overall fascinating reactivity, they also reveal super Lewis acidic character, which is classified by a fluoride ion affinity (FIA) of roughly more than 500 kJ/mol.[57]

Lastly, recent developments in high valent pnictogen chemistry showed for example the possibility to isolate highly charged Sb(V) cations (**VII**, Scheme 6)[58] and even the first monomeric stibine oxide (**VIII**).[59] The first trisubstituted P(V) dication (**IX**) was described in 2019[60] by *Dielmann* and coworkers and more recent work by the same group focused on the synthesis and reactivity of oxo-,[61] thio-[62] and methylene-phosphonium[63] cations.

1.2.2. Neutral and Anionic Polypnictogen Compounds

Unsubstituted polynuclear anions of group 15 elements have been reported for all five elements from nitrogen to bismuth. Many pnictides with lower degree of aggregation are obtained in solid state compounds (compare M_3Pn, where M is an alkali metal).[1] In contrast, the azide anion (N_3^-), first described by *Curtius* in 1890,[64] can be obtained in form of soluble salts. Another highly interesting polynitrogen species is the pentazolate anion, which is the all-nitrogen analog of cyclopentadienide, a prototypical organometallic ligand. However, the synthesis of salts of this highly sensitive anion, which are stable under normal conditions could only be achieved within the past decade.[65] The polynuclear anions of the heavier pnictogens are far more numerous.[1] Notably, several groups but especially *Marianne Baudler* (in nearly 250 “contributions to phosphorus chemistry”) intensively studied the chemistry of polyphosphides and -phosphines over the past 60 years.[66] Covering this comprehensively would exceed the scope of this thesis. Thus only selected examples are presented.

One of these fascinating classes of polypnictogen anions are the cyclic tetrapnictides [*cyclo*-$Pn_4]^{2-}$ (**X**, Scheme 7), which are known for Pn = P,[67] As,[68] Sb[69] and Bi.[70] These four membered cyclic species are planar and show 6π aromaticity, expressing their close relationship to cyclo-butadienides ($[C_4H_4]^{2-}$). The seminal cyclopentadienide homolog [*cyclo*-$P_5]^-$[71] (**XI**) was initially obtained in mixtures of various polyphosphides,[72] but its synthesis could later be refined to give the title anion in good yields.[73] The even larger [*cyclo*-$P_6]^{4-}$ anion (**XII**) could be obtained in the solid state, but rapidly disproportionates upon

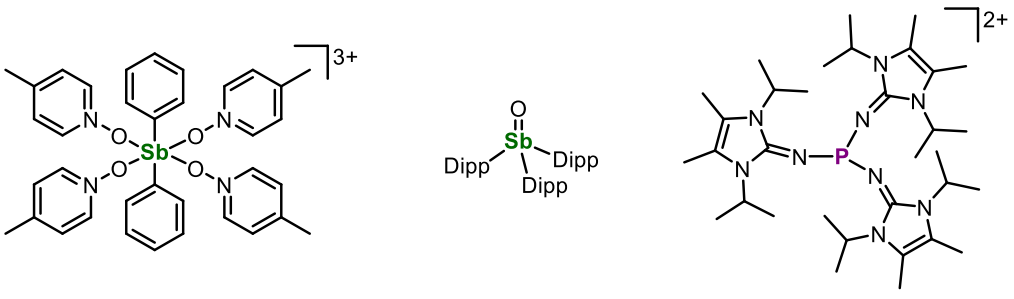

VII **VIII** **IX**

*Scheme 6: A highly charged Sb(V) cation (**VII**), the first isolated stibine oxide (**VIII**) and a planar three-coordinate P(V) cation (**IX**).*

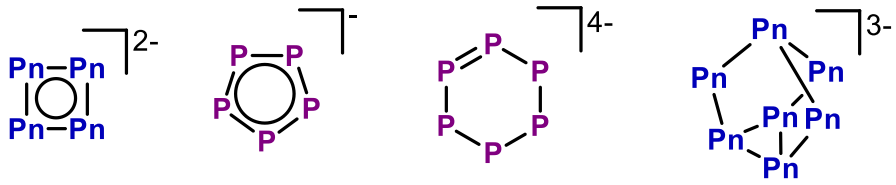

X (P, As, Sb, Bi) **XI** **XII** **XIII (P, As, Sb)**

Scheme 7: Selected structurally characterized polypnictide anions drawn with delocalized charges.

dissolution.[74] While its planar structure and 10 π electron count hint towards the aromatic character of this anion, this was later disproven on the basis of solid state ^{31}P-MAS-NMR spectroscopy.[75] The Zintl phases[76] M_3Pn_7 (**XIII**, M = alkali metal, Pn = P,[77] As,[78] Sb[69,79]) reveal a nortricyclane type framework, which can also be found in several ionogenic polypnictogen complexes of the TMs (*vide infra*). While the groups of *Baudler* and *von Schnering* were able to prepare even larger polycyclic phosphides[80] with up to 26 P atoms,[81] polyanions of the heavier pnictogens (As, Sb and Bi) are less studied and more exotic due to the lack of critical ^{31}P NMR spectroscopy.[82] However, the latter technique has proven essential in the study of complex phosphide/phosphine mixtures and has facilitated the preparation of numerous cyclic and polycyclic polyphosphines including species with P_7,[83] P_8,[84] P_9,[85] P_{10},[85b,86] P_{11},[87] P_{12},[88] P_{13},[88a,89] P_{14},[83a,90] P_{16},[90c] P_{18},[91] P_{20},[92] and P_{21}[93] scaffolds.[94] While highly polar and often protic solvents, such as ethylene diamine or DMF (dimethyl formamide) are common in this field, the group of *Korber* even utilized liquid ammonia to prepare highly reduced polypnictogen species, such as three membered *catena*-phosphides.[95] Renewed interest into polyphosphine chemistry was found by the groups of *Hey-Hawkins* and *Wolf*, who investigated the synthesis and reactivity of small four- and five-membered *catena*- as well as *cyclo*-phosphines and -phosphanides.[96] The group of *Lammertsma* was even able to trap the initial addition product of an organo-nucleophile to P_4 by means of coordination to a Lewis acid.[97] Furthermore, the multifaceted coordination chemistry of cyclic polyphosphines was studied in great detail.[98] While (poly-)cyclic arsines[84a,87a,99] and stibines[100] have become available over the past decades as well, recent focus is on the preparation of interpnictides. These are compounds featuring chemical bonds between two or even more different pnictogen

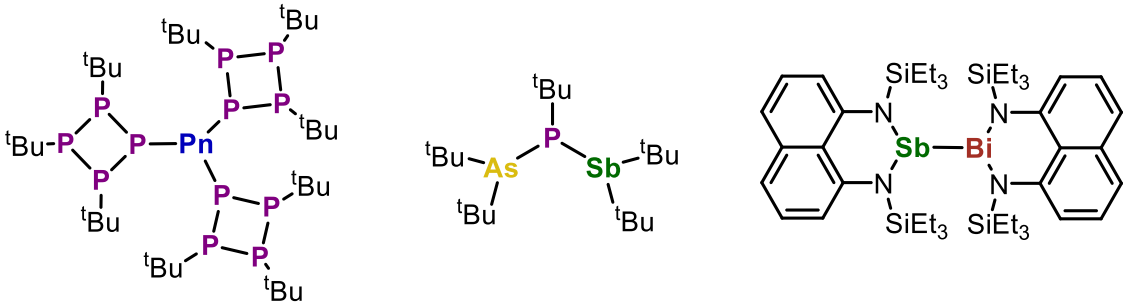

XIV (Pn = As, Sb, Bi) **XV** **XVI**

*Scheme 8: Neutral mixed interpnictogen compounds bearing cyclo-P_4 substituents (**XIV**), featuring multiple (>2) catenated pnictogens (**XV**) and an example of the first stable bismuthanyl-stibines (**XVI**).*

elements. Thus, the group of *Hey-Hawkins* was able to prepare complex polyphospha-pnictines (**XIV**, Scheme 8),[101] while the *von Hänisch* group was able to develop rational syntheses for *catena*-interpnictogen compounds (e. g. **XV**).[102] Fascinatingly, the same group could demonstrate the synthesis of a compound featuring all five pnictogen atoms (N, P, As, Sb and Bi) in a row.[103] Notably, a compound featuring a Sb–Bi bond stable against scrambling was only reported in 2020 (**XVI**).[104]

The above mentioned compounds are centered around the heavier pnictogens P – Bi. Yet, the chemistry of polynitrogen species is a vivid field of research and has furnished numerous useful and intriguing compounds. However, these species generally fall into the category of high-energy materials, which shall not be a point of discussion within this thesis. Thus, only the outstanding compounds C_2N_{14} (**XXIII**, Scheme 9)[105] and C_2N_{16} (**XXIV**)[106] shall be mentioned here, which are two of the most nitrogen rich organic molecules known to date. Notably, a heavier analog of prototypical dinitrogen (N_2), namely phosphorus mononitride (PN), was recently shown to be liberated from a suitable precursor in synthetically useful fashion.[107]

In addition to saturated compounds, the past decades have seen a dramatic increase in the number of multiply bonded species of the heavy main group elements, a field heavily advanced by the group of *Power*. This can largely be attributed to the availability of sterically protecting substituents, which allowed the isolation of dipnictenes (e. g. **XIX**, Scheme 10).[108] In case of phosphorus, a second class of neutral doubly bonded species is known, which are phosphanylidenephosphoranes (e.g. **XX**), acting as masked phosphinidenes and thus are also regarded as Phospha-Wittig reagents.[109] Impressively, the group of *Hering-Junghans* recently utilized these for the synthesis of unprecedented group 13/15 compounds,[110] including rare Al/Ga=P double bonded species.[111]

In addition, the transformation of white phosphorus (P_4)[66f] as well as yellow arsenic (As_4)[21] by low valent main group species has furnished numerous polyphosphorus/-arsenic species. The most versatile reactivity has been observed for the reaction of P_4 with various-heterocyclic carbenes, yielding several P_2,[112] P_4,[113] P_8[114] and P_{12}[115] products. Carbene stabilized diphosphorus $(NHC)_2P_2$ has previously been isolated by the reduction of a PCl_3 precursor.[116]

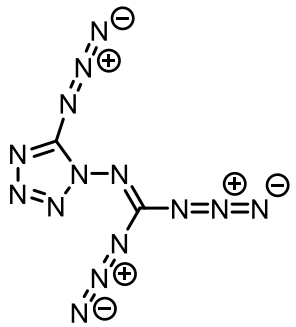

1-Diazidocarbamoyl-5-azidotetrazole

XVII

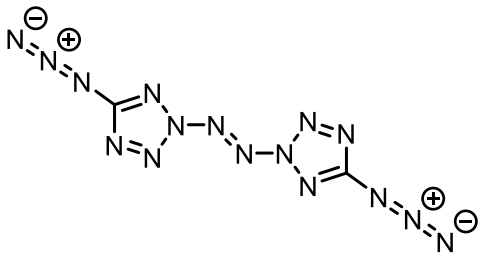

2,2′-Azobis(5-azidotetrazole)

XVIII

Scheme 9: Two selected nitrogen rich organic molecules.

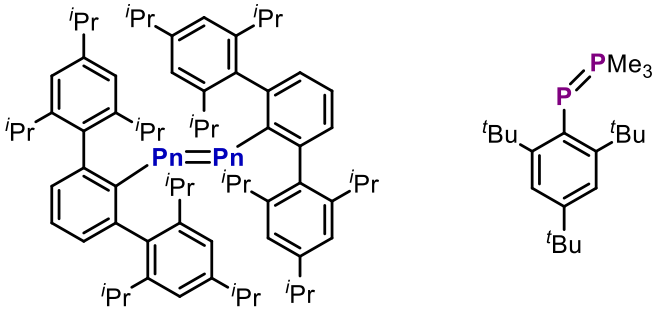

XIX (**Pn** = **P**, **As**, **Sb**, **Bi**) **XX**

*Scheme 10: Neutral doubly bonded dipnictenes (**XIX**) and phosphanylidenephosphorane (**XX**).*

Recently, this reactivity was transferred to yellow arsenic revealing similar structural motifs.[117] While reaction of P_4 with low valent group 13 reagents commonly result in the formation of mixed group 13/15 cage compounds,[118] highly reactive alyminyl anions afford the direct reduction to a *catena*-P_4 species.[119] In contrast, the acetylacetonato derived nacnac ($HC(CMeNAr)_2$) ligand platform allowed for the rational preparation of group 13 derivatives featuring singly[120] and doubly[121] P–P bond inserted species **XXVII** and **XXVIII** (Scheme 11), respectively. Again, this reactivity could be transferred to As_4 and even the interpnictogen compound AsP_3.[122] The structural motives **XXVII**[123] and **XXVIII**[123a] are common within the group 14 mediated transformation of P_4. However, formation of butterfly type P_4R_2 frameworks[124] as well as fragmentation of the P_4 tetrahedron[125] are also common pathways in these reactions. In contrast, As_4 reacts with silylenes either under aggregation to an As_{10} unit or fragmentation to an $As_2(SiR_2)_2$ butterfly species.[126]

Finally, the recent years have shown that the isolobal analogy between P_4 and the class of tetrahedranes, initially discovered by the group of *Maier*,[127] is not limited to the homopolyatomic compounds (**XXIII**, Scheme 12). Impressively, the group of *Wolf* demonstrated the synthesis of diphospha-tetrahedrane (**XXV**) via catalytic dimerization of a phosphaalkyne.[128] Later, the group of *Cummins* developed elegant synthetic procedures towards the missing phospha- (**XXIV**)[129] as well as triphospha-tetrahedrane (**XXVI**).[130] Thus, the series of mixed carbon phosphorus tetrahedranes has been completed and future challenge is on the introduction of heavier group 14 and 15 elements into this structural motif.

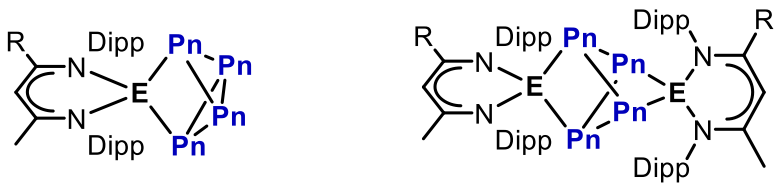

E = **Al**, **Ga** (R = Me)
E = **Si** (R = CH_2

XXI (**Pn** = **P**, **As**)

E = **Al** (R = Me)
E = **Si** (R = CH_2

XXII (**Pn** = **P**, **As**)

Scheme 11: Polypnictogen compounds arising from the insertion of low valent group 13 and 14 species into the Pn_4 tetrahedron.

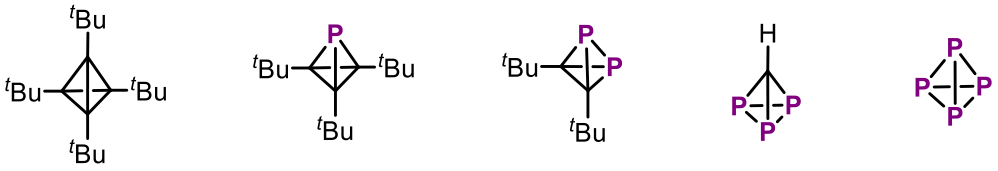

Maier 1978 **XXIII** | *Cummins* 2020 **XXIV** | *Wolf* 2019 **XXV** | *Cummins* 2021 **XXVI** | *Brand* 1669

*Scheme 12: Phosphatetrahedranes **XXIV** – **XXVI**, P_4 and their isolobal all-carbon analog tetrakis-tertbutyl-tetrahedrane **XXIII**.*

1.2.3. Cationic Polypnictogen Compounds

As demonstrated above, the chemistry of neutral as well as anionic polypnictogen compounds has been well established over the past six decades. In contrast, polypnictogen cations are far less common and have received considerable interest only since the early 2000s. For instance, several polyatomic bismuth cations could be isolated, due to the metallic character of this element.[1,131] For the lighter homologs, these species are extremely rare, however.[132] Thus, salts of the $[N_5]^+$ cation (**XXVII**, Scheme 13)[133] and $[Sb_8][GaCl_4]$ (**XXIX**)[134] are the only known polyhomoatomic cations for nitrogen and antimony, respectively. The $[P_9]^+$ cation (**XXVIII**),[135] which was previously identified in solution could be crystallographically characterized only last year[136] and a homopolyatomic cation of arsenic remains unknown to date. While the latter proceeds via the formal oxidation of P_4 with $[NO]^+$ salts,[137] the prototypical protonation of P_4 (**XXX**) could be achieved utilizing a sophisticated weakly coordinating anion (*vide infra*).[138] Dipnictogen cations[139] could be realized via oxidation of the corresponding carbene stabilized precursors for phosphorus arsenic and even the mixed NP derivative,[140] while the heavier antimony and bismuth analogs relied on the stabilization by anionic carbene ligands[141] or a gallyl substituent.[142] Triply bonded polypnictogen compounds can be found in seminal diazonium salts,[143] which arguably represented the first polypnictogen cations to ever be isolated in 1858. Only about 150 years after their first report the corresponding phospha-[144] and arsa-diazonium[145] analogs became available, featuring the respective N≡P/As triple bond.

However, the largest progress in the field of polypnictogen cations, especially polyphosphorus cations, was made by the groups of *Burford*, *Weigand* and *Krossing* among other teams, who utilized the functionalization of (poly)pnictogen species with main group electrophiles.[146] The

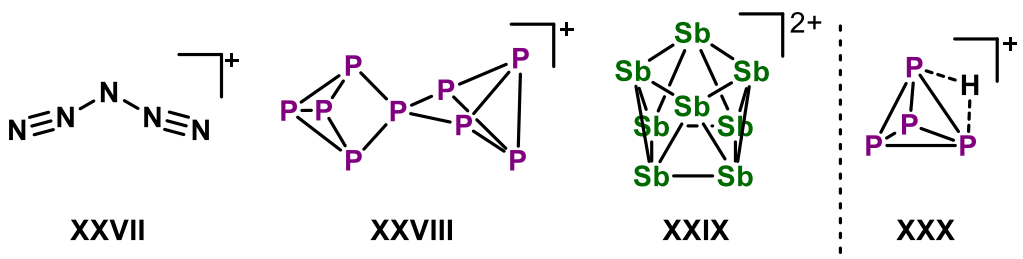

XXVII | **XXVIII** | **XXIX** | **XXX**

*Scheme 13: Left: Only known homopolyatomic cations of nitrogen (**XXVII**), phosphorus (**XXVIII**) and antimony (**XXIX**) characterized in condensed phases; Right: protonated white phosphorus (**XXX**).*

key intermediates in the majority of these reactions are highly reactive pnictogenium cations, which represent the cationic group 15 analoga of carbenes (*vide supra*). Seminal work by *Burford* and coworkers focused on the synthesis of simple catenated phosphino-phosphonium cations (e. g. **XXXI**, Scheme 14) via coordination of phosphines to phosphenium cations.[147] Reduction of halo-phosphino-phosphonium cations was then rapidly demonstrated to afford elongated *catena*-phosphino-phosphonium cations.[148] However, three-membered *catena*-bis-phosphino-phosphonium cations have also been obtained via insertion of phosphenium ions into the P–P bond of diphosphines (**XXXII**).[149] The functionalization of the latter with simple alkyl electrophiles even afforded diphosphonium cations (e. g. **XXXIII**), which constitute the phosphorus analogs of ethane.[150] Harnessing the insertion reactivity of phosphenium cations, cyclic phosphino-posphonium cations could also be prepared.[151] Utilizing an elaborate melt approach *Weigand* and *Burford* were able to isolate six-membered cyclic polyphosphorus dications (e. g. **XXXIV**).[152] Later, this approach could be transferred to P_4 itself. Besides the cage compound $[P_5Ph_2]^+$ (**XXXV**), whose derivatives are also accessible by different synthetic strategies,[153] this even gave the dicationic $[P_6Ph_4]^{2+}$ as well as the tricationic $[P_7Ph_6]^{3+}$ polyphosphorus cages.[154] Besides these fascinating insertion reactions, other cyclic phosphino-phosphonium cations can also be accessed via electrophilic addition reactions.[151,155]

While in-depth studies of the reactivity of such polyphosphorus cations are relatively scarce, the latter *cyclo*-phosphino-phosphonium ions reveal intriguing ring opening/expansion reactivity towards nucleophiles (Scheme 15a).[156] Notably, the halogen substituted $[P_5RCl]^+$ cages also show fascinating reactivity when exposed to nucleophiles. Thus, a unique [3+2] fragmentation is observed, when these compounds are exposed to NHCs (Scheme 15b).[157] The resulting diphosphanide (Scheme 15b, top) could then be transformed into an unsymmetrical and cationic diphosphene by chloride abstraction.[158] This highly polarized diphosphene undergoes (cyclo-)addition reactions with azides providing various unprecedented aza-diphosphorus species.[159] Latest entries into the synthesis of cationic polyphosphorus frameworks have been demonstrated by the group of *Weigand*, who utilized cationic pyrazolyl substituted P_1 building blocks to access complex cationic polyphosphorus species.[160] The same group was able to prepare cationic imidazolium substituted *cyclo*-tetraphosphines[161] and later used them to synthesize cationic phospha-Wittig reagents as well as phospha-olefins.[162] Finally, the synthetic procedures developed for polyphosphorus cations

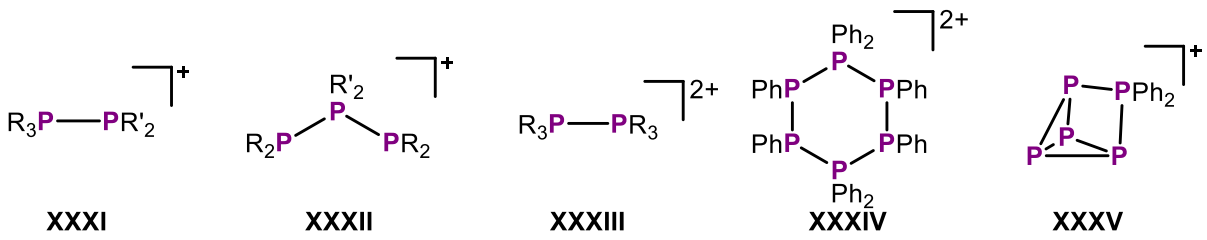

XXXI **XXXII** **XXXIII** **XXXIV** **XXXV**

Scheme 14: Selected polyphosphorus cations arising from the insertion of phosphenium cations into, or electrophile addition to neutral polyphosphorus compounds.

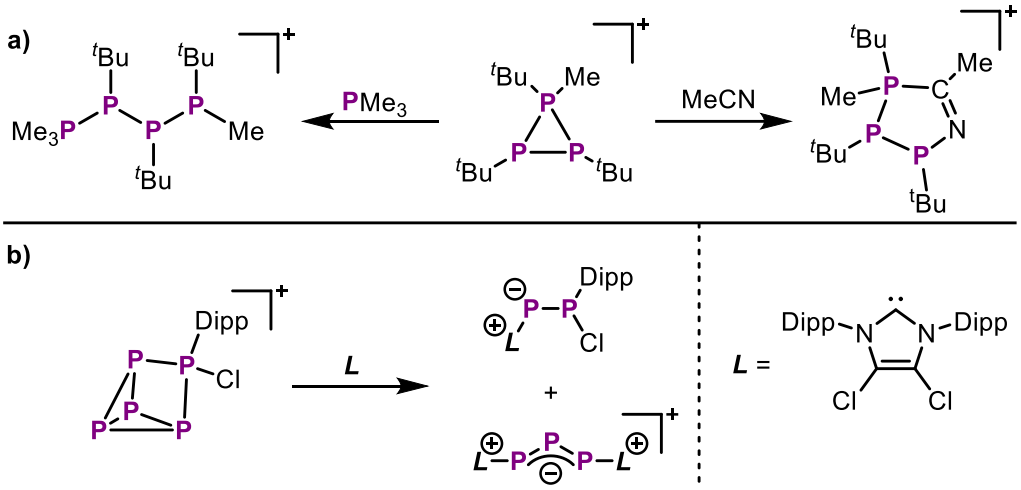

Scheme 15: Selected examples for the reactivity of organo-polyphosphorus cations; a) ring opening and expansion of a P_3 cycle and b) the fragmentation of a P_5 cage compound mediated by an NHC; Dipp = 2,6-diisopropylphenyl.

were transferred and applied to the synthesis of heavier *catena*-polypnictogen cations, including species incorporating mixed pnictogens.[163] Thus, even complex interpnictogen cations could be accessed bearing cyclic and polycyclic structural motifs.[164]

Excursion: Weakly Coordinating Anions

The advances made in the synthesis and study of polyphosphorus cations are unthinkable of without the concurrent rise of weakly coordinating anions (WCAs). While small polyatomic anions of p-block elements, such as $[GaCl_4]^-$, $[PF_6]^-$, $[SbF_6]^-$, $[SO_3CF_3]^-$ $[ClO_4]^-$ were long believed to have truly “non-coordinating” properties, this assumption was rapidly proven wrong by the preparation of ever more electrophilic cationic TM complexes by the end of the last century.[165] Ever since, the development of new and more powerful, thus less coordinating, weakly coordinating anions is a highly active field of research.[166] It spans multiple disciplines of chemistry ranging from TM catalysis[167] over the preparation of ionic liquids[168] to the stabilization of exotic and extremely reactive main group cations.[169] Generally, suitable candidates to be useful weakly coordinating anions should have the following properties, which have in part been summarized before:[167e]

- The WCA should have minimal charge (optimally -1) and maximal size, which both help to minimize the electrostatic interaction between anion and cation.
- The charge of the WCA should be dispersed across the whole anion to avoid nucleophilic sites, which could lead to its degradation.
- The WCA needs to be constructed from chemically inert and highly robust moieties to avoid electrophilic degradation.
- The polarizability of the WCA should be as low as possible to avoid interaction with the corresponding cation.
- The WCA should have reasonably simple synthetic access from readily available starting materials and a suitable way to introduce the WCA into the targeted compound.

With these design principles in mind, numerous WCAs have been developed over the past decades. However, there are three classes of WCAs, which have shown to be the most versatile and synthetically useful. On the one hand, carborate anions (**XXXVI**, Scheme 16)[170] were demonstrated to be among the most chemically robust WCAs even allowing the isolation of salts of protonated benzene.[171] However, their synthesis is tedious, and they have been shown to possess remaining Lewis basicity.[170] In contrast, fluorinated tetra-aryl-borates (e. g. **XXXVII**) and fluorinated alkoxy-aluminates (e. g. **XXXVIII**) are readily accessible and partially even surpass the WCA properties of carborates. Recently, the largest and yet "least-coordinating" anion (**XXXIX**) could be prepared in high yields and again represents an alkoxy-aluminate based compound.[172] With their invention affecting chemistry as a whole, WCAs also proved inevitable for the isolation and study of extremely reactive (poly-)pnictogen cations (*vide supra*). Conclusively, the robust perfluorinated anions $[B(C_6F_5)_4]^-$ ($[BAr^F]^-$)[173] and $[Al\{OC(CF_3)_3\}_4]^-$ ($[TEF]^-$)[174] were also used to stabilize several of the most reactive and unstable cations presented within this thesis (*vide infra*).

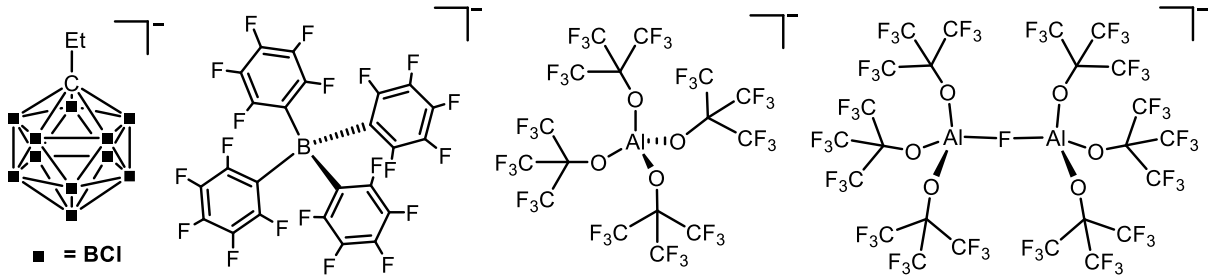

XXXVI **XXXVII** **XXXVIII** **XXXIX**

Scheme 16: Selected carborate, tetraaryl-borate and aluminate based WCAs.

1.3. Polypnictogen (Pn_n) Ligand Complexes

The first part of this introduction (2.1 – 2.3) demonstrated the tremendous progress that has been made in organo- and main-group polypnictogen chemistry over the past decades and highlighted their significance for the preparation of poly-pnictogen cations. However, the seminal reports by *Dahl* and co-workers in 1969 on the synthesis of $[\{Co(CO)_3\}_nAs_{4-n}]$ (n = 1, 2)[175] demonstrated that polypnictogen frameworks could also be stabilized within the coordination sphere of a TM without the need for additional substituents. This founded the field of polypnictogen (Pn_n) ligand complexes (Pn = P, As, Sb, Bi), which are defined by at least one ligand solely built from Pn atoms, which are only bound to the TM or another Pn atom.[176] These Pn_n ligands spark interest as they share an isolobal relationship with aromatic hydrocarbons (n = 3 – 6), acetylene (n = 2) or the CH fragment itself (n = 1) as shown in Scheme 17 and offer unprecedented insight into the structural chemistry of the group 15 elements. Lastly, the element nitrogen is largely excluded from this discussion, as the field of TM mediated dinitrogen activation stands on its own,[177] although recent developments show that expanded nitrogen frameworks ($[N_5]^-$) can be coordinated to TMs.[178]

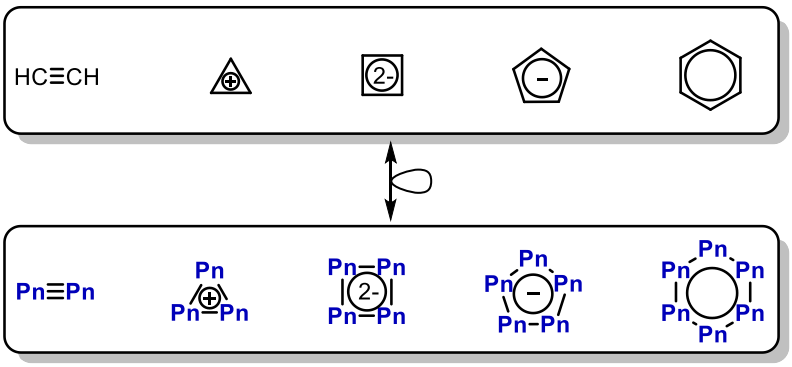

Scheme 17: Isolobal relationship between aromatic hydrocarbons (and acetylene) and cyclo-Pn_n ligands commonly found within Pn_n ligand complexes.

1.3.1. Synthesis of Pn_n Ligand Complexes

Due to the inherent interest these once exotic Pn_n ligand complexes received, synthetic procedures towards them are now well established and comprise several general methods. The first, and most utilized, of these methods can be described as the reaction of a coordinatively unsaturated TM precursor with a suitable (poly-)pnictogen source. While this includes the classic co-thermolysis as well as -photolysis of TM carbonyls with Pn_n precursors (*vide infra*),[176] modern approaches utilize more labile (compared to CO) ligands, e. g. toluene, allowing for more controlled reaction conditions as during the preparation of **XL** (Scheme 18).[179] A closely related approach towards Pn_n ligand complexes is the *in situ* reduction of TM halide precursors in the presence of a suitable polypnictogem source, as has been exploited in the synthesis of **XLI**.[180] Similarly, the reaction of d- and f-block metal halides with Zintl anions[181] or smaller anionic Pn transfer reagents (e. g. $[PnR_2]^-$, $[PnCO]^-$, [*cyclo*-$P_5]^-$)[182] displays a suitable entry into Pn_n ligand complexes, especially for smaller Pn_n (n = 1, 2) units

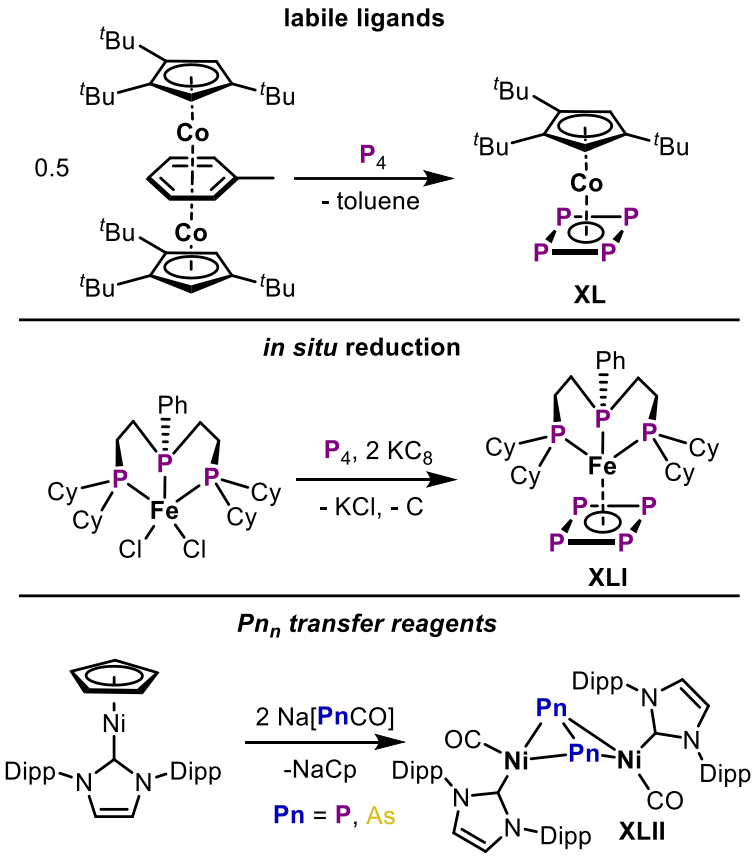

Scheme 18: Selected synthetic approaches towards Pn_n ligand complexes.

as in **XLII**.[183] Reversing the roles, the reaction of anionic metalates with pnictogen trihalides has been heavily utilized in the synthesis of Pn_1 and other small Pn_n complexes.[184] However, recent reports focus on the sequential assembly of the desired Pn_n ligand within the coordination sphere of the TM,[185] as has been demonstrated for the first side-on complex of P_2. Furthermore, photolysis of the platinum azide precursor was shown to produce a metallonitrene.[186] Similarly, a complex featuring the rare Bi_2 ligand could also be rationalized via photolysis, highlighting the importance of this approach very early on.[187] However, white phosphorus (P_4) and yellow arsenic (As_4) remain the most versatile precursors for the preparation of larger P_n and As_n ligand complexes, respectively (*vide infra*). In contrast, the preparation of expanded polyantimony and -bismuth ligands (and sometimes As) often relies on the utilization of more exotic compounds, such as organo-polypnictines or -pnictides,[188] poly-anionic Zintl clusters[189] or even the insoluble allotropes of these elements.[190] An illustrative example of the complicated access into poly-bismuth complexes is the multi-step procedure towards a compound featuring a Bi_4 tetrahedron and its derivatives.[182a,191]

1.3.2. Pn_4 Transformation by TM Complexes

The most versatile Pn_n surrogates for the preparation of P_n and As_n ligand complexes are P_4 and As_4. While they have been used since the infancy of this field,[176] especially the lighter P_4 received renewed interest in the context of a more sustainable production of organo-phosphorus compounds. Besides the extremely energy intensive production of P_4 itself,[192] the

conventional synthetic procedures for producing organo-phosphines from P_4 (Scheme 19) involve highly toxic and corrosive intermediates and cause enormous amounts of waste.[193] Recent developments by the groups of *Cummins*, *Wolf* and *Weigand* try to avoid most of these issues by employing the transformation of P_4 by radical species (**XLIII**),[194] strong oxidants (**XLV**),[195] photocatalysis (**XLIV**)[196] or electrochemistry,[197] or avoid the necessity of P_4 all along.[198] Yet, while these approaches offer an exciting, highly efficient, and benign entry into mono-phosphorus compounds, they rarely allow for insight into the stepwise cleavage of P–P bonds (Scheme 20) or even the isolation of potential intermediates. In contrast, TM mediated P_4 activation allows both, insight into the stepwise degradation of the P_4 tetrahedron as well as the isolation of polyphosphorus species, which may display intermediates on the way to the desired phosphine products.[199] Furthermore, the transformation of P_4 by TM species can lead to even larger polyphosphorus compounds, which would otherwise be inaccessible. All of these benefits lead to TM mediated P_4 transformation developing into one of the most fruitful areas within phosphorus chemistry over the past decades. Similarly, the interest into the transformation of isostructural As_4 by TM complexes received an influx of interest and displays a way to study arsenic's rich structural chemistry, which is otherwise often hard to access.[21] The following provides an overview of structural motives arising from Pn_4 (Pn = P, As) transformation by TM complexes and aims to show their immense potential for the preparation of polypnictogen cations.

While P_1 and As_1 complexes are readily prepared from small Pn_1 precursors (*vide supra*), the synthesis of such compounds starting from P_4 or As_4 is much less common. This can largely be attributed to the fact that all six Pn–Pn bonds of the Pn_4 tetrahedron have to be cleaved within this process. Yet, cubane-type complexes (**XLVI**, Scheme 21)[200] could be prepared from Pn_4 and suitable TM precursors, while a tetrahedral complex with a capping phosphide[201] was obtained using a tungsten alkoxide precursor. Related amido and siloxido precursors could later be utilized to access compounds featuring bridging (**XLVII**)[202] and finally terminal (**XLVIII**)[203] pnictide complexes starting from P_4 or As_4. Notably, all of the latter compounds are based on group 5 and mostly group 6 metals, highlighting their importance for the field.

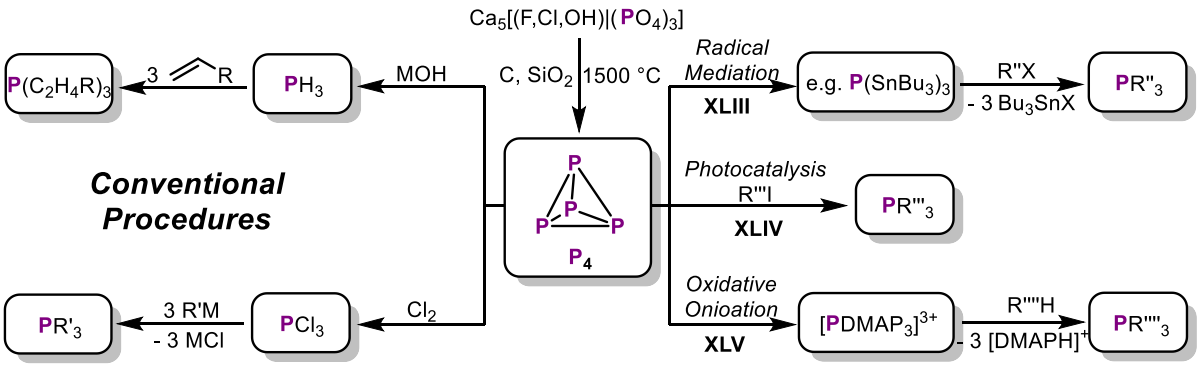

Scheme 19: Conventional synthetic route towards organo-phosphines (left) and novel approaches towards this challenge (right); R = usually alkyl residues, R' = usually aryl residues, R'' = various alkyl and aryl groups, R''' = aryl groups, R'''' = substituents derived from relatively acidic functional groups.

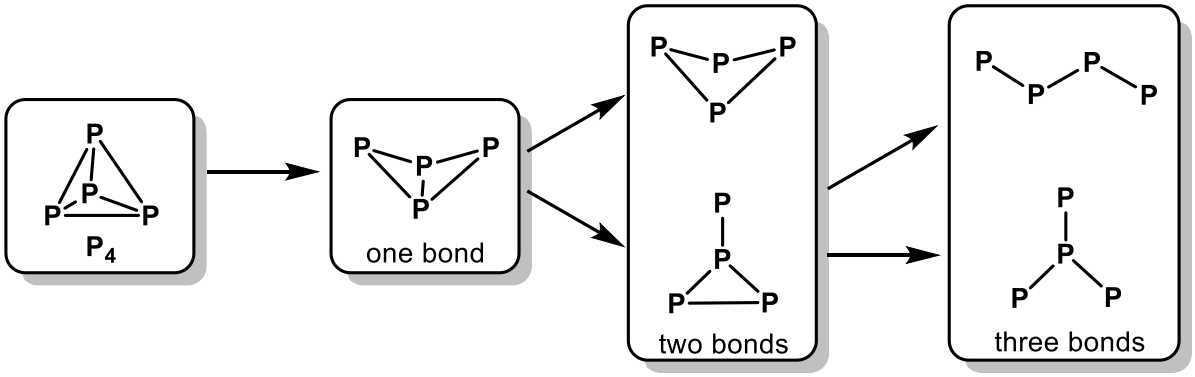

Scheme 20: Schematic representation of the stepwise degradation of P_4 via sequential P–P bond cleavage; Lone pairs of electrons and charges are neglected.

In contrast, P_4 and As_4 have been utilized numerously in the synthesis of Pn_2 complexes. The Pn_2 units in these compounds commonly act as bridging ligands between two metals. Thus, complexes with one bridging Pn_2 ligand are usually obtained in a tetrahedral (**IL**, Scheme 22)[204] or butterfly (**L**)[202b,205] conformation depending on the presence of a respective M–M bond. Notably, the former are isolobal to the respective Pn_4 tetrahedra themselves, as they are usually formed with TM fragments possessing 15 valence electrons (VE). Two Pn_2 ligands are incorporated within triple-decker compounds (**LI**)[204b,206] or cluster type arrangements,[207] while three Pn_2 units are found within prismatic TM clusters.[206f] Exceptions to these structural motives are the end-on bridging ($\mu,\eta^{1:1}$) P_2 unit in a Nb siloxide complex,[208] or a phosphido-phosphinidene P_2 ligand bridging three Ta centers.[209]

Pn_3 complexes obtained by the activation of P_4 or As_4 are similarly numerous. Most commonly, the respective products contain a *cyclo*-Pn_3 ligand in either bridging or end-deck coordination mode. Again, the combination of a TM moiety with 15 VE and the *cyclo*-Pn_3 ligand leads to compounds which are isolobal to Pn_4 (**LII**, Scheme 23),[204a–c,210] yet other end-deck *cyclo*-Pn_3 compounds are readily available as well.[211] In contrast, the bridging mode of the *cyclo*-Pn_3 ligand is commonly realized within triple-decker complexes or related species (**LIII**).[210b,210d,210j,211f,212] Furthermore, compounds with *catena*-Pn_3 ligands are known,[206i,206j,213] but not obtained from Pn_4 as readily as *cyclo*-Pn_3 complexes.

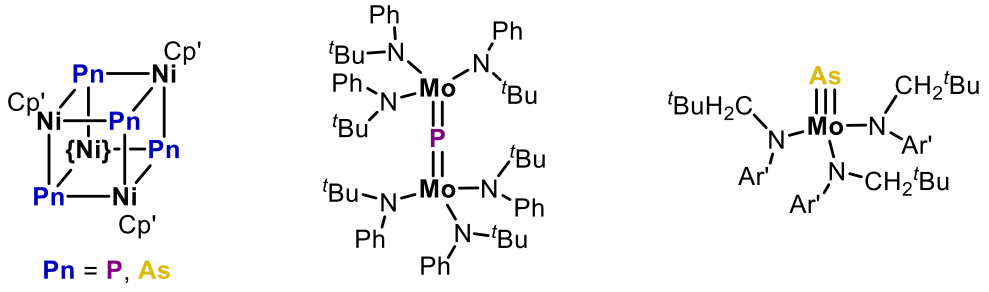

XLVI **XLVII** **XLVIII**

Scheme 21: Selected Pn_1 complexes prepared from Pn_4; Cp' = C_5H_4Me, {Ni} = Cp'Ni, Ar' = 3,5-dimethylphenyl.

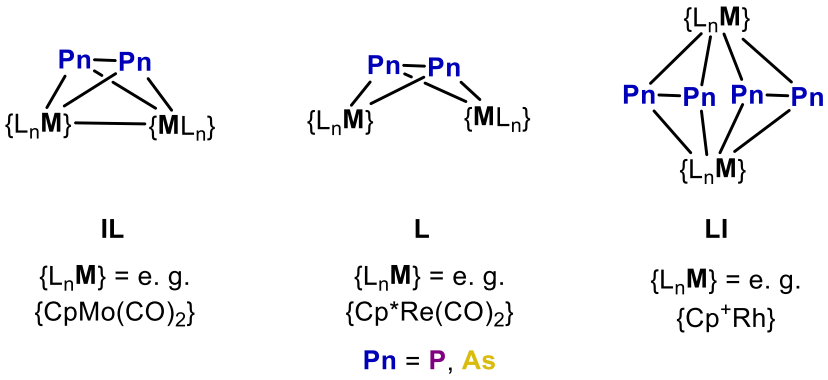

Scheme 22: Selected Pn_2 complexes prepared from Pn_4; Cp = C_5Me_5, Cp^+ = C_5Me_4Et.*

Complexes featuring Pn_4 ligands are by far the most accessible Pn_n ligand complexes (from P_4/As_4) which can be attributed to the comparably small number of Pn–Pn bonds that need to be cleaved/rearranged. Additionally, Pn_4 ligands show the greatest structural diversity compared to their smaller (n = 1-3) and larger (n = 5-8) congeners and can usually be obtained in various coordination modes. While the lone pairs of electrons at each of the Pn atoms in P_4 and As_4 allowed the synthesis of various η^1 coordinated complexes (e. g. **LIV,** Scheme 24) of intact Pn_4 tetrahedra,[210d,210e,214] η^2 coordinated side-on complexes (e. g. **LV**)[215] could also be obtained especially with coinage metals. Notably, this is due to the HOMO of uncoordinated Pn_4 being located at a Pn–Pn bond rather than the lone pairs, which possess significant s-orbital character. The more common observation of η^1 bound Pn_4 is thus attributed to a more complex electronic interaction between the TM and the Pn_4 tetrahedron.[214l] Cleavage of one Pn–Pn bond affords the butterfly Pn_4 motif, which is usually obtained by insertion of a TM moiety ($\eta^{1:1}$, e. g. **LVI**)[214e,216] or the addition of TM units to the wing-tip Pn atoms ($\mu,\eta^{1:1}$, e. g. **LVII**).[216j,216k,217] When a second Pn–Pn bond is cleaved, there are two possibilities to do so. Most commonly, this affords the formation of *cyclo*-Pn_4 ligand complexes, in which the *cyclo*-Pn_4 ligand can bind in end-deck (**LVIII**),[179,180,206g,206i,206j,218] bridging (e. g. **LIX**)[212g,212h,216d,216f,216m,216n,216j,218c,219] or even more complicated coordination

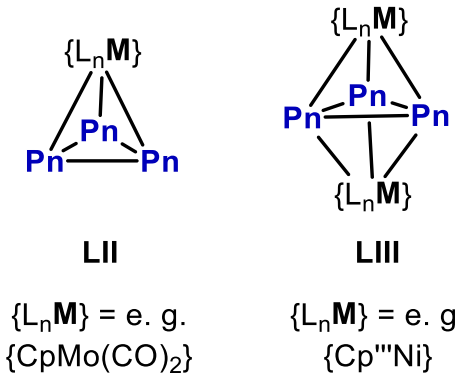

Scheme 23: Selected end-deck and triple-decker cyclo-Pn_3 ligand complexes prepared from Pn_4; Cp''' = 1,2,4-$^tBu_3C_5H_2$.

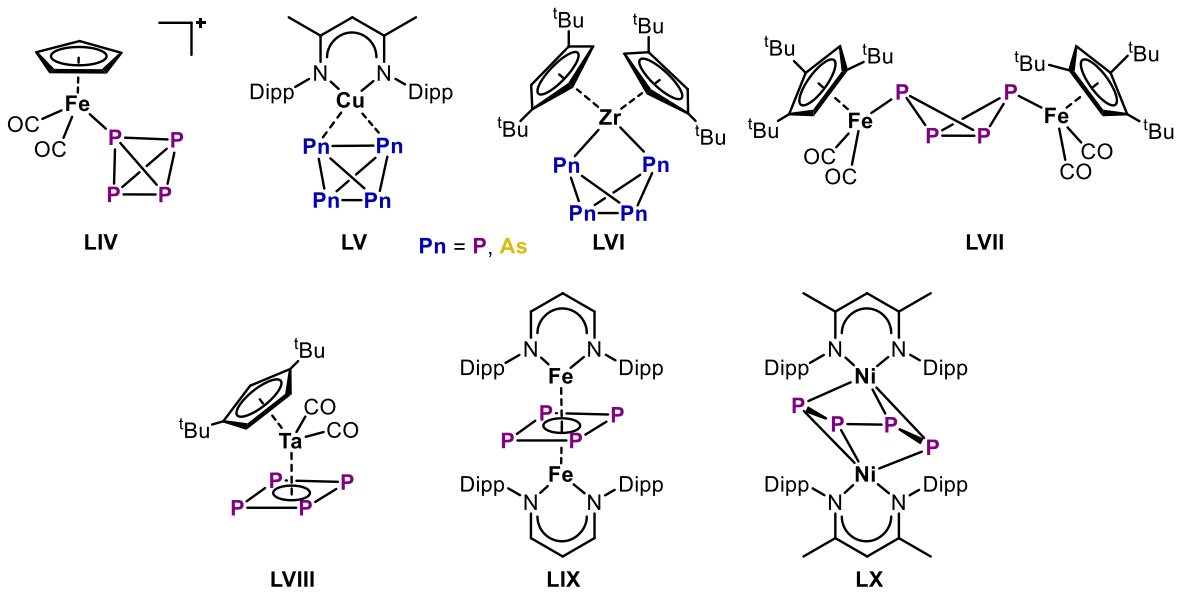

Scheme 24: Selected examples of Pn_4 complexes prepared from Pn_4; Dipp = 2,6-diisopropylphenyl.

mode.[206h,216g,216h,216k,216l,220] In contrast, compounds with a *cyclo*-Pn_3-Pn ligand are far less known and only obtained upon simultaneous substitution.[210i,221] Finally, cleavage of a third Pn–Pn bond affords either *catena*-Pn_4 ligand complexes (e. g. **LX**)[211g,212i,216c,216f,216j,216m,217a,222] or compounds with the rarer branched $Pn(Pn)_3$ ligand.[200b,209,223]

The *cyclo*-Pn_5 ligand could first be stabilized within the triple decker complex **LXI** (Scheme 25),[224] which was however obtained by utilizing $(MeAs)_5$ as As source. While several triple-decker and inverse sandwich complexes of *cyclo*-Pn_5 are accessible from both P_4 as well as As_4,[206l,210h,217e,225] sandwich compounds with an end-deck *cyclo*-Pn_5 ligand[217a,219j,226] also became available within a short time. Importantly, the *cyclo*-Pn_5 ligand takes a special place, as it displays the isolobal counterpart to the cyclopentadienide anion ($C_5H_5^-$),[19] arguably one of the most important ligands in organometallic chemistry. While the carbon-free sandwich compound **LXII**[227] surely displays a landmark within this field, the seminal pentaphosphaferrocene **LXIII**,[226a] featured only one *cyclo*-P_5 ligand. Similarly to the *cyclo*-Pn_5 ligand, the *cyclo*-Pn_6 ligand owes its significance to its isolobal carbocyclic counterpart,[19]

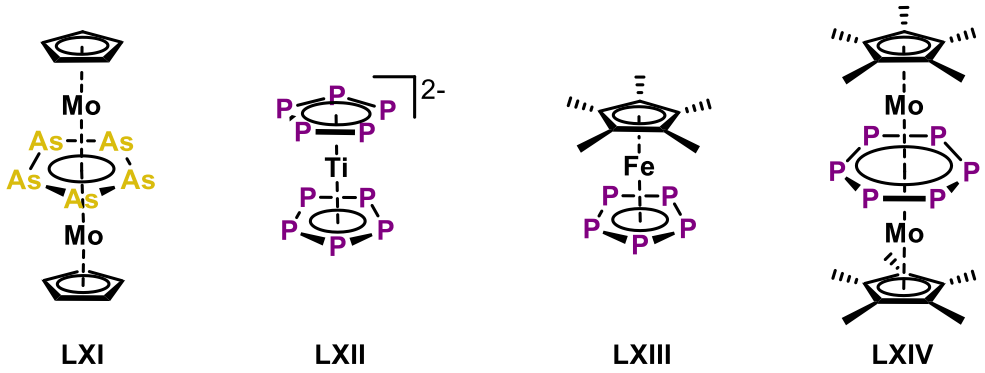

Scheme 25: Selected examples of cyclo-Pn_5 and cyclo-P_6 ligand complexes prepared from Pn_4.

namely prototypical benzene. Both, the *cyclo*-P_6[204b,206i,206j,218a,228] as well as the *cyclo*-As_6[206d] ligand could be stabilized within triple decker complexes (**LXIV**, Scheme 25) synthesized from P_4 and As_4, respectively. However, complexes featuring Pn_6 ligands with different structural motives could also be obtained in this way.[208] Thus, compounds with e. g. prismatic[219j,229] or bicyclic[212e,230] Pn_6 ligands are available as well.

In comparison to the compounds above, larger Pn_n ligands become even rarer with the number of Pn atoms present. Only few Pn_7 ligand complexes are known, mostly featuring a nortricyclan-type scaffold and group 3 or f-block metals (**LXV**, Scheme 26).[231] In contrast, the group of Pn_8 ligands makes up the majority of these larger compounds. The most common structural motif within this group are cunean/realgar-type Pn_8 ligand complexes (**LXVII**),[216i,219g,231a,232] but more complex (e. g. bicyclic) arrangements[179,225d,233] and even *cyclo*-As_8 ligand complexes (**LXVII**)[234] could be realized within the past decades. Even larger Pn_n ligand scaffolds with up to 24 P atoms[235] and 12 As atoms[236] are accessible from the controlled reaction of unsaturated Co complexes with P_4 and As_4, respectively. Finally, several exotic complexes featuring extended Pn_{10}[237] or P_{11}[219e] ligands could also be obtained from the activation of the Pn_4 tetrahedra.

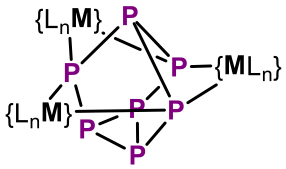

LXV

{L_n**M**} = e. g. {1,1′-Fc(NSi^{t}BuMe$_2$)$_2$**Sc**}

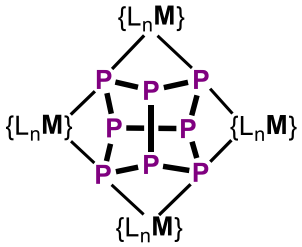

LXVI

{L_n**M**} = e. g. {Cp*$_2$**Sm**}

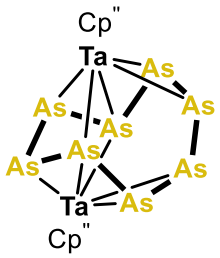

LXVII

Scheme 26: Selected P_7 and Pn_8 ligand complexes prepared from Pn_4.

1.3.3. Reactivity

Coordination

The most obvious difference between Pn_n ligand complexes and their carbocyclic counterparts are the free lone pairs of electrons at each of the respective Pn atoms. The availability of these lone pairs enables Pn_n ligand complexes to engage in further coordination chemistry. While this has in part been demonstrated already during the initial synthesis of these compounds (*vide supra*), reaction of uncoordinated Pn_n ligand complexes with coordinatively unsaturated (transition-) metal compounds displays a more general approach towards Pn_n ligand based coordination compounds. Examples for simple molecular coordination complexes of this type are **LXVIII**[238] and **LXIX**[239] (Scheme 27), arising from the coordination of AuCl or a second {CpFe} unit to the respective P_1 and *cyclo*-P_5 complex. Notably, in the latter the π-donor

capability of the *cyclo*-P_5 ligand overshadows the donating capability of the lone pairs at the P atoms and thus leads to formation of a triple-decker complex. Related triple-decker compounds and other molecular coordination compounds could be isolated numerously from reactions of Pn_n ligand complexes with suitable (transition-) metal precursors.[240] However, the *Scheer* group could expand this concept to achieve the synthesis of 1D-, 2D-, and even 3D coordination polymers by reacting Pn_n ligand complexes with coinage metal[241] and group 13 salts.[241e,242] While the initial focus was on the lighter P_n ligand complexes, arguably due to their stronger donating character, latest results on heavier Pn_n (e. g. As_n)[243] ligand complexes highlight their capacity to assemble within unprecedented supramolecular aggregates. Furthermore, the additional integration of organic linking units could be achieved, which afforded the formation of organometallic-organic hybrid materials.[244] However, the reaction of Pn_n ligand complexes with coinage metal salts can also lead to the formation of spherical supramolecular aggregates with C_{60} topology and beyond.[245] Outstandingly, these compounds display all-inorganic counterparts to fullerenes and demonstrate the immense potential of Pn_n ligand complexes in coordination chemistry, which has been highlighted in several review articles.[246]

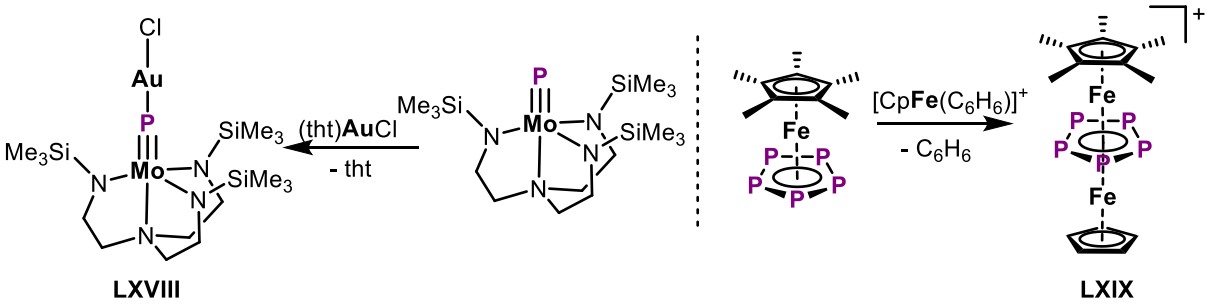

*Scheme 27: Selected examples of further coordination reactivity of P_n ligand complexes leading to bridging phosphido (**LXVIII**) and triple decker (**LXIX**) complexes.*

Besides their rich coordination chemistry, Pn_n ligand complexes also exhibit interesting redox reactivity. Especially, the reduction of Pn_n ligand complexes to anionic TM stabilized polypnictides has been studied over the past decades. The utilization of common, alkali metal based, reduction agents (e. g. KC_8) may lead to a doubly reduced species (e. g. **LXX**, Scheme 28),[247] dimeric products (e. g. **LXXI**),[247a,248] or even scrambling/fragmentation reactions and thus the formation of unexpected anionic Pn_n ligand complexes (e. g. **LXXII**).[248a,249] Consequently, the reaction of Pn_n ligand complexes with highly reducing lanthanide compounds has been found to serve as a useful way to access mixed d-/f-block polypnictides (e. g. **LXXIII**).[250] Similarly, conversion of Pn_n complexes with group 2 based reductants allows the preparation of TM polypnictides, in which the group 2 metal is closely assembled with the Pn_n framework.[251] The closely associated functionalization of Pn_n ligand complexes with nucleophiles is equally well developed. Both, anionic as well as neutral nucleophiles can simply add to the Pn_n ligands and thus provide functionalized complexes (e. g. **LXXIV**, Scheme 29), respectively.[211e,248b,252] However, the nucleophilic addition can also trigger rearrangement of the Pn_n ligand,[248b,253] as in **LXXV**, or even fragmentation reactions (e. g. **LXXVI**).[254] A highly selective fragmentation reaction can for example be observed in the NHC mediated ring contraction of several *cyclo*- Pn_n ligands.[48b] Furthermore, studies on the controlled hydrolysis and halogenation of TM coordinated P_4 by the group of *Peruzzini* gave invaluable insight into the mechanism of this fundamental fragmentation reaction of P_4 itself.[255] Similarly, the halogenation of Pn_n ligand complexes provided crucial understanding of the highly relevant process of e. g. P_4 halogenation.[256] Lastly, the reaction of Pn_n ligand complexes with low valent main group compounds has been demonstrated to afford unprecedented mixed main group compounds stabilized within the coordination sphere of the TM. This allowed the preparation of TM bound polypnictogen ligands incorporating Al,[257] Ga,[258] Si,[259] Ge,[260] Sn,[260a,261] and Pb.[260a,261b] The reaction of a Zr bound Pn_4 ligand with a halide substituted silylene even provided access to the TM free **LXXVII**, which are Pn/Si analogs (Pn = P, As) of benzene

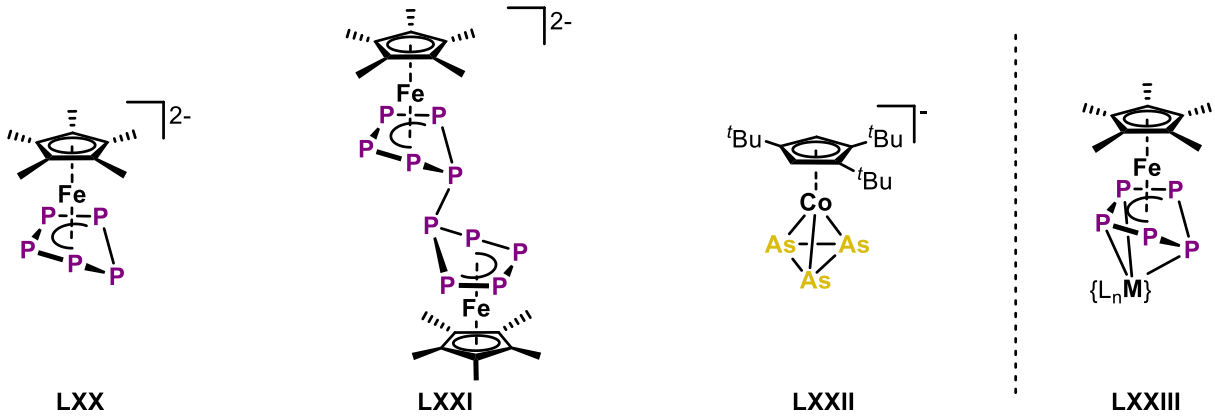

Scheme 28: Selected TM stabilized polypnictide anions arising from the reduction of Pn_n ligand complexes (left) and a mixed d-/f-metal triple decker complex with a P_5 middle deck (right); $\{L_nM\}$ = {(2,5-bis{N-(2,6-diisopropylphenyl)iminomethyl}pyrrolyl)Sm}.

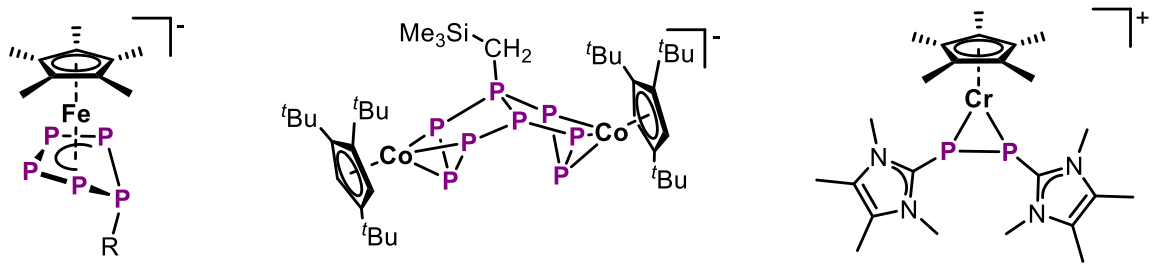

LXXIV **LXXV** **LXXVI**

*Scheme 29: Selected example of nucleophilically functionalized P_n ligand complexes resulting from addition (**LXXIV**), aggregation (**LXXV**) or fragmentation (**LXXVI**); R = alkyl, dialkylamino, aryl.*

(Scheme 30).[262] Notably, the nucleophilic functionalization of Pn_n ligand complexes has mainly focused on the phosphorus derivatives, while As_n ligands have rarely been studied and the nucleophilic functionalization of the heavier congeners is virtually unknown.

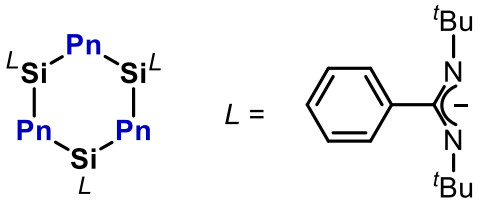

LXXVII **Pn** = **P**, **As**

*Scheme 30: Inorganic Pn/Si benzene analogs (**LXVII**) arising from the reaction of a chloro-silylene with **LVI**.*

However, the subsequent addition of electrophiles to anionic Pn_n, but especially P_n ligand complexes, is comparably well established. Simple salt-metathesis reactions facilitate the introduction of further substituents (e. g. **LXXVIII**, Scheme 31),[263] rearrangement reactions (e. g. **LXXIX**),[253g] or expansion of the P_n ligand (e. g. **LXXX**),[249,253h,264] when a Pn based electrophile is used. Prominently, the sequential nucleophilic/electrophilic functionalization of pentaphosphaferrocene **LXIII**[226a] recently allowed the preparation of asymmetric

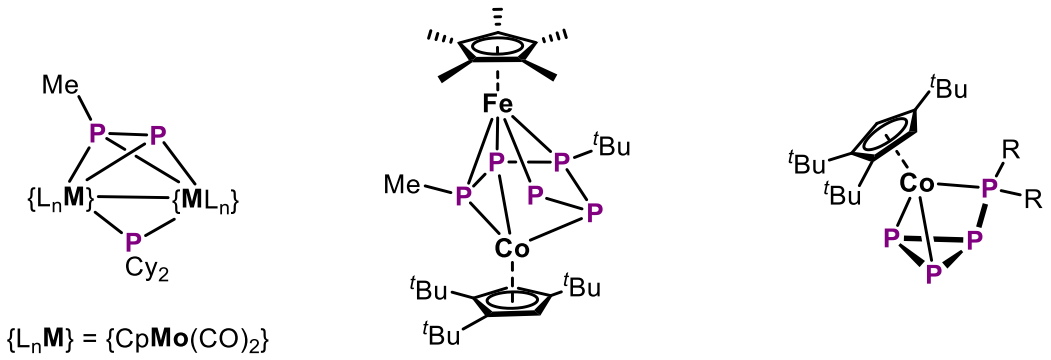

$\{L_nM\} = \{CpMo(CO)_2\}$

LXXVIII **LXXIX** **LXXX**

*Scheme 31: Selected examples of functionalized Pn_n ligand complexes arising from electrophile addition (**LXXVIII**), rearrangement (**LXXIX**) or expansion (**LXXX**) to anionic polypnictogen complexes.*

phosphines.[265] Further reactivity of Pn_n ligands involves their transfer between TM centers (e. g. *cyclo*-P_5),[266] or reactivity towards unsaturated substrates, such as phosphaalkynes. The latter was shown to afford Fe coordinated phospholyl ligands[267] or highly extended organo-polyphosphorus frameworks coordinated to early TMs.[268] Interestingly, P_1 ligand complexes also display a potential synthetic entry into phosphaalkynes.[269] Finally, several P_2 complexes can serve as sources for the transient P_2 molecule under suitable conditions,[270] which has been utilized for the synthesis of valuable organic molecules containing a P_2 unit.

Cationic Polypnictogen Complexes: Challenges and New Potential

In striking contrast to the above discussion, cationic Pn_n ligand complexes have been investigated to a far lower extent. As this closely resembles the situation of TM free polypnictogen species (*vide supra*), the decreased availability of TM coordinated polypnictogen cations may as well be attributed to their high reactivity as well as challenging preparation. However, these compounds display intriguing synthetic targets, as the coordinated TM may allow the isolation of otherwise unstable polypnictogen cations. Furthermore, this route displays another entry into the functionalization of Pn_n ligand complexes and thus give valuable insight into the transformation of P_4/As_4. Consecutive nucleophilic or reductive transformation of TM coordinated polypnictogen cations could facilitate the preparation of yet unprecedented polypnictogen compounds. With this in mind, the potential synthetic pathways towards TM bound polypnictogen cations can be grouped into three distinct categories (Scheme 32).

The presence of a TM in Pn_n ligand complexes usually allows for their oxidation. Thus, neutral Pn_n ligand complexes can be transformed into the respective cations by addition of a suitable oxidation reagent. While this pathway is rarely applicable to TM free polypnictogen cations, besides e. g. **XXVIII**,[135,136] it has already seen utilization for the synthesis of TM bound Pn_n cations. Small Pn_2 complexes can be oxidized to form Pn_4 chains (**LXXXI**, Scheme 33),

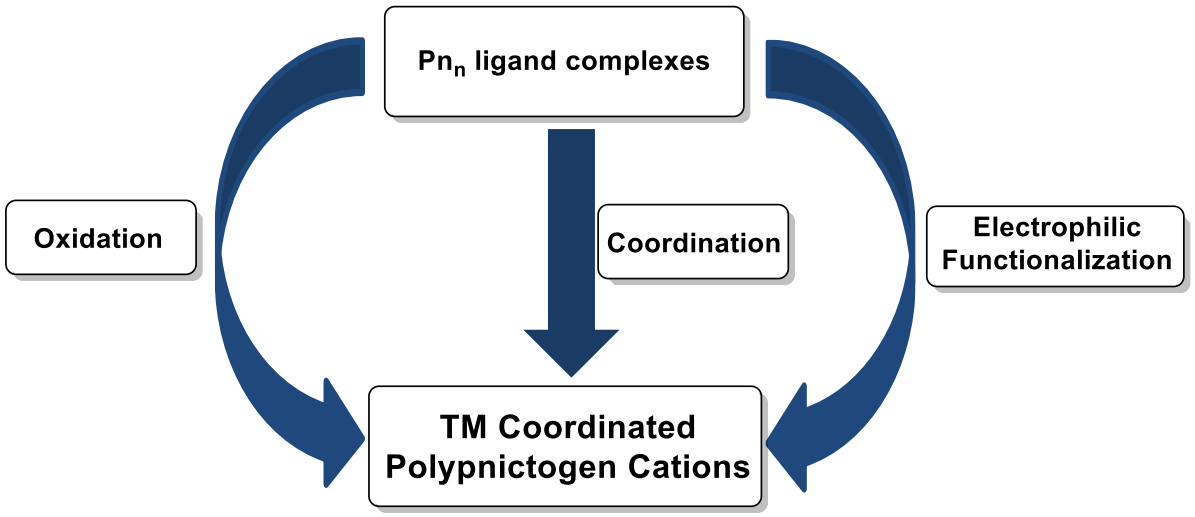

Scheme 32: Conceptual access to TM coordinated polypnictogen cations via oxidation, coordination or electrophilic functionalization.

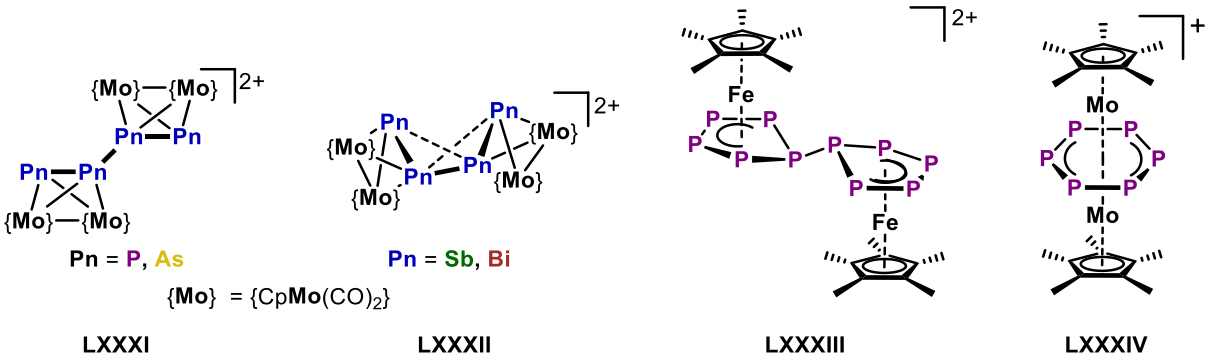

Scheme 33: Selected TM stabilized polypnictogen cations arising from the oxidation of Pn_n ligand complexes.

cages (**LXXXII**),[271] and even hetero-polypnictogen cations.[272] Similarly, the *cyclo*-P_5 complex **LXIII**[226a] can be oxidized under P–P bond formation to yield a P_{10} ligand complex (**LXXXIII**).[247a,273] In contrast, the oxidation of *cyclo*-Pn_6[241e,274] and other Pn_n triple-decker[247b,247c] complexes only leads to distortion of the ligand (e. g. **LXXXIV**). Lastly, oxidation of Pn_n ligand complexes can also lead to fragmentation.[247c,275]

The second pathway towards cationic Pn_n ligand complexes is the coordination of cationic/neutral polyphosphorus species to neutral or cationic TM units, respectively. Most of these compounds fall along the lines of complexes of intact P_4 or As_4 tetrahedra (e. g. **LIV**) as well as few examples of rearranged Pn_n moieties (*vide supra*). However, the coordination of polyphosphorus cations to neutral TM species can also lead to rearrangement within the polyphosphorus unit as in the *cyclo*-P_5R_2 complex **LXXXV** (Scheme 34).[276] Furthermore, the coordination of additional TM units to preformed TM bound polypnictogen cations has been demonstrated to furnish intriguing species, such as the azide analogs **LXXXVI**.[277]

The third and last potential way towards TM bound polypnictogen cations is the functionalization of neutral Pn_n ligand complexes with cationic electrophiles. While the potential of this approach has been utilized very early on within the investigation of Pn_n ligand complexes, it did not receive significant attention within the past decades. Thus, examples of

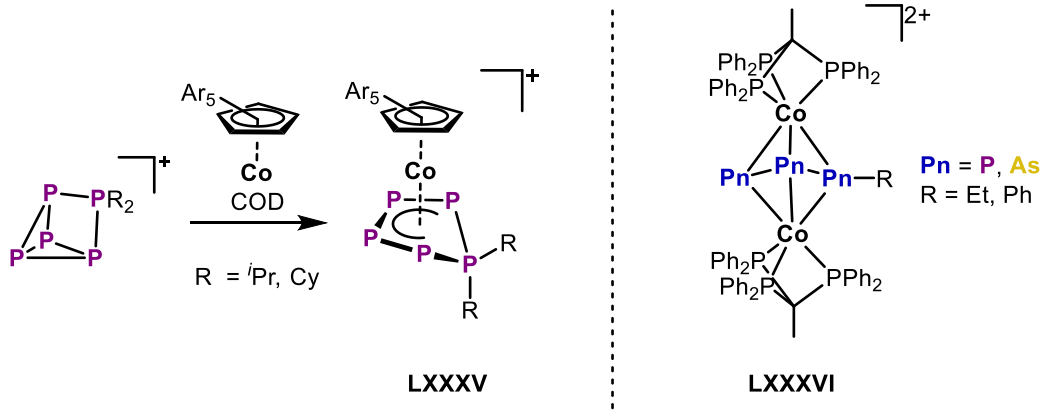

*Scheme 34: Synthesis of the TM coordinated polyphosphorus cation **LXXXV** via coordination of a $Cp^{Ar5}Co$ unit (left) and the heavy azide analogs **LXXXVI** (right); COD = cyclo-octadiene, $Cp^{Ar5} = C_5(C_6H_4\text{-}4\text{-}Et)_5$.*

it being utilized are restricted to the alkylation and protonation reactions of a *cyclo*-Pn_3 ligand leading to e. g. **LXXXVII** (Scheme 35),[278] and related prefunctionalized species.[279] While salt metathesis reactions between anionic P_n ligand complexes and halo-phosphines are well established,[249] e. g. affording *cyclo*-P_5R_2 ligands,[254a,258a] the electrophilic functionalization with pnictogenium cations has only recently been transferred to neutral P_n ligand complexes.[275] Thus, *in situ* generated phosphenium cations readily insert into one of the P–P bonds of a butterfly P_4 complex to afford **LXXXVIII**.[280] Notably, neutral Pn centered electrophiles have previously been shown to insert into non-polar *cyclo*-Pn_n ligands as well.[281]

Conclusively, the chemistry of TM stabilized polypnictogen cations is highly underdeveloped compared to their neutral as well as anionic TM homologs (*vide supra*). While three potential synthetic pathways towards TM bound polypnictogen cations have been pointed out, these have seen variable utilization. Oxidation of neutral Pn_n ligand complexes has been proven to be a valuable tool in accessing TM stabilized polypnictogen cations with novel structural and bonding motifs. Coordination to cationic TM units has often been utilized to access complexes featuring intact Pn_4 tetrahedra but this does not always facilitate further transformation to other Pn_n scaffolds. Most notably, the potential of the electrophilic functionalization of Pn_n ligand complexes has substantially been overlooked for the past decades.

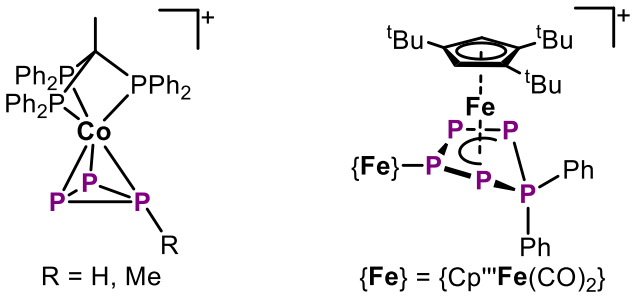

Scheme 35: Rare examples of TM coordinated polyphosphorus cations arising directly from the electrophilic functionalization of neutral P_n ligand complexes.

1.4. References

[1] A. F. Holleman, N. Wiberg in *Lehrbuch der anorganischen Chemie*, De Gruyter, Berlin (DE), **2007**, 651–860.

[2] Y. T. Oganessian, V. K. Utyonkoy, Y. V. Lobanov, F. S. Abdullin, A. N. Polyakov, I. V. Shirokovsky, Y. S. Tsyganov, G. G. Gulbekian, S. L. Bogomolov, A. N. Mezentsev, S. Iliev, V. G. Subbotin, A. M. Sukhov, A. A. Voinov, G. V. Buklanov, K. Subotic, V. I. Zagrebaev, M. G. Itkis, J. B. Patin, K. J. Moody, J. F. Wild, M. A. Stoyer, N. J. Stoyer, D. A. Shaughnessy, J. M. Kenneally, R. W. Lougheed, *Phys. Rev. C* **2004**, *69*.

[3] A. F. Holleman, N. Wiberg in *Lehrbuch der anorganischen Chemie*, De Gruyter, Berlin (DE), **2007**, 302.

[4] L. Pauling, *The Nature of the Chemical Bond and the Structure of Molecules & Crystals*, Cornell University Press, Ithaca, **1973**.

[5] A. F. Holleman, N. Wiberg in *Lehrbuch der anorganischen Chemie*, De Gruyter, Berlin (DE), **2007**, 2145–2148.

[6] J. W. Erisman, M. A. Sutton, J. Galloway, Z. Klimont, W. Winiwarter, *Nat. Geosci.* **2008**, *1*, 636–639.

[7] a) F. Haber, R. Le Rossignol, “Production of ammonia”, U. S. Patent 1202995A, **1909**; b) C. Bosch, “Process of producing ammonia”, U. S. Patent 990191, **1908**.

[8] F. Haber, *Nobel Lecture* **1920**.

[9] C. Bosch, *Nobel Lecture* **1932**.

[10] V. Smil, *Enriching the earth*. *Fritz Haber, Carl Bosch, and the transformation of world food production*, MIT Press, Cambridge, **2004**.

[11] D. E. C. Corbridge, *Phosphorus*. *Chemistry, biochemistry and technology*, CRC Press, Boca Raton, **2013**.

[12] D. E. C. Corbridge, E. J. LOWE, *Nature* **1952**, *170*, 629.

[13] X. Ling, H. Wang, S. Huang, F. Xia, M. S. Dresselhaus, *Proc. Natl. Acad. Sci. U.S.A.* **2015**, *112*, 4523–4530.

[14] A. Carvalho, M. Wang, X. Zhu, A. S. Rodin, H. Su, A. H. Castro Neto, *Nat. Rev. Mater.* **2016**, *1*, 1–16.

[15] A. Pfitzner, M. F. Bräu, J. Zweck, G. Brunklaus, H. Eckert, *Angew. Chem. Int. Ed.* **2004**, *43*, 4228–4231.

[16] W. Jansen, M. Ducci, *CHEMKON* **2006**, *13*, 133–142.

[17] J. A. Osborn, F. H. Jardine, J. F. Young, G. Wilkinson, *J. Chem. Soc. A* **1966**, 1711.

[18] a) P. Schwab, M. B. France, J. W. Ziller, R. H. Grubbs, *Angew. Chem. Int. Ed. Engl.* **1995**, *34*, 2039–2041; b) M. Scholl, S. Ding, C. W. Lee, R. H. Grubbs, *Org. Lett.* **1999**, *1*, 953–956.

[19] R. Hoffmann, *Angew. Chem. Int. Ed. Engl.* **1982**, *21*, 711–724.

[20] a) K. B. Dillon, F. Mathey, J. F. Nixon, *Phosphorus*. *The carbon copy: from organophosphorus to phospha-organic chemistry*, John Wiley & Sons, Chichester (UK),

New York (US), Weinheim (DE), Brisbane (AU), Singapore (SG) Toronto (CA), **2022**; b) F. Mathey, *Angew. Chem. Int. Ed.* **2003**, *42*, 1578–1604.

[21] M. Seidl, G. Balázs, M. Scheer, *Chem. Rev.* **2019**, *119*, 8406–8434.

[22] A. E. Seitz, F. Hippauf, W. Kremer, S. Kaskel, M. Scheer, *Nat. Commun.* **2018**, *9*, 361–367.

[23] D. W. Bierer, *Clin. Infect. Dis.* **1990**, *12*, 3-8.

[24] M. Mato, D. Spinnato, M. Leutzsch, H. W. Moon, E. J. Reijerse, J. Cornella, *Nat. Chem.* **2023**, *15*, 1138–1145.

[25] H. W. Moon, J. Cornella, *ACS Catal.* **2022**, *12*, 1382–1393.

[26] a) M. N. Hopkinson, C. Richter, M. Schedler, F. Glorius, *Nature* **2014**, *510*, 485–496; b) V. Nesterov, D. Reiter, P. Bag, P. Frisch, R. Holzner, A. Porzelt, S. Inoue, *Chem. Rev.* **2018**, *118*, 9678–9842.

[27] F. Dielmann, O. Back, M. Henry-Ellinger, P. Jerabek, G. Frenking, G. Bertrand, *Science* **2012**, *337*, 1526–1528.

[28] L. Liu, D. A. Ruiz, D. Munz, G. Bertrand, *Chem.* **2016**, *1*, 147–153.

[29] a) A. Velian, C. C. Cummins, *J. Am. Chem. Soc.* **2012**, *134*, 13978–13981; b) W. J. Transue, A. Velian, M. Nava, C. García-Iriepa, M. Temprado, C. C. Cummins, *J. Am. Chem. Soc.* **2017**, *139*, 10822–10831.

[30] A. Velian, M. Nava, M. Temprado, Y. Zhou, R. W. Field, C. C. Cummins, *J. Am. Chem. Soc.* **2014**, *136*, 13586–13589.

[31] Y. Pang, N. Nöthling, M. Leutzsch, L. Kang, E. Bill, M. van Gastel, E. Reijerse, R. Goddard, L. Wagner, D. SantaLucia, S. DeBeer, F. Neese, J. Cornella, *Science* **2023**, *380*, 1043–1048.

[32] P. Simon, F. de Proft, R. Jambor, A. Růzicka, L. Dostál, *Angew. Chem. Int. Ed.* **2010**, *49*, 5468–5471.

[33] K. Hansen, T. Szilvási, B. Blom, S. Inoue, J. Epping, M. Driess, *J. Am. Chem. Soc.* **2013**, *135*, 11795–11798.

[34] A. Doddi, M. Weinhart, A. Hinz, D. Bockfeld, J. M. Goicoechea, M. Scheer, M. Tamm, *Chem. Commun.* **2017**, *53*, 6069–6072.

[35] R. Kretschmer, D. A. Ruiz, C. E. Moore, A. L. Rheingold, G. Bertrand, *Angew. Chem. Int. Ed.* **2014**, *53*, 8176–8179.

[36] G. Wang, L. A. Freeman, D. A. Dickie, R. Mokrai, Z. Benkő, R. J. Gilliard, *Chem. Eur. J.* **2019**, *25*, 4335–4339.

[37] M. Regitz, *Chem. Rev.* **1990**, *90*, 191–213.

[38] P. B. Hitchcock, C. Jones, J. F. Nixon, *J. Chem. Soc., Chem. Commun.* **1994**, *18*, 2061–2062.

[39] T. Görlich, P. Coburger, E. S. Yang, J. M. Goicoechea, H. Grützmacher, C. Müller, *Angew. Chem. Int. Ed.* **2023**, *62*, e202217749.

[40] H. Jun, V. G. Young, R. J. Angelici, *J. Am. Chem. Soc.* **1992**, *114*, 10064–10065.

[41] D. W. N. Wilson, S. J. Urwin, E. S. Yang, J. M. Goicoechea, *J. Am. Chem. Soc.* **2021**, *143*, 10367–10373.

[42] E. S. Yang, J. M. Goicoechea, *Angew. Chem. Int. Ed.* **2022**, *61*, e202206783.

[43] E. S. Yang, D. W. N. Wilson, J. M. Goicoechea, *Angew. Chem. Int. Ed.* **2023**, *62*, e202218047.

[44] N. T. Coles, A. Sofie Abels, J. Leitl, R. Wolf, H. Grützmacher, C. Müller, *Coord. Chem. Rev.* **2021**, *433*, 213729–213754.

[45] G. Märkl, *Angew. Chem. Int. Ed. Engl.* **1966**, *5*, 846–847.

[46] a) K.-C. Schwan, A. Y. Timoskin, M. Zabel, M. Scheer, *Chem. Eur. J.* **2006**, *12*, 4900–4908; b) C. Marquardt, A. Adolf, A. Stauber, M. Bodensteiner, A. V. Virovets, A. Y. Timoshkin, M. Scheer, *Chem. Eur. J.* **2013**, *19*, 11887–11891; c) C. Marquardt, O. Hegen, M. Hautmann, G. Balázs, M. Bodensteiner, A. V. Virovets, A. Y. Timoshkin, M. Scheer, *Angew. Chem. Int. Ed.* **2015**, *54*, 13122–13125; d) M. A. K. Weinhart, A. S. Lisovenko, A. Y. Timoshkin, M. Scheer, *Angew. Chem. Int. Ed.* **2020**, *59*, 5541–5545; e) M. A. K. Weinhart, M. Seidl, A. Y. Timoshkin, M. Scheer, *Angew. Chem. Int. Ed.* **2021**, *60*, 3806–3811.

[47] Z. Feng, S. Tang, Y. Su, X. Wang, *Chem. Soc. Rev.* **2022**, *51*, 5930–5973.

[48] a) C. L. B. Macdonald, J. F. Binder, A. Swidan, J. H. Nguyen, S. C. Kosnik, B. D. Ellis, *Inorg. Chem.* **2016**, *55*, 7152–7166; b) M. Piesch, S. Reichl, M. Seidl, G. Balázs, M. Scheer, *Angew. Chem. Int. Ed.* **2019**, *58*, 16563–16568; c) M. M. Siddiqui, S. K. Sarkar, M. Nazish, M. Morganti, C. Köhler, J. Cai, L. Zhao, R. Herbst-Irmer, D. Stalke, G. Frenking, H. W. Roesky, *J. Am. Chem. Soc.* **2021**, *143*, 1301–1306.

[49] a) A. Schmidpeter, S. Lochschmidt, W. S. Sheldrick, *Angew. Chem. Int. Ed. Engl.* **1982**, *21*, 63–64; b) A. Schmidpeter, S. Lochschmidt, W. S. Sheldrick, *Angew. Chem. Int. Ed. Engl.* **1985**, *24*, 226–227; c) B. D. Ellis, C. L. B. Macdonald, *Inorg. Chem.* **2004**, *43*, 5981–5986; d) B. D. Ellis, C. L. B. Macdonald, *Inorg. Chem.* **2006**, *45*, 6864–6874; e) E. L. Norton, K. L. S. Szekely, J. W. Dube, P. G. Bomben, C. L. B. Macdonald, *Inorg. Chem.* **2008**, *47*, 1196–1203; f) P. K. Coffer, K. B. Dillon, *Coord. Chem. Rev.* **2013**, *257*, 910–923; g) J. W. Dube, C. L. B. Macdonald, B. D. Ellis, P. J. Ragogna, *Inorg. Chem.* **2013**, *52*, 11438–11449; h) S. C. Kosnik, C. L. B. Macdonald, *Dalton Trans.* **2016**, *45*, 6251–6258.

[50] X. Wang, B. Lei, Z. Zhang, M. Chen, H. Rong, H. Song, L. Zhao, Z. Mo, *Nat. Commun.* **2023**, *14*, 2968–2979.

[51] a) S. Fleming, M. K. Lupton, K. Jekot, *Inorg. Chem.* **1972**, *11*, 2534–2540; b) B. E. Maryanoff, R. O. Hutchins, *J. Org. Chem.* **1972**, *37*, 3475–3480; c) A. H. Cowley, M. C. Cushner, M. Lattman, M. L. McKee, J. S. Szobota, J. C. Wilburn, *Pure Appl. Chem.* **1980**, *52*, 789–797.

[52] a) G. Boche, P. Andrews, K. Harms, M. Marsch, K. S. Rangappa, M. Schimeczek, C. Willeke, *J. Am. Chem. Soc.* **1996**, *118*, 4925–4930; b) Y. Tulchinsky, M. A. Iron, M. Botoshansky, M. Gandelman, *Nat. Chem.* **2011**, *3*, 525–531.

[53] a) S. G. Baxter, R. L. Collins, A. H. Cowley, S. F. Sena, *J. Am. Chem. Soc.* **1981**, *103*, 714–715; b) M. Olaru, A. Mischin, L. A. Malaspina, S. Mebs, J. Beckmann, *Angew. Chem. Int. Ed.* **2020**, *59*, 1581–1584.

[54] M. Olaru, D. Duvinage, E. Lork, S. Mebs, J. Beckmann, *Angew. Chem. Int. Ed.* **2018**, *57*, 10080–10084.

[55] M. Olaru, S. Mebs, J. Beckmann, *Angew. Chem. Int. Ed.* **2021**, *60*, 19133–19138.

[56] a) C. Üffing, A. Ecker, E. Baum, H. Schnöckel, *Z. Anorg. Allg. Chem.* **1999**, *625*, 1354–1356; b) J. Zhou, L. L. Liu, L. L. Cao, D. W. Stephan, *Chem.* **2018**, *4*, 2699–2708; c) J. Zhou, L. L. Liu, L. L. Cao, D. W. Stephan, *Angew. Chem. Int. Ed.* **2019**, *58*, 5407–5412; d) J. Zhou, H. Kim, L. L. Liu, L. L. Cao, D. W. Stephan, *Chem. Commun.* **2020**, *56*, 12953–12956.

[57] L. Greb, *Chem. Eur. J.* **2018**, *24*, 17881–17896.

[58] C. Frazee, N. Burford, R. McDonald, M. J. Ferguson, A. Decken, B. O. Patrick, *Chem. Eur. J.* **2018**, *24*, 4011–4013.

[59] J. S. Wenger, M. Weng, G. N. George, T. C. Johnstone, *Nat. Chem.* **2023**, *15*, 633–640.

[60] P. Mehlmann, T. Witteler, L. F. B. Wilm, F. Dielmann, *Nat. Chem.* **2019**, *11*, 1139–1143.

[61] P. Löwe, M. Feldt, M. A. Wünsche, L. F. B. Wilm, F. Dielmann, *J. Am. Chem. Soc.* **2020**, *142*, 9818–9826.

[62] P. Löwe, T. Witteler, F. Dielmann, *Chem. Commun.* **2021**, *57*, 5043–5046.

[63] P. Löwe, M. A. Wünsche, F. R. S. Purtscher, J. Gamper, T. S. Hofer, L. F. B. Wilm, M. B. Röthel, F. Dielmann, *Chem. Sci.* **2023**, *14*, 7928–7935.

[64] T. Curtius, *Ber. Dtsch. Chem. Ges.* **1890**, *23*, 3023–3033.

[65] a) B. Bazanov, U. Geiger, R. Carmieli, D. Grinstein, S. Welner, Y. Haas, *Angew. Chem. Int. Ed.* **2016**, *55*, 13233–13235; b) C. Zhang, C. Sun, B. Hu, C. Yu, M. Lu, *Science* **2017**, *355*, 374–376; c) C. Yang, C. Zhang, Z. Zheng, C. Jiang, J. Luo, Y. Du, B. Hu, C. Sun, K. O. Christe, *J. Am. Chem. Soc.* **2018**, *140*, 16488–16494.

[66] a) M. Baudler, *Angew. Chem. Int. Ed. Engl.* **1987**, *26*, 419–441; b) H. G. von Schnering, W. Hoenle, *Chem. Rev.* **1988**, *88*, 243–273; c) M. Baudler, K. Glinka, *Chem. Rev.* **1993**, *93*, 1623–1667; d) M. Baudler, K. Glinka, *Chem. Rev.* **1994**, *94*, 1273–1297; e) M. E. Schlesinger, *Chem. Rev.* **2002**, *102*, 4267–4301; f) M. Scheer, G. Balázs, A. Seitz, *Chem. Rev.* **2010**, *110*, 4236–4256; g) T. Wellnitz, C. Hering-Junghans, *Eur. J. Inorg. Chem.* **2021**, *2021*, 8–21.

[67] F. Kraus, J. C. Aschenbrenner, N. Korber, *Angew. Chem. Int. Ed.* **2003**, *42*, 4030–4033.

[68] a) F. Kraus, T. Hanauer, N. Korber, *Inorg. Chem.* **2006**, *45*, 1117–1123; b) N. Korber, M. Reil, *Chem. Commun.* **2002**, *1*, 84–85.

[69] S. C. Critchlow, J. D. Corbett, *Inorg. Chem.* **1984**, *23*, 770–774.

[70] A. Cisar, J. D. Corbett, *Inorg. Chem.* **1977**, *16*, 2482–2487.

[71] H. Grützmacher, *Z. Anorg. Allg. Chem.* **2012**, *638*, 1877–1879.

[72] a) M. Baudler, D. Düster, D. Ouzounis, *Z. Anorg. Allg. Chem.* **1987**, *544*, 87–94; b) M. Baudler, S. Akpapoglou, D. Ouzounis, F. Wasgestian, B. Meinigke, H. Budzikiewicz, H. Münster, *Angew. Chem. Int. Ed. Engl.* **1988**, *27*, 280–281.

[73] V. A. Milyukov, A. V. Kataev, O. G. Sinyashin, E. Hey-Hawkins, *Russ. Chem. Bull.* **2006**, *55*, 1297–1299.

[74] a) W. Schmettow, A. Lipka, H. G. von Schnering, *Angew. Chem. Int. Ed. Engl.* **1974**, *13*, 345; b) H. G. von Schnering, W. Hönle, W. Bauhofer, G. Kliche, T. Meyer, W. Schmettow, U. Hinze, *Z. Anorg. Allg. Chem.* **1987**, *553*, 261–279.

[75] F. Kraus, J. Schmedt Auf der Günne, B. F. DiSalle, N. Korber, *Chem. Commun.* **2006**, *2*, 218–219.

[76] E. Zintl, *Angew. Chem.* **1939**, *52*, 1–6.

[77] M. Baudler, W. Faber, *Chem. Ber.* **1980**, *113*, 3394–3395.

[78] F. Emmerling, C. Röhr, *Z. Naturforsch. B* **2002**, *57*, 963–975.

[79] a) C. Hirschle, C. Röhr, *Z. Anorg. Allg. Chem.* **2000**, *626*, 1992–1998; b) F. Mutzbauer, N. Korber, *Acta Crystallogr. E* **2011**, *67*, 1551-1551.

[80] a) W. Dahlmann, H. G. v. Schnering, *Sci. Nat.* **1972**, *59*, 420; b) H. G. von Schnering, V. Manriquez, W. Hönle, *Angew. Chem. Int. Ed. Engl.* **1981**, *20*, 594–595; c) M. Baudler, O. Exner, *Chem. Ber.* **1983**, *116*, 1268–1270; d) M. Baudler, D. Düster, K. Langerbeins, J. Germeshausen, *Angew. Chem. Int. Ed. Engl.* **1984**, *23*, 317–318; e) M. Baudler, D. Düster, J. Germeshausen, *Z. Anorg. Allg. Chem.* **1986**, *534*, 19–26.

[81] M. Baudler, R. Heumller, D. Dster, J. Germeshausen, J. Hahn, *Z. Anorg. Allg. Chem.* **1984**, *518*, 7–13.

[82] a) U. Bolle, W. Tremel, *J. Chem. Soc., Chem. Commun.* **1992**, *2*, 91–93; b) N. Korber, F. Richter, *Angew. Chem. Int. Ed. Engl.* **1997**, *36*, 1512–1514; c) L. Xu, S. Bobev, J. El-Bahraoui, S. C. Sevov, *J. Am. Chem. Soc.* **2000**, *122*, 1838–1839; d) F. Gascoin, S. C. Sevov, *J. Am. Chem. Soc.* **2000**, *122*, 10251–10252; e) F. Gascoin, S. C. Sevov, *Inorg. Chem.* **2001**, *40*, 5177–5181; f) T. Hanauer, J. C. Aschenbrenner, N. Korber, *Inorg. Chem.* **2006**, *45*, 6723–6727; g) T. Hanauer, N. Korber, *Z. Anorg. Allg. Chem.* **2006**, *632*, 1135–1140; h) M. Reil, N. Korber, *Z. Anorg. Allg. Chem.* **2007**, *633*, 1599–1602; i) M. Kaas, N. Korber, *Z. Anorg. Allg. Chem.* **2017**, *643*, 1331–1334.

[83] a) G. Fritz, W. Hölderich, *Sci. Nat.* **1975**, *62*, 573–575; b) W. Hönle, H. G. V. Schnering, *Z. Anorg. Allg. Chem.* **1978**, *440*, 171–182.

[84] a) M. Baudler, J. Hellmann, P. Bachmann, K.-F. Tebbe, R. Fröhlich, M. Fehér, *Angew. Chem. Int. Ed. Engl.* **1981**, *20*, 406–408; b) M. Baudler, B. Koll, C. Adamek, R. Gleiter, *Angew. Chem. Int. Ed. Engl.* **1987**, *26*, 347–348.

[85] a) M. Baudler, J. Hahn, V. Arndt, B. Koll, K. Kazmierczak, E. Drr, *Z. Anorg. Allg. Chem.* **1986**, *538*, 7–20; b) M. Baudler, M. Schnalke, C. Wiaterek, *Z. Anorg. Allg. Chem.* **1990**, *585*, 7–17.

[86] M. Baudler, S. Schlitte, J. Hasenbach, *Z. Anorg. Allg. Chem.* **1988**, *560*, 7–17.

[87] a) H. G. von Schnering, D. Fenske, W. Hönle, M. Binnewies, K. Peters, *Angew. Chem. Int. Ed. Engl.* **1979**, *18*, 679; b) M. Baudler, H. Jachow, J. Germeshausen, *Z. Anorg. Allg. Chem.* **1987**, *553*, 15–23; c) M. Baudler, H. Jachow, A. Floruss, J. Hasenbach, *Chem. Ber.* **1991**, *124*, 1153–1157.

[88] a) M. Baudler, Y. Aktalay, V. Arndt, K.-F. Tebbe, M. Fehér, *Angew. Chem. Int. Ed. Engl.* **1983**, *22*, 1002–1003; b) M. Baudler, H. Jachow, K.-F. Tebbe, *Z. Anorg. Allg. Chem.* **1991**, *593*, 9–16.

[89] M. Baudler, M. Schnalke, *Z. Anorg. Allg. Chem.* **1990**, *585*, 18–26.
[90] a) M. Baudler, H. Jachow, B. Lieser, K.-F. Tebbe, M. Fehér, *Angew. Chem. Int. Ed. Engl.* **1989**, *28*, 1231–1232; b) M. Baudler, H. Jachow, *Z. Anorg. Allg. Chem.* **1990**, *580*, 27–35; c) M. Baudler, J. Hasenbach, H. Jachow, *Z. Anorg. Allg. Chem.* **1994**, *620*, 2021–2025.
[91] M. Baudler, W. Oehlert, A. Kmieciak, A. Floruss, *Z. Anorg. Allg. Chem.* **1992**, *611*, 43–49.
[92] M. Baudler, H. Jachow, W. Oehlert, A. Kmieciak, A. Floruss, *Z. Anorg. Allg. Chem.* **1992**, *616*, 19–26.
[93] M. Baudler, R. Becher, J. Germeshausen, *Chem. Ber.* **1986**, *119*, 2510–2516.
[94] M. Baudler, V. Arndt, *Z. Naturforsch. B* **1984**, *39*, 275–283.
[95] a) N. Korber, J. Aschenbrenner, *J. Chem. Soc., Dalton Trans.* **2001**, *8*, 1165–1166; b) F. Kraus, J. C. Aschenbrenner, T. Klamroth, N. Korber, *Inorg. Chem.* **2009**, *48*, 1911–1919.
[96] a) A. Schisler, P. Lönnecke, T. Gelbrich, E. Hey-Hawkins, *Dalton Trans.* **2004**, *18*, 2895–2898; b) R. Wolf, E. Hey-Hawkins, *Chem. Commun.* **2004**, *22*, 2626–2627; c) R. Wolf, A. Schisler, P. Lönnecke, C. Jones, E. Hey-Hawkins, *Eur. J. Inorg. Chem.* **2004**, *2004*, 3277–3286; d) R. Wolf, S. Gomez-Ruiz, J. Reinhold, W. Böhlmann, E. Hey-Hawkins, *Inorg. Chem.* **2006**, *45*, 9107–9113; e) R. Wolf, E. Hey-Hawkins, *Z. Anorg. Allg. Chem.* **2006**, *632*, 727–734.
[97] J. E. Borger, A. W. Ehlers, M. Lutz, J. C. Slootweg, K. Lammertsma, *Angew. Chem. Int. Ed.* **2014**, *53*, 12836–12839.
[98] V. J. Eilrich, E. Hey-Hawkins, *Coord. Chem. Rev.* **2021**, *437*, 213749–213762.
[99] a) W. Hönle, J. Wolf, H. G. von Schnering, *Z. Naturforsch. B* **1988**, *43*, 219–223; b) S. Heinl, G. Balázs, A. Stauber, M. Scheer, *Angew. Chem. Int. Ed.* **2016**, *55*, 15524–15527.
[100] a) K. Issleib, B. Hamann, L. Schmidt, *Z. Anorg. Allg. Chem.* **1965**, *339*, 298–303; b) H. J. Breunig, *Z. Naturforsch. B* **1978**, *33*, 242–243; c) H. J. Breunig, H. Kischkel, *Z. Anorg. Allg. Chem.* **1983**, *502*, 175–177; d) T. F. Berlitz, H. Sinning, J. Lorberth, U. Müller, *Z. Naturforsch. B* **1988**, *43*, 744–748; e) L. Tuscher, C. Ganesamoorthy, D. Bläser, C. Wölper, S. Schulz, *Angew. Chem. Int. Ed.* **2015**, *54*, 10657–10661; f) C. Ganesamoorthy, C. Wölper, A. S. Nizovtsev, S. Schulz, *Angew. Chem. Int. Ed.* **2016**, *55*, 4204–4209; g) C. Ganesamoorthy, J. Krüger, C. Wölper, A. S. Nizovtsev, S. Schulz, *Chem. Eur. J.* **2017**, *23*, 2461–2468.
[101] V. J. Eilrich, T. Grell, P. Lönnecke, E. Hey-Hawkins, *Dalton Trans.* **2021**, *50*, 14144–14155.
[102] a) S. Traut, A. P. Hähnel, C. von Hänisch, *Dalton Trans.* **2011**, *40*, 1365–1371; b) B. Ringler, M. Müller, C. von Hänisch, *Eur. J. Inorg. Chem.* **2018**, *2018*, 640–646; c) C. Ritter, N. Michel, A. Rinow, B. Ringler, C. Hänisch, *Eur. J. Inorg. Chem.* **2021**, *2021*, 2514–2522; d) T. Dunaj, C. von Hänisch, *Chem. Eur. J.* **2022**, *28*, e202202932.
[103] C. Ritter, F. Weigend, C. von Hänisch, *Chem. Eur. J.* **2020**, *26*, 8536–8540.
[104] K. M. Marczenko, S. S. Chitnis, *Chem. Commun.* **2020**, *56*, 8015–8018.
[105] T. M. Klapötke, F. A. Martin, J. Stierstorfer, *Angew. Chem. Int. Ed.* **2011**, *50*, 4227–4229.
[106] M. Benz, T. M. Klapötke, J. Stierstorfer, M. Voggenreiter, *J. Am. Chem. Soc.* **2022**, *144*, 6143–6147.

[107] A. K. Eckhardt, M.-L. Y. Riu, M. Ye, P. Müller, G. Bistoni, C. C. Cummins, *Nat. Chem.* **2022**, *14*, 928–934.

[108] a) M. Yoshifuji, I. Shima, N. Inamoto, K. Hirotsu, T. Higuchi, *J. Am. Chem. Soc.* **1981**, *103*, 4587–4589; b) A. H. Cowley, J. G. Lasch, N. C. Norman, M. Pakulski, *J. Am. Chem. Soc.* **1983**, *105*, 5506–5507; c) N. Tokitoh, Y. Arai, R. Okazaki, S. Nagase, *Science* **1997**, *277*, 78–80; d) N. Tokitoh, Y. Arai, T. Sasamori, R. Okazaki, S. Nagase, H. Uekusa, Y. Ohashi, *J. Am. Chem. Soc.* **1998**, *120*, 433–434; e) B. Twamley, C. D. Sofield, M. M. Olmstead, P. P. Power, *J. Am. Chem. Soc.* **1999**, *121*, 3357–3367; f) G. Sieg, M. Fischer, F. Dankert, J.-E. Siewert, C. Hering-Junghans, C. G. Werncke, *Chem. Commun.* **2022**, *58*, 9786–9789; g) Y. Pang, M. Leutzsch, N. Nöthling, J. Cornella, *Angew. Chem. Int. Ed.* **2023**, e202302071.

[109] a) S. Shah, J. D. Protasiewicz, *Chem. Commun.* **1998**, *15*, 1585–1586; b) J. D. Protasiewicz, *Eur. J. Inorg. Chem.* **2012**, *2012*, 4539–4549.

[110] S. Nees, F. Fantuzzi, T. Wellnitz, M. Fischer, J.-E. Siewert, J. T. Goettel, A. Hofmann, M. Härterich, H. Braunschweig, C. Hering-Junghans, *Angew. Chem. Int. Ed.* **2021**, *60*, 24318–24325.

[111] a) M. Fischer, S. Nees, T. Kupfer, J. T. Goettel, H. Braunschweig, C. Hering-Junghans, *J. Am. Chem. Soc.* **2021**, *143*, 4106–4111; b) T. Taeufer, F. Dankert, D. Michalik, J. Pospech, J. Bresien, C. Hering-Junghans, *Chem. Sci.* **2023**, *14*, 3018–3023; c) S. Nees, T. Wellnitz, F. Dankert, M. Härterich, S. Dotzauer, M. Feldt, H. Braunschweig, C. Hering-Junghans, *Angew. Chem. Int. Ed.* **2023**, *62*, e202215838.

[112] O. Back, G. Kuchenbeiser, B. Donnadieu, G. Bertrand, *Angew. Chem. Int. Ed.* **2009**, *48*, 5530–5533.

[113] J. D. Masuda, W. W. Schoeller, B. Donnadieu, G. Bertrand, *Angew. Chem. Int. Ed.* **2007**, *46*, 7052–7055.

[114] C. D. Martin, C. M. Weinstein, C. E. Moore, A. L. Rheingold, G. Bertrand, *Chem. Commun.* **2013**, *49*, 4486–4488.

[115] J. D. Masuda, W. W. Schoeller, B. Donnadieu, G. Bertrand, *J. Am. Chem. Soc.* **2007**, *129*, 14180–14181.

[116] Y. Wang, Y. Xie, P. Wei, R. B. King, H. F. Schaefer, P. V. R. Schleyer, G. H. Robinson, *J. Am. Chem. Soc.* **2008**, *130*, 14970–14971.

[117] M. Haimerl, C. Schwarzmaier, C. Riesinger, A. Y. Timoshkin, M. Melaimi, G. Bertrand, M. Scheer, *Chem. Eur. J.* **2023**, *29*, e202300280.

[118] a) M. B. Power, A. R. Barron, *Angew. Chem. Int. Ed. Engl.* **1991**, *30*, 1353–1354; b) C. Dohmeier, H. Schnöckel, C. Robl, U. Schneider, R. Ahlrichs, *Angew. Chem. Int. Ed. Engl.* **1994**, *33*, 199–200; c) W. Uhl, M. Benter, *Chem. Commun.* **1999**, *9*, 771–772; d) A. R. Fox, R. J. Wright, E. Rivard, P. P. Power, *Angew. Chem. Int. Ed.* **2005**, *44*, 7729–7733.

[119] M. M. D. Roy, A. Heilmann, M. A. Ellwanger, S. Aldridge, *Angew. Chem. Int. Ed.* **2021**, *60*, 26550–26554.

[120] G. Prabusankar, A. Doddi, C. Gemel, M. Winter, R. A. Fischer, *Inorg. Chem.* **2010**, *49*, 7976–7980.

[121] Y. Peng, H. Fan, H. Zhu, H. W. Roesky, J. Magull, C. E. Hughes, *Angew. Chem. Int. Ed.* **2004**, *43*, 3443–3445.

[122] M. Haimerl, M. Piesch, R. Yadav, P. W. Roesky, M. Scheer, *Chem. Eur. J.* **2023**, *29*, e202202529.

[123] a) Y. Xiong, S. Yao, M. Brym, M. Driess, *Angew. Chem. Int. Ed.* **2007**, *46*, 4511–4513; b) J. W. Dube, C. M. E. Graham, C. L. B. Macdonald, Z. D. Brown, P. P. Power, P. J. Ragogna, *Chem. Eur. J.* **2014**, *20*, 6739–6744; c) D. Sarkar, C. Weetman, D. Munz, S. Inoue, *Angew. Chem. Int. Ed.* **2021**, *60*, 3519–3523.

[124] S. Khan, R. Michel, J. M. Dieterich, R. A. Mata, H. W. Roesky, J.-P. Demers, A. Lange, D. Stalke, *J. Am. Chem. Soc.* **2011**, *133*, 17889–17894.

[125] a) M. Driess, A. D. Fanta, D. R. Powell, R. West, *Angew. Chem. Int. Ed. Engl.* **1989**, *28*, 1038–1040; b) M. Drieß, *Angew. Chem. Int. Ed. Engl.* **1991**, *30*, 1022–1024; c) S. S. Sen, S. Khan, H. W. Roesky, D. Kratzert, K. Meindl, J. Henn, D. Stalke, J.-P. Demers, A. Lange, *Angew. Chem. Int. Ed.* **2011**, *50*, 2322–2325; d) M. M. D. Roy, M. J. Ferguson, R. McDonald, Y. Zhou, E. Rivard, *Chem. Sci.* **2019**, *10*, 6476–6481; e) Y. Wang, T. Szilvási, S. Yao, M. Driess, *Nat. Chem.* **2020**, *12*, 801–807; f) Y. Xiong, S. Dong, S. Yao, J. Zhu, M. Driess, *Angew. Chem. Int. Ed.* **2022**, *61*, e202205358.

[126] A. E. Seitz, M. Eckhardt, S. S. Sen, A. Erlebach, E. V. Peresypkina, H. W. Roesky, M. Sierka, M. Scheer, *Angew. Chem. Int. Ed.* **2017**, *56*, 6655–6659.

[127] G. Maier, S. Pfriem, U. Schäfer, R. Matusch, *Angew. Chem. Int. Ed. Engl.* **1978**, *17*, 520–521.

[128] G. Hierlmeier, P. Coburger, M. Bodensteiner, R. Wolf, *Angew. Chem. Int. Ed.* **2019**, *58*, 16918–16922.

[129] M.-L. Y. Riu, R. L. Jones, W. J. Transue, P. Müller, C. C. Cummins, *Sci. Adv.* **2020**, *6*, eaaz3168.

[130] M.-L. Y. Riu, M. Ye, C. C. Cummins, *J. Am. Chem. Soc.* **2021**, *143*, 16354–16357.

[131] a) M. Ruck, F. Locherer, *Coord. Chem. Rev.* **2015**, *285*, 1–10; b) E. Ahmed, M. Ruck, *Coord. Chem. Rev.* **2011**, *255*, 2892–2903; c) M. Drieß, H. Nöth (Eds.) *Molecular Clusters of the Main Group Elements*, Wiley-VCH, Weinheim (DE), **2008**.

[132] T. A. Engesser, I. Krossing, *Coord. Chem. Rev.* **2013**, *257*, 946–955.

[133] a) K. O. Christe, W. W. Wilson, J. A. Sheehy, J. A. Boatz, *Angew. Chem. Int. Ed.* **1999**, *38*, 2004–2009; b) A. Vij, W. W. Wilson, V. Vij, F. S. Tham, J. A. Sheehy, K. O. Christe, *J. Am. Chem. Soc.* **2001**, *123*, 6308–6313.

[134] M. Lindsjö, A. Fischer, L. Kloo, *Angew. Chem. Int. Ed.* **2004**, *43*, 2540–2543.

[135] T. Köchner, T. A. Engesser, H. Scherer, D. A. Plattner, A. Steffani, I. Krossing, *Angew. Chem. Int. Ed.* **2012**, *51*, 6529–6531.

[136] J. Frötschel-Rittmeyer, M. Holthausen, C. Friedmann, D. Röhner, I. Krossing, J. J. Weigand, *Sci. Adv.* **2022**, *8*, eabq8613.

[137] T. Köchner, S. Riedel, A. J. Lehner, H. Scherer, I. Raabe, T. A. Engesser, F. W. Scholz, U. Gellrich, P. Eiden, R. A. Paz Schmidt, D. A. Plattner, I. Krossing, *Angew. Chem. Int. Ed.* **2010**, *49*, 8139–8143.

[138] A. Wiesner, S. Steinhauer, H. Beckers, C. Müller, S. Riedel, *Chem. Sci.* **2018**, *9*, 7169–7173.

[139] a) M. Y. Abraham, Y. Wang, Y. Xie, R. J. Gilliard, P. Wei, B. J. Vaccaro, M. K. Johnson, H. F. Schaefer, P. V. R. Schleyer, G. H. Robinson, *J. Am. Chem. Soc.* **2013**, *135*, 2486–2488; b) O. Back, B. Donnadieu, P. Parameswaran, G. Frenking, G. Bertrand, *Nat. Chem.* **2010**, *2*, 369–373.

[140] R. Kinjo, B. Donnadieu, G. Bertrand, *Angew. Chem. Int. Ed.* **2010**, *49*, 5930–5933.

[141] a) L. P. Ho, A. Nasr, P. G. Jones, A. Altun, F. Neese, G. Bistoni, M. Tamm, *Chem. Eur. J.* **2018**, *24*, 18922–18932; b) L. P. Ho, M. Tamm, *Dalton Trans.* **2021**, *50*, 1202–1205.

[142] H. M. Weinert, Y. Schulte, A. Gehlhaar, C. Wölper, G. Haberhauer, S. Schulz, *Chem. Commun.* **2023**, *59*, 7755–7758.

[143] P. Griefs, *Ann. Chem. Pharm.* **1858**, *106*, 123–125.

[144] a) E. Niecke, M. Nieger, F. Reichert, *Angew. Chem. Int. Ed.* **1988**, *27*, 1715–1716; b) N. Burford, J. A. C. Clyburne, P. K. Bakshi, T. S. Cameron, *J. Am. Chem. Soc.* **1993**, *115*, 8829–8830; c) N. Burford, A. D. Phillips, H. A. Spinney, M. Lumsden, U. Werner-Zwanziger, M. J. Ferguson, R. McDonald, *J. Am. Chem. Soc.* **2005**, *127*, 3921–3927.

[145] M. Kuprat, A. Schulz, A. Villinger, *Angew. Chem. Int. Ed.* **2013**, *52*, 7126–7130.

[146] a) N. Burford, P. J. Ragogna in *ACS Symposium Series*, American Chemical Society, Washington, DC, **2005**, 280–292; b) C. A. Dyker, N. Burford, *Chem. Asian J.* **2008**, *3*, 28–36; c) M. H. Holthausen, J. J. Weigand, *Chem. Soc. Rev.* **2014**, *43*, 6639–6657; d) A. P. M. Robertson, P. A. Gray, N. Burford, *Angew. Chem. Int. Ed.* **2014**, *53*, 6050–6069; e) M. Donath, F. Hennersdorf, J. J. Weigand, *Chem. Soc. Rev.* **2016**, *45*, 1145–1172.

[147] a) N. Burford, T. S. Cameron, P. J. Ragogna, E. Ocando-Mavarez, M. Gee, R. McDonald, R. E. Wasylishen, *J. Am. Chem. Soc.* **2001**, *123*, 7947–7948; b) N. Burford, P. J. Ragogna, R. McDonald, M. J. Ferguson, *Chem. Commun.* **2003**, *16*, 2066–2067; c) N. Burford, P. J. Ragogna, R. McDonald, M. J. Ferguson, *J. Am. Chem. Soc.* **2003**, *125*, 14404–14410; d) N. Burford, D. E. Herbert, P. J. Ragogna, R. McDonald, M. J. Ferguson, *J. Am. Chem. Soc.* **2004**, *126*, 17067–17073; e) R. J. Davidson, J. J. Weigand, N. Burford, T. S. Cameron, A. Decken, U. Werner-Zwanziger, *Chem. Commun.* **2007**, *44*, 4671–4673; f) J. J. Weigand, N. Burford, D. Mahnke, A. Decken, *Inorg. Chem.* **2007**, *46*, 7689–7691; g) S. S. Chitnis, E. MacDonald, N. Burford, U. Werner-Zwanziger, R. McDonald, *Chem. Commun.* **2012**, *48*, 7359–7361; h) P. A. Gray, Y. Carpenter, N. Burford, R. McDonald, *Dalton Trans.* **2016**, *45*, 2124–2129; i) J. Possart, A. Martens, M. Schleep, A. Ripp, H. Scherer, D. Kratzert, I. Krossing, *Chem. Eur. J.* **2017**, *23*, 12305–12313.

[148] a) C. A. Dyker, N. Burford, M. D. Lumsden, A. Decken, *J. Am. Chem. Soc.* **2006**, *128*, 9632–9633; b) Y. Carpenter, C. A. Dyker, N. Burford, M. D. Lumsden, A. Decken, *J. Am. Chem. Soc.* **2008**, *130*, 15732–15741; c) Y. Carpenter, N. Burford, M. D. Lumsden, R. McDonald, *Inorg. Chem.* **2011**, *50*, 3342–3353.

[149] N. Burford, C. A. Dyker, A. Decken, *Angew. Chem. Int. Ed.* **2005**, *44*, 2364–2367.

[150] J. J. Weigand, S. D. Riegel, N. Burford, A. Decken, *J. Am. Chem. Soc.* **2007**, *129*, 7969–7976.

[151] a) N. Burford, C. A. Dyker, M. Lumsden, A. Decken, *Angew. Chem. Int. Ed.* **2005**, *44*, 6196–6199; b) C. A. Dyker, S. D. Riegel, N. Burford, M. D. Lumsden, A. Decken, *J. Am. Chem. Soc.* **2007**, *129*, 7464–7474; c) M. H. Holthausen, D. Knackstedt, N. Burford, J. J. Weigand, *Aust. J. Chem.* **2013**, *66*, 1155–1162.

[152] a) J. J. Weigand, N. Burford, M. D. Lumsden, A. Decken, *Angew. Chem. Int. Ed.* **2006**, *45*, 6733–6737; b) J. J. Weigand, N. Burford, A. Decken, *Eur. J. Inorg. Chem.* **2008**, *2008*, 4343–4347.

[153] a) I. Krossing, I. Raabe, *Angew. Chem. Int. Ed.* **2001**, *40*, 4406–4409; b) I. Krossing, *J. Chem. Soc., Dalton Trans.* **2002**, *4*, 500–512; c) M. H. Holthausen, J. J. Weigand, *J. Am. Chem. Soc.* **2009**, *131*, 14210–14211; d) M. H. Holthausen, K.-O. Feldmann, S. Schulz, A. Hepp, J. J. Weigand, *Inorg. Chem.* **2012**, *51*, 3374–3387; e) M. H. Holthausen, J. J. Weigand, *Z. Anorg. Allg. Chem.* **2012**, *638*, 1103–1108; f) M. H. Holthausen, A. Hepp, J. J. Weigand, *Chem. Eur. J.* **2013**, *19*, 9895–9907.

[154] J. J. Weigand, M. Holthausen, R. Fröhlich, *Angew. Chem. Int. Ed.* **2009**, *48*, 295–298.

[155] a) J. J. Weigand, N. Burford, R. J. Davidson, T. S. Cameron, P. Seelheim, *J. Am. Chem. Soc.* **2009**, *131*, 17943–17953; b) R. Schoemaker, P. Kossatz, K. Schwedtmann, F. Hennersdorf, J. J. Weigand, *Chem. Eur. J.* **2020**, *26*, 11734–11741; c) C. A. Dyker, N. Burford, G. Menard, M. D. Lumsden, A. Decken, *Inorg. Chem.* **2007**, *46*, 4277–4285; d) S. D. Riegel, N. Burford, M. D. Lumsden, A. Decken, *Chem. Commun.* **2007**, *44*, 4668–4670.

[156] a) A. P. M. Robertson, C. A. Dyker, P. A. Gray, B. O. Patrick, A. Decken, N. Burford, *J. Am. Chem. Soc.* **2014**, *136*, 14941–14950; b) S. S. Chitnis, R. A. Musgrave, H. A. Sparkes, N. E. Pridmore, V. T. Annibale, I. Manners, *Inorg. Chem.* **2017**, *56*, 4522–4538.

[157] M. H. Holthausen, S. K. Surmiak, P. Jerabek, G. Frenking, J. J. Weigand, *Angew. Chem. Int. Ed.* **2013**, *52*, 11078–11082.

[158] K. Schwedtmann, M. H. Holthausen, C. H. Sala, F. Hennersdorf, R. Fröhlich, J. J. Weigand, *Chem. Commun.* **2016**, *52*, 1409–1412.

[159] K. Schwedtmann, F. Hennersdorf, A. Bauzá, A. Frontera, R. Fischer, J. J. Weigand, *Angew. Chem. Int. Ed.* **2017**, *56*, 6218–6222.

[160] a) K.-O. Feldmann, J. J. Weigand, *Angew. Chem. Int. Ed.* **2012**, *51*, 6566–6568; b) K.-O. Feldmann, J. J. Weigand, *Angew. Chem. Int. Ed.* **2012**, *51*, 7545–7549; c) C. Taube, K. Schwedtmann, M. Noikham, E. Somsook, F. Hennersdorf, R. Wolf, J. J. Weigand, *Angew. Chem. Int. Ed.* **2020**, *59*, 3585–3591.

[161] K. Schwedtmann, J. Haberstroh, S. Roediger, A. Bauzá, A. Frontera, F. Hennersdorf, J. J. Weigand, *Chem. Sci.* **2019**, *10*, 6868–6875.

[162] P. Royla, K. Schwedtmann, Z. Han, J. Fidelius, D. P. Gates, R. M. Gomila, A. Frontera, J. J. Weigand, *J. Am. Chem. Soc.* **2023**, *145*, 10364–10375.

[163] a) H. Althaus, H. J. Breunig, E. Lork, *Chem. Commun.* **1999**, *19*, 1971–1972; b) N. Burford, P. J. Ragogna, K. Sharp, R. McDonald, M. J. Ferguson, *Inorg. Chem.* **2005**, *44*, 9453–9460; c) N. L. Kilah, M. L. Weir, S. B. Wild, *Dalton Trans.* **2008**, *18*, 2480–2486; d) E. Conrad, N. Burford, R. McDonald, M. J. Ferguson, *Inorg. Chem.* **2008**, *47*, 2952–2954; e) E. Conrad, N. Burford, R. McDonald, M. J. Ferguson, *J. Am. Chem. Soc.* **2009**, *131*, 5066–

5067; f) E. Conrad, N. Burford, R. McDonald, M. J. Ferguson, *J. Am. Chem. Soc.* **2009**, *131*, 17000–17008; g) E. Conrad, N. Burford, R. McDonald, M. J. Ferguson, *Chem. Commun.* **2010**, *46*, 4598–4600; h) S. S. Chitnis, B. Peters, E. Conrad, N. Burford, R. McDonald, M. J. Ferguson, *Chem. Commun.* **2011**, *47*, 12331–12333; i) S. S. Chitnis, N. Burford, R. McDonald, M. J. Ferguson, *Inorg. Chem.* **2014**, *53*, 5359–5372; j) S. S. Chitnis, K. A. Vos, N. Burford, R. McDonald, M. J. Ferguson, *Chem. Commun.* **2016**, *52*, 685–688.

[164] a) E. Conrad, N. Burford, U. Werner-Zwanziger, R. McDonald, M. J. Ferguson, *Chem. Commun.* **2010**, *46*, 2465–2467; b) M. Donath, E. Conrad, P. Jerabek, G. Frenking, R. Fröhlich, N. Burford, J. J. Weigand, *Angew. Chem. Int. Ed.* **2012**, *51*, 2964–2967; c) S. S. Chitnis, Y. Carpenter, N. Burford, R. McDonald, M. J. Ferguson, *Angew. Chem. Int. Ed.* **2013**, *52*, 4863–4866; d) M. Donath, M. Bodensteiner, J. J. Weigand, *Chem. Eur. J.* **2014**, *20*, 17306–17310; e) S. S. Chitnis, N. Burford, J. J. Weigand, R. McDonald, *Angew. Chem. Int. Ed.* **2015**, *54*, 7828–7832; f) S. S. Chitnis, A. P. M. Robertson, N. Burford, J. J. Weigand, R. Fischer, *Chem. Sci.* **2015**, *6*, 2559–2574.

[165] W. Beck, K. Suenkel, *Chem. Rev.* **1988**, *88*, 1405–1421.

[166] a) S. H. Strauss, *Chem. Rev.* **1993**, *93*, 927–942; b) I. Krossing, I. Raabe, *Angew. Chem. Int. Ed.* **2004**, *43*, 2066–2090.

[167] a) E. Y. Chen, T. J. Marks, *Chem. Rev.* **2000**, *100*, 1391–1434; b) C. Knapp in *Comprehensive Inorganic Chemistry II*, Elsevier, Amsterdam (NL), Oxford (UK), Waltham (US), **2013**, 651–679; c) I. Krossing in *Comprehensive Inorganic Chemistry II*, Elsevier, Amsterdam (NL), Oxford (UK), Waltham (US), **2013**, 681–705; d) E.-X. Chen, S. J. Lancaster in *Comprehensive Inorganic Chemistry II*, Elsevier, Amsterdam (NL), Oxford (UK), Waltham (US), **2013**, 707–754; e) I. M. Riddlestone, A. Kraft, J. Schaefer, I. Krossing, *Angew. Chem. Int. Ed.* **2018**, *57*, 13982–14024; f) A. Barthélemy, P. Dabringhaus, E. Jacob, H. Koger, D. Röhner, M. Schmitt, M. Sellin, K. Ingo in *Comprehensive Inorganic Chemistry III*, Elsevier, Amsterdam (NL), Oxford (UK), Cambridge (US), **2023**, 378–438.

[168] a) A. B. A. Rupp, I. Krossing, *Acc. Chem. Res.* **2015**, *48*, 2537–2546; b) S. Bulut, P. Klose, M.-M. Huang, H. Weingärtner, P. J. Dyson, G. Laurenczy, C. Friedrich, J. Menz, K. Kümmerer, I. Krossing, *Chem. Eur. J.* **2010**, *16*, 13139–13154.

[169] T. A. Engesser, M. R. Lichtenthaler, M. Schleep, I. Krossing, *Chem. Soc. Rev.* **2016**, *45*, 789–899.

[170] C. A. Reed, *Acc. Chem. Res.* **1998**, *31*, 133–139.

[171] C. A. Reed, K.-C. Kim, E. S. Stoyanov, D. Stasko, F. S. Tham, L. J. Mueller, P. D. W. Boyd, *J. Am. Chem. Soc.* **2003**, *125*, 1796–1804.

[172] A. Martens, P. Weis, M. C. Krummer, M. Kreuzer, A. Meierhöfer, S. C. Meier, J. Bohnenberger, H. Scherer, I. Riddlestone, I. Krossing, *Chem. Sci.* **2018**, *9*, 7058–7068.

[173] A. G. Massey, A. J. Park, *J. Organomet. Chem.* **1964**, *2*, 245–250.

[174] S. M. Ivanova, B. G. Nolan, Y. Kobayashi, S. M. Miller, O. P. Anderson, S. H. Strauss, *Chem. Eur. J.* **2001**, *7*, 503–510.

[175] a) A. S. Foust, M. S. Foster, L. F. Dahl, *J. Am. Chem. Soc.* **1969**, *91*, 5631–5633; b) A. S. Foust, M. S. Foster, L. F. Dahl, *J. Am. Chem. Soc.* **1969**, *91*, 5633–5635.

[176] a) M. Di Vaira, P. Stoppioni, M. Peruzzini, *Polyhedron* **1987**, *6*, 351–382; b) O. J. Scherer, *Angew. Chem. Int. Ed. Engl.* **1990**, *29*, 1104–1122; c) O. J. Scherer, *Acc. Chem. Res.* **1999**, *32*, 751–762.

[177] M. P. Shaver, M. D. Fryzuk, *Adv. Synth. Catal.* **2003**, *345*, 1061–1076.

[178] C. Zhang, C. Yang, B. Hu, C. Yu, Z. Zheng, C. Sun, *Angew. Chem. Int. Ed.* **2017**, *56*, 4512–4514.

[179] F. Dielmann, A. Timoshkin, M. Piesch, G. Balázs, M. Scheer, *Angew. Chem. Int. Ed.* **2017**, *56*, 1671–1675.

[180] A. Cavaillé, N. Saffon-Merceron, N. Nebra, M. Fustier-Boutignon, N. Mézailles, *Angew. Chem. Int. Ed.* **2018**, *57*, 1874–1878.

[181] a) S. Charles, B. W. Eichhorn, A. L. Rheingold, S. G. Bott, *J. Am. Chem. Soc.* **1994**, *116*, 8077–8086; b) B. Kesanli, J. Fettinger, B. Eichhorn, *J. Am. Chem. Soc.* **2003**, *125*, 7367–7376; c) B. Kesanli, J. Fettinger, B. Scott, B. Eichhorn, *Inorg. Chem.* **2004**, *43*, 3840–3846; d) Z.-C. Wang, L. Qiao, Z.-M. Sun, M. Scheer, *J. Am. Chem. Soc.* **2022**, *144*, 6698–6702.

[182] a) K. H. Whitmire, C. B. Lagrone, M. R. Churchill, J. C. Fettinger, L. V. Biondi, *Inorg. Chem.* **1984**, *23*, 4227–4232; b) M. Baudler, T. Etzbach, *Angew. Chem. Int. Ed. Engl.* **1991**, *30*, 580–582; c) N. C. Zanetti, R. R. Schrock, W. M. Davis, *Angew. Chem. Int. Ed. Engl.* **1995**, *34*, 2044–2046; d) M. Scheer, J. Müller, M. Häser, *Angew. Chem. Int. Ed. Engl.* **1996**, *35*, 2492–2496; e) G. Balázs, M. Sierka, M. Scheer, *Angew. Chem. Int. Ed.* **2005**, *44*, 4920–4924; f) B. M. Gardner, G. Balázs, M. Scheer, F. Tuna, E. J. L. McInnes, J. McMaster, W. Lewis, A. J. Blake, S. T. Liddle, *Nat. Chem.* **2015**, *7*, 582–590; g) E. P. Wildman, G. Balázs, A. J. Wooles, M. Scheer, S. T. Liddle, *Nat. Commun.* **2016**, *7*, 12884–12895; h) E. P. Wildman, G. Balázs, A. J. Wooles, M. Scheer, S. T. Liddle, *Nat. Commun.* **2017**, *8*, 14769–14778; i) T. M. Rookes, B. M. Gardner, G. Balázs, M. Gregson, F. Tuna, A. J. Wooles, M. Scheer, S. T. Liddle, *Angew. Chem. Int. Ed.* **2017**, *56*, 10495–10500; j) G. Hierlmeier, A. Hinz, R. Wolf, J. M. Goicoechea, *Angew. Chem. Int. Ed.* **2018**, *57*, 431–436; k) R. Magnall, G. Balázs, E. Lu, M. Kern, J. van Slageren, F. Tuna, A. J. Wooles, M. Scheer, S. T. Liddle, *Chem. Eur. J.* **2019**, *25*, 14246–14252; l) S. Senthil, S. Kwon, D. Fehn, H. Im, M. R. Gau, P. J. Carroll, M.-H. Baik, K. Meyer, D. J. Mindiola, *Angew. Chem. Int. Ed.* **2022**, *61*, e202212488.

[183] a) O. J. Scherer, *Angew. Chem. Int. Ed. Engl.* **1985**, *24*, 924–943; b) B. P. Johnson, G. Balázs, M. Scheer, *Coord. Chem. Rev.* **2006**, *250*, 1178–1195; c) G. Balázs, L. J. Gregoriades, M. Scheer, *Organometallics* **2007**, *26*, 3058–3075.

[184] a) L. F. Dahl, A. S. Foust, *J. Am. Chem. Soc.* **1970**, *92*, 7337–7341; b) A. Vizi-Orosz, G. Pályi, L. Markó, *J. Organomet. Chem.* **1973**, *60*, C25-C26; c) A. Vizi-Orosz, V. Galamb, G. Pályi, L. Markó, G. Bor, G. Natile, *J. Organomet. Chem.* **1976**, *107*, 235–240; d) A. Vizi-Orosz, *J. Organomet. Chem.* **1976**, *111*, 61–64; e) W. Malisch, P. Panster, *Angew. Chem. Int. Ed. Engl.* **1976**, *15*, 618–619; f) C. F. Campana, A. Vizi-Orosz, G. Palyi, L. Marko, L. F. Dahl, *Inorg. Chem.* **1979**, *18*, 3054–3059; g) G. Huttner, U. Weber, B. Sigwarth, O.

Scheidsteger, *Angew. Chem. Int. Ed. Engl.* **1982**, *21*, 215–216; h) G. Huttner, U. Weber, B. Sigwarth, O. Scheidsteger, H. Lang, L. Zsolnai, *J. Organomet. Chem.* **1985**, *282*, 331–348; i) S. Martinengo, G. Ciani, *J. Chem. Soc., Chem. Commun.* **1987**, *20*, 1589–1591; j) J. M. Wallis, G. Mueller, H. Schmidbaur, *Inorg. Chem.* **1987**, *26*, 458–459; k) J. M. Wallis, G. Müller, H. Schmidbaur, *J. Organomet. Chem.* **1987**, *325*, 159–168; l) V. Grossbruchhaus, D. Rehder, *Inorg. Chim. Acta* **1988**, *141*, 9–10; m) A. Strube, J. Heuser, G. Huttner, H. Lang, *J. Organomet. Chem.* **1988**, *356*, C9-C11; n) A. Strube, G. Huttner, L. Zsolnai, *Angew. Chem. Int. Ed. Engl.* **1988**, *27*, 1529–1530; o) W. Clegg, N. A. Compton, R. J. Errington, N. C. Norman, *J. Chem. Soc., Dalton Trans.* **1988**, *6*, 1671–1678; p) W. Clegg, N. A. Compton, R. J. Errington, N. C. Norman, A. J. Tucker, M. J. Winter, *J. Chem. Soc., Dalton Trans.* **1988**, *12*, 2941–2951; q) A. M. Barr, M. D. Kerlogue, N. C. Norman, P. M. Webster, L. J. Farrugia, *Polyhedron* **1989**, *8*, 2495–2505; r) S. Luo, K. H. Whitmire, *Inorg. Chem.* **1989**, *28*, 1424–1431.

[185] a) L. Dütsch, C. Riesinger, G. Balázs, M. Scheer, *Chem. Eur. J.* **2021**, *27*, 8804–8810; b) S. Wang, J. D. Sears, C. E. Moore, A. L. Rheingold, M. L. Neidig, J. S. Figueroa, *Science* **2022**, *375*, 1393–1397.

[186] J. Sun, J. Abbenseth, H. Verplancke, M. Diefenbach, B. de Bruin, D. Hunger, C. Würtele, J. van Slageren, M. C. Holthausen, S. Schneider, *Nat. Chem.* **2020**, *12*, 1054–1059.

[187] W. Clegg, N. A. Compton, R. Errington, N. C. Norman, *Polyhedron* **1988**, *7*, 2239–2241.

[188] a) P. J. Sullivan, A. L. Rheingold, *Organometallics* **1982**, *1*, 1547–1549; b) H. J. Breunig, R. Rösler, E. Lork, *Angew. Chem. Int. Ed. Engl.* **1997**, *36*, 2819–2821; c) H. J. Breunig, N. Burford, R. Rösler, *Angew. Chem. Int. Ed.* **2000**, *39*, 4148–4150; d) V. Heinl, A. E. Seitz, G. Balázs, M. Seidl, M. Scheer, *Chem. Sci.* **2021**, *12*, 9726–9732; e) V. Heinl, G. Balázs, M. Seidl, M. Scheer, *Chem. Commun.* **2022**, *58*, 2484–2487.

[189] a) Y. Wang, P. Zavalij, B. Eichhorn, *Chem. Commun.* **2018**, *54*, 11917–11920; b) N. Lichtenberger, N. Spang, A. Eichhöfer, S. Dehnen, *Angew. Chem. Int. Ed.* **2017**, *56*, 13253–13258; c) M. Kaas, N. Korber, *Z. Anorg. Allg. Chem.* **2019**, *645*, 146–148; d) A. R. Eulenstein, Y. J. Franzke, N. Lichtenberger, R. J. Wilson, H. L. Deubner, F. Kraus, R. Clérac, F. Weigend, S. Dehnen, *Nat. Chem.* **2021**, *13*, 149–155; e) F. Pan, S. Wei, L. Guggolz, A. R. Eulenstein, F. Tambornino, S. Dehnen, *J. Am. Chem. Soc.* **2021**, *143*, 7176–7188; f) F. Pan, B. Peerless, S. Dehnen, *Acc. Chem. Res.* **2023**, *56*, 1018–1030; g) B. Peerless, A. Schmidt, Y. J. Franzke, S. Dehnen, *Nat. Chem.* **2023**, *15*, 347–356.

[190] a) K. Blechschmitt, H. Pfisterer, T. Zahn, M. L. Ziegler, *Angew. Chem. Int. Ed. Engl.* **1985**, *24*, 66–67; b) C. Schoo, S. Bestgen, A. Egeberg, S. Klementyeva, C. Feldmann, S. N. Konchenko, P. W. Roesky, *Angew. Chem. Int. Ed.* **2018**, *57*, 5912–5916; c) G. Etzrodt, R. B. Und, G. Schmid, *Chem. Ber.* **1979**, *112*, 2574–2580.

[191] a) K. H. Whitmire, M. R. Churchill, J. C. Fettinger, *J. Am. Chem. Soc.* **1985**, *107*, 1056–1057; b) K. H. Whitmire, J. S. Leigh, M. E. Gross, *J. Chem. Soc., Chem. Commun.* **1987**, *12*, 926–927; c) K. H. Whitmire, J. R. Eveland, *J. Chem. Soc., Chem. Commun.* **1994**, *11*, 1335–1336.

[192] H. Diskowski, T. Hofmann in *Ullmann's Encyclopedia of Industrial Chemistry*, Wiley-VCH, Weinheim (DE), **2000**.

[193] a) G. Bettermann, W. Krause, G. Riess, T. Hofmann in *Ullmann's Encyclopedia of Industrial Chemistry*, Wiley-VCH, Weinheim (DE), **2000**; b) J. Svara, N. Weferling, T. Hofmann in *Ullmann's Encyclopedia of Industrial Chemistry*, Wiley-VCH, Weinheim (DE), **2000**.

[194] a) D. H. R. Barton, J. Zhu in *World Scientific Series in 20th Century Chemistry*, IMPERIAL COLLEGE PRESS, **1996**, 658–659; b) D. H. Barton, R. A. Vonder Embse, *Tetrahedron* **1998**, *54*, 12475–12496; c) B. M. Cossairt, C. C. Cummins, *New J. Chem.* **2010**, *34*, 1533–1536; d) S. Heinl, S. Reisinger, C. Schwarzmaier, M. Bodensteiner, M. Scheer, *Angew. Chem. Int. Ed.* **2014**, *53*, 7639–7642; e) D. J. Scott, J. Cammarata, M. Schimpf, R. Wolf, *Nat. Chem.* **2021**, *13*, 458–464; f) J. Cammarata, D. J. Scott, R. Wolf, *Chem. Eur. J.* **2022**, *28*, e202202456.

[195] M. Donath, K. Schwedtmann, T. Schneider, F. Hennersdorf, A. Bauzá, A. Frontera, J. J. Weigand, *Nat. Chem.* **2022**, *14*, 384–391.

[196] a) U. Lennert, P. B. Arockiam, V. Streitferdt, D. J. Scott, C. Rödl, R. M. Gschwind, R. Wolf, *Nat. Cat.* **2019**, *2*, 1101–1106; b) P. B. Arockiam, U. Lennert, C. Graf, R. Rothfelder, D. J. Scott, T. G. Fischer, K. Zeitler, R. Wolf, *Chem. Eur. J.* **2020**, *26*, 16374–16382; c) R. Rothfelder, V. Streitferdt, U. Lennert, J. Cammarata, D. J. Scott, K. Zeitler, R. M. Gschwind, R. Wolf, *Angew. Chem. Int. Ed.* **2021**, *60*, 24650–24658; d) M. Till, J. Cammarata, R. Wolf, D. J. Scott, *Chem. Commun.* **2022**, *58*, 8986–8989; e) M. Till, V. Streitferdt, D. J. Scott, M. Mende, R. M. Gschwind, R. Wolf, *Chem. Commun.* **2022**, *58*, 1100–1103.

[197] a) Y. G. Budnikova, D. G. Yakhvarov, Y. M. Kargin, *Mendeleev Commun.* **1997**, *7*, 67–68; b) D. G. Yakhvarov, Y. H. Budnikova, D. I. Tazeev, O. G. Sinyashin, *Russ. Chem. Bull.* **2002**, *51*, 2059–2064; c) D. G. Yakhvarov, Y. G. Budnikova, O. G. Sinyashin, *Russ. J. Electrochem.* **2003**, *39*, 1261–1270; d) Y. H. Budnikova, D. G. Yakhvarov, O. G. Sinyashin, *J. Organomet. Chem.* **2005**, *690*, 2416–2425; e) Y. G. Budnikova, D. I. Tazeev, A. G. Kafiyatullina, D. G. Yakhvarov, V. I. Morozov, N. K. Gusarova, B. A. Trofimov, O. G. Sinyashin, *Russ. Chem. Bull.* **2005**, *54*, 942–947; f) D. G. Yakhvarov, E. V. Gorbachuk, R. M. Kagirov, O. G. Sinyashin, *Russ. Chem. Bull.* **2012**, *61*, 1300–1312; g) D. G. Yakhvarov, E. V. Gorbachuk, O. G. Sinyashin, *Eur. J. Inorg. Chem.* **2013**, *2013*, 4709–4726; h) Y. H. Budnikova, T. V. Gryaznova, V. V. Grinenko, Y. B. Dudkina, M. N. Khrizanforov, *Pure Appl. Chem.* **2017**, *89*, 311–330.

[198] a) M. B. Geeson, C. C. Cummins, *Science* **2018**, *359*, 1383–1385; b) M. B. Geeson, P. Ríos, W. J. Transue, C. C. Cummins, *J. Am. Chem. Soc.* **2019**, *141*, 6375–6384; c) M. B. Geeson, C. C. Cummins, *ACS Cent. Sci.* **2020**, *6*, 848–860; d) F. Zhai, T. Xin, M. B. Geeson, C. C. Cummins, *ACS Cent. Sci.* **2022**, *8*, 332–339.

[199] a) M. Scheer, *Coord. Chem. Rev.* **1997**, *163*, 271–286; b) M. Ehses, A. Romerosa, M. Peruzzini in *Topics in Current Chemistry*, Springer, Berlin, Heidelberg (DE), **2002**, 107–140; c) B. P. Johnson, G. Balazs, M. Scheer in *Topics in Current Chemistry*, Springer, Berlin, Heidelberg (DE), **2004**, 1–23; d) M. Peruzzini, L. Gonsalvi, A. Romerosa, *Chem.*

Soc. Rev. **2005**, *34*, 1038–1047; e) C. C. Cummins, *Angew. Chem. Int. Ed.* **2006**, *45*, 862–870; f) B. M. Cossairt, N. A. Piro, C. C. Cummins, *Chem. Rev.* **2010**, *110*, 4164–4177; g) M. Caporali, L. Gonsalvi, A. Rossin, M. Peruzzini, *Chem. Rev.* **2010**, *110*, 4178–4235; h) L. Giusti, V. R. Landaeta, M. Vanni, J. A. Kelly, R. Wolf, M. Caporali, *Coord. Chem. Rev.* **2021**, *441*, 213927–214019; i) C. M. Hoidn, D. J. Scott, R. Wolf, *Chem. Eur. J.* **2021**, *27*, 1886–1902.

[200] a) G. L. Simon, L. F. Dahl, *J. Am. Chem. Soc.* **1973**, *95*, 2175–2183; b) O. J. Scherer, J. Braun, G. Wolmershäuser, *Chem. Ber.* **1990**, *123*, 471–475; c) S. Heinl, K. Kiefer, G. Balázs, C. Wickleder, M. Scheer, *Chem. Commun.* **2015**, *51*, 13474–13477.

[201] M. H. Chisholm, K. Folting, J. W. Pasterczyk, *Inorg. Chem.* **1988**, *27*, 3057–3058.

[202] a) M. J. A. Johnson, P. M. Lee, A. L. Odom, W. M. Davis, C. C. Cummins, *Angew. Chem. Int. Ed. Engl.* **1997**, *36*, 87–91; b) J. S. Figueroa, C. C. Cummins, *J. Am. Chem. Soc.* **2003**, *125*, 4020–4021.

[203] a) C. E. Laplaza, W. M. Davis, C. C. Cummins, *Angew. Chem. Int. Ed. Engl.* **1995**, *34*, 2042–2044; b) J. P. Cherry, A. R. Johnson, L. M. Baraldo, Y. C. Tsai, C. C. Cummins, S. V. Kryatov, E. V. Rybak-Akimova, K. B. Capps, C. D. Hoff, C. M. Haar, S. P. Nolan, *J. Am. Chem. Soc.* **2001**, *123*, 7271–7286; c) J. P. Cherry, F. H. Stephens, M. J. Johnson, P. L. Diaconescu, C. C. Cummins, *Inorg. Chem.* **2001**, *40*, 6860–6862; d) D. S. Kuiper, P. T. Wolczanski, E. B. Lobkovsky, T. R. Cundari, *J. Am. Chem. Soc.* **2008**, *130*, 12931–12943; e) J. J. Curley, N. A. Piro, C. C. Cummins, *Inorg. Chem.* **2009**, *48*, 9599–9601; f) H. A. Spinney, N. A. Piro, C. C. Cummins, *J. Am. Chem. Soc.* **2009**, *131*, 16233–16243.

[204] a) O. J. Scherer, H. Sitzmann, G. Wolmershäuser, *J. Organomet. Chem.* **1984**, *268*, C9-C12; b) O. J. Scherer, H. Sitzmann, G. Wolmershäuser, *Angew. Chem. Int. Ed. Engl.* **1985**, *24*, 351–353; c) L. Y. Goh, C. K. Chu, R. C. S. Wong, T. W. Hambley, *J. Chem. Soc., Dalton Trans.* **1989**, *10*, 1951–1956; d) O. J. Scherer, M. Ehses, G. Wolmershäuser, *Angew. Chem. Int. Ed.* **1998**, *37*, 507–510; e) C. Eichhorn, O. J. Scherer, T. Sögding, G. Wolmershäuser, *Angew. Chem. Int. Ed.* **2001**, *40*, 2859–2861; f) Y.-C. Shi, *J. Coord. Chem.* **2004**, *57*, 393–400; g) M. A. Alvarez, M. E. García, D. García-Vivó, A. Ramos, M. A. Ruiz, *Inorg. Chem.* **2011**, *50*, 2064–2066; h) M. Caporali, L. Gonsalvi, V. Mirabello, A. Ienco, G. Manca, F. Zanobini, M. Peruzzini, *Eur. J. Inorg. Chem.* **2014**, *2014*, 1652–1659; i) M. A. Alvarez, M. E. García, D. García-Vivó, M. A. Ruiz, M. F. Vega, *Organometallics* **2015**, *34*, 870–878.

[205] a) O. J. Scherer, M. Ehses, G. Wolmershäuser, *J. Organomet. Chem.* **1997**, *531*, 217–221; b) M. Demange, X.-F. Le Goff, P. Le Floch, N. Mézailles, *Chem. Eur. J.* **2010**, *16*, 12064–12068; c) B. Zarzycki, T. Zell, D. Schmidt, U. Radius, *Eur. J. Inorg. Chem.* **2013**, *2013*, 2051–2058.

[206] a) O. J. Scherer, H. Sitzmann, G. Wolmershäuser, *J. Organomet. Chem.* **1986**, *309*, 77–86; b) A.-J. DiMaio, A. L. Rheingold, *J. Chem. Soc., Chem. Commun.* **1987**, *6*, 404–405; c) O. J. Scherer, M. Swarowsky, G. Wolmershäuser, *Angew. Chem. Int. Ed. Engl.* **1988**, *27*, 405–406; d) O. J. Scherer, H. Sitzmann, G. Wolmershäuser, *Angew. Chem. Int. Ed. Engl.* **1989**, *28*, 212–213; e) M. E. Barr, L. F. Dahl, *Organometallics* **1991**, *10*, 3991–3996;

f) O. J. Scherer, K. Pfeiffer, G. Heckmann, G. Wolmershäuser, *J. Organomet. Chem.* **1992**, *425*, 141–149; g) O. J. Scherer, R. Winter, G. Wolmershäuser, *Z. Anorg. Allg. Chem.* **1993**, *619*, 827–835; h) M. Scheer, U. Becker, *Phosphorus Sulfur Silicon Relat. Elem.* **1994**, *93*, 391–392; i) M. Herberhold, G. Frohmader, W. Milius, *Phosphorus Sulfur Silicon Relat. Elem.* **1994**, *93*, 205–208; j) M. Herberhold, G. Frohmader, W. Milius, *J. Organomet. Chem.* **1996**, *522*, 185–196; k) S. Yao, T. Szilvási, N. Lindenmaier, Y. Xiong, S. Inoue, M. Adelhardt, J. Sutter, K. Meyer, M. Driess, *Chem. Commun.* **2015**, *51*, 6153–6156; l) S. Heinl, G. Balázs, M. Bodensteiner, M. Scheer, *Dalton Trans.* **2016**, *45*, 1962–1966.

[207] O. J. Scherer, G. Kemény, G. Wolmershäuser, *Chem. Ber.* **1995**, *128*, 1145–1148.

[208] E. B. Hulley, P. T. Wolczanski, E. B. Lobkovsky, *Chem. Commun.* **2009**, *42*, 6412–6414.

[209] O. J. Scherer, R. Winter, G. Wolmershäuser, *J. Chem. Soc., Chem. Commun.* **1993**, *3*, 313–314.

[210] a) F. Cecconi, P. Dapporto, S. Midollini, L. Sacconi, *Inorg. Chem.* **1978**, *17*, 3292–3294; b) M. Di Vaira, C. A. Ghilardi, S. Midollini, L. Sacconi, *J. Am. Chem. Soc.* **1978**, *100*, 2550–2551; c) C. Bianchini, C. Mealli, A. Meli, L. Sacconi, *Inorg. Chim. Acta* **1979**, *37*, 543-544; d) P. Dapporto, L. Sacconi, P. Stoppioni, F. Zanobini, *Inorg. Chem.* **1981**, *20*, 3834–3839; e) M. Di Vaira, L. Sacconi, *Angew. Chem. Int. Ed. Engl.* **1982**, *21*, 330–342; f) M. Di Vaira, L. Sacconi, P. Stoppioni, *J. Organomet. Chem.* **1983**, *250*, 183–195; g) O. J. Scherer, T. Dave, J. Braun, G. Wolmershäuser, *J. Organomet. Chem.* **1988**, *350*, C20-C24; h) O. J. Scherer, W. Wiedemann, G. Wolmershäuser, *Chem. Ber.* **1990**, *123*, 3–6; i) M. Peruzzini, J. A. Ramirez, F. Vizza, *Angew. Chem. Int. Ed.* **1998**, *37*, 2255–2257; j) E. Mädl, G. Balázs, E. V. Peresypkina, M. Scheer, *Angew. Chem. Int. Ed.* **2016**, *55*, 7702–7707; k) T. D. Lohrey, G. Rao, R. D. Britt, R. G. Bergman, J. Arnold, *Inorg. Chem.* **2019**, *58*, 13492–13501.

[211] a) M. H. Chisholm, J. C. Huffman, J. W. Pasterczyk, *Inorg. Chim. Acta* **1987**, *133*, 17–18; b) O. J. Scherer, C. Blath, G. Heckmann, G. Wolmershäuser, *J. Organomet. Chem.* **1991**, *409*, C15-C18; c) B. M. Cossairt, M.-C. Diawara, C. C. Cummins, *Science* **2009**, *323*, 602; d) B. L. Tran, M. Singhal, H. Park, O. P. Lam, M. Pink, J. Krzystek, A. Ozarowski, J. Telser, K. Meyer, D. J. Mindiola, *Angew. Chem. Int. Ed.* **2010**, *49*, 9871–9875; e) D. Tofan, B. M. Cossairt, C. C. Cummins, *Inorg. Chem.* **2011**, *50*, 12349–12358; f) B. Pinter, K. T. Smith, M. Kamitani, E. M. Zolnhofer, B. L. Tran, S. Fortier, M. Pink, G. Wu, B. C. Manor, K. Meyer, M.-H. Baik, D. J. Mindiola, *J. Am. Chem. Soc.* **2015**, *137*, 15247–15261; g) P. Coburger, J. Leitl, D. J. Scott, G. Hierlmeier, I. G. Shenderovich, E. Hey-Hawkins, R. Wolf, *Chem. Sci.* **2021**, *12*, 11225–11235.

[212] a) M. Di Vaira, S. Midollini, L. Sacconi, F. Zanobini, *Angew. Chem. Int. Ed. Engl.* **1978**, *17*, 676–677; b) M. Di Vaira, S. Midollini, L. Sacconi, *J. Am. Chem. Soc.* **1979**, *101*, 1757–1763; c) C. Bianchini, M. Di Vaira, A. Meli, L. Sacconi, *Angew. Chem. Int. Ed. Engl.* **1980**, *19*, 405–406; d) C. Bianchini, M. Di Vaira, A. Meli, L. Sacconi, *J. Am. Chem. Soc.* **1981**, *103*, 1448–1452; e) O. J. Scherer, B. Werner, G. Heckmann, G. Wolmershäuser, *Angew. Chem. Int. Ed.* **1991**, *30*, 553–555; f) Y. Nakanishi, Y. Ishida, H. Kawaguchi, *Inorg. Chem.* **2016**, *55*, 3967–3973; g) F. Spitzer, C. Graßl, G. Balázs, E. Mädl, M. Keilwerth, E. M.

Zolnhofer, K. Meyer, M. Scheer, *Chem. Eur. J.* **2017**, *23*, 2716–2721; h) F. Spitzer, G. Balázs, C. Graßl, M. Keilwerth, K. Meyer, M. Scheer, *Angew. Chem. Int. Ed.* **2018**, *57*, 8760–8764; i) M. Haimerl, C. Graßl, M. Seidl, M. Piesch, M. Scheer, *Chem. Eur. J.* **2021**, *27*, 18129–18134.

[213] M. A. Alvarez, M. Casado-Ruano, M. E. García, D. García-Vivó, M. A. Ruiz, *Chem. Eur. J.* **2018**, *24*, 9504–9507.

[214] a) P. Dapporto, S. Midollini, L. Sacconi, *Angew. Chem. Int. Ed. Engl.* **1979**, *18*, 469; b) T. Gröer, G. Baum, M. Scheer, *Organometallics* **1998**, *17*, 5916–5919; c) M. Peruzzini, L. Marvelli, A. Romerosa, R. Rossi, F. Vizza, F. Zanobini, *Eur. J. Inorg. Chem.* **1999**, *1999*, 931–933; d) M. Peruzzini, S. Mañas, A. Romerosa, A. Vacca, *Mendeleev Commun.* **2000**, *10*, 134–135; e) M. Di Vaira, M. P. Ehses, M. Peruzzini, P. Stoppioni, *Eur. J. Inorg. Chem.* **2000**, *2000*, 2193–2198; f) I. de los Rios, J.-R. Hamon, P. Hamon, C. Lapinte, L. Toupet, A. Romerosa, M. Peruzzini, *Angew. Chem. Int. Ed.* **2001**, *40*, 3910–3912; g) M. Di Vaira, M. Peruzzini, S. S. Costantini, P. Stoppioni, *J. Organomet. Chem.* **2010**, *695*, 816–820; h) M. Caporali, M. Di Vaira, M. Peruzzini, S. Seniori Costantini, P. Stoppioni, F. Zanobini, *Eur. J. Inorg. Chem.* **2010**, *2010*, 152–158; i) V. Mirabello, M. Caporali, V. Gallo, L. Gonsalvi, A. Ienco, M. Latronico, P. Mastrorilli, M. Peruzzini, *Dalton Trans.* **2011**, *40*, 9668–9671; j) V. Mirabello, M. Caporali, V. Gallo, L. Gonsalvi, D. Gudat, W. Frey, A. Ienco, M. Latronico, P. Mastrorilli, M. Peruzzini, *Chem. Eur. J.* **2012**, *18*, 11238–11250; k) S. Heinl, E. V. Peresypkina, A. Y. Timoshkin, P. Mastrorilli, V. Gallo, M. Scheer, *Angew. Chem. Int. Ed.* **2013**, *52*, 10887–10891; l) I. M. Riddlestone, P. Weis, A. Martens, M. Schorpp, H. Scherer, I. Krossing, *Chem. Eur. J.* **2019**, *25*, 10546–10551.

[215] a) D. N. Akbayeva, O. J. Scherer, *Z. Anorg. Allg. Chem.* **2001**, *627*, 1429–1430; b) I. Krossing, *J. Am. Chem. Soc.* **2001**, *123*, 4603–4604; c) I. Krossing, L. van Wüllen, *Chem. Eur. J.* **2002**, *8*, 700–711; d) G. Santiso-Quiñones, A. Reisinger, J. Slattery, I. Krossing, *Chem. Commun.* **2007**, *47*, 5046–5048; e) L. C. Forfar, T. J. Clark, M. Green, S. M. Mansell, C. A. Russell, R. A. Sanguramath, J. M. Slattery, *Chem. Commun.* **2012**, *48*, 1970–1972; f) C. Schwarzmaier, M. Sierka, M. Scheer, *Angew. Chem. Int. Ed.* **2013**, *52*, 858–861; g) F. Spitzer, M. Sierka, M. Latronico, P. Mastrorilli, A. V. Virovets, M. Scheer, *Angew. Chem. Int. Ed.* **2015**, *54*, 4392–4396; h) L. C. Forfar, D. Zeng, M. Green, J. E. McGrady, C. A. Russell, *Chem. Eur. J.* **2016**, *22*, 5397–5403.

[216] a) A. P. Ginsberg, W. E. Lindsell, *J. Am. Chem. Soc.* **1971**, *93*, 2082–2084; b) A. P. Ginsberg, W. E. Lindsell, K. J. McCullough, C. R. Sprinkle, A. J. Welch, *J. Am. Chem. Soc.* **1986**, *108*, 403–416; c) O. J. Scherer, M. Swarowsky, H. Swarowsky, G. Wolmershäuser, *Angew. Chem. Int. Ed. Engl.* **1988**, *27*, 694–695; d) O. J. Scherer, M. Swarowsky, G. Wolmershäuser, *Organometallics* **1989**, *8*, 841–842; e) M. Scheer, M. Dargatz, A. Rufińska, *J. Organomet. Chem.* **1992**, *440*, 327–334; f) O. J. Scherer, K. Pfeiffer, G. Wolmershäuser, *Chem. Ber.* **1992**, *125*, 2367–2372; g) M. Scheer, C. Troitzsch, P. G. Jones, *Angew. Chem. Int. Ed. Engl.* **1992**, *31*, 1377–1379; h) M. Scheer, C. Troitzsch, L. Hilfert, M. Dargatz, E. Kleinpeter, P. G. Jones, J. Sieler, *Chem. Ber.* **1995**, *128*, 251–257; i) M. Scheer, U. Becker, E. Matern, *Chem. Ber.* **1996**, *129*, 721–724; j) O. J. Scherer, G.

Schwarz, G. Wolmershäuser, *Z. Anorg. Allg. Chem.* **1996**, *622*, 951–957; k) M. Scheer, K. Schuster, U. Becker, *Phosphorus Sulfur Silicon Relat. Elem.* **1996**, *109*, 141–144; l) M. Scheer, U. Becker, *J. Organomet. Chem.* **1997**, *545*, 451–460; m) S. Dürr, D. Ertler, U. Radius, *Inorg. Chem.* **2012**, *51*, 3904–3909; n) C. C. Mokhtarzadeh, A. L. Rheingold, J. S. Figueroa, *Dalton Trans.* **2016**, *45*, 14561–14569; o) M. Schmidt, A. E. Seitz, M. Eckhardt, G. Balázs, E. V. Peresypkina, A. V. Virovets, F. Riedlberger, M. Bodensteiner, E. M. Zolnhofer, K. Meyer, M. Scheer, *J. Am. Chem. Soc.* **2017**, *139*, 13981–13984; p) M. J. Drance, S. Wang, M. Gembicky, A. L. Rheingold, J. S. Figueroa, *Organometallics* **2020**, *39*, 3394–3402.

[217] a) O. J. Scherer, T. Hilt, G. Wolmershäuser, *Organometallics* **1998**, *17*, 4110–4112; b) S. Heinl, M. Scheer, *Chem. Sci.* **2014**, *5*, 3221–3225; c) S. Pelties, D. Herrmann, B. de Bruin, F. Hartl, R. Wolf, *Chem. Commun.* **2014**, *50*, 7014–7016; d) C. Schwarzmaier, A. Y. Timoshkin, G. Balázs, M. Scheer, *Angew. Chem. Int. Ed.* **2014**, *53*, 9077–9081; e) S. Heinl, G. Balázs, M. Scheer, *Phosphorus Sulfur Silicon Relat. Elem.* **2014**, *189*, 924–932; f) J. E. Borger, M. K. Jongkind, A. W. Ehlers, M. Lutz, J. C. Slootweg, K. Lammertsma, *ChemistryOpen* **2017**, *6*, 350–353.

[218] a) O. J. Scherer, J. Vondung, G. Wolmershäuser, *Angew. Chem. Int. Ed. Engl.* **1989**, *28*, 1355–1357; b) O. J. Scherer, J. Vondung, G. Wolmershäuser, *J. Organomet. Chem.* **1989**, *376*, C35-C38; c) U. Chakraborty, J. Leitl, B. Mühldorf, M. Bodensteiner, S. Pelties, R. Wolf, *Dalton Trans.* **2018**, *47*, 3693–3697; d) K. A. Mandla, C. E. Moore, A. L. Rheingold, J. S. Figueroa, *Angew. Chem. Int. Ed.* **2019**, *58*, 1779–1783; e) K. A. Mandla, M. L. Neville, C. E. Moore, A. L. Rheingold, J. S. Figueroa, *Angew. Chem. Int. Ed.* **2019**, *58*, 15329–15333; f) M. Dietz, M. Arrowsmith, S. Reichl, L. I. Lugo-Fuentes, J. O. C. Jiménez-Halla, M. Scheer, H. Braunschweig, *Angew. Chem. Int. Ed.* **2022**, *61*, e202206840.

[219] a) W. W. Seidel, O. T. Summerscales, B. O. Patrick, M. D. Fryzuk, *Angew. Chem. Int. Ed.* **2009**, *48*, 115–117; b) A. S. P. Frey, F. G. N. Cloke, P. B. Hitchcock, J. C. Green, *New J. Chem.* **2011**, *35*, 2022–2026; c) M. D. Walter, J. Grunenberg, P. S. White, *Chem. Sci.* **2011**, *2*, 2120–2130; d) C. Schwarzmaier, A. Noor, G. Glatz, M. Zabel, A. Y. Timoshkin, B. M. Cossairt, C. C. Cummins, R. Kempe, M. Scheer, *Angew. Chem. Int. Ed.* **2011**, *50*, 7283–7286; e) C. Camp, L. Maron, R. G. Bergman, J. Arnold, *J. Am. Chem. Soc.* **2014**, *136*, 17652–17661; f) S. Yao, N. Lindenmaier, Y. Xiong, S. Inoue, T. Szilvási, M. Adelhardt, J. Sutter, K. Meyer, M. Driess, *Angew. Chem. Int. Ed.* **2015**, *54*, 1250–1254; g) F. Spitzer, C. Graßl, G. Balázs, E. M. Zolnhofer, K. Meyer, M. Scheer, *Angew. Chem. Int. Ed.* **2016**, *55*, 4340–4344; h) A. Formanuik, F. Ortu, R. Beekmeyer, A. Kerridge, R. W. Adams, D. P. Mills, *Dalton Trans.* **2016**, *45*, 2390–2393; i) S. Pelties, T. Maier, D. Herrmann, B. de Bruin, C. Rebreyend, S. Gärtner, I. G. Shenderovich, R. Wolf, *Chem. Eur. J.* **2017**, *23*, 6094–6102; j) S. Heinl, A. Y. Timoshkin, J. Müller, M. Scheer, *Chem. Commun.* **2018**, *54*, 2244–2247; k) C. Schoo, S. Bestgen, R. Köppe, S. N. Konchenko, P. W. Roesky, *Chem. Commun.* **2018**, *54*, 4770–4773.

[220] a) M. E. Barr, S. K. Smith, B. Spencer, L. F. Dahl, *Organometallics* **1991**, *10*, 3983–3991; b) M. Scheer, M. Dargatz, K. Schenzel, P. G. Jones, *J. Organomet. Chem.* **1992**, *435*,

123–132; c) M. Scheer, U. Becker, J. C. Huffman, M. H. Chisholm, *J. Organomet. Chem.* **1993**, *461*, C1-C3; d) M. Scheer, U. Becker, *Phosphorus Sulfur Silicon Relat. Elem.* **1994**, *93*, 257–260; e) M. Scheer, U. Becker, M. H. Chisholm, J. C. Huffman, F. Lemoigno, O. Eisenstein, *Inorg. Chem.* **1995**, *34*, 3117–3119; f) M. Scheer, U. Becker, *Chem. Ber.* **1996**, *129*, 1307–1310.

[221] P. Barbaro, M. Peruzzini, J. A. Ramirez, F. Vizza, *Organometallics* **1999**, *18*, 4237–4240.

[222] a) F. Cecconi, C. A. Ghilardi, S. Midollini, A. Orlandini, *J. Am. Chem. Soc.* **1984**, *106*, 3667–3668; b) F. Cecconi, C. A. Ghilardi, S. Midollini, A. Orlandini, *Inorg. Chem.* **1986**, *25*, 1766–1770; c) O. J. Scherer, J. Braun, P. Walther, G. Wolmershäuser, *Chem. Ber.* **1992**, *125*, 2661–2665; d) S. Yao, Y. Xiong, C. Milsmann, E. Bill, S. Pfirrmann, C. Limberg, M. Driess, *Chem. Eur. J.* **2010**, *16*, 436–439; e) S. Yao, M. Driess, *Acc. Chem. Res.* **2012**, *45*, 276–287.

[223] D. Yakhvarov, P. Barbaro, L. Gonsalvi, S. Mañas Carpio, S. Midollini, A. Orlandini, M. Peruzzini, O. Sinyashin, F. Zanobini, *Angew. Chem. Int. Ed.* **2006**, *45*, 4182–4185.

[224] A. L. Rheingold, M. J. Foley, P. J. Sullivan, *J. Am. Chem. Soc.* **1982**, *104*, 4727–4729.

[225] a) O. J. Scherer, J. Schwalb, G. Wolmershäuser, W. Kaim, R. Gross, *Angew. Chem. Int. Ed. Engl.* **1986**, *25*, 363–364; b) O. J. Scherer, W. Wiedemann, G. Wolmershäuser, *J. Organomet. Chem.* **1989**, *361*, C11-C14; c) B. M. Gardner, F. Tuna, E. J. L. McInnes, J. McMaster, W. Lewis, A. J. Blake, S. T. Liddle, *Angew. Chem. Int. Ed.* **2015**, *54*, 7068–7072; d) G. Hierlmeier, P. Coburger, N. P. van Leest, B. de Bruin, R. Wolf, *Angew. Chem. Int. Ed.* **2020**, *59*, 14148–14153.

[226] a) O. J. Scherer, T. Brück, *Angew. Chem. Int. Ed. Engl.* **1987**, *26*, 59; b) O. J. Scherer, T. Brück, G. Wolmershäuser, *Chem. Ber.* **1988**, *121*, 935–938; c) O. J. Scherer, C. Blath, G. Wolmershäuser, *J. Organomet. Chem.* **1990**, *387*, C21-C24; d) C. Heinl, E. Peresypkina, G. Balázs, E. Mädl, A. V. Virovets, M. Scheer, *Chem. Eur. J.* **2021**, *27*, 7542–7548.

[227] E. Urnius, W. W. Brennessel, C. J. Cramer, J. E. Ellis, P. v. R. Schleyer, *Science* **2002**, *295*, 832–834.

[228] a) O. J. Scherer, J. Schwalb, H. Swarowsky, G. Wolmershäuser, W. Kaim, R. Gross, *Chem. Ber.* **1988**, *121*, 443–449; b) A. C. Reddy, E. D. Jemmis, O. J. Scherer, R. Winter, G. Heckmann, G. Wolmershäuser, *Organometallics* **1992**, *11*, 3894–3900; c) O. J. Scherer, H. Swarowsky, G. Wolmershäuser, W. Kaim, S. Kohlmann, *Angew. Chem. Int. Ed. Engl.* **1987**, *26*, 1153–1155.

[229] E.-M. Schnöckelborg, J. J. Weigand, R. Wolf, *Angew. Chem. Int. Ed.* **2011**, *50*, 6657–6660.

[230] O. J. Scherer, J. Schulze, G. Wolmershäuser, *J. Organomet. Chem.* **1994**, *484*, C5-C7.

[231] a) W. Huang, P. L. Diaconescu, *Chem. Commun.* **2012**, *48*, 2216–2218; b) W. Huang, P. L. Diaconescu, *Eur. J. Inorg. Chem.* **2013**, *2013*, 4090–4096; c) D. Patel, F. Tuna, E. J. L. McInnes, W. Lewis, A. J. Blake, S. T. Liddle, *Angew. Chem. Int. Ed.* **2013**, *52*, 13334–13337; d) A. N. Selikhov, T. V. Mahrova, A. V. Cherkasov, G. K. Fukin, E. Kirillov, C. Alvarez Lamsfus, L. Maron, A. A. Trifonov, *Organometallics* **2016**, *35*, 2401–2409; e) F. Zhang, J. Zhang, Z. Chen, L. Weng, X. Zhou, *Inorg. Chem.* **2019**, *58*, 8451–8459.

[232] S. N. Konchenko, N. A. Pushkarevsky, M. T. Gamer, R. Köppe, H. Schnöckel, P. W. Roesky, *J. Am. Chem. Soc.* **2009**, *131*, 5740–5741.

[233] a) M. E. Barr, B. R. Adams, R. R. Weller, L. F. Dahl, *J. Am. Chem. Soc.* **1991**, *113*, 3052–3060; b) O. J. Scherer, G. Berg, G. Wolmershäuser, *Chem. Ber.* **1996**, *129*, 53–58; c) B. M. Cossairt, C. C. Cummins, *Angew. Chem. Int. Ed.* **2008**, *47*, 169–172.

[234] a) O. J. Scherer, R. Winter, G. Heckmann, G. Wolmershäuser, *Angew. Chem. Int. Ed.* **1991**, *30*, 850–852; b) K. Mast, J. Meiers, O. J. Scherer, G. Wolmershäuser, *Z. Anorg. Allg. Chem.* **1999**, *625*, 70–74.

[235] F. Dielmann, M. Sierka, A. V. Virovets, M. Scheer, *Angew. Chem. Int. Ed.* **2010**, *49*, 6860–6864.

[236] C. Graßl, M. Bodensteiner, M. Zabel, M. Scheer, *Chem. Sci.* **2015**, *6*, 1379–1382.

[237] a) L. Y. Goh, R. C. S. Wong, E. Sinn, *J. Chem. Soc., Chem. Commun.* **1990**, *21*, 1484–1485; b) O. J. Scherer, B. Höbel, G. Wolmershäuser, *Angew. Chem. Int. Ed. Engl.* **1992**, *31*, 1027–1028; c) O. J. Scherer, T. Völmecke, G. Wolmershäuser, *Eur. J. Inorg. Chem.* **1999**, *1999*, 945–949.

[238] G. Balázs, M. Hautmann, M. Seidl, M. Scheer, *Inorg. Chim. Acta* **2018**, *475*, 47–52.

[239] O. J. Scherer, T. Brück, G. Wolmershäuser, *Chem. Ber.* **1989**, *122*, 2049–2054.

[240] a) S. Midollini, A. Orlandini, L. Sacconi, *Angew. Chem. Int. Ed. Engl.* **1979**, *18*, 81–82; b) C. A. Ghilardi, S. Midollini, A. Orlandini, L. Sacconi, *Inorg. Chem.* **1980**, *19*, 301–306; c) C. Bianchini, M. Di Vaira, A. Meli, L. Sacconi, *Inorg. Chem.* **1981**, *20*, 1169–1173; d) F. Cecconi, C. A. Ghilardi, S. Midollini, A. Orlandini, *J. Chem. Soc., Chem. Commun.* **1982**, *4*, 229–230; e) A. Vizi-Orosz, G. Pályi, L. Markó, R. Boese, G. Schmid, *J. Organomet. Chem.* **1985**, *288*, 179–187; f) M. Di Vaira, P. Stoppioni, M. Peruzzini, *J. Chem. Soc., Dalton Trans.* **1990**, *1*, 109–113; g) B. Rink, O. J. Scherer, G. Heckmann, G. Wolmershäuser, *Chem. Ber.* **1992**, *125*, 1011–1016; h) M. Detzel, T. Mohr, O. J. Scherer, G. Wolmershäuser, *Angew. Chem. Int. Ed. Engl.* **1994**, *33*, 1110–1112; i) O. J. Scherer, G. Berg, G. Wolmershäuser, *Chem. Ber.* **1995**, *128*, 635–639; j) M. Detzel, G. Friedrich, O. J. Scherer, G. Wolmershäuser, *Angew. Chem. Int. Ed. Engl.* **1995**, *34*, 1321–1323; k) G. Friedrich, O. J. Scherer, G. Wolmershäuser, *Z. Anorg. Allg. Chem.* **1996**, *622*, 1478–1486; l) O. J. Scherer, S. Weigel, G. Wolmershäuser, *Chem. Eur. J.* **1998**, *4*, 1910–1916; m) A. R. Kudinov, P. V. Petrovskii, M. I. Rybinskaya, *Russ. Chem. Bull.* **1999**, *48*, 1362–1364; n) M. Di Vaira, M. P. Ehses, M. Peruzzini, P. Stoppioni, *Polyhedron* **1999**, *18*, 2331–2336; o) M. Di Vaira, M. P. Ehses, P. Stoppioni, M. Peruzzini, *Inorg. Chem.* **2000**, *39*, 2199–2205; p) A. R. Kudinov, D. A. Loginov, Z. A. Starikova, P. V. Petrovskii, M. Corsini, P. Zanello, *Eur. J. Inorg. Chem.* **2002**, *2002*, 3018–3027; q) M. Scheer, L. J. Gregoriades, M. Zabel, J. Bai, I. Krossing, G. Brunklaus, H. Eckert, *Chem. Eur. J.* **2008**, *14*, 282–295; r) M. Fleischmann, J. S. Jones, F. P. Gabbaï, M. Scheer, *Chem. Sci.* **2015**, *6*, 132–139; s) A. E. Seitz, U. Vogel, M. Eberl, M. Eckhardt, G. Balázs, E. V. Peresypkina, M. Bodensteiner, M. Zabel, M. Scheer, *Chem. Eur. J.* **2017**, *23*, 10319–10327; t) J. Müller, S. Heinl, C. Schwarzmaier, G. Balázs, M. Keilwerth, K. Meyer, M. Scheer, *Angew. Chem. Int. Ed.* **2017**, *56*, 7312–7317; u) M. Modl, S. Heinl, G. Balázs, F. Delgado Calvo, M. Caporali,

G. Manca, M. Keilwerth, K. Meyer, M. Peruzzini, M. Scheer, *Chem. Eur. J.* **2019**, *25*, 6300–6305; v) V. Heinl, G. Balázs, S. Koschabek, M. Eckhardt, M. Piesch, M. Seidl, M. Scheer, *Molecules* **2021**, *26*, 2966–2978; w) P. A. Shelyganov, M. Elsayed Moussa, M. Seidl, M. Scheer, *Angew. Chem. Int. Ed.* **2023**, *62*, e202215650.

[241] a) J. Bai, E. Leiner, M. Scheer, *Angew. Chem. Int. Ed.* **2002**, *41*, 783–786; b) J. Bai, A. V. Virovets, M. Scheer, *Angew. Chem. Int. Ed.* **2002**, *41*, 1737–1740; c) M. Scheer, L. J. Gregoriades, A. V. Virovets, W. Kunz, R. Neueder, I. Krossing, *Angew. Chem. Int. Ed.* **2006**, *45*, 5689–5693; d) L. J. Gregoriades, B. K. Wegley, M. Sierka, E. Brunner, C. Gröger, E. V. Peresypkina, A. V. Virovets, M. Zabel, M. Scheer, *Chem. Asian J.* **2009**, *4*, 1578–1587; e) M. Fleischmann, F. Dielmann, L. J. Gregoriades, E. V. Peresypkina, A. V. Virovets, S. Huber, A. Y. Timoshkin, G. Balázs, M. Scheer, *Angew. Chem. Int. Ed.* **2015**, *54*, 13110–13115; f) M. Fleischmann, S. Welsch, E. V. Peresypkina, A. V. Virovets, M. Scheer, *Chem. Eur. J.* **2015**, *21*, 14332–14336; g) C. Heindl, E. V. Peresypkina, D. Lüdeker, G. Brunklaus, A. V. Virovets, M. Scheer, *Chem. Eur. J.* **2016**, *22*, 2599–2604.

[242] a) M. Fleischmann, S. Welsch, L. J. Gregoriades, C. Gröger, M. Scheer, *Z. Naturforsch. B* **2014**, *69*, 1348–1356; b) M. Fleischmann, S. Welsch, H. Krauss, M. Schmidt, M. Bodensteiner, E. V. Peresypkina, M. Sierka, C. Gröger, M. Scheer, *Chem. Eur. J.* **2014**, *20*, 3759–3768; c) T. N. Sevastianova, M. Bodensteiner, A. F. Maulieva, E. I. Davydova, A. V. Virovets, E. V. Peresypkina, G. Balázs, C. Graßl, M. Seidl, M. Scheer, G. Frenking, E. A. Berezovskaya, I. V. Kazakov, O. V. Khoroshilova, A. Y. Timoshkin, *Dalton Trans.* **2015**, *44*, 20648–20658.

[243] a) H. Krauss, G. Balázs, M. Bodensteiner, M. Scheer, *Chem. Sci.* **2010**, *1*, 337–342; b) M. E. Moussa, J. Schiller, E. Peresypkina, M. Seidl, G. Balázs, P. Shelyganov, M. Scheer, *Chem. Eur. J.* **2020**, *26*, 14315–14319.

[244] a) B. Attenberger, S. Welsch, M. Zabel, E. Peresypkina, M. Scheer, *Angew. Chem. Int. Ed.* **2011**, *50*, 11516–11519; b) M. Elsayed Moussa, B. Attenberger, E. V. Peresypkina, M. Fleischmann, G. Balázs, M. Scheer, *Chem. Commun.* **2016**, *52*, 10004–10007; c) P. A. Shelyganov, M. Elsayed Moussa, M. Seidl, M. Scheer, *Chem. Eur. J.* **2023**, *29*, e202300610.

[245] a) J. Bai, A. V. Virovets, M. Scheer, *Science* **2003**, *300*, 781–783; b) M. Scheer, J. Bai, B. P. Johnson, R. Merkle, A. V. Virovets, C. E. Anson, *Eur. J. Inorg. Chem.* **2005**, *2005*, 4023–4026; c) B. P. Johnson, F. Dielmann, G. Balázs, M. Sierka, M. Scheer, *Angew. Chem. Int. Ed.* **2006**, *45*, 2473–2475; d) M. Scheer, A. Schindler, R. Merkle, B. P. Johnson, M. Linseis, R. Winter, C. E. Anson, A. V. Virovets, *J. Am. Chem. Soc.* **2007**, *129*, 13386–13387; e) M. Scheer, L. J. Gregoriades, R. Merkle, B. P. Johnson, F. Dielmann, *Phosphorus Sulfur Silicon Relat. Elem.* **2008**, *183*, 504–508; f) M. Scheer, A. Schindler, C. Gröger, A. V. Virovets, E. V. Peresypkina, *Angew. Chem. Int. Ed.* **2009**, *48*, 5046–5049; g) S. Welsch, C. Gröger, M. Sierka, M. Scheer, *Angew. Chem. Int. Ed.* **2011**, *50*, 1435–1438; h) C. Schwarzmaier, A. Schindler, C. Heindl, S. Scheuermayer, E. V. Peresypkina, A. V. Virovets, M. Neumeier, R. Gschwind, M. Scheer, *Angew. Chem. Int. Ed.* **2013**, *52*, 10896–10899; i) F. Dielmann, C. Heindl, F. Hastreiter, E. V. Peresypkina, A. V. Virovets, R. M.

Gschwind, M. Scheer, *Angew. Chem. Int. Ed.* **2014**, *53*, 13605–13608; j) F. Dielmann, M. Fleischmann, C. Heindl, E. V. Peresypkina, A. V. Virovets, R. M. Gschwind, M. Scheer, *Chem. Eur. J.* **2015**, *21*, 6208–6214; k) C. Heindl, E. V. Peresypkina, A. V. Virovets, W. Kremer, M. Scheer, *J. Am. Chem. Soc.* **2015**, *137*, 10938–10941; l) S. Heinl, E. Peresypkina, J. Sutter, M. Scheer, *Angew. Chem. Int. Ed.* **2015**, *54*, 13431–13435; m) E. Peresypkina, K. Grill, B. Hiltl, A. V. Virovets, W. Kremer, J. Hilgert, W. Tremel, M. Scheer, *Angew. Chem. Int. Ed.* **2021**, *60*, 12132–12142.

[246] a) M. Scheer, *Dalton Trans.* **2008**, *33*, 4372–4386; b) E. Peresypkina, A. Virovets, M. Scheer, *Coord. Chem. Rev.* **2021**, *446*, 213995–214036; c) A. V. Virovets, E. Peresypkina, M. Scheer, *Chem. Rev.* **2021**, *121*, 14485–14554.

[247] a) M. V. Butovskiy, G. Balázs, M. Bodensteiner, E. V. Peresypkina, A. V. Virovets, J. Sutter, M. Scheer, *Angew. Chem. Int. Ed.* **2013**, *52*, 2972–2976; b) M. Piesch, C. Graßl, M. Scheer, *Angew. Chem. Int. Ed.* **2020**, *59*, 7154–7160; c) M. Piesch, S. Reichl, C. Riesinger, M. Seidl, G. Balazs, M. Scheer, *Chem. Eur. J.* **2021**, *27*, 9129–9140.

[248] a) M. Schmidt, D. Konieczny, E. V. Peresypkina, A. V. Virovets, G. Balázs, M. Bodensteiner, F. Riedlberger, H. Krauss, M. Scheer, *Angew. Chem. Int. Ed.* **2017**, *56*, 7307–7311; b) M. Piesch, M. Seidl, M. Scheer, *Chem. Sci.* **2020**, *11*, 6745–6751.

[249] M. Piesch, S. Reichl, M. Seidl, G. Balázs, M. Scheer, *Angew. Chem. Int. Ed.* **2021**, *60*, 15101–15108.

[250] a) T. Li, J. Wiecko, N. A. Pushkarevsky, M. T. Gamer, R. Köppe, S. N. Konchenko, M. Scheer, P. W. Roesky, *Angew. Chem. Int. Ed.* **2011**, *50*, 9491–9495; b) T. Li, M. T. Gamer, M. Scheer, S. N. Konchenko, P. W. Roesky, *Chem. Commun.* **2013**, *49*, 2183–2185; c) T. Li, N. Arleth, M. T. Gamer, R. Köppe, T. Augenstein, F. Dielmann, M. Scheer, S. N. Konchenko, P. W. Roesky, *Inorg. Chem.* **2013**, *52*, 14231–14236; d) N. Arleth, M. T. Gamer, R. Köppe, N. A. Pushkarevsky, S. N. Konchenko, M. Fleischmann, M. Bodensteiner, M. Scheer, P. W. Roesky, *Chem. Sci.* **2015**, *6*, 7179–7184; e) N. Arleth, M. T. Gamer, R. Köppe, S. N. Konchenko, M. Fleischmann, M. Scheer, P. W. Roesky, *Angew. Chem. Int. Ed.* **2016**, *55*, 1557–1560; f) C. Schoo, R. Köppe, M. Piesch, M. T. Gamer, S. N. Konchenko, M. Scheer, P. W. Roesky, *Chem. Eur. J.* **2018**, *24*, 7890–7895; g) N. Reinfandt, N. Michenfelder, C. Schoo, R. Yadav, S. Reichl, S. N. Konchenko, A. N. Unterreiner, M. Scheer, P. W. Roesky, *Chem. Eur. J.* **2021**, *27*, 7862–7871; h) N. Reinfandt, C. Schoo, L. Dütsch, R. Köppe, S. N. Konchenko, M. Scheer, P. W. Roesky, *Chem. Eur. J.* **2021**, *27*, 3974–3978.

[251] R. Yadav, M. Weber, A. K. Singh, L. Münzfeld, J. Gramüller, R. M. Gschwind, M. Scheer, P. W. Roesky, *Chem. Eur. J.* **2021**, *27*, 14128–14137.

[252] a) E. Mädl, M. V. Butovskii, G. Balázs, E. V. Peresypkina, A. V. Virovets, M. Seidl, M. Scheer, *Angew. Chem. Int. Ed.* **2014**, *53*, 7643–7646; b) F. Riedlberger, M. Seidl, M. Scheer, *Chem. Commun.* **2020**, *56*, 13836–13839; c) F. Riedlberger, S. Todisco, P. Mastrorilli, A. Y. Timoshkin, M. Seidl, M. Scheer, *Chem. Eur. J.* **2020**, *26*, 16251–16255.

[253] a) J. C. Green, M. L. H. Green, G. E. Morris, *J. Chem. Soc., Chem. Commun.* **1974**, *6*, 212–213; b) E. Hey, M. F. Lappert, J. L. Atwood, S. G. Bott, *J. Chem. Soc., Chem.*

Commun. **1987**, *8*, 597–598; c) P. J. Chirik, J. A. Pool, E. Lobkovsky, *Angew. Chem. Int. Ed.* **2002**, *41*, 3463–3465; d) S. Pelties, A. W. Ehlers, R. Wolf, *Chem. Commun.* **2016**, *52*, 6601–6604; e) J. E. Borger, M. S. Bakker, A. W. Ehlers, M. Lutz, J. C. Slootweg, K. Lammertsma, *Chem. Commun.* **2016**, *52*, 3284–3287; f) M. Piesch, A. Nicolay, M. Haimerl, M. Seidl, G. Balázs, T. Don Tilley, M. Scheer, *Chem. Eur. J.* **2022**, *28*, e202201144; g) S. B. Dinauer, M. Piesch, R. Szlosek, M. Seidl, G. Balázs, M. Scheer, *Chem. Eur. J.* **2023**, *29*, e202300459; h) V. Heinl, M. Seidl, G. Balázs, M. Scheer, *Chem. Eur. J.* **2023**, *29*, e202301016.

[254] a) C. M. Hoidn, T. M. Maier, K. Trabitsch, J. J. Weigand, R. Wolf, *Angew. Chem. Int. Ed.* **2019**, *58*, 18931–18936; b) S. Reichl, R. Grünbauer, G. Balázs, M. Scheer, *Chem. Commun.* **2021**, *57*, 3383–3386.

[255] a) M. Di Vaira, P. Frediani, S. S. Costantini, M. Peruzzini, P. Stoppioni, *Dalton Trans.* **2005**, *13*, 2234–2236; b) M. Di Vaira, M. Peruzzini, S. Seniori Costantini, P. Stoppioni, *J. Organomet. Chem.* **2006**, *691*, 3931–3937; c) P. Barbaro, M. Di Vaira, M. Peruzzini, S. Seniori Costantini, P. Stoppioni, *Chem. Eur. J.* **2007**, *13*, 6682–6690; d) P. Barbaro, M. Di Vaira, M. Peruzzini, S. Seniori Costantini, P. Stoppioni, *Angew. Chem. Int. Ed.* **2008**, *47*, 4425–4427; e) P. Barbaro, M. Di Vaira, M. Peruzzini, S. Seniori Costantini, P. Stoppioni, *Inorg. Chem.* **2009**, *48*, 1091–1096; f) P. Barbaro, C. Bazzicalupi, M. Peruzzini, S. Seniori Costantini, P. Stoppioni, *Angew. Chem. Int. Ed.* **2012**, *51*, 8628–8631.

[256] a) M. Scheer, M. Dargatz, P. G. Jones, *J. Organomet. Chem.* **1993**, *447*, 259–264; b) M. Bispinghoff, Z. Benkő, H. Grützmacher, F. D. Calvo, M. Caporali, M. Peruzzini, *Dalton Trans.* **2019**, *48*, 3593–3600; c) H. Brake, E. Peresypkina, A. V. Virovets, M. Piesch, W. Kremer, L. Zimmermann, C. Klimas, M. Scheer, *Angew. Chem. Int. Ed.* **2020**, *59*, 16241–16246; d) A. Garbagnati, M. Seidl, G. Balázs, M. Scheer, *Inorg. Chem.* **2021**, *60*, 5163–5171; e) A. Garbagnati, M. Seidl, G. Balázs, M. Scheer, *Chem. Eur. J.* **2022**, *28*, e202200669; f) A. Garbagnati, M. Piesch, M. Seidl, G. Balázs, M. Scheer, *Chem. Eur. J.* **2022**, *28*, e202201026; g) A. Garbagnati, M. Seidl, M. Piesch, G. Balázs, M. Scheer, *Polyhedron* **2022**, *221*, 115854.

[257] R. Yadav, T. Simler, B. Goswami, C. Schoo, R. Köppe, S. Dey, P. W. Roesky, *Angew. Chem. Int. Ed.* **2020**, *59*, 9443–9447.

[258] a) C. G. P. Ziegler, T. M. Maier, S. Pelties, C. Taube, F. Hennersdorf, A. W. Ehlers, J. J. Weigand, R. Wolf, *Chem. Sci.* **2019**, *10*, 1302–1308; b) C. G. P. Ziegler, F. Hennersdorf, J. J. Weigand, R. Wolf, *Z. Anorg. Allg. Chem.* **2020**, *646*, 552–557.

[259] a) Y. Xiong, S. Yao, E. Bill, M. Driess, *Inorg. Chem.* **2009**, *48*, 7522–7524; b) T. Arnold, H. Braunschweig, J. O. C. Jimenez-Halla, K. Radacki, S. S. Sen, *Chem. Eur. J.* **2013**, *19*, 9114–9117; c) R. Yadav, T. Simler, S. Reichl, B. Goswami, C. Schoo, R. Köppe, M. Scheer, P. W. Roesky, *J. Am. Chem. Soc.* **2020**, *142*, 1190–1195; d) C. G. P. Ziegler, C. Taube, J. A. Kelly, G. Hierlmeier, M. Uttendorfer, J. J. Weigand, R. Wolf, *Chem. Commun.* **2020**, *56*, 14071–14074.

[260] a) J. S. Figueroa, C. C. Cummins, *Angew. Chem. Int. Ed.* **2005**, *44*, 4592–4596; b) R. Yadav, B. Goswami, T. Simler, C. Schoo, S. Reichl, M. Scheer, P. W. Roesky, *Chem. Commun.* **2020**, *56*, 10207–10210.

[261] a) C. M. Hoidn, C. Rödl, M. L. McCrea-Hendrick, T. Block, R. Pöttgen, A. W. Ehlers, P. P. Power, R. Wolf, *J. Am. Chem. Soc.* **2018**, *140*, 13195–13199; b) J. A. Kelly, V. Streitferdt, M. Dimitrova, F. F. Westermair, R. M. Gschwind, R. J. F. Berger, R. Wolf, *J. Am. Chem. Soc.* **2022**, *144*, 20434–20441.

[262] A. E. Seitz, M. Eckhardt, A. Erlebach, E. V. Peresypkina, M. Sierka, M. Scheer, *J. Am. Chem. Soc.* **2016**, *138*, 10433–10436.

[263] M. A. Alvarez, M. E. García, D. García-Vivó, A. Ramos, M. A. Ruiz, *Inorg. Chem.* **2012**, *51*, 11061–11075.

[264] a) J. S. Figueroa, C. C. Cummins, *Angew. Chem. Int. Ed.* **2004**, *43*, 984–988; b) C. M. Hoidn, K. Trabitsch, K. Schwedtmann, C. Taube, J. J. Weigand, R. Wolf, *Chem. Eur. J.* **2023**, e202301930.

[265] S. Reichl, E. Mädl, F. Riedlberger, M. Piesch, G. Balázs, M. Seidl, M. Scheer, *Nat. Commun.* **2021**, *12*, 5774–5783.

[266] a) B. Rink, O. J. Scherer, G. Wolmershäuser, *Chem. Ber.* **1995**, *128*, 71–73; b) B. M. Cossairt, C. C. Cummins, *Angew. Chem. Int. Ed.* **2010**, *49*, 1595–1598.

[267] a) O. J. Scherer, T. Hilt, G. Wolmershäuser, *Angew. Chem. Int. Ed.* **2000**, *39*, 1425–1427; b) M. Scheer, S. Deng, O. J. Scherer, M. Sierka, *Angew. Chem. Int. Ed.* **2005**, *44*, 3755–3758.

[268] a) B. M. Cossairt, C. C. Cummins, *Angew. Chem. Int. Ed.* **2008**, *47*, 8863–8866; b) B. M. Cossairt, C. C. Cummins, *Inorg. Chem.* **2008**, *47*, 9363–9371; c) N. A. Piro, C. C. Cummins, *Angew. Chem. Int. Ed.* **2009**, *48*, 934–938; d) U. Vogel, M. Eberl, M. Eckhardt, A. Seitz, E.-M. Rummel, A. Y. Timoshkin, E. V. Peresypkina, M. Scheer, *Angew. Chem. Int. Ed.* **2011**, *50*, 8982–8985.

[269] a) J. S. Figueroa, C. C. Cummins, *J. Am. Chem. Soc.* **2004**, *126*, 13916–13917; b) I. Krummenacher, C. C. Cummins, *Polyhedron* **2012**, *32*, 10–13.

[270] a) N. A. Piro, J. S. Figueroa, J. T. McKellar, C. C. Cummins, *Science* **2006**, *313*, 1276–1279; b) N. A. Piro, C. C. Cummins, *Inorg. Chem.* **2007**, *46*, 7387–7393; c) N. A. Piro, C. C. Cummins, *J. Am. Chem. Soc.* **2008**, *130*, 9524–9535; d) A. Velian, C. C. Cummins, *Chem. Sci.* **2012**, *3*, 1003–1006; e) G. Hierlmeier, R. Wolf, *Eur. J. Inorg. Chem.* **2022**, *2022*, e202101057.

[271] L. Dütsch, M. Fleischmann, S. Welsch, G. Balázs, W. Kremer, M. Scheer, *Angew. Chem. Int. Ed.* **2018**, *57*, 3256–3261.

[272] L. Dütsch, C. Riesinger, G. Balázs, M. Seidl, M. Scheer, *Chem. Sci.* **2021**, *12*, 14531–14539.

[273] R. F. Winter, W. E. Geiger, *Organometallics* **1999**, *18*, 1827–1833.

[274] M. Fleischmann, F. Dielmann, G. Balázs, M. Scheer, *Chem. Eur. J.* **2016**, *22*, 15248–15251.

[275] L. Dütsch, *Dissertation* **2022**, University of Regensburg.

[276] A. K. Adhikari, C. G. P. Ziegler, K. Schwedtmann, C. Taube, J. J. Weigand, R. Wolf, *Angew. Chem. Int. Ed.* **2019**, *58*, 18584–18590.

[277] A. Barth, G. Huttner, M. Fritz, L. Zsolnai, *Angew. Chem. Int. Ed.* **1990**, *29*, 929–931.

[278] a) G. Capozzi, L. Chiti, M. Di Vaira, M. Peruzzini, P. Stoppioni, *J. Chem. Soc., Chem. Commun.* **1986**, *24*, 1799–1800; b) M. Di Vaira, P. Stoppioni, S. Midollini, F. Laschi, P. Zanello, *Polyhedron* **1991**, *10*, 2123–2129.

[279] a) P. Barbaro, M. Caporali, A. Ienco, C. Mealli, M. Peruzzini, F. Vizza, *Eur. J. Inorg. Chem.* **2008**, *2008*, 1392–1399; b) P. Barbaro, A. Ienco, C. Mealli, M. Peruzzini, O. J. Scherer, G. Schmitt, F. Vizza, G. Wolmershäuser, *Chem. Eur. J.* **2003**, *9*, 5196–5210.

[280] M. Weber, G. Balázs, A. V. Virovets, E. Peresypkina, M. Scheer, *Molecules* **2021**, *26*, 3920-3933.

[281] M. Piesch, M. Seidl, M. Stubenhofer, M. Scheer, *Chem. Eur. J.* **2019**, *25*, 6311–6316.

2. Research Objectives

Based on the above, the synthetic entries to access transition metal stabilized polypnictogen cations as well as studies on their reactivity are highly limited. However, increasing the accessibility of such species would greatly aid the development of fundamentally important concepts in group 15 chemistry and grant insight into the chemistry of the pnictogens. Thus, three distinct main objectives were defined within this thesis to accomplish this goal:

Firstly, the systematic study of the reactivity of *cyclo*-P_n (n = 3, 4, 5, 8) ligand complexes towards cationic electrophiles should provide a synthetic entry into transition metal stabilized polyphosphorus cations, which has substantially been overlooked within the past decades. Moreover, it may enable the preparation of species with yet unprecedented structural and bonding motifs. To realize this objective, the following tasks are at hand:

- Transfer of the insertion reactivity of phosphenium cations towards P_4 to the isolobal *cyclo*-P_3 complex [Cp'''Ni(η^3-P_3)], granting access to cationic *cyclo*-P_4R_2 units.

- Expanding the insertion reactivity of phosphenium cations to the larger *cyclo*-P_4 complexes [Cp^RTa$(CO)_2$(η^4-P_4)] (Cp^R = Cp'' or Cp''') and investigation of the reactivity of these complexes towards heavier pnictogenium cations, namely arsenium and stibenium cations.

- Functionalization of the *cyclo*-P_5 complex [Cp*Fe(η^5-P_5)] with electrophiles from across the p-block to access a broad range of coordinatively stabilized pentaphosphole ligands, including the parent compound *cyclo*-P_5H.

- Investigation of the reactivity of [Cp*Fe(η^5-P_5)] towards the cationic transition metal species $\{Cp'''M\}^+$ (M = Cr – Ni) and $[M(C_6H_6)_2]^{n+}$ (M = Fe, Co, n = 1, 2) to access novel triple- and quadruple-decker complexes bearing *cyclo*-P_5 moieties.

- Electrophilic functionalization of [{Cp'''Ta}$_2$(μ,$\eta^{2:2:2:2:1:1}$-P_8)] bearing the largest monocyclic P_n unit known to date (*cyclo*-P_8) and further studies on the reactivity (coordination, redox) of this unprecedented compound.

Secondly, the redox chemistry of Pn_n ligand complexes should be further expanded to As_n complexes. Of particular interest are end-deck *cyclo*-As_3 as well as cluster type As_n ligand complexes, as the former display an obvious gap in the existing literature and the redox properties of cluster type As_n ligand complexes are promising in terms of observing multiple stable redox states within one structural motif. Thus, the following issues have been targeted:

- Investigation of the redox chemistry of the *cyclo*-As_3 complex [Cp'''Ni(η^3-As_3)] and potential fragmentation products.

- Synthesis and electrochemical as well as synthetic investigation of the redox properties of the cluster compound [{Cp*Fe}$_3$As$_6$].

Lastly, the synthetic utilization of transition metal stabilized polypnictogen cations in terms of their nucleophilic functionalization remains only scarcely explored. However, it bears great potential for the targeted preparation of complex and highly functionalized polypnictogen compounds. As the reactivity of stable singlet carbenes and their analogs with polyphosphorus compounds is well established, they appear to be promising candidates for the functionalization of polypnictogen cations as well. The resulting products then may still serve as valuable starting materials for further nucleophilic quenching with anionic nucleophiles. Thus, the two most accessible classes of polyphosphorus cations prepared within this thesis should be investigated in terms of their nucleophilic functionalization:

- Reactivity studies of the methylated pentaphosphole derivative [Cp*Fe(η^5-P$_5$Me)][OTf] towards carbenes and their analogs. Identification of reactivity trends and exploiting the cationic charge in the starting material for functionalization with even weakly nucleophilic species.

- Functionalization of the Ni stabilized *cyclo*-P$_4$R$_2$ units in [Cp'''Ni(η^3-P$_4$R$_2$)]$^+$ with NHCs and investigation of the resulting products towards their further charge quenching reactivity with simple organic nucleophiles, like [EtO]$^-$, [CN]$^-$ and the more elaborate [ECO]$^-$ (E = P, As).

3. Cationic Functionalization by Phosphenium Ion Insertion

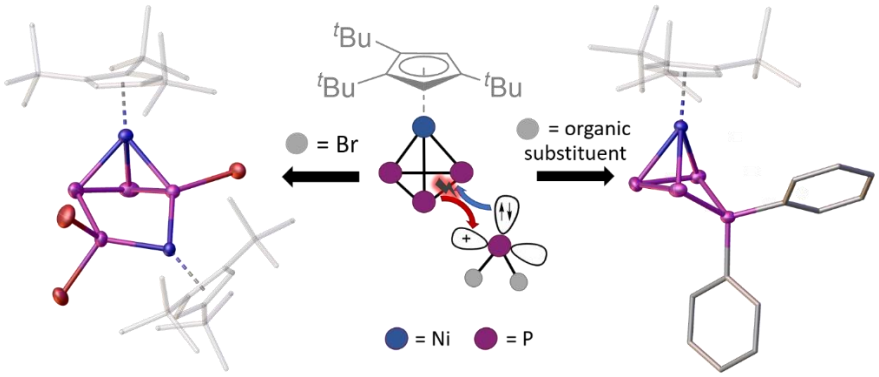

Preface

The following chapter has already been published. The article is reprinted with permission from Wiley-VCH. License Number: 5637020010433

"Cationic Functionalization by Phosphenium Ion Insertion"

Chem. Eur. J. **2020**, *26*, 17165–17170.

Parts of this chapter have already been described within the MSc thesis of the first author (Christoph Riesinger).

Authors

Christoph Riesinger, Luis Dütsch, Gábor Balázs, Michael Bodensteiner and Manfred Scheer

Author Contributions

Christoph Riesinger – Conceptualization, Synthesis of compounds **2**, **3** and **4**, Writing of original draft.
Luis Dütsch – Conceptualization, Writing of original draft.
Gábor Balázs – Interpretation of computational data.
Michael Bodensteiner – Interpretation of crystallographic data.
Manfred Scheer – Project administration, Funding acquisition, Co-writing final manuscript.

Acknowledgements

This work was supported by the Deutsche Forschungsgemeinschaft (DFG) within the project Sche 384/36-1.

3.1. Abstract

*The reaction of [Cp'''Ni(η^3-P_3)] (**1**) with in situ generated phosphenium ions [RR´P]$^+$ yields the unprecedented polyphosphorus cations of the type [Cp'''Ni(η^3-P_4R_2)][X] (R = Ph (**2a**), Mes (**2b**), Cy (**2c**), 2,2´-biphen (**2d**), Me (**2e**); [X]$^-$ = [OTf]$^-$, [SbF_6]$^-$, [$GaCl_4$]$^-$, [BAr^F]$^-$, [TEF]$^-$)) and [Cp'''Ni(η^3-P_4RCl)][TEF] (R =Ph (**2f**), ^{t}Bu (**2g**)). In the reaction of **1** with [Br_2P]$^+$, an analogous compound is observed only as an intermediate and the final product is an unexpected dinuclear complex [{Cp'''Ni}$_2$(μ,η^3:η^1:η^1-P_4Br_3)][TEF] (**3a**). A similar product [{Cp'''Ni}$_2$(μ,η^3:η^1:η^1-P_4(2,2´-biphen)Cl)][$GaCl_4$] (**3b**) is obtained, when **2d**[$GaCl_4$] is kept in solution for prolonged times. While the central structural motif of **2a**-**g** consists of a "butterfly-like" folded P_4 ring attached to a {Cp'''Ni} fragment, the structures of **3a** and **3b** exhibit a unique asymmetrically substituted and distorted P_4 chain stabilized by two {Cp'''Ni} fragments. Additional DFT calculations shed light on the reaction pathway for the formation of **2a**-**2g** and the bonding situation in **3a**.*

3.2. Introduction

The structural diversity observed in organic chemistry is immense, and it is based on the high tendency of carbon to form homoatomic bonds, due to the high C–C single and multiple bond energies.[1] Due to its diagonal relationship to carbon and the isolobality of CH fragments to P,[2] a similar chemical behaviour is predicted for phosphorus. Thus, a broad variety of anionic and neutral polyphosphorus compounds was reported.[3] In contrast, the area of polyphosphorus cations is still underdeveloped. Important efforts in view of the synthesis of organosubstituted polyphosphorus cations were made by the groups of *Burford* and *Weigand*, respectively, who were able to isolate catenated[4] as well as ring-[5] and cage-type (**I**, **III**)[6] polyphosphorus cations (Scheme 1), the latter representing mostly unsubstituted polyphosphorus moieties. The *Krossing* group was able to extend these results by isolating halogen-substituted cages (**II**),[7] and they even succeeded in demonstrating the formation of the first homoleptic polyatomic phosphorus cation (**IV**) in solution.[8] The syntheses of the cations **I**, **II** and **III** could be achieved by the reaction of P_4 with phosphenium cations [RR´P]$^+$, which have proven to be very useful electrophiles for this purpose. While donor-substituted

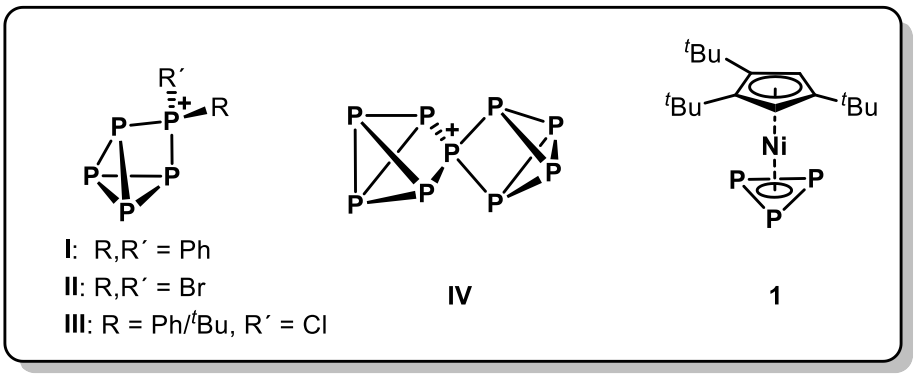

*Scheme 1: Left: Selected polyphosphorus cations (**I**, **II** and **III**) derived from the reaction of P_4 with suitable phosphenium ions. Middle: The first homoatomic polyphosphorus cation **IV** generated upon the reaction of P_4 with [NO][TEF]. Right: The starting compound **1**, which is isolobal to P_4.*

derivatives of these heavy carbene analogues can be isolated,[9] phosphenium cations bearing alkyl, aryl or halogen substituents are too reactive[10] so that they can only be generated *in situ* by the reaction of halogenophosphines with a suitable halide-abstracting agent. A general reactivity pattern of these phosphenium cations is their insertion into P–P bonds affording expanded polyphosphorus structures.

On the other hand, polypnictogen units can also serve as ligands (E_n ligands; E = P, As, Sb, Bi) stabilized in the coordination sphere of transition metals. Reductive[11] and nucleophilic[11e] functionalizations of these units have proven to be promising routes to obtain large polypnictogen frameworks. Furthermore, initial studies on their oxidation chemistry revealed the potential in the formation of larger cationic polypnictogen structures.[11a,12] While the reaction of such complexes with electrophilic pnictinidenes [Cp*E{$W(CO)_5$}$_2$] (E = P, As)[13] and the condensation of an anionic bimetallic complex with halogenophosphines[14] lead to neutral E_n ring-expanded products, their functionalization with cationic electrophiles has only been scarcely explored. Examples of the latter are alkylation reactions of [(L)Co(η^3-P_3)][15] or [(L)Rh(η^1:η^2-P_4R)][16] (L = $MeC(CH_2PPh_2)_3$). Furthermore, it was shown only recently that derivatives of **I** can be reacted with highly reduced metal units to yield cationic polyphosphorus compounds.[17] An alternative approach, however, the reactivity of polyphosphorus complexes towards phosphenium cations, has not been investigated so far. Therefore, the question arises if this would be a general way for the synthesis of a large variety of novel cationic polyphosphorus frameworks. This way would open a huge variety of functionalization possibilities by the used phosphenium cations as well as afterwards by having introduced suitable functional groups. Moreover, also the question as to a possible mechanism between addition and insertion on the one hand or the immediate insertion on the other came up. Inspired by the results obtained on the electrophilic functionalization of P_4 by the Krossing group (*vide supra*), we envisioned the P_4 isolobal polyphosphorus complex [Cp'''Ni(η^3-P_3)] (**1**, Cp''' = 1,2,4-^{t}Bu$_3$-C_5H_2)[11e] (Scheme 1) as a suitable starting material for such investigations. While the recently reported coordinative transformation of derivatives of **I** is so far limited to P_5R_2 moieties,[17] our approach would allow for the preparation of yet unknown *cyclo*-P_4R_2 units. Moreover, if we could demonstrate this reactivity on **1** with success, this approach would potentially open a general way to cationic polyphosphorus ligands of different sizes, since a large variety of polyphosphorus ligand complexes does already exist. Additionally, this approach allows for the simple exchange of substituents in the final products, if e.g. halogen substituents are present and, therefore, the obtained compounds could serve as valuable starting materials in the preparation of novel functionalized polyphosphorus compounds.

3.3. Results and Discussion

When **1** is reacted with [Ph_2P][OTf] (Ph = phenyl, [OTf]$^-$ = [SO_3CF_3]$^-$), *in situ* generated by the reaction of Tl[OTf] as the halide-abstracting agent and Ph_2PCl in *o*-DFB (1,2-difluorobenzene), a colour change from bright orange to dark red and the formation of a white precipitate (TlCl) can be observed over the course of 20 h. Upon workup and recrystallization, [Cp'''Ni(η^3-P_4Ph_2)][OTf] (**2a**[OTf]) can be isolated in 63% crystalline yield (Scheme 2).

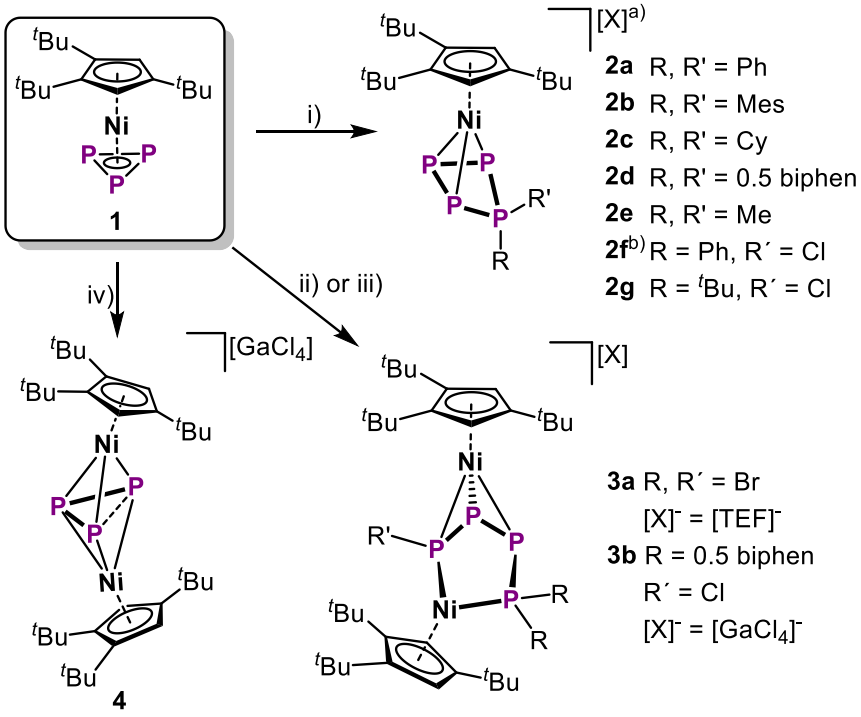

*Scheme 2: Reaction of **1** with phosphenium and halogenophosphenium ions: i) "[RR'P][X]" in situ generated from RR'PCl and Tl[TEF] (for other abstracting agents see SI); ii) "[Br$_2$P][TEF]" from PBr$_3$ and Tl[TEF]; iii) "[biphenP][GaCl$_4$]" from biphenPCl and GaCl$_3$ with prolonged reaction time (14 d); iv) GaCl$_3$.[a] All compounds **2a-g** were prepared as their [TEF]$^-$ salts and **2a-d** additionally as their [GaCl$_4$]$^-$ salts; [b] Isolated as an isomeric mixture of **2f$_{endo}$**:**2f$_{exo}$** = 7:1 with endo and exo referring to the position of the Ph group at the folded P$_4$ ring.*

As we had anticipated the halide-abstracting agent to have crucial impact on this reaction, we evaluated other compounds applicable for this purpose. Performing the same reaction in the presence of Ag[SbF$_6$], M[TEF] (M$^+$ = Ag$^+$ or Tl$^+$, [TEF]$^-$ = [Al(OC(CF$_3$)$_3$)$_4$]$^-$)[18] or [(Et$_3$Si)$_2$(μ-H)][BAr^F][19] ([BAr^F]$^-$ = [B(C$_6$F$_5$)$_4$]$^-$) yielded **2a**[X] ([X]$^-$ = [SbF$_6$]$^-$, [TEF]$^-$, [BAr^F]$^-$) in comparably lower yields (for details see SI). The exchange of these ionic halide-abstracting agents for the neutral GaCl$_3$, however, gave **2a**[GaCl$_4$] in 71% yield after only 4 h of reaction. With these results in hand, we turned our interest towards exchanging the Ph substituents at the phosphenium ion against other organic groups, while performing the reactions either with GaCl$_3$ or Tl[TEF] (enhanced stabilization). Notably, replacing Ph$_2$PCl with the sterically very demanding ^{t}Bu$_2$PCl (^{t}Bu = *tert*-butyl) or the electronically deactivated (Et$_2$N)$_2$PCl does not lead to any reaction with **1**. Instead, using Mes$_2$PCl, Cy$_2$PCl or (biphen)PCl (Mes = mesityl, Cy = cyclohexyl, biphen = 2,2´-biphenyl) gives the products [Cp'''Ni(η^3-P$_4$R$_2$)][X] (R = Mes (**2b**: 53% [X]$^-$ = [GaCl$_4$]$^-$/46% [X]$^-$ = [TEF]$^-$), Cy (**2c**: 59/57%); R$_2$ = biphen (**2d**: 70/55%); [X]$^-$ = [GaCl$_4$]$^-$/[TEF]$^-$) in moderate to good yields. When employing the highly reactive Me$_2$PCl, only the [TEF]$^-$ salt is stable enough to isolate [Cp'''Ni(η^3-P$_4$Me$_2$)][TEF] (**2e**: 52%). The insertion of multiple [Ph$_2$P]$^+$ entities into **1** is not observed, not even when using two or more equivalents of Ph$_2$PCl and Tl[TEF]. By expanding the scope of our approach, we replaced halogenophosphines with dihalogenophosphines RPCl$_2$. When **1** is reacted with the respective dihalogenophosphine (PhPCl$_2$ or ^{t}BuPCl$_2$) under similar conditions, a colour change from bright

orange to brownish red and again the formation of a white precipitate (TlCl) are observed. After workup, the products [Cp'''Ni(η^3-P_4RCl)][TEF] (R = Ph (**2f**: 60%), R = ^{t}Bu (**2g**: 50%)), can be isolated as brownish red powders. While for **2g** the formation of a single product is observed, NMR data (*vide infra*) suggest the formation of two isomers of **2f** (Ph-substituent in *endo*/*exo* position; see Figures S2 and 3). Furthermore, when we implemented PBr_3 as the phosphenium ion precursor, the expected [Cp'''Ni(η^3-P_4Br_2)]$^+$ (**2h**) was only observed as an intermediate (see Figures SI 8-10 for the $^{31}P\{^1H\}$ NMR spectra) that cannot be isolated. However, stirring the reaction mixture for three days at room temperature leads to the formation of the dinuclear complex [{Cp'''Ni}$_2$(μ,η^3:η^1:η^1-P_4Br_3)][TEF] (**3a**, Scheme 2). The additional detection of P_4 hints at a fragmentation pathway for the formation of **3a**, which, after workup and crystallization, is isolated as dark brown blocks in high yields (90%, based on **1**). Intriguingly, we discovered that keeping **2d**[$GaCl_4$] in *o*-DFB solution at room temperature for two weeks yields a similar dinuclear complex [{Cp'''Ni}$_2$(μ,η^3:η^1-P_4(biphen)Cl)][$GaCl_4$] (**3b**) in 74 % yield (based on **1**). When we tried to further increase the yield of reactions involving $GaCl_3$ by varying the order of addition, we found that **1** also reacts with $GaCl_3$ alone in the absence of R_2PCl. Investigating this new reaction pattern revealed that the formation of the novel triple-decker complex [{Cp'''Ni}$_2$(μ,η^3:η^3-P_3)][$GaCl_4$] (**4**) can be achieved that way. To the best of our knowledge, **4** represents the first cationic representative of a Ni/Ni triple-decker complex with an η^3:η^3-P_3 middle deck. Thus, it completes the series of previously reported anionic and neutral complexes [{Cp'''Ni}$_2$(μ,η^3:η^3-P_3)]$^{-/0}$.[11e] Except for **2b** and **2g**, all obtained products could be crystallized as their [$GaCl_4$]$^-$ (**2a**, **2c**, **2d**) or [TEF]$^-$ (**2e**, **2f**) salt, allowing their X-ray crystallographic characterization (Figure 1). For **2f**, only the *endo*-Ph (regarding the P_4 ring) isomer could be characterized crystallographically. Additional solid-state structures of **2a**[X] ([X] = [OTf]$^-$, [SbF_6]$^-$ or [TEF]$^-$) hint at a negligible influence of the anion on the structure of **2a** (see Figures SI 12-15). The central structural motif of **2** consists of a bent *cyclo*-P_4 unit, which is attached to a {Cp'''Ni} fragment, carrying two substituents at one of the P atoms. This structural motif arises from the formal insertion of the corresponding phosphenium cation into one of the P–P bonds of **1** and represents a rare example of a ring expansion reaction from a

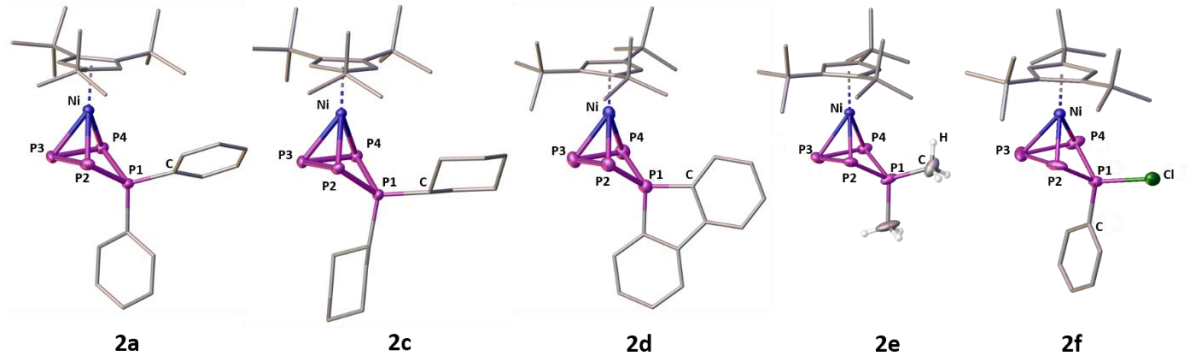

*Figure 1: Solid-state structures of **2a** and **2c**-**f**; Hydrogen atoms (except Me in **2e**), solvent molecules (0.5 o-DFB (**2c**), 0.4 n-hexane (**2d**)) and counter anions ([$GaCl_4$]$^-$ (**2a**, **2c**, **2d**), [TEF]$^-$ (**2e**, **2f**)) are omitted for clarity and ADPs are drawn at 50 % probability level. The cation denoted with Ni1 is displayed for the structures of **2d** and **2e**, as the respective crystal structures contain five and four molar equivalents in the asymmetric unit, respectively.*

strained 3-membered ring to a 4-membered one.[5b,20] The P–P bond lengths in the P_4 ring (**2a**: 2.173(1) - 2.194(2) Å, **2c**: 2.174(1) - 2.195(1) Å, **2d**: 2.162(1) - 2.208(1) Å, **2e**: 2.149(2) – 2.195(2) Å, **2f**: 2.146(1) - 2.204(2) Å) are all well within the range of P–P single bonds,[20] and comparably shorter than found in **I** or **III**.[6a,b] Along the lines of the latter, the shortest P–P bonds are those involving the atom P1. These bond lengths are the shortest in **2f** (2.146(1)/2.147(1) Å), increase according to the steric bulk of the substituents (**2f** < **2e** < **2d** < **2a** < **2c**) and are the longest in **2c** (2.174(1)/2.183(1) Å). A similar trend is not observed for the dihedral angle P1–P2–P4–P3, which is the smallest in **2e** (40.75(9)°) but the largest in **2f** (49.48(7)°). The former P–P bond of **1** is clearly broken in these compounds, which is indicated by the elongated P2–P4 distances (**2a**: 3.028(5) Å, **2c**: 3.020(1) Å, **2d**: 3.044(2) Å, **2e**: 3.031(3) Å, **2f**: 3.078(1) Å).[20,21] The solid-state structures of the cations **3a** and **3b** could be established as their $[TEF]^-$ and $[GaCl_4]^-$ salt, respectively (Figure 2). The central structural motif within both cations is the unprecedented, unsymmetrically substituted P_4 chain, which is coordinated to two {Cp'''Ni} fragments. The structure of these products can be formally described by the insertion of a second {Cp'''Ni} fragment into a P–P bond of the cations **2** and the addition of a halide substituent to the P_4 unit. The P–P bond lengths in **3a** (2.162(1) - 2.223(1) Å) and **3b** (2.144(2) - 2.239(2) Å) match the expected values for P–P single bonds,[20] where the longest ones are those between P1 and P2. While the Ni1–P bond lengths (**3a**: 2.221(1) - 2.269(1) Å, **3b**: 2.217(1) - 2.262(1) Å) are close to the values found for the starting material **1** (2.236(1) - 2.246(1) Å),[11e] the Ni2–P1/P4 distances are comparably shorter (**3a**: 2.104(1) - 2.157(1) Å, **3b**: 2.142(1) - 2.147(1) Å). The formulation as a P_4 chain is clearly manifested in the large P1–P4 distances of 2.878(1) Å and 2.919(2) Å in **3a** and **3b**, respectively.[20] With P3–P4–P2–P1 dihedral angles of 135.30(6)° (**3a**) and 130.58(9)° (**3b**) the P1 atom is located below the plane spanned by the other P atoms, and the halide substituents are situated above that plane (P2–P4–P3–X = 163.09(5) (**3a**), 162.14(8)° (**3b**)). The solid-state structure of **4** reveals an allylically distorted P_3 ligand in-between two {Cp'''Ni} fragments (Figure 2). The P1–P2 (2.202(1) Å) and P2–P3 (2.198(1) Å) bonds are within common P–P single bonds,[20] while the P1–P3 (2.539(1) Å) distance is clearly elongated. The elongation of the P1–P3 distance is more pronounced than in the neutral (2.398(1) and anionic (2.241(1) Å) derivatives of **4**,[11e] with the anion

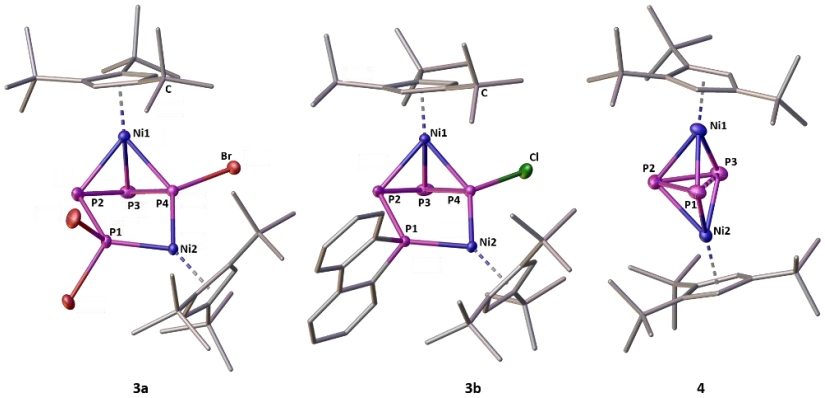

*Figure 2: Solid state structures of the cations in **3a**, **3b** and **4**; H atoms and the counter anions are omitted for clarity; ADPs are drawn at 50% probability level.*

showing a nearly triangular P_3 ligand. Furthermore, the P1–P2–P3 angles in the anionic (61.16(2)°) and neutral (66.60(2)°) derivatives[11e] are comparably smaller than the one in **4** (70.48(5)°). According to DFT calculations, the increasing allylic distortion going from the anion $[\{Cp'''Ni\}_2(\mu,\eta^3{:}\eta^3\text{-}P_3)]^-$ over the neutral species $[\{Cp'''Ni\}_2(\mu,\eta^3{:}\eta^3\text{-}P_3)]$ to the cation **4** is caused by the stepwise depopulation of the HOMO of the anion, which has a large P–P bonding contribution.[11e]

The ^{31}P and $^{31}P\{^1H\}$ NMR spectra of the isolated products **2** in CD_2Cl_2 show AA´MX (**2b**, **2d**, **2f**), AMM´X (**2a**, **2e**, **2g**) or AMXX´ (**2c**) spin systems (Figure 3), which are in agreement with the cyclic P_4R_2 ligand found in these compounds. For **2f,** an additional set of signals is found, as both isomers (*endo*-Ph and *exo*-Ph) are present in a 7:1 ratio (see Figures S2 and 3). The chemical shifts of the signals are found between δ = –10 and 120 ppm (exact values are provided in the SI) and their assignment is simplified by additional P–H coupling of the signal corresponding to the former phosphenium cation in the ^{31}P NMR spectrum. While the $^1J_{P-P}$ coupling constants in **2a**-**g** (see SI) are slightly larger compared to the isolobal **I/III**,[6a,b] the

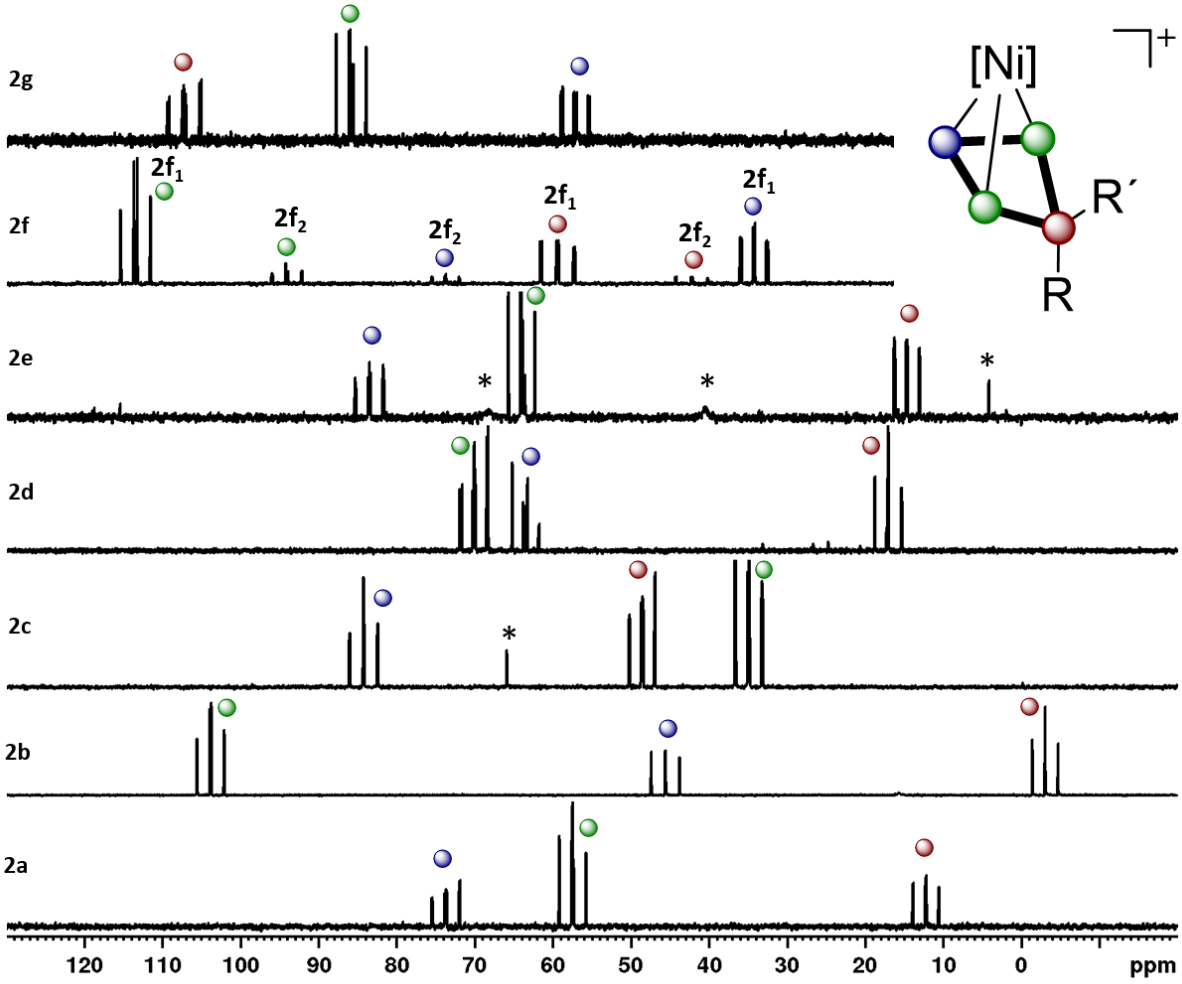

*Figure 3: $^{31}P\{^1H\}$ NMR spectra of isolated **2a**-**g** in CD_2Cl_2 recorded at 298 K with signal assignment according to the colour code. The two sets of signals observed for **2f** are labelled with **$2f_1$** and **$2f_2$**, with the former being most probably the endo-Ph isomer due to steric reasons. * = unidentified minor impurities.*

varying sequence of signals (in addition to electronic effects) may be attributed to similar "cross-ring through space" interactions as reported for derivatives of **III**.[6b] The ^{1}H NMR spectrum of **3a** in CD_2Cl_2 shows five signals for the ^{t}Bu groups and four signals for the residual protons of the Cp''' ligands, respectively. The ^{1}H NMR spectrum of **3b** in CD_2Cl_2 is similar but shows six signals for the ^{t}Bu groups and additional resonances for the 2,2´-biphen substituent. Thus, a hindered rotation of the Cp''' ligands can be assumed in both cases at ambient temperatures. The ^{31}P NMR spectrum of **3a** in CD_2Cl_2 reveals an AMNX spin system with signals at δ = –1.1 (P^X), 128.0 (P^N), 134.2 (P^M) and 182.0 (P^A) ppm, which is consistent with an asymmetric P_4 chain. An unexpectedly large $^{2}J_{P–P}$ coupling constant (281.7 Hz) of the P atoms at each end of the chain may however hint at possible orbital interactions between those atoms in **3a** (*vide infra*). The ^{31}P NMR spectra of **3b** in CD_2Cl_2 recorded at room temperature only reveal two moderately resolved and two very broad resonances at δ = –31.9 (br), 80.6 (br), 84.1 and 146.6 ppm. Upon cooling to –80 °C, these signals split into two separate, well-resolved sets indicating the presence of two isomers which we assume to arise from a hindered rotation of the Cp''' ligands at this temperature. Again, unusually high $^{2}J_{P–P}$ coupling constants are found between the P atoms at each end of the chain for both isomers (**3b$_1$**: $^{2}J_{P–P}$ = 108.2 Hz, **3b$_2$**: $^{2}J_{P–P}$ = 113.2 Hz). The ^{1}H NMR spectrum of **4** in CD_2Cl_2 shows three signals consistent with two symmetrical Cp''' ligands. Accordingly, its ^{31}P NMR spectrum reveals only one singlet at δ = 139.3 ppm, which does not change even upon cooling to –80 °C. Thus, we assume a rapid dynamic behaviour for the allylic P_3 ligand.

ESI(+) mass spectrometry studies on salts of the cations **2a**-**g** reveal their high stability towards fragmentation, as the only observed peaks are those attributed to the molecular cations (*m/z* = 569.1 (**2a**), 653.2 (**2b**), 581.2 (**2c**), 567.1 (**2d**), 445.1 (**2e**), 527.1 (**2f**), 507.1 (**2g**)). Only for **2d**[$GaCl_4$], a second peak at *m/z* = 895.2 (**3b**) is observed, which is in agreement with our experimental finding of a (slow) fragmentation/rearrangement process of **2d**. When isolated samples of **3a** or **3b** in *o*-DFB are subjected to ESI(+) MS experiments, only the molecular ion peaks are found (*m/z* = 947.0 (**3a**), 895.2 (**3b**)). The ESI(+) mass spectrum of **4** also shows the molecular ion peak (*m/z* = 675.2).

To obtain insight into the formation of the cations **2,** we carried out DFT calculations (BP86/def2-TZVP, PCM solvent correction for CH_2Cl_2, see SI for details) on the model system consisting of [CpNi(η^3-P_3)] (**1'**) and $[Me_2P]^+$ (Figure 4). While the crucial impact of the $[GaCl_4]^–$ anion on the formation of the isolobal compounds **III** has been pointed out for reactions involving $GaCl_3$ as halide abstracting agent,[6b] this seems unfeasible for reactions involving the weakly coordinating $[TEF]^–$ anion. Furthermore, investigations of the solution chemistry of the PBr_3/Ag[TEF] couple showed that the formation of free phosphenium cations is unlikely,[22] but, to our knowledge, similar reactivity has not been studied for Tl^+. Thus, we assume the formation of a free phosphenium cation ($[Me_2P]^+$) in the first step of the reaction. **1'** reacts with $[Me_2P]^+$ in an exergonic reaction (ΔG_{298K} = –24.08 kcal/mol) and without a transition state to yield the intermediate **I2** in which $[Me_2P]^+$ is coordinated to the *cyclo*-P_3 ligand of **1'** in an η^1 fashion. This reaction proceeds via **TS2** (ΔG_{298K} = –18.31 kcal/mol, $\Delta\Delta G^{‡}_{298K}$ = 5.77 kcal/mol) in which the $[Me_2P]^+$ fragment is coordinated to one of the P–P bonds of **1'** and finally gives

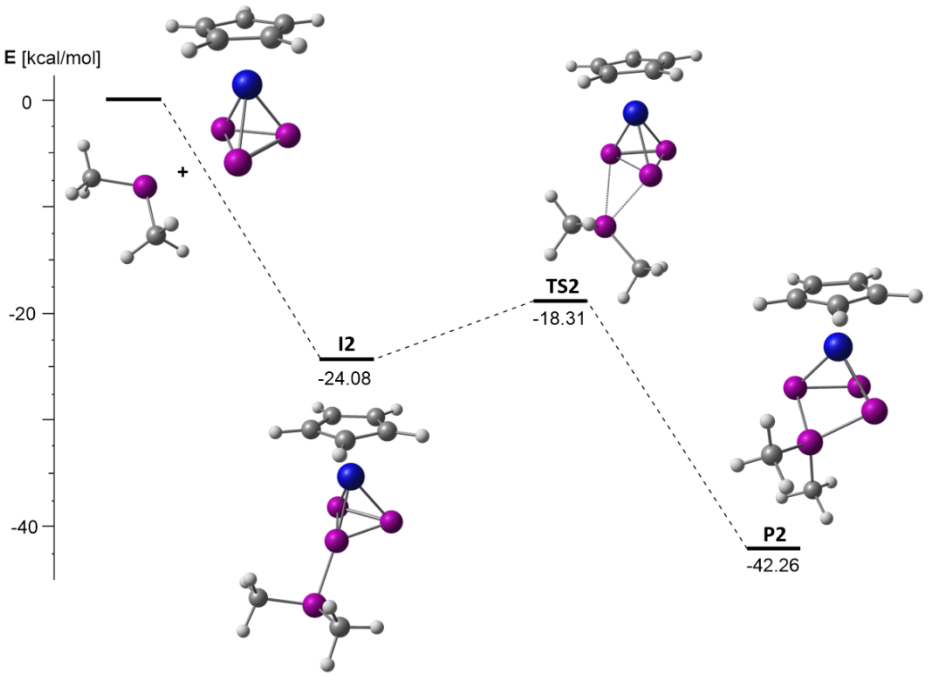

*Figure 4: Calculated (BP86/def2-TZVP, PCM solvent correction for CH_2Cl_2) energy profile of the reaction between the model compound **1´** and $[Me_2P]^+$; stationary points were verified by analytical frequency calculations, energies are given in kcal/mol and the couple **1´**+$[Me_2P]^+$ was arbitrarily set to an energy of 0 kcal/mol.*

the product **P2**, which shows the complete insertion of $[Me_2P]^+$ into the respective P–P bond. The overall reaction is exergonic (ΔG_{298K} = –42.26 kcal/mol), which is caused by the assumption of free $[Me_2P]^+$ being initially formed.

Finally, we also investigated the electronic and bonding properties of **3a**/**b** computationally (B3LYP/def2-SVP, PCM solvent correction for CH_2Cl_2). The observed geometric parameters for **3a** and **3b** obtained from these calculations match well with the experimental values, which corroborates the formulation of the P_4X_3 ligands as chains. Furthermore, the Wiberg Bond Indices (WBIs) for both compounds, obtained from NBO analyses, are in line with this formulation (**3a**: 0.87 (P1–P2), 1.12 (P2–P3), 1.04 (P3–P4); **3b**: 0.84 (P1–P2), 1.14 (P2–P3), 1.05 (P3–P4)). When we examined the canonical frontier orbitals of **3a**, we found an allylic-type interaction between P1, Ni2 and P4 within the HOMO-4 (see Figure S24 for details). The comparably small but significant orbital contributions of both P1 (7%) and P4 (6%) may explain the large $^2J_{P–P}$ coupling constant found in the ^{31}P NMR spectra of **3a** and **3b**.

3.4. Conclusions

In conclusion, the reaction of **1** with a variety of phosphenium cations yields numerous cationic polyphosphorus scaffolds, which are stabilized by coordination to {Cp'''Ni} moieties. While the cations **2** contain novel P_4R_2 ligands, **3a** and **3b** display a P_4X_3 chain motif that is unprecedented to date. DFT calculations revealed the reaction pathway leading to **2** as an addition/insertion mechanism and gave insight into the electronic structure of **3a**/**b**. Thus, we could show that the combination of phosphenium cations with polyphosphorus ligand complexes (such as **1**) is an additional possibility to design polyphosphorus cations of the

desired size in a rational way. While we demonstrate this for the *cyclo*-P_3 complex **1**, we expect our approach to be transferrable to other polyphosphorus ligand complexes as well. The presented simple synthetic route allows for large diversification regarding the substitution pattern of the product by simply exchanging the phosphenium ion precursor. While the discussed reactivity is exemplified by the P_3 ligand complex **1**, our approach should also be transferrable to other neutral polyphosphorus and other polypnictogen ligand complexes, and investigations in this direction are in progress. Furthermore, the obtained products hold great potential for functionalizations via reduction, nucleophilic functionalization, or displacement of the {Cp'''Ni} fragments, paving the way for even more elaborate substituted polyphosphorus compounds.

3.5. Supporting Information

3.5.1. Experimental Procedures

General Considerations

All manipulations were carried out using standard Schlenk techniques at a Stock apparatus with N_2 as an inert gas or in a glove box with Ar atmosphere. All glassware was dried with a heat gun (600 °C) for at least 30 min prior to use. *o*-DFB was distilled from P_2O_5, CD_2Cl_2 was distilled from CaH_2 and other solvents were directly taken from an MB SPS-800 solvent purification system and degassed at room temperature. Solution ^{1}H (400.130 MHz), ^{19}F (376.498 MHz) and ^{31}P (161.976 MHz) NMR spectra were recorded at an Avance400 (Bruker) spectrometer using $(H_3C)_4Si$ (^{1}H), $CFCl_3$ (^{19}F) or 85% phosphoric acid (^{31}P), respectively, as external standards. Chemical shifts (δ) are provided in parts per million (ppm) and coupling constants (*J*) are reported in Hertz (Hz). Chemical shifts and coupling constants for all $^{31}P\{^{1}H\}$ and ^{31}P NMR spectra were derived from spectral simulation. The following abbreviations are used: s = singlet, d = doublet, dd = doublet of doublets, ddd = doublet of doublets of doublets, t = triplet, br = broad and m = multiplet. ESI mass spectra were recorded at the internal mass spectrometry department using a ThermoQuest Finnigan TSQ 7000 mass spectrometer and peak assignment was performed using the Molecular weight calculator 6.50.[23] Elemental analysis of the products was conducted by the elemental analysis department at the University of Regensburg using an Elementar Vario EL. The starting materials [Cp'''Ni(η^3-P_3)] (**1**),[11e] Tl[TEF],[18b] [$(Et_3Si)_2(\mu$-H)][BAr^F],[19] (2,2´-biphen)PCl[24] and ^{t}BuPCl$_2$[25] were synthesized following literature procedures. All other chemicals were purchased from commercial vendors. $GaCl_3$ was sublimed and all purchased halogenophosphanes were distilled before use.

*[Cp'''Ni(η^3-P_4Ph_2)][OTf] (**2a**[OTf])*

A colourless solution of Ph_2PCl (0.1 mmol, 22 mg, 17.9 μL, 1 eq.) in 1 mL of toluene was added to an orange solution of **1** (0.1 mmol, 38 mg, 1 eq.) and Tl[OTf] (0.1 mmol, 35 mg, 1 eq.) in 5 mL of *o*-DFB at room temperature. Immediate precipitation of small amounts of white solid occurred and a colour change to dark red could be observed upon stirring for 24 h. The mixture was then filtered through glass fibre filter paper and upon addition of 50 mL of *n*-hexane a dark red oil was precipitated. This oil was washed three times with 10 mL of *n*-hexane, each, and dried under reduced pressure (10^{-3} mbar). Dissolving the residue in *o*-DFB and layering with *n*-hexane (ratio of 1:8) yielded [Cp´´´Ni(η^3-P_4Ph_2)][OTf] (**2a**[OTf]) after five days at room temperature as small red plates suitable for single crystal X-ray analysis.

Yield: 45 mg (0.063 mmol, 63%)

Elemental analysis: calc. (%) for [Cp´´´Ni(η^3-P_4Ph_2)][OTf] ($C_{30}H_{41}O_3F_3P_4SNi$): C: 50.09 H: 5.47; found (%): C: 50.01 H: 5.32

ESI(+) MS (*o*-DFB): *m/z* (%) = 569.1 (100%) [Cp´´´Ni(η^3-P_4Ph_2)]$^+$

NMR (CD_2Cl_2, 298 K): **^{1}H**: δ/ppm = 1.21 (s, 9 H, $C(CH_3)_3$), 1.31 (s, 18 H, $C(CH_3)_3$), 5.92 (s, 2 H, $C_5H_2{}^t Bu_3$), 7.54–7.86 (br, 10 H, Ph)

^{31}P{^{1}H}: (AMM'X spin system) δ/ppm = 12.4 (ddd, $^1J_{PX\text{-}PM/PM´}$ = 270.3 Hz, $^2J_{PX\text{-}PA}$ = 14.2 Hz, 1 P, P^X), 57.8 (ddd, $^1J_{PM/PM´\text{-}PX}$ = 270.3 Hz, $^1J_{PM/PM´\text{-}PA}$ = 288.1 Hz, 2 P, $P^{M/M´}$), 73.8 (ddd, $^1J_{PA\text{-}PM/PM´}$ = 288.1 Hz, $^2J_{PA\text{-}PX}$ = 14.2 Hz, 1 P, P^A)

^{31}P: (AMM'X spin system) δ/ppm = 12.4 (t, $^1J_{Px\text{-}PM/PM´}$ = 270.3 Hz, 1 P, P^X), 57.8 (ddd, $^1J_{PM/PM´\text{-}PX}$ = 270.3 Hz, $^1J_{PM/PM´\text{-}PA}$ = 288.1 Hz, 2 P, $P^{M/M´}$), 73.8 (ddd, $^1J_{PA\text{-}PM/PM´}$ = 288.1 Hz, $^2J_{PA\text{-}PX}$ = 14.2 Hz, 1 P, P^A)

^{19}F{^{1}H}: δ/ppm = –78.75 (s, $[OTf]^-$)

*[Cp´´´Ni(η^3-P_4Ph_2)][SbF_6] (**2a**[SbF_6])*

A colourless solution of Ph_2PCl (0.1 mmol, 22 mg, 17.9 μL, 1 eq.) in 1 mL of toluene was added to an orange solution of [Cp´´´Ni(η^3-P_3)] (0.1 mmol, 38 mg, 1 eq.) and Ag[SbF_6] (0.1 mmol, 34 mg, 1 eq.) in 5 mL of *o*-DFB at room temperature. Immediate precipitation of small amounts of white solid and a colour change to red could be observed. After stirring for 24 h at room temperature the mixture was filtered through glass fibre filter paper and upon addition of 50 mL of *n*-hexane, a dark red solid precipitated. The precipitate was washed three times with 10 mL of *n*-hexane, each, and dried under reduced pressure (10^{-3} mbar). Recrystallisation from *o*-DFB/*n*-hexane (1:8) at room temperature yielded [Cp´´´Ni(η^3-P_4Ph_2)][SbF_6] (**2a**[SbF_6]) as red platelets, suitable for X-ray analysis after one week.

Yield: 27 mg (0.037 mmol, 37%)

Elemental analysis: calc. (%) for [Cp´´´Ni(η^3-P_4Ph_2)][SbF_6] ($C_{29}H_{41}F_6P_4NiSb$): C: 43.22 H: 4.88; found (%): C: 43.55 H: 4.62

ESI(+) MS (*o*-DFB): *m/z* (%) = 569.1 (100%) [Cp´´´Ni(η^3-P_4Ph_2)]$^+$

NMR (CD_2Cl_2, 298 K): **^{1}H**: δ/ppm = 1.21 (s, 9 H, $C(CH_3)_3$), 1.31 (s, 18 H, $C(CH_3)_3$), 5.92 (s, 2 H, $C_5H_2{}^tBu_3$), 7.54–7.86 (br, 10 H, Ph)

^{31}P{^{1}H}: (AMM'X spin system) δ/ppm = 12.4 (ddd, $^1J_{PX\text{-}PM/PM´}$ = 270.3 Hz, $^2J_{PX\text{-}PA}$ = 14.2 Hz, 1 P, P^X), 57.8 (ddd, $^1J_{PM/PM´\text{-}PX}$ = 270.3 Hz, $^1J_{PM/PM´\text{-}PA}$ = 288.1 Hz, 2 P, $P^{M/M´}$), 73.8 (ddd, $^1J_{PA\text{-}PM/PM´}$ = 288.1 Hz, $^2J_{PA\text{-}PX}$ = 14.2 Hz, 1 P, P^A)

^{31}P: (AMM'X spin system) δ/ppm = 12.4 (t, $^1J_{Px\text{-}PM/PM´}$ = 270.3 Hz, 1 P, P^X), 57.8 (ddd, $^1J_{PM/PM´\text{-}PX}$ = 270.3 Hz, $^1J_{PM/PM´\text{-}PA}$ = 288.1 Hz, 2 P, $P^{M/M´}$), 73.8 (ddd, $^1J_{PA\text{-}PM/PM´}$ = 288.1 Hz, $^2J_{PA\text{-}PX}$ = 14.2 Hz, 1 P, P^A)

^{19}F{^{1}H}: δ/ppm = –122.7 (br, $[SbF_6]^-$)

*[Cp´´´Ni(η^3-P_4Ph_2)][TEF] (**2a**[TEF])*

A colourless solution of Ph_2PCl (0.1 mmol, 22 mg, 17.9 μL, 1 eq.) in 1 mL of toluene was added to an orange solution of **1** (0.1 mmol, 38 mg, 1 eq.) and Tl[TEF] (0.1 mmol, 117 mg, 1 eq., $[TEF]^- = [Al(OC(CF_3)_3)_4]^-$) in 5 mL of *o*-DFB at room temperature. Immediate precipitation of small amounts of white solid and a slow colour change to red could be observed. After stirring for 24 h at room temperature the mixture was filtered through glass fibre filter paper and the solvent was removed *in vacuo*. The oily red residue was washed three times with 10 mL of *n*-hexane, each, and dried under reduced pressure (10^{-3} mbar). Dark red crystals of [Cp´´´Ni(η^3-P_4Ph_2)][TEF] (**2a**[TEF]), suitable for X-ray analysis could be obtained by slowly evaporating CH_2Cl_2 from a concentrated solution. Performing the same reaction with Ag[TEF] instead of Tl[TEF] results in diminished yields.

Yield: 80 mg (0.052 mmol, 52%)

Elemental analysis: calc. (%) for [Cp´´´Ni(η^3-P_4Ph_2)][TEF] ($C_{45}H_{41}O_4F_{36}AlP_4Ni$): C: 35.16 H: 2.56; found (%): C: 35.17 H: 2.53

ESI(+) MS (*o*-DFB): *m/z* (%) = 569.1 (100%) [Cp´´´Ni(η^3-P_4Ph_2)]$^+$

NMR (CD_2Cl_2, 298 K): **^{1}H**: δ/ppm = 1.21 (s, 9 H, $C(CH_3)_3$), 1.31 (s, 18 H, $C(CH_3)_3$), 5.92 (s, 2 H, $C_5H_2{}^tBu_3$), 7.54–7.86 (br, 10 H, Ph)

^{31}P{^{1}H}: (AMM'X spin system) δ/ppm = 12.4 (ddd, $^1J_{PX\text{-}PM/PM´}$ = 270.3 Hz, $^2J_{PX\text{-}PA}$ = 14.2 Hz, 1 P, P^X), 57.8 (ddd, $^1J_{PM/PM´\text{-}PX}$ = 270.3 Hz, $^1J_{PM/PM´\text{-}PA}$ = 288.1 Hz, 2 P, $P^{M/M´}$), 73.8 (ddd, $^1J_{PA\text{-}PM/PM´}$ = 288.1 Hz, $^2J_{PA\text{-}PX}$ = 14.2 Hz, 1 P, P^A)

^{31}P: (AMM'X spin system) δ/ppm = 12.4 (t, $^1J_{Px\text{-}PM/PM´}$ = 270.3 Hz, 1 P, P^X), 57.8 (ddd, $^1J_{PM/PM´\text{-}PX}$ = 270.3 Hz, $^1J_{PM/PM´\text{-}PA}$ = 288.1 Hz, 2 P, $P^{M/M´}$), 73.8 (ddd, $^1J_{PA\text{-}PM/PM´}$ = 288.1 Hz, $^2J_{PA\text{-}PX}$ = 14.2 Hz, 1 P, P^A)

^{19}F{^{1}H}: δ/ppm = –75.62 (s, $[TEF]^-$)

*[Cp´´´Ni(η^3-P_4Ph_2)][BAr^F] (**2a**[BAr^F])*

A colourless solution of [$(Et_3Si)_2(\mu$-H)][BAr^F] (0.1 mmol, 91 mg, 1 eq., [BAr^F]$^-$ = [$B(C_6F_5)_4$]$^-$) in 3 mL of *o*-DFB was added to an orange solution of **1** (0.1 mmol, 38 mg, 1 eq.) and Ph_2PCl (0.1 mmol, 22 mg, 17.9 µL, 1 eq.) in 4 mL of *o*-DFB at room temperature. Immediate colour change to red could be observed. After stirring for 6 h at room temperature the solvent was removed *in vacuo*. The oily red residue was washed three times with 10 mL of *n*-hexane, each, and dried under reduced pressure (10^{-3} mbar) leading to solidification. [Cp´´´Ni(η^3-P_4Ph_2)][BAr^F] (**2a**[BAr^F]) was isolated as an orange to red powder. All attempts to obtain (**2a**[BAr^F]) as a single crystallin material failed.

Yield: 45 mg (0.037 mmol, 37%)

Elemental analysis: calc. (%) for [Cp´´´Ni(η^3-P_4Ph_2)][BAr^F]·$(C_6H_4F_2)_{1.5}$ ($C_{62}H_{47}BF_{23}P_4Ni$): C: 51.98 H: 3.18; found (%): C: 52.35 H: 2.87 (Signals for $C_6H_4F_2$ are also found in the ^{1}H NMR of the isolated product)

ESI(+) MS (*o*-DFB): *m/z* (%) = 569.1 (100%) [Cp´´´Ni(η^3-P_4Ph_2)]$^+$

NMR (CD_2Cl_2, 298 K): **^{1}H**: δ/ppm = 1.21 (s, 9 H, $C(CH_3)_3$), 1.31 (s, 18 H, $C(CH_3)_3$), 5.92 (s, 2 H, $C_5H_2{}^t Bu_3$), 7.54–7.86 (br, 10 H, Ph)

^{31}P{^{1}H}: (AMM'X spin system) δ/ppm = 12.4 (ddd, $^1J_{PX\text{-}PM/PM´}$ = 270.3 Hz, $^2J_{PX\text{-}PA}$ = 14.2 Hz, 1 P, P^X), 57.8 (ddd, $^1J_{PM/PM´\text{-}PX}$ = 270.3 Hz, $^1J_{PM/PM´\text{-}PA}$ = 288.1 Hz, 2 P, $P^{M/M´}$), 73.8 (ddd, $^1J_{PA\text{-}PM/PM´}$ = 288.1 Hz, $^2J_{PA\text{-}PX}$ = 14.2 Hz, 1 P, PA)

^{31}P: (AMM'X spin system) δ/ppm = 12.4 (t, $^1J_{Px\text{-}PM/PM´}$ = 270.3 Hz, 1 P, P^X), 57.8 (ddd, $^1J_{PM/PM´\text{-}PX}$ = 270.3 Hz, $^1J_{PM/PM´\text{-}PA}$ = 288.1 Hz, 2 P, $P^{M/M´}$), 73.8 (ddd, $^1J_{PA\text{-}PM/PM´}$ = 288.1 Hz, $^2J_{PA\text{-}PX}$ = 14.2 Hz, 1 P, P^A)

^{19}F{^{1}H}: δ/ppm = –167.4 (t, 2 F, [BAr^F]$^-$), –163.6 (t, 1 F, [BAr^F]$^-$), –133.0 (br, 2 F, [BAr^F]$^-$)

*[Cp´´´Ni(η^3-P_4Ph_2)][$GaCl_4$] (**2a**[$GaCl_4$])*

A colourless solution of $GaCl_3$ (0.1 mmol, 18 mg, 1 eq.) in 4 mL of *o*-DFB was added to an orange solution of **1** (0.1 mmol, 38 mg, 1 eq.) and Ph_2PCl (0.1 mmol, 22 mg, 17.9 µL, 1 eq.) in 3 mL of *o*-DFB at room temperature. A rapid colour change to dark red occurred. After stirring for 4 h at room temperature the solvent was removed *in vacuo* and the oily red residue was washed three times with 10 mL of *n*-hexane, each. Drying under reduced pressure (10^{-3} mbar) lead to solidification and dark red crystals of [Cp´´´Ni(η^3-P_4Ph_2)][$GaCl_4$] (**2a**[$GaCl_4$]), suitable for X-ray analysis could be obtained by recrystallisation from *o*-DFB/*n*-hexane (1:6) at room temperature after seven days.

Yield: 55 mg (0.071 mmol, 71%)

Elemental analysis: calc. (%) for [Cp´´´Ni(η^3-P_4Ph_2)][$GaCl_4$] ($C_{29}H_{41}P_4Cl_4NiGa$): C: 44.56 H: 5.03; found (%): C: 44.49 H: 5.11

ESI(+) MS (*o*-DFB): *m/z* (%) = 569.1 (100%) [Cp´´´Ni(η^3-P_4Ph_2)]$^+$

NMR (CD_2Cl_2, 298 K): ^{1}H: δ/ppm = 1.21 (s, 9 H, $C(CH_3)_3$), 1.31 (s, 18 H, $C(CH_3)_3$), 5.92 (s, 2 H, $C_5H_2{}^tBu_3$), 7.54–7.86 (br, 10 H, Ph)

^{31}P{^{1}H}: (AMM'X spin system) δ/ppm = 12.4 (ddd, $^1J_{PX\text{-}PM/PM´}$ = 270.3 Hz, $^2J_{PX\text{-}PA}$ = 14.2 Hz, 1 P, P^X), 57.8 (ddd, $^1J_{PM/PM´\text{-}PX}$ = 270.3 Hz, $^1J_{PM/PM´\text{-}PA}$ = 288.1 Hz, 2 P, $P^{M/M´}$), 73.8 (ddd, $^1J_{PA\text{-}PM/PM´}$ = 288.1 Hz, $^2J_{PA\text{-}PX}$ = 14.2 Hz, 1 P, P^A)

^{31}P: (AMM'X spin system) δ/ppm = 12.4 (t, $^1J_{Px\text{-}PM/PM´}$ = 270.3 Hz, 1 P, P^X), 57.8 (ddd, $^1J_{PM/PM´\text{-}PX}$ = 270.3 Hz, $^1J_{PM/PM´\text{-}PA}$ = 288.1 Hz, 2 P, $P^{M/M´}$), 73.8 (ddd, $^1J_{PA\text{-}PM/PM´}$ = 288.1 Hz, $^2J_{PA\text{-}PX}$ = 14.2 Hz, 1 P, P^A)

*[Cp´´´Ni(η³-P₄Mes₂)][GaCl₄] (**2b**[GaCl₄])*

A colourless solution of $GaCl_3$ (0.1 mmol, 18 mg, 1 eq.) in 4 mL of *o*-DFB was added to an orange solution of **1** (0.1 mmol, 38 mg, 1 eq.) and Mes_2PCl (0.1 mmol, 30 mg, 1 eq.) in 3 mL of *o*-DFB at room temperature. A rapid colour change to red occurred. After stirring for 6 h at room temperature the solvent was removed *in vacuo* and the oily red residue was washed three times with 10 mL of *n*-hexane, each. Drying under reduced pressure (10^{-3} mbar) lead to solidification of the product [Cp´´´Ni(η³-P_4Mes_2)][$GaCl_4$] (**2b**[$GaCl_4$]), which was isolated as a red powder. All attempts to recrystallise the product ended in the formation of red oil at the bottom of the flask.

Yield: 46 mg (0.053 mmol, 53%)

Elemental analysis: calc. (%) for [Cp´´´Ni(η³-P_4Mes_2)][$GaCl_4$] ($C_{35}H_{51}P_4Cl_4NiGa$): C: 48.72 H: 5.96; found (%): C: 48.29 H: 5.79

ESI(+) MS (*o*-DFB): *m/z* (%) = 653.2 (100%) [Cp´´´Ni(η³-P_4Mes_2)]⁺

NMR (CD_2Cl_2, 298 K): **^{1}H**: δ/ppm = 1.14 (s, 9 H, $C(CH_3)_3$), 1.29 (s, 18 H, $C(CH_3)_3$), 2.32 (s, 6 H, Me), 2.64 (s, 6 H, Me), 2.73 (s, 6 H, Me) 5.92 (d, ^4J = 1.4 Hz, 2 H, $C_5H_2{}^tBu_3$), 6.98 (d, ^4J = 4.2 Hz, 2 H, Mes), 7.01 (d, ^4J = 4.6 Hz, 2 H, Mes)

^{31}P{^{1}H}: (AA'MX spin system) δ/ppm = –3.1 (t, $^1J_{PX\text{-}PA/PA´}$ = 267.7 Hz, 1 P, P^X), 45.6 (t, $^1J_{PM\text{-}PA/PA´}$= 294.8 Hz, 1 P, P^M), 103.7 (dd, $^1J_{PA/PA´\text{-}PX}$ = 267.7 Hz, $^1J_{PA/PA´\text{-}PM}$ = 294.8 Hz, 2 P, $P^{A/A´}$)

^{31}P{^{1}H}: (AA'MX spin system) δ/ppm = –3.1 (t, $^1J_{PX\text{-}PA/PA´}$ = 267.7 Hz, 1 P, P^X), 45.6 (t, $^1J_{PM\text{-}PA/PA´}$= 294.8 Hz, 1 P, P^M), 103.7 (dd, $^1J_{PA/PA´\text{-}PX}$ = 267.7 Hz, $^1J_{PA/PA´\text{-}PM}$ = 294.8 Hz, 2 P, $P^{A/A´}$)

*[Cp´´´Ni(η³-P₄Mes₂)][TEF] (**2b**[TEF])*

A colourless solution of Tl[TEF] (0.1 mmol, 117 mg, 1 eq., $[TEF]^- = [Al(OC(CF_3)_3)_4]^-$) in 2 mL of *o*-DFB was added to an orange solution of **1** (0.1 mmol, 38 mg, 1 eq.) and Mes_2PCl (0.1 mmol, 30 mg, 1 eq.) in 3 mL of *o*-DFB at room temperature. A rapid colour change to red occurred and formation of white solid could be observed. After stirring for 24 h at room temperature, the mixture was filtered, and the solvent removed *in vacuo.* The oily red residue was washed three times with 10 mL of *n*-hexane, each. Drying under reduced pressure (10^{-3} mbar) lead to solidification of the product [Cp´´´Ni(η³-P_4Mes_2)][TEF] (**2b**[TEF]), which was isolated as a red powder. All attempts to recrystallise the product ended in the formation of red oil at the bottom of the flask.

Yield: 75 mg (0.046 mmol, 46%)

Elemental analysis: calc. (%) for [Cp´´´Ni(η³-P_4Mes_2)][TEF] ($C_{51}H_{51}O_4F_{36}AlP_4Ni$): C: 37.77 H: 3.17; found (%): C: 38.05 H: 3.08

ESI(+) MS (*o*-DFB): *m/z* (%) = 653.2 (100%) [Cp´´´Ni(η³-P_4Mes_2)]⁺

NMR (CD_2Cl_2, 298 K): **^{1}H**: δ/ppm = 1.14 (s, 9 H, $C(CH_3)_3$), 1.29 (s, 18 H, $C(CH_3)_3$), 2.32 (s, 6 H, Me), 2.64 (s, 6 H, Me), 2.73 (s, 6 H, Me) 5.92 (d, ^4J = 1.4 Hz, 2 H, $C_5H_2{}^tBu_3$), 6.98 (d, ^4J = 4.2 Hz, 2 H, Mes), 7.01 (d, ^4J = 4.6 Hz, 2 H, Mes)

^{31}P{^{1}H}: (AA'MX spin system) δ/ppm = –3.1 (t, $^1J_{PX\text{-}PA/PA´}$ = 267.7 Hz, 1 P, P^X), 45.6 (t, $^1J_{PM\text{-}PA/PA´}$= 294.8 Hz, 1 P, P^M), 103.7 (dd, $^1J_{PA/PA´\text{-}PX}$ = 267.7 Hz, $^1J_{PA/PA´\text{-}PM}$ = 294.8 Hz, 2 P, $P^{A/A´}$)

^{31}P{^{1}H}:(AA'MX spin system) δ/ppm = –3.1 (t, $^1J_{PX\text{-}PA/PA´}$ = 267.7 Hz, 1 P, P^X), 45.6 (t, $^1J_{PM\text{-}PA/PA´}$= 294.8 Hz, 1 P, P^M), 103.7 (dd, $^1J_{PA/PA´\text{-}PX}$ = 267.7 Hz, $^1J_{PA/PA´\text{-}PM}$ = 294.8 Hz, 2 P, $P^{A/A´}$)

^{19}F{^{1}H}: δ/ppm = – 75.62 (s, $[TEF]^-$)

*[Cp´´´Ni(η³-P₄Cy₂)][GaCl₄] (**2c**[GaCl₄])*

A colourless solution of $GaCl_3$ (0.1 mmol, 18 mg, 1 eq.) in 4 mL of *o*-DFB was added to an orange solution of **1** (0.1 mmol, 38 mg, 1 eq.) and Cy_2PCl (0.1 mmol, 23 mg, 22 μL, 1 eq.) in 3 mL of *o*-DFB at room temperature. A rapid colour change to red occurred. After stirring for 6 h at room temperature the solvent was removed *in vacuo* and the oily red residue was washed three times with 10 mL of *n*-hexane, each. Drying under reduced pressure (10^{-3} mbar) lead to solidification of the product [Cp´´´Ni(η³-P_4Cy_2)][$GaCl_4$] (**2c**[$GaCl_4$]), which was then recrystallised from *o*-DFB/*n*-hexane (1:8) at – 30 °C to give dark red crystals of X-ray analysis quality after two weeks.

Yield: 47 mg (0.059 mmol, 59%)

Elemental analysis: calc. (%) for [Cp´´´Ni(η³-P_4Cy_2)][$GaCl_4$]·$(C_6H_4F_2)_{0.2}$ ($C_{30.2}H_{51.8}P_4Cl_4NiGa$): C: 44.42 H: 6.39; found (%): C: 44.38 H: 6.12

ESI(+) MS (*o*-DFB): *m/z* (%) = 581.2 (100%) [Cp´´´Ni(η³-P_4Cy_2)]⁺

NMR (CD_2Cl_2, 298 K): **^{1}H**: δ/ppm = 1.26 – 2.56 (several broad multiplets, 22 H, Cy), 1.29 (s, 9 H, $C(CH_3)_3$), 1.45 (s, 18 H, $C(CH_3)_3$), 5.92 (d, ^4J = 1.4 Hz, 2 H, $C_5H_2{}^tBu_3$)

^{31}P{^{1}H}: (AMXX' spin system) δ/ppm = 35.0 (m, $^1J_{PX\text{-}PM}$ = 270.9 Hz, $^1J_{PX'\text{-}PM}$ = 261.8 Hz, $^1J_{PX\text{-}PA}$ = 286.6 Hz, $^1J_{PX'\text{-}PA}$ = 296.7 Hz, $^2J_{PX\text{-}PX'}$ = 22.7 Hz, 2 P, $P^{X/X'}$), 48.5 (ddd, $^1J_{PM\text{-}PX}$ = 270.9 Hz, $^1J_{PM\text{-}PX'}$ = 261.8 Hz, $^2J_{PM\text{-}PA}$ = 12.3 Hz, 1 P, P^M), 84.3 (ddd, $^1J_{PA\text{-}PX}$ = 286.6 Hz, $^1J_{PA\text{-}PX'}$ = 296.7 Hz, $^2J_{PA\text{-}PM}$ = 12.3 Hz, 1 P, P^A)

^{31}P: (AMXX' spin system) δ/ppm = 35.0 (m, $^1J_{PX\text{-}PM}$ = 270.9 Hz, $^1J_{PX'\text{-}PM}$ = 261.8 Hz, $^1J_{PX\text{-}PM}$ = 286.6 Hz, $^1J_{PX'\text{-}PA}$ = 296.7 Hz, $^2J_{PX\text{-}PX'}$ = 22.7 Hz, 2 P, $P^{X/X'}$), 48.5 (m, 1 P, P^M), 84.3 (ddd, $^1J_{PA\text{-}PX}$ = 286.6 Hz, $^1J_{PA\text{-}PX'}$ = 296.7 Hz, $^2J_{PA\text{-}PM}$ = 12.3 Hz, 1 P, P^A)

*[Cp´´´Ni(η^3-P_4Cy_2)][TEF] (**2c**[TEF])*

A colourless solution of Tl[TEF] (0.1 mmol, 117 mg, 1 eq.) in 2 mL of *o*-DFB was added to an orange solution of **1** (0.1 mmol, 38 mg, 1 eq.) and Cy_2PCl (0.1 mmol, 23 mg, 22 μL, 1 eq.) in 3 mL of *o*-DFB at room temperature. A rapid colour change to red occurred and formation of white solid could be observed. After stirring for 24 h at room temperature, the mixture was filtered, and the solvent removed *in vacuo.* The oily red residue was dissolved in 3 mL of CH_2Cl_2, precipitated with 30 mL of *n* -hexane and washed three times with 10 mL of *n*-hexane, each. Drying under reduced pressure (10^{-3} mbar) lead to solidification of the product [Cp´´´Ni(η^3-P_4Cy_2)][TEF] (**2c**[TEF]), which was isolated as an orange to red powder. All attempts to recrystallise the product ended in the formation of red oil at the bottom of the flask.

Yield: 88 mg (0.057 mmol, 57%)

Elemental analysis: calc. (%) for [Cp´´´Ni(η^3-P_4Cy_2)][TEF] ($C_{45}H_{51}O_4F_{36}AlP_4Ni$): C: 35.16 H: 2.56; found (%): C: 35.04 H: 3.06

ESI(+) MS (CH_2Cl_2): *m/z* (%) = 581.2 (100%) [Cp´´´Ni(η^3-P_4Cy_2)]$^+$

NMR (CD_2Cl_2, 298 K): **^{1}H**: δ/ppm = 1.26 – 2.56 (several broad multiplets, 22 H, Cy), 1.29 (s, 9 H, $C(CH_3)_3$), 1.45 (s, 18 H, $C(CH_3)_3$), 5.92 (d, ^4J = 1.4 Hz, 2 H, $C_5H_2{}^tBu_3$)

^{31}P{^{1}H}: (AMXX' spin system) δ/ppm = 35.0 (m, $^1J_{PX\text{-}PM}$ = 270.9 Hz, $^1J_{PX'\text{-}PM}$ = 261.8 Hz, $^1J_{PX\text{-}PA}$ = 286.6 Hz, $^1J_{PX'\text{-}PA}$ = 296.7 Hz, $^2J_{PX\text{-}PX'}$ = 22.7 Hz, 2 P, $P^{X/X'}$), 48.5 (ddd, $^1J_{PM\text{-}PX}$ = 270.9 Hz, $^1J_{PM\text{-}PX'}$ = 261.8 Hz, $^2J_{PM\text{-}PA}$ = 12.3 Hz, 1 P, P^M), 84.3 (ddd, $^1J_{PA\text{-}PX}$ = 286.6 Hz, $^1J_{PA\text{-}PX'}$ = 296.7 Hz, $^2J_{PA\text{-}PM}$ = 12.3 Hz, 1 P, P^A)

^{31}P: (AMXX' spin system) δ/ppm = 35.0 (m, $^1J_{PX\text{-}PM}$ = 270.9 Hz, $^1J_{PX'\text{-}PM}$ = 261.8 Hz, $^1J_{PX\text{-}PM}$ = 286.6 Hz, $^1J_{PX'\text{-}PA}$ = 296.7 Hz, $^2J_{PX\text{-}PX'}$ = 22.7 Hz, 2 P, $P^{X/X'}$), 48.5 (m, 1 P, P^M), 84.3 (ddd, $^1J_{PA\text{-}PX}$ = 286.6 Hz, $^1J_{PA\text{-}PX'}$ = 296.7 Hz, $^2J_{PA\text{-}PM}$ = 12.3 Hz, 1 P, P^A)

^{19}F{^{1}H}: δ/ppm = –75.62 (s, $[TEF]^-$)

*[Cp´´´Ni(η^3-P_4biphen)][$GaCl_4$] (**2d**[$GaCl_4$])*

A colourless solution of $GaCl_3$ (0.1 mmol, 18 mg, 1 eq.) in 4 mL of CH_2Cl_2 was added to an orange solution of **1** (0.1 mmol, 38 mg, 1 eq.) and biphenPCl (0.1 mmol, 22 mg, 1 eq.) in 3 mL of CH_2Cl_2 at room temperature. Rapid colour change to dark red occurred. After stirring the solution for 1.5 h, it was constrained to a total of 4 mL, layered with 20 mL of *n*-hexane, and stored at – 30 °C. After one week, formation of red microcrystalline [Cp´´´Ni(η^3-P_4biphen)][$GaCl_4$] (**2d**[$GaCl_4$]) could be observed. Recrystallisation from CH_2Cl_2/n-hexane (1:5) at –30 °C yielded light red crystals of X-ray quality after two weeks.

Yield: 55 mg (0.07 mmol, 70 %)

Elemental analysis: calc. (%) for [Cp´´´Ni(η^3-P_4biphen)][$GaCl_4$]·$(C_6H_{14})_{0.6}$ ($C_{32.6}H_{45.4}P_4Cl_4NiGa$): C: 47.09 H: 5.50; found (%): C: 47.56 H: 5.11

ESI(+) MS (*o*-DFB): *m/z* (%) = 567.1 (100%) [Cp´´´Ni(□^{3}-P_4biphen)]$^+$, 895.2 (8%) [(Cp´´´Ni)$_2$(μ;η^3:η^1:η^1-P_4biphenCl)]$^+$

NMR (CD_2Cl_2, 298 K): **^{1}H**: δ/ppm = 1.36 (s, 9 H, $C(CH_3)_3$), 1.52 (s, 18 H, $C(CH_3)_3$), 6.25 (d, $^4J_{H\text{-}H}$ = 1.5 Hz, 2 H, $C_5H_2{}^tBu_3$), 7.72 (m, 2 H, biphen), 7.83 (m, 2 H, biphen), 7.96 (m, 2 H, biphen), 8.28 (m, 2 H, biphen)

^{31}P{^{1}H}: (AA'MX spin system) δ/ppm = 17.1 (m, $^1J_{PX\text{-}PA}$ = 292.8 Hz, $^1J_{PX\text{-}PA´}$ = 274.2 Hz, $^2J_{PX\text{-}PM}$ = 24.8 Hz, 1 P, P^X), 63.8 (m, $^1J_{PM\text{-}PA}$ = 277.2 Hz, $^1J_{PM\text{-}PA´}$ = 282.5 Hz, $^2J_{PM\text{-}PX}$ = 24.8 Hz, 1 P, P^M), 70.0 (m, $^1J_{PA\text{-}PX}$ = 292.8 Hz, $^1J_{PA´\text{-}PX}$ = 274.2 Hz, $^1J_{PA\text{-}PM}$ = 277.2 Hz, $^1J_{PA´\text{-}PM}$ = 282.5 Hz, 2 P, $P^{A/A´}$)

^{31}P: (AA'MX spin system) δ/ppm = 17.1 (t, $^1J_{PX\text{-}PA/A´}$ = 282.4 Hz, 1 P, P^X), 63.8 (m, $^1J_{PM\text{-}PA}$ = 277.2 Hz, $^1J_{PM\text{-}PA´}$ = , $^2J_{PM\text{-}PX}$ = 24.8 Hz, 1 P, P^M), 70.0 (m, $^1J_{PA\text{-}PX}$ = 292.8 Hz, $^1J_{PA´\text{-}PX}$ = 274.2 Hz, $^1J_{PA\text{-}PM}$ = 277.2 Hz, $^1J_{PA´\text{-}PM}$ = 282.5 Hz, 2 P, $P^{A/A´}$)

*[Cp´´´Ni(η³-P₄biphen)][TEF] (**2d**[TEF])*

A colourless solution of Tl[TEF] (0.1 mmol, 117 mg, 1 eq.) in 2 mL of *o*-DFB was added to an orange solution of **1** (0.1 mmol, 38 mg, 1 eq.) and biphenPCl (0.1 mmol, 22 mg, 1 eq.) in 3 mL of *o*-DFB at room temperature. A rapid colour change to dark red occurred and formation of white solid could be observed. After stirring for 24 h at room temperature, the mixture was filtered, and the solvent removed *in vacuo.* The dark red residue was washed three times with 10 mL of *n*-hexane, each, and then dried under reduced pressure (10^{-3} mbar) to yield [Cp´´´Ni(η³-P₄biphen)][TEF] (**2d**[TEF]) as an orange to red powder.

Yield: 84 mg (0.055 mmol, 55%)

Elemental analysis: calc. (%) for [Cp´´´Ni(η³-P₄biphen)][TEF] ($C_{45}H_{37}O_4F_{36}AlP_4Ni$): C: 35.20 H: 2.43; found (%): C: 35.02 H: 2.47

ESI(+) MS (CH_2Cl_2): *m/z* (%) = 567.1 (100%) $[Cp´´´Ni(\eta^3\text{-}P_4biphen)]^+$

NMR (CD_2Cl_2, 298 K): **^{1}H**: δ/ppm = 1.36 (s, 9 H, $C(CH_3)_3$), 1.52 (s, 18 H, $C(CH_3)_3$), 6.25 (d, $^4J_{H\text{-}H}$ = 1.5 Hz, 2 H, $C_5H_2{}^tBu_3$), 7.72 (m, 2 H, biphen), 7.83 (m, 2 H, biphen), 7.96 (m, 2 H, biphen), 8.28 (m, 2 H, biphen)

^{31}P{^{1}H}: (AA'MX spin system) □/ppm = 17.1 (m, $^1J_{PX\text{-}PA}$ = 292.8 Hz, $^1J_{PX\text{-}PA´}$ = 274.2 Hz, $^2J_{PX\text{-}PM}$ = 24.8 Hz, 1 P, P^X), 63.8 (m, $^1J_{PM\text{-}PA}$ = 277.2 Hz, $^1J_{PM\text{-}PA´}$ = 282.5 Hz, $^2J_{PM\text{-}PX}$ = 24.8 Hz, 1 P, P^M), 70.0 (m, $^1J_{PA\text{-}PX}$ = 292.8 Hz, $^1J_{PA´\text{-}PX}$ = 274.2 Hz, $^1J_{PA\text{-}PM}$ = 277.2 Hz, $^1J_{PA´\text{-}PM}$ = 282.5 Hz, 2 P, $P^{A/A´}$)

^{31}P: (AA'MX spin system) δ/ppm = 17.1 (t, $^1J_{PX\text{-}PA/A´}$ = 282.4 Hz, 1 P, P^X), 63.8 (m, $^1J_{PM\text{-}PA}$ = 277.2 Hz, $^1J_{PM\text{-}PA´}$ = , $^2J_{PM\text{-}PX}$ = 24.8 Hz, 1 P, P^M), 70.0 (m, $^1J_{PA\text{-}PX}$ = 292.8 Hz, $^1J_{PA´\text{-}PX}$ = 274.2 Hz, $^1J_{PA\text{-}PM}$ = 277.2 Hz, $^1J_{PA´\text{-}PM}$ = 282.5 Hz, 2 P, $P^{A/A´}$)

^{19}F{^{1}H}: δ/ppm = –75.54 (s, $[TEF]^-$)

*[Cp´´´Ni(η^3-P_4Me_2)][TEF] (**2e**[TEF])*

A colourless solution of Tl[TEF] (0.1 mmol, 117 mg, 1 eq.) in 2 mL of *o*-DFB was added to an orange solution of **1** (0.1 mmol, 38 mg, 1 eq.) and Me_2PCl (0.1 mmol, 10 mg, 10 µL, 1 eq.) in 3 mL of *o*-DFB at room temperature. A rapid colour change to red occurred and formation of white solid could be observed. After stirring for 24 h at room temperature, the mixture was filtered, and the solvent removed *in vacuo.* The oily red residue was washed three times with 10 mL of *n*-hexane, each. Drying under reduced pressure (10^{-3} mbar) lead to solidification. Recrystallisation from *o*-DFB/*n*-hexane (1:10) at 4 °C gave [Cp´´´Ni(η^3-P_4Me_2)][TEF] (**2e**[TEF]) as a single crystalline material after 10 days.

Yield: 73 mg (0.052 mmol, 52%)

Elemental analysis: calc. (%) for [Cp´´´Ni(η^3-P_4Me_2)][TEF] ($C_{35}H_{35}O_4F_{36}AlP_4Ni$): C: 29.74 H: 2.50; found (%): C: 29.95 H: 2.42

ESI(+) MS (CH_2Cl_2): *m/z* (%) = 445.1 (100%) [Cp´´´Ni(η^3-P_4Me_2)]$^+$

NMR (CD_2Cl_2, 298 K): **^{1}H**: δ/ppm = 1.30 (s, 9 H, $C(CH_3)_3$), 1.44 (s, 18 H, $C(CH_3)_3$), 2.01 (d, $^2J_{HP}$ = 12.2 Hz, 3 H, Me), 2.30 (d, $^2J_{HP}$ = 12.4 Hz, 3 H, Me), 5.96 (s, 2 H, $C_5H_2{}^tBu_3$)

^{31}P{^{1}H}: (AMM'X spin system) δ/ppm = 14.7 (ddd, $^1J_{PX\text{-}PM}$ = 257.1 Hz, $^1J_{PX\text{-}PM´}$ = 255.4 Hz, $^2J_{PX\text{-}PA}$ = 18.6 Hz, 1 P, P^X), 64.0 (m, $^1J_{PM\text{-}PX}$ = 257.1 Hz, $^1J_{PM´\text{-}PX}$ = 255.4 Hz, $^1J_{PM\text{-}PA}$ = 295.4 Hz, $^1J_{PM´\text{-}PA}$ = 279.5 Hz, 2 P, $P^{M/M´}$), 83.5 (ddd, $^1J_{PA\text{-}PM}$ = 295.4 Hz, $^1J_{PA\text{-}PM´}$ = 279.5 Hz, $^2J_{PA\text{-}PX}$ = 18.6 Hz, 1 P, P^A)

^{31}P: (AMM'X spin system) δ/ppm = 14.7 (m, 1 P, P^X), 64.0 (m, $^1J_{PM\text{-}PX}$ = 257.1 Hz, $^1J_{PM´\text{-}PX}$ = 255.4 Hz, $^1J_{PM\text{-}PA}$ = 295.4 Hz, $^1J_{PM´\text{-}PA}$ = 279.5 Hz, 2 P, $P^{M/M´}$), 83.5 (ddd, $^1J_{PA\text{-}PM}$ = 295.4 Hz, $^1J_{PA\text{-}PM´}$ = 279.5 Hz, $^2J_{PA\text{-}PX}$ = 18.6 Hz, 1 P, P^A)

^{19}F{^{1}H}: δ/ppm = – 75.60 (s, $[TEF]^-$)

*[Cp´´´Ni(η³-P₄PhCl)][TEF] (**2f**[TEF])*

A colourless solution of Tl[TEF] (0.1 mmol, 117 mg, 1 eq.) in 2 mL of *o*-DFB was added to an orange solution of **1** (0.1 mmol, 38 mg, 1 eq.) and $PhPCl_2$ (0.1 mmol, 18 mg, 14 μL, 1 eq.) in 3 mL of *o*-DFB at room temperature. A rapid colour change to dark red occurred and formation of white solid could be observed. After stirring for 20 h at room temperature, the mixture was filtered, and the solvent removed *in vacuo.* The oily red residue was washed three times with 10 mL of *n*-hexane, each. Drying under reduced pressure (10^{-3} mbar) lead to formation of [Cp´´´Ni(η³-P_4ClPh)][TEF] (**2f**[TEF]) as a brownish red solid. NMR spectroscopy studies revealed that **2f**[TEF] is formed in two isomeric forms, endo-Ph and exo-Ph, respectively. According to the ^{1}H and ^{31}P NMR spectrum the two isomers are formed in a ratio of 1:7. Crystals of the *endo*-Ph isomer of **2f**[TEF] could be obtained in X-ray analysis quality, by recrystallisation from *o*-DFB/*n*-hexane (1:6) at 4 °C for two weeks.

Yield: 93 mg (0.06 mmol, 60%)

Elemental analysis: calc. (%) for [Cp´´´Ni(η³-P_4Me_2)][TEF]·$(C_6H_4F_2)_{0,6}$ ($C_{42.6}H_{36.4}O_4F_{37.2}AlP_4Ni$): C: 32.72 H: 2.35; found (%): C: 32.89 H: 2.52 (Signals for $C_6H_4F_2$ are also found in the ^{1}H NMR of the isolated product)

ESI(+) MS (*o*-DFB): *m/z* (%) = 527.1 (100%) [Cp´´´Ni(η³-P_4PhCl)]$^+$

NMR (CD_2Cl_2, 298 K): **^{1}H**: δ/ppm = 1.21 (s, 9 H, $C(CH_3)_3$ (**2f$^+_{exo}$**)), 1.29 (s, 18 H, $C(CH_3)_3$ (**2f$^+_{exo}$**)), 1.39 (s, 9 H, $C(CH_3)_3$ (**2f$^+_{endo}$**)), 1.49 (s, 18 H, $C(CH_3)_3$ (**2f$^+_{endo}$**)), 5.91 (d, $^4J_{H\text{-}H}$ = 2.7 Hz, 2 H, $C_5H_2{}^tBu_3$ (**2f$^+_{exo}$**)), 6.05 (s, 2 H, $C_5H_2{}^tBu_3$ (**2f$^+_{endo}$**)), 7.73 (m, 2.3 H, Ph (**2f$^+$**)), 7.81 (m, 1.1 H, Ph (**2f$^+$**)), 7.9 ─ 8.0 (m, 2.3 H, Ph (**2f$^+$**)), **2f$^+_{endo}$**: **2f$^+_{exo}$** = 7:1
^{31}P{^{1}H}: (two AA'MX spin systems) δ/ppm = 34.3 (ddd, $^1J_{PX\text{-}PA}$ = 274.1 Hz, $^1J_{PX\text{-}PA´}$ = 273.6 Hz, $^2J_{PX\text{-}PM}$ = 36.8 Hz, 1 P, P^X (**2f$^+_{endo}$**)), 42.3 (ddd, $^1J_{PX\text{-}PA}$ = 331.1 Hz, $^1J_{PX\text{-}PA´}$ = 330.2 Hz, $^2J_{PX\text{-}PM}$ = 18.7 Hz, 1 P, P^X (**2f$^+_{exo}$**)), 59.5 (ddd, $^1J_{PM\text{-}PA}$ = 346.4 Hz, $^1J_{PM\text{-}PA´}$ = 338.5 Hz, $^2J_{PM\text{-}PX}$ = 36.8 Hz, 1 P, P^M (**2f$^+_{endo}$**)), 73.9 (ddd, $^1J_{PM\text{-}PA}$ = 285.0 Hz, $^1J_{PM\text{-}PA´}$ = 282.3 Hz, $^2J_{PM\text{-}PX}$ = 18.7 Hz, 1 P, P^M (**2f$^+_{exo}$**)), 94.1 (m, $^1J_{PA\text{-}PX}$ = 331.1 Hz, $^1J_{PA´\text{-}PX}$ = 330.2 Hz, $^1J_{PA\text{-}PM}$ = 285.0 Hz, $^1J_{PA´\text{-}PM}$ = 282.3 Hz, 2 P, $P^{A/A´}$ (**2f$^+_{exo}$**)), 113.5 (ddd, $^1P_{PA\text{-}PM}$ = 346.4 Hz, $^1J_{PA´\text{-}PM}$ = 338.5 Hz, $^1J_{P2\text{-}PX}$ = 274.1 Hz, $^1J_{P4\text{-}PX}$ = 273.6 Hz, 2 P, $P^{A/A´}$ (**2f$^+_{endo}$**))
^{31}P: (two AA'MX spin systems) δ/ppm = 34.3 (ddd, $^1J_{PX\text{-}PA}$ = 274.1 Hz, $^1J_{PX\text{-}PA´}$ = 273.6 Hz, $^2J_{PX\text{-}PM}$ = 36.8 Hz, 1 P, P^X (**2f$^+_{endo}$**)), 42.3 (t (broad), $^1J_{P\text{-}P}$ = 339.8 Hz, 1 P, P^X (**2f$^+_{exo}$**)), 59.5 (t (broad), $^1J_{P\text{-}P}$ = 342.4 Hz, 1 P, P^M (**2f$^+_{endo}$**)), 73.9 (ddd, $^1J_{PM\text{-}PA}$ = 285.0 Hz, $^1J_{PM\text{-}PA´}$ = 282.3 Hz, $^2J_{PM\text{-}PX}$ = 18.7 Hz, 1 P, P^M (**2f$^+_{exo}$**)), 94.1 (m, $^1J_{PA\text{-}PX}$ = 331.1 Hz, $^1J_{PA´\text{-}PX}$ = 330.2 Hz, $^1J_{PA\text{-}PM}$ = 285.0 Hz, $^1J_{PA´\text{-}PM}$ = 282.3 Hz, 2 P, $P^{A/A´}$ (**2f$^+_{exo}$**)), 113.5 (ddd, $^1P_{PA\text{-}PM}$ = 346.4 Hz, $^1J_{PA´\text{-}PM}$ = 338.5 Hz, $^1J_{PA\text{-}PX}$ = 274.1 Hz, $^1J_{PA´\text{-}PX}$ = 273.6 Hz, 2 P, $P^{A/A´}$ (**2f$^+_{endo}$**)), Integration: **2f$^+_{endo}$**: **2f$^+_{exo}$** = 7:1
^{19}F{^{1}H}: δ/ppm = ─75.57 (s, $[TEF]^-$)

*[Cp´´´Ni(η³-P₄ᵗBuCl)][TEF] (**2g**[TEF])*

A colourless solution of Tl[TEF] (0.1 mmol, 117 mg, 1 eq.) in 2 mL of *o*-DFB was added to an orange solution of **1** (0.1 mmol, 38 mg, 1 eq.) and ^{t}BuPCl$_2$ (0.1 mmol, 16 mg, 1 eq.) in 3 mL of *o*-DFB at room temperature. Precipitation of white solid and a colour change to red could be observed within one hour. Stirring for 20 h lead to darkening of the mixture. The solution was then filtered of the white solid, and the solvent removed *in vacuo*. The dark red to brown precipitate was washed three times with 10 mL of *n*-hexane, each. After drying under vacuum (10^{-3} mbar) [Cp´´´Ni(η^3-P$_4$Cl^{t}Bu)][TEF] (**2g**[TEF]) could be isolated as a brown powder.

Yield: 74 mg (0.05 mmol, 50%)

Elemental analysis: calc. (%) for [Cp´´´Ni(η^3-P$_4$^{t}BuCl)][TEF]·(C$_6$H$_4$F$_2$)$_{0.4}$ (C$_{39.4}$H$_{39.6}$O$_4$F$_{36.8}$AlP$_4$ClNi): C: 31.11 H: 2.63; found (%): C: 31.01 H: 2.50 (Signals for C$_6$H$_4$F$_2$ are also found in the ^{1}H NMR of the isolated product)

ESI(+) MS (*o*-DFB): *m/z* (%) = 507.1 (100%) [Cp´´´Ni(η^3-P$_4$^{t}BuCl)]$^+$

NMR (CD$_2$Cl$_2$, 298 K): **^{1}H**: δ/ppm = 1.32 (s, 9 H, C(CH$_3$)$_3$), 1.46 (s, 18 H, C(CH$_3$)$_3$), 1.47 (d, $^3J_{PH}$ = 22.0 Hz, 9 H, ^{t}Bu), 6.01 (s, 2 H, C$_5$H$_2$^{t}Bu$_3$)

^{31}P{^{1}H}: δ/ppm = 57.1 (ddd, $^1J_{PX\text{-}PM}$ = 288.6 Hz, $^1J_{PX\text{-}PM´}$ = 270.0 Hz, $^2J_{PX\text{-}PA}$ = 41.9 Hz, 1 P, P^X), 85.9 (ddd, $^1J_{PM\text{-}PA}$ = 357.9 Hz, $^1J_{PM´\text{-}PA}$ = 324.8 Hz, $^1J_{PM\text{-}PX}$ = 288.6 Hz, $^1J_{PM´\text{-}PX}$ = 270.0 Hz, 2 P, P$^{M/M´}$), 107.2 (ddd, $^1J_{PA\text{-}PM}$ = 357.9 Hz, $^1J_{PA\text{-}PM´}$ = 324.8 Hz, $^2J_{PA\text{-}PX}$ = 41.9 Hz, 1 P, P^A)

^{31}P: δ/ppm = 57.1 (ddd, $^1J_{PX\text{-}PM}$ = 288.6 Hz, $^1J_{PX\text{-}PM´}$ = 270.0 Hz, $^2J_{PX\text{-}PA}$ = 41.9 Hz, 1 P, P^X), 85.9 (ddd, $^1J_{PM\text{-}PA}$ = 357.9 Hz, $^1J_{PM´\text{-}PA}$ = 324.8 Hz, $^1J_{PM\text{-}PX}$ = 288.6 Hz, $^1J_{PM´\text{-}PX}$ = 270.0 Hz, 2 P, P$^{M/M´}$), 107.2 (br, 1 P, P^A)

^{19}F{^{1}H}: δ/ppm = –75.60 (s, [TEF]$^-$)

*[(Cp´´´Ni)$_2$(μ;η^3:η^1:η^1-P$_4$Br$_3$)][TEF] (**3a**[TEF])*

Addition of a solution of Tl[TEF] (0.1 mmol, 117 mg, 1 eq.) in 3 mL of CH_2Cl_2 to a solution of **1** (0.1 mmol, 38 mg, 1 eq.) and PBr_3 (0.1 mmol, 27 mg, 10 μL, 1 eq.) in 4 mL of CH_2Cl_2 at – 80 °C lead to an immediate colour change to dark red and the precipitation of white solid. ^{31}P NMR spectra (*o*-DFB/tol-*d*^{8} capillary, r. t., Figure SI 7) taken 1 h after the addition revealed the initial formation of [Cp´´´Ni(η^3-P$_4$Br$_2$)][TEF] (**2h**[TEF]) besides P_4 and the final product [(Cp´´´Ni)$_2$(μ;η^3:η^1:η^1-P$_4$Br$_3$)][TEF] (**3a**[TEF]). Attempts to isolate the intermediate **2h**[TEF] by filtration of the cold (–80 °C) solution and washing three times with cold *n*-hexane (10 mL each, –80 °C) failed. Isolated batches of (**2h**[TEF]) always carried impurities of the final product **3a**[TEF]. The latter was obtained, by letting the reaction mixture warm to room temperature overnight and stirring for three more days. The now dark brown mixture was filtered, and the solvent removed *in vacuo*. The brown precipitate was washed with 10 mL of *n*-hexane, each, and then dried under reduced pressure (10^{-3} mbar). Recrystallisation from CH_2Cl_2/*n*-hexane (1:6) at room temperature for six days yielded large blackish red crystals of **3a**[TEF] in X-ray quality. These crystals were washed with toluene, dried under reduced pressure and then isolated. Conducting the reaction in *o*-DFB, but only cooling to –30 °C yielded similar results.

Yield: 92 mg (0.048 mmol, 90% based on **1**)

Elemental analysis: calc. (%) for [(Cp´´´Ni)$_2$(μ;η^3:η^1:η^1-P$_4$Br$_3$)][TEF]·(TlBr)$_{0.5}$ ($C_{50}H_{58}O_4F_{36}AlP_4Ni_2Br_{3.5}Tl_{0.5}$): C: 29.24 H: 2.85; found (%): C: 29.16 H: 2.56 (even after several filtration steps, TlBr precipitates after layering *o*-DFB solutions of the product and covers the surface of the crystals)

ESI(+) MS (*o*-DFB): *m/z* (%) = 332.2 (100) [Cp´´´Ni(H$_3$CCN)]$^+$, 373.2 (20) [Cp´´´Ni(H$_3$CCN)$_2$]$^+$, 947.0 (5) [(Cp´´´Ni)$_2$(μ;η^3:η^1:η^1-P$_4$Br$_3$)]$^+$; Acetonitrile molecules are from the purging solution of the diffractometer.

NMR (CD_2Cl_2, 298 K): **^{1}H**: δ/ppm = 1.25 (s, 9 H, C(CH$_3$)$_3$), 1.41 (s, 9 H, C(CH$_3$)$_3$), 1.42 (s, 9 H, C(CH$_3$)$_3$), 1.46 (s, 18 H, C(CH$_3$)$_3$), 1.48 (s, 9 H, C(CH$_3$)$_3$), 4.91 (m, 1 H, C$_5$H$_2$^{t}Bu$_3$), 5.35 (m, 1 H, C$_5$H$_2$^{t}Bu$_3$), 5.43 (s, 1 H, C$_5$H$_2$^{t}Bu$_3$), 5.91 (s, 1 H, C$_5$H$_2$^{t}Bu$_3$)
^{31}P{^{1}H}: (AMNX spin system) δ/ppm = –1.1 (t (br), $^1J_{PX\text{-}PN}$ = 347.0 Hz, $^1J_{PX\text{-}PM}$ = 379.2 Hz, 1 P, P^X), 128.0 (td, $^1J_{P2\text{-}PA}$ = 353.1 Hz, $^1J_{PN\text{-}PX}$ = 347.0 Hz, $^2J_{PN\text{-}PM}$ = 71.3 Hz, 1 P, P^N), 134.2 (ddd, $^1J_{PM\text{-}PX}$ = 379.2 Hz, $^2J_{PM\text{-}PA}$ = 281.7 Hz, $^2J_{PM\text{-}PN}$ = 71.3 Hz, 1 P, P^M), 182.0 (dd, $^1J_{PA\text{-}PN}$ = 353.1, $^2J_{PA\text{-}PM}$ = 281.7 Hz, 1 P, P^A)
^{31}P{^{1}H}: (AMNX spin system) δ/ppm = –1.1 (t (br), $^1J_{PX\text{-}PN}$ = 347.0 Hz, $^1J_{PX\text{-}PM}$ = 379.2 Hz, 1 P, P^X), 128.0 (td, $^1J_{P2\text{-}PA}$ = 353.1 Hz, $^1J_{PN\text{-}PX}$ = 347.0 Hz, $^2J_{PN\text{-}PM}$ = 71.3 Hz, 1 P, P^N), 134.2 (ddd, $^1J_{PM\text{-}PX}$ = 379.2 Hz, $^2J_{PM\text{-}PA}$ = 281.7 Hz, $^2J_{PM\text{-}PN}$ = 71.3 Hz, 1 P, P^M), 182.0 (dd, $^1J_{PA\text{-}PN}$ = 353.1, $^2J_{PA\text{-}PM}$ = 281.7 Hz, 1 P, P^A)
^{19}F{^{1}H}: δ/ppm = –75.50 (s, [TEF]$^-$)

*[(Cp´´´Ni)$_2$(μ;η^3:η^1:η^1-P$_4$biphenCl)][GaCl$_4$] (**3b**[GaCl$_4$])*

Following the same synthetic protocol as for (**2d**[GaCl$_4$]) but performing the reaction in *o*-DFB and stirring for 20 h again leads to a dark red solution of (**2d**[GaCl$_4$], by NMR spectroscopy). When this solution was concentrated to 4 mL, layered with *n*-hexane (6:1), and then stored at room temperature for two weeks [(Cp´´´Ni)$_2$(μ;η^3:η^1:η^1-P$_4$biphenCl)][GaCl$_4$] (**3b**[GaCl$_4$]) crystallised as light brown plates of X-ray quality. Alternatively, **2d**[GaCl$_4$] can be stirred in *o*-DFB solution (4 mL) for two weeks. When the resulting solution is layered with *n*-hexane, crystals of **3b**[GaCl$_4$] can be obtained in similar yield. Decanting off the solvent followed by washing steps (3 x 10 mL *n*-hexane) and drying under reduced pressure (10^{-3} mbar) gives pure **3b**[GaCl$_4$].

Yield: 41 mg (0.037 mmol, 74% based on **1**)

Elemental analysis: calc. (%) for [(Cp´´´Ni)$_2$(μ;η^3:η^1:η^1-P$_4$biphenCl)][GaCl$_4$] ($C_{46}H_{66}P_4Cl_5NiGa$): C: 49.90 H: 6.01; found (%): C: 50.02 H: 5.94

ESI(+) MS (*o*-DFB): *m/z* (%) = 895.2 (100) [(Cp´´´Ni)$_2$(μ;η^3:η^1:η^1-P$_4$biphenCl)]$^+$

NMR (CD_2Cl_2, 298 K): **^{1}H**: δ/ppm = 0.89 (s, 9 H, $C(CH_3)_3$), 1.11 (s, 9 H, $C(CH_3)_3$), 1.25 (s, 9 H, $C(CH_3)_3$), 1.38 (s, 9 H, $C(CH_3)_3$), 1.40 (s, 9 H, $C(CH_3)_3$), 1.42 (s, 9 H, $C(CH_3)_3$), 4.69 (s, 1 H, $C_5H_2{}^tBu_3$), 5.20 (s, 1 H, $C_5H_2{}^tBu_3$), 5.54 (s, 1 H, $C_5H_2{}^tBu_3$), 5.60 (s, 1 H, $C_5H_2{}^tBu_3$), 7.53 (m, 2 H, biphen), 7.61 – 7.80 (m (br), 4 H, biphen), 8.00 (m, 2 H, biphen)

^{31}P{^{1}H}: δ/ppm = - 31.9 (br, 1 P), 80.6 (br, 1 P), 84.1 (dd, $^1J_{PP}$ = 246.9, $^2J_{PP}$ = 112.1 Hz, 1 P), 146.6 (ddd, $^1J_{PP}$ = 392.2 Hz, $^2J_{PP}$ = 112.1 Hz, $^2J_{PP}$ = 69 Hz, 1 P)

^{31}P: δ/ppm = 84.1 (br, 1 P), 146.6 (m, 1 P); other signals are not observed due to significant line broadening

*[(Cp´´´Ni)$_2$(μ;η^3-η^3-P$_3$)][GaCl$_4$] (**4**)*

A colourless solution of $GaCl_3$ (36 mg, 0.2 mmol, 1 eq.) in *o*-DFB (4 mL) was added to a bright orange solution of **1** (78 mg, 0.2 mmol, 1 eq.) in *o*-DFB (4 mL), which resulted in an immediate colour change to a dark greenish brown. This solution was stirred for 1 h and then 40 mL of *n*-pentane were added to precipitate a dark brown oil. The slightly yellowish solvent mixture was decanted, the oil washed three times with 10 mL of toluene and another three times with 10 mL of *n*-pentane, each and then dissolved in 3 mL of o-DFB again. This solution was layered with 25 mL of *n*-pentane and stored for four weeks at room temperature, affording dark greenish brown crystals of [(Cp´´´Ni)$_2$(μ;η^3:η^3-P$_3$)][GaCl$_4$] (**4**) in X-ray analysis quality.

Yield: 72 mg (0.074 mmol, 74% based on **1**)

Elemental analysis: calc. (%) for [(Cp´´´Ni)$_2$(μ;η^3:η^3-P$_3$)][GaCl$_4$]·(GaCl$_3$)$_{0.5}$ ($C_{34}H_{58}P_3Cl_{5.5}Ni_2Ga_{1.5}$): C: 41.81 H: 5.99; found (%): C: 42.17 H: 5.82

ESI(+) MS (*o*-DFB): *m/z* (%) = 675.2 (80) [(Cp´´´Ni)$_2$(μ;η^3:η^3-P$_3$)]$^+$, below 300 (several peaks that could not be assigned to certain molecular fragments)

NMR (CD_2Cl_2, 298 K): **^{1}H**: □/ppm = 1.02 (s, 18 H, C(CH$_3$)$_3$), 1.36 (s, 36 H, C(CH$_3$)$_3$), 4.66 (s, 2 H, C$_5$H$_2$^{t}Bu$_3$)

^{31}P{^{1}H}: δ/ppm = 139.5 (s)

^{31}P: δ/ppm = 139.5 (s)

Tested Reactions and Conditions

Attempts to employ $^{t}Bu_2PCl$ or $(Et_2N)_2PCl$ under identical conditions (*o*-DFB, Tl[TEF] equimolar) as for the synthesis of **2a**-**2e**[TEF] failed as no observable colour change or precipitation of a white solid occurred. ^{31}P NMR spectra of the reaction mixtures revealed unreacted halogenophosphanes and **1** at δ = –168.8 ppm. Using two equivalents of Ph_2PCl (0.2 mmol, 44 mg, 35.8 μL, 2 eq.) and Tl[TEF] (0.2 mmol, 234 mg, 2 eq.) with only one equivalent of **1** (0.1 mmol, 38 mg, 1 eq.) under identical conditions did not lead to the anticipated second insertion of $[Ph_2P]^+$ into **2a**$^+$. This reaction rather yielded **2a**[TEF] in similar yields to the reported procedure (*vide supra*) accompanied by $[Ph_2ClPPPh_2]$[TEF], identified by ^{31}P NMR spectra of the reaction solutions. When **1** (0.1 mmol, 38 mg, 1 eq.) is reacted with dihalogenophosphanes $RPCl_2$ (R = Ph, ^{t}Bu; 0.1 mmol) in the presence of two equivalents of Tl[TEF] (0.2 mmol, 234 mg, 2 eq.) the second chloride atom is not abstracted and the reaction outcome are the products **2f**[TEF] and **2g**[TEF]. Excess of Tl[TEF] crystallises from the reaction mixtures upon layering with *n*-hexane and cooling to –30 °C.

3.5.2. X-ray Crystallographic Data

The crystallographic data for all synthesised compounds was collected on either an Xcalibur Gemini (Agilent technologies, AT) with an Atlas^{S2} detector using Mo–K_α (**2a**[SbF_6], **2a**[$GaCl_4$], **2a**[TEF], **2g**[TEF], **3a**[TEF]) radiation (sealed tube), on a SuperNova diffractometer (AT) with a Titan^{S2} detector using Cu–K_β radiation (**2a**[OTf], **2c**[$GaCl_4$], **2e**[TEF], **3b**[$GaCl_4$], **4**[$GaCl_4$]), obtained by using customised optics, or on another SuperNova diffractometer (AT) with a Titan^{S2} detector using a standard Cu–K_α (**2d**[$GaCl_4$]) sealed tube microfocus source. Data reduction and absorption correction were performed with the CrysAlisPro software package.[26] Structure solution and refinement was conducted in Olex2 (1.3-alpha)[27] with ShelXT[28] (solution) and ShelXL-2014[29] (least squares refinement (F^2)) or olex2.refine (Gauss-Newton).[27] All non-H atoms were refined with anisotropic displacement parameters and H atoms were treated as riding models with isotropic displacement parameters and fixed C–H bond lengths (sp^3: 0.96 (CH_3), 0.97 (CH_2); sp^2: 0.93 (CH)). Residual electron density arising from disordered solvent molecules was treated with the integrated solvent mask procedure of Olex2 (1.3 alpha) and visualisation of the crystal structures was done with this program as well.[27]

CCDC-2015036 (**1**), CCDC-2015037 (**2a**[OTf]), CCDC-2015038 (**2a**[SbF_6]), CCDC-2015039 (**2a**[TEF]), CCDC-2015040 (**2a**[$GaCl_4$]), CCDC-2015041 (**2c**[$GaCl_4$] *o*DFB), CCDC-2015042 (**2d**[$GaCl_4$]), CCDC-2015043 (**2e**[TEF]), CCDC-2015044 (**2f$_{endo}$**[$GaCl_4$]), CCDC-2015045 (**3a**[TEF]), CCDC-2015046 (**3b**[$GaCl_4$]) and CCDC-2015047 (**4**[$GaCl_4$] *o*DFB), contain the supplementary crystallographic data for this paper. These data can be obtained free of charge at www.ccdc.cam.ac.uk/contents/retrieving.html (or from the Cambridge Crystallographic Data Centre, 12 Union Road, Cambridge CB2 1EZ, UK; Fax: +44-1223-336-033; e-mail: deposit@ccdc.com.ac.uk).

*Table S 1: Crystallographic and refinement details for compounds **1**, **2a**[OTF], **2a**[SbF_6] and **2a**[TEF].*

Compound	**1**[30]	**2a**[OTf]	**2a**[SbF_6]	**2a**[TEF]
Empirical formula	$C_{17}H_{29}NiP_3$	$C_{30}H_{39}F_3NiO_3P_4S$	$C_{29}H_{39}F_6NiP_4Sb$	$C_{90}H_{78}Al_2F_{72}Ni_2O_8P_8$
Formula weight	385.02	719.26	805.94	3074.66
Temperature/K	123.00(10)	122.98(17)	293(2)	122.7(4)
Crystal system	monoclinic	monoclinic	monoclinic	monoclinic
Space group	$P2_1/n$	$P2_1/n$	$P2_1/n$	$P2_1/n$
a/Å	19.2653(9)	10.49870(10)	10.6938(2)	20.99150(10)
b/Å	14.6055(3)	26.0828(2)	25.2128(4)	22.23550(10)
c/Å	9.2674(4)	12.95300(10)	13.2668(2)	25.32560(10)
α/°	90	90	90	90
β/°	133.487(8)	109.4820(10)	110.963(2)	96.6970(10)
γ/°	90	90	90	90
Volume/Å3	1891.9(2)	3343.91(5)	3340.25(10)	11740.23(9)
Z	4	4	4	4
ρcalcg/cm3	1.352	1.429	1.603	1.740
μ/mm-1	7.840	5.520	1.616	3.115
F(000)	816.0	1496.0	1624.0	6128.0
Crystal size/mm3	0.352 × 0.245 × 0.151	0.383 × 0.293 × 0.111	0.402 × 0.224 × 0.165	0.322 × 0.208 × 0.175
Radiation	Cu Kβ (λ = 1.39222)	Cu Kβ (λ = 1.39222)	Mo Kα (λ = 0.71073)	Cu Kα (λ = 1.54184)
2Θ range for data collection/°	7.906 to 149.05	6.12 to 148.27	6.582 to 64.626	7.028 to 147.352
Index ranges	-26 ≤ h ≤ 22, -12 ≤ k ≤ 20, -11 ≤ l ≤ 12	-13 ≤ h ≤ 14, -35 ≤ k ≤ 30, -17 ≤ l ≤ 16	-15 ≤ h ≤ 15, -34 ≤ k ≤ 37, -19 ≤ l ≤ 19	-24 ≤ h ≤ 26, -27 ≤ k ≤ 27, -23 ≤ l ≤ 31
Reflections collected	10908	28827	31775	101791
Independent reflections	5090 [R_{int} = 0.0372, R_{sigma} = 0.0466]	9012 [R_{int} = 0.0409, R_{sigma} = 0.0359]	10913 [R_{int} = 0.0322, R_{sigma} = 0.0417]	23503 [R_{int} = 0.0302, R_{sigma} = 0.0226]
Data/restraints/parameters	5090/0/199	9012/63/420	10913/0/379	23503/655/2095
Goodness-of-fit on F2	1.017	1.044	1.061	1.019
Final R indexes [I>=2σ (I)]	R_1 = 0.0345, wR_2 = 0.0864	R_1 = 0.0380, wR_2 = 0.1046	R_1 = 0.0343, wR_2 = 0.0702	R_1 = 0.0351, wR_2 = 0.0873
Final R indexes [all data]	R_1 = 0.0386, wR_2 = 0.0906	R_1 = 0.0396, wR_2 = 0.1064	R_1 = 0.0501, wR_2 = 0.0773	R_1 = 0.0382, wR_2 = 0.0900
Largest diff. peak/hole / e Å-3	0.65/-0.49	0.54/-0.73	0.87/-1.15	0.62/-0.41

*Table S 2: Crystallogrraphic and refinement details for compounds **2a**[GaCl4], **2c**[GaCl4], **2d**[GaCl4] and **2e**[TEF].*

Compound	**2a**[$GaCl_4$]	**2c**[$GaCl_4$]	**2d**[$GaCl_4$]	**2e**[TEF]
Empirical formula	$C_{29}H_{39}Cl_4GaNiP_4$	$C_{64}H_{106}Cl_8F_2Ga_2Ni_2P_8$	$C_{157}Cl_{20}Ga_5H_{213}Ni_5P_{20}$	$C_{140}H_{140}Al_4F_{144}Ni_4O_{16}P_{16}$
Formula weight	781.71	1701.70	4070.81	5652.79
Temperature/K	293(2)	123.00(12)	122.9(3)	123.01(10)
Crystal system	monoclinic	monoclinic	monoclinic	triclinic
Space group	$P2_1/n$	$P2_1/n$	$P2_1/n$	P-1
a/Å	10.3088(18)	10.30213(12)	23.5978(3)	19.4947(11)
b/Å	37.3289(11)	16.4498(2)	26.0263(3)	24.9584(14)
c/Å	17.239(3)	23.1565(3)	31.9826(3)	25.7834(14)
α/°	90	90	90	64.002(6)
β/°	149.06(5)	95.0842(12)	107.3890(10)	73.289(5)
γ/°	90	90	90	71.681(5)
Volume/Å3	3411(2)	3908.84(9)	18744.8(4)	10538.0(12)
Z	4	2	4	2
ρcalcg/cm3	1.522	1.446	1.442	1.781
μ/mm-1	1.862	6.657	5.898	4.384
F(000)	1600.0	1764.0	8360.0	5616.0
Crystal size/mm3	0.681 × 0.324 × 0.126	0.339 × 0.205 × 0.082	0.272 × 0.077 × 0.057	0.242 × 0.23 × 0.179
Radiation	Mo Kα (λ = 0.71073)	Cu Kβ (λ = 1.39222)	Cu Kα (λ = 1.54184)	Cu Kβ (λ = 1.39222)
2Θ range for data collection/°	7.028 to 64.43	5.958 to 139.876	6.792 to 148.454	4.752 to 150.572
Index ranges	$-14 \le h \le 15$, $-30 \le k \le 53$, $-24 \le l \le 18$	$-13 \le h \le 13$, $-21 \le k \le 18$, $-30 \le l \le 30$	$-29 \le h \le 29$, $-23 \le k \le 32$, $-29 \le l \le 39$	$-21 \le h \le 27$, $-33 \le k \le 34$, $-35 \le l \le 34$
Reflections collected	18408	27605	104837	110292
Independent reflections	10619 [R_{int} = 0.0384, R_{sigma} = 0.0815]	9585 [R_{int} = 0.0304, R_{sigma} = 0.0298]	36561 [R_{int} = 0.0598, R_{sigma} = 0.0597]	56269 [R_{int} = 0.0648, R_{sigma} = 0.0843]
Data/restraints/parameters	10619/0/361	9585/36/458	36561/288/1975	56269/4534/4740
Goodness-of-fit on F2	1.076	1.028	1.022	1.029
Final R indexes [I>=2σ (I)]	R_1 = 0.0514, wR_2 = 0.0861	R_1 = 0.0309, wR_2 = 0.0824	R_1 = 0.0543, wR_2 = 0.1327	R_1 = 0.0714, wR_2 = 0.1818
Final R indexes [all data]	R_1 = 0.0744, wR_2 = 0.0965	R_1 = 0.0336, wR_2 = 0.0845	R_1 = 0.0739, wR_2 = 0.1437	R_1 = 0.1111, wR_2 = 0.2293
Largest diff. peak/hole / e Å-3	0.88/-0.66	0.57/-0.51	0.92/-0.73	0.99/-0.91

*Table S 3: Crystallogrraphic and refinement details for compounds **2f**$_{endo}$[TEF], **3a**[TEF], **3b**[$GaCl_4$] and **4**[$GaCl_4$].*

Compound	**2f**$_{endo}$[TEF]	**3a**[TEF]	**3b**[$GaCl_4$]	**4**[$GaCl_4$]
Empirical formula	$C_{39}H_{34}AlClF_{36}NiO_4P_4$	$C_{50}H_{58}AlBr_3F_{36}Ni_2O_4P_4$	$C_{46}H_{66}Cl_5GaNi_2P_4$	$C_{113}Cl_{12}F_2Ga_3H_{190}Ni_6P_9$
Formula weight	1495.68	1914.97	1107.25	2852.19
Temperature/K	293(2)	293(2)	122.99(13)	293(2)
Crystal system	monoclinic	triclinic	triclinic	trigonal
Space group	$P2_1/n$	$P\bar{1}$	P-1	R-3
a/Å	15.4562(5)	10.5753(4)	10.4773(5)	62.3366(8)
b/Å	12.8245(4)	17.8782(7)	14.5388(8)	62.3366(8)
c/Å	28.0794(11)	20.7325(8)	18.7053(11)	17.8833(5)
α/°	90	108.035(3)	105.393(5)	90
β/°	96.820(3)	103.509(3)	105.799(5)	90
γ/°	90	101.557(3)	97.951(5)	120
Volume/Å3	5526.5(3)	3462.9(2)	2574.3(3)	60182(2)
Z	4	2	2	18
ρcalcg/cm3	1.798	1.837	1.428	1.417
μ/mm-1	0.693	2.518	7.587	5.121
F(000)	2968.0	1896	1148.0	26748.0
Crystal size/mm3	0.702 × 0.659 × 0.368	0.328 × 0.177 × 0.141	0.3 × 0.2 × 0.1 (estimated	0.538 × 0.351 × 0.292
Radiation	Mo Kα (λ = 0.71073)	Mo Kα (λ = 0.71073)	Cu Kβ (λ = 1.39222)	CuKα (λ = 1.54184)
2Θ range for data collection/°	6.568 to 64.97	6.538 to 64.868	4.676 to 119.1	6.572 to 149.804
Index ranges	$-19 \le h \le 22$, $-18 \le k \le 19$, $-42 \le l \le 40$	$-13 \le h \le 15$, $-18 \le k \le 26$, $-31 \le l \le 29$	$-11 \le h \le 12$, $-17 \le k \le 17$, $-22 \le l \le 12$	$-75 \le h \le 76$, $-71 \le k \le 77$, $-20 \le l \le 17$
Reflections collected	53485	31980	16125	98135
Independent reflections	18349 [R_{int} = 0.0236, R_{sigma} = 0.0300]	21606 [R_{int} = 0.0258, R_{sigma} = 0.0680]	9775 [R_{int} = 0.0394, R_{sigma} = 0.0718]	26099 [R_{int} = 0.0603, R_{sigma} = 0.0432]
Data/restraints/parameters	18349/1072/1457	21606/18/974	9775/151/646	26099/408/1556
Goodness-of-fit on F2	1.038	1.053	1.026	1.047
Final R indexes [I>=2σ (I)]	R_1 = 0.0778, wR_2 = 0.2092	R_1 = 0.0497, wR_2 = 0.0865	R_1 = 0.0561, wR_2 = 0.1344	R_1 = 0.0477, wR_2 = 0.1250
Final R indexes [all data]	R_1 = 0.0958, wR_2 = 0.2252	R_1 = 0.0799, wR_2 = 0.0978	R_1 = 0.0761, wR_2 = 0.1493	R_1 = 0.0532, wR_2 = 0.1326
Largest diff. peak/hole / e Å-3	1.85/-1.30	1.00/-0.58	0.83/-0.51	0.92/-0.63

1

A different polymorph of **1** has already been described previously.[30] Compound **1** crystallized from a concentrated *n*-hexane solution, which was stored at –30 °C for one day. It forms large bright red blocks with the space group $P2_1/n$ containing a single molecule in the asymmetric unit. The respective solid state structure is shown in Figures S1.

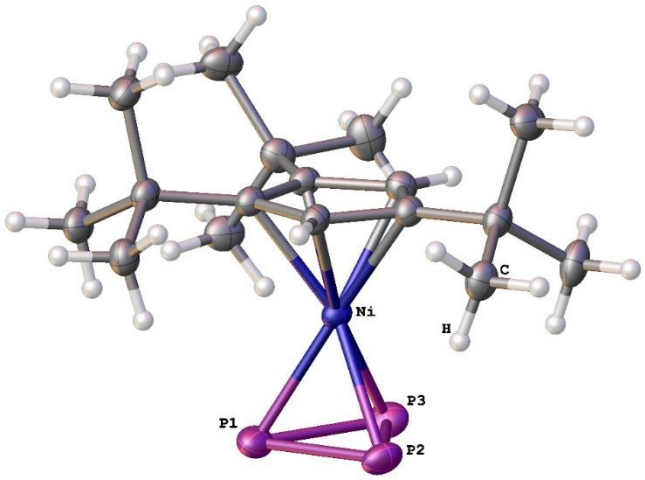

*Figure S 1: The asymmetric unit of **1**, ADPs are drawn at the 50% probability level; Selected bond lengths [Å] and angles [°]: P1-P2 2.1410(8), P1-P3 2.1425(7), P2-P3 2.1488(8), Ni-P1 2.2427(5), Ni-P2 2.2455(6), Ni-P3 2.2357(6), P1-P2-P3 59.93(3), P2-P3-P1 59.86(3), P2-P1-P3 60.22(3).*

***2a**[OTf]*

Compound **2a**[OTf] crystallised from a concentrated solution in *o*-DFB, which was layered with *n*-hexane (8:1) and stored for several days at room temperature. It crystallizes as large dark red plates with the space group $P2_1/n$ containing one anion and one cation in the asymmetric unit. The solid state structure is shown in Figure S2.

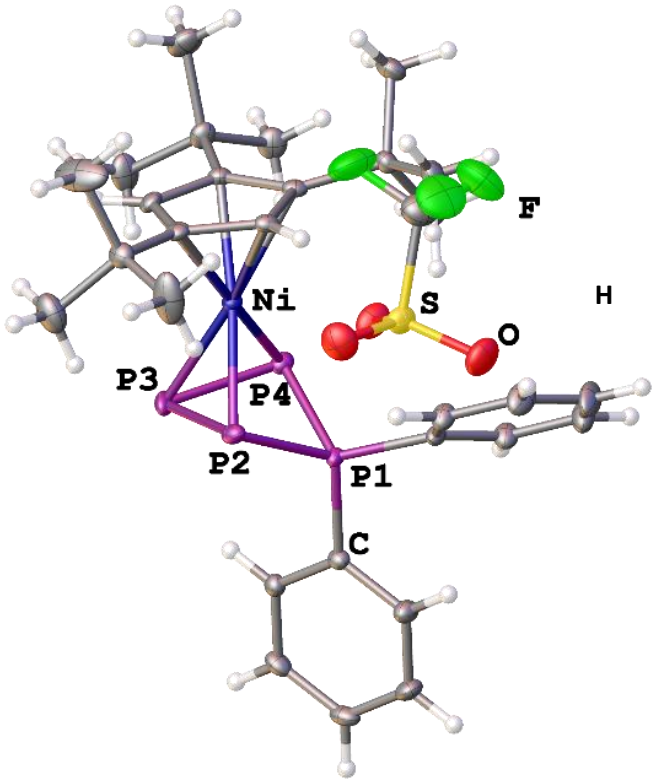

Figure S 2: The asymmetric unit of 2a[OTf], ADPs are drawn at the 50% probability level; Selected bond lengths [Å] and angles [°]: P1-P2 2.1723(6), P1-P4 2.1740(5), P2-P3 2.1984(6), P3-P4 2.1889(6), P2-Ni 2.2743(5), P3-Ni 2.2154(5), P4-Ni 2.2778(5), P1-P2-P3 83.66(2), P2-P3-P4 87.48(2), P3-P4-P1 83.84(2), P2-P1-P4 88.51(2), P3-P4-P2-P1 136.21(4).

***2a**[SbF$_6$]*

Compound **2a**[SbF_6] crystallised from a concentrated solution in *o*-DFB, which was layered with *n*-hexane (8:1) and stored for several days at room temperature. It crystallizes as large dark red plates with the space group $P2_1/n$ containing one anion and one cation in the asymmetric unit. The solid state structure is shown in Figure S3.

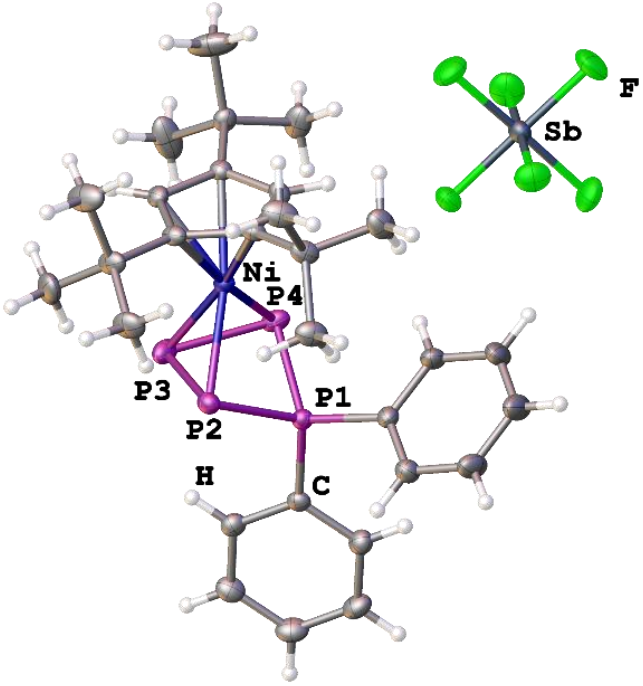

*Figure S 3: Asymmetric unit of **2a**[SbF$_6$], ADPs are drawn at the 50% probability level; Selected bond lengths [Å] and angles [°]: P1-P2 2.1727(7), P1-P4 2.1737(7), P2-P3 2.1946(8), P3-P4 2.2002(8), P2-Ni 2.2787(6), P3-Ni 2.2130(6), P4-Ni 2.2786(6), P1-P2-P3 83.39(3), P2-P3-P4 87.58(3), P3-P4-P1 83.23(3), P2-P1-P4 88.80(3), P3-P4-P2-P1 135.47(4).*

***2a**[TEF]*

Compound **2a**[TEF] crystallised by slowly evaporating the solvent of a CH_2Cl_2 solution. Thus, a few red platelets of **2a**[TEF] could be obtained, which crystallizes in the monoclinic space group $P2_1/n$ with two anions and two cations in the asymmetric unit. The structure in solid state is shown in Figure S4. The severe disorder within one of the anions was treated with restraints. The cations are enantiomers to each other and besides that their structural parameters differ only very slightly. Thus, these structural parameters are given for only one of them.

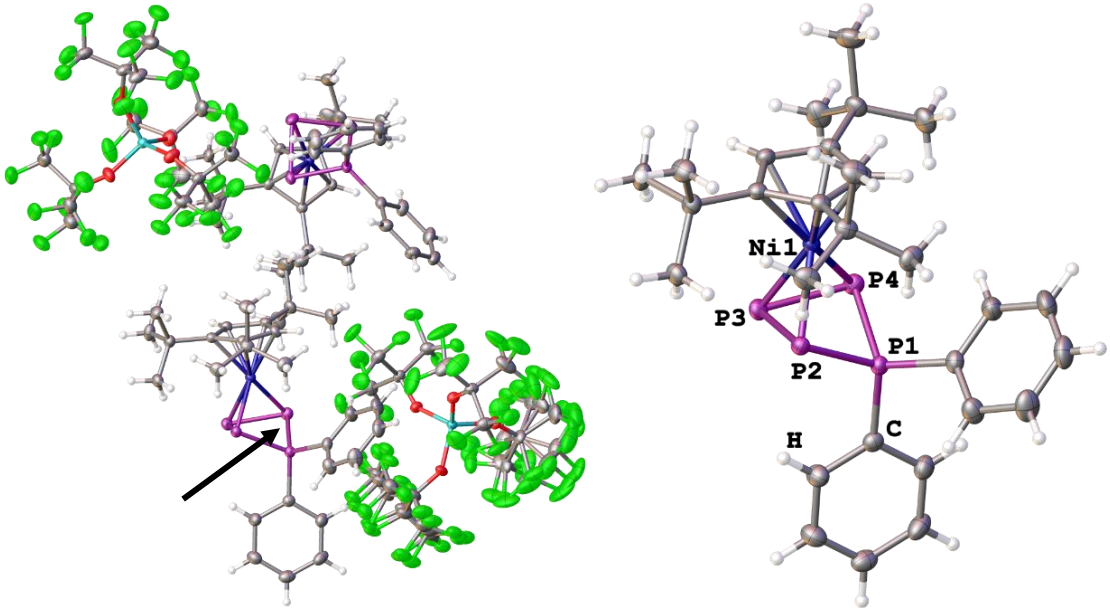

*Figure S 4: Asymmetric unit of **2a**[TEF] (left) and the marked cation denoted with Ni1 (right), ADPs are drawn at the 50% probability level; Selected bond lengths [Å] and angles [°]: P1-P2 2.1659(6), P1-P4 2.1733(6), P2-P3 2.1988(6), P3-P4 2.1967(6), P2-Ni1 2.2598(5), P3-Ni1 2.2192(5), P4-Ni1 2.2867(5), P1-P2-P3 83.56(2), P2-P3-P4 86.93(3), P3-P4-P1 83.44(2), P2-P1-P4 88.35(3), P3-P4-P2-P1 134.70(3).*

***2a**[GaCl₄]*

Compound **2a**[$GaCl_4$] crystallised from a concentrated solution in *o*-DFB, which was layered with *n*-hexane (6:1) and stored for several days at room temperature. It crystallises as large dark red plates with the space group $P2_1/n$ containing one anion and one cation in the asymmetric unit. The structure in solid state is shown in Figure S5.

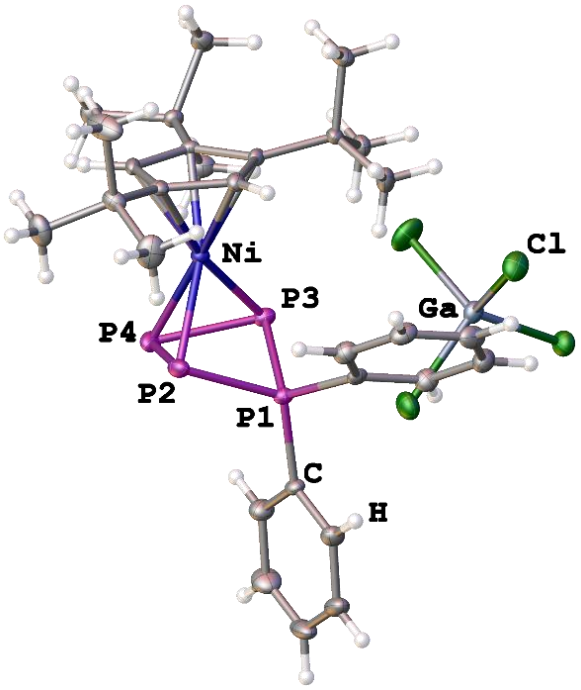

*Figure S 5: Asymmetric unit of **2a**[$GaCl_4$], ADPs are drawn at the 50% probability level; Selected bond lengths [Å] and angles [°]: P1-P2 2.1790(20), P1-P4 2.1731(14), P2-P3 2.1862(16), P3-P4 2.1940(20), P2-Ni 2.2873(12), P3-Ni 2.2281(9), P4-Ni 2.2780(20), P1-P2-P3 84.85(9), P2-P3-P4 87.54 (11), P3-P4-P1 84.80(8), P2-P1-P4 88.17(9), P3-P4-P2-P1 138.83(11).*

***2c**[GaCl$_4$]·(o-DFB)$_{0.5}$*

Compound **2c**[$GaCl_4$] crystallised as an o-DFB solvate from a concentrated solution in *o*-DFB, which was layered with *n*-hexane (6:1) and stored at –30 °C for several days. It forms large dark red plates with the space group $P2_1/n$ containing one anion, one cation and half a molecule of o-DFB in the asymmetric unit. Slight disorder within the $[GaCl_4]^-$ anion could be refined without restraints, but DFIX restraints were used for two of the C–H bonds in the disordered *o*-DFB molecule. The structure in solid state is shown in Figure S6.

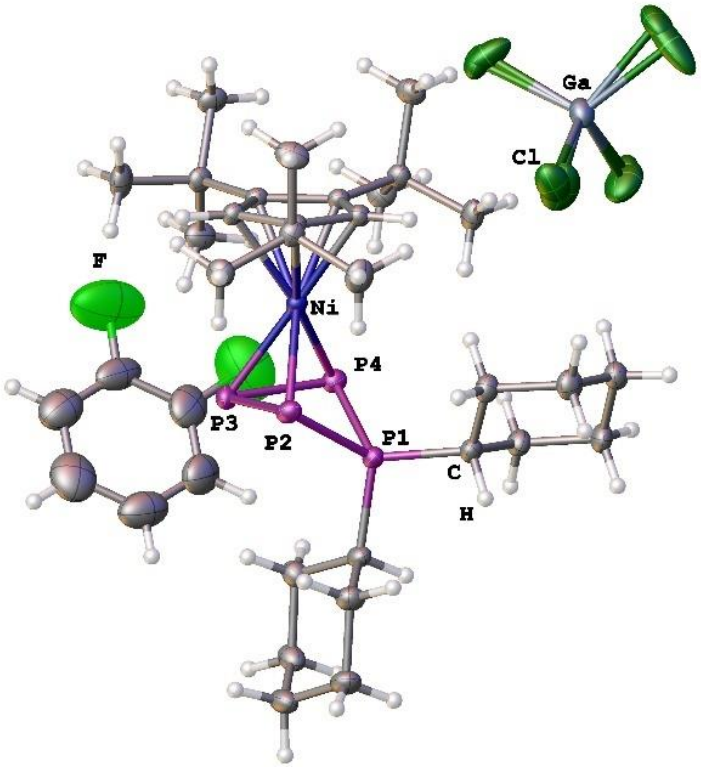

*Figure S 6 Asymmetric unit of **2c**[GaCl$_4$]·(o-DFB)$_{0.5}$, ADPs are drawn at the 50% probability level; Selected bond lengths [Å] and angles [°]: P1-P2 2.1738(6), P1-P4 2.1827(5), P2-P3 2.1922(5), P3-P4 2.1951(6), P2-Ni 2.2788(4), P3-Ni 2.2186(5), P4-Ni 2.2854(4), P1-P2-P3 83.59(2), P2-P3-P4 86.98(2), P3-P4-P1 83.32(2), P2-P1-P4 87.75(2), P3-P4-P2-P1 133.96(3).*

***2d**[GaCl$_4$]·(n-hex)$_{0.4}$*

Layering a concentrated CH_2Cl_2 solution of **2d**[$GaCl_4$] with *n*-hexane (5:1) and storing it at –30 °C for two weeks leads to formation of light red crystals of **2d**[$GaCl_4$]·(*n*-hex)$_{0.4}$. It crystallises in the monoclinic space group P21/n with five cations, five anions and two n-hexane molecules in the asymmetric unit. Disorder within the $[GaCl_4]^-$ anions and one of the Cp´´´ ligands was treated with restraints. Both *n*-hexane molecules are too disordered for proper modelling and thus have been treated with the implemented solvent mask procedure in Olex2.[9] As the structural parameters within the cations only differ very slightly, just those for one of them (Ni1) are given and the structure of the asymmetric unit and the respective cation are provided in Figure S7.

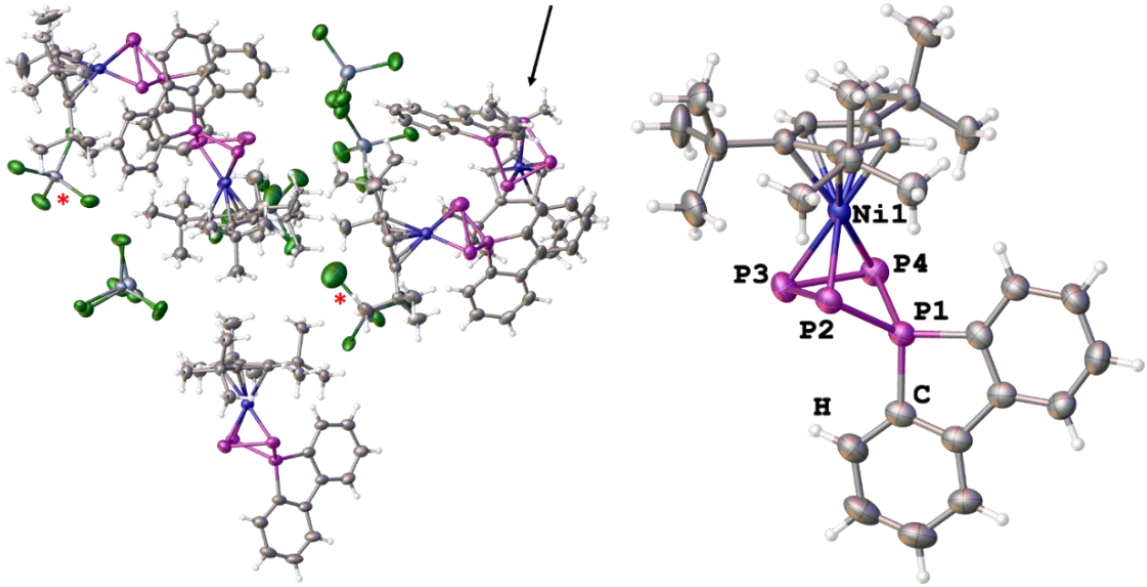

*Figure S 7: Asymmetric unit of **2d**[GaCl$_4$](n-hex)$_{0.4}$, where * marks two disordered parts of one $[GaCl_4]^-$ anion and the arrow points to the cation denoted with Ni1 (left) and the respective structure of this cation (right), ADPs are drawn at the 50% probability level; Selected bond lengths [Å] and angles [°]: P1-P2 2.1629(14), P1-P4 2.1620(14), P2-P3 2.2078(15), P3-P4 2.1919(14), P2-Ni 2.2642(12), P3-Ni 2.2343(13), P4-Ni 2.2952(12), P1-P2-P3 82.59(6), P2-P3-P4 87.53(5), P3-P4-P1 82.97(6), P2-P1-P4 89.46(5), P3-P4-P2-P1 134.74(8).*

***2e**[TEF]*

Red crystals of **2e**[TEF] could be obtained from layering a concentrated solution in *o*-DFB with *n*-hexane (1:10) and storing it at 4 °C for ten days. **2e**[TEF] crystallises in the triclinic space group $P\bar{1}$ with four cations and four anions in the asymmetric unit. Heavy disorder within the anions was treated with restraints, but still leads to comparably bad R values. Thus, structural parameters were considered carefully. As the structural parameters within the cations only differ very slightly, just those for one of them (Ni1) are given and the structure of the asymmetric unit and the respective cation are provided in Figure S8.

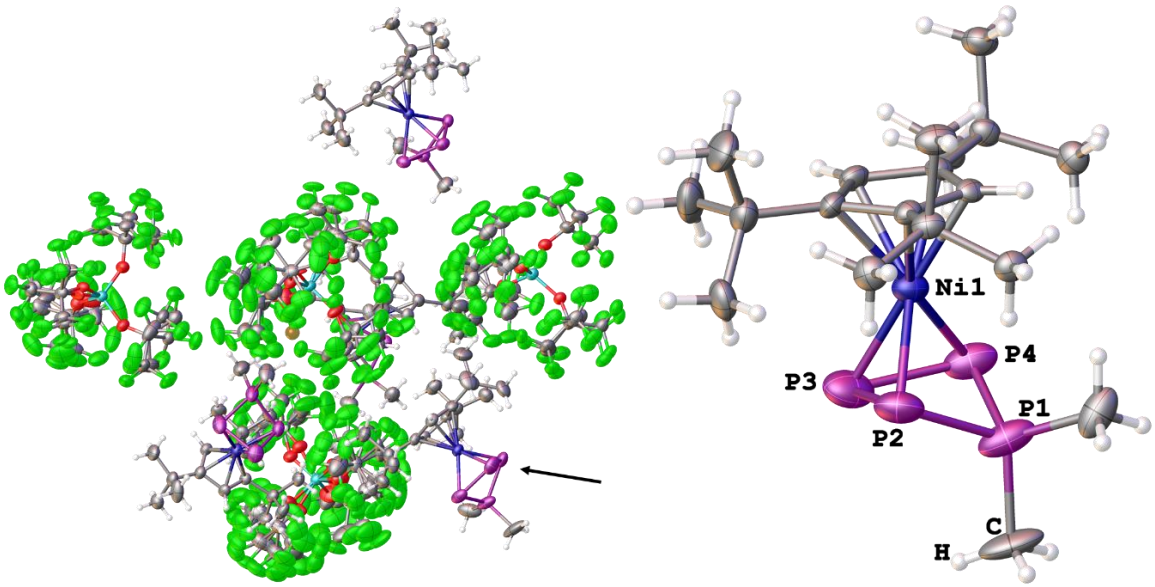

*Figure S 8: Asymmetric unit of **2e**[TEF], where the arrow points to the cation denoted with Ni1 (left) and the respective structure of this cation (right), ADPs are drawn at the 50% probability level; Selected bond lengths [Å] and angles [°]: P1-P2 2.153(2), P1-P4 2.149(2), P2-P3 2.188(2), P3-P4 2.195(2), P2-Ni 2.260(1), P3-Ni 2.199(1), P4-Ni 2.274(1), P1-P2-P3 84.37(9), P2-P3-P4 87.50(8), P3-P4-P1 84.28(10), P2-P1-P4 89.58(7), P3-P4-P2-P1 139.25(9).*

2f$_{endo}$[TEF]

Layering a concentrated solution of **2f**[TEF] in *o*-DFB with *n*-hexane and storing the solution at 4 °C for two weeks, yields bright red crystals of the *endo*-Ph isomer of **2f**[TEF] (Figure S9). The X-ray structural analysis of **2f$_{endo}$**[TEF] revealed its incommensurate modulated structure in the solid state (Figure S10), but the solution and refinement of the average structure yielded a reasonable structural model (R_1 = 7.8%), which may be discussed. Structural parameters were considered carefully. The average structure of **2f$_{endo}$**[TEF] forms a monoclinic lattice with the space group $P2_1/n$, where the asymmetric unit contains one anion and one cation. As a result of the modulation, the structure appears heavily disordered, which especially counts for the $[TEF]^-$ anion. Disorder has been treated with restraints.

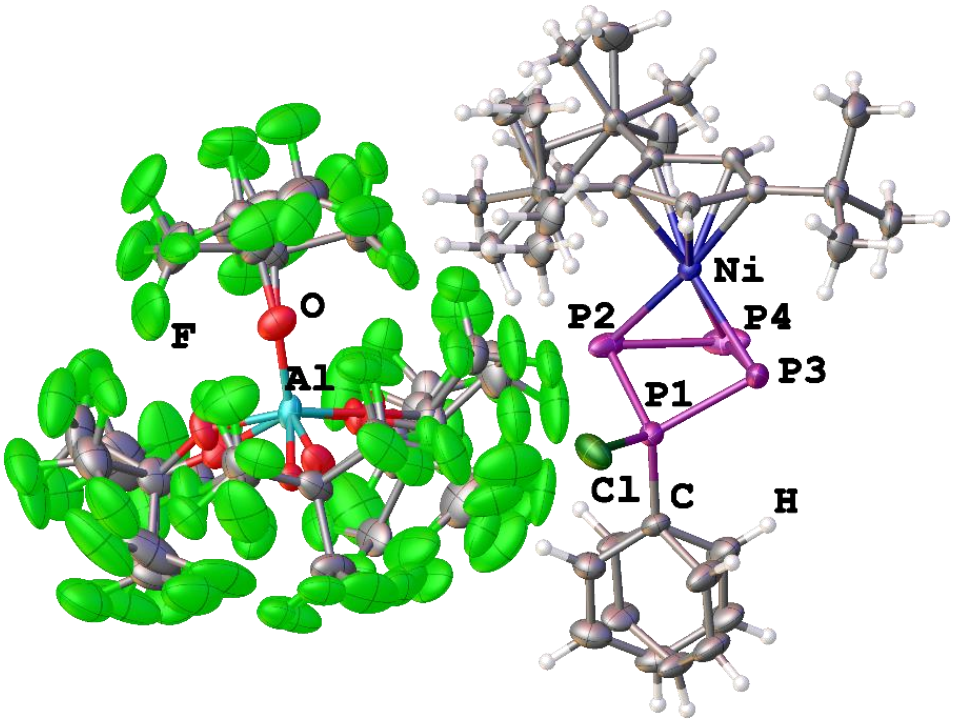

*Figure S 9: Asymmetric unit of the average structure solution of **2f$_{endo}$**[TEF] with ADPs drawn at the 50% probability level; Selected bond lengths [Å] and angles [°]: P1-P2 2.1462(11), P1-P4 2.1471(11), P2-P3 2.1966(17), P3-P4 2.2038(16), P2-Ni 2.2684(9), P3-Ni 2.2141(9), P4-Ni 2.2708(9), P1-Cl 2.0227(11), P1-P2-P3 79.86(5), P2-P3-P4 88.76(5), P3-P4-P1 79.68(4), P2-P1-P4 91.60 (5), P2-P3-P4-P1 130.52(7).*

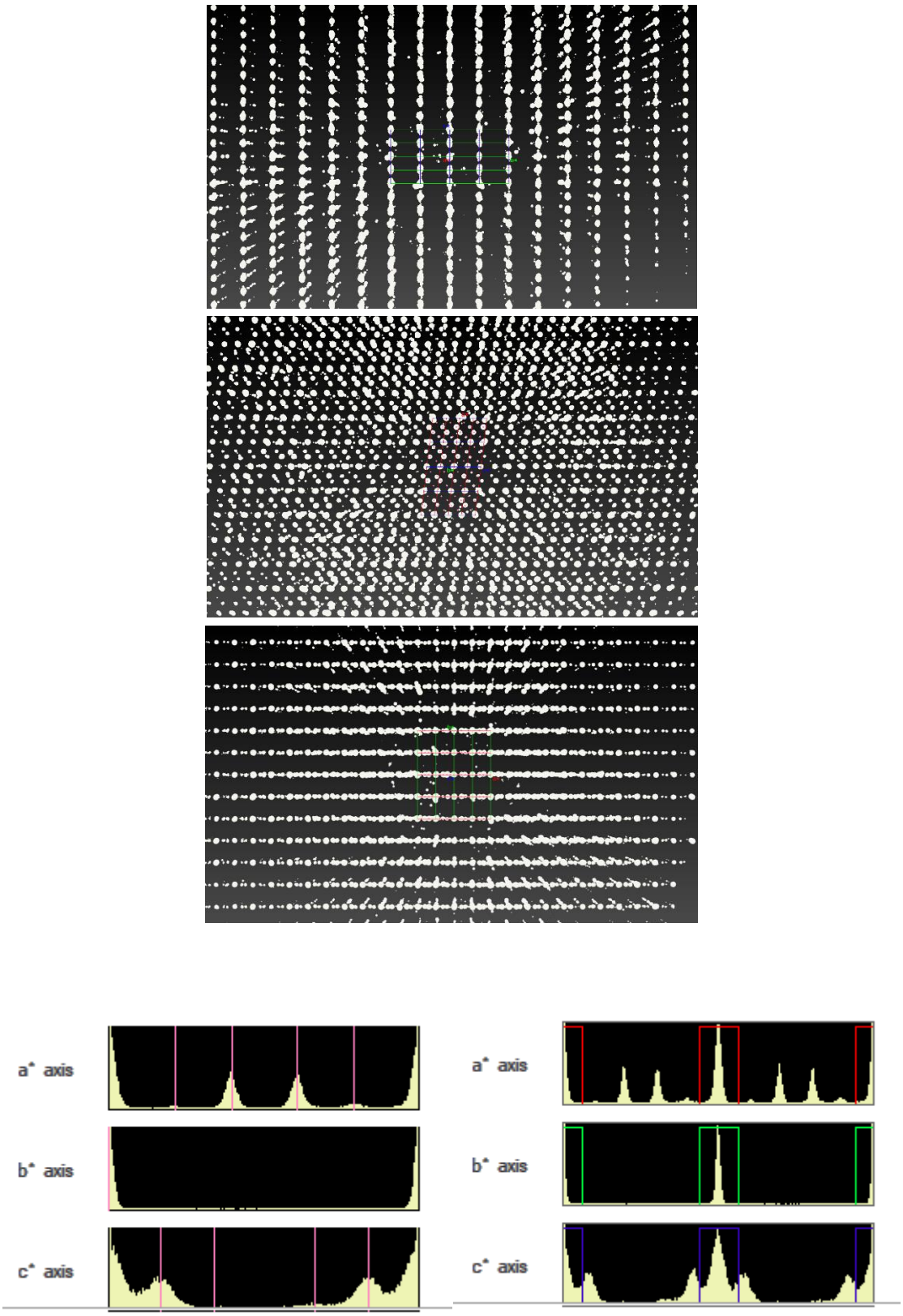

Figure S 10: Views of the reciprocal space of ***2f*** $_{endo}$*[TEF] along the a*(top), b*(middle) and c*(bottom) axis, with clearly visible satellite peaks (along a* and c*) arising from the incommensurate structure of this compound; Bottom: Intensity distribution histograms with (left) and without (right) the refined modulation vector 0.393, 0.0, 0.169 of order 2.*

3a[TEF]

Storing a solution of **3a**[TEF] in CH_2Cl_2 layered with *n*-hexane at room temperature for six days yield dark blackish red crystals. **3a**[TEF] crystallises in the triclinic space group $P\bar{1}$ with one cation and one anion in the asymmetric unit. Disorder within the $[TEF]^-$ anion was treated with SIMU restraints and the solid state structure is shown in Figure S11.

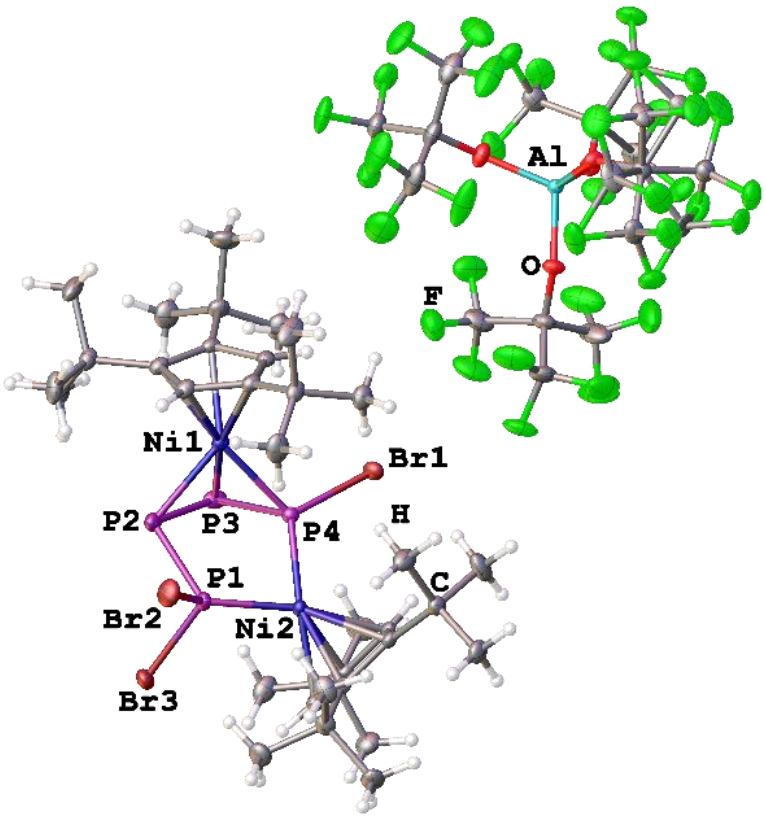

*Figure S 11: Asymmetric unit of **3a**[TEF], ADPs are drawn at the 50% probability level; Selected bond lengths [Å] and angles [°]: P1-P2 2.2228(11), P2-P3 2.1653(12), P3-P4 2.1623(10), P2-Ni1 2.2562(8), P3-Ni1 2.2691(8), P4-Ni1 2.2209(8), P1-Ni2 2.1035(8), P4-Ni2 2.1573(8), P1-Br2 2.2161(8), P1-Br3 2.2194(8), P4-Br1 2.2146(8), P1-P2-P3 100.82(4), P2-P3-P4 86.47(4), P3-P4-Ni2 116.62(4), P1-Ni2-P4 84.96(3), P2-P1-Ni2 117.12(4), Br2-P1-Br3 100.82(3), P3-P4-P2-P1 135.30(6), P3-P4-P2-Ni2 126.93(7).*

3b[GaCl$_4$]

Brownish crystals of **3b**[GaCl$_4$] are obtained from layering a concentrated solution in *o*-DFB with *n*-hexane (6:1) and storing it for two weeks at room temperature. **3b**[GaCl$_4$] crystallises in the triclinic space group $P\bar{1}$ with one cation and one anion in the asymmetric unit (Figure S12). Disorder within the ^{t}Bu groups and the anion were treated with DFIX and SIMU restraints. The crystal movie recording before the X-ray diffraction experiment failed due to issues with the camera. Thus, the dimensions of the crystal are therefore estimated and only multi-scan absorption correction was applied.

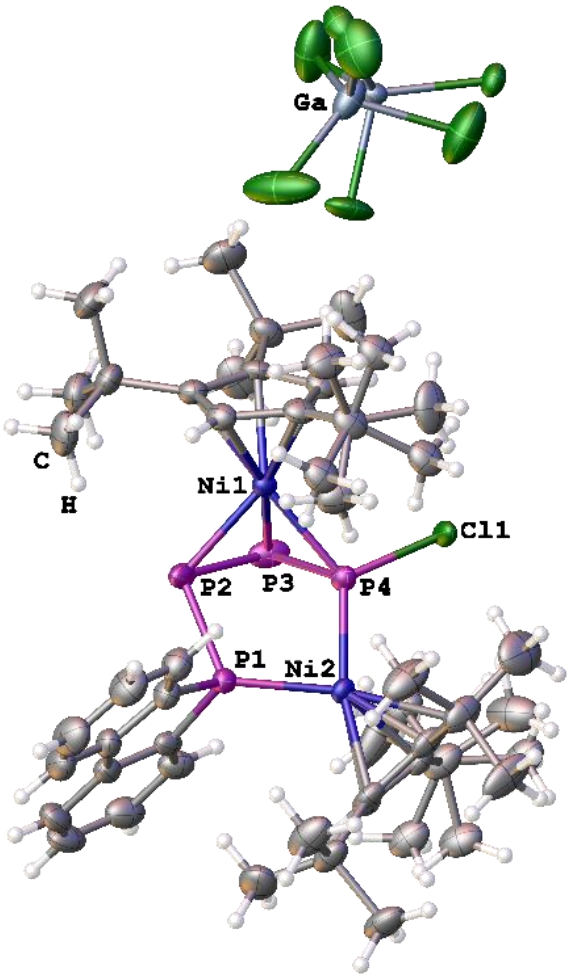

*Figure S 12: Asymmetric unit of **3b**[GaCl$_4$], ADPs are drawn at the 50% probability level; Selected bond lengths [Å] and angles [°]: P1-P2 2.2387(16), P2-P3 2.1450 (20), P3-P4 2.1444(16), P2-Ni1 2.2525(13), P3-Ni1 2.2617(13), P4-Ni1 2.2167(12), P1-Ni2 2.1420(12), P4-Ni2 2.1470(13), P4-Cl1 2.0738(16), P1-P2-P3 100.66(7), P2-P3-P4 85.34(6), P3-P4-Ni2 116.16(7), P1-Ni2-P4 85.79(5), P2-P1-Ni2 113.88(5), P3-P4-P2-P1 –130.58(8), P3-P4-P2-Ni2 –124.67(9).*

4[$GaCl_4$]·(*o*-DFB)$_{0.33}$·(*n*-pent)$_{0.33}$

Layering a concentrated solution of **4**[$GaCl_4$] with *n*-pentane (8:1) and storing it for four weeks at room temperature afforded dark brownish green crystals of the solvate **4**[$GaCl_4$]·(*o*-DFB)$_{0.33}$·(*n*-pent)$_{0.33}$. This compound has the space group $R\bar{3}$ and the asymmetric unit contains three cations, three anions, an *o*-DFB and a strongly disordered *n*-pentane molecule, which was treated with the implemented solvent mask procedure in Olex2 (Figure S13).[9] Disorder within the Cp´´´ ligands, the anions and two of the three P_3 middle decks was treated with restraints and the cation without disorder is selected for description of structural parameters.

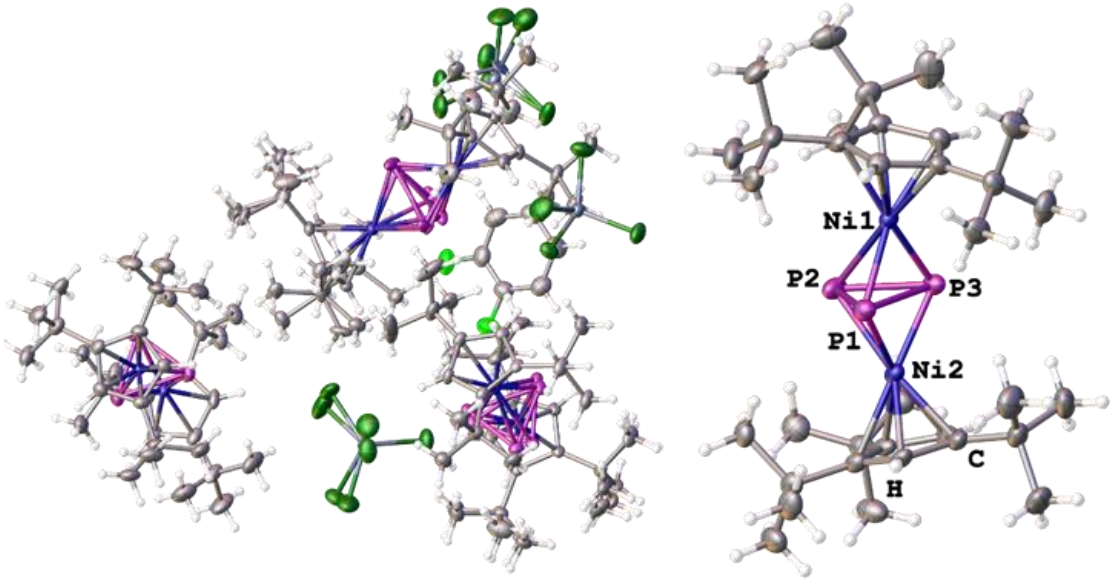

*Figure S 13: Asymmetric unit of **4**[GaCl4]·(o-DFB)0.33·(n-pent)0.33 (left) and the cation without disorder (right), ADPs are drawn at the 50% probability level; Selected bond lengths [Å] and angles [°]: P1-P2 2.2021(11), P1-P3 2.5385(10), P2-P3 2.1975(11), P1-Ni1 2.1842(9), P2-Ni1 2.3566(9), P3-Ni1 2.1831(9), P1-Ni2 2.1746(8), P2-Ni2 2.3920(9), P3-Ni2 2.1786(9), P1-P2-P3 70.48(5), P2-P3-P1 54.84(4), P3-P1-P2 54.68(5), P2-P1-P3-Ni1 82.51(5), P2-P3-P1-Ni2 84.28(6), fold angle in between the planes of the Cp´´´ ligands: 24.48(15).*

3.5.3. NMR Spectroscopic Investigations

Assignment of the signals in the ^{31}P NMR spectra (CD_2Cl_2, r. t.) of the compounds **2a**-**g** is simplified by the broadening of the signal of the former phosphenium ion (P1) compared to the $^{31}P\{^1H\}$ NMR spectrum. The other signals can then be assigned by following the $^1J_{PP}$ couplings around the P_4 ring. For simplification, the $^{31}P\{^1H\}$ and ^{31}P NMR spectra of **2a**-**e** and **2f**/**g** are compared in Figure S14 and Figure S15, respectively. The signals are labelled according to Figure S1b.

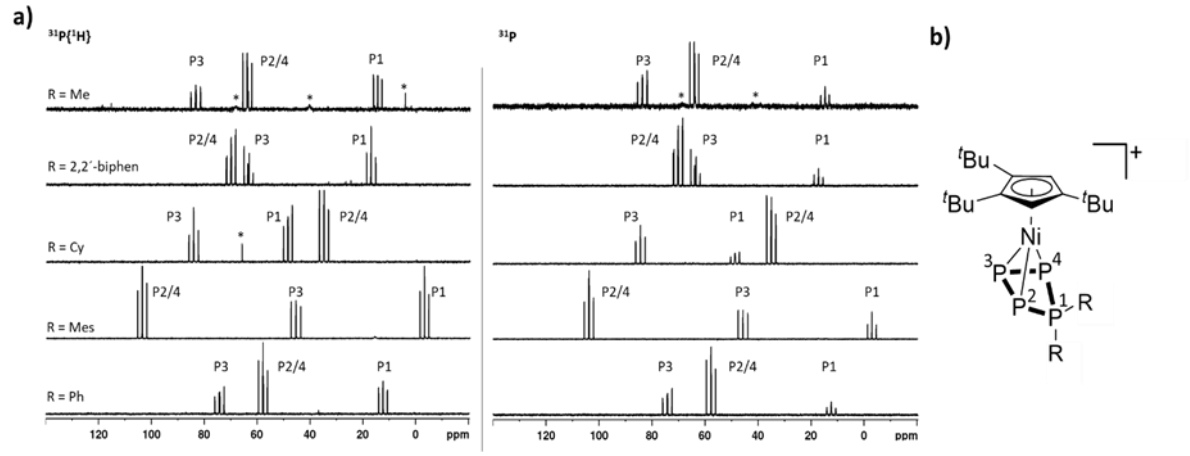

*Figure S 14: ^{31}P and $^{31}P\{^1H\}$ NMR spectra of **2f**-**2g**[TEF] in CD_2Cl_2 recorded at 298 K with signal assignment corresponding to Figure S1b); The endo/exo labelling for **2f** refers to the position of the Ph ring on the P_4 ring.*

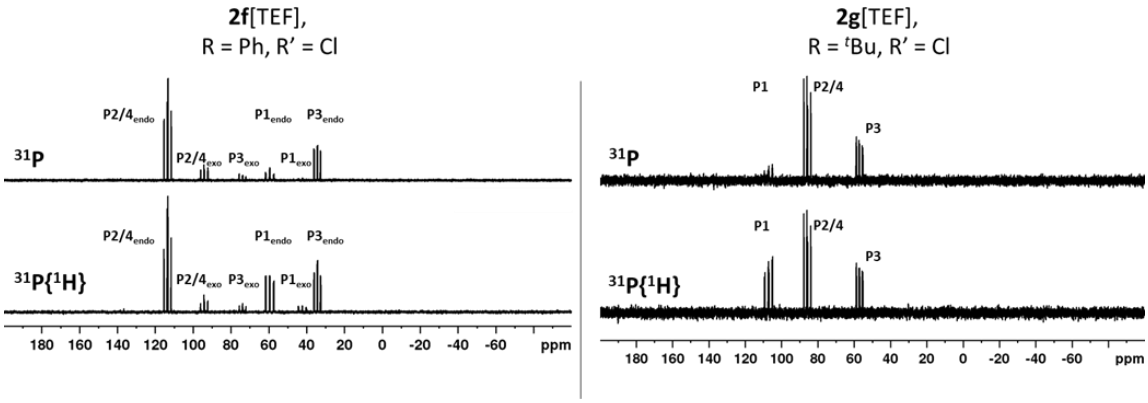

*Figure S 15: a) $^{31}P\{^1H\}$ (left) and ^{31}P NMR spectra (right) of **2a**-**2e**[TEF] in CD_2Cl_2 recorded at 298 K; signal assignment is done according to the structure shown in b) to illustrate the variation of the sequence of the signals with the corresponding P atoms.*

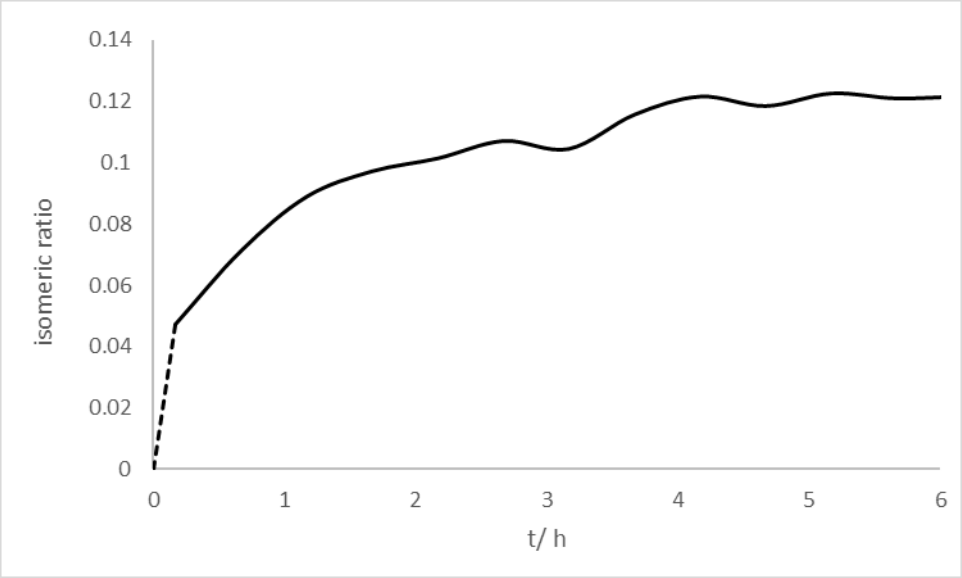

*Figure S 16: Plot of the isomeric ratio **2f**$_{endo}$:**2f**$_{exo}$ against the time after dissolving crystals of **2f**$_{endo}$[TEF] in CD_2Cl_2 obtained from ^{31}P NMR spectra recorded every 30 min for 6 h; The final ratio after 6 h is 8:1, which is very close to that observed for spectra of precipitated **2f** (7:1).*

As both isomers of **2f** are formed during the reaction of **1** with Ph_2PCl and Tl[TEF], the question arises if they exist in equilibrium or if the observed isomeric ratio of 7:1 (**2f**$_{endo}$:**2f**$_{exo}$) is due to kinetic factors during the reaction. Thus, crystals of **2f**$_{endo}$[TEF] were subjected to ^{31}P NMR spectroscopic measurements to gather information about the formation of both isomers of **2f**. Crystals of **2f**$_{endo}$[TEF] were dissolved in 0.8 mL of CD_2Cl_2 and ^{31}P NMR spectra of this sample were recorded every 30 min for 6 h. The plot of the isomeric ratio during this time (Figure S16) shows that the initially present endo isomer slowly interconverts to the exo isomer until an isomeric ratio of 7:1 (**2f**$_{endo}$:**2f**$_{exo}$) is approached after 6 h. This clearly supports the assumption that both isomers exist in equilibrium (in solution) and their formation is not based on kinetic factors during the initial synthesis of **2f**.

The room temperature ^{31}P and $^{31}P\{^1H\}$ NMR spectra of **3a** in CD_2Cl_2 are identical and express an AMNX spin system. An expected similar spectrum is not observed for **3b** in CD_2Cl_2, which

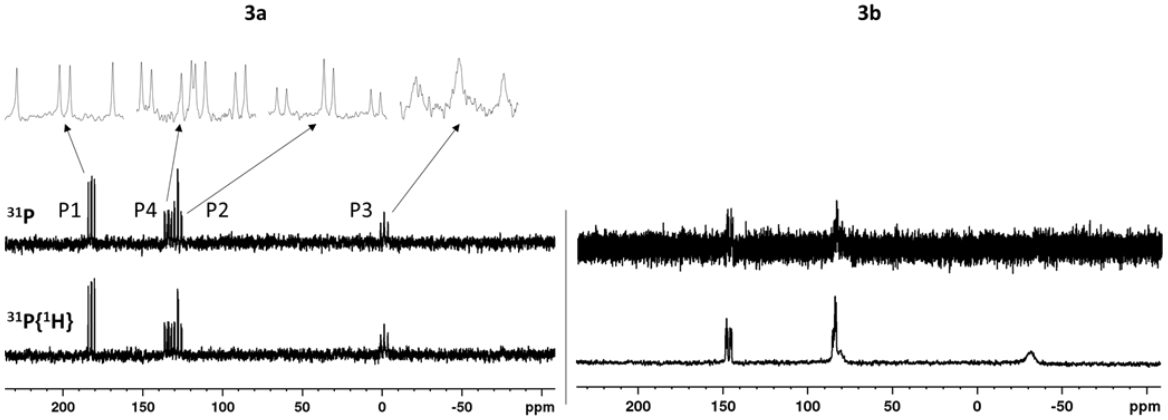

*Figure S 17: ^{31}P (top) and $^{31}P\{^1H\}$ (bottom) NMR spectra of **3a** and **3b** in CD_2Cl_2 recorded at 298 K with zoomed in signals for the spectra of **3a**; The $^{31}P\{^1H\}$ NMR spectrum of **3b** was recorded with 6144 scans to be able to see the full set of four signals, which is not visible for the ^{31}P NMR spectrum (512 scans).*

is probably caused by a dynamic effect involving rotation of the Cp´´´ ligands. Thus, the complete set of four resonances in the spectrum of **3b** is only observed at very high scan numbers (6144), but two of them are significantly broadened (Figure S17).

Only when the solution is cooled to –80 °C sharp signals can be observed. However, at this temperature two sets of signals are found in the $^{31}P\{^{1}H\}$ NMR spectrum (Figure S18), thus indicating the presence of two isomeric forms of **3b$_{1/2}$**. We attribute these isomers to differently rotated Cp´´´ ligands at both Ni centres. As the number of scans needed for recording this spectrum was still very high (8192), the corresponding ^{31}P spectrum could not be recorded and signal assignment was conducted as for **3a** (most downfield shifted signal should be that of P^A due to the similarity with the starting material (2,2´-biphen)PCl). However, the corresponding ^{1}H NMR shows signals in accordance with two isomers of **3b** being present. While the respective signals of the ^{t}Bu and the biphen moieties overlap and thus avoid further interpretation, the region for the $C_5\underline{H}_2{}^{t}Bu_3$ protons is well resolved and allows for integration (Figure S19), which affords an isomeric ratio of 1:1.25.

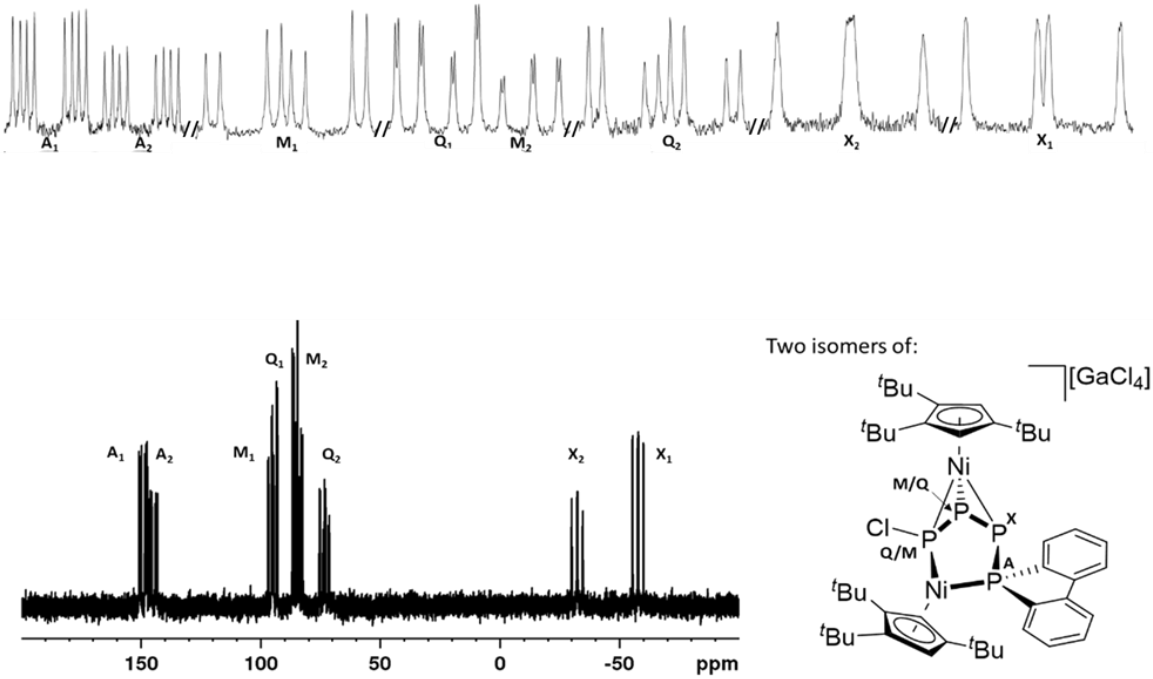

*Figure S 18: $^{31}P\{^{1}H\}$ NMR spectrum of **3b** in CD_2Cl_2 recorded at 193 K with 8192 scans (bottom), zoomed in signal with assignment (top) and structure of **3b** with assigned P atoms (right); Isomerism in the cation **3b** is most probably caused by hindered rotation of the Cp´´´ ligands at this temperature; Spectral parameters: **3b$_1$**: δ/ppm = 149.1 (ddd, $^{1}J_{PA\text{-}PX}$ = 397.1 Hz, $^{2}J_{PA\text{-}PQ}$ = 108.2 Hz, $^{2}J_{PA\text{-}PM}$ = 57.3 Hz, 1 P, P^A), 94.8 (ddd, $^{1}J_{PM\text{-}PX}$ = 346.9 Hz, $^{1}J_{PM\text{-}PQ}$ = 247.2 Hz, $^{2}J_{PM\text{-}PA}$ = 57.3 Hz, 1 P, P^M), 85.7 (ddd, $^{1}J_{PQ\text{-}PM}$ = 247.2 Hz, $^{2}J_{PQ\text{-}PA}$ = 108.2 Hz, $^{2}J_{PQ\text{-}PX}$ = 11.7 Hz, 1 P, P^Q), –57.8 (ddd, $^{1}J_{PX\text{-}PA}$ = 397.13 Hz, $^{1}J_{PX\text{-}PM}$ = 346.9 Hz, $^{2}J_{PX\text{-}PQ}$ = 11.7 Hz, 1 P, P^X); **3b$_2$**: δ/ppm = 144.7 (ddd, $^{1}J_{PA\text{-}PX}$ = 391.2 Hz, $^{2}J_{PA\text{-}PM}$ = 113.2 Hz, $^{2}J_{PA\text{-}PQ}$ = 60.6 Hz, 1 P, P^A), 83.4 (ddd, $^{1}J_{PM\text{-}PQ}$ = 246.2 Hz, $^{2}J_{PM\text{-}PA}$ = 113.2, $^{2}J_{PM\text{-}PX}$ = 11.7 Hz, 1 P, P^M), 73.4 (ddd, $^{1}J_{PQ\text{-}PX}$ = 360.4 Hz, $^{1}J_{PQ\text{-}PM}$ = 246.2 Hz, $^{2}J_{PQ\text{-}PA}$ = 60.6 Hz, 1 P, P^Q), –32.4 (ddd, $^{1}J_{PX\text{-}PA}$ = 391.2 Hz, $^{1}J_{PX\text{-}PQ}$ = 360.4 Hz, $^{2}J_{PX\text{-}PM}$ = 11.7 Hz, 1 P, P^X).*

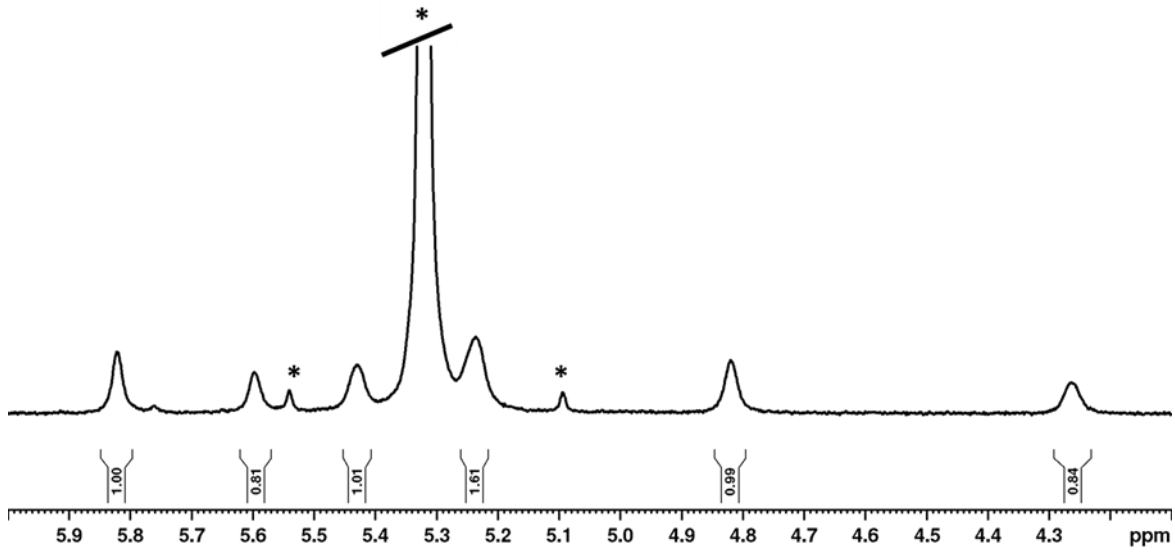

*Figure S 19: ^{1}H NMR spectrum of **3b** in CD_2Cl_2 recorded at 193 K showing two sets of signals for the $C_5\underline{H}_2{}^tBu_3$ protons, thus indicating the presence of two isomers of **3b**$_{1/2}$ in a ratio of 1.25:1; One of the expected signals is probably overlapped by the large solvent signal caused by residual CH_2Cl_2 (*).*

The allylic distortion of the P_3 middle deck in **4** leads to inequivalent P atoms and thus its ^{31}P NMR spectrum should show multiple (two) signals. Similar behaviour is found for the isoelectronic complex [(Cp´´´Co)(Cp´´´Ni)(μ,η^3-P_3)].[31] However, in the room temperature ^{31}P NMR spectrum of **4** in CD_2Cl_2 only one sharp singlet is found, located at δ = 139.5 ppm, which hints towards a dynamic process of the P_3 middle deck in solution. A $^{31}P\{^{1}H\}$ VT NMR study of **4** in CD_2Cl_2 (Figure S20) revealed that this dynamic behaviour is retained even at temperatures as low as 193 K. The only noticeable change in these spectra is the slight shift of the singlet upon cooling of the sample.

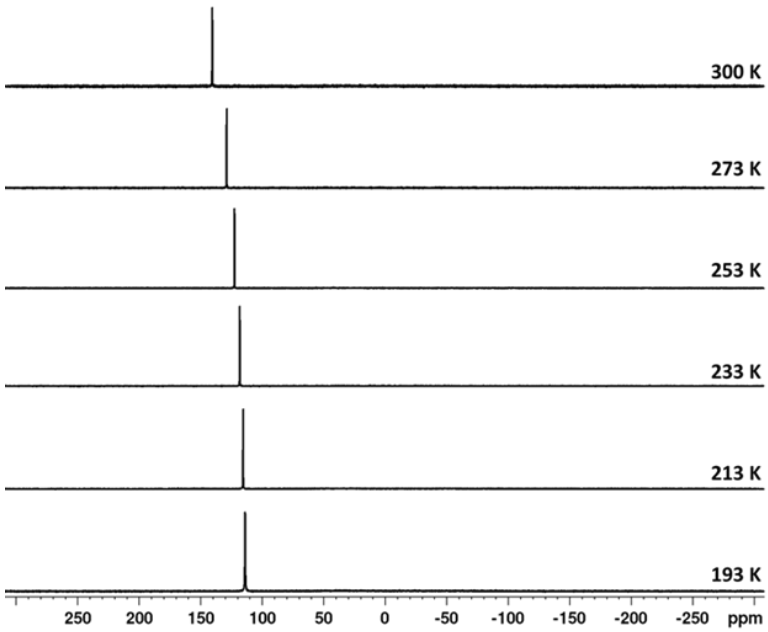

*Figure S 20: $^{31}P\{^{1}H\}$ NMR spectra of **4** in CD_2Cl_2 recorded at different temperatures.*

To get insight into the formation of the dinuclear products **3** an NMR study was carried out to elucidate possible intermediates. Thus, PBr_3 (10 μL, 0.1 mmol, 1 eq.) was added to a freshly prepared solution of **1** (38 mg, 0.1 mmol, 1 eq.) and Tl[TEF] (117 mg, 0.1 mmol, 1 eq.) in 1 mL of *o*-DFB. A capillary with toluene-d^8 and PPh_3 (standard) was added, the NMR tube closed and then shaken. Immediately the solution turned dark brown and the sample was subjected

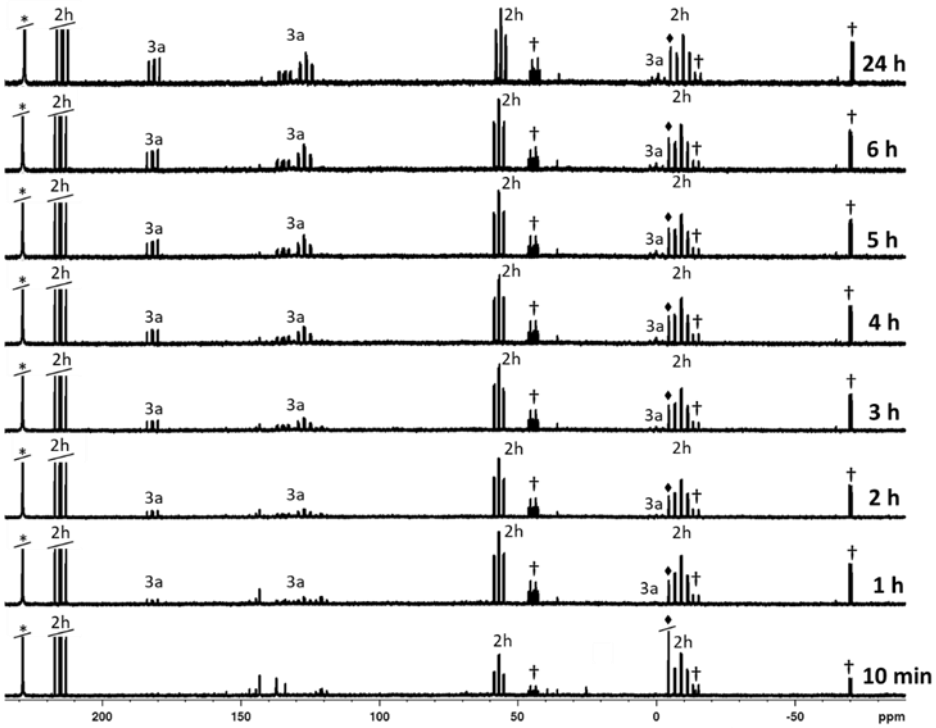

*Figure S 21: $^{31}P\{^1H\}$ NMR spectra of a reaction solution containing 0.1 mmol of **1**, PBr_3 and Tl[TEF] in o-DFB with a capillary containing tol-d^8 and PPh_3 (σ); Spectra were measured hour-wise and additionally another spectrum was measured 24 h after addition of PBr_3; Signals are assigned to the corresponding species **2h**, **3a**, **†** (unidentified side product) and ***** (residual PBr_3).*

to the first measurement (10 min). Afterwards, $^{31}P\{^1H\}$ NMR spectra of the solution were recorded every hour and a final one was collected 24 h after the reaction was started (Figure S21). In the first spectrum the immediate formation of **2h** can be seen, alongside the complete consumption of the starting material **1**. After one hour the formation of **3a** is visible in the spectra and a third species (**†**) also appears but so far eludes structural assignment.

While the intensity of the signals corresponding to **2h** slowly decrease, the ones for **3a** increase and that of **†** stays the same (Figure S22). This data may suggest that **2h** is an intermediate during the reaction of **1** with "$[Br_2P][TEF]$" which finally affords **3a**. Further insight into this reaction could however not be obtained as the precipitation of TlCl and the elongated reaction times (three days with stirring) caused severe problems during NMR spectroscopic investigations. Thus, the plot in figure SI 7 can only be seen having qualitative character.

In one more attempt to get an understanding of this reaction we recorded $^{31}P\{^1H\}$ NMR spectra of reaction solutions (*o*-DFB, C_6D_6 capillary) with a very broad ppm range (Figure S23). Thus, we were able to find P_4 as one of the by-products of the reaction yielding **3a**. Accordingly, a

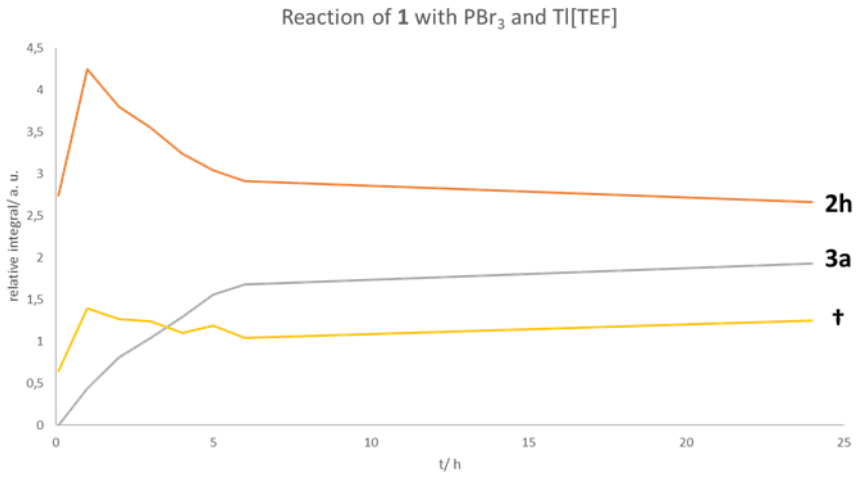

*Figure S 22: Relative signal intensities of **2h**, **3a** and **†** compared to the standard PPh_3 over the course of 24 h; The flattening of the plot is probably caused by the absence of mixing in between the measurements.*

reaction mechanism involving the initial formation of **2h** followed by its fragmentation into P_4 and a {Cp´´´Ni} containing species and the formation of **3a** from this species and another equivalent of **2h** seems to be plausible. However, this complicated reaction pathway involving several species eludes further study so far.

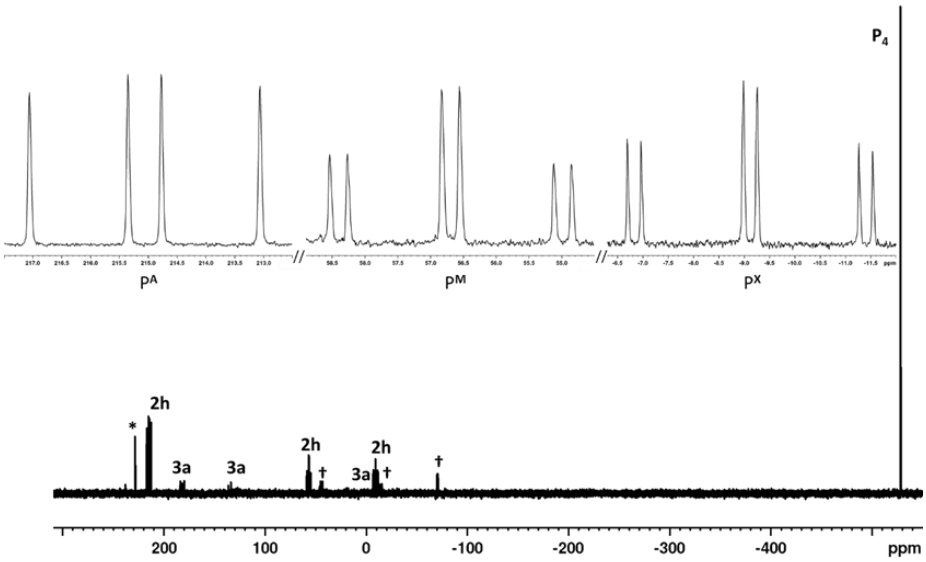

*Figure S 23: Bottom: $^{31}P\{^1H\}$ NMR spectrum of the reaction mixture (0.1 mmol **1**, PBr_3 and Tl[TEF]) in o-DFB (C_6D_6 capillary) recorded at 298 K with a broad ppm range; The singlet at δ = –528.3 ppm clearly shows the formation of P_4 during the reaction; Top: Zoomed in signals assigned to **2h**, which shows a typical A_2MX spectrum; Spectral parameters: δ/ppm = 215.1 (dd, $^1J_{PA-PX}$ = 370.6 Hz, $^1J_{PA-PM}$ = 277.5 Hz, 2P, P^A), 56.7 (td, $^1J_{PM-PA}$ = 277.5 Hz, $^2J_{PM-PX}$ = 44.1 Hz, 1P, P^M), –9.1 (td, $^1J_{PX-PA}$ = 370.6 Hz, $^2J_{PX-PM}$ = 44.1 Hz, 1P, P^X).*

3.5.4. Computational Details

General Considerations

Calculations were carried out using the Gaussian09 software package[31] at the DFT level by means of either the density functional BP86[32] or the hybrid density functional B3LYP.[33] The def2SVP[16] basis set was used for calculations involving both isomers of **2f** and **2g** and the structures of **3a** and **3b**. The def2TZVP[34] basis set was used for calculations on the possible reaction mechanism. Implicit solvent correction was applied via a polarisable continuum model for CH_2Cl_2.[35] NBO analysis of **3a** and **3b** was conducted with the NBO6 software package.[36] Stationary points were verified by analytical frequency calculations. The transition state **TS2** was verified by slightly changing its molecular geometry along its imaginary frequency and then performing geometry optimisations on the obtained structures.

*Selected canonical molecular orbitals of **3a***

To obtain further insight into the electronic structure of **3a** we performed a Mulliken population analysis on its optimized geometry. While most of the canonical frontier orbitals (HOMO-5 to LUMO+1, Figure S24) are smeared across large parts of the cation, the orbital contributions of P1 and P4 in the HOMO-4 (Significant orbital contributions: Ni2(d) = 20 %, P1(p) = 7 %, P4(p) = 6 %) may yield a possible explanation for the relatively high $^2J_{P-P}$ coupling constant found in the ^{31}P NMR spectra of **3a**. The bonding motif found for P1-Ni2-P4 in the HOMO-4 resembles an allylic-type interaction.

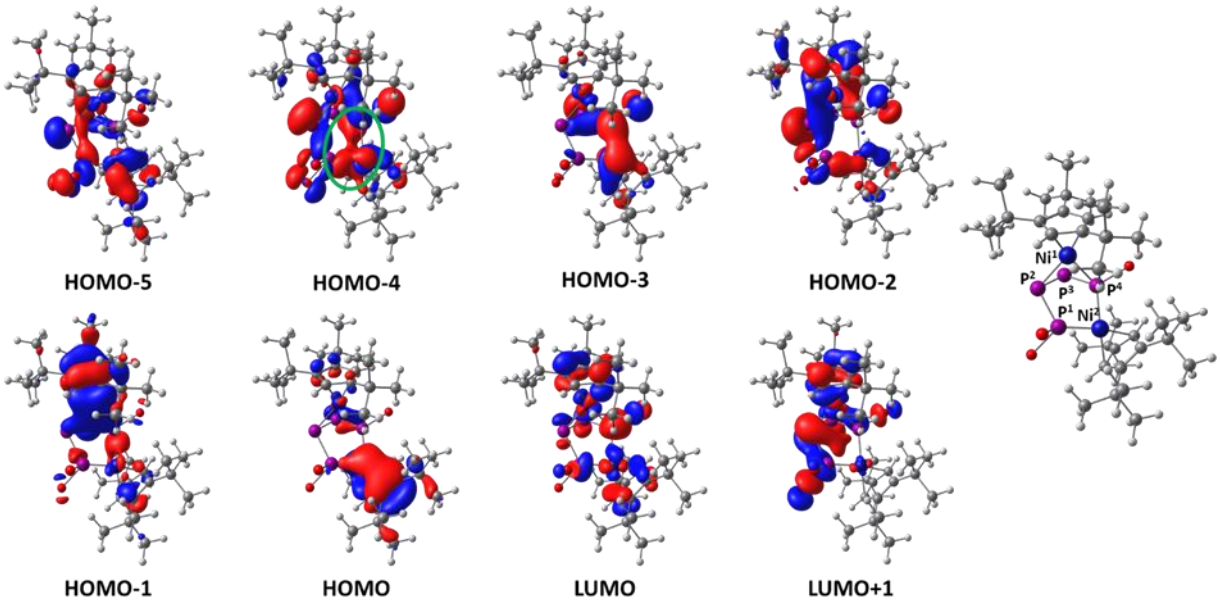

*Figure S 24: Canonical frontier orbitals of **3a**; The allylic part of the HOMO-4, which is stretched across P1, Ni2 and P4 is marked in green, isosurfaces are drawn with both signs and at a 0.03 contour value.*

Optimized Geometries

[CpNi(η^3-P_3)]:

BP86/def2TZVP: Energies/H = –2726.415940, Enthalpies/H = –2726.414996, Free Energies/H = –2726.462662, ZPVE/ kJ/mol = 227.85 (ZPVE = zero point vibrational energies)

Symbol	X	Y	Z
Ni	0.2315880	0.0003550	-0.0002530
P	-1.6581020	0.1405030	1.2453800
P	-1.6588170	-1.1486330	-0.5009340
P	-1.6599450	1.0076390	-0.7439290
C	1.9482110	-1.2180120	-0.0684430
C	1.9470460	0.9456500	0.7719540
C	1.9476030	-0.4439540	1.1363480
H	1.9453280	-0.8386160	2.1488960
C	1.9472350	-0.3099050	-1.1810320
C	1.9493720	1.0258080	-0.6589600
H	1.9451030	1.9402720	-1.2462460
H	1.9476710	1.7873270	1.4593890
H	1.9452950	-2.3031370	-0.1298310
H	1.9483070	-0.5859450	-2.2320710

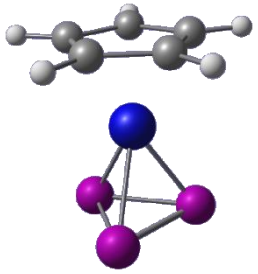

[Me_2P]$^+$:

BP86/def2TZVP: Energies/H = –420.933417, Enthalpies/H = –420.932473, Free Energies/H = –420.966318, ZPVE/ kJ/mol = 182.86

Symbol	X	Y	Z
C	1.3970920	-0.4638670	-0.0245410
H	2.2782590	-0.0007810	-0.4883890
H	1.6232810	-0.5021650	1.0746510
H	1.2053900	-1.4928920	-0.3534430
C	-1.3971220	-0.4638380	0.0245590
H	-2.2786000	-0.0005020	0.4875270
H	-1.6224530	-0.5030140	-1.0747920
H	-1.2055490	-1.4926400	0.3542600

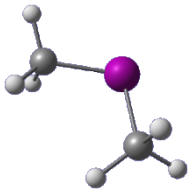

*[CpNi(η^3-P_4Me_2)]$^+$ (**I2**):*

BP86/def2TZVP: Energies/H = –3147.407361, Enthalpies/H = –3147.406417, Free Energies/H = –3147.467349, ZPVE/ kJ/mol = 424.86

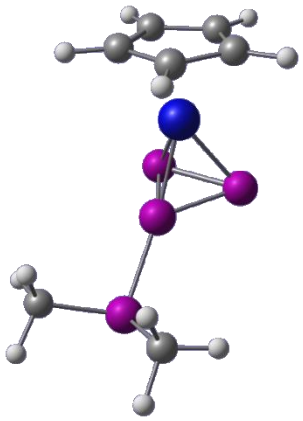

Symbol	X	Y	Z
Ni	-1.1354880	0.0281460	-0.0004480
P	3.2133650	-0.0222500	0.0308580
P	-0.1746150	-1.7721380	1.1066150
P	1.0156070	-0.3347520	0.0516700
P	-0.1268880	-1.7511780	-1.0851130
C	-2.0787760	1.6676670	0.9182250
C	-3.2114140	0.0616430	-0.3109570
C	-2.9171680	0.5176520	1.0209600
H	-3.2587120	0.0533110	1.9418490
C	-1.8646440	1.9345840	-0.4837250
C	-2.5725560	0.9507550	-1.2396520
H	-2.6069620	0.8771180	-2.3228540
C	3.3926220	1.2146770	1.3918260
C	3.3771280	1.0295710	-1.4799650
H	4.4457130	1.2900930	-1.5432480
H	3.1137260	0.4437930	-2.3698380
H	2.7870510	1.9536960	-1.4392070
H	2.7873060	2.1181790	1.2467240
H	3.1569080	0.7450120	2.3551140
H	4.4580050	1.4950690	1.3970920
H	-3.8151020	-0.8044620	-0.5682400
H	-1.6742630	2.2431000	1.7461380
H	-1.2631750	2.7424850	-0.8917120

*[CpNi(η^3-P_4Me_2)]$^+$ (**TS2**):*

BP86/def2TZVP: Energies/H = –3147.399502, Enthalpies/H = –3147.398558, Free Energies/H = –3147.458166, ZPVE/ kJ/mol = 422.58

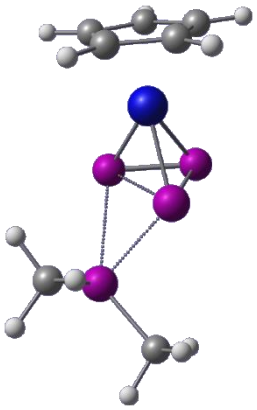

Symbol	X	Y	Z
Ni	-1.1158950	-0.0587770	-0.0207480
P	2.8839640	0.2073760	0.4226840
P	0.4276800	-0.7474120	1.3923110
P	0.9364150	-0.3681810	-0.8503960
P	-0.0803630	-2.1539330	-0.1211310
C	-1.9847070	1.8377560	-0.2372500
C	-3.1046150	-0.0092440	0.5885650
C	-2.4581740	1.2220070	0.9584250
H	-2.3363370	1.6004450	1.9692870
C	-2.3647010	1.0024850	-1.3555270
C	-3.0651360	-0.1246470	-0.8465860
H	-3.4696500	-0.9472030	-1.4295780
C	2.5662740	2.0261340	0.5041300
C	3.9787380	0.0923470	-1.0732940
H	4.9648770	0.4650240	-0.7501060
H	4.0908910	-0.9586340	-1.3696080
H	3.6188640	0.6901840	-1.9218420
H	2.2284000	2.4575710	-0.4478800
H	1.8372730	2.2453140	1.2949390
H	3.5258180	2.4904640	0.7824410
H	-3.5588960	-0.7209510	1.2727400
H	-1.4342030	2.7723220	-0.3019010
H	-2.1434750	1.2024630	-2.4003390

*[CpNi(η^3-P_4Me_2)]$^+$ (**P2**):*

BP86/def2TZVP: Energies/H = –3147.439393, Enthalpies/H = –3147.438449, Free Energies/H = –3147.496319, ZPVE/ kJ/mol = 427.63

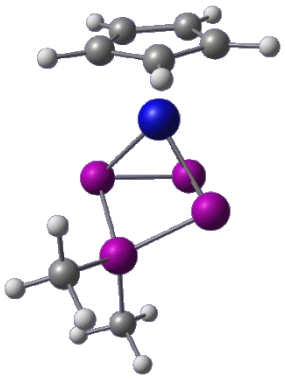

Symbol	X	Y	Z
Ni	-0.9306060	-0.1157720	-0.0000030
P	2.0928060	0.4372400	0.0000010
P	0.7404110	-0.3961710	1.5208370
P	0.7404220	-0.3961780	-1.5208400
P	0.3468100	-1.9608900	-0.0000010
C	-2.1183220	1.4635440	-0.7131780
C	-2.6708930	0.2064030	1.1546360
C	-2.1182840	1.4636190	0.7130680
H	-1.7690020	2.2662400	1.3563070
C	-2.6709550	0.2062820	-1.1545870
C	-3.0272070	-0.5552070	0.0000740
H	-3.4612400	-1.5511810	0.0001370
C	2.2680680	2.2462300	-0.0000080
C	3.7713560	-0.2658940	0.0000130
H	4.3042870	0.0786920	0.8975770
H	3.7115030	-1.3609100	0.0000340
H	4.3042880	0.0786580	-0.8975650
H	2.8222660	2.5580460	-0.8969830
H	1.2723840	2.7059170	-0.0000470
H	2.8222020	2.5580630	0.8970000
H	-2.7949230	-0.1038260	2.1886960
H	-1.7690700	2.2660940	-1.3565210
H	-2.7950410	-0.1040530	-2.1886090

*[Cp´´´Ni(η^3-P_4PhCl)]$^+$ (**2f$_{endo}$**):*

B3LYP/def2SVP: Energies/H = –4228.944626, Enthalpies/H = –4228.943682, Free Energies/H = –4229.043422, ZPVE/ kJ/mol = 1366.27

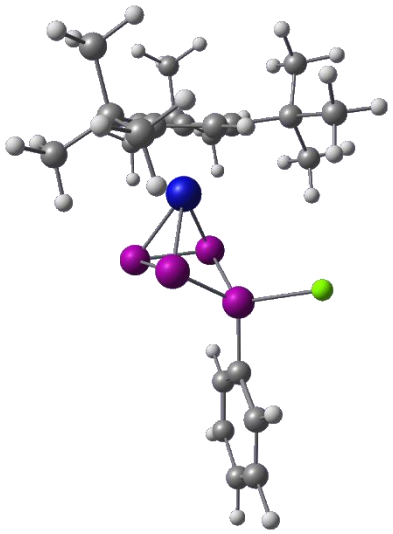

Symbol	X	Y	Z
Ni	-0.6055810	0.3257590	0.2996010
P	2.3200890	-0.1159040	-0.3697060
P	1.1873620	1.7385380	-0.0530340
P	0.9835470	-1.1957870	1.0023560
P	0.8255180	0.8235620	1.9506710
C	-2.1020130	-0.7204590	-0.8298670
C	-2.2643850	1.5495960	-0.1990790
C	-1.9589300	0.6314310	-1.2641200
H	-1.6844300	0.9353530	-2.2679190
C	-2.4753900	-0.6482140	0.6082740
C	-2.5828850	0.7454250	0.9280690
H	-2.8612410	1.1340260	1.9026140
C	-0.9531250	-2.9411430	-1.5459320
H	0.0504950	-2.5024910	-1.6366150
H	-1.0267580	-3.7547360	-2.2844480
H	-1.0423020	-3.3869200	-0.5518670
C	-3.4336080	-2.5463150	-1.9283720
H	-3.7116930	-3.0679380	-1.0045050
H	-3.4386780	-3.2895510	-2.7406870
H	-4.2138290	-1.8010640	-2.1484150
C	-2.4510790	3.0575910	-0.3087710
C	-1.7222180	-1.3331080	-3.2592330
H	-2.4997510	-0.6438630	-3.6209460
H	-1.6742010	-2.1745300	-3.9662250
H	-0.7504160	-0.8188220	-3.2940880
C	-2.9443040	-1.6769070	1.6613270
C	-2.0363220	-1.8823080	-1.8476140
C	-2.3765040	-3.0998510	1.5236260
H	-2.6894100	-3.5995850	0.6004040
H	-2.7487530	-3.7104360	2.3598750
H	-1.2775800	-3.1081160	1.5750620
C	-2.5742190	-1.1931200	3.0856490
H	-1.4871860	-1.0604040	3.1995990
H	-2.8973080	-1.9475840	3.8181040
H	-3.0653600	-0.2500370	3.3620850
C	-4.4927450	-1.7350610	1.5649240
H	-4.9402480	-0.7468370	1.7510980
H	-4.8845480	-2.4339630	2.3207990
H	-4.8300640	-2.0792030	0.5773860
C	-1.9241810	3.7824970	0.9451240
H	-2.3976780	3.4129770	1.8672570
H	-2.1393160	4.8596460	0.8721990
H	-0.8339770	3.6684830	1.0517830
C	-1.7662080	3.6269620	-1.5647850
H	-0.6811120	3.4441440	-1.5596020
H	-1.9226690	4.7154700	-1.6101620
H	-2.1836190	3.1976540	-2.4884310
C	-3.9802170	3.2938340	-0.4255060
H	-4.3979650	2.7716860	-1.3002640
H	-4.1827090	4.3703100	-0.5414580
H	-4.5120830	2.9401360	0.4709930
C	4.0852880	-0.1212200	0.0449840

C	4.9879660	0.6182050	-0.7412350
C	4.5373350	-0.8409800	1.1630630
C	6.3398140	0.6352540	-0.3994720
C	5.8953480	-0.8195110	1.4915170
C	6.7934410	-0.0823820	0.7143870
H	7.0428510	1.2093740	-1.0068600
H	6.2493380	-1.3831770	2.3573140
Cl	2.2879980	-0.7214080	-2.3554720
H	4.6432220	1.1720540	-1.6172070
H	7.8541170	-0.0674110	0.9755350
H	3.8422460	-1.4193830	1.7757340

*[Cp´´´Ni(η^3-P_4ClPh)]$^+$ (**2f$_{exo}$**):*

B3LYP/def2SVP: Energies/H = –4228.942000, Enthalpies/H = –4228.941056, Free Energies/H = –4229.037902, ZPVE/ kJ/mol = 1368.80

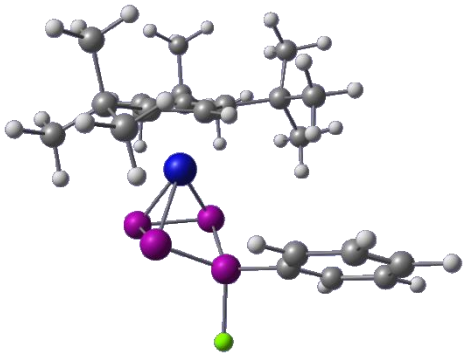

Symbol	X	Y	Z
Ni	-0.5924970	-0.5354360	-0.3188020
P	2.2987130	-0.8281050	-0.8802510
P	0.8914180	-2.3023750	-0.0791030
P	0.7229040	0.0512030	-2.1315490
P	-0.1978040	-1.9732490	-1.9991920
C	-1.3172230	1.2739020	0.6013300
C	-1.9622430	-0.8991660	1.2606660
C	-1.1242600	0.2315880	1.5565660
H	-0.4665750	0.2931250	2.4159140
C	-2.2904240	0.7439970	-0.3906760
C	-2.6654090	-0.5617320	0.0717010
H	-3.3851690	-1.2062250	-0.4230900
C	0.3127610	3.0969480	-0.2652300
H	1.1999490	2.4476560	-0.2398050
H	0.6504170	4.1268040	-0.0695810
H	-0.1026880	3.0687780	-1.2770620
C	-1.8273830	3.7215140	0.9518750
H	-2.3635330	3.8896240	0.0109470
H	-1.3942530	4.6859990	1.2586160
H	-2.5603310	3.4233500	1.7175640
C	-2.2343680	-2.0982030	2.1596430
C	0.0748100	2.7006570	2.1665510
H	-0.5814870	2.4925680	3.0249400
H	0.4999780	3.7046650	2.3117350
H	0.9114840	1.9876160	2.1809720
C	-3.0641310	1.3593220	-1.5776220
C	-0.6948950	2.6727470	0.8253740
C	-2.3009480	2.4187330	-2.3915220
H	-2.0616760	3.3180370	-1.8143040
H	-2.9271340	2.7380770	-3.2380930
H	-1.3667760	2.0126180	-2.8073570
C	-3.4895820	0.2573820	-2.5795990
H	-2.6238100	-0.2864420	-2.9871760
H	-4.0169930	0.7255310	-3.4237380
H	-4.1801070	-0.4775610	-2.1429100
C	-4.3612800	1.9828220	-0.9946610
H	-4.9678780	1.2229200	-0.4785880
H	-4.9671580	2.4033320	-1.8127310
H	-4.1489510	2.7889240	-0.2802840
C	-2.4663360	-3.3806280	1.3372400
H	-3.2952760	-3.2707780	0.6217270
H	-2.7202680	-4.2137350	2.0103620
H	-1.5650280	-3.6705740	0.7745870
C	-1.0940070	-2.3258120	3.1685750
H	-0.1389900	-2.5377080	2.6646410
H	-1.3337390	-3.1877030	3.8094660
H	-0.9523890	-1.4566060	3.8288580
C	-3.5316780	-1.7578470	2.9408240
H	-3.4116900	-0.8380340	3.5340340
H	-3.7756030	-2.5804180	3.6314050
H	-4.3851700	-1.6179840	2.2599770
C	3.1938150	0.2012260	0.3105940

C	3.0677800	-0.0519830	1.6864110
C	4.0175420	1.2438370	-0.1510770
C	3.7664900	0.7429500	2.5988170
H	2.4370400	-0.8653510	2.0525140
C	4.7026150	2.0359820	0.7703150
H	4.1291110	1.4340430	-1.2209340
C	4.5784540	1.7858140	2.1425520
H	3.6757300	0.5435340	3.6687000
H	5.3395940	2.8490820	0.4155940
H	5.1210290	2.4062810	2.8595070
Cl	3.8146580	-1.6433910	-2.0441400

*[Cp´´´Ni(η^3-$P_4{}^tBuCl$)]$^+$ (**2g$_{endo}$**):*

B3LYP/def2SVP: Energies/H = –4155.171882, Enthalpies/H = –4155.170938, Free Energies/H = –4155.268938, ZPVE/ kJ/mol = 1447.38

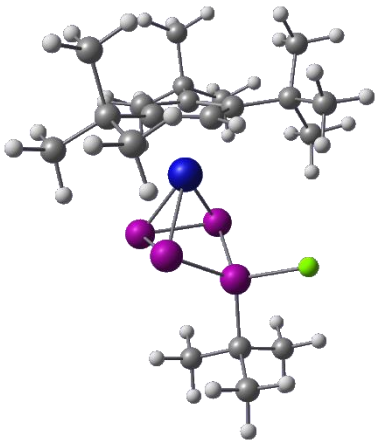

Symbol	X	Y	Z
Ni	0.3450650	0.3379170	-0.3107430
P	-2.6130210	-0.1260560	0.1254290
P	-1.4803510	1.7430840	-0.0630890
P	-1.1860410	-1.1562480	-1.1961550
P	-0.9432860	0.8906860	-2.0547910
C	1.7742210	-0.7775190	0.8474630
C	1.9318960	1.5388610	0.4222660
C	1.5662680	0.5286320	1.3803290
H	1.2081460	0.7408260	2.3813360
C	2.2514060	-0.5774700	-0.5484570
C	2.3566820	0.8397270	-0.7394940
H	2.7045670	1.3150820	-1.6516350
C	0.6140420	-3.0589030	1.2988150
H	-0.3987300	-2.6367910	1.3647250
H	0.6523480	-3.9349950	1.9652270
H	0.7684270	-3.4130250	0.2761870
C	3.0623970	-2.6804860	1.8692860
H	3.4009340	-3.1307440	0.9284750
H	3.0298370	-3.4811880	2.6242450
H	3.8192240	-1.9471500	2.1887540
C	2.0731570	3.0348110	0.6738410
C	1.2605170	-1.5992300	3.1890340
H	2.0054400	-0.9344860	3.6516520
H	1.1855170	-2.4979110	3.8189560
H	0.2805960	-1.1005800	3.2115440
C	2.8167530	-1.5087930	-1.6439330
C	1.6637630	-2.0233300	1.7569640
C	2.2629970	-2.9442160	-1.6688200
H	2.5091990	-3.5183670	-0.7690850
H	2.7078480	-3.4791420	-2.5213400
H	1.1715850	-2.9578430	-1.8068610
C	2.5466900	-0.9154120	-3.0487220
H	1.4688550	-0.7994850	-3.2408350
H	2.9493970	-1.5986550	-3.8110240
H	3.0295700	0.0584270	-3.2076120
C	4.3542640	-1.5583080	-1.4347680
H	4.7978210	-0.5529580	-1.4987940
H	4.8139610	-2.1839510	-2.2161460
H	4.6221340	-1.9841670	-0.4579380
C	1.6291500	3.8569360	-0.5522310
H	2.1791330	3.5743100	-1.4624890
H	1.8161460	4.9266670	-0.3717540
H	0.5528370	3.7375650	-0.7527110
C	1.2767130	3.4805610	1.9137670
H	0.2014180	3.2732340	1.8053740
H	1.3964950	4.5645940	2.0614090
H	1.6329110	2.9840230	2.8292200
C	3.5823690	3.2859900	0.9305200
H	3.9449670	2.6977300	1.7878360
H	3.7504860	4.3518480	1.1519640
H	4.1885350	3.0193580	0.0511030
C	-4.4503060	-0.1260410	-0.3434640

C	-5.1880790	0.8062220	0.6328760
H	-6.2498610	0.8412420	0.3404750
H	-5.1354180	0.4458720	1.6696590
H	-4.7981060	1.8352600	0.5954950
C	-4.9665680	-1.5716440	-0.2470600
H	-6.0308590	-1.5779220	-0.5319960
H	-4.4340690	-2.2468020	-0.9343200
H	-4.8884900	-1.9719840	0.7734590
C	-4.5640320	0.3989300	-1.7853670
H	-4.2010630	1.4328590	-1.8840210
H	-4.0305520	-0.2362450	-2.5081320
H	-5.6299310	0.3944690	-2.0640580
Cl	-2.6140240	-0.8422690	2.0780280

*[Cp´´´Ni(η^3-P_4Cl^tBu)]$^+$ (**2g$_{exo}$**):*

B3LYP/def2SVP: Energies/H = –4155.165046, Enthalpies/H = –4155.164101, Free Energies/H = –4155.262553, ZPVE/ kJ/mol = 1446.79

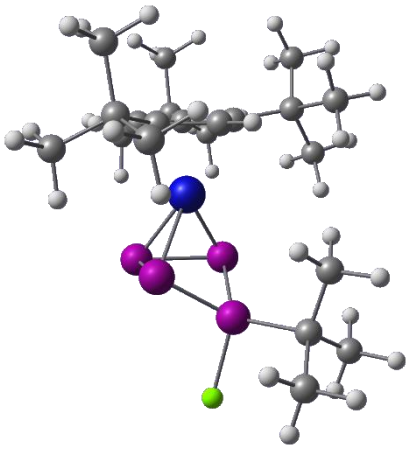

Symbol	X	Y	Z
Ni	0.2879420	0.2664310	-0.3633960
P	-2.7704400	-0.1484860	-0.3778990
P	-1.5501270	1.6531000	-0.6850400
P	-1.1247550	-1.3807440	-1.1777160
P	-0.6867860	0.4592850	-2.3649790
C	1.7526130	-0.6891830	0.9283690
C	1.6663240	1.6305590	0.5141100
C	1.3479750	0.5830030	1.4390620
H	0.9063680	0.7463630	2.4152940
C	2.3065340	-0.4329150	-0.4236380
C	2.2437440	0.9876080	-0.6187650
H	2.5984670	1.5033870	-1.5056020
C	0.7809730	-3.0620100	1.3390580
H	-0.2703010	-2.7429600	1.3983090
H	0.8955080	-3.9491710	1.9813680
H	0.9784290	-3.3676090	0.3070110
C	3.1626300	-2.4976380	1.9957330
H	3.5505490	-2.9552530	1.0787890
H	3.1634160	-3.2762000	2.7738540
H	3.8615240	-1.7076310	2.3113960
C	1.6462730	3.1287370	0.7877300
C	1.2551660	-1.5627420	3.2595320
H	1.9306010	-0.8366700	3.7364080
H	1.2460960	-2.4669500	3.8858620
H	0.2371160	-1.1493440	3.2723590
C	3.0730650	-1.2937290	-1.4524940
C	1.7244940	-1.9441170	1.8353820
C	2.6066680	-2.7562830	-1.5699770
H	2.7698240	-3.3370550	-0.6558690
H	3.1785110	-3.2504650	-2.3697750
H	1.5412670	-2.8235440	-1.8391500
C	2.9649510	-0.6821850	-2.8708060
H	1.9211560	-0.6127830	-3.2119780
H	3.5070560	-1.3259930	-3.5790190
H	3.4167950	0.3169910	-2.9414100
C	4.5736350	-1.2501180	-1.0539700
H	4.9478750	-0.2148760	-1.0492950
H	5.1657730	-1.8219030	-1.7858510
H	4.7566480	-1.6788910	-0.0607700
C	1.3927230	3.9389190	-0.4980710
H	2.1494190	3.7361820	-1.2708700
H	1.4347060	5.0154490	-0.2725450
H	0.4003010	3.7285140	-0.9260090
C	0.6028110	3.5023190	1.8567740
H	-0.4181650	3.2421210	1.5396090
H	0.6321670	4.5871620	2.0404980
H	0.8036020	3.0038360	2.8174180
C	3.0601330	3.4751270	1.3278350
H	3.2872770	2.9124650	2.2466450
H	3.1151470	4.5498190	1.5629610
H	3.8398640	3.2470710	0.5849090
C	-3.5906340	-0.4868140	1.2909720

Cl	-4.3624740	-0.1877760	-1.7149600
C	-2.5039500	-0.3957630	2.3744590
H	-1.7108750	-1.1410780	2.2271030
H	-2.0465350	0.6034340	2.4246500
H	-2.9740320	-0.5981620	3.3500010
C	-4.1984760	-1.8997750	1.2436040
H	-4.6837520	-2.1005480	2.2121690
H	-4.9606340	-1.9956930	0.4574230
H	-3.4302550	-2.6732110	1.0890160
C	-4.6705170	0.5853590	1.5219060
H	-5.1232350	0.4070080	2.5104870
H	-4.2496910	1.6028400	1.5279590
H	-5.4694980	0.5379690	0.7697260

*[(Cp´´´Ni)$_2$(μ;η^3:η^1:η^1-P_4Br_3)]$^+$ (**3a**):*

B3LYP/def2SVP: Energies/H = –13431.720505, Enthalpies/H = –13431.719561, Free Energies/H = –13431.862697, ZPVE/ kJ/mol = 2238.06

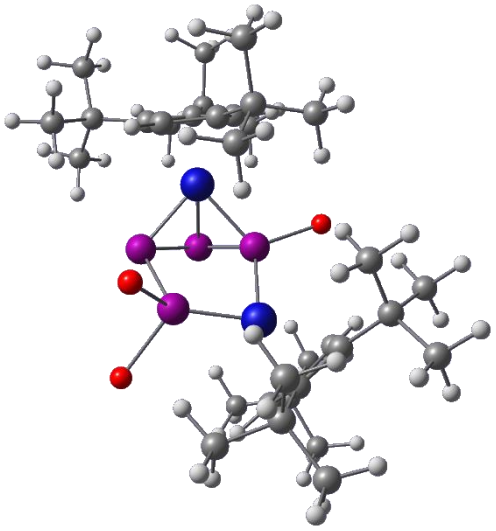

Symbol	X	Y	Z
Br	0.4276270	-3.2108310	-0.9767950
Br	-1.7734950	3.3687370	-1.5796430
Br	-0.6430860	2.9114590	1.6925810
Ni	-1.8540770	-0.1688950	-0.2675090
Ni	2.1710910	-0.0228290	-0.0661190
P	0.1980350	-0.9820290	-0.6017910
P	-0.8911990	1.7716430	-0.2492840
P	1.3179120	-0.0123730	-2.2139420
P	1.2345360	1.8252680	-1.0197630
C	3.4205370	-1.4313050	0.8363200
H	3.2623850	-2.5039240	0.7874840
C	-3.0242700	-1.8426840	-0.6265850
H	-2.5916550	-2.8078670	-0.8690220
C	-3.9084590	-0.1140010	0.6083700
C	-3.4107050	-0.8753860	-1.6010230
C	2.8770810	-0.5844290	1.8626970
C	3.2912630	0.7248010	1.5205670
H	3.0378520	1.6191450	2.0795770
C	-3.8282730	0.2271790	-0.8311640
H	-4.1441360	1.1824360	-1.2405390
C	-3.4187640	-1.4442860	0.7290730
C	4.2594910	-0.6958510	-0.0646960
C	4.1589260	0.7025420	0.3508660
C	-4.6960960	-2.6624210	2.5641490
H	-5.0633030	-1.7702650	3.0836780
H	-4.6242010	-3.4684010	3.3113430
H	-5.4510330	-2.9610250	1.8200690
C	2.2029600	-1.0280920	3.1517760
C	-3.4431690	-1.0231490	-3.1187470
C	-3.3153400	-2.4498120	1.9012450
C	-4.6533930	0.8526050	1.5540420
C	4.9198790	1.9817780	-0.0711430
C	-4.5913220	2.3077910	1.0320210
H	-3.5589460	2.6709310	0.9393660
H	-5.1066760	2.9660850	1.7472070
H	-5.0934360	2.4365280	0.0631470
C	-6.1499040	0.4395600	1.5415840
H	-6.5556660	0.4642540	0.5180080
H	-6.7342260	1.1466270	2.1522560
H	-6.3096540	-0.5689330	1.9427560
C	5.1288540	-1.4808300	-1.0723170
C	-2.2728050	-2.0199370	2.9547360
H	-1.2709930	-1.9831270	2.5058010
H	-2.2442500	-2.7526420	3.7774690
H	-2.4820930	-1.0363460	3.3875310
C	-2.5349950	-2.1738960	-3.5874350
H	-1.4842700	-2.0012590	-3.3096920
H	-2.5822380	-2.2640960	-4.6836930
H	-2.8459890	-3.1420080	-3.1652020
C	5.5338770	-0.7277690	-2.3508350
H	4.6514900	-0.3854440	-2.9118970
H	6.0949470	-1.4140600	-3.0029610

H	6.1863690	0.1311660	-2.1585190
C	1.6353250	-2.4520490	3.0216280
H	0.9002250	-2.5244640	2.2070410
H	1.1332100	-2.7420510	3.9567910
H	2.4276160	-3.1920400	2.8315870
C	-4.1233050	0.8852340	2.9992700
H	-4.2643170	-0.0616260	3.5316530
H	-4.6664240	1.6559750	3.5675920
H	-3.0539110	1.1433490	3.0230520
C	-4.9058930	-1.3466870	-3.5128670
H	-5.2533470	-2.2729310	-3.0285990
H	-4.9867790	-1.4808200	-4.6037350
H	-5.5870660	-0.5330860	-3.2179560
C	4.6832390	2.4195240	-1.5339210
H	4.8420150	1.6193670	-2.2601970
H	5.3721620	3.2421890	-1.7814440
H	3.6600060	2.7998790	-1.6672780
C	-3.0095780	0.2795880	-3.8163990
H	-3.6439150	1.1318350	-3.5288780
H	-3.0864120	0.1658160	-4.9092460
H	-1.9666850	0.5349590	-3.5735480
C	1.0906600	-0.0495900	3.5674840
H	1.4743060	0.9729990	3.7024280
H	0.6515840	-0.3663490	4.5260690
H	0.2868540	-0.0126910	2.8184120
C	6.4066120	-1.9196250	-0.3067730
H	6.9964770	-1.0604520	0.0411210
H	7.0455020	-2.5243300	-0.9697650
H	6.1523900	-2.5334960	0.5709580
C	6.4308260	1.7475600	0.1820480
H	6.6137380	1.4067340	1.2131700
H	6.9751150	2.6937570	0.0381030
H	6.8651350	1.0101780	-0.5038180
C	3.3088850	-1.0306570	4.2403680
H	4.1333600	-1.7095730	3.9724240
H	2.8857580	-1.3701790	5.1990260
H	3.7281170	-0.0237090	4.3890610
C	-2.8723070	-3.8369780	1.3793830
H	-3.5805460	-4.2474080	0.6430760
H	-2.8296990	-4.5408810	2.2241950
H	-1.8715110	-3.8114640	0.9247150
C	4.3968950	-2.7620210	-1.5401390
H	4.1924790	-3.4667760	-0.7223020
H	5.0332140	-3.2927250	-2.2637680
H	3.4452370	-2.5248940	-2.0381780
C	4.4998360	3.1780070	0.8151450
H	3.4238050	3.3940030	0.7356980
H	5.0397530	4.0756460	0.4792960
H	4.7506020	3.0220540	1.8749860

*[(Cp´´´Ni)$_2$(μ;η^3:η^1:η^1-P$_4$biphenC)]$^+$ (**3b**):*

B3LYP/def2SVP: Energies/H = –6631.766303, Enthalpies/H = –6631.765358, Free Energies/H = –6631.918303, ZPVE/ kJ/mol = 2656.45

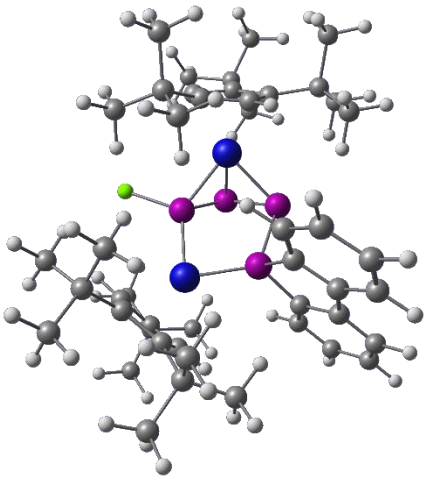

Symbol	X	Y	Z
Ni	1.7698811	-0.6463039	0.3271271
Ni	-2.2512149	-0.2667362	0.2133180
P	-0.3025568	-1.3049820	0.6963321
P	0.9694810	1.4211141	0.2737259
Cl	-0.6460077	-3.3539850	1.1295232
P	-1.1571260	1.5448410	1.0978159
P	-1.3107119	-0.2578070	2.3183080
C	1.3617919	3.7259250	-1.0405592
C	3.2041432	-1.9757749	-0.7643889
C	2.8035032	-2.4268218	0.5666302
H	2.2939133	-3.3654998	0.7576772
C	3.2920552	-1.5626357	1.5936841
C	3.8073211	-0.6999218	-0.5681399
C	-4.4141279	-0.5917233	0.3922930
C	-4.1248510	0.6537597	-0.3320301
C	-3.1503128	-1.1158433	-1.5423280
C	1.7132639	2.8284541	1.1800609
C	3.7877081	-0.4494687	0.8925381
H	4.1963920	0.4450003	1.3542470
C	-3.3400579	0.2840407	-1.4945790
H	-3.0059810	0.9846567	-2.2521171
C	1.8341388	3.9599281	0.3368958
C	0.8673889	2.4172270	-1.2558541
C	-3.7547268	-1.6275203	-0.3390229
H	-3.7507147	-2.6755873	-0.0598149
C	3.3434802	-1.8282657	3.0953121
C	0.3893940	2.0251269	-2.5078851
H	0.0169260	1.0128058	-2.6668630
C	2.0992179	2.8867512	2.5208989
H	1.9926019	2.0166203	3.1693069
C	-5.3011689	-0.9340623	1.6141710
C	1.3651528	4.6385639	-2.1042492
H	1.7429047	5.6532800	-1.9620353
C	2.3663338	5.1467272	0.8575897
H	2.4725117	6.0299691	0.2242127
C	-2.6872788	-1.9343243	-2.7387249
C	-4.6992660	2.0867277	-0.2659811
C	2.6262158	4.0796503	3.0279208
H	2.9336578	4.1347464	4.0745848
C	2.7606557	5.1999693	2.1976487
H	3.1751977	6.1270043	2.6006517
C	4.6336011	0.2468582	-1.4659290
C	0.3970179	2.9466778	-3.5604791
H	0.0272470	2.6505517	-4.5447491
C	2.9642553	-2.8775609	-1.9987178
C	-4.8595749	-0.2626062	2.9341580
H	-4.7045130	0.8163058	2.8441459
H	-5.6298719	-0.4296232	3.7037240
H	-3.9222739	-0.7053041	3.2988010
C	0.8829018	4.2451039	-3.3558342
H	0.8881468	4.9583708	-4.1833983
C	6.0772141	-0.3209127	-1.5224219

H	6.1196192	-1.3044698	-2.0066919
H	6.7260161	0.3666463	-2.0891100
H	6.4984861	-0.4237306	-0.5099979
C	1.9313862	-2.2669811	-2.9700379
H	2.2352872	-1.2880671	-3.3564329
H	1.7750663	-2.9374681	-3.8307048
H	0.9656892	-2.1405461	-2.4607479
C	4.7356650	1.6580612	-0.8415531
H	5.2873750	1.6633493	0.1089200
H	5.2808970	2.3197922	-1.5310581
H	3.7474740	2.1034742	-0.6685311
C	-4.9553281	2.6411257	1.1463878
H	-4.0337621	2.6540688	1.7477838
H	-5.3116472	3.6792377	1.0635968
H	-5.7234981	2.0820647	1.6919129
C	4.0877331	0.4385281	-2.8928500
H	3.0614551	0.8343890	-2.8761730
H	4.7175570	1.1659721	-3.4282200
H	4.0937451	-0.4840730	-3.4831159
C	-1.7074758	-1.1415173	-3.6187259
H	-0.7951908	-0.8841872	-3.0621130
H	-1.4100158	-1.7460863	-4.4889389
H	-2.1545389	-0.2119324	-4.0018950
C	-6.0336530	2.0573675	-1.0626691
H	-6.7759980	1.3863205	-0.6126551
H	-6.4641681	3.0709075	-1.0916142
H	-5.8663450	1.7311705	-2.1007661
C	4.2885013	-3.1772959	-2.7376988
H	5.0324243	-3.6150148	-2.0537358
H	4.1038424	-3.9049420	-3.5438808
H	4.7321502	-2.2876189	-3.1989068
C	-3.7725591	3.0984657	-0.9832482
H	-3.6674931	2.8929256	-2.0576322
H	-4.2087132	4.1044737	-0.8942852
H	-2.7698811	3.1269068	-0.5339052
C	-3.9697578	-2.2359365	-3.5603789
H	-4.4540858	-1.3075715	-3.9001120
H	-3.7113157	-2.8337475	-4.4489669
H	-4.7004647	-2.8065535	-2.9665649
C	2.4003674	-4.2491240	-1.5575448
H	1.4263123	-4.1589210	-1.0553788
H	2.2542714	-4.8815270	-2.4463937
H	3.0898794	-4.7805869	-0.8835567
C	-6.7711989	-0.5634974	1.2984990
H	-7.0949309	-0.9946694	0.3382680
H	-7.4265719	-0.9652234	2.0868000
H	-6.9340490	0.5206516	1.2612559
C	-5.2721468	-2.4579383	1.8770181
H	-4.2545018	-2.8182992	2.0920751
H	-5.8926108	-2.6804222	2.7580401
H	-5.6791857	-3.0355673	1.0333451
C	-2.0462177	-3.2662223	-2.3151788
H	-2.7414827	-3.8941193	-1.7376488
H	-1.7505637	-3.8384973	-3.2076798
H	-1.1499747	-3.1047782	-1.7012088
C	4.8016552	-2.2151875	3.4461382
H	5.5005441	-1.3980905	3.2076281
H	4.8913882	-2.4377415	4.5220102
H	5.1204943	-3.1084856	2.8861432

C	2.4159572	-2.9916287	3.4898962
H	2.7026823	-3.9299297	2.9901782
H	2.4766142	-3.1662196	4.5754452
H	1.3657722	-2.7811458	3.2395522
C	2.9493471	-0.5748056	3.8977601
H	1.9124671	-0.2762537	3.6761390
H	3.0231811	-0.7743756	4.9785541
H	3.6113460	0.2758134	3.6745730

3.6. References

[1] a) Y.-R. Luo, "Comprehensive handbook of chemical bond energies, *CRC Press*, Boca Raton, *Fla.* **2007**; b) S. W. Benson, *J. Chem. Educ.* **1965**, *42*, 502.

[2] R. Hoffmann, *Angew. Chem. Int. Ed. Engl.* **1982**, *21*, 711–724.

[3] a) M. Baudler, K. Glinka, *Chem. Rev.* **1993**, *4*, 1623–1667; b) M. Baudler, K. Glinka, *Chem. Rev.* **1994**, *5*, 1273–1297.

[4] a) N. Burford, T. S. Cameron, P. J. Ragogna, E. Ocando-Mavarez, M. Gee, R. McDonald, R. E. Wasylishen, *J. Am. Chem. Soc.* **2001**, *123*, 7947–7948; b) N. Burford, P. J. Ragogna, R. McDonald, M. J. Ferguson, *J. Am. Chem. Soc.* **2003**, *125*, 14404–14410; c) N. Burford, C. A. Dyker, A. Decken, *Angew. Chem. Int. Ed.* **2005**, *44*, 2364–2367; d) J. Possart, A. Martens, M. Schleep, A. Ripp, H. Scherer, D. Kratzert, I. Krossing, *Chem. Eur. J.* **2017**, *23*, 12305–12313.

[5] a) N. Burford, C. A. Dyker, M. Lumsden, A. Decken, *Angew. Chem. Int. Ed.* **2005**, *44*, 6196–6199; b) J. J. Weigand, N. Burford, M. D. Lumsden, A. Decken, *Angew. Chem. Int. Ed.* **2006**, *45*, 6733–6737; c) C. A. Dyker, N. Burford, *Chem. Asian J.* **2008**, *3*, 28-36.

[6] a) J. J. Weigand, M. Holthausen, R. Fröhlich, *Angew. Chem. Int. Ed.* **2009**, *48*, 295–298; b) M. H. Holthausen, K. O. Feldmann, S. Schulz, A. Hepp, J. J. Weigand, *Inorg. Chem.* **2012**, *51*, 3374–3387; c) M. H. Holthausen, J. J. Weigand, *Chem. Soc. Rev.* **2014**, *43*, 6639–6657.

[7] a) I. Krossing, I. Raabe, *Angew. Chem. Int. Ed.* **2001**, *40*, 4406–4409; b) M. Gonsior, I. Krossing, Müller, Lutz, I. Raabe, M. Jansen, L. v. Wüllen, *Chem. Eur. J.* **2002**, *8*, 4475–4492.

[8] T. Köchner, T. A. Engesser, H. Scherer, D. A. Plattner, A. Steffani, I. Krossing, *Angew. Chem. Int. Ed.* **2012**, *51*, 6529–6531.

[9] a) A. H. Cowley, M. C. Cushner, M. Lattman, M. L. McKee, J. S. Szobota, J. C. Wilburn, *Pure Appl. Chem.* **1980**, *52*, 789–797; b) A. H. Cowley, R. A. Kemp, *Chem. Rev.* **1985**, *85*, 367–382; c) H. A. Spinney, I. Korobkov, G. A. DiLabio, G. P. A. Yap, D. S. Richeson, *Organometallics* **2007**, *26*, 4972–4982.

[10] J. M. Slattery, S. Hussein, *Dalton Trans.* **2012**, *41*, 1808–1815.

[11] a) M. V. Butovskiy, G. Balázs, M.Bodensteiner, E. V. Peresypkina, A. V. Virovets, J. Sutter, M. Scheer, *Angew. Chem. Int. Ed.* **2013**, *52*, 2972–2976; b) T. Li, M. T. Gamer, M. Scheer, S. N. Konchenko, P. W. Roesky, *ChemComm* **2013**, *49*, 2183–2185; c) N. Arleth, M. T. Gamer, R. Köppe, N. A. Pushkarevsky, S. N. Konchenko, M. Fleischmann, M. Bodensteiner, M. Scheer, P. W. Roesky, *Chem. Sci.* **2015**, *6*, 7179–7184; d) N. Arleth, M. T. Gamer, R. Köppe, S. N. Konchenko, M. Fleischmann, M. Scheer, P. W. Roesky, *Angew. Chem. Int. Ed.* **2016**, *55*, 1557–1560; e) E. Mädl, G. Balázs, E. V. Peresypkina, M. Scheer, *Angew. Chem. Int. Ed.* **2016**, *55*, 7702–7707; f) C. Schoo, S. Bestgen, M. Schmidt, S. N. Konchenko, M. Scheer, P. W. Roesky, *ChemComm* **2016**, *52*, 13217–13220; g) M. Schmidt, D. Konieczny, E. V. Peresypkina, A. V. Virovets, G.

Balázs, M. Bodensteiner, F. Riedlberger, H. Krauss, M. Scheer, *Angew. Chem. Int. Ed.* **2017**, *56*, 7307–7311.

[12] a) M. Fleischmann, F. Dielmann, L. J. Gregoriades, E. V. Peresypkina, A. V. Virovets, S. Huber, A. Y. Timoshkin, G. Balázs, M. Scheer, *Angew. Chem. Int. Ed.* **2015**, *54*, 13110–13115; b) L. Dütsch, M. Fleischmann, S. Welsch, G. Balázs, W. Kremer, M. Scheer, *Angew. Chem. Int. Ed.* **2018**, *57*, 3256–3261.

[13] M. Piesch, M. Seidl, M. Stubenhofer, M. Scheer, *Chem. Eur. J.* **2019**, *25*, 6311–6316.

[14] C. G. P. Ziegler, T. M. Maier, S. Pelties, C. Taube, F. Hennersdorf, A. W. Ehlers, J. J. Weigand, R. Wolf, *Chem. Sci.* **2019**, *10*, 1302–1308.

[15] a) G. Capozzi, L. Chiti, M. Di Vaira, M. Peruzzini, P. Stoppioni, *ChemComm* **1986**, *24*, 1799–1800; b) A. Barth, G. Huttner, M. Fritz, L. Zsolnai, *Angew. Chem. Int. Ed.* **1990**, *29*, 929–931; c) M. Peruzzini, R. R. Abdreimova, Y. Budnikova, A. Romerosa, O. J. Scherer, H. Sitzmann, *J. Organomet. Chem.* **2004**, *689*, 4319–4331.

[16] P. Barbaro, A. Ienco, C. Mealli, M. Peruzzini, O. J. Scherer, G. Schmitt, F. Vizza, G. Wolmershäuser, *Chem. Eur. J.* **2003**, *9*, 5196–5210.

[17] A. K. Adhikari, C. G. P. Ziegler, K. Schwedtmann, C. Taube, J. J. Weigand, R. Wolf, *Angew. Chem. Int. Ed.* **2019**, *58*, 18584-18590.

[18] a) I. Krossing, *Chem. Eur. J.* **2001**, *7*, 490–502; b) M. Gonsior, I. Krossing, N. Mitzel, *Z. Anorg. Allg. Chem.* **2002**, *628*, 1821–1830.

[19] S. J. Connelly, W. Kaminsky, D. M. Heinekey, *Organometallics* **2013**, *32*, 7478–7481.

[20] a) P. Pyykkö, M. Atsumi, *Chem. Eur. J.* **2009**, *15*, 186–197; b) P. Pyykkö, *J. Phys. Chem. A* **2015**, *119*, 2326–2337.

[21] M. Mantina, A. C. Chamberlin, R. Valero, C. J. Cramer, D. G. Truhlar, *J. Phys. Chem. A* **2009**, *113*, 5806–5812.

[22] a) M. Gonsior, I. Krossing, *Dalton Trans.* **2005**, *11*, 2022–2030; b) M. Gonsior, I. Krossing, *Dalton Trans.* **2005**, *7,* 1203–1213; c) M. Gonsior, I. Krossing, E. Matern, *Chem. Eur. J.* **2006**, *12*, 1703–1714.

[23] https://omics.pnl.gov/software/molecular-weight-calculator, (27.12.2019).

[24] H. T. Teunissen, C. B. Hansen, F. Bickelhaupt, *Phosphorus, Sulfur, and Silicon and the Relat. Elem.* **1996**, *118*, 309–312.

[25] M. Fild, O. Stelzer, R. Schmutzler, G. O. Doak, "Tert-butyldichlorophosphine and Di-tert-butylchlorophosphine" in (A.Wold, J. K. Ruff, *Inorganic Syntheses* **1973**, 12 - Wiley-Interscience, Hoboken, N. J.), 4–9.

[26] Agilent (**2014**). CrysAlis PRO. Agilent Technologies Ltd, Yarnton, Oxfordshire, England.

[27] O. V. Dolomanov, L. J. Bourhis, R. J. Gildea, J. A. K. Howard, H. Puschmann, *J. Appl. Crystallogr.* **2009**, *42*, 339–341.

[28] G. M. Sheldrick, *Acta Crystallogr. A* **2015**, *71*, 3–8.

[29] a) G. M. Sheldrick, *Acta Crystallogr. C* **2015**, *71*, 3–8; b) G. M. Sheldrick*, Acta Crystallogr. A* **2008**, *64*, 112–122.

[30] Miriam Eberl, Dissertation, University of Regensburg **2011**.

[31] M. Piesch, F. Dielmann, S. Reichl, M. Scheer, *Chem. Eur. J.* **2020**, *24*, 1518–1524.

[32] M. J. Frisch, G. W. Trucks, H. B. Schlegel, G. E. Scuseria, M. A. Robb, J. R. Cheeseman, G. Scalmani, V. Barone, B. Mennucci, G. A. Petersson, H. Nakatsuji, M. Caricato, X. Li, H. P. Hratchian,A. F. Izmaylov, J. Bloino, G. Zheng, J. L. Sonnenberg, M. Hada, M. Ehara, K. Toyota, R. Fukuda, J. Hasegawa, M. Ishida, T. Nakajima, Y. Honda, O. Kitao, H. Nakai, T. Vreven, J. A. Montgomery Jr., J. E. Peralta, F. Ogliaro, M. Bearpark, J. J. Heyd, E. Brothers, K. N. Kudin, V. N. Staroverov, T. Keith, R. Kobayashi, J. Normand, K. Raghavachari, A. Rendell, J. C. Burant, S. S. Iyengar, J. Tomasi, M. Cossi, N. Rega, J. M. Millam, M. Klene, J. E. Knox, J. B. Cross, V. Bakken, C. Adamo, J. Jaramillo, R. Gomperts, R. E. Stratmann, O. Yazyev, A. J. Austin, R. Cammi, C. Pomelli, J. W. Ochterski, R. L. Martin, K. Morokuma, V. G. Zakrzewski, G. A. Voth, P. Salvador, J. J. Dannenberg, S. Dapprich, A. D. Daniels, O. Farkas, J. B. Foresman, J. V. Ortiz, J. Cioslowski, D. J. Fox, "Gaussian 09", Revision E.01, Gaussian Inc., Wallingford CT **2013**.

[33] A. D. Becke, *Phys. Rev. A* **1988**, *38*, 3098–3100.

[34] C. Lee, W. Yang, R. G. Parr, *Phys. Rev. B* **1988**, *37*, 785–789.

[35] F. Weigend, R. Ahlrichs, *Phys. Chem. Chem. Phys.* **2005**, *7*, 3297–3305.

[36] J. Tomasi, B. Mennucci, R. Cammi, *Chem. Rev.* **2005**, *105*, 2999–3093.

[37] E. D. Glendening, C. R. Landis, F. Weinhold, *J. Comput. Chem.* **2013**, *34*, 1363–1374.

4. Ring Expansion vs. Addition – Reactivity of a *cyclo*-P_4 Complex Towards Pnictogenium Cations

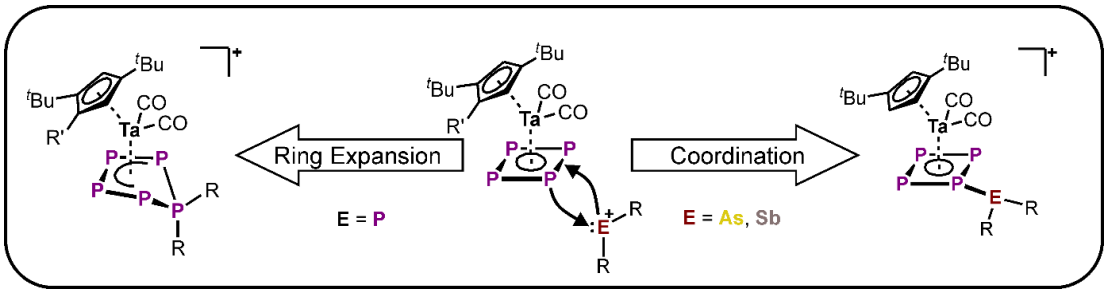

Preface

The following chapter has already been published. The article is reproduced with permission from the Royal Society of Chemistry.

"Ring expansion vs. addition – reactivity of a cyclo-P_4 complex towards pnictogenium cations" *Chem. Commun.* **2023**, *59*, 10117–10120.

Parts of this chapter have already been described within the BSc thesis of Alexander Erhard.

Authors

Christoph Riesinger, Alexander Erhard and Manfred Scheer

Author Contributions

Christoph Riesinger – Conceptualization, Synthesis of compounds **2**, **3** and **5**, Acquisition and interpretation of crystallographic data, Interpretation of computational data, Writing of original draft.
Alexander Erhard – Synthesis of compounds **1** and **4**.
Manfred Scheer – Project administration, Funding acquisition, Co-writing final manuscript.

Acknowledgements

This work was supported by the Deutsche Forschungsgemeinschaft (DFG) within the project Sche 384/36-2. C. R. is grateful to the Studienstiftung des Deutschen Volkes for a PhD fellowship. We thank Lisa Zimmermann for her assistance with recording the IR spectra of **1** – **5**.

4.1. Abstract

A systematic reactivity study of the cyclo-P_4 complexes [$Cp^RTa(CO)2(\eta^4$-$P_4)$] towards pnictogenium cations results in the formation of functionalised interpnictogen cations. Phosphenium ions insert into one of the P–P bonds to give ring-expanded cyclo-P_5R_2 products. In contrast, the arsenium-functionalised P_4AsCy_2 ligand displays an interesting borderline case between ring expansion and coordination, while stibenium cations afford addition products. Tuning of steric and electronic properties of the stibenium ion shows drastic influence on the reaction outcome.

4.2. Introduction

Carbenes are an essential class of compounds in which the central divalent carbon atom has two substituents and bears a lone pair of electrons.[1] They find use as ligands in transition metal catalysis,[2] as organocatalysts[3] or for the stabilisation of highly reactive (main group) species.[4] In contrast to the well-explored chemistry of carbenes (CR_2), the isolobally [5] related phosphenium cations ($[PR_2]^+$) and their heavier congeners ($[ER_2]^+$, E = As, Sb, Bi) received considerably less attention. However, phosphenium substituents have been employed with great success by the groups of *Bertrand* and *Liu* as e. g. in the stabilisation of a singlet phosphinidene,[6] of carbyne anions[7] or stable ketenyl anions.[8] Furthermore, the first salts of unstabilised phosphenium and arsenium cations have only been isolated very recently by the group of *Beckmann*,[9] with the heavier stibenium and bismuthenium cations only known shortly longer.[10] Nevertheless, phosphenium ions and their homologues are key intermediates in the synthesis of extended cationic polyphosphorus frameworks. Thus, catenated linear polyphosphorus cations (**I**)[11] as well as ring- (**II**, **III**)[12] and cage-type (**IV**)[13] compounds could be obtained (Scheme 1), displaying the phosphorus analogues of ubiquitous organic carbo(cyclic) species. Similarly, cations with mixed and heavier pnictogens are accessible by the exchange of the phosphenium ion for its heavier homologues.[14] The express carbene-like

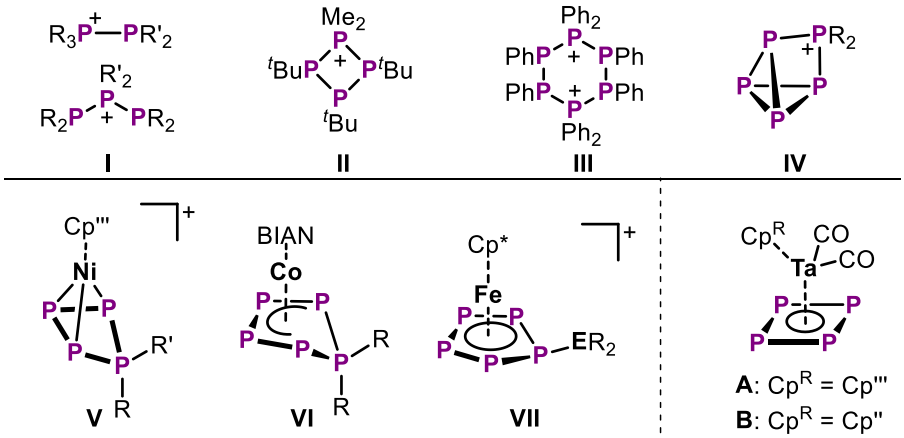

*Scheme 1: Organophosphorus cations (**I** – **IV**) arising from the insertion of phosphenium ions into P–P bonds, selected transition metal complexes arising from phosphenium ion insertion (**V**), halophosphane condensation (**VI**) or pnictogenium addition (**VII**, ER_2 = PBr_2 or $AsCy_2$), and the cyclo-P_4 compounds **A** and **B**; Cp''' = 1,2,4-^{t}Bu$_3$C$_5$H$_2$, Cp'' = 1,3-^{t}Bu$_2$C$_5$H$_3$, Cp* = C_5Me_5, BIAN = 1,2-bis((C$_6$H$_3$^{i}Pr$_2$-2,6)imino)acenaphthene.*

character of phosphenium ions leads to P–P bond insertion (e. g. ring expansion) reactions being the primary reactivity pattern of these species. In contrast, the reactivity of heavier pnictogenium ions is far less explored, but the decreased similarity to carbenes (e. g. s-p separation) should lead to addition reactions being preferred over insertion reactions.[14e] Recent investigations transferred the reactivity of pnictogenium ions to transition metal polyphosphorus complexes. Phosphenium ions were found to insert into small strained *cyclo*-E_3 (E = P, As) ligands to afford ring-expanded products such as $[Cp'''Ni(\eta^3\text{-}P_4R_2)]^+$ (**V**, R = alkyl, aryl; Cp‴ = 1,2,4-^{t}Bu$_3$C$_5$H$_2$).[15] The neutral [(BIAN)Co(η^4-P_5R_2)] (**VI**, R = alkyl, aryl, BIAN = 1,2-bis((C$_6$H$_3$^{i}Pr$_2$-2,6)imino)acenaphthene) is not a product of phosphenium ion insertion but is formed by the replacement of a [(nacnac)Ga] (nacnac = N(C$_6$H$_3$^{i}Pr$_2$-2,6)C(Me)}$_2$CH)) moiety via salt metathesis of chlorophosphines with the respective cobalt-P_4 precursor (Scheme 1).[16] In contrast, both phosphenium and arsenium ions do not insert into the *cyclo*-P_5 ligand of pentaphosphaferrocene but instead yield functionalised pnictino-pentaphosphole complexes $[Cp^*Fe(\eta^5\text{-}P_5ER_2)]^+$ (**VII**, ER_2 = PBr_2, $AsCy_2$; Cp* = C_5Me_5).[17] Surprisingly, a much larger *cyclo*-P_8 complex can be functionalised with arsenium ions in an addition reaction, affording salts of the exotic cation $[\{Cp'''Ta\}_2(\mu,\eta^{2:2:2:2:1:1:1:1}\text{-}P_8AsCy_2)]^+$.[18] Despite the precedent for the synthetic utility of pnictogenium ions for the preparation of transition metal-stabilised polyphosphorus cations, a systematic evaluation of the reactivity trend from lighter phosphenium to their heavier homologues is still missing. Most notably, the reactivity of polyphosphorus complexes towards stibenium ions is completely unexplored to the best of our knowledge. With respect to the above results, a neutral *cyclo*-P_4 complex should be optimally suited for the purpose of evaluating the addition or insertion behaviour of pnictogenium ions. Herein we report the functionalisation of $[Cp^RTa(CO)_2(\eta^4\text{-}P_4)]$ (**A**: Cp^R = Cp‴; **B**: Cp^R = Cp″)[19] with a variety of aryl-

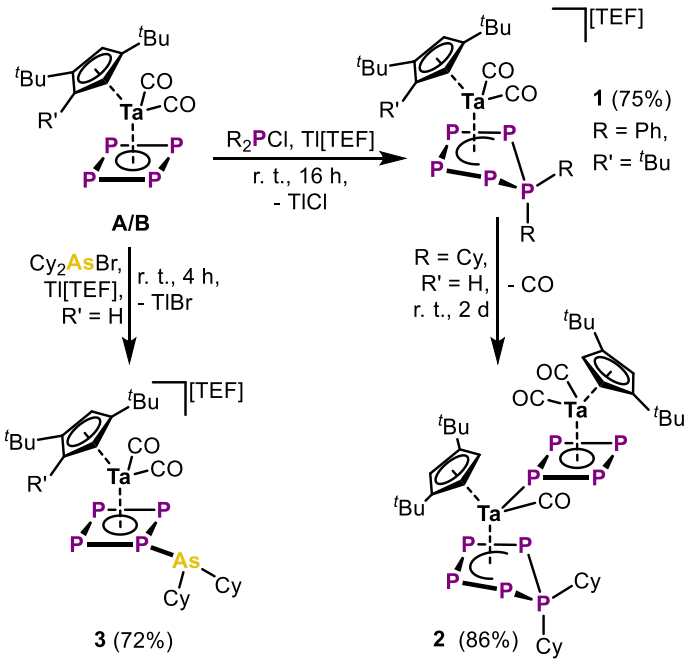

*Scheme 2: Synthesis of **1** and **2** from **A/B** via phosphenium ion insertion/ring expansion and **3** via arsenium ion addition.*

and alkyl-substituted pnictogenium ions. While the tendency towards either addition or insertion is primarily governed by the pnictogen present, variation of substituents and reaction conditions influence the reaction outcome as well. Additionally, the exchange of the bulkier Cp‴ (in **A**) for the sterically less demanding Cp″ (in **B**) is demonstrated to trigger an additional aggregation reaction upon insertion of a phosphenium ion.[20]

4.3. Results and Discussion

Initially, **A** and **B** were reacted with alkyl- and aryl-substituted phosphenium cations, generated *in situ* via halide abstraction from chlorophosphines and Tl[TEF] ([TEF]$^-$ = [Al{OC(CF$_3$)$_3$}$_4$]$^-$).[21] Similar mixtures of R$_2$EX (E = P, As, X = Br, I) and Ag$^+$ ions were found to provide free pnictogenium cations.[22] Interestingly, the aryl-substituted [Ph$_2$P]$^+$ cleanly inserts into one of the P–P bonds of **A** to give rise to the *cyclo*-P$_5$R$_2$ compound [Cp‴Ta(CO)$_2$(η^4-P$_5$Ph$_2$)][TEF] (**1**, Scheme 2) in 75% yield. In contrast, the reaction of the alkyl phosphenium cation [Cy$_2$P]$^+$ with **B** only intermediately leads to an isostructural species **2$_{int}$** compared to **1** (via NMR, see ESI). Choice of the sterically less demanding Cp″ ligand in **B** causes **2$_{int}$** to rapidly decarbonylate and addition of a second unit of **B** occurs to finally afford the dinuclear complex [Cp″Ta(CO){Cp″Ta(CO)$_2$(μ,$\eta^{4:1}$-P$_4$}(η^4-P$_5$Ph$_2$)][TEF] (**2**) in good yields of 86%. However, when the electrophile is exchanged for the heavier arsenium ion [Cy$_2$As]$^+$, the product [Cp″Ta(CO)$_2$(η^4-P$_4$AsCy$_2$)][TEF] (**3**) is obtained in 72% yield. Notably, **3** displays a borderline case as it shows a *cyclo*-P$_4$ ligand with an exocyclic Cy$_2$As substituent in the solid state, while multinuclear solution NMR spectroscopic studies are in line with the arsenium ion being inserted into the P$_4$ ring (*vide infra*). The central structural motif in **1** and **2** is the *cyclo*-P$_5$R$_2$ ligand coordinated to the Ta centre (Figure 1). While the latter still bears two CO ligands in **1**, one of these ligands is displaced by a second moiety of **B** in **2**. However, this substitution has only minor implications on the structure of both the *cyclo*-P$_5$Cy$_2$ (P1 – P5) and the *cyclo*-P$_4$ (P6 – P9) ligand in **2**, as can be seen in the P–P bond lengths of 2.157(1) – 2.165(1) Å (**B**: 2.150(2) – 2.173(3) Å).[19] The *cyclo*-P$_5$R$_2$ ring in both compounds can best be described showing partial

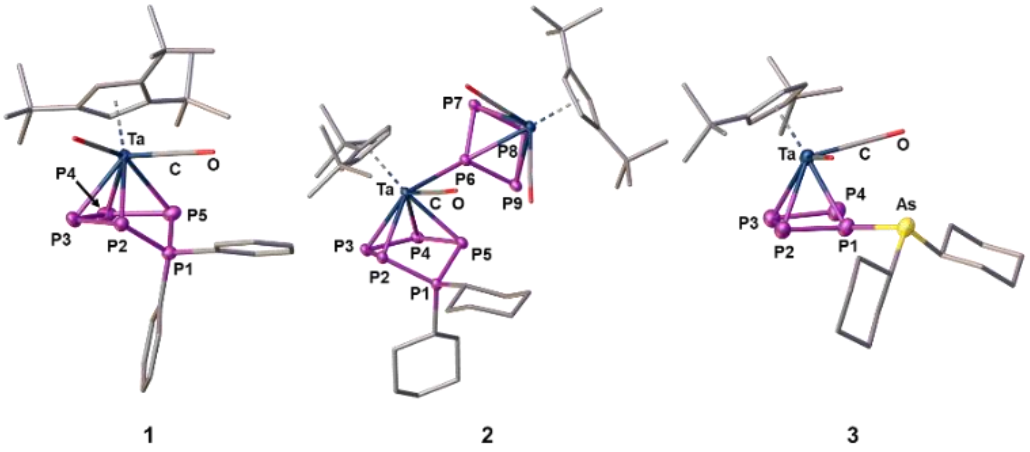

*Figure 1: Solid-state structures of **1** – **3**; counter anions and H atoms are omitted for clarity and ellipsoids are drawn the 50% probability level.*

double-bond character for the P2–P3 (**1**: 2.150(2) Å, **2**: 2.138(1) Å) and the P4–P5 (**1**: 2.141(2) Å, **2**: 2.160(1) Å) bonds,[23] with the P1 atom bent out of the plane of the residual four P atoms by 52.7(1)° (**1**) and 57.0(1)° (**2**), respectively. Thus, a typical envelope structural motif is obtained, which has been observed for similar neutral *cyclo*-P_5R_2 as well as anionic *cyclo*-P_5R^- ligands.[16,24] In contrast, the solid-state structure of **3** reveals an intact *cyclo*-P_4 ligand which is functionalised via the addition of the Cy_2As moiety to P1 (Figure 1). The new P1–As bond length (2.348(1) Å) is in the range of a single bond,[23] while the P–P bonds (2.141(2) – 2.176(2) Å) remain nearly unchanged compared to **B**.[19] The ^{1}H NMR spectra of **1** – **3** reveal the hindered rotation of the respective Cp^R ligands and thus the asymmetric nature of the compounds. Accordingly, the $^{31}P\{^1H\}$ NMR spectrum of **1** (CD_2Cl_2, r. t.) reveals an AMNXY spin system with five chemically different P atoms, where P^A shows the signal broadening expected for the PPh_2 moiety in the ^{31}P NMR spectrum. Furthermore, **2** shows similar $^{31}P\{^1H\}$ and ^{31}P NMR spectra with additional four signals arising from the additional moiety of **B** coordinated to the Ta centre. Lastly, the $^{31}P\{^1H\}$ NMR spectrum of **3** does not show the expected set of signals for an intact and substituted P_4 cycle. In contrast, the AMXY spin system is reminiscent of the insertion of the $AsCy_2$ moiety into the *cyclo*-P_4 ligand. This behaviour is observed even when dissolving crystalline **3** in cold *o*-DFB. Accordingly, a rapid transformation of the addition product to the inserted one seems to take place upon dissolution, while the coordination of the $AsCy_2$ fragment to the *cyclo*-P_4 ligand likely stems from packing effects in the solid state. The latter agrees with DFT calculations on this isomerisation process (*vide infra*) and the observation that redissolved **3** forms the addition product upon crystallisation repeatedly. Additionally, **A** and **B** were exposed to two different stibenium cations. Interestingly, the simple $[SbPh_2]^+$ needs two moieties of **B** for its coordinative stabilisation. After simple workup, the complex $[\{Cp''Ta(CO)_2(\eta^4\text{-}P_4)\}_2SbPh_2][TEF]$ (**4**, Figure 2a) can be isolated as an orange brown powder in good yields of 73%. In contrast, steric and electronic tuning of the stibenium electrophile as well as the choice of the bulkier Cp‴ ligand allowed the isolation of a singly coordinated species. Reaction of **A** with one equivalent of [Cp‴SbI][TEF][17] yields $[Cp''Ta(CO)_2(\eta^4\text{-}P_4)Sb(I)Cp''][TEF]$ (**5**) with an intact, functionalised *cyclo*-P_4 ligand in 56% yield.

The solid-state structure of **4** (Figure 2b) features the central stibenium cation being coordinated by two units of **B**. While the P–P bond lengths (2.154(2) – 2.174(2) Å) remain nearly unchanged compared to the starting material, the new Sb–P distances (2.760(1)/2.891(1) Å) are longer than the sum of the respective covalent radii,[19] hinting towards the coordinative nature of these bonds. Furthermore, the planes of both *cyclo*-P_4 ligands are tilted against each other by 100.4(1)°. In contrast, the $[Cp'''SbI]^+$ cation in **5** is only coordinated by one unit of **A**, which is attributed to the larger steric demand of the Cp‴ substituent and the higher electronic stabilisation it invokes at the Sb centre. Again, the P–P bonds (2.154(3) – 2.170(3) Å) undergo only minor changes upon coordination of the stibenium ion and the Sb–P distance (2.772(2) Å) is slightly elongated compared to the sum of the respective covalent radii. In agreement, the ^{1}H NMR spectra of **4** and **5** reveal signals in accordance with rotationally unhindered Cp^R ligands. Furthermore, the ^{31}P NMR spectra of

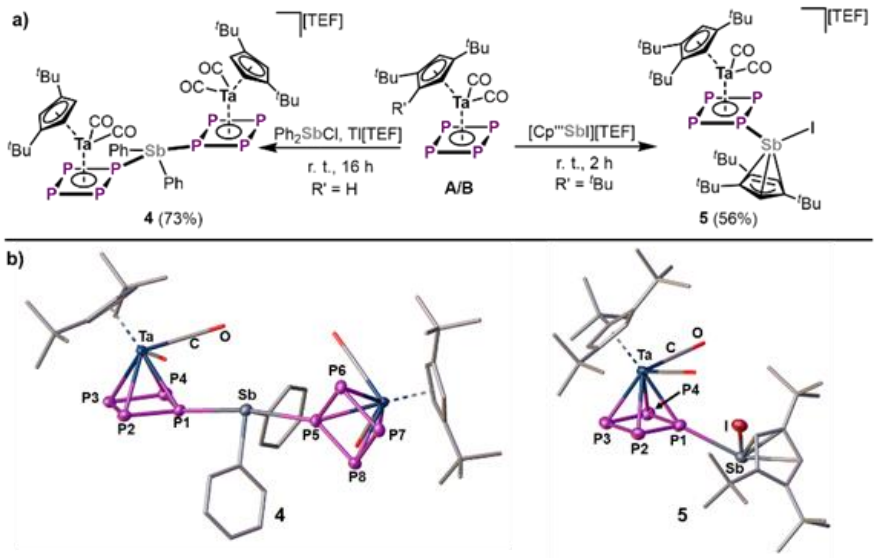

*Figure 2: a) Synthesis of **4** and **5** via coordination of stibenium ions to **A** and **B**; b) Solid-state structures of **4** and **5**; counter anions and H atoms are omitted for clarity and ellipsoids are drawn the 50% probability level.*

both compounds show AMX_2 spin systems reminiscent of the starting materials **A** and **B**. However, the signals are shifted due to the coordination to the respective stibenium cation in **4** and **5**.

To shed further light onto the distinct addition or insertion reactivities of pnictogenium ions towards the *cyclo*-P_4 complexes **A** and **B**, DFT calculations (ωB97X-D4[25]/def2-TZVP[26]) were performed to elaborate the thermodynamic relation between inserted and coordinated species. The sterically demanding Cp^R groups were replaced with standard Cp ligands and simple $[EMe_2]^+$ (E = P, As, Sb) cations were used in the model systems **1′** – **4′** to save computational resources. In contrast to the experimental results, the insertion of $[EMe_2]^+$ into the *cyclo*-P_4 is found to be exergonic for the model systems **1′** – **4′** (see ESI, Table S3). More precisely, the insertion (**1′$_{Ins}$**) of the phosphenium ion is strongly exergonic by 86.0 kJ/mol compared to its coordination (**1′$_{Coord}$**), while both species are closer (43.9 kJ/mol) or similar (1.5 kJ/mol) in energy for the arsenium and stibenium cations, respectively. However, the electronic structure of the coordinated isomers drastically changes upon exchange of the phosphino group for its heavier analogues (for details see ESI). While **1′$_{Coord}$** features a covalent P–P bond (Figure 3) with similar orbital contributions of both P atoms and a WBI of 0.90, the latter decreases over **3′$_{Coord}$** (0.83) to **4″$_{Coord}$** (0.71) accompanied by the increased polarisation of the P–E bond (E = As, Sb). This trend highlights the tendency of the heavier pnictogenium ions to engage in dative bonding and thus a stabilisation of the coordinated species compared to the insertion products. Furthermore, the lone pair of electrons located at the coordinated pnictogenium cation shows increased s-character going from **1′$_{Coord}$** (52%) over **3′$_{Coord}$** (63%) to **4″$_{Coord}$** (70%). Summing up, the covalency of the P1–E bond as well as the availability of the E-centred lone pair of electrons increase from **4″$_{Coord}$** to **1′$_{Coord}$** explaining the ring expansion tendency of the latter, compared to its heavier analogues. At last, the bonding interaction within **4′** was investigated and shown to be of mostly electrostatic nature. Two lone pairs of the respective

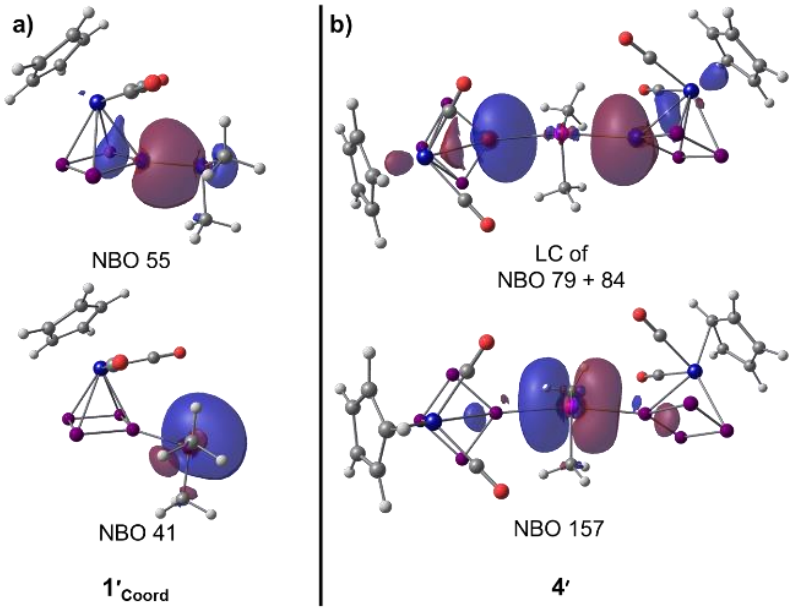

Figure 4: a) Selected NBOs representing the P–E bond as well as the lone electron pair in ***1'Coord****,* ***3'Coord*** *and* ***4''Coord*** *exemplarily shown for* ***1'Coord****; b) bonding interaction within* ***4'*** *caused by the interaction of a linear combination of two P-centred lone electron pairs with an empty p-type orbital at Sb; LC = linear combination.*

cyclo-P_4 ligands form a bonding interaction with an empty p-orbital at the stibenium cation. Notably, similar interaction has been observed for phosphine complexes of simple stibenium cations and has been studied in great detail.[27]

4.4. Conclusion

In conclusion, this systematic study of the reactivity of pnictogenium cations towards the *cyclo*-P_4 complexes **A** and **B** provides an overview of the distinct insertion and addition trends of these interesting carbene analogues. Phosphenium cations readily insert into one of the P–P bonds of **A** and **B** to afford the ring-expanded *cyclo*-P_5R_2 compounds **1** and **2**. In contrast, arsenium cations reveal their ambivalent character, as the solid-state structure of **3** clearly shows addition to the *cyclo*-P_4 ligand, while its spectroscopic data in solution hints towards the insertion of the arsenium cation into the *cyclo*-P_4 ligand. Furthermore, the sterically unstabilised $[SbPh_2]^+$ simply adds to the *cyclo*-P_4 ligand of **B**. However, addition of a second unit of **B** is necessary to stabilise the highly electrophilic and sterically unshielded stibenium cation in **4**. Lastly, employing the sterically tuned stibenium cation $[Cp'''SbI]^+$ affords the monocoordinated complex **5**. These findings are supported by DFT calculations, providing insight into the reaction pathway, and thus explaining the distinct reactivities within this system. Accordingly, this work may suit as a point of reference for future research into the reactivity of pnictogenium cations and heavier carbene analogues in general. Moreover, compounds **1** – **5** could serve as useful starting materials for the synthesis of polyphosphorus compounds incorporating heteroatoms.

4.5. Supporting Information

4.5.1. Experimental Procedures

General Considerations

All manipulations were carried out using standard Schlenk techniques at a Stock apparatus under N_2 as an inert gas or in a glove box with Ar atmosphere. All glassware was dried with a heat gun (600 °C) for at least 30 min prior to use. *o*-DFB (1,2-difluorobenzene) was distilled from P_2O_5, CD_2Cl_2 was distilled from CaH_2 and other solvents were directly taken from an MBraun SPS-800 solvent purification system and degassed at room temperature. Solution ^{1}H (400.130 MHz), ^{19}F (376.498 MHz)a and ^{31}P (161.976 MHz) NMR spectra were recorded at an Avance400 (Bruker) spectrometer using $(H_3C)_4Si$ (^{1}H, ^{13}C), $CFCl_3$ (^{19}F) or 85% phosphoric acid (^{31}P), respectively, as external standards. Chemical shifts (δ) are provided in parts per million (ppm) and coupling constants (*J*) are reported in Hertz (Hz). The following abbreviations are used: s = singlet, d = doublet, dd = doublet of doublets, dt = doublet of triplets, t = triplet, td = triplet of doublets br = broad and m = multiplet. Mass spectra were recorded at the internal mass spectrometry department using a ThermoQuest Finnigan TSQ 7000 (ESI) or Finnigan MAT 95 (LIFDI) mass spectrometer or by the first author on a Waters Micromass LCT ESI-TOF mass-spectrometer and peak assignment was performed using the Molecular weight calculator 6.50.[27] Elemental analysis of the products was conducted by the elemental analysis department at the University of Regensburg using an Elementar Vario EL. The starting materials $[Cp'''Ta(CO)_2(\eta^4\text{-}P_4)]$ (**A**), $[Cp''Ta(CO)_2(\eta^4\text{-}P_4)]$ (**B**),[19] Tl[TEF],[28] Cy_2AsBr[29] and [Cp‴SbI][TEF][30] were synthesized according to literature procedures. All other chemicals were purchased from commercial vendors and used without further purification.

*[Cp'''Ta(CO)$_2$(η^4-P$_5$Ph$_2$)][TEF] (**1**)*

A solution of Tl[TEF] (117 mg, 0.1 mmol, 1 eq.) in 4 mL *o*-DFB was added to a solution of **A** (59 mg, 0.1 mmol, 1 eq.) and Ph_2PCl (0.5 mL stock solution in toluene (c = 0.2 M), 0.1 mmol, 1 eq.) resulting in the rapid precipitation of colourless solid and a slow colour change to orange. After stirring the mixture for 2 h, 50 mL of *n*-hexane were added to precipitate a yellow solid. The supernatant was decanted, the solid dried and then resuspended in 4 mL of CH_2Cl_2. The yellow solution was filtered, constrained to 2 mL and again 50 mL of *n*-hexane were added to precipitate the product [Cp'''Ta(CO)$_2$(η^4-P$_5$Ph$_2$)][TEF] (**1**) as a yellow solid. After drying, **1** could be isolated as a yellow powder. Single crystals suitable for X-ray diffraction studies can be obtained by layering a concentrated solution of **1** in 3 mL of *o*-DFB with 15 mL of *n*-hexane and storing the mixture at -30 °C for 10 days.

Yield:	130 mg (0.075 mmol, 75%).
Elemental analysis:	calc. (%) for $C_{47}H_{39}O_6F_{36}AlP_5Ta\bullet(C_6H_{14})_{0.3}$: C: 33.07, H: 2.46. found (%): C: 33.12, H: 2.28. Notably, *n*-hexane is not found in the crystal structure of **1**. However, the ^{1}H NMR spectrum of crystalline **1** reveals signals in agreement with the presence of *n*-hexane, even after extensive drying under reduced pressure.
ESI(+) MS (*o*-DFB):	*m/z* (%) = 779.1 (90, [**1**]$^+$), 751.1 (100, [**1**-CO]$^+$), 723.2 (20, [**2**-2CO]$^+$).
NMR (CD_2Cl_2, r.t.):	**^{1}H**: *δ*/ppm = 1.27 (s, 9 H, $C_5H_2{}^t\underline{Bu_3}$), 1.37 (s, 9 H, $C_5H_2{}^t\underline{Bu_3}$), 1.54 (s, 9 H, $C_5H_2{}^t\underline{Bu_3}$), 5.65 (s, 1 H, $C_5\underline{H_2}{}^tBu_3$), 6.02 (m, 1 H, $C_5\underline{H_2}{}^tBu_3$), 7.21 (m, 2 H, Ph), 7.44 (m, 2 H, Ph), 7.54 (m, 1 H, Ph), 7.66 (m, 2 H, Ph), 7.78 (m, 1 H, Ph), 8.16 (m, 2 H, Ph). **^{31}P{^{1}H}**: *δ*/ppm = 119.6 (m, 1 P, P^A), -7.0 (m, 1 P, P^M), -25.9 (m, 1 P, P^N), -104.9 (m, 1 P, P^X), -108.3 (m, 1 P, P^Y), coupling constants given with the spectral simulation (*vide infra*). **^{31}P**: *δ*/ppm = 119.6 (m (broadened), 1 P, P^A), -7.0 (m, 1 P, P^M), -25.9 (m, 1 P, P^N), -104.9 (m, 1 P, P^X), -108.3 (m, 1 P, P^Y), coupling constants given with the spectral simulation (*vide infra*). **^{19}F{^{1}H}**: *δ*/ppm = -75.6 (s, [TEF]$^-$).
IR (ATR, r. t.):	$\tilde{\nu}$/cm^{-1} = 2975 (w), 2045 (m), 2008 (m), 1352 (m), 1297 (m), 1274 (s), 1238 (vs), 1209 (vs), 1163 (s), 1096 (m), 969 (vs), 831 (w), 742 (w), 726 (s), 701 (m), 689 (m)

*[Cp''Ta(CO){Cp''Ta(CO)$_2$(μ,$\eta^{4:1}$-P$_4$)}(η^4-P$_5$Cy$_2$)][TEF] (**2**)*

Cy_2PBr (29 μL stock solution in toluene (c = 1.07 M), 0.05 mmol, 0.5 eq.) was added to a solution of **B** (54 mg, 0.1mmol, 1 eq.) and Tl[TEF] (58 mg, 0.05 mmol, 0.5 eq.) in 3 mL *o*-DFB resulting in the rapid precipitation of colourless solid and a slow colour change to orange-red. After stirring the mixture for one day, 50 mL of *n*-hexane were added to precipitate an orange solid. The supernatant was decanted, the solid dried and then resuspended in 3 mL of *o*-DFB. The solution was filtered, and again 60 mL of *n*-hexane were added to precipitate the product [Cp″Ta(CO){Cp″Ta(CO)$_2$(μ,η$^{4:1}$-P$_4$}(η^4-P$_5$Cy$_2$)][TEF] (**2**) as an orange-red solid. Single crystals suitable for X-ray diffraction studies could be obtained by layering a concentrated solution of **2** in 4 mL of *o*-DFB with 30 mL of *n*-hexane and storing the mixture at r. t. for 8 days.

Yield:	98 mg (0.043 mmol, 86%).
Elemental analysis:	calc. (%) for $C_{57}H_{64}O_7F_{36}AlP_9Ta_2$: C: 30.94, H: 2.92. found (%): C: 30.55, H: 2.91.
ESI(+) MS (*o*-DFB):	*m/z* (%) = 1244.9 (70, [**2**]$^+$), 1217.1 (10, [**2**-CO]$^+$), 707.0 (100, [**2**-**B**]$^+$), 679.1 (15, [**2**-**B**-CO]$^+$).
NMR (CD_2Cl_2, r.t.):	**^{1}H**: *δ*/ppm = 1.09 (s, 9 H, $C_5H_3{}^tBu_2$), 1.12 (s, 9 H, $C_5H_3{}^tBu_2$), 1.14 (s, 9 H, $C_5H_3{}^tBu_2$), 1.52 (s, 9 H, $C_5H_3{}^tBu_2$), 0.8 - 2.3 (several overlapping multiplets, Cy), 4.33 (m, 1 H, $C_5\underline{H_3}{}^tBu_2$), 5.37 ((m, 1 H, $C_5\underline{H_3}{}^tBu_2$), 5.82 (m, 1 H, $C_5\underline{H_3}{}^tBu_2$), 6.10 (m, 1 H, $C_5\underline{H_3}{}^tBu_2$), 6.16 (m, 1 H, $C_5\underline{H_3}{}^tBu_2$), 6.33 (m, 1 H, $C_5\underline{H_3}{}^tBu_2$). **^{31}P{^{1}H}**: *δ*/ppm = 129.7 (m, 1 P, P^A), 3.3 (m, 1 P, P^M), -12.1 (m, 1 P, P^N), -22.0 (m, 1 P, P^O), -43.9 (m, 1 P, P^P), -70.9 (m, 1 P, P^Q), -74.7 (m, 1 P, P^R), -127.4 (m, 1 P, P^X), -129.3 (m, 1 P, P^Y), coupling information is discussed below (*vide infra*). **^{31}P**: *δ*/ppm = *δ*/ppm = 129.7 (m, 1 P, P^A), 3.3 (m, 1 P, P^M), -12.1 (m, 1 P, P^N), -22.0 (m, 1 P, P^O), -43.9 (m, 1 P, P^P), -70.9 (m, 1 P, P^Q), -74.7 (m, 1 P, P^R), -127.4 (m, 1 P, P^X), -129.3 (m, 1 P, P^Y), coupling information is discussed below (*vide infra*). **^{19}F{^{1}H}**: *δ*/ppm = -75.6 (s, [TEF]$^-$).
IR (ATR, r. t.):	$\tilde{\nu}$/cm^{-1} = 2963 (w), 2023 (m), 2022 (m), 1971 (m), 1352 (w), 1297 (m), 1274 (s), 1239 (s), 1209 (vs), 1164 (s), 969 (vs), 886 (w), 862 (w), 820 (w), 755 (w), 726 (vs)

*[Cp''Ta(CO)$_2$(η^4-P$_4$AsCy$_2$)][TEF] (**3**)*

Cy_2AsBr (15 µL, 0.1 mmol, 1 eq.) was added to a solution of **B** (54 mg, 0.1 mmol, 1 eq.) and Tl[TEF] (117 mg, 0.1 mmol, 1 eq.) in 4 mL *o*-DFB resulting in the rapid precipitation of colourless solid and a slow colour change to orange. After stirring the mixture for 3 h, the solution was constrained to 1 mL and 50 mL of *n*-hexane were added to precipitate an orange solid. The supernatant was decanted, the solid dried and then resuspended in 4 mL of *o*-DFB. The solution was filtered, and again 30 mL of *n*-hexane were added to precipitate the product [Cp″Ta(CO)$_2$(η^4-P$_4$AsCy$_2$)][TEF] (**3**) as a red oil. This oil was washed with 5 mL of toluene and two times with 10 mL of *n*-hexane, each, affording **3** as a red solid, which could be isolated after drying under reduced pressure (10^{-3} mbar). Single crystals suitable for X-ray diffraction studies could be obtained by layering a concentrated solution of **3** in 2 mL of *o*-DFB with 20 mL of *n*-hexane and storing the mixture at -30 °C for one month.

Yield:	125 mg (0.072 mmol, 72%).
Elemental analysis:	calc. (%) for $C_{43}H_{43}O_6F_{36}AlP_4AsTa\bullet(C_6H_4F_2)_{0.4}$: C: 30.43, H: 2.51. found (%): C: 30.33, H: 2.54.
ESI(+) MS (*o*-DFB):	*m/z* (%) = 779.1 (40, [**3**]$^+$), 751.1 (100, [**3**-CO]$^+$), 723.2 (40, [**2**-2CO]$^+$), 483.2 (90, [**B**-2CO+H]$^+$).
NMR (*o*-DFB/C_6D_6, r.t.):	**^{1}H**: *δ*/ppm = 1.28 (s, 9 H, $C_5H_3{}^t\underline{Bu_2}$), 1.39 (s, 9 H, $C_5H_3{}^t\underline{Bu_2}$), 1.0 – 2.5 (several overlapping multiplets, Cy), 5.12 (m, 1 H, $C_5\underline{H_3}{}^tBu_2$), 5.74 (m, 1 H, $C_5\underline{H_3}{}^tBu_2$), 5.89 (m, 1 H, $C_5\underline{H_3}{}^tBu_2$). **^{31}P{^{1}H}**: *δ*/ppm = -11.7 (td, $^1J_{PA\text{-}PM}$ = 361 Hz, $^1J_{PA\text{-}PX}$ = 359 Hz, $^2J_{PA\text{-}PY}$ = 46 Hz, 1 P, P^A), -33.7 (ddd, $^1J_{PM\text{-}PY}$ = 388 Hz, $^1J_{PM\text{-}PA}$ = 361 Hz, $^2J_{PM\text{-}PX}$ = 48 Hz, 1 P, P^M), -108.2 (dd, $^1J_{PX\text{-}PA}$ = 359 Hz, $^2J_{PX\text{-}PM}$ = 48 Hz, 1 P, P^X), -111.0 (dd, $^1J_{PY\text{-}PM}$ = 388 Hz, $^2J_{PY\text{-}PA}$ = 46 Hz, 1 P, P^Y). **^{31}P**: *δ*/ppm = -11.7 (td, $^1J_{PA\text{-}PM}$ = 361 Hz, $^1J_{PA\text{-}PX}$ = 359 Hz, $^2J_{PA\text{-}PY}$ = 46 Hz, 1 P, P^A), -33.7 (ddd, $^1J_{PM\text{-}PY}$ = 388 Hz, $^1J_{PM\text{-}PA}$ = 361 Hz, $^2J_{PM\text{-}PX}$ = 48 Hz, 1 P, P^M), -108.2 (dd, $^1J_{PX\text{-}PA}$ = 359 Hz, $^2J_{PX\text{-}PM}$ = 48 Hz, 1 P, P^X), -111.0 (dd, $^1J_{PY\text{-}PM}$ = 388 Hz, $^2J_{PY\text{-}PA}$ = 46 Hz, 1 P, P^Y). **^{19}F{^{1}H}**: *δ*/ppm = -75.5 (s, [TEF]$^-$).
IR (ATR, r. t.):	$\tilde{\nu}$/cm^{-1} = 2933 (w), 2039 (w), 2001 (w), 1351 (m), 1297 (m), 1274 (s), 1210 (vs), 1164 (s), 969 (vs), 8857 (m), 831 (w), 756 (w), 726 (s)

*[{Cp''Ta(CO)$_2$(η^4-P$_4$)}$_2$SbPh$_2$][TEF] (**4**)*

A solution of Ph_2SbCl (31 mg, 0.01 mmol, 1 eq.) in 2 mL *o*-DFB was added to a solution of **B** (108 mg, 0.2 mmol, 2 eq.) and Tl[TEF] (117 mg, 0.1 mmol, 1 eq.) in 4 mL of *o*-DFB resulting in the rapid precipitation of colourless solid and a slow colour change to brownish yellow. After stirring the mixture for 2 h, 50 mL of *n*-hexane were added to precipitate a yellow solid. The supernatant was decanted, the solid dried and then resuspended in 4 mL of CH_2Cl_2. The yellowish solution was filtered, constrained to 2 mL and again 50 mL of *n*-hexane were added to precipitate the product [{Cp″Ta(CO)$_2$(η^4-P$_4$)}$_2$SbPh$_2$][TEF] (**4**) as a brownish yellow solid. After drying, **4** could be isolated as a brownish yellow powder. Single crystals suitable for X-ray diffraction studies could be obtained by slow addition of 20 mL of *n*-hexane to a concentrated solution of **4** in 2 mL of *o*-DFB.

Yield:	170 mg (0.073 mmol, 73%).
Elemental analysis:	calc. (%) for $C_{58}H_{52}O_8F_{36}AlP_8SbTa_2$: C: 30.03, H: 2.26. found (%): C: 30.15, H: 2.28.
ESI(+) MS (*o*-DFB):	*m/z* (%) = 1323.1 (20, [**4**-CO]$^+$), 813.0 (100, [**4**-**B**]$^+$), 539.1 (70, [**B**+H]$^+$), 483.1 (60, [**B**-2CO+H]$^+$), several unidentified fragmentation products.
NMR (CD_2Cl_2, r.t.):	**^{1}H**: *δ*/ppm = 1.11 (s, 36 H, $C_5H_3{}^t\underline{Bu_2}$), 6.15 (m, 4 H, $C_5\underline{H_3}{}^tBu_2$), 6.45 (m, 2 H, $C_5\underline{H_3}{}^tBu_2$), 7.62 (m (br), 6 H, Ph), 7.79 (m (br), 4 H, Ph). **^{31}P{^{1}H}**: *δ*/ppm = 40.1 (t (br), $^1J_{PA\text{-}PX}$ = 297 Hz, 1 P, P^A), 16.7 (t (br), $^1J_{PM\text{-}PX}$ = 247 Hz, 1 P, P^M), -4.7 (dd (br), $^1J_{PX\text{-}PA}$ = 297 Hz, $^1J_{PX\text{-}PM}$ = 247 Hz, 2 P, P^X). **^{31}P**: *δ*/ppm = 40.1 (t (br), $^1J_{PA\text{-}PX}$ = 297 Hz, 1 P, P^A), 16.7 (t (br), $^1J_{PM\text{-}PX}$ = 247 Hz, 1 P, P^M), -4.7 (dd (br), $^1J_{PX\text{-}PA}$ = 297 Hz, $^1J_{PX\text{-}PM}$ = 247 Hz, 2 P, P^X). **^{19}F{^{1}H}**: *δ*/ppm = -75.6 (s, [TEF]$^-$).
IR (ATR, r. t.):	$\tilde{\nu}$/cm^{-1} = 2963 (w), 2030 (m), 2020 (s), 1986 (s), 1367 (m), 1351 (m), 1296 (s), 1274 (s), 1239 (s), 1211 (vs), 1164 (s), 1061 (m), 971 (vs), 919 (m), 880 (m), 859 (m), 830 (m), 726 (vs), 693 (m)

*[Cp‴Ta(CO)$_2$(η^4-P$_4$Sb(I)Cp‴)][TEF] (**5**)*

A solution of Cp‴SbI$_2$ (61 mg, 0.1 mmol, 1 eq.) in 2 mL *o*-DFB was added to a solution of **A** (59 mg, 0.1 mmol, 1 eq.) and Tl[TEF] (117 mg, 0.1 mmol, 1 eq.) in 4 mL of *o*-DFB resulting in the rapid precipitation of pale yellow solid and a slow colour change to clear red. After stirring the mixture for 2 h, 50 mL of *n*-hexane were added to precipitate a red solid. The supernatant was decanted, the solid dried and then resuspended in 4 mL of CH_2Cl_2. The red solution was filtered, constrained to 2 mL and again 50 mL of *n*-hexane were added to precipitate the product [Cp‴Ta(CO)$_2$(η^4-P$_4$Sb(I)Cp‴)][TEF] (**5**) as a clear red solid. After drying, **5** could be isolated as a red powder. Single crystals suitable for X-ray diffraction studies could be obtained by layering a concentrated solution of **5** in 3 mL of CH_2Cl_2 with 30 mL of *n*-hexane and storing the mixture at -30 °C for two weeks.

Yield:	115 mg (0.056 mmol, 56%).
Elemental analysis:	calc. (%) for $C_{52}H_{58}O_6F_{36}AlP_4SbITa$: C: 30.56, H: 2.86. found (%): C: 30.92, H: 2.95.
ESI(+) MS (*o*-DFB):	*m/z* (%) = 404.3 (70), 279.2 (100), **5** undergoes complete fragmentation leading to decomposition under mass spectrometric conditions.
NMR (CD_2Cl_2, r.t.):	**^{1}H**: *δ*/ppm = 1.05 (s, 9 H, $C_5H_2{}^tBu_3$), 1.45 (s, 9 H, $C_5H_2{}^tBu_3$), 1.52 (s, 18 H, $C_5H_2{}^tBu_3$), 1.56 (s, 18 H, $C_5H_2{}^tBu_3$), 6.38 (s, 2 H, $C_5H_2{}^tBu_3$), 6.71 (s, 2 H, $C_5H_2{}^tBu_3$). **^{31}P{^{1}H}**: *δ*/ppm = 39.4 (t (br), $^1J_{PA\text{-}PX}$ = 300 Hz, 1 P, P^A), 10.8 (t (br), $^1J_{PM\text{-}PX}$ = 253 Hz, 1 P, P^M), -1.1 (dd (br), $^1J_{PX\text{-}PA}$ = 300 Hz, $^1J_{PX\text{-}PM}$ = 253 Hz, 2 P, P^X). **^{31}P**: *δ*/ppm = 39.4 (t (br), $^1J_{PA\text{-}PX}$ = 300 Hz, 1 P, P^A), 10.8 (t (br), $^1J_{PM\text{-}PX}$ = 253 Hz, 1 P, P^M), -1.1 (dd (br), $^1J_{PX\text{-}PA}$ = 300 Hz, $^1J_{PX\text{-}PM}$ = 253 Hz, 2 P, P^X). **^{19}F{^{1}H}**: *δ*/ppm = -75.6 (s, $[TEF]^-$).
IR (ATR, r. t.):	$\tilde{\nu}$/cm^{-1} = 2975 (w), 2025 (m), 1988 (m), 1352 (m), 1297 (m), 1274 (s), 1239 (s), 1211 (vs), 1163 (s), 1061 (w), 970 (vs), 878 (w), 833 (w), 726 (vs), 693 (w), 680 (w)

4.5.2. X-ray Crystallographic Data

General Considerations

The crystallographic data for all described compounds were collected on a SuperNova diffractometer (Rigaku) with a Titan^{S2} detector using Cu–K$_\alpha$ radiation (**3**, **5**), on an Xcalibur Gemini (Rigaku) with an Atlas^{S2} detector using Cu–K$_\alpha$ (**1**, **4**) radiation, or an XtaLAB Synergy R, DW System (Rigaku) with a HyPix-Arc 150 detector using Cu-K$_\alpha$ radiation from a rotating anode (**2**). Data reduction and absorption correction were performed with the CrysAlisPro software package.[31] Structure solution and refinement was conducted in Olex2 (1.5-alpha)[32] with ShelXT[33] (solution) and ShelXL-2018/3[34] (least squares refinement (F^2)). All non-H atoms were refined with anisotropic displacement parameters and H atoms were treated as riding models with isotropic displacement parameters and fixed C–H bond lengths (sp^3: 0.96 (CH_3), 0.97 (CH_2); sp^2: 0.93 (CH)). Visualisation of the crystal structures was performed with Olex2 (1.5-alpha).[32]

CCDC-2280522 (**1**), CCDC-2280523 (**2**), CCDC-2280524 (**3**), CCDC-2280525 (**4**), and CCDC2280526 (**5**) contain the supplementary crystallographic data for this paper. These data can be obtained free of charge at www.ccdc.cam.ac.uk/conts/retrieving.html (or from the Cambridge Crystallographic Data Centre, 12 Union Road, Cambridge CB2 1EZ, UK; Fax: + 44-1223-336-033; email: deposit@ccdc.cam.ac.uk).

*Table S 1: Crystallographic and refinement data for compounds **1** – **5**.*

Compound	1	2	3	4	5
Empirical formula	$C_{47}H_{39}AlF_{36}O_6P_5Ta$	$C_{57}H_{64}O_7F_{36}AlP_9Ta_2$	$C_{46}H_{45}AlAsF_{37}O_6P_4Ta$	$C_{58}H_{52}O_8F_{36}AlP_8SbTa_2$	$C_{52}H_{58}O_6F_{36}AlP_4SbITa$
Formula weight	1746.71	2212.69	1803.55	2319.38	2043.44
Temperature/K	293(2)	123.01(10)	122.98(14)	123(2)	123.00(10)
Crystal system	triclinic	triclinic	triclinic	triclinic	triclinic
Space group	$P\bar{1}$	$P\bar{1}$	$P\bar{1}$	$P\bar{1}$	$P\bar{1}$
a/Å	14.9785(3)	15.59941(8)	10.4865(2)	11.8387(3)	10.6596(4)
b/Å	15.3177(3)	16.56789(7)	14.5949(3)	17.1357(3)	16.9425(5)
c/Å	15.6939(3)	16.90000(7)	21.4991(5)	20.9703(5)	21.4058(7)
α/°	95.299(2)	112.5307(4)	79.473(2)	111.931(2)	109.867(3)
β/°	108.400(2)	99.2052(4)	79.942(2)	96.332(2)	91.228(3)
γ/°	110.628(2)	91.6604(4)	85.7070(10)	90.449(2)	98.222(3)
Volume/Å3	3112.47(12)	3962.89(3)	3182.19(12)	3916.65(16)	3588.2(2)
Z	2	2	2	2	2
ρcalcg/cm3	1.864	1.854	1.882	1.967	1.891
μ/mm-1	6.048	8.043	6.282	10.640	11.365
F(000)	1708.0	2160.0	1762.0	2236.0	1984.0
Crystal size/mm3	0.444 × 0.175 × 0.048	0.34 × 0.24 × 0.13	0.31 × 0.196 × 0.124	0.322 × 0.102 × 0.034	0.093 × 0.061 × 0.044
Radiation	Cu Kα (λ = 1.54184)	Cu Kα (λ = 1.54184)	Cu Kα (λ = 1.54184)	CuKα (λ = 1.54184)	CuKα (λ = 1.54184)
2Θ range for data collection/°	7.182 to 143.762	5.762 to 148.126	6.852 to 133.874	7.524 to 143.92	8.256 to 134.154
Index ranges	-17 ≤ h ≤ 18, -18 ≤ k ≤ 18, -19 ≤ l ≤ 19	-19 ≤ h ≤ 19, -20 ≤ k ≤ 20, -21 ≤ l ≤ 20	-12 ≤ h ≤ 11, -14 ≤ k ≤ 17, -25 ≤ l ≤ 25	-14 ≤ h ≤ 14, -16 ≤ k ≤ 21, -25 ≤ l ≤ 25	-12 ≤ h ≤ 12, -20 ≤ k ≤ 20, -25 ≤ l ≤ 25
Reflections collected	34318	148006	55899	43183	38301
Independent reflections	11896 [Rint = 0.0369, Rsigma = 0.0368]	15538 [Rint = 0.0387, Rsigma = 0.0141]	11297 [Rint = 0.0361, Rsigma = 0.0227]	15015 [Rint = 0.0477, Rsigma = 0.0512]	12796 [Rint = 0.0980, Rsigma = 0.0931]
Data/restraints /parameters	11896/6336/1478	15538/660/1248	11297/404/1268	15015/78/1233	12796/146/1019
Goodness-of-fit on F2	1.038	1.149	1.064	1.024	1.012
Final R indexes [I>=2σ (I)]	R1 = 0.0358, wR2 = 0.0929	R1 = 0.0249, wR2 = 0.0628	R1 = 0.0389, wR2 = 0.1024	R1 = 0.0381, wR2 = 0.0985	R1 = 0.0545, wR2 = 0.1290
Final R indexes [all data]	R1 = 0.0389, wR2 = 0.0953	R1 = 0.0250, wR2 = 0.0628	R1 = 0.0392, wR2 = 0.1026	R1 = 0.0441, wR2 = 0.1035	R1 = 0.0724, wR2 = 0.1427
Largest diff. peak/hole / e Å-3	1.70/-0.63	0.89/-1.14	3.41/-0.98	1.77/-1.65	2.18/-1.94

*[Cp'''Ta(CO)$_2$(η^4-P$_5$Ph$_2$)][TEF] (**1**)*

Compound **1** crystallizes in the triclinnic space group $P\bar{1}$ forming yellowish-orange plates from *o*-DFB/*n*-hexane mixtures at -30 °C (Figure S1). The asymmetric unit contains the cation and one anion. All non-hydrogen atoms were refined anisotropically and the H atoms were treated as riding models. Disorder within the anion and the cation was treated with appropriate restraints.

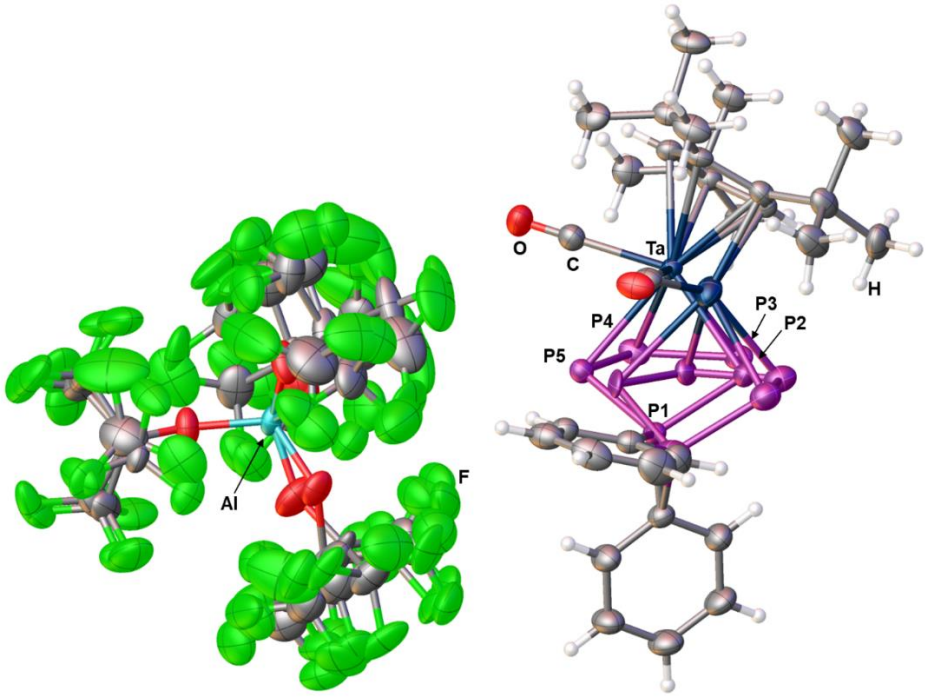

*Figure S 1: Solid state structure of **1**; Shown is the asymmetric unit containing one cation and one anion; ellipsoids are drawn at the 50% probability level.*

*[Cp''Ta(CO){Cp''Ta(CO)$_2$(μ,$\eta^{4:1}$-P$_4$)}(η^4-P$_5$Cy$_2$)][TEF] (**2**)*

Compound **2** crystallizes in the triclinnic space group $P\bar{1}$ forming clear orange blocks from *o*-DFB/*n*-hexane mixtures at room temperature (Figure S2). The asymmetric unit contains the cation and one anion. All non-hydrogen atoms were refined anisotropically and the H atoms were treated as riding models. Disorder within the anion was treated with appropriate restraints.

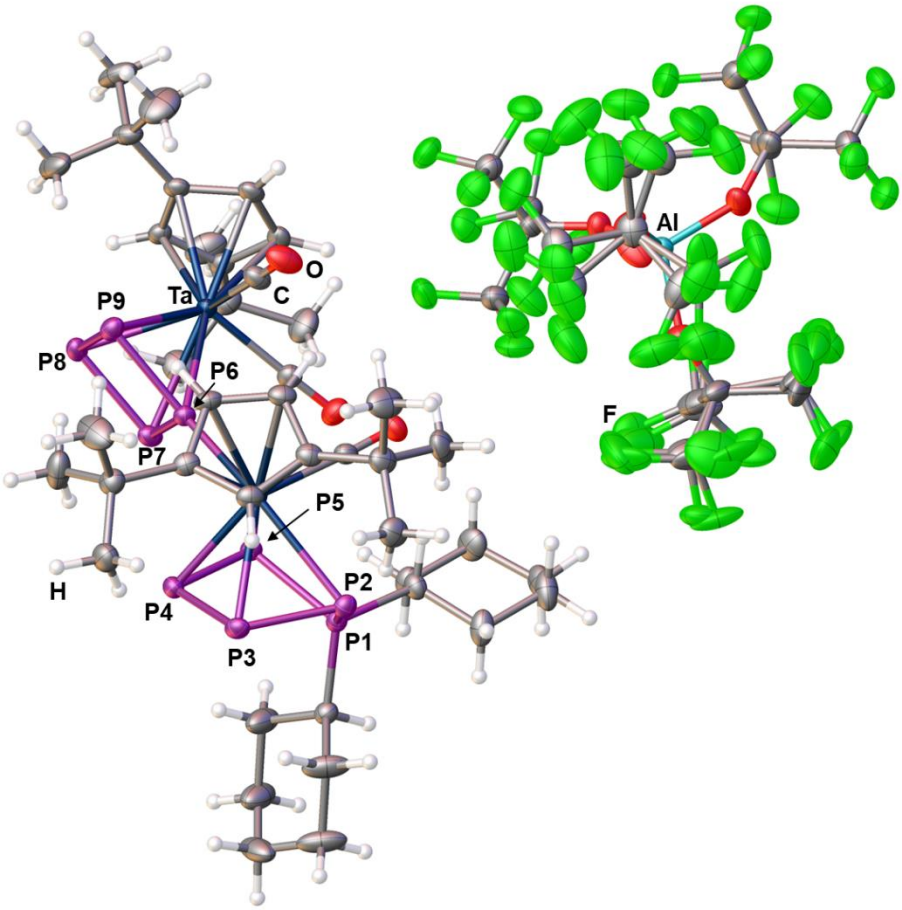

*Figure S 2: Solid state structure of **2**; Shown is the asymmetric unit containing one cation and one anion; ellipsoids are drawn at the 50% probability level.*

*[Cp"Ta(CO)$_2$(η^4-P$_4$AsCy$_2$)][TEF] (**3**)*

Compound **3** crystallizes in the triclinnic space group $P\bar{1}$ forming clear orange blocks from *o*-DFB/*n*-hexane mixtures at -30 °C (Figure S3). The asymmetric unit contains the cation, one anion and 0.4 *o*-DFB. All non-hydrogen atoms were refined anisotropically and the H atoms were treated as riding models. Disorder within the anion was treated with appropriate restraints.

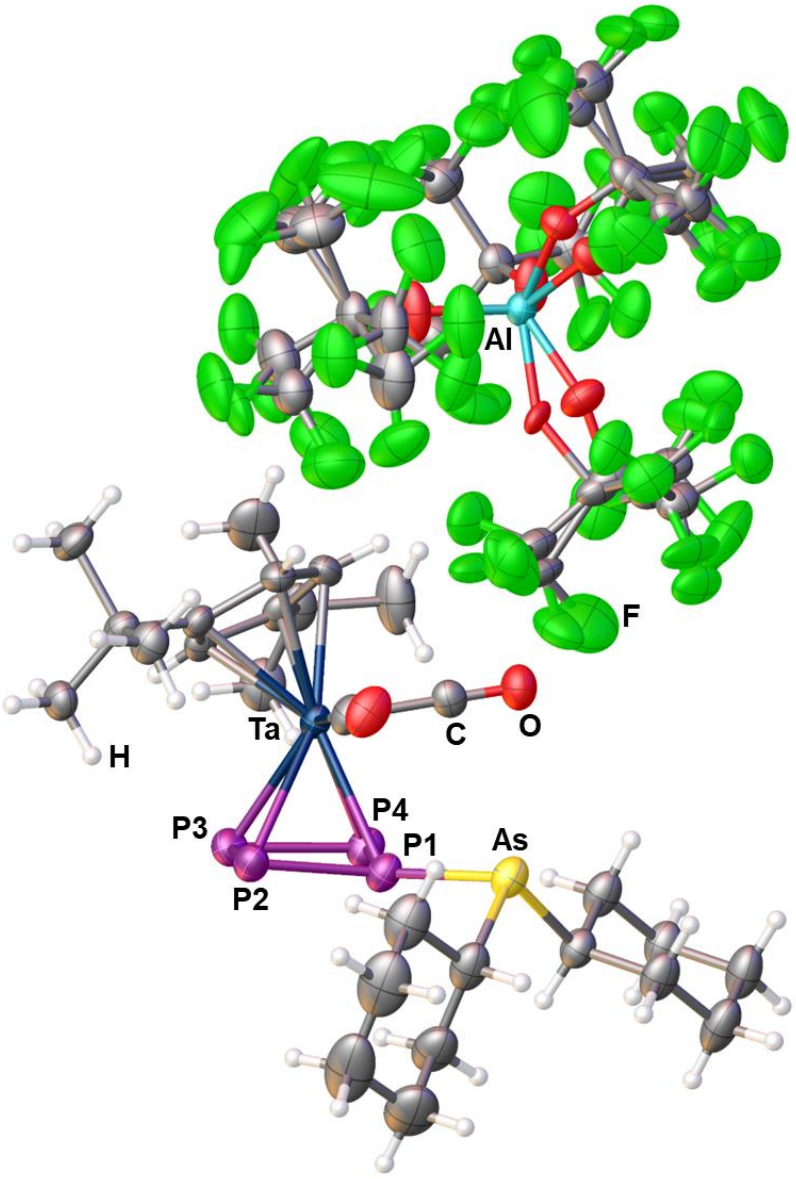

*Figure S 3: Solid state structure of **3**; Shown is the asymmetric unit containing one cation, one anion and 0.4 o-DFB (treated with a solvent mask); ellipsoids are drawn at the 50% probability level.*

*[{Cp''Ta(CO)$_2$(η^4-P$_4$)}$_2$SbPh$_2$][TEF] (**4**)*

Compound **4** crystallizes in the triclinnic space group $P\bar{1}$ forming dark orange plates upon addition of *n*-hexane to a concentrated solution in *o*-DFB at room temperature (Figure S4). The asymmetric unit contains the cation and one anion. All non-hydrogen atoms were refined anisotropically and the H atoms were treated as riding models. Disorder within the anion was treated with appropriate restraints.

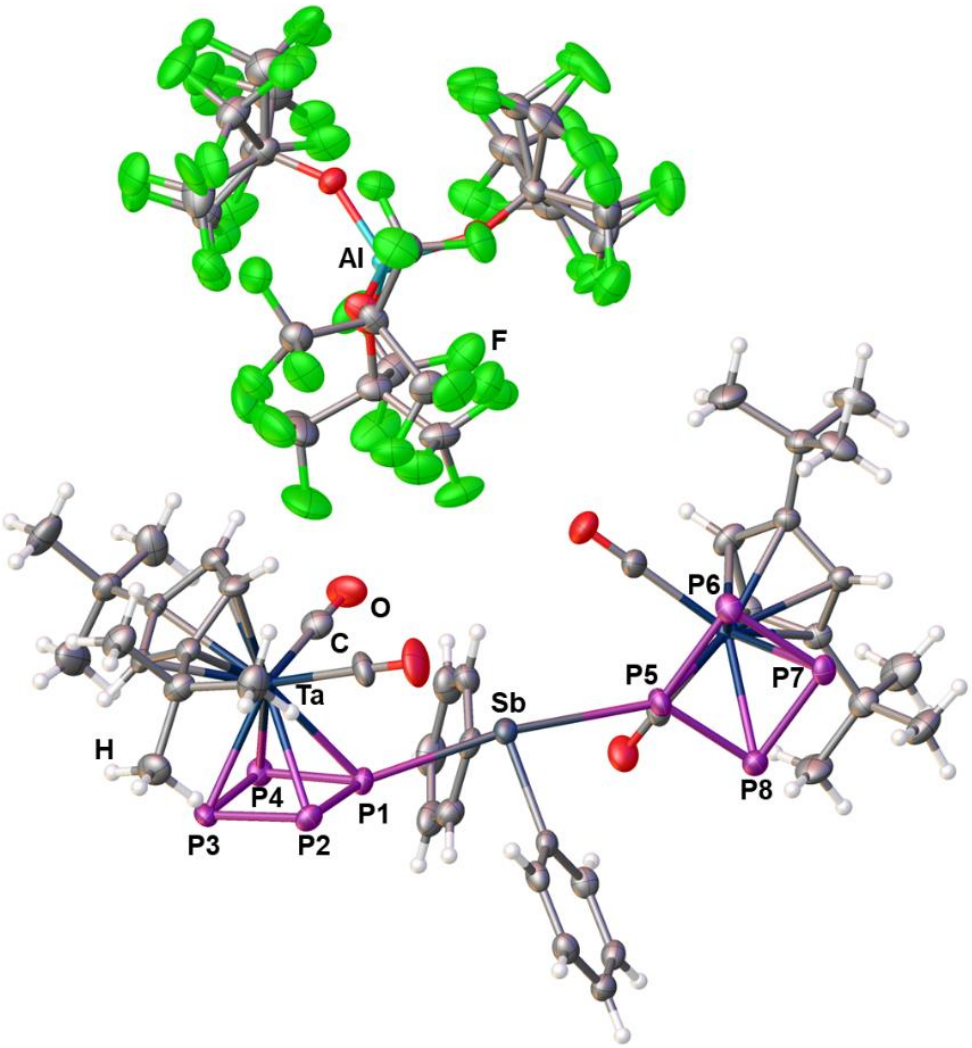

*Figure S 4: Solid state structure of **4**; Shown is the asymmetric unit containing one cation and one anion; ellipsoids are drawn at the 50% probability level.*

*[Cp'''Ta(CO)$_2$(η^4-P$_4$Sb(I)Cp''')][TEF] (**5**)*

Compound **5** crystallizes in the triclinnic space group $P\bar{1}$ forming intense yellow blocks from *o*-DFB/*n*-hexane mixtures at -30 °C (Figure S5). The asymmetric unit contains the cation and one anion. All non-hydrogen atoms were refined anisotropically and the H atoms were treated as riding models. Disorder within the anion was treated with appropriate restraints.

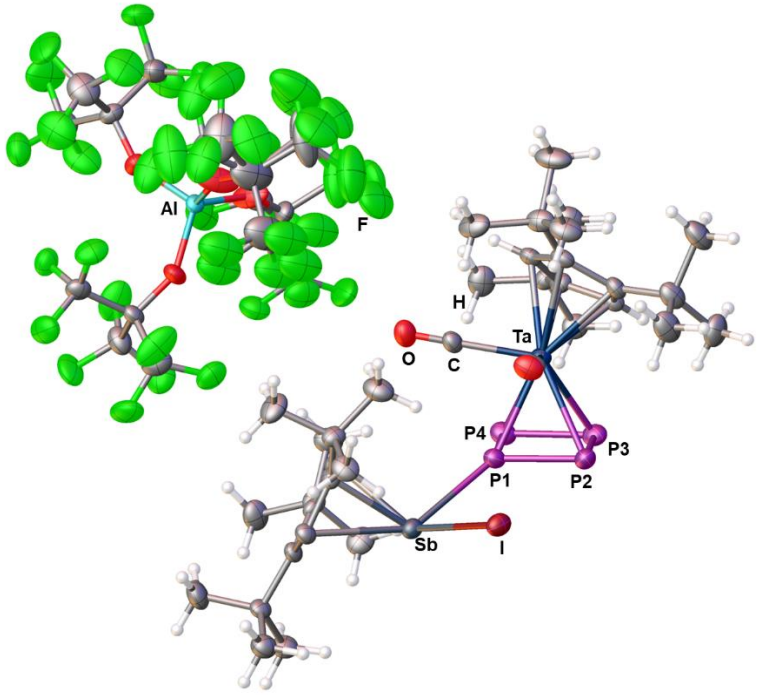

*Figure S 5: Solid state structure of **5**; Shown is the asymmetric unit containing one cation and one anion; ellipsoids are drawn at the 50% probability level.*

4.5.3. NMR Spectroscopic Investigations

*[Cp'''Ta(CO)$_2$(η^4-P$_5$Ph$_2$)][TEF] (**1**)*

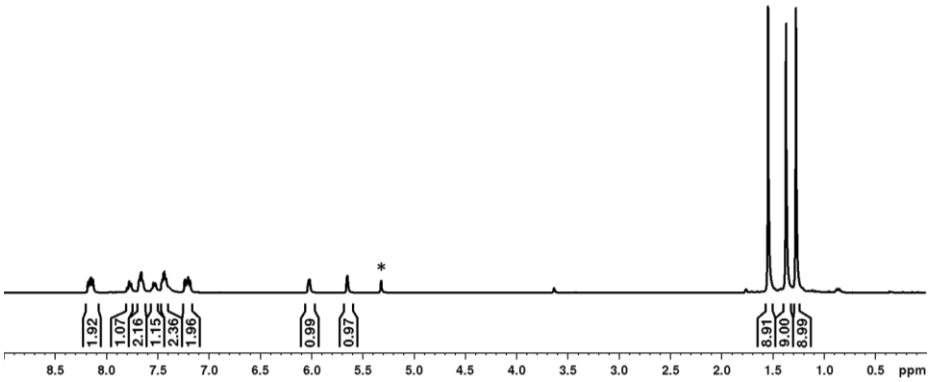

*Figure S 6: ^{1}H NMR spectrum of **1** in CD_2Cl_2 recorded at room temperature; * marks the residual solvent signal of CH_2Cl_2.*

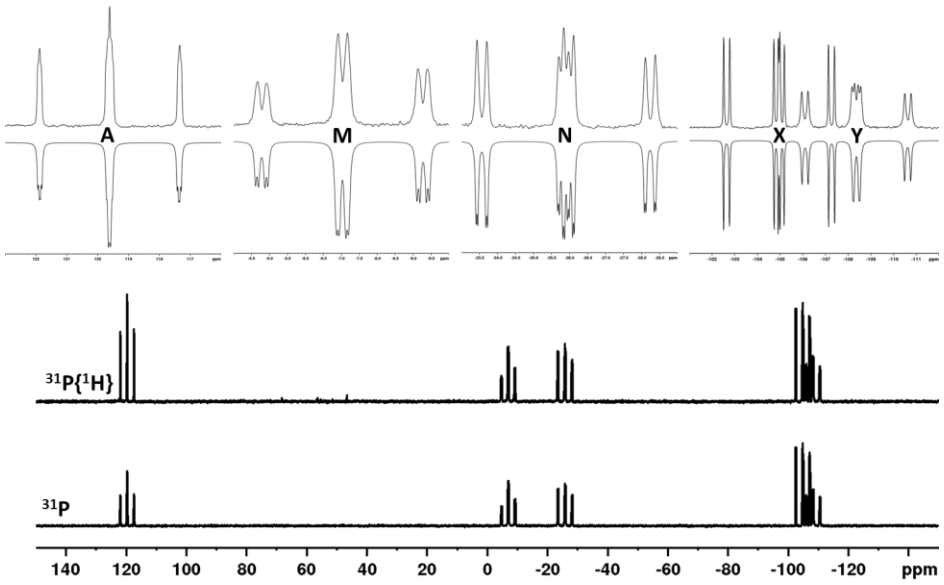

*Figure S 7: ^{31}P and ^{31}P{^{1}H} NMR spectra of **1** in CD_2Cl_2 recorded at room temperature and experimental (top) as well as simulated (bottom) spectra shown in the enlarged inserts.*

*Table S 2: Spectral parameters of the ^{31}P{^{1}H} NMR spectrum of **1** in CD_2Cl_2 recorded at room temperature.*

J/ Hz		*δ/ ppm*	
$^1J_{PA\text{-}PX}$	*360.9*	P^A	*119.6*
$^1J_{PA\text{-}PY}$	*370.7*	P^M	*-7.1*
$^1J_{PM\text{-}PN}$	*366.8*	P^N	*-25.9*
$^1J_{PM\text{-}PY}$	*362.7*	P^X	*-104.9*
$^1J_{PN\text{-}PX}$	*391.4*	P^Y	*-108.3*
$^2J_{PA\text{-}PM}$	*11.0*		
$^2J_{PA\text{-}PN}$	*7.1*		
$^2J_{PM\text{-}PN}$	*40.6*		
$^2J_{PN\text{-}PY}$	*41.4*		
$^2J_{PX\text{-}PY}$	*1.8*		
R-factor (%)	*6.8*		

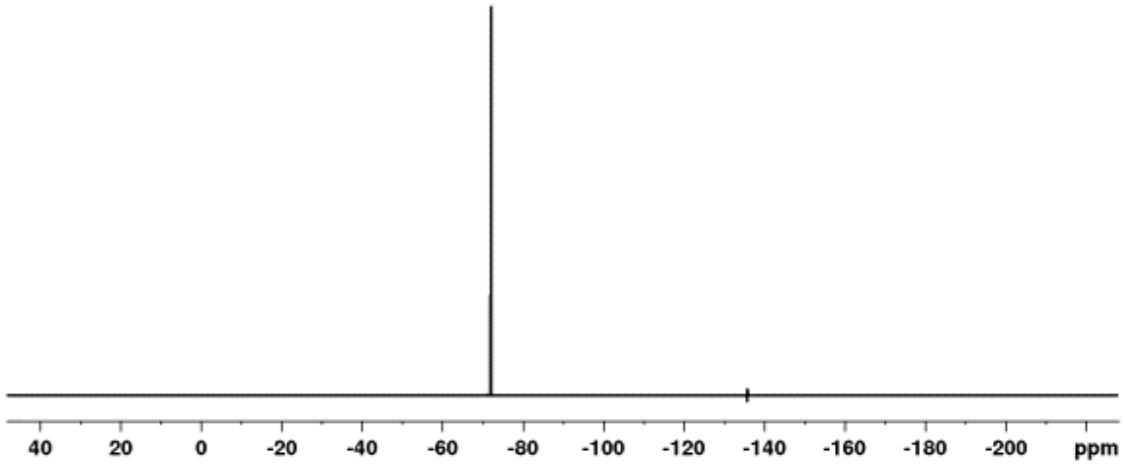

*Figure S 8: $^{19}F\{^{1}H\}$ NMR spectrum of **1** in CD_2Cl_2 recorded at room temperature.*

*[Cp"Ta(CO){Cp"Ta(CO)$_2$(μ,$\eta^{4:1}$-P$_4$)}(η^4-P$_5$Cy$_2$)][TEF] (**2**)*

The formation of **2** via an intermediate, which is isostructural to **1**, is highly plausible and should then be followed by decarbonylation accompanied by addition of a second equivalent of **B**. However, already after one hour signals corresponding to **2** are clearly visible in the ^{31}P NMR spectrum of the reaction mixture without any traces of an intermediate. This strongly points towards the rapid decarbonylation of the hypothetical intermediate under the reaction conditions (room temperature, *o*-DFB). Furthermore, this is supported by our observation of formation of **2** even in reactions of equimolar amounts of starting materials.

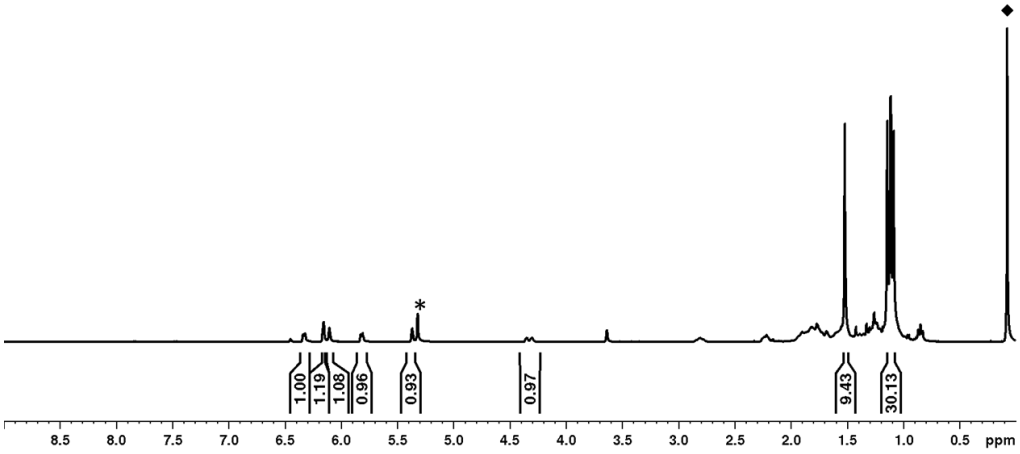

*Figure S 9: ^{1}H NMR spectrum of **2** in CD_2Cl_2 recorded at room temperature; * marks the residual solvent signal of CH_2Cl_2 and ◆ the signal from residual H-grease.*

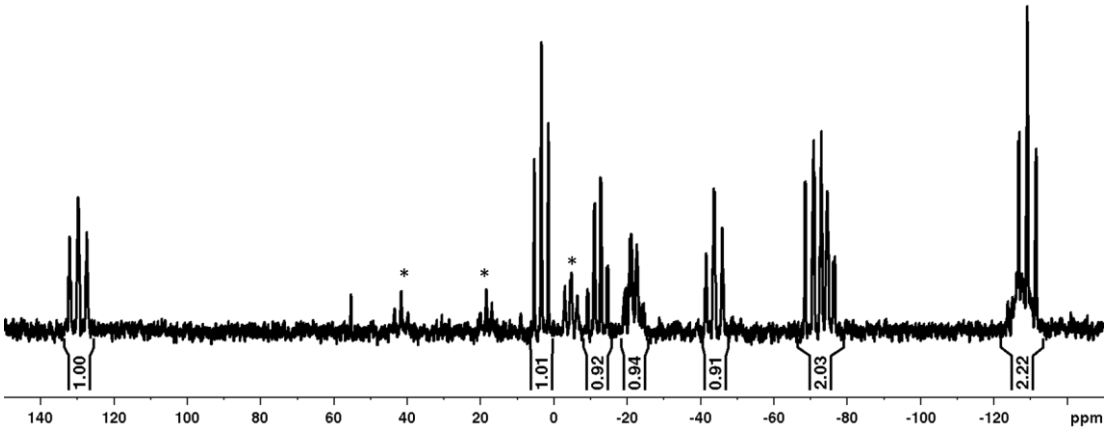

*Figure S 10: $^{31}P\{^1H\}$ NMR spectrum of **2** in CD_2Cl_2 recorded at room temperature; * marks the signals of traces of unreacted **B**.*

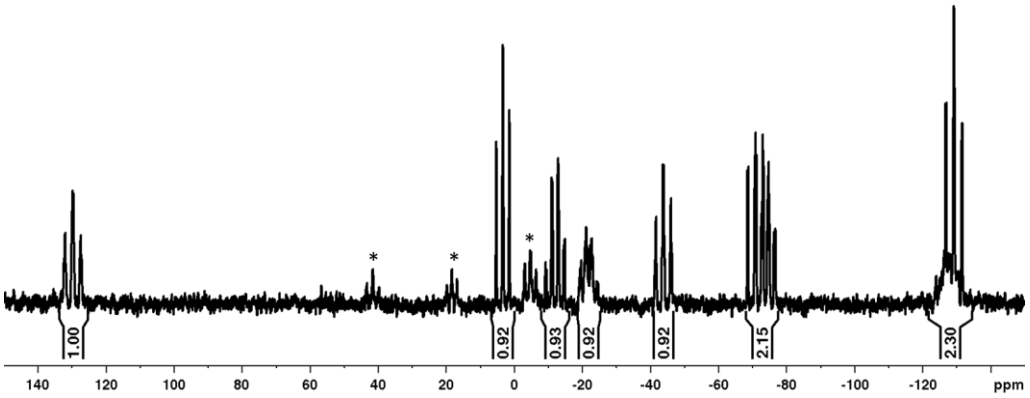

*Figure S 11: ^{31}P NMR spectrum of **2** in CD_2Cl_2 recorded at room temperature; * marks the signals of traces of unreacted **B**.*

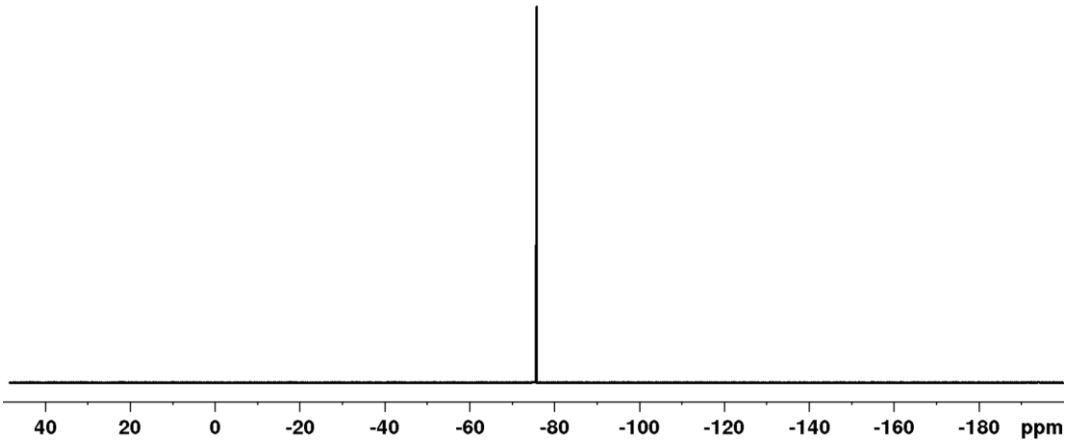

*Figure S 12: $^{19}F\{^1H\}$ NMR spectrum of **2** in CD_2Cl_2 recorded at room temperature.*

*[Cp"Ta(CO)$_2$(η^4-P$_4$AsCy$_2$)][TEF] (**3**)*

While the solid state structure of **3** (Figure S3) clearly shows a coordinated arsenium residue at the *cyclo*-P$_4$ ligand, the ^{31}P NMR spectra in *o*-DFB point towards the insertion of the arsenium ion into the P$_4$ cycle and thus formation of a *cyclo*-P$_4$AsCy$_2$ ligand. The presence of four chemically inequivalent ^{31}P nuclei of which two only show one $^1J_{P\text{-}P}$ coupling is clear indication for this insertion taking place in solution. The spectra are well reproduced even upon dissolving crystalline **3** in cold *o*-DFB. However, **3** rapidly degrades in CD_2Cl_2 solution limiting the temperature range to -30 °C.

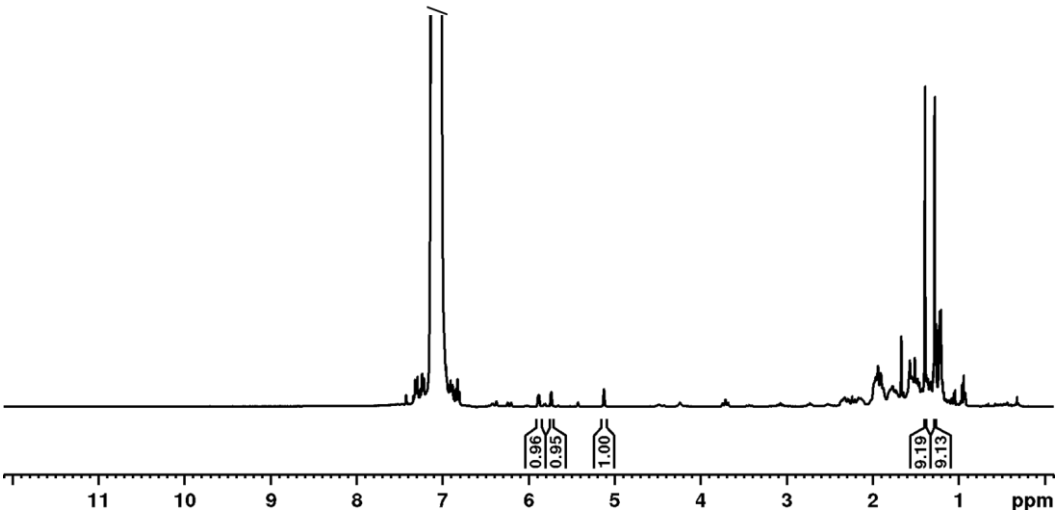

*Figure S 13: ^{1}H NMR spectrum of **3** in o-DFB with C_6D_6 capillary recorded at room temperature; the signal of o-DFB is cut off for clarity.*

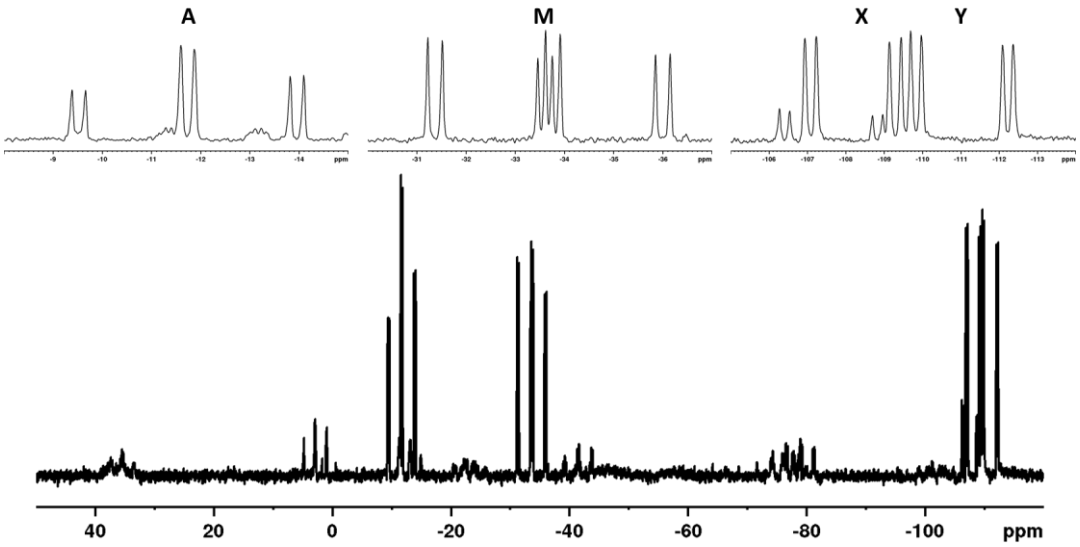

*Figure S 14: $^{31}P\{^1H\}$ NMR spectrum of **3** in o-DFB (with C_6D_6 capillary) recorded at room temperature; small additional signals indicate the rapid degradation of this compound in solution at room temperature.*

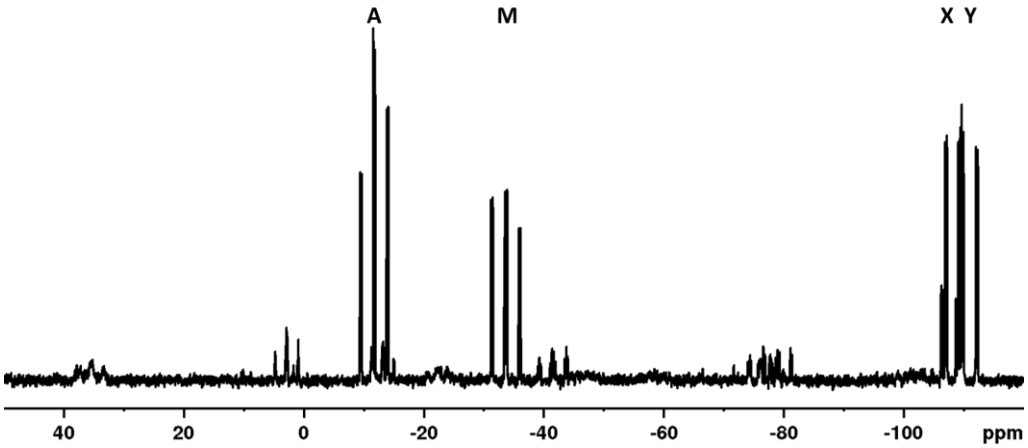

*Figure S 15: ^{31}P NMR spectrum of **3** in o-DFB (with C_6D_6 capillary) recorded at room temperature; small additional signals indicate the rapid degradation of this compound in solution at room temperature.*

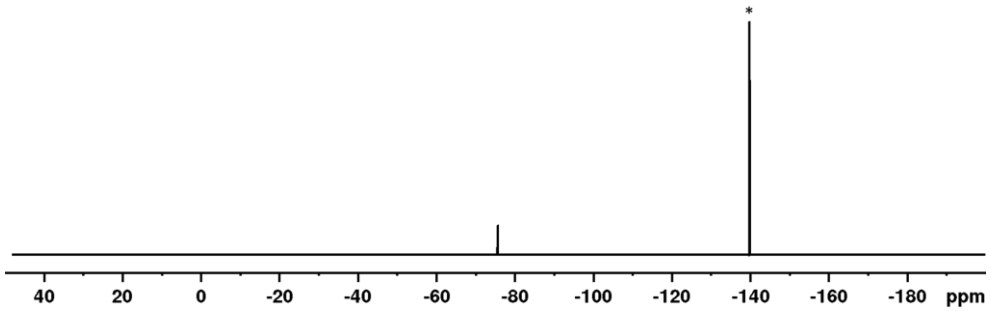

*Figure S 16: $^{19}F\{^1H\}$ NMR spectrum of **3** in CD_2Cl_2 recorded at room temperature; * marks the signal of o-DFB.*

*[{Cp"Ta(CO)$_2$(η^4-P$_4$)}$_2$SbPh$_2$][TEF] (**4**)*

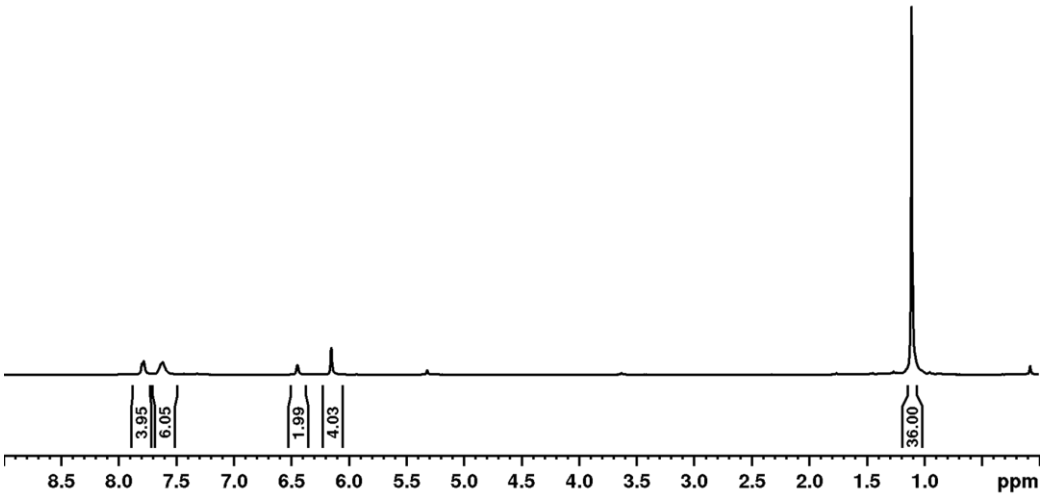

*Figure S 17: ^{1}H NMR spectrum of **4** in CD_2Cl_2 recorded at room temperature.*

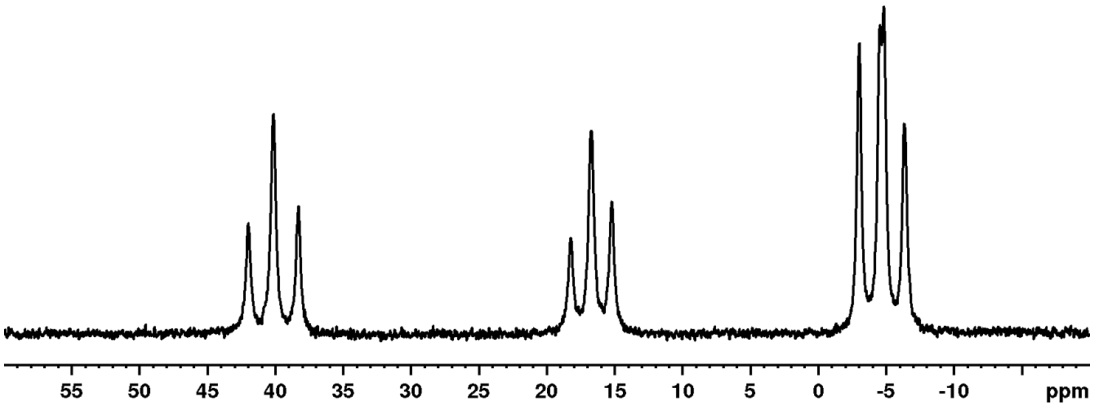

*Figure S 18: $^{31}P\{^1H\}$ NMR spectrum of **4** in CD_2Cl_2 recorded at room temperature.*

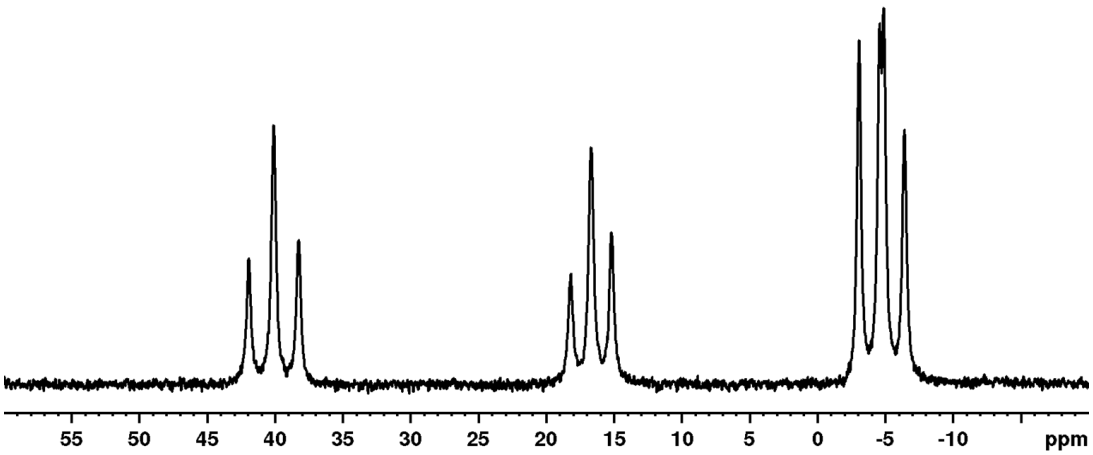

*Figure S 19: ^{31}P NMR spectrum of **4** in CD_2Cl_2 recorded at room temperature.*

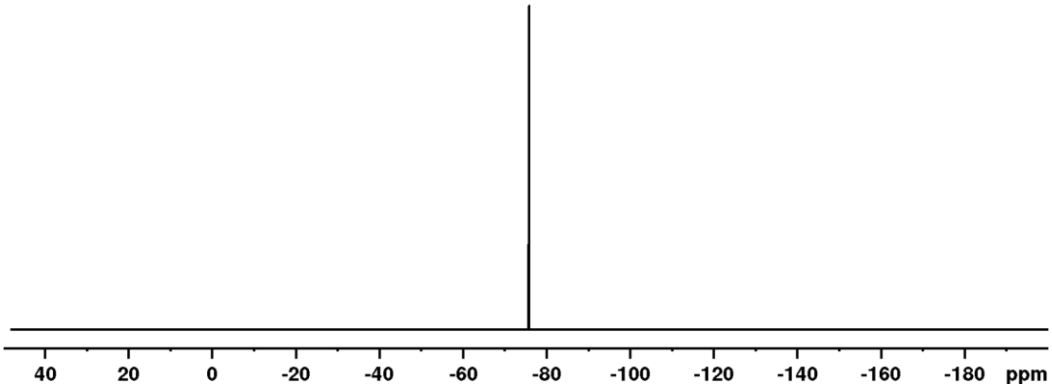

*Figure S 20: $^{19}F\{^{1}H\}$ NMR spectrum of **4** in CD_2Cl_2 recorded at room temperature.*

*[Cp'''Ta(CO)$_2$(η^4-P$_4$Sb(I)Cp''')][TEF] (**5**)*

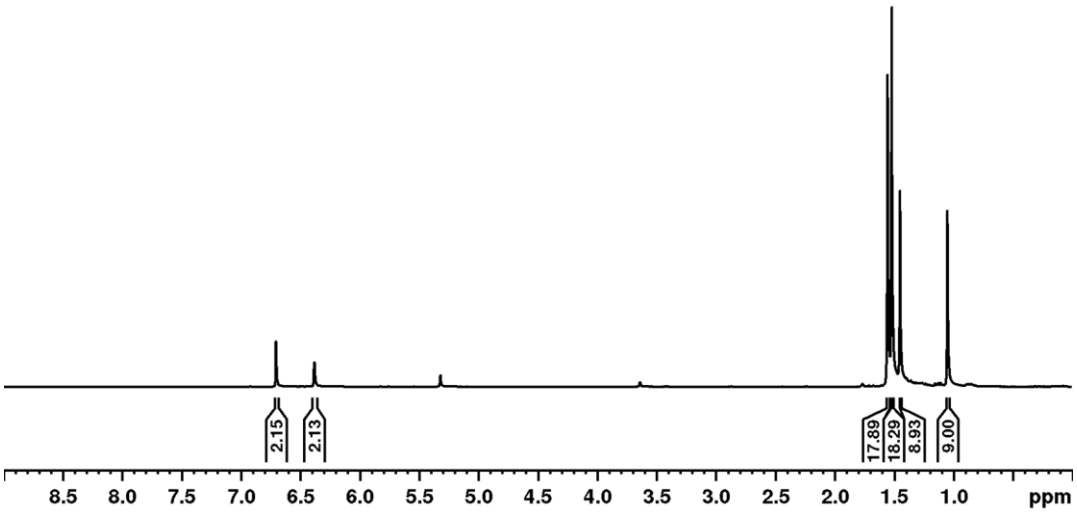

*Figure S 21 ^{1}H NMR spectrum of **5** in CD_2Cl_2 recorded at room temperature.*

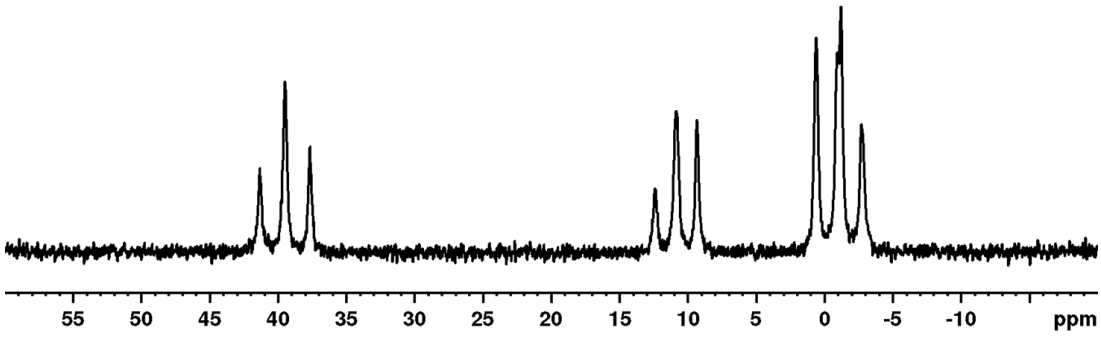

*Figure S 22: $^{31}P\{^1H\}$ NMR spectrum of **5** in CD_2Cl_2 recorded at room temperature.*

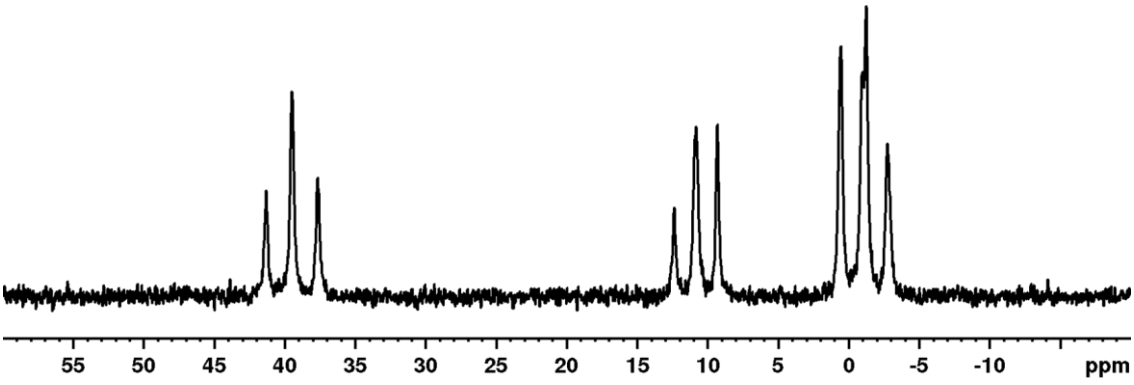

*Figure S 23: ^{31}P NMR spectrum of **5** in CD_2Cl_2 recorded at room temperature.*

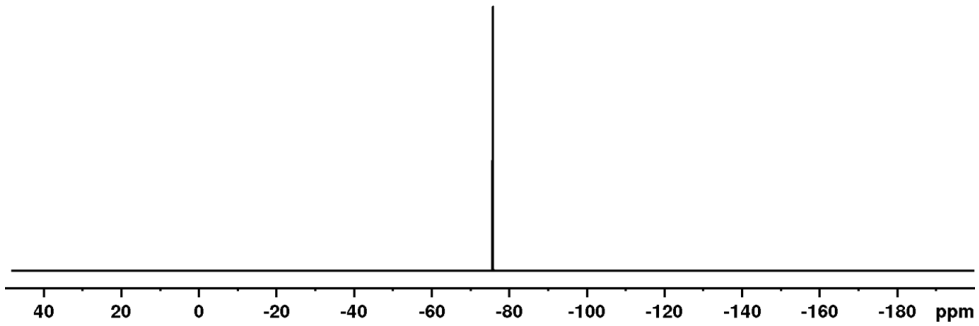

*Figure S 24: $^{19}F\{^{1}H\}$ NMR spectrum of **5** in CD_2Cl_2 recorded at room temperature.*

4.5.4. Computational Details

General Considerations

DFT calculations were performed using the Orca 5.0 software package.[35] The sterically demanding Cp^R were replaced with unsubstituted Cp ligands and the dimethylpnictogenium cations $[Me_2E]^+$ (E = P, As, Sb) were used to save computational resources. Geometry optimizations were performed at the ωB97X-D4[24]/def2-TZVP[25] level of theory with PCM solvent correction for CH_2Cl_2.[36] Stationary points were verified by analytical frequency calculations. Single point calculations were performed at the ωB97X-D4/def2-TZVP level of theory with solvent correction as described above. Imaginary modes with a value higher than -30 cm^{-1} were not considered due to approximations implemented in Orca 5.0. The differences in energy between the ring expanded insertion products and the respective coordination products **1′** – **4″** are listed in Table S3.

*Table S 3: Computed (@ωB97X-D4/def2-TZVP) energy differences between the ring expanded and the coordinated species in the model systems **1′** – **4″**.*

	1′	**3′**	**4″**
$\Delta G_{(Ins\text{-}Coord)}$ [kJ/mol]	-86.0	-43.9	-1.5

NBO Analysis

NBO analyses were performed using the NBO7.0 software package.[37] To gain further insight into the electronic structure of the coordinated species, NBO analysis was performed. Representative NBOs for **1′$_{Coord}$**, **3′$_{Coord}$**, **4″$_{Coord}$** and **4′** are provided in Figure S25. While the monocoordinated compounds all feature expressed P-E (E = P, As, Sb) bonding (WBI: 0.90 (**1′$_{Coord}$**), 0.83 (**3′$_{Coord}$**) and 0.71 (**4″$_{Coord}$**)), this bond becomes more polar going down the group. This is supported by NLMO analysis providing orbital contributions of 62% P: 38% P (**1′$_{Coord}$**), 68% P:32% As (**3′$_{Coord}$**) and 74% P: 26% Sb (**4″$_{Coord}$**). Accordingly, the WBIs decrease (0.90 (**1′$_{Coord}$**), 0.83 (**3′$_{Coord}$**), 0.71 (**4″$_{Coord}$**)) and the s-character of the lone-pair at the former pnictogenium cation increases (52% (**1′$_{Coord}$**), 63% (**3′$_{Coord}$**), 70% (**4″$_{Coord}$**)). This again is in line with the decreased “carbene-like” character of heavy pnictogenium cations and thus supports the formation of a ring expanded product for phosphenium ions, while their heavier congeners yield addition products. Furthermore, the bonding situation within **4′** is more complicated, as there are no directly bonding NBOs to be found for the P-Sb interactions. However, the linear combination of NBOs 79 and 84 fits the symmetry of an empty p-orbital at Sb (NBO 157), supporting a more electrostatic attractive interaction within **4′**. This is in line with significantly decreased WBIs (P-Sb: 0.41/0.38) and earlier investigations on phosphine complexes of stibenium cations.[26]

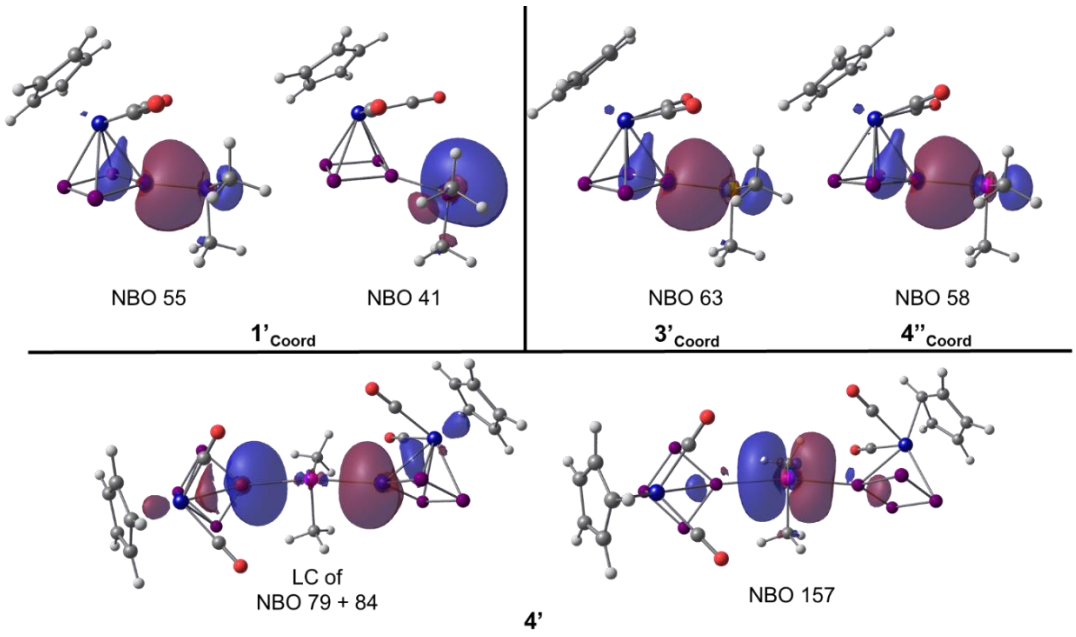

*Figure S 25: Selected NBOs for **1' – 4'** from DFT calculations at the ωB97X-D4/def2-TZVP level of theory.*

Optimized Geometries

1'$_{Ins}$

ωB97XD/def2TZVP (CPCM (CH_2Cl_2)): Energies/H = -2264.25837190, Enthalpies/H = -2264.25742769, Free Energies/H = -2264.32298419, ZPVE/ kcal/mol = 130.86

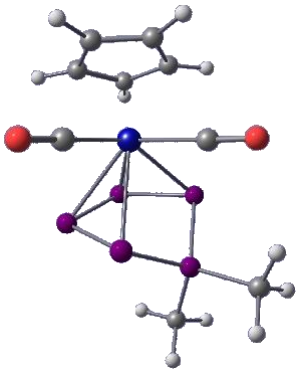

Symbol	X	Y	Z
Ta	-10.77671291793124	6.29787527240214	-7.42909739228838
P	-11.10429388134577	7.05392501628582	-4.12706015106119
P	-9.45330932400105	6.11678109868220	-5.09528164783389
P	-12.31295509064916	7.68006741957999	-5.77438840169302
P	-8.91454344452395	7.75790104564301	-6.37034894919594
P	-10.76295008544286	8.77057031367188	-6.73653142328607
O	-12.40649387566078	3.90747604733310	-5.93092995179368
O	-8.08575327051028	4.42379493023690	-7.65677429163008
C	-11.76658822186292	7.40750696193785	-9.30264803056991
H	-12.02612168260922	8.45321813323559	-9.27688737809766
C	-12.61850388169845	6.32932866517455	-8.94251740691240
C	-11.82841714630421	4.74052372265521	-6.43549663015612
C	-11.95666607103136	5.85986074138507	-3.07940937472289
C	-10.52825136552373	6.86626837713934	-9.74203313229785
C	-11.91687898324245	5.11636806572546	-9.20392029826678
C	-10.64018991227360	5.45014958143115	-9.70139792685786
H	-9.88376441976254	4.74590397773516	-10.01627474975063
C	-9.01709032090912	5.06216927483211	-7.58285584649716
C	-10.64187216191904	8.41002922025766	-3.04311666867286
H	-9.67116551939285	7.42693148244136	-10.08458110261657
H	-12.30106067424965	4.11583756579365	-9.06818626727832
H	-13.63312672352465	6.41180957330057	-8.58200325934625
H	-12.26016783036029	4.97775011952750	-3.63874996625421
H	-11.27666039275378	5.56803332210560	-2.27636692966675
H	-12.83692184943411	6.34509237644253	-2.65320924262597
H	-10.09638125722726	9.16546004940720	-3.60732127216327
H	-10.01242333244285	8.01572770220917	-2.24173186187671
H	-11.55115500541251	8.84404370442804	-2.62033134458743

1'Coord

ωB97XD/def2TZVP (CPCM (CH_2Cl_2)): Energies/H = -2264.22439225, Enthalpies/H = -2264.22344804, Free Energies/H = -2264.29024895, ZPVE/ kcal/mol = 130.69

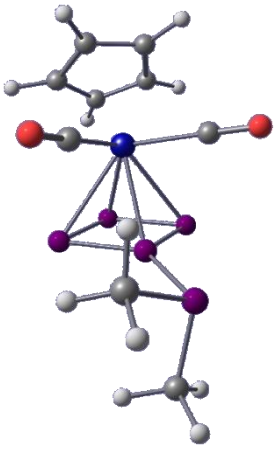

Symbol	X	Y	Z
Ta	0.93684224305866	11.62218082005737	14.75481474368288
P	-0.85870520576502	11.66300802145568	18.68350023998215
P	-0.54007190430828	12.41330091728528	16.67609433592016
P	-0.65346585926345	13.52245914650123	14.08611963796423
P	0.52491049408842	14.03209654763291	15.80895052825066
P	-1.69266436413892	11.87210941696067	14.98730354318340
O	-0.15171438128351	8.84403005905352	16.05815679317590
O	3.17629341911207	12.02372970175340	17.08203561739180
C	0.23974920297009	9.80600730285957	15.60465497429614
C	2.38318623533120	11.87060655154194	16.28654244322665
C	2.69069747247705	12.07478074612465	13.21172977979770
C	2.00432637744132	9.89325676238276	13.43286953789614
H	1.96976999024223	8.85190063855423	13.71962993993326
C	1.05300120229670	10.56777136319440	12.61908056413734
C	3.00781412353697	10.81584296003625	13.79795922171451
H	3.87362883501240	10.59770297155577	14.40646918250802
C	1.49485321627997	11.91053423927887	12.46024684375717
H	1.02108967293260	12.66397646384400	11.85252331098147
H	0.17492249687586	10.12678761959643	12.17055668621495
H	3.27848652346274	12.97762828142597	13.28834017184631
C	-1.87963277581704	13.05210023403303	19.31426597972325
H	-2.82977972077705	13.07967714226700	18.77827226424055
H	-2.08388327733685	12.84567419899212	20.36820205182973
H	-1.37359247119919	14.01461130315964	19.22660713940468
C	0.77700923757643	12.04761658734154	19.41706467987557
H	0.64449215796510	11.98284143326108	20.50038123967777
H	1.50788660571476	11.29752728460184	19.11688128056745
H	1.13285579551472	13.04899076624827	19.16694709681925

3'Ins

ωB97XD/def2TZVP (CPCM (CH_2Cl_2)): Energies/H = -4158.68068398, Enthalpies/H = -4158.67973977, Free Energies/H = -4158.74917894, ZPVE/ kcal/mol = 130.85

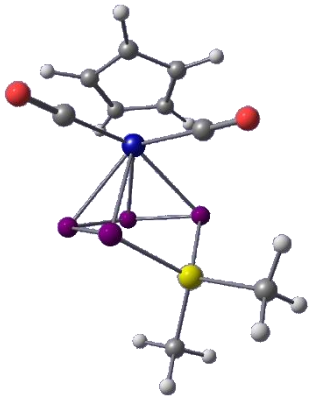

Symbol	X	Y	Z
Ta	-10.76545389970606	6.35203105425269	-7.48178231547535
As	-11.14025775518313	6.98220576484593	-4.06954223700013
P	-9.32529414395121	6.32772679046288	-5.20987286718577
P	-12.49251347421188	7.44862314547225	-5.79819020094191
P	-9.13361705614616	8.06953434934127	-6.44353109705950
P	-11.13133277481053	8.78260855892637	-6.73708789196408
O	-11.87685983086575	3.69613278905108	-5.95641857593015
O	-7.86503602425393	4.87270309443159	-7.89286493263317
C	-11.35979088548063	7.42292830542121	-9.56900531894278
H	-11.22301734528950	8.48299150500114	-9.71286773018842
C	-12.53774719775664	6.79373723214070	-9.08453155454157
C	-11.48740562254246	4.62462378110092	-6.47533830354510
C	-11.81987689707721	5.58533360753680	-2.93908474757694
C	-10.40063218293233	6.41858620398381	-9.82703539891975
C	-12.32028460795525	5.39712333465616	-9.07144392274151
C	-10.99445555593595	5.15275385969627	-9.51194696124180
H	-10.53815948736267	4.18294916627447	-9.64495716300122
C	-8.86167598395194	5.38714953202538	-7.74050801778153
C	-10.85515248507778	8.49654605862436	-2.92938966372164
H	-9.41121178043398	6.57615863655791	-10.23078854684661
H	-13.04109893337638	4.64874368618566	-8.77422815253284
H	-13.44565649005928	7.29662707459789	-8.78478484010052
H	-11.99337822761166	4.67798285318604	-3.51285625290072
H	-11.08495382944024	5.40120930112723	-2.15526737369578
H	-12.75395339886139	5.94022632497070	-2.50251447053359
H	-10.42250378040889	9.30470441523515	-3.51675330026407
H	-10.17821802355299	8.20155408127397	-2.12685810635540
H	-11.82088096776333	8.79690925461964	-2.52000095437769

3'Coord

ωB97XD/def2TZVP (CPCM (CH_2Cl_2)): Energies/H = -4158.66504282, Enthalpies/H = -4158.66409861, Free Energies/H = -4158.73246870, ZPVE/ kcal/mol = 130.11

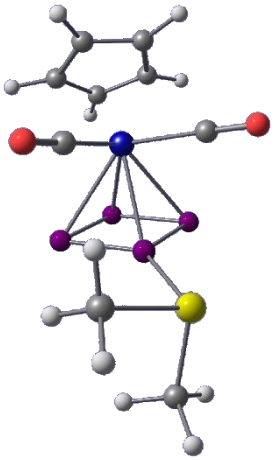

Symbol	X	Y	Z
Ta	0.94070287191774	11.61114590654289	14.73063420680986
As	-0.82907175030898	11.55168316839394	18.79444899591147
P	-0.53481746150933	12.37424666077960	16.67102643419237
P	-0.65919533075694	13.51240561496483	14.08399141053547
P	0.52215729303163	14.00250884184918	15.81010387441973
P	-1.68556085638836	11.84871157963155	14.97286514098012
O	-0.13965028043737	8.81739253326705	16.00485142151332
O	3.16192296691067	11.97818364917467	17.07973712827355
C	0.25004792776328	9.78448554163872	15.55973630514270
C	2.37733468534956	11.83715065175684	16.27318032488928
C	2.70174313898708	12.08227790490528	13.20095168284461
C	2.00430468565437	9.90041530542826	13.38243453412719
H	1.96536719153665	8.85388795981807	13.64923964299645
C	1.05939208566837	10.59279915358325	12.57685478062621
C	3.01031776278942	10.81225740833193	13.76800740979682
H	3.87406865557078	10.57881678671616	14.37380050825383
C	1.50737011187729	11.93658825963530	12.44342300066112
H	1.04044493455422	12.70199965825094	11.84536823504198
H	0.18070665418899	10.16365120640163	12.11811145916517
H	3.29411050340750	12.98063402237341	13.29346651087731
C	-1.99762285206619	13.00386191335119	19.38421977942871
H	-2.94620943992593	12.94581211431806	18.85038270722615
H	-2.17833387667529	12.84989204593992	20.45023248165501
H	-1.53344705290096	13.97746267027959	19.22832659125152
C	0.85537571891327	12.22481600767523	19.51924674962334
H	0.72681920490664	12.24723054890582	20.60342392705581
H	1.66560391979620	11.54151660261389	19.27203029172533
H	1.07835829214563	13.23158684147218	19.16419191697481

4"Ins

ωB97XD/def2TZVP (CPCM (CH_2Cl_2)): Energies/H = -2163.18677742, Enthalpies/H = -2163.18583321, Free Energies/H = -2163.25728000, ZPVE/ kcal/mol = 130.11

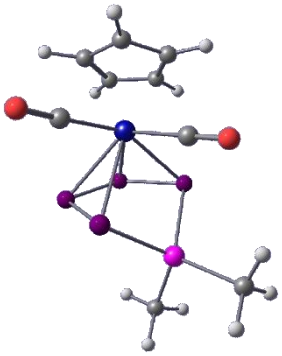

Symbol	X	Y	Z
Ta	-10.75199789554422	6.34266287255867	-7.54419496315230
Sb	-11.15084606846920	6.96397293677675	-3.99955675150600
P	-9.24501110432233	6.27317411469600	-5.30769184762453
P	-12.52615027686681	7.45530439953257	-5.91821839114480
P	-9.10790666697178	8.04440510707212	-6.50478677204104
P	-11.10623659289750	8.77122023801611	-6.79535422523882
O	-11.86420033546302	3.71354379182049	-5.96915619615331
O	-7.86292753779993	4.85273917608671	-8.01801228783167
C	-11.35075885443675	7.41964612335973	-9.63036363560886
H	-11.21103855583630	8.47936146816003	-9.77345375529501
C	-12.52894046472884	6.79357233695036	-9.14515127802565
C	-11.47454804096616	4.62709790544788	-6.51425932326153
C	-11.91712276725933	5.45822446651066	-2.74562651712571
C	-10.39509634229458	6.41217766364058	-9.89076274336853
C	-12.31538166067885	5.39587902505314	-9.13166103454819
C	-10.99260602051471	5.14799376262371	-9.57701213824001
H	-10.53943213967520	4.17691536697798	-9.71124278774766
C	-8.85332030998599	5.37032878646925	-7.83679982694997
C	-10.80905660987705	8.65559929324449	-2.80366512592336
H	-9.40631775327047	6.56690407954586	-10.29710251559221
H	-13.03704395957370	4.64972136619328	-8.83101582261298
H	-13.43501096465162	7.29853420268936	-8.84433812669819
H	-12.14159960427044	4.57016689946742	-3.33299970601442
H	-11.16751101841051	5.23695596637749	-1.98620857825113
H	-12.82368143109095	5.84713213077867	-2.28184214108322
H	-10.35943536224129	9.42583989036909	-3.42868706143035
H	-10.13865462044486	8.37895106462428	-1.99010473529786
H	-11.76858568345681	8.99237932595674	-2.41018261023219

4"Coord

ωB97XD/def2TZVP (CPCM (CH_2Cl_2)): Energies/H = -4006.37272524, Enthalpies/H = -4006.37178103, Free Energies/H = -4006.47815535, ZPVE/ kcal/mol = 209.74

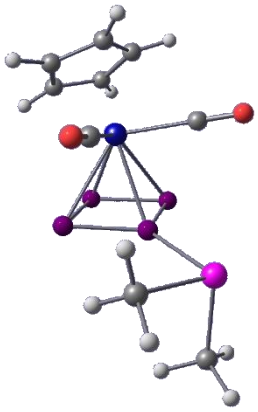

Symbol	X	Y	Z
Ta	0.94578620509559	11.50546148787121	14.67930611904885
Sb	-0.52852953487125	11.36946841017280	19.03205153439098
P	-0.57137314851128	12.17389335875307	16.64285785021037
P	-0.87808331833939	13.18544044495526	13.99872217693818
P	0.27982272045401	13.86487828394044	15.67450806719082
P	-1.67784531700315	11.45140978785162	14.98007507540905
O	0.28071011428434	8.63354996971546	16.05517547308328
O	3.17370342521769	12.10590348379073	16.96787331315283
C	0.51820088984737	9.63289420863720	15.57445872653502
C	2.38408401692455	11.89357201838262	16.18160236812489
C	2.94332304201257	11.78975221699277	13.40523429421168
C	1.62972622333096	9.94380577429825	12.98507054764856
H	1.25092783853908	8.93197827990246	12.96929934008751
C	1.06491650753365	11.04720186206009	12.31203754712793
C	2.78367230435182	10.39723890784028	13.68971920935553
H	3.45530012669333	9.78464806843096	14.27284117125650
C	1.87964153433277	12.18701332566169	12.56737128703453
H	1.70699588075956	13.18352002511461	12.18902798255870
H	0.16584806037777	11.03483159179868	11.71321785424592
H	3.74373883658557	12.42417734237296	13.75693747511141
C	-2.15466993419090	12.63866690934234	19.58464335914860
H	-3.07506543317125	12.28253495074692	19.12187498281628
H	-2.25364442009112	12.58284239778143	20.67079822163102
H	-1.95319588315438	13.66714739508864	19.28648593101009
C	0.99349899673333	12.77470620653965	19.55568747270655
H	0.87945600147076	12.95613151872408	20.62658809472874
H	1.98181875289385	12.36191732810540	19.36401601809667
H	0.85954085389406	13.71416392612728	19.01871833513806

4'

ωB97XD/def2TZVP (CPCM (CH_2Cl_2)): Energies/H = -2163.18547273, Enthalpies/H = -2163.18452852, Free Energies/H = -2163.25672647, ZPVE/ kcal/mol = 129.88

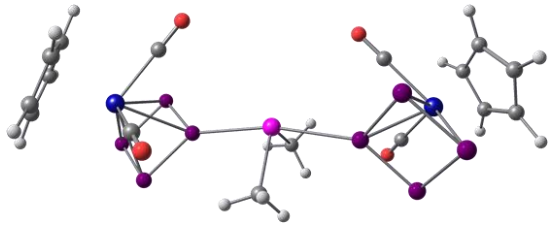

Symbol	X	Y	Z
Ta	9.348003000	9.301170000	9.261573000
Ta	2.388836000	12.873858000	3.580541000
Sb	5.743139000	11.634669000	6.840147000
P	8.214897000	11.213538000	7.945028000
P	0.647871000	13.655534000	5.314065000
P	9.737447000	10.212249000	6.829228000
P	11.102512000	10.934805000	8.311191000
P	9.576849000	11.920868000	9.442327000
P	3.272638000	12.571684000	5.995515000
P	2.570674000	14.554699000	5.593106000
P	1.357777000	11.667809000	5.672490000
O	3.649884000	9.881939000	3.588530000
O	5.389465000	14.106918000	3.428976000
O	7.104039000	7.831717000	7.434023000
O	7.070479000	10.291019000	11.355595000
C	7.891018000	8.342138000	8.076426000
C	4.339869000	13.673505000	3.479299000
C	9.289272000	7.272765000	10.476970000
H	8.355669000	6.780568000	10.705802000
C	7.855248000	9.942082000	10.611616000
C	11.176277000	8.567536000	10.667973000
C	10.109834000	7.034461000	9.331903000
C	11.261520000	7.842007000	9.446214000
H	12.066833000	7.905181000	8.729475000
C	1.017503000	14.159534000	2.059243000
C	3.210866000	10.930207000	3.579882000
C	1.432309000	11.951524000	1.586517000
C	9.973343000	8.207394000	11.309912000
H	9.633000000	8.572887000	12.267866000
C	0.472952000	12.845005000	2.107259000
H	-0.503438000	12.579803000	2.485355000
C	2.313627000	14.079178000	1.508488000
H	2.975526000	14.912802000	1.324007000
C	2.592260000	12.706043000	1.232577000
H	3.488433000	12.318064000	0.771580000
H	0.523930000	15.059000000	2.396599000
H	1.307119000	10.884706000	1.471473000
H	9.892275000	6.351745000	8.523391000
H	11.904396000	9.277252000	11.032172000
C	4.929168000	11.418544000	8.808078000
H	5.095531000	10.393447000	9.139548000
H	3.859558000	11.624539000	8.791776000
H	5.425882000	12.112435000	9.485916000
C	6.279533000	13.706899000	6.941921000
H	6.556425000	13.947836000	7.968005000
H	7.127976000	13.880577000	6.279601000
H	5.448729000	14.343068000	6.636866000

4.6. References

[1] M. N. Hopkinson, C. Richter, M. Schedler, F. Glorius, *Nature* **2014**, *510*, 485–496.

[2] a) F. Glorius, N-heterocyclic carbenes in transition metal catalysis, *Springer*, Berlin, New York, **2007**; b) S. Díez-González, N. Marion, S. P. Nolan, *Chem. Rev.* **2009**, *109*, 3612–3676.

[3] D. Enders, O. Niemeier, A. Henseler, *Chem. Rev.* **2007**, *107*, 5606–5655.

[4] V. Nesterov, D. Reiter, P. Bag, P. Frisch, R. Holzner, A. Porzelt, S. Inoue, *Chem. Rev.* **2018**, *118*, 9678–9842.

[5] R. Hoffmann, *Angew. Chem. Int. Ed. Engl.* **1982**, *21*, 711–724.

[6] a) L. Liu, D. A. Ruiz, D. Munz, G. Bertrand, *Chem* **2016**, *1*, 147–153; b) M. M. Hansmann, R. Jazzar, G. Bertrand, *J. Am. Chem. Soc.* **2016**, *138*, 8356–8359.

[7] R. Wei, X.-F. Wang, C. Hu, L. L. Liu, *Nat. Synth.* **2023**, *2*, 357–363.

[8] R. Wei, X.-F. Wang, D. A. Ruiz, L. L. Liu, *Angew. Chem. Int. Ed.* **2023**, *62*, e202219211.

[9] M. Olaru, S. Mebs, J. Beckmann, *Angew. Chem. Int. Ed.* **2021**, *60*, 19133–19138.

[10] M. Olaru, D. Duvinage, E. Lork, S. Mebs, J. Beckmann, *Angew. Chem. Int. Ed.* **2018**, *57*, 10080–10084.

[11] a) N. Burford, T. S. Cameron, P. J. Ragogna, E. Ocando-Mavarez, M. Gee, R. McDonald, R. E. Wasylishen, *J. Am. Chem. Soc.* **2001**, *123*, 7947–7948; b) N. Burford, P. J. Ragogna, R. McDonald, M. J. Ferguson, *J. Am. Chem. Soc.* **2003**, *125*, 14404–14410; c) N. Burford, C. A. Dyker, A. Decken, *Angew. Chem. Int. Ed.* **2005**, *44*, 2364–2367; d) J. Possart, A. Martens, M. Schleep, A. Ripp, H. Scherer, D. Kratzert, I. Krossing, *Chem. Eur. J.* **2017**, *23*, 12305–12313.

[12] a) N. Burford, C. A. Dyker, M. Lumsden, A. Decken, *Angew. Chem. Int. Ed.* **2005**, *44*, 6196–6199; b) J. J. Weigand, N. Burford, M. D. Lumsden, A. Decken, *Angew. Chem. Int. Ed.* **2006**, *45*, 6733–6737.

[13] a) I. Krossing, I. Raabe, *Angew. Chem. Int. Ed.* **2001**, *40*, 4406; b) M. Gonsior, I. Krossing, L. Müller, I. Raabe, M. Jansen, L. van Wüllen, *Chem. Eur. J.* **2002**, *8*, 4475–4492; c) J. J. Weigand, M. Holthausen, R. Fröhlich, *Angew. Chem. Int. Ed.* **2009**, *48*, 295–298; d) M. H. Holthausen, K.-O. Feldmann, S. Schulz, A. Hepp, J. J. Weigand, *Inorg. Chem.* **2012**, *51*, 3374–3387; e) M. H. Holthausen, J. J. Weigand, *Chem. Soc. Rev.* **2014**, *43*, 6639–6657.

[14] a) H. Althaus, H. J. Breunig, E. Lork, *Chem. Commun.* **1999**, *19*, 1971–1972; b) K. A. Porter, A. C. Willis, J. Zank, S. B. Wild, *Inorg. Chem.* **2002**, *41*, 6380–6386; c) N. L. Kilah, S. Petrie, R. Stranger, J. W. Wielandt, A. C. Willis, S. B. Wild, *Organometallics* **2007**, *26*, 6106–6113; d) N. L. Kilah, M. L. Weir, S. B. Wild, *Dalton Trans.* **2008**, *18*, 2480–2486; e) E. Conrad, N. Burford, U. Werner-Zwanziger, R. McDonald, M. J. Ferguson, *Chem. Commun.* **2010**, *46*, 2465–2467.

[15] a) C. Riesinger, L. Dütsch, G. Balázs, M. Bodensteiner, M. Scheer, *Chem. Eur. J.* **2020**, *26*, 17165–17170; b) M. Piesch, S. Reichl, M. Seidl, G. Balázs, M. Scheer, *Angew. Chem. Int. Ed.* **2021**, *60*, 15101–15108.

[16] a) C. M. Hoidn, T. M. Maier, K. Trabitsch, J. J. Weigand, R. Wolf, *Angew. Chem. Int. Ed.* **2019**, *58*, 18931–18936; b) C. G. P. Ziegler, T. M. Maier, S. Pelties, C. Taube, F. Hennersdorf, A. W. Ehlers, J. J. Weigand, R. Wolf, *Chem. Sci.* **2019**, *10*, 1302–1308.

[17] C. Riesinger, G. Balázs, M. Seidl, M. Scheer, *Chem. Sci.* **2021**, *12*, 13037–13044.

[18] C. Riesinger, F. Dielmann, R. Szlosek, A. V. Virovets, M. Scheer, *Angew. Chem. Int. Ed.* **2023**, *62*, e202218828.

[19] O. J. Scherer, R. Winter, G. Wolmershuser, *Z. Anorg. Allg. Chem.* **1993**, *619*, 827–835; Notably, the exchange of Cp‴ for Cp″ and *vice versa* does not influence the insertion/addition reactivity of these compounds towards pnictogenium ions.

[20] M. Gonsior, I. Krossing, N. Mitzel, *Z. Anorg. Allg. Chem.* **2002**, *628*, 1821–1830.

[21] M. Gonsior, I. Krossing, *Dalton Trans.* **2005**, *11*, 2022–2030.

[22] P. Pyykkö, *J. Phys. Chem. A* **2015**, *119*, 2326−2337.

[23] a) E. Mädl, M. V. Butovskii, G. Balázs, E. V. Peresypkina, A.V. Virovets, M. Seidl, M. Scheer, *Angew. Chem. Int. Ed.* **2014**, *53*, 7643–7646; b) A. K. Adhikari, C. G. P. Ziegler, K. Schwedtmann, C. Taube, J. J. Weigand, R. Wolf, *Angew. Chem. Int. Ed.* **2019**, 58, 18584–18590; c) S. Reichl, E. Mädl, F. Riedlberger, M. Piesch, G. Balázs, M. Seidl, M. Scheer, *Nat. Commun.* **2021**, 12, 5774–5782.

[24] a) Y.-S. Lin, G.-D. Li, S.-P. Mao, J. D. Chai, *J. Chem. Theory Comput.* **2013**, *9*, 263–272; b) E. Caldeweyher, S. Ehlert, A. Hansen, H. Neugebauer, S. Spicher, C. Bannwarth, S. Grimme, *J. Chem. Phys.* **2019**, *150*, 154122–154141.

[25] F. Weigend, R. Ahlrichs, *Phys. Chem. Chem. Phys.* **2005**, *7*, 3297–3305.

[26] N. L. Kilah, S. Petrie, R. Stranger, J. W. Wielandt, A. C. Willis, S. B. Wild, *Organometallics* **2007**, *26*, 6106–6113.

[27] *https://omics.pnl.gov/software/molecular-weight-calculator (25.04.2023)*.

[28] M. Gonsior, I. Krossing and N. Mitzel, *Z. anorg. allg. Chem.*, **2002**, *628*, 1821–1830.

[29] W. Steinkopf, H. Dudek, S. Schmidt, *Ber. dtsch. Chem. Ges. A/B* **1928**, *61*, 1911–1918.

[30] C. Riesinger, G. Balázs, M. Seid, M. Scheer, *Chem. Sci.* **2021**, *12*, 13037–13044.

[31] Agilent Technologies Ltd, *CrysAlis PRO*, Yarnton, Oxfordshire, England, **2014**.

[32] O. V. Dolomanov, L. J. Bourhis, R. J. Gildea, J. A. K. Howard and H. Puschmann, *J. Appl. Crystallogr.* **2009**, *42*, 339–341.

[33] G. M. Sheldrick, *Acta Cryst. A* **2015**, *71*, 3–8.

[34] a) G. M. Sheldrick, *Acta Cryst. A* **2008**, *64*, 112–122; b) G. M. Sheldrick, *Acta Cryst. C* **2015**, *71*, 3–8.

[35] a) F. Neese, F. Wennmohs, U. Becker, C. Rieplinger, *J. Chem. Phys.* **2020**, *152*, 224108–224125; b) F. Neese, *WIREs Comput. Mol. Sci.* **2022**, *12*, 1606–1620.

[36] J. Tomasi, B. Mennucci, R. Cammi, *Chem. Rev.* **2005**, *105*, 2999–3093.

[37] NBO 7.0. E. D. Glendening, J. K. Badenhoop, A. E. Reed, J. E. Carpenter, J. A. Bohmann, C. M. Morales, P. Karafiloglou, C. R. Landis, F. Weinhold, Theoretical Chemistry Institute, University of Wisconsin, Madison, WI (**2018**).

5. Stabilization of Pentaphospholes as η^5-Coordinating Ligands

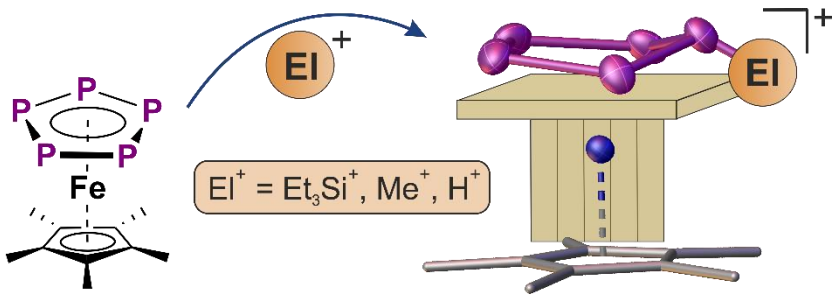

Coordinative Stabilization of Pentaphospholes

Preface

The following chapter has already been published. The article is reproduced with permission from Wiley-VCH. License Number: 5637011186594

"Stabilization of Pentaphospholes as η^5-Coordinating Ligands"

Angew. Chem. Int. Ed. **2020**, *59*, 23879–23884.

Angew. Chem. **2020**, *132*, 24088–24094.

Parts of this chapter have already been described within the MSc thesis of the first author (Christoph Riesinger).

Authors

Christoph Riesinger, Gábor Balázs, Michael Bodensteiner and Manfred Scheer

Author Contributions

Christoph Riesinger – Conceptualization, Synthesis of compounds **2**, **3** and **4**, Writing of original draft.
Gábor Balázs – Interpretation of computational data.
Michael Bodensteiner – Interpretation of crystallographic data.
Manfred Scheer – Project administration, Funding acquisition, Co-writing final manuscript.

Acknowledgements

This work was supported by the Deutsche Forschungsgemeinschaft (DFG) within the project Sche 384/36-1.

5.1. Abstract

*Electrophilic functionalisation of [Cp*Fe(η^5-P_5)] (**1**) yields the first transition metal complexes of pentaphospholes (cyclo-P_5R). Silylation of **1** with [($Et_3Si)_2$(μ-H)][$B(C_6F_5)_4$] leads to the ionic species [Cp*Fe(η^5-P_5SiEt_3)][$B(C_6F_5)_4$] (**2**), whose subsequent reaction with H_2O yields the parent compound [Cp*Fe(η^5-P_5H)][$B(C_6F_5)_4$] (**3**). The synthesis of a carbon-substituted derivative [Cp*Fe(η^5-P_5Me)][X] ([X]$^-$ = [$FB(C_6F_5)_3$]$^-$ (**4a**), [X]$^-$ = [$B(C_6F_5)_4$]$^-$ (**4b**)) is achieved by methylation of **1** employing [Me_3O][BF_4] and $B(C_6F_5)_3$ or a combination of MeOTf and [$Li(OEt_2)_2$][$B(C_6F_5)_4$]. The structural characterisation of these compounds reveals a slight envelope structure for the cyclo-P_5R ligand. Detailed NMR spectroscopic studies suggest a highly dynamic behaviour and thus a distinct lability for **2** and **3** in solution. DFT calculations shed light on the electronic structure and bonding situation of this unprecedented class of compounds.*

5.2. Introduction

The Cyclopentadienide anion (Cp^-, $C_5H_5^-$) and its derivatives are some of the most utilised ligands in organometallic chemistry. They are widely used in designing catalysts, e.g. group 4 metallocene derivatives for olefin polymerisation,[1] and in the stabilisation of highly reactive and thus uncommon species (e.g. the isoelectronic series of Cp^RAl (Cp^R = Cp*,[2] Cp^R = Cp‴[3]), $[Cp^*Si]^+$,[4] and $[Cp^*P]^{2+}$[5] (Cp‴ = 1,2,4-^{t}Bu$_3C_5H_2^-$, Cp* = $C_5Me_5^-$). The powerful concept of isolobality[6] relates the exotic pentaphospholide anion ([*cyclo*-P_5]$^-$) to Cp^- (Scheme 1). *Scherer* et al. were able to isolate the first transition metal complexes bearing such a *cyclo*-P_5 ligand in bridging (μ_2,$\eta^{5:5}$)[7] or end-deck (η^5)[8] coordination. In 1987, the group of *Baudler* succeeded in synthesising the first alkali metal salts of [*cyclo*-P_5]$^-$ (**II'**) in solution.[9] The synthesis for such solutions could later be optimized,[10] and initial reactivity studies revealed their potential in the preparation of polyphosphorus compounds.[11] In the following decades, complexes of various transition metals with *cyclo*-P_5 ligands in bridging[12] or end-deck[13] coordination modes could be obtained and it was even possible to synthesise an all-phosphorus sandwich dianion

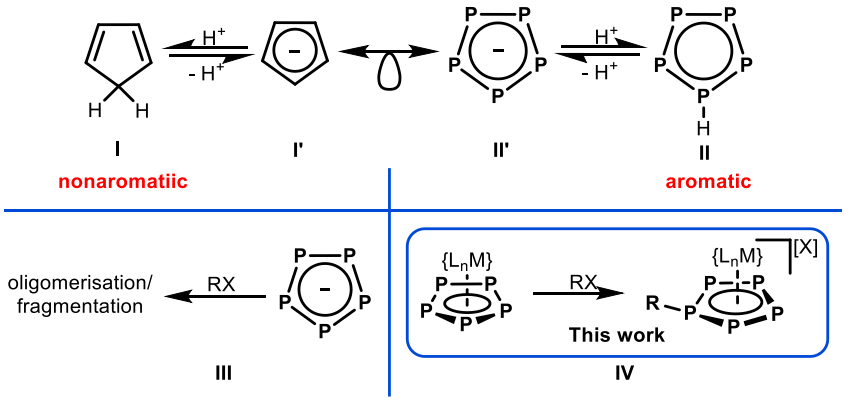

*Scheme 1: Formal protonation/deprotonation reactions (**I** and **II**) of the isolobal Cp^- and cyclo-P_5^- moieties, reactivity studies on cyclo-P_5^- with organohalides (**III**) and our approach of stabilising pentaphospholes in the coordination sphere of transition metals (**IV**).*

$[(\eta^5\text{-}P_5)_2Ti]^{2-}$.[14] While the synthetic strategy for these compounds usually involves the reaction of a transition metal precursor with a reactive source of phosphorus (e.g. P_4 or K_3P_7), a common way to introduce the Cp^- ligand (**I'**) is by salt metathesis with [Cat][Cp] ($[Cat]^+ = [Li]^+$, $[Na]^+$, $[K]^+$), which is obtained by deprotonation of cyclopentadiene (CpH, C_5H_6, Scheme 1, **I**). Because CpH is metastable at ambient temperatures and undergoes [2+4] Diels-Alder cyclisation (dimerisation), the question arises as to the existence of the isolobal parent pentaphosphole (*cyclo*-P_5H), its derivatives (*cyclo*-P_5R), and their stability (Scheme 1, **II**). In view of the high reactivity of CpH, less stability can be assumed for *cyclo*-P_5R. Consequently, attempts by *Baudler* et al. to obtain pentaphospholes by reacting solutions of $[Cat][P_5]$ with alkyl halides only yielded further aggregated polyphosphines (Scheme 1, **III**).[15] Moreover, reports on functionalised P_5 ligands coordinated to transition metal fragments are relatively scarce[16] and there are no reports on neutral pentaphosphole ligand complexes **II**.[17] Thus, the current literature on pentaphospholes is mostly limited to computational studies dealing with the predicted planar structure of the aromatic parent *cyclo*-P_5H, which is in contradiction with the nonaromaticity of CpH (**I**).[18] Therefore, the generation and stabilisation of such a moiety seems to be a valuable target and we report herein a first access to complexes possessing a parent-aromatic *cyclo*-P_5H ligand and related *cyclo*-P_5R ligands, respectively.

One of the key interests of our group is the synthesis of novel polyphosphorus (P_n) ligand complexes and the evaluation of their reactivity. We could demonstrate that pentamethyl-pentaphosphaferrocene ([Cp*Fe(η^5-P_5)], **1**)[8] readily reacts with a variety of Lewis acids to form coordination compounds.[19] It was found that **1** can be oxidised and reduced under P–P bond formation to yield a dimeric dication and dianion, respectively. Doubly reducing **1** even provides a monomeric dianion with an extremely folded *cyclo*-P_5 ligand.[20] **1** also reacts with charged main group nucleophiles to give products bearing an η^4-coordinated *cyclo*-P_5R ligand with an envelope structure, representing the coordinated anionic form of the isolobal CpH moiety **I**.[16a] However, the reactivity of **1** towards cationic main group electrophiles (Scheme 1, **IV**) remains unexplored. Inspired by recent reports on the protonation of the P_4-butterfly complex [{Cp‴Fe$(CO)_2$}$_2$(μ,$\eta^{2:2}$-P_4)][21] and even P_4 (white phosphorus),[22] the question as to the possible protonation of **1** came up. Interestingly, the protonation of ferrocene[23] or the P_4 complexes [$^{Ph}PP_2^{Cy}$Fe(η^4-P_4)] ($^{Ph}PP_2^{Cy}$ = PhP$(C_2H_4PCy_2)_2$)[24] and [$Na_2(THF)_5(Cp^{Ar}Fe)_2$(μ,$\eta^{4:4}$-P_4)] (Cp^{Ar} = $C_5(C_6H_4$-4-Et$)_5$)[25] occurs at the iron and not on the polyphosphorus ligand. In contrast, if the protonation of **1** were to occur at the *cyclo*-P_5 ligand, this would yield the first transition metal complex of the parent *cyclo*-P_5H (**II**). However, the comparably low proton affinity of **1** labels common acids such as HBF_4 (in Et_2O) or even $[H(OEt_2)_2]$[TEF] ($[TEF]^-$ = $[Al\{OC(CF_3)_3\}_4]^-$)[26] unsuitable for this purpose (for details see SI). Thus, we envisioned a two-step process in which **1** would react with an electrophile to yield a metastable intermediate, subsequently to be quenched with a suitable proton source. With this in mind, silylium cations, sometimes referred to as masked protons,[27] seemed to be promising electrophiles to obtain the desired reactivity.

5.3. Results and Discussion

When **1** is reacted with the silylium ion precursor $[(Et_3Si)_2(\mu\text{-}H)][B(C_6F_5)_4]$[28] in *o*-DFB (1,2-difluorobenzene), a colour change to brownish green marks a rapid reaction providing $[Cp^*Fe(\eta^5\text{-}P_5SiEt_3)][B(C_6F_5)_4]$ (**2**) in 71 % yield (Scheme 2). **2** is stable in *o*-DFB solution at room temperature but decomposes slowly in CH_2Cl_2 and is insoluble in toluene or aliphatic hydrocarbons. Furthermore, the slightest traces of moisture immediately decompose **2**. When **2** is treated with half an equivalent of H_2O in *o*-DFB, a rapid colour change to bright red is observed and after workup the protonated complex $[Cp^*Fe(\eta^5\text{-}P_5H)][B(C_6F_5)_4]$ (**3**) can be isolated in 61 % yield. **3** represents the first transition metal complex of the parent pentaphosphole P_5H. It is well soluble and stable in *o*-DFB and CH_2Cl_2 at room temperature and can be stored as a solid under inert atmosphere for several weeks. Similar to **2**, **3** is highly sensitive towards moisture and air and has to be handled with great care. Thus, we also searched for ways to avoid H_2O during the synthesis of **3**, as slight errors in stoichiometry lead to the decomposition of the product. However, when **2** was reacted with MeOH as a proton source, the ^{31}P NMR spectrum of the corresponding reaction solution suggested that, besides **3**, a second species ($[Cp^*Fe(\eta^5\text{-}P_5Me)][B(C_6F_5)_4]$, **4b**) with a substituted P_5 ligand is formed, which we assume to be caused by C–O bond cleavage of MeOH induced by the silylium cation (*vide infra*, Figure 2d). The respective product mixture could, however, not be separated. Thus, we sought for an alternative way to access the methylated derivative **4** which we found in the stoichiometric reaction of **1** with a trimethyloxonium salt. When **1** is reacted with $[Me_3O][BF_4]$ and $B(C_6F_5)_3$ in *o*-DFB at room temperature, a slow colour change of the solution from clear

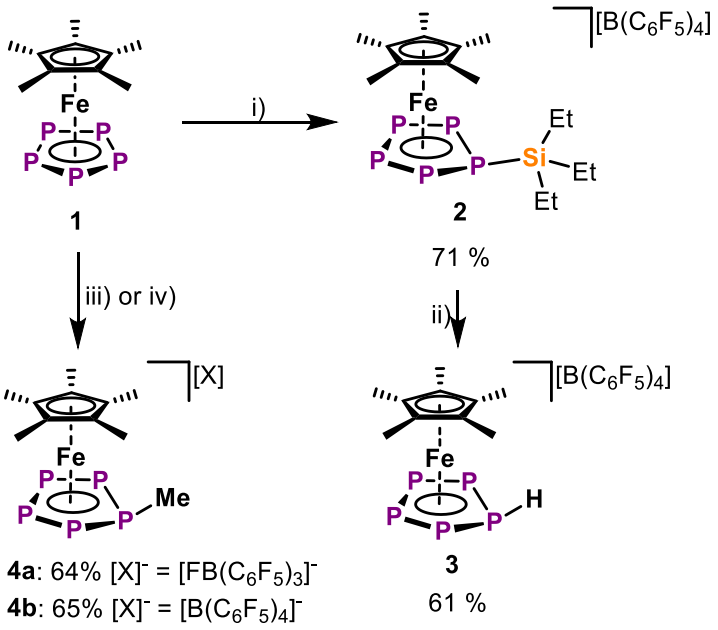

*Scheme 2: Reaction of **1** with cationic main group electrophiles to yield silylated (**2**), protonated (**3**) and methylated (**4**) pentaphosphole complexes: i) 1 eq. $[(Et_3Si)_2(\mu\text{-}H)][B(C_6F_5)_4]$, o-DFB, r.t., 1 h; ii) 0.5 eq. H_2O, o-DFB, r.t., 1 h; iii) 1. 1 eq. $[Me_3O][BF_4]$ in o-DFB, 2. 1 eq. $B(C_6F_5)_3$, o-DFB, r. t., 3 h; iv) 1. 1 eq. MeOTf in o-DFB, r.t., 1 h, 2. 1 eq. $[Li(OEt_2)_2][B(C_6F_5)_4]$, o-DFB, r.t., 18 h.*

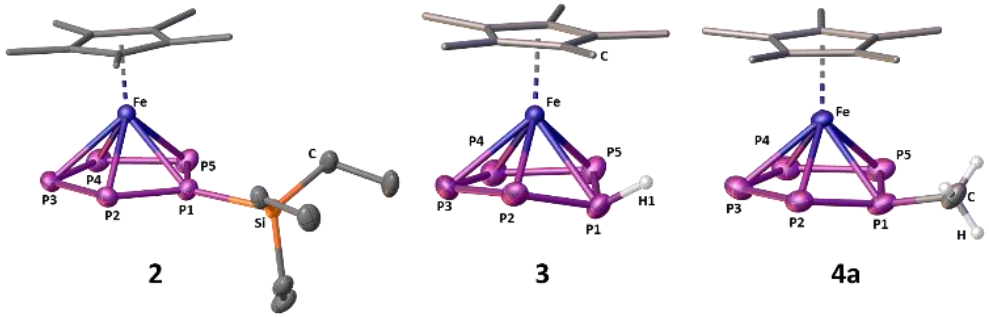

*Figure 1: Solid state structures of the cations in **2**, **3** and **4**; Hydrogen atoms at the Cp* ligand and the Et groups in **2**, the anions $[B(C_6F_5)_4]^-$ (**2** and **3**) and $[FB(C_6F_5)_3]^-$ (**4a**) and cocrystallised $[H][FB(C_6F_5)_3]$ (**4a**) are omitted for clarity. As the cyclo-P_5Me ligand in **4b** is disordered, only structural parameters within **4a** are discussed; ADPs are drawn at the 50 % probability level.*

green to brownish red can be observed. After workup and crystallisation, [Cp*Fe(η^5-P_5Me)][$FB(C_6F_5)_3$]·{$HFB(C_6F_5)_3$}$_{0.5}$ (**4a**·{$HFB(C_6F_5)_3$}$_{0.5}$), a carbon-substituted pentaphosphole transition metal complex, can be isolated as dark red crystals in 64 % yield (Scheme 2). In addition, we found an even easier way to access the methylated derivative **4** and avoided the stoichiometric formation of $HFB(C_6F_5)_3$ by reacting **1** with MeOTf followed by the addition of one equivalent of $[Li(OEt_2)_2][B(C_6F_5)_4]$. After workup, the product **4b** can then be isolated as dark red crystals in 65% yield (Scheme 2).

Compounds **2**, **3** and **4** crystallise from mixtures of *o*-DFB or CH_2Cl_2 and *n*-hexane at -30 °C (**2** and **3**) or at room temperature (**4**) as dark green plates (**2**) and red blocks (**3**, **4**), respectively, which allowed for their X-ray crystallographic investigation. The core-structural motif of the cations is a slightly bent *cyclo*-P_5R (R = $SiEt_3$ (**2**), H (**3**), Me (**4**)) ligand coordinating to the $\{Cp^*Fe\}^+$ moiety in η^5 mode (Figure 1). In contrast to the previously reported anionic compounds [Cp*Fe(η^4-P_5R)]$^-$,[16a] the substituents at the P1 atom in **2**, **3** and **4** are oriented in exo-fashion with regard to the envelope of the P_5 ring (towards the $\{Cp^*Fe\}^+$ moiety). The P–P bond lengths in **2** (2.099(1)-2.122(1) Å) are similar to each other, and those in **3** (2.115(1)-2.130(1) Å) and **4** (2.108(4)-2.133(4) Å) are only slightly longer and in-between the expected values for P–P single (2.22 Å) and double (2.04 Å) bonds.[29] The deviation of the P1 atom from the plane spanned by the other P atoms is less pronounced in **2** (7.44(6)°) than in **3** (25.38(5)°) and **4** (18.1(2)°), which may be attributed to the sterically demanding $SiEt_3$ group in **2**. The P1–Fe distances are only slightly longer (**2**: 2.3010(7) Å, **3**: 2.3729(5) Å, **4**: 2.306(3) Å) than the sum of the covalent radii (2.27 Å), which we attribute to the bonding interaction between the Fe centre and the back lobe of an occupied p-orbital of P1 (*vide infra*). The P1–Si bond in **2** (2.308(1) Å) is slightly longer than the expected P–Si single bond (2.27 Å),[29] which may again be caused by the steric bulk of the $SiEt_3$ group and points towards a comparably weak bond between these atoms. In contrast, the P1–C bond length in **4** (1.848(9) Å) is well within the expected values for a P–C single bond (1.86 Å). The position of H1 in **3** is clearly visible in the difference electron density map, but standard refinement of hydrogen positions from X-ray diffraction data is known to underestimate their distance to adjacent atoms. Thus, it is not surprising that the determined P1-H1 bond length for **3** is only 1.29(3) Å, which is distinctly

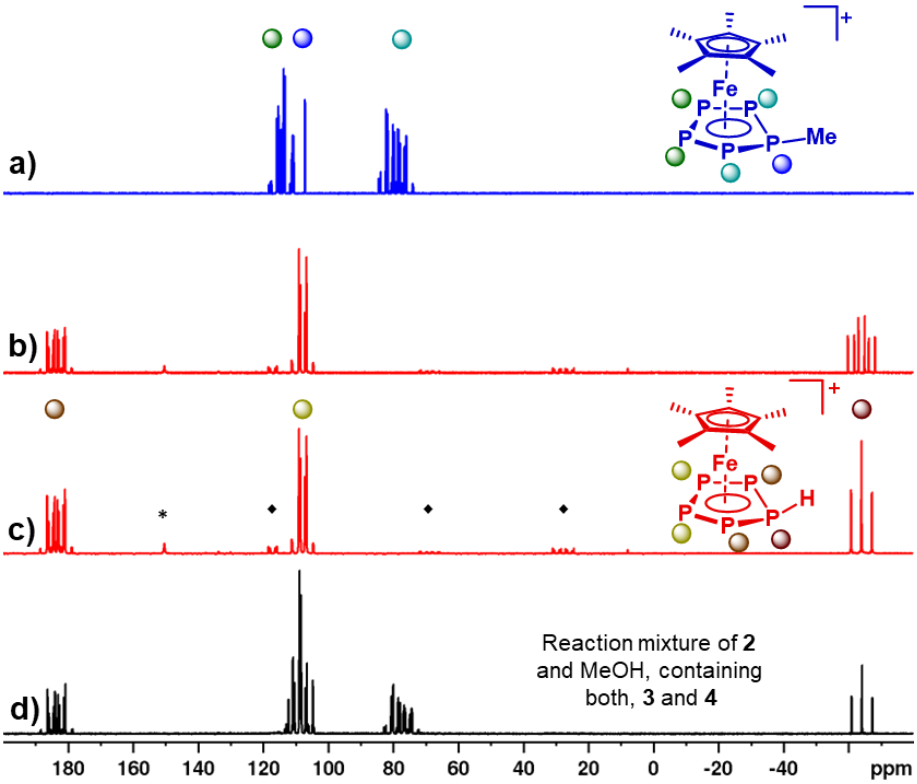

*Figure 2: a) $^{31}P\{^{1}H\}$ NMR spectrum of isolated **4** in CD_2Cl_2 at r. t., b) ^{31}P and c) $^{31}P\{^{1}H\}$ NMR spectra of isolated **3** in CD_2Cl_2 at –80 °C and d) $^{31}P\{^{1}H\}$ NMR spectrum of the product mixture obtained from the reaction of **2** with MeOH in CD_2Cl_2 at –80 °C; assignment of P atoms to the molecular structures of **3** and **4** is provided by the colour code of the signals; * marks the signal for residual **1** and ◆ a group of signals assigned to trace impurities of an unidentified side product.*

shorter than the sum of the covalent radii (1.43 Å).[29] Consequently, neutron diffraction data obtained on compounds containing P–H bonds shows P–H distances much closer to the expected value of 1.43 Å,[30] even when there is a positive charge localisation at the P atom as in $[PH_4][I]$.[31]

NMR spectroscopic investigations of **2** in *o*-DFB revealed its dynamic behaviour in solution at room temperature (see SI). The respective ^{31}P NMR spectrum shows three broad signals centred at 87.6, 102.7 and 149.8 ppm. Upon cooling, the signals sharpen up and at –30 °C a clear AA´MXX´ spin system can be observed, which proves the structural integrity of **2** in solution. Additionally, the signal for P^M shows the expected ^{29}Si satellites and the $^{29}Si\{^{1}H\}$ NMR spectrum reveals a doublet ($^{1}J_{Si\text{-}P}$ = 61 Hz) at 42 ppm, which is slightly upfield shifted compared to the starting material (δ = 57 ppm).[28] Similar to **2**, **3** expresses dynamic behaviour in solution (CD_2Cl_2) at room temperature, which is indicated by three broad resonances centred at –60.9, 112.6 and 179.6 ppm in the ^{31}P NMR spectrum. Consequently, the respective ^{1}H NMR spectrum shows a broad resonance at 1.56 ppm for the Cp* ligand and an additional very broad signal for the proton of the phosphole ligand (δ = 4.6 ppm). Upon cooling the sample, the signals in the $^{31}P\{^{1}H\}$ NMR spectrum become sharper and at –80 °C a well resolved AA´MM´X spin system is observed (Figure 2c). While these signals are only slightly shifted compared to the room temperature spectrum, the P^X signal shows additional coupling in the

^{31}P NMR spectrum ($^{1}J_{P\text{-}H}$ = 316 Hz, Figure 2b). The same coupling constant is found for the P_5H signal (δ = 4.6 ppm) in the ^{1}H NMR spectrum at –80 °C. Neither the ^{11}B nor the ^{19}F NMR spectrum of **3** reveal an interaction of the $[B(C_6F_5)_4]^-$ counteranion with the proton. However, traces of **1** can be detected in the ^{31}P NMR spectrum of **3** (even after several recrystallisation steps). We thus attribute the observed dynamic behaviour to a "bond-breaking/bond-forming" process between **3** itself and **1** (see SI for further details). In contrast to **2** and **3**, **4** shows a well-resolved AA´BXX´ spin system with signals centred at 78.7, 111.8 and 114.2 ppm in the ^{31}P NMR spectrum (CD_2Cl_2, Figure 2a). Thus, dynamic behaviour (on the NMR time scale) of **4** in solution at room temperature can be ruled out. In keeping with that, the ^{1}H NMR spectrum (CD_2Cl_2, r. t.) of **4** shows a singlet for the Cp* ligand (δ = 1.7 ppm) and a doublet of triplets for the methyl group of the P_5Me ligand (δ = 2.68 ppm, $^{2}J_{H\text{-}P}$ = 11.2 Hz, $^{3}J_{H\text{-}P}$ = 3.8 Hz). Consistent with the dynamic behaviour in solution, **3** undergoes partial fragmentation under ESI-MS conditions, and several other species are detected besides the molecular ion $\mathbf{3}^+$ (m/z = 347). This behaviour is even more pronounced for **2**, for which the molecular ion peak is absent and of which only fragments can be detected in the ESI mass spectrum. In contrast, for **4**, the molecular ion peak is detected at m/z = 361 ($\mathbf{4}^+$) and only minor hints of fragmentation are observed under ESI MS conditions.

To obtain further insight into the reaction energetics and the electronic structure of the obtained products **2**–**4**, DFT calculations were carried out at the B3LYP[32]/def2-TZVP[33] level of theory (see SI for details). The silylation reaction ((*1*), Figure 3) of **1** is only slightly exothermic with a reaction enthalpy of ΔH = –31.41 kJ/mol, which is in line with the experimentally observed dynamic behaviour and instability of **2**. However, the follow-up hydrolysis (*2*) of **2** is highly exothermic (ΔH = –89.49 kJ/mol), which is also the case for the methylation (*3*) of **1** (ΔH = –122.96 kJ/mol). The latter is in line with the calculated methyl cation affinity[34] of **1** (see Scheme S 1). NBO analysis[35] revealed sigma bonding interaction between the P1 atom and the respective substituent in **2**, **3** and **4** (Figure 3). While the Wiberg bond indices (WBI) for the P–

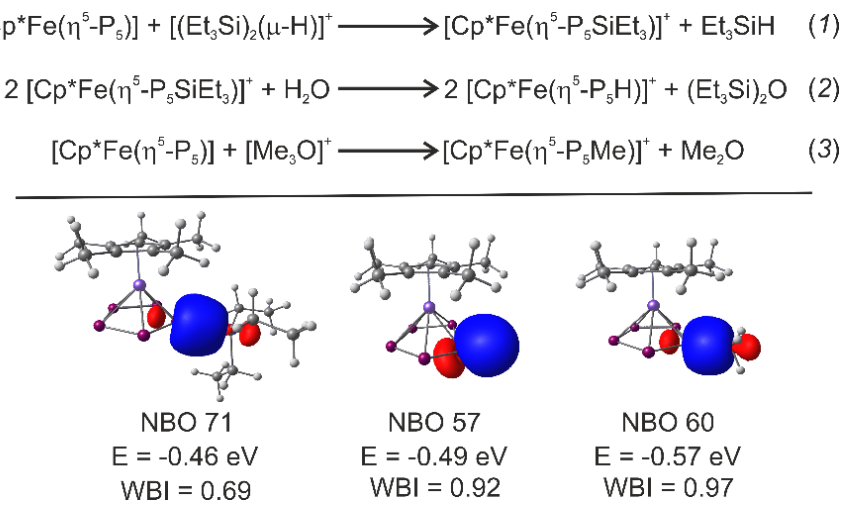

*Figure 3: Reaction equations for the formation of **2**, **3** and **4** (top); NBO orbitals representing the bond between the P_5 moiety and the respective substituent in **2**, **3** and **4**, respectively (isosurfaces drawn at 0.04 contour value), the energies of these orbitals and the respective WBIs (bottom).*

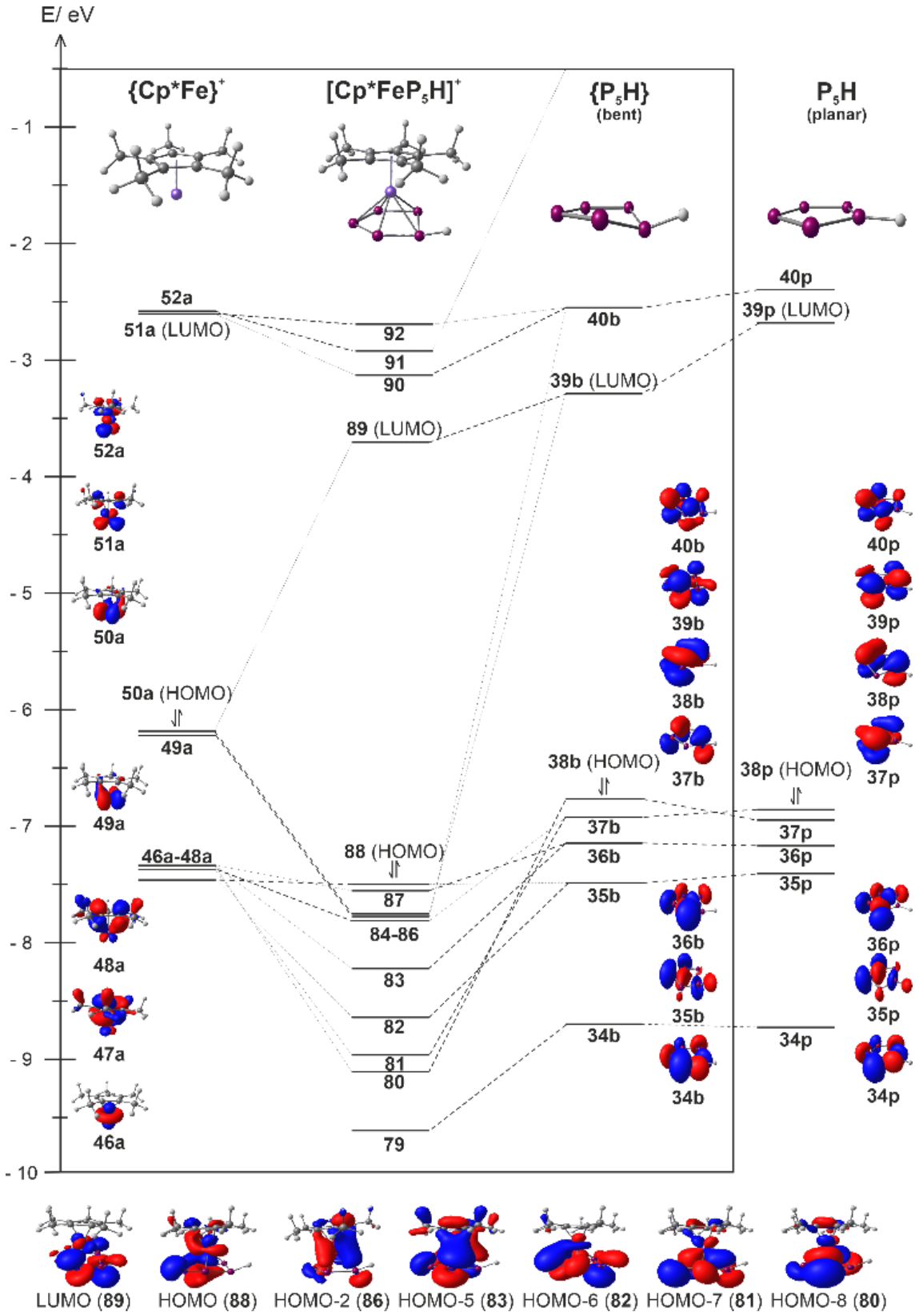

*Figure 4: Section of the orbital interaction diagram for **3**⁺, which is split into the cationic {Cp*Fe}⁺ and the neutral cyclo-P₅H fragments; as well as selected frontier orbitals of both fragments (isosurfaces at 0.04 contour value), and **3**⁺. Additionally, the frontier orbitals of the bent geometry of the P₅H ligand observed in **3**⁺ are compared to those of the planar geometry (global minimum structure of free cyclo-P₅H).*

H bond in **3** (WBI = 0.92) and the P–C bond in **4** (WBI = 0.97) are in line with the formulation as single bonds, the one for the P–Si bond in **2** (WBI = 0.69) is significantly smaller. Additionally, the charge distribution between the {Cp*Fe(η^5-P_5)} moiety and the respective substituent suggests a more polar bond for **2** than for **3** and **4**. This corresponds with the dynamic behaviour of **2** in solution and the elongated P–Si distance observed in the solid state, underlining the weak character of this bond and the high instability of **2**. As **3** displays the first isolated coordination complex of the parent pentaphosphole *cyclo*-P_5H and the molecular structure of free *cyclo*-P_5H has been subject to numerous computational studies,[18] we were especially interested in the orbital interactions within the cation [Cp*Fe(η^5-P_5H)]$^+$ (Figure 4, see SI for details). While the global minimum geometry of free P_5H is planar, the coordination to the {Cp*Fe}$^+$ fragment in **3** leads to a bent geometry for the P_5H ligand. However, we found that the differences regarding the orbital energy and the symmetry of the frontier molecular orbitals (MOs) of both geometries are minor. Namely, the HOMO and HOMO-1 switch places by going from planar P_5H to the bent geometry, and the LUMO experiences a lowering in energy of 0.61 eV (Figure 4). Additionally, the aromatic character of the P_5H moiety is largely preserved in the bent geometry as indicated by a comparison of NICS(1/-1)$_{zz}$[36] values of -31.71/-30.92 and -37.19 for the bent and planar geometry of P_5H, respectively, obtained at the PBE0[37]/aug-pcSseg-2[38] level of theory. While the HOMO (88) and HOMO-1 (87) in **3** can be considered as non-bonding, bonding interaction can be found for the MOs 84 (π bond), 85 (δ bond) and 86 (δ bond). The strongest bonding interactions, however, become manifest in the HOMO-7 (81) and HOMO-8 (80) which display large contributions from the HOMO (38b) and HOMO-1 (37b) of the P_5H ligand. The LUMO (89) of **3** is mainly located at the P_5H ligand, which goes hand in hand with the large contribution of the LUMO (39b) of the P_5H ligand itself. As 37b itself shows a large contribution from one of the p orbitals localised at P1 and contributes to the bonding MOs 86 and 81 in **3**, the hapticity of the P_5H ligand in **3** can be regarded as η^5. A related bonding motif has already been found in the oxidation product[20] of **1** and is consistent with the short P1–Fe distances found in the solid state structure of **2**-**4** (*vide supra*). In account of the bonding situation in **3** and the aromaticity of the bent *cyclo*-P_5H ligand, the description of **3** as a coordination complex of neutral *cyclo*-P_5H and the {Cp*Fe}$^+$ fragment seems appropriate, despite the high degree of covalency between the *cyclo*-P_5H and the {Cp*Fe}$^+$ fragment.

5.4. Conclusion

In conclusion, we were able to isolate and fully characterise the first transition metal complexes bearing pentaphosphole (*cyclo*-P_5R) ligands. Silylation and methylation of [Cp*Fe(η^5-P_5)] (**1**) afforded the respective products [Cp*Fe(η^5-P_5R)][X] (R = $SiEt_3$, [X]$^-$ = [B(C_6F_5)$_4$]$^-$ (**2**); R = Me, [X]$^-$ = [FB(C_6F_5)$_3$]$^-$ (**4a**), [X]$^-$ = [B(C_6F_5)$_4$]$^-$ (**4b**)). Selective hydrolysis of **2** results in P–Si bond cleavage and yields the protonated compound [Cp*Fe(η^5-P_5H)][B(C_6F_5)$_4$] (**3**), which bears the parent *cyclo*-P_5H ligand. Crystallographic characterisation of these compounds revealed that the P_5R unit, in contrast to earlier computational predictions,[18] shows a slight envelope

structure, which we attribute to the coordination to the $\{Cp^*Fe\}^+$ fragment. Detailed computational analysis of the parent compound **3** highlights the preservation of the aromatic character of the *cyclo*-P_5H ligand upon coordination and slightly bending and sheds light on the covalent bonding situation within the cation $[Cp^*Fe(\eta^5\text{-}P_5H)]^+$. Furthermore, the cationic charge of the obtained compounds may allow for the functionalisation of the *cyclo*-P_5R ligand, which could lead to further advances in polyphosphorus chemistry.

5.5. Supporting Information

5.5.1. Experimental Procedures

General Considerations

All manipulations were carried out using standard Schlenk techniques at a Stock apparatus under N_2 as an inert gas or in a glove box with Ar atmosphere. All glassware was dried with a heat gun (600 °C) for at least 1 h prior to use. *o*-DFB was distilled from P_2O_5, CD_2Cl_2 was distilled from CaH_2 and other solvents were directly taken from an MBraun SPS-800 solvent purification system and degassed at room temperature. Solution ^{1}H (400.130 MHz), ^{13}C (100.627 MHz), ^{19}F (376.498 MHz), ^{29}Si (79.485 MHz) and ^{31}P (161.976 MHz) NMR spectra were recorded at an Avance400 (Bruker) spectrometer using $(H_3C)_4Si$ (^{1}H, ^{13}C, ^{29}Si), $CFCl_3$ (^{19}F) or 85% phosphoric acid (^{31}P), respectively, as external standards. Chemical shifts (δ) are provided in parts per million (ppm) and coupling constants (*J*) are reported in Hertz (Hz). Chemical shifts and coupling constants for all $^{31}P\{^{1}H\}$ and ^{31}P NMR spectra were derived from spectral simulation using the built-in simulation package of TopSpin4.0. The following abbreviations are used: s = singlet, d = doublet, dd = doublet of doublets, dt = doublet of triplets, t = triplet, td = triplet of doublets br = broad and m = multiplet. ESI mass spectra were recorded at the internal mass spectrometry department using a ThermoQuest Finnigan TSQ 7000 mass spectrometer and peak assignment was performed using the Molecular weight calculator 6.50.[39] Elemental analysis of the products was conducted by the elemental analysis department at the University of Regensburg using an Elementar Vario EL. The starting materials Cp*Fe(η^5-P_5) (**1**),[8] $[(Et_3Si)_2(\mu\text{-}H)][B(C_6F_5)_4]$[28] and $B(C_6F_5)_3$[40] were synthesized following literature procedures. All other chemicals were purchased from commercial vendors.

*[Cp*Fe(η^5-P$_5$SiEt$_3$)][B(C$_6$F$_5$)$_4$] (**2**)*

Addition of a colourless solution of [(Et$_3$Si)$_2$(μ-H)][B(C$_6$F$_5$)$_4$][28] (156 mg, 0.171 mmol, 1 eq.) in 3 mL of *o*-DFB (1,2-difluorobenzene, C$_6$H$_4$F$_2$) to a green solution of [Cp*Fe(η^5-P$_5$)][8] (59 mg, 0.171 mmol, 1 eq.) in 3 mL of *o*-DFB at room temperature immediately resulted in a greenish brown reaction solution. After stirring this solution for 1 h 30 mL of *n*-pentane were added under vigorous stirring, which resulted in the precipitation of [Cp*Fe(η^5-P$_5$SiEt$_3$)][B(C$_6$F$_5$)$_4$] (**2**) as a light greenish brown powder. **2** was washed two times with 20 mL of *n*-pentane each, then dried under reduced pressure (10^{-3} mbar) and isolated as a light greenish brown powder (134 mg, 0.12 mmol, 71%). Crystallisation from a solution in *o*-DFB (2 mL) which was layered with *n*-hexane (18 mL) leads to the formation of dark green crystals of **2** as large plates.

Yield:	134 mg (0.12 mmol, 71%)
Elemental Analysis:	calc. (%) for [Cp*Fe(η^5-P$_5$SiEt$_3$)][B(C$_6$F$_5$)$_4$] (C$_{40}$H$_{30}$BF$_{20}$SiP$_5$Fe): C: 42.13 H: 2.65
	found (%): C: 42.43 H: 2.38 (powder)
	found (%): C: 42.27 H: 2.80 (crystalline sample)
ESI(+) MS (*o*-DFB):	*m/z* (%) = 346.9 (55%) [Cp*Fe(η^5-P$_5$H)]$^+$, 345.9 (40%) [Cp*Fe(η^5-P$_5$)]$^+$, 156.1 (100%) [Et$_3$Si(MeCN)]$^+$, 115.1 (13%) [Et$_3$Si]$^+$ (acetonitrile arises from the cleansing solution of the mass spectrometer)
NMR (r. t., *o*-DFB):	^{1}H δ/ ppm = 1.13 (t, $^3J_{H\text{-}H}$ = 7.6 Hz, 9 H, Si(CH$_2$C**H**$_3$)$_3$), 1.25 (q, $^3J_{H\text{-}H}$ = 7.6 Hz, 6 H, Si(C**H**$_2$CH$_3$)$_3$), 1.32 (br, 15 H, Cp*)
	^{19}F{^{1}H} δ/ ppm = –167.67 (t, $^3J_{F\text{-}F}$ = 20 Hz, 8 F, m-C$_6$F$_5$), –163.90 (t, $^3J_{F\text{-}F}$ = 18 Hz, 4 F, p-C$_6$F$_5$), –132.55 (br, 8 F, o-C$_6$F$_5$)
	^{31}P{^{1}H} δ/ ppm = 87.6 (br), 102.7 (br), 149.8 (br)
NMR (-30°C, *o*-DFB):	^{1}H δ/ ppm = 1.00 (t, $^3J_{H\text{-}H}$ = 7.8 Hz, 9 H, Si(CH$_2$C**H**$_3$)$_3$), 1.08 (q, $^3J_{H\text{-}H}$ = 7.8 Hz, 6 H, Si(C**H**$_2$CH$_3$)$_3$), 1.18 (s, 15 H, Cp*)
	^{31}P δ/ ppm = 84.32 (m, $^1J_{PX\text{-}PM}$ = 558.5 Hz, $^1J_{PX'\text{-}PM}$ = 557.9 Hz, $^1J_{PX\text{-}PA}$ = 435.2 Hz, $^1J_{PX'\text{-}PA'}$ = 421.9 Hz, $^2J_{PX\text{-}PX'}$ = 22.2 Hz, $^2J_{PX\text{-}PA'}$ = -54.9 Hz, $^2J_{PX'\text{-}PA}$ = -46.3 Hz, 2P, P$^{X/X'}$), 101.69 (m, $^1J_{PM\text{-}PX}$ = 558.5 Hz, $^1J_{PM\text{-}PX'}$ = 557.9 Hz, $^1J_{PM\text{-}Si}$ = 62.1 Hz, $^2J_{PM\text{-}PA}$ = 14.1 Hz, $^2J_{PM\text{-}PA'}$ = 10.9 Hz, 1P, P^M), 146.28 (m, $^1J_{PA\text{-}PX}$ = 435.2 Hz, $^1J_{PA'\text{-}PX'}$ = 421.9 Hz, $^1J_{PA\text{-}PA'}$ = 415.1 Hz, $^2J_{PA\text{-}PX'}$ = -46.3 Hz, $^1J_{PA'\text{-}PX}$ = -54.9 Hz, $^2J_{PA\text{-}PM}$ = 14.1 Hz, $^2J_{PA\text{-}PM'}$ = 10.9 Hz, 2P, P$^{A/A'}$)

$^{31}P\{^{1}H\}$ δ/ ppm = 84.32 (m, $^{1}J_{PX\text{-}PM}$ = 558.5 Hz, $^{1}J_{PX'\text{-}PM}$ = 557.9 Hz, $^{1}J_{PX\text{-}PA}$ = 435.2 Hz, $^{1}J_{PX'\text{-}PA'}$ = 421.9 Hz, $^{2}J_{PX\text{-}PX'}$ = 22.2 Hz, $^{2}J_{PX\text{-}PA'}$ = -54.9 Hz, $^{2}J_{PX'\text{-}PA}$ = -46.3 Hz, 2P, $P^{X/X'}$), 101.69 (m, $^{1}J_{PM\text{-}PX}$ = 558.5 Hz, $^{1}J_{PM\text{-}PX'}$ = 557.9 Hz, $^{1}J_{PM\text{-}Si}$ = 62.1 Hz, $^{2}J_{PM\text{-}PA}$ = 14.1 Hz, $^{2}J_{PM\text{-}PA'}$ = 10.9 Hz, 1P, P^{M}), 146.28 (m, $^{1}J_{PA\text{-}PX}$ = 435.2 Hz, $^{1}J_{PA'\text{-}PX'}$ = 421.9 Hz, $^{1}J_{PA\text{-}PA'}$ = 415.1 Hz, $^{2}J_{PA\text{-}PX'}$ = -46.3 Hz, $^{1}J_{PA'\text{-}PX}$ = -54.9 Hz, $^{2}J_{PA\text{-}PM}$ = 14.1 Hz, $^{2}J_{PA\text{-}PM'}$ = 10.9 Hz, 2P, $P^{A/A'}$)

$^{29}Si\{^{1}H\}$ δ/ ppm = 42 (d, $^{1}J_{Si\text{-}P}$ = 60.7 Hz)

*[Cp*Fe(η^5-P$_5$H)][B(C$_6$F$_5$)$_4$] (**3**)*

[Cp*Fe(η^5-P$_5$SiEt$_3$)][B(C$_6$F$_5$)$_4$] (**2**, 114 mg, 0.1 mmol, 1 eq.) was dissolved in 4 mL of *o*-DFB and H_2O (1 μL, 0.05 mmol, 0.5 eq.) was added with a syringe. The resulting mixture was stirred for 1 h, upon which a gradual colour change from brownish green to clear red could be observed. 20 mL of *n*-pentane were added to precipitate a brownish red powder, which was then washed three times with 10 mL of *n*-pentane each. After drying under reduced pressure (10^{-3} mbar) [Cp*Fe(η^5-P$_5$H)][B(C$_6$F$_5$)$_4$] (**3**) could be isolated as a pale brownish red powder. Recrystallisation of **3** from *o*-DFB (4 mL) solution layered with *n*-hexane (32 mL) gave after 5 days large red blocks, suitable for single crystals X-ray analysis.

Yield: 38 mg (0.037 mmol, 74 %)

Elemental Analysis: calc. (%) for [Cp*Fe(η^5-P$_5$H)][B(C$_6$F$_5$)$_4$] (C$_{34}$H$_{16}$BF$_{20}$P$_5$Fe):
C: 39.80 H: 1.57

found (%): C: 40.28 H: 1.72

ESI(+) MS (*o*-DFB): *m/z* (%) = 346.9 (55%) [Cp*Fe(η^5-P$_5$H)]$^+$, 345.9 (45%) [Cp*Fe(η^5-P$_5$)]$^+$, 156.1 (60%) [Et$_3$Si(MeCN)]$^+$, (acetonitrile arises from the cleansing solution of the mass spectrometer)

NMR (r. t., CD_2Cl_2): ^{1}H δ/ ppm = 1.55 (s, 15 H, Cp*), 4.58 (br, 1 H, P$_5$**H**)

^{19}F{^{1}H} δ/ ppm = –167.30 (t, $^3J_{F\text{-}F}$ = 18 Hz, 8 F, m-C$_6$F$_5$), –163.50 (t, $^3J_{F\text{-}F}$ = 18 Hz, 4 F, p-C$_6$F$_5$), –132.80 (br, 8 F, o-C$_6$F$_5$)

^{31}P{^{1}H} δ/ ppm = –60.9 (br), 112.6 (br), 179.6 (br)

NMR (-80°C, CD_2Cl_2): ^{1}H δ/ ppm = 1.53 (s, 15 H, Cp*), 4.47 (d, $^1J_{H\text{-}P}$ = 315.8 Hz, 1 H, P$_5$**H**)

^{19}F{^{1}H} δ/ ppm = –166.0 (br, 2 F, [B(C$_6$F$_5$)$_4$]$^-$), –162.1 (br, 1 F, [B(C$_6$F$_5$)$_4$]$^-$), –133.4 (br, 2 F, [B(C$_6$F$_5$)$_4$]$^-$)

^{31}P{^{1}H} δ/ ppm = –64.13 (t, $^1J_{PX\text{-}PA}$ = 517.37 Hz, $^1J_{PX\text{-}PA'}$ = 516.60 Hz, $^2J_{PX\text{-}PM}$ = 5.67 Hz, $^2J_{PX\text{-}PM'}$ = 3.19 Hz, 1P, P^X), 107.75 (m, $^1J_{PM\text{-}PA}$ = 436.76 Hz, $^1J_{PM'\text{-}PA'}$ = 427.80 Hz, $^1J_{PM\text{-}PM'}$ = 416.61 Hz, $^2J_{PM\text{-}PA'}$ = –61.77 Hz, $^2J_{PM'\text{-}PA}$ = –54.41 Hz, $^2J_{PM\text{-}PX}$ = 5.67 Hz, $^2J_{PM'\text{-}PX}$ = 3.19 Hz, 2P, P$^{M/M'}$), 183.95 (m, $^1J_{PA\text{-}PX}$ = 517.37 Hz, $^1J_{PA'\text{-}PX}$ = 516.60 Hz, $^1J_{PA\text{-}PM}$ = 436.76 Hz, $^1J_{PA'\text{-}PM'}$ = 427.80 Hz, $^2J_{PA\text{-}PM'}$ = –61.77 Hz, $^2J_{PA'\text{-}PM}$ = –54.41 Hz, $^2J_{PA\text{-}PA'}$ = 18.16 Hz, 2P, P$^{A/A'}$)

^{31}P δ/ ppm = –64.14 (td, $^1J_{PX\text{-}PA}$ = 516.99 Hz, $^1J_{PX\text{-}PA'}$ = 516.94 Hz, $^1J_{PX\text{-}H}$ = 315.82 Hz, $^2J_{PX\text{-}PM}$ = 5.32 Hz, $^2J_{PX\text{-}PM'}$ = 4.20 Hz, 1P, P^X), 107.67 (m, $^1J_{PM\text{-}PA}$ = 436.75 Hz, $^1J_{PM'\text{-}PA'}$ = 428.24 Hz, $^1J_{PM\text{-}PM'}$ =

416.91 Hz, $^{2}J_{PM\text{-}PA'}$ = –63.45 Hz, $^{2}J_{PM'\text{-}PA}$ = –52.76 Hz, $^{2}J_{PM\text{-}PX}$ = 5.32 Hz, $^{2}J_{PM'\text{-}PX}$ = 4.20 Hz, 2P, $P^{M/M'}$), 183.95 (m, $^{1}J_{PA\text{-}PX}$ = 516.99 Hz, $^{1}J_{PA'\text{-}PX}$ = 516.94 Hz, $^{1}J_{PA\text{-}PM}$ = 436.75 Hz, $^{1}J_{PA'\text{-}PM'}$ = 428.24 Hz, $^{2}J_{PA\text{-}PM'}$ = –63.45 Hz, $^{2}J_{PA'\text{-}PM}$ = –52.76 Hz, $^{2}J_{PA\text{-}PA'}$ = 18.53 Hz, 2P, $P^{A/A'}$)

*[Cp*Fe(η^5-P$_5$Me)][FB(C$_6$F$_5$)$_3$]·{HFB(C$_6$F$_5$)$_3$}$_{0.5}$ (**4a**)*

[Cp*Fe(η^5-P$_5$)] (**1**, 70 mg, 0.2 mmol, 1 eq.) and [Me$_3$O][BF$_4$] (30 mg, 0.2 mmol, 1 eq.) were weighed into a Schlenk flask and 6 mL of *o*-DFB were added ([Me$_3$O][BF$_4$] does not dissolve). Then a solution of B(C$_6$F$_5$)$_3$[40] (102 mg, 0.2 mmol, 1 eq.) in 2 mL of *o*-DFB was added. Upon stirring the resulting mixture for 3 h a gradual colour change from clear green to brownish red could be observed (after 2 hours there was no solid [Me$_3$O][BF$_4$] left in the flask). 30 mL of *n*-pentane were added to precipitate a brownish red oil, which was washed three times with 20 mL of *n*-pentane each. Recrystallisation from *o*-DFB (5 mL) solution by layering with *n*-pentane (20 mL) gave after two weeks [Cp*Fe(η^5-P$_5$Me)][FB(C$_6$F$_5$)$_3$] (**4a**) as brownish red stick-shaped crystals.

Yield:	147 mg (0.127 mmol, 64%)
Elemental Analysis:	calc. (%) for [Cp*Fe(η^5-P$_5$Me)][FB(C$_6$F$_5$)$_3$]·{[H][FB(C$_6$F$_5$)$_3$]}$_{0.5}$ (C$_{38}$H$_{18.5}$B$_{1.5}$F$_{24}$FeP$_5$): C: 39.42 H: 1.61
	found (%): C: 39.16 H: 1.79
ESI(+) MS:	*m/z* (%) =, 360.9 (100%) [Cp*Fe(η^5-P$_5$Me)]$^+$, 377.9 (25%) [Cp*Fe(η^5-P$_5$Me)+OH]$^+$, 326.2 (60%) unidentified species
ESI(-) MS:	*m/z* (%) = 531.0 (90%) [FB(C$_6$F$_5$)$_3$]$^-$, 1100.9 (35%) [{FB(C$_6$F$_5$)$_3$}$_2$(H$_2$F)(H$_2$O)]$^-$, 1080.0 (100%) [{FB(C$_6$F$_5$)$_3$}$_2$(H$_3$O)]$^-$, 1059.0 (20%) [F{B(C$_6$F$_5$)$_3$}$_2$+O]$^-$.
NMR (r. t., CD$_2$Cl$_2$):	^{1}H δ/ ppm = 1.69 (s, 15 H, Cp*), 2.68 (dt, $^2J_{H\text{-}PB}$ = 11.2 Hz $^3J_{H\text{-}PX/X'}$ = 3.8 Hz, 3 H, P$_5$C**H$_3$**)
	^{11}B{^{1}H} δ/ ppm = –0.1 (br, [FB(C$_6$F$_5$)$_3$]$^-$)
	^{13}C{^{1}H} δ/ ppm = 1.8 (dt, $^1J_{C\text{-}P}$ = 15.9 Hz, $^2J_{C\text{-}P}$ = 4.5 Hz, P$_5$CH$_3$), 11.1 (s, C$_5$(CH$_3$)$_5$), 97.8 (s, C$_5$(CH$_3$)$_5$), 117.3 (br, [H][FB(C$_6$F$_5$)$_3$]$_{geminal}$), 122.6 (br, [FB(C$_6$F$_5$)$_3$]$^-_{geminal}$), 137.1 (dm, [FB(C$_6$F$_5$)$_3$]$^-_{meta}$), 137.4 (dm, [H][FB(C$_6$F$_5$)$_3$]$_{meta}$), 140.0 (dm, [FB(C$_6$F$_5$)$_3$]$^-_{para}$), 141.2 (dm, [H][FB(C$_6$F$_5$)$_3$]$_{para}$) 148.2 (dm, [FB(C$_6$F$_5$)$_3$]$^-_{ortho}$/[H][FB(C$_6$F$_5$)$_3$]$_{ortho}$). The determination of coupling constants for the [FB(C$_6$F$_5$)$_3$]$^-$ anion is hampered by strong overlap and broadening of the signals.
	^{19}F δ/ ppm = –184.25 (br, 1.5 F, [FB(C$_6$F$_5$)$_3$]$^-$/ [H][FB(C$_6$F$_5$)$_3$]), –166.32 (m, 6 F, [FB(C$_6$F$_5$)$_3$]$^-_{meta}$), –164.67 (m, 3 F, [H][FB(C$_6$F$_5$)$_3$]$_{meta}$), –161.46 (t, $^3J_{F\text{-}F}$ = 20.1 Hz, 3 F, [FB(C$_6$F$_5$)$_3$]$^-_{para}$), –157.91 (m, 1.5 F, [H][FB(C$_6$F$_5$)$_3$]$_{para}$) –135.62 (m, 6 F, [FB(C$_6$F$_5$)$_3$]$^-_{ortho}$), –135.34 (m, 3 F, [H][FB(C$_6$F$_5$)$_3$]$_{ortho}$)

$^{31}P\{^{1}H\}$ δ/ ppm = 78.74 (m, $^{1}J_{PX\text{-}PB}$ = 607.74 Hz, $^{1}J_{PX\text{-}PB}$ = 605.96 Hz, $^{1}J_{PX\text{-}PA}$ = 462.34 Hz, $^{1}J_{PX'\text{-}PA'}$ = 448.15 Hz, $^{2}J_{PX\text{-}PA'}$ = –61.40 Hz, $^{2}J_{PX'\text{-}PA}$ = –48.99 Hz, $^{2}J_{PX\text{-}PX'}$ = 42.11 Hz, 2P, $P^{X/X'}$), 111.79 (m, $^{1}J_{PB\text{-}PX}$ = 607.74 Hz, $^{1}J_{PB\text{-}PX'}$ = 605.96 Hz, $^{2}J_{PB\text{-}PA}$ = 11.82 Hz, $^{2}J_{PB\text{-}PA'}$ = 9.42 Hz, 1P, P^{B}), 114.24 (m, $^{1}J_{PA\text{-}PX}$ = 462.34 Hz, $^{1}J_{PA'\text{-}PX'}$ = 448.15 Hz, $^{1}J_{PA\text{-}PA'}$ = 405.82 Hz, $^{2}J_{PA\text{-}PB}$ = 11.82 Hz, $^{2}J_{PA'\text{-}PB}$ = 9.42 Hz, 2P, $P^{A/A'}$)

^{31}P δ/ ppm = 78.73 (m, $^{1}J_{PX\text{-}PB}$ = 607.66 Hz, $^{1}J_{PX\text{-}PB}$ = 606.05 Hz, $^{1}J_{PX\text{-}PA}$ = 461.98 Hz, $^{1}J_{PX'\text{-}PA'}$ = 448.49 Hz, $^{2}J_{PX\text{-}PA'}$ = –60.90 Hz, $^{2}J_{PX'\text{-}PA}$ = –49.45 Hz, $^{2}J_{PX\text{-}PX'}$ = 42.11 Hz, $^{3}J_{PX\text{-}H(Me)}$ = 3.59 Hz, $^{3}J_{PX'\text{-}H(Me)}$ = 2.87 Hz, 2P, $P^{X/X'}$), 111.79 (m, $^{1}J_{PB\text{-}PX}$ = 607.66 Hz, $^{1}J_{PB\text{-}PX'}$ = 606.05 Hz, $^{2}J_{PB\text{-}PA}$ = 10.72 Hz, $^{2}J_{PB\text{-}PA'}$ = 10.47 Hz, $^{2}J_{PB\text{-}H(Me)}$ = 11.33 Hz, 1P, P^{B}), 114.23 (m, $^{1}J_{PA\text{-}PX}$ = 461.98 Hz, $^{1}J_{PA'\text{-}PX'}$ = 448.49 Hz, $^{1}J_{PA\text{-}PA'}$ = 405.90 Hz, $^{2}J_{PA\text{-}PB}$ = 10.72 Hz, $^{2}J_{PA'\text{-}PB}$ = 10.47 Hz, 2P, $P^{A/A'}$)

*[Cp*Fe(η^5-P$_5$Me)][B(C$_6$F$_5$)$_4$] (**4b**)*

[Cp*Fe(η^5-P$_5$)] (**1**, 70 mg, 0.2 mmol, 1 eq.) was weighed into a Schlenk flask and 4 mL of *o*-DFB and MeOTf (22 μL, 0.2 mmol, 1 eq.) were added. After stirring the solution for 1 h a solution of [(Li(OEt$_2$)$_2$][B(C$_6$F$_5$)$_4$] (167 mg, 0.2 mmol, 1 eq.) in 2 mL of *o*-DFB was added. Upon stirring the resulting mixture for 3 h a gradual colour change from clear green to brownish red could be observed and the solution was then stirred for another 15 h. Then, 30 mL of *n*-pentane were added to precipitate a brownish red solid, which was washed three times with 10 mL of *n*-pentane each. 2 mL of CH_2Cl_2 were added and the resulting red solution was filtered from the formes white precipitate (LiOTf). Layering this red solution with 16 mL of *n*-pentane and storing it at room temperature afforded [Cp*Fe(η^5-P$_5$Me)][B(C$_6$F$_5$)$_4$] (**4b**) as brownish red block shaped crystals after one day.

Yield:	135 mg (0.13 mmol, 65%)
Elemental Analysis:	calc. (%) for [Cp*Fe(□^{5}-P$_5$Me)][B(C$_6$F$_5$)$_4$] (C$_{35}$H$_{18}$BF$_{20}$P$_5$Fe): C: 40.42 H: 1.74
	found (%): C: 40.97 H: 1.92
ESI(+) MS:	*m/z* (%) = 360.9 (20%) [Cp*Fe(η^5-P$_5$Me)]$^+$, 474.0 (80%) unidentified species, 326.2 (30%) unidentified species, 187.2 (100%) unidentified species
ESI(-) MS:	*m/z* (%) = 679.0 (100%) [B(C$_6$F$_5$)$_4$]$^-$
NMR (r. t., CD_2Cl_2):	^{1}H δ/ ppm = 1.69 (s, 15 H, Cp*), 2.68 (dt, $^2J_{H\text{-}PB}$ = 11.2 Hz $^3J_{H\text{-}PX/X'}$ = 3.8 Hz, 3 H, P$_5$C**H$_3$**)
	^{11}B{^{1}H} δ/ ppm = –16.9 (s, [B(C$_6$F$_5$)$_4$]$^-$)
	^{13}C{^{1}H} δ/ ppm = 1.8 (dt, $^1J_{C\text{-}P}$ = 15.9 Hz, $^2J_{C\text{-}P}$ = 4.5 Hz, P$_5$CH$_3$), 11.1 (s, C$_5$(CH$_3$)$_5$), 97.8 (s, C$_5$(CH$_3$)$_5$), 123.7 (br, gem-C$_6$F$_5$), 136.3 (dm, $^1J_{C\text{-}F}$ = 247 Hz, o-C$_6$F$_5$), 138.2 (dm, $^1J_{C\text{-}F}$ = 245 Hz, p-C$_6$F$_5$), 148.2 (dm, $^1J_{C\text{-}F}$ = 243 Hz, m-C$_6$F$_5$)
	^{19}F δ/ ppm = –167.11 (t, $^3J_{F\text{-}F}$ = 19 Hz, 8 F, m-C$_6$F$_5$), –163.26 (t, $^3J_{F\text{-}F}$ = 19 Hz, 4 F, p-C$_6$F$_5$), –132.74 (br, 8 F, o-C$_6$F$_5$)
	^{31}P{^{1}H} δ/ ppm = 78.74 (m, $^1J_{PX\text{-}PB}$ = 607.74 Hz, $^1J_{PX\text{-}PB}$ = 605.96 Hz, $^1J_{PX\text{-}PA}$ = 462.34 Hz, $^1J_{PX'\text{-}PA'}$ = 448.15 Hz, $^2J_{PX\text{-}PA'}$ = –61.40 Hz, $^2J_{PX'\text{-}PA}$ = –48.99 Hz, $^2J_{PX\text{-}PX'}$ = 42.11 Hz, 2P, P$^{X/X'}$), 111.79 (m, $^1J_{PB\text{-}PX}$ = 607.74 Hz, $^1J_{PB\text{-}PX'}$ = 605.96 Hz, $^2J_{PB\text{-}PA}$ = 11.82 Hz, $^2J_{PB\text{-}PA'}$ = 9.42

Hz, 1P, P^{B}), 114.24 (m, $^{1}J_{PA-PX}$ = 462.34 Hz, $^{1}J_{PA'-PX'}$ = 448.15 Hz, $^{1}J_{PA-PA'}$ = 405.82 Hz, $^{2}J_{PA-PB}$ = 11.82 Hz, $^{2}J_{PA'-PB}$ = 9.42 Hz, 2P, $P^{A/A'}$)

^{31}P δ/ ppm = 78.73 (m, $^{1}J_{PX-PB}$ = 607.66 Hz, $^{1}J_{PX-PB}$ = 606.05 Hz, $^{1}J_{PX-PA}$ = 461.98 Hz, $^{1}J_{PX'-PA'}$ = 448.49 Hz, $^{2}J_{PX-PA'}$ = –60.90 Hz, $^{2}J_{PX'-PA}$ = –49.45 Hz, $^{2}J_{PX-PX'}$ = 42.11 Hz, $^{3}J_{PX-H(Me)}$ = 3.59 Hz, $^{3}J_{PX'-H(Me)}$ = 2.87 Hz, 2P, $P^{X/X'}$), 111.79 (m, $^{1}J_{PB-PX}$ = 607.66 Hz, $^{1}J_{PB-PX'}$ = 606.05 Hz, $^{2}J_{PB-PA}$ = 10.72 Hz, $^{2}J_{PB-PA'}$ = 10.47 Hz, $^{2}J_{PB-H(Me)}$ = 11.33 Hz, 1P, P^{B}), 114.23 (m, $^{1}J_{PA-PX}$ = 461.98 Hz, $^{1}J_{PA'-PX'}$ = 448.49 Hz, $^{1}J_{PA-PA'}$ = 405.90 Hz, $^{2}J_{PA-PB}$ = 10.72 Hz, $^{2}J_{PA'-PB}$ = 10.47 Hz, 2P, $P^{A/A'}$)

5.5.2. X-ray Crystallographic Data

The crystallographic data for all synthesised compounds was collected on either an Xcalibur Gemini (Rigaku Oxford Diffraction) with an Atlas^{S2} detector using Mo–K_α (**2**) or Cu–K_α (**4b**) radiation (sealed tube), on a SuperNova diffractometer (Rigaku) with a Titan^{S2} detector using Cu–K_β radiation (**3**), obtained by using customised optics, or on another SuperNova diffractometer (Rigaku) with a Titan^{S2} detector using a standard Cu–K_α (**4a**) sealed tube microfocus source. Data reduction and absorption correction were performed with the CrysAlisPro software package.[41] Structure solution and refinement was conducted in Olex2 (1.3-alpha)[42] with ShelXT[43] (solution) and ShelXL-2014[44] (least squares refinement (F^2)) or olex2.refine (Gauss-Newton).[42] All non-H atoms were refined with anisotropic displacement parameters and H atoms were treated as riding models with isotropic displacement parameters and fixed C–H bond lengths (sp^3: 0.96 (CH_3), 0.97 (CH_2); sp^2: 0.93 (CH)). Visualisation of the crystal structures was performed with Olex2 (1.3-alpha).[42]

CIF files with comprehensive information on the details of the diffraction experiments and full tables of bond lengths and angles for **2**, **3**, **4a** and **4b** are deposited in Cambridge Crystallographic Data Centre under the deposition codes CCDC-2022440, CCDC-2022441, CCDC-2022442 and CCDC-2022443, respectively.

*Table S 1: X-ray crystallographic and refinement data on compounds **2**, **3**, **4a** and **4b**.*

Compound	2	3	4a	4b
Empirical formula	$C_{40}H_{30}BF_{20}FeP_5Si$	$C_{34}H_{16}BF_{20}P_5Fe$	$C_{304}H_{144}B_{12}F_{192}Fe_8P_{40}$	$C_{35}H_{18}BF_{20}P_5Fe$
Formula weight	1140.24	1025.98	9258.95	1040.00
Temperature/K	123(2)	123.00(10)	89.9(4)	123(2)
Crystal system	monoclinic	triclinic	monoclinic	triclinic
Space group	$I2/a$	$P\bar{1}$	Cc	$P\bar{1}$
a/Å	17.8248(4)	10.3611(2)	24.7070(2)	10.4794(3)
b/Å	18.3720(4)	12.6558(2)	29.0546(2)	12.6253(4)
c/Å	28.7731(7)	14.0360(3)	47.1012(3)	14.3041(4)
α/°	90	94.696(2)	90	85.003(2)
β/°	106.865(3)	90.009(2)	93.7920(10)	88.481(2)
γ/°	90	98.632(2)	90	83.202(2)
Volume/Å^3	9017.3(4)	1813.41(6)	33737.7(4)	1871.81(10)
Z	8	2	4	2
ρ_{calc}g/cm^3	1.680	1.879	1.823	1.845
μ/mm^{-1}	0.653	4.964	5.957	6.471
F(000)	4560.0	1012.0	18255.0	1028.0
Crystal size/mm^3	0.347 × 0.207 × 0.114	0.465 × 0.269 × 0.165	0.259 × 0.211 × 0.172	0.432 × 0.26 × 0.186
Radiation	Mo Kα (λ = 0.71073)	Cu Kβ (λ = 1.39222)	Cu Kα (λ = 1.54184)	Cu Kα (λ = 1.54184)
2Θ range for data collection/°	6.816 to 58.202	5.706 to 148.828	7.154 to 148.394	7.076 to 144.032
Index ranges	-24 ≤ h ≤ 16, -21 ≤ k ≤ 23, -38 ≤ l ≤ 37	-14 ≤ h ≤ 14, -17 ≤ k ≤ 16, -19 ≤ l ≤ 19	-30 ≤ h ≤ 29, -36 ≤ k ≤ 36, -58 ≤ l ≤ 55	-12 ≤ h ≤ 9, -15 ≤ k ≤ 14, -16 ≤ l ≤ 17
Reflections collected	17646	28063	142942	20735
Independent reflections	10205 [R_{int} = 0.0232, R_{sigma} = 0.0434]	9759 [R_{int} = 0.0298, R_{sigma} = 0.0272]	53933 [R_{int} = 0.0345, R_{sigma} = 0.0329]	7190 [R_{int} = 0.0393, R_{sigma} = 0.0368]
Data/restraints/parameters	10205/0/621	9759/0/559	53933/1050/5338	7190/0/603
Goodness-of-fit on F^2	1.050	1.039	1.051	1.021
Final R indexes [I>=2σ (I)]	R_1 = 0.0429, wR_2 = 0.0835	R_1 = 0.0340, wR_2 = 0.0913	R_1 = 0.0578, wR_2 = 0.1553	R_1 = 0.0406, wR_2 = 0.1098
Final R indexes [all data]	R_1 = 0.0590, wR_2 = 0.0897	R_1 = 0.0354, wR_2 = 0.0926	R_1 = 0.0632, wR_2 = 0.1621	R_1 = 0.0424, wR_2 = 0.1116
Largest diff. peak/hole / e Å^{-3}	0.46/-0.35	0.56/-0.53	1.26/-0.45	0.55/-0.49

*[Cp*Fe(η^5-P$_5$SiEt$_3$)][B(C$_6$F$_5$)$_4$] (**2**)*

Large green prism shaped crystals of [Cp*Fe(η^5-P$_5$SiEt$_3$)][B(C$_6$F$_5$)$_4$] (**2**) are obtained by layering a concentrated solution in *o*-DFB with *n*-hexane (1:7) and storing it at room temperature for two weeks. **2** crystallises in the monoclinic space group *I*2/a with one cation and one anion in the asymmetric unit (Figure S1).

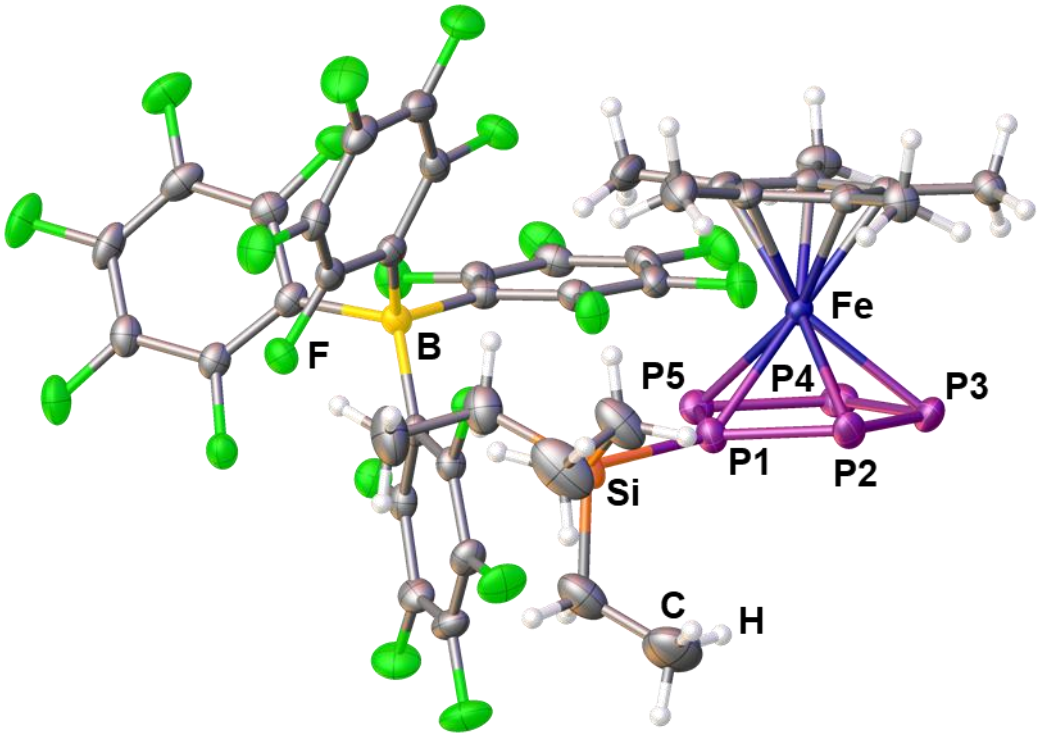

*Figure S 1: Solid state structure of **2**; Depicted is the asymmetric unit and ADPs (anisotropic displacement parameters) are drawn at 50% probability); Selected bond lengths and angles: d(P1-P2) = 2.1062 (9) Å, d(P2-P3) = 2.1177(9) Å, d(P3-P4) = 2.1216(10) Å, d(P4-P5) = 2.1145(9) Å, d(P1-P5) = 2.0993(9) Å, d(P1-Fe) = 2.3010(7) Å, d(P2-Fe) = 2.3947(7) Å, d(P3-Fe) = 2.3852(7) Å, d(P4-Fe) = 2.3855(7) Å, d(P5-Fe) = 2.3979(7) Å, d(P1-Si) = 2.3085(9) Å), ∢(P1-P2-P3) = 101.70(3)°, ∢(P2-P3-P4) = 109.91(4)°, ∢(P3-P4-P5) = 110.02(4)°, ∢(P4-P5-P1) = 101.83(4)°, ∢(P5-P1-P2) = 116.02(4)°, ∢(Si-P1-P2) = 123.82(4)°, ∢(Si-P1-P5) = 120.14(4)°, ∢(Si-P1-Fe) = 140.16(4)°, ∂(P4-P5-P2-P1) = 172.31(8)°, ∂(P3-P2-P5-P1) = –172.54(6)°.*

*[Cp*Fe(η^5-P_5H)][$B(C_6F_5)_4$] (**3**)*

Large red crystalline blocks of [Cp*Fe(η^5-P_5H)][$B(C_6F_5)_4$] (**3**) are obtained by layering a concentrated solution in *o*-DFB with *n*-hexane (1:10) and storing it at –30 °C for five days. **3** crystallises in the triclinic space group $P\bar{1}$ with one cation and one anion in the asymmetric unit (Figure S2).

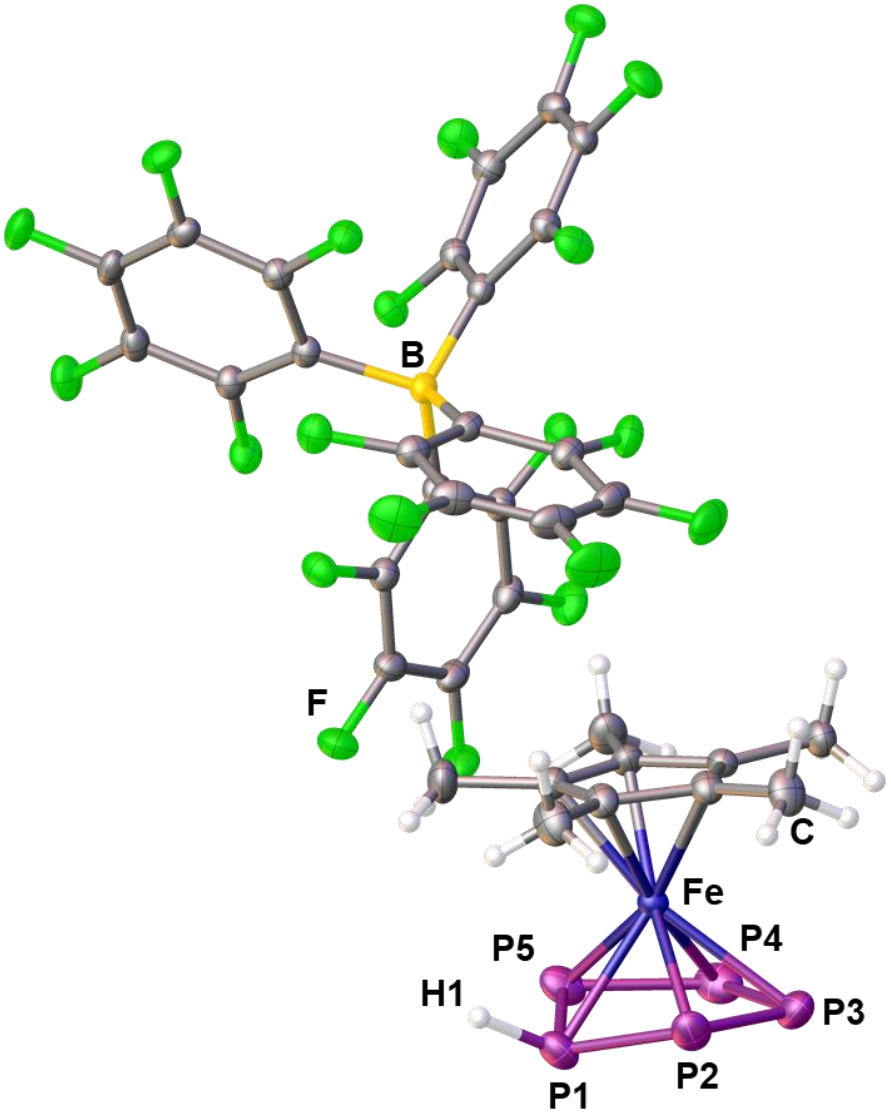

*Figure S 2: Solid state structure of **3**; Depicted is the asymmetric unit and ADPs are drawn at 50% probability; Selected bond lengths and angles: d(P1-P2) = 2.1241(6) Å, d(P2-P3) = 2.1179(7) Å, d(P3-P4) = 2.1295(8) Å, d(P4-P5) = 2.1155(7) Å, d(P1-P5) = 2.1242(7) Å, d(P1-Fe) = 2.3729(5) Å, d(P2-Fe) = 2.3076(5) Å, d(P3-Fe) = 2.3903(5) Å, d(P4-Fe) = 2.3926(5) Å, d(P5-Fe) = 2.3067(5) Å, d(P1-H1) = 1.29(3) Å, ∢(P1-P2-P3) = 99.84(3)°, ∢(P2-P3-P4) = 110.11(3)°, ∢(P3-P4-P5) = 109.73(3)°, ∢(P4-P5-P1) = 100.17(3)°, ∢(P5-P1-P2) = 114.44(3)°, ∢(H1-P1-P2) = 108.8(17)°, ∢(H1-P1-P5) = 112.1(14)°, ∢(H1-P1-Fe) = 102.2(14)°, δ(P2-P5-P1-H1) = -124.5(18)°, δ(P4-P2-P5-P1) = -154.77(4)°, δ(P3-P5-P2-P1) = 154.62(4)°.*

*[Cp*Fe(η^5-P$_5$Me)][FB(C$_6$F$_5$)$_3$] (**4a**)*

[Cp*Fe(η^5-P$_5$Me)][FB(C$_6$F$_5$)$_3$] (**4a**) crystallises as a {[H][FB(C$_6$F$_5$)$_3$]} solvate from *o*-DFB solution layered with *n*-hexane (1:6) after 4 days at room temperature. The obtained dark red to brown block shaped crystals adopt the space group *Cc* with eight formula units and four equivalents of [H][FB(C$_6$F$_5$)$_3$] in the asymmetric unit (Figure S3). Together with the acid, two equivalents of the anion [FB(C$_6$F$_5$)$_3$]$^-$ form a dianionic agglomerate, in which the exact position of the proton could not be determined. Furthermore, several of the cations [Cp*Fe(η^5-P$_5$Me)]$^+$ are disordered. The disorder for these cations could however only be resolved for the Fe atoms and the P$_5$Me ligand (distance and ADP restraints were applied), but the disorder within the Cp* ligands of these cations could not be resolved. Thus, one of the cations, which was not disordered is discussed regarding its structure.

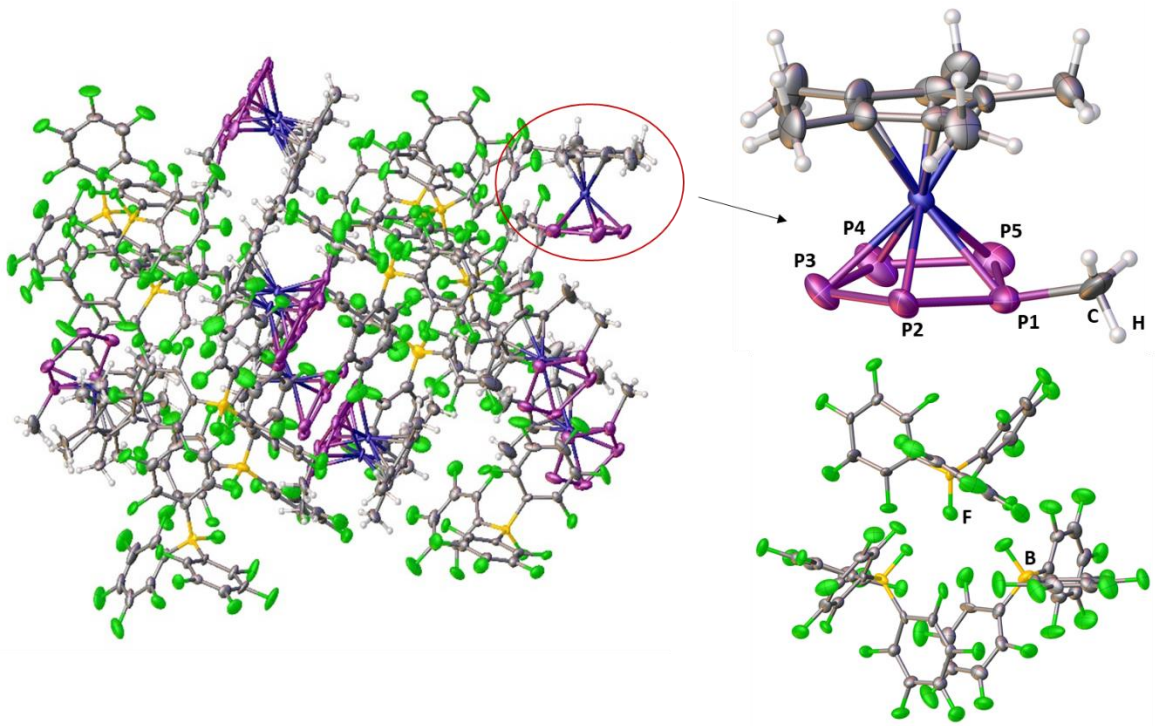

*Figure S 3: Asymmetric unit of **4a**·[H][FB(C$_6$F$_5$)$_3$]$_{0.5}$ with the cation discussed structurally marked in red (left), the respective cation (top right) and one of the dianionic aggregates {[H][FB(C$_6$F$_5$)$_3$]$_3$}$^{2-}$ (bottom right); ADPs are drawn at the 50 % probability level; Selected bond lengths and angles: d(P1-P2) = 2.108(4) Å, d(P2-P3) = 2.101(4) Å, d(P3-P4) = 2.123(5) Å, d(P4-P5) = 2.084(5) Å, d(P1-P5) = 2.106(4) Å, d(P1-Fe) = 2.306(3) Å, d(P2-Fe) = 2.351(3) Å, d(P3-Fe) = 2.382(3) Å, d(P4-Fe) = 2.364(3) Å, d(P5-Fe) = 2.354 (3) Å, d(P1-C) = 1.799(11) Å, ∢(P1-P2-P3) = 100.31(16)°, ∢(P2-P3-P4) = 110.09(19)°, ∢(P3-P4-P5) = 110.70(20)°, ∢(P4-P5-P1) = 100.58(18)°, ∢(P5-P1-P2) = 116.37(18)°, ∢(C-P1-P2) = 121.3(4)°, ∢(C-P1-P5) = 116.5(4)°, ∢(C-P1-Fe) = 122.0(4)°, δ(P2-P5-P1-C) = –153.6(4)°, δ(P4-P2-P5-P1) = –165.4(2)°, δ(P3-P5-P2-P1) = 164.7(2)°.*

*[Cp*Fe(η^5-P$_5$Me)][B(C$_6$F$_5$)$_4$] (**4b**)*

[Cp*Fe(η^5-P$_5$Me)][B(C$_6$F$_5$)$_4$] (**4b**) crystallises as dark red blocks from concentrated CH_2Cl_2 solutions, layered with *n*-pentane (1:10) and stored for one day at room temperature. The formed crystals adopt the triclinic space group $P\bar{1}$ with one cation and one anion in the asymmetric unit (Figure S4). Disorder within the cyclo-P$_5$Me ligand was refined using distance and ADP constraints and restraints.

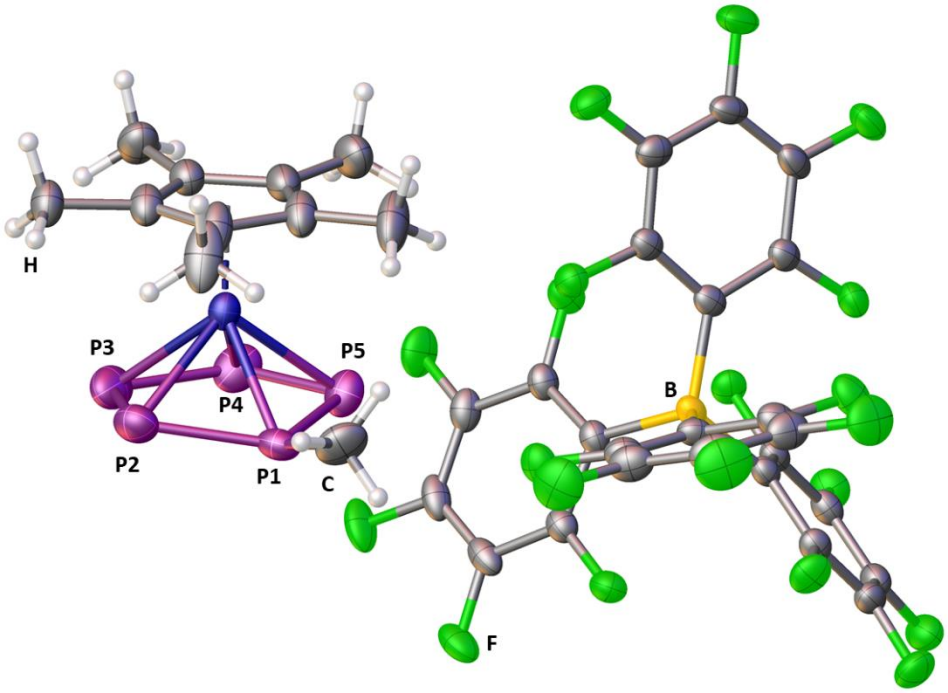

*Figure S 4: Asymmetric unit of **4b**, with only one part oft he disordered cation displayed; ADPs are drawn at the 50 % probability level; Selected bond lengths and angles: d(P1-P2) = 2.131(9) Å, d(P2-P3) = 2.260(4) Å, d(P3-P4) = 2.110(6) Å, d(P4-P5) = 2.050(5) Å, d(P1-P5) = 2.170(3) Å, d(P1-Fe) = 2.282(7) Å, d(P2-Fe) = 2.291(2) Å, d(P3-Fe) = 2.390(4) Å, d(P4-Fe) = 2.380(4) Å, d(P5-Fe) = 2.350(3) Å, d(P1-C) = 1.750(1) Å, ∢(P1-P2-P3) = 99.80(1)°, ∢(P2-P3-P4) = 108.30(2)°, ∢(P3-P4-P5) = 113.0(2)°, ∢(P4-P5-P1) = 102.9(2)°, ∢(P5-P1-P2) = 114.4(8)°, ∢(C-P1-P2) = 120.3(4)°, ∢(C-P1-P5) = 117.3(9)°, ∢(C-P1-Fe) = 119.2(4)°, δ(P2-P5-P1-C) = –148.9(9)°, δ(P4-P2-P5-P1) = –166.0(2)°, δ(P3-P5-P2-P1) = 164.8(2)°.*

5.5.3. NMR Spectroscopic Investigations

*[Cp*Fe(η^5-P$_5$SiEt$_3$)][B(C$_6$F$_5$)$_4$] (**2**)*

[Cp*Fe(η^5-P$_5$SiEt$_3$)][B(C$_6$F$_5$)$_4$] (**2**) is highly unstable towards hydrolysis and reacts even with traces of water left on the surface of meticulously dried glassware (heated to 600 °C at 10^{-3} mbar for 3 h and then stored in a glove box for 7 days). Thus, exposing isolated **2** to fresh glassware/solvents usually leads to partial decomposition. As **2** shows highly dynamic behaviour in solution at room temperature, we carried out a VT NMR study (Figure S5) of this compound by preparing it in the NMR tube itself. However, the stoichiometry of the reaction could not be accurately controlled under these circumstances and there was residual **1** left in the reaction mixture, which can be clearly seen in the ^{31}P{^{1}H} NMR spectra (Figure S5).

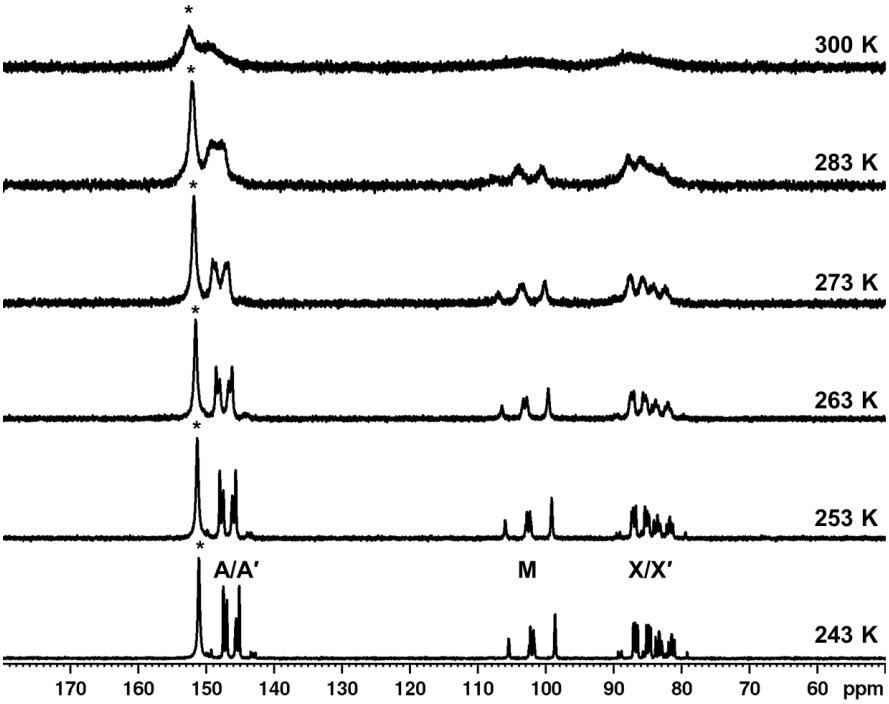

*Figure S 5: ^{31}P{^{1}H} VT NMR spectra of **2** in o-DFB (with a toluene-d^8 capillary and PPh$_3$ as external standard). The spin system is labelled according to the Scheme in Figure S. * = **1**.*

When a crystalline sample of **2** is dissolved in *o*-DFB in a NMR tube and then subjected to NMR spectroscopic analysis, the respective ^{31}P{^{1}H} NMR spectrum (at –30 °C) reveals small signs of degradation (Figure S6), but obviously there is no **1** left in the sample. While these degradation products may imply the impurity of **2**, elemental analysis (*vide supra*) confirmed the purity of **2**. Simulation of this spectrum allowed the determination of the coupling constants (Table S2) within the *cyclo*-P$_5$SiEt$_3$ ligand in **2**. In accordance with the observed signal in the ^{29}Si{^{1}H} NMR spectrum (Figure S7, $^1J_{PM\text{-}Si}$ ≈ 60 Hz), simulation of the ^{29}Si satellites in the ^{31}P{^{1}H} NMR spectrum yields a $^1J_{PM\text{-}Si}$ coupling constant of 62.1 Hz.

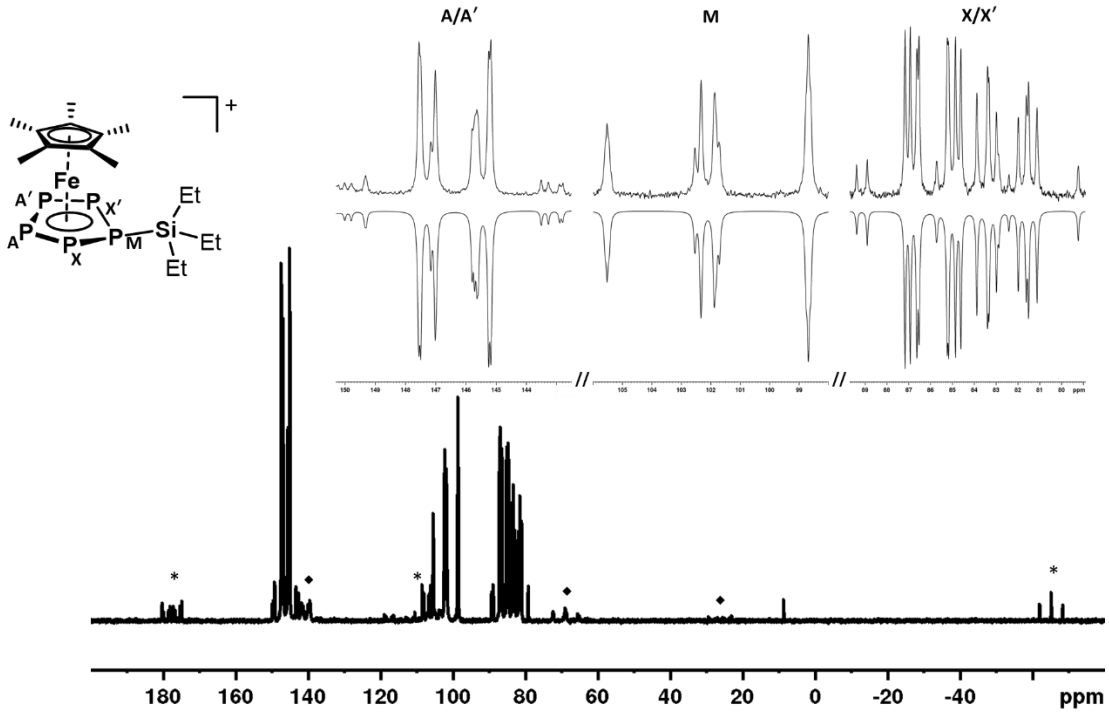

*Figure S 6: Experimental (top) and simulated (bottom) $^{31}P\{^{1}H\}$ NMR spectrum of isolated **2** in o-DFB at 243 K and assignment of the spin system (left); * = **3**, which is formed due to the slightest traces of H_2O in the NMR tube. ◆ = unidentified side product.*

*Table S 2: Spectral parameters of the $^{31}P\{^{1}H\}$ NMR spectrum of **2** in o-DFB (toluene-d^8 capillary) recorded at 243 K extracted from spectral simulation.*

J/ Hz		*δ/ ppm*	
$^{1}J_{PA/A'-PX/X'}$	435.2/421.92	$P^{A/A'}$	146.28
$^{1}J_{PM-PX/X'}$	558.5/557.9	P^{M}	101.69
$^{1}J_{PA-PA'}$	415.1	$P^{X/X'}$	84.31
$^{2}J_{PA/A'-PX'/X}$	–54.9/–46.3		
$^{2}J_{PA/A'-PM}$	14.1/10.9		
$^{2}J_{PX-X'}$	22.2		
$^{1}J_{PM-Si}$	62.1		
R-factor (%)	16.6		

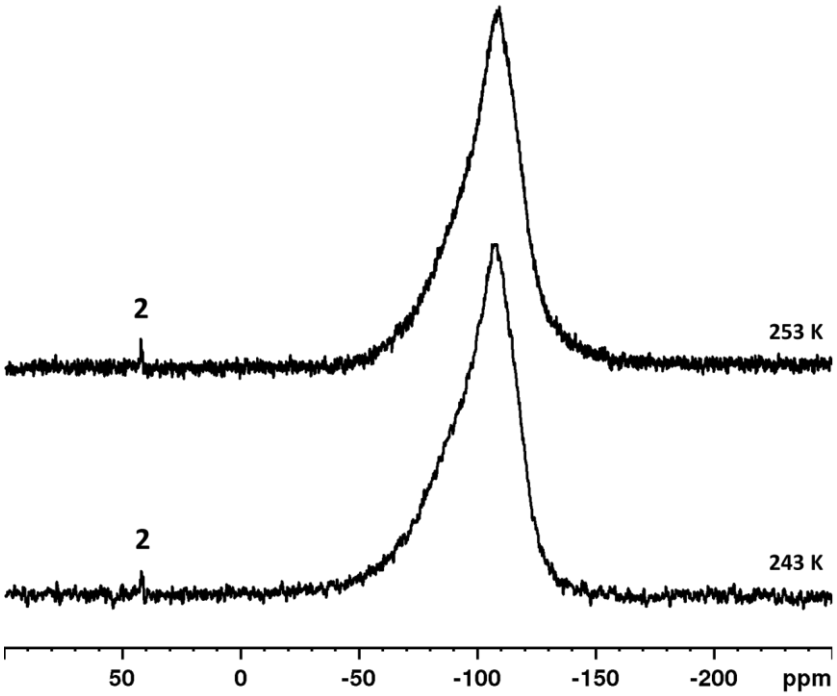

*Figure S 7: $^{29}Si\{^{1}H\}$ NMR spectra of **2** in o-DFB recorded at different temperatures; The spectrum at 243 K was collected with 2000, the one at 253 K with 4000 scans.*

*[Cp*Fe(η^5-P$_5$H)][B(C$_6$F$_5$)$_4$] (**3**)*

Similarly to **2**, [Cp*Fe(η^5-P$_5$H)][B(C$_6$F$_5$)$_4$] (**3**) is highly moisture sensitive and easily reacts with traces of moisture left on the surface of glass ware. Thus, small impurities of **1** and an unidentified product, already formed during hydrolysis of **2**, can be detected in the NMR spectra of isolated **3**. **2** also expresses significant dynamic behaviour in CD_2Cl_2 solution at room temperature as seen from the respective ^{31}P NMR spectra. VT ^{31}P{^{1}H} NMR spectroscopic investigations (Figure S8) however show that this dynamic behaviour is not expressed at lower temperatures and at –80 °C a well resolved spectrum is observed (Figure S9). Spectral simulation of the latter revealed the coupling constants (Table S2) within the *cyclo*-P$_5$H ligand and the additional coupling (Table S3) to the proton of this ligand can be observed in the respective ^{31}P NMR spectrum (Figure S10). Accordingly, the ^{1}H NMR spectrum of **3** in CD_2Cl_2 recorded at room temperature only shows a broad resonance for the *cyclo*-P$_5$H ligand but at –80 °C a well resolved doublet can be observed (Figure S11). As both, the ^{11}B and ^{19}F NMR spectra (at r. t.) of **3** do not show similar signs of dynamic effects, we do not attribute this behaviour to exchange of the proton between **1** and the [B(C$_6$F$_5$)$_4$]$^-$ anion. Furthermore, we observed the formation of small quantities of **3** in other reactions involving the electrophilic functionalisation of **1** as well, and the respective ^{31}P NMR spectra are already well resolved at

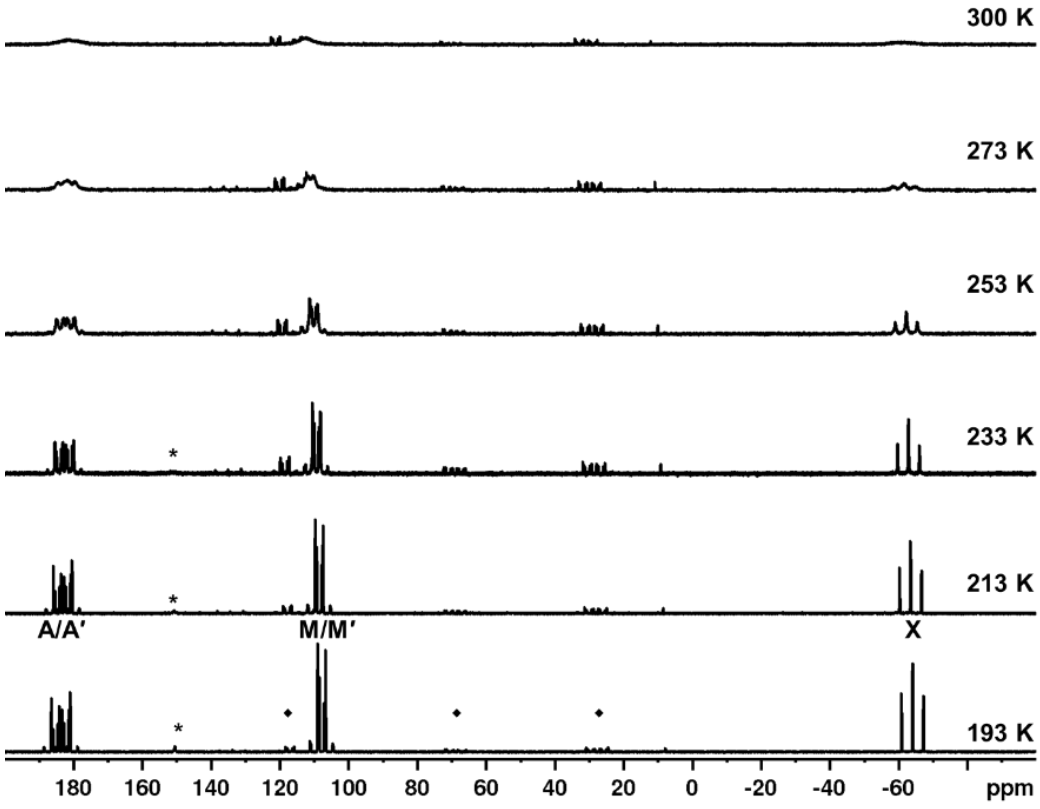

*Figure S 8: ^{31}P{^{1}H} VT NMR spectra of **3** in CD_2Cl_2. The spin system is labelled according to the Scheme in Figure S, * = residual **1**, which is probably formed due to slight traces of moisture on the NMR tube and ◆ = trace impurities of an unidentified side product.*

room temperature. It has to be noted that in these cases no traces of free 1 are detected in the ^{1}H or ^{31}P NMR spectra. Thus, we attribute the highly dynamic behaviour of isolated **3** to the small quantities of **1**, which are formed upon exposure to fresh glass ware (when dissolved in the NMR tube). This dynamic process can then be understood as a constant "bond-braking/bond-forming" mechanism and based upon the above we exclude a mechanism, in which the proton would migrate around a single molecule of **1**.

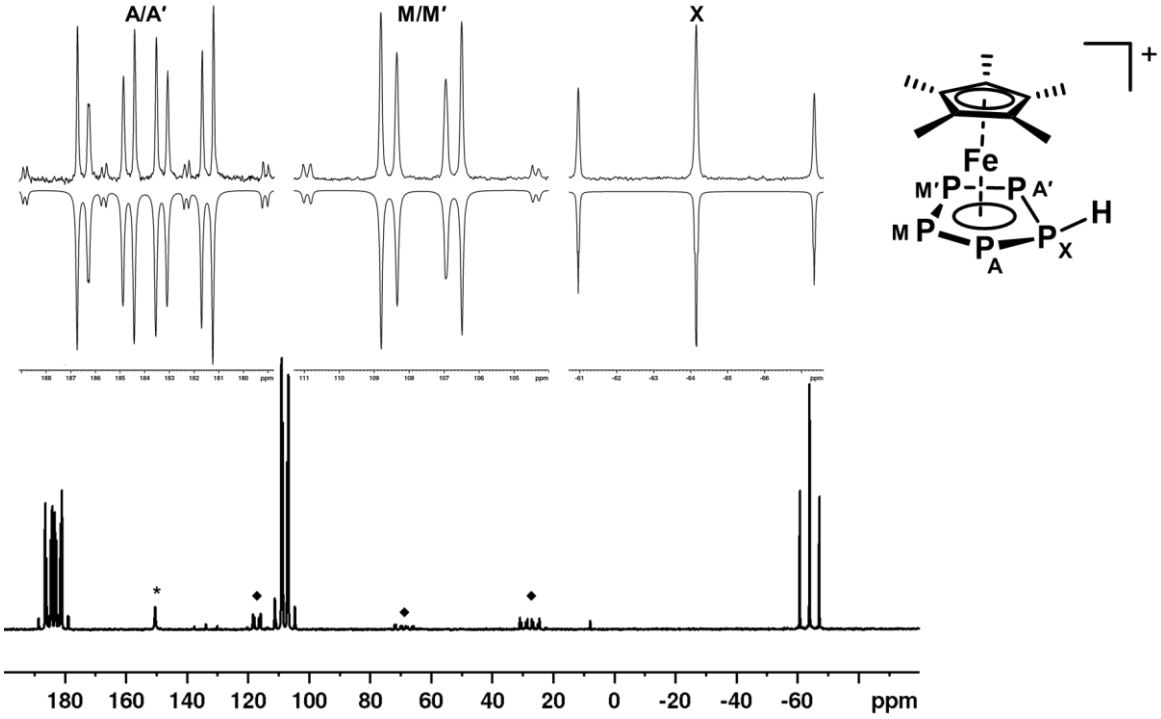

*Figure S 9: Experimental (top) and simulated (bottom) $^{31}P\{^{1}H\}$ NMR spectrum of **3** in CD_2Cl_2 at 193 K and assignment of the spin system (right); * = residual **1** and ◆ = trace impurities of an unidentified side product.*

*Table S 2: Spectral parameters of the $^{31}P\{^{1}H\}$ NMR spectrum of **3** in CD_2Cl_2 recorded at 193 K extracted from spectral simulation.*

J/ Hz		*δ/ ppm*	
$^{1}J_{PA/A'-PM/M'}$	*436.76/427.80*	$P^{A/A'}$	*183.95*
$^{1}J_{PA/A'-PX}$	*517.37/516.60*	$P^{M/M'}$	*107.75*
$^{1}J_{PM-PM'}$	*416.61*	P^{X}	*–64.13*
$^{2}J_{PA/A'-PM'/M}$	*–61.77/–54.41*		
$^{2}J_{PM/M'-PX}$	*5.67/3.19*		
$^{2}J_{PA-A'}$	*18.16*		
R-factor (%)	*9.9*		

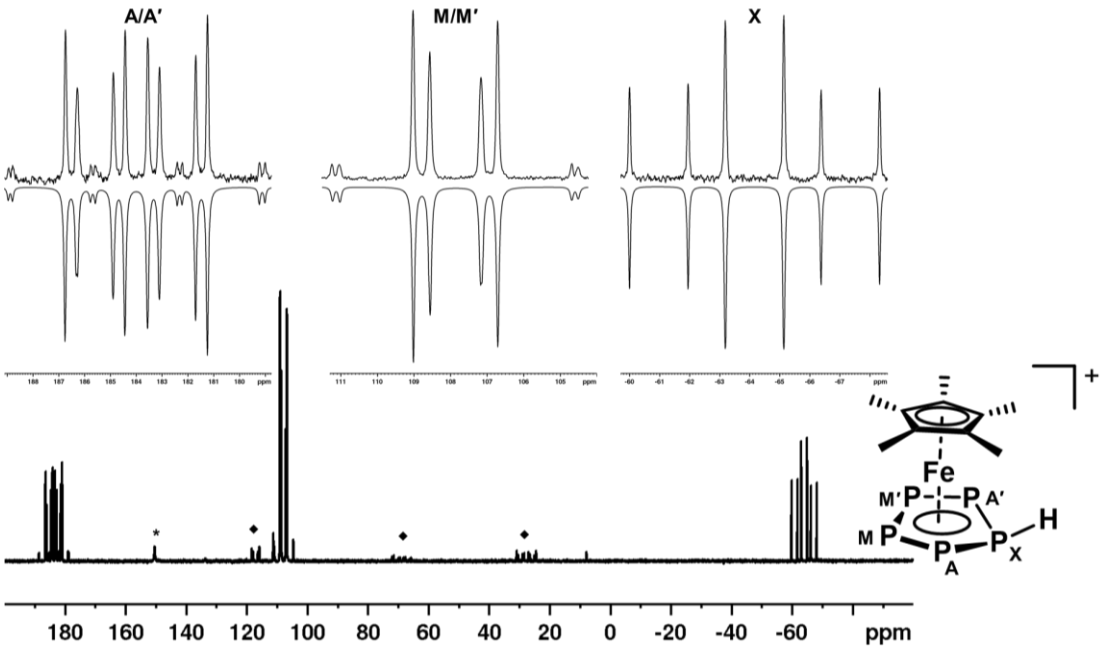

*Figure S 10: Experimental (top) and simulated (bottom) ^{31}P NMR spectrum of **3** in CD_2Cl_2 at 193 K and assignment of the spin system (right); * = residual **1** and ◆ = trace impurities of an unidentified side product.*

*Table S 3: Spectral parameters of the ^{31}P NMR spectrum of **3** in CD_2Cl_2 recorded at 193 K extracted from spectral simulation.*

J/ Hz		*δ/ ppm*	
$^1J_{PA/A'-PM/M'}$	*436.75/428.24*	$P^{A/A'}$	*183.96*
$^1J_{PA/A'-PX}$	*516.99/516.94*	$P^{M/M'}$	*107.67*
$^1J_{PM-PM'}$	*416.91*	P^{X}	*–64.14*
$^2J_{PA/A'-PM'/M}$	*–63.45/–52.76*		
$^2J_{PM/M'-PX}$	*5.32/4.20*		
$^2J_{PA-A'}$	*18.53*		
$^1J_{PX-H}$	*315.82*		
R-factor (%)	*1.2*		

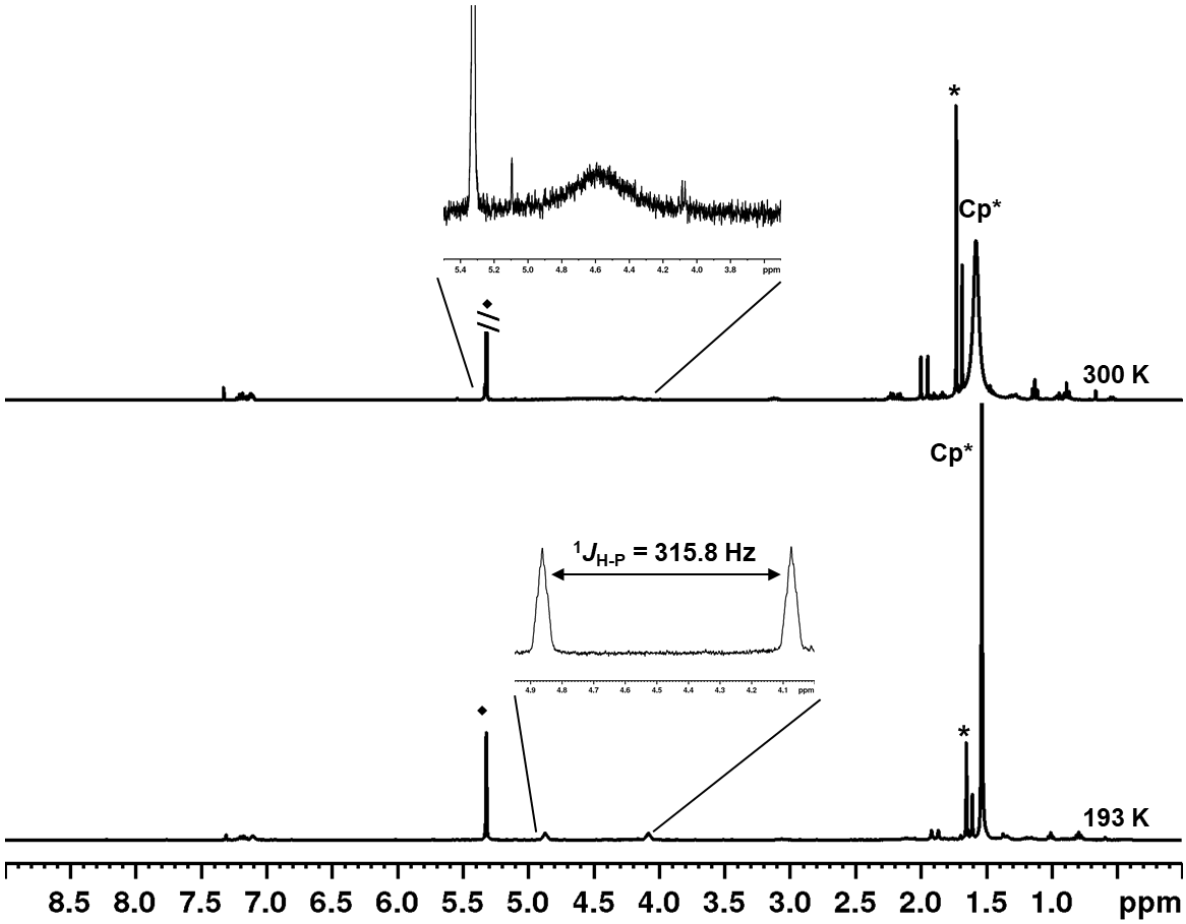

*Figure S 11: ^{1}H VT NMR spectrum of **3** in CD_2Cl_2. * = residual **1**, Cp* is the signal arising from the Cp* ligand in **3** and ◆ = residual CH_2Cl_2.*

*[Cp*Fe(η^5-P$_5$Me)][X] (**4a/b**)*

In contrast to **2** and **3**, [Cp*Fe(η^5-P$_5$Me)][X] (**4a** [X]$^-$ = [FB(C$_6$F$_5$)$_3$]$^-$/**4b** [X]$^-$ = [B(C$_6$F$_5$)$_4$]$^-$) do not show signs of dynamic behaviour in CD_2Cl_2 at room temperature. Thus, the corresponding NMR spectra can easily be obtained (depicted are only the ones for **4a**, as those obtained for **4b** are similar) and show the expected signals for the cation **4**$^+$ in the ^{1}H (Figure S14), ^{13}C{^{1}H} (Figure S 11), ^{31}P (Figure S13) and ^{31}P{^{1}H} (Figure S12) NMR spectra. The coupling constants within the *cyclo*-P$_5$Me ligand could be obtained by simulation (Table S4 and S5) of the ^{31}P and ^{31}P{^{1}H} NMR spectra and extracted from the ^{1}H and ^{13}C{^{1}H} (Figure S15) NMR spectra. The ^{19}F and ^{19}F{^{1}H} and ^{11}B NMR spectra of **4a** reveal two sets of signals for species containing the B(C$_6$F$_5$)$_3$ moiety, of which one can clearly be attributed to the [FB(C$_6$F$_5$)$_3$]$^-$ anion. In accordance with the solid state structure of **4a** and the obtained ESI(-) mass spectra, we attribute the second set of signals to B(C$_6$F$_5$)$_3$·HF. The respective ^{19}F and ^{11}B NMR spectra of **4b** reveal the sole presence of the [B(C$_6$F$_5$)$_4$]$^-$ anion, which is in agreement with the solid state structure of this compound and the respective mass spectra and elemental analysis.

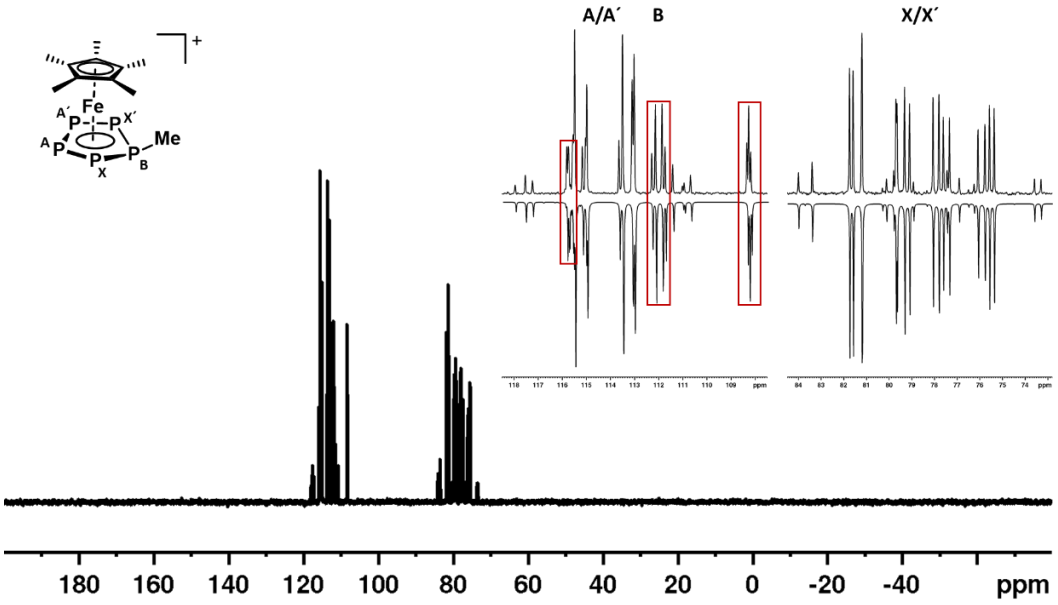

*Figure S 12: Experimental (top) and simulated (bottom) ^{31}P{^{1}H} NMR spectrum of **4a** in CD_2Cl_2 at r. t. and assignment of the spin system (left).*

*Table S 4: Spectral parameters of the ^{31}P{^{1}H} NMR spectrum of **4a** in CD_2Cl_2 recorded at r. t. extracted from spectral simulation.*

J/ Hz		*δ/ ppm*	
$^1J_{PA/A'-PX/X'}$	*462.34/448.15*	$P^{A/A'}$	*114.24*
$^1J_{PB-PX/X'}$	*607.74/605.96*	P^{B}	*111.79*
$^1J_{PA-PA'}$	*405.82*	$P^{X/X'}$	*78.74*
$^2J_{PA/A'-PX'/X}$	*–61.40/–48.99*		
$^2J_{PA/A'-PB}$	*11.82/9.42*		
$^2J_{PX-X'}$	*42.11*		
R-factor (%)	*2.9*		

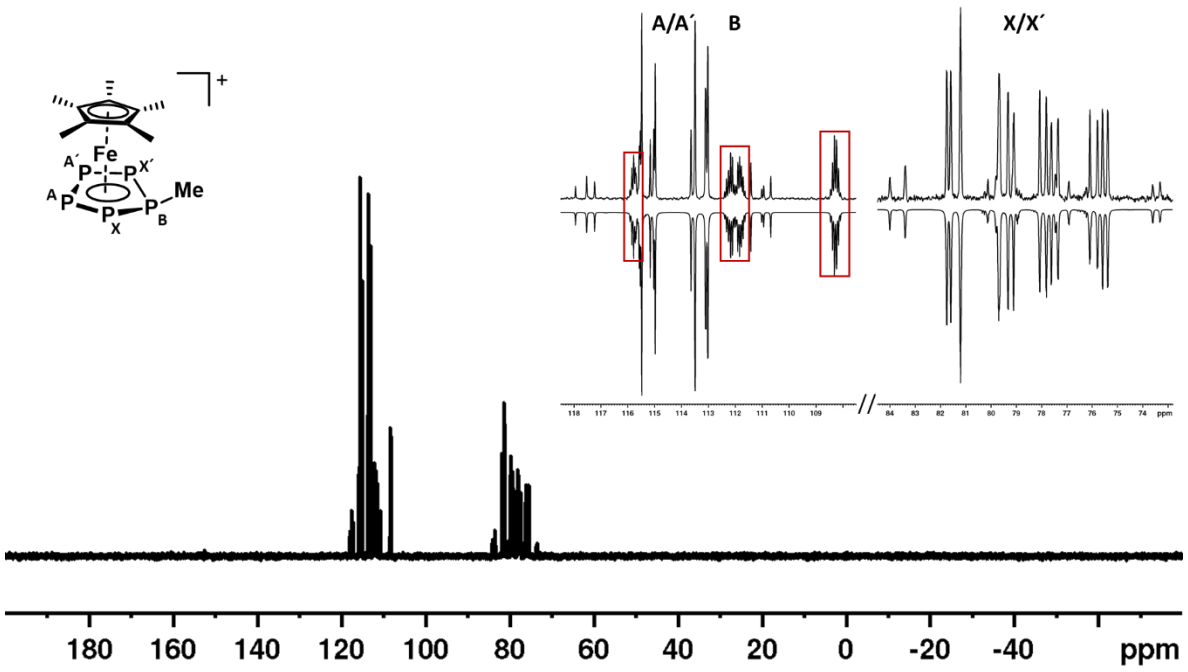

*Figure S 13: Experimental (top) and simulated (bottom) ^{31}P NMR spectrum of **4a** in CD_2Cl_2 at r. t. and assignment of the spin system (left).*

*Table S 5: Spectral parameters of the ^{31}P NMR spectrum of **4a** in CD_2Cl_2 recorded at r.t. extracted from spectral simulation.*

J/ Hz		*δ/ ppm*	
$^1J_{PA/A'-PX/X'}$	461.98/448.49	$P^{A/A'}$	114.23
$^1J_{PB-PX/X'}$	607.66/606.05	P^{B}	111.79
$^1J_{PA-PA'}$	405.90	$P^{X/X'}$	78.73
$^2J_{PA/A'-PX'/X}$	–60.90/–49.45		
$^2J_{PA/A'-PB}$	10.72/10.47		
$^2J_{PX-X'}$	42.11		
$^2J_{PB-H(Me)}$	11.33		
$^3J_{PX/X'-H(Me)}$	3.59/2.87		
R-factor (%)	1.4		

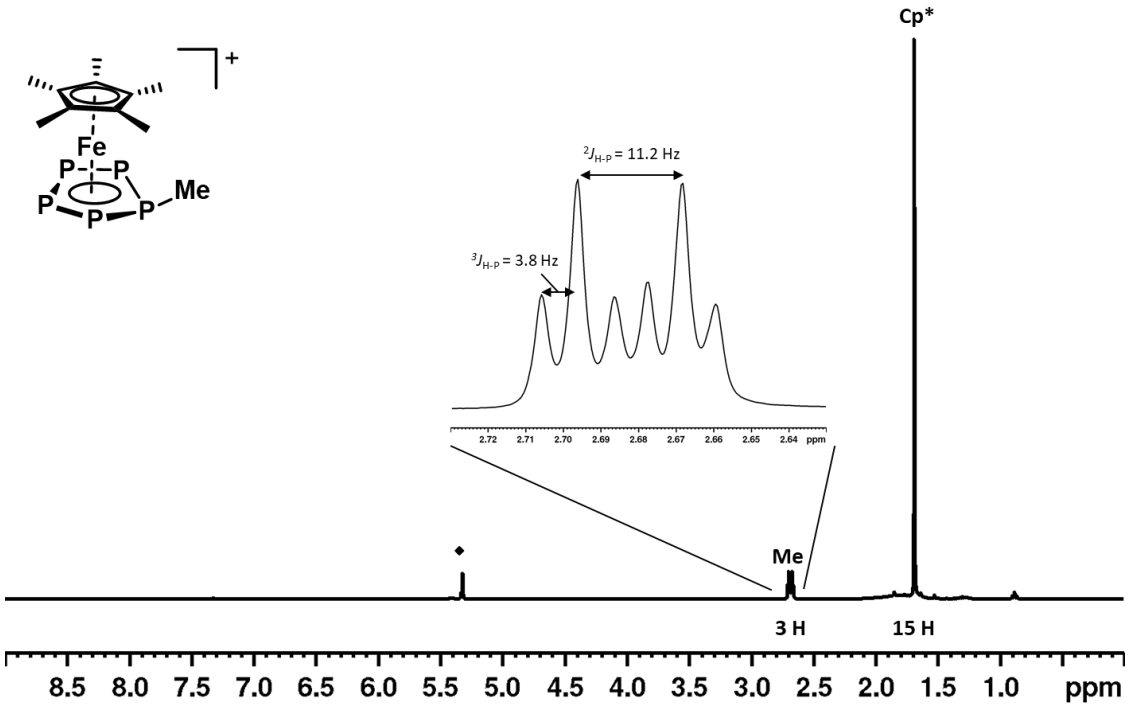

*Figure S 14: ^{1}H NMR spectrum of **4a** in CD_2Cl_2 at r.t.; "Cp*" and "Me" mark the signals for the respective protons in **4** and ◆ is the signal from residual CH_2Cl_2.*

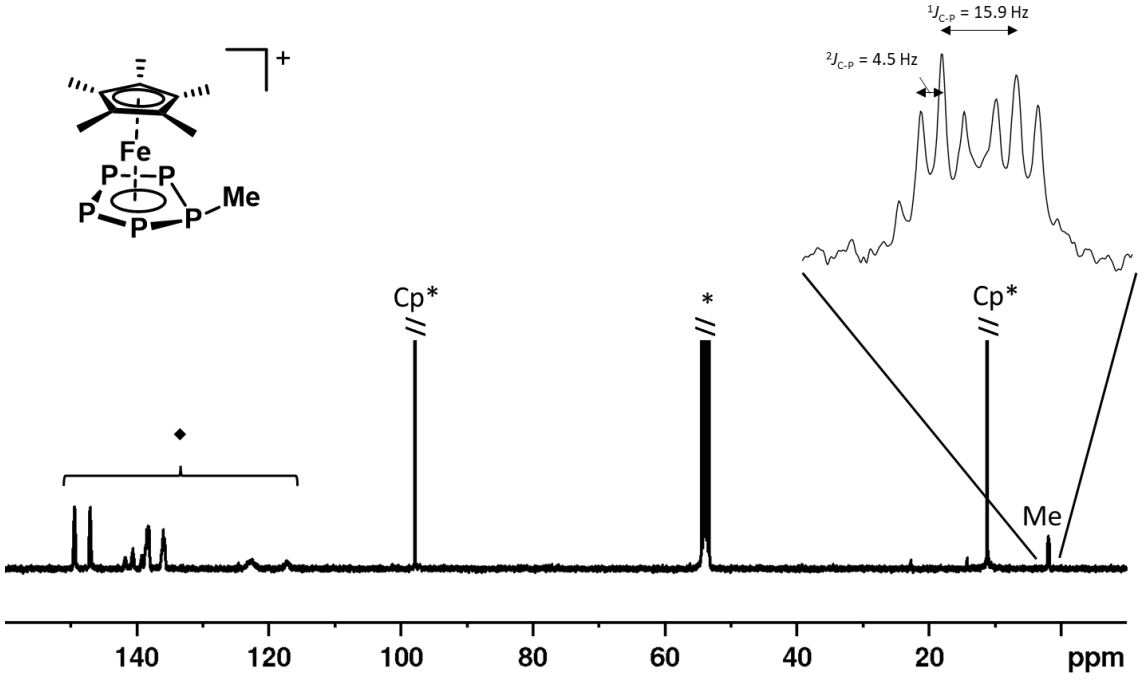

*Figure S 15: $^{13}C\{^1H\}$ NMR spectrum of **4a** in CD_2Cl_2 at r.t.; "Cp*" and "Me" mark the signals for the respective protons in **4**, ◆ marks the signals for the $[FB(C_6F_5)_3]^-$ anion and $H[FB(C_6F_5)_3]$ and * is the solvent residual signal.*

Additional NMR Spectroscopic Investigations

MeOH Quenching

In search of milder quenching reagents for **2** to form **3**, we thought MeOH would be a suitable substrate. Adding MeOH (0.1 mmol, 4 μL, 1 eq.) to a solution of **2** (0.1 mmol, 114 mg, 1 eq.) in *o*-DFB (4 mL) leads to the desired colour change to red within seconds. The solvent was then removed under reduced pressure and the red residue dissolved in 1 mL of CD_2Cl_2. Subjecting this sample to low temperature (–80 °C) NMR spectroscopic studies (Figure S16) revealed the presence of both, $\mathbf{3}^+$ and $\mathbf{4}^+$ in solution. As this product mixture could however not be separated, MeOH seems unsuitable for preparing salts of either $\mathbf{3}^+$ or $\mathbf{4}^+$, respectively.

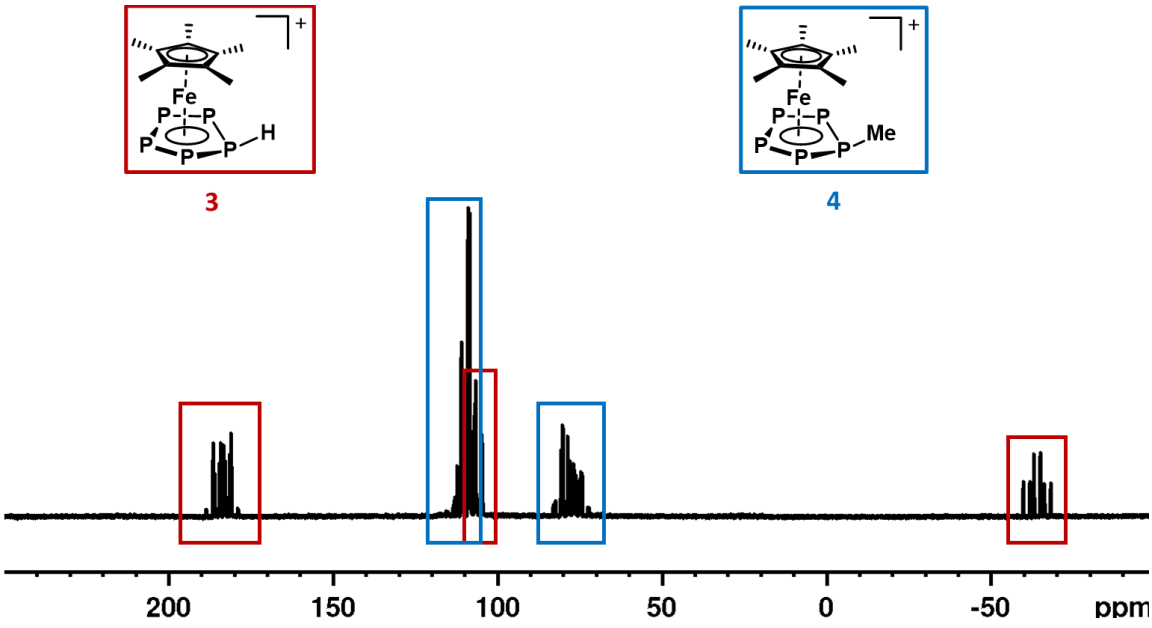

*Figure S 16: ^{31}P NMR spectrum of the reaction solution of **2** and MeOH in CD_2Cl_2 recorded at 193 K, which indicates the formation of two species, namely **3** and **4** (assignment according to colour scheme).*

5.5.4. Computational Details

General Considerations

DFT calculations were performed using the Gaussian09 software package.[45] The geometry optimizations were performed at the B3LYP[32]/def2-TZVP[33] level of theory with PCM solvent correction for CH_2Cl_2.[46] The gas phase energy values for the calculation of proton affinities were obtained on the B3LYP/def2-TZVPD[33,47] level of theory without solvent correction. Orbital interaction schemes were created using single point calculations at the B3LYP/def2-TZVP level of theory (PCM solvent correction for CH_2Cl_2)[46] and the AOMix program.[48] Magnetic shielding tensors were calculated at the PBE0[37]/aug-pcSseg-2[38] level of theory (PCM solvent correction for CH_2Cl_2).[46] NICS(0/1/-1)$_{zz}$ values[49] and ring critical points were derived using Multiwfn.[50] The basis sets def2-TZVPD and aug-pcSseg-2 were generated with the help of the open access "basis set exchange" web page.[51]

*Proton and Methyl Cation Affinities of **1***

As we were experimentally unsuccessful in direct protonation of **1** with acids, such as $H[BF_4]$ in ether or $[H(OEt_2)_2][TEF]$,[26] we computed the gas phase proton affinities[52] of **1** and Et_2O at the B3LYP/def2-TZVPD (pre optimized structures at B3LYP/def2-TZVP) level of theory. For the latter, we assumed formation of the $[H(OEt_2)_2]^+$ cation, as it is found in the crystal structure of $[H(OEt_2)_2][TEF]$. Proton affinities (PA) were calculated using equation (*1)*.[52,53] For **1** we calculated a proton affinity of 875.42 kJ/mol, which is 11.31 kJ/mol lower than that found for Et_2O (886.73 kJ/mol), thus yielding a theoretical explanation for our experimental finding that **1** cannot be protonated in the presence of Et_2O.

$$PA = \Delta E_{ele} + \Delta E_{vib} + \frac{5}{2}RT \qquad (1)$$

Additionally, we computed the methyl cation affinity[34] of **1** according to Scheme S1 at the B3LYP/def2-TZVP level of theory with implicit solvent correction (PCM model for CH_2Cl_2 implemented in Gaussian09). Thus, we calculated a methyl cation affinity of 355.27 kJ/mol for **1**.

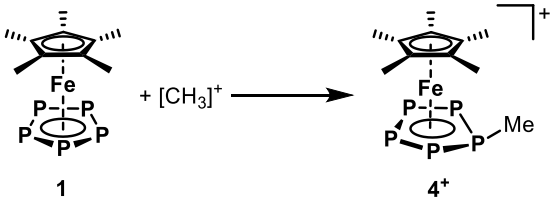

*Scheme S 1: Reaction equation used for calculating the methyl cation affinity[23] of **1**.*

*Reaction Energetics for the Formation of **2**, **3** and **4***

The molecular structures of all involved species for the reactions yielding **2**, **3** and **4** were optimized at the B3LYP/def2-TZVP level of theory with implicit solvent correction (PCM model

for CH_2Cl_2 implemented in Gaussian09). Reaction enthalpies were then extracted by summation across all involved species according to equations *2*, *3* and *4*.

$$[Cp^*Fe(\eta^5\text{-}P_5)] + [(Et_3Si)_2(\mu\text{-}H)]^+ \longrightarrow [Cp^*Fe(\eta^5\text{-}P_5SiEt_3)]^+ + Et_3SiH \quad (2)$$

$$2\,[Cp^*Fe(\eta^5\text{-}P_5SiEt_3)]^+ + H_2O \longrightarrow 2\,[Cp^*Fe(\eta^5\text{-}P_5H)]^+ + (Et_3Si)_2O \quad (3)$$

$$[Cp^*Fe(\eta^5\text{-}P_5)] + [Me_3O]^+ \longrightarrow [Cp^*Fe(\eta^5\text{-}P_5Me)]^+ + Me_2O \quad (4)$$

*NBO Analysis of **2**, **3** and **4***

NBO analysis was performed on the pre-optimized (B3LYP/def2-TZVP, PCM solvent correction for CH_2Cl_2) molecular structures of **2**, **3** and **4** using the NBO6.0[35] software package and its implementation in Gaussian09 (Figure S17). Wiberg bond indices (WBI) and orbital energies for the respective P1-R (R= $SiEt_3$ (**2**), H (**3**) and Me (**4**)) bond have also been obtained from these calculations. While the WBIs suggest proper single bonds for **3** (0.92) and **4** (0.97), the one for the P1-Si bond in **2** (0.69) is significantly lower, which may hint towards the dative character of this bond. This is also represented in the orbital contributions for the discussed bonds:

P1-Si (NBO 71) in **2**: s(P1) = 27%, p(P1) = 47%, s(Si) = 4%, p(Si) = 22%, overall contribution (P1: 75%, Si: 25%)

P1-H (NBO 57) in **3**: s(P1) = 6%, p(P1) = 47%, s(H) = 45%, overall contribution (P1: 54%, H: 46 %)

P1-Me (NBO 60) in **4**: s(P1) = 14%, p(P1) = 30%, s(C) = 14%, p(C) = 42%, overall contribution (P1: 44%, C: 56%)

Additional Mulliken population analysis on the optimized structures of **2**, **3** and **4** revealed the charge distribution for these compounds. Summation of the partial charges on the {$Cp^*Fe(\eta^5\text{-}P_5)$} moiety and the respective substituent R (R = $SiEt_3$ (**2**), H (**3**), Me (**4**)) shows that the charge transfer from the substituent is much less pronounced in **2** than it is in **3** and **4** (Table S6). This goes in hand with a more polar P–Si bond in **2** and more covalent P–H and P–C bonds in **3** and **4**.

*Table S 6: Summed up Mulliken charges of the {$Cp^*Fe(\eta^5\text{-}P_5)$} moiety and the respective substituent (R) for the compounds **2**, **3** and **4**.*

Compound	{$Cp^*Fe(\eta^5\text{-}P_5)$}	R
2 (R = $SiEt_3$)	0.627	0.373
3 (R = H)	0.889	0.111
4 (R = Me)	0.908	0.092

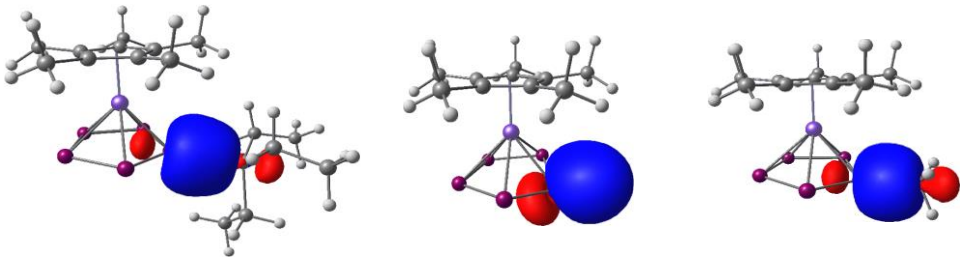

NBO 71
E = -0.46 eV
WBI = 0.69

NBO 57
E = -0.49 eV
WBI = 0.92

NBO 60
E = -0.57 eV
WBI = 0.97

*Figure S 17: P1-R bonding NBOs of **2** (R = $SiEt_3$, left), **3** (R = H, middle) and **4** (R = Me, right), the respective orbital energies and WBIs.*

*Orbital Interaction in **3***

The orbital interaction diagram (Figure S18) for **3**$^+$ has been created using single point calculations performed at the B3LYP/def2-TZVP level of theory (PCM solvent correction for CH_2Cl_2) using Gaussian09 and the AOMix program. The geometries of **3**$^+$ and free *cyclo*-P_5H were optimized at the same level of theory and the fragments $\{Cp^*Fe\}^+$ and bent *cyclo*-P_5H were extracted from the optimized structure of **3**$^+$. As indicated by the schematic representations of the MOs in Figure S 18, the P1 atom (the one the H atom is bonded to) in the bent geometry of *cyclo*-P_5H has strong contributions to the HOMO-1 (37b, the atomic contribution of P1 is p(P1) = 34 %), which itself shows strong overlap MOs of the $\{Cp^*Fe\}^+$ fragment to form the HOMO-2 (86, p(P1) < 10 %) and HOMO-7 (81, p(P1) = 14 %) of **3**$^+$. This strong contribution manifests the *cyclo*-P_5H ligands hapticity in **3**$^+$ as η^5. Orbital energies of selected MOs of the $\{Cp^*Fe\}^+$ fragment, **3**$^+$, bent *cyclo*-P_5H and planar *cyclo*-P_5H are provided in Table S 8.

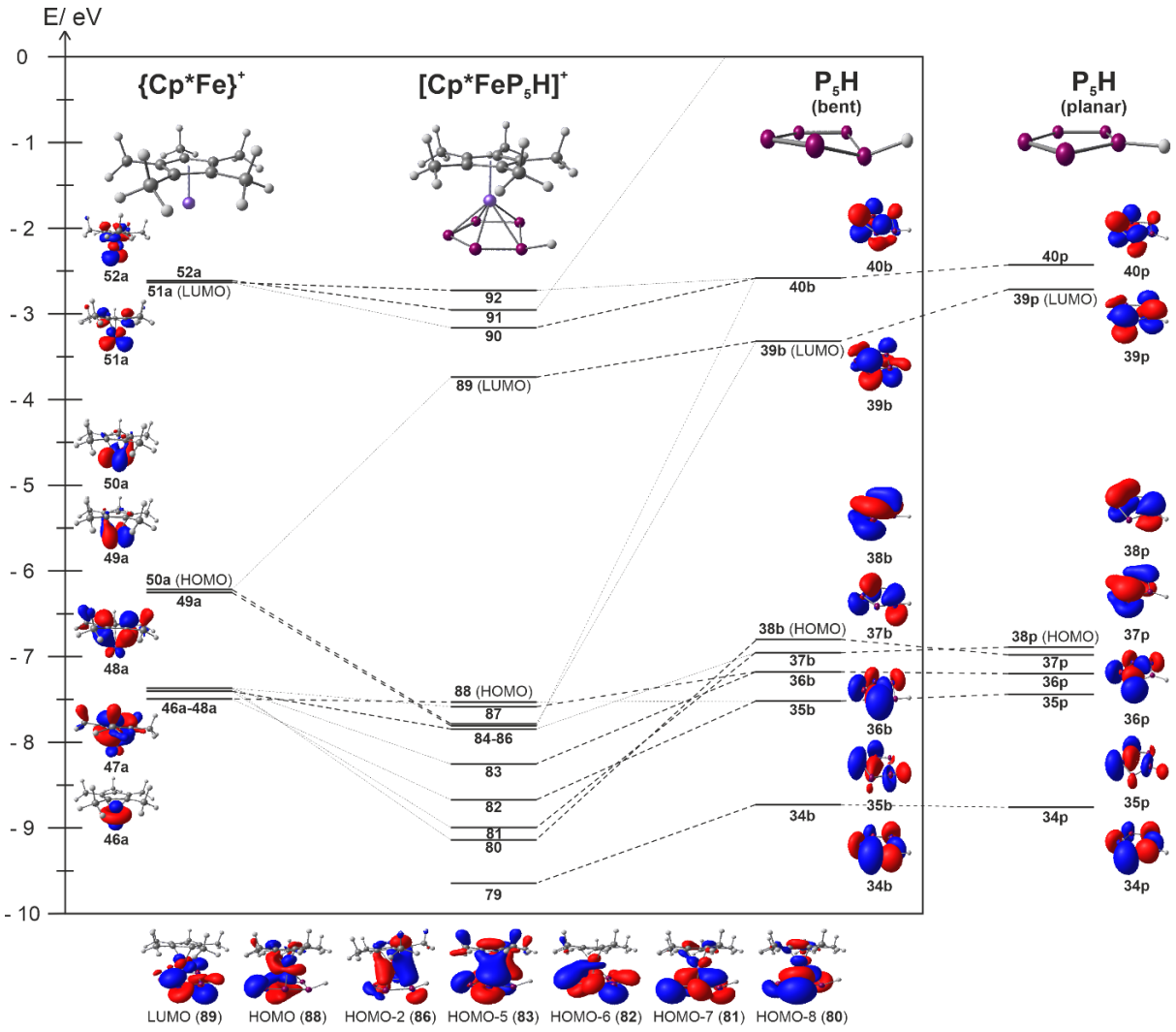

*Figure S 18: Orbital interaction diagram for **3**$^+$ as parted into the $\{Cp^*Fe\}^+$ fragment and the cyclo-P_5H ligand (left box) and changes in the molecular orbitals of the cyclo-P_5H ligand upon bending into the geometry found in **3**$^+$.*

*Table S 7: Orbital energies in eV for selected frontier orbitals of planar (free) cyclo-P_5H, bent (coordinated) cyclo-P_5H, the $\{Cp^*Fe\}^+$ fragment and of **3**$^+$.*

Orbital	**free *cyclo*-P_5H**		**bent *cyclo*-P_5H**		**$\{Cp^*Fe\}^+$**		**3$^+$**	
	index	E/ eV	index	E/ eV	index	E/ eV	index	E/ eV
HOMO-9	29	-14.2835015	29	-14.222548	41	-10.9419161	79	-9.60915683
HOMO-8	30	-13.3404365	30	-13.2228833	42	-10.8791939	80	-9.10465772
HOMO-7	31	-11.3309301	31	-11.1431171	43	-9.97487786	81	-8.95989315
HOMO-6	32	-9.15959751	32	-9.12550165	44	-9.96755799	82	-8.63771034
HOMO-5	33	-9.11529738	33	-8.96253265	45	-9.96391167	83	-8.21919922
HOMO-4	34	-8.72407928	34	-8.69518078	46	-7.45874982	84	-7.80993997
HOMO-3	35	-7.40457195	35	-7.48397477	47	-7.36930599	85	-7.75932679
HOMO-2	36	-7.1652478	36	-7.14366917	48	-7.33393119	86	-7.74953069
HOMO-1	37	-6.94562471	37	-6.91963783	49	-6.18484877	87	-7.55061546
HOMO	38	-6.85490194	38	-6.7637438	50	-6.18212763	88	-7.49728114
LUMO	39	-2.67887934	39	-3.28572047	51	-2.58173469	89	-3.70292544
LUMO+1	40	-2.39446593	40	-2.54772046	52	-2.57762577	90	-3.12794885
LUMO+2	41	-1.06089032	41	-0.9772153	53	-1.67559553	91	-2.91978174
LUMO+3	42	-0.67361787	42	-0.60237846	54	0.61696376	92	-2.69038976
LUMO+4	43	-0.52381919	43	-0.33608783	55	0.77927968	93	-1.55240959
LUMO+5	44	0.28882165	44	0.21703802	56	0.79789227	94	-1.26641792
LUMO+6	45	0.81119864	45	0.62052845	57	0.86815207	95	-1.04709414
LUMO+7	46	3.23905294	46	2.60676917	58	0.87149907	96	-0.59647359
LUMO+8	47	3.23995091	47	3.35138154	59	1.89647035	97	-0.51783268
LUMO+9	48	3.6583804	48	3.58161708	60	1.93304246	98	0.34640095

NICS Values for cyclo-P_5H

We calculated the NICS values for the bent geometry of the *cyclo*-P_5H ligand found in **3**$^+$ to assess its aromaticity and compared them with the values obtained for the planar geometry of hypothetical free *cyclo*-P_5H and two geometries of [*cyclo*-P_5]$^-$ for which a highly aromatic character can safely be stated (Table S8). Calculation of these NICS values has been performed on optimized (B3LYP/def2-TZVP, PCM solvent correction for CH_2Cl_2) molecular structures of free *cyclo*-P_5H, [*cyclo*-P_5]$^-$, the bent geometry of the *cyclo*-P_5H ligand in **3**$^+$ and the coordinated [*cyclo*-P_5]$^-$ ligand in **1**. Calculation of magnetic shielding tensors for dummy atoms placed at the centre (ring critical point), 1 Å above this centre and 1 Å below this centre have been performed on the PBE0/aug-pcSseg-2 level of theory. MultiWFN was used to obtain the ring critical point for these species and to extract the corresponding NICS(0/1/-1)$_{zz}$ values. The obtained values show clearly that the aromatic character of *cyclo*-P_5H is retained upon bending into the geometry found in **3**$^+$. While the decrease in all three NICS values is larger for this bending, than what is found for the geometric changes within the [*cyclo*-P_5]$^-$ upon coordination, the obtained NICS values are still negative indicating a high degree of aromaticity for the system.

*Table S 8: NICS(0/1/-1)$_{zz}$ of various species whose aromaticity can safely be stated and those obtained for the bent geometry of the cyclo-P_5H ligand in **3**$^+$, revealing decreased aromaticity for this geometry, while maintaining the largest part of it.*

Species	*NICS(0)*	*NICS(0)$_{zz}$*	*NICS(1)$_{zz}$*	*NICS(-1)$_{zz}$*
cyclo-P_5H (bent)	*–13.10*	*–20.96*	*–31.71*	*–30.92*
cyclo-P_5H (free)	*–17.03*	*–27.92*	*–37.19*	*–37.19*
[cyclo-P_5]$^-$ (ligand)	*–15.95*	*–31.90*	*–39.98*	*–39.98*
[cyclo-P_5]$^-$ (free)	*–16.25*	*–33.12*	*–41.10*	*–41.10*

Optimized Geometries

*[Cp*Fe(η^5-P_5)] (**1**)*

B3LYP/def2TZVP: Energies/H = –3360.782830, Enthalpies/H = –3360.781885, Free Energies/H = –3360.850077, ZPVE/ kJ/mol = 610.65

B3LYP/def2TZVPD: Energies/H = –3360.781850, Enthalpies/H = –3360.780905, Free Energies/H = –3360.848996, ZPVE/ kJ/mol = 610.99

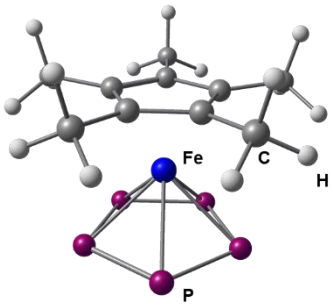

Symbol	X	Y	Z
Fe	0.0907820	0.0001340	-0.0004200
P	1.6788700	0.7449760	-1.6476410
P	1.6789650	-1.3356420	-1.2187340
P	1.6790230	1.7963410	0.1985620
P	1.6811750	-1.5701690	0.8927190
P	1.6810900	0.3653270	1.7686030
C	-1.6470920	-1.2064340	-0.1482740
C	-1.6458170	-0.5151290	1.1023450
C	-1.6467260	0.8878400	0.8312760
C	-1.6481730	1.0637610	-0.5868840
C	-1.6486720	-0.2306910	-1.1922690
C	-1.7384330	-1.1484340	2.4533840
C	-1.7394940	1.9787350	1.8493280
C	-1.7441380	2.3700220	-1.3074480
C	-1.7428180	-2.6872710	-0.3305700
C	-1.7448980	-0.5142630	-2.6570370
H	-1.2575250	-2.1255820	2.4751130
H	-1.2758620	-0.5305200	3.2220760
H	-1.2681930	1.6953900	2.7896440
H	-1.2949470	-3.0087260	-1.2700400
H	-1.2582440	3.1731220	-0.7545040
H	-1.2499760	-3.2266820	0.4774400
H	-2.7880280	-1.2899790	2.7293270
H	-1.2716310	-1.4601910	-2.9175540
H	-2.7928810	-2.9957100	-0.3419380
H	-2.7891990	2.2055810	2.0603880
H	-1.2771270	0.2688120	-3.2524780
H	-1.2676960	2.8971080	1.5019960
H	-2.7953310	-0.5759870	-2.9580780
H	-1.2886150	2.3207090	-2.2956440
H	-2.7943510	2.6478750	-1.4405750

*[Cp*Fe(η^5-P$_5$SiEt$_3$)]$^+$ (**2**$^+$)*

B3LYP/def2TZVP: Energies/H = –3887.722003, Enthalpies/H = –3887.721059, Free Energies/H = –3887.814994, ZPVE/ kJ/mol = 1136.93

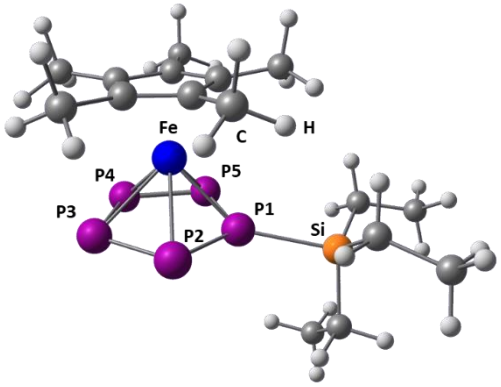

Symbol	X	Y	Z
Fe	1.324578	-0.105551	-0.01182
P	-0.914722	-0.777765	-0.188888
P	0.177455	-0.935106	-1.99369
P	0.076203	-1.533599	1.52032
P	1.898082	-2.015912	-1.396412
P	1.839168	-2.370392	0.700751
Si	-3.112785	0.094463	-0.09863
C	2.307397	1.093776	1.442468
C	3.239954	0.705871	0.430627
C	1.55396	1.925941	-0.579785
C	2.773663	1.220552	-0.819064
C	1.270175	1.85319	0.81993
C	4.540497	0.00663	0.656949
H	4.506235	-0.646025	1.527479
H	5.326095	0.748261	0.830226
H	4.837324	-0.590924	-0.203514
C	3.502029	1.150219	-2.121502
H	4.13132	0.2646	-2.189214
H	4.150825	2.025417	-2.222592
H	2.820703	1.148185	-2.970875
C	2.464362	0.864308	2.910268
H	1.503788	0.82441	3.421166
H	3.037595	1.686606	3.348901
H	3.001334	-0.058823	3.122852
C	0.79581	2.720816	-1.592454
H	0.883369	2.296632	-2.591463
H	1.194082	3.739091	-1.63154
H	-0.261801	2.791557	-1.346823
C	0.180934	2.577919	1.541019
H	-0.646598	2.833557	0.882695
H	0.576967	3.514831	1.944076
H	-0.208486	2.004178	2.380835
C	-3.132935	1.618566	-1.202432
H	-2.62671	2.429273	-0.671658
H	-2.532046	1.411211	-2.091744
C	-3.403039	0.40641	1.733059
H	-3.170102	-0.511719	2.279406
H	-2.684808	1.155178	2.076175
C	-4.124468	-1.323748	-0.805484
H	-5.147569	-0.939047	-0.888352
H	-3.793828	-1.495469	-1.83414
C	-4.540369	2.072646	-1.632609
H	-4.474049	2.96944	-2.251014
H	-5.173601	2.310324	-0.77706
H	-5.048086	1.306168	-2.219549
C	-4.128243	-2.638014	-0.014222
H	-3.128749	-3.070915	0.057996
H	-4.769754	-3.376141	-0.498567
H	-4.500575	-2.496925	1.001706
C	-4.833964	0.861789	2.075321
H	-5.076546	1.81868	1.611409
H	-4.941817	0.985361	3.154311
H	-5.581911	0.135268	1.753255

*[Cp*Fe(η^5-P_5H)]$^+$ (**3$^+$**)*

B3LYP/def2TZVP: Energies/H = –3361.177444, Enthalpies/H = –3361.176500, Free Energies/H = –3361.245504, ZPVE/ kJ/mol = 633.43

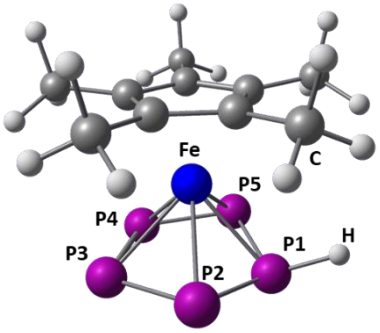

Symbbol	X	Y	Z
Fe	0.096073	-0.000213	-0.013797
P	1.857892	-0.003782	-1.649798
P	1.508684	-1.801993	-0.561563
P	1.514179	1.796783	-0.563676
P	1.747788	-1.071771	1.415056
P	1.750964	1.06813	1.413816
C	-1.64483	-1.152797	0.405463
C	-1.618831	0.001878	1.246547
C	-1.640794	1.157788	0.40697
C	-1.667318	0.717722	-0.955803
C	-1.670965	-0.711013	-0.956598
C	-1.68047	0.000885	2.739003
C	-1.743913	2.572231	0.874719
C	-1.808451	1.597653	-2.155461
C	-1.752141	-2.567793	0.870633
C	-1.822362	-1.589846	-2.155817
H	-1.206523	-0.881864	3.165049
H	-1.204112	0.881671	3.166393
H	-1.240491	2.724632	1.828164
H	-1.340566	-3.269884	0.147208
H	-1.342646	2.570636	-2.00693
H	-1.247786	-2.723823	1.823014
H	-2.725797	0.002062	3.061337
H	-1.333775	-2.553981	-2.022729
H	-2.806655	-2.822405	1.011464
H	1.240225	-0.003393	-2.915215
H	-2.797824	2.829883	1.01454
H	-1.423688	-1.12652	-3.056825
H	-1.329044	3.274611	0.153534
H	-2.88467	-1.783146	-2.331128
H	-1.376962	1.14654	-3.047645
H	-2.869726	1.769762	-2.35695

*[Cp*Fe(η^5-P$_5$Me)]$^+$ (**4**$^+$)*

B3LYP/def2TZVP: Energies/H = –3400.488573, Enthalpies/H = –3400.487629, Free Energies/H = –3400.560708, ZPVE/ kJ/mol = 710.48

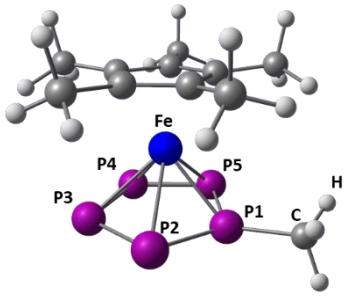

Symbol	X	Y	Z
Fe	-0.048181	-0.108942	-0.000338
P	2.215598	0.369174	0.004563
P	1.551908	-0.48332	-1.803392
P	1.542083	-0.476443	1.811754
P	0.562034	-2.203472	-1.064812
P	0.556989	-2.199831	1.072762
C	-1.738676	0.430048	-1.165216
C	-2.168144	-0.313232	-0.022747
C	-1.76121	0.40204	1.145221
C	-1.090194	1.594041	0.725368
C	-1.075564	1.611484	-0.703409
C	-3.000569	-1.553601	-0.044674
C	-2.099575	0.046328	2.55607
C	-0.617682	2.6817	1.634897
C	-2.049564	0.105319	-2.589917
C	-0.584533	2.721977	-1.574631
H	-2.814251	-2.153539	-0.933829
H	-2.824082	-2.17752	0.829972
H	-2.177259	-1.030084	2.700158
H	-1.299397	0.50337	-3.271394
H	-0.149796	2.287391	2.53641
H	-2.126819	-0.967729	-2.757636
H	-4.059813	-1.279946	-0.046955
H	-0.154783	2.350812	-2.504045
H	-3.01045	0.551599	-2.862724
H	-3.066687	0.485073	2.819038
H	0.161678	3.337322	-1.075416
H	-1.363706	0.432302	3.25986
H	-1.421174	3.374844	-1.839835
H	0.089993	3.346967	1.144418
H	-1.470564	3.290047	1.94933
C	3.015034	2.009543	-0.000786
H	4.088394	1.864807	0.112851
H	2.811106	2.502442	-0.949323
H	2.635181	2.608825	0.823737

[(Et$_3$Si)$_2$(μ-H)]$^+$

B3LYP/def2TZVP: Energies/H = –1054.628352, Enthalpies/H = –1054.627408, Free Energies/H = – 1054.704688, ZPVE/ kJ/mol = 1063.67

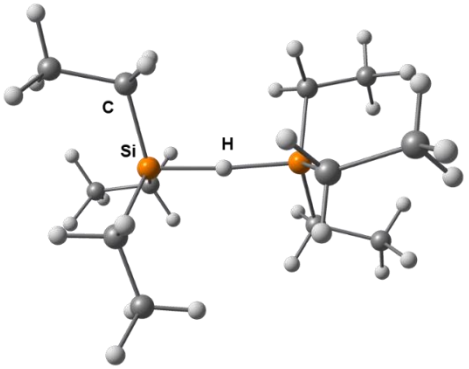

Symbol	X	Y	Z
C	-3.4769920	-2.2452780	-0.8026890
H	-3.5524950	-3.3089980	-1.0328720
H	-3.8350970	-1.6946430	-1.6735770
H	-4.1567980	-2.0404450	0.0252570
C	-2.0202160	-1.8815980	-0.4552650
H	-1.6817740	-2.4677160	0.4034150
H	-1.3671150	-2.1505350	-1.2905850
C	-2.1639910	0.5211870	1.6507210
H	-1.6551930	1.4757020	1.8133750
H	-1.7269780	-0.1860160	2.3620020
C	-3.6718590	0.6806620	1.9250470
H	-4.2015350	-0.2695230	1.8477080
H	-3.8302310	1.0617430	2.9349610
H	-4.1405310	1.3816890	1.2326810
C	-2.1338930	1.0876790	-1.4870040
H	-1.6685970	0.6748780	-2.3870170
H	-3.2150050	0.9954630	-1.6496340
C	-1.7574120	2.5645300	-1.3107600
H	-2.0778950	3.1458230	-2.1766160
H	-2.2285510	3.0018210	-0.4295090
H	-0.6789280	2.6964470	-1.2115490
C	1.7929120	-1.6523950	0.9708530
H	1.0848830	-1.6732340	1.8044250
H	1.5125050	-2.4741800	0.3059800
C	3.2193160	-1.8729960	1.5109920
H	3.4976080	-1.1085300	2.2372220
H	3.2804340	-2.8391460	2.0141870
H	3.9669660	-1.8691980	0.7170790
C	1.9170600	-0.0411520	-1.7824500
H	1.1942550	-0.6888060	-2.2866280
H	1.7375370	0.9697680	-2.1593360
C	3.3455310	-0.4959590	-2.1384080
H	4.1045170	0.1421600	-1.6841310
H	3.5324570	-1.5209390	-1.8153880
H	3.4914460	-0.4606790	-3.2190230
C	1.8859890	1.5333110	0.9798940
H	1.2836940	2.3292900	0.5326850
H	1.5283000	1.4150780	2.0066450
C	3.3690930	1.9524810	0.9761660
H	4.0092470	1.2029070	1.4422990
H	3.7368110	2.1231000	-0.0366260
H	3.4954800	2.8830590	1.5314440
Si	1.5219690	-0.0479420	0.0473920
Si	-1.7476380	-0.0700230	-0.0742810
H	-0.1132820	0.0023400	-0.0049920

Et_3SiH

B3LYP/def2TZVP: Energies/H = –527.701140, Enthalpies/H = –527.700196, Free Energies/H = –527.750313, ZPVE/ kJ/mol = 536.82

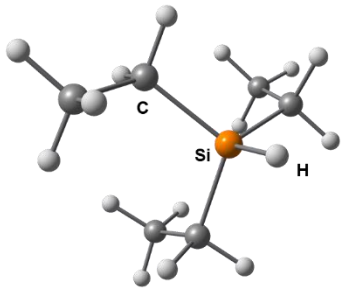

Symbol	X	Y	Z
C	-2.4019700	-0.7208310	-0.8476060
H	-3.4169770	-1.1259300	-0.8501840
H	-1.8348750	-1.2611950	-1.6087120
H	-2.4677930	0.3202470	-1.1688570
C	-1.7537420	-0.8495860	0.5388400
H	-2.3590400	-0.3186950	1.2819230
H	-1.7667280	-1.9004770	0.8493970
C	0.2183720	1.6274940	0.6626620
H	1.2247440	1.8614000	1.0272770
H	-0.4649440	2.0498300	1.4077280
C	-0.0031530	2.3120570	-0.6944270
H	-1.0232180	2.1733050	-1.0572570
H	0.1741680	3.3885130	-0.6296490
H	0.6700440	1.9178790	-1.4590170
C	1.1634450	-1.1118580	-0.5255240
H	0.9691870	-2.1881490	-0.4619500
H	0.8607980	-0.8169600	-1.5358580
C	2.6634850	-0.8441910	-0.3345200
H	3.2648030	-1.3887030	-1.0667940
H	2.9006540	0.2164340	-0.4442180
H	3.0000280	-1.1511490	0.6586140
Si	0.0340670	-0.2560300	0.7262260
H	0.4736040	-0.6704430	2.0938450

$(Et_3Si)_2O$

B3LYP/def2TZVP: Energies/H = –1129.581330, Enthalpies/H = –1129.580386, Free Energies/H = –1129.663504, ZPVE/ kJ/mol = 1045.45

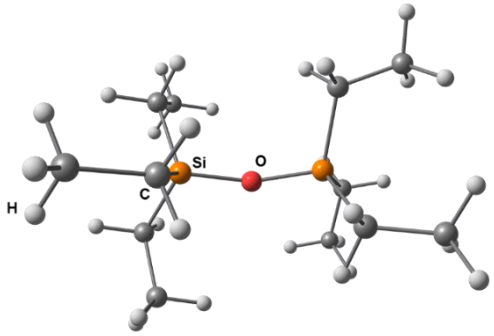

Symbol	X	Y	Z
C	3.2793150	2.3347630	0.5481400
H	3.3415830	3.4005500	0.7817670
H	3.8144230	2.1768720	-0.3907850
H	3.8264180	1.8014710	1.3276550
C	1.8189940	1.8678180	0.4521850
H	1.3066710	2.0623630	1.4013990
H	1.2929020	2.4743300	-0.2939760
C	1.9586300	-1.1407690	1.3708520
H	1.5110590	-2.1048500	1.1044620
H	1.4342300	-0.8177640	2.2771950
C	3.4505170	-1.3402440	1.6783160
H	3.9208800	-0.4194080	2.0280320
H	3.5990450	-2.0933140	2.4562870
H	4.0033560	-1.6722920	0.7965850
C	2.4153460	-0.3657910	-1.6075630
H	2.1403820	0.3847640	-2.3574380
H	3.4897980	-0.2337060	-1.4401430
C	2.1452010	-1.7727030	-2.1604630
H	2.6796860	-1.9464890	-3.0978130
H	2.4607150	-2.5481220	-1.4584910
H	1.0817250	-1.9241290	-2.3560080
Si	1.5044340	0.0632300	-0.0132110
O	-0.1105540	-0.1130330	-0.3000330
C	-2.6729550	-1.2054590	-0.9213600
H	-3.7425990	-0.9957060	-0.8077140
H	-2.4636290	-1.0904520	-1.9903290
C	-2.3767040	-2.6494250	-0.4905920
H	-2.9522040	-3.3706320	-1.0763680
H	-1.3199600	-2.8932760	-0.6187070
H	-2.6235760	-2.8136720	0.5608070
C	-2.2173840	1.8374560	-0.6313760
H	-3.2790570	1.9819990	-0.4018000
H	-1.6834610	2.5854190	-0.0341140
C	-1.9719510	2.0977680	-2.1248240
H	-2.5481060	1.4141920	-2.7523290
H	-2.2551120	3.1147590	-2.4077310
H	-0.9190920	1.9672990	-2.3841580
C	-2.0043660	0.0205790	1.8612210
H	-1.6138550	-0.9437110	2.2042320
H	-1.3743040	0.7790160	2.3396040
C	-3.4583730	0.1857920	2.3298360
H	-4.1099990	-0.5780550	1.8990550
H	-3.5405690	0.1055870	3.4165970
H	-3.8659330	1.1584570	2.0453400
Si	-1.7133340	0.1313440	-0.0008660

H_2O

B3LYP/def2TZVP: Energies/H = –76.445378, Enthalpies/H = –76.444434, Free Energies/H = –76.465863, ZPVE/ kJ/mol = 55.42

Symbol	X	Y	Z
O	0.0000000	0.0000000	0.1177390
H	0.0000000	0.7631970	-0.4709540
H	0.0000000	-0.7631970	-0.4709540

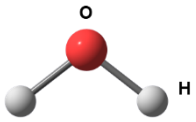

Me_2O

B3LYP/def2TZVP: Energies/H = –155.012573, Enthalpies/H = –155.012573, Free Energies/H = –155.042385, ZPVE/ kJ/mol = 208.17

Symbol	X	Y	Z
C	1.1762010	-0.1960170	0.0000000
H	2.0261580	0.4851680	0.0003490
H	1.2290150	-0.8347970	-0.8905680
H	1.2286910	-0.8353050	0.8902240
C	-1.1762010	-0.1960170	0.0000000
H	-1.2286050	-0.8354300	0.8901390
H	-2.0261580	0.4851680	0.0005280
H	-1.2291010	-0.8346710	-0.8906520
O	0.0000000	0.5902590	-0.0000030

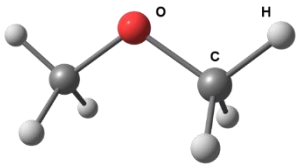

$[Me_3O]^+$

B3LYP/def2TZVP: Energies/H = –194.684233, Enthalpies/H = –194.683289, Free Energies/H = –194.718687, ZPVE/ kJ/mol = 317.88

Symbol	X	Y	Z
C	-0.4519470	-1.3591690	0.0651410
H	0.2637340	-2.0420890	-0.3784080
H	-1.4330190	-1.4753870	-0.3807600
H	-0.4835490	-1.4480290	1.1485390
C	-0.9520730	1.0704720	0.0653180
H	-1.0096680	1.1450250	1.1488780
H	-0.5687210	1.9791350	-0.3847650
H	-1.9013910	0.7869130	-0.3746420
C	1.4037020	0.2885640	0.0652530
H	1.9960770	-0.5029690	-0.3787610
H	1.6384320	1.2488740	-0.3795850
H	1.4954570	0.3068040	1.1487120
O	0.0005700	0.0003150	-0.2929350

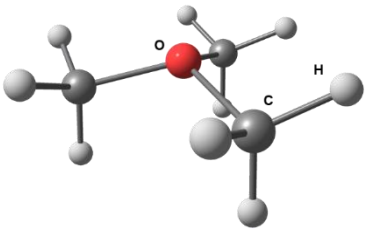

cyclo-P_5H (free)

B3LYP/def2TZVP: Energies/H = –1707.509978, Enthalpies/H = –1707.509034, Free Energies/H = –1707.548299, ZPVE/ kJ/mol = 41.90

Symbol	X	Y	Z
P	-0.0001190	-1.4181550	-1.0583310
P	-0.0001190	-1.4181550	1.0583310
P	-0.0001190	0.5490970	-1.8160170
P	0.0004610	1.5416710	0.0000000
H	0.0002280	2.9467030	0.0000000
P	-0.0001190	0.5490970	1.8160170

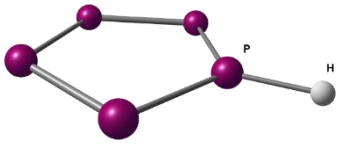

[cyclo-P_5]$^-$ (free)

B3LYP/def2TZVP: Energies/H = –1707.08315, Enthalpies/H = –1707.082210, Free Energies/H = –1707.12035, ZPVE/ kJ/mol = 20.55

Symbol	X	Y	Z
P	-1.1419970	1.3794220	0.0000340
P	0.9591780	1.5122790	0.0001100
P	-1.6650010	-0.6597200	-0.0001660
P	1.7348780	-0.4448980	-0.0002130
P	0.1129430	-1.7870840	0.0002340

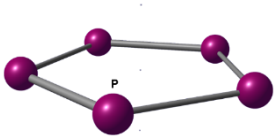

$[H(Et_2O)_2]^+$

B3LYP/def2TZVPD: Energies/H = –467.587972, Enthalpies/H = –467.587028, Free Energies/H = –467.647942, ZPVE/ kJ/mol = 747.04

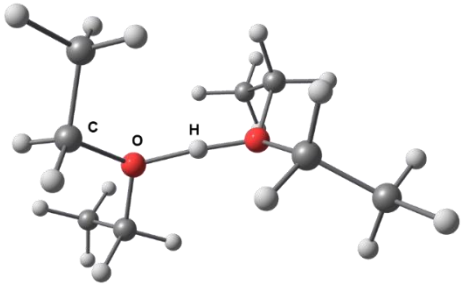

Symbol	X	Y	Z
C	-3.1023330	0.2879020	-1.5643740
H	-3.8415050	-0.1960270	-0.9262620
H	-3.6119460	1.0854360	-2.1079710
H	-2.7320280	-0.4359030	-2.2899430
C	-1.9706760	0.8936160	-0.7704180
H	-2.3151640	1.6189260	-0.0319090
H	-1.2379890	1.3730670	-1.4180880
C	-1.7525980	-0.5820300	1.2463880
H	-2.8145840	-0.7475320	1.0804220
H	-1.6240570	0.2420540	1.9501700
C	-1.0540250	-1.8423010	1.6916420
H	-1.4804990	-2.1563740	2.6455030
H	-1.1996680	-2.6496150	0.9741150
H	0.0138510	-1.6830410	1.8419640
C	1.8827490	1.3793710	0.1648250
H	2.9264090	1.1335820	0.3558990
H	1.8317850	2.0258250	-0.7150540
C	1.7866550	-0.6586590	-1.2321290
H	2.0499060	0.0261690	-2.0411930
H	0.9794340	-1.3040540	-1.5773250
C	2.9734440	-1.4717840	-0.7654870
H	3.3359090	-2.0751200	-1.5996910
H	3.8008620	-0.8448260	-0.4336780
H	2.6946810	-2.1461550	0.0442350
C	1.2501990	2.0235630	1.3757220
H	1.7947480	2.9379310	1.6142890
H	0.2110030	2.3043870	1.1950380
H	1.3002120	1.3683230	2.2458270
O	-1.2063090	-0.1438100	-0.0519120
O	1.1970970	0.1322080	-0.1506920
H	-0.0881420	0.0376900	-0.0625290

Et_2O

B3LYP/def2TZVPD: Energies/H = –233.619297, Enthalpies/H = –233.618353, Free Energies/H = –233.656271, ZPVE/ kJ/mol = 357.00

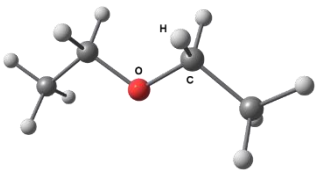

Symbol	X	Y	Z
C	-2.3794560	0.4127000	0.0000070
H	-2.3689380	1.0517910	-0.8841620
H	-3.3079000	-0.1617670	0.0000240
H	-2.3689160	1.0518080	0.8841620
C	-1.1845980	-0.5178840	0.0000000
H	-1.2034130	-1.1709230	-0.8849940
H	-1.2033920	-1.1709070	0.8850070
C	1.1845980	-0.5178840	0.0000020
H	1.2033930	-1.1709030	0.8850100
H	1.2034120	-1.1709270	-0.8849900
C	2.3794560	0.4127000	0.0000060
H	3.3079000	-0.1617670	0.0000280
H	2.3689400	1.0517870	-0.8841650
H	2.3689140	1.0518120	0.8841590
O	0.0000000	0.2577750	-0.0000210

5.6. References

[1] a) W. Kaminsky, *J. Chem. Soc., Dalton Trans.* **1998**, 1413–1418; b) G. G. Hlatky, *Coord. Chem. Rev.* **1999**, *181*, 243–296; c) W. Kaminsky, *Stud. Surf. Sci. Catal.* **1999**, *121*, 3–12; d) W. Kaminsky, A. Funck, H. Hähnsen, *Dalton. Trans.* **2009**, 8803–8810.

[2] a) C. Dohmeier, C. Robl, M. Tacke, H. Schnöckel, *Angew. Chem. Int. Ed. Engl.* **1991**, *30*, 564–565; b) S. Schulz, H. W. Roesky, H. J. Koch, G. M. Sheldrick, D. Stalke, A. Kuhn, *Angew. Chem. Int. Ed. Engl.* **1993**, *32*, 1729–1731.

[3] A. Hofmann, T. Tröster, T. Kupfer, H. Braunschweig, *Chem. Sci.* **2019**, *10*, 3421–3428.

[4] P. Jutzi, A. Mix, B. Rummel, W. W. Schoeller, B. Neumann, H.-G. Stammler, *Science* **2004**, *305*, 849–851.

[5] J. Zhou, L. L. Liu, L. L. Cao, D. W. Stephan, *Chem* **2018**, *4*, 2699–2708.

[6] R. Hoffmann, *Angew. Chem. Int. Ed. Engl.* **1982**, *21*, 711–724.

[7] O. J. Scherer, J. Schwalb, G. Wolmershäuser, W. Kaim, R. Gross, *Angew. Chem. Int. Ed. Engl.* **1986**, *25*, 363–364.

[8] O. J. Scherer, T. Brück, *Angew. Chem. Int. Ed. Engl.* **1987**, *26*, 59.

[9] M. Baudler, D. Düster, D. Ouzounis, *Z. Anorg. Allg. Chem.* **1987**, *544*, 87–94.

[10] V. A. Milyuko, A. V. Kataev, O. G. Sinyashin, E. Hey-Hawkins, *Russ. Chem. Bull.* **2006**, *55*, 1297–1299.

[11] a) V. A. Miluykov, O. G. Sinyashin, O. J. Scherer, E. Hey-Hawkins, *Mendeleev Commun.* **2002**, *12*, 1–2; b) V. A. Miluykov, A. Kataev, O. Sinyashin, P. Lönnecke, E. Hey-Hawkins, *Organometallics* **2005**, *24*, 2233–2236.

[12] a) A. R. Kudinov, D. A. Loginov, Z. A. Starikova, P. V. Petrovskii, M. Corsini, P. Zanello, Eur. *J. Inorg. Chem.* **2002**, *2002*, 3018–3027; b) S. Heinl, G. Balázs, M. Bodensteiner, M. Scheer, *Dalton Trans.* **2016**, *45*, 1962–1966; c) D. A. Loginov, Y. V. Nelyubina, A. R. Kudinov, *J. Organomet. Chem.* **2018**, *870*, 130–135.

[13] a) O. J. Scherer, T. Brück, G. Wolmershäuser, *Chem. Ber.* **1988**, *121*, 935–938; b) M. Baudler, T. Etzbach, *Angew. Chem. Int. Ed. Engl.* **1991**, *30*, 580–582; c) B. Rink, O. J. Scherer, G. Wolmershäuser, *Chem. Ber.* **1995**, *128*, 71–73; d) C. M. Knapp, B. H. Westcott, M. A. C. Raybould, J. E. McGrady, J. M. Goicoechea, *Angew. Chem. Int. Ed.* **2012**, *51*, 9097–9100.

[14] E. Urnius, W. W. Brennessel, C. J. Cramer, J. E. Ellis, P. v. R. Schleyer, *Science* **2002**, *295*, 832–834.

[15] M. Baudler, S. Akpapoglou, D. Ouzounis, F. Wasgestian, B. Meinigke, H. Budzikiewicz, H. Münster, *Angew. Chem. Int. Ed. Engl.* **1988**, *27*, 280–281.

[16] a) E. Mädl, M. V. Butovskii, G. Balázs, E. V. Peresypkina, A. V. Virovets, M. Seidl, M. Scheer, *Angew. Chem. Int. Ed.* **2014**, *53*, 7643–7646; b) A. K. Adhikari, C. G. P. Ziegler, K. Schwedtmann, C. Taube, J. J. Weigand, R. Wolf, *Angew. Chem. Int. Ed.* **2019**, *58*, 18584–18590; c) M. Piesch, M. Seidl, M. Stubenhofer, M. Scheer, *Chem. Eur. J.* **2019**, *25*, 6311–6316; d) C. G. P. Ziegler, T. M. Maier, S. Pelties, C. Taube, F. Hennersdorf, A. W. Ehlers, J. J. Weigand, R. Wolf, *Chem. Sci.* **2019**, *10*, 1302–1308.

[17] Note that there is a compound formulated as $[Me_3Si(\eta^5\text{-}P_5)W(CO)_3]$ in [13c], which is only characterised NMR-spectroscopically. The fact that in the ^{31}P NMR spectrum it shows only a singlet at -23 ppm renders silylation at the *cyclo*-P_5 ligand unlikely.

[18] a) L. Nyulászi, *Inorg. Chem.* **1996**, *35*, 4690–4693; b) M. N. Glukhovtsev, A. Dransfeld, P. v. R. Schleyer, *J. Phys. Chem.* **1996**, *100*, 13447–13454; c) A. Dransfeld, L. Nyulászi, P. v. R. Schleyer, *Inorg. Chem.* **1998**, *37*, 4413–4420; d) M. K. Cyrański, P. v. R. Schleyer, T. M. Krygowski, H. Jiao, Haijun, G. Hohlneicher, *Tetrahedron* **2003**, *59*, 1657–1665; e) W. P. Ozimiński, J. C. Dobrowolski, *Chem. Phys.* **2005**, *313*, 123–132; f) L. Wang, H. J. Wang, W. B. Dong, Q. Y. Ge, L. Lin, *Struct. Chem.* **2007**, *18*, 25–31; g) W.-Q. Li, L.-L. Liu J.-K. Feng, Z.-Z. Liu, A.-M. Ren, G. Zhang, C.-C. Sun, *J. Theor. Comput. Chem.* **2008**, *07*, 1203–1214; h) D. Josa, A. Peña-Gallego, J. Rodríguez-Otero, E. M. Cabaleiro-Lago, *J. Mol. Model.* **2011**, *17*, 1267–1272.

[19] a) J. Bai, A. V. Virovets, M. Scheer, *Angew. Chem. Int. Ed.* **2002**, *41*, 1737–1740; b) J. Bai, A. V. Virovets, M. Scheer, *Science* **2003**, *300*, 781–783; c) M. Scheer, J. Bai, B. P. Johnson, R. Merkle, A. V. Virovets, C. E. Anson, *Eur. J. Inorg. Chem.* **2005**, *2005*, 4023–4026; d) M. Scheer, L. J. Gregoriades, A. V. Virovets, W. Kunz, R. Neueder, I. Krossing, *Angew. Chem. Int. Ed.* **2006**, *45*, 5689–5693; e) S. Welsch, L. J. Gregoriades, M. Sierka, M. Zabel, A. V. Virovets, M. Scheer, *Angew. Chem. Int. Ed.* **2007**, *46*, 9323–9326; f) M. Scheer, A. Schindler, R. Merkle, B. P. Johnson, M. Linseis, R. Winter, C. E. Anson, A. V. Virovets, *J. Am. Chem. Soc.* **2007**, *129*, 13386–13387; g) M. Scheer, L. J. Gregoriades, R. Merkle, B. P. Johnson, F. Dielmann, *Phosphorus, Sulfur, Silicon Relat. Elem.* **2008**, *183*, 504–508; h) M. Scheer, A. Schindler, C. Gröger, A. V. Virovets, E. V. Peresypkina, *Angew. Chem. Int. Ed.* **2009**, *48*, 5046–5049; i) M. Scheer, A. Schindler, J. Bai, B. P. Johnson, R. Merkle, R. Winter, A. V. Virovets, E. V. Peresypkina, V. A. Blatov, M. Sierka, H. Eckert, *Chem. Eur. J.* **2010**, *16*, 2092–2107; j) E. Peresypkina, C. Heindl, A. Virovets, H. Brake, E. Mädl, M. Scheer, *Chem. Eur. J.* **2018**, *24*, 2503–2508.

[20] M. V. Butovskiy, G. Balázs, M. Bodensteiner, E. V. Peresypkina, A. V. Virovets, J. Sutter, M. Scheer, *Angew. Chem. Int. Ed.* **2013**, *52*, 2972–2976.

[21] C. Schwarzmaier, S. Heinl, G. Balázs, M. Scheer, *Angew. Chem. Int. Ed.* **2015**, *54*, 13116–13121.

[22] A. Wiesner, S. Steinhauer, H. Beckers, C. Müller, S. Riedel, *Chem. Sci.* **2018**, *9*, 7169–7173.

[23] M. Malischewski, K. Seppelt, J. Sutter, F. W. Heinemann, B. Dittrich, K. Meyer, *Angew. Chem. Int. Ed.* **2017**, *56*, 13372–13376.

[24] A. Cavaillé, N. Saffon-Merceron, N. Nebra, M. Fustier-Boutignon, N. Mézailles, *Angew. Chem. Int. Ed.* **2017**, *57*, 1874–1878.

[25] U. Chakraborty, J. Leitl, B. Mühldorf, M. Bodensteiner, S. Pelties, Stefan, R. Wolf, *Dalton Trans.* **2018**, *47*, 3693–3697.

[26] I. Krossing, A. Reisinger, *Eur. J. Inorg. Chem.* **2005**, *10*, 1979–1989.

[27] C. Marquardt, A. Adolf, A. Stauber, M. Bodensteiner, A. V. Virovets, A. Y. Timoshkin, M. Scheer, *Chem. Eur. J.* **2013**, *19*, 11887–11891.

[28] S. J. Connelly, W. Kaminsky, D. M. Heinekey, *Organometallics* **2013**, *32*, 7478–7481.
[29] a) M. A. P. Pyykkö, *Chem. Eur. J.* 2009, *15*, 186–197; b) P. Pyykkö, *J. Phys. Chem. A* **2015**, *119*, 2326–2337.
[30] G. Becker, H.-D. Hausen, O. Mundt, W. Schwarz, C. T. Wagner, T. Vogt, *Z. Anorg. Allg. Chem.* **1990**, *591*, 17–31.
[31] A. Sequeira, W. C. Hamilton, *J. Chem. Phys.* **1967**, *47*, 1818–1822.
[32] a) P. A. M. Dirac, *Proc. R. Soc. Lond. A* **1929**, *123*, 714–733; b) J. C. Slater, *Phys. Rev.* **1951**, *81*, 385–390; c) S. H. Vosko, L. Wilk, M. Nusair, *Can. J. Phys.* **1980**, *58*, 1200–1211; d) C. Lee, W. Yang, R. G. Parr, *Phys. Rev. B* **1988**, *37*, 785–789; e) A. D. Becke, *Phys. Rev. A* **1988**, *38*, 3098–3100; f) A. D. Becke, *J. Chem. Phys.* **1993**, *98*, 5648–5652.
[33] a) R. A. F. Weigend, *Phys. Chem. Chem. Phys.* **2005**, *7*, 3297–3305; b) F. Weigend, *Phys. Chem. Chem. Phys.* **2006**, *8*, 1057–1065.
[34] S. Hämmerling, P. Voßnacker, S. Steinhauer, H. Beckers, S. Riedel, *Chem. Eur. J.* **2020**, *26*, 14377–14384.
[35] E. D. Glendening, C. R. Landis, F. Weinhold, *J. Comput. Chem.* **2013**, *34*, 1363–1374.
[36] a) P. v. R. Schleyer, C. Maerker, A. Dransfeld, H. Jiao, N. J. R. v. E. Hommes, *J. Am. Chem. Soc.* **1996**, *118*, 6317–6318; b) Z. Chen, C. S. Wannere, C. Corminboeuf, R. Puchta, P. v. R. Schleyer, *Chem. Rev.* **2005**, *105*, 3842–3888.
[37] a) J. P. Perdew, K. Burke, M. Ernzerhof, *Phys. Rev. Lett.* **1996**, *77*, 3865–3868; b) J. P. Perdew, K. Burke, M. Ernzerhof, *Phys. Rev. Lett.* **1997**, *78*, 1396; c) V. B. C. Adamo, *J. Chem. Phys.* **1999**, *110*, 6158–6170.
[38] F. Jensen, *J. Chem. Theory Comput.* **2015**, *11*, 132–138.
[39] https://omics.pnl.gov/software/molecular-weight-calculator, (14.07.2020).
[40] Y. Soltani, L. C. Wilkins, R. L. Melen, *Angew. Chem. Int. Ed.* **2017**, *56*, 11995–11999.
[41] Agilent (**2014**). CrysAlis PRO. Agilent Technologies Ltd, Yarnton, Oxfordshire, England.
[42] O. V. Dolomanov, L. J. Bourhis, R. J. Gildea, J. A. K. Howard, H. Puschmann, *J. Appl. Crystallogr.* **2009**, *42*, 339–341.
[43] G. M. Sheldrick, *Acta Crystallogr. A* **2015**, *71*, 3–8.
[44] a) G. M. Sheldrick, *Acta Crystallogr. C* **2015**, *71*, 3–8; b) G. M. Sheldrick, *Acta Crystallogr. A* **2008**, *64*, 112–122.
[45] M. J. Frisch, G. W. Trucks, H. B. Schlegel, G. E. Scuseria, M. A. Robb, J. R. Cheeseman, G. Scalmani, V. Barone, B. Mennucci, G. A. Petersson, H. Nakatsuji, M. Caricato, X. Li, H. P. Hratchian,A. F. Izmaylov, J. Bloino, G. Zheng, J. L. Sonnenberg, M. Hada, M. Ehara, K. Toyota, R. Fukuda, J. Hasegawa, M. Ishida, T. Nakajima, Y. Honda, O. Kitao, H. Nakai, T. Vreven, J. A. Montgomery Jr., J. E. Peralta, F. Ogliaro, M. Bearpark, J. J. Heyd, E. Brothers, K. N. Kudin, V. N. Staroverov, T. Keith, R. Kobayashi, J. Normand, K. Raghavachari, A. Rendell, J. C. Burant, S. S. Iyengar, J. Tomasi, M. Cossi, N. Rega, J. M. Millam, M. Klene, J. E. Knox, J. B. Cross, V. Bakken, C. Adamo, J. Jaramillo, R. Gomperts, R. E. Stratmann, O. Yazyev, A. J. Austin, R. Cammi, C. Pomelli, J. W. Ochterski, R. L. Martin, K. Morokuma, V. G. Zakrzewski, G. A. Voth, P. Salvador, J. J.

Dannenberg, S. Dapprich, A. D. Daniels, O. Farkas, J. B. Foresman, J. V. Ortiz, J. Cioslowski, D. J. Fox, "Gaussian 09", Revision E.01, Gaussian Inc., Wallingford CT **2013**.

[46] J. Tomasi, B. Mennucci, R. Cammi, *Chem. Rev.* **2005**, *105*, 2999–3093.

[47] F. F. D. Rappoport, *J. Chem. Phys.* **2010**, *133*, 134105–134116.

[48] a) S. I. Gorelsky, AOMix: Program for Molecular Orbital Analysis; **2017**, version 6.90, http://www.sg-chem.net; b) S. I. Gorelsky, A. B. P. Lever, *J. Organomet. Chem.* **2001**, *635*, 187–196.

[49] a) P. v. R. Schleyer, C. Maerker, A. Dransfeld, H. Jiao, N. J. R. v. Eikema Hommes, *J. Am. Chem. Soc.* **1996**, *118*, 6317–6318; b) Z. Chen, C. S. Wannere, C. Corminboeuf, R. Puchta, P. v. R. Schleyer, *Chem. Rev.* **2005**, *105*, 3842–3888.

[50] T. Lu, F. Chen, *J. Comput. Chem.* **2012**, *33*, 580–592.

[51] a) D. Feller, *J. Comput. Chem.* **1996**, *17*, 1571–1586; b) K. L. Schuchardt, B. T. Didier, T. Elsethagen, L. Sun, V. Gurumoorthi, J. Chase, J. Li, T. L. Windus, *J. Chem. Infor. Model.* **2007**, 47, 1045–1052; c) B. P. Pritchard, D. Altarawy, B. T. Didier, D. Gibson, T. L. Windus, *J. Chem. Infor. Model.* **2019**, *59*, 4814–4820.

[52] A. K. Chandra, A. Goursot, *J. Phys. Chem.* **1996**, *100*, 11596–11599.

[53] B. Kovacević, Z. B. Maksić, *Chem. Commun.* **2006**, 1524–1526.

6. Substituted Aromatic Pentaphosphole Ligands – A Journey Across the p-Block

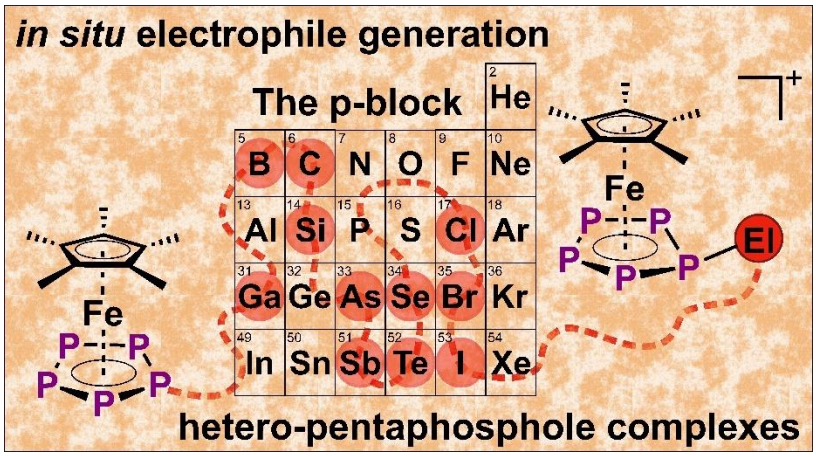

Preface

The following chapter has already been published. The article is reproduced with permission from the Royal Society of Chemistry.

"Substituted Aromatic Pentaphosphole Ligands – A Journey Across the p-Block"

Chem. Sci. **2021,** *12***,** 13037–13044.

Authors

Christoph Riesinger, Gábor Balázs, Michael Seidl and Manfred Scheer

Author Contributions

Christoph Riesinger – Conceptualization, Synthesis of compounds **2** – **13** and **15**, Writing of original draft.
Gábor Balázs – Interpretation of computational data.
Michael Seidl – Interpretation of crystallographic data.
Manfred Scheer – Project administration, Funding acquisition, Co-writing final manuscript.

Acknowledgements

This work was supported by the Deutsche Forschungsgemeinschaft (DFG) in the project Sche 384/36-1. C. R. is grateful to the Studienstiftung des Deutschen Volkes for a PhD fellowship.

6.1. Abstract

*The functionalization of Pentaphosphaferrocene [Cp*Fe(η^5-P_5)] (**1**) with cationic group 13 – 17 electrophiles is shown to be a general synthetic strategy towards P–E bond formation of unprecedented diversity. The products of these reactions are dinuclear [{Cp*Fe}$_2${$\mu,\eta^{5:5}$-(P_5)$_2$$EX_2$}][TEF] ($EX_2$ = BBr_2 (**2**), GaI_2 (**3**), $[TEF]^-$ = $[Al\{OC(CF_3)_3\}_4]^-$) or mononuclear [Cp*Fe(η^5-P_5E)][X] (E = CH_2Ph (**4**), $CHPh_2$ (**5**), $SiHPh_2$ (**6**), $AsCy_2$ (**7**), SePh (**9**), TeMes (**10**), Cl (**11**), Br (**12**), I (**13**)) complexes of hetero-bis-pentaphosphole ((cyclo-P_5)$_2$R) or hetero-pentaphosphole ligands (cyclo-P_5R), the aromatic all-phosphorus analogs of prototypical cyclopentadienes. Further, modifying the steric and electronic properties of the electrophile has a drastic impact on its reactivity and leads to the formation of [Cp*Fe($\mu,\eta^{5:2}$-P_5)SbICp'''][TEF] (**8**) which possesses a triple-decker-like structure. X-ray crystallographic characterization reveals the slightly twisted conformation of the cyclo-P_5R ligands in these compounds and multinuclear NMR spectroscopy confirms their integrity in solution. DFT calculations shed light on the bonding situation of these compounds and confirm the aromatic character of the pentaphosphole ligands on a journey across the p-block.*

6.2. Introduction

Electrophilic aromatic substitution is one of the most basic and widely applied reactions for the functionalization of aromatic organic compounds. While Friedel-Crafts alkylation and acylation are in fact textbook examples for the reactivity of benzene derivatives,[1] they can also be applied to smaller ring systems.[2] In contrast, derivatives of the carbocyclic aromatic cyclopentadienide anion (Cp^-, $C_5H_5^-$) form non-aromatic cyclopentadiene derivatives (CpR, C_5H_5R) upon salt metathesis with element halogenides. Compared to their alkali metal salts, transition metal (TM) bound Cp^-

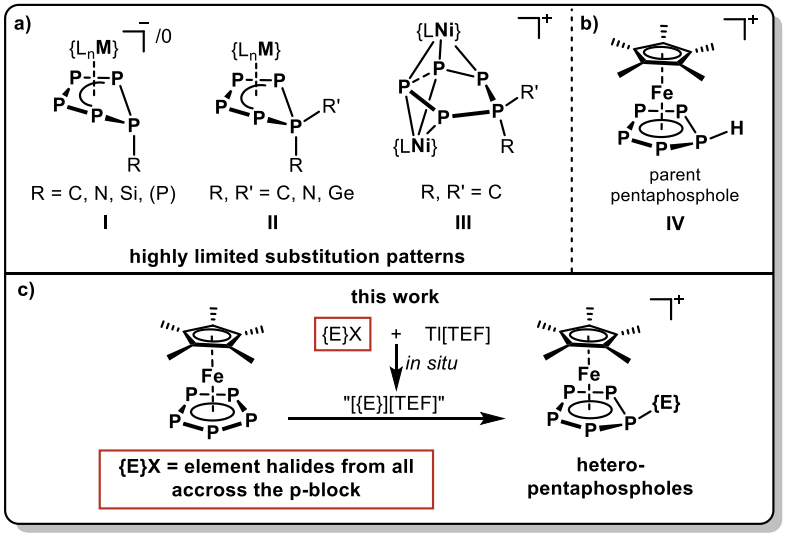

*Scheme 1: a) Known substituted cyclo-P_5 ligand architectures **I** ({L_nM} = {($Mes^{neo}PentN$)$_2$Nb} or {Cp*Fe}), **II** ({L_nM} = {Cp*Fe}, {$Cp^{PEt}Co$}$^+$, {(BIAN)Co}), **III** (L = Cp^{PEt}); b) The parent pentaphosphole complex **IV**; c) Targeted functionalization of an iron bound pentaphospholide ion with in situ generated cationic electrophiles from across the p-block to yield unprecedented coordinatively stabilized hetero-pentaphospholes.*

ligands (e. g. in Cp_2Fe)[3] exhibit different reactivity towards electrophiles mimicking that of benzene derivatives (e.g. $(C_6H_6)Cr(CO)_3$).[4] The isolobal relationship between the CH fragment and the P atom[5] and the diagonal relationship between carbon and phosphorus suggest a comparable reactivity for the pentaphospholide anion *cyclo*-P_5^-.[6] However, investigations on the reactivity of the salts of *cyclo*-P_5^- towards alkylhalogenides showed further aggregation to polyphosphides,[7] leaving the chemistry of pentaphospholes *cyclo*-P_5R to theoretical studies for decades.[8] Similar to Cp^-, *cyclo*-P_5^- can be stabilized within the coordination sphere of different TMs[9] and is thus closely associated with the TM-mediated conversion of P_4.[10] One of the most prominent examples of such complexes is pentaphosphaferrocene [Cp*Fe(η^5-P_5)] (**1**).[9a] While **1** readily reacts with various monovalent metal salts to form coordination compounds,[11] we could also demonstrate both its redox reactivity[12] and its behavior towards anionic[13] and neutral nucleophiles.[14] These reactions yielded complexes with bent *cyclo*-P_5R ligands (**I**, Scheme 1),[13,14] which are also accessible by the reaction of a Niobium phosphorus triple bond complex with P_4.[15] Disubstituted *cyclo*-P_5R_2 moieties (**II** and **III**, Scheme 1) could be obtained via the coordination of the respective $[P_5R_2]^+$ cations[16] to low-valent transition metal fragments.[17] The formation of the structural motif **II** was also observed upon condensation of an anionic *cyclo*-P_4 complex with chlorophosphines.[18] The introduction of germylene substituents has recently been achieved by the reaction of **1** with a digermylene.[19] While their structural motifs are remarkable, the respective *cyclo*-P_5R_n ligands (n = 1, 2) within types **I** – **III** do not show any aromatic character, since they do not represent pentaphospholes (**IV**).[8] Only recently, we succeeded in the synthesis of the first transition metal complexes [Cp*Fe(η^5-P_5R)][$B(C_6F_5)_4$] (**IV**, R = H, Me, $SiEt_3$) featuring such pentaphosphole ligands.[20] While our previous approach is well-suited to prepare the parent compound with a *cyclo*-P_5H ligand, it is limited to group 14 electrophiles (such as CH_3/$SiEt_3$) as introducible substituents.[21] Thus, we sought a more general strategy to electrophilically functionalize **1** which may also be applicable beyond the synthesis of the targeted hetero-pentaphosphole complexes to other heteroaromatic ligands. Such a strategy would represent a valuable contribution to electrophilic substitution reactions in general. We hypothesized that the *in situ* generation of cationic electrophiles from p-block element halogenides and a suitable halide-abstracting reagent, as has for example been utilized for the functionalization of coordinated chlorophosphines,[22] and subsequent reaction with **1** could provide this reactivity. Such an approach would allow P–E bond formation with a nearly unlimited choice of electrophiles and would thus overcome the limitations of known synthetic strategies towards the P–E bond formation in the vicinity of transition metals.[14,15,23] Indeed, the major drawback of the so far used strategies is their immensely limited applicability to a very narrow range of electrophile/nucleophile combinations. This is usually reflected in the use of rather exotic low-valent main group species such as tetrylenes,[14b,18] $\{Cp^*Al\}_4$,[24] or the utilization of highly reactive, e.g. anionic, polyphosphorus ligand complexes.[23e,f] While

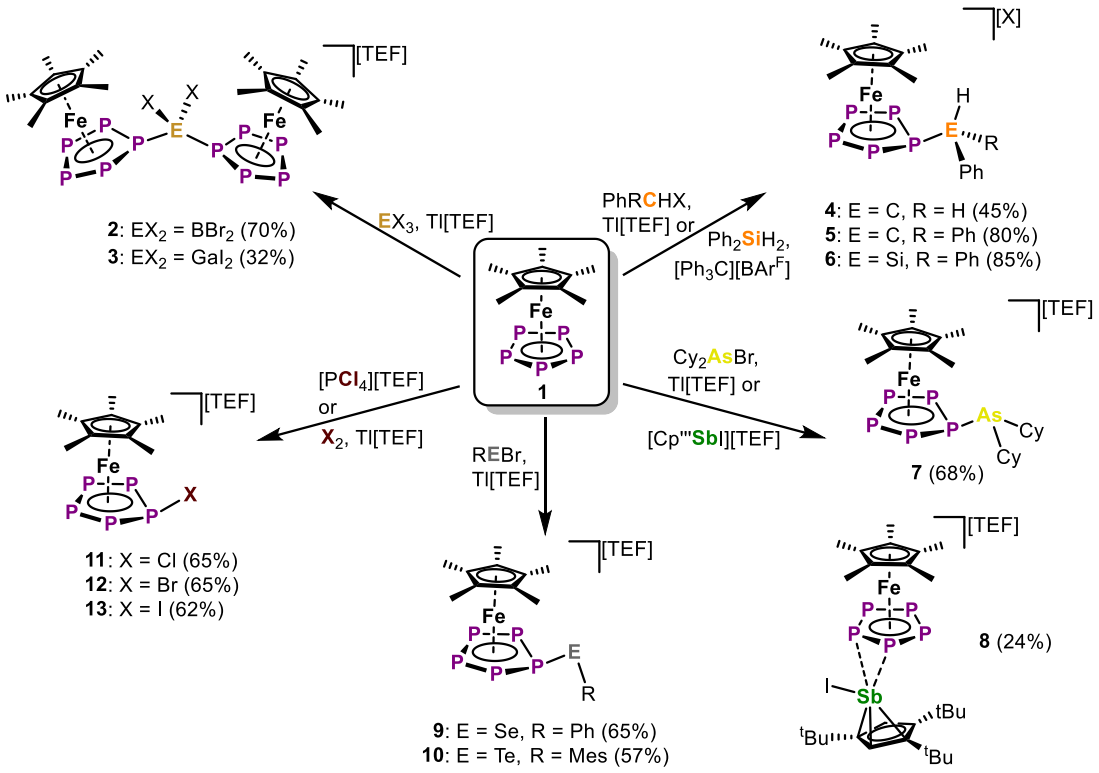

*Scheme 2: Reactivity of Pentaphosphaferrocene **1** with different cationic p-block electrophiles; Reactions were carried out in o-DFB and stirred at room temperature for several hours (for details see SI); While all other compounds are obtained as their [TEF]⁻ salt, **6** has a [B(C6F5)4]⁻ counterion; [TEF]⁻ = [Al{OC(CF3)3}4]⁻; While all displayed reactions are quantitative (by NMR), the yields provided are those for the crystalline compounds.*

our goal is the functionalization of **1** to obtain unprecedented hetero-pentaphosphole ligands, namely the aromatic all-P congeners of cyclopentadienes, we expect our approach to also be applicable to polyphosphorus ligand complexes of various sizes. Furthermore, this idea merges the functionalization of TM polyphosphorus complexes with the concept of electrophilic substitution,[2] a classic organic or organometallic (for e.g. Cp_2Fe[3] or $(C_6H_6)Cr(CO)_3$[4]) reaction. Thus, it may be transferred back to these fields and allow the electrophilic functionalization of still challenging substrates such as multifunctionalized CpR derivatives.[25] To achieve the *in situ* generation of the desired electrophiles from the respective halogenides, Tl[TEF] ([TEF]⁻ = [Al{OC(CF$_3$)$_3$}$_4$]⁻)[26] was chosen to facilitate efficient halide abstraction and simultaneously introduce the weakly coordinating [TEF]⁻ anion. However, for some cases, we also provide an easily accessible alternative avoiding Tl^+ salts by the reaction of simple element hydrides with $[Ph_3C][B(C_6F_5)_4]$ for *in situ* electrophile generation. This method has been employed e. g. for the generation of the highly reactive silylium ion precursor $[(Et_3Si)_2(\mu\text{-}H)][B(C_6F_5)_4]$.[21] However, the question arises as to how broad, if successful, the applicability of this approach would actually be, and which electrophiles could be introduced by employing it. We herein report on a synthetic strategy allowing the functionalization and P–E bond formation of **1** with twelve distinct cationic electrophiles all across the p-block elements and compare their structural and electronic properties.

6.3. Results and Discussion

Starting with group 13 electrophiles, we investigated the reactivity of **1** towards BBr_3 in the presence of Tl[TEF]. However, performing the reaction in a 1:1:1 stoichiometry leads to a reaction of the *in situ* prepared borinium cation $[BBr_2]^+$ with the solvent, resulting in a mixture of products (see SI). Repeating the reaction in the presence of a second equivalent of **1** afforded the bimetallic compound [{Cp*Fe}$_2${$\mu,\eta^{5:5}$-$(P_5)_2BBr_2$}][TEF] (**2**), featuring an unprecedented{(cyclo-$P_5)_2BBr_2$} ligand (Scheme 2). After workup, **2** could be isolated in 70% yield. To our pleasure, exchanging BBr_3 for the heavier analog GaI_3 affords the isostructural compound [{Cp*Fe}$_2${$\mu,\eta^{5:5}$-$(P_5)_2GaI_2$}][TEF] (**3**) in 32% yield. While we had already been able to demonstrate the silylation and methylation of **1**,[20] we now wanted to broaden the scope of group 14 functionalized pentaphosphole derivatives, by using better accessible and easier-to-handle electrophile precursors. In both cases, the reaction of **1** with $PhCH_2Br$ and Ph_2CHCl in the presence of Tl[TEF] affords the pentaphosphole complexes [Cp*Fe(η^5-P_5CH_2Ph)][TEF] (**4**) and [Cp*Fe(η^5-P_5CHPh_2)][TEF] (**5**) in a yield of 45% and 80%, respectively. To demonstrate an easily accessible alternative pathway towards the electrophile generation avoiding the use of Tl^+ salts, we chose to react **1** with Ph_2SiH_2 in the presence of one equivalent of $[Ph_3C][B(C_6F_5)_4]$. A rapid reaction is indicated by the color change of the solution from green to greenish red and, after simple workup, the product [Cp*Fe(η^5-P_5SiHPh_2)][$B(C_6F_5)_4$] (**6**) could be isolated in an astonishing 85% yield. In principle, it should be possible to prepare phosphino-pentaphosphole complexes similarly well as they benefit from the additional stabilization caused by P-P bond formation. However, attempts to prepare such phosphino-functionalized species are seriously affected by

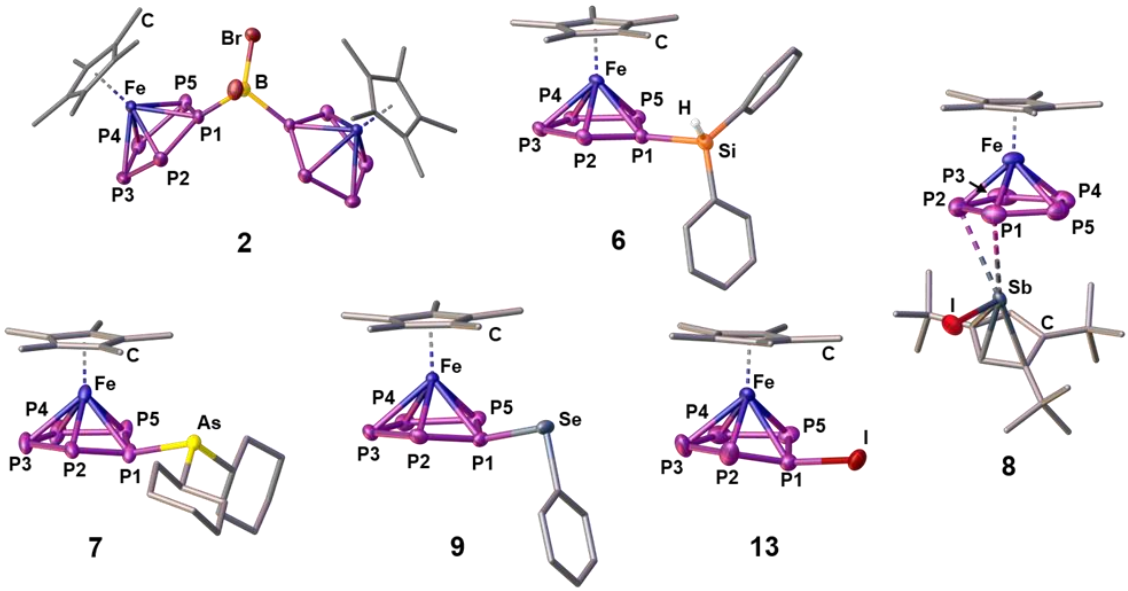

*Figure 1: Molecular structures of the cations in **2**, **6**, **7**, **8**, **9** and **13** in the solid state; Structural models for the cations in **3**, **4**, **5**, **10** and **12** as well as a list of selected structural parameters (bond lengths and angles) for all compounds can be found in the SI.*

the inherently high tendency of halogenophosphines to form phosphinophosphonium ions under Lewis acidic conditions.[27] We were able to observe the desired cation $[Cp^*Fe(\eta^5\text{-}P_5PBr_2)]^+$ spectroscopically only after reacting **1** with PBr_3 and Tl[TEF] at −80 °C (see SI). This cation, however, undergoes rapid fragmentation and rearrangement processes above –60 °C, affording a complex mixture of several polyphosphorus compounds and thus prohibiting its isolation even at low temperatures. In contrast, the reaction of **1**, Cy_2AsBr and Tl[TEF] proceeds smoothly, and from the filtered solution, the arsino-pentaphosphole complex $[Cp^*Fe(\eta^5\text{-}P_5AsCy_2)][TEF]$ (**7**) could be isolated in 68% yield. When both the electronic and steric properties of the pnictogenium cation were changed and **1** was reacted with $Cp'''SbI_2$ ($Cp''' = 1,2,4\text{-}{}^tBu_3C_5H_2$) and Tl[TEF], the unique triple-decker-like complex $[Cp^*Fe(\mu,\eta^{5:2}\text{-}P_5)SbICp'''][TEF]$ (**8**) with a P_5 middle deck could be obtained in 24% yield. The molecular structure of **8** may provide insight into the mechanism of electrophilic functionalization of **1**, which initially seems to occur through the π-system and not by

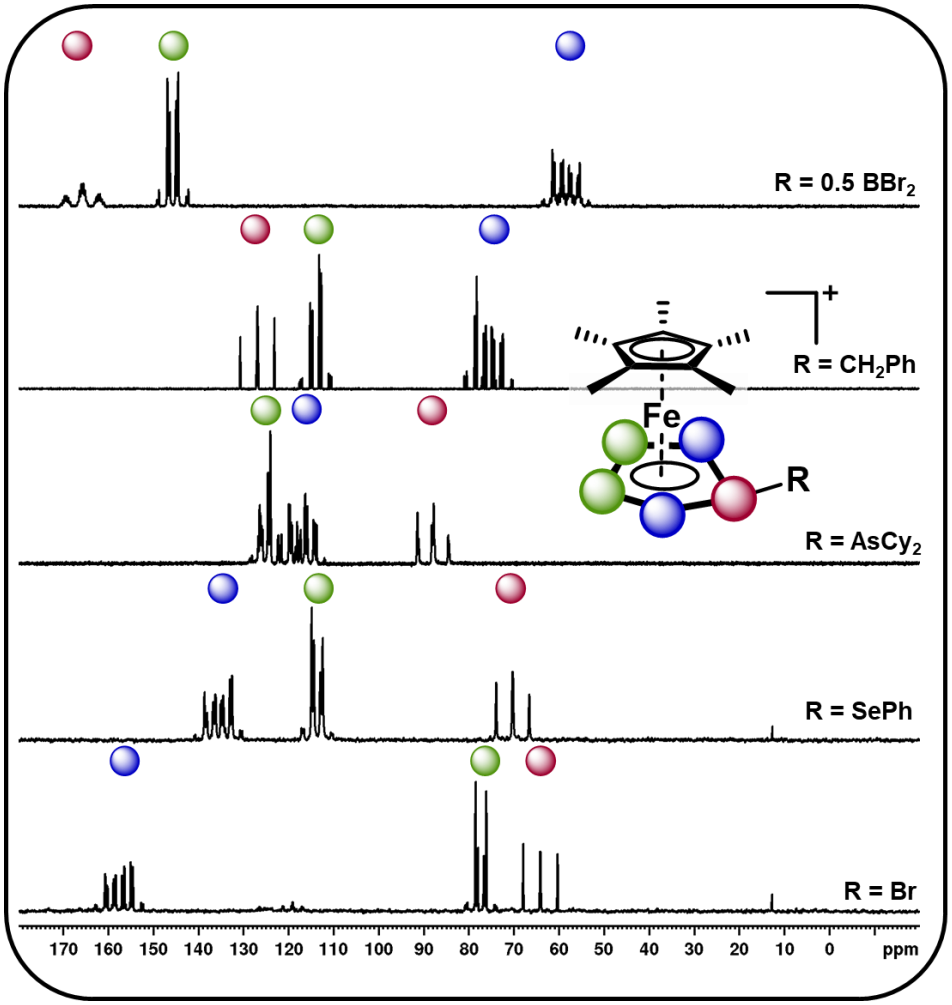

*Figure 2: $^{31}P\{^1H\}$ NMR spectra of **2**, **4**, **7**, **9** and **12** (from top to bottom, representing substitution with electrophiles from each group within the p-block) recorded in CD_2Cl_2 at room temperature and signal assignment according to the color code; respective NMR spectra of all other compounds are given in the SI.*

the lone pairs of one of the P atoms of the cyclo-P_5 ligand. Functionalization of **1** with group 16 electrophiles could be achieved by the reaction with Tl[TEF] and PhSeBr or MesTeBr, respectively. The products [Cp*Fe(η^5-P_5ER)][TEF] (**9**: E = Se, R = Ph; **10**: E = Te, R = Mes) could be isolated in 65% and 57% yield, respectively, and reveal novel seleno- or telluro-pentaphosphole ligands. To date, there is no synthetic pathway for a rational and selective monohalogenation of unsubstituted polyphosphorus frameworks, although the products would provide both insight into the mechanism of P_n halogenation reactions[28] and a high potential for further functionalization. After recently investigating the complex iodination chemistry of **1**[29] and of the diphosphorus complex [{CpMo(CO)$_2$}$_2$(μ,$\eta^{2:2}$-P_2)],[30] we were wondering if electrophilic halogen transfer could lead to the desired reactivity. Indeed, when a solution of [PCl_4][TEF] is added to **1** in *o*-DFB, the NMR spectra of the crude solution indicate the clean conversion to [Cp*Fe(η^5-P_5Cl)][TEF] (**11**) and PCl_3. After workup, **11** can be isolated in 65% yield. Similarly, the addition of X_2 to mixtures of **1** and Tl[TEF] leads to the formation of [Cp*Fe(η^5-P_5X)][TEF] (**12**: X = Br; **13**: X = I), which could be isolated in 65% and 62% yield, respectively. Notably, these halogenation reactions can be scaled up to at least 2 mmol, allowing the gram scale preparation of **11** – **13**, which opens broad perspectives for their further functionalization. While the starting material **1** is comparably robust, the pentaphosphole complexes **2** – **13** are highly sensitive towards both, moisture and air, while retaining decent thermal stability. All compounds **2** – **13** can be crystallized from mixtures of *o*-DFB or CH_2Cl_2 and *n*-hexane either at room temperature or at –30 °C. However, incommensurate modulation (**11**) or extreme disorder of anion and cation (**12**) within **11** and **12** prohibit a satisfactory refinement of their crystal structure. Compound **8** reveals a triple-decker-like arrangement (Figure 1) of the cation [Cp*Fe(μ,$\eta^{5:2}$-P_5)SbICp'''$]^+$ with elongated P-Sb interactions (3.236(2)/3.400(2) Å) and a planar P_5 ligand. The cations in **4** – **7** and **9** – **13** show the anticipated pentaphosphole complex structure with a slightly bent *cyclo*-P_5R ligand (Figure 1). In contrast, the cations in **2** and **3** are dinuclear complexes in which two {Cp*Fe} units are bridged by the respective {(*cyclo*-P_5)$_2$EX_2} (**2**: E = B, X = Br, **3**: E = Ga, X = I) ligand. The P–P bond lengths within **2** – **13** are similar and in between the sum of the covalent radii of P–P single and double bonds.[31] As observed for the parent compound [Cp*Fe(η^5-P_5H)]$^+$,[20] the substituents in the hetero-pentaphosphole complexes **2** – **7** and **9** – **13** are oriented in exo-fashion regarding the envelope of the P_5 ring (Figure 1). The respective P–E bond lengths (**2**: 1.985(7) Å, **4**: 1.853(4) Å, **5**: 1.866(4) Å, **7**: 2.348(1) Å, **9**: 2.2234(7) Å, **10**: 2.438(2) Å, **13**: 2.385(1) Å) are in the range of single bonds, whereas those in **3** (2.410(1)/2.387(1) Å) and **6** (2.3053(8) Å) are elongated compared to the sum of the respective covalent radii (P–Ga: 2.35 Å, P–Si: 2.27 Å).[31] The slight folding of the P_5 ring in these pentaphosphole complexes is far less pronounced than in anionic or neutral substituted *cyclo*-P_5R ligands possessing an envelope structure (type **I**, Scheme 1).[13,14] Interestingly, this slight folding, represented by the pyramidalization at the P1 atom (359.94° (**2**) - 350.41°(**13**)), gradually increases when going from group 13 to group 17

substituents at the pentaphosphole ligand. To elaborate the molecular structure of the obtained pentaphosphole complexes **2** – **13** in CD_2Cl_2 solution, they were investigated by multinuclear NMR spectroscopy. In general, all of them reveal the expected signals for the Cp* ligand and the respective substituents in the ^{1}H NMR spectra. Furthermore, the signals for the benzylic hydrogen atoms in **4** (δ = 4.42 ppm) and **5** (δ = 5.93 ppm) show a coupling to the P_5 moiety (**4**: $^2J_{H\text{-}P}$ = 11.2 Hz, $^3J_{H\text{-}P}$ = 3.2 Hz, **5**: $^2J_{H\text{-}P}$ = 17.3 Hz). Interestingly, the isostructural **6** does not show a similar coupling for the hydrogen atom bound to silicon, which we attribute to the dynamic behavior of this compound in solution. Accordingly, the ^{13}C{^{1}H} NMR spectra of **4** and **5** both reveal signals for the benzylic carbon atoms, which show $^1J_{C\text{-}P}$ coupling of 23 Hz for both compounds. The ^{31}P{^{1}H} NMR spectra of most of the obtained products reveal complex AMM´XX´ (**4**, **5**), AA´BB´X (**7**), AA´MXX´ (**11**), AA´MM´X (**6**, **9**, **12**) or even AA´M_2M´$_2$X$_2$X´$_2$ (**2**) spin systems (see SI). However, **3**, **8**, **10** and **13** show a highly dynamic behavior in CD_2Cl_2 solution, which cannot be resolved, not even at –80 °C. Similar dynamic broadening of signals has been observed for the parent compound[20] and might be caused by a tumbling process of the respective substituent around the P_5 ring. When comparing the ^{31}P{1H} NMR spectra (Figure 2), the signal assigned to P1 (according to Figure 1) gradually shifts to higher fields going from group 13 to group 17 substituents at the pentaphosphole moiety. Similarly, the signal assigned to P2/5 is downfield shifted following the same order, whereas the effect on the P3/4 signal is rather small (for assignment see Figure 1). While this trend should depend on various electronic and steric factors, it correlates well with the folding of the P_5 moiety (*vide supra*). The $^nJ_{P\text{-}P}$ (n = 1-2) coupling constants for all compounds are within the expected range (see SI). Additional $^1J_{P\text{-}B}$ coupling of 64 Hz is clearly visible in the ^{31}P NMR spectrum of **2** and is confirmed in its ^{11}B{^{1}H} NMR spectrum. While the dynamic behavior of the Si-substituted compound **6** in CD_2Cl_2 solution, even at –80 °C, does not allow for determination of P-P coupling constants, its ^{29}Si(DEPT135) NMR spectrum shows a clear doublet of multiplets at δ = –20 ppm with a $^1J_{Si\text{-}P}$ = 239 Hz coupling constant. Compared to the $SiEt_3$-substituted derivative ($^1J_{P\text{-}Si}$ = 61 Hz) this rather high $^1J_{P\text{-}Si}$ coupling constant may be the result of the difference in substitution at Si and the resulting change in the orbital contribution to the P-Si bonding interaction. Furthermore, the ^{31}P NMR spectrum of **9** reveals ^{77}Se satellites for the P^X signal and a clear doublet ($^1J_{P\text{-}Se}$ = 418 Hz) at δ = 287.3 ppm in the ^{77}Se{^{1}H} NMR spectrum.

To attain a better understanding of the electronic structure of the obtained complexes **2** – **13**, computational analyses at the B3LYP[32]/def2-TZVP[33] level of theory were performed. Employing solvent correction,[34] the molecular structures, determined in the solid state, are well reproduced by these computations. NBO analysis[35] indicates the interaction between the [Cp'''SbI]$^+$ fragment and **1** in **8** to be of a mostly electrostatic and dispersive nature as shown by the absence of bonding MOs and the low charge transfer from the electrophile (see SI). Furthermore, the Wiberg Bond Indices (WBIs)

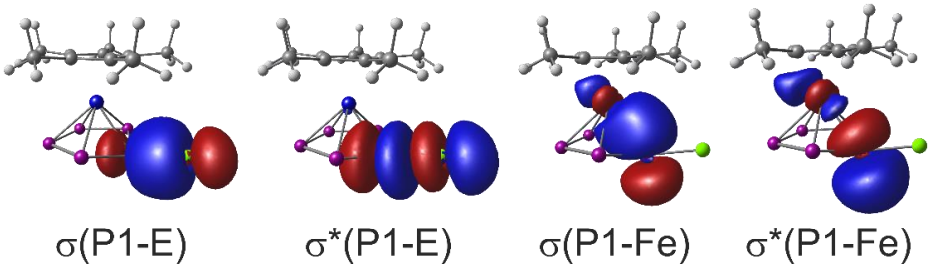

*Figure 3: Selected representative NBOs for the bonding and antibonding molecular orbitals for the P1–E and P1–Fe interactions found in the pentaphosphole complexes **2** – **7** and **9** – **13** exemplified at **11**; The σ* orbitals are unoccupied.*

for the P1–E bonds in **3** (E = Ga, WBI = 0.58/0.57) and **6** (E = Si, WBI = 0.72) suggest these bonds to be of polar single bond character. This is substantiated by the respective orbital contributions to the P1–E bonding (**3**: 79%P/21%Ga, **6**: 72%P/28%Si) and unoccupied antibonding (**3**: 21%P/79%Ga, **6**: 28%P/72%Si) molecular orbitals and agrees with the respective bond lengths determined for **3** (2.410(1)/2.387(1) Å) and **6** (2.3053(8) Å). In contrast, the WBIs of all other pentaphosphole complexes corroborate the P1–E single bonds (WBI = 0.82 – 0.99) determined from their respective solid-state structures (Table 1, column 3). Accordingly, the orbital contributions to the respective

*Table 1: Selected computational and experimental parameters for the pentaphosphole complexes **2** – **7** and **9** – **13**.*

Com-pound	WBI (P1-E)	Orbital contribution P1-E	*d*(P1-E)/ Å		Charge Transfer {**1**}→{E}[b]	NICS(+/-1)$_{zz}$[c]
			Exp.	Theo.		
2[a]	0.89	57/43	1.985(7)	2.01	0.57[d]	-31.2/-30.5
3[a]	0.58	79/21	2.399(1)	2.46	0.56[d]	-34.7/-34.3
4	0.92	45/55	1.853(4)	1.86	0.85	-33.7/-32.8
5	0.88	45/55	1.866(4)	1.89	0.84	-31.2/-32.1
6	0.72	72/28	2.3053(8)	2.35	0.68	-34.3/-34.7
7	0.82	67/33	2.348(1)	2.38	0.63	-34.0/-33.4
9	0.98	53/47	2.2234(7)	2.25	0.83	-33.5/-32.6
10	0.92	62/38	2.438(2)	2.48	0.74	-34.9/-34.0
11	0.96	36/64	-	2.03	1.09	-31.0/-30.9
12	0.98	41/59	-	2.21	1.05	-31.8/-31.7
13	0.99	51/49	2.385(1)	2.42	0.94	-34.3/-34.2

*[a] As **2** and **3** are dinuclear complexes the average of the actual values is provided for clarity, NICS values have only been obtained on one the P_5 rings; [b] The charge transfer from fragment {**1**} to the respective fragments {E} is obtained by ECDA; [c] NICS(+/-1)$_{zz}$ values are computed on the ligand geometries from the optimized structures of the complexes **2** – **7** and **9** – **13** after removal of the {Cp*Fe}$^+$ fragments; [d] The charge transfer is given per fragment {**1**}.*

P1–E bonding and antibonding molecular orbitals (Figure 3, left) are more balanced (Table 1, column 2), suggesting more covalent bonding in these cases. Analyzing the summed up natural charges for the fragments {Cp*Fe(η^5-P_5)} ({**1**}) and {R_nE} ({E}, n = 1 – 3) (see SI) of **2** – **13** reveals correlation between the positive charge accumulation at {**1**} and the electronegativity of the central atom of the electrophiles. As **3** and **6** incorporate the least electronegative central atoms in the respective electrophile, they show the lowest charge accumulation at {**1**} in the series of the herein reported pentaphosphole complexes (see Table S 13). The charge transfer from {**1**} to {E} (Table 1, column 5) obtained by an extended charge decomposition analysis (ECDA)[36] on the optimized structures of **2** – **13** shows a similar trend but hints towards other factors to be of relevance as well. Thus, effective charge transfer seems to be at least one of the governing factors for the formation of covalent P1–E bonds and consequently less labile pentaphosphole ligands, which is in line with the highly dynamic behavior of **3** and **6** in CD_2Cl_2 solution (*vide supra*). Similar to the parent compound [Cp*Fe(η^5-P_5H)]$^+$,[20] the pentaphosphole complexes **2** – **7** and **9** – **13** exhibit a pronounced P1-Fe bonding interaction (Figure 3, right), which is represented by WBIs of 0.34 – 0.36. This interaction manifests their η^5-binding mode and hints towards the aromatic character of the pentaphosphole ligands. To clarify the latter point, we computed the NICS(0/1/–1)$_{zz}$[37] values for the ligand geometries from the optimized structures of the cations **2** – **7** and **9** – **13** on the PBE0[38]/aug-pcSseg-1[39]/def2-TZVPPD[33,40] level of theory. Consequently, these NICS(+/–1)$_{zz}$ values (Table 1) corroborate the aromaticity of the *cyclo*-P_5R ligands but are smaller than the ones for the *cyclo*-P_5^- ligand in **1** (NICS(+/–1)$_{zz}$ = –40.5). However, they compare well with that determined for the parent pentaphosphole complex [Cp*Fe(η^5-P_5H)]$^+$ (NICS(+/–1)$_{zz}$ = –32.1/–31.2).[20] A rough correlation between the pyramidalization at P1 and the computed NICS values is observed, although this effect is not accentuated and has minor exceptions (see SI).

Thus, we demonstrate *in situ* electrophilic functionalization of **1** to be a highly versatile approach towards a variety of unprecedented hetero-pentaphosphole complexes. However, to provide a first insight into the generality of this synthetic strategy, we expanded our investigations on the electrophilic functionalization of [Cp'''Ta(CO)$_2$(η^4-P_4)] (**14**)[41] bearing an aromatic tetra-phospha-*cyclo*-butadiendiide (*cyclo*-P_4^{2-}) ligand. Initial reactivity studies reveal that two equivalents of **14** react with BBr_3 in the presence of Tl[TEF] to afford [{Cp'''Ta(CO)$_2$}$_2${μ,$\eta^{4:4}$-((P_4)$_2$$BBr_2$})][TEF] (**15**) in 74% yield. Compound **15** crystallizes as orange blocks and shows a similar dinuclear structure as found in **2**, which was confirmed by X-ray structural analysis. Interestingly, the metal fragments in **15** are rotated by nearly 180° compared to those in **2** and the P1/P5 atoms are bent out of the former P_4 plane by only 1.2(2)/0.7(2)°, respectively. The P–P bond lengths (2.124(4) – 2.171(4) Å) in the {(*cyclo*-P_4)$_2$$BBr_2$} ligand are slightly shortened compared to the starting material **14** (2.1555(15) – 2.1800(15) Å),[41] but still in between covalent P–P single (2.22 Å) and double bonds (2.04 Å).[31] The P1/P5-B bond lengths (1.997(10)/1.996(9) Å) are within the expected range for P–B single bonds (1.96 Å) and

the P1–B–P5 angle of 112.3(5)° leads to a slightly distorted tetrahedral geometry around the B atom. The ^{31}P NMR spectrum of **15** in CD_2Cl_2 reveals a complicated $A_2A'_2MM'XX'Z$ (Z = B) spin systems with resonances located at –15.4, –37.1 and –80.8 ppm, agreeing with its structure being retained in solution. $^1J_{P\text{-}B}$ coupling is clearly visible for the $P^{M/M'}$ resonance and consequently the respective $^{11}B\{^1H\}$ NMR spectrum shows a triplet at –10.2 ppm with a $^1J_{P\text{-}B}$ coupling constant of 60 Hz.

The solid state structure of **15** is well reproduced by DFT calculations (B3LYP[32]/def2-TZVP[33], PCM solvent correction for CH_2Cl_2), which give further insight into its electronic structure. The WBIs for the P1/P5–B bonds (0.88/0.86) in **15** are in agreement with covalent P–B single bonds. Furthermore, the orbital contributions to these P–B bonds (58%P/42%B%) are in line with this formulation. While the positive charge within **15** is distributed across both {**14**} fragments, the B atom shows negative charge accumulation (natural charge of –0.44), labelling the $\{(cyclo\text{-}P_4)_2BBr_2\}$ ligand in **15** as a borate bridged bis-tetra-phospha butadiendiide. At last, the respective $NICS(+/-1)_{zz}$ values indicate the aromaticity of the *cyclo*-P_4 ligand of **14** (–3.3/–3.5) to be preserved within the ligand geometry in **15** (–9.5/–9.7, –10.8/–9.6), although it is less expressed as in the pentaphosphole complexes **2**–**7** and **9**–**13**.

6.4. Conclusions

In conclusion, we demonstrated a general synthetic strategy to obtain a broad range of hetero-pentaphosphole coordination complexes bearing substituents from across the whole p-block of the periodic table. While the group 14 – 17 substituted species $[Cp^*Fe(\eta^5\text{-}P_5E)]^+$ (E = CH_2Ph (**4**), $CHPh_2$ (**5**), $SiHPh_2$ (**6**), $AsCy_2$ (**7**), SePh (**9**), TeMes (**10**), Cl (**11**), Br (**12**), I (**13**)) reveal the desired mononuclear aromatic pentaphosphole complexes, the group 13 functionalized species result in unexpected dinuclear complexes $[\{Cp^*Fe\}_2\{\mu,\eta^{5:5}\text{-}(P_5)_2EX_2\}][TEF]$ (EX_2 = BBr_2 (**2**), GaI_2 (**3**)) with bridging bis-pentaphosphole $\{(cyclo\text{-}P_5)_2EX_2\}$ ligands. In contrast, the alternation of the electronic

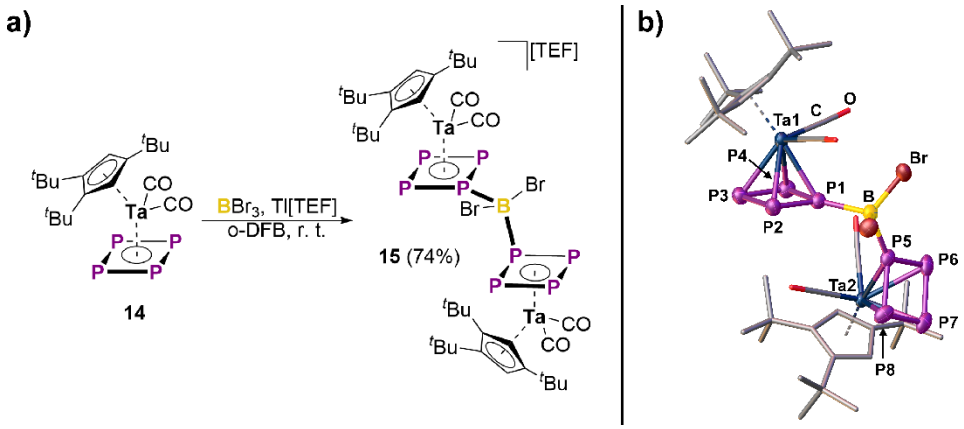

*Figure 4: a) Reactivity of **14** towards the in situ formed dibromoborinium ion "$[BBr_2][TEF]$"; b) Molecular structure of **15** in the solid state (hydrogen atoms and the counter ion are omitted for clarity and thermal ellipsoids are drawn at the 50% probability level).*

and steric properties of the employed electrophile, as in $[Cp'''SbI]^+$, leads to the formation of the triple-decker-like arrangement observed in $[Cp^*Fe(\mu,\eta^{5:2}\text{-}P_5)SbICp''']$[TEF] (**8**). This paves the way towards the investigation of the chemical, physical and electronic properties of these all-P congeners of prototypical cyclopentadienes, which have raised considerable theoretical interest over the past decades.[8] Furthermore, this report highlights the versatility of the electrophilic functionalization of transition metal-stabilized polyphosphorus frameworks. While some P–E bond formation processes at such compounds have been observed, these are highly specific towards certain electrophile/nucleophile combinations (*vide supra*). In contrast, our approach shows an unprecedented diversity and thus allows P–E bond formation for elements all across the p-block. The generality of this approach is proven by the additional electrophilic aromatic functionalization of the *cyclo*-P_4 ligand of **14**, which furnishes $[\{Cp'''Ta(CO)_2\}_2(\mu,\eta^{4:4}\text{-}(P_4)_2BBr_2)]$[TEF] (**15**), bearing a unique borate bridged bis-tetra-phospha butadiendiide ligand. Finally, the obtained cationic pentaphosphole complexes **2** – **13** represent highly interesting starting materials (e.g. the halogen derivatives **11** – **13**) towards even further functionalized polyphosphorus frameworks, which is underlined by the gram scale synthesis of selected representatives (**5**, **11** – **13**).

6.5. Supporting Information

6.5.1. Experimental Procedures

General Considerations

All manipulations were carried out using standard Schlenk techniques at a Stock apparatus under N_2 as an inert gas or in a glove box with Ar atmosphere. All glassware was dried with a heat gun (600 °C) for at least 30 min prior to use. *o*-DFB (1,2-difluorobenzene) was distilled from P_2O_5, CD_2Cl_2 was distilled from CaH_2 and other solvents were directly taken from an MBraun SPS-800 solvent purification system and degassed at room temperature. Solution ^{1}H (400.130 MHz), ^{11}B (128.432 MHz) ^{13}C (100.627 MHz), ^{19}F (376.498 MHz), ^{29}Si (79.485 MHz), ^{31}P (161.976 MHz) and ^{77}Se (76.334 MHz) NMR spectra were recorded at an Avance400 (Bruker) spectrometer using $(H_3C)_4Si$ (^{1}H, ^{13}C, ^{29}Si), $BF_3{\cdot}OEt_2$ (^{11}B) $CFCl_3$ (^{19}F), $SeMe_2$ (^{77}Se) or 85% phosphoric acid (^{31}P), respectively, as external standards. Chemical shifts (δ) are provided in parts per million (ppm) and coupling constants (*J*) are reported in Hertz (Hz). Chemical shifts and coupling constants for all $^{31}P\{^{1}H\}$ and ^{31}P NMR spectra were derived from spectral simulation using the built-in simulation package of TopSpin3.2. The following abbreviations are used: s = singlet, d = doublet, dd = doublet of doublets, dt = doublet of triplets, t = triplet, td = triplet of doublets br = broad and m = multiplet. ESI mass spectra were recorded at the internal mass spectrometry department using a ThermoQuest Finnigan TSQ 7000 mass spectrometer or by the first author on a Waters Micromass LCT ESI-TOF mass-spectrometer and peak assignment was performed using the Molecular weight calculator 6.50.[42] Elemental analysis of the products was conducted by the elemental analysis department at the University of Regensburg using an Elementar Vario EL. The starting materials $[Cp^*Fe(\eta^5\text{-}P_5)]$ (**1**),[9a] Tl[TEF],[26b] $[Ph_3C][B(C_6F_5)_4]$,[43] Cy_2AsCl,[44] PhSeBr,[45] MesTeBr,[46] NaCp''',[47] $[Cp'''Ta(CO)_2(\eta^4\text{-}P_4)]$ (**14**)[41] were synthesized following literature procedures. All other chemicals were purchased from commercial vendors and used without further purification.

*[{Cp*Fe}$_2${(η^5-P$_5$)$_2$BBr$_2$}][TEF] (**2**)*

[Cp*Fe(η^5-P$_5$)] (0.2 mmol, 70 mg, 2 eq.) and Tl[TEF] (0.1 mmol, 117 mg, 1 eq.) were dissolved in 4 mL of *o*-DFB and cooled to -30 °C. BBr_3 (0.1 mmol, 10 µL, 1 eq.) was added with a syringe which afforded a rapid colour change to brownish green and the precipitation of white solid (TlBr). The resulting solution was stirred for 1.5 h, filtered, and then layered with 40 mL of *n*-hexane. After storage for eight days the product [{Cp*Fe}$_2${(η^5-P$_5$)$_2$BBr$_2$}][TEF] (**2**) could be isolated as crystalline dark brownish green sticks, which were of X-ray quality.

Yield: 130 mg (0.070 mmol, 70%)

Elemental analysis: calc. (%) for [{Cp*Fe}$_2${(η^5-P$_5$)$_2$BBr$_2$}][TEF]·(*n*-hex)$_{0.4}$ ($C_{38.4}H_{35.6}BO_4F_{36}AlP_{10}Fe_2Br_2$): C: 24.74 H: 1.92

found (%): C: 25.13 H: 1.76

ESI(+) MS (*o*-DFB): *m/z* (%) = 345.92 (30%) [Cp*Fe(η^5-P$_5$)]$^+$, 417.98 (100%) [Cp*FeP$_6$·MeCN]$^+$, (strong fragmentation)

NMR (CD_2Cl_2, 298 K): **^{1}H**: δ/ppm = 1.76 (s, 15 H, Cp*)

^{31}P{^{1}H}: AA´M$_2$M´$_2$X$_2$X´$_2$ spin system δ/ppm = 165.8 (m, $^1J_{PA\text{-}PX/X´}$ = 604.5/589.8 Hz, $^2J_{PA\text{-}PM/M´}$ = 6.8/3.8 Hz, $^2J_{PA\text{-}PA´}$ = 123.6 Hz, $^1J_{PA/A´\text{-}B}$ = 64 Hz, 2 P, P$^{A/A´}$), 145.6 (m, $^1J_{PM/M´\text{-}PX/X´}$ = 447.5/436.8 Hz, $^1J_{PM\text{-}PM´}$ = 415.3 Hz, $^2J_{PM/M´\text{-}PX´/X}$ = -58.4/-47.0 Hz, $^2J_{PM/M´\text{-}PA}$ = 6.8/3.8 Hz, 4 P, P$^{M/M´}$), 58.4 (m, $^1J_{PX/X´\text{-}PA}$ = 604.5/589.8 Hz, $^1J_{PX/X´\text{-}PM/M´}$ = 447.5/436.8 Hz, $^2J_{PX/X´\text{-}PM´/M}$ = -58.4/-47.0 Hz, $^2J_{PX\text{-}PX´}$ = 36.9 Hz, 4 P, P$^{X/X´}$)

^{31}P: AA´M$_2$M´$_2$X$_2$X´$_2$ spin system δ/ppm = 165.8 (m, $^1J_{PA\text{-}PX/X´}$ = 604.5/589.8 Hz, $^2J_{PA\text{-}PM/M´}$ = 6.8/3.8 Hz, $^2J_{PA\text{-}PA´}$ = 123.6 Hz, $^1J_{PA/A´\text{-}B}$ = 64 Hz, 2 P, P$^{A/A´}$), 145.6 (m, $^1J_{PM/M´\text{-}PX/X´}$ = 447.5/436.8 Hz, $^1J_{PM\text{-}PM´}$ = 415.3 Hz, $^2J_{PM/M´\text{-}PX´/X}$ = -58.4/-47.0 Hz, $^2J_{PM/M´\text{-}PA}$ = 6.8/3.8 Hz, 4 P, P$^{M/M´}$), 58.4 (m, $^1J_{PX/X´\text{-}PA}$ = 604.5/589.8 Hz, $^1J_{PX/X´\text{-}PM/M´}$ = 447.5/436.8 Hz, $^2J_{PX/X´\text{-}PM´/M}$ = -58.4/-47.0 Hz, $^2J_{PX\text{-}PX´}$ = 36.9 Hz, 4 P, P$^{X/X´}$)

^{11}B: δ/ppm = -15.6 (t, $^1J_{B\text{-}PA/A´}$ = 64 Hz, 1 B, {BBr_2})

^{19}F{^{1}H}: δ/ppm = - 75.6 (s, [TEF]$^-$)

*[{Cp*Fe}$_2${(η^5-P_5)$_2$$GaI_2$}][TEF] (**3**)*

[Cp*Fe(η^5-P_5)] (0.2 mmol, 70 mg, 2 eq.), Tl[TEF] (0.1 mmol, 117 mg, 1 eq.) and GaI_3 (0.1 mmol, 45 mg, 1 eq.) were dissolved in 5 mL of *o*-DFB, which afforded a brown solution, with the GaI_3 still being suspended. Stirring this solution for three days lead to a colour change to brownish green and the formation of a yellow precipitate (TlI). After filtration, this solution was layered with 50 mL of *n*-hexane, which after nine days afforded [{Cp*Fe}$_2${(η^5-P_5)$_2$$GaI_2$}][TEF] (**3**) as dark brownish green stick shaped crystals of X-ray quality.

Yield: 63 mg (0.032 mmol, 32%)

Elemental analysis: calc. (%) for [{Cp*Fe}$_2${(η^5-P_5)$_2$$GaI_2$}][TEF] ($C_{36}H_{30}O_4F_{36}AlP_{10}Fe_2GaI_2$): C: 21.81 H: 1.53

found (%): C: 22.17 H: 1.37

ESI(+) MS (*o*-DFB): *m/z* (%) = 345.92 (60%) [Cp*Fe(η^5-P_5)]$^+$, (strong fragmentation)

NMR (CD_2Cl_2, 298 K): **^{1}H**: δ/ppm = 1.63 (s, 15 H, Cp*)

^{31}P{^{1}H}: δ/ppm = 117.2 (br)

^{31}P: δ/ppm = 117.2 (br)

^{19}F{^{1}H}: δ/ppm = -75.6 (s, [TEF]$^-$)

NMR (CD_2Cl_2, 193 K): **^{1}H**: δ/ppm = 1.62 (s, 15 H, Cp*)

^{31}P{^{1}H}: δ/ppm = 92.7 (m(br), 6 P), 141.6 (m(br), 4 P)

*[Cp*Fe(η^5-P_5CH_2Ph)][TEF] (**4**)*

$PhCH_2Br$ (0.2 mmol, 24 μL, 1 eq.) was added dropwise to a solution of [Cp*Fe(η^5-P_5)] (0.2 mmol, 70 mg, 1 eq.) and Tl[TEF] (0.1 mmol, 117 mg, 1 eq.) in 4 mL *o*-DFB, which resulted in a gradual colour change from brownish green to red and the formation of a white precipitate (TlBr) over the course of 24 h. The resulting mixture was filtered and 20 mL of *n*-hexane were added, which afforded the precipitation of [Cp*Fe(η^5-P_5CH_2Ph)][TEF] (**4**) as a dark red solid. This solid was washed two times with 10 mL of *n*-hexane, each, dried and then dissolved in 2 mL of *o*-DFB. Layering this solution with 20 mL of *n*-hexane and storing it for one week resulted in the formation of large red crystals of **4** in X-ray quality.

Yield: 127 mg (0.09 mmol, 45%)

Elemental analysis: calc. (%) for [Cp*Fe(η^5-P_5CH_2Ph)][TEF] ($C_{33}H_{22}O_4F_{36}AlP_5Fe$): C: 28.23 H: 1.58

found (%): C: 28.73 H: 1.36

ESI(+) MS (*o*-DFB): *m/z* (%) = 437.03 (100%) [Cp*Fe(η^5-P_5CH_2Ph)]$^+$

NMR (CD_2Cl_2, 298 K): **^{1}H**: δ/ppm = 1.73, (s, 15 H, Cp*), 4.42 (dt, $^2J_{H\text{-}PA}$ = 11.2 Hz, $^3J_{H\text{-}PX/X'}$ = 3.2 Hz, 2 H, C$\underline{H_2}$Ph), 7.40–7.55 (m, 5 H, Ph)

^{31}P{^{1}H}: δ/ppm = 126.8 (m, $^1J_{PA\text{-}PX/X'}$ = 615.4/615.2 Hz, $^2J_{PA\text{-}PM/M'}$ = 10.2/9.0 Hz, 1 P, P^A), 113.9 (m, $^1J_{PM/M'\text{-}PX/X'}$ = 455.4/454.6 Hz, $^1J_{PM\text{-}PM'}$ = 407.0 Hz, $^2J_{PM/M'\text{-}PX'/X}$ = -56.0/-55.7 Hz, $^2J_{PM/M'\text{-}PA}$ = 10.2/9.0 Hz, 2 P, $P^{M/M'}$), 75.7 (m, $^1J_{PX/X'\text{-}PA}$ = 615.4/615.2 Hz, $^1J_{PX/X'\text{-}PM/M'}$ = 455.4/454.6 Hz, $^2J_{PX/X'\text{-}PM'/M}$ = -56.0/-55.7 Hz, $^2J_{PX\text{-}PX'}$ = 42.3 Hz, 2 P, $P^{X/X'}$)

^{31}P: δ/ppm = 126.8 (m, $^1J_{PA\text{-}PX/X'}$ = 617.1/613.6Hz, $^2J_{PA\text{-}PM/M'}$ = 10.5/9.1 Hz, $^2J_{PA\text{-}H}$ = 11.3 Hz, 1 P, P^A), 113.9 (m, $^1J_{PM/M'\text{-}PX/X'}$ = 459.3/450.9 Hz, $^1J_{PM\text{-}PM'}$ = 407.0 Hz, $^2J_{PM/M'\text{-}PX'/X}$ = -60.6/-51.2 Hz, $^2J_{PM/M'\text{-}PA}$ = 10.5/9.1 Hz, 2 P, $P^{M/M'}$), 75.7 (m, $^1J_{PX/X'\text{-}PA}$ = 617.1/613.6 Hz, $^1J_{PX/X'\text{-}PM/M'}$ = 459.3/450.9 Hz, $^2J_{PX/X'\text{-}PM'/M}$ = -60.6/-51.2 Hz, $^2J_{PX\text{-}PX'}$ = 42.1Hz, 2 P, $P^{X/X'}$)

^{13}C{^{1}H}: δ/ppm = 11.0 (s, $C_5\underline{Me_5}$), 26.1 (d, $^1J_{C\text{-}PA}$ = 23 Hz, $\underline{C}H_2Ph$), 97.7 (s, $\underline{C_5}Me_5$), 121.3 (q, $^1J_{C\text{-}F}$ = 292 Hz, [Al{OC($\underline{C}F_3$)$_3$}$_4$]$^-$), 129.2 (s, Ph), 129.3 (s, Ph), 130.2 (s, Ph), 132.4 (s, Ph)

^{19}F{^{1}H}: δ/ppm = –75.6 (s, [TEF]$^-$)

*[Cp*Fe(η^5-P_5CHPh_2)][TEF] (**5**)*

Ph_2CHCl (0.2 mmol, 36 μL, 1 eq.) was added dropwise to a solution of [Cp*Fe(η^5-P_5)] (0.2 mmol, 70 mg, 1 eq.) and Tl[TEF] (0.1 mmol, 117 mg, 1 eq.) in 4 mL *o*-DFB, which resulted in a gradual colour change from brownish green to red and the formation of a white precipitate (TlCl) over the course of 3 h. The resulting mixture was filtered and 20 mL of *n*-hexane were added, which afforded the precipitation of [Cp*Fe(η^5-P_5CHPh_2)][TEF] (**5**) as a dark red solid. This solid was washed two times with 10 mL of *n*-hexane, each, dried and then dissolved in 2 mL of *o*-DFB. Layering this solution with 40 mL of *n*-hexane and storing it for one week resulted in the formation of large red crystals of **5** in X-ray quality.

Note: The order of addition in this reaction can be exchanged and the reaction could be scaled up to 2 mmol, which allows the gram scale isolation of **5**.

Yield: 230 mg (0.16 mmol, 80%)

Elemental analysis: calc. (%) for [Cp*Fe(η^5-P_5CHPh_2)][TEF]·$(C_6H_4F_2)_{0.4}$ ($C_{41.4}H_{27.6}O_4F_{36.8}AlP_5Fe$): C: 32.59 H: 1.82

found (%): C: 32.80 H: 1.89 (traces of *o*-DFB are also detected in the ^{1}H NMR spectrum of isolated crystals)

ESI(+) MS (*o*-DFB): *m/z* (%) = 513.02 (100%) [Cp*Fe(η^5-P_5CHPh_2)]$^+$

NMR (CD_2Cl_2, 298 K): **^{1}H**: δ/ppm = 1.64 (s, 15 H, Cp*), 5.93 (d, $^2J_{H\text{-}P}$ = 17.3 Hz, 1 H, C<u>H</u>Ph_2), 7.43-7.72 (br, 10 H, CH<u>Ph_2</u>)

^{31}P{^{1}H}: δ/ppm = 156.2 (m, $^1J_{PA\text{-}PX/X'}$ = 629.8/625.3 Hz, $^2J_{PA\text{-}PM/M'}$ = 17.5/6.0 Hz, 1 P, P^A), 115.0 (m, $^1J_{PM/M'\text{-}PX/X'}$ = 450.4/449.5 Hz, $^1J_{PM\text{-}PM'}$ = 412.2 Hz, $^2J_{PM/M'\text{-}PX'/X}$ = -54.5/-54.0 Hz, $^2J_{PM/M'\text{-}PA}$ = 17.5/6.0 Hz, 2 P, $P^{M/M'}$), 77.0 (m, $^1J_{PX/X'\text{-}PA}$ = 629.8/625.3 Hz, $^1J_{PX/X'\text{-}PM/M'}$ = 450.4/449.5 Hz, $^2J_{PX/X'\text{-}PM'/M}$ = -54.5/-54.0 Hz, $^2J_{PX\text{-}PX'}$ = 43.1 Hz, 2 P, $P^{X/X'}$)

^{31}P: δ/ppm = 156.2 (m, $^1J_{PA\text{-}PX/X'}$ = 628.5/626.4 Hz, $^2J_{PA\text{-}PM/M'}$ = 14.9/9.6 Hz, $^2J_{PA\text{-}H}$ = 17.3 Hz, 1 P, P^A), 115.0 (m, $^1J_{PM/M'\text{-}PX/X'}$ = 452.7/447.1 Hz, $^1J_{PM\text{-}PM'}$ = 412.1 Hz, $^2J_{PM/M'\text{-}PX'/X}$ = -56.5/-52.1 Hz, $^2J_{PM/M'\text{-}PA}$ = 14.9/9.6 Hz, 2 P, $P^{M/M'}$), 77.0 (m, $^1J_{PX/X'\text{-}PA}$ = 628.5/626.4 Hz, $^1J_{PX/X'\text{-}PM/M'}$ = 452.7/447.1 Hz, $^2J_{PX/X'\text{-}PM'/M}$ = -56.5/-52.1 Hz, $^2J_{PX\text{-}PX'}$ = $^2J_{PX\text{-}PX'}$ = 42.9 Hz, 2 P, $P^{X/X'}$)

^{13}C{^{1}H}: δ/ppm = 11.0 (s, C_5<u>Me_5</u>), 49.3 (d, $^1J_{C\text{-}P}$ = 23 Hz, <u>C</u>HPh_2), 97.9 (s, <u>C_5</u>Me_5), 121.3 (q, $^1J_{C\text{-}F}$ = 292 Hz, [Al{OC(<u>C</u>F_3)$_3$}$_4$]$^-$), 128.7 (d, $^2J_{C\text{-}P}$ = 8 Hz, Ph), 129.6 (s, Ph), 130.1 (s, Ph)

^{19}F{^{1}H}: δ/ppm = –75.6 (s, [TEF]$^-$)

*[Cp*Fe(η^5-P_5SiHPh_2)][$B(C_6F_5)_4$] (**6**)*

Ph_2SiH_2 (0.2 mmol, 37 μL, 1 eq.) were added to a mixture of [Cp*Fe(η^5-P_5)] (0.2 mmol, 70 mg, 1 eq.) and [Ph_3C][$B(C_6F_5)_4$] (0.2 mmol, 185 mg, 1 eq.) in 3 mL of *o*-DFB which afforded a rapid colour change to brownish green. The mixture was stirred for one hour and then directly layered with 30 mL of n-hexane. Storing this mixture for one day at room temperature afforded [Cp*Fe(η^5-P_5SiHPh_2)][$B(C_6F_5)_4$] (**6**) as brownish green plate shaped crystals of X-ray quality. After decanting the solution and thoroughly drying the crystals under reduced pressure (10^{-3} mbar), **6** could be isolated as a pure compound.

Yield: 205 mg (0.17 mmol, 85%)

Elemental analysis: calc. (%) for [Cp*Fe(η^5-P_5SiHPh_2)][$B(C_6F_5)_4$] ($C_{46}H_{26}BF_{20}SiP_5Fe$): C: 45.73 H: 2.17

found (%): C: 45.38 H: 1.84

ESI(+) MS (*o*-DFB): *m/z* (%) = 347.01 (100%) [Cp*Fe(h^5-P_5H)]$^+$ (formed by fragmentation in the mass spectrometer)

NMR (CD_2Cl_2, 300 K): **^{1}H**: δ/ppm = 1.51 (s(br), 15 H, Cp*), 6.45 (s, $^1J_{H\text{-}Si}$ = 237.5 Hz, 1 H, Si<u>H</u>Ph_2), 7.63 (m, 4 H, SiH<u>Ph</u>$_2^m$), 7.70 (m, 2 H SiH<u>Ph</u>$_2^p$), 8.00 (m, 4 H, SiH<u>Ph</u>$_2^o$)

^{31}P{^{1}H}, 300 K: δ/ppm = 83.6 (br, $\omega_{1/2}$ = 1300 Hz, P^X), 104.0 (br, , $\omega_{1/2}$ = 1600 Hz, $P^{M/M'}$), 145.6 (br, $\omega_{1/2}$ = 1400 Hz, $P^{A/A'}$)

^{19}F{^{1}H}: δ/ppm = –167.1 (t, $^3J_{F\text{-}F}$ = 19 Hz, 8 F, m-C_6<u>F</u>$_5$), –163.2 (t, $^3J_{F\text{-}F}$ = 19 Hz, 4 F, p-C_6<u>F</u>$_5$), –132.6 (br, 8 F, o-C_6<u>F</u>$_5$)

NMR (CD_2Cl_2, 243 K): **^{29}Si(DEPT135)**: δ/ppm = –20 (dm, $^1J_{Si\text{-}P}$ = 239 Hz, $SiHPh_2$)

NMR (CD_2Cl_2, 193 K): **^{1}H**: δ/ppm = 1.40 (s(br), 15 H, Cp*), 6.39 (s, $^1J_{H\text{-}Si}$ = 237.5 Hz, 1 H, Si<u>H</u>Ph_2), 7.59 (m, 4 H, SiH<u>Ph</u>$_2^m$), 7.65 (m, 2 H SiH<u>Ph</u>$_2^p$), 7.97 (m, 4 H, SiH<u>Ph</u>$_2^o$)

^{31}P{^{1}H}: δ/ppm = 76.4 (t (br), P^X), 102.6 (m, $P^{M/M'}$), 141.1 (m, $P^{A/A'}$)

^{31}P: δ/ppm = 76.4 (t (br), 1 P, P^X), 102.6 (m, 2 P, $P^{M/M'}$), 141.1 (m, 2 P, $P^{A/A'}$)

*[Cp*Fe(η^5-P_5AsCy_2)][TEF] (**7**)*

Cy_2AsCl (0.2 mmol, 39 μL, 1 eq.) was added to a suspension of LiBr (3 mmol, 261 mg, 15 eq.) in 2 mL of toluene (Similar halogen exchange has been described for chlorophosphanes).[48] The mixture was stirred for two hours and the white precipitate allowed to settle. The resulting solution was filtered to a mixture of [Cp*Fe(η^5-P_5)] (0.2 mmol, 70 mg, 1 eq.) and Tl[TEF] (0.2 mmol, 234 mg, 1 eq.) in 3 mL of *o*-DFB which afforded a rapid colour change to dark red and the precipitation of a colourless solid (TlBr). The suspension was stirred for 3 h and 20 mL of *n*-hexane were added to precipitate [Cp*Fe(η^5-P_5AsCy_2)][TEF] (**7**) as a dark red solid. The supernatant was decanted, the solid washed two times with 10 mL of toluene, each, one time with 10 mL of *n*-hexane, and then dried at reduced pressure (10^{-3} mbar). 2 mL of *o*-DFB were added to give a dark red solution above a colourless solid. The solution was filtered and 20 mL of *n*-hexane were added to precipitate **7** as a red solid, which was isolated after drying at reduced pressure (10^{-3} mbar). **7** could be recrystallized from *o*-DFB/*n*-hexane mixtures as red block shaped crystals of X-ray quality.

Yield: 210 mg (0.135 mmol, 68%)

Elemental analysis: calc. (%) for [Cp*Fe(η^5-P_5AsCy_2)][TEF] ($C_{38}H_{37}O_4F_{36}AlP_5FeAs$): C: 29.36 H: 2.40

found (%): C: 28.89 H: 2.28

ESI(+) MS (*o*-DFB): *m/z* (%) = 587.00 (100%) [Cp*Fe(η^5-P_5AsCy_2)]$^+$

NMR (CD_2Cl_2, 298 K)):**^{1}H** (298 K): δ/ppm = 1.62 (s, 15 H, Cp*), 1.34-2.94 (br, 22 H, As<u>Cy</u>$_2$)

^{31}P{^{1}H} (273 K): δ/ppm = 123.9 (m, $^1J_{PA/A'-PB/B'}$ = 432.9/430.0 Hz, $^1J_{PA-PA'}$ = 420.1 Hz, $^2J_{PA/A'-PB'/PB}$ = -52.0/-50.5 Hz, $^2J_{PA/A'-PX}$ = 10.2/3.8 Hz, 2 P, $P^{A/A'}$), 117.1 (m, $^1J_{PB/B'-PX}$ = 576.0/574.5 Hz, $^1J_{PB/B'-PA/A'}$ = 432.9/430.0 Hz, $^2J_{PB/B'-PA'/PA}$ = -52.0/-50.5 Hz, $^2J_{PB-PB'}$ = 22.2 Hz, 2 P, $P^{B/B'}$), 86.6 (m, $^1J_{PX-PB/B'}$ = 576.0/574.5 Hz, $^2J_{PX-PA/A'}$ = 10.2/3.8 Hz, 1 P, P^X)

^{31}P (298 K): δ/ppm = 123.9 (m, $^1J_{PA/A'-PB/B'}$ = 432.9/430.0 Hz, $^1J_{PA-PA'}$ = 420.1 Hz, $^2J_{PA/A'-PB'/PB}$ = -52.0/-50.5 Hz, $^2J_{PA/A'-PX}$ = 10.2/3.8 Hz, 2 P, $P^{A/A'}$), 117.1 (m, $^1J_{PB/B'-PX}$ = 576.0/574.5 Hz, $^1J_{PB/B'-PA/A'}$ = 432.9/430.0 Hz, $^2J_{PB/B'-PA'/PA}$ = -52.0/-50.5 Hz, $^2J_{PB-PB'}$ = 22.2 Hz, 2 P, $P^{B/B'}$), 86.6 (m, $^1J_{PX-PB/B'}$ = 576.0/574.5 Hz, $^2J_{PX-PA/A'}$ = 10.2/3.8 Hz, 1 P, P^X)

^{19}F{^{1}H} (298 K): δ/ppm = - 75.6 (s, $[TEF]^-$)

*[{Cp*Fe(μ,η$^{5:2}$-P$_5$)}SbICp'''][TEF] (**8**)*

[Cp*Fe(η^5-P$_5$)] (0.2 mmol, 70 mg, 1 eq.), Cp'''SbI$_2$ (0.2 mmol, 122 mg, 1 eq.) and Tl[TEF] (0.2 mmol, 234 mg, 1 eq.) were dissolved in 5 mL of *o*-DFB, which gave a light brown solution and a pale yellow precipitate (TlI). This mixture was stirred for 1 h, filtered and then directly layered with 50 mL of *n*-hexane. After 13 days of storage at room temperature [{Cp*Fe(η$^{5:2}$-P$_5$)}SbICp'''][TEF] (**8**) could be isolated as dark brown rod shaped crystals of X-ray quality.

Yield: 85 mg (0.048 mmol, 24%)

Elemental analysis: calc. (%) for [{Cp*Fe(η$^{5:2}$-P$_5$)}SbICp'''][TEF] ($C_{43}H_{44}O_4F_{36}AlP_5FeSbI$): C: 28.77 H: 2.47

found (%): C: 28.62 H: 2.25

ESI(+) MS (*o*-DFB): *m/z* (%) = 481.03 (5%) [Cp'''SbI]$^+$, 587.36 (10%) [Cp'''$_2$Sb]$^+$ (strong fragmentation)

NMR (CD_2Cl_2, 298 K): **^{1}H**: δ/ppm = 1.41 (s, 15 H, Cp*), 1.51 (s, 9 H, C(CH$_3$)$_3$), 1.55 (s, 18 H, C(CH$_3$)$_3$), 6.72 (s, 2 H, C$_5$H$_2$^{t}Bu$_3$)

^{31}P{^{1}H}: δ/ppm = 164.7 (s, 5 P, P$_5$)

^{31}P: δ/ppm = 164.7 (s, 5 P, P$_5$)

^{19}F{^{1}H}: δ/ppm = - 75.6 (s, [TEF]$^-$)

*[Cp*Fe(η^5-P_5SePh)][TEF] (**9**)*

[Cp*Fe(η^5-P_5)] (0.1 mmol, 35 mg, 1 eq.) and PhSeBr (0.1 mmol, 24 mg, 1 eq.) were dissolved in 4 mL of *o*-DFB to give an orange-green solution. Tl[TEF] (0.1 mmol, 117 mg, 1 eq.), dissolved in 2 mL of *o*-DFB, was added to afford a rapid colour change to dark brown and the precipitation of a white solid (TlBr). This mixture was stirred for 5 h at room temperature and then filtered. The resulting dark reddish-brown solution was concentrated to 2 mL under reduced pressure (10^{-3} mbar) and 20 mL of *n*-hexane were added to precipitate [Cp*Fe(η^5-P_5SePh)][TEF] (**9**) as a dark brown solid. This solid was washed two times with 10 mL of *n*-hexane, each, and then dissolved in 3 mL of *o*-DFB. Layering this solution with 20 mL of *n*-hexane and storing it for 12 days at room temperature afforded dark brown rod shaped crystals of **9** in X-ray quality.

Yield: 95 mg (0.065 mmol, 65%)

Elemental analysis: calc. (%) for [Cp*Fe(η^5-P_5SePh)][TEF] ($C_{32}H_{20}O_4F_{36}AlP_5FeSe$): C: 26.16 H: 1.37

found (%): C: 26.49 H: 1.43

ESI(+) MS (*o*-DFB): *m/z* (%) = 502.96 (100%) [Cp*Fe(h^5-P_5SePh)]$^+$

NMR (CD_2Cl_2, 298 K): **^{1}H**: δ/ppm = 1.75 (s, 15 H, Cp*), 7.47-7.90(m, 5 H, Ph)

^{31}P{^{1}H}: δ/ppm = 135.5 (m, $^1J_{PA/A´-PX}$ = 596.9/595.4 Hz, $^1J_{PA/A´-PM/M´}$ = 448.4/441.1 Hz, $^2J_{PA/A´-PM´/M}$ = -54.2/-48.3 Hz, $^2J_{PA-PA´}$ = 37.3 Hz, 2 P, $P^{A/A´}$), 113.8 (m, $^1J_{PM/M´-PA/A´}$ = 448.4/441.1 Hz, $^1J_{PM-PM´}$ = 413.3 Hz, $^2J_{PM/M´-PA´/A}$ = -54.2/-48.3 Hz, $^2J_{PM/M´-PX}$ = -1.9/-0.6 Hz, 2 P, $P^{M/M´}$), 70.4 (m, $^1J_{PX-PA/A´}$ = 596.9/595.4 Hz, $^2J_{PX-PM/M´}$ = 7.8/2.4 Hz, $^1J_{PX-Se}$ = 418 Hz, 1 P, P^X)

^{31}P: δ/ppm = 135.5 (m, $^1J_{PA/A´-PX}$ = 596.9/595.4 Hz, $^1J_{PA/A´-PM/M´}$ = 448.4/441.1 Hz, $^2J_{PA/A´-PM´/M}$ = -54.2/-48.3 Hz, $^2J_{PA-PA´}$ = 37.3 Hz, 2 P, $P^{A/A´}$), 113.8 (m, $^1J_{PM/M´-PA/A´}$ = 448.4/441.1 Hz, $^1J_{PM-PM´}$ = 413.3 Hz, $^2J_{PM/M´-PA´/A}$ = -54.2/-48.3 Hz, $^2J_{PM/M´-PX}$ = -1.9/-0.6 Hz, 2 P, $P^{M/M´}$), 70.4 (m, $^1J_{PX-PA/A´}$ = 596.9/595.4 Hz, $^2J_{PX-PM/M´}$ = 7.8/2.4 Hz, $^1J_{PX-Se}$ = 418 Hz, 1 P, P^X)

^{77}Se{^{1}H}: δ/ppm = 287.3 (d, $^1J_{Se-P}$ = 418 Hz, SePh)

^{19}F{^{1}H}: d/ppm = - 75.5 (s, $[TEF]^-$)

*[Cp*Fe(η^5-P_5TeMes)][TEF] (**10**)*

[Cp*Fe(η^5-P_5)] (0.2 mmol, 70 mg, 1 eq.) and MesTeBr (0.2 mmol, 65 mg, 1 eq.) were dissolved in 4 mL of *o*-DFB to give a brownish-green solution. Tl[TEF] (0.2 mmol, 234 mg, 1 eq.), dissolved in 2 mL of *o*-DFB, was added to afford a rapid colour change to dark brown and the precipitation of a white solid (TlBr). This mixture was stirred for 18 h at room temperature and then filtered. The resulting dark reddish-brown solution was concentrated to 4 mL under reduced pressure (10^{-3} mbar) and 20 mL of *n*-hexane were added to precipitate [Cp*Fe(η^5-P_5TeMes)][TEF] (**10**) as a dark brown solid. This solid was washed two times with 10 mL o toluene and two times with 10 mL of *n*-hexane and then dried under reduced pressure to afford **10** as a pure compound. Dissolving **10** in 3 mL of *o*-DFB and layering the solution with 20 mL of *n*-hexane after storage for 12 days at room temperature afforded dark brownish red rod shaped crystals in X-ray quality.

Yield: 177 mg (0.114 mmol, 57%)

Elemental analysis: calc. (%) for [Cp*Fe(η^5-P_5TeMes)][TEF] ($C_{35}H_{26}O_4F_{36}AlP_5FeTe$): C: 26.95 H: 1.68

found (%): C: 27.19 H: 1.68

ESI(+) MS (*o*-DFB): *m/z* (%) = 537.02 (100%) [$(Cp^*Fe)_2(\mu,\eta^{5:5}$-$P_5)]^+$, 593.00 (5%) [Cp*Fe($\eta^5$-$P_5$TeMes)]$^+$

NMR (CD_2Cl_2, 298 K): **^{1}H**: δ/ppm = 1.70 (s, 15 H, Cp*), 2.27 (s, 3 H, $Mes_{para)}$, 2.84 (s, 6 H, Mes_{ortho}), 7.12 (s, 2 H, Mes_{meta})

^{31}P{^{1}H}: δ/ppm = 126.3 (br, $\omega_{1/2}$ = 2500 Hz)

^{31}P: δ/ppm = 126.3 (br, $\omega_{1/2}$ = 2500 Hz)

^{19}F{^{1}H}: d/ppm = -75.5 (s, $[TEF]^-$)

NMR (CD_2Cl_2, 193 K): **^{31}P{^{1}H}**: δ/ppm =10.0 (br, $\omega_{1/2}$ = 1100 Hz), 124.9 (br, $\omega_{1/2}$ = 1000 Hz), 139.3 (br, $\omega_{1/2}$ = 1500 Hz)

*[Cp*Fe(η^5-P_5Cl)][TEF] (**11**)*

PCl_5 (0.2 mmol, 42 mg, 1 eq.) and Tl[TEF] (0.2 mmol, 234 mg, 1 eq.) were dissolved in 4 mL of *o*-DFB and stirred for 1.5 h. The resulting colourless solid (TlCl) was allowed to settle from the clear solution. The latter was then filtered into a solution of [Cp*Fe(η^5-P_5)] (0.2 mmol, 70 mg, 1 eq.) in 2 mL of *o*-DFB resulting in an immediate colour change from green to dark brownish red. This solution was stirred for 2 h, concentrated under reduced pressure (10^{-3} mbar) and then 30 mL of *n*-hexane were added to precipitate [Cp*Fe(η^5-P_5Cl)][TEF] (**11**) as a dark brownish red solid. The solid was washed two times with 10 mL of *n*-hexane, each, then dried and dissolved in 2 mL of *o*-DFB. The resulting solution was layered with 20 mL of *n*-hexane and then stored at -30 °C for five days, which afforded dark red block shaped crystals of **11** in X-ray quality.

Yield: 175 mg (0.13 mmol, 65%)

Elemental analysis: calc. (%) for [Cp*Fe(η^5-P_5Cl)][TEF]·$(C_6H_4F_2)_{0.1}$ ($C_{26.6}H_{15.4}O_4F_{36.2}AlP_5FeCl$): C: 23.49 H: 1.14

found (%): C: 23.84 H: 0.95

ESI(+) MS (*o*-DFB): *m/z* (%) = 536.97 (100%) $[(Cp^*Fe)_2(\mu,\eta^{5:5}\text{-}P_5)]^+$

NMR (CD_2Cl_2, 300 K): **^{1}H**: δ/ppm = 1.73 (s, Cp*)

^{31}P{^{1}H}: δ/ppm = 156.1 (m, $^1J_{PA/A'\text{-}PM}$ = 637.3/626.9 Hz, $^1J_{PA/A'\text{-}PX/X'}$ = 461.8/426.0 Hz, $^2J_{PA/A'\text{-}PX'/X}$ = -71.2/-37.6 Hz, $^2J_{PA\text{-}PA'}$ = 41.7 Hz, 2 P, $P^{A/A'}$), 84.9 (m, $^1J_{PM\text{-}PA/A'}$ = 637.3/626.9 Hz, $^2J_{PM\text{-}PX/X'}$ = 6.1/2.0 Hz, 1 P, P^M), 70.7 (m, $^1J_{PX/X'\text{-}PA/A'}$ = 461.8/426.0 Hz, $^1J_{PX\text{-}PX'}$ = 406.2Hz, $^2J_{PX/X'\text{-}PA'/A}$ = -71.2/-37.6 Hz, $^2J_{PX/X'\text{-}PM}$ = 6.1/2.0 Hz, 2 P, $P^{X/X'}$)

^{31}P: δ/ppm = 156.1 (m, $^1J_{PA/A'\text{-}PM}$ = 637.3/626.9 Hz, $^1J_{PA/A'\text{-}PX/X'}$ = 461.8/426.0 Hz, $^2J_{PA/A'\text{-}PX'/X}$ = -71.2/-37.6 Hz, $^2J_{PA\text{-}PA'}$ = 41.7 Hz, 2 P, $P^{A/A'}$), 84.9 (m, $^1J_{PM\text{-}PA/A'}$ = 637.3/626.9 Hz, $^2J_{PM\text{-}PX/X'}$ = 6.1/2.0 Hz, 1 P, P^M), 70.7 (m, $^1J_{PX/X'\text{-}PA/A'}$ = 461.8/426.0 Hz, $^1J_{PX\text{-}PX'}$ = 406.2Hz, $^2J_{PX/X'\text{-}PA'/A}$ = -71.2/-37.6 Hz, $^2J_{PX/X'\text{-}PM}$ = 6.1/2.0 Hz, 2 P, $P^{X/X'}$)

^{19}F{^{1}H}: δ/ppm = -75.5 (s, $[TEF]^-$)

*[Cp*Fe(η^5-P_5Br)][TEF] (**12**)*

Br_2 (0.2 mmol, 10 μL, 1 eq.) was added dropwise to a solution of [Cp*Fe(η^5-P_5)] (0.2 mmol, 70 mg, 1 eq.) and Tl[TEF] (0.1 mmol, 117 mg, 1 eq.) in 3 mL of CH_2Cl_2 at – 80 °C affording an immediate colour change to dark brownish red and the precipitation of a white solid (TlBr). The resulting mixture was stirred at room temperature for 1.5 h, then filtered and addition of 20 mL of *n*-pentane afforded the precipitation of [Cp*Fe(η^5-P_5Br)][TEF] (**12**) as a dark brown powder. This powder was dissolved in 3 mL of *o*-DFB to give a dark brown solution, which was layered with 30 mL of *n*-pentane and stored for 7 days to afford dark reddish brown crystals (rod shaped) of **12** in X-ray quality.

Yield: 181 mg (0.13 mmol, 65%)

Elemental analysis: calc. (%) for [Cp*Fe(η^5-P_5Br)][TEF] ($C_{26}H_{15}O_4F_{36}AlP_5FeBr$):

C: 22.42 H: 1.09

found (%): C: 22.71 H: 0.72

ESI(+) MS (*o*-DFB): *m/z* (%) = 536.97 (100%) $[(Cp^*Fe)_2(\mu,\eta^{5:5}\text{-}P_5)]^+$

NMR (CD_2Cl_2, 300 K): **^{1}H**: δ/ppm = 1.73 (s, Cp*)

^{31}P{^{1}H}: δ/ppm = 157.6 (m, $^1J_{PA/A´\text{-}PX}$ = 616.4/615.2 Hz, $^1J_{PA/A´\text{-}PM/M´}$ = 439.0/436.5 Hz, $^2J_{PA/A´\text{-}PM´/M}$ = -58.0/-49.4 Hz, $^2J_{PA\text{-}PA´}$ = 34.4 Hz, 2 P, $P^{A/A´}$), 77.4 (m, $^1J_{PM/M´\text{-}PA/A´}$ = 439.0/436.5 Hz, $^1J_{PM\text{-}PM´}$ = 415.6 Hz, $^2J_{PM/M´\text{-}PA´/A}$ = -58.0/-49.4 Hz, $^2J_{PM/M´\text{-}PX}$ = -1.8/-1.4 Hz, 2 P, $P^{M/M´}$), 64.2 (m, $^1J_{PX\text{-}PA/A´}$ = 616.4/615.2 Hz, $^2J_{PX\text{-}PM/M´}$ = -1.8/-1.4 Hz, 1 P, P^X)

^{31}P: δ/ppm = 157.6 (m, $^1J_{PA/A´\text{-}PX}$ = 616.4/615.2 Hz, $^1J_{PA/A´\text{-}PM/M´}$ = 439.0/436.5 Hz, $^2J_{PA/A´\text{-}PM´/M}$ = -58.0/-49.4 Hz, $^2J_{PA\text{-}PA´}$ = 34.4 Hz, 2 P, $P^{A/A´}$), 77.4 (m, $^1J_{PM/M´\text{-}PA/A´}$ = 439.0/436.5 Hz, $^1J_{PM\text{-}PM´}$ = 415.6 Hz, $^2J_{PM/M´\text{-}PA´/A}$ = -58.0/-49.4 Hz, $^2J_{PM/M´\text{-}PX}$ = -1.8/-1.4 Hz, 2 P, $P^{M/M´}$), 64.2 (m, $^1J_{PX\text{-}PA/A´}$ = 616.4/615.2 Hz, $^2J_{PX\text{-}PM/M´}$ = -1.8/-1.4 Hz, 1 P, P^X)

^{19}F{^{1}H}: δ/ppm = –75.5 (s, $[TEF]^-$)

*[Cp*Fe(η^5-P_5I)][TEF] (**13**)*

I_2 (0.2 mmol, 51 mg, 1 eq.) and Tl[TEF] (0.2 mmol, 234 mg, 1 eq.) were dissolved in 8 mL of *o*-DFB and cooled to – 30 °C. Addition of this solution to another solution of [Cp*Fe(η^5-P_5)] (0.2 mmol, 70 mg, 1 eq.) in 3 mL of *o*-DFB (– 30 °C) afforded a rapid colour change to brown and the formation of a yellow precipitate (TlI). This mixture was stirred for another 2 h at – 30 °C and then the solvent was removed under reduced pressure (10^{-3} mbar). The resulting dark brown residue was washed two times with 20 mL of *n*-pentane, each, and then dissolved in 3 mL of cold (– 30 °C) *o*-DFB. After filtration, this solution was layered with 30 mL of *n*-pentane and stored at – 30 °C, which after 14 days afforded formation [Cp*Fe(η^5-P_5I)][TEF] (**13**) as dark brown crystals in X-ray quality.

Yield: 178 mg (0.124 mmol, 62%)

Elemental analysis: calc. (%) for [Cp*Fe(η^5-P_5I][TEF] ($C_{26}H_{15}O_4F_{36}AlP_5FeI$):

C: 21.69 H: 1.05

found (%): C: 22.14 H: 1.06

ESI(+) MS (*o*-DFB): *m/z* (%) = 536.97 (80%) $[(Cp^*Fe)_2(\mu,\eta^{5:5}\text{-}P_5)]^+$

NMR (CD_2Cl_2, 300 K): **^{1}H**: δ/ppm = 1.67 (s (br), Cp*)

^{31}P{^{1}H}: δ/ppm = 106 (br, $\omega_{1/2}$ = 5600 Hz)

^{31}P: δ/ppm = 106 (br, $\omega_{1/2}$ = 5600 Hz)

^{19}F{^{1}H}: δ/ppm = –75.5 (s, $[TEF]^-$)

NMR (CD_2Cl_2, 193 K): **^{1}H**: δ/ppm = 1.60 (s, Cp*)

^{31}P{^{1}H}: δ/ppm = 153 (br, $\omega_{1/2}$ = 4100 Hz), 90 (br, $\omega_{1/2}$ = 1060 Hz) 19 (br, $\omega_{1/2}$ = 4350 Hz)

*[{Cp'''Ta(CO)$_2$}$_2${μ,η$^{4:4}$-((P$_4$)$_2$BBr$_2$)}][TEF] (**15**)*

[Cp'''Ta(CO)$_2$(η^4-P$_4$)] (59 mg, 0.1 mmol, 2 eq.) and BBr_3 (5 μL, 0.05 mmol, 1 eq.) were dissolved in 5 mL of *o*-DFB to give a yellow solution. Tl[TEF] (59 mg, 0.05 mmol, 1 eq.) dissolved in 2 ml of *o*-DFB was added slowly under strong stirring. An immediate colour change to pale orange occurred and precipitation of a white solid (TlBr) can be observed. The mixture was stirred for six hours, then filtered and directly layered with 40 mL of *n*-pentane. Storage of this mixture for one day at room temperature affords [{Cp'''Ta(CO)$_2$}$_2${μ,η$^{4:4}$-((P$_4$)$_2$BBr$_2$})][TEF] (**15**) as clear yellow crystals in X-ray quality. Further storage at –30 °C for several weeks leads to quantitative precipitation of **15** as orange powder.

Yield: 87 mg (0.037 mmol, 74%)

Elemental analysis: calc. (%) for [{Cp'''Ta(CO)$_2$}$_2${μ,η$^{4:4}$-((P$_4$)$_2$BBr$_2$)}][TEF] ($C_{54}H_{58}BO_8F_{36}AlP_8Br_2Ta_2$): C: 27.88 H: 2.51

calc. (%) for [{Cp'''Ta(CO)$_2$}$_2${μ,η$^{4:4}$-((P$_4$)$_2$BBr$_2$)][TEF]·(TlBr)$_{0.4}$ ($C_{54}H_{58}BO_8F_{36}AlP_8Br_2Ta_2$)]·(TlBr)$_{0.4}$: C: 26.58 H: 2.40

found (%): C: 26.23 H: 2.11

Traces of TlBr are inseparable from the product by filtration due to weak interaction of **15** with the soft Tl^+ ion.

NMR (CD_2Cl_2, 300 K): **^{1}H**: δ/ppm = 1.12 (s, 9 H, $C_5H_2{}^t\underline{Bu}_3$), 1.56 (s, 18 H, $C_5H_2{}^t\underline{Bu}_3$), 6.33 (s, 1 H, $C_5\underline{H}_2{}^tBu_3$), 6.34 (s, 1 H, $C_5\underline{H}_2{}^tBu_3$)

^{31}P{^{1}H}: δ/ppm = –15.4 (m, $^1J_{PA/A'\text{-}PM/M'}$ = 350 Hz, $^1J_{PA/A'\text{-}PX/X'}$ = 293 Hz, 4 P, $P^{A/A'}$), –37.1 (m (br), $^1J_{PM/M'\text{-}PA/A'}$ = 350 Hz, $^2J_{PM/M'\text{-}PX/X'}$ = 117 Hz, , $^2J_{PM\text{-}M'}$ = 120 Hz, $^1J_{PM\text{-}B}$ = 61 Hz, 2 P, $P^{A/A'}$) and –80.8 (m, $^1J_{PX/X'\text{-}PA/A'}$ = 293 Hz, $^1J_{PX/X'\text{-}PM/M'}$ = 117 Hz)

^{31}P: δ/ppm = –15.4 (m, $^1J_{PA/A'\text{-}PM/M'}$ = 350 Hz, $^1J_{PA/A'\text{-}PX/X'}$ = 293 Hz, 4 P, $P^{A/A'}$), –37.1 (m (br), $^1J_{PM/M'\text{-}PA/A'}$ = 350 Hz, $^2J_{PM/M'\text{-}PX/X'}$ = 117 Hz, , $^2J_{PM\text{-}M'}$ = 120 Hz, $^1J_{PM\text{-}B}$ = 61 Hz, 2 P, $P^{A/A'}$) and –80.8 (m, $^1J_{PX/X'\text{-}PA/A'}$ = 293 Hz, $^1J_{PX/X'\text{-}PM/M'}$ = 117 Hz)

^{11}B{^{1}H}: δ/ppm = –10.2 (t, 1 B, $^1J_{B\text{-}P}$ = 61 Hz, {$\underline{B}Br_2$})

^{19}F{^{1}H}: δ/ppm = –75.6 (s, $[TEF]^-$)

Cp'''SbI_2

To a solution of 9.80 g (19.5 mmol) SbI_3 in 200 mL THF a solution of 5.00 g (19.5 mmol) Cp'''Na in 100 mL THF was added at −80°C. The reaction mixture was warmed to room temperature and stirred for 18 hours. The solvent was removed in vacuo and the residue extracted with hexane. The hexane solution was concentrated until beginning of crystallization and stored over night at −28°C. Large orange crystals were formed. Yield 10.03 g (85%).

Elemental analysis: calc. (%) for Cp'''SbI_2 ($C_{17}H_{29}SbI_2$): C: 33.53 H: 4.80

found (%): C: 33.43 H: 4.73

NMR (C_6D_6, 300 K): **^{1}H**: δ/ppm = 1.22 (s, 18H, $C(CH_3)_3$), 1.29 (s, 9 H, $C(CH_3)_3$), 6.55 (s, 2H, CH).

^{13}C{^{1}H}: δ/ppm = 30.59 (s, $C(CH_3)_3$), 32.99 (s, $C(CH_3)_3$), 34.31 (s, $C(CH_3)_3$), 35.30 (s, $C(CH_3)_3$), 116.76 (s, $CSbI_2$), 123.65 (s, CCH), 145.97 (s, $CC(CH_3)_3$)

6.5.2. Xray Crystallographic Data

General Considerations

The crystallographic data for all described compounds were collected on a SuperNova diffractometer (Rigaku) with a Titan^{S2} detector using Cu–K_α radiation (micro-focus sealed tube) (**7**), on a GV50 diffractometer (Rigaku) with a Titan^{S2} detector using Cu–K_β radiation obtained by using customised optics (**13**), an Xcalibur Gemini Ultra diffractometer with an Atlas^{S2} detector using Mo-K_α (**9**) radiation (sealed tube) or a standard Cu-K_α sealed tube (**2**, **3**, **5**, **8**), or an XtaLAB Synergy R, DW System with a HyPix-Arc 150 detector using Cu-K_α radiation from a rotating anode (**4**, **6**, **10**, **12**). Data reduction and absorption correction were performed with the CrysAlisPro software package.[49] Structure solution and refinement was conducted in Olex2 (1.3-alpha)[50] with ShelXT[51] (solution) and ShelXL-2018/3[52] (least squares refinement (F^2)). All non-H atoms were refined with anisotropic displacement parameters (except the minor disordered part of **7**) and H atoms were treated as riding models with isotropic displacement parameters and fixed C–H bond lengths (sp^3: 0.96 (CH_3), 0.97 (CH_2); sp^2: 0.93 (CH)). Visualisation of the crystal structures was performed with Olex2 (1.3-alpha).[50]

CIF files with comprehensive information on the details of the diffraction experiments and full tables of bond lengths and angles for **2**, **3**, **4**, **5**, **6**, **7**, **8**, **9**, **10**, **13** and **15** are deposited in Cambridge Crystallographic Data Centre under the deposition codes CCDC-2083554, CCDC-2083555, CCDC-2083556, CCDC-2083557, CCDC-2083558, CCDC-2083559, CCDC-2083560, CCDC-2083561, CCDC-2083562, CCDC-2083563, respectively.

*Table S 1: Crystallographic and refinement details on compounds **2**, **3**, **4** and **5**.*

Compound	2	3	4	5
Formula	$C_{39.6}H_{38.4}AlBBr_2F_{36}Fe_2O_4P_{10}$	$C_{36}H_{30}AlF_{36}Fe_2GaI_2O_4P_{10}$	$C_{33}H_{22}AlF_{36}FeO_4P_5$	$C_{39}H_{26}AlF_{36}FeO_4P_5$
$D_{calc.}$/ g cm^{-3}	1.937	2.074	1.896	1.830
μ/mm^{-1}	8.892	15.621	4.279	5.382
Formula Weight	1881.31	1982.50	1404.18	1480.28
Colour	clear light green	dark brown	clear dark red	clear dark red
Shape	prism	plate	block	block-shaped
Size/mm^3	0.36×0.12×0.06	0.42×0.37×0.12	0.32×0.28×0.19	0.63×0.38×0.21
T/K	123(1)	123(1)	123.00(10)	123(1)
Crystal System	monoclinic	triclinic	monoclinic	triclinic
Space Group	$C2$	$P\bar{1}$	$P2_1/n$	$P\bar{1}$
a/Å	40.0184(7)	12.8777(2)	15.0993(7)	15.4816(4)
b/Å	9.73790(10)	16.0557(2)	18.0632(8)	16.9548(5)
c/Å	18.3964(4)	18.4470(3)	18.8351(10)	21.6022(6)
α/°	90	112.4860(10)	90	86.014(2)
β/°	115.870(2)	95.1250(10)	106.706(5)	71.751(2)
γ/°	90	110.9810(10)	90	88.928(2)
V/Å^3	6450.6(2)	3175.29(9)	4920.3(4)	5372.1(3)
Z	4	2	4	4
Z'	1	1	1	2
Wavelength/Å	1.54184	1.54184	1.39222	1.54184
Radiation type	Cu K$_\alpha$	Cu K$_\alpha$	Cu K$_\beta$	Cu K$_\alpha$
Θ_{min}/°	4.346	3.830	2.999	3.500
Θ_{max}/°	72.039	71.666	75.377	71.857
Measured Refl's.	23789	33614	26352	58001
Indep't Refl's	12143	12088	13101	20392
Refl's I≥2 σ(I)	11912	11702	10904	18475
R_{int}	0.0362	0.0473	0.0306	0.0433
Parameters	921	1145	1385	2252
Restraints	88	851	608	1556
Largest Peak	0.730	1.421	0.612	1.211
Deepest Hole	-0.429	-1.030	-0.667	-0.506
GooF	1.037	1.035	1.087	1.044
wR_2 (all data)	0.1117	0.1314	0.1640	0.1939
wR_2	0.1109	0.1301	0.1462	0.1882
R_1 (all data)	0.0432	0.0487	0.0667	0.0722
R_1	0.0425	0.0477	0.0559	0.0675
Flack Parameter	0.386(5)	/	/	/
Hooft Parameter	0.387(2)	/	/	/

*Table S 2: Crystallographic and refinement details on compounds **6**, **7**, **8** and **9**.*

Compound	6	7	8	9
Formula	$C_{46}H_{26}BF_{20}FeP_5Si$	$AlAsC_{41.5}F_{36}FeH_{41}O_4P_5$	$Al_2C_{92}F_{72}Fe_2H_{98}I_2O_8P_{10}Sb_2$	$C_{32}H_{20}AlF_{36}FeO_4P_5Se$
$D_{calc.}$/ g cm^{-3}	1.707	1.812	1.837	1.944
μ/mm^{-1}	5.490	5.578	11.213	1.374
Formula Weight	1208.27	1600.34	3672.36	1469.12
Colour	clear light green	clear dark red	light brown	clear dark red
Shape	plate	block-shaped	rod-shaped	block-shaped
Size/mm^3	0.22×0.15×0.05	0.48×0.28×0.22	0.53×0.10×0.08	0.52×0.44×0.28
T/K	123.00(10)	123.15(1)	123(1)	123(1)
Crystal System	monoclinic	monoclinic	monoclinic	triclinic
Space Group	$P2_1/c$	$P2_1/n$	$P2_1/n$	$P\bar{1}$
a/Å	17.0141(2)	28.0092(2)	21.0539(2)	12.1286(4)
b/Å	14.79290(10)	21.7375(2)	16.5834(2)	12.6674(5)
c/Å	20.3007(3)	10.53850(10)	38.0631(4)	17.2846(8)
α/°	90	90	90	107.670(4)
β/°	113.070(2)	113.8980(10)	92.2010(10)	96.922(3)
γ/°	90	90	90	90.247(3)
V/Å^3	4700.82(11)	5866.28(10)	13279.7(2)	2509.49(18)
Z	4	4	4	2
Z'	1	1	1	1
Wavelength/Å	1.54184	1.54184	1.54184	0.71073
Radiation type	Cu K$_\alpha$	Cu K$_\alpha$	Cu K$_\alpha$	Mo K$_\alpha$
Θ_{min}/°	2.823	4.007	3.394	3.379
Θ_{max}/°	73.459	66.906	71.750	32.286
Measured Refl's.	33445	61278	75069	22005
Indep't Refl's	9127	10404	25253	15499
Refl's I≥2 σ(I)	8217	9640	18923	11637
R_{int}	0.0288	0.0393	0.0782	0.0296
Parameters	696	1182	2570	924
Restraints	48	368	1318	164
Largest Peak	0.649	0.842	1.024	0.770
Deepest Hole	-0.540	-0.807	-0.980	-0.555
GooF	1.091	1.024	1.008	1.059
wR_2 (all data)	0.1029	0.1469	0.1737	0.1329
wR_2	0.1008	0.1429	0.1570	0.1169
R_1 (all data)	0.0396	0.0572	0.0875	0.0743
R_1	0.0359	0.0537	0.0649	0.0508

*Table S 3: Crystallographic and refinement details on compounds **10**, **13** and **15**.*

Compound	**10**	**13**	**15**
Formula	$Al_3C_{123}F_{114}Fe_3H_{90}O_{12}P_{15}Te_3$	$C_{29}H_{17}AlF_{37}FeIO_4P_5$	$C_{54}H_{58}AlBBr_2F_{36}O_8P_8Ta_2$
$D_{calc.}$/ g cm^{-3}	1.917	2.071	1.973
μ/mm^{-1}	8.965	8.267	9.149
Formula Weight	5021.78	1497.01	2326.27
Colour	dark red	dark brown	clear yellow
Shape	block-shaped	block-shaped	rods-shaped
Size/mm^3	0.21×0.17×0.14	0.41×0.28×0.14	0.38×0.14×0.07
T/K	122.99(10)	122.99(10)	122.93(19)
Crystal System	triclinic	monoclinic	triclinic
Space Group	$P\bar{1}$	$C2/c$	$P\bar{1}$
a/Å	18.1681(7)	31.0024(8)	10.70454(17)
b/Å	19.4877(7)	19.5946(3)	17.1553(4)
c/Å	28.8463(10)	19.9635(6)	22.3411(6)
α/°	77.316(3)	90	73.344(2)
β/°	72.113(3)	127.644(4)	86.2377(16)
γ/°	64.085(4)	90	85.9405(15)
V/Å^3	8698.6(6)	9602.7(6)	3916.28(15)
Z	2	8	2
Z'	1	1	1
Wavelength/Å	1.54184	1.39222	1.54184
Radiation type	Cu K$_\alpha$	Cu K$_\beta$	Cu K$_\alpha$
Θ_{min}/°	3.543	2.605	3.832
Θ_{max}/°	73.781	74.464	74.898
Measured Refl's.	59952	39627	54888
Indep't Refl's	33498	13047	15822
Refl's I≥2 σ(I)	25725	11680	14586
R_{int}	0.0555	0.0295	0.0744
Parameters	3526	942	1297
Restraints	1862	173	328
Largest Peak	1.133	0.662	3.643
Deepest Hole	-1.172	-0.479	-5.026
GooF	1.010	1.021	1.037
wR_2 (all data)	0.1815	0.1174	0.1950
wR_2	0.1662	0.1133	0.1915
R_1 (all data)	0.0844	0.0478	0.0775
R_1	0.0675	0.0431	0.0736

*[{Cp*Fe}$_2${(η^5-P_5)$_2$$BBr_2$}][TEF] (**2**)*

Large pale greenish brown rod shaped crystals of [{Cp*Fe(η^5-P_5)}$_2$$BBr_2$][TEF] (**2**) are obtained by layering a concentrated solution in *o*-DFB with *n*-hexane (1:7) and storing it at room temperature for two weeks. **2** crystallises as inversion twins in the monoclinic space group *C*2 with one cation, one anion and 0.6 hexane solvent molecules present in the asymmetric unit (Figure S1). Due to the heavy disorder of the hexane molecule a solvent mask was calculated with the in Olex2 implemented masking tool and 120 electrons were found in a volume of 550 Å^3 in 2 voids per unit cell. This is consistent with the presence of 0.6 hexane molecules per asymmetric unit, which account for 120 electrons per unit cell. Disorder within the anion was treated with appropriate geometric and ADP (Anisotropic Displacement Parameter) restraints.

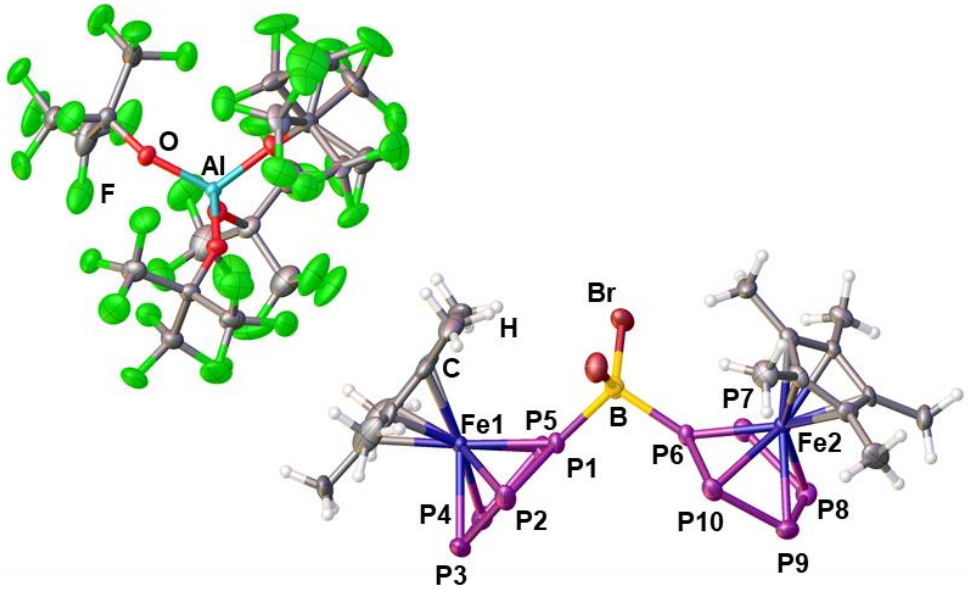

*Figure S 1: Solid state structure of **2**; Depicted is the asymmetric unit and ADPs are drawn at 50% probability; Selected bond lengths and angles: d(P1-P2) = 2.098(2) Å, d(P2-P3) = 2.117(3) Å, d(P3-P4) = 2.121(4) Å, d(P4-P5) = 2.103(3) Å, d(P1-P5) = 2.108(2) Å, d(P6-P7) = 2.105(2) Å, d(P7-P8) = 2.110(3) Å, d(P8-P9) = 2.120(3) Å, d(P9-P10) = 2.111(3) Å, d(P6-P10) = 2.110(2) Å, d(P1-B) = 1.985(7) Å, d(P6-B) = 1.985(8) Å, d(P1-Fe1) = 2.289(2) Å, d(P2-Fe1) = 2.408(2) Å, d(P3-Fe1) = 2.383(2) Å, d(P4-Fe1) = 2.379(3) Å, d(P5-Fe1) = 2.395(2) Å, d(P6-Fe2) = 2.275(2) Å, d(P7-Fe2) = 2.289(2) Å, d(P8-Fe2) = 2.380(3) Å, d(P9-Fe2) = 2.387(2) Å, d(P10-Fe2) = 2.397(2) Å, ∢(P1-B-P6) = 100.9(3)°, ∢(P3-P5-P2-P1) = 174.31(18)°, ∢(P8-P10-P7-P6) = 173.10(14)°.*

*[{Cp*Fe}$_2${(η^5-P_5)$_2$$GaI_2$}][TEF] (**3**)*

Dark brown crystalline plates of [{Cp*Fe(η^5-P_5)}$_2$$GaI_2$][TEF] (**3**) are obtained by layering a concentrated solution in *o*-DFB with *n*-hexane (1:7) and storing it at room temperature for one week. **3** crystallises in the triclinic space group $P\bar{1}$ with one cation and one anion present in the asymmetric unit (Figure S2). Disorder within the anion was treated with appropriate geometric and ADP restraints.

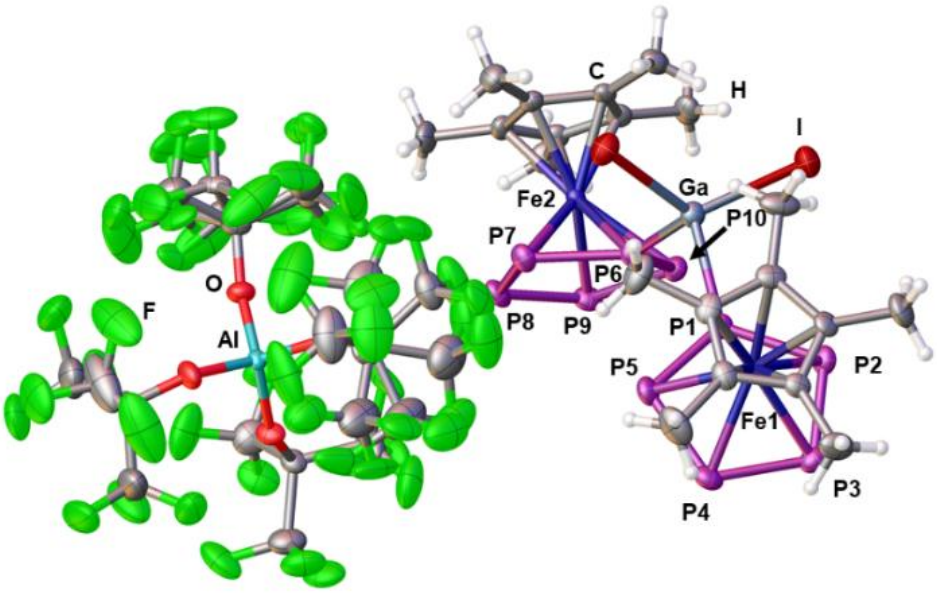

*Figure S 2: Solid state structure of **3**; Depicted is the asymmetric unit and ADPs are drawn at 50% probability; Selected bond lengths and angles: d(P1-P2) = 2.1054(15) Å, d(P2-P3) = 2.1076(16) Å, d(P3-P4) = 2.1175(17) Å, d(P4-P5) = 2.1179(15) Å, d(P1-P5) = 2.1076(16) Å, d(P6-P7) = 2.1116(15) Å, d(P7-P8) = 2.1174(17) Å, d(P8-P9) = 2.1123(17) Å, d(P9-P10) = 2.1127(17) Å, d(P6-P10) = 2.1044(15) Å, d(P1-Ga) = 2.3871(11) Å, d(P6-Ga) = 2.4102(12) Å, d(P1-Fe1) = 2.310(1) Å, d(P2-Fe1) = 2.375(2) Å, d(P3-Fe1) = 2.394(1) Å, d(P4-Fe1) = 2.368(2) Å, d(P5-Fe1) = 2.370(1) Å, d(P6-Fe2) = 2.308(1) Å, d(P7-Fe2) = 2.367(2) Å, d(P8-Fe2) = 2.391(2) Å, d(P9-Fe2) = 2.386(1) Å, d(P10-Fe2) = 2.375(1) Å ∢(P1-Ga-P6) = 97.31(4)°, ∢(P3-P5-P2-P1) = 170.04(10)°, ∢(P8-P10-P7-P6) = 171.61(12)°.*

*[Cp*Fe(η^5-P_5CH_2Ph)][TEF] (**4**)*

[Cp*Fe(η^5-P_5CH_2Ph)][TEF] (**4**) can be obtained as dark red crystalline blocks after layering a concentrated solution in *o*-DFB with *n*-hexane (1:8) and storing it at room temperature for one week. **4** crystallises in the monoclinic space group $P2_1/n$ with one cation and one anion present in the asymmetric unit (Figure S3). Disorder within the anion and the cation was treated with appropriate geometric and ADP restraints.

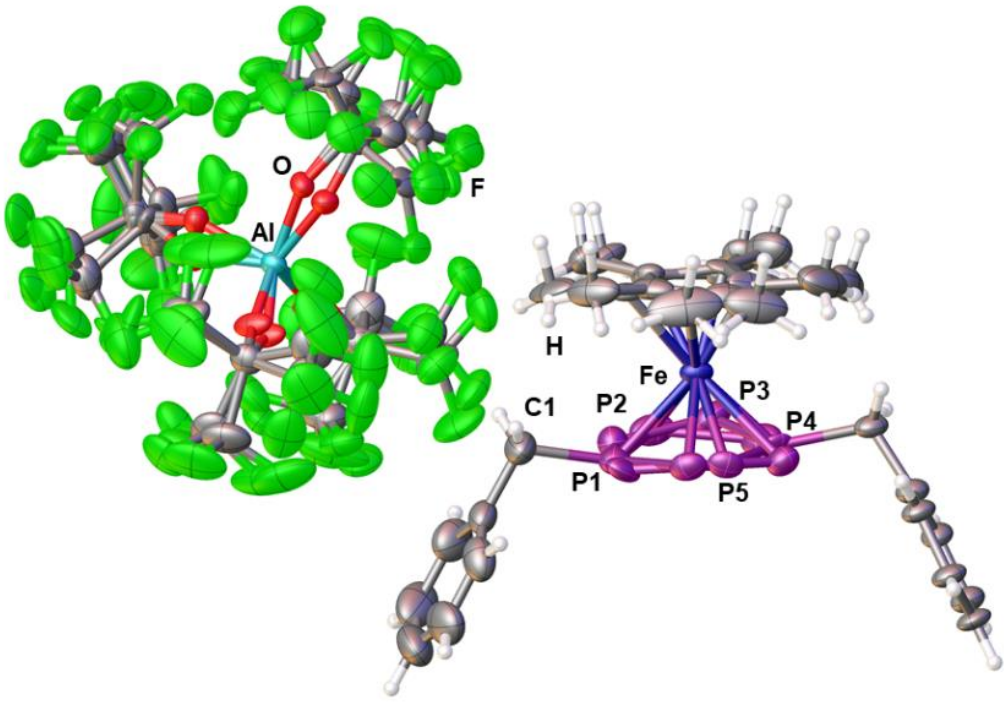

*Figure S 3: Solid state structure of **4**; Depicted is the asymmetric unit and ADPs are drawn at 50% probability; Selected bond lengths and angles: d(P1-P2) = 2.0893(18) Å, d(P2-P3) = 2.1091(17) Å, d(P3-P4) = 2.1273(14) Å, d(P4-P5) = 2.1032(15) Å, d(P1-P5) = 2.0928(17) Å, d(P1-C1) = 1.853(4) Å, d(P1-Fe1) = 2.282(1) Å, d(P2-Fe1) = 2.358(1) Å, d(P3-Fe1) = 2.391(1) Å, d(P4-Fe1) = 2.389(1) Å, d(P5-Fe1) = 2.359(1) Å, ∢(P1-C1-C2) = 109.6(3)°, ∢(P3-P5-P2-P1) = 166.00(9)°.*

*[Cp*Fe(η^5-P_5CHPh_2)][TEF] (**5**)*

[Cp*Fe(η^5-P_5CHPh_2)][TEF] (**5**) can also be obtained as red crystalline blocks after layering a concentrated solution in *o*-DFB with *n*-hexane (1:8) and storing it at -30 °C for eleven days. **5** crystallises in the triclinic space group $P\bar{1}$ with two cations and two anions present in the asymmetric unit (Figure S4). Disorder within the anions was treated with appropriate geometric and ADP restraints.

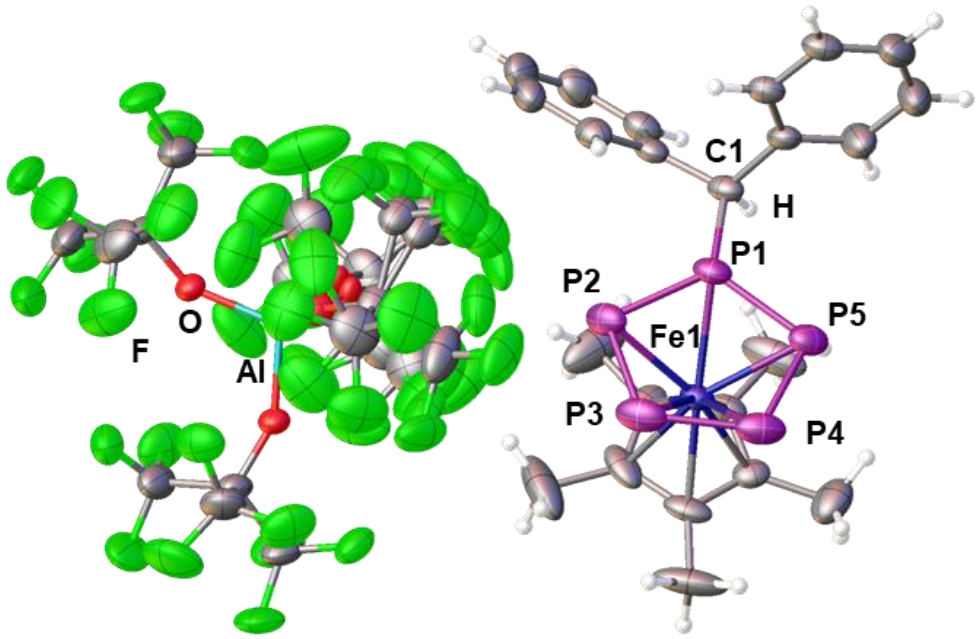

*Figure S 4: Solid state structure of **5**; Depicted is half of the asymmetric unit and ADPs are drawn at 50% probability; Selected bond lengths and angles: d(P1-P2) = 2.0957(13) Å, d(P2-P3) = 2.1198(18) Å, d(P3-P4) = 2.1195(17) Å, d(P4-P5) = 2.1170(20) Å, d(P1-P5) = 2.0984(15) Å, d(P1-C1) = 1.866(4) Å, d(P1*-Fe1*) = 2.2944(10) Å, d(P2-Fe1) = 2.3679(13) Å, d(P3-Fe1) = 2.3829(12) Å, d(P4-Fe1) = 2.3863(18) Å, d(P5-Fe1) = 2.3520(12) Å, ∢(P1-C1-C2) = 107.0(3)°, ∢(P3-P5-P2-P1) = 162.96(10)°.*

*[Cp*Fe(η^5-P_5SiHPh_2)][$B(C_6F_5)_4$] (**6**)*

Crystals of [Cp*Fe(η^5-P_5SiHPh_2)][$B(C_6F_5)_4$] (**6**) can be obtained as clear greenish brown plates after layering a concentrated solution in *o*-DFB with *n*-hexane (1:10) and storing it at room temperature for two days. **6** crystallises in the monoclinic space group $P2_1/c$ with one cation and one anion present in the asymmetric unit (Figure S5). Disorder within the Cp* ligand was treated with appropriate geometric and ADP restraints.

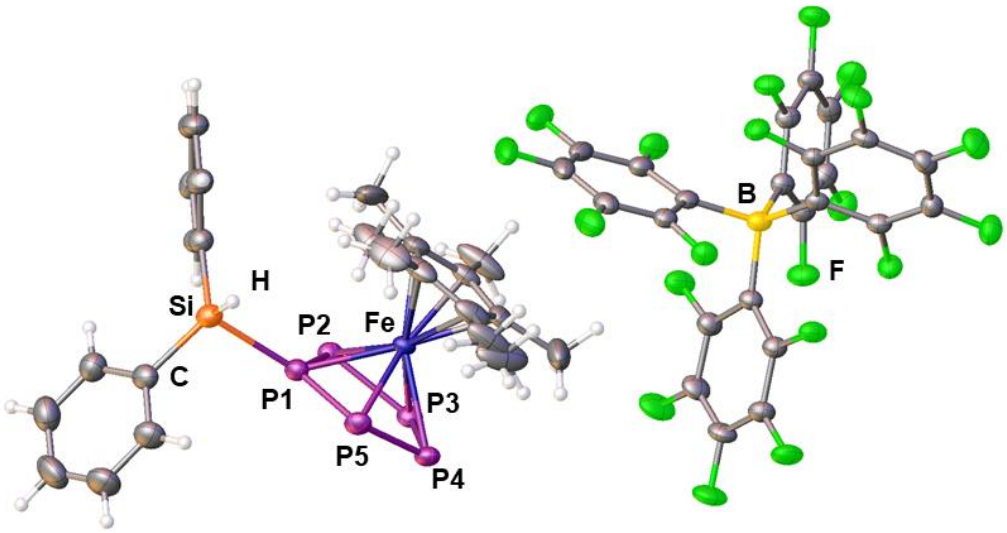

*Figure S 5: Solid state structure of **6**; Depicted is the asymmetric unit and ADPs are drawn at 50% probability; Selected bond lengths and angles: d(P1-P2) = 2.1047(8) Å, d(P2-P3) = 2.1124(8) Å, d(P3-P4) = 2.1150(8) Å, d(P4-P5) = 2.1151(8) Å, d(P1-P5) = 2.1027(8) Å, d(P1-Si) = 2.3053(8) Å, d(P1*-Fe1*) = 2.3080(8) Å, d(P2-Fe1) = 2.3640(8) Å, d(P3-Fe1) = 2.3683(6) Å, d(P4-Fe1) = 2.3963(6) Å, d(P5-Fe1) = 2.3544(7) Å, ∢(P1-Si-H1) = 97.4(12)°, ∢(P3-P5-P2-P1) = 167.74(5)°.*

*[Cp*Fe(η^5-P_5AsCy_2)][TEF] (**7**)*

Dark red block shaped crystals of [Cp*Fe(η^5-P_5AsCy_2)][TEF] (**7**) can be obtained after layering a concentrated solution in *o*-DFB with *n*-hexane (1:10) and storing it at -30 °C for two weeks. **7** crystallises in the monoclinic space group $P2_1/n$ with one cation, one anion and one half of a toluene molecule present in the asymmetric unit (Figure S6). The toluene could not be modelled properly and was therefore treated with the in Olex2 implemented masking tool. A solvent mask was calculated and 100 electrons were found in a volume of 348 Å^3 in 1 void per unit cell. This is consistent with the presence of half a toluene molecule per asymmetric unit, which accounts for 100 electrons per unit cell. Disorder within the anion and one of the cyclohexyl groups was treated with appropriate geometric and ADP restraints. Further, is the complete cationic part disordered over two positions (0.96 : 0.4). Due to the low occupancy of the second part it was only possible to model the heavy atom framework consisting of FeP_5As.

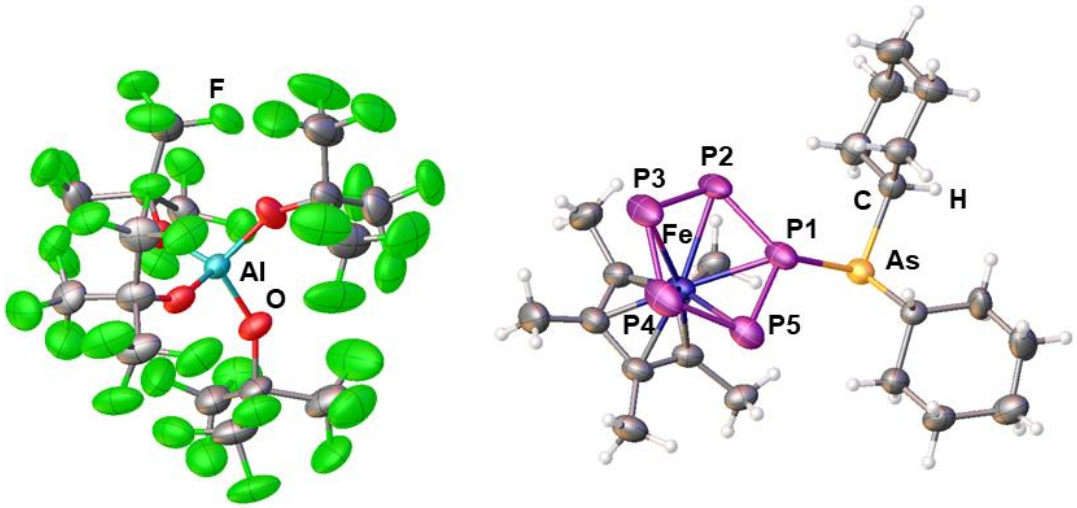

*Figure S 6: Solid state structure of **7**; Depicted is the asymmetric unit and ADPs are drawn at 50% probability; Selected bond lengths and angles: d(P1-P2) = 2.110(2) Å, d(P2-P3) = 2.119(2) Å, d(P3-P4) = 2.121(3) Å, d(P4-P5) = 2.106(2) Å, d(P1-P5) = 2.116(2) Å, d(P1-As) = 2.348(1) Å, d(P1*-Fe1*) = 2.353(1) Å, d(P2-Fe1) = 2.335(2) Å, d(P3-Fe1) = 2.393(1) Å, d(P4-Fe1) = 2.386(2) Å, d(P5-Fe1) = 2.335(1) Å, ∢(P3-P5-P2-P1) = 162.66(8)°.*

*[{Cp*Fe(μ,η$^{5:2}$-P$_5$)}SbICp'''][TEF] (**8**)*

Clear light greenish brown crystalline plates of [{Cp*Fe(η$^{5:2}$-P$_5$)}SbICp'''][TEF] (**8**) can be obtained after layering a concentrated solution in *o*-DFB with *n*-hexane (1:10) and storing it at room temperature for ten days. **8** crystallises in the monoclinic space group *P*2$_1$/*n* with two formula units and two times half a hexane molecule present in the asymmetric unit (Figure S7). Disorder within the anions and the cations was treated with appropriate geometric and ADP restraints. The *n*-hexane molecules could not be modelled appropriately and therefore were treated with the in Olex2 implemented masking tool. A solvent mask was calculated and 204 electrons were found in a volume of 1206 Å^3 in 3 voids per unit cell. This is consistent with the presence of two half hexane molecules per asymmetric unit, which account for 200 electrons per unit cell.

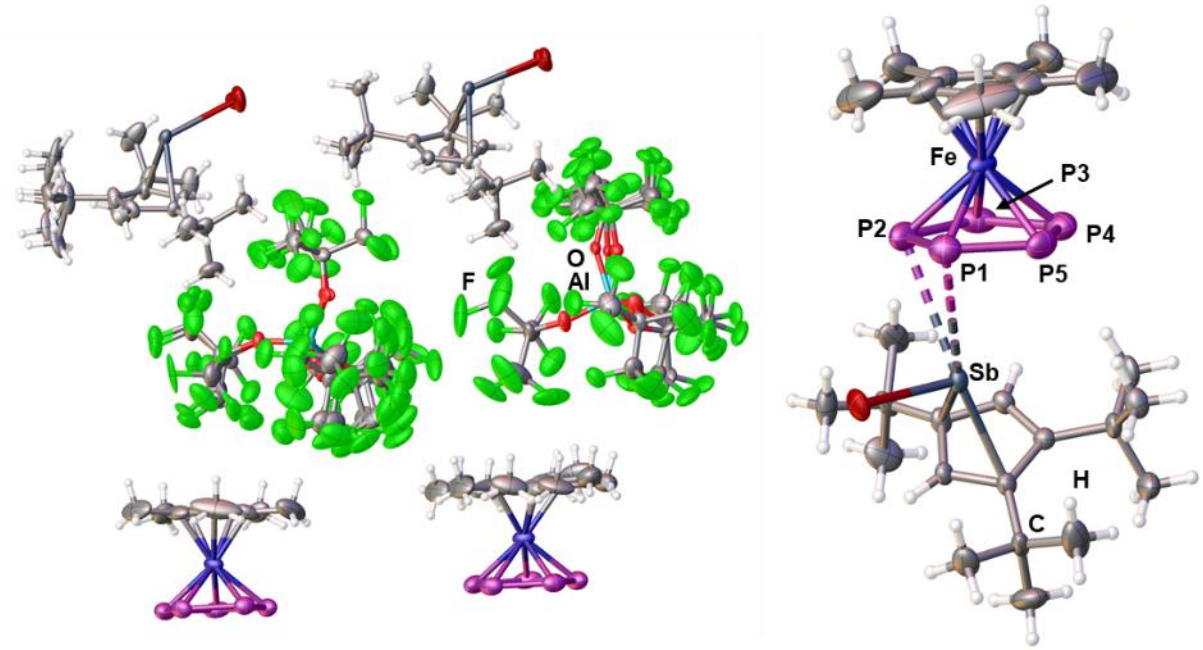

*Figure S 7: Solid state structure of **8**; Depicted is the asymmetric unit (left), an excerpt of the cation (right) and ADPs are drawn at 50% probability; Selected bond lengths and angles: d(P1-P2) = 2.105(3) Å, d(P2-P3) = 2.137(4) Å, d(P3-P4) = 2.143(3) Å, d(P4-P5) = 2.119(3) Å, d(P1-P5) = 2.107(3) Å, d(P3-Sb) = 3.236(2) Å, d(P4-Sb) = 3.400(2) Å, d(Sb-I) = 2.787(3) Å, d(P1*-Fe1*) = 2.348(3) Å, d(P2-Fe1) = 2.329(2) Å, d(P3-Fe1) = 2.347(2) Å, d(P4-Fe1) = 2.328(2) Å, d(P5-Fe1) = 2.345(2) Å, ∢(cent(P$_5$)-Sb-cent(C$_5$)) = 128.51(8)°.*

*[Cp*Fe(η^5-P_5SePh)][TEF] (**9**)*

Clear dark red block shaped crystals of [Cp*Fe(η^5-P_5SePh)][TEF] (**9**) can be obtained after layering a concentrated solution in *o*-DFB with *n*-hexane (1:7) and storing it at room temperature for twelve days. **9** crystallises in the triclinic space group $P\bar{1}$ with one cation and one anion present in the asymmetric unit (Figure S8). Disorder within the anion was treated with appropriate geometric and ADP restraints.

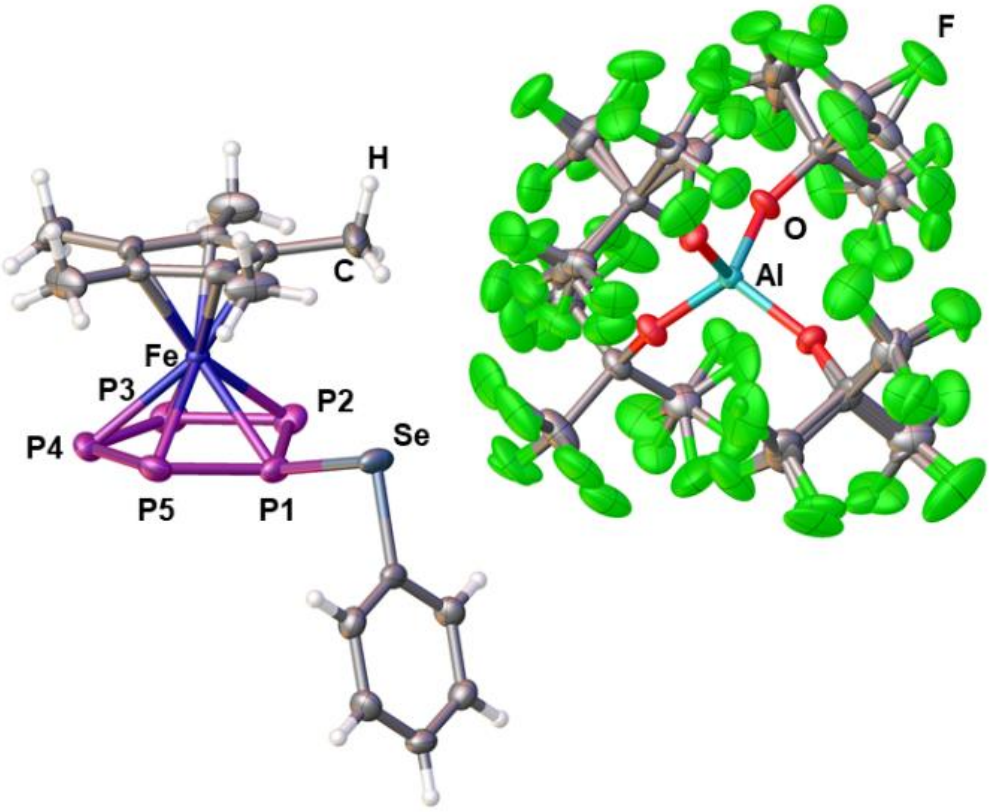

*Figure S 8: Solid state structure of **9**; Depicted is the asymmetric unit and ADPs are drawn at 50% probability; Selected bond lengths and angles: d(P1-P2) = 2.1201(11) Å, d(P2-P3) = 2.1109(11) Å, d(P3-P4) = 2.1395(12) Å, d(P4-P5) = 2.1098(12) Å, d(P1-P5) = 2.1220(10) Å, d(P1-Se) = 2.2234(7) Å, d(P1*-Fe1*) = 2.3061(9) Å, d(P2-Fe1) = 2.3489(8) Å, d(P3-Fe1) = 2.3923(8) Å, d(P4-Fe1) = 2.3967(8) Å, d(P5-Fe1) = 2.3401(10) Å, ∢(P3-P5-P2-P1) = 163.19(6)°.*

*[Cp*Fe(η^5-P_5TeMes)][TEF] (**10**)*

[Cp*Fe(η^5-P_5TeMes)][TEF] (**10**) can be obtained as crystalline dark red blocks after layering a concentrated solution in *o*-DFB with *n*-pentane (1:6) and storing it at room temperature for two weeks. **10** crystallises in the triclinic space group $P\bar{1}$ with three cations, three anions and one *o*-DFB molecule present in the asymmetric unit (Figure S9). Disorder within the anions and the solvent molecule was treated with appropriate geometric and ADP restraints.

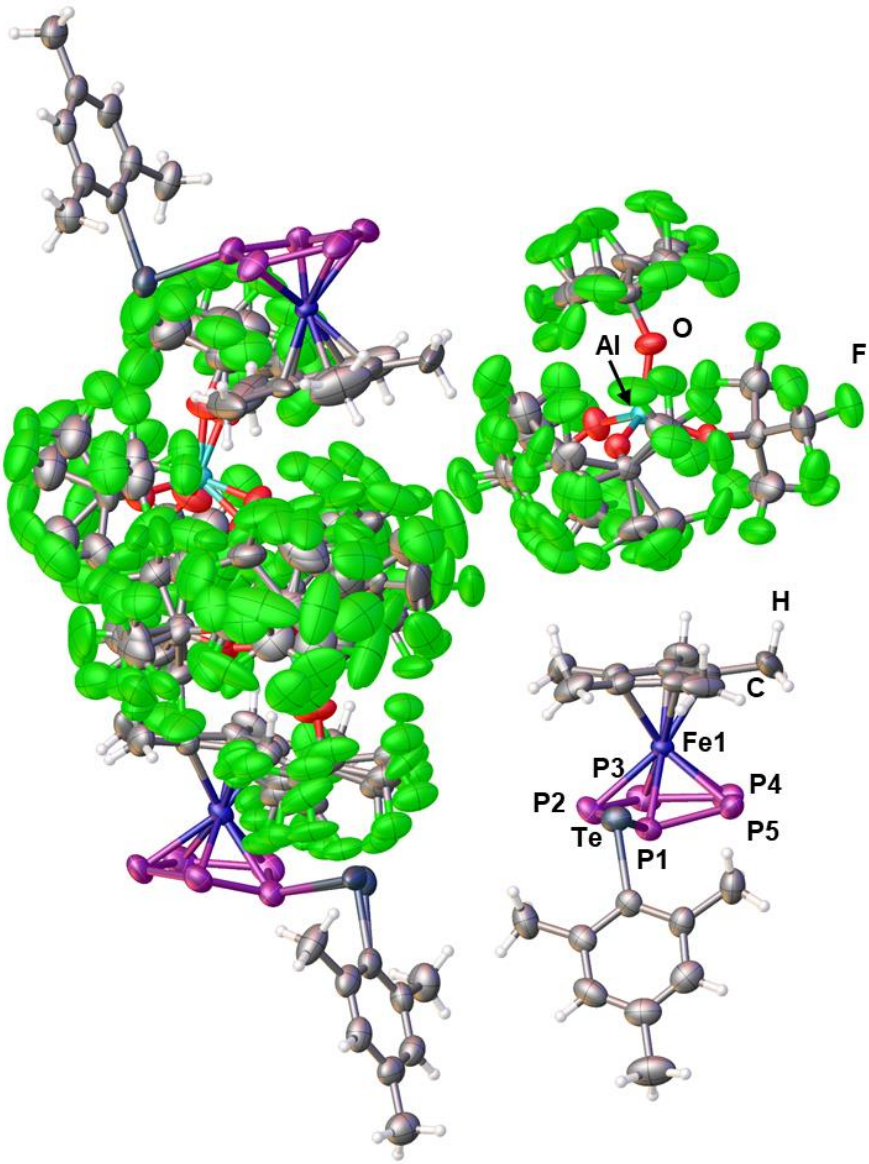

*Figure S 9: Solid state structure of **10**; Depicted is the asymmetric unit and ADPs are drawn at 50% probability; Selected bond lengths and angles within the labelled cation: d(P1-P2) = 2.123(3) Å, d(P2-P3) = 2.092(4) Å, d(P3-P4) = 2.126(3) Å, d(P4-P5) = 2.123(4) Å, d(P1-P5) = 2.105(2) Å, d(P1-Te) = 2.438(2) Å, d(P1*-Fe1*) = 2.314(2) Å, d(P2-Fe1) = 2.340(2) Å, d(P3-Fe1) = 2.393(3) Å, d(P4-Fe1) = 2.376(2) Å, d(P5-Fe1) = 2.344(2) Å, ∢(P3-P5-P2-P1) = 164.93(13)°.*

*[Cp*Fe(η^5-P_5Cl)][TEF] (**11**)*

Dark red block shaped crystals of [Cp*Fe(η^5-P_5Cl)][TEF] (**11**) can easily be obtained from storing mixtures of concentrated solutions in *o*-DFB or CH_2Cl_2 and *n*-hexane at -30 °C for several days. However, the crystal structure of **11** appears to be incommensurate modulated with a 1st order modulation vector of (0.201/-0.032/-0.230). Despite many attempts of recrystallisation and variation of experiment parameters during data collection (e. g. temperature), this modulation could not be resolved. Thus, the solid state structure of **11** cannot be provided within this report and only the cell parameters are given within Table S4.

*Table S 4: Cell parameters for the average unit cell of **11**.*

Empirical formula	$C_{26}H_{15}O_4F_{36}AlP_5ClFe$
Formula weight	1348.51
Temperature/K	122.96(13)
Crystal system	monoclinic
Space group	*P*c
a/Å	20.4081(10)
b/Å	20.4729(11)
c/Å	21.4055(9)
α/°	90
β/°	93.162(4)
γ/°	90
Volume/Å^3	8929.9(8)

*[Cp*Fe(η^5-P_5Br)][TEF] (**12**)*

[Cp*Fe(η^5-P_5Br)][TEF] (**12**) can be obtained as crystalline dark brownish red plates after layering a concentrated solution in CH_2Cl_2 with *n*-hexane (1:7) and storing it at -30 °C for three weeks. **12** crystallises in the monoclinic space group *C*2/*c* with one cation, one anion and one third of a CH_2Cl_2 molecule present in the asymmetric unit. Despite using appropriate geometric and ADP restraints and constraints for handling the severe disorder within both the anion and the cation, proper refinement of the crystal structure was not feasible. Thus, only the major disordered parts of the anion and the cation are depicted in Figure S10 as structural proof. The unit cell parameters of **12** are provided in Table S5.

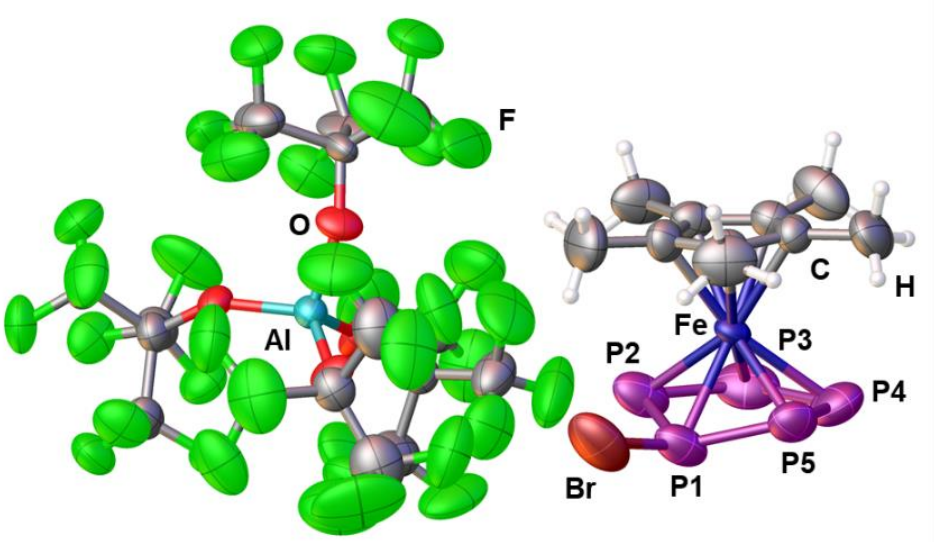

*Figure S 10: Solid state structure of **12**; Depicted is the asymmetric unit and disorder, and solvent molecules are omitted for clarity.*

*Table S 5: Cell parameters for the unit cell of **12**.*

Empirical formula	$C_{26.33}H_{15.66}AlBrCl_{0.66}F_{36}FeO_4P_5$
Formula weight	1420.99
Temperature/K	123.01(10)
Crystal system	monoclinic
Space group	*C*2/*c*
a/Å	30.3586(19)
b/Å	19.7750(4)
c/Å	23.3649(16)
α/°	90
β/°	138.494(13)
γ/°	90
Volume/Å^3	9295.6(18)

*[Cp*Fe(η^5-P_5I)][TEF] (**13**)*

[Cp*Fe(η^5-P_5I)][TEF] (**13**) can be obtained as crystalline dark brown blocks after layering a concentrated solution in *o*-DFB with *n*-pentane (1:10) and storing it at -30 °C for three days. **13** crystallises in the monoclinic space group *C*2/*c* with one cation, one anion and half an equivalent of *o*-DFB present in the asymmetric unit (Figure S11). Disorder within the anion was treated with appropriate geometric and ADP restraints.

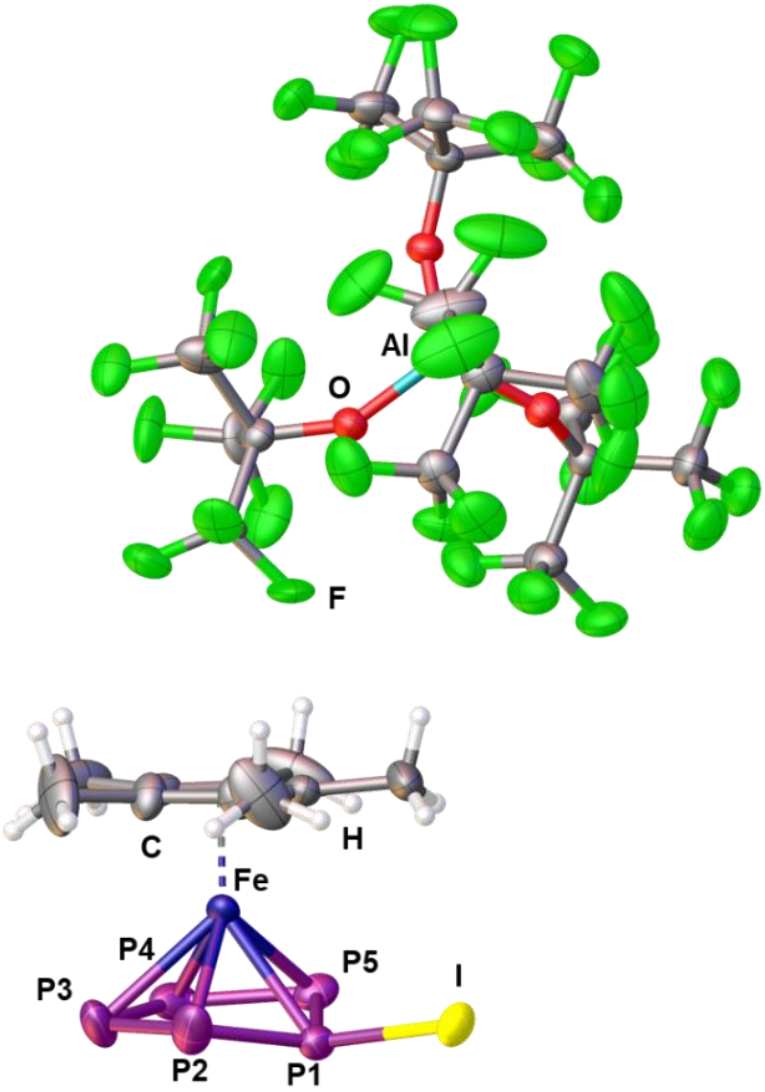

*Figure S 11: Solid state structure of **13**; Depicted is the asymmetric unit and ADPs are drawn at 50% probability; Selected bond lengths and angles within the labelled cation: d(P1-P2) = 2.107(4) Å, d(P2-P3) = 2.106(6) Å, d(P3-P4) = 2.147(6) Å, d(P4-P5) = 2.102(3) Å, d(P1-P5) = 2.112(3) Å, d(P1-I) = 2.385(1) Å, d(P1*-Fe1*) = 2.363(1) Å, d(P2-Fe1) = 2.301(6) Å, d(P3-Fe1) = 2.422(4) Å, d(P4-Fe1) = 2.494(3) Å, d(P5-Fe1) = 2.403(2) Å, ∢(P3-P5-P2-P1) = 156.4(3)°.*

*[{Cp'''Ta(CO)$_2$}$_2${μ,η$^{4:4}$-((P$_4$)$_2$BBr$_2$})][TEF] (**15**)*

[{Cp'''Ta(CO)$_2$}$_2${μ,η$^{4:4}$-((P$_4$)$_2$BBr$_2$})][TEF] (**15**) can be obtained as clear yellow crystals after layering a concentrated solution in *o*-DFB with *n*-pentane (1:6) and storing it at room temperature for one day. **15** crystallises in the triclinic space group $P\bar{1}$ with one cation and one anion in the asymmetric unit (Figure S12). Disorder within the anion was treated with appropriate geometric and ADP restraints.

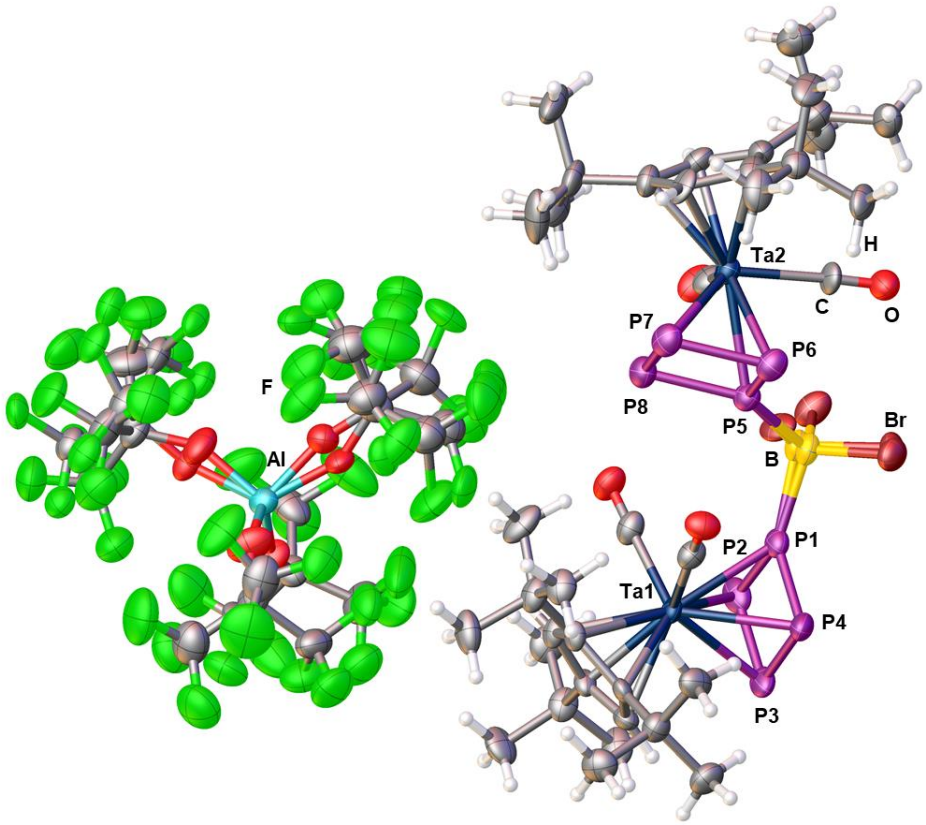

*Figure S 12: Solid state structure of **15**; Depicted is the asymmetric unit and ADPs are drawn at 50% probability; Selected bond lengths and angles within the labelled cation: d(P1-P2) = 2.133(4) Å, d(P2-P3) = 2.171(4) Å, d(P3-P4) = 2.164(4) Å, d(P1-P4) = 2.124(4) Å, d(P5-P6) = 2.129(4) Å, d(P6-P7) = 2.171(4) Å, d(P7-P8) = 2.170(4) Å, d(P5-P8) = 2.149(3) Å, d(P1-B) = 1.997(10) Å, d(P5-B) = 1.996(9) Å, , ∢(P1-B-P5) = 112.3(5)°.*

6.5.3. NMR Spectroscopic Investigations

*[{Cp*Fe}$_2${(η^5-P$_5$)$_2$BBr$_2$}][TEF] (**2**)*

While the ^{1}H NMR spectrum recorded at room temperature only shows one singlet at δ = 1.76 ppm for the Cp* ligands, its´ ^{31}P NMR spectrum (Figure S13) reveals a complex AA'M$_2$M'$_2$X$_2$X'$_2$ spin system with an additional ^{11}B-P coupling (chemical shifts and coupling constants provided in Table S6). Consistently, the ^{11}B{^{1}H} NMR spectrum (Figure S14) of **2** reveals a triplet at δ = -15.6 with a $^1J_{B\text{-}P}$ = 64 Hz coupling constant.

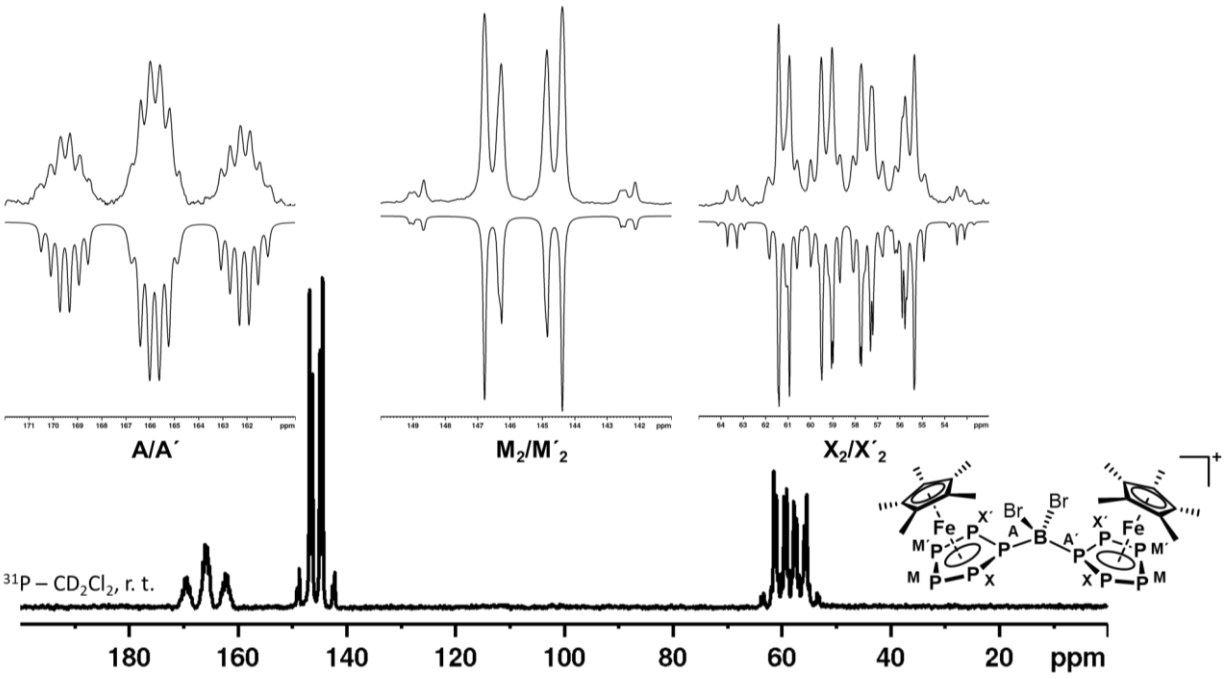

*Figure S 13: Experimental (top) and simulated (bottom) ^{31}P NMR spectrum of **2** in CD_2Cl_2 at room temperature and assignment of the spin system (right).*

*Table S 6: Coupling constants (left) and chemical shifts (right) of **2** in CD_2Cl_2 solution obtained from spectral simulation of the respective ^{31}P NMR spectrum.*

J/ Hz		*δ/ ppm*	
$^1J_{PA/A'\text{-}PX/X'}$	*604.5/589.8*	$P^{A/A'}$	*165.8*
$^1J_{PM/M'\text{-}PX/X'}$	*447.5/436.8*	$P^{M/M'}$	*145.6*
$^1J_{PM\text{-}PM'}$	*415.3*	$P^{X/X'}$	*58.4*
$^2J_{PM/M'\text{-}PX'/X}$	*–58.4/–47.0*		
$^2J_{PA/A'\text{-}PM/M'}$	*6.8/3.8*		
$^2J_{PX\text{-}X'}$	*36.9*		
$^1J_{PA\text{-}A'}$	*123.6*		
$^1J_{PA/A'\text{-}B}$	*64*		

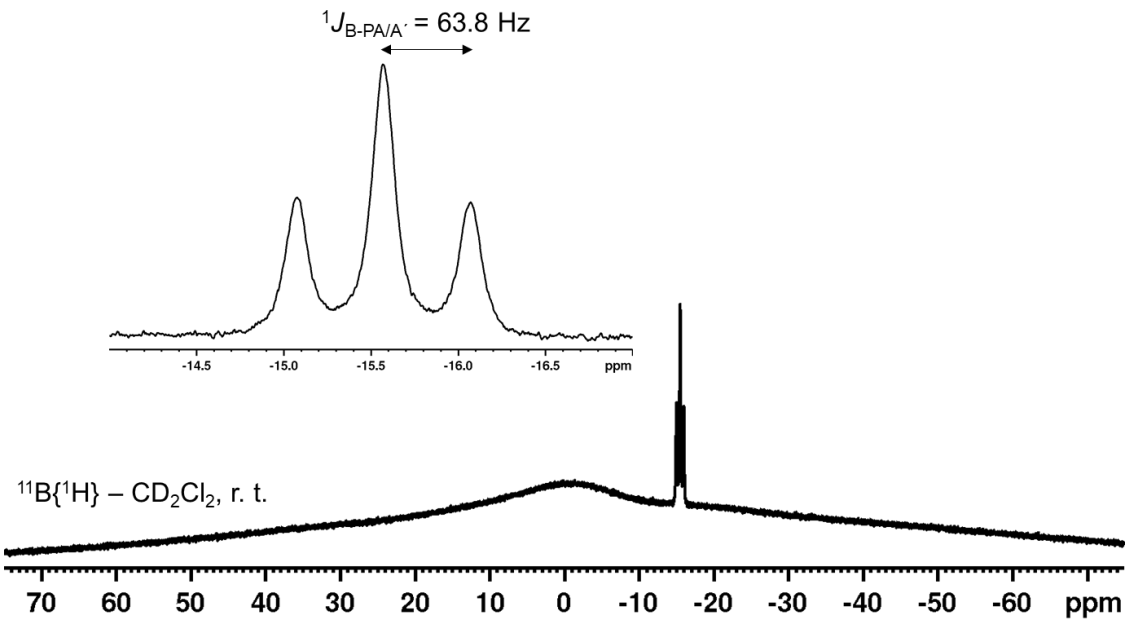

*Figure S 14: $^{11}B\{^1H\}$ NMR spectrum of **2** in CD_2Cl_2 at room temperature.*

*[{Cp*Fe}$_2${(η^5-P_5)$_2$GaI_2}][TEF] (**3**)*

3 is well soluble in *o*-DFB, but shows rapid dynamic behaviour in solution, leading to observation of only one broad signal at room temperature. Even when a crystalline sample of **3**, dissolved in CD_2Cl_2, is cooled to -80 °C this dynamic behaviour is not completely resolved. The $^{31}P\{^1H\}$ NMR spectrum of **3** recorded at -80 °C shows two signals **I** and **II** (Figure S15) at δ = 92.7 and 141.6 ppm integrating in a ratio of 4:6, respectively, thus indicating overlap of two out of the three expected signals. However, **3** slowly decomposes in CD_2Cl_2 solution, which is indicated by the presence of degradation products, such as $[Cp^*Fe(\eta^5\text{-}P_5H)]^+$,[20] in its $^{31}P\{^1H\}$ NMR spectrum.

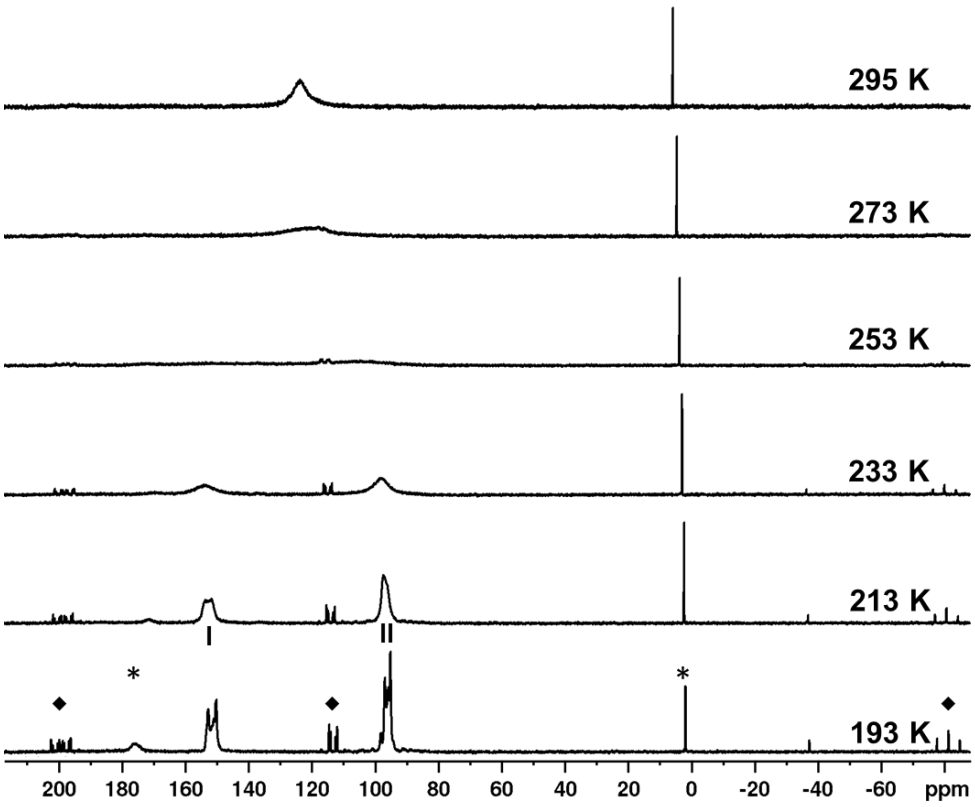

*Figure S 15: $^{31}P\{^1H\}$ NMR spectra of **3** in CD_2Cl_2 recorded at indicated temperatures, revealing its dynamic behaviour in solution (even at –80 °C); ◆ marks the signals assigned to $[Cp^*Fe(\eta^5\text{-}P_5H)]^+$ and * those assigned to corresponding, yet unidentified decomposition products.*

*[Cp*Fe(η^5-P_5CH_2Ph)][TEF] (**4**)*

4 is well soluble in CD_2Cl_2, allowing its NMR spectra to be recorded easily. The ^{1}H NMR spectrum (Figure S18) recorded at room temperature reveals a singlet at δ = 1.73 ppm for the Cp* ligand, a doublet of triplets at δ = 4.42 ppm for the benzylic protons and a multiplet of at δ = 7.40–7.55 ppm for the Ph group. Its´ ^{31}P{^{1}H} NMR spectrum (Figure S16) reveals an AMM'XX' spin system (chemical shifts and coupling constants provided in Table S7), of which the signals for P^A shows additional coupling in the ^{31}P NMR spectrum (Figure S17 and Table S8). The ^{13}C{^{1}H} NMR spectrum (Figure S19) of **4** additionally reveals a small doublet (δ = 26.1 ppm) for the benzylic carbon with a $^1J_{C\text{-}P}$ = 23 Hz coupling constant.

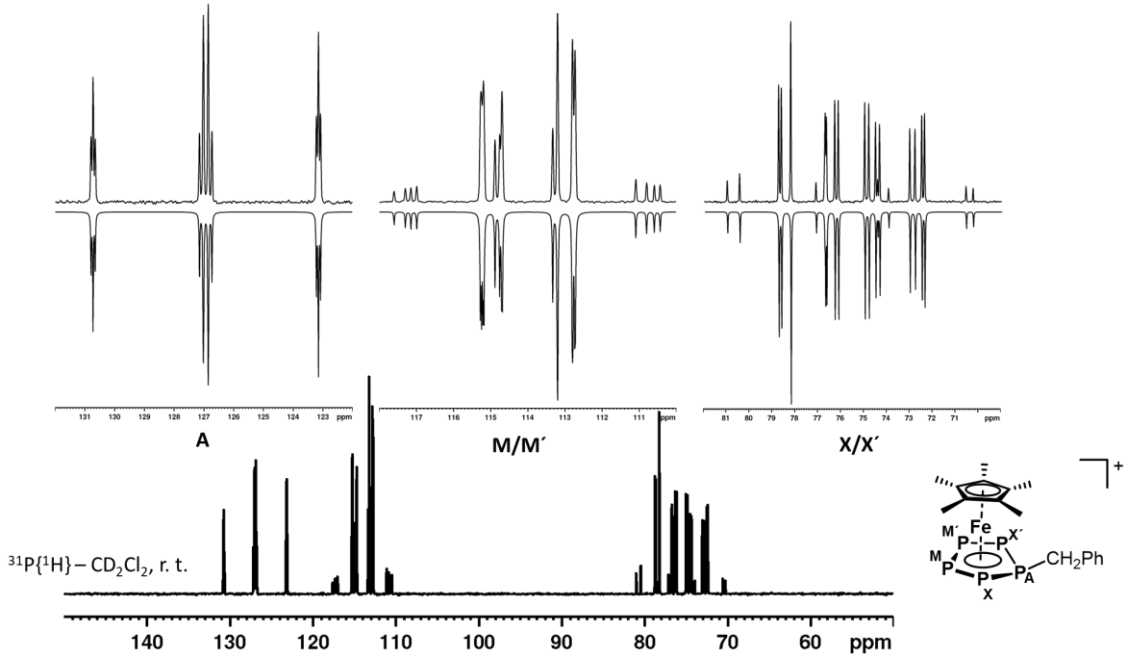

*Figure S 16: Experimental (top) and simulated (bottom) $^{31}P\{^1H\}$ NMR spectrum of **4** in CD_2Cl_2 at room temperature and assignment of the spin system (right).*

*Table S 7: Coupling constants (left) and chemical shifts (right) of **4** in CD_2Cl_2 solution obtained from spectral simulation of the respective $^{31}P\{^1H\}$ NMR spectrum.*

J/ Hz		*δ/ ppm*	
$^1J_{PA\text{-}PX/X'}$	615.4/615.2	P^A	126.8
$^1J_{PM/M'\text{-}PX/X'}$	455.4/454.6	$P^{M/M'}$	113.9
$^1J_{PM\text{-}PM'}$	407.0	$P^{X/X'}$	75.7
$^2J_{PM/M'\text{-}PX'/X}$	–56.0/–55.7		
$^2J_{PA\text{-}PM/M'}$	10.2/9.0		
$^2J_{PX\text{-}X'}$	42.3		

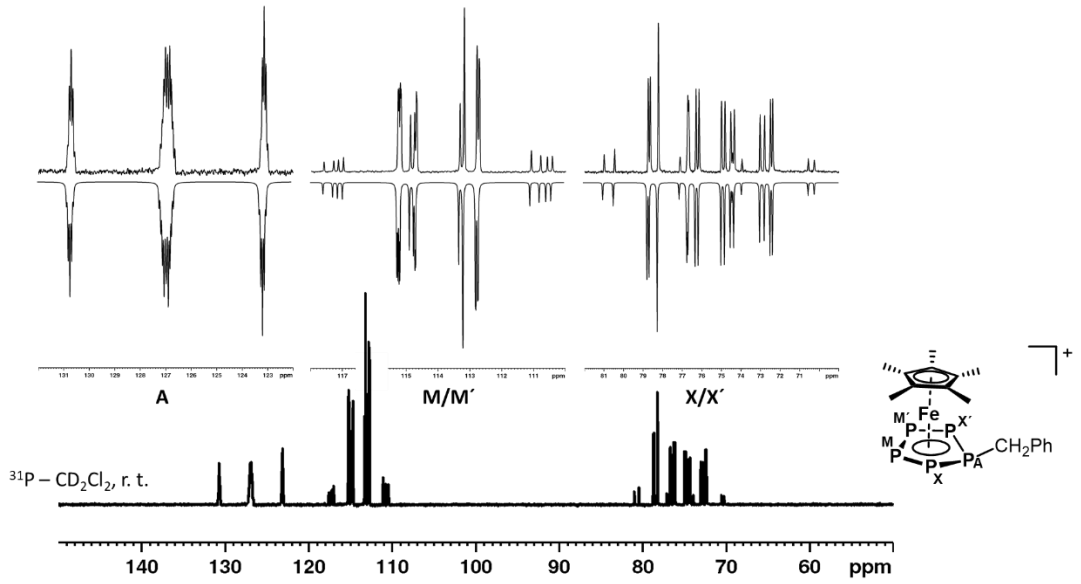

*Figure S 17: Experimental (top) and simulated (bottom) ^{31}P NMR spectrum of **4** in CD_2Cl_2 at room temperature and assignment of the spin system (right).*

*Table S 8: Coupling constants (left) and chemical shifts (right) of **4** in CD_2Cl_2 solution obtained from spectral simulation of the respective ^{31}P NMR spectrum.*

J/ Hz		*δ/ ppm*	
$^1J_{PA\text{-}PX/X'}$	*617.1/613.6*	P^A	*126.8*
$^1J_{PM/M'\text{-}PX/X'}$	*459.3/450.9*	$P^{M/M'}$	*113.9*
$^1J_{PM\text{-}PM'}$	*407.0*	$P^{X/X'}$	*75.7*
$^2J_{PM/M'\text{-}PX'/X}$	*–60.6/–51.2*		
$^2J_{PA\text{-}PM/M'}$	*10.5/9.1*		
$^2J_{PX\text{-}X'}$	*42.1*		
$^2J_{PA\text{-}H}$	*11.3*		

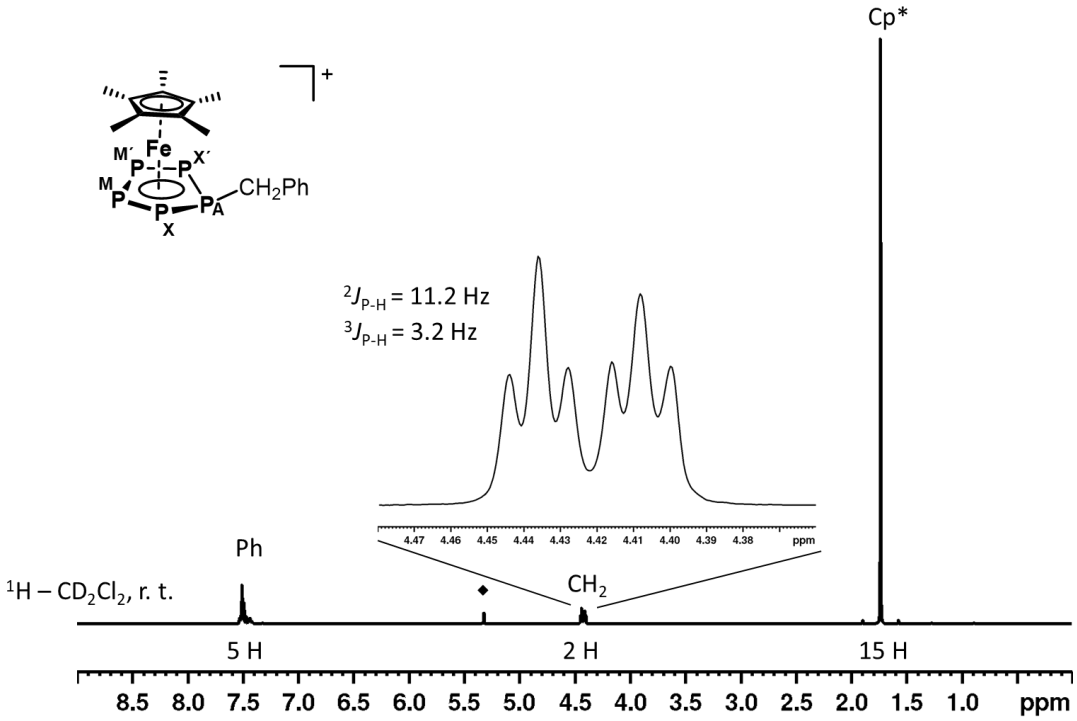

*Figure S 18: ^{1}H NMR spectrum of **4** in CD_2Cl_2 at room temperature; ◆ marks the residual solvent signal for CD_2Cl_2.*

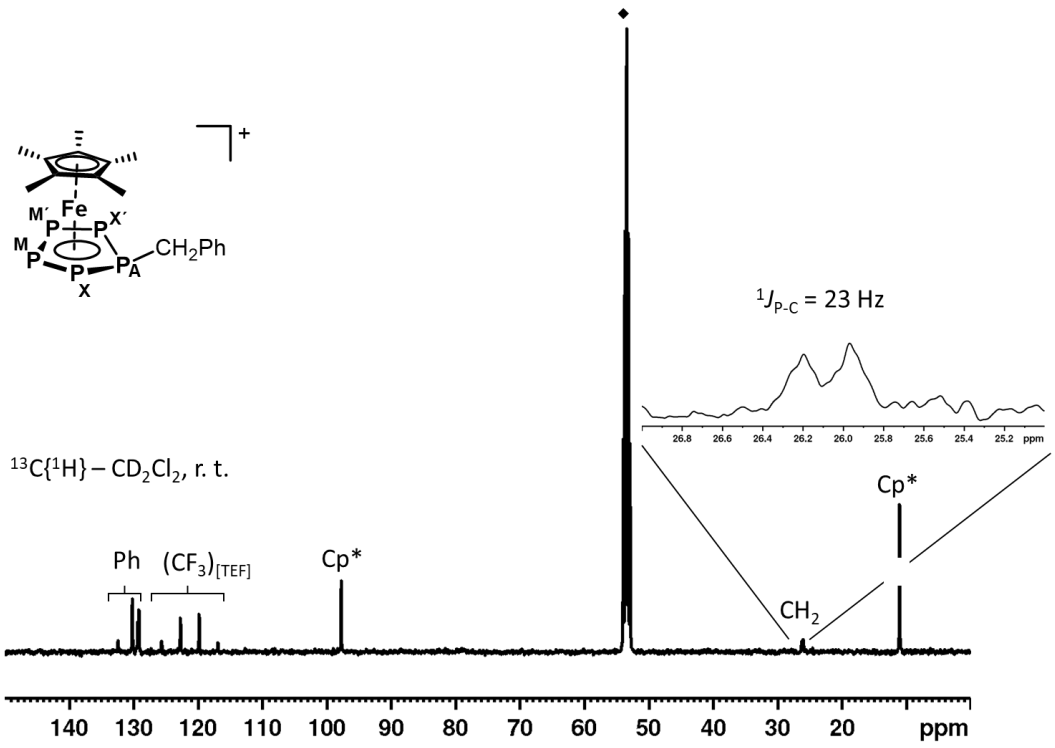

*Figure S 19: $^{13}C\{^1H\}$ NMR spectrum of **4** in CD_2Cl_2 at room temperature; ◆ marks the residual solvent signal for CD_2Cl_2.*

*[Cp*Fe(η^5-P_5CHPh_2)][TEF] (**5**)*

Similar to **4**, compound **5** is well soluble in CD_2Cl_2 and its ^1H NMR spectrum (Figure S22) recorded at room temperature reveals a sharp singlet at δ = 1.64 ppm for the Cp* ligand, a doublet of triplets at δ = 5.93 ppm for the benzylic proton and a set of multiplets in between δ = 7.43-7.72 ppm for the Ph groups. The $^{31}P\{^1H\}$ NMR spectrum (Figure S20) again shows an AMM´XX´ spin system (chemical shifts and coupling constants provided in Table S9), of which the P^A signal shows further coupling in the ^{31}P NMR spectrum (Figure S21 and Table S10). In agreement, the $^{13}C\{^1H\}$ NMR spectrum (Figure S23) of **5** reveals a doublet at δ = 49.3 ppm with a distinct $^1J_{C\text{-}P}$ = 23 Hz coupling constant.

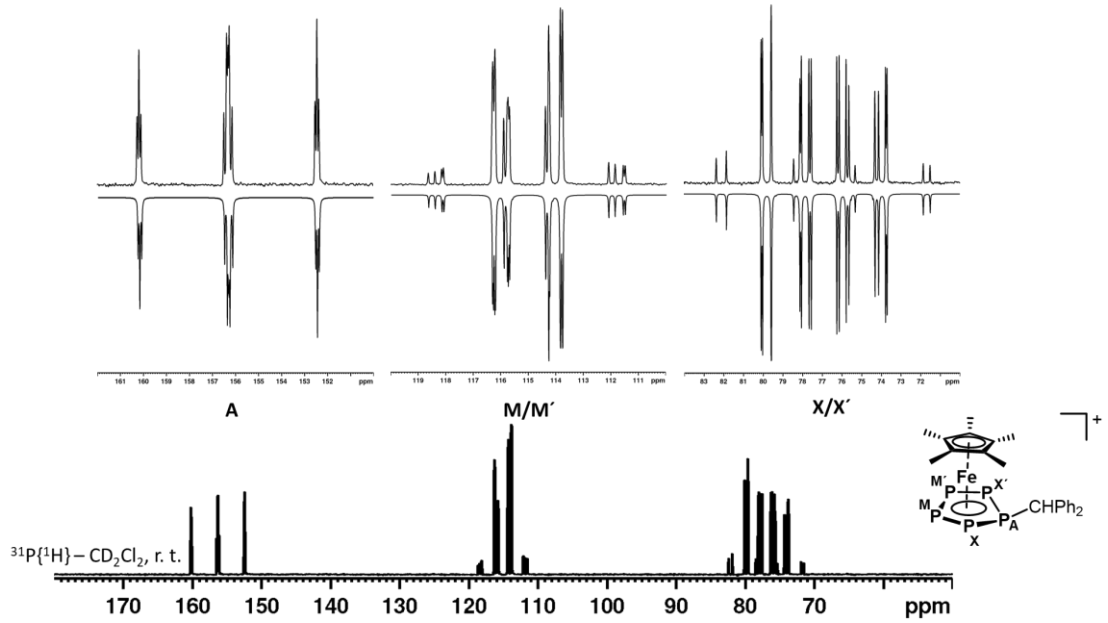

*Figure S 20: Experimental (top) and simulated (bottom) $^{31}P\{^1H\}$ NMR spectrum of **5** in CD_2Cl_2 at room temperature and assignment of the spin system (right).*

*Table S 9: Coupling constants (left) and chemical shifts (right) of **5** in CD_2Cl_2 solution obtained from spectral simulation of the respective $^{31}P\{^1H\}$ NMR spectrum.*

J/ Hz		*δ/ ppm*	
$^1J_{PA\text{-}PX/X'}$	629.8/625.3	P^A	156.2
$^1J_{PM/M'\text{-}PX/X'}$	450.4/449.5	$P^{M/M'}$	115.0
$^1J_{PM\text{-}PM'}$	412.2	$P^{X/X'}$	77.0
$^2J_{PM/M'\text{-}PX'/X}$	–54.5/–54.0		
$^2J_{PA\text{-}PM/M'}$	17.5/6.0		
$^2J_{PX\text{-}X'}$	43.1		

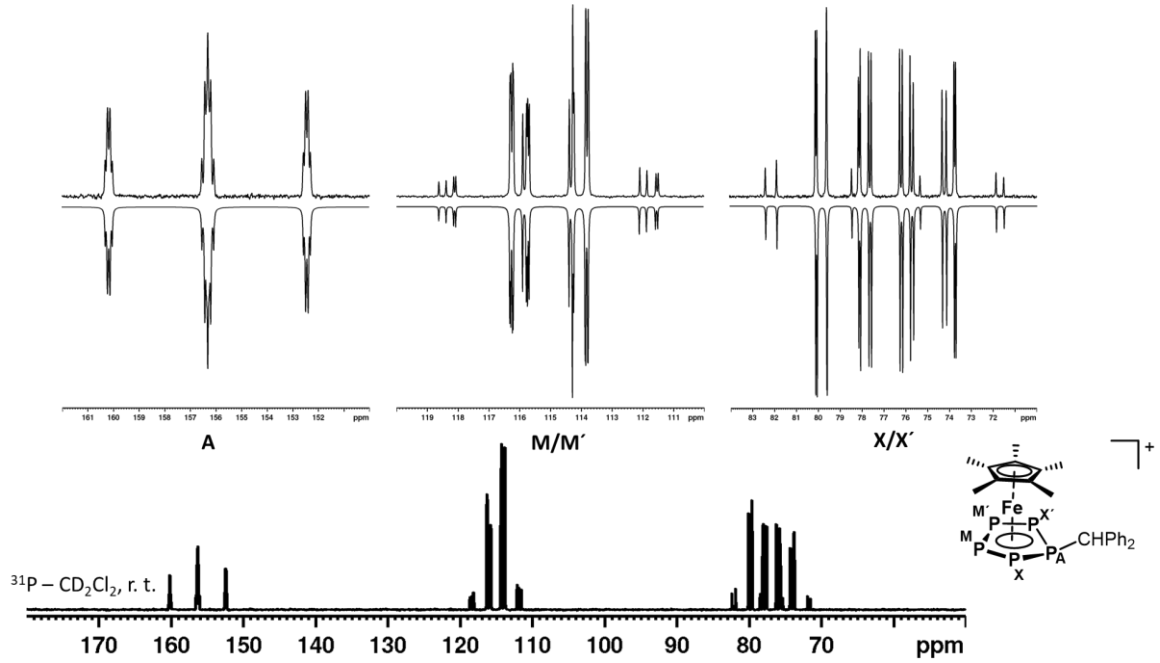

*Figure S 21: Experimental (top) and simulated (bottom) ^{31}P NMR spectrum of **5** in CD_2Cl_2 at room temperature and assignment of the spin system (right).*

*Table S 10: Coupling constants (left) and chemical shifts (right) of **5** in CD_2Cl_2 solution obtained from spectral simulation of the respective ^{31}P NMR spectrum.*

J/ Hz		*δ/ ppm*	
$^1J_{PA\text{-}PX/X'}$	*628.5/626.4*	P^A	*156.2*
$^1J_{PM/M'\text{-}PX/X'}$	*452.7/447.1*	$P^{M/M'}$	*115.0*
$^1J_{PM\text{-}PM'}$	*412.1*	$P^{X/X'}$	*77.0*
$^2J_{PM/M'\text{-}PX'/X}$	*–56.5/–52.1*		
$^2J_{PA\text{-}PM/M'}$	*14.9/9.6*		
$^2J_{PX\text{-}X'}$	*42.9*		
$^2J_{PA\text{-}H}$	*17.3*		

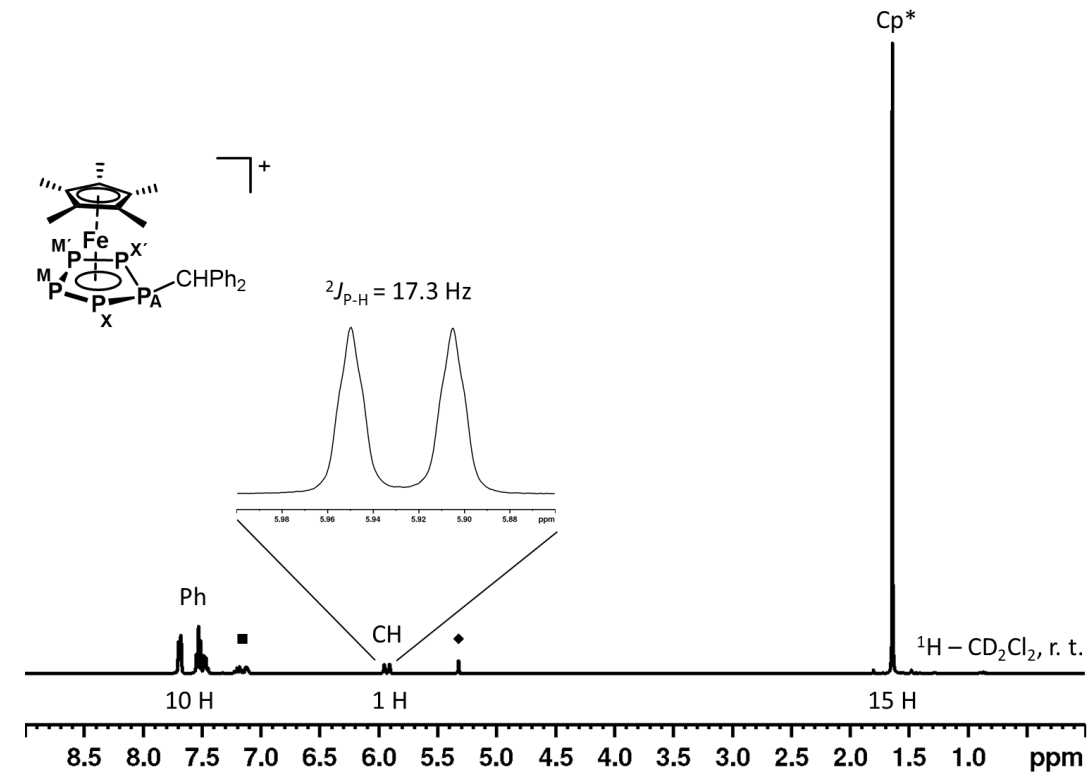

*Figure S 22: ^1H NMR spectrum of **5** in CD_2Cl_2 at room temperature; ◆ marks the residual solvent signal for CD_2Cl_2, ■ marks the signal for residual o-DFB.*

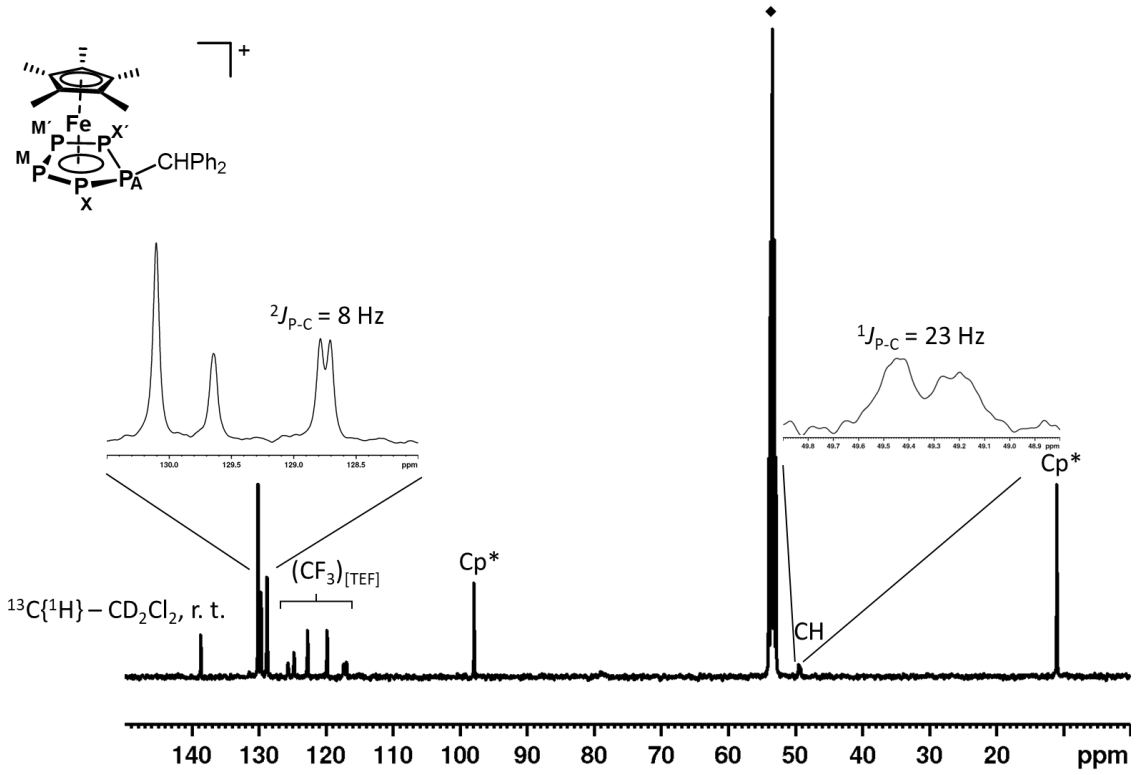

*Figure S 23: $^{13}C\{^1H\}$ NMR spectrum of **5** in CD_2Cl_2 at room temperature; ◆ marks the residual solvent signal for CD_2Cl_2.*

*[Cp*Fe(η^5-P_5SiHPh_2)][$B(C_6F_5)_4$] (**6**)*

While **6** is well soluble in *o*-DFB, its ^{31}P NMR spectrum at room temperature reveals significant dynamic behaviour as indicated by the presence of three broad signals at δ = 76.4,102.6 and 141.1 ppm. However, even cooling a sample of **6** in CD_2Cl_2 to –80 °C does not resolve this dynamic behaviour and additionally leads to partial degradation by the solvent (Figure S24). The product of this degradation may be formulated as $[Cp^*Fe(\eta^5\text{-}P_5CH_2Cl)]^+$ due to the similarity of its $^{31}P\{^1H\}$ NMR spectrum with that of $[Cp^*Fe(\eta^5\text{-}P_5Me)]^+$.[20] Thus, obtaining a well resolved spectrum of **6** cannot be achieved and no coupling information could be extracted from its ^{31}P and $^{31}P\{^1H\}$ spectra. Peak assignment is still possible by comparison of the peak shape with similar compounds reported herein. In contrast, the ^{29}Si(DEPT135) spectrum of **6** in CD_2Cl_2 recorded at –30 °C shows a doublet of multiplets ($^1J_{Si\text{-}P}$ = 239 Hz) at –20 ppm manifesting its integrity (although dynamic) in solution (Figure S25).

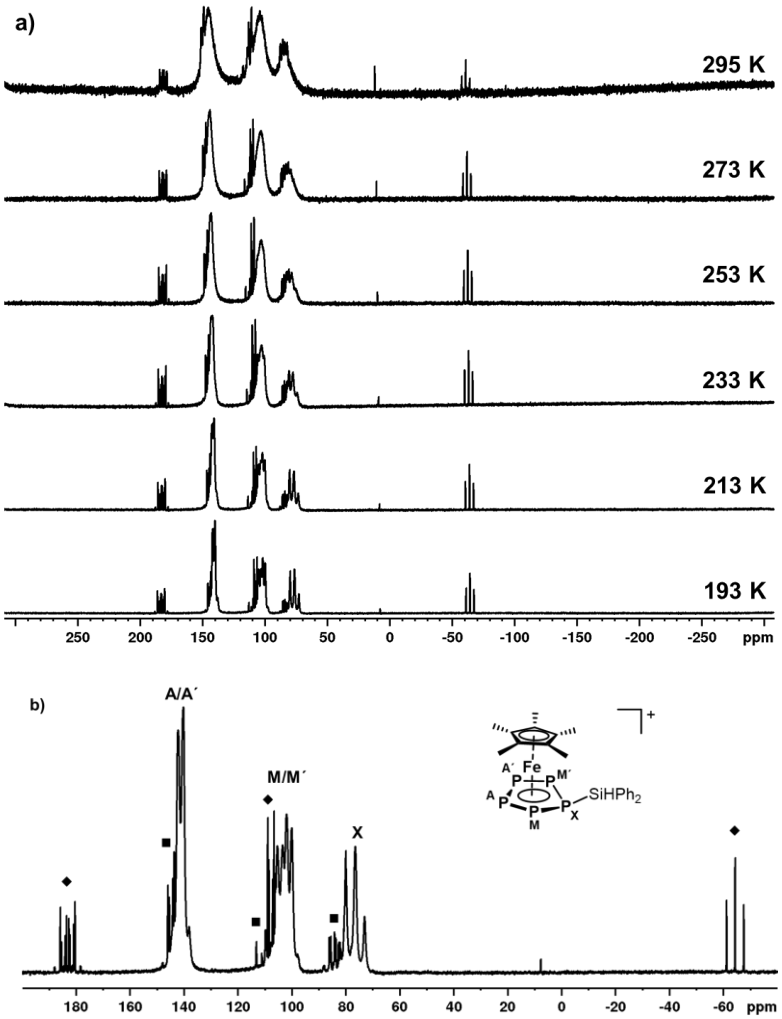

*Figure S 24: a) $^{31}P\{^1H\}$ NMR spectra of **6** in CD_2Cl_2 recorded at indicated temperatures, revealing its dynamic behaviour in solution (even at –80 °C); b) $^{31}P\{^1H\}$ NMR spectrum of **6** in CD_2Cl_2 at –80 °C with assignment of the spin system; ◆ marks the signals for $[Cp^*Fe(\eta^5\text{-}P_5H]^+$, which is formed in the presence of traces of moisture (< 3 ppm in solvents and on glass surfaces), ■ marks a group of signals, which is assigned to $[Cp^*Fe(\eta^5\text{-}P_5CH_2Cl]^+$ arising from degradation of **6** in CD_2Cl_2.*

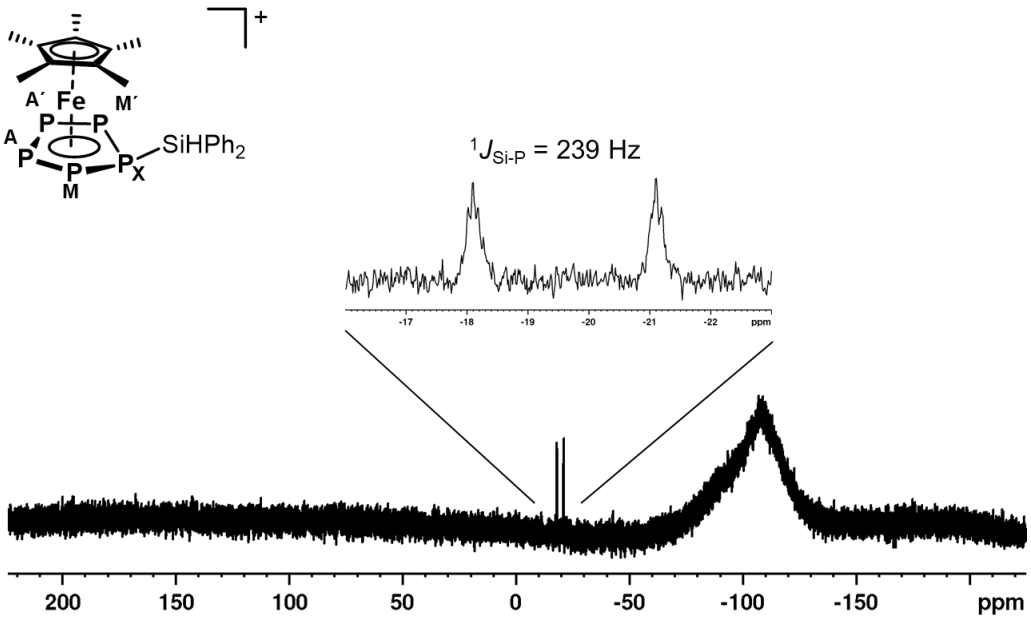

*Figure S 25: ^{29}Si(DEPT135) NMR spectrum of **6** in CD_2Cl_2 recorded at –30 °C with 4096 scans.*

*[Cp*Fe(η^5-P_5AsCy_2)][TEF] (**7**)*

The ^{1}H NMR spectrum of **7** in CD_2Cl_2 shows a signal at δ = 1.62 ppm for the Cp* ligand and multiple broad signals in between δ = 1.34-2.94 for the Cy groups. The corresponding ^{31}P NMR spectrum reveals a complex AA´BB´X spin system with slight line broadening. Cooling the sample to 273 K leads to an even better resolved ^{31}P NMR spectrum (Figure S26, chemical shifts and coupling constants provided in Table S11), which agrees with the molecular structure of **7**.

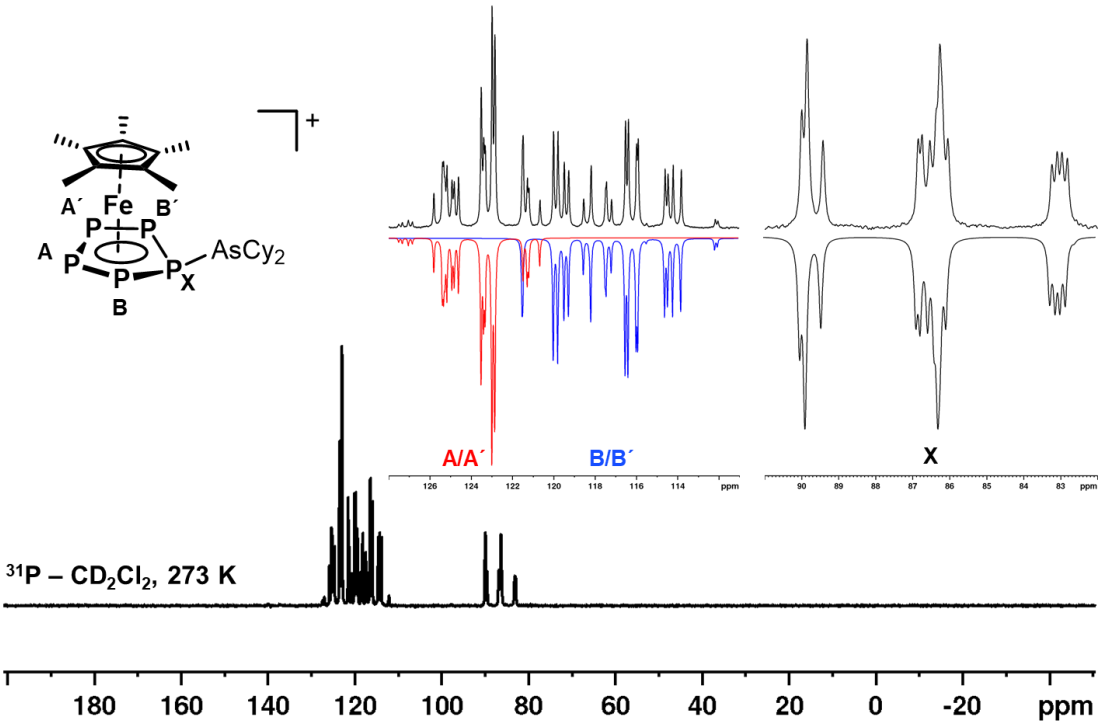

*Figure S 26: Experimental (top) and simulated (bottom) ^{31}P NMR spectrum of **7** in CD_2Cl_2 at 273 K and assignment of the spin system (top left).*

*Table S 11: Coupling constants (left) and chemical shifts (right) of **7** in CD_2Cl_2 solution obtained from spectral simulation of the respective ^{31}P NMR spectrum.*

J/ Hz		*δ/ ppm*	
$^1J_{PX\text{-}PB/B'}$	576.0/574.5	$P^{A/A'}$	123.9
$^1J_{PA/A'\text{-}PB/B'}$	432.9/430.0	$P^{B/B'}$	117.1
$^1J_{PA\text{-}PA'}$	420.1	P^{X}	86.6
$^2J_{PA/A'\text{-}PB'/B}$	–52.0/–50.5		
$^2J_{PX\text{-}PA/A'}$	10.2/3.8		
$^2J_{PB\text{-}B'}$	22.2		

*[{Cp*Fe(μ,η$^{5:2}$-P$_5$)}SbICp'''][TEF] (**8**)*

While the ^{1}H NMR spectrum of **8** in CD_2Cl_2 recorded at room temperature reveals the signals for the respective Cp* and Cp''' groups, the respective ^{31}P NMR spectrum only shows a singlet at δ = 164.7 ppm. We thus carried out a VT NMR study (Figure S27) on **8**, but even at -80°C the signal, now located at δ = 172.9 ppm, does not show any splitting. This highlights the extreme dynamic behaviour of **8** in solution.

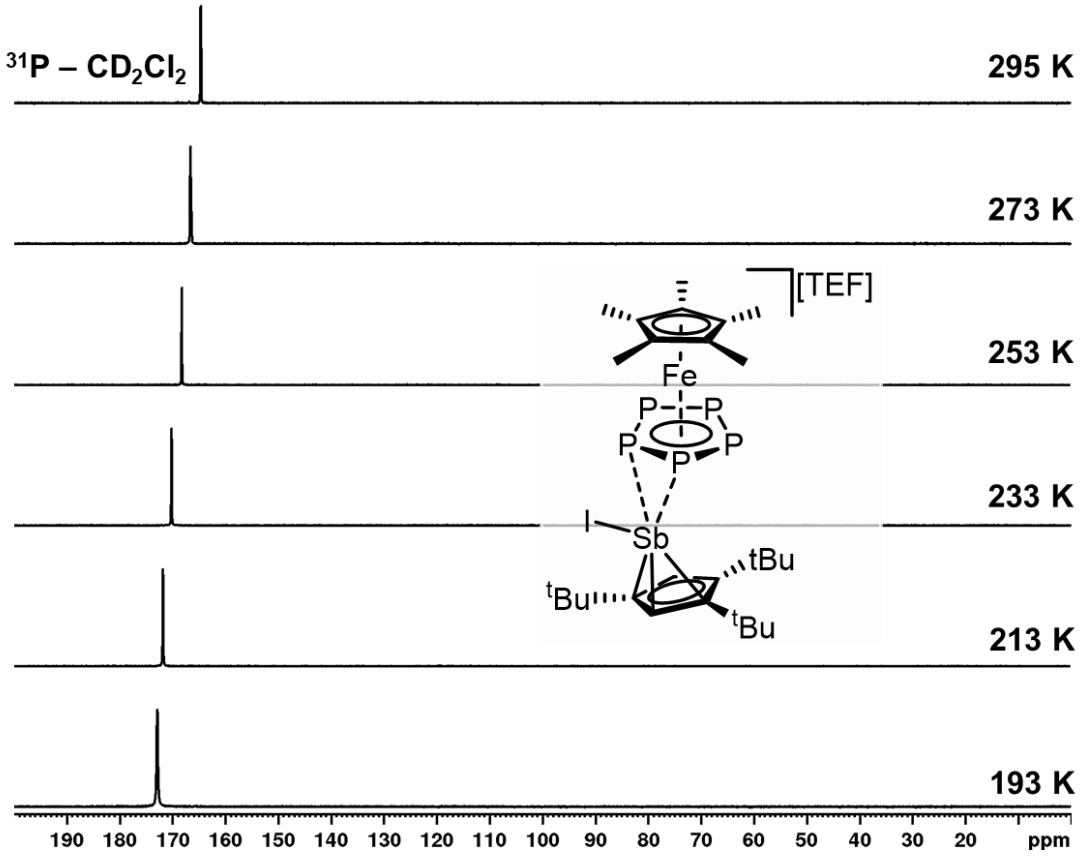

*Figure S 27: ^{31}P NMR spectra of **8** in CD_2Cl_2 at specified temperatures.*

*[Cp*Fe(η^5-P_5SePh)][TEF] (**9**)*

The ^{1}H NMR spectrum of **9** in CD_2Cl_2 at room temperature shows the expected signals for the Cp* ligand and the Ph group at δ = 1.75 and 7.47-7.90 ppm, respectively. The corresponding ^{31}P NMR spectrum (Figure S28) reveals an AA´MM´X spin system (chemical shifts and coupling constants provided in Table S12), in which the P^X signal has additional ^{77}Se satellites with a $^1J_{P\text{-}Se}$ = 418 Hz coupling constant. This coupling constant is corroborated by the ^{77}Se{^{1}H} NMR spectrum (Figure S29) of **9** in CD_2Cl_2 solution, which shows a doublet at δ = 287.3 ppm.

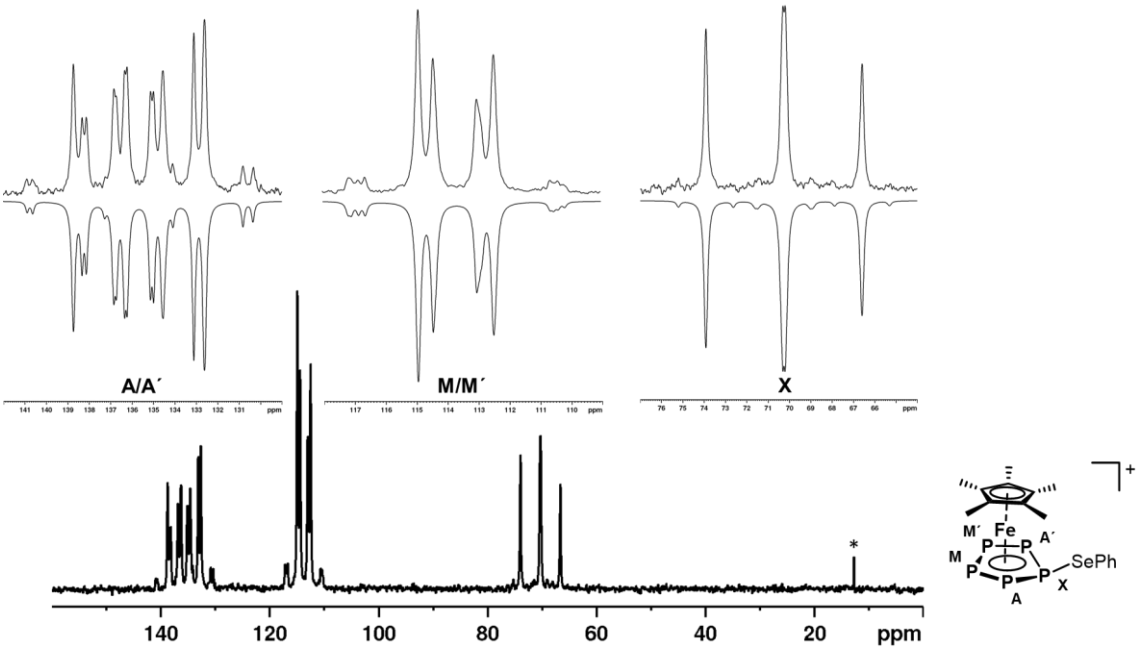

*Figure S 28: Experimental (top) and simulated (bottom) ^{31}P NMR spectrum of **9** in CD_2Cl_2 at room temperature and assignment of the spin system (right); * marks the signal for trace impurities of an unidentified species.*

*Table S 12: Coupling constants (left) and chemical shifts (right) of **9** in CD_2Cl_2 solution obtained from spectral simulation of the respective ^{31}P NMR spectrum.*

J/ Hz		*δ/ ppm*	
$^1J_{PA/A´\text{-}PX}$	*596.9/595.4*	$P^{A/A´}$	*135.5*
$^1J_{PA/A'\text{-}PM/M'}$	*448.4/441.1*	$P^{M/M'}$	*113.8*
$^1J_{PM\text{-}PM'}$	*413.3*	P^X	*70.4*
$^2J_{PA/A'\text{-}PM'/M}$	*–54.2/–48.3*		
$^2J_{PM/M´\text{-}PX}$	*7.8/2.4*		
$^2J_{PA\text{-}A'}$	*37.3*		
$^1J_{PX\text{-}Se}$	*418*		

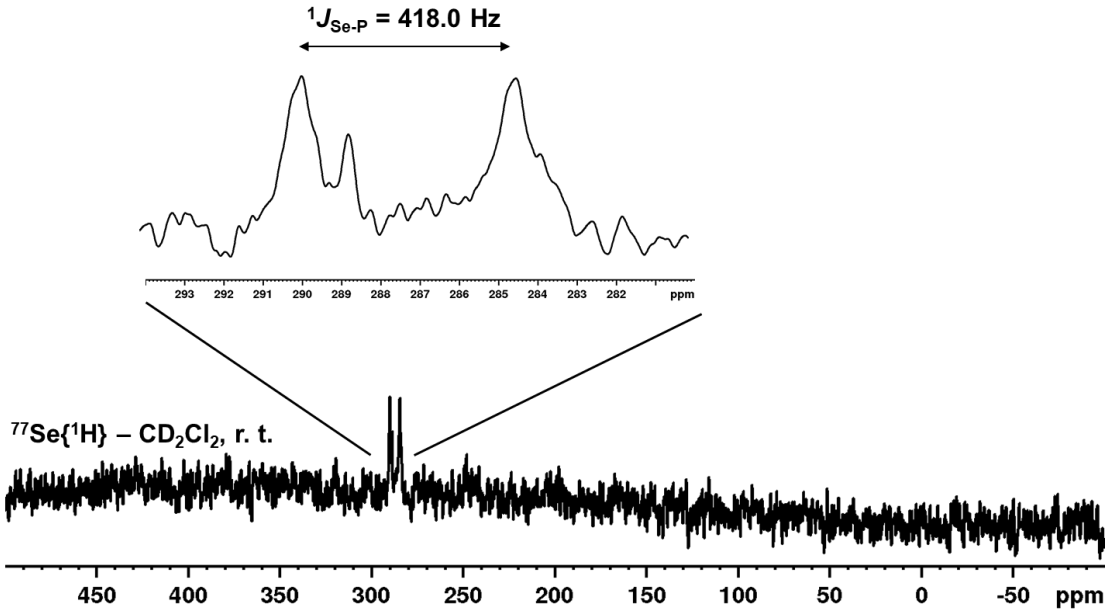

*Figure S 29: $^{77}Se\{^1H\}$ NMR spectrum of **9** in CD_2Cl_2 recorded at room temperature with 11000 scans and a dwell time of 6.6 s.*

*[Cp*Fe(η^5-P_5TeMes)][TEF] (**10**)*

While **10** is well soluble in *o*-DFB, its ^{31}P NMR spectrum at room temperature reveals significant dynamic behaviour as indicated by the presence of one extremely broadened signal at δ = 126.3 ppm. Cooling a sample of **10** in CD_2Cl_2 to –80 °C leads to splitting into three signals (Figure S30) located at δ = 10.0, 124.9 and 139.3 ppm but also to partial degradation. Thus, obtaining a well resolved spectrum of **10** cannot be achieved and no coupling information could be extracted from its ^{31}P and ^{31}P{^{1}H} spectra.

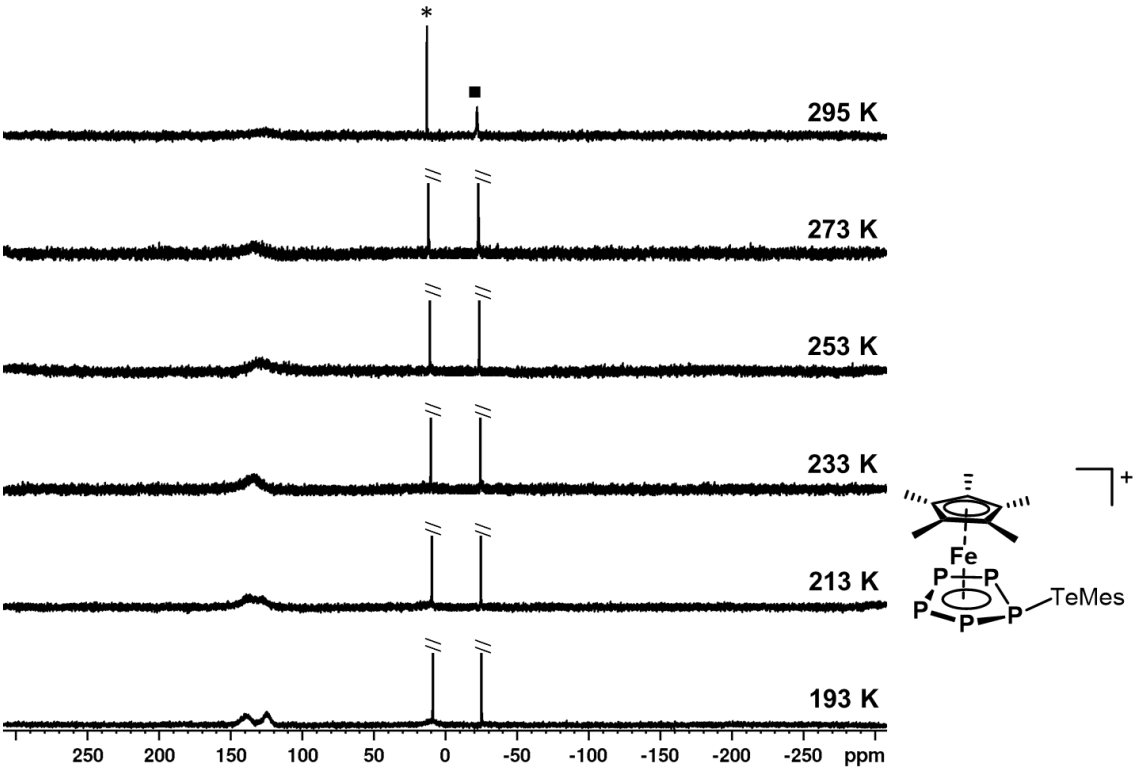

*Figure S 30: ^{31}P{^{1}H} NMR spectra of **10** in CD_2Cl_2 recorded at specified temperatures * marks the signals for trace impurities of two unidentified species arising from degradation of **10**.*

*[Cp*Fe(η^5-P_5Cl)][TEF] (**11**)*

As compound **11** is well soluble in CD_2Cl_2, its NMR spectra can easily be recorded. Its ^{1}H NMR spectrum recorded at room temperature only reveals one singlet for the Cp* ligand at δ = 1.73 ppm. The respective ^{31}P NMR spectrum (Figure S31) shows an AA´MXX´ spin system (chemical shifts and coupling constants provided in Table S13), manifesting the structure of **11** in solution.

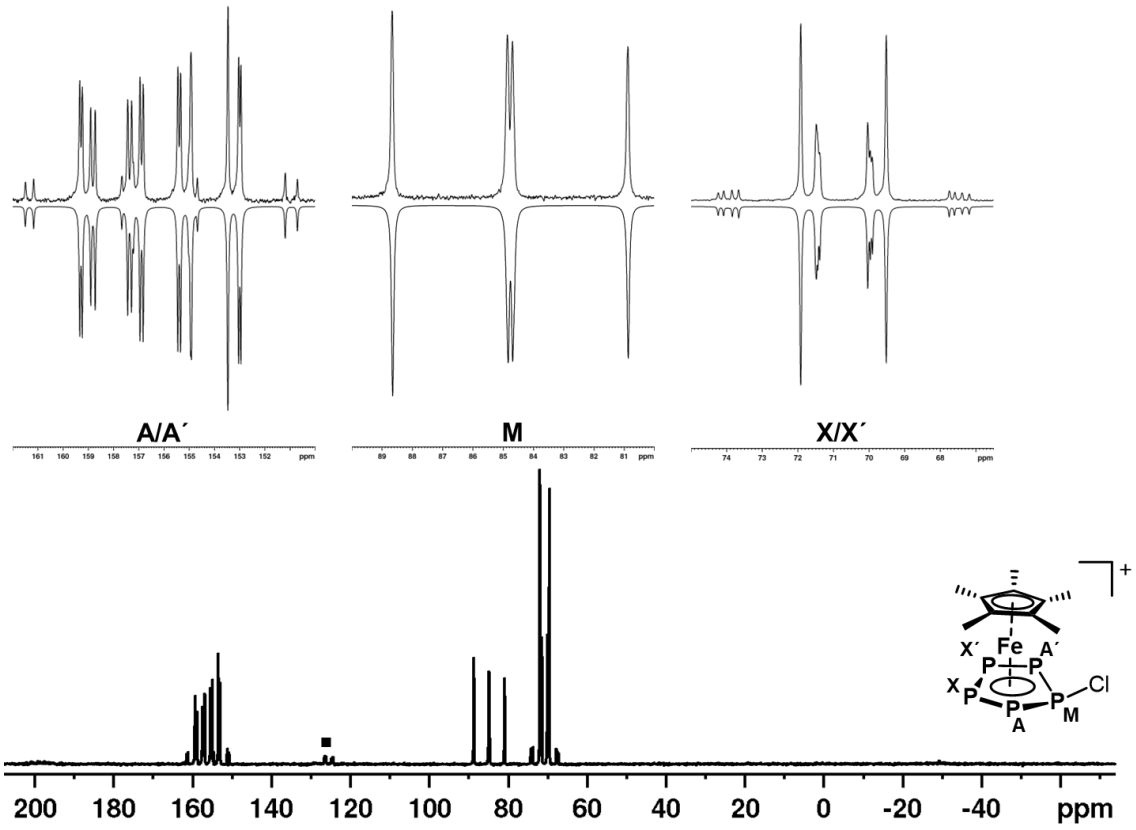

*Figure S 31: Experimental (top) and simulated (bottom) ^{31}P NMR spectrum of **11** in CD_2Cl_2 at room temperature and assignment of the spin system (right); ■ marks a signal for trace impurities of [{Cp*Fe}$_2$(μ,$\eta^{5:5}$-P_{10})]$^{2+}$.*

*Table S 13: Coupling constants (left) and chemical shifts (right) of **11** in CD_2Cl_2 solution obtained from spectral simulation of the respective ^{31}P NMR spectrum.*

J/ Hz		*δ/ ppm*	
$^1J_{PA/A´-PM}$	*637.3/626.9*	$P^{A/A´}$	*156.6*
$^1J_{PA/A'-PX/X´}$	*461.8/426.0*	P^{M}	*84.9*
$^1J_{PX-PX'}$	*406.2*	$P^{X/X´}$	*70.7*
$^2J_{PA/A´-PX'/X}$	*–71.2/–37.6*		
$^2J_{PM-PX/X´}$	*6.1/2.0*		
$^2J_{PA-A'}$	*41.7*		

*[Cp*Fe(η^5-P_5Br)][TEF] (**12**)*

Compound **12** is well soluble in CD_2Cl_2, its NMR spectra can easily be recorded. Its ^{1}H NMR spectrum recorded at room temperature only reveals one singlet for the Cp* ligand at δ = 1.73 ppm. The respective ^{31}P NMR spectrum (Figure S32) shows an AA´MM´X spin system (chemical shifts and coupling constants provided in Table S14), manifesting the structure of **12** in solution.

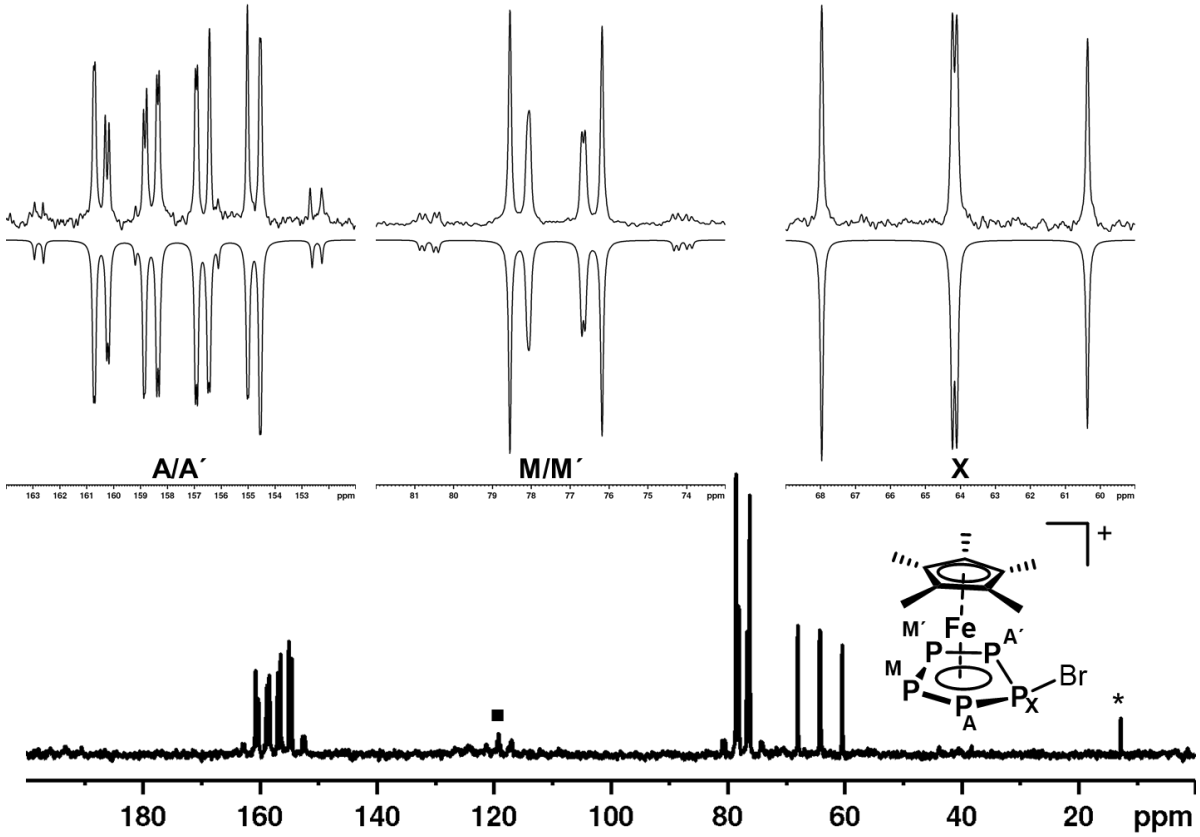

*Figure S 32: Experimental (top) and simulated (bottom) ^{31}P NMR spectrum of **12** in CD_2Cl_2 at room temperature and assignment of the spin system (right); ■ marks a signal for trace impurities of [{Cp*Fe}$_2$(μ,$\eta^{5:5}$-P_{10})]$^{2+}$, and * marks the signalfor trace impurities of an unidentified species.*

*Table S 14: Coupling constants (left) and chemical shifts (right) of **12** in CD_2Cl_2 solution obtained from spectral simulation of the respective ^{31}P NMR spectrum.*

J/ Hz		*δ/ ppm*	
$^1J_{PA/A´-PX}$	*616.4/615.2*	$P^{A/A´}$	*135.5*
$^1J_{PA/A'-PM/M'}$	*439.0/436.5*	$P^{M/M'}$	*113.8*
$^1J_{PM-PM'}$	*415.6*	P^{X}	*70.4*
$^2J_{PA/A'-PM'/M}$	*–58.0/–49.4*		
$^2J_{PM/M´-PX}$	*-1.8/-1.4*		
$^2J_{PA-A'}$	*34.4*		

*[Cp*Fe(η^5-P_5I)][TEF] (**13**)*

As compound **13** is well soluble in CD_2Cl_2, its NMR spectra can easily be recorded. Its ^{1}H NMR spectrum recorded at room temperature only reveals one singlet for the Cp* ligand at δ = 1.67 ppm. The respective ^{31}P NMR spectrum however only shows a broad signal at room temperature. We thus carried out a VT NMR study (Figure S33) on **13**, which revealed splitting of the signal upon cooling. However, the dynamic behaviour of **13** in solution is manifested in the persistent broadening of the observed signals, even at -80 °C. Assignment of the signals to certain P Atoms in **13** (Figure S33, bottom right) has been carried out by comparison with the spectra of its lighter homologs **11** and **12**.

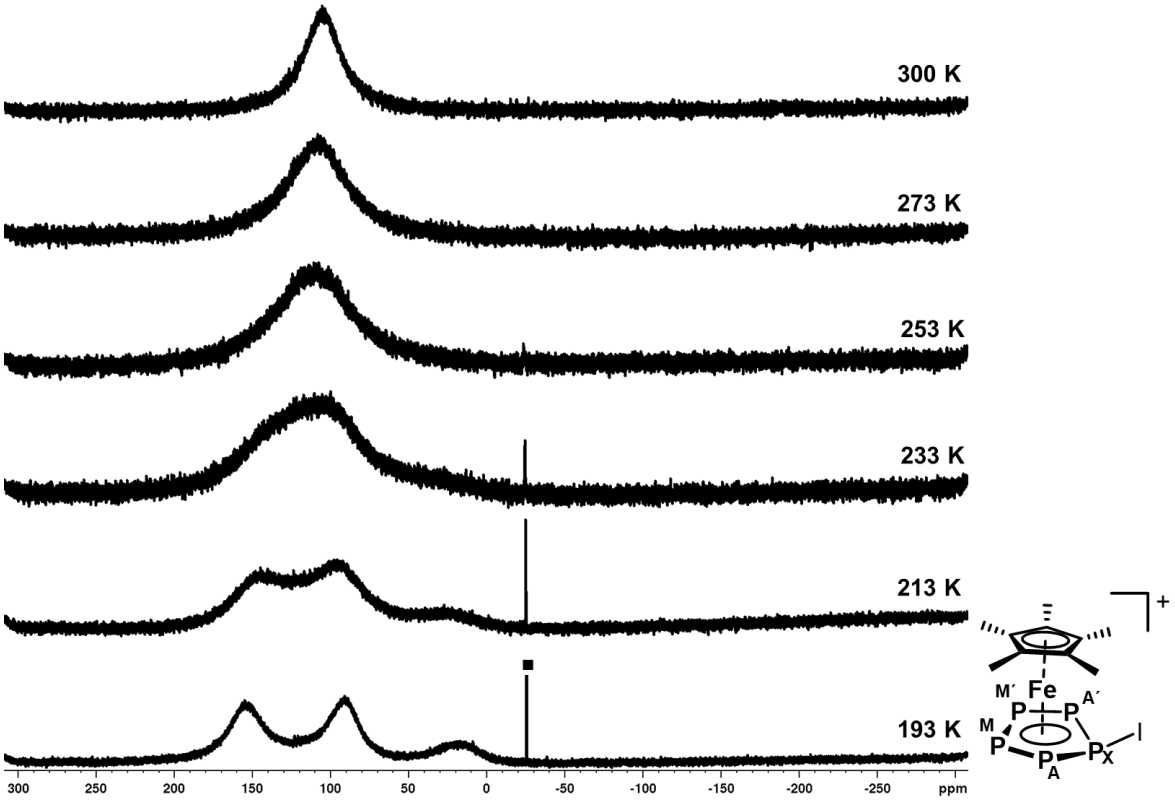

*Figure S 33: $^{31}P\{^1H\}$ NMR spectra of **13** in CD_2Cl_2 recorded at specified temperatures and assignment of the spin system (bottom right); * marks a signal for trace impurities of an unidentified species.*

*[{Cp'''Ta(CO)$_2$}$_2${$\mu,\eta^{4:4}$-((P$_4$)$_2$BBr$_2$})][TEF] (**15**)*

As compound **15** is well soluble in CD_2Cl_2, its NMR spectra can easily be recorded. Its ^{1}H NMR spectrum recorded at room temperature reveals four signals at δ = 1.12, 1.56, 6.33 and 6.34 ppm in agreement with the presence of two chemically equivalent (on the NMR time scale) Cp''' ligands. The ^{31}P NMR spectrum (Figure S34) shows a complex $A_2A'_2MM'XX'Z$ spin system (chemical shift and coupling constants provided in Table S15) and the ^{11}B{^{1}H} NNMR spectrum (Figure S35) corroborates the $^1J_{B\text{-}PM/M'}$ = 61 Hz coupling constant.

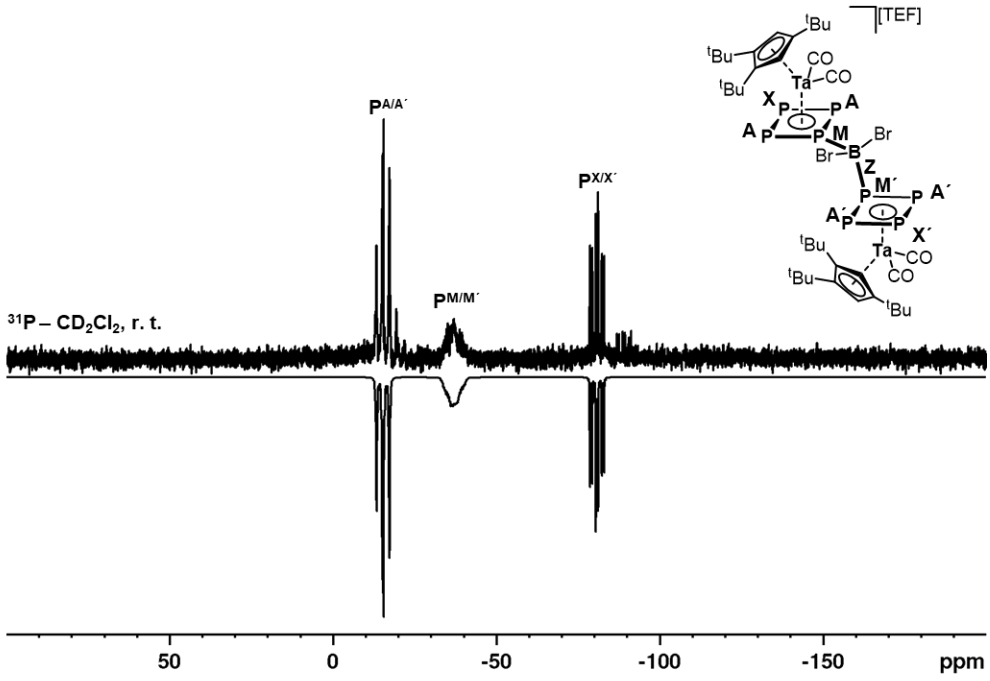

*Figure S 34: Experimental (top) and simulated (bottom) ^{31}P NMR spectrum of **15** in CD_2Cl_2 recorded at room temperature and assignment of the spin system according to the scheme on the right.*

*Table S 15: Coupling constants (left) and chemical shifts (right) of **15** in CD_2Cl_2 solution obtained from spectral simulation of the respective ^{31}P NMR spectrum; Simulation was performed manually and thus coupling constants arre provided without decimals.*

J/ Hz		*δ/ ppm*	
$^1J_{PA/A'\text{-}PM/M'}$	350	$P^{A/A'}$	–15.4
$^1J_{PA/A'\text{-}PX/X'}$	293	$P^{M/M'}$	–37.08 ($\omega_{1/2}$ = 50 Hz)
$^2J_{PM\text{-}PM'}$	120	$P^{X/X'}$	–80.81
$^2J_{PX/X'\text{-}PM/M'}$	117		

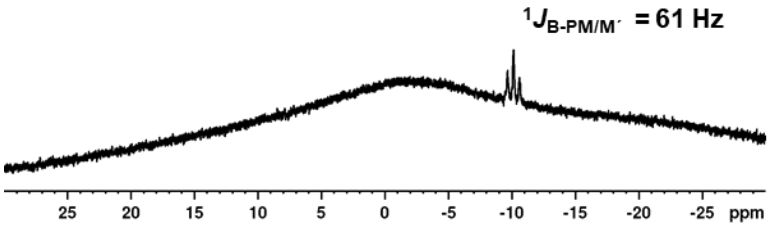

*Figure S 35: $^{11}B\{^1H\}$ NMR spectrum of **15** in CD_2Cl_2 recorded at room temperature.*

Additional Data

When **1** (0.2 mmol, 70 mg, 1 eq.) is reacted with equimolar amounts of BBr_3 (0.2 mmol, 19 μL, 1 eq.) and Tl[TEF] (0.2 mmol, 234 mg, 1 eq.) in *o*-DFB at room temperature, two products can be observed in the $^{31}P\{^1H\}$ NMR spectrum (Figure S36) of the crude reaction mixture. While one of them can clearly be identified as compound **2**, the major product is the protonated species $[Cp^*Fe(\eta^5\text{-}P_5H)]^+$,[20] which we hypothesize to be formed from the reaction of excess borinium species $[BBr_2]^+$ with the solvent *o*-DFB.

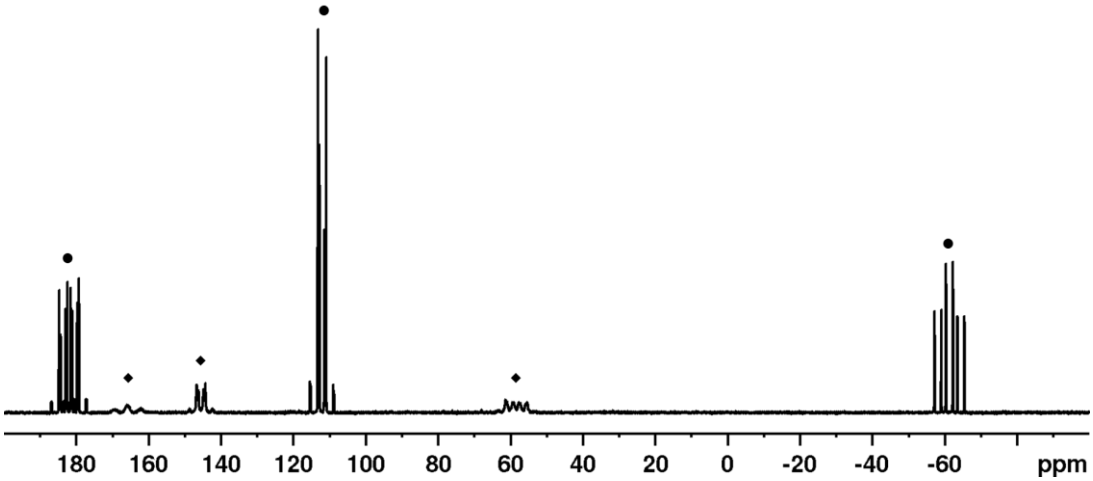

*Figure S 36: ^{31}P NMR spectrum of the crude mixture of **1**, BBr_3 and Tl[TEF] in o-DFB; ◆ marks the signals for compound **2** and ● marks those assigned to the protonated species $[Cp^*Fe(\eta^5\text{-}P_5H)]^+$.*

Attempts to functionalize $[Cp^*Fe(\eta^5\text{-}P_5)]$ (**1**) with *in situ* generated phosphenium ions suffer from the high tendency of phosphinophposphonium ion ($[R_2P\text{-}P(Cl)R_2]^+$) formation upon exposing Chlorophosphanes (R_2PCl, R = Aryl, Alkyl) to Lewis acidic conditions.[27a] As this behavior can be attributed to the high (compared to e. g. the respective Chloroarsines) Lewis basicity of most Chlorophosphanes, we thought PBr_3 could be a suitable phosphenium ion precursor for the functionalization of **1**. Indeed, the desired product $[Cp^*Fe(\eta^5\text{-}P_5PBr_2)]^+$ can

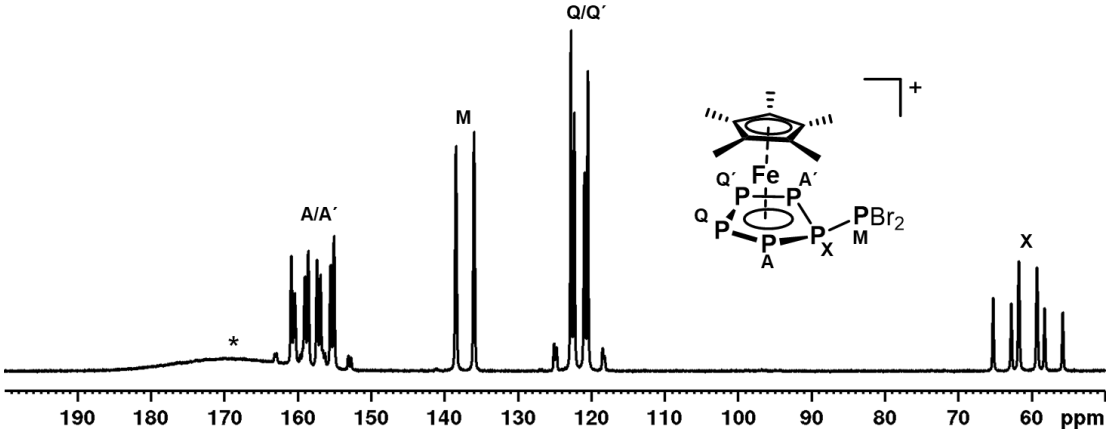

*Figure S 37: $^{31}P\{^1H\}$ NMR spectrum of the reaction mixture containing **1**, PBr_3 and Tl[TEF] (1:1:1) in CD_2Cl_2 recorded at 193 K and signal assignment; * marks the broad signal for **1**, which coordinates to Tl^+ in solution.*

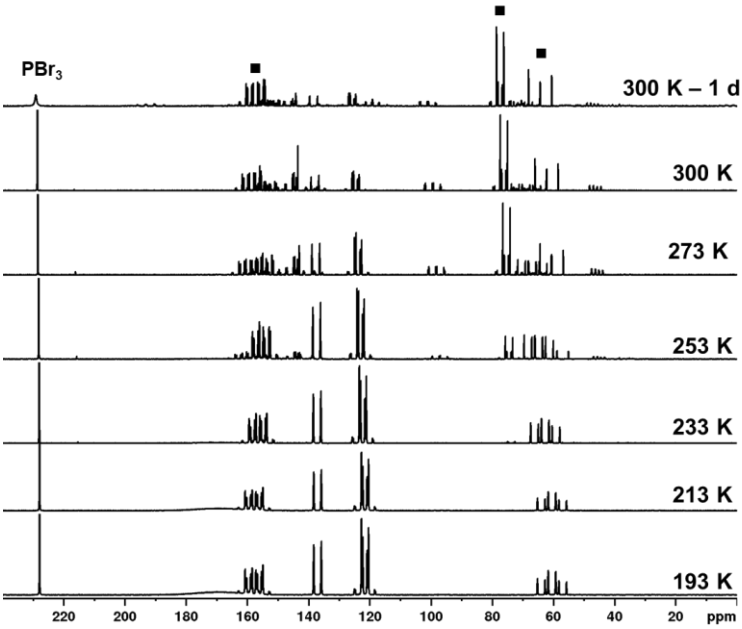

*Figure S 38: $^{31}P\{^{1}H\}$ NMR spectra of the 1:1:1 mixture of **1**, PBr_3 and Tl[TEF] in CD_2Cl_2 recorded at different temperatures and times (right); ■ marks the group of signals assigned to **12**.*

be detected NMR spectroscopically (Figure S37) in mixtures of **1**, PBr_3 and Tl[TEF] in CD_2Cl_2, which are cooled to -80 °C (already after ~10min, the reaction seems to be nearly complete). However, this compound appears to be highly unstable in solution and decomposes above −60 °C, prohibiting its isolation and further characterization. When the sample is allowed to warm from -80 °C to room temperature over the course of 6 h, this decomposition process can be monitored (Figure S38), revealing [Cp*Fe(η^5-P_5Br)][TEF] (**12**) as the major product of this decomposition. However, formation of several other P-containing (and probably ionic) products is visible. Despite various attempts, separation of this product mixture was not possible.

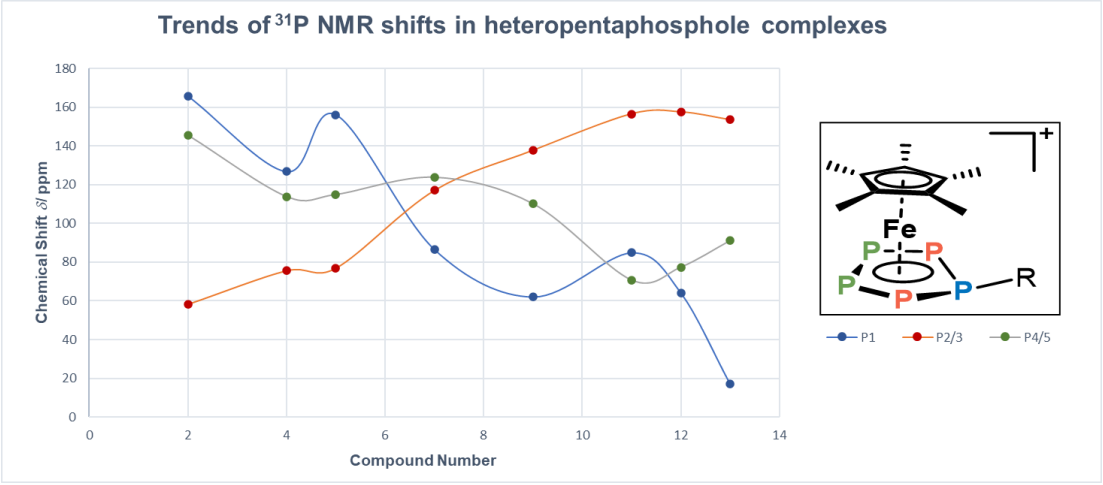

*Figure S 39: ^{31}P Chemical shifts within the pentaphosphole complexes **2**, **4**, **5**, **7**, **9** and **11** – **13** showing a significant upfield shift for P1, while the signal for P2/3 experiences a downfield shift; Spectra of all other pentaphospholes complexes reported herein are not considered as they do not show resolved ^{31}P NMR spectra at room temperature.*

Comparison of the ^{31}P NMR spectra of the obtained pentaphosphole complexes reveals a periodic trend (Figure S39) according to which, the signal assigned to P1 is shifted upfield with the main group of the central atom of the electrophile. Similarly, the signal assigned to P2/3 is shifted downfield in the same order. Note that compounds **3**, **6**, **8** and **10** are not included in this consideration, as they do not show well resolved ^{31}P NMR spectra at room temperature.
Comparison of the above shown NMR spectroscopic data to structural parameters of the respective compounds reveals a very similar periodic trend for the pyramidalization at the P1 atom (which also represents the folding angle of the envelope cyclo-P_5 structure, Figure S40). Both, data from X-ray structural analysis (blue) and computational data (red) show an increase of the pyramidalization at the P1 atom, where the computational data slightly overestimates the experimentally derived values. This may suggest a dependency of the ^{31}P NMR chemical shifts within the studied pentaphosphole complexes on the observed pyramidalization at P1.

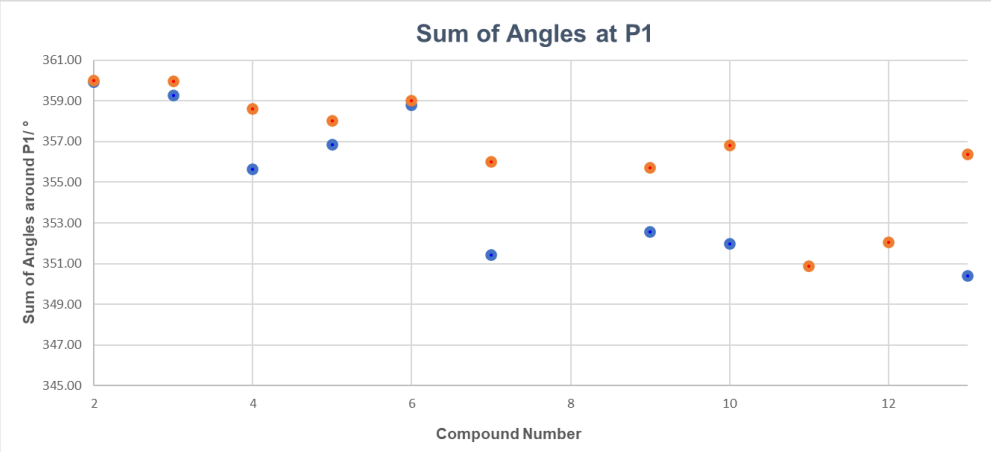

Figure S 40: Summed up ∢(P2-P1-E), ∢(P5-P1-E) and ∢(P2-P1-P1) angles around P1 decreasing with the main group of the central atom of the electrophile determined from Xray crystallographic data (blue) and from the computationally optimized structures (vide infra, red).

6.5.4. Computational Details

General Considerations

DFT calculations were performed using the Gaussian09 software package.[53] Geometry optimizations were performed at the B3LYP[32]/def2-TZVP[33] (or B3LYP/def2-SVP[33] for compounds **14** and **15**) level of theory with PCM solvent correction for CH_2Cl_2.[34] Stationary points were verified by analytical frequency calculations. Magnetic shielding tensors were calculated using the PBE0[38] functional and the basis sets aug-pcSseg-1[39] (for P) and def2-TZVPPD[33,40] (all other atoms). Ring critical points were derived using MultiWFN.[37c] Charge decomposition analysis (CDA)[36] was also performed utilizing MultiWFN. The basis sets def2-TZVPPD and aug-pcSseg-1 were generated with the help of the open access "basis set exchange" web page.[54]

NBO Analyses

NBO analysis was performed on the pre-optimized (B3LYP/def2-TZVP, PCM solvent correction for CH_2Cl_2) molecular structures of **2** – **15** using the NBO6.0 software package[35] and its implementation in Gaussian09. Wiberg bond indices (WBI, Table S16) for the respective P1-E and P1-Fe bonds have also been obtained from these calculations. These WBIs suggest covalent P1-E single bonds for most of the obtained pentaphosphole complexes. However, the WBIs for the P1-Ga and P1-Si bonds in **3** and **6**, respectively, suggest weaker and more polar bonds in these cases. The more expressed bond polarity in these cases is also expressed by the orbital contributions (from P1 and the central atom of the electrophile) to the respective bonding NBO. The P1-E bond lengths determined in the solid state are generally well reproduced by our calculations. However, the closest P-Sb contact in **8** is highly overestimated and no orbital interaction between both fragments could be found. Thus, the structure of **8** seems to mostly depend on electrostatic and dispersive interactions, which is also indicated by its highly dynamic behaviour in solution (*vide supra*). Analysing the natural charges within **2** – **13** reveals a clear trend (Figure S41) for the charge accumulation at the fragment {**1**} and the respective electrophile fragment {E} upon formation of the pentaphosphole complex. Thus, charge transfer, computed via extended charge decomposition analysis (ECDA), increases, the higher the electronegativity (Allred/Rochow) of the central atom of the electrophile is (Figure S42). Again, **8** does not follow this trend, which we attribute to its significantly different molecular structure. Furthermore, the charge transfer in **2** and **3** is more expressed, as the positive charge can be distributed across two units of {**1**}.

*Table S 16: Selected computational and experimental parameters for the pentaphosphole complexes **2 – 7** and **9 – 13**; [a] As **2** and **3** are dinuclear complexes the average of the actual values is provided for clarity; [b] The charge transfer from fragment {**1**} to the respective fragments {E} is obtained by ECDA; [c] The cations in **2** and **3** were dissected into two fragments (Fragment 1 = 2*{**1**}, Fragment 2 = $\{EX_2\}^+$) for ECDA and the value in brackets is simply the charge transfer per {**1**} unit.*

Compound	WBI (P1-E)	Orbital contribution P1-E to σ(P1-E) NBO	*d*(P1-E)/ Å		∑charge		Charge Transfer {**1**}→{E}[b]
			Exp.	Theo.	{**1**}	{E}	
2	0.89[a]	57/43[a]	1.985(7)[a]	2.01[a]	0.79[a]	-0.58[a]	1.13(0.57)[c]
3	0.58[a]	79/21[a]	2.399(1)[a]	2.46[a]	0.43[a]	0.14[a]	1.11(0.56)[c]
4	0.92	45/55	1.853(4)	1.86	1.09	-0.09	0.85
5	0.88	45/55	1.866(4)	1.89	1.09	-0.09	0.84
6	0.72	72/28	2.3053(8)	2.35	0.57	0.43	0.68
7	0.82	67/33	2.348(1)	2.38	0.63	0.37	0.63
8	-	-	3.236(2)	4.53	0.01	0.99	0.02
9	0.98	53/47	2.2234(7)	2.25	0.84	0.16	0.83
10	0.92	62/38	2.438(2)	2.48	0.67	0.33	0.74
11	0.96	36/64	-	2.03	1.17	-0.17	1.09
12	0.98	41/59	-	2.21	1.06	-0.06	1.05
13	0.99	51/49	2.385(1)	2.42	0.89	0.11	0.94

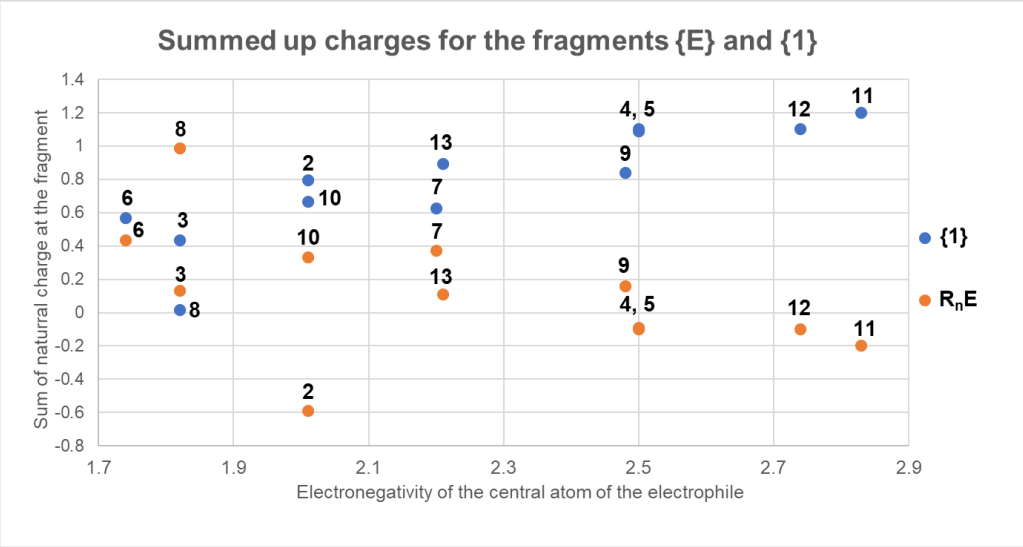

*Figure S 41: Natural charge accumulation at {**1**} and the employed electrophile {E} against the electronegativity of the central atom of the electrophile.*

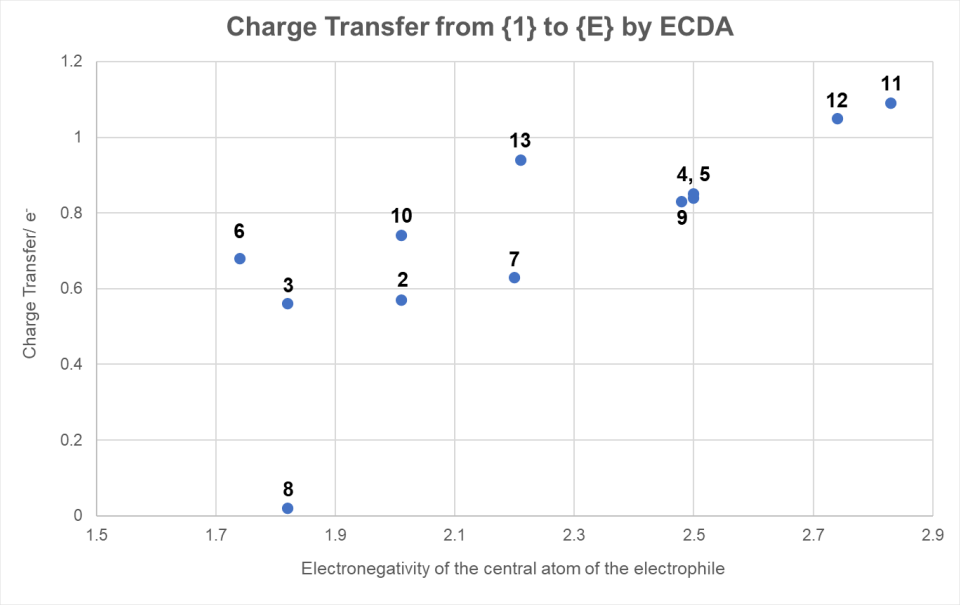

*Figure S 42: Charge transfer from {**1**} to the respective electrophile {E} within in cations **2** – **13**, computed via ECDA of their optimized geometries (vide supra, against the electronegativity of the central atom of the electrophile.*

NICS Values

NICS[37] values (Table S17) were obtained on the ligand geometries from the optimized structures of the cationic pentaphosphole complexes as well as **1**, **14** and **15**. The computed values derived for the (*cyclo*-P_5)$^-$ ligand in **1** and the parent pentaphosphole ligand compare well with those previously calculated on a different level of theory. Ring critical points and the points above and below the ring plane, respectively, were derived using MultiWFN. Magnetic shielding tensors were calculated using the correlation functional PBE0 and the basis sets aug-pcSseg-1 (for P atoms) and def2-TZVPPD (for all other atoms: C, H, B, Ga, Si, As, Se, Te, Cl, Br, I; in case of **15**, the aug-pcSseg-1 basis set was used for B and Br). The negative of the eigenvalue (z) of the magnetic shielding tensor at the respective position (RCP (0), one angstrom above (+1) and one angstrom below (-1)) represents the corresponding NICS value.

*Table S 17: NICS values for compounds **2** – **7** and **9** – **15** obtained on the PBE1/aug-pcSseg-1/def2-TZVPPD level of theory; NICS values of the ligand geometries in **1** and [Cp*Fe(η^5-P_5H)]$^+$ were recalculated for better comparison; for **15**, the NICS values for both P_4-rings are listed, as they are chemically distinct within the solid state structure of this compound.*

Compound	$NICS(0)_{zz}$	$NICS(1)_{zz}$	$NICS(-1)_{zz}$
1	-32.5205	-40.5356	-40.5356
2	-19.48	-31.19	-30.47
3	-24.23	-34.73	-34.28
4	-21.31	-33.67	-32.84
5	-20.26	-32.05	-31.22
6	-24.11	-34.66	-34.33
7	-22.91	-34.03	-33.42
9	-24.31	-33.46	-32.62
10	-26.17	-34.92	-34.02
11	-22.47	-31.05	-30.89
12	-23.28	-31.79	-31.66
13	-26.25	-34.26	-34.20
14	-22.37	-3.27	-3.47
15	-29.06/-29.30	-9.53/-10.75	-9.73/-9.61
[Cp*Fe(η^5-P_5H)]$^+$	-21.6272	-32.1365	-31.2407

To evaluate possible correlation between the calculated $NICS(1/-1)_{zz}$ values and the pyramidalization at P1, the former values are plotted against the sum of the respective P2-P1-R, P5-P1-R and P2-P1-P5 bond angles at P1 (Figure S43). While a general trend of decreasing $NICS(1/-1)_{zz}$ values (thus increasing aromaticity) for increasing planarization of P1 can be observed within this plot, the presence of two outliers, namely compounds **2** and **5**, suggests a more complicated electronic situation for the pentaphosphole complexes in question.

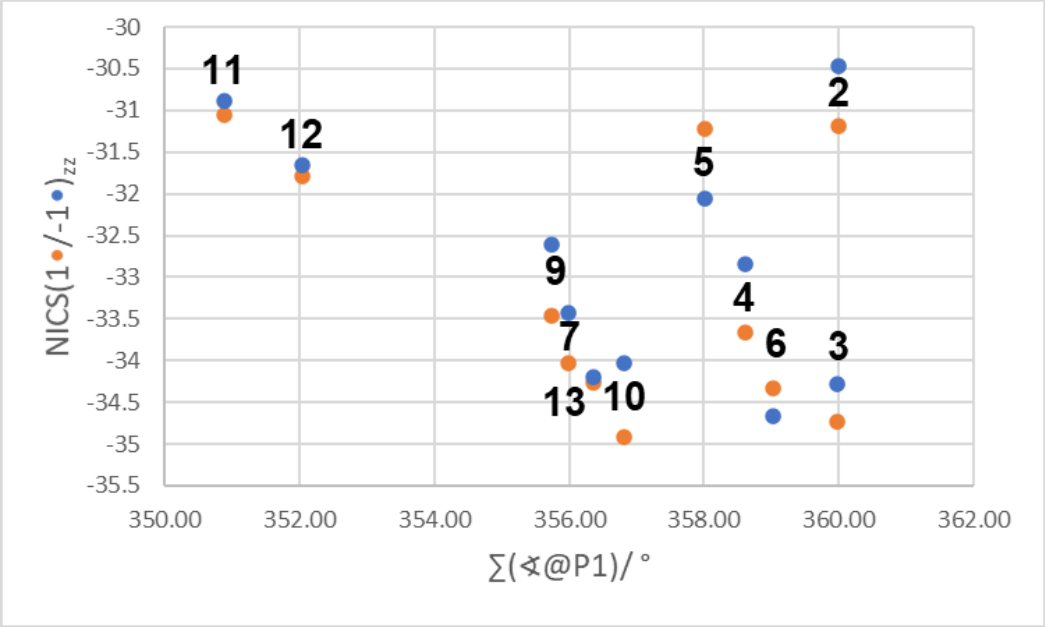

*Figure S 43: Plot of the calculated NICS(1/-1)$_{zz}$ for compounds **2** – **7** and **9** – **13** against the sum of the bond angles at P1 of the respective compound; Labelling according to color code and compound number.*

Optimized Geometries

[2]$^+$

B3LYP/def2TZVP: Energies/H = -11894.674338, Enthalpies/H = -11894.673394, Free Energies/H = -11894.802066, ZPVE/ kJ/mol = 1241.735

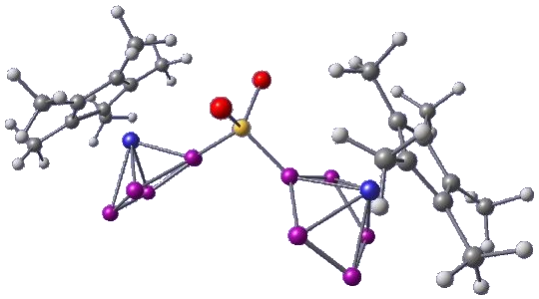

Symbol	X	Y	Z
Br	0.0667610	1.8324550	1.6797950
Br	-0.0730920	1.8412310	-1.7100220
Fe	3.8926080	-0.3980390	-0.0156470
Fe	-3.8904920	-0.3994770	0.0197000
P	1.5684480	-0.4961750	-0.0970090
P	-1.5660080	-0.5013370	0.0488110
P	-2.4517260	-1.1063740	1.8704230
P	-2.4184870	-1.3052410	-1.7106870
P	2.3828040	-1.3587820	1.6519830
P	-3.8549720	-2.6434570	-0.9207760
P	-3.8777420	-2.5216000	1.2061960
P	2.4931830	-1.0397500	-1.9188070
P	3.8352680	-2.6720830	0.8488390
P	3.9023000	-2.4799920	-1.2720460
C	4.6981500	1.1304370	1.2140870
C	-4.3186080	1.6853940	0.0715130
C	-4.7589400	1.1277390	-1.1691670
C	-4.9446210	1.3729820	2.5784240
H	-5.1545690	0.5162150	3.2167830
H	-5.6891000	2.1423510	2.8048030
H	-3.9685330	1.7695150	2.8528160
C	-5.0160420	1.0219390	1.1275480
C	-3.4264920	2.8722010	0.2299270
H	-2.8742780	2.8470930	1.1667380
H	-4.0374630	3.7804720	0.2306380
H	-2.7103340	2.9583370	-0.5841540
C	-5.8993360	0.0632120	0.5401940
C	5.9304020	0.0565140	-0.4241100
C	5.0851050	1.0155550	-1.0638830
C	-4.3747340	1.6111570	-2.5300020
H	-3.3502090	1.9783450	-2.5566260
H	-5.0305960	2.4367910	-2.8227420
H	-4.4747360	0.8304230	-3.2820960
C	5.6910280	0.1277580	0.9846290
C	-5.7400160	0.1287750	-0.8802690
C	-6.9213220	-0.7471090	1.2693310
H	-7.1486610	-1.6790260	0.7547090
H	-7.8512270	-0.1745860	1.3412440
H	-6.6047030	-0.9881090	2.2825430
C	6.4526500	-0.6053380	2.0406210
H	5.8544790	-0.7710660	2.9351630
H	7.3254210	-0.0137750	2.3336500
H	6.8119590	-1.5710530	1.6899590
C	4.3291290	1.6834910	-0.0520120
C	-6.5621060	-0.6034620	-1.8905870
H	-6.0112380	-0.7799480	-2.8130750
H	-7.4427840	-0.0047130	-2.1426000
H	-6.9127160	-1.5634120	-1.5161160
C	4.2395840	1.6197560	2.5493840
H	3.2148690	1.9854480	2.5175950

H	4.8777090	2.4474530	2.8737440
H	4.2989690	0.8424160	3.3092390
B	-0.0006470	0.7556230	-0.0182980
C	6.9887380	-0.7603170	-1.0914240
H	7.1949290	-1.6830870	-0.5520240
H	7.9190430	-0.1850580	-1.1274560
H	6.7217740	-1.0180150	-2.1147680
C	3.4445050	2.8668820	-0.2690500
H	4.0542100	3.7759170	-0.2626190
H	2.6958980	2.9673260	0.5136130
H	2.9304990	2.8230260	-1.2270470
C	5.1004740	1.3631320	-2.5171040
H	4.1426080	1.7580570	-2.8512790
H	5.3508930	0.5055060	-3.1395180
H	5.8564020	2.1331310	-2.6992240

[3]$^{+}$

B3LYP/def2TZVP: Energies/H = -9242.030969, Enthalpies/H = -9242.030024, Free Energies/H = -9242.164203, ZPVE/ kJ/mol = 1233.115

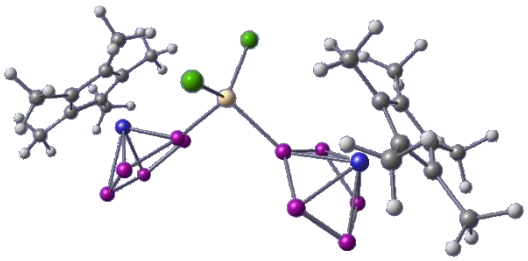

Symbol	X	Y	Z
Ga	-0.0032500	-0.8622180	-0.0374390
Fe	-4.1824360	0.7588690	-0.0284490
Fe	4.1879380	0.7573810	0.0016060
P	1.8432860	0.7632060	-0.0500600
P	-1.8440310	0.7567690	-0.2167960
P	2.7518600	1.4614330	-1.8313740
P	-2.5828960	1.8502430	1.4393890
P	2.6784970	1.5494770	1.7315320
P	-2.8633560	1.1201530	-2.0387000
P	4.1235860	2.9087460	-1.1211240
P	-4.0376920	3.1104300	0.5575600
P	-4.2039720	2.6740670	-1.5198520
P	4.0784970	2.9628380	1.0065550
C	-6.2494280	0.3132060	-0.2566830
C	-5.4653430	-0.7216330	-0.8558550
C	4.6538660	-1.3181060	-0.0545890
C	-4.9270800	-0.6282650	1.3922210
C	6.1931520	0.3336320	-0.5555920
C	5.3172050	-0.6429970	-1.1253620
C	-4.6518110	-1.3053020	0.1630880
C	5.1100880	-0.7534550	1.1765550
C	-7.3320420	1.0934970	-0.9292030
H	-7.1312810	1.2422740	-1.9887380
H	-7.4763130	2.0707510	-0.4712660
H	-8.2770820	0.5480620	-0.8454400
C	-5.9166200	0.3705460	1.1330870
C	5.2243820	-0.9980250	-2.5741830
H	4.2419370	-1.3876780	-2.8360960
H	5.9603270	-1.7732350	-2.8082220
H	5.4321110	-0.1440360	-3.2168700
C	3.7708440	-2.5140530	-0.1938330
H	3.0724110	-2.6076380	0.6356830
H	4.3877930	-3.4181090	-0.2036870
H	3.2025250	-2.4980830	-1.1214920
C	6.0650780	0.2645970	0.8673420
C	-6.5904660	1.2204010	2.1607710
H	-6.9634940	2.1521980	1.7395650
H	-5.9260770	1.4646770	2.9880690
H	-7.4464230	0.6787350	2.5746760
C	7.1793420	1.1706570	-1.3035730
H	6.8428110	1.3929880	-2.3145830
H	8.1279210	0.6306970	-1.3818460
H	7.3788220	2.1141920	-0.7986400
C	6.8862780	1.0193040	1.8616710
H	7.2364900	1.9703440	1.4647020
H	7.7671460	0.4278310	2.1295700
H	6.3333160	1.2187320	2.7782540
C	-4.3885490	-1.0008930	2.7354860
H	-3.3674040	-1.3746750	2.6772640
H	-5.0062010	-1.7935090	3.1688110
H	-4.4024750	-0.1599930	3.4267740
C	-5.5882400	-1.2081840	-2.2634700
H	-6.3774000	-1.9642750	-2.3185000

H	-4.6677600	-1.6692650	-2.6171660
H	-5.8545730	-0.4080430	-2.9522840
C	4.7651410	-1.2433480	2.5454910
H	4.8682420	-0.4604700	3.2951020
H	5.4425780	-2.0566110	2.8233770
H	3.7487280	-1.6306080	2.5964810
C	-3.7901650	-2.5144940	0.0014080
H	-3.3104580	-2.5515940	-0.9751700
H	-4.4070770	-3.4134830	0.0966610
H	-3.0170250	-2.5691230	0.7652500
I	-0.0042570	-2.2705500	-2.1630990
I	-0.0184770	-2.0635580	2.2129600

[4]$^{+}$

B3LYP/def2TZVP: Energies/H = -3631.534317, Enthalpies/H = -3631.533373, Free Energies/H = -3631.616864, ZPVE/ kJ/mol = 925.420

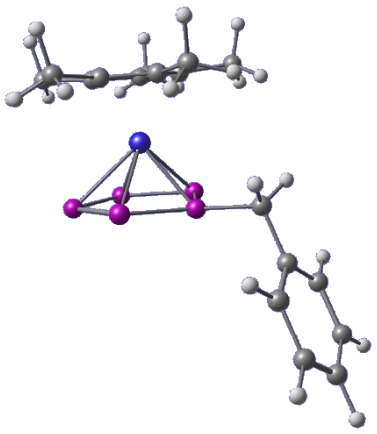

Symbol	X	Y	Z
Fe	1.1938160	-0.1232520	-0.0173070
P	-1.1207140	-0.2411500	0.0488410
P	-0.1861600	-1.1767020	1.6905910
P	-0.3232960	-0.5794790	-1.8710540
P	1.1665180	-2.4511880	0.6757060
P	1.0873860	-2.0958100	-1.4308700
C	2.8701610	0.5045910	1.1271760
C	3.2808370	0.2474060	-0.2174250
C	2.5486500	1.1242060	-1.0761020
C	1.6891620	1.9278780	-0.2623450
C	1.8891610	1.5456570	1.1002490
C	4.3725740	-0.6816570	-0.6377390
C	2.7483480	1.2715880	-2.5492270
C	0.8573640	3.0696960	-0.7511710
C	3.4587900	-0.1073530	2.3563800
C	1.2995980	2.2090820	2.3023270
H	4.4660670	-1.5316320	0.0361950
H	4.2175420	-1.0625670	-1.6458440
H	3.0235300	0.3291550	-3.0206020
H	2.7477830	-0.1307150	3.1809990
H	0.3759820	2.8499800	-1.7035480
H	3.8080340	-1.1230920	2.1792070
H	5.3274460	-0.1476830	-0.6291270
H	1.1731240	1.5132420	3.1302410
H	4.3187230	0.4856820	2.6815200
H	3.5592510	1.9818080	-2.7366520
H	0.3348520	2.6662150	2.0906010
H	1.8577260	1.6536590	-3.0455240
H	1.9695960	3.0041480	2.6427200
H	0.0900740	3.3547310	-0.0341070
H	1.4968660	3.9436460	-0.9059120
C	-2.3503340	1.1242870	0.3085160
H	-2.1068940	1.8975960	-0.4192260
C	-3.7687880	0.6354930	0.1569960
C	-4.3959120	0.6636310	-1.0893490
C	-4.4699880	0.1484480	1.2610910
C	-5.7048800	0.2174450	-1.2277640
H	-3.8620970	1.0416260	-1.9531840
C	-5.7789610	-0.2975200	1.1220780
H	-3.9942770	0.1247420	2.2342890
C	-6.3988360	-0.2651160	-0.1228450
H	-6.1833460	0.2498530	-2.1981170
H	-6.3149770	-0.6666640	1.9869560
H	-7.4188210	-0.6107110	-0.2307740
H	-2.1630770	1.5198870	1.3065890

[5]$^{+}$

B3LYP/def2TZVP: Energies/H = -3862.572624, Enthalpies/H = -3862.571680, Free Energies/H = -3862.665852, ZPVE/ kJ/mol = 1137.939

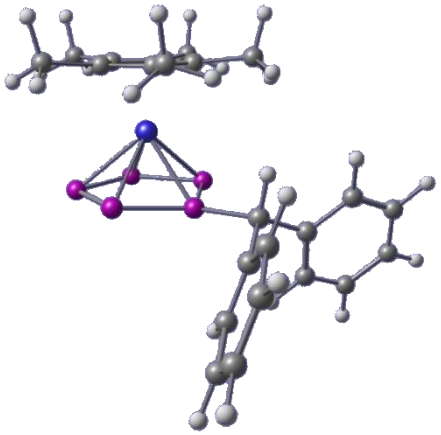

Symbol	X	Y	Z
Fe	1.6880580	0.0174600	-0.1262580
P	-0.5765820	0.0358180	-0.7257040
P	0.4318820	-1.7579410	-1.2029240
P	0.4350400	1.8523250	-1.1027350
P	2.0718720	-0.9911510	-2.3012280
P	2.0726870	1.1447500	-2.2437180
C	2.9406270	-1.1936760	1.0894420
C	3.6862350	-0.0746500	0.6051250
C	3.0522170	1.1148850	1.0790140
C	1.9186010	0.7323120	1.8619460
C	1.8492850	-0.6957200	1.8682790
C	4.9724030	-0.1373360	-0.1517750
C	3.5600010	2.5085470	0.9042730
C	1.0614620	1.6686440	2.6504410
C	3.3108650	-2.6314820	0.9233940
C	0.9056850	-1.5353490	2.6677970
H	5.0438670	-1.0365880	-0.7609220
H	5.1054000	0.7258200	-0.8020560
H	4.0870910	2.6362730	-0.0396500
H	2.4418600	-3.2846330	0.9865610
H	0.8561870	2.5910890	2.1090540
H	3.8090950	-2.8185520	-0.0267660
H	5.8079390	-0.1498920	0.5543660
H	0.6236450	-2.4489090	2.1461940
H	4.0009670	-2.9237750	1.7203680
H	4.2632570	2.7425030	1.7091020
H	-0.0025850	-0.9959050	2.9285530
H	2.7569770	3.2427730	0.9483230
H	1.3863030	-1.8296810	3.6053490
H	0.1111330	1.2178670	2.9288360
H	1.5765420	1.9401260	3.5764000
C	-2.0917130	0.0001070	0.4028620
H	-1.6819080	-0.0011810	1.4105520
C	-2.8574440	-1.3016570	0.2186590
C	-3.4025700	-1.6918560	-1.0066500
C	-3.0483970	-2.1234540	1.3306190
C	-4.1245620	-2.8736960	-1.1131090
H	-3.2673000	-1.0814440	-1.8894620
C	-3.7746250	-3.3045000	1.2253130
H	-2.6339980	-1.8362500	2.2890750
C	-4.3142310	-3.6835480	0.0022260
H	-4.5393220	-3.1616500	-2.0704710
H	-3.9160480	-3.9261430	2.1000130
H	-4.8777830	-4.6035500	-0.0833060
C	-2.9112780	1.2715490	0.2418940
C	-3.2312050	2.0022060	1.3879190
C	-3.3883030	1.7164690	-0.9931010
C	-4.0198050	3.1441560	1.3047810
H	-2.8712340	1.6729920	2.3549760
C	-4.1737430	2.8592350	-1.0765470
H	-3.1466000	1.1828010	-1.9029370
C	-4.4938270	3.5760660	0.0718490
H	-4.2605090	3.6951340	2.2048220
H	-4.5343590	3.1900810	-2.0419460
H	-5.1056760	4.4662300	0.0044090

[6]$^{+}$

B3LYP/def2TZVP: Energies/H = -4114.014234, Enthalpies/H = -4114.013290, Free Energies/H = -4114.013290, ZPVE/ kJ/mol = 1115.353

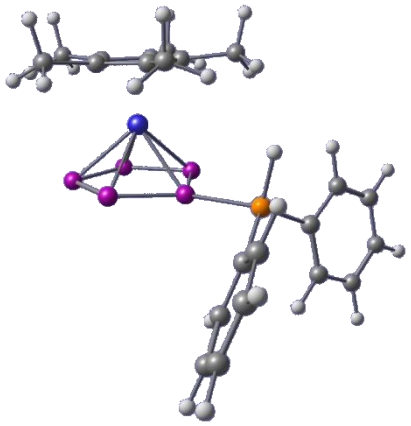

Symbol	X	Y	Z
Fe	1.9051020	0.0370700	-0.1471990
P	-0.3945050	0.0369380	-0.6637860
P	0.6400010	-1.7209090	-1.2313700
P	0.6099340	1.8526100	-1.0908200
P	2.2653110	-0.9391190	-2.3409610
P	2.2459460	1.1891080	-2.2595570
C	3.2709650	-1.1397640	0.9769460
C	3.9127860	0.0654320	0.5555910
C	3.1918340	1.1663800	1.1138690
C	2.1058870	0.6420010	1.8811730
C	2.1551750	-0.7849910	1.7966860
C	5.1866760	0.1540860	-0.2193390
C	3.5834310	2.6045620	1.0164080
C	1.1831350	1.4485310	2.7365340
C	3.7570680	-2.5282850	0.7175200
C	1.2969670	-1.7503590	2.5483720
H	5.3087360	-0.6862790	-0.9007150
H	5.2483100	1.0733590	-0.7994040
H	4.0906420	2.8244520	0.0782820
H	2.9453000	-3.2538480	0.7353950
H	0.9606100	2.4184030	2.2940460
H	4.2659830	-2.6112130	-0.2414600
H	6.0342400	0.1434130	0.4724290
H	1.0728340	-2.6418440	1.9638650
H	4.4712870	-2.8150650	1.4952330
H	4.2733430	2.8500310	1.8292270
H	0.3564880	-1.3024380	2.8619100
H	2.7248490	3.2685430	1.1033930
H	1.8218150	-2.0755980	3.4513290
H	0.2421580	0.9353090	2.9225260
H	1.6535540	1.6318080	3.7070860
C	-3.1491680	-1.6422780	0.2985780
C	-4.1022360	-1.7620380	-0.7222600
C	-2.8383250	-2.7780180	1.0606920
C	-4.7225390	-2.9795390	-0.9738110
H	-4.3758110	-0.9024930	-1.3208320
C	-3.4591520	-3.9953050	0.8087370
H	-2.1127370	-2.7147790	1.8628400
C	-4.4007570	-4.0972340	-0.2100150
H	-5.4596210	-3.0549220	-1.7629460
H	-3.2117300	-4.8612430	1.4093260
H	-4.8865660	-5.0446930	-0.4055890
C	-3.2211450	1.5471190	0.3316600
C	-3.5736190	2.3707440	1.4109460
C	-3.6045040	1.9381450	-0.9597400
C	-4.2955000	3.5412810	1.2067350
H	-3.2859480	2.0993370	2.4196260
C	-4.3243040	3.1082220	-1.1628360
H	-3.3380880	1.3370990	-1.8207640
C	-4.6721020	3.9101580	-0.0796460
H	-4.5610340	4.1642550	2.0511800
H	-4.6124450	3.3955430	-2.1658820
H	-5.2327730	4.8222540	-0.2396550
Si	-2.3081580	-0.0312640	0.6963710
H	-1.7955580	-0.0380600	2.0781410

[7]$^{+}$

B3LYP/def2TZVP: Energies/H = -6066.908076, Enthalpies/H = -6066.907131, Free Energies/H = -6067.010590, ZPVE/ kJ/mol = 1455.621

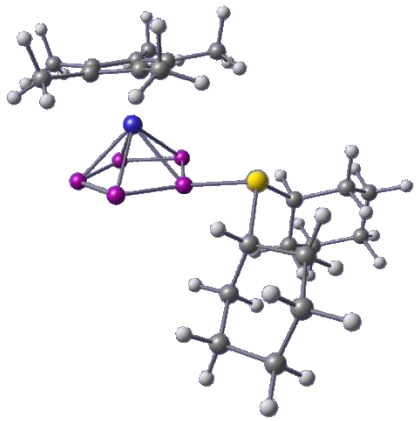

Symbol	X	Y	Z
Fe	-2.2944020	-0.0014260	-0.1511160
P	0.0102680	-0.0303850	-0.7092890
P	-1.0227400	1.7520850	-1.2069470
P	-1.0441590	-1.8248820	-1.1086060
P	-2.6602400	1.0062860	-2.3273520
P	-2.6735910	-1.1240750	-2.2687050
C	-3.6080970	1.1865110	1.0224630
C	-4.2870840	0.0037390	0.5954550
C	-3.5799060	-1.1229030	1.1181190
C	-2.4648870	-0.6368630	1.8698150
C	-2.4821860	0.7914240	1.8105840
C	-5.5781590	-0.0434750	-0.1547190
C	-4.0056510	-2.5502570	1.0053620
C	-1.5389060	-1.4731530	2.6923800
C	-4.0670890	2.5894220	0.7930850
C	-1.5754880	1.7144420	2.5581720
H	-5.6926420	0.8078310	-0.8237350
H	-5.6730740	-0.9538420	-0.7442840
H	-4.5284080	-2.7461370	0.0704150
H	-3.2380730	3.2953170	0.7967500
H	-1.3772860	-2.4559710	2.2517430
H	-4.5985610	2.6953190	-0.1512600
H	-6.4118050	-0.0209230	0.5534520
H	-1.4475840	2.6655970	2.0434730
H	-4.7534720	2.8841570	1.5924290
H	-4.6908550	-2.7922800	1.8231500
H	-0.5911680	1.2784960	2.7200180
H	-3.1606990	-3.2336940	1.0729670
H	-2.0048480	1.9295450	3.5412600
H	-0.5697330	-0.9967040	2.8293170
H	-1.9723400	-1.6266480	3.6851500
C	2.7162000	-1.6671020	0.3257020
C	3.0444390	-1.9204930	-1.1477410
C	3.9666570	-1.8211390	1.2090810
H	1.9842450	-2.4150470	0.6501750
C	3.6568200	-3.3178040	-1.3239490
H	3.7563820	-1.1753640	-1.5057290
H	2.1527520	-1.8311110	-1.7712260
C	4.5900640	-3.2121210	1.0241490
H	4.7049780	-1.0600880	0.9378040
H	3.7203420	-1.6636170	2.2624290
C	4.8963140	-3.5064060	-0.4459510
H	3.9090390	-3.4728920	-2.3759310
H	2.9081240	-4.0747420	-1.0658040
H	5.4996720	-3.2837450	1.6255100
H	3.8971810	-3.9670610	1.4111350
H	5.2823040	-4.5231610	-0.5520080
H	5.6888460	-2.8332800	-0.7916070
C	2.7137460	1.6524020	0.1619440
C	3.6978250	2.1400130	1.2394570
C	3.3820910	1.5913980	-1.2124840
H	1.8873590	2.3705240	0.1176990
C	4.2871710	3.5051680	0.8563060

H	4.5118660	1.4166080	1.3510510
H	3.2024040	2.2104870	2.2108620
C	3.9530410	2.9661560	-1.5913100
H	4.2006710	0.8678920	-1.1930490
H	2.6787140	1.2574240	-1.9778900
C	4.9303530	3.4801560	-0.5318840
H	5.0175100	3.8091190	1.6102370
H	3.4878260	4.2541200	0.8733340
H	4.4465620	2.8990700	-2.5640690
H	3.1290320	3.6790280	-1.7054020
H	5.2842790	4.4789840	-0.7986230
H	5.8131880	2.8313480	-0.5110320
As	1.7628800	0.0228000	0.8939270

[8]$^{+}$

B3LYP/def2TZVP: Energies/H = -4563.845732, Enthalpies/H = -4563.844788, Free Energies/H = -4563.976174, ZPVE/ kJ/mol = 1716.721

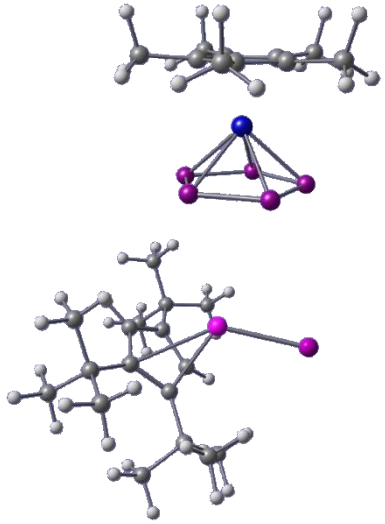

Symbol	X	Y	Z
Fe	-3.947394000	-0.130964000	0.099206000
Sb	1.979679000	0.454908000	0.025960000
I	2.064682000	3.217810000	0.267696000
P	-2.540770000	0.721371000	1.853883000
P	-2.154268000	-1.270204000	1.216645000
P	-2.726821000	1.941046000	0.123575000
P	-2.448421000	0.706996000	-1.584497000
P	-2.099663000	-1.279855000	-0.909982000
C	-5.618481000	-0.802548000	1.220758000
C	-5.857237000	0.526094000	0.751747000
C	-5.556730000	-0.838638000	-1.090411000
C	-5.818502000	0.503861000	-0.676338000
C	-5.433425000	-1.646246000	0.082221000
C	-6.110126000	1.659155000	-1.578748000
H	-5.622749000	1.548770000	-2.546314000
H	-5.784611000	2.603980000	-1.145338000
H	-7.187419000	1.730337000	-1.757017000
C	-6.198373000	1.708123000	1.600436000
H	-5.892771000	2.643246000	1.132951000
H	-5.726533000	1.652838000	2.580603000
H	-7.280503000	1.754364000	1.756402000
C	-5.664002000	-1.249840000	2.646175000
H	-5.335447000	-0.465330000	3.326539000
H	-5.037836000	-2.124849000	2.815154000
H	-6.688803000	-1.518143000	2.920332000
C	-5.529579000	-1.330310000	-2.501764000
H	-4.910837000	-2.220261000	-2.608256000
H	-5.150299000	-0.573454000	-3.187353000
H	-6.542119000	-1.591018000	-2.824581000
C	-5.249614000	-3.129382000	0.110618000
H	-4.731654000	-3.454999000	1.011795000
H	-4.681657000	-3.482767000	-0.749036000
H	-6.223920000	-3.627154000	0.090791000
C	3.998453000	-0.050063000	-0.962266000
H	4.520207000	0.808747000	-1.346329000
C	3.454818000	-1.878788000	0.378952000
C	3.240095000	-0.969917000	-1.762975000
C	2.995013000	0.574496000	-3.742567000
H	2.184734000	1.147192000	-3.286474000
H	3.936211000	1.084033000	-3.533583000
H	2.846544000	0.594005000	-4.822524000
C	2.923622000	-2.048948000	-0.909959000
H	2.319798000	-2.886623000	-1.210332000
C	4.174459000	-0.584032000	0.378354000
C	5.221217000	0.040137000	1.331470000
C	2.999125000	-0.881309000	-3.253360000
C	1.885528000	-3.669340000	1.231158000
H	1.776406000	-4.156939000	0.264008000
H	1.768076000	-4.441982000	1.991359000
H	1.070798000	-2.953959000	1.353916000
C	1.677281000	-1.558258000	-3.650528000
H	1.651574000	-2.609629000	-3.362831000
H	0.821178000	-1.056120000	-3.196765000

H	1.558381000	-1.512640000	-4.733770000
C	4.177446000	-1.637033000	-3.923367000
H	4.056520000	-1.595877000	-5.006896000
H	5.137225000	-1.184728000	-3.669809000
H	4.199116000	-2.684601000	-3.620862000
C	5.916614000	1.239914000	0.653928000
H	5.218092000	2.037772000	0.399830000
H	6.640517000	1.657327000	1.353757000
H	6.460275000	0.945533000	-0.244526000
C	3.266644000	-2.997679000	1.416866000
C	4.626026000	0.566974000	2.652714000
H	4.064196000	-0.180070000	3.201163000
H	5.435627000	0.916342000	3.295367000
H	3.969156000	1.418865000	2.466626000
C	6.324665000	-1.004774000	1.608658000
H	6.742783000	-1.389472000	0.677007000
H	7.131363000	-0.525314000	2.164808000
H	5.974256000	-1.845335000	2.199393000
C	3.340815000	-2.570577000	2.889133000
H	2.592890000	-1.812813000	3.126645000
H	3.130785000	-3.441179000	3.511430000
H	4.318889000	-2.202385000	3.181672000
C	4.350981000	-4.070182000	1.136929000
H	5.359261000	-3.680664000	1.265478000
H	4.217596000	-4.901353000	1.831480000
H	4.263901000	-4.458499000	0.121538000

[9]$^{+}$

B3LYP/def2TZVP: Energies/H = -3658.406358, Enthalpies/H = -3658.405413, Free Energies/H = -3658.481294, ZPVE/ kJ/mol = 612.879

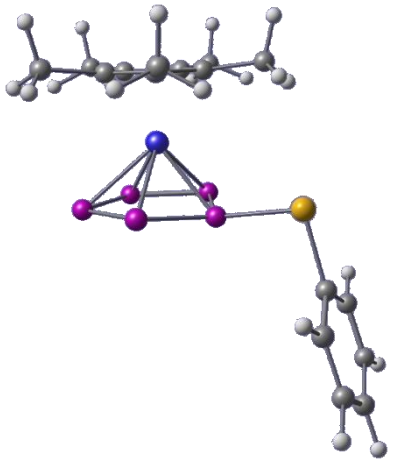

Symbol	X	Y	Z
Fe	1.5155710	-0.2184240	-0.0087880
P	-0.8186570	-0.4260130	-0.0163240
P	0.1383470	-1.0681000	1.7746470
P	0.1374190	-0.9560060	-1.8428580
P	1.5388320	-2.4396470	0.9960810
P	1.5404160	-2.3706580	-1.1491680
C	2.6795780	1.0510670	1.2438700
C	3.5448080	0.2346710	0.4502790
C	3.2837990	0.5235260	-0.9253820
C	2.2547180	1.5165520	-0.9820510
C	1.8854290	1.8448550	0.3596900
C	4.6294850	-0.6521460	0.9686540
C	4.0521170	-0.0051420	-2.0920650
C	1.7631980	2.2008570	-2.2161080
C	2.7091930	1.1704270	2.7328190
C	0.9660500	2.9471210	0.7739030
H	4.3917080	-1.0530600	1.9522650
H	4.8299530	-1.4876930	0.3002400
H	4.4627450	-0.9941220	-1.8971690
H	1.7476290	1.4842250	3.1354640
H	1.8467690	1.5650140	-3.0959100
H	2.9938100	0.2367240	3.2154550
H	5.5543570	-0.0749130	1.0619350
H	0.4266740	2.7133920	1.6904530
H	3.4475270	1.9254570	3.0194470
H	4.8905310	0.6649290	-2.3047590
H	0.2429190	3.1905260	-0.0021270
H	3.4422970	-0.0618690	-2.9922800
H	1.5528400	3.8511980	0.9630060
H	0.7251990	2.5157660	-2.1213990
H	2.3639500	3.0967560	-2.3992660
C	-3.8857370	0.3470040	0.0152140
C	-4.5384950	0.1431390	-1.1981440
C	-4.4475260	-0.0869920	1.2136130
C	-5.7671560	-0.5085130	-1.2072880
H	-4.0969050	0.4876530	-2.1232120
C	-5.6745390	-0.7404660	1.1916520
H	-3.9370920	0.0826630	2.1517660
C	-6.3329590	-0.9509520	-0.0159150
H	-6.2797420	-0.6693390	-2.1467560
H	-6.1153630	-1.0811970	2.1194480
H	-7.2888510	-1.4583390	-0.0280730
Se	-2.2171450	1.3365170	0.0417010

[10]$^{+}$

B3LYP/def2TZVP: Energies/H = -3978.258935, Enthalpies/H = -3978.257990, Free Energies/H = -3978.359390, ZPVE/ kJ/mol = 1065.305

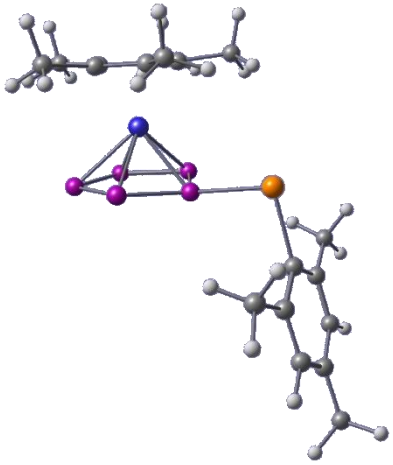

Symbol	X	Y	Z
Fe	2.1688790	-0.3178170	-0.0363820
P	-0.1812110	-0.4462170	-0.0937990
P	0.7326150	-1.3057140	1.6277440
P	0.7945370	-0.8605680	-1.9418070
P	2.1322800	-2.6213800	0.7554610
P	2.1696900	-2.3551550	-1.3692430
C	3.6267360	0.5138020	1.2730440
C	4.2698870	0.0155350	0.0980440
C	3.7396990	0.7204690	-1.0261950
C	2.7706390	1.6562940	-0.5469960
C	2.7009350	1.5282350	0.8761600
C	5.3921940	-0.9694830	0.0648020
C	4.2090430	0.5963640	-2.4388700
C	2.0745990	2.6795520	-1.3844750
C	3.9590520	0.1331230	2.6785910
C	1.9207140	2.3944500	1.8108440
H	5.3298120	-1.6873910	0.8809120
H	5.4231570	-1.5219330	-0.8728230
H	4.5512600	-0.4113780	-2.6689570
H	3.1156060	0.2811370	3.3510670
H	1.8014580	2.2884000	-2.3636140
H	4.2779780	-0.9051950	2.7541910
H	6.3432810	-0.4381380	0.1653640
H	1.5664150	1.8416560	2.6798190
H	4.7813660	0.7577460	3.0398460
H	5.0504150	1.2760960	-2.6031740
H	1.0617510	2.8552840	1.3273480
H	3.4299080	0.8622960	-3.1515870
H	2.5603470	3.2034410	2.1758490
H	1.1728560	3.0589760	-0.9081610
H	2.7413790	3.5315200	-1.5463550
C	-3.5438310	0.3287330	0.0360350
C	-4.1831530	0.1491800	-1.2054010
C	-4.1001120	-0.1698640	1.2282130
C	-5.3890060	-0.5497040	-1.2219730
C	-5.3080970	-0.8623800	1.1452370
C	-5.9680990	-1.0623130	-0.0636020
H	-5.8890550	-0.6968910	-2.1722280
H	-5.7434660	-1.2551510	2.0565460
Te	-1.7325510	1.4716740	0.1268920
C	-3.4649770	0.0007680	2.5843530
H	-2.4860160	-0.4794940	2.6365720
H	-3.3188470	1.0534880	2.8318900
H	-4.0954490	-0.4420160	3.3540640
C	-3.6377640	0.6670730	-2.5115590
H	-3.4820800	1.7467630	-2.4858310
H	-2.6775650	0.2103910	-2.7584600
H	-4.3307070	0.4458860	-3.3220840
C	-7.2850140	-1.7868460	-0.1175620
H	-8.1151460	-1.0747020	-0.1205490
H	-7.3704540	-2.3867660	-1.0243970
H	-7.4157480	-2.4402840	0.7448350

[11]$^{+}$

B3LYP/def2TZVP: Energies/H = -3820.828078, Enthalpies/H = -3820.827134, Free Energies/H = -3820.902382, ZPVE/ kJ/mol = 613.509

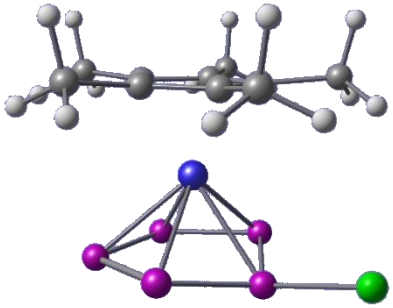

Symbol	X	Y	Z
Fe	-0.2265480	-0.1485790	0.0000400
P	2.0971580	-0.5895230	-0.0005900
P	1.0664590	-0.9689980	-1.8247800
P	1.0669590	-0.9716320	1.8234020
P	-0.3743200	-2.3246800	-1.0779350
P	-0.3739980	-2.3262500	1.0750260
C	-1.6244260	0.9662670	-1.1553320
C	-2.2766290	0.4311680	-0.0017910
C	-1.6275880	0.9618790	1.1555630
C	-0.5693180	1.8216540	0.7173720
C	-0.5673810	1.8243500	-0.7110410
C	-3.4993740	-0.4271230	-0.0051690
C	-2.0643310	0.7655940	2.5702370
C	0.2790200	2.6817160	1.5959350
C	-2.0573840	0.7758620	-2.5719490
C	0.2824290	2.6880580	-1.5846230
H	-3.5493250	-1.0625820	-0.8876770
H	-3.5530810	-1.0641310	0.8759830
H	-2.5379260	-0.2026050	2.7235050
H	-1.2272860	0.8672370	-3.2709260
H	0.4333580	2.2392450	2.5784960
H	-2.5329390	-0.1906030	-2.7298880
H	-4.3890340	0.2093040	-0.0064770
H	0.4498930	2.2433560	-2.5640780
H	-2.7885060	1.5474490	-2.8305940
H	-2.7981350	1.5344540	2.8293880
H	1.2503370	2.8994530	-1.1344750
H	-1.2364960	0.8565490	3.2719480
H	-0.2217950	3.6460570	-1.7423530
H	1.2530880	2.8830490	1.1544720
H	-0.2185070	3.6445420	1.7451510
Cl	3.3925070	0.9759980	0.0002610

[12]$^{+}$

B3LYP/def2TZVP: Energies/H = -5934.784939, Enthalpies/H = -5934.783995, Free Energies/H = -5934.858303, ZPVE/ kJ/mol = 613.138

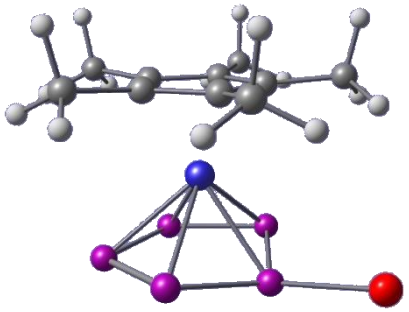

Symbol	X	Y	Z
Fe	-0.5751750	-0.1361500	0.0012240
P	1.6307580	-1.0021170	-0.0061200
P	0.5426040	-1.1813000	-1.8271720
P	0.5497140	-1.2010980	1.8168380
P	-1.1266840	-2.2448730	-1.0829130
P	-1.1230920	-2.2554310	1.0677370
C	-1.6819060	1.2508340	-1.1737540
C	-2.4876030	0.7980130	-0.0836640
C	-1.8280990	1.1609110	1.1311220
C	-0.6114560	1.8359690	0.7922990
C	-0.5219560	1.8922000	-0.6331450
C	-3.8405070	0.1749910	-0.1951940
C	-2.3795100	0.9848690	2.5077480
C	0.3213350	2.4952020	1.7553370
C	-2.0540750	1.1893400	-2.6187780
C	0.5162240	2.6207350	-1.4217170
H	-3.9455250	-0.4118460	-1.1061040
H	-4.0645160	-0.4696090	0.6529200
H	-3.0134710	0.1030350	2.5837010
H	-1.1795790	1.2093670	-3.2673170
H	0.3266250	2.0010780	2.7253420
H	-2.6363610	0.3000760	-2.8551140
H	-4.6003070	0.9616410	-0.2206310
H	0.6936590	2.1591330	-2.3919310
H	-2.6678670	2.0594030	-2.8698580
H	-2.9919770	1.8542050	2.7643800
H	1.4651810	2.6791570	-0.8931590
H	-1.5944640	0.9065670	3.2580230
H	0.1774770	3.6449730	-1.6032070
H	1.3431710	2.5238530	1.3814590
H	0.0024740	3.5292690	1.9161440
Br	3.3698810	0.3526720	0.0001850

[13]$^{+}$

B3LYP/def2TZVP: Energies/H = -3658.406358, Enthalpies/H = -3658.405413, Free Energies/H = -3658.481294, ZPVE/ kJ/mol = 612.879

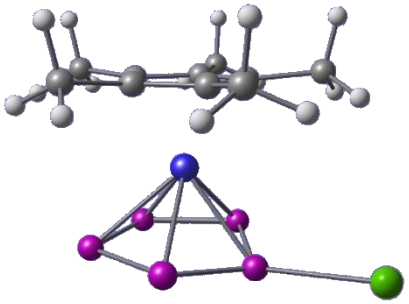

Symbol	X	Y	Z
Fe	0.8989940	-0.1248060	0.0001740
P	-1.2617830	-1.0356970	0.0025800
P	-0.1904870	-1.2636370	1.8228410
P	-0.1936720	-1.2648490	-1.8188450
P	1.5440580	-2.2105720	1.0740480
P	1.5425150	-2.2112310	-1.0716410
C	1.8932350	1.3287030	1.1979380
C	2.7810840	0.8578870	0.1810250
C	2.1978710	1.1630940	-1.0877630
C	0.9491670	1.8219050	-0.8558860
C	0.7615170	1.9248300	0.5579810
C	4.1391080	0.2756820	0.4009400
C	2.8432590	0.9581380	-2.4188680
C	0.0800030	2.4348830	-1.9050670
C	2.1680700	1.3278970	2.6660200
C	-0.3381330	2.6624680	1.2481430
H	4.2076360	-0.2538600	1.3494800
H	4.4220380	-0.4121860	-0.3942070
H	3.5076260	0.0958620	-2.4231510
H	1.2518950	1.3122140	3.2541470
H	0.1226500	1.8866010	-2.8447730
H	2.7829270	0.4813500	2.9673650
H	4.8792390	1.0811150	0.4181470
H	-0.5659070	2.2386620	2.2250360
H	2.7122470	2.2391790	2.9312740
H	3.4435730	1.8381920	-2.6678100
H	-1.2533040	2.6780000	0.6602260
H	2.1099810	0.8281150	-3.2132380
H	-0.0317950	3.7010350	1.4051420
H	-0.9605510	2.4970890	-1.5922910
H	0.4231090	3.4543730	-2.1053570
I	-3.3374670	0.2044540	-0.0003030

14

B3LYP/def2SVP: Energies/H = -2312.831455, Enthalpies/H = -2312.830511, Free Energies/H = -2312.924899, ZPVE/ kJ/mol = 1164.342

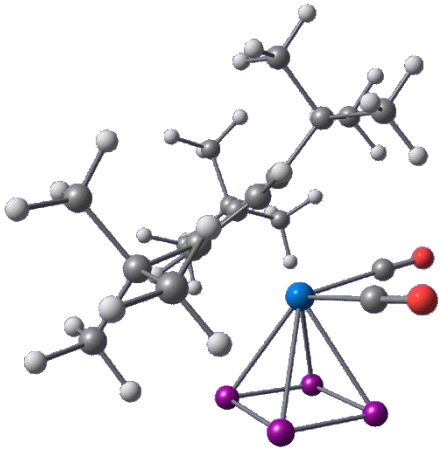

Symbol	X	Y	Z
Ta	0.577394000	-0.290233000	-0.226926000
P	2.738341000	-1.833228000	-0.881675000
P	1.752908000	-2.403754000	1.020978000
P	3.236452000	0.161214000	-0.049693000
P	2.260494000	-0.430286000	1.826807000
O	-0.621992000	-3.004082000	-1.558715000
O	1.476547000	0.704602000	-3.191682000
C	-0.197535000	-2.044343000	-1.083159000
C	-1.017844000	1.496527000	-0.784256000
H	-1.026748000	1.987648000	-1.753089000
C	-0.612623000	1.062016000	1.394652000
H	-0.252127000	1.156546000	2.411771000
C	-1.573810000	0.079464000	0.962072000
C	0.444373000	3.300833000	0.458718000
C	1.175448000	0.338094000	-2.143731000
C	-0.276749000	1.956227000	0.336974000
C	-2.268536000	-0.836610000	2.005121000
C	-1.843625000	0.373965000	-0.447924000
C	1.487940000	3.290111000	1.589940000
H	1.041929000	3.034759000	2.563272000
H	1.941694000	4.288698000	1.688159000
H	2.297887000	2.574036000	1.383964000
C	-2.969939000	-0.002446000	-1.454033000
C	-3.720225000	-0.338536000	2.213776000
H	-3.733330000	0.727849000	2.489189000
H	-4.195088000	-0.904414000	3.031162000
H	-4.344855000	-0.463161000	1.320713000
C	1.132952000	3.703659000	-0.858141000
H	1.934414000	2.997693000	-1.121201000
H	1.582353000	4.703438000	-0.752589000
H	0.424142000	3.752596000	-1.699224000
C	-4.052365000	1.101256000	-1.300714000
H	-4.465569000	1.124269000	-0.281804000
H	-4.882921000	0.911962000	-1.999489000
H	-3.643747000	2.098951000	-1.521597000
C	-2.450570000	0.037965000	-2.912021000
H	-2.041144000	1.016220000	-3.199682000
H	-3.286651000	-0.169693000	-3.596975000
H	-1.677277000	-0.723594000	-3.091715000
C	-1.565234000	-0.720177000	3.378514000
H	-0.499826000	-0.990103000	3.324254000
H	-2.045478000	-1.413893000	4.084978000
H	-1.646702000	0.289208000	3.808433000
C	-2.255066000	-2.337196000	1.644921000
H	-2.696493000	-2.554393000	0.668574000
H	-2.826095000	-2.900853000	2.399899000
H	-1.225110000	-2.722409000	1.642982000
C	-0.647609000	4.348363000	0.797726000
H	-1.407754000	4.403471000	0.002834000
H	-0.195398000	5.347213000	0.907995000
H	-1.159119000	4.099201000	1.740681000
C	-3.658534000	-1.367669000	-1.276112000
H	-2.966048000	-2.209366000	-1.400763000

H	-4.432602000	-1.468589000	-2.052451000
H	-4.164166000	-1.468635000	-0.309716000

[15]$^{+}$

B3LYP/def2SVP: Energies/H = -9798.557610, Enthalpies/H = -9798.556666, Free Energies/H = -9798.733683, ZPVE/ kJ/mol = 2349.701

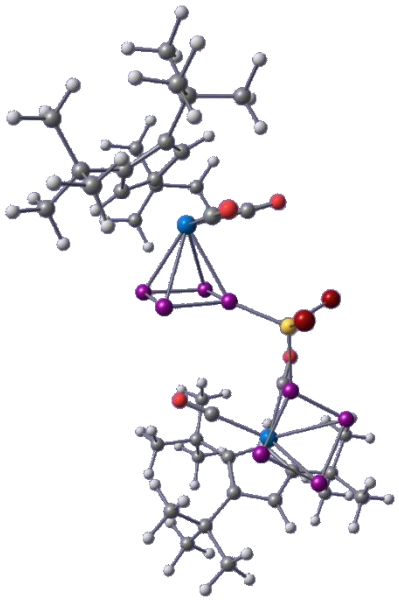

Symbol	X	Y	Z
Ta	3.870701000	-0.158907000	-0.080086000
Ta	-3.670091000	0.266379000	0.075639000
Br	-0.747014000	-3.622675000	-1.247428000
Br	-0.050137000	-2.722825000	1.960431000
P	1.863380000	-1.876914000	-0.432854000
P	-1.161017000	-0.582493000	-0.228570000
P	2.896458000	-1.538017000	-2.316371000
P	-1.890939000	0.288143000	-2.079599000
P	3.512136000	-2.810825000	0.623164000
P	4.608457000	-2.409658000	-1.250752000
P	-1.238204000	1.220359000	0.982363000
P	-2.040267000	2.118687000	-0.865166000
O	2.310014000	0.012470000	2.779398000
O	1.607889000	1.740601000	-1.449645000
O	-4.133121000	-2.562400000	-1.475595000
O	-3.218384000	-1.317065000	2.891677000
C	2.845446000	-0.066553000	1.770672000
C	4.936251000	2.118192000	0.147104000
C	-5.210321000	2.110895000	-0.174254000
H	-4.903663000	3.036075000	-0.647428000
C	6.235442000	0.260337000	-0.354202000
H	6.868757000	-0.434375000	-0.892918000
C	-3.350938000	-0.770192000	1.895636000
C	4.385670000	3.559484000	0.351715000
C	6.021993000	0.225131000	1.054336000
C	-6.183266000	0.029808000	0.163773000
C	-6.249613000	1.177032000	-2.355372000
C	5.595146000	1.405292000	-0.951151000
C	-5.843311000	1.016154000	-0.866212000
C	5.194906000	1.347801000	1.330323000
H	4.887348000	1.646632000	2.328426000
C	5.903733000	1.780929000	-2.425090000
C	2.405711000	1.072404000	-0.966062000
C	-3.965507000	-1.568021000	-0.932557000
C	-5.144843000	1.866821000	1.228462000
C	-5.842073000	-0.002210000	-3.262500000
H	-4.747295000	-0.071147000	-3.343110000
H	-6.240663000	0.163078000	-4.275589000
H	-6.218926000	-0.967847000	-2.916324000
C	7.235064000	-1.965280000	1.501530000
H	7.870555000	-1.840744000	0.611837000
H	6.379692000	-2.601872000	1.227831000
H	7.825288000	-2.512799000	2.252091000
C	-5.711048000	0.575490000	1.404621000
H	-5.868518000	0.105495000	2.371163000
C	3.266167000	3.577619000	1.420484000
H	2.386801000	2.998380000	1.101741000
H	2.937840000	4.615672000	1.578772000
H	3.592570000	3.197361000	2.398219000
C	6.779159000	-0.616095000	2.084239000
C	-7.160092000	-1.179092000	0.256559000
C	-4.855038000	2.885157000	2.333859000
C	-5.589330000	2.437394000	-2.963222000
H	-5.936609000	3.366691000	-2.488466000

H	-5.856490000	2.499531000	-4.028543000
H	-4.490497000	2.404025000	-2.902773000
C	3.828320000	4.296808000	-0.879593000
H	4.573997000	4.438790000	-1.669212000
H	3.507846000	5.300340000	-0.561562000
H	2.948661000	3.802187000	-1.309792000
C	4.656976000	2.068585000	-3.287186000
H	4.058756000	1.155472000	-3.423261000
H	4.974672000	2.409655000	-4.284858000
H	4.007050000	2.841284000	-2.868552000
C	-7.780556000	1.408721000	-2.415457000
H	-8.356560000	0.534561000	-2.087684000
H	-8.080592000	1.634013000	-3.450877000
H	-8.073789000	2.262819000	-1.785123000
C	6.861531000	2.998934000	-2.424935000
H	6.395043000	3.909032000	-2.028293000
H	7.185350000	3.214930000	-3.455155000
H	7.761055000	2.790573000	-1.824799000
B	-0.065949000	-2.224161000	0.016814000
C	8.035571000	0.211125000	2.464565000
H	8.638749000	-0.339576000	3.203646000
H	7.757770000	1.181104000	2.905172000
H	8.667470000	0.404133000	1.583742000
C	5.940293000	-0.864543000	3.350985000
H	5.053108000	-1.477262000	3.132163000
H	5.607471000	0.074728000	3.818740000
H	6.545034000	-1.402500000	4.096947000
C	5.586743000	4.382130000	0.896180000
H	5.965640000	3.967789000	1.842504000
H	5.271276000	5.420792000	1.082772000
H	6.420516000	4.405291000	0.179612000
C	-4.267354000	2.219095000	3.591519000
H	-4.923995000	1.430723000	3.990281000
H	-4.144573000	2.971377000	4.385686000
H	-3.279309000	1.779109000	3.389675000
C	-6.656569000	-2.219359000	1.286357000
H	-5.707685000	-2.679390000	0.972943000
H	-7.399957000	-3.025501000	1.374401000
H	-6.520580000	-1.803637000	2.294182000
C	-7.469594000	-1.955606000	-1.036257000
H	-7.935834000	-1.334389000	-1.808663000
H	-8.188615000	-2.752236000	-0.792700000
H	-6.584730000	-2.444385000	-1.462007000
C	-8.495728000	-0.583624000	0.783434000
H	-8.367331000	-0.105574000	1.766149000
H	-9.241966000	-1.386299000	0.891962000
H	-8.905289000	0.167777000	0.092655000
C	6.659389000	0.629282000	-3.129552000
H	7.650009000	0.443640000	-2.689194000
H	6.819868000	0.901840000	-4.183207000
H	6.089976000	-0.312632000	-3.117394000
C	-6.224648000	3.519864000	2.692752000
H	-6.675813000	4.016029000	1.819531000
H	-6.093479000	4.274129000	3.484708000
H	-6.933436000	2.760924000	3.058353000
C	-3.905284000	3.998122000	1.856994000
H	-2.904883000	3.607270000	1.615325000
H	-3.781199000	4.745700000	2.655267000
H	-4.292020000	4.524856000	0.971535000

6.6. References

[1] a) C. Friedel, J. M. Crafts, *Compt. Rend.***1877**, *84*, 1392; b) C. Friedel, J. M. Crafts, *Compt. Rend.* **1877**, *84*, 1450.

[2] a) R. Brückner, *Reaktionsmechanismen*, Springer, Berlin, Heidelberg, **2004**, 203-235; b) P. Y. Bruice, *Organische Chemie*, Pearson Studium, Hallbergmoos, **2013**, 627-642.

[3] a) T. J. Kealy, P. L. Pauson, *Nature* **1951**, *168*, 1039–1040; b) R. B. Woodward, M. Rosenblum, M. C. Whiting, *J. Am. Chem. Soc.* **1952**, *74*, 3458–3459.

[4] E. O. Fischer, K. Öfele, *Chem. Ber.* **1957**, *90*, 2532–2535.

[5] R. Hoffmann, *Angew. Chem. Int. Ed. Engl.* **1982**, *21*, 711–724.

[6] a) M. Baudler, T. Etzbach, *Chem. Ber.* **1991**, *124*, 1159–1160; b) V. A. Milyukov, A. V. Kataev, O. G. Sinyashin, E. Hey-Hawkins, *Russ. Chem. Bull.* **2006**, *55*, 1297–1299; c) M. Jo, A. Dragulescu-Andrasi, L. Z. Miller, C. Pak, M. Shatruk, *Inorg. Chem.* **2020**, *59*, 5483–5489.

[7] M. Baudler, S. Akpapoglou, D. Ouzounis, F. Wasgestian, B. Meinigke, H. Budzikiewic, H. Münster, *Angew. Chem. Int. Ed. Engl.* **1988**, *27*, 280–281.

[8] a) L. Nyulászi, *Inorg. Chem.* **1996**, *35*, 4690–4693; b) M. N. Glukhovtsev, A. Dransfeld, P. v. R. Schleyer, *J. Phys. Chem.* **1996**, *100*, 13447–13454; c) A. Dransfeld, L. Nyulászi, P. v. R. Schleyer, *Inorg. Chem.* **1998**, *37*, 4413–4420; d) M. K. Cyrański, P. v. R. Schleyer, T. M. Krygowski, H. Jiao, G. Hohlneicher, *Tetrahedron* **2003**, *59*, 1657–1665; e) W. P. Ozimiński, J. C. Dobrowolski, *Chem. Phys.* **2005**, *313*, 123–132; f) L. Wang, H. J. Wang, W. B. Dong, Q. Y. Ge, L. Lin, *Struct. Chem.* **2007**, *18*, 25–31; g) W.-Q. Li, L.-L. Liu, J.-K. Feng, Z.-Z. Liu, A.-M. Ren, G. Zhang, C.-C. Sun, *J. Theor. Comput. Chem.* **2008**, *07*, 1203–1214; (h) D. Josa, A. Peña-Gallego, J. Rodríguez-Otero, E. M. Cabaleiro-Lago, *J. Mol. Model.* **2011**, *17*, 1267–1272.

[9] a) O. J. Scherer, T. Brück, *Angew. Chem. Int. Ed. Engl.* **1987**, *26*, 59; b) M. Baudler, T. Etzbach, *Angew. Chem. Int. Ed. Engl.* **1991**, *30*, 580–582; c) A. R. Kudinov, D. A. Loginov, Z. A. Starikova, P. V. Petrovskii, M. Corsini, P. Zanello, *Eur. J. Inorg. Chem.* **2002**, *2002*, 3018–3027; d) E. Urnius, W. W. Brennessel, C. J. Cramer, J. E. Ellis, P. v. R. Schleyer, *Science* **2002**, *295*, 832–834; e) C. M. Knapp, B. H. Westcott, M. A. C. Raybould, J. E. McGrady, J. M. Goicoechea, *Angew. Chem. Int. Ed.* **2012**, *51*, 9097–9100; f) S. Heinl, G. Balázs, M. Bodensteiner, M. Scheer, *Dalton Trans.* **2016**, *45*, 1962–1966.

[10] a) B. M. Cossairt, N. A. Piro, C. C. Cummins, *Chem. Rev.* **2010**, *110*, 4164–4177; b) M. Caporali, L. Gonsalvi, A. Rossin, M. Peruzzini, *Chem. Rev.* **2010**, *110*, 4178–4235; c) C. M. Hoidn, D. J. Scott, R. Wolf, *Chem. Eur. J.* **2021**, *27*, 1886–1902.

[11] a) J. Bai, A. V. Virovets, M. Scheer, *Angew. Chem. Int. Ed.* **2002**, *41*, 1737–1740; b) J. Bai, A. V. Virovets, M. Scheer, *Science* **2003**, *300*, 781–783; c) M. Scheer, J. Bai, B. P. Johnson, R. Merkle, A. V. Virovets, C. E. Anson, *Eur. J. Inorg. Chem.*

2005, *2005*, 4023–4026; d) M. Scheer, L. J. Gregoriades, A. V. Virovets, W. Kunz, R. Neueder, I. Krossing, *Angew. Chem. Int. Ed.* **2006**, *45*, 5689–5693; e) M. Scheer, A. Schindler, R. Merkle, B. P. Johnson, M. Linseis, R. Winter, C. E. Anson, A. V. Virovets, *J. Am. Chem. Soc.* **2007**, *129*, 13386–13387; f) S. Welsch, L. J. Gregoriades, M. Sierka, M. Zabel, A. V. Virovets, M. Scheer, *Angew. Chem. Int. Ed.* **2007**, *46*, 9323–9326; g) M. Scheer, L. J. Gregoriades, R. Merkle, B. P. Johnson, F. Dielmann, *Phosphorus, Sulfur, Silicon, Relat. Elem.* **2008**, *183*, 504–508; h) M. Scheer, A. Schindler, C. Gröger, A. V. Virovets, E. V. Peresypkina, *Angew. Chem. Int. Ed.* **2009**, *48*, 5046–5049; i) M. Scheer, A. Schindler, J. Bai, B. P. Johnson, R. Merkle, R. Winter, A. V. Virovets, E. V. Peresypkina, V. A. Blatov, M. Sierka, H. Eckert, *Chem. Eur. J.* **2010**, *16*, 2092–2107; j) F. Dielmann, A. Schindler, S. Scheuermayer, J. Bai, R. Merkle, M. Zabel, A. V. Virovets, E. V. Peresypkina, G. Brunklaus, H. Eckert, M. Scheer, *Chem. Eur. J.* **2012**, *18*, 1168–1179; k) E. Peresypkina, C. Heindl, A. Virovets, H. Brake, E. Mädl, M. Scheer, *Chem. Eur. J.* **2018**, *24*, 2503–2508.

[12] M. V. Butovskiy, G. Balázs, M. Bodensteiner, E. V. Peresypkina, A. V. Virovets, J. Sutter, M. Scheer, *Angew. Chem. Int. Ed.* **2013**, *52*, 2972–2976.

[13] E. Mädl, M. V. Butovskii, G. Balázs, E. V. Peresypkina, A. V. Virovets, M. Seidl, M. Scheer, *Angew. Chem. Int. Ed.* **2014**, *53*, 7643–7646.

[14] a) F. Riedlberger, S. Todisco, P. Mastrorilli, A. Y. Timoshkin, M. Seidl, M. Scheer, *Chem. Eur. J.* **2020**, *26*, 16251–16255; b) R. Yadav, T. Simler, S. Reichl, B. Goswami, C. Schoo, R. Köppe, M. Scheer, P. W. Roesky, *J. Am. Chem. Soc.* **2020**, *142*, 1190–1195.

[15] D. Tofan, B. M. Cossairt, C. C. Cummins, *Inorg. Chem.* **2011**, *50*, 12349–12358.

[16] a) J. J. Weigand, M. Holthausen, R. Fröhlich, *Angew. Chem. Int. Ed.* **2009**, *48*, 295–298; b) M. H. Holthausen, J. J. Weigand, *Chem. Soc. Rev.* **2014**, *43*, 6639–6657.

[17] A. K. Adhikari, C. G. P. Ziegler, K. Schwedtmann, C. Taube, J. J. Weigand, R. Wolf, *Angew. Chem. Int. Ed.* **2019**, *58*, 18584–18590.

[18] C. G. P. Ziegler, T. M. Maier, S. Pelties, C. Taube, F. Hennersdorf, A. W. Ehlers, J. J. Weigand, R. Wolf, *Chem. Sci.* **2019**, *10*, 1302–1308.

[19] R. Yadav, B. Goswami, T. Simler, C. Schoo, S. Reichl, M. Scheer, P. W. Roesky, *Chem. Commun.* **2020**, *56*, 10207–10210.

[20] C. Riesinger, G. Balázs, M. Bodensteiner, M. Scheer, *Angew. Chem. Int. Ed.* **2020**, *59*, 23879–23884.

[21] S. J. Connelly, W. Kaminsky, D. M. Heinekey, *Organometallics* **2013**, *32*, 7478–7481.

[22] a) A. Jayaraman, T. V. Jacob, J. Bisskey, B. T. Sterenberg, *Dalton Trans.* **2015**, *44*, 8788-8791; b) A. Jayaraman, B. T. Sterenberg, *Organometallics* **2016**, *35*, 14, 2367–2377; c) A. Jayaraman, S. Nilewar, T. V. Jacob, B. T. Sterenberg, *ACS Omega* **2017**, *2*, 7849–7861.

[23] a) G. Capozzi, L. Chiti, M. Di Vaira, M. Peruzzini, P. Stoppioni, *Chem. Commun.* **1986**, *24*, 1799–1800; b) A. Barth, G. Huttner, M. Fritz, L. Zsolnai, *Angew. Chem. Int. Ed. Engl.* **1990**, *29*, 929–931; c) P. Barbaro, A. Ienco, C. Mealli, M. Peruzzini, O. J. Scherer, G. Schmitt, F. Vizza, G. Wolmershäuser, *Chem. Eur. J.* **2003**, *9*, 5196–5210; d) M. Peruzzini, R. R. Abdreimova, Y. Budnikova, A. Romerosa, O. J. Scherer, H. Sitzmann, *J. Organomet. Chem.* **2004**, *689*, 4319–4331; e) B. M. Cossairt, M.-C. Diawara, C. C. Cummins, *Science* **2009**, *323*, 602; f) P. Barbaro, C. Bazzicalupi, M. Peruzzini, S. Seniori Costantini, P. Stoppioni, *Angew. Chem. Int. Ed.* **2012**, *51*, 8628–8631; g) C. Schwarzmaier, S. Heinl, G. Balázs, M. Scheer, *Angew. Chem. Int. Ed.* **2015**, *54*, 13116–13121; h) E. Mädl, G. Balázs, E. V. Peresypkina, M. Scheer, *Angew. Chem. Int. Ed.* **2016**, *55*, 7702–7707; i) A. Cavaillé, N. Saffon-Merceron, N. Nebra, M. Fustier-Boutignon, N. Mézailles, *Angew. Chem. Int. Ed.* **2018**, *57*, 1874–1878; j) C. M. Hoidn, T. M. Maier, K. Trabitsch, J. J. Weigand, R. Wolf, *Angew. Chem. Int. Ed.* **2019**, *58*, 18931–18936; k) U. Chakraborty, J. Leitl, B. Mühldorf, M. Bodensteiner, S. Pelties, R. Wolf, *Dalton Trans.* **2018**, *47*, 3693–3697.

[24] a) C. Dohmeier, C. Robl, M. Tacke, H. Schnöckel, *Angew. Chem. Int. Ed. Engl.* **1991**, *30*, 564–565; b) S. Schulz, H. W. Roesky, H. J. Koch, G. M. Sheldrick, D. Stalke, A. Kuhn, *Angew. Chem. Int. Ed. Engl.* **1993**, *32*, 1729–1731; c) R. Yadav, T. Simler, B. Goswami, C. Schoo, R. Köppe, S. Dey, P. W. Roesky, *Angew. Chem. Int. Ed.* **2020**, *59*, 9443–9447.

[25] A. Frei, *Chem. Eur. J.* **2019**, *25*, 7074–7090.

[26] a) I. Krossing, *Chem. Eur. J.* **2001**, *7*, 490–502; b) M. Gonsior, I. Krossing, N. Mitzel, *Z. anorg. allg. Chem.* **2002**, *628*, 1821–1830.

[27] a) N. Burford, P. J. Ragogna, R. McDonald, M. J. Ferguson, *J. Am. Chem. Soc.* **2003**, *125*, 14404–14410; b) M. Gonsior, I. Krossing, L. Müller, I. Raabe, M. Jansen, L. van Wüllen, *Chem. Eur. J.* **2002**, *8*, 4475–4492; c) J. Possart, A. Martens, M. Schleep, A. Ripp, H. Scherer, D. Kratzert, I. Krossing, *Chem. Eur. J.* **2017**, *23*, 12305–12313.

[28] G. Manca, A. Ienco, *Inorg. Chim. Acta* **2021**, *517*, 120205.

[29] H. Brake, E. Peresypkina, A. V. Virovets, M. Piesch, W. Kremer, L. Zimmermann, C. Klimas, M. Scheer, *Angew. Chem. Int. Ed.* **2020**, *59*, 16241–16246.

[30] A. Garbagnati, M. Seidl, G. Balázs, M. Scheer, *Inorg. Chem.* **2021**, *60*, 5163–5171.

[31] a) P. Pyykkö, M. Atsumi, *Chem. Eur. J.* **2009**, *15*, 186–197; b) P. Pyykkö, M. Atsumi, *Chem. Eur. J.* **2009**, *15*, 12770–12779; c) P. Pyykkö, *J. Phys. Chem. A* **2015**, *119*, 2326–2337.

[32] a) P. A. M. Dirac, *Proc. Roy. Soc. Lond. A* **1929**, *123*, 714–733; b) J. C. Slater, *Phys. Rev.* **1951**, *81*, 385–390; c) S. H. Vosko, L. Wilk, M. Nusair, *Can. J. Phys.* **1980**, *58*, 1200–1211; d) C. Lee, W. Yang, R. G. Parr, *Phys. Rev. B* **1988**, *37*, 785–789; e) A. D. Becke, *Phys. Rev. A* **1988**, *38*, 3098–3100; f) A. D. Becke, *J. Chem. Phys.* **1993**, *98*, 5648–5652.

[33] a) F. Weigend, R. Ahlrichs, *Phys. Chem. Chem. Phys.* **2005**, *7*, 3297–3305; b) F. Weigend, *Phys. Chem. Chem. Phys.* **2006**, *8*, 1057–1065.

[34] J. Tomasi, B. Mennucci, R. Cammi, *Chem. Rev.* **2005**, *105*, 2999–3093.

[35] a) E. D. Glendening, C. R. Landis, F. Weinhold, *J. Comput. Chem.* **2013**, *34*, 1363–1374; b) E. D. Glendening, C. R. Landis, F. Weinhold, *J. Comput. Chem.* **2013**, *34*, 2134.

[36] a) S. Dapprich, G. Frenking, *J. Phys. Chem.* **1995**, *99*, 9352–9362; b) M. Xiao, T. Lu, *J. Adv. Phys. Chem.* **2015**, *04*, 111–124.

[37] a) P. v. R. Schleyer, C. Maerker, A. Dransfeld, H. Jiao, N. J. R. van Eikema Hommes, *J. Am. Chem. Soc.* **1996**, *118*, 6317–6318; b) Z. Chen, C. S. Wannere, C. Corminboeuf, R. Puchta, P. v. R. Schleyer, *Chem. Rev.* **2005**, *105*, 3842–3888; c) T. Lu, F. Chen, *J. Comput. Chem.* **2012**, *33*, 580–592.

[38] a) J. P. Perdew, K. Burke, M. Ernzerhof, *Phys. Rev. Lett.* **1996**, *77*, 3865–3868; b) J. P. Perdew, K. Burke, M. Ernzerhof, *Phys. Rev. Lett.* **1997**, *78*, 1396; c) C. Adamo, V. Barone, *J. Chem. Phys.* **1999**, *110*, 6158–6170.

[39] F. Jensen, *J. Chem. Theory Comput.* **2015**, *11*, 132–138.

[40] a) B. Metz, H. Stoll, M. Dolg, *J. Chem. Phys.* **2000**, *113*, 2563–2569; b) K. A. Peterson, D. Figgen, E. Goll, H. Stoll, M. Dolg, *J. Chem. Phys.* **2003**, *119*, 11113–11123; c) D. Rappoport, F. Furche, *J. Chem. Phys.* **2010**, *133*, 134105–134116.

[41] F. Dielmann, E. V. Peresypkina, B. Krämer, F. Hastreiter, B. P. Johnson, M. Zabel, C. Heindl, M. Scheer, *Angew. Chem. Int. Ed.* **2016**, *55*, 14833-14837.

[42] *https://omics.pnl.gov/software/molecular-weight-calculator (30.03.2021)*.

[43] P. Romanato, S. Duttwyler, A. Linden, K. K. Baldridge and J. S. Siegel, *J. Am. Chem. Soc.* **2010**, *132*, 7828–7829.

[44] W. Steinkopf, H. Dudek and S. Schmidt, *Ber. dtsch. Chem. Ges. A/B* **1928**, *61*, 1911–1918.

[45] O. Behaghel and H. Seibert, *Ber. dtsch. Chem. Ges. A/B* **1932**, *65*, 812–816.

[46] A. K. S. Chauhan, P. Singh, A. Kumar, R. C. Srivastava, R. J. Butcher and A. Duthie, *Organometallics* **2007**, *26*, 1955–1959.

[47] a) H. Sitzmann, P. Zhou and G. Wolmershäuser, *Chem. Ber.* **1994**, *127*, 3–9; b) M. D. Walter, C. D. Sofield, C. H. Booth and R. A. Andersen, *Organometallics* **2009**, *28*, 2005–2019.

[48] S. Humbel, C. Bertrand, C. Darcel, C. Bauduin and S. Jugé, *Inorg. Chem.* **2003**, *42*, 420–427.

[49] Agilent Technologies Ltd, *CrysAlis PRO*, Yarnton, Oxfordshire, England, **2014**.

[50] O. V. Dolomanov, L. J. Bourhis, R. J. Gildea, J. A. K. Howard and H. Puschmann, *J. Appl. Crystallogr.* **2009**, *42*, 339–341.

[51] G. M. Sheldrick, *Acta Cryst. A* **2015**, *71*, 3–8.

[52] a) G. M. Sheldrick, *Acta Cryst. A* **2008**, *64*, 112–122; b) G. M. Sheldrick, *Acta Cryst. C,* **2015**, *71*, 3–8.

[53] M. J. Frisch, G. W. Trucks, H. B. Schlegel, G. E. Scuseria, M. A. Robb, J. R. Cheeseman, G. Scalmani, V. Barone, B. Mennucci, G. A. Petersson, H. Nakatsuji, M. Caricato, X. Li, H. P. Hratchian,A. F. Izmaylov, J. Bloino, G. Zheng, J. L. Sonnenberg, M. Hada, M. Ehara, K. Toyota, R. Fukuda, J. Hasegawa, M. Ishida, T. Nakajima, Y. Honda, O. Kitao, H. Nakai, T. Vreven, J. A. Montgomery Jr., J. E. Peralta, F. Ogliaro, M. Bearpark, J. J. Heyd, E. Brothers, K. N. Kudin, V. N. Staroverov, T. Keith, R. Kobayashi, J. Normand, K. Raghavachari, A. Rendell, J. C. Burant, S. S. Iyengar, J. Tomasi, M. Cossi, N. Rega, J. M. Millam, M. Klene, J. E. Knox, J. B. Cross, V. Bakken, C. Adamo, J. Jaramillo, R. Gomperts, R. E. Stratmann, O. Yazyev, A. J. Austin, R. Cammi, C. Pomelli, J. W. Ochterski, R. L. Martin, K. Morokuma, V. G. Zakrzewski, G. A. Voth, P. Salvador, J. J. Dannenberg, S. Dapprich, A. D. Daniels, O. Farkas, J. B. Foresman, J. V. Ortiz, J. Cioslowski and D. J. Fox, *"Gaussian 09", Revision E.01, Gaussian Inc.*, Wallingford CT, **2013**.

[54] a) D. Feller, *J. Comput. Chem.* **1996**, *17*, 1571–1586; b) K. L. Schuchardt, B. T. Didier, T. Elsethagen, L. Sun, V. Gurumoorthi, J. Chase, J. Li and T. L. Windus, *J. Chem. Inf. Model.* **2007**, *47*, 1045–1052; c) B. P. Pritchard, D. Altarawy, B. Didier, T. D. Gibson and T. L. Windus, *J. Chem. Inf. Model.* **2019**, *59*, 4814–4820.

7. Teaching Old Tricks to New Dogs – Rational Synthesis of Multi-Decker Complexes Featuring *cyclo*-P_5 Decks

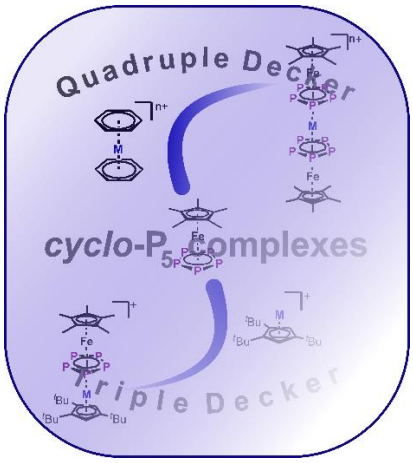

Preface

The following chapter has already been published. The article is reproduced with permission from the Royal Society of Chemistry.

"Teaching Old Tricks to New Dogs – Rational Synthesis of Multi-Decker Complexes Featuring cyclo-P_5 Decks"

Chem. Commun. **2023,** *59***,** 4495–4498.

Parts of this chapter have already been described within the BSc thesis of Adrian Stadler.

Authors

Christoph Riesinger, David Röhner, Ingo Krossing and Manfred Scheer

Author Contributions

Christoph Riesinger – Conceptualization, Synthesis of compounds **1**, **2-Fe** and **3**, Interpretation of computational data, Interpretation of crystallographic data, Writing of original draft.
David Röhner – Synthesis of **2-Co**, Writing of original draft
Ingo Krossing – Project administration, Funding acquisition, Co-writing final manuscript.
Manfred Scheer – Project administration, Funding acquisition, Co-writing final manuscript.

Acknowledgements

This work was supported by the Deutsche Forschungsgemeinschaft (DFG) within the projects Sche 384/36-2 and Sche 384/32-2. C. R. is grateful to the Studienstiftung des Deutschen Volkes for a PhD fellowship.

7.1. Abstract

*A rational synthetic pathway towards a series of cyclo-P_5-bearing multi-decker complexes was developed. The combination of [Cp*Fe($\mu,\eta^{5:5}$-P_5)] (A) with low-valent transition metal cations yields a series of triple-decker complexes [Cp*Fe($\mu,\eta^{5:5}$-P_5)MCp'''][WCA] (M = Cr – Ni; WCA = weakly coordinating anion). Utilizing the arene complexes [M(C_6R_6)$_2$][WCA]$_n$ (M = Fe, Co) instead allowed the synthesis of the unprecedented cyclo-P_5-containing quadruple-decker complexes [{Cp*Fe($\mu,\eta^{5:5}$-P_5)}$_2$M][pf]$_n$ (M = Fe, Co).*

7.2. Introduction

Since the first isolations of ferrocene[1] and bis-benzene chromium[2] in 1951 and 1955, respectively, sandwich complexes have become a staple in organometallic and even organic chemistry, being applied in e. g. electrochemistry,[3] catalysis[4] or in the stabilisation of exotic compounds as recently reported for a U(I) species.[5] While the intriguing physical properties (e. g. magnetism)[6] of these species have attracted considerable scientific interest over the past decades, the classic sandwich structure was rapidly expanded to triple-decker compounds, when Salzer and Werner isolated salts of the $[Cp_3Ni_2]^+$ cation (**I**) in 1972 (Scheme 1).[7] Since then, the synthesis, reactivity and use of organometallic multi-decker compounds have been an ever-growing field, yielding complexes with up to six decks (**III**).[8] However, while triple-decker complexes are comparatively well-known, the number of reported compounds drastically decreases when it comes to larger multi-decker systems. Their inherently challenging synthesis further diminishes their availability and often deviates from rational synthetic pathways, e. g. as has recently been described for the archetypical [(COT$^{1,4\text{-}Si\textit{i}Pr3}$)$_4Sm_3$] (**II**).[9]

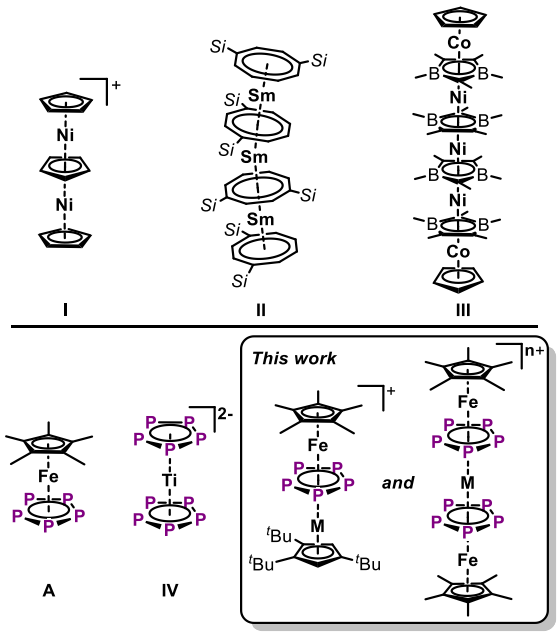

Scheme 1: Selected multi-decker complexes (top) and relevant sandwich as well as multi-decker species bearing cyclo-P_5 ligands; Si = Si^iPr_3.

Besides multi-decker complexes based purely on carbocyclic ligands,[10] compounds bearing heteroatomic ligands are of great importance to the field.[11] Especially, cyclic polyphosphorus (*cyclo*-P_n) ligands received significant attention very early on, which is due to their isolobal relationship with their carbocyclic analogs. Thus, sandwich and triple-decker complexes with *cyclo*-P_n ligands (n = 3,[12] 4,[13] 5,[14] 6[15]) are well studied species, even finding their way into the use as e. g. building blocks for supramolecular chemistry.[16] The arguably most prominent one of these complexes is [Cp*Fe(η^5-P_5)] (**A**, Cp* = C_5Me_5, Scheme 1),[14b] the *cyclo*-P_5 analog to prototypical ferrocene, first described by the group of Scherer. Furthermore, the *cyclo*-P_5 ligand was also used to stabilise the purely inorganic metallocene [Ti(*cyclo*-P_5)$_2$]$^{2-}$ (**IV**)[17] as well as numerous triple-decker species with planar[18] and bent[19] *cyclo*-P_5 middle decks. However, various synthetic protocols were used for their preparation which resulted in rather low-yielding syntheses. A general synthetic pathway towards *cyclo*-P_5 triple-decker complexes in high yields is still missing and quadruple-decker compounds bearing *cyclo*-P_5 ligands are completely unknown to the best of our knowledge. However, **A** displays a promising building block for the synthesis of *cyclo*-P_5-bearing multi-decker systems. With its great potential in coordination chemistry already demonstrated for coinage metal[20] and heavy group 13 ions,[21] a combination of **A** and suitable transition metal precursors, such as the arene complexes [M(C_6R_6)$_2$][WCA]$_n$ (M = Fe,[22] Co;[23] n = 1, 2; WCA = weakly coordinating anion), could allow the preparation of *cyclo*-P_5 multi-decker complexes. Herein, a general and high-yielding synthetic approach towards such complexes is reported for new hetero-bimetallic triple-decker compounds and then transferred to a series of unprecedented *cyclo*-P_5-based quadruple-decker complexes.

7.3. Results and Discussion

As the reactivity of unsaturated cationic transition metal species has played a key role in the synthesis of triple-decker compounds ever since their first synthesised in 1972,[7] this methodology could be called an “old trick”, which had been envisioned to systematically yield

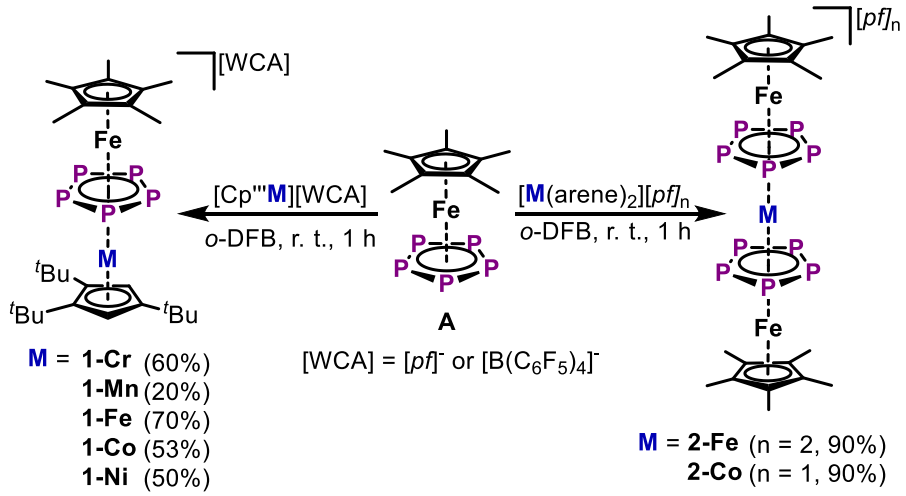

Scheme 2: Rational synthesis of cationic triple- (left) and quadruple-decker (right) complexes bearing cyclo-P_5 ligands; yields are reported in parantheses.

cationic *cyclo*-P_5-bearing triple-decker complexes of various metals in combination with **A**, a "new player" in the field of expanded multi-decker systems. Interestingly, *in situ* halide abstraction from $[Cp'''M(\mu\text{-}X)]_2$ (M = Cr – Ni, X = Cl, Br, Cp''' = 1,2,4-^{t}Bu$_3$C$_5$H$_2$)[24] and reaction with **A** was found to even provide a general straightforward access to the triple-decker compounds of the type $[Cp^*Fe(\mu,\eta^{5:5}\text{-}P_5)MCp'''][WCA]$ (**1-Cr** – **1-Ni**, $[WCA]^-$ = $[BAr^F]^-$ or [*pf*]$^-$, $[BAr^F]^-$ = $[B(C_6F_5)_4]^-$, [*pf*]$^-$ = $[Al\{OC(CF_3)_3\}_4]^-$; Scheme 2). The compounds **1-Cr** – **1-Ni** can be isolated as crystalline solids in good yields of up to 70% after a simple workup. Only the paramagnetic **1-Mn** is obtainable in diminished yields of 20%, due to its complicated separation from side products (see SI). Moving forward, the Cp''' ligands in these complexes may be pictured to be replaced with another moiety of **A** to form unprecedented *cyclo*-P_5 based quadruple-decker complexes. However, halide abstraction reactions between $FeBr_2$ or $CoCl_2$ and Tl[*pf*] in the presence of **A** failed to provide the desired products. In contrast, the reaction of two equivalents of **A** with $[Fe(tol)_2][pf]_2$ yields the new homometallic quadruple-decker species $[\{Cp^*Fe(\mu,\eta^{5:5}\text{-}P_5)\}_2Fe][pf]_2$ (**2-Fe**) in a straightforward and clean reaction (Scheme 2). Even more interestingly, $[Co(o\text{-dfb})_2][pf]$ readily reacts with **A** to afford a novel heterometallic quadruple-decker complex $[\{Cp^*Fe(\mu,\eta^{5:5}\text{-}P_5)\}_2Co][pf]$ (**2-Co**). Both species can be isolated in excellent crystalline yields of 90% enabling the investigation of their physical properties. While both compounds **2-Fe** and **2-Co** display unprecedented quadruple-deckers bearing *cyclo*-P_5 ligands, the recent exploration of cationic arene complexes of more and more transition metals may allow the preparation of a whole series of such complexes.[22,23,25]

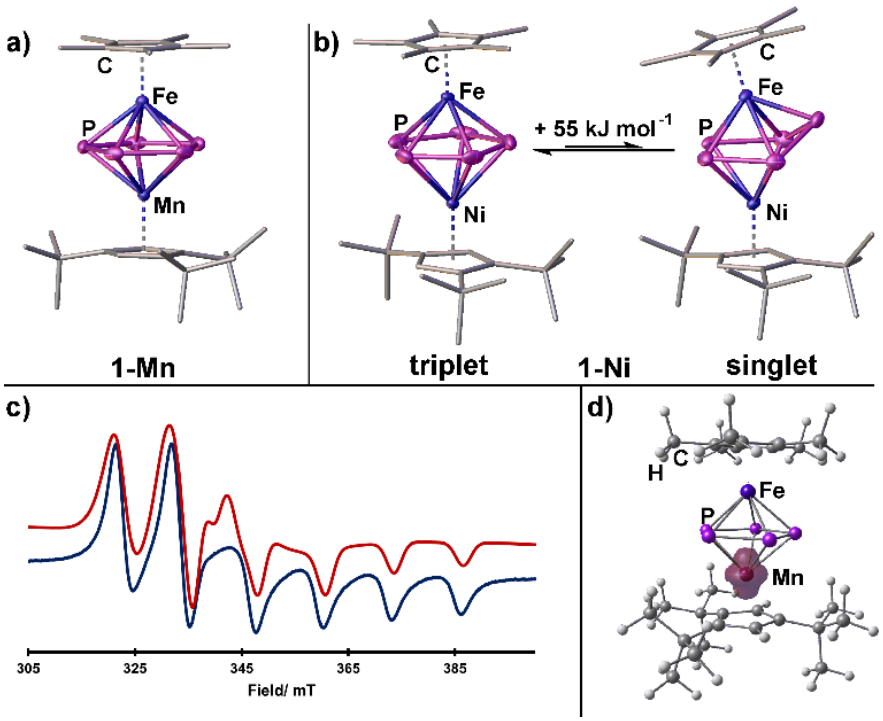

*Figure 1: a) Solid-state structure of the triple-decker complexes exemplified for **1-Mn**; b) Both structures of **1-Ni** in the solid state with the assignment of spin states and their energy difference (H atoms and counterions are omitted for clarity); c) Experimental (blue) and simulated (red) X-band EPR spectrum of **1-Mn** in frozen o-DFB solution at 77 K; d) Calculated spin density of **1-Mn** (at ωB97X-D3/def2-TZVP), cut-off at 0.01 a.u.*

Structurally, the triple-decker complexes **1** reveal a cationic central framework of a *cyclo*-P_5 ligand sandwiched between a {Cp*Fe} moiety and another {Cp‴M} (M = Cr – Ni) unit (Figure 1a for **1-Mn**). While the *cyclo*-P_5 ligand is oriented in a staggered conformation towards the Cp* ligand, it is aligned in an eclipsed fashion to the Cp‴ ligand. Moreover, the Fe–M distances expand from 2.666(1) Å (**1-Cr**, 28 VE) to 3.293(1) Å (**1-Ni**, 32 VE). The opposite trend is observed for the P–P bond lengths, which are elongated in **1-Cr** (2.198(5) – 2.235(9) Å) compared to the starting material **A** (2.088(3) – 2.108(3) Å) and gradually decrease down to **1-Ni** (2.115(2) – 2.130(2) Å). Both trends are in line with the increasing number of valence electrons (VE) in the triple-decker system. Furthermore, the solid-state structure of **1-Ni** features two distinct molecular geometries, one of which shows a planar and the other one a bent *cyclo*-P_5 middle deck. This is attributed to a rapid dynamic behaviour of the *cyclo*-P_5 ligand within **1-Ni** and was already observed in the isoelectronic compound [Cp*Fe($\mu,\eta^{5:5}$-P_5)CoCp‴][19b] (Figure 1b). However, spectroscopic investigations suggest the planar conformation of the *cyclo*-P_5 ligand to be the dominant one for **1-Ni** in solution (*vide infra*). Spectroscopically, the well-resolved ^{1}H NMR spectra of the complexes **1-Cr** and **1-Fe** reveal their singlet character and agree with rotationally free Cp* and Cp‴ ligands. Furthermore, **1-Cr** and **1-Fe** show sharp singlets at δ/ppm = 14.2 and –12.5 in the ^{31}P NMR spectrum, respectively. In contrast, the NMR spectra of **1-Mn** indicate its paramagnetic character, which is confirmed by its X-band EPR spectrum. The axial signal with exceptionally hyperfine coupling to the Mn nucleus (Figure 1c) is well reproduced by its simulation and in good agreement with DFT calculations showing the localisation of the spin density at the Mn atom (Figure 1d). Similar behaviour was observed for the cation in **1-Co**.[18c] Despite its even number of VE (32), **1-Ni** is silent in both the NMR and the X-band EPR spectrum, suggesting a triplet ground state in solution. This is further supported by DFT calculations revealing the planar conformation of **1-Ni** (triplet) to be 55 kJ mol^{-1} more stable than the bent form (singlet, ωB97X-D3/def2-TZVP, see SI). Finally, the Evans method imparts two unpaired electrons for **1-Ni** (see SI), disclosing its triplet ground state. Notably, the isoelectronic neutral compound [Cp*Fe($\mu,\eta^{5:5}$-P_5)CoCp‴] is a singlet.[19b]

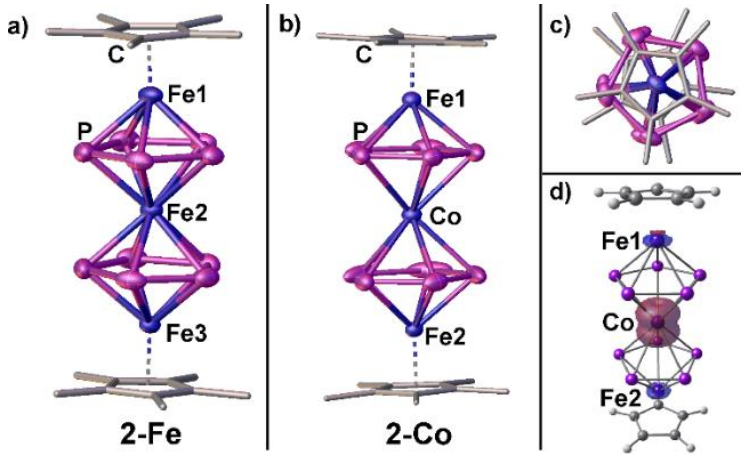

*Figure 2: a) and b) Side view of the solid-state structures of **2-Fe** and **2-Co**, respectively; c) Top view of the solid-state structure **2-Co** (H atoms and counterions omitted for clarity); d) Calculated spin density of **2-Co** (at □B97X-D3/def2-TZVP), cut-off at 0.01 a.u..*

Similarly to the triple-decker species **1**, the Fe–M distance in the quadruple-decker complexes **2** increases from 3.101(1)/3.103(1) Å (**2-Fe**, 42 VE, Figure 2a) to 3.286(1)/3.287(1) Å (**2-Co**, 44 VE, Figure 2b,c) upon addition of two valence electrons. However, the P–P bond lengths remain nearly unchanged going from **2-Fe** (2.122(2) – 2.160(2) Å) to **2-Co** (2.112(2) – 2.141(2) Å) and are only slightly elongated compared to those in **A**.[14b] In both species, the *cyclo*-P_5 ligands are arranged in an ecliptic conformation with the Cp* ligands being oriented in a staggered fashion relative to them. While **2-Fe** is a diamagnetic quadruple-decker-species showing a sharp singlet in the ^{31}P NMR spectrum at δ/ppm = 12.9, **2-Co** shows paramagnetic character despite its 44 VE. The X-band EPR spectrum of **2-Co** remains silent, suggesting a triplet ground state. DFT calculations reveal a highly distorted and energetically unfavored (127 kJ mol^{-1}, ωB97X-D3/def2-TZVP) molecular geometry for a hypothetical singlet configuration, thus pointing towards the triplet character of **2-Co** as well (see SI). Consequently, the Evans method reveals two unpaired electrons, corroborating that indeed **2-Co** has a triplet ground state, with the spin density being highly localised at the Co atom (Figure 2d).

To demonstrate the generalisability of the presented quadruple-decker synthesis even beyond the variation of the central metal atom, the starting material **A** was exchanged for its heavier analog [Cp*Fe(η^5-As_5)] (**B**)[26] bearing a *cyclo*-As_5 ligand. Interestingly, two equivalents of **B** cleanly react with [Fe(tol)$_2$][*pf*]$_2$ (tol = toluene) to afford the unprecedented *cyclo*-As_5 containing quadruple-decker compound [{Cp*Fe(μ,$\eta^{5:5}$-As_5)}$_2$Fe][*pf*]$_2$ (**3**) in almost quantitative 96% crystalline yield (Figure 3a). The dication in **3** shows a quadruple- decker structural motif similar to **2-Fe**, featuring, however, two perfectly eclipsed *cyclo*-As_5 ligands on the central Fe atom (Figure 3b). The Fe–Fe distances (3.166(1)/3.173(1) Å) in **3** are longer than in **2-Fe** but still shorter compared to the Fe-Co distance in **2-Co**, thus allowing careful tuning of this crucial structural parameter within the series of herein reported quadruple-decker complexes. Furthermore, the As–As bonds in **3** (2.346(1) – 2.356(1) Å) are only slightly elongated compared to those in the starting material **B** (2.317(1) – 2.330(1) Å). The ^{1}H NMR spectrum of **3** reveals only one singlet corresponding to chemically equivalent Cp* ligands and indicating its diamagnetic character.

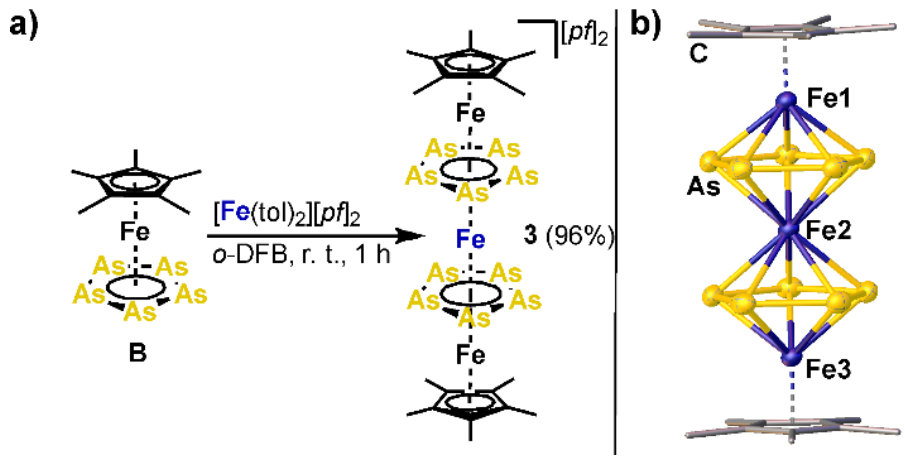

*Figure 3: a) Synthesis of **3**, a quadruple- decker complex bearing cyclo-As_5 ligands; b) Its solid-state structure, H atoms and counterions omitted for clarity; tol = toluene.*

7.4. Conclusion

In summary, a general synthetic approach towards new *cyclo*-P_5 bearing triple-decker complexes was developed utilising the reactivity of **A** with *in situ* generated $[Cp'''M]^+$ cations (M = Cr – Ni). The respective products $[Cp^*Fe(\mu,\eta^{5:5}\text{-}P_5)MCp'''][WCA]$ (**1-Cr** – **1-Ni**) show intriguing spectroscopic and magnetic properties rendering them promising candidates for further applications. Systematic replacement of $[Cp'''M]^+$ by arene-coordinated transition metal cations $[M(arene)]^{n+}$ (n = 1, 2) enabled the synthesis of the unprecedented *cyclo*-P_5 containing quadruple-decker complexes $[\{Cp^*Fe(\mu,\eta^{5:5}\text{-}P_5)\}_2M][pf]_n$ (**2-Fe**, **2-Co**). While compounds **2** are the first representatives of this class of compounds, the generality of the herein described approach should allow for the preparation of a wide variety of *cyclo*-P_5-based quadruple-decker species. Finally, this method is not limited to *cyclo*-P_5 ligands but can even be transferred to the preparation of *cyclo*-As_5 quadruple-decker compounds. Thus, replacing **A** with $[Cp^*Fe(\eta^5\text{-}As_5)]$ (**B**) enables the synthesis of $[\{Cp^*Fe(\mu,\eta^{5:5}\text{-}As_5)\}_2Fe][pf]_2$ (**3**), the first *cyclo*-As_5-containing quadruple-decker species. Notably, the structural and spectroscopic properties of the quadruple-decker species **2** and **3** can easily be varied via the exchange of the central metal ion or middle-deck ligand. Finally, compared to their carbocyclic analogs, the quadruple-decker complexes **2** and **3** bear great potential for further application in e. g. coordination chemistry due to the availability of lone pairs of electrons centered at the pnictogen atoms.

7.5. Supporting Information

7.5.1. Experimental Procedures

General Considerations

All manipulations were carried out using standard Schlenk techniques at a Stock apparatus under N_2 as an inert gas or in a glove box with Ar atmosphere. All glassware was dried with a heat gun (600 °C) for at least 30 min prior to use. *o*-DFB (1,2-difluorobenzene) was distilled from P_2O_5, CD_2Cl_2 was distilled from CaH_2 and other solvents were directly taken from an MBraun SPS-800 solvent purification system and degassed at room temperature. Solution ^{1}H (400.130 MHz), ^{11}B (128.432 MHz), ^{19}F (376.498 MHz)a and ^{31}P (161.976 MHz) NMR spectra were recorded at an Avance400 (Bruker) spectrometer using $(H_3C)_4Si$ (^{1}H, ^{13}C), $BF_3{\cdot}OEt_2$ (^{11}B) $CFCl_3$ (^{19}F) or 85% phosphoric acid (^{31}P), respectively, as external standards. Chemical shifts (δ) are provided in parts per million (ppm) and coupling constants (*J*) are reported in Hertz (Hz). The following abbreviations are used: s = singlet, d = doublet, dd = doublet of doublets, dt = doublet of triplets, t = triplet, td = triplet of doublets br = broad and m = multiplet. Mass spectra were recorded at the internal mass spectrometry department using a ThermoQuest Finnigan TSQ 7000 (ESI) or Finnigan MAT 95 (LIFDI) mass spectrometer or by the first author on a Waters Micromass LCT ESI-TOF mass-spectrometer and peak assignment was performed using the Molecular weight calculator 6.50.[27] Elemental analysis of the products was conducted by the elemental analysis department at the University of Regensburg using an Elementar Vario EL. The starting materials [Cp*Fe(η^5-P_5)],[14b] [Cp*Fe(η^5-As_5)],[26] [Cp‴M(μ-X)]$_2$ (M = Cr,[24e] Mn,[24c] Fe,[24b] Co,[24a] Ni,[24d] X = Cl, Br), K[BAr^F],[28] Tl[*pf*][29] and [Co(*o*-dfb)$_2$][*pf*][23] were synthesized according to literature procedures. All other chemicals were purchased from commercial vendors and used without further purification.

1-Cr

A dark blue solution of $[Cp'''Cr(\mu\text{-}Cl)]_2$ (64 mg, 0.1 mmol, 1 eq.) in 6 mL of *o*-DFB was added to a dark green solution of $[Cp^*Fe(\eta^5\text{-}P_5)]$ (70 mg, 0.2 mmol, 2 eq.) and $K[BAr^F]$ (144 mg, 0.2 mmol, 2 eq.) in 6 mL of *o*-DFB. A rapid colour change to red and formation of a colourless solid was observed and the reaction was completed by stirring the solution at room temperature for 1 h. Afterwards the solution was filtered, constricted to 3 mL and layered with 15 mL of *n*-hexane. Storage of this mixture at room temperature for 4 days yielded dark red plate shaped crystals of $[Cp^*Fe(\mu;\eta^{5:5}\text{-}P_5)CrCp'''][BAr^F]$ (**1-Cr**), which were isolated by decanting the solvent and drying under reduced pressure (10^{-3} mbar).

Yield:	140 mg (0.12 mmol, 60%)
Elemental Analysis:	calculated (%) for $[Cp^*Fe(\mu;\eta^{5:5}\text{-}P_5)CrCp'''][BAr^F]$: C: 46.72 H: 3.38, found: C: 47.17 H: 3.24
ESI(+)-MS (*o*-DFB):	m/z (%) = 631.3 (100, [**1-Cr**]$^+$)
^{1}H-NMR (CD_2Cl_2, 300 K):	δ/ ppm = 1.10 (s, 9 H, $^t\underline{Bu}_3C_5H_2$), 1.26 (s, 18 H, $^t\underline{Bu}_3C_5H_2$), 1.53 (s, 15 H, Cp*), 4.41 (s, 2 H, $^tBu_3C_5\underline{H}_2$)
^{31}P{^{1}H}-NMR (CD_2Cl_2, 300 K):	δ/ ppm = 14.2 ppm (s, *cyclo*-P_5)
^{31}P-NMR (CD_2Cl_2, 300 K):	δ/ ppm = 14.2 ppm (s, *cyclo*-P_5)
^{19}F{^{1}H}-NMR (CD_2Cl_2, 300 K):	δ/ ppm = - 167.3 (br, 8 F, $[BAr^F]^-$), - 163.4 (br, 4 F, $[BAr^F]^-$), - 133.0 (br, 8 F, $[BAr^F]^-$)
^{11}B{^{1}H}-NMR (CD_2Cl_2, 300 K):	δ/ ppm = - 16.9 ppm (s, $[BAr^F]^-$)

1-Mn

[Cp‴Mn(thf)(μ-Cl)]$_2$ (79 mg, 0.1 mmol, 1 eq.), [Cp*Fe(η^5-P$_5$)] (70 mg, 0.2 mmol, 2 eq.) and Tl[*pf*] (234 mg, 0.2 mmol, 2 eq.) were suspended in 4 mL of *o*-DFB to afford a clear green solution and formation of a colourless precipitate. The solution was stirred for 17 h and the solvent was removed under reduced pressure (10^{-3} mbar). 3 mL of CH_2Cl_2 were added to the mixture and the solution was then filtered. The now green solution was layered with 20 mL of *n*-hexane. Storage of this mixture for 2 weeks yielded dark green block shaped crystals of [Cp*Fe(μ;$\eta^{5:5}$-P$_5$)MnCp‴][*pf*] (**1-Mn**). As the formation of a polymeric coordination compound of [Cp*Fe(η^5-P$_5$)] and Tl[*pf*] during this reaction cannot be suppressed, the product has to be isolated by mechanical separation of the crystals of **1-Mn**, which results in decreased yields.

Yield:	65 mg (0.04 mmol, 20%)
Elemental Analysis:	calculated (%) for [Cp*Fe(μ;$\eta^{5:5}$-P$_5$)MnCp‴][*pf*]: C: 32.25 H: 2.77, found: C: 32.21 H: 2.97
ESI(+)-MS (*o*-DFB):	m/z (%) = 634.0 (100, [**1-Mn**]$^+$)
^{1}H-NMR (CD_2Cl_2, 300 K):	δ/ ppm = broad signal between 1 – 3 ppm
^{31}P{^{1}H}-NMR (CD_2Cl_2, 300 K):	δ/ ppm = no signal observed between +/-500 ppm
^{19}F{^{1}H}-NMR (CD_2Cl_2, 300 K):	δ/ ppm = - 75.7 (s, [*pf*]$^-$)

1-Fe

$[Cp'''Fe(\mu\text{-}Br)]_2$ (74 mg, 0.1 mmol, 1 eq.), $[Cp^*Fe(\eta^5\text{-}P_5)]$ (70 mg, 0.2 mmol, 2 eq.) and $Tl[BAr^F]$ (277 mg, 0.2 mmol, 2 eq.) were suspended in 4 mL of *o*-DFB to afford a rapid colour change to greenish blue and formation of a colourless solid. The reaction was completed by stirring the solution at room temperature for 2 h and then the solvent was constrained to 2 mL. Afterwards the solution was filtered, the solvent removed, the residue dissolved in 3 mL of CH_2Cl_2 and layered with 30 mL of *n*-hexane. Storage of this mixture for 7 days yielded dark brownish blue block shaped crystals of $[Cp^*Fe(\mu;\eta^{5:5}\text{-}P_5)FeCp'''][BAr^F]$ (**1-Fe**), which were isolated by decanting the solvent and drying under reduced pressure (10^{-3} mbar).

Yield:	185 mg (0.14 mmol, 70%)
Elemental Analysis:	calculated (%) for $[Cp^*Fe(\mu;\eta^{5:5}\text{-}P_5)FeCp'''][BAr^F]$: C: 46.61 H: 3.37, found: C: 46.27 H: 3.50
ESI(+)-MS (*o*-DFB):	m/z (%) = 635.1 (100, [**1-Fe**]$^+$)
^{1}H-NMR (CD_2Cl_2, 300 K):	δ/ ppm = 1.10 (s, 15 H, Cp*), 1.19 (s, 9 H, $^t\underline{Bu}_3C_5H_2$), 1.31 (s, 18 H, $^t\underline{Bu}_3C_5H_2$), 3.36 (s, 2 H, $^tBu_3C_5\underline{H}_2$)
^{31}P{^{1}H}-NMR (CD_2Cl_2, 300 K):	δ/ ppm = - 12.5 ppm (s, *cyclo*-P_5)
^{31}P-NMR (CD_2Cl_2, 300 K):	δ/ ppm = - 12.5 ppm (s, *cyclo*-P_5)
^{19}F{^{1}H}-NMR (CD_2Cl_2, 300 K):	δ/ ppm = - 167.4 (br, 8 F, $[BAr^F]^-$), - 163.6 (br, 4 F, $[BAr^F]^-$), - 132.9 (br, 8 F, $[BAr^F]^-$)
^{11}B{^{1}H}-NMR (CD_2Cl_2, 300 K):	δ/ ppm = - 16.8 (s, $[BAr^F]^-$)

1-Co

1-Co has already been prepared on a different route, we reported previously.[18c]

[Cp‴Co(μ-Cl)]$_2$ (33 mg, 0.05 mmol, 1 eq.), [Cp*Fe(η^5-P$_5$)] (35 mg, 0.1 mmol, 2 eq.) and Tl[*pf*] (134 mg, 0.1 mmol, 2 eq.) were suspended in 4 mL of *o*-DFB to afford arapid colour change to dark olive green and formation of a colourless solid. The reaction was completed by stirring the solution at room temperature for 4 h. The solution was filtered and 40 mL of *n*-hexane were added to precipitate [Cp*Fe(μ;$\eta^{5:5}$-P$_5$)CoCp‴][*pf*] (**1-Co**) as an olive green powder, which could be isolated in 53% yield (85 mg, 0.085 mmol). Spectroscopic data of this product matches that reported earlier.

1-Ni

$[Cp'''Ni(\mu\text{-}Br)]_2$ (74 mg, 0.1 mmol, 1 eq.), $[Cp^*Fe(\eta^5\text{-}P_5)]$ (70 mg, 0.2 mmol, 2 eq.) and $K[BAr^F]$ (144 mg, 0.2 mmol, 2 eq.) were suspended in 6 mL of *o*-DFB to afford a rapid colour change to brown and formation of a colourless solid. The reaction was completed by stirring the solution at 90 °C for 4 h. Afterwards the solution was filtered, the solvent removed, and the residue washed two times with 15 mL of *n*-hexane, each. The residue was dissolved in 2 mL of *o*-DFB and layered with 10 mL of *n*-hexane. Storage of this mixture at room temperature for 4 days yielded dark brownish block shaped crystals of $[Cp^*Fe(\mu;\eta^{5:5}\text{-}P_5)NiCp'''][BAr^F]$ (**1-Ni**), which were isolated by decanting the solvent and drying under reduced pressure (10^{-3} mbar).

Yield:	108 mg (0.1 mmol, 50%)
Elemental Analysis:	calculated (%) for $[Cp^*Fe(\mu;\eta^{5:5}\text{-}P_5)NiCp'''][BAr^F]$: C: 46.50 H: 3.37, found: C: 46.62 H: 3.26
ESI(+)-MS (*o*-DFB):	m/z (%) = 637.1 (70, [**1-Ni**]$^+$), 332.2 (100, [**A**]$^+$)
^{1}H-NMR (CD_2Cl_2, 300 K):	δ/ ppm = 15.83 (br, 9 H, $^t\underline{Bu}_3C_5H_2$), 12.19 (br, 18 H, $^t\underline{Bu}_3C_5H_2$), 9.21 (br, 15 H, Cp*), signals for the $^tBu_3C_5H_2$ could not be found within the ^{1}H NMR spectrum of **1-Ni**
$^{31}P\{^1H\}$-NMR (CD_2Cl_2, 300 K):	δ/ ppm = no signals observed within +/- 500 ppm
^{31}P-NMR (CD_2Cl_2, 300 K):	δ/ ppm = no signals observed within +/- 500 ppm
$^{19}F\{^1H\}$-NMR (CD_2Cl_2, 300 K):	δ/ ppm = - 166.3 (br, 8 F, $[BAr^F]^-$), - 162.7 (br, 4 F, $[BAr^F]^-$), - 132.3 (br, 8 F, $[BAr^F]^-$)
$^{11}B\{^1H\}$-NMR (CD_2Cl_2, 300 K):	δ/ ppm = - 16.8 (s, $[BAr^F]^-$)

2-Fe

$[Fe(tol)_2][pf]_2$ (217 mg, 0.1 mmol, 1 eq.) and $[Cp^*Fe(\eta^5\text{-}P_5)]$ (70 mg, 0.2 mmol, 2 eq.) were dissolved in 3 mL of *o*-DFB affording a dark green solution, which was stirred for 10 min. Afterwards the solution was layered with 20 mL of *n*-hexane and stored at 4 °C for three days, yielding dark green plate shaped crystals of $[\{Cp^*Fe(\eta^5\text{-}P_5)\}_2Fe][pf]_2$ (**2-Fe**).

As crystal quality of **2-Fe** could not be improved to a level suitable for single crystal X-ray diffractometry, its´ $[BAr^F]^-$ salt was prepared by sonication of $[Cp^*Fe(\eta^5\text{-}P_5)]$, $K[BAr^F]$ and $FeBr_2$•dme in *o*-DFB and crystallized from a CH_2Cl_2/*n*-hexane layering (3mL/20mL). Notably, the turnover and yield of **2-Fe** in this reaction is drastically decreased compared to the procedure using $[Fe(tol)_2][pf]_2$. Spectroscopic data for both compounds matches.

Yield:	240 mg (0.09 mmol, 90%)
Elemental Analysis:	calculated (%) for $[\{Cp^*Fe(\eta^5\text{-}P_5)\}_2Fe][pf]_2$•$(C_6H_4F_2)$: C: 24.91 H: 1.23, found: C: 24.46 H: 1.30
ESI(+)-MS (*o*-DFB):	m/z (%) = 373.8 (100, $[\mathbf{2\text{-}Fe}]^{2+}$), 747.7 (20, $[\{Cp^*Fe(\eta^5\text{-}P_5)\}_2Fe]^+$)
^{1}H-NMR (CD_2Cl_2, 300 K):	δ/ ppm = 0.70 (s, Cp*)
$^{31}P\{^1H\}$-NMR (CD_2Cl_2, 300 K):	δ/ ppm = 12.9 (s, *cyclo*-P_5)
^{31}P-NMR (CD_2Cl_2, 300 K):	δ/ ppm = 12.9 (s, *cyclo*-P_5)
$^{19}F\{^1H\}$-NMR (CD_2Cl_2, 300 K):	δ/ ppm = - 75.4 (s, $[pf]^-$)

2-Co

$[Co(dfb)_2][pf]$ (125 mg, 0.1 mmol, 1 eq.) dissolved in 2 mL of *o*-DFB was slowly added to $[Cp^*Fe(\eta^5\text{-}P_5)]$ (70 mg, 0.2 mmol, 2 eq.) dissolved in 2 mL of *o*-DFB at -30 °C. A rapid colour change to dark green was observed, the solution stirred for 1 h at room temperature and then constrained to 1 mL. 30 mL of *n*-hexane were added to precipitate a dark green powder, which was dried under reduced pressure (10^{-3} mbar). 3 mL of *o*-DFB were added, and the solution was layered with 30 mL of *n*-hexane. Storage at room temperature for two days yielded dark green plate shaped crystals of $[\{Cp^*Fe(\eta^5\text{-}P_5)\}_2Co][pf]$ (**2-Co**).

Yield:	154 mg (0.09 mmol, 90%)
Elemental Analysis:	calculated (%) for $[\{Cp^*Fe(\eta^5\text{-}P_5)\}_2Co][pf]_2\bullet(C_6H_4F_2)$: C: 27.54 H: 1.87, found: C: 27.59 H: 1.98
ESI(+)-MS (*o*-DFB):	m/z (%) = 750.8 (100, [**2-Co**]$^+$)
^{1}H-NMR (*o*-DFB/C_6D_6, 300 K):	δ/ ppm = 11.81 (br, Cp*)
$^{31}P\{^1H\}$-NMR (*o*-DFB/C_6D_6, 300 K):	δ/ ppm = no signals observed within +/- 500 ppm
^{31}P-NMR (*o*-DFB/C_6D_6, 300 K):	δ/ ppm = no signals observed within +/- 500 ppm
$^{19}F\{^1H\}$-NMR (*o*-DFB/C_6D_6, 300 K):	δ/ ppm = - 74.1 (s, $[pf]^-$)

3

$[Fe(tol)_2][pf]_2$ (24 mg, 0.01 mmol, 1 eq.) and $[Cp^*Fe(\eta^5\text{-}As_5)]$ (11 mg, 0.02 mmol, 2 eq.) were dissolved in 3 mL of *o*-DFB affording a dark brown solution, which was stirred for 2 h. Afterwards the solution was layered with 50 mL of *n*-hexane and stored at room temperature for three days, yielding dark brownish green plate shaped crystals of $[\{Cp^*Fe(\eta^5\text{-}As_5)\}_2Fe][TEF]_2$ (**3**).

Yield:	30 mg (0.0096 mmol, 96%)
Elemental Analysis:	calculated (%) for $[\{Cp^*Fe(\eta^5\text{-}As_5)\}_2Fe][pf]_2 \bullet (C_6H_4F_2)$: C: 21.53 H: 1.06, found: C: 21.30 H: 1.24
ESI(+)-MS (*o*-DFB):	m/z (%) = 593.6 (100, $[\mathbf{2\text{-}Fe}]^{2+}$), 1187.2 (20, $[\{Cp^*Fe(\eta^5\text{-}As_5)\}_2Fe]^+$)
^{1}H-NMR (*o*-DFB/C_6D_6, 300 K):	δ ppm = 0.36 (s, Cp*)
$^{19}F\{^1H\}$-NMR (*o*-DFB/C_6D_6, 300 K):	δ ppm = - 75.4 (s, $[pf]^-$)

[Fe(tol)$_2$][pf]$_2$

$Fe(CO)_5$ in 1.3 mL of toluene (1.96 mmol, 384 mg, 1 eq.) was added to a purple suspension of $[Ag(CH_2Cl_2)_2][pf]$ (3.92 mmol, 4.88 g, 2 eq.) and I_2 (497 mg, 1.96 mmol, 1 eq.) in 20 mL of *o*-DFB, which resulted in a rapid colour change to dark red and precipitation of colourless solid. Stirring at 90 °C for 16 hours completed the reaction, after which an orange solution with colourless precipitate was obtained. Filtration and precipitation with *n*-hexane afforded $[Fe(tol)_2][pf]_2$ as analytically pure compound. Crystals suitable for X-ray diffraction studies could be obtained by layering a concentrated solution in *o*-DFB with *n*-hexane and storage at room temperature for two days.

Yield:	3.45 g (1.6 mmol, 82%)
Elemental Analysis:	calculated (%) for $[Fe(tol)_2][pf]_2$: C: 25.39 H: 0.76, found: C: 25.77 H: 0.93
ESI(+)-MS (*o*-DFB):	m/z (%) = 239.0 (10, $[Fe(tol)_2]$-H^+), 240.1 (10, $[\mathbf{Fe(tol)_2}]^+$)
^{1}H-NMR (*o*-DFB/C_6D_6, 300 K):	δ/ ppm = 7.49 (m, 3 H, PhMe), 7.41 (m, 2 H, PhMe), 3.21 (s, 3 H, PhMe)
$^{19}F\{^1H\}$-NMR (*o*-DFB/C_6D_6, 300 K):	δ/ ppm = -75.5 (s, $[pf]^-$)

7.5.2. X-ray Crystallographic Data

General Considerations

The crystallographic data for all described compounds were collected on a GV50 diffractometer (Rigaku) with a Titan^{S2} detector using Cu–K_α radiation (**1-Cr**, **1-Mn**, **1-Ni, 2-Co**) or an XtaLAB Synergy R, DW System with a HyPix-Arc 150 detector using Cu-K_α radiation from a rotating anode (**1-Fe**, **2-Fe**[BAr^F], **3)**. Data reduction and absorption correction were performed with the CrysAlisPro software package.[30] Structure solution and refinement was conducted in Olex2 (1.5-alpha)[31] with ShelXT[32] (solution) and ShelXL-2018/3[33] (least squares refinement (F^2)). All non-H atoms were refined with anisotropic displacement parameters and H atoms were treated as riding models with isotropic displacement parameters and fixed C–H bond lengths (sp^3: 0.96 (CH_3), 0.97 (CH_2); sp^2: 0.93 (CH)). Visualisation of the crystal structures was performed with Olex2 (1.5-alpha).[31]

CIF files with comprehensive information on the details of the diffraction experiments and full tables of bond lengths and angles for **1-Cr**, **1-Mn**, **1-Fe**, **1-Ni**, **2-Fe**, **2-Co**, **3 and [Fe(tol)$_2$][*pf*]$_2$** are deposited in Cambridge Crystallographic Data Centre under the deposition codes CCDC 2242844-2242851.

*Table S 1: Crystallographic and refinement data for compounds **1-Cr** – **1-Ni**.*

Compound	1-Cr	1-Mn	1-Fe	1-Ni
Empirical formula	$C_{54}H_{46}BCrF_{21}FeP_5$	$C_{43}H_{44}AlF_{36}FeMnO_4P_5$	$C_{51.5}H_{45}BClF_{20}Fe_2P_5$	$C_{102}H_{88}B_2F_{40}Fe_2Ni_2P_{10}$
Formula weight	1367.42	1601.40	1356.68	2634.16
Temperature/K	122.99(10)	123.00(10)	123.00(10)	122.99(10)
Crystal system	monoclinic	monoclinic	monoclinic	monoclinic
Space group	$P2_1/c$	$P2_1/c$	$P2_1/c$	$P2_1$
a/Å	15.7984(2)	11.95740(10)	15.6478(3)	15.8271(2)
b/Å	19.8256(2)	21.6035(2)	19.8608(3)	19.95370(10)
c/Å	18.1573(2)	23.2630(2)	18.1588(2)	17.9342(2)
α/°	90	90	90	90
β/°	104.2570(10)	93.7580(10)	104.7420(10)	105.1610(10)
γ/°	90	90	90	90
Volume/Å3	5511.94(11)	5996.42(9)	5457.58(15)	5466.65(10)
Z	4	4	4	2
ρcalcg/cm3	1.648	1.774	1.651	1.600
μ/mm-1	6.102	6.488	7.058	4.886
F(000)	2756.0	3188.0	2732.0	2656.0
Crystal size/mm3	0.38 × 0.22 × 0.04	0.259 × 0.2 × 0.163	0.29 × 0.23 × 0.06	0.293 × 0.248 × 0.219
Radiation	Cu Kα (λ = 1.54184)	Cu Kα (λ = 1.54184)	Cu Kα (λ = 1.54184)	Cu Kα (λ = 1.54184)
2Θ range for data collection/°	7.294 to 133.46	7.41 to 133.506	5.84 to 144.244	7.288 to 133.626
Index ranges	-18 ≤ h ≤ 18, -23 ≤ k ≤ 23, -20 ≤ l ≤ 21	-13 ≤ h ≤ 14, -25 ≤ k ≤ 25, -27 ≤ l ≤ 27	-19 ≤ h ≤ 17, -24 ≤ k ≤ 23, -21 ≤ l ≤ 22	-18 ≤ h ≤ 18, -20 ≤ k ≤ 23, -21 ≤ l ≤ 20
Reflections collected	57435	63995	52174	52429
Independent reflections	9708 [Rint = 0.0577, Rsigma = 0.0324]	10585 [Rint = 0.0488, Rsigma = 0.0256]	10344 [Rint = 0.0479, Rsigma = 0.0331]	15560 [Rint = 0.0533, Rsigma = 0.0411]
Data/restraints/parameters	9708/200/906	10585/1041/1179	10344/18/803	15560/0/1449
Goodness-of-fit on F2	1.046	1.019	1.099	1.018
Final R indexes [I>=2σ (I)]	R1 = 0.0384, wR2 = 0.1067	R1 = 0.0370, wR2 = 0.0943	R1 = 0.0446, wR2 = 0.1226	R1 = 0.0363, wR2 = 0.0914
Final R indexes [all data]	R1 = 0.0427, wR2 = 0.1114	R1 = 0.0389, wR2 = 0.0961	R1 = 0.0541, wR2 = 0.1286	R1 = 0.0377, wR2 = 0.0928
Largest diff. peak/hole / e Å-3	0.45/-0.62	0.71/-0.37	0.67/-0.72	0.57/-0.44
Flack parameter	/	/	/	0.488(5)

*Table S 2: Crystallographic and refinement details on **2-Fe**, **2-Co** and **3**.*

Compound	2-Fe	2-Co	3	$[Fe(tol)_2][pf]_2$
Empirical formula	$C_{69}H_{32}B_2Cl_2F_{40}Fe_3P_{10}$	$C_{39}H_{32}AlCoF_{37}Fe_2O_4P_{10}$	$C_{70}H_{42}Al_2As_{10}F_{78}Fe_3O_8$	$C_{92}H_{32}Al_4F_{144}Fe_2O_{16}$
Formula weight	2190.71	1774.95	3463.74	4348.79
Temperature/K	123.02(10)	123.00(10)	123.01(10)	123.00(10)
Crystal system	monoclinic	monoclinic	monoclinic	triclinic
Space group	$P2_1/c$	$P2_1/c$	$P2_1/c$	$P\bar{1}$
a/Å	19.4743(2)	10.87740(10)	33.7409(2)	15.9325(4)
b/Å	20.2790(2)	28.6587(3)	14.01600(10)	16.1088(4)
c/Å	20.0413(2)	20.0246(2)	22.6687(2)	26.3304(6)
α/°	90	90	90	92.872(2)
β/°	91.7850(10)	96.7550(10)	102.8080(10)	91.023(2)
γ/°	90	90	90	94.758(2)
Volume/Å3	7910.86(14)	6198.98(11)	10453.57(14)	6724.4(3)
Z	4	4	4	2
ρcalcg/cm3	1.839	1.902	2.201	2.148
μ/mm-1	8.166	9.782	8.760	4.454
F(000)	4312.0	3492.0	6648.0	4224.0
Crystal size/mm3	0.22 × 0.14 × 0.03	0.29 × 0.23 × 0.09	0.19 × 0.17 × 0.07	0.251 × 0.166 × 0.112
Radiation	Cu Kα (λ = 1.54184)	Cu Kα (λ = 1.54184)	Cu Kα (λ = 1.54184)	Cu Kα (λ = 1.54184)
2Θ range for data collection/°	6.202 to 150.304	7.604 to 133.968	5.372 to 143.816	7.502 to 134.246
Index ranges	-23 ≤ h ≤ 24, -24 ≤ k ≤ 17, -24 ≤ l ≤ 24	-12 ≤ h ≤ 12, -34 ≤ k ≤ 33, -18 ≤ l ≤ 23	-39 ≤ h ≤ 41, -17 ≤ k ≤ 15, -26 ≤ l ≤ 27	-18 ≤ h ≤ 18, -19 ≤ k ≤ 19, -31 ≤ l ≤ 31
Reflections collected	85089	66406	103420	42141
Independent reflections	15714 [Rint = 0.0379, Rsigma = 0.0302]	10977 [Rint = 0.0698, Rsigma = 0.0392]	20045 [Rint = 0.0521, Rsigma = 0.0336]	42141 [Rint = ?, Rsigma = 0.0374]
Data/restraints/parameters	15714/280/1236	10977/1392/1244	20045/1584/2363	42141/2636/2870
Goodness-of-fit on F2	1.044	1.028	1.069	0.997
Final R indexes [I>=2σ (I)]	R1 = 0.0543, wR2 = 0.1477	R1 = 0.0470, wR2 = 0.1154	R1 = 0.0411, wR2 = 0.1087	R1 = 0.0579, wR2 = 0.1540
Final R indexes [all data]	R1 = 0.0708, wR2 = 0.1582	R1 = 0.0570, wR2 = 0.1235	R1 = 0.0534, wR2 = 0.1155	R1 = 0.0795, wR2 = 0.1642
Largest diff. peak/hole / e Å-3	0.91/-0.92	0.93/-0.70	0.99/-0.58	1.52/-0.68
Flack parameter	/	/	/	/

1-Cr

Compound **1-Cr** crystallizes in the monoclinic space group $P2_1/c$ forming dark red plates from *o*-DFB/*n*-hexane mixtures at room temperature. The asymmetric unit (Figure S1) contains the cation, one anion and one *o*-DFB molecule. All non-hydrogen atoms were refined anisotropically and the H atoms were treated as riding models.

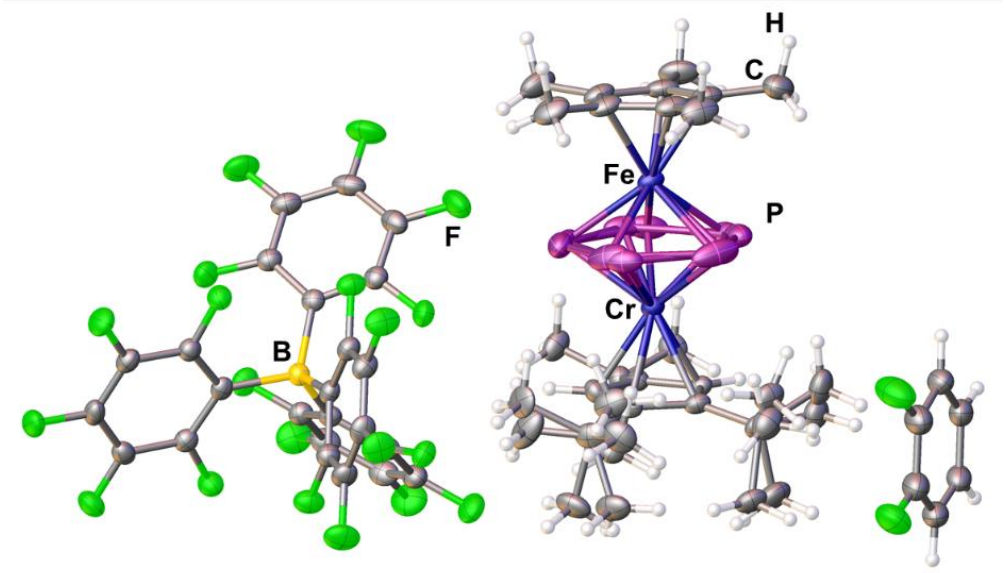

*Figure S 1: Solid state structure of **1-Cr**; Shown is the asymmetric unit containing one cation, one anion as well as one o-DFB molecule; thermal ellipsoids are drawn at the 50% probability level.*

1-Mn

Compound **1-Mn** crystallizes in the monoclinic space group $P2_1/c$ forming dark green blocks from CH_2Cl_2/*n*-hexane mixtures at room temperature. The asymmetric unit (Figure S2) contains the cation and one anion. All non-hydrogen atoms were refined anisotropically and the H atoms were treated as riding models. Disorder within the anion was treated with appropriate restraints.

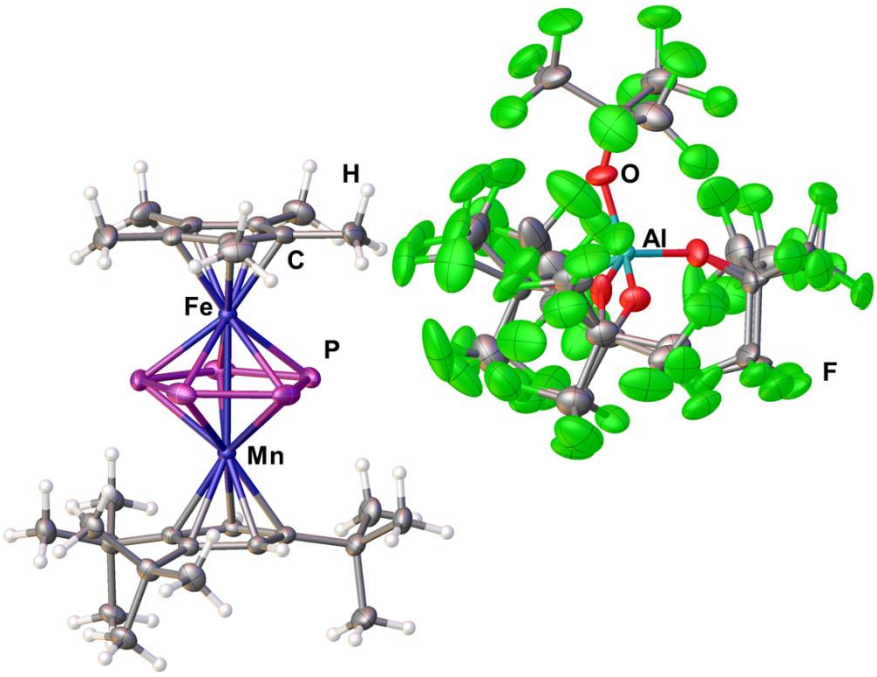

*Figure S 2: Solid state structure of **1-Mn**; Shown is the asymmetric unit containing one cation and one anion; thermal ellipsoids are drawn at the 50% probability level.*

1-Fe

Compound **1-Fe** crystallizes in the monoclinic space group $P2_1/c$ forming dark brownish-blue blocks from CH_2Cl_2/*n*-hexane mixtures at room temperature. The asymmetric unit (Figure S3) contains the cation and one anion. All non-hydrogen atoms were refined anisotropically and the H atoms were treated as riding models. Disorder within on ^{t}Bu group was treated with appropriate restraints.

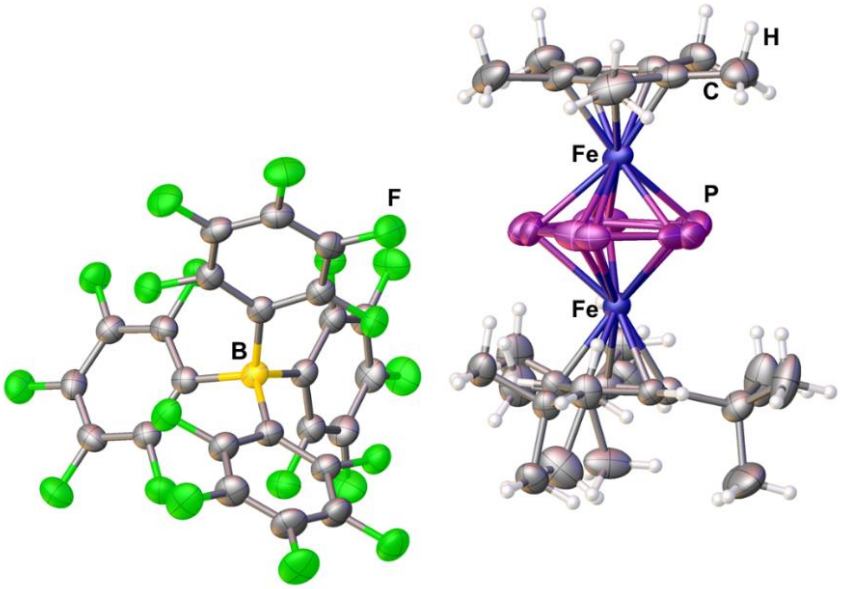

*Figure S 3: Solid state structure of **1-Fe**; Shown is the asymmetric unit containing one cation and one anion; thermal ellipsoids are drawn at the 50% probability level.*

1-Ni

Compound **1-Ni** crystallizes in the monoclinic space group $P2_1$ forming dark brown blocks from *o*-DFB/*n*-hexane mixtures at room temperature. The asymmetric unit (Figure S4) contains two distinct cations and two anions. All non-hydrogen atoms were refined anisotropically and the H atoms were treated as riding models.

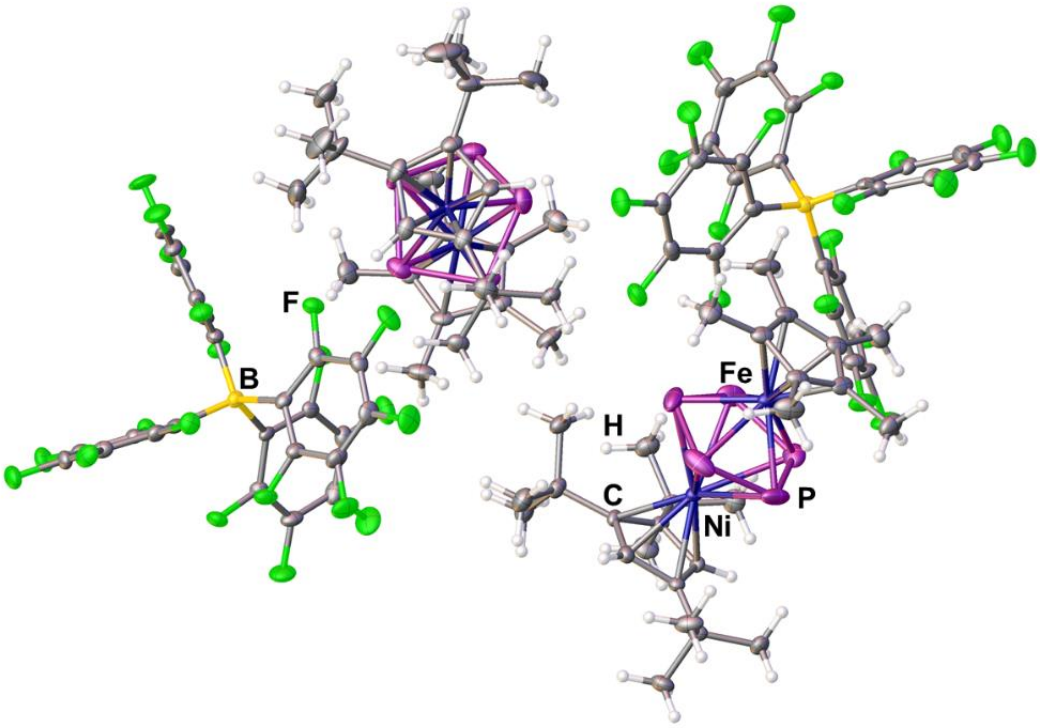

*Figure S 4: Solid state structure of **1-Ni**; Shown is the asymmetric unit containing two distinct cations and two anions; thermal ellipsoids are drawn at the 50% probability level.*

2-Fe

Compound **2-Fe** crystallizes in the monoclinic space group $P2_1/c$ forming dark green plates from CH_2Cl_2/*n*-hexane mixtures at room temperature. The asymmetric unit (Figure S5) contains one cation and two anions, as well 0.9 CH_2Cl_2 molecules. All non-hydrogen atoms were refined anisotropically and the H atoms were treated as riding models. Disorder within the *cyclo*-P_5 ligands was treated with appropriate restraints.

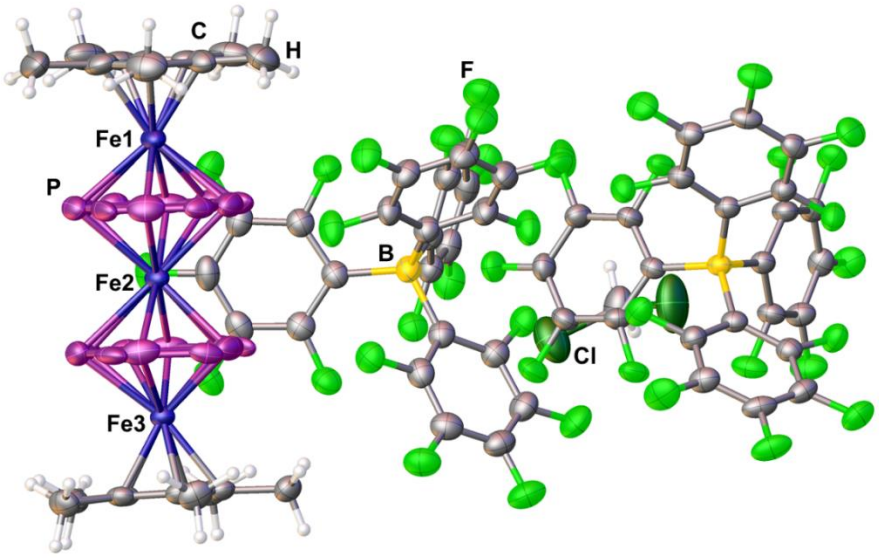

*Figure S 5: Solid state structure of **2-Fe**; Shown is the asymmetric unit containing one dication, two anions as well as one CH_2Cl_2 molecule; thermal ellipsoids are drawn at the 50% probability level.*

2-Co

Compound **2-Co** crystallizes in the monoclinic space group $P2_1/c$ forming dark green plates from *o*-DFB/*n*-hexane mixtures at room temperature. The asymmetric unit (Figure S6) contains one cation and one anion and an *o*-DFB molecule. All non-hydrogen atoms were refined anisotropically and the H atoms were treated as riding models. Disorder within the anion was treated with appropriate restraints.

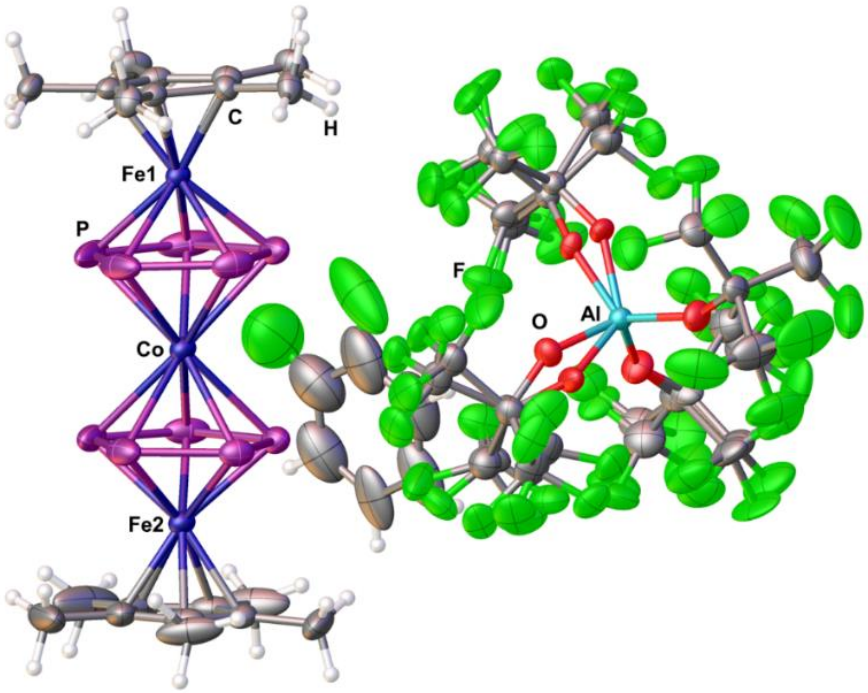

*Figure S 6: Solid state structure of **2-Co**; Shown is the asymmetric unit containing one cation, one anion as well as one o-DFB molecule; thermal ellipsoids are drawn at the 50% probability level.*

3

Compound **3** crystallizes in the monoclinic space group $P2_1/c$ forming dark brownish green plates from *o*-DFB/*n*-hexane mixtures at room temperature. The asymmetric unit (Figure S7) contains one cation, two anions and three *o*-DFB molecules. All non-hydrogen atoms were refined anisotropically and the H atoms were treated as riding models. Disorder within the anions and solvent molecules was treated with appropriate restraints.

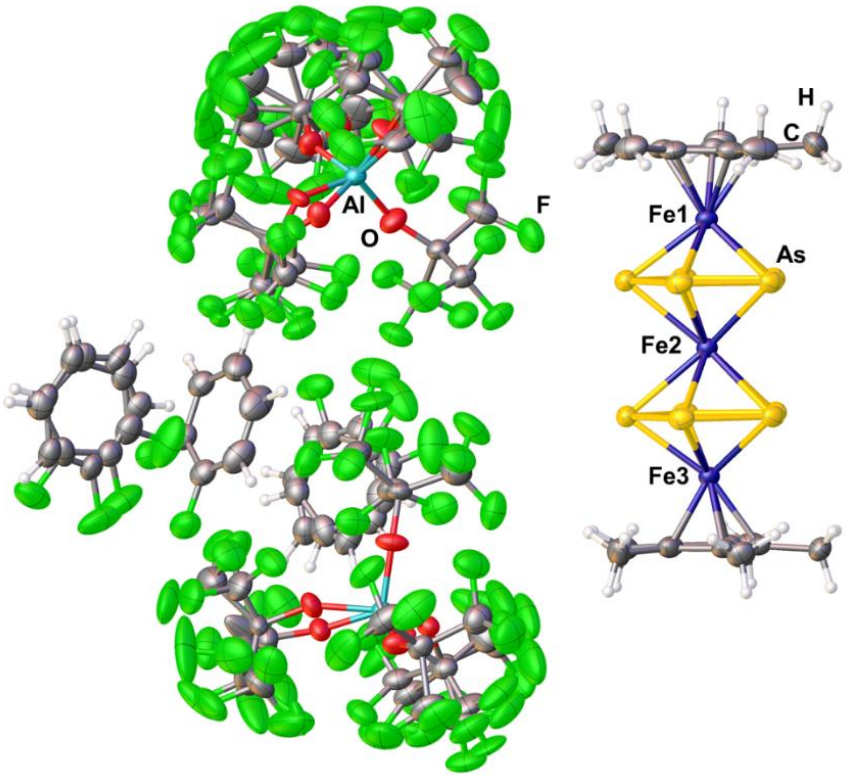

*Figure S 7: Solid state structure of **3**; Shown is the asymmetric unit containing one dication, two anions as well as three o-DFB molecules; thermal ellipsoids are drawn at the 50% probability level.*

[Fe(tol)$_2$][pf]$_2$

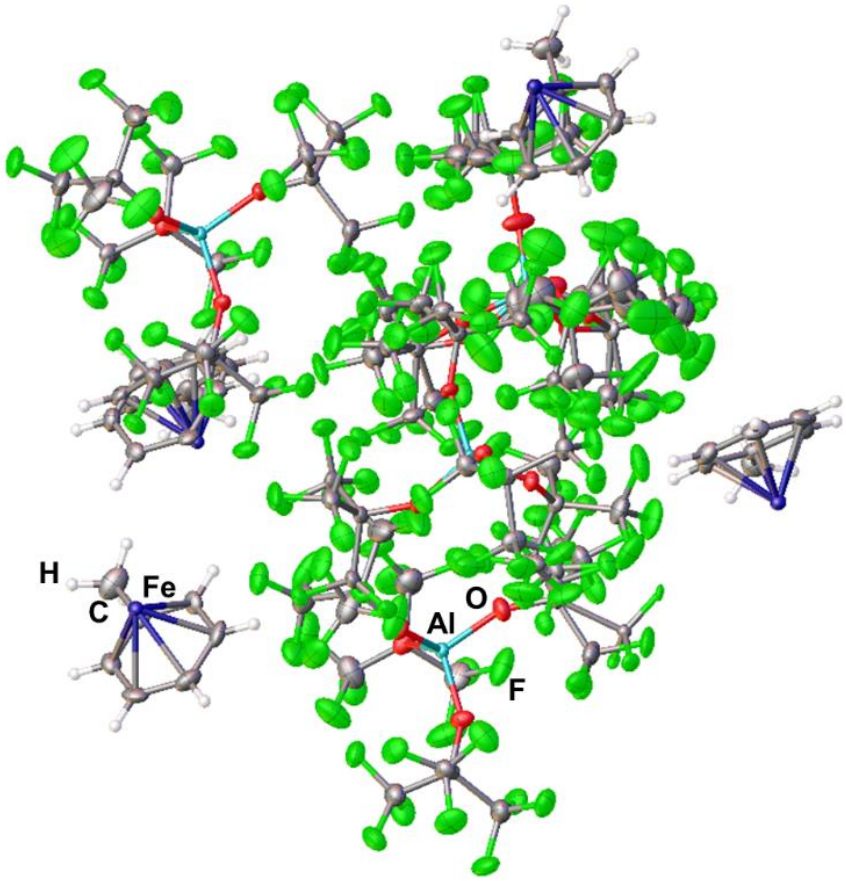

*Figure S 8: Solid state structure of **[Fe(tol)$_2$][pf]$_2$**; Shown is the asymmetric unit containing four half dications and four anions; thermal ellipsoids are drawn at the 50% probability level.*

7.5.3. NMR Spectroscopic Investigations and EPR Studies

1-Cr

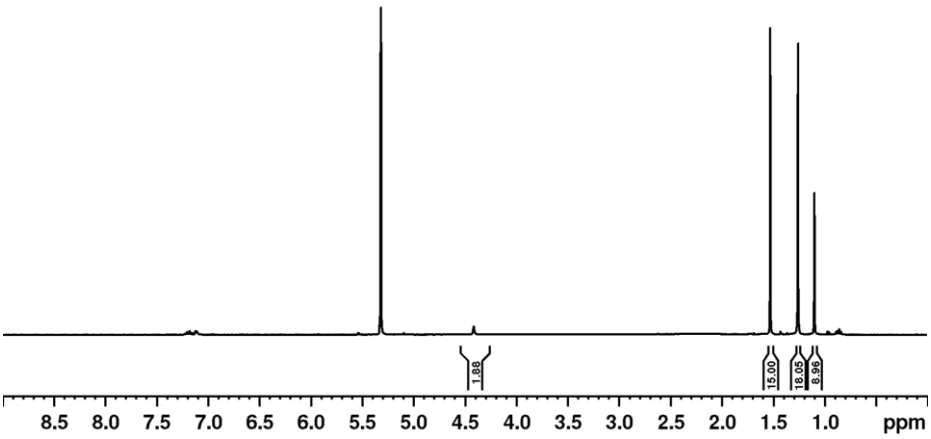

*Figure S 9: ^{1}H NMR spectrum of **1-Cr** in CD_2Cl_2 recorded at room temperature.*

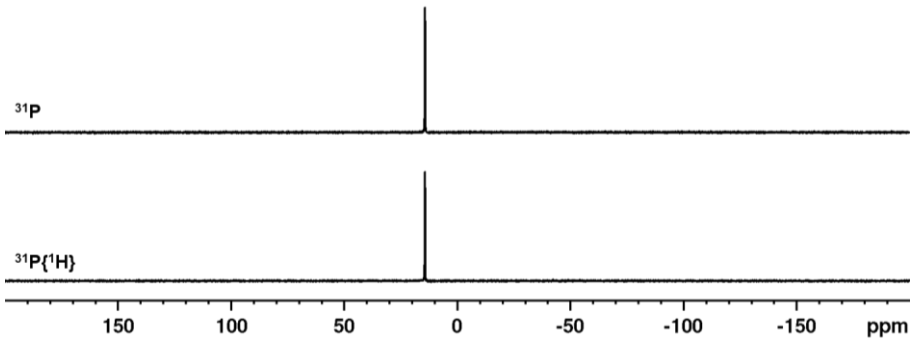

*Figure S 10: ^{31}P (top) and $^{31}P\{^{1}H\}$ (bottom) NMR spectrum of **1-Cr** in CD_2Cl_2 recorded at room temperature.*

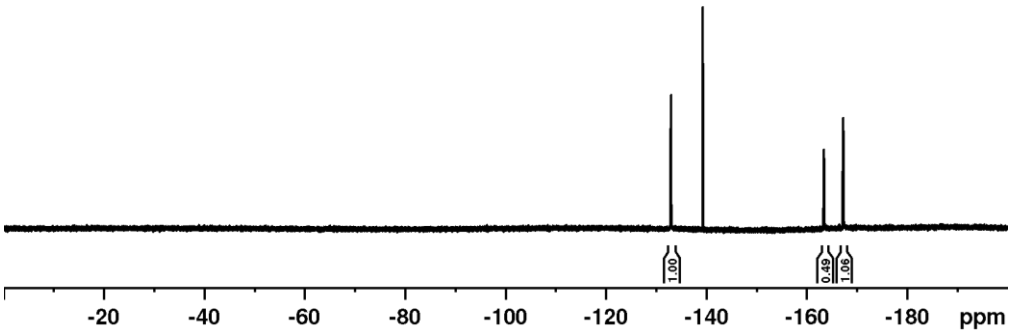

*Figure S 11: $^{19}F\{^{1}H\}$ NMR spectrum of **1-Cr** in CD_2Cl_2 recorded at room temperature.*

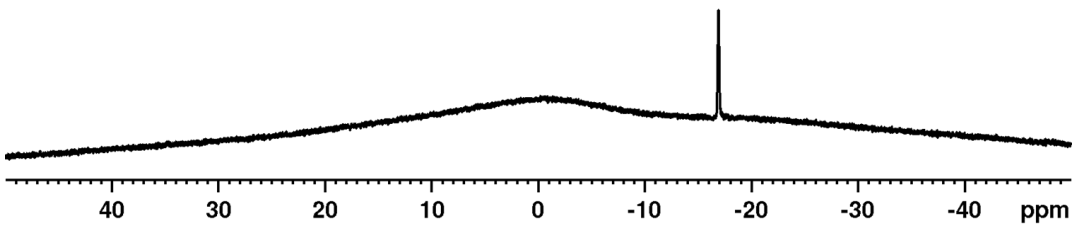

*Figure S 12: $^{11}B\{^{1}H\}$ NMR spectrum of **1-Cr** in CD_2Cl_2 recorded at room temperature.*

1-Mn

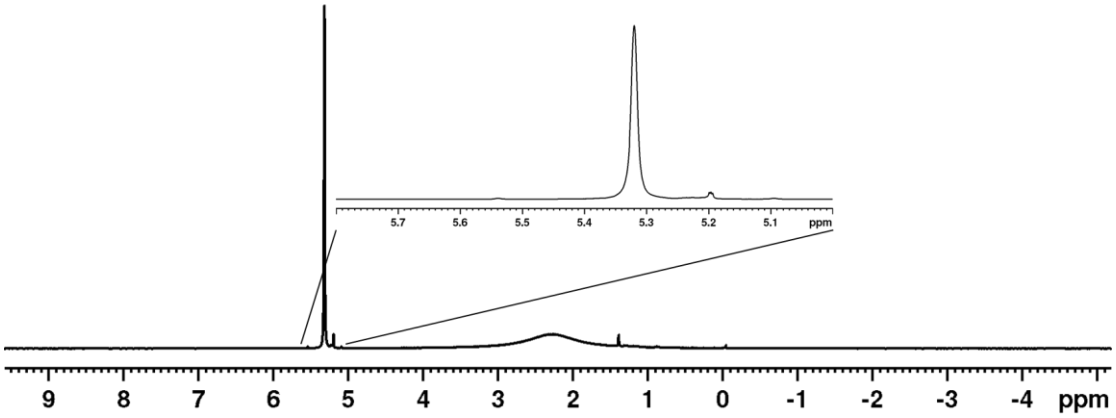

*Figure S 13: ^{1}H NMR spectrum of **1-Mn** in CD_2Cl_2 recorded at room temperature; 32 mg of substance were dissolved in 0.6 mL of CD_2Cl_2 inside the NMR tube and a coaxial capillary filled with CD_2Cl_2 was added to determine the number of unpaired electrons in **1-Mn** via the Evans method.*

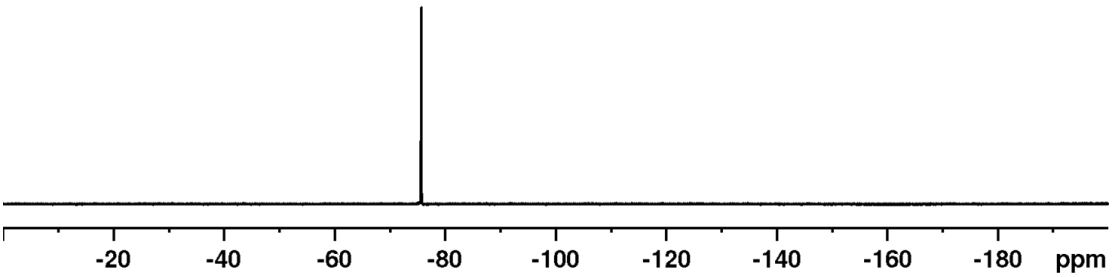

*Figure S 14: $^{19}F\{^{1}H\}$ NMR spectrum of **1-Mn** in CD_2Cl_2 recorded at room temperature.*

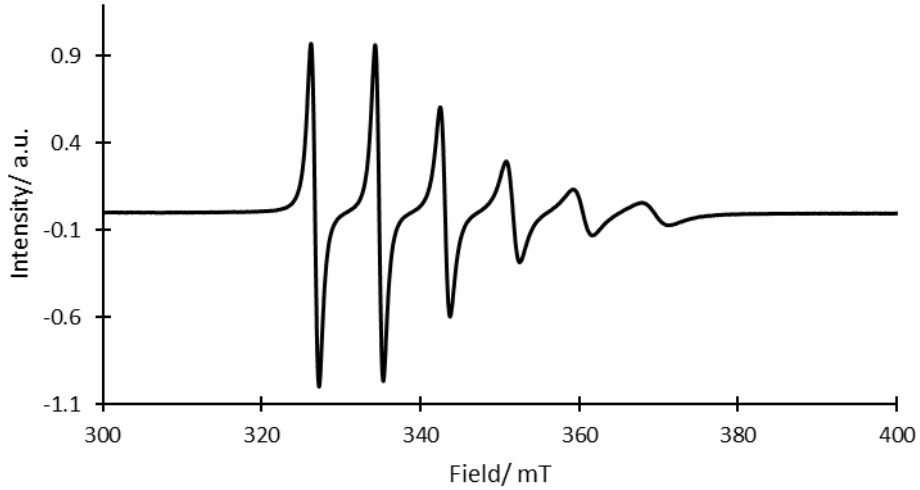

*Figure S 15: X-band EPR spectrum of **1-Mn** in o-DFB recorded at room temperature.*

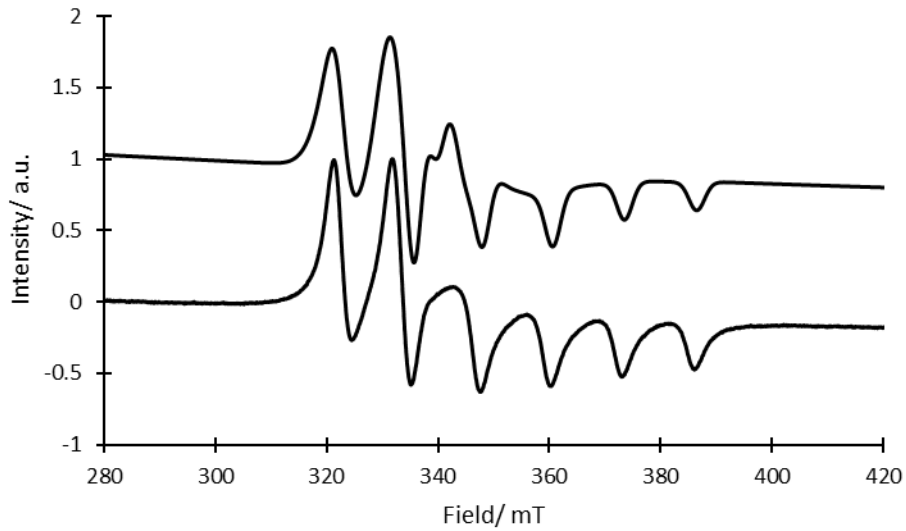

*Figure S 16: Experimental (bottom) and simulated (top) X-band EPR spectrum of **1-Mn** in frozen o-DFB solution recorded at 77 K; Simulation: $g_{\parallel}$ = 1.976, $g_{\perp}$ = 1.902, $A_{\parallel}$ = 125.17 MHz, $A_{\perp}$ = 337.73 MHz, lw = 0.53 mT, $HStrain_{\parallel}$ = 114.60 MHz, $HStrain_{\perp}$ = 84.05 MHz, $AStrain_{\parallel}$ = 114.20 MHz, $AStrain_{\perp}$ = 0 MHz.*

Simulation of the X-band EPR spectrum of **1-Mn** in frozen *o*-DFB solution at 77 K allowed the determination of g-values and coupling constants, which are given in Figure S16. Minor errors in the simulation persist due to the anisotropy of the signal.

1-Fe

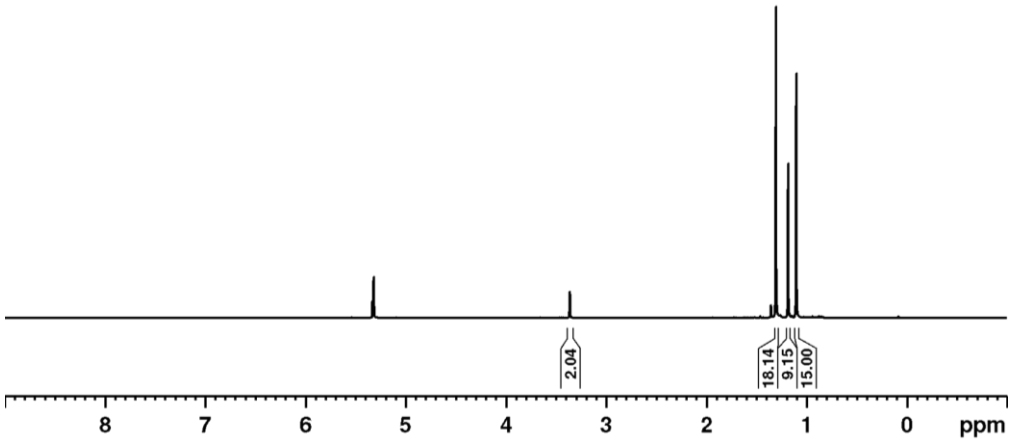

*Figure S 17: ^{1}H NMR spectrum of **1-Fe** in CD_2Cl_2 recorded at room temperature.*

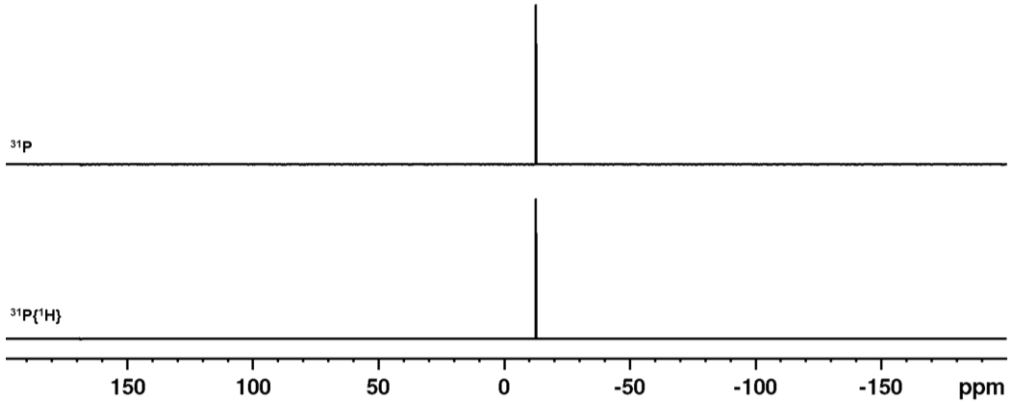

*Figure S 18: ^{31}P (top) and $^{31}P\{^{1}H\}$ (bottom) NMR spectrum of **1-Fe** in CD_2Cl_2 recorded at room temperature.*

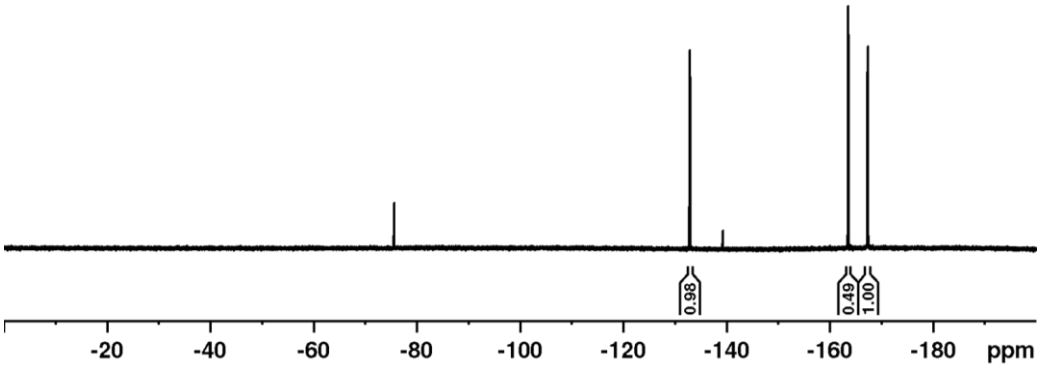

*Figure S 19: $^{19}F\{^{1}H\}$ NMR spectrum of **1-Fe** in CD_2Cl_2 recorded at room temperature.*

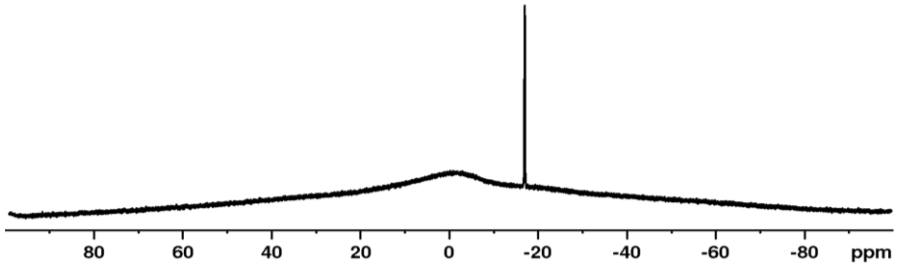

*Figure S 20: $^{11}B\{^{1}H\}$ NMR spectrum of **1-Fe** in CD_2Cl_2 recorded at room temperature.*

1-Co

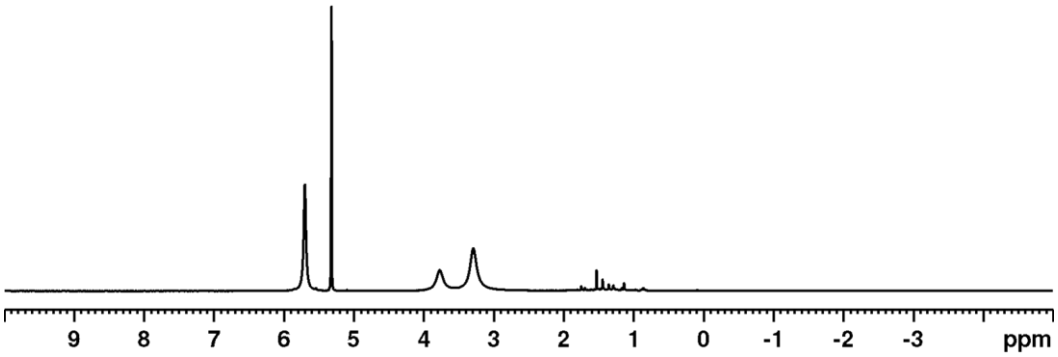

*Figure S 21: ^{1}H NMR spectrum of **1-Co** in CD_2Cl_2 recorded at room temperature.*

1-Ni

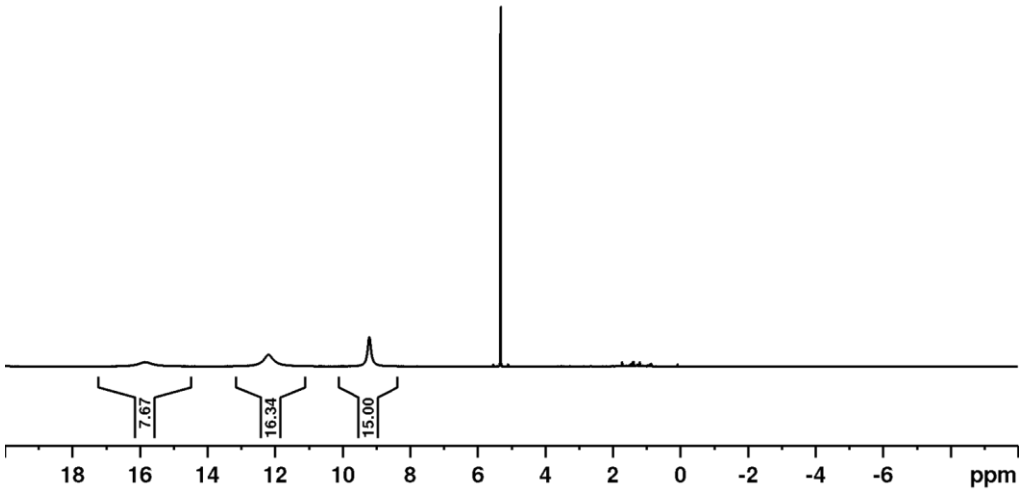

*Figure S 22: ^{1}H NMR spectrum of **1-Ni** in CD_2Cl_2 recorded at room temperature.*

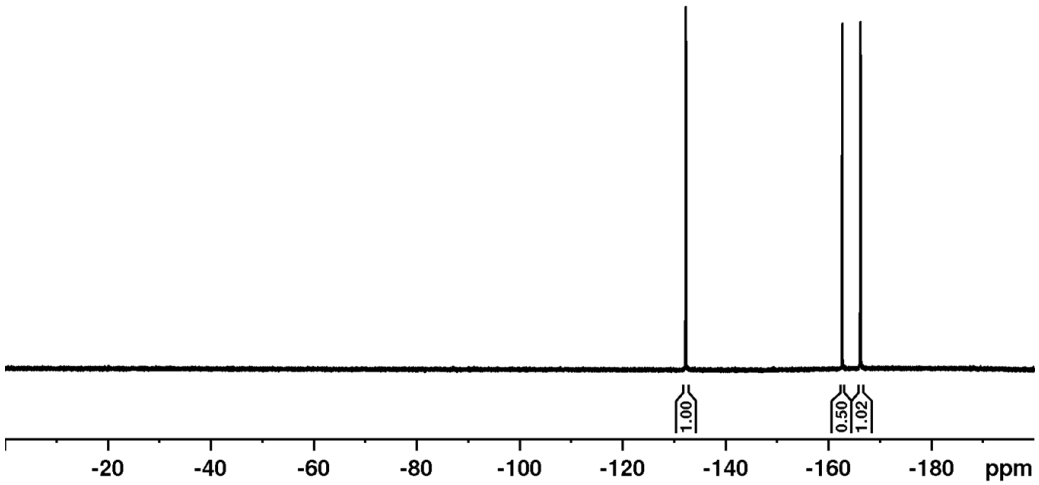

*Figure S 23: $^{19}F\{^{1}H\}$ NMR spectrum of **1-Ni** in CD_2Cl_2 recorded at room temperature.*

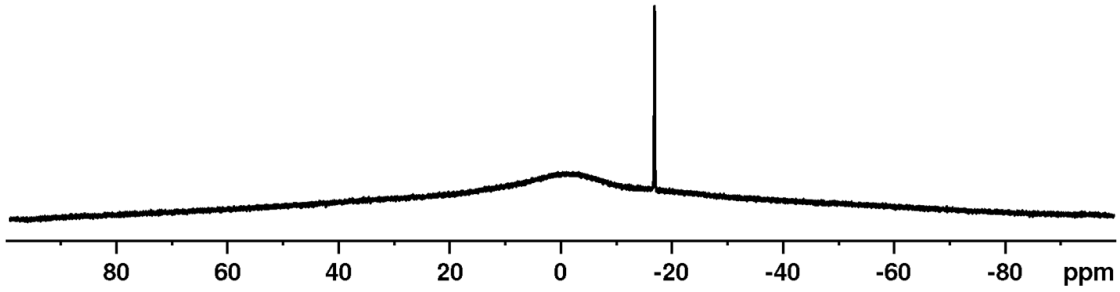

*Figure S 24: $^{11}B\{^{1}H\}$ NMR spectrum of **1-Ni** in CD_2Cl_2 recorded at room temperature.*

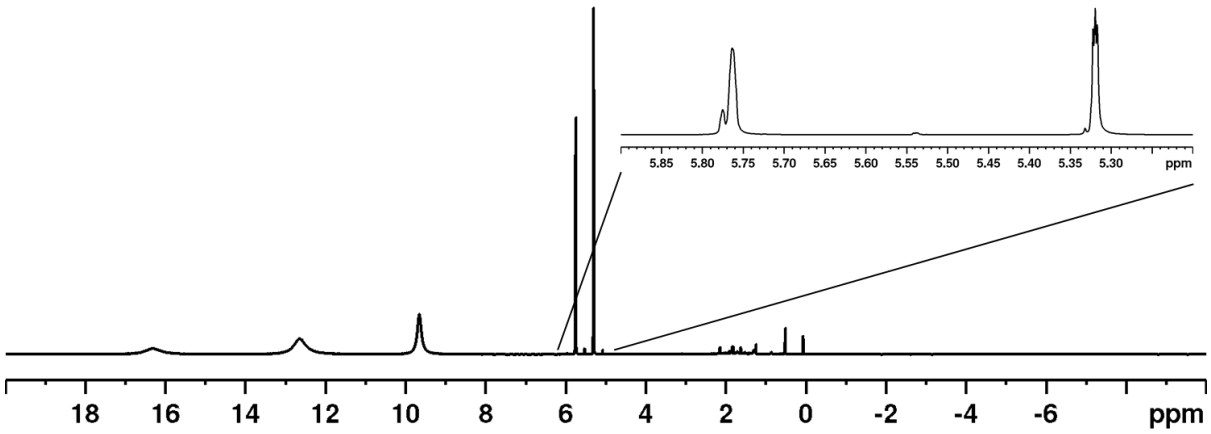

*Figure S 25: ^{1}H NMR spectrum of **1-Ni** in CD_2Cl_2 recorded at room temperature; 18 mg of substance were dissolved in 0.6 mL of CD_2Cl_2 inside the NMR tube and a coaxial capillary filled with CD_2Cl_2 was added to determine the number of unpaired electrons in **1-Ni** via the Evans method.*

2-Fe

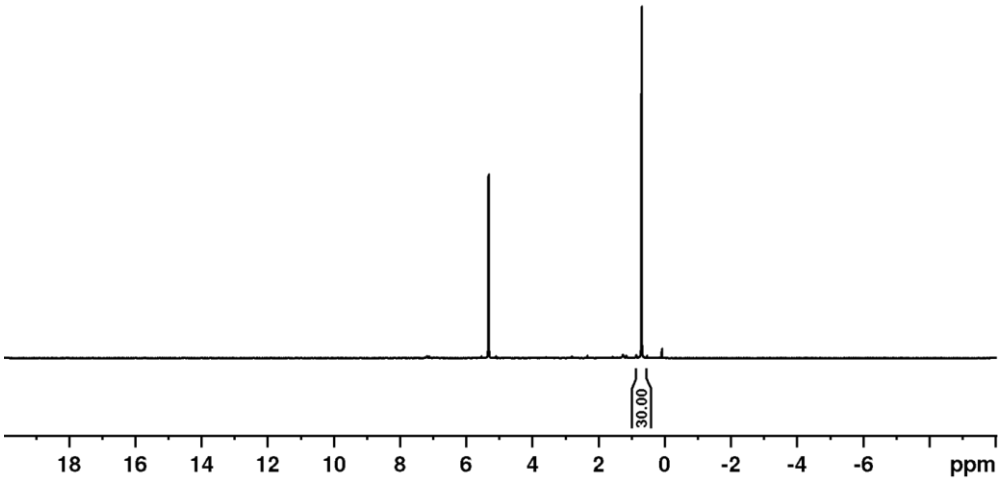

*Figure S 26: ^{1}H NMR spectrum of **2-Fe** in CD_2Cl_2 recorded at room temperature.*

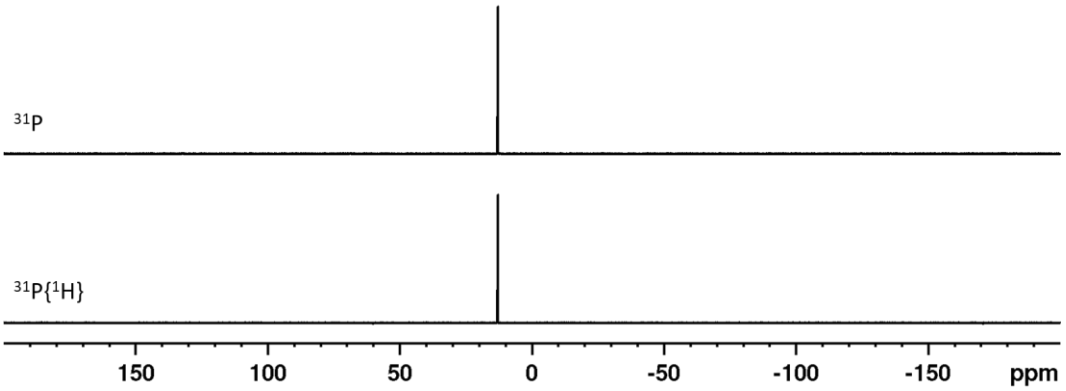

*Figure S 27: ^{31}P (top) and $^{31}P\{^{1}H\}$ (bottom) NMR spectrum of **2-Fe** in CD_2Cl_2 recorded at room temperature.*

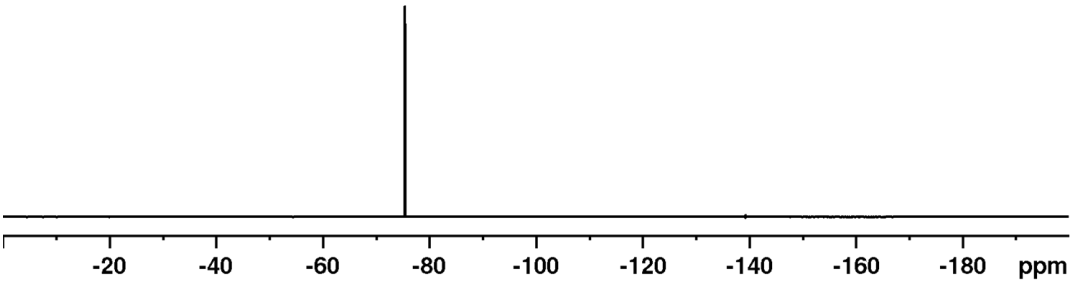

*Figure S 28: $^{19}F\{^{1}H\}$ NMR spectrum of **2-Fe** in CD_2Cl_2 recorded at room temperature.*

2-Co

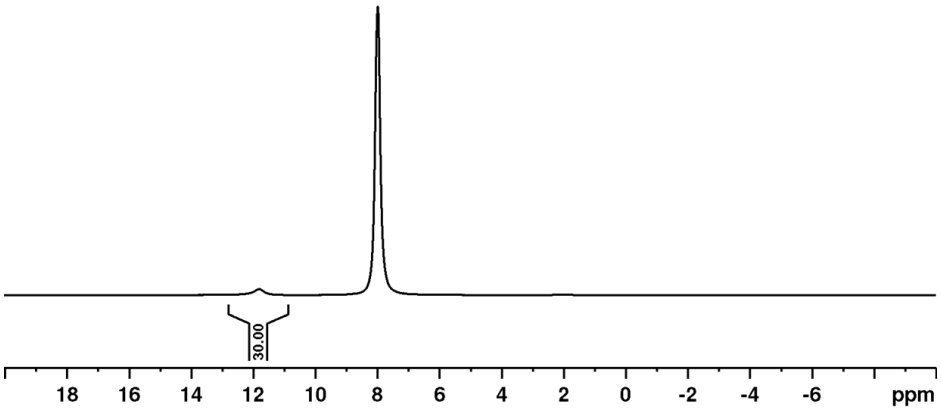

*Figure S 29: ^{1}H NMR spectrum of **2-Co** in o-DFB with added C_6D_6* capillary *recorded at room temperature.*

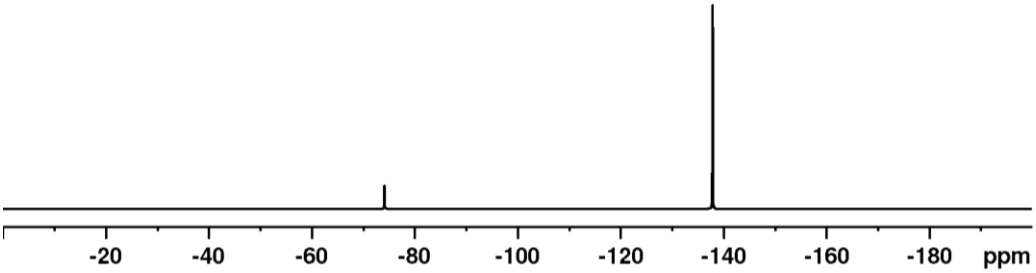

*Figure S 30: $^{19}F\{^{1}H\}$ NMR spectrum of **2-Co** in o-DFB with added C_6D_6* capillary *recorded at room temperature.*

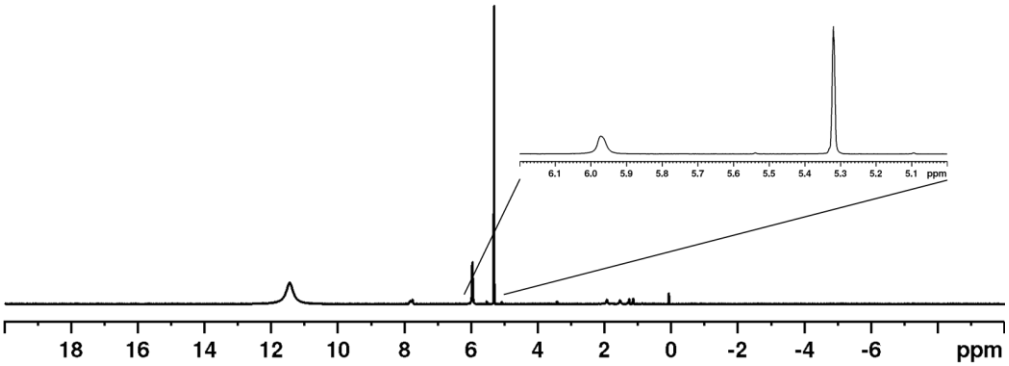

*Figure S 31: ^{1}H NMR spectrum of **2-Co** in CD_2Cl_2 recorded at room temperature; 20 mg of substance were dissolved in 0.2 mL of CD_2Cl_2 inside the NMR tube and a coaxial capillary filled with CD_2Cl_2 was added to determine the number of unpaired electrons in **2-Co** via the Evans method.*

3

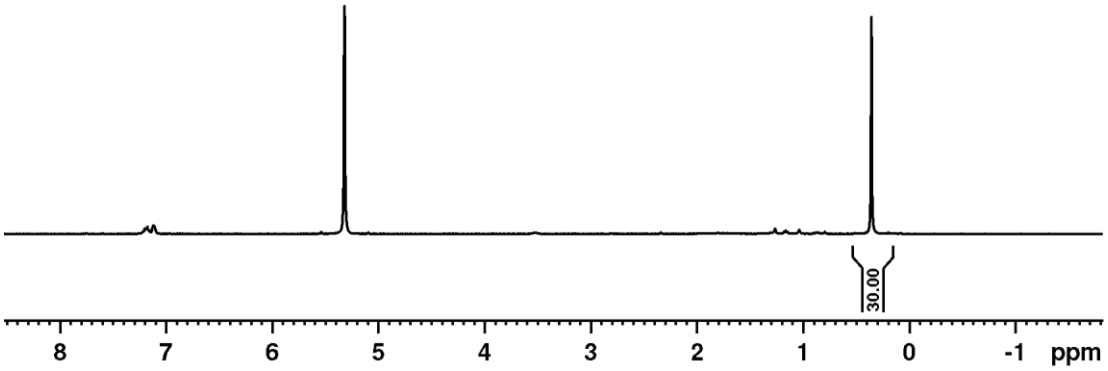

*Figure S 32: ^{1}H NMR spectrum of **3** in CD_2Cl_2 recorded at room temperature with traces of o-DFB at δ = 7.1 ppm.*

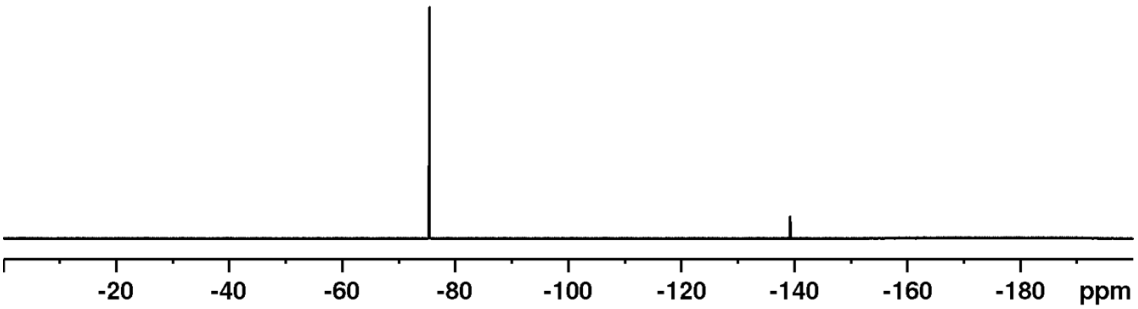

*Figure S 33: $^{19}F\{^{1}H\}$ NMR spectrum of **3** in CD_2Cl_2 recorded at room temperature with traces of o-DFB at δ = 140 ppm.*

[Fe(tol)$_2$][pf]$_2$

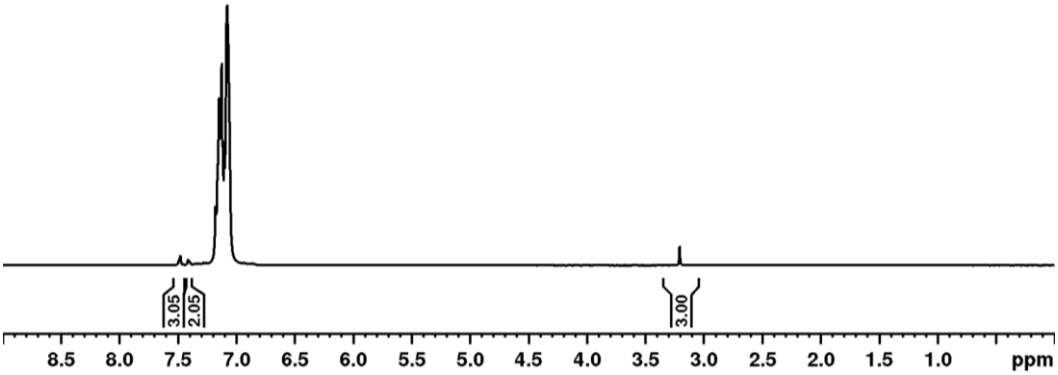

*Figure S 34: ^{1}H NMR spectrum of **[Fe(tol)$_2$][pf]$_2$** in o-DFB with added C_6D_6* capillary *recorded at room temperature.*

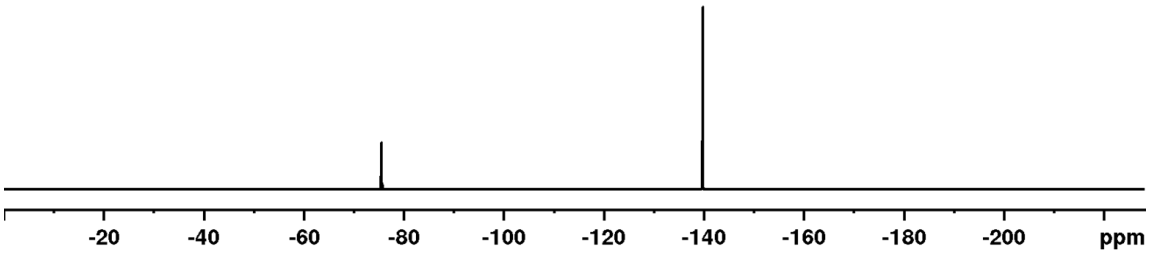

*Figure S 35: $^{19}F\{^1H\}$ NMR spectrum of **[Fe(tol)$_2$][pf]$_2$** in o-DFB with added C_6D_6* capillary *recorded at room temperature.*

7.5.4. Computational Details

General Considerations

DFT calculations were performed using the Orca 5.0 software package.[34] The sterically demanding Cp* ligands in **2-Fe** and **2-Co** were replaced with unsubstituted Cp ligands to save computational resources. Geometry optimizations were performed at the ωB97X-D3[35]/def2-TZVP[36] level of theory with PCM solvent correction for CH_2Cl_2.[37] Stationary points were verified by analytical frequency calculations. Single point calculations were performed at the ωB97X-D3/def2-TZVP level of theory with solvent correction as described above.

Spin Density Distribution and Energetic Comparison

To gain insight into the electronic structure of especially the paramagnetic species **1-Mn**, **1-Ni** and **2-Co**, their spin densities were analysed (Figure S36). While the spin density in **1-Mn** is clearly localized at the Mn atom, the two unpaired electrons in **1-Ni** and **2-Co** are centred at the Ni and Co atoms, respectively. Only in **1-Ni**, minor contributions from the Cp‴ ligand are apparent. As for both latter species a hypothetical singlet electron configuration would be possible and is transiently even observed for **1-Ni** in the solid state, the energetic separation between this singlet configuration and the experimentally observed triplet ground state was of interest. Thus, both the compounds **1-Ni** and **2-Co** were optimized as singlet as well as triplet configuration, the geometries compared, and the energetic separation determined (Figure S37). In both cases, the triplet configuration is 55 kJ/mol (**1-Ni**) and 127 kJ/mol (**2-Co**) more stable, respectively.

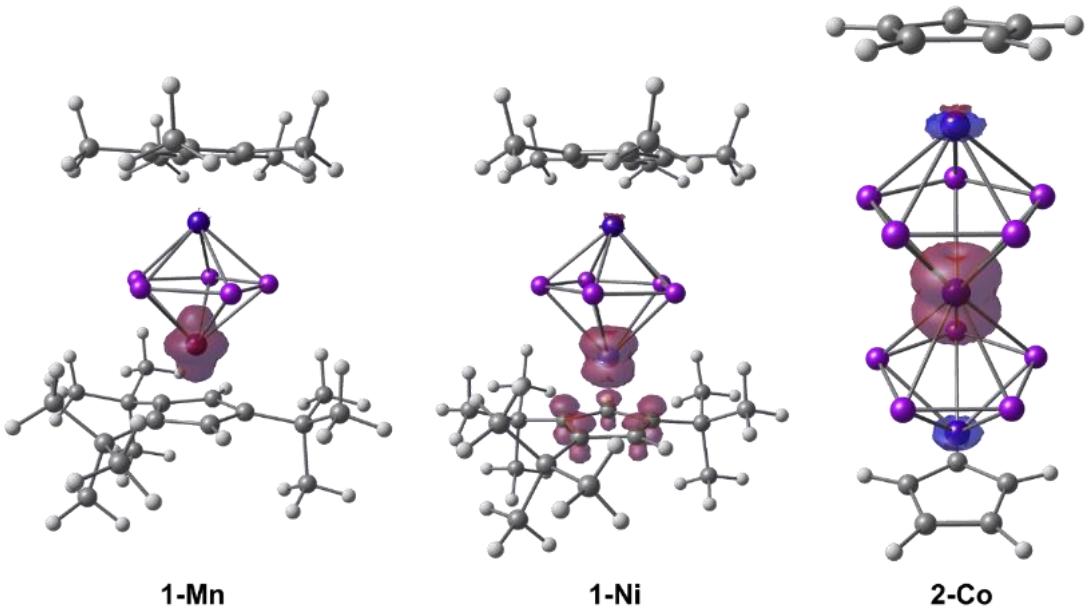

*Figure S 36: Calculated spin density distribution for **1-Mn**, **1-Ni** and **2-Co**; cutoff: 0.01 a. u.*

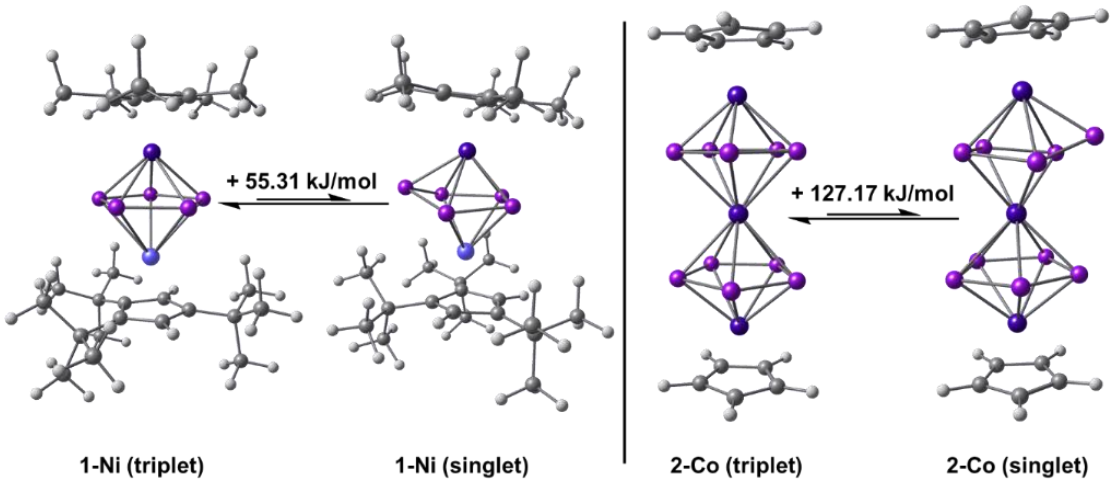

*Figure S 37: Comparison of optimized molecular structures for **1-Ni** (left) and **2-Co** (right) in case of a singlet or triplet electronic configuration, each.*

Optimized Geometries

1-Mn

ωB97XD/def2TZVP (CPCM (CH_2Cl_2)): Energies/H = -5176.41492301, Enthalpies/H = -5176.41397880, Free Energies/H = -5176.51963493, ZPVE/ kcal/mol = 441.30

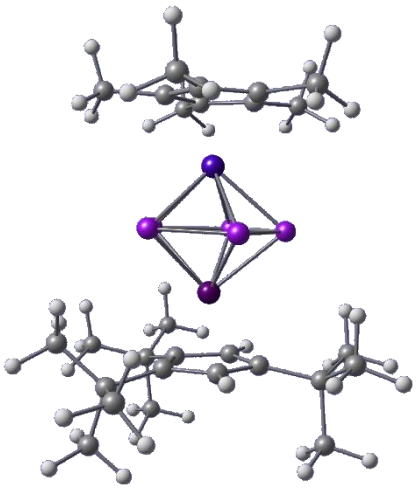

Symbol	X	Y	Z
Fe	11.537949000	7.691020000	21.194182000
Mn	9.749845000	6.152922000	23.176102000
P	11.907417000	7.105424000	23.481035000
P	10.299426000	8.466773000	23.081553000
P	11.776838000	5.500057000	22.072764000
P	9.180285000	7.685969000	21.436635000
P	10.067029000	5.830692000	20.840639000
C	7.707775000	5.666106000	23.631510000
C	8.481336000	4.499285000	23.434186000
H	8.294496000	3.766067000	22.668105000
C	6.349321000	5.958460000	23.023769000
C	9.520927000	4.405682000	24.410581000
C	8.319411000	6.347626000	24.705442000
H	7.980915000	7.291468000	25.098481000
C	11.753465000	9.480438000	20.164545000
C	12.877701000	9.264115000	21.013326000
C	10.315698000	3.096722000	24.561365000
C	11.679533000	8.393674000	19.246168000
C	9.415428000	5.597417000	25.230491000
C	8.983985000	5.515516000	27.640096000
H	8.873435000	4.432065000	27.601079000
H	7.999267000	5.960832000	27.484914000
H	9.326815000	5.788155000	28.640442000
C	11.845267000	3.233284000	24.580950000
H	12.238938000	3.291853000	23.566848000
H	12.278019000	2.343569000	25.043475000
H	12.201043000	4.101243000	25.123190000
C	5.967831000	7.433335000	23.158982000
H	5.949269000	7.749406000	24.203420000
H	4.967972000	7.588491000	22.749361000
H	6.655441000	8.083454000	22.615632000
C	12.760610000	7.507749000	19.524673000
C	9.989981000	6.029348000	26.590508000
C	9.826442000	2.415849000	25.852270000
H	10.160820000	2.933762000	26.748914000
H	10.218806000	1.397799000	25.893751000
H	8.735694000	2.362603000	25.875222000
C	11.384119000	5.512854000	26.939925000
H	12.129597000	5.850583000	26.218129000
H	11.431544000	4.429610000	27.011260000
H	11.666948000	5.913297000	27.915079000
C	6.256293000	5.524214000	21.559866000
H	6.874707000	6.144987000	20.910846000
H	5.223087000	5.617728000	21.220225000
H	6.555989000	4.483371000	21.425665000
C	13.501481000	8.045873000	20.615666000
C	5.357138000	5.116252000	23.848131000
H	5.573529000	4.050375000	23.751083000
H	4.339466000	5.294105000	23.494166000
H	5.403869000	5.381109000	24.906589000

C	10.050439000	7.559772000	26.718892000
H	10.384654000	7.809413000	27.727202000
H	9.084507000	8.042354000	26.574528000
H	10.764397000	7.996559000	26.019554000
C	9.988068000	2.140934000	23.403942000
H	8.940845000	1.834105000	23.404428000
H	10.595973000	1.241337000	23.513156000
H	10.223105000	2.583901000	22.433244000
C	10.686905000	8.244623000	18.141129000
H	10.480124000	7.196329000	17.926000000
H	11.079955000	8.700634000	17.229366000
H	9.744094000	8.736103000	18.380669000
C	13.095331000	6.270670000	18.760023000
H	13.600447000	5.535076000	19.385384000
H	13.761922000	6.519648000	17.930916000
H	12.202406000	5.806418000	18.341789000
C	13.356450000	10.184382000	22.087288000
H	12.531814000	10.734421000	22.540154000
H	14.055816000	10.912161000	21.669261000
H	13.874111000	9.641536000	22.877936000
C	10.854121000	10.671616000	20.187289000
H	9.838075000	10.414405000	19.887723000
H	11.226169000	11.426169000	19.490172000
H	10.813034000	11.123557000	21.177985000
C	14.751667000	7.470743000	21.192736000
H	14.846302000	7.697020000	22.254706000
H	15.620157000	7.894430000	20.682877000
H	14.788716000	6.388397000	21.071914000

1-Ni *(triplet)*

ωB97XD/def2TZVP (CPCM (CH_2Cl_2)): Energies/H = -5533.77609673, Enthalpies/H = -5533.77515253, Free Energies/H = -5533.88116412, ZPVE/ kcal/mol = 439.97

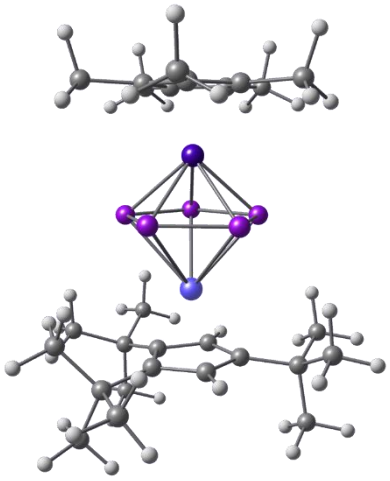

Symbol	X	Y	Z
C	5.323371000	8.615463000	20.265968000
Ni	7.803515000	4.062555000	19.865378000
P	7.868925000	5.829919000	17.999674000
P	5.678036000	5.291258000	20.574025000
P	5.937916000	5.113278000	18.479408000
P	8.811134000	6.435977000	19.793535000
C	9.327822000	2.633908000	19.166084000
C	9.463603000	2.858590000	20.554932000
H	10.337472000	3.282306000	21.020783000
C	8.036736000	2.093799000	18.990014000
H	7.616448000	1.815418000	18.037675000
C	8.302529000	2.418407000	21.254779000
C	7.381517000	1.925414000	20.246051000
Fe	6.580160000	7.171919000	19.450461000
P	7.453088000	6.121182000	21.379291000
C	10.421801000	2.738547000	18.123754000
C	8.292278000	2.378036000	22.790797000
C	6.073489000	1.121453000	20.286401000
C	6.999883000	9.088230000	18.754917000
C	6.642798000	9.137330000	20.133956000
C	5.901665000	8.535282000	18.035096000
C	4.865399000	8.242130000	18.968734000
C	9.845313000	2.868315000	16.712243000
H	9.220054000	2.012231000	16.452597000
H	10.659149000	2.918204000	15.986023000
H	9.245230000	3.773499000	16.603146000
C	11.225432000	1.427804000	18.209436000
H	11.672226000	1.308229000	19.198692000
H	12.028281000	1.431150000	17.468379000
H	10.584211000	0.564925000	18.017468000
C	11.365329000	3.910753000	18.404663000
H	10.854947000	4.870768000	18.312838000
H	12.187569000	3.901319000	17.686255000
H	11.798574000	3.850691000	19.404595000
C	7.158599000	3.177534000	23.448501000
H	7.366833000	4.246797000	23.394861000
H	7.095698000	2.912333000	24.506333000
H	6.186786000	3.006188000	22.999325000
C	9.598467000	2.969080000	23.344033000
H	10.472812000	2.390257000	23.041203000
H	9.553831000	2.959048000	24.434602000
H	9.738380000	4.005333000	23.028086000
C	8.246458000	0.910515000	23.246565000
H	7.287232000	0.438159000	23.046530000
H	8.420987000	0.857097000	24.323466000
H	9.023210000	0.327779000	22.746362000
C	5.252733000	1.354011000	19.007236000
H	4.975628000	2.403728000	18.894620000
H	4.331360000	0.772182000	19.066978000
H	5.775057000	1.037090000	18.105352000
C	6.466503000	-0.367251000	20.320219000
H	7.060564000	-0.628497000	19.442077000
H	5.567453000	-0.988216000	20.322023000

H	7.051039000	-0.613213000	21.206439000
C	5.134196000	1.421218000	21.454426000
H	5.561507000	1.167921000	22.420736000
H	4.227779000	0.824393000	21.336264000
H	4.836895000	2.471897000	21.466877000
C	8.267035000	9.599290000	18.155115000
H	9.096899000	9.541603000	18.858619000
H	8.139248000	10.646583000	17.871311000
H	8.539090000	9.040281000	17.259958000
C	7.472840000	9.711802000	21.233234000
H	7.261271000	10.779207000	21.331082000
H	8.537954000	9.599235000	21.032455000
H	7.254964000	9.239062000	22.190523000
C	5.820920000	8.365410000	16.554673000
H	6.803758000	8.195217000	16.116179000
H	5.406724000	9.271757000	16.106727000
H	5.174806000	7.531842000	16.280469000
C	3.511007000	7.710305000	18.638618000
H	3.109755000	7.101782000	19.448897000
H	3.528911000	7.104436000	17.733158000
H	2.821911000	8.541589000	18.472248000
C	4.531625000	8.548623000	21.529197000
H	3.797649000	7.743895000	21.500069000
H	3.994011000	9.488967000	21.671654000
H	5.173315000	8.395043000	22.396549000

1-Ni *(singlet)*

ωB97XD/def2TZVP (CPCM (CH_2Cl_2)): Energies/H = -5533.75348611, Enthalpies/H = -5533.75254190, Free Energies/H = -5533.86009630, ZPVE/ kcal/mol = 440.62

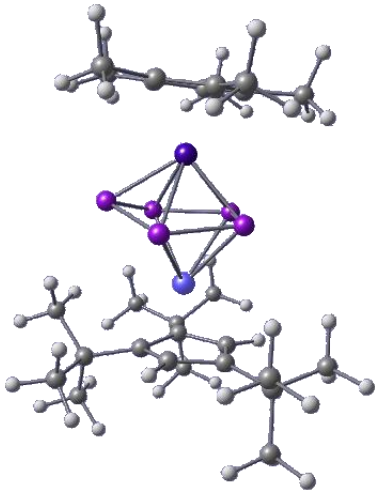

Symbol	X	Y	Z
C	5.323371000	8.615463000	20.265968000
Ni	7.803515000	4.062555000	19.865378000
P	7.868925000	5.829919000	17.999674000
P	5.678036000	5.291258000	20.574025000
P	5.937916000	5.113278000	18.479408000
P	8.811134000	6.435977000	19.793535000
C	9.327822000	2.633908000	19.166084000
C	9.463603000	2.858590000	20.554932000
H	10.337472000	3.282306000	21.020783000
C	8.036736000	2.093799000	18.990014000
H	7.616448000	1.815418000	18.037675000
C	8.302529000	2.418407000	21.254779000
C	7.381517000	1.925414000	20.246051000
Fe	6.580160000	7.171919000	19.450461000
P	7.453088000	6.121182000	21.379291000
C	10.421801000	2.738547000	18.123754000
C	8.292278000	2.378036000	22.790797000
C	6.073489000	1.121453000	20.286401000
C	6.999883000	9.088230000	18.754917000
C	6.642798000	9.137330000	20.133956000
C	5.901665000	8.535282000	18.035096000
C	4.865399000	8.242130000	18.968734000
C	9.845313000	2.868315000	16.712243000
H	9.220054000	2.012231000	16.452597000
H	10.659149000	2.918204000	15.986023000
H	9.245230000	3.773499000	16.603146000
C	11.225432000	1.427804000	18.209436000
H	11.672226000	1.308229000	19.198692000
H	12.028281000	1.431150000	17.468379000
H	10.584211000	0.564925000	18.017468000
C	11.365329000	3.910753000	18.404663000
H	10.854947000	4.870768000	18.312838000
H	12.187569000	3.901319000	17.686255000
H	11.798574000	3.850691000	19.404595000
C	7.158599000	3.177534000	23.448501000
H	7.366833000	4.246797000	23.394861000
H	7.095698000	2.912333000	24.506333000
H	6.186786000	3.006188000	22.999325000
C	9.598467000	2.969080000	23.344033000
H	10.472812000	2.390257000	23.041203000
H	9.553831000	2.959048000	24.434602000
H	9.738380000	4.005333000	23.028086000
C	8.246458000	0.910515000	23.246565000
H	7.287232000	0.438159000	23.046530000
H	8.420987000	0.857097000	24.323466000
H	9.023210000	0.327779000	22.746362000
C	5.252733000	1.354011000	19.007236000
H	4.975628000	2.403728000	18.894620000
H	4.331360000	0.772182000	19.066978000
H	5.775057000	1.037090000	18.105352000
C	6.466503000	-0.367251000	20.320219000
H	7.060564000	-0.628497000	19.442077000
H	5.567453000	-0.988216000	20.322023000

H	7.051039000	-0.613213000	21.206439000
C	5.134196000	1.421218000	21.454426000
H	5.561507000	1.167921000	22.420736000
H	4.227779000	0.824393000	21.336264000
H	4.836895000	2.471897000	21.466877000
C	8.267035000	9.599290000	18.155115000
H	9.096899000	9.541603000	18.858619000
H	8.139248000	10.646583000	17.871311000
H	8.539090000	9.040281000	17.259958000
C	7.472840000	9.711802000	21.233234000
H	7.261271000	10.779207000	21.331082000
H	8.537954000	9.599235000	21.032455000
H	7.254964000	9.239062000	22.190523000
C	5.820920000	8.365410000	16.554673000
H	6.803758000	8.195217000	16.116179000
H	5.406724000	9.271757000	16.106727000
H	5.174806000	7.531842000	16.280469000
C	3.511007000	7.710305000	18.638618000
H	3.109755000	7.101782000	19.448897000
H	3.528911000	7.104436000	17.733158000
H	2.821911000	8.541589000	18.472248000
C	4.531625000	8.548623000	21.529197000
H	3.797649000	7.743895000	21.500069000
H	3.994011000	9.488967000	21.671654000
H	5.173315000	8.395043000	22.396549000

2-Fe'

ωB97XD/def2TZVP (CPCM (CH_2Cl_2)): Energies/H = -7591.66093026, Enthalpies/H = -7591.65998606, Free Energies/H = -7591.73656363, ZPVE/ kcal/mol = 124.09

Symbol	X	Y	Z
Fe	3.832713000	2.015632000	14.356746000
Fe	3.813755000	5.201005000	14.509974000
Fe	3.790546000	8.385606000	14.662908000
P	2.222021000	3.502489000	15.265999000
P	2.532311000	3.603941000	13.166905000
P	2.509027000	6.903730000	13.329164000
P	2.202119000	6.799588000	15.429352000
P	4.603273000	6.933537000	12.971410000
P	4.126091000	3.465271000	16.209118000
P	4.627220000	3.632686000	12.812439000
P	5.590300000	6.852922000	14.851766000
P	5.612336000	3.549021000	14.692867000
P	4.106910000	6.767194000	16.370100000
C	2.995844000	0.370799000	13.418235000
C	4.021607000	0.280729000	15.469761000
C	4.398681000	0.388197000	13.208236000
C	2.762899000	0.303750000	14.816011000
C	5.032479000	0.332946000	14.476081000
H	4.896448000	0.453919000	12.252641000
H	6.097009000	0.349619000	14.654507000
C	4.970652000	10.066872000	14.910977000
H	2.238500000	0.421224000	12.650655000
C	2.909602000	10.097164000	13.901483000
C	4.306971000	10.119792000	13.658353000
H	4.181687000	0.251168000	16.536923000
C	2.709780000	10.030880000	15.304277000
H	1.797225000	0.294329000	15.298293000
C	3.983600000	10.011946000	15.928175000
H	6.039332000	10.048992000	15.062015000
H	4.781597000	10.148373000	12.689268000
H	1.756099000	9.980607000	15.807564000
H	4.168903000	9.945178000	16.989501000
H	2.134565000	10.105497000	13.150093000

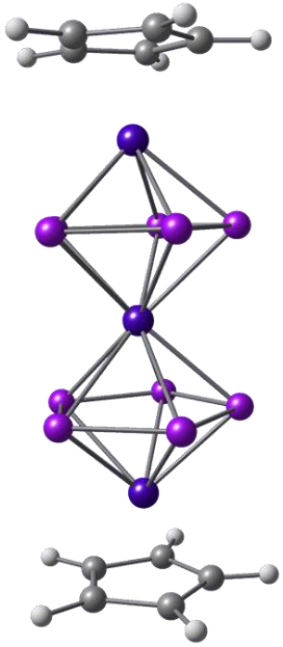

2-Co' *(triplet)*

ωB97XD/def2TZVP (CPCM (CH_2Cl_2)): Energies/H = -7710.95679967, Enthalpies/H = -7710.95585546, Free Energies/H = -7711.03591349, ZPVE/ kcal/mol = 123.19

Symbol	X	Y	Z
Fe	7.522234000	12.483643000	12.579632000
Fe	11.974036000	16.328787000	15.913898000
Co	9.750639000	14.405681000	14.243586000
P	10.911286000	14.284925000	16.524974000
P	12.225338000	14.203733000	14.865862000
P	8.524832000	12.208109000	14.724003000
P	9.831632000	12.136245000	13.058601000
P	11.771595000	15.833612000	13.590770000
P	9.647310000	15.966567000	16.277686000
P	10.177761000	16.921645000	14.463326000
P	7.255268000	13.887160000	14.488150000
P	9.368022000	13.769000000	11.791424000
P	7.776578000	14.851581000	12.675701000
C	6.959468000	11.799005000	10.711671000
C	7.272053000	10.704155000	11.557324000
C	5.893657000	12.521672000	11.306074000
C	13.050173000	16.513178000	17.669842000
C	6.399380000	10.750102000	12.674434000
C	5.547800000	11.873657000	12.519350000
H	7.461076000	12.052135000	9.790523000
H	8.052992000	9.978227000	11.391954000
C	13.933523000	16.448977000	16.562042000
C	12.208608000	17.641176000	17.494659000
H	5.443043000	13.420839000	10.915281000
H	4.787046000	12.193986000	13.214224000
H	6.400238000	10.065498000	13.508416000
C	13.637854000	17.537589000	15.702246000
C	12.571691000	18.274274000	16.278426000
H	13.009032000	15.812440000	18.489295000
H	14.682248000	15.691048000	16.391219000
H	11.414847000	17.948222000	18.157875000
H	12.102553000	19.148237000	15.853800000
H	14.122589000	17.752394000	14.762531000

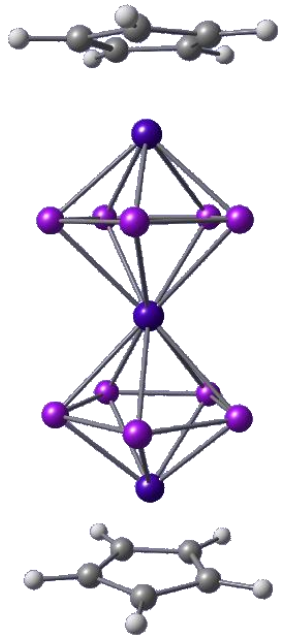

2-Co' *(singlet)*

ωB97XD/def2TZVP (CPCM (CH_2Cl_2)): Energies/H = -7710.90921936, Enthalpies/H = -7710.90827516, Free Energies/H = -7710.98747581, ZPVE/ kcal/mol = 123.07

Symbol	X	Y	Z
Fe	7.619011000	12.475142000	12.650199000
Fe	11.864829000	16.385590000	15.837958000
Co	9.736019000	14.309834000	14.246688000
P	10.822598000	14.337733000	16.381160000
P	12.084765000	14.329193000	14.695537000
P	8.632946000	12.114136000	14.781731000
P	9.913733000	12.055851000	13.119032000
P	11.335827000	15.938651000	13.464929000
P	9.436045000	15.948722000	15.998734000
P	10.179517000	17.329122000	14.572449000
P	7.399194000	13.851844000	14.585855000
P	9.486059000	13.774950000	11.920305000
P	7.856161000	14.839078000	12.766486000
C	7.091087000	11.780117000	10.774894000
C	7.306979000	10.688882000	11.653649000
C	6.045552000	12.574159000	11.311462000
C	12.981564000	16.368799000	17.579902000
C	6.395003000	10.808255000	12.734193000
C	5.616445000	11.973846000	12.523170000
H	7.643621000	11.983655000	9.870517000
H	8.051455000	9.917081000	11.533334000
C	13.840617000	16.342441000	16.448713000
C	12.202101000	17.549931000	17.510693000
H	5.659136000	13.486928000	10.884889000
H	4.850460000	12.352351000	13.182473000
H	6.324454000	10.144951000	13.582455000
C	13.591422000	17.508108000	15.682126000
C	12.582396000	18.257366000	16.340461000
H	12.921057000	15.613502000	18.348226000
H	14.549166000	15.564680000	16.208785000
H	11.434367000	17.843859000	18.209641000
H	12.168242000	19.193545000	16.001336000
H	14.064572000	17.765196000	14.746815000

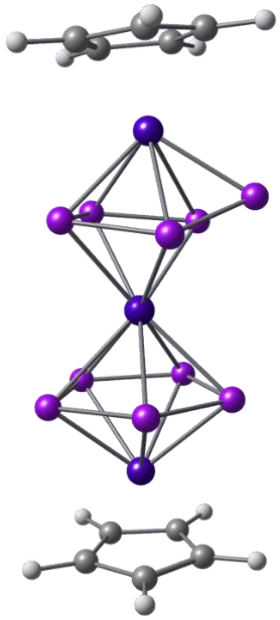

7.6. References

[1] a) T. J. Kealy, P. L. Pauson, *Nature* **1951**, *168*, 1039–1040; b) G. Wilkinson, M. Rosenblum, M. C. Whiting, R. B. Woodward, *J. Am. Chem. Soc.* **1952**, *74*, 2125–2126; c) E. O. Fischer, W. Pfab, *Z. Naturforsch. B* **1952**, *7*, 377–379.

[2] E. O. Fischer, W. Hafner, *Z. Naturforsch. B* **1955**, *10*, 665–668.

[3] G. Gritzner, J. Kuta, *Pure Appl. Chem.* **1984**, *56*, 461–466.

[4] G. G. Hlatky, *Coord. Chem. Rev.* **1999**, *181*, 243–296.

[5] L. Barluzzi, S. R. Giblin, A. Mansikkamäki, R. A. Layfield, *J. Am. Chem. Soc.* **2022**, *144*, 18229–18233.

[6] a) F.-S. Guo, B. M. Day, Y.-C. Chen, M.-L. Tong, A. Mansikkamäki, R. A. Layfield, *Science* **2018**, *362*, 1400–1403; b) F. T. Edelmann, *New J. Chem.* **2011**, *35*, 517–528.

[7] a) A. Salzer, H. Werner, *Angew. Chem. Int. Ed. Engl.* **1972**, *11*, 930–932; b) E. Dubler, M. Textor, H.-R. Oswald, A. Salzer, *Angew. Chem. Int. Ed. Engl.* **1974**, *13*, 135–136.

[8] T. Kuhlmann, W. Siebert, *Z. Naturforsch. B* **1985**, *40*, 167–170.

[9] L. Münzfeld, A. Hauser, P. Hädinger, F. Weigend, P. W. Roesky, *Angew. Chem. Int. Ed.* **2021**, *60*, 24493–24499.

[10] V. Beck, D. O'Hare, *J. Organomet. Chem.* **2004**, *689*, 3920–3938.

[11] a) O. J. Scherer, H. Sitzmann, G. Wolmershäuser, *Angew. Chem. Int. Ed. Engl.* **1989**, *28*, 212–213; b) X. Wang, M. Sabat, R. N. Grimes, *J. Am. Chem. Soc.* **1995**, *117*, 12218–12226; c) M. Piesch, M. Scheer, *Organometallics* **2020**, *39*, 4247–4252; d) C. Rödl, G. Hierlmeier, R. Wolf, *Chem. Commun.* **2022**, *58*, 12212–12215.

[12] a) O. J. Scherer, J. Braun, G. Wolmershäuser, *Chem. Ber.* **1990**, *123*, 471–475; b) E. Mädl, G. Balázs, E. V. Peresypkina, M. Scheer, *Angew. Chem. Int. Ed.* **2016**, *55*, 7702–7707.

[13] F. Dielmann, A. Timoshkin, M. Piesch, G. Balázs, M. Scheer, *Angew. Chem. Int. Ed.* **2017**, *56*, 1671–1675.

[14] a) O. J. Scherer, J. Schwalb, G. Wolmershäuser, W. Kaim, R. Gross, *Angew. Chem. Int. Ed. Engl.* **1986**, *25*, 363–364; b) O. J. Scherer, T. Brück, *Angew. Chem. Int. Ed. Engl.* **1987**, *26*, 59.

[15] a) O. J. Scherer, H. Sitzmannn, G. Wolmershäuser, *Angew. Chem. Int. Ed. Engl*. **1985**, *24*, 351–353; b) O. J. Scherer, H. Swarowsky, G. Wolmershäuser, W. Kaim, S. Kohlmann, *Angew. Chem. Int. Ed. Engl.* **1987**, *26*, 1153–1155; c) O. J. Scherer, J. Schwalb, H. Swarowsky, G. Wolmershäuser, W. Kaim, R. Gross, *Chem. Ber.* **1988**, *121*, 443–449.

[16] E. Peresypkina, A. Virovets, M. Scheer, *Coord. Chem. Rev.* **2021**, *446*, 213995.

[17] E. Urne˙žius, W. W. Brennessel, C. J. Cramer, J. E. Ellis, P. v. R. Schleyer, *Science* **2002**, *295*, 832–834.

[18] a) O. J. Scherer, T. Brück, G. Wolmershäuser, *Chem. Ber.* **1989**, *122*, 2049–2054; b) B. Rink, O. J. Scherer, G. Heckmann, G. Wolmershäuser, *Chem. Ber.* **1992**, *125*,

1011–1016; c) M. Piesch, S. Reichl, C. Riesinger, M. Seidl, G. Balazs, M. Scheer, *Chem. Eur. J.* **2021**, *27*, 9129–9140.

[19] a) T. Li, J. Wiecko, N. A. Pushkarevsky, M. T. Gamer, R. Köppe, S. N. Konchenko, M. Scheer, P. W. Roesky, *Angew. Chem. Int. Ed.* **2011**, *50*, 9491–9495; b) M. Piesch, F. Dielmann, S. Reichl, M. Scheer, *Chem. Eur. J.* **2020**, *26*, 1518–1524; c) X. Sun, A. K. Singh, R. Yadav, D. Jin, M. Haimerl, M. Scheer, P. W. Roesky, *Chem. Commmun.* **2022**, *58*, 673–676.

[20] a) S. Welsch, C. Gröger, M. Sierka, M. Scheer, *Angew. Chem. Int. Ed.* **2011**, *50*, 1435–1438; b) F. Dielmann, A. Schindler, S. Scheuermayer, J. Bai, R. Merkle, M. Zabel, A. V. Virovets, E. V. Peresypkina, G. Brunklaus, H. Eckert, M. Scheer, *Chem. Eur. J.* **2012**, *18*, 1168–1179; c) C. Heindl, E. V. Peresypkina, A. V. Virovets, W. Kremer, M. Scheer, *J. Am. Chem. Soc.* **2015**, *137*, 10938–10941; d) M. Fleischmann, S. Welsch, E. V. Peresypkina, A. V. Virovets, M. Scheer, *Chem. Eur. J.* **2015**, *21*, 14332–14336; e) E. Peresypkina, K. Grill, B. Hiltl, A. V. Virovets, W. Kremer, J. Hilgert, W. Tremel, M. Scheer, *Angew. Chem. Int. Ed.* **2021**, *60*, 12132–12142; f) M. Haimerl, M. Piesch, G. Balázs, P. Mastrorilli, W. Kremer, M. Scheer, *Inorg. Chem.* **2021**, *60*, 5840–5850; g) H. Brake, E. Peresypkina, A. V. Virovets, W. Kremer, C. Klimas, C. Schwarzmaier, M. Scheer, *Inorg. Chem.* **2021**, *60*, 6027–6039.

[21] a) S. Welsch, L. J. Gregoriades, M. Sierka, M. Zabel, A. V. Virovets, M. Scheer, *Angew. Chem. Int. Ed.* **2007**, *46*, 9323–9326; b) M. Fleischmann, S. Welsch, H. Krauss, M. Schmidt, M. Bodensteiner, E. V. Peresypkina, M. Sierka, C. Gröger, M. Scheer, *Chem. Eur. J.* **2014**, *20*, 3759–3768.

[22] E. O. Fischer, R. Böttcher, *Chem. Ber.* **1956**, *89*, 2397–2400.

[23] S. C. Meier, A. Holz, J. Kulenkampff, A. Schmidt, D. Kratzert, D. Himmel, D. Schmitz, E.-W. Scheidt, W. Scherer, C. Bülow, M. Timm, R. Lindblad, S. T. Akin, V. Zamudio-Bayer, B. v. Issendorff, M. A. Duncan, J. T. Lau, I. Krossing, *Angew. Chem. Int. Ed.* **2018**, *57*, 9310–9314.

[24] a) F. Baumann, E. Dormann, Y. Ehleiter, W. Kaim, J. Kärcher, M. Kelemen, R. Krammer, D. Saurenz, D. Stalke, C. Wachter, G. Wolmershäuser, H. Sitzmann, *J. Organomet. Chem.* **1999**, *587*, 267–283; b) M. Wallasch, G. Wolmershäuser, H. Sitzmann, *Angew. Chem. Int. Ed.* **2005**, *44*, 2597–2599; c) M. Maekawa, M. Römelt, C. G. Daniliuc, P. G. Jones, P. S. White, F. Neese, M. D. Walter, *Chem. Sci.* **2012**, *3*, 2972–2979; d) M. Schär, D. Saurenz, F. Zimmer, I. Schädlich, G. Wolmershäuser, S. Demeshko, F. Meyer, H. Sitzmann, O. M. Heigl, F. H. Köhler, *Organometallics* **2013**, *32*, 6298–6305; e) M. Kreye, C. G. Daniliuc, M. Freytag, P. G. Jones, M. D. Walter, *Dalt. Trans.* **2014**, *43*, 9052–9060.

[25] M. Schmitt, M. Mayländer, T. Heizmann, S. Richert, C. Bülow, K. Hirsch, V. Zamudio-Bayer, J. T. Lau, I. Krossing, *Angew. Chem. Int. Ed.* **2022**, *134*, e202211555.

[26] O. J. Scherer, C. Blath, G. Wolmershäuser, *J.Organomet. Chem.* **1990**, *387*, C21–C24.

[27] *https://omics.pnl.gov/software/molecular-weight-calculator* (30.01.2023).

[28] V. D. Makhaev, A. N. Galiullin, E. E. Faingol´d, N. M. Bravaya, L. A. Petrova, *Russ. Chem. Bull.* **2014**, *63*, 651–656.
[29] M. Gonsior, I. Krossing, N. Mitzel, *Z. anorg. allg. Chem.* **2002**, *628*, 1821–1830.
[30] Agilent Technologies Ltd, *CrysAlis PRO*, Yarnton, Oxfordshire, England, **2014**.
[31] O. V. Dolomanov, L. J. Bourhis, R. J. Gildea, J. A. K. Howard, H. Puschmann, *J. Appl. Crystallogr.* **2009**, *42*, 339–341.
[32] G. M. Sheldrick, *Acta Cryst. A* **2015**, *71*, 3–8.
[33] a) G. M. Sheldrick, *Acta Cryst. A* **2008**, *64*, 112–122; b) G. M. Sheldrick, *Acta Cryst. C* **2015**, *71*, 3–8.
[34] a) F. Neese, F. Wennmohs, U. Becker, C. Rieplinger, *J. Chem. Phys.* **2020**, *152*, 224108–224126; b) F. Neese, *WIREs Comput. Mol. Sci.* **2022**, *12*, 1606–1621.
[35] Y.-S. Lin, G.-D. Li, S.-P. Mao, J. D. Chai, *J. Chem. Theory Comput.* **2013**, *9*, 263–272.
[36] F. Weigend, R. Ahlrichs, *Phys. Chem. Chem. Phys.* **2005**, *7*, 3297–3305.
[37] J. Tomasi, B. Mennucci, R. Cammi, *Chem. Rev.* **2005**, *105*, 2999–3094.

8. Synthesis and Reactivity of a Cyclooctatetraene-Like Polyphosphorus Ligand Complex [*Cyclo*-P_8]

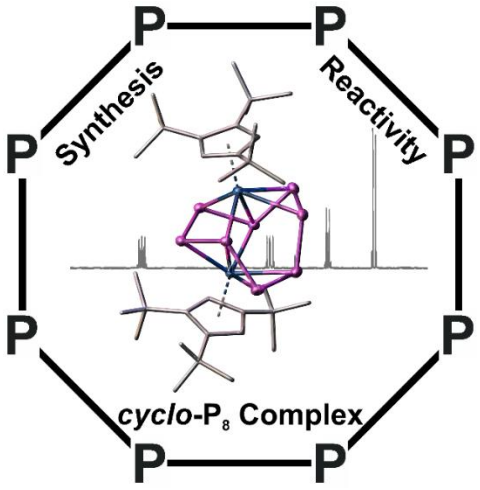

Preface

The following chapter has already been published. The article is reproduced with permission from Wiley-VCH. License Number: 5637011373493

"Synthesis and Reactivity of a Cyclooctatetraene-Like Polyphosphorus Ligand Complex [Cyclo-P_8]"

Angew. Chem. Int. Ed. **2023**, *62,* e202218828.

Angew. Chem. **2023**, *135,* e202218828.

Parts of this chapter have already been described within the PhD thesis of Dr. Fabian Dielmann.

Authors

Christoph Riesinger, Fabian Dielmann, Robert Szlosek, Alexander V. Virovets and Manfred Scheer

Author Contributions

Christoph Riesinger – Synthesis of **3** ,**4**, **5** and further reactivity studies, Interpretation of crystallographic data (**3**, **4**, **5**), Interpretation of computational data, writing of original draft.
Fabian Dielmann – Synthesis of **A**, **B**, **1**, **2** and **2a**, writing of original draft.
Robert Szlosek – Performance and interpretation of electrochemical investigations.
Alexander V. Virovets – X-ray data acquisition, Interpretation of crystallographic data (**A**, **B**, **1**).
Manfred Scheer – Project administration, Funding acquisition, Co-writing final manuscript.

Acknowledgements

This work was supported by the Deutsche Forschungsgemeinschaft (DFG) within the projects Sche 384/36-2 and Sche 384/32-2. C. R. is grateful to the Studienstiftung des Deutschen Volkes for a PhD fellowship. R. S. is grateful to the Fonds der Chemischen Industrie for a PhD fellowship. The authors thank Prof. Dr. Karaghiosoff (LMU Munich) for the measurement of 2D-31P NMR experiments.

8.1. Abstract

*The thermolysis of Cp'''Ta(CO)$_4$ with white phosphorus (P$_4$) gives access to [{Cp'''Ta}$_2$(μ,$\eta^{2:2:2:2:1:1}$-P$_8$)] (**A**), representing the first complex containing a cyclo-octatetraene-like (COT) cyclo-P$_8$ ligand. While ring sizes of n > 6 have remained elusive for cyclo-P$_n$ structural motifs, the choice of the transition metal, co-ligand and reaction conditions allowed the isolation of **A**. Reactivity investigations reveal its versatile coordination behaviour as well as its redox properties. Oxidation leads to dimerization to afford [{Cp'''Ta}$_4$(μ_4,$\eta^{2:2:2:2:2:2:2:2:1:1:1:1}$-P$_{16}$)][TEF]$_2$ (**4**, TEF = [Al(OC{CF$_3$}$_3$)$_4$]$^-$). Reduction, however, leads to the fission of one P–P bond in **A** followed by rapid dimerization to form [K@[2.2.2]cryptand]$_2$[{Cp'''Ta}$_4$(μ_4,$\eta^{2:2:2:2:2:2:2:2:1:1:1:1}$-P$_{16}$)] (**5**), which features an unprecedented chain-type P$_{16}$ ligand. Lastly, **A** serves as a P$_2$ synthon, via ring contraction to the triple-decker complex [{Cp'''Ta}$_2$(μ,$\eta^{6:6}$-P$_6$)] (**B**).*

8.2. Introduction

Carbocyclic compounds are of tremendous importance as e. g. in organic drug-like molecules or ligands in transition metal catalysts. Closely related cyclic oligo-phosphorus compounds, although synthetically more challenging, have also gained considerable attention over the past decades.[1] This development was initiated by the fundamental interest in the close relationship (cross relation, isolobality between P and CH)[2] of oligo-phosphorus compounds with carbon-based species. In addition, the field of white phosphorus (P$_4$) activation has been growing significantly in recent years and has thus raised additional interest in these compounds from

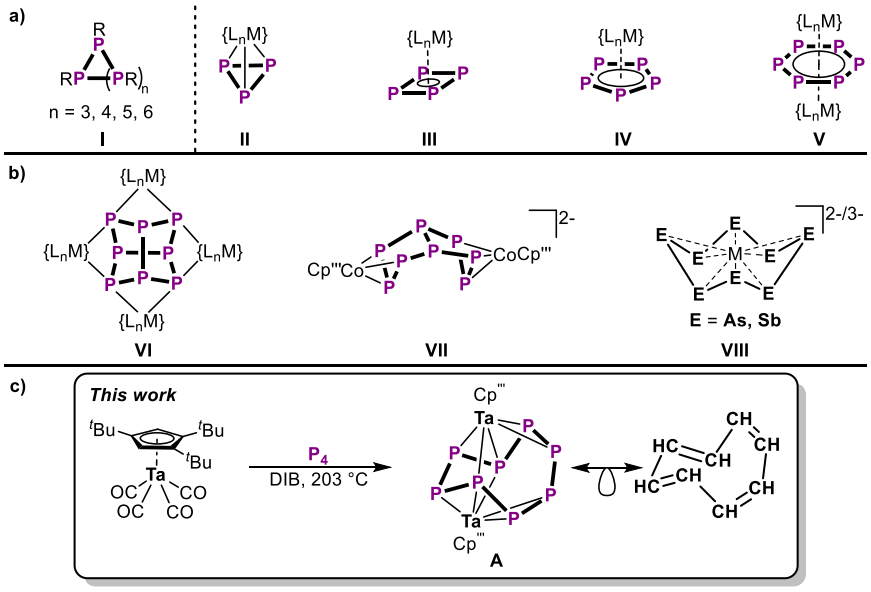

*Scheme 1: a) Known cyclo-(PR)$_n$ (**I**, R = alkyl or aryl) and cyclo-P$_n$ structural motifs for n = 3 – 6 (**II** – **V**), b) selected P$_8$ species (**VI** – **VII**, {L$_n$M} = {Cp*$_2$Sm}, {(^{dmp}nacnac)Fe} (^{dmp}nacnac = [{N(C$_6$H$_3$Me$_2$-2,6)C(Me)}$_2$CH]$^-$), {(1,1'-Fc(NSi^{t}BuMe$_2$)$_2$)Sc}) and crown-shaped cyclo-E$_8^{8-}$-containing compounds (**VIII**, E = As, Sb, M = Cr, Mo, Nb, Ta), c) synthesis of [{Cp'''Ta}$_2$(μ,$\eta^{2:2:2:2:1:1}$-P$_8$)] (**A**).*

an application-oriented perspective.[3] Simple organically substituted cyclic oligo-phosphines $(RP)_n$ (**I**, Scheme 1a) were already prepared as early as 1877.[4] Since then, development of various synthetic protocols has yielded $(RP)_n$ compounds (n = 3 – 6), in which the sterics of R govern the overall ring size.[1a-c, 5] Notably, however, the ring size of n = 6 could not be exceeded and larger organo-polyphosphines, such as $^t Bu_6P_8$, form bicyclic systems.[6]
Besides organic substitution, oligo-phosphorus species can also be stabilized via coordination to transition metals. Very prominently, the Figueroa group recently was able to stabilize the elusive P_2 at a mononuclear iron center.[7] Besides, several completely unsubstituted cyclic P_n ligands (n = 3 – 6), could be stabilized within the coordination sphere of transition metals (Scheme 1a). While *cyclo*-P_n (n = 3 – 5) ligands can be obtained within sandwich type complexes (**II**,[8], **III**,[9] **IV**[10]), *cyclo*-P_6 (**V**)[11] could this far only be obtained within triple-decker complexes. Even though complexes with far larger oligo-phosphorus moieties (up to 24 P-atoms) are known, such species unexceptionally feature aggregated polycyclic structural motifs.[12] Thus, monocyclic all-phosphorus species with more than six ring atoms are unknown to date. These facts raised the question whether compounds featuring larger all-phosphorus rings are accessible and how such species can be stabilized. Such compounds would be optimal starting materials on the way towards extended oligo-phosphorus frameworks. Additionally, their large ring size could allow for their use as transfer reagents of smaller P_n units under ring contraction. While the isolobal relationship of *cyclo*-P_8 to *cyclo*-octatetraene (COT) renders its coordinative stabilization viable, known P_8 ligand complexes feature polycyclic arrangements,[13] as e. g. the cunean type (**VI**)[14] or related (**VII**)[15] structures (Scheme 1b). While highly ionic crown-shaped *cyclo*-E_8^{8-} structural motifs (**VIII**)[16] could be obtained for the heavier congeners arsenic and antimony, their transfer to phosphorus has not yet been possible. However, a neutral *cyclo*-As_8 ligand could be stabilized within a niobium complex,[17] which provides a good starting point for investigations to realize a group 5 *cyclo*-P_8 ligand complex. Herein the synthesis and isolation of a tantalum complex are presented featuring an unprecedented COT-like *cyclo*-P_8 ligand, which notably is the largest cyclic all-phosphorus species known to date. Moreover, the reactivity of this exotic compound demonstrates its versatility as building block for large entities in phosphorus chemistry and as a P_2 source by ring contraction reactions.

8.3. Results and Discussion

Careful choice of the metal, the Cp^R ligand and the reaction conditions enabled the synthesis of $[\{Cp'''Ta\}_2(\mu,\eta^{2:2:2:2:1:1}\text{-}P_8)]$ (**A**, Cp''' = 1,2,4-$tBu_3C_5H_2$) via co-thermolysis of P_4 with $Cp'''Ta(CO)_4$ in boiling 1,3-diisopropyl-benzene (Scheme 1c). After chromatographic separation (see SI) from the byproducts, $[\{Cp'''Ta\}_2(\mu,\eta^{6:6}\text{-}P_6)]$ (**B**, 20%) and $[\{Cp'''Ta\}_3(\mu_3,\eta^{1:1:1:1:1:1}\text{-}P_4)(\mu_3,\eta^{1:1:1}\text{-}P_2)]$ (**C**, 7%), **A** was isolated as a dark red solid in 41% yield. Assessing the *cyclo*-P_8 ligand´s potential for coordination chemistry, it was reacted with excess $[W(CO)_5(thf)]$ (Scheme 2). The major product of this reaction is the tetranuclear $[\{Cp'''Ta\}_2(\mu_4,\eta^{2:2:2:2:1:1:1:1}\text{-}P_8)\{W(CO)_5\}_2]$ (**1**). However, the chromatographic separation of **1**

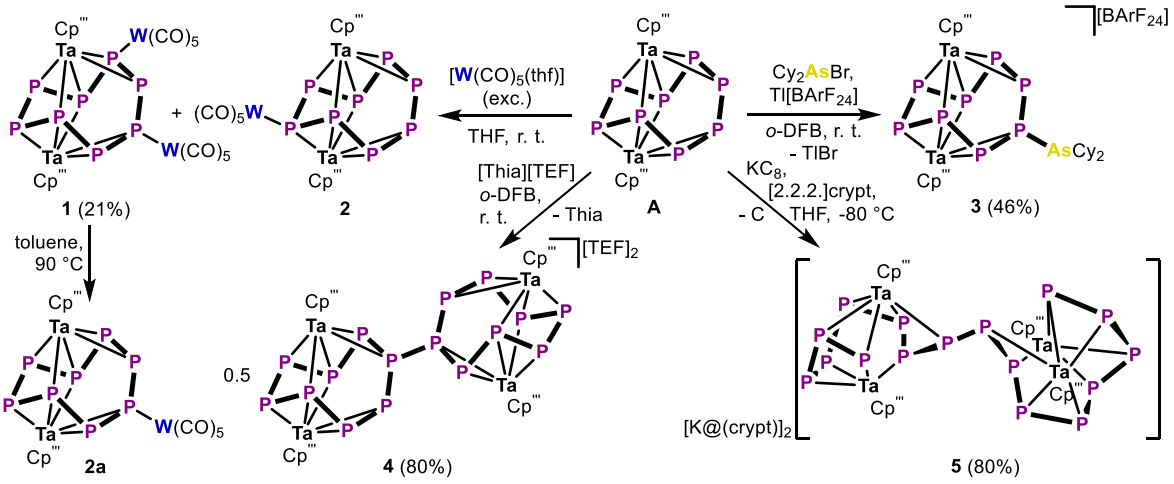

*Scheme 2: Reactivity of **A** towards the Lewis acid [W(CO)$_5$(thf)], its electrophilic functionalization with [AsCy$_2$]$^+$, and its redox chemistry.*

from the trinuclear side product [{Cp'''Ta}$_2$(μ_3,$\eta^{2:2:2:2:1:1:1}$-P$_8$){4-W(CO)$_5$}] (**2**), which decomposes during workup, is difficult and results in rather low isolated yields of 21%. Interestingly, thermolysis of **1** affords cleavage of only one {W(CO)$_5$} fragment, and formation of [{Cp'''Ta}$_2$(μ_3,$\eta^{2:2:2:2:1:1:1}$-P$_8$){1-W(CO)$_5$}] (**2a**), which can be followed spectroscopically. These results suggested that the selective functionalization of **A** could also be achieved with Lewis-acidic cationic main group electrophiles. Indeed, **A** reacts with the *in situ* generated [Cy$_2$As]$^+$ to form [{Cp'''Ta}$_2$(μ,$\eta^{2:2:2:2:1:1}$-P$_8$(1-AsCy$_2$)][BArF$_{24}$] (**3**, [BArF$_{24}$]$^-$ = [B{3,5-(CF$_3$)$_2$C$_6$H$_3$}$_4$]$^-$) in 46% crystalline yield. As redox-mediated aggregation/dimerization has been observed for smaller P$_n$ ligand complexes,[15,18] utilization of **A** would allow the preparation of extended polyphosphorus structures. Chemical oxidation of **A** affords the dimeric [{Cp'''Ta}$_4$(μ_4,$\eta^{2:2:2:2:2:2:2:1:1:1:1}$-P$_{16}$)][TEF]$_2$ (**4**, (80%), [TEF]$^-$ = [Al{OC(CF$_3$)$_3$}$_4$]$^-$) which shows a newly formed P1–P1' bond. Notably, **4** displays the largest cationic polyphosphorus arrangement known to date. On the other hand, the reduction of **A** with KC$_8$ also results in dimerization, furnishing [K@[2.2.2]cryptand]$_2$[{Cp'''Ta}$_4$(μ_4,$\eta^{2:2:2:2:2:2:2:2:1:1:1:1}$-P$_{16}$)] (**5**, 80%, Scheme 2). **5**, however, reveals a bond formation via the more encumbered P4 atoms, accompanied by the cleavage of the former P4–P4' bond within **A**. Thus, **5** features an unprecedented P$_{16}$ chain, which is solely stabilized by the coordination to the {Cp'''Ta} moieties. Crystallization of the compounds **A**, **1**, **3**, **4** and **5** allowed their X-ray crystallographic structure determination (Figure 1).[19] The central structural motif of **A** is a puckered *cyclo*-P$_8$ ligand coordinated by the two Ta atoms. The P–P bond lengths within the P$_8$ cycle are roughly alternating in length (P1–P1´ = 2.243(1) Å, P1–P2 = 2.145(1) Å, P2–P3 = 2.196(1) Å, P3–P4 = 2.170(1) Å, P4–P4´ = 2.444(2) Å), reminiscent of the isolobal relationship to COT. Thus, the more coordinated P1–P2 and P3–P4 bonds are closer to the expected bond lengths for a P–P double bond than the residual P–P single bonds. The newly formed P–W bonds in **1** are in the expected range (2.510(2) – 2.570(2) Å),[20] while the structural core remains intact upon coordination of the {W(CO)$_5$} moieties. Similarly, the arsenium functionalization in **3** has only a minor impact on the structure of the *cyclo*-P$_8$ ligand with the newly formed P1–As bond length

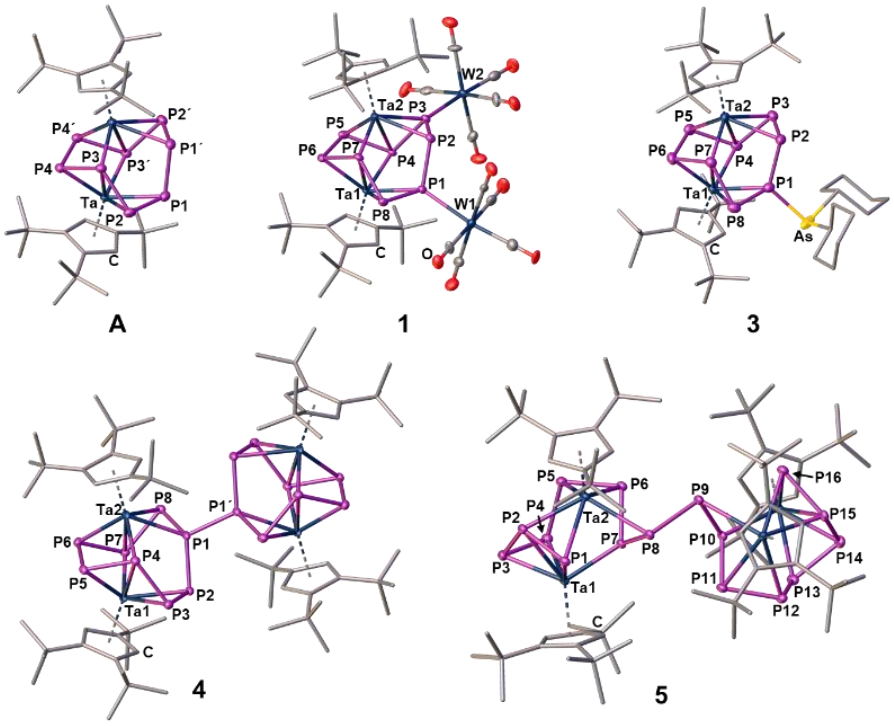

*Figure 1: Molecular structures of **A**, **1**, **3**, **4** and **5** in the solid state, H atoms and counterions are omitted for clarity and ellipsoids are drawn at the 50% probability level.*

(2.301(4) Å) agreeing with a single bond.[20] The oxidized species **4** features a large bicyclic P_{16} ligand, comprising two *cyclo*-P_8 moieties linked via a central P–P single bond (2.201(2) Å).[20] The P1–P2 bond in **4** is shortened (2.178(1) Å), while the residual P–P bonds remain similar in length upon oxidation. In contrast, the dianion in **5** also arises from the dimerization of **A**, however, the new P8–P9 bond (2.269(1) Å) is formed via the former P4 (in **A**) atoms. Additionally, the P1–P8 (3.222(1) Å) as well as the P9–P16 (3.263(2) Å) distances indicate complete P–P bond fission, thus leading to an unsubstituted P_{16} chain. Notably, while long chain-type polyphosphides have been described,[21] the P_{16} ligand in **5** is by far the longest linear polyphosphorus chain known to date.

Multinuclear NMR studies of **A** in CD_2Cl_2 reveal the preservation of its C_2 symmetry in solution. Moreover, the $^{31}P\{^1H\}$ NMR spectrum of **A** features an AA'MM'QQ'XX' spin system for the symmetrical *cyclo*-P_8 ligand. In contrast, this symmetry is revoked within the $\{W(CO)_5\}$ coordinated species **1**, **2a** and **2**. The $^{31}P\{^1H\}$ NMR spectrum of **1** reveals the presence of two species in solution at –80 °C which, however, coalesce at room temperature (see SI). As both species feature similar ABMNOPQX spin systems, this behavior is attributed to rotationally hindered Cp''' ligands consistent with the presence of two diastereomers (see SI), which are in rapid exchange at room temperature. Additional $^1J_{P\text{-}W}$ coupling for P_A and P_X corroborates the structural integrity of **1** in solution. Similarly, the $^{31}P\{^1H\}$ NMR spectra of **2a** and **2** show complex ACGMNSTX and AMNQRSTU spin systems, respectively, yet with only one $^1J_{P\text{-}W}$ coupling each. This allows the determination of **2a** as the respective 1-$\{W(CO)_5\}$ and **2** as the 4-$\{W(CO)_5\}$ isomer. Analogously, the arsenium functionalization in **3** leads to an AMNOPQRX spin system in the $^{31}P\{^1H\}$ NMR spectrum, bearing the $\{AsCy_2\}$ substituent at P_M.

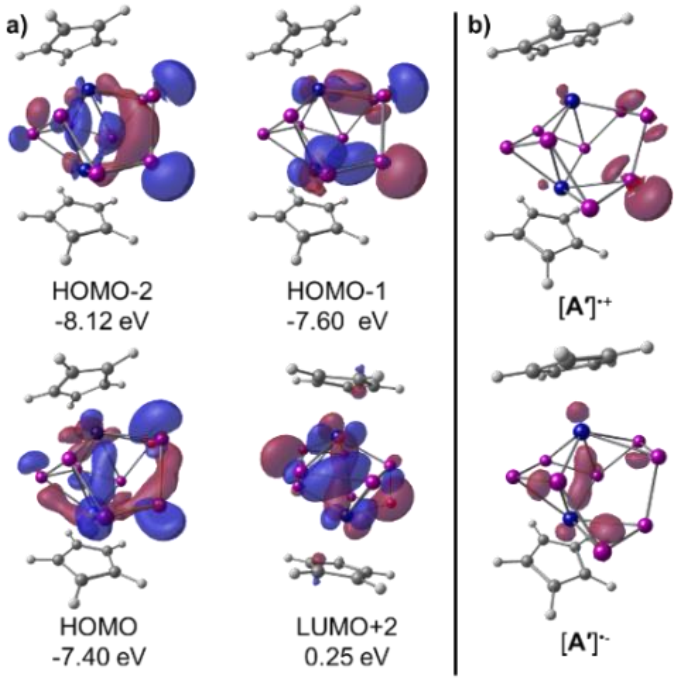

*Figure 2: a) Molecular frontier orbitals of **A'**; b) Spin densities of [**A'**]$^+$ and [**A'**]$^-$; calculated at the ωB97X-D3/def2-TZVP level of theory, surfaces are drawn at isovalues of 0.005 (MOs) and 0.008 (spin densities).*

The much larger dicationic complex **4** reveals broad and overlapping signals in the $^{31}P\{^1H\}$ NMR spectrum as well as a set of signals consistent with rotationally fixed Cp''' ligands in the ^1H NMR spectrum. This is in line with a rapid exchange between two diastereomers formed by rotationally hindered Cp''' ligands as in **1** (see SI). However, this exchange process cannot be resolved for **4**, not even at low temperatures (–80 °C, see SI). In contrast, **5** rapidly decomposes upon dissolution in common solvents, hampering its spectroscopic characterization. However, the combustion analysis of crystalline **5** confirms its composition.

To obtain insight into the electronic structure and reactivity of **A**, DFT calculations on the model system [{CpTa}$_2$(μ,$\eta^{2:2:2:2:1:1}$-P_8)] (**A'**) were performed (see SI). The WBIs for the P–P bonds in **A'** (0.85 – 1.06) corroborate its formulation as a *cyclo*-P_8 ligand complex, with only the P4–P4' bond exhibiting slightly lower values (0.51). The HOMOs of **A'** demonstrate a strong p(P1/1') contribution (Figure 2a), explaining the reactivity of **A** towards Lewis acids and cationic electrophiles. On the other hand, the P4–P4' character of the LUMO+2 of **A'** as well as the calculated spin density for the initial reduction product [**A'**]$^{\bullet-}$ (Figure 2, right) reveal a tendency for the cleavage of the latter bond. Thus, both the oxidation and the reduction of **A'** lead to a dimerization via P–P bond formation involving P1 or P4, and the newly formed P–P bonds showing WBIs of 0.86 and 0.94, respectively. However, the comparably low calculated bond dissociation energy for **5** (ΔG = -74.55 kJ/mol, see SI) corroborates its labile character.

Moreover, the large *cyclo*-P_8 ligand in **A** was hypothesized to potentially serve as a source of extremely reactive P_2 via ring contraction to **B**. Although P_2 is a highly versatile building block in organophosphorus chemistry, only a handful of compounds are known to liberate molecular P_2 under certain conditions,[22] while remaining stable enough to be stored. Indeed, the mild

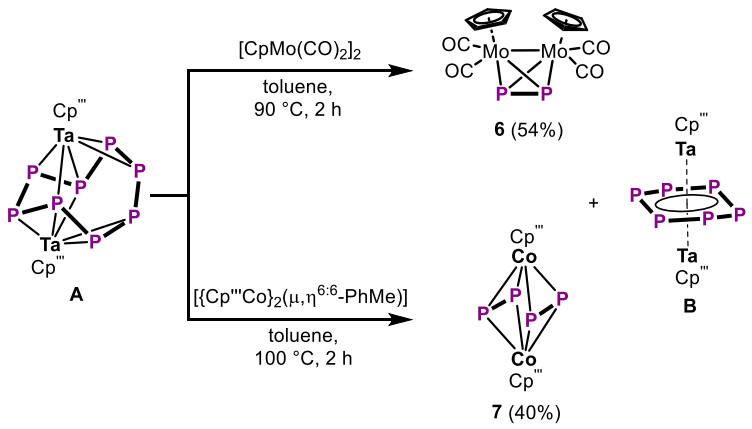

*Scheme 3: Thermolysis of **A** with [{Cp'''Co}$_2$(μ,η$^{6:6}$-PhMe)] demonstrating the potential of **A** as a P$_2$ synthon.*

thermolysis of **A** with [CpMo(CO)$_2$]$_2$[23] or [{Cp'''Co}$_2$(μ,η$^{6:6}$-PhMe)][24] proceeds rapidly affording [{CpMo(CO)$_2$}$_2$(μ,η$^{2:2}$-P$_2$)][8a] (**6**, 54% by NMR)[25] or [{Cp'''Co}$_2$(μ,η$^{2:2}$-P$_2$)$_2$][12c] (**7**, 40% by NMR), respectively (Scheme 3). Accordingly, the formation of **B** is observed spectroscopically, indicating the clean release of P$_2$ from **A**.

8.4. Conclusion

In summary, the synthesis and characterization of [{Cp'''Ta}$_2$(μ,η$^{2:2:2:2:1:1}$-P$_8$)] (**A**) is reported. **A** is the first compound featuring a *cyclo*-P$_8$ ligand, which is the largest monocyclic polyphosphorus species known to date revealing a COT-like arrangement and bonding character. Reaction of **A** with [W(CO)$_5$(thf)] combined with computational studies discloses the energetically most accessible P-centered lone pairs. These findings allowed the selective electrophilic functionalization of **A** yielding [{Cp'''Ta}$_2$(μ,η$^{2:2:2:2:1:1}$-P$_8$(1-AsCy$_2$))][BArF$_{24}$] (**3**). Exploiting the redox reactivity of **A** allowed the isolation of dicationic [{Cp'''Ta}$_4$(μ$_4$,η$^{2:2:2:2:2:2:2:1:1:1:1}$-P$_{16}$)][TEF]$_2$ (**4**) as well as dianionic [K@[2.2.2]cryptand]$_2$[{Cp'''Ta}$_4$(μ$_4$,η$^{2:2:2:2:2:2:2:2:1:1:1:1}$-P$_{16}$)] (**5**) compounds. While **4** represents the largest cationic polyphosphorus cage species reported to date, the P$_{16}$ chain in **5** constitutes the longest unsubstituted polyphosphorus chain so far. This highlights the synthetic utility of **A** as a building block for even larger polyphosphorus architectures. Completing this synthetic survey, **A** was demonstrated to be an efficient precursor transferring molecular P$_2$ units upon ring contraction.

8.5. Supporting Information

8.5.1. Experimental Procedures

General Considerations

All manipulations were carried out using standard Schlenk techniques at a Stock apparatus under N_2 as an inert gas or in a glove box with Ar atmosphere. All glassware was dried with a heat gun (600 °C) for at least 30 min prior to use. *o*-DFB (1,2-difluorobenzene) was distilled from P_2O_5, CD_2Cl_2 was distilled from CaH_2 and other solvents were directly taken from an MBraun SPS-800 solvent purification system and degassed at room temperature. Solution ^{1}H (400.130 MHz), ^{11}B (128.432 MHz) ^{13}C (100.627 MHz), ^{19}F (376.498 MHz), ^{29}Si (79.485 MHz), ^{31}P (161.976 MHz) and ^{77}Se (76.334 MHz) NMR spectra were recorded at an Avance400 (Bruker) spectrometer using $(H_3C)_4Si$ (^{1}H, ^{13}C, ^{29}Si), $BF_3{\cdot}OEt_2$ (^{11}B) $CFCl_3$ (^{19}F), $SeMe_2$ (^{77}Se) or 85% phosphoric acid (^{31}P), respectively, as external standards. Chemical shifts (δ) are provided in parts per million (ppm) and coupling constants (*J*) are reported in Hertz (Hz). Chemical shifts and coupling constants for all $^{31}P\{^{1}H\}$ and ^{31}P NMR spectra were derived from spectral simulation using the built-in simulation package of TopSpin3.2. The following abbreviations are used: s = singlet, d = doublet, dd = doublet of doublets, dt = doublet of triplets, t = triplet, td = triplet of doublets br = broad and m = multiplet. Mass spectra were recorded at the internal mass spectrometry department using a ThermoQuest Finnigan TSQ 7000 (ESI), Finnigan MAT 95 (LIFDI), or Finnigan MAT SSQ 710 A (EI) mass spectrometer or by the first author on a Waters Micromass LCT ESI-TOF mass-spectrometer and peak assignment was performed using the Molecular weight calculator 6.50.[26] IR spectra were recorded on a VARIAN FTS-800 FT-IR spectrometer, in the form of KBr discs or in solution. Cyclic voltammetry measurements were performed in *o*-DFB solution with $[NBu_4][PF_6]$ (0.1 M) as supporting electrolyte. The redox pair of ferrocene ($Fc^{0/+}$ = 0.000 V) was applied as reference. Elemental analysis of the products was conducted by the elemental analysis department at the University of Regensburg using an Elementar Vario EL. The starting materials Tl[TEF],[27] Cy_2AsCl,[28] [Thia][TEF][18b], [{Cp'''Co}(C_7H_8)][24], Tl[$BArF_{24}$][29] and [$CpMo(CO)_2]_2$[23] were synthesized according to literature procedures. Cp'''$Ta(CO)_4$ was prepared following the protocol developed for the previously reported Cp'' analog.[30] All other chemicals were purchased from commercial vendors and used without further purification.

Thermolysis of [Cp'''Ta(CO)$_4$] with P$_4$

A solution of [Cp'''Ta(CO)$_4$] (1.10 g, 2.09 mmol) in 50 mL DIB was slowly added to a refluxing solution of P$_4$ (1.29 g, 10.45 mmol) in 70 mL DIB through the reflux condenser. The mixture was refluxed for 2 h until the carbonyl bands in the IR spectrum had disappeared. After stirring for 30 min at room temperature the solvent was removed at 60 °C upon distillation under vacuum. In the $^{31}P\{^1H\}$ NMR spectrum (C_6D_6) of the reaction mixture the signals of complexes **A**, **B** and **C** were observed. The resulting brown residue was adsorbed on silica gel. A subsequent column chromatographic separation of the solid (hexane, 21 × 3 cm) eluted traces of unreacted **A** (35 mg) first. This was followed by a yellow fraction of **B** (209 mg). With hexane/toluene (5:1) a green fraction was eluted containing complex **C** (72 mg). Finally, toluene eluted a reddish brown fraction of **A** (456 mg). Crystals of **A** and **B** suitable for X-ray diffraction analysis were obtained for both compounds from CH_2Cl_2 solutions.

Analytical data of [(Cp'''Ta)$_2$(μ;$\eta^{6:6}$ -P$_6$)] (**B**):

Yield:	209 mg (20%)
^{1}H-NMR (C_6D_6, 300 K):	δ [ppm] = 5.04 (s, 4 H; C*H*), 1.22 (s, 36 H; *t*Bu), 1.13 (s, 18 H; *t*Bu)
^{31}P{^{1}H}-NMR (C_6D_6, 300 K):	δ [ppm] = 28.4 (s)
LIFDI-MS (toluene):	*m/z* (%) = 1014.2 (100) [M^+]
Elemental analysis:	Calculated (%) for $C_{34}H_{58}P_6Ta_2$ (1014.56 g/mol): C 40.25, H 5.76; found: C 39.99, H 5.60

Analytical data of [(Cp'''Ta)$_3$(μ_3-$\eta^{1:1:1:1:1:1}$-P$_4$)(μ_3-$\eta^{1:1:1}$-P$_2$)] (**C**):

Yield:	72 mg (7%)
^{1}H-NMR (C_6D_6, 300 K):	δ [ppm] = 6.17 (s, 2 H; C*H*), 5.19 (s, 2 H; C*H*), 5.15 (s, 2 H; C*H*), 1.66 (s, 18 H; *t*Bu), 1.46 (s, 18 H; *t*Bu), 1.42 (s, 9 H; *t*Bu), 1.26 (s, 18 H; *t*Bu), 1.18 (s, 18 H; *t*Bu)
^{31}P{^{1}H}-NMR (C_6D_6, 300 K):	δ [ppm] = 701.7 (d, $^1J_{PP}$ = 467 Hz, 1 P), 261.2 (d, $^1J_{PP}$ = 357 Hz, 2 P), 166.2 (d, $^1J_{PP}$ = 347 Hz, $^2J_{PP}$ = 14 Hz, 1 P), −25.5 (d, $^1J_{PP}$ = 467 Hz, $^2J_{PP}$ = 14 Hz, 1 P), −444.2 (dt, $^1J_{PP}$ = 357 Hz, $^1J_{PP}$ = 347 Hz, 1 P)
LIFDI-MS (toluene/CH_2Cl_2):	*m/z* (%) = 1428.5 (86) [M^+], 1460.4 (100) [M^++O_2] (injection done in air)

Analytical data of [(Cp'''Ta)$_2$(μ-$\eta^{2:2:2:2:1:1}$-P$_8$)] (**A**):

Yield:	456 mg (41%)
^{1}H-NMR (CD_2Cl_2, 300 K):	δ [ppm] = 5.31 (s, 2 H; C*H*), 4.42 (s, 2 H; C*H*), 1.44 (s, 18 H; *t*Bu), 1.28 (s, 18 H; *t*Bu), 1.17 (s, 18 H; *t*Bu)
^{1}H-NMR (C_6D_6, 300 K):	δ [ppm] = 5.29 (s, 2 H; C*H*), 4.44 (s, 2 H; C*H*), 1.39 (s, 18 H; *t*Bu), 1.21 (s, 18 H; *t*Bu), 1.13 (s, 18 H; *t*Bu)

$^{31}P\{^{1}H\}$-NMR (CD_2Cl_2, 300 K):	δ [ppm] = 148.1 (m, 2 P; $P_A/P_{A'}$), 46.7 (m, 2 P; $P_M/P_{M'}$), 0.8 (m, 2 P; $P_R/P_{R'}$), −35.9 (m, 2 P; $P_X/P_{X'}$) (coupling constants are listed in Table S 1)
$^{31}P\{^{1}H\}$-NMR (C_6D_6, 300 K):	δ [ppm] = 152.3 (m, 2 P; $P_A/P_{A'}$), 48.6 (m, 2 P; $P_M/P_{M'}$), 4.6 (m, 2 P; $P_R/P_{R'}$), −39.2 (m, 2 P; $P_X/P_{X'}$)
EI-MS (70 eV, toluene/CH_2Cl_2):	*m/z* (%) = 1075.9 (59) [M^+], 1014.1 (100) [M^+-P_2], 983.1 (10) [M^+-P_3], 952.2 (30) [M^+-P_4], 538.1 (7) [M^{2+}], 507.1 (41) [M^{2+}-P_2], 123.9 (2) $[P_4]^+$
LIFDI-MS (toluene/CH_2Cl_2):	*m/z* (%) = 1076.2 (100) [M^+]
Elemental analysis:	Calculated (%) for $C_{34}H_{58}P_8Ta_2 \cdot 0.33\ CH_2Cl_2$: C 37.32 H 5.35; found: C 37.31 H 5.17

*Reaction of **A** with [W(CO)$_5$(thf)]*

A freshly prepared solution of [W(CO)$_5$(thf)] (0.028 mol/L, 0.56 mmol) in 20 mL THF was added to a stirred solution of **A** (203 mg, 0.189 mmol) in 20 mL THF at room temperature. After stirring the mixture over 2 h at room temperature the solvent was removed under reduced pressure. A thin-layer chromatography of a small part of the reaction mixture in a glove box revealed the presence of two reaction products: a brown-yellow spot (**2**) (toluene/hexane (1:2); R_f = 0.71), a brown-green spot (**1**) (toluene/hexane (1:2); R_f = 0.63). The NMR spectroscopic analysis of the reaction mixture showed a composition of **1** and **2** in a ratio of 1.7:1. During the column chromatographic workup (hexane/toluene (5:1), 26 × 3 cm) of the brown solid on silica gel compound **2** decomposed. Only a brown-green fraction of **1** could be isolated. After removal of the solvent under vacuum the resulting brown solid was dissolved in CH_2Cl_2, layered with hexane and stored in a freezer at −35°C. Dark brown sticks of **1** deposited within two weeks in the vessel. The crystals were isolated, washed with pentane (3 × 3 mL) and dried under vacuum at room temperature.

Analytical data of [(Cp'''Ta)$_2$(μ_4-$\eta^{2:2:2:2:1:1:1:1}$-P$_8$){W(CO)$_5$}$_2$] (**1**):

Yield:	67 mg (21%)
^{1}H-NMR (CD_2Cl_2, 300 K):	δ [ppm] = 5.75 (s, 1 H; C*H*), 5.52 (s, 1 H; C*H*), 5.38 (s, 1 H; C*H*), 4.69 (s, 1 H; C*H*), 1.56 (s, 9 H; *t*Bu), 1.49 (s, 9 H; *t*Bu), 1.40 (s, 9 H; *t*Bu), 1.38 (s, 9 H; *t*Bu), 1.37 (s, 9 H; *t*Bu), 1.17 (s, 9 H; *t*Bu)
^{31}P{^{1}H}-NMR (CD_2Cl_2, 300 K):	δ [ppm] = 125.8 (m, 1 P; P_A), 91.1 (m {br}, 1 P; P_B), 45.5 (m, 1 P; P_M), 29.0 (m, 1 P; P_N), 7.4 (m {br}, 2 P; P_O/P_P), −5.1 (m, 1 P; P_Q), −28.3 (m, 1 P; P_X). (coupling constants are listed in Table S 2**Fehler! Verweisquelle konnte nicht gefunden werden.**)
LIFDI-MS (toluene):	*m/z* (%) = 1723.8 (100) [M^+]
EI-MS (70 eV, toluene):	*m/z* (%) = 1400.0 (0.03) [*M*-W(CO)$_5$]$^+$, 1372.1 (0.05) [(Cp'''Ta)$_2$P$_8$W(CO)$_4$]$^+$, 1338.0 (0.03) [(Cp'''Ta)$_2$P$_6$W(CO)$_5$]$^+$, 1287.9 (0.07) [(Cp'''Ta)$_2$P$_8$W(CO)]$^+$, 1260.0 (2) [(Cp'''Ta)$_2$P$_8$W]$^+$, 1076.0 (5) [(Cp'''Ta)$_2$P$_8$]$^+$, 1014.0 (100) [(Cp'''Ta)$_2$P$_6$]$^+$, 507.2 (17) [(Cp'''Ta)$_2$P$_6$]$^{2+}$
IR (KBr):	$\tilde{\nu}$ [cm^{-1}] = 2067 (vs; CO), 2060 (vs; CO), 1987 (s; CO), 1979 (s; CO), 1920 (vs {br}; CO)
Elemental analysis:	Calculated (%) for $C_{44}H_{58}O_{10}P_8Ta_2W_2$: C 30.65, H 3.39; found: C 31.38, H 3.32

Analytical data of [(Cp'''Ta)$_2$(μ_3-$\eta^{2:2:2:2:1:1:1}$-P$_8$){4-W(CO)$_5$}] (**2**):

^{1}H-NMR (CD_2Cl_2, 300 K):	δ [ppm] = 5.94 (m, 1 H; C*H*), 5.66 (d, $^4J_{HH}$ = 3 Hz, 1 H; C*H*), 5.47 (m, 1 H; C*H*), 4.62 (m, 1 H; C*H*), 1.72 (s, 9 H; *t*Bu), 1.63 (s, 9 H; *t*Bu), 1.58 (s, 9 H; *t*Bu), 1.43 (s, 9 H; *t*Bu), 1.25 (s, 9 H; *t*Bu), 1.24 (s, 9 H; *t*Bu)
^{31}P{^{1}H}-NMR (CD_2Cl_2, 300 K):	δ [ppm] = 123.6 (m, 1 P; P_A), 63.7 (m, 1 P; P_M), 48.9 (m, 1 P; P_N), 20.3 (m, 1 P; P_Q), 10.3 (m, 1 P; P_R), −1.8 (m, 1 P; P_S), −5.4 (m, 1 P; P_T), −14.4 (m, 1 P; P_U)
LIFDI-MS (toluene):	*m/z* (%) = 1400.4 (100) [M^+]

*Thermolysis of **1***

A solution of **1** in toluene (0.7 mL) was heated to 90 °C in an NMR tube over 3 h. Thereby, the green-brown solution became brown and the signals of **1** disappeared. Concomitant, new signals of the thermolysis product **2a** appeared in the ^{31}P{^{1}H} NMR spectrum.

Analytical data of [(Cp'''Ta)$_2$(μ_3-$\eta^{2:2:2:2:1:1:1}$-P$_8$){1-W(CO)$_5$}] (**2a**):

^{1}H-NMR (toluene-d^8, 300 K):	δ [ppm] = 5.43 (d, $^4J_{HH}$ = 3 Hz, 1 H; C*H*), 5.08 (m, 1 H; C*H*), 4.62 (m, 1 H; C*H*), 4.47 (m, 1 H; C*H*), 1.37 (s, 18 H; *t*Bu), 1.27 (s, 9 H; *t*Bu), 1.24 (s, 9 H; *t*Bu), 1.10 (s, 9 H; *t*Bu), 1.05 (s, 9 H; *t*Bu)
^{31}P{^{1}H}-NMR (toluene-d^8, 300 K):	δ [ppm] = 136.7 (m, 1 P; P_A), 111.5 (m, 1 P; P_C), 61.6 (m, 1 P; P_G), 27.3 (m, 1 P; P_M), 23.6 (m, 1 P; P_N), −13.7 (m, 1 P; P_S), −15.9 (m, 1 P; P_T), −58.9 (m, 1 P; P_X)
LIFDI-MS (toluene):	*m/z* (%) = 1400.2 (100) [M^+]

*Synthesis of [{Cp'''Ta}$_2$(μ_3;$\eta^{2:2:2:2:1:1}$-P$_8$(1-AsCy$_2$))][BArF$_{24}$] (**3**)*

A (108 mg, 0.1 mmol, 1 eq.) and Tl[BArF$_{24}$] (107 mg, 0.1 mmol, 1 eq.) were dissolved in 2 mL of *o*-DFB and Cy$_2$AsBr (10 µL) was added carefully at room temperature. Immediate precipitation of white solid (TlBr) and a colour change of the solution to dark brown could be observed. The mixture was stirred for one hour at room temperature. Afterwards, 20 mL of *n*-pentane were added to precipitate a brownish oil. The supernatant was decanted, and the oily residue washed two times with 10 mL of *n*-pentane, each. After drying, the residue was dissolved in 2 mL of *o*-DFB, filtered and the resulting solution carefully layered with 20 mL of *n*-hexane. Storage for at room temperature for three weeks afforded dark brownish red crystals of [{Cp'''Ta}$_2$(μ_3;$\eta^{2:2:2:2:1:1}$-P$_8$(1-AsCy$_2$))][BArF$_{24}$] (**3**) in X-ray quality, which could be isolated upon decanting the supernatant and drying under reduced pressure (10^{-3} mbar).

Yield:	100 mg (46%)
^{1}H-NMR (CD_2Cl_2, 300 K):	δ [ppm] = 7.73 (br, 8 H, [BAr^F]$^-$), 7.57 (s, 4 H, [BAr^F]$^-$), 5.62 (m, 1 H, 1,2,4-^{t}Bu$_3$C$_5$H$_2$), 5.33 (m, 1 H, 1,2,4-^{t}Bu$_3$C$_5$H$_2$), 4.86 (m, 1 H, 1,2,4-^{t}Bu$_3$C$_5$H$_2$), 4.47 (m, 1 H, 1,2,4-^{t}Bu$_3$C$_5$H$_2$), 2.6–1.7 (several multiplets, 14 H, Cy), 1.55 (s, 9 H, 1,2,4-^{t}Bu$_3$C$_5$H$_2$), 1.44 (s, 9 H, 1,2,4-^{t}Bu$_3$C$_5$H$_2$), 1.34 (s, 9 H, 1,2,4-^{t}Bu$_3$C$_5$H$_2$), 1.31 (s, 9 H, 1,2,4-^{t}Bu$_3$C$_5$H$_2$), 1.30 (s, 9 H, 1,2,4-^{t}Bu$_3$C$_5$H$_2$), 1.22 (s, 9 H, 1,2,4-^{t}Bu$_3$C$_5$H$_2$)
^{31}P{^{1}H}-NMR (CD_2Cl_2, 300 K):	δ [ppm] = 160.9 (m, 1 P, P$_A$), 66.5 (m, 1 P, P$_M$), 65.0 (m, 1 P, P$_N$), 15.2 (m, 1 P, P$_O$), 7.5 (m, 1 P, P$_P$), -5.9 (m, 1 P, P$_Q$), -14.4 (m, 1 P, P$_R$), -45.3 (m, 1 P, P$_X$) (coupling constants are listed in Table S 3**Fehler! Verweisquelle konnte nicht gefunden werden.**)
^{31}P-NMR (CD_2Cl_2, 300 K):	δ [ppm] = 160.9 (m, 1 P, P$_A$), 66.5 (m, 1 P, P$_M$), 65.0 (m, 1 P, P$_N$), 15.2 (m, 1 P, P$_O$), 7.5 (m, 1 P, P$_P$), -5.9 (m, 1 P, P$_Q$), -14.4 (m, 1 P, P$_R$), -45.3 (m, 1 P, P$_X$)
ESI(+)-MS (*o*-DFB):	*m/z* (%) = 1317.5 (100) [*M*$^+$]
Elemental analysis:	Calculated (%) for $C_{78}H_{92}BF_{24}P_8AsTa_2$: C: 42.96, H: 4.25; found: C: 42.94, H: 3.79

*Oxidation of A to [{Cp'''Ta}$_4$(μ_4;$\eta^{2:2:2:2:2:2:2:2:1:1:1:1}$-P$_{16}$)][TEF]$_2$ (**4**)*

A (54 m, 0.05 mmol, 1 eq.) and [Thia][TEF] (59 mg, 0.05 mmol, 1 eq.) were weighed into one flask and 2 mL of CH_2Cl_2 were added to afford a rapid colour change to brownish red. After 10 min of stirring 30 mL of *n*-pentane were added to precipitate [{Cp'''Ta}$_4$(μ_4;$\eta^{2:2:2:2:2:2:2:2:1:1:1:1}$-P$_{16}$)][TEF]$_2$ (**4**) as a brown powder. The powder was washed with 10 mL of toluene and 10 mL of *n*-pentane three times, each, and then dried under reduced pressure (10^{-3} mar). The brown residue was dissolved in 1 mL of CD_2Cl_2 and subjected to multinuclear NMR spectroscopy. Afterwards, the solution was layered with 20 mL of *n*-pentane and stored at room temperature over night to give crystals of **4** in X-ray quality, which could be isolated after decanting the solution and drying under reduced pressure (10^{-3} mbar).

Yield:	82 mg (80%)
^{1}H-NMR (CD_2Cl_2, 300 K):	δ [ppm] = 6.03 (s, 1 H, 1,2,4-^{t}Bu$_3$C$_5$H$_2$), 5.86 (s, 1 H, 1,2,4-^{t}Bu$_3$C$_5$H$_2$), 5.80 (s, 1 H, 1,2,4-^{t}Bu$_3$C$_5$H$_2$), 5.42 (s, 1 H, 1,2,4-^{t}Bu$_3$C$_5$H$_2$), 5.40 (s, 1 H, 1,2,4-^{t}Bu$_3$C$_5$H$_2$), 5.30 (s, 1 H, 1,2,4-^{t}Bu$_3$C$_5$H$_2$), 5.05 (s, 1 H, 1,2,4-^{t}Bu$_3$C$_5$H$_2$), 5.01 (s, 1 H, 1,2,4-^{t}Bu$_3$C$_5$H$_2$), 1.62 (s, 9 H, 1,2,4-^{t}Bu$_3$C$_5$H$_2$), 1.61 (s, 9 H, 1,2,4-^{t}Bu$_3$C$_5$H$_2$), 1.53 (s, 9 H, 1,2,4-^{t}Bu$_3$C$_5$H$_2$), 1.45 (s, 18 H, 1,2,4-^{t}Bu$_3$C$_5$H$_2$), 1.42 (s, 9 H, 1,2,4-^{t}Bu$_3$C$_5$H$_2$), 1.35 (s, 9 H, 1,2,4-^{t}Bu$_3$C$_5$H$_2$), 1.32 (s, 27 H, 1,2,4-^{t}Bu$_3$C$_5$H$_2$), 1.22 (s, 18 H, 1,2,4-^{t}Bu$_3$C$_5$H$_2$)
^{31}P{^{1}H}-NMR (CD_2Cl_2, 300 K):	δ [ppm] = 173.2 (m), 153.7 (m), 66.4 (m), 40.9 (m), 31.7 (m), 12.7 (m), -0.6 (m), -21.2 (m), -26.5 (m), -29.7 (m) (see Figure S 19)
^{31}P-NMR (CD_2Cl_2, 300 K):	δ [ppm] = 173.2 (m), 153.7 (m), 66.4 (m), 40.9 (m), 31.7 (m), 12.7 (m), -0.6 (m), -21.2 (m), -26.5 (m), -29.7 (m)
ESI(+)-MS (*o*-DFB):	*m/z* (%) = 1076.1(100) [M^{2+}] (no signals for the mono cation are detected)
Elemental analysis:	Calculated (%) for $C_{100}H_{116}O_8F_{72}Al_2P_{16}Ta_4$: C 29.39, H 2.86; found: C 29.68, H 2.67

*Reduction of A to [K@crypt]$_2$[{Cp'''Ta}$_4$(μ_4;$\eta^{2:2:2:2:2:2:2:2:1:1:1:1}$-$P_{16}$)] (**5**)*

A (54 mg, 0.05 mmol, 1 eq.) and KC_8 (10 mg, 0.075 mmol, 1.5 eq.) were weighed into a Schlenk flask and 5 mL of THF were condensed upon the solids at –196°C. The mixture was allowed to slowly reach –80 °C and then stirred for 20 min resulting in a gradual colour change to dark grey/black. [2.2.2]-cryptand (19 mg, 0.05 mmol, 1 eq.) dissolved in 2 mL of precooled (–80°C) THF was added to the solution, which was then stirred at –80 °C for additional 30 min. Afterwards the solution was slowly warmed to room temperature, constrained to 2 mL under reduced pressure (10^{-3}mbar), and 30 mL of *n*-hexane added to afford precipitation of a dark solid. The supernatant was decanted, the solid dried and then redissolved in 3 mL of THF. Filtration gave a dark grey solution of [K@crypt]$_2$[{Cp'''Ta}$_4$(μ_4;$\eta^{2:2:2:2:2:2:2:2:1:1:1:1}$-$P_{16}$)] (**5**), which was layered with 20 mL of toluene and stored at room temperature for several hours. From this mixture **5** crystallized in X-ray quality and could be isolated after decanting the solvent and drying under reduced pressure (10^{-3} mbar).

Yield:	60 mg (80%)
Elemental analysis:	Calculated (%) for $C_{104}H_{188}N_4O_{12}P_{16}K_2Ta_4$ ·3 THF: C 43.53, H 6.68, N 1.75; found: C 43.24, H 6.47 N 1.82

As **5** decomposes rapidly upon dissolving crystals of this compound, no further spectroscopic or mass spectrometric details can be provided.

*Thermolysis of **A** with $[CpMo(CO)_2]_2$ and $[\{Cp'''Co\}_2(\mu,\eta^{6:6}\text{-PhMe})]$*

A (0.04 mmol, 43 mg, 1 eq.) and $[CpMo(CO)_2]_2$ (0.04 mmol, 17 mg, 1 eq.) were weighed into a Schlenk flask and dissolved in 5 mL of toluene. The brown solution was then heated to 90 °C for 2 h, constrained to 1 mL and then subjected to NMR spectroscopic analysis with a C_6D_6 capillary containing 0.002 mmol PPh_3. The ^{31}P NMR spectrum (Figure S21) of this solution clearly indicates the formation of $[\{CpMo(CO)_2\}_2(\mu,\eta^{2:2}\text{-}P_2)]$[8a] (**6**) in 54% yield. Additionally, the complex $[\{CpMo(CO)_2\}(\eta^3\text{-}P_3)]$[9] can be observed as a side product, which probably arises from the further reaction of **6** with the liberated P_2 from **A**.

A (0.05 mmol, 54 mg, 1 eq.) and $[\{Cp'''Co\}_2(\mu,\eta^{6:6}\text{-PhMe})]$ (0.05 mmol, 17 mg, 1 eq.) were weighed into a Schlenk flask and dissolved in 2 mL of toluene. The brown solution was then heated to 100 °C for 2 h, and 0.5 mL of this solution were subjected to NMR spectroscopic analysis with a C_6D_6 capillary containing 0.01 mmol PPh_3. The ^{31}P NMR spectrum (Figure S22) of this solution clearly indicates the formation of $[\{Cp'''Co\}_2(\mu,\eta^{2:2}\text{-}P_2)_2]$[12c] (**7**) in 40% yield.

8.5.2. X-ray Crystallographic Data

General Considerations

The crystallographic data for all described compounds were collected on a SuperNova diffractometer (Rigaku) with a Atlas^{S2} detector using Cu–K$_\alpha$ radiation (micro-focus sealed tube) (**A**), on a GV50 diffractometer (Rigaku) with a Titan^{S2} detector using Cu–K$_\alpha$ (**5**) or Cu–K$_\beta$ radiation obtained by using customised optics (**4**), an Xcalibur Gemini Ultra diffractometer with an Atlas^{S2} detector using Cu-K$_\alpha$ (**B**, **1**) radiation (sealed tube), or an XtaLAB Synergy R, DW System with a HyPix-Arc 150 detector using Cu-K$_\alpha$ radiation from a rotating anode (**3**). Data reduction and absorption correction were performed with the CrysAlisPro software package.[31] Structure solution and refinement was conducted in Olex2 (1.5-alpha)[32] with ShelXT[33] (solution) and ShelXL-2018/3[34] (least squares refinement (F^2)). All non-H atoms were refined with anisotropic displacement parameters and H atoms were treated as riding models with isotropic displacement parameters and fixed C–H bond lengths (sp^3: 0.96 (CH_3), 0.97 (CH_2); sp^2: 0.93 (CH)). Visualisation of the crystal structures was performed with Olex2 (1.5-alpha).[32]

CIF files with comprehensive information on the details of the diffraction experiments and full tables of bond lengths and angles for **A**, **B**, **1**, **3**, **4**, and **5** are deposited in Cambridge Crystallographic Data Centre under the deposition codes CCDC-2225834 (**A**), CCDC-2225835 (**B**), CCDC-2225836 (**1**), CCDC-2225837 (**3**), CCDC-2225838 (**4**) and CCDC-2225839 (**5**).

*Table S 1: Crystallographic and refinement details for compounds **A**, **B** and **1**.*

Compound	A	B	1
Empirical formula	$C_{41}H_{66}P_8Ta_2$	$C_{34}H_{58}P_6Ta_2$	$C_{44}H_{58}O_{10}P_8Ta_2W_2$
Formula weight	1168.60	1014.52	1724.25
Temperature/K	123.0(2)	123.0(10)	123(1)
Crystal system	monoclinic	monoclinic	orthorhombic
Space group	$C2/c$	$P2_1/n$	$Pna2_1$
a/Å	15.0257(4)	8.5617(1)	36.6216(8)
b/Å	25.8432(4)	11.8881(1)	11.2823(2)
c/Å	13.6833(4)	18.5854(1)	26.8981(10)
α/°	90.00	90	90
β/°	122.327(4)	92.030(1)	90
γ/°	90.00	90	90
Volume/Å3	4489.87(28)	1890.48(3)	11113.7(5)
Z	4	2	8
ρcalcg/cm3	1.729	1.782	2.061
μ/mm-1	11.739	13.052	17.109
F(000)	2312.0	996.0	6528.0
Crystal size/mm3	0.2169 × 0.166 × 0.0171	0.1 × 0.056 × 0.056	0.226 × 0.048 × 0.02
Radiation	CuKα (λ = 1.54178)	CuKα (λ = 1.54178)	CuKα (λ = 1.54178)
2Θ range for data collection/°	6.84 to 145.86	12.1 to 133.36	5.84 to 133.82
Index ranges	-18 ≤ h ≤ 17, -31 ≤ k ≤ 31, -16 ≤ l ≤ 16	-10 ≤ h ≤ 9, -14 ≤ k ≤ 13, -22 ≤ l ≤ 19	-42 ≤ h ≤ 28, -11 ≤ k ≤ 13, -30 ≤ l ≤ 31
Reflections collected	17525	13016	29918
Independent reflections	4444 [Rint = 0.0241, Rsigma = 0.0166]	3220 [Rint = 0.0321, Rsigma = 0.0231]	16247 [Rint = 0.0373, Rsigma = 0.0507]
Data/restraints/parameters	4444/0/253	3220/0/199	16247/67/1226
Goodness-of-fit on F2	1.039	1.058	1.023
Final R indexes [I>=2σ (I)]	R1 = 0.0197, wR2 = 0.0465	R1 = 0.0221, wR2 = 0.0514	R1 = 0.0303, wR2 = 0.0687
Final R indexes [all data]	R1 = 0.0220, wR2 = 0.0472	R1 = 0.0263, wR2 = 0.0528	R1 = 0.0353, wR2 = 0.0709
Largest diff. peak/hole / e Å-3	1.96/-0.97	1.14/-0.76	2.52/-0.77
Flack parameter	/	/	0.445(9)

*Table S 2: Crystallographic and rrefinement details foor compounds **A**, **B** and **1**.*

Compound	**3**	**4**	**5**
Empirical formula	$C_{78}H_{92}BF_{24}P_8AsTa2$	$C_{55}H_{70}AlF_{36}O_4P_8Ta_2$	$C_{104}H_{188}N_4O_{12}P_{16}K_2Ta_4$
Formula weight	2180.90	2115.75	2984.09
Temperature/K	100.00(10)	123.00(10)	123.01(10)
Crystal system	triclinic	monoclinic	triclinic
Space group	$P\bar{1}$	$P2_1/c$	$P\bar{1}$
a/Å	12.5850(2)	13.8517(2)	14.1190(2)
b/Å	18.4172(2)	17.3944(3)	15.4930(2)
c/Å	19.4711(3)	31.2933(5)	35.0834(4)
α/°	74.9520(10)	90	87.9770(10)
β/°	87.9360(10)	94.5120(10)	81.4590(10)
γ/°	88.7680(10)	90	74.8080(10)
Volume/Å3	4355.09(11)	7516.5(2)	7323.96(17)
Z	2	4	2
ρcalcg/cm3	1.663	1.870	1.353
μ/mm-1	7.182	6.114	7.884
F(000)	2160.0	4140.0	3012.0
Crystal size/mm3	0.15 × 0.1 × 0.08	0.53 × 0.38 × 0.06	0.392 × 0.158 × 0.062
Radiation	Cu Kα (λ = 1.54184)	Cu Kβ (λ = 1.39222)	Cu Kα (λ = 1.54184)
2Θ range for data collection/°	4.702 to 146.208	5.252 to 144.774	7.37 to 133.75
Index ranges	-14 ≤ h ≤ 15, -22 ≤ k ≤ 22, -21 ≤ l ≤ 24	-18 ≤ h ≤ 16, -23 ≤ k ≤ 22, -35 ≤ l ≤ 42	-16 ≤ h ≤ 16, -18 ≤ k ≤ 15, -41 ≤ l ≤ 40
Reflections collected	56080	36487	147906
Independent reflections	16743 [Rint = 0.0362, Rsigma = 0.0260]	18981 [Rint = 0.0514, Rsigma = 0.0546]	25840 [Rint = 0.1005, Rsigma = 0.0547]
Data/restraints/parameters	16743/286/1210	18981/0/928	25840/0/1315
Goodness-of-fit on F2	1.133	1.038	0.977
Final R indexes [I>=2σ (I)]	R1 = 0.0449, wR2 = 0.1270	R1 = 0.0439, wR2 = 0.1188	R1 = 0.0417, wR2 = 0.1040
Final R indexes [all data]	R1 = 0.0478, wR2 = 0.1289	R1 = 0.0469, wR2 = 0.1227	R1 = 0.0508, wR2 = 0.1101
Largest diff. peak/hole / e Å-3	1.32/-1.44	1.54/-1.17	1.48/-1.55
	/		

*[(Cp'''Ta)$_2$(μ-η^2:η^2:η^2:η^1:η^1-P$_8$)] (**A**)*

Complex **A** crystallizes in the monoclinic space group *C*2/*c* forming brown plates from toluene solutions at −35 °C. The asymmetric unit (Figure S1) contains half a molecule of **A** and half a toluene molecule, which is disordered over two positions. All non-hydrogen atoms were refined anisotropically and the H atoms were treated as riding models.

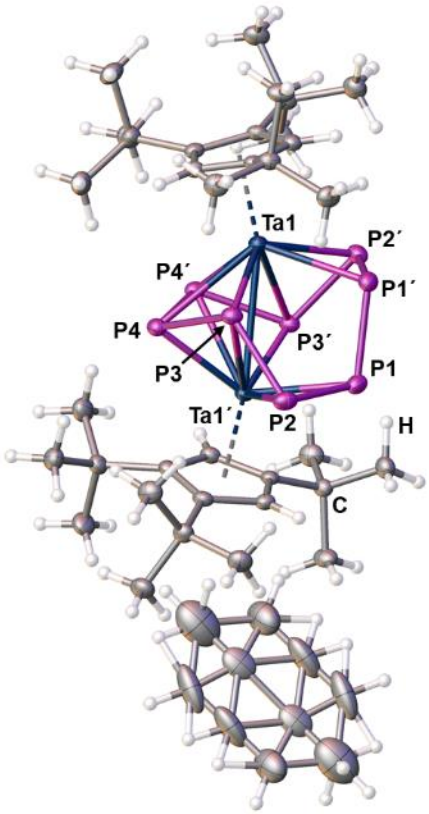

*Figure S 1: Solid state structure of **A**; Shown is the asymmetric unit containing one molecule **A** as well as one disordered toluene; thermal ellipsoids are drawn at the 50% probability level.*

*[(Cp'''Ta)$_2$(μ;η^6:η^6-P$_6$)] (**B**)*

Complex **B** crystallizes in the monoclinic space group *P*2$_1$/*n* forming yellow blocks from concentrated CH_2Cl_2 solutions. The asymmetric unit (Figure S2) contains half a molecule of **B**. All non-hydrogen atoms were refined anisotropically and the H atoms were treated as riding models.

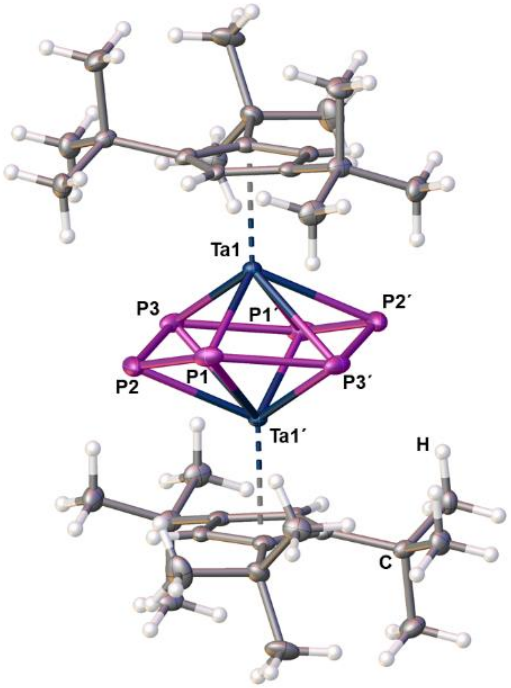

*Figure S 2: Solid state structure of **B**; Shown is the asymmetric unit containing one molecule **B**; thermal ellipsoids are drawn at the 50% probability level.*

*[(Cp'''Ta)$_2$(μ_4-η^2:η^2:η^2:η^1:η^1:η^1-P$_8$){W(CO)$_5$}$_2$] (**1**)*

Complex **1** crystallizes in the orthorhombic space group *Pna*2$_1$ forming brown rods from a CH_2Cl_2/pentane mixture at −35°C. The asymmetric unit (Figure S3) contains two enantiomeric molecules of **1**. All non-hydrogen atoms were refined anisotropically and the H atoms were treated as riding models.

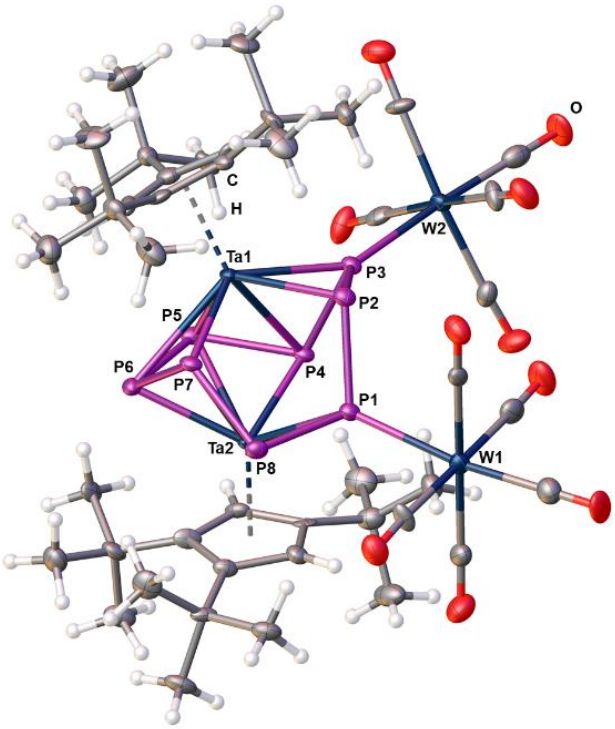

*Figure S 3: Solid state structure of **1**; Shown is half of the asymmetric unit, which contains two enantiomeric molecules of **1**; thermal ellipsoids are drawn at the 50% probability level.*

[{Cp'''Ta}$_2$(μ_3;$\eta^{2:2:2:2:1:1}$-P$_8$(1-AsCy$_2$))][BArF$_{24}$] (***3***)

Compound **3** crystallizes in the triclinic space group $P\bar{1}$ forming brownish red blocks from a *o*-DFB/*n*-hexane mixture at room temperature. The asymmetric unit (Figure S4) contains one anion and one cation. All non-hydrogen atoms were refined anisotropically and the H atoms were treated as riding models. Disorder within the anion as well as the –AsCy$_2$ moiety was refined using adequate restraints.

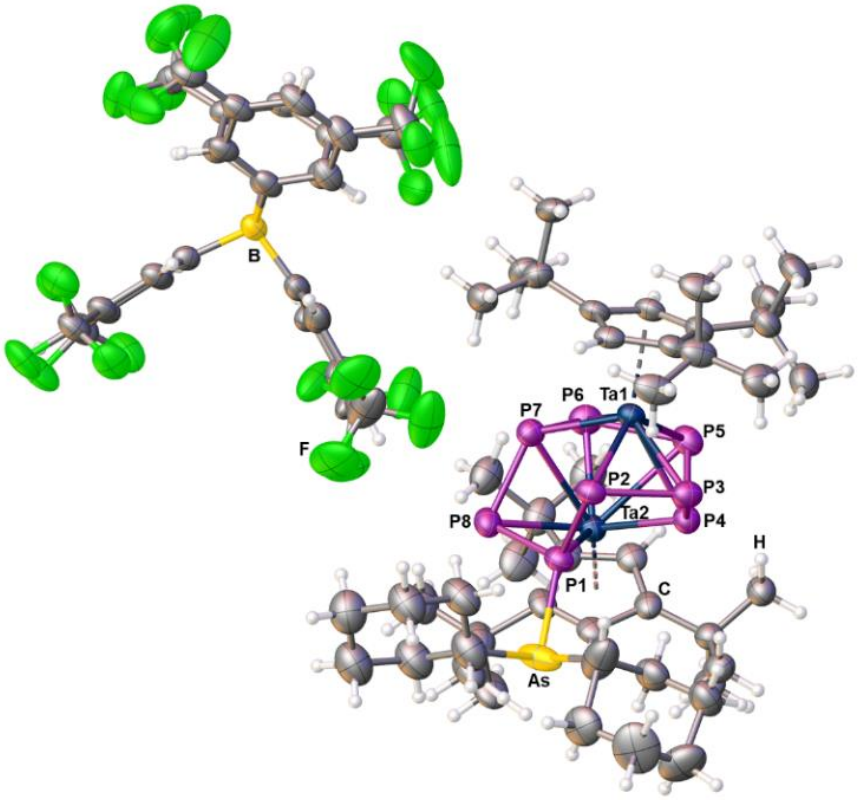

*Figure S 4: Solid state structure of **3**; Shown is the asymmetric unit containing one cation [**3**]$^+$ and one [BAr^F]$^-$ counter anion; thermal ellipsoids are drawn at the 50% probability level.*

[{Cp'''Ta}$_4$(μ_4;$\eta^{2:2:2:2:2:2:2:2:1:1:1:1}$-$P_{16}$)][TEF]$_2$ (***4***)

Compound **4** crystallizes in the monoclinic space group $P2_1/c$ forming dark brown plates from a CH_2Cl_2/*n*-pentane mixture at room temperature. The asymmetric unit (Figure S5) contains one anion, one half of the dication and one *n*-pentane molecule, which was treated with a solvent mask. All non-hydrogen atoms were refined anisotropically and the H atoms were treated as riding models.

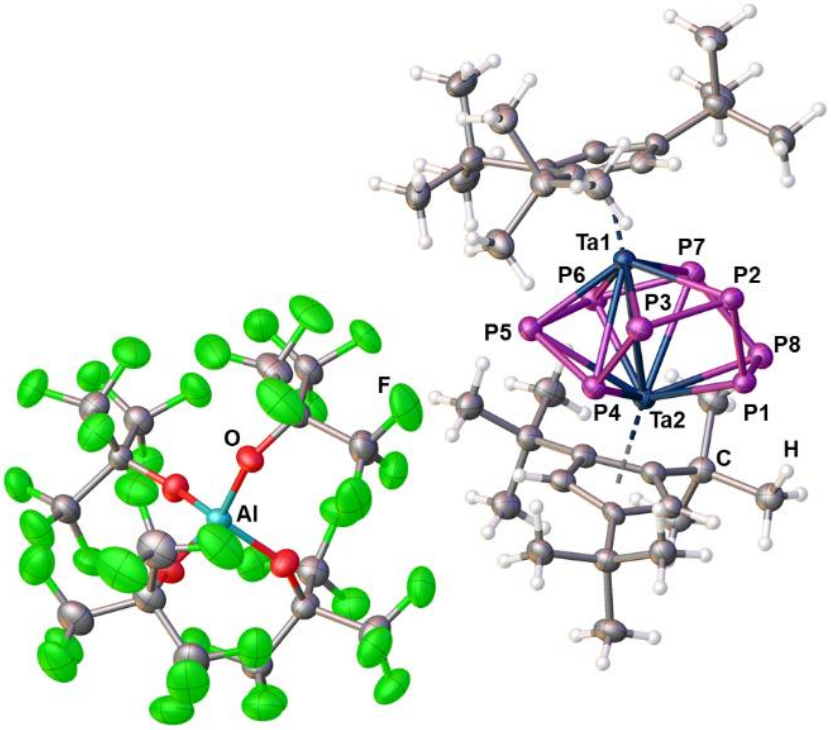

*Figure S 5: Solid state structure of **4**; Shown is the asymmetric unit containing half of the dication [**4**]$^{2+}$, one anion and one n-pentane molecule, which is omitted for clarity; thermal ellipsoids are drawn at the 50% probability level.*

[K@crypt]$_2$[{Cp'''Ta}$_4$(μ_4;$\eta^{2:2:2:2:2:2:2:2:1:1:1:1}$-P$_{16}$)] (***5***)

Compound **5** crystallizes in the triclinic space group $P\bar{1}$ forming greyish brown plates from a THF/toluene mixture at room temperature. The asymmetric unit (Figure S6) contains the dianion, two cations and five THF molecules, which were treated with a solvent mask. All non-hydrogen atoms were refined anisotropically and the H atoms were treated as riding models.

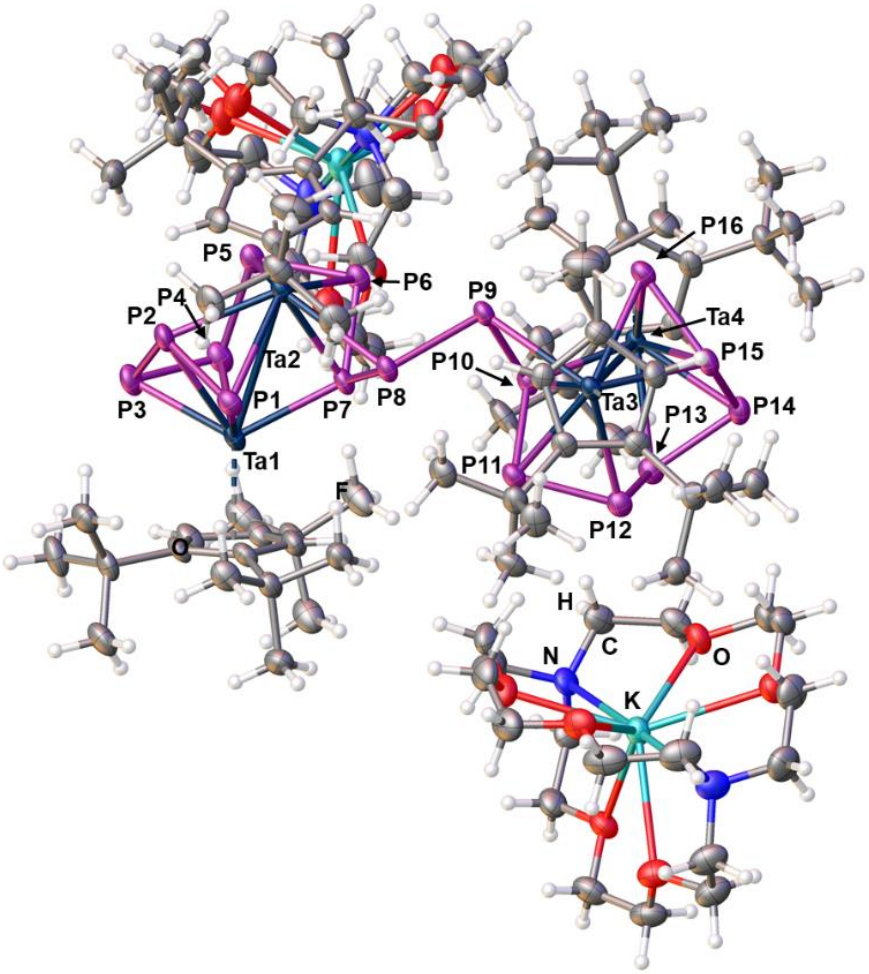

*Figure S 6: Solid state structure of **5**; Shown is the asymmetric unit containing one dianion [**5**]$^{2-}$ and two [K@crypt]$^+$ cations; five cocrystallized THF molecules are omitted for clarity; thermal ellipsoids are drawn at the 50% probability level.*

8.5.3. NMR Spectroscopic Investigations

*[(Cp'''Ta)$_2$(μ-η^2:η^2:η^2:η^1:η^1-P$_8$)] (**A**)*

The $^{31}P\{^1H\}$ as well as the ^{31}P NMR spectra of **A** in CD_2Cl_2 recorded at room temperature (Figure S7 and S8) reveal an AA´MM´QQ´XX´ spin system with signals centered at δ ppm = 148.1, 46.7, 0.8 and −35.9 for the C_2 symmetric *cyclo*-P_8 ligand. Spectral simulation of the $^{31}P\{^1H\}$ NMR spectrum allows to derive the $^nJ_{P-P}$ (n = 1, 2) coupling constants (Table S3). The corresponding $^{31}P\{^1H\}$-$^{31}P\{^1H\}$ COSY NMR spectrum (Figure S9) corroborates the connectivity of the P_8 ring.

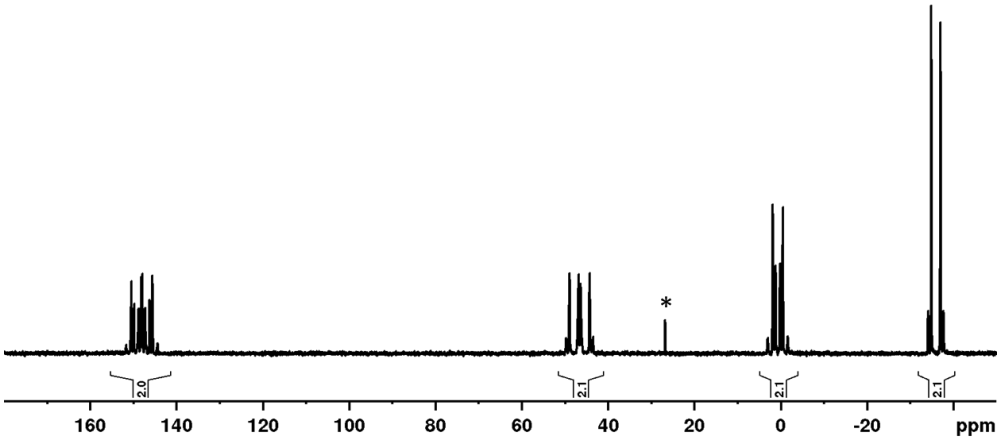

*Figure S 7: ^{31}P NMR spectrum of **A** in CD_2Cl_2 recorded at room temperature; * marks the signal of trace impurities of **B**.*

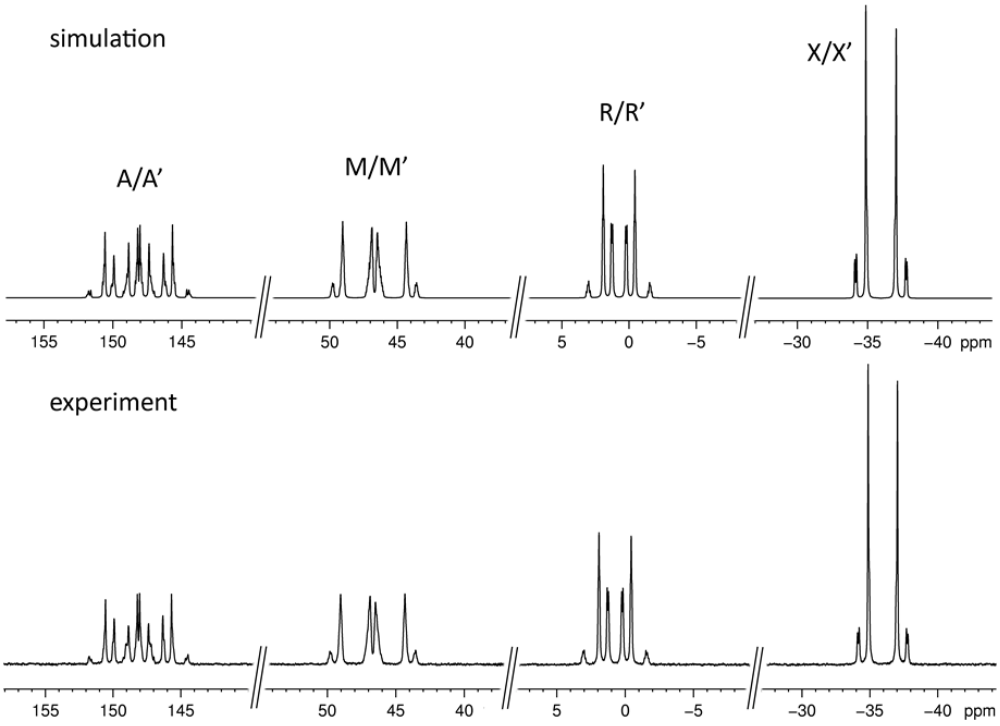

*Figure S 8: Simulated (top) and experimental (bottom) $^{31}P\{^1H\}$ NMR spectra of **A** in CD_2Cl_2 at room temperature.*

*Table S 3: Coupling constants derived from the simulation of the $^{31}P\{^{1}H\}$ NMR spectrum of **A**.*

$^{1}J_{PXPM}$ = 394.2 Hz	$^{1}J_{PMPA}$ = 421.4 Hz	$^{1}J_{PAPR}$ = 369.5 Hz
$^{1}J_{PRPR'}$ = −285.8 Hz	$^{1}J_{PXPX'}$ = 125.9 Hz	$^{2}J_{PXPA}$ = 7.2 Hz
$^{2}J_{PMPR}$ = 0.3 Hz	$^{2}J_{PAPR'}$ = 12.3 Hz	$^{2}J_{PXPM'}$ = −43.3 Hz
$^{3}J_{PXPR}$ = 1.6 Hz	$^{3}J_{PXPA'}$ = −12.5 Hz	$^{3}J_{PMPR'}$ = 19.2 Hz
$^{3}J_{PAPA'}$ = 16.0 Hz	$^{3}J_{PMPM'}$ = 12.1 Hz	$^{4}J_{PXPR'}$ = −6.4 Hz
$^{4}J_{PMPA'}$ = −12.4 Hz		

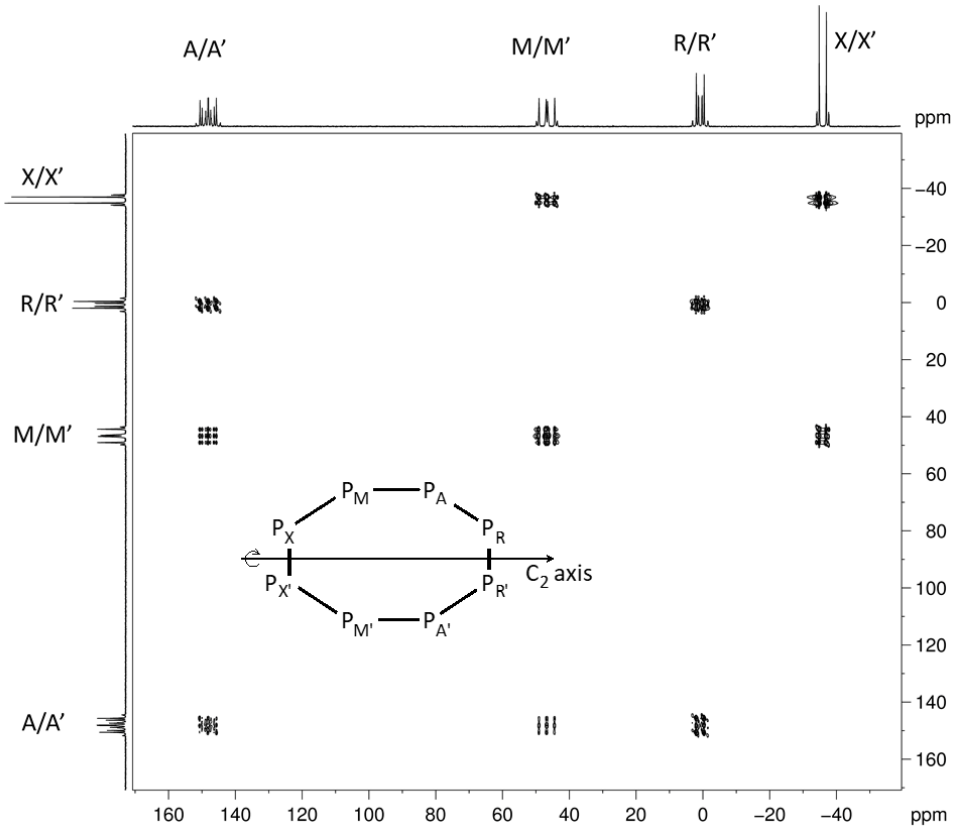

*Figure S 9: $^{31}P\{^{1}H\}$-$^{31}P\{^{1}H\}$ COSY NMR spectrum of **A** in CD_2Cl_2 at room temperature.*

*[(Cp'''Ta)$_2$(μ;η^6:η^6-P$_6$)] (**B**)*

The $^{31}P\{^1H\}$ NMR spectrum of **B** in C_6D_6 (Figure S10) reveals only one sharp singlet at δ/ ppm = 28.4 reminiscent of the rotational symmetry of its central *cyclo*-P_6 ligand.

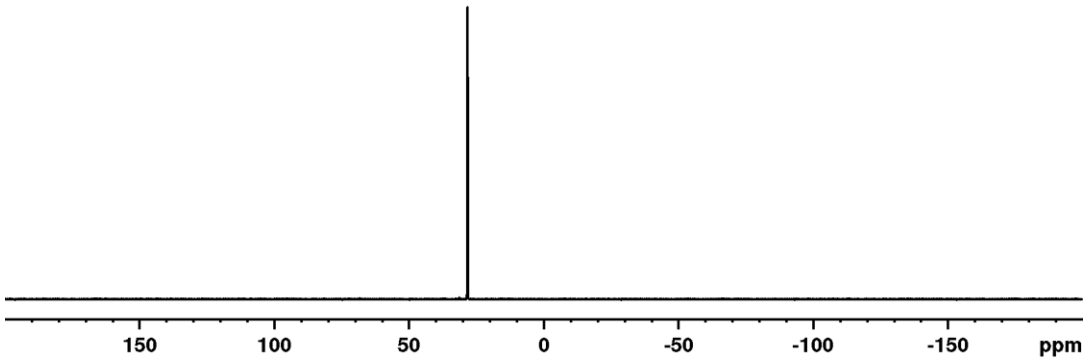

*Figure S 10: $^{31}P\{^1H\}$ NMR spectrum of **B** in C_6D_6 recorded at room temperature.*

*[(Cp'''Ta)$_3$(μ_3-$\eta^{1:1:1:1:1:1}$-P_4)(μ_3-$\eta^{1:1:1}$-P_2)] (**C**)*

The $^{31}P\{^1H\}$ NMR spectrum of **C** in C_6D_6 reveals five multiplets which agree with the structural assignment presented in Figure S11. Notably, the Cp'' derivative of this compound has already been reported previously.[35]

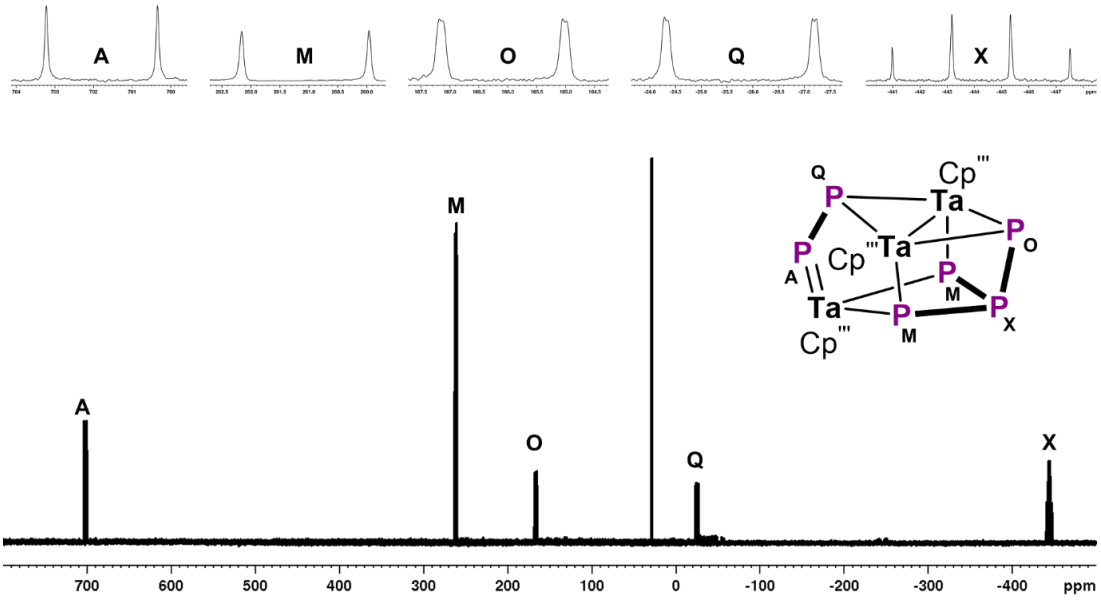

*Figure S 11: $^{31}P\{^1H\}$ NMR spectrum of **C** in C_6D_6 recorded at room temperature.*

*[(Cp'''Ta)$_2$(μ_4-$\eta^{2:2:2:2:1:1:1:1}$-P_8){W(CO)$_5$}$_2$] (**1**) and its thermolysis to [(Cp'''Ta)$_2$(μ_3-$\eta^{2:2:2:2:1:1:1}$-P_8){1-W(CO)$_5$}] (**2a**)*

The $^{31}P\{^1H\}$ NMR spectrum of **1** in CD_2Cl_2 (Figure S12) reveals the presence of two diastereomers **1I** and **1II** in solution, which arise from the hindered rotation of the planar chiral Cp''' ligands. While those dynamically interconvert at room temperature, this dynamic process (Figure S14) can be suppressed by cooling the solution to –80 °C. This allows the spectral simulation of the ABMNOPQX spin system of the major isomer **1I** and thus to derive the respective $^nJ_{P–P}$ (n = 1, 2) as well as $^1J_{P–W}$ coupling constants (Table S4). The connectivity of **1** is corroborated by the $^{31}P\{^1H\}$-$^{31}P\{^1H\}$ COSY NMR spectrum in CD_2Cl_2 recorded at –80 °C (Figure S13). Changing the solvent to tol-d^8 and heating the sample to 55 °C and then 90 °C leads to slow and then more rapid formation of **2a** under the release of one {W(CO)$_5$} moiety (Figure S15). This is indicated by observation of a new set of signals in the respective $^{31}P\{^1H\}$ NMR spectra consistent with an intact *cyclo*-P_8 ligand, which persist upon cooling the solution to room temperature (Scheme S1). Interestingly, the signals remain sharp at room temperature indicating unhindered rotation of the Cp''' ligands, which in conjunction with the W satellites allows the structural assignment of **2a**.

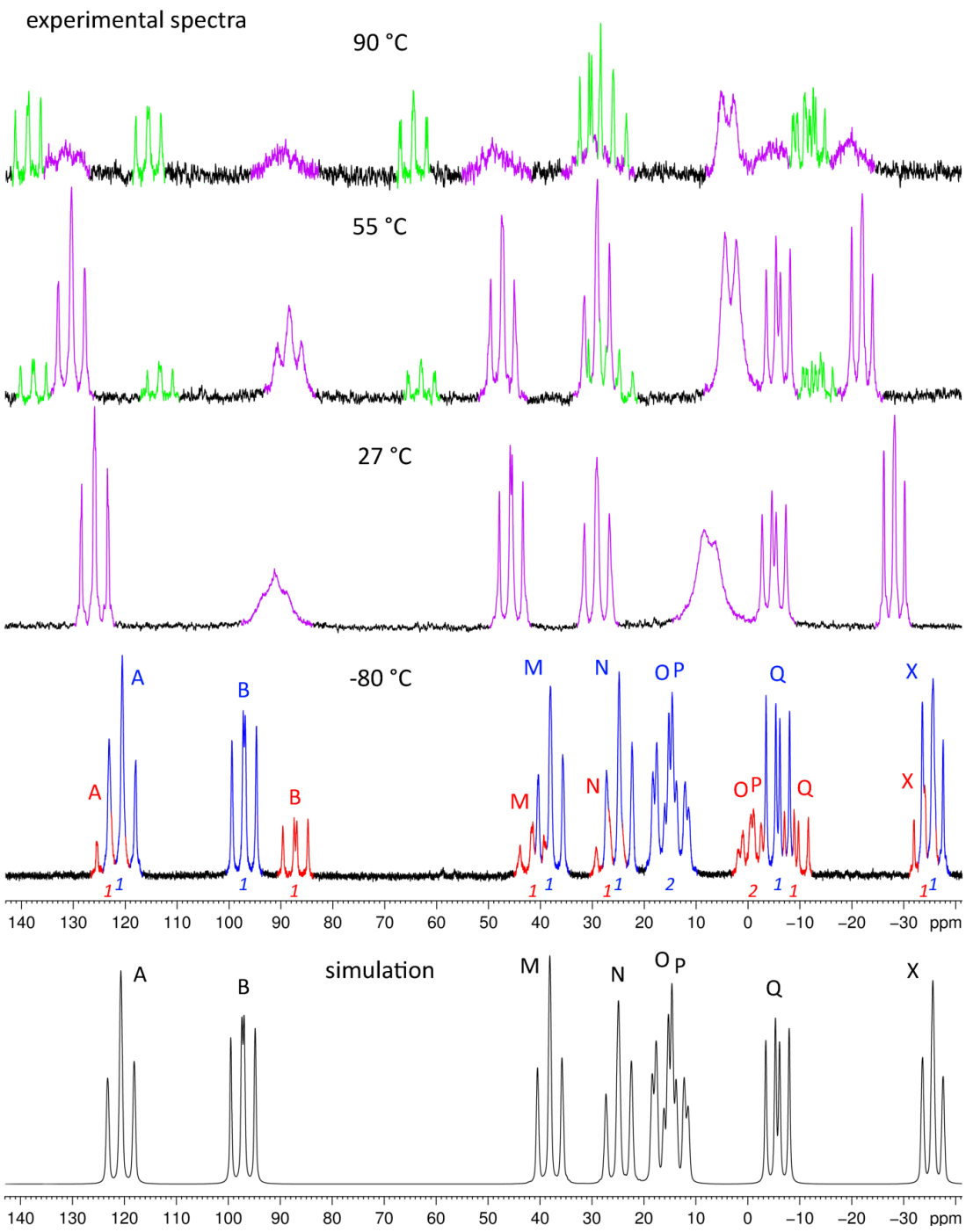

*Figure S 12: Selected temperature dependent $^{31}P\{^{1}H\}$ NMR spectra of **1** (−80 °C and 27 °C in CD_2Cl_2, 55 °C and 90 °C in tol-d^8) and the simulated spectrum (below) of the major species **1'** (blue) in the experimental spectrum at −80 °C. The blue and red signals belong to two diastereomers of **1**; The green signals belong to the decomposition product **2a**; Relative intensities are given below the signals.*

*Table S 4: Coupling constants determined from the simulated $^{31}P\{^{1}H\}$ NMR spectrum (Figure S 12) of the major species **1'** (blue) in the experimental spectrum of **1** at −80 °C; Due to the large linewidths of the signals only the coupling constants exceeding 40 Hz are given; The $^{1}J_{P\text{-}W}$ coupling constants were estimated from the experimental $^{31}P\{^{1}H\}$ NMR spectrum at 27 °C.*

$^{1}J_{PAPQ}$ = 429.8 Hz	$^{1}J_{PAPM}$ = 397.2 Hz	$^{1}J_{PMPO}$ = 378.2 Hz
$^{1}J_{POPP}$ = 126.1 Hz	$^{1}J_{PNPP}$ = 381.9 Hz	$^{1}J_{PBPN}$ = 420.1 Hz
$^{1}J_{PBPX}$ = 342.9 Hz	$^{1}J_{PQPX}$ = 299.8 Hz	$^{2}J_{PNPO}$ = −45.1 Hz
$^{2}J_{PMPP}$ = −42.0 Hz	$^{1}J_{PAW}$ = 218 Hz	$^{1}J_{PXW}$ = 165 Hz

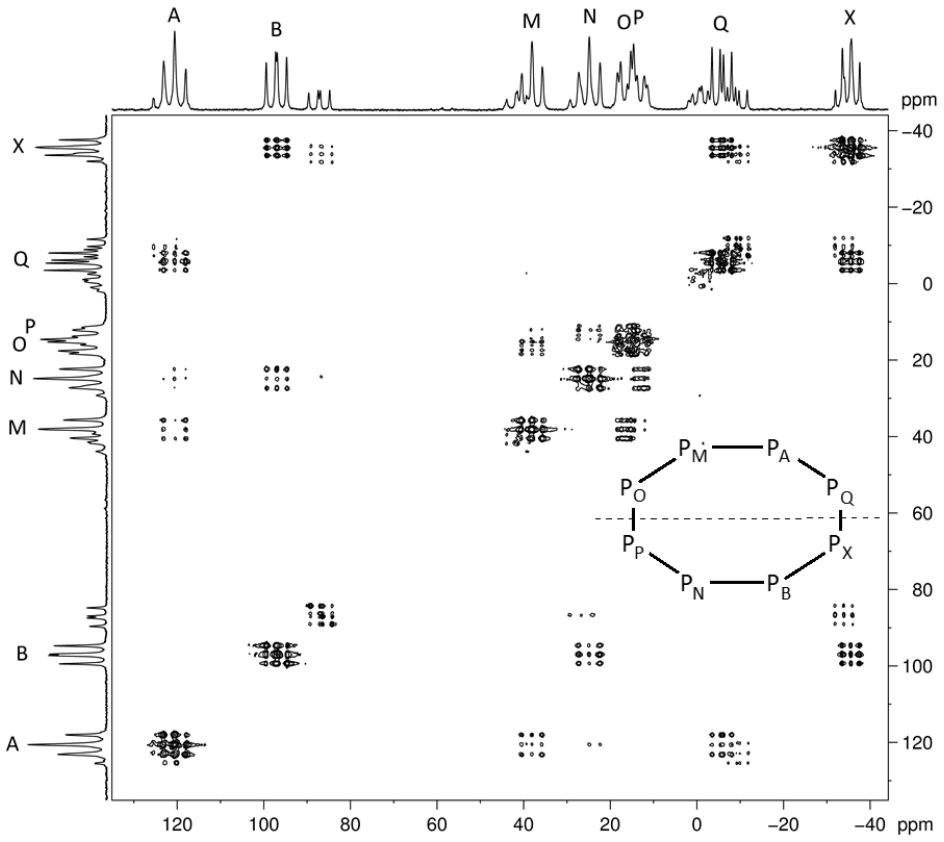

*Figure S 13: $^{31}P\{^{1}H\}$-$^{31}P\{^{1}H\}$ COSY NMR spectrum of **1** in CD_2Cl_2 recorded at room temperature.*

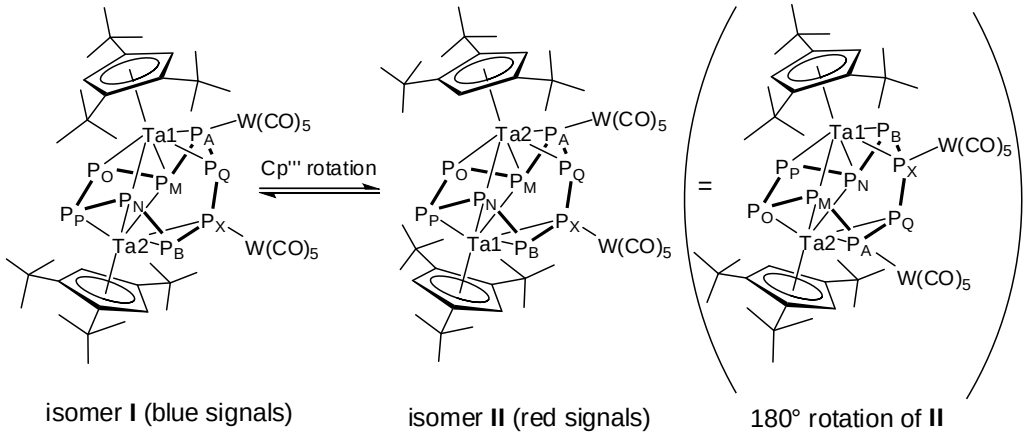

*Figure S 14: Dynamic process of complex **1**; Due to the C_2 symmetric Ta_2P_8 core isomer **1^I** can convert into isomer **1^{II}** by rotation of its Cp''' ligands or a simultaneous 1,2 shift of both {$W(CO)_5$} groups.*

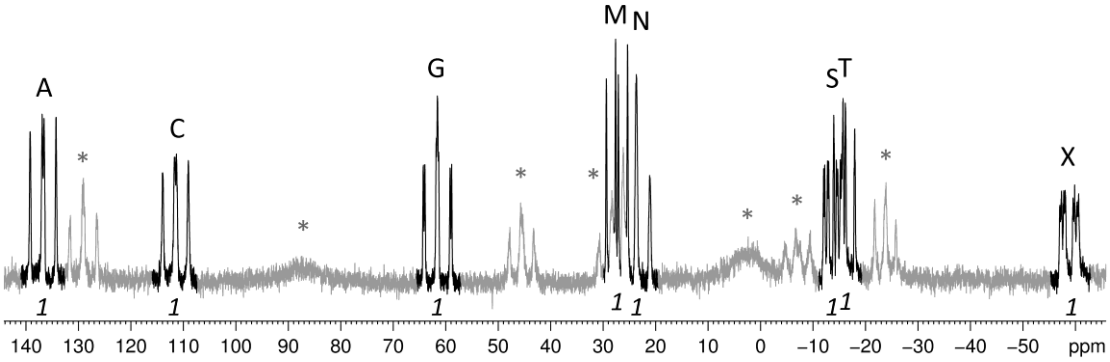

*Figure S 15: $^{31}P\{^1H\}$ NMR spectrum of the thermolysis product **2a** in tol-d^8 recorded at room temperature; Relative intensities are given in italic numbers under the signals; * marks signals of residual **1**.*

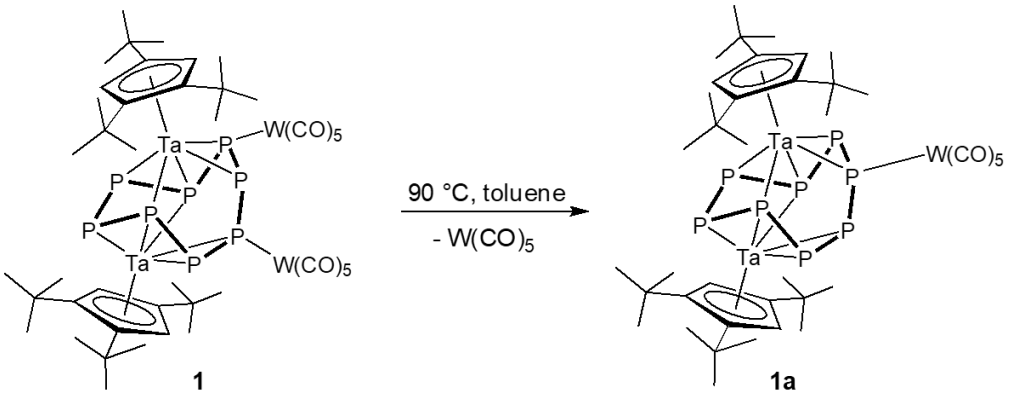

*Scheme S 1: Formation of **2a** from **1** by loss of a $W(CO)_5$ group at 90 °C.*

*[(Cp'''Ta)$_2$(μ_3-$\eta^{2:2:2:2:1:1:1}$-P$_8$){4-W(CO)$_5$}] (**2**)*

Since complex **2** decomposes during workup of the reaction mixture (*vide supra*), it can only be characterized spectroscopically, aside of complex **1**. In the FD mass spectrum of the reaction mixture the W(CO)$_5$ mono- and di-adduct were detected, whereas in the FD mass spectrum of pure **1** only its molecule ion peak was observed. This suggests **2** to be a W(CO)$_5$ mono-adduct [(Cp'''Ta)$_2$(μ_3-$\eta^{2:2:2:2:1:1:1}$-P$_8$){W(CO)$_5$}]. Since the ^{31}P{^{1}H} NMR spectrum of **1** is known (Figure S12), the signals of complex **2** can be assigned (Figure S16). In the ^{31}P{^{1}H} NMR spectrum complex **2** shows a AMNQRSTU spin system with the signals being in the same range like those of **1** and **A**, which suggests no difference in the connectivity of the Ta$_2$P$_8$ core. Signal U additionally shows tungsten satellites ($^1J_{PU\text{-}W}$ = 163 Hz), just as found for **1**, where signals A and X also show small tungsten satellites due to the coordination to the {W(CO)$_5$} fragments. By comparing the chemical shift of signal U with the signals of **A** (Figure S7), it can be assigned to P1/P1' or P4/P4' using the numbering of Figure S1. However, a primary coordination of a {W(CO)$_5$} fragment to P1 would give isomer **2a** and moreover would have allowed a coordination of a second fragment to P2' due to the excess of [W(CO)$_5$(thf)] in the reaction. Consequently, the primary coordination of the {W(CO)$_5$} fragment to P4 or P4' apparently inhibits additional coordination of other {W(CO)$_5$} groups and the connectivity of **2a** is corroborated as [(Cp'''Ta)$_2$(μ_3-$\eta^{2:2:2:2:1:1:1}$-P$_8$){4-W(CO)$_5$}].

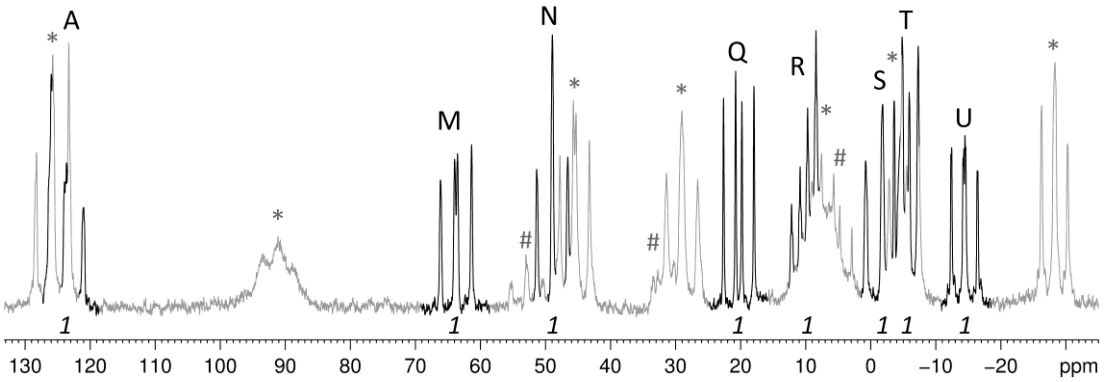

*Figure S 16: ^{31}P{^{1}H} NMR spectrum of the reaction mixture containing **1** and **2** in CD_2Cl_2 recorded at room temperature; the signals of **2** are highlighted, those of **1** faded and relative intensities are given in italic numbers under the signals. * marks the signals for **1** and # those of an unknown impurity.*

*[{Cp'''Ta}$_2$(μ_3;$\eta^{2:2:2:2:1:1}$-P$_8$(1-AsCy$_2$))][BArF$_{24}$] (**3**)*

As **3** has good solubility in CD_2Cl_2, its NMR spectra can easily be obtained. While signal assignment in the ^{31}P{^{1}H} NMR spectra of **1**, **2a** and **2** is simplified due to the respective ^{183}W satellites, it is more complicated for **3**. However, the characteristically small $^1J_{pp\text{-}px}$ = 119.4 Hz coupling (*vide supra*) observed in the ^{31}P{^{1}H} NMR spectrum (Figure S17) provides a good starting point for spectral simulation. Additional broadening of P^O , which we attribute to small $^4J_{P\text{-}H}$ coupling with the Cy residues, in the ^{31}P NMR spectrum (Figure S18) finally allows complete assignment of the functionalized *cyclo*-P$_8$ ligand. Moreover, spectral simulation of the ^{31}P{^{1}H} NMR spectrum delivered the $^1J_{P\text{-}P}$ and $^2J_{P\text{-}P}$ coupling constants for **3** (Table S5). Interestingly, only one set of signals for the *cyclo*-P$_8$ ligand is observed in these spectra (in

contrast to **1**), which points towards less hindered rotation of the Cp''' ligands. However, the substitution of the P_8 ligand still leads to a decreased symmetry for the Cp''' ligands, as the ^{1}H NMR spectrum reveals six signals for the ^{t}Bu groups, and four signals are found for the Cp-H protons.

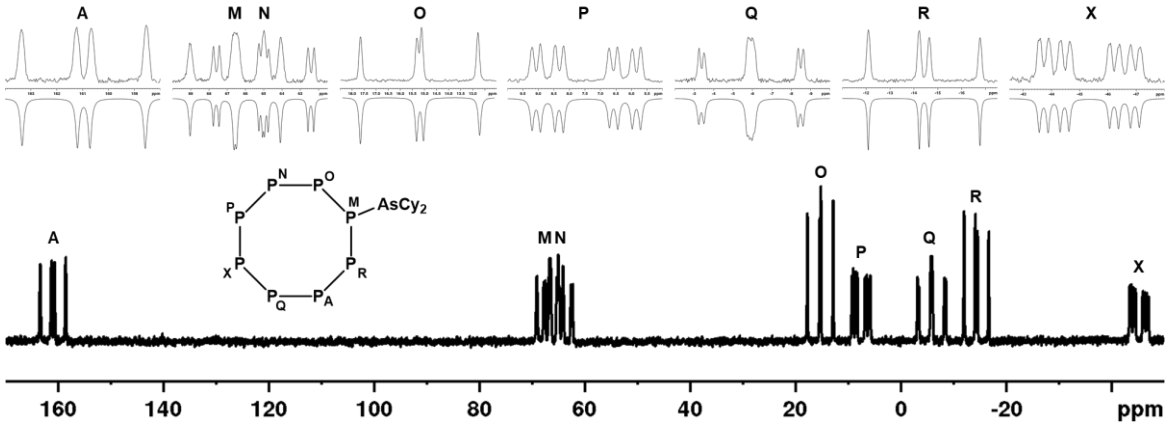

*Figure S 17: $^{31}P\{^1H\}$ NMR spectrum of **3** in CD_2Cl_2 recorded at room temperature; Experimental spectrum (top) and simulated spectrum (below).*

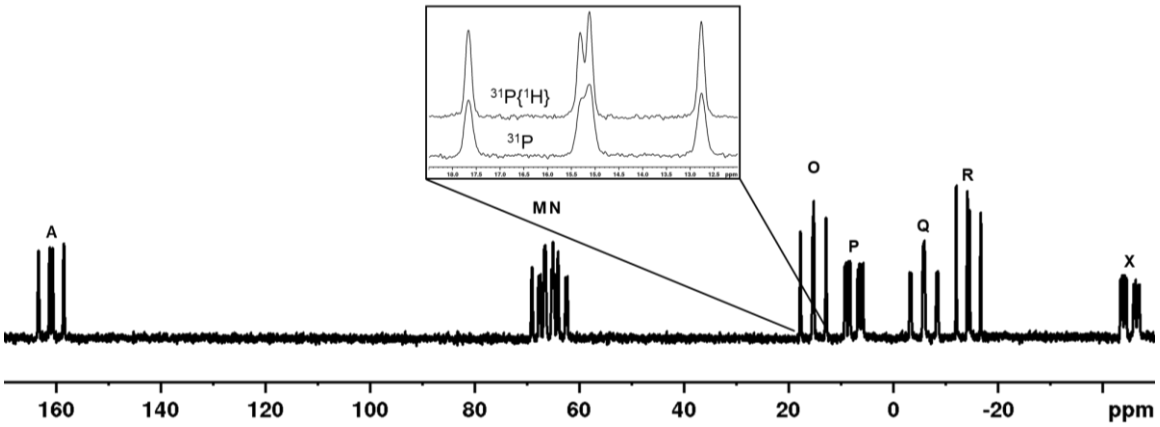

*Figure S 18: ^{31}P NMR spectrum of **3** in CD_2Cl_2 recorded at room temperature; The inlet shows the signal broadening for P^O in the ^{31}P NMR spectrum compared to the decoupled $^{31}P\{^1H\}$ MR spectrum.#*

*Table S5: $^1J_{P-P}$ and $^2J_{P-P}$ coupling constants derived from the simulation of the $^{31}P\{^1H\}$ NMR spectrum of **3**.*

$^1J_{PAPP}$ = 425.4 Hz	$^1J_{PAPR}$ = 346.6 Hz	$^1J_{PMPO}$ = 388.6 Hz
$^1J_{PMPR}$ = 412.0 Hz	$^1J_{PNPO}$ = 436.5 Hz	$^1J_{PNPP}$ = 403.9 Hz
$^1J_{PPPX}$ = 119.4 Hz	$^1J_{PQPX}$ = 402.7 Hz	$^2J_{PNPX}$ = 50.6 Hz
$^2J_{PPPQ}$ = 43.4 Hz		

[{Cp'''Ta}$_4$(μ_4;$\eta^{2:2:2:2:2:2:2:2:1:1:1:1}$-$P_{16}$)][TEF]$_2$ (***4***)

The ^{1}H NMR spectrum of **4** in CD_2Cl_2 reveals twelve singlets for the ^{t}Bu groups and eight signals for the CpH protons clearly pointing towards the asymmetric character of this compound. However, the respective $^{31}P\{^1H\}$ NMR spectrum (Figure S19) reveals several strongly overlapping multiplets in between δ/ ppm = –40 - 180 of which only two can reasonably be integrated. Their integral ratio of 1.4:1 hints towards the presence of two isomers of **4** in solution, which are detected due to the slower time scale of $^{31}P\{^1H\}$ compared to ^{1}H NMR spectroscopy. Similarly to **1**, this isomerism is most probably caused by the hindered rotation of the Cp''' ligands, making them planar chiral, thus affording several diastereomers of **4**, which slowly interconvert. Notably, this is supported by multinuclear variable temperature NMR studies (Figure S20). While the $^{31}P\{^1H\}$ NMR spectra experience only minor changes upon cooling a solution of **4** to –80 °C, the signals in the respective ^{1}H NMR spectra experience significant broadening, pointing towards a slower exchange rate at this temperature.

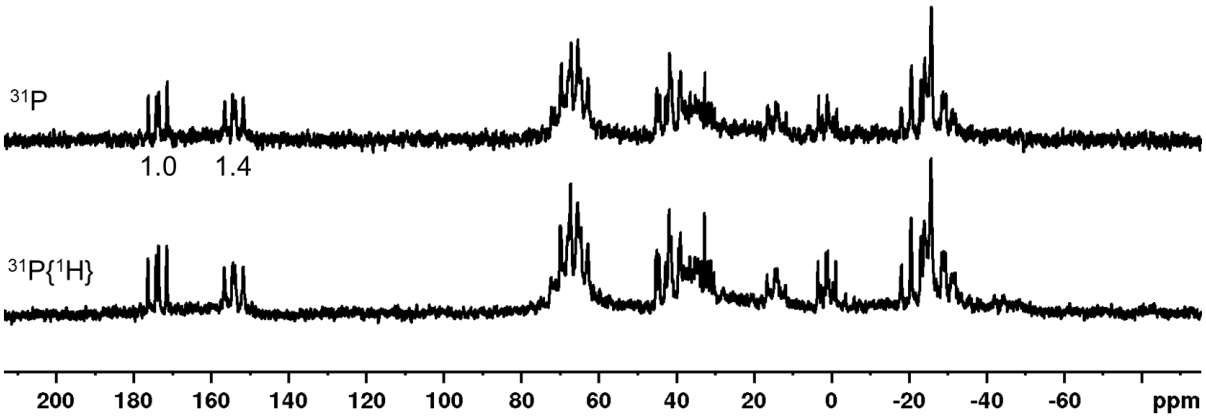

*Figure S 19: $^{31}P\{^1H\}$ (bottom) and ^{31}P (top) NMR spectrum of **4** in CD_2Cl_2 recorded at room temperature with integral values for the two most downfield shifted signals.*

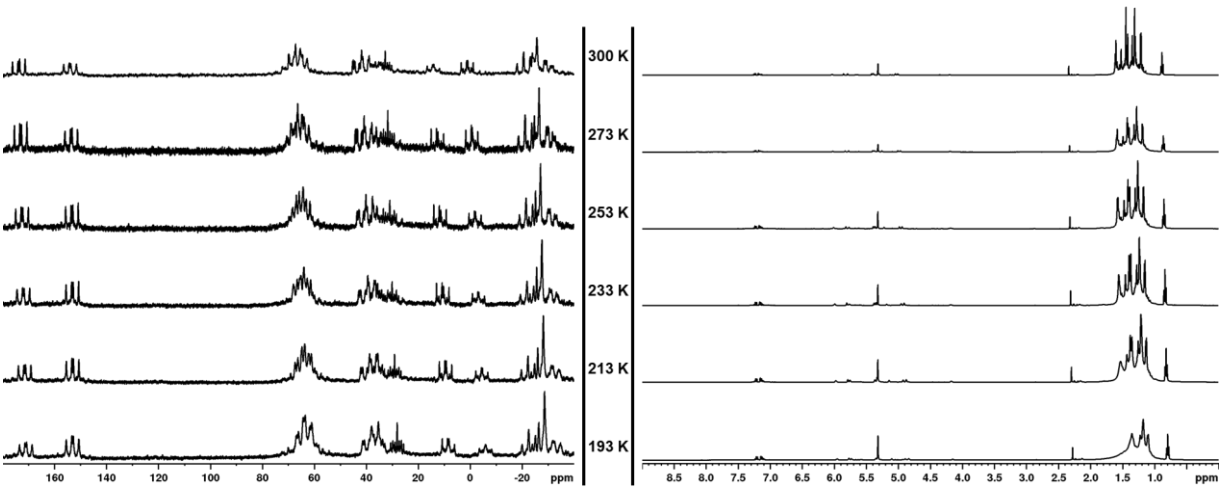

*Figure S 20: $^{31}P\{^1H\}$ (left) and ^1H (right) NMR spectra of **4** in CD_2Cl_2 recorded at indicated temperatures.*

*Thermolysis of **A** with $[CpMo(CO)_2]_2$ and $[\{Cp'''Co\}_2(\mu,\eta^{6:6}\text{-PhMe})]$*

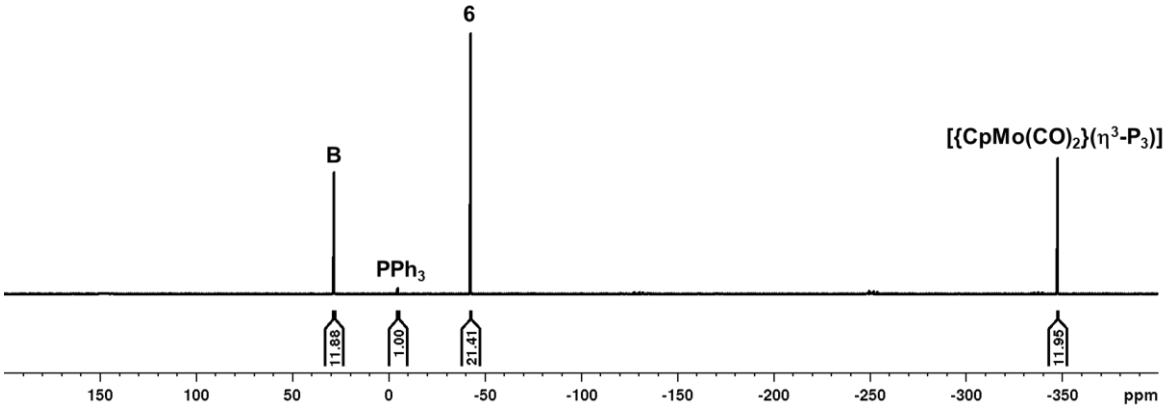

*Figure S 21: ^{31}P NMR spectrum of the reaction mixture of **A** and $[CpMo(CO)_2]_2$ after 2 h at 90 °C in toluene with a C_6D_6 capillary containing 0.002 mmol PPh_3; the integral ratio between the product **6** and PPh_3 indicates the yield of 54% yield.*

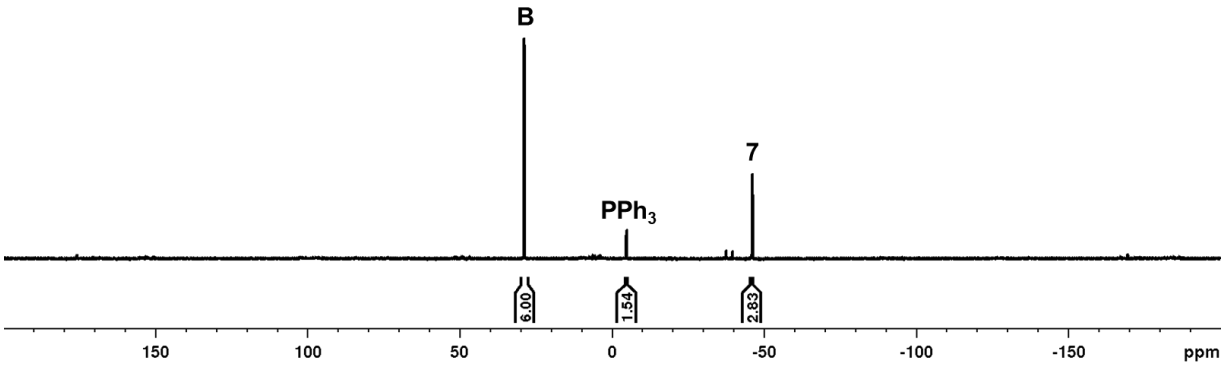

*Figure S 22: ^{31}P NMR spectrum of the reaction mixture of **A** and $[\{Cp'''Co\}_2(\mu,\eta^{6:6}\text{-PhMe})]$ after 2 h at 100 °C in toluene with a C_6D_6 capillary containing 0.01 mmol PPh_3; the integral ratio between the product **7** and PPh_3 indicates the yield of 40% yield.*

8.5.4. Electrochemical Investigations on A

To get an initial idea of the redox behavior of **A** in solution, cyclovoltammetric (CV) measurements were performed. Thus, **A** (50 mg) were dissolved in 5 mL of *o*-DFB, 750 mg of [^{n}Bu$_4$N][PF$_6$] were added and the measurements performed on these solutions. The CV of **A** in between +1 V and –1.5 V (vs. Fc/Fc$^+$, Figure S23) reveals one irreversible oxidative, as well as one irreversible reductive process. An additional reductive event can be observed when scanning to even lower potentials (Figure S24), which is however accompanied by decomposition.

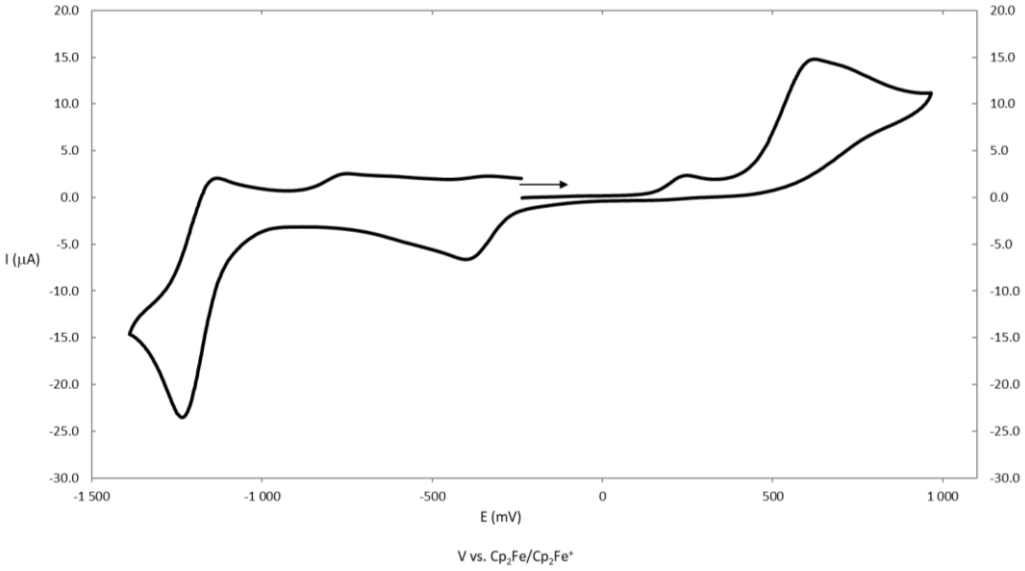

*Figure S 23: Cyclovoltammogram of **A** from –1.5 V to 1.0 V (50 mg in 5 mL o-DFB with 750 mg [^{n}Bu$_4$N][PF$_6$] as supporting electrolyte).*

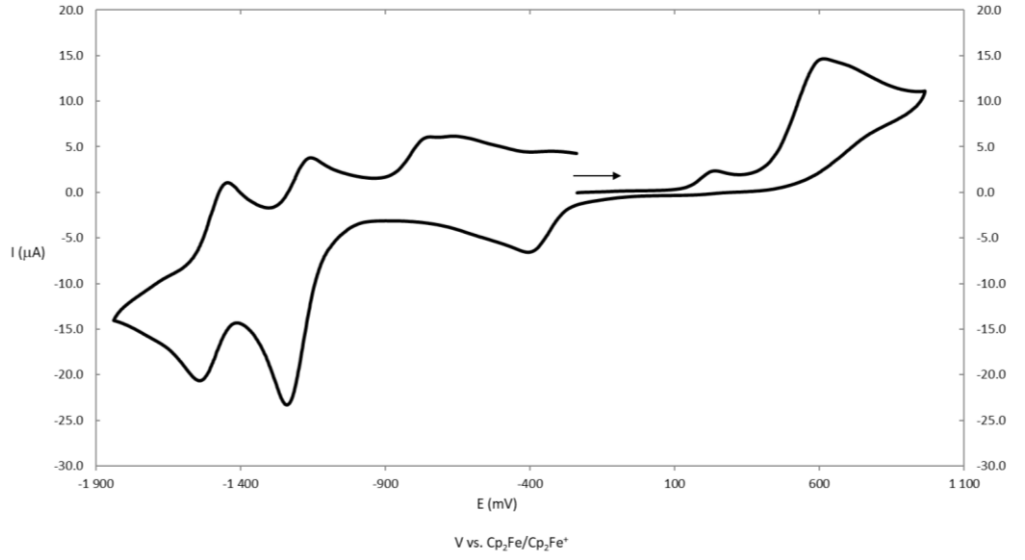

*Figure S 24: Cyclovoltammogram of **A** from –1.9 V to 1.0 V (50 mg in 5 mL o-DFB with 750 mg [^{n}Bu$_4$N][PF$_6$] as supporting electrolyte).*

8.5.5. Computational Details

General Considerations

DFT calculations were performed using the Orca 5.0 software package.[36] The sterically demanding Cp''' ligands were replaced with unsubstituted Cp ligands to save computational resources on the large molecular structures described herein. Geometry optimizations were performed at the BP86[37]/def2-TZVP[38] level of theory with PCM solvent correction for CH_2Cl_2 (**A'**, [**A'**]$^{\bullet+}$, [**4'**]$^{2+}$) or THF ([**A'**]$^{\bullet-}$, [**5'**]$^{2-}$).[39] Stationary points were verified by analytical frequency calculations. Single point calculations were performed at the ωB97X-D3/def2-TZVP[38] level of theory with solvent correction as described above. NBO analyses were performed using the NBO7.0 software package.[40]

Molecular Orbitals and WBIs

The highest molecular orbitals of **A'** are centred at the *cyclo*-P_8 ligand (Figure S25). While the HOMO shows great contribution from the P1-P1' bond, the HOMO-1 and HOMO-2 both have high p(P1/1') character. Additionally, the HOMO-4 also features high contributions from the P2/2' atoms. In contrast, the LUMO+2 is mainly centred at the P4-P4' bond. These observations indicate that oxidative/electrophilic reactivity should largely take place at the more exposed P1/1' and P2/2' atoms, while reductive processes may rather impact the encumbered P4/4' bond.

Additionally, we investigated the spin density distributions (Figure S26) within the hypothetical radical cation [**A'**]$^{\bullet+}$ and anion [**A'**]$^{\bullet-}$ intermediates, which should be formed upon either one electron oxidation or reduction of **A'**, respectively. While the spin density within the radical cation [**A'**]$^{\bullet+}$ is clearly centered at P1 (43%), the spin density within the radical anion [**A'**]$^{\bullet-}$ is distributed more diffusely (17% at P4). This agrees with our experimental findings of oxidatively induced dimerization via P1 and reductive dimerization via P4.

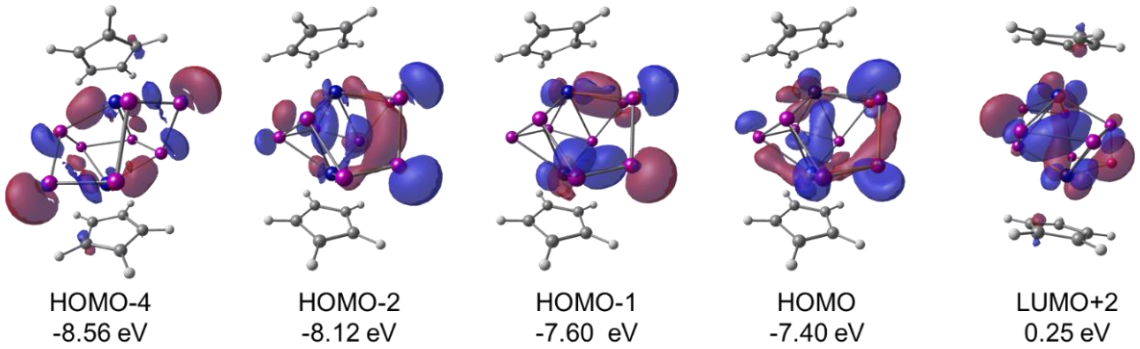

*Figure S 25: Frontier molecular orbitals of **A'** computed at the ωB97XD/def2-TZVP level of theory; isosurfaces drawn at a contour value of 0.005.*

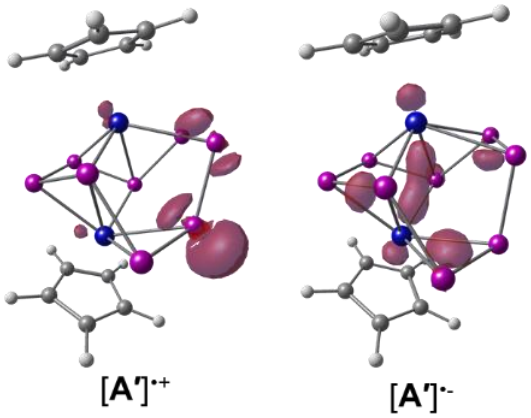

*Figure S 26: Total spin density distributions of [**A'**]•+ and [**A'**]•- computed at the ωB97XD/def2-TZVP level of theory; isosurfaces drawn at a contour value of 0.008.*

While generally being slightly overestimated, the calculated bond lengths within **A'** agree well with those found in the solid state structure of **A**. Moreover, the Wiberg bond indices (WBI) indicate the presence of P–P single bonds throughout the cyclo-P_8 ligand, with slightly higher bond order observed for the P1–P2/P1'–P2' bond and greatly decreased bond order for the P4–P4' bond (Table S6). Upon oxidation to [**A'**]•+ a shortening of all P–P bonds as well as a slight increase in bond order are observed, while reduction to [**A'**]•- leads to a distortion of the cyclo-P_8 ligand.

*Table S 6: Wiberg bond indices for **A'**, [**A'**]•+ and [**A'**]•- computed at the ωB97X-D3/def2-TZVP level of theory.*

Bond Length/ Å (WBI)	**A'**	[**A'**]•+	[**A'**]•-
P1-P1'	2.27056 (0.92)	2.21164 (1.00)	2.24710 (0.93)
P1-P2	2.17037/2.16985 (1.06)	2.17634/2.18211 (1.05/1.01)	2.17440/2.17385 (1.03)
P2-P3	2.22456/2.22522 (0.86)	2.20731/2.21780 (0.90/0.88)	2.22463/2.22502 (0.88/0.89)
P3-P4	2.19794/2.19777 (0.85)	2.19202/2.18908 (0.87/0.85)	2.24835/2.24592 (0.71)
P4-P4'	2.43423 (0.51)	2.40799 (0.52)	2.29968 (0.66)

Both dimerization reactions are highly exergonic. Thus, dimerization of [**A'**]•+ to [**4'**]$^{2+}$ is exergonic by ΔG = -182.91 kJ/mol, while the dimerization of [**A'**]•- to [**5'**]$^{2-}$ is exergonic by ΔG = -74.55 kJ/mol. The newly formed P–P bonds are in the range of single bonds as indicated by WBIs of 0.86 ([**4'**]$^{2+}$) and 0.94 ([**5'**]$^{2-}$).

Optimized Geometries

A'

ωB97XD/def2TZVP (CPCM (CH_2Cl_2)): Energies/H = -3233.20088307, Enthalpies/H = -3232.99701806, Free Energies/H = -3233.07081305, ZPVE/ kcal/mol = 127.33

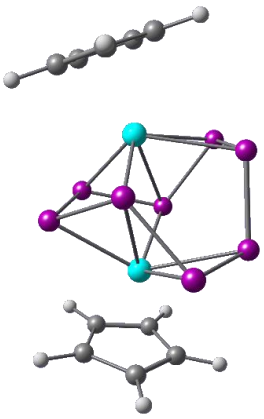

Symbol	X	Y	Z
Ta	12.087508000	19.794345000	5.109550000
Ta	9.827074000	17.602996000	5.878095000
P	13.602549000	17.781967000	5.873158000
P	11.022038000	17.711666000	3.760830000
P	11.187232000	19.420713000	7.339956000
P	11.007353000	17.349258000	8.132622000
P	12.017206000	16.294190000	6.527861000
P	9.933251000	19.619517000	3.835626000
P	13.232560000	17.960458000	3.742019000
P	9.436460000	20.063002000	6.176996000
C	14.119116000	21.096335000	5.374787000
H	15.023509000	20.620189000	5.741988000
C	8.769686000	15.424870000	6.055609000
H	9.365436000	14.557376000	6.324413000
C	7.709197000	17.059807000	4.825644000
H	7.357866000	17.660005000	3.991596000
C	13.120515000	21.726627000	6.173951000
C	7.443632000	17.307153000	6.206912000
C	8.091509000	16.291781000	6.967759000
C	8.523379000	15.893259000	4.731942000
C	13.728776000	21.211213000	4.004386000
C	12.479348000	21.893847000	3.960501000
C	12.104477000	22.213184000	5.300839000
H	11.198643000	22.730179000	5.603302000
H	14.289180000	20.847138000	3.149545000
H	11.916792000	22.139947000	3.064925000
H	13.138391000	21.826794000	7.254439000
H	6.841378000	18.117934000	6.605416000
H	8.073117000	16.190359000	8.047995000
H	8.885717000	15.436520000	3.816499000

[A']•+

ωB97XD/def2TZVP (CPCM (CH_2Cl_2)): Energies/H = -3232.80467482, Enthalpies/H = -3232.80373061, Free Energies/H = -3232.87830324, ZPVE/ kcal/mol = 127.59

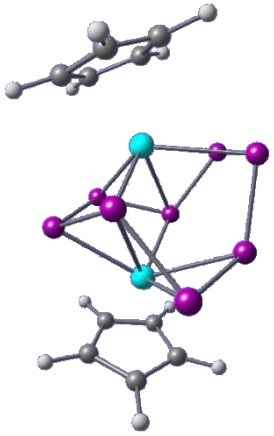

Symbol	X	Y	Z
Ta	12.097536000	19.811845000	5.138513000
Ta	9.883768000	17.577337000	5.898851000
P	13.326468000	17.680141000	5.792964000
P	10.961796000	17.752771000	3.675728000
P	11.214295000	19.397165000	7.386785000
P	10.982795000	17.346697000	8.199580000
P	11.985947000	16.155780000	6.670859000
P	9.905056000	19.655422000	3.936810000
P	13.156880000	17.982681000	3.644440000
P	9.435682000	20.016307000	6.270878000
C	14.114714000	21.109063000	5.371729000
H	15.017506000	20.633312000	5.746018000
C	8.785706000	15.420877000	6.057910000
H	9.347883000	14.535017000	6.340158000
C	7.784518000	17.074949000	4.804168000
H	7.450039000	17.672876000	3.961232000
C	13.116640000	21.753498000	6.162372000
C	7.505198000	17.337422000	6.180085000
C	8.114269000	16.307534000	6.954628000
C	8.571735000	15.888512000	4.728861000
C	13.726609000	21.211455000	3.999159000
C	12.482298000	21.900145000	3.944038000
C	12.104585000	22.233786000	5.280302000
H	11.200345000	22.759274000	5.575372000
H	14.288871000	20.838001000	3.149113000
H	11.922285000	22.137099000	3.044131000
H	13.133020000	21.868956000	7.241794000
H	6.907013000	18.157254000	6.565748000
H	8.075133000	16.212175000	8.035252000
H	8.934303000	15.415280000	3.821684000

[4']$^{2+}$

ωB97XD/def2TZVP (CPCM (CH_2Cl_2)): Energies/H = -6465.70685560, Enthalpies/H = -6465.70591139, Free Energies/H = -6465.82627164, ZPVE/ kcal/mol = 256.79

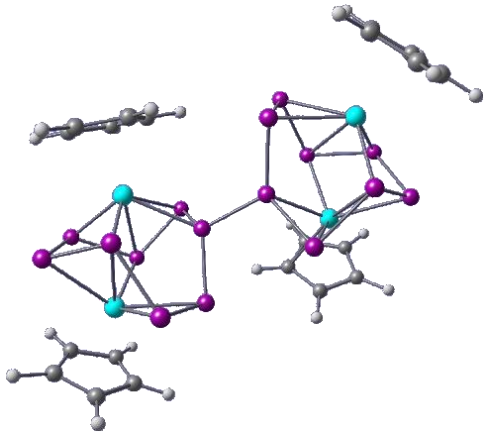

Symbol	X	Y	Z
Ta	-2.693091000	1.717066000	-0.346441000
Ta	-4.327779000	-0.997593000	0.435313000
P	-1.056869000	-0.056325000	0.379484000
P	-3.488438000	0.645826000	2.062724000
P	-3.214168000	-0.117852000	-1.890821000
P	-2.927883000	-2.231747000	-1.296748000
P	-1.920339000	-2.049085000	0.652704000
P	-4.886147000	1.814871000	0.833764000
P	-1.429358000	1.444452000	1.908981000
P	-5.181044000	0.637379000	-1.260533000
C	-1.012443000	3.038205000	-1.459050000
H	-0.000051000	2.659465000	-1.568510000
C	-4.949308000	-2.998254000	1.655188000
H	-4.191826000	-3.699561000	1.993703000
C	-6.438239000	-1.240243000	1.595737000
H	-7.007951000	-0.358487000	1.874886000
C	-2.073965000	2.858187000	-2.394304000
C	-6.543080000	-1.948322000	0.358967000
C	-5.631383000	-3.042764000	0.400643000
C	-5.456658000	-1.890738000	2.397324000
C	-1.501015000	3.832558000	-0.376603000
C	-2.871634000	4.123263000	-0.630850000
C	-3.224695000	3.521166000	-1.878124000
H	-4.201940000	3.562863000	-2.350804000
Ta	2.725905000	-1.713246000	-0.463506000
Ta	4.318232000	1.019412000	0.358105000
P	1.065575000	0.146996000	-0.103461000
P	3.473523000	0.513953000	-1.895566000
P	3.234497000	-1.011108000	1.833320000
P	2.915327000	1.081490000	2.485548000
P	1.899089000	1.982329000	0.755230000
P	4.907422000	-1.106011000	-1.504480000
P	1.432464000	-0.275140000	-2.204023000
P	5.206363000	-1.257896000	0.896820000
C	1.110941000	-3.447152000	-0.977571000
H	0.112666000	-3.177609000	-1.310228000
C	4.900371000	3.371100000	0.493276000
H	4.132844000	4.124259000	0.647654000
C	6.380691000	1.927234000	-0.523351000
H	6.934878000	1.378491000	-1.279574000
C	1.520573000	-3.636934000	0.374100000
C	6.538213000	1.795640000	0.890536000
C	5.629953000	2.696429000	1.519211000
C	5.370848000	2.901874000	-0.768816000
C	2.240431000	-3.677515000	-1.819618000
C	3.346924000	-4.011523000	-0.990770000
C	2.906396000	-3.976963000	0.366688000
H	3.517117000	-4.184650000	1.240838000
H	2.253285000	-3.594678000	-2.903016000
H	4.351406000	-4.248690000	-1.329289000
H	0.891686000	-3.532241000	1.253680000
H	7.246044000	1.146090000	1.396460000
H	5.517441000	2.850851000	2.587595000

H	5.027319000	3.239180000	-1.741959000
H	-0.923106000	4.160727000	0.481839000
H	-3.529699000	4.709610000	0.003509000
H	-2.009136000	2.323218000	-3.336515000
H	-5.154526000	-1.604830000	3.400080000
H	-5.486526000	-3.785850000	-0.376970000
H	-7.218561000	-1.709936000	-0.457056000

[A']$^{\bullet-}$

ωB97XD/def2TZVP (CPCM (THF)): Energies/H = -3233.12408579, Enthalpies/H = -3233.12314158, Free Energies/H = -3233.19780651, ZPVE/ kcal/mol = 126.84

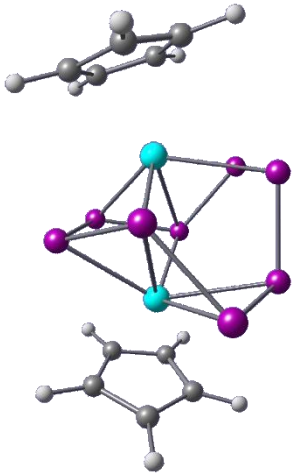

Symbol	X	Y	Z
Ta	12.044887000	19.776621000	5.159642000
Ta	9.857830000	17.631971000	5.828007000
P	13.575524000	17.812850000	5.943175000
P	11.055180000	17.710778000	3.683242000
P	11.149941000	19.429560000	7.421549000
P	11.058730000	17.325530000	8.139512000
P	12.004356000	16.296676000	6.474315000
P	9.835623000	19.587856000	3.893771000
P	13.268811000	17.902897000	3.792400000
P	9.482880000	20.144256000	6.097064000
C	14.102456000	21.064430000	5.352939000
H	15.012151000	20.577523000	5.691539000
C	8.795177000	15.454199000	6.061615000
H	9.393499000	14.594943000	6.349969000
C	7.734218000	17.061834000	4.797166000
H	7.379761000	17.642603000	3.951723000
C	13.133094000	21.701497000	6.182851000
C	7.466272000	17.335926000	6.173710000
C	8.113101000	16.337015000	6.954737000
C	8.551502000	15.895596000	4.727537000
C	13.673961000	21.185467000	3.994879000
C	12.429929000	21.876670000	3.987950000
C	12.096869000	22.198503000	5.339811000
H	11.207064000	22.726147000	5.668053000
H	14.201929000	20.807922000	3.125645000
H	11.841584000	22.125517000	3.109969000
H	13.181436000	21.796942000	7.262739000
H	6.865916000	18.156445000	6.554725000
H	8.102764000	16.262480000	8.037009000
H	8.916451000	15.421978000	3.821919000

[5']$^{2-}$

ωB97XD/def2TZVP (CPCM (THF)): Energies/H = -6466.30353101, Enthalpies/H = -6466.30258680, Free Energies/H = -6466.42400744, ZPVE/ kcal/mol = 255.18

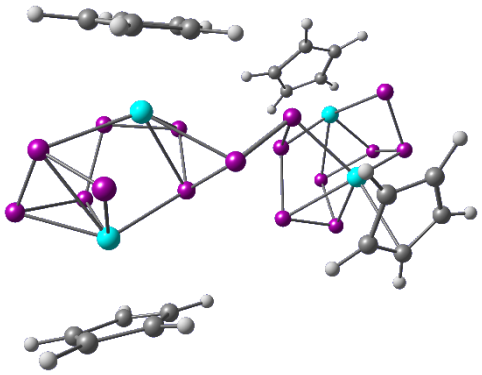

Symbol	X	Y	Z
Ta	16.263287000	12.799102000	11.410868000
Ta	15.335913000	10.806916000	5.534932000
Ta	19.216906000	13.695487000	10.487475000
Ta	14.474707000	7.949776000	6.747232000
P	15.943133000	9.628587000	7.747762000
P	16.061962000	12.989365000	8.767378000
P	14.677392000	11.372470000	8.049026000
P	14.174390000	8.973699000	4.260540000
P	17.809242000	11.943956000	9.530610000
P	16.882515000	10.368232000	10.766403000
P	12.906680000	9.647464000	5.927264000
P	16.774425000	7.329526000	5.689620000
P	17.650679000	10.500578000	6.654702000
P	17.391514000	9.322439000	4.843809000
P	17.317709000	15.221114000	10.765030000
P	17.743988000	11.020044000	12.654604000
P	14.977925000	6.870914000	4.545162000
P	17.800803000	14.310679000	12.709663000
P	19.803542000	11.663212000	12.009772000
P	19.967002000	13.655155000	12.875144000
C	20.223995000	13.609474000	8.248848000
H	19.839356000	12.904639000	7.516755000
H	13.837792000	10.848749000	11.424883000
C	21.263023000	13.350428000	9.195373000
C	14.309890000	14.111612000	12.056169000
C	14.855989000	13.178709000	5.317400000
H	14.495782000	13.745868000	6.169984000
C	14.051388000	12.510431000	4.348571000
C	13.687416000	5.736134000	7.474708000
H	13.741160000	4.895096000	6.790893000
C	14.233767000	7.283645000	9.100070000
H	14.779104000	7.826222000	9.867384000
C	20.536181000	15.515476000	9.508162000
C	16.264053000	12.195360000	3.778410000
C	14.920890000	11.908506000	3.391147000
H	14.616285000	11.340844000	2.517978000
C	19.771337000	14.941041000	8.445121000
C	14.079849000	11.824751000	11.832242000
C	14.810424000	13.502951000	13.245507000
H	15.208117000	14.022305000	14.111272000
H	11.668843000	6.609828000	7.046679000
H	12.309940000	8.416753000	8.956656000
C	14.712383000	6.145665000	8.380393000
H	18.972604000	15.429490000	7.895237000
C	12.595169000	6.637215000	7.613438000
C	13.859390000	13.075570000	11.185976000
H	13.411125000	13.209583000	10.206470000
H	17.078185000	13.382409000	5.507331000
C	12.932107000	7.591705000	8.623292000
C	21.466721000	14.538733000	9.960267000
H	22.191637000	14.665261000	10.758154000
H	15.681976000	5.672268000	8.506910000
H	12.967088000	12.462507000	4.343604000

H	14.971767000	11.344646000	13.837013000
H	20.420194000	16.520055000	9.904945000
C	14.681262000	12.088835000	13.101745000
H	17.159834000	11.877698000	3.253546000
H	21.807180000	12.416753000	9.306576000
C	16.224066000	12.992719000	4.963785000
H	14.282819000	15.176548000	11.847808000

8.6. References

[1] a) M. Baudler, *Angew. Chem. Int. Ed. Engl.* **1982**, *21*, 492–512, b) M. Baudler, K. Glinka, *Chem. Rev.* **1993**, *93*, 1623–1667, c) T. Wellnitz, C. Hering‐Junghans, *Eur. J. Inorg. Chem.* **2021**, *2021*, 8–21, d) O. J. Scherer, *Nachr. Chem.* **1987**, *35*, 1140–1144, e) O. J. Scherer, *Angew. Chem. Int. Ed. Engl.* **1990**, *29*, 1104–1122.

[2] R. Hoffmann, *Angew. Chem. Int. Ed. Engl.* **1982**, *21*, 711–724.

[3] a) B. M. Cossairt, N. A. Piro, C. C. Cummins, *Chem. Rev.* **2010**, *110*, 4164–4177, b) M. Caporali, L. Gonsalvi, A. Rossin, M. Peruzzini, *Chem. Rev.* **2010**, *110*, 4178–4235, c) M. Scheer, G. Balázs, A. Seitz, *Chem. Rev.* **2010**, *110*, 4236–4256, d) C. M. Hoidn, D. J. Scott, R. Wolf, *Chem. Eur. J.* **2021**, *27*, 1886–1902, e) L. Giusti, V. R. Landaeta, M. Vanni, J. A. Kelly, R. Wolf, M. Caporali, *Coord. Chem. Rev.* **2021**, *441*, 213927.

[4] a) H. Köhler, A. Michaelis, *Ber. Dtsch. Chem. Ges.* **1877**, *10*, 807–814, b) J. J. Daly, L. Maier, *Nature* **1964**, *203*, 1167–1168, c) J. J. Daly, *J. Chem. Soc.* **1964**, 6147.

[5] K. Schwedtmann, J. Haberstroh, S. Roediger, A. Bauzá, A. Frontera, F. Hennersdorf, J. J. Weigand, *Chem. Sci.* **2019**, *10*, 6868–6875.

[6] a) M. Baudler, J. Hellmann, P. Bachmann, K.-F. Tebbe, R. Fröhlich, M. Fehér, *Angew. Chem. Int. Ed. Engl.* **1981**, *20*, 406–408, b) T. Grell, E. Hey-Hawkins, *Chem. Eur. J.* **2020**, *26*, 1008–1012, c) V. J. Eilrich, T. Grell, P. Lönnecke, E. Hey-Hawkins, *Dalton Trans.* **2021**, *50*, 14144–14155.

[7] S. Wang, J. D. Sears, C. E. Moore, A. L. Rheingold, M. L. Niedig, J. S. Figueroa, *Science* **2022**, *375*, 1393–1397.

[8] a) O. J. Scherer, H. Sitzmann, G. Wolmershäuser, *J. Organomet. Chem.* **1984**, *268*, C9-C12, b) O. J. Scherer, J. Braun, G. Wolmershäuser, *Chem. Ber.* **1990**, *123*, 471–475.

[9] a) O. J. Scherer, J. Vondung, G. Wolmershäuser, *Angew. Chem. Int. Ed. Engl.* **1989**, *28*, 1355–1357, b) F. Dielmann, A. Timoshkin, M. Piesch, G. Balázs, M. Scheer, *Angew. Chem. Int. Ed.* **2017**, *56*, 1671–1675, c) A. Cavaillé, N. Saffon-Merceron, N. Nebra, M. Fustier-Boutignon, N. Mézailles, *Angew. Chem. Int. Ed.* **2018**, *57*, 1874–1878.

[10] a) O. J. Scherer, T. Brück, *Angew. Chem. Int. Ed. Engl.* **1987**, *26*, 59, b) E. Urnius, W. W. Brennessel, C. J. Cramer, J. E. Ellis, P. v. R. Schleyer, *Science* **2002**, *295*, 832–834, c) C. M. Knapp, B. H. Westcott, M. A. C. Raybould, J. E. McGrady, J. M. Goicoechea, *Angew. Chem. Int. Ed.* **2012**, *51*, 9097–9100.

[11] O. J. Scherer, H. Sitzmann, G. Wolmershäuser, *Angew. Chem. Int. Ed. Engl.* **1985**, *24*, 351–353.

[12] a) O. J. Scherer, G. Berg, G. Wolmershäuser, *Chem. Ber.* **1996**, *129*, 53–58, b) J. D. Masuda, W. W. Schoeller, B. Donnadieu, G. Bertrand, *J. Am. Chem. Soc.* **2007**, *129*, 14180–14181, c) F. Dielmann, M. Sierka, A. V. Virovets, M. Scheer, *Angew. Chem. Int. Ed.* **2010**, *49*, 6860–6864.

[13] a) B. M. Cossairt, C. C. Cummins, *Angew. Chem. Int. Ed. Engl.* **2008**, *47*, 169–172, b) G. Hierlmeier, P. Coburger, N. P. van Leest, B. de Bruin, R. Wolf, *Angew. Chem. Int. Ed. Engl.* **2020**, *59*, 14148–14153, c) C. Yang, X. Jiang, Q. Chen, X. Leng, J. Xiao, S. Ye, L. Deng, *J. Am. Chem. Soc.* **2022**, doi.org/10.1021/jacs.2c08647.

[14] a) M. E. Barr, B. R. Adams, R. R. Weller, L. F. Dahl, *J. Am. Chem. Soc.* **1991**, *113*, 3052–3060, b) M. Scheer, U. Becker, E. Matern, *Chem. Ber.* **1996**, *129*, 721–724, c) S. N. Konchenko, N. A. Pushkarevsky, M. T. Gamer, R. Köppe, H. Schnöckel, P. W. Roesky, *J. Am. Chem. Soc.* **2009**, *131*, 5740–5741, d) W. Huang, P. L. Diaconescu, *Chem. Commun.* **2012**, *48*, 2216–2218, e) F. Spitzer, C. Graßl, G. Balázs, E. M. Zolnhofer, K. Meyer, M. Scheer, *Angew. Chem. Int. Ed.* **2016**, *55*, 4340–4344.

[15] M. Piesch, M. Seidl, M. Scheer, *Chem. Sci.* **2020**, *11*, 6745–6751.

[16] a) H.-G. von Schnering, J. Wolf, D. Weber, R. Ramirez, T. Meyer, *Angew. Chem. Int. Ed. Engl.* **1986**, *25*, 353–354, b) B. W. Eichhorn, S. P. Mattamana, D. R. Gardner, J. C. Fettinger, *J. Am. Chem. Soc.* **1998**, *120*, 9708–9709, c) B. Kesanli, J. Fettinger, B. Eichhorn, *J. Am. Chem. Soc.* **2003**, *125*, 7367–7376, d) B. Kesanli, J. Fettinger, B. Scott, B. Eichhorn, *Inorg. Chem.* **2004**, *43*, 3840–3846.

[17] O. J. Scherer, R. Winter, G. Heckmann, G. Wolmershäuser, *Angew. Chem. Int. Ed. Engl.* **1991**, *30*, 850–852.

[18] a) M. V. Butovskiy, G. Balázs, M. Bodensteiner, E. V. Peresypkina, A. V. Virovets, J. Sutter, M. Scheer, *Angew. Chem. Int. Ed.* **2013**, *52*, 2972–2976, b) L. Dütsch, M. Fleischmann, S. Welsch, G. Balázs, W. Kremer, M. Scheer, *Angew. Chem. Int. Ed.* **2018**, *57*, 3256–3261.

[19] Deposition numbers 2225834 (**A**), 2225835 (**B**), 2225836 (**1**), 2225837 (**3**), 2225838 (**4**) and 2225839 (**5**) contain supplementary crystallographic data for this paper. These data are provided free of charge by the joint CCDC and FIZ Karlsruhe Access Structures service.

[20] P. Pyykkö, *J. Phys. Chem. A* **2015**, *119*, 2326–2337.

[21] S. Du, J. Hu, Z. Chai, W.-X. Zhang, Z. Xi, *Chin. J. Chem.* **2019**, *37*, 71–75.

[22] a) N. A. Piro, J. S. Figueroa, J. T. McKellar, C. C. Cummins, *Science* **2006**, *313*, 1276–1279, b) A. Velian, M. Nava, M. Temprado, Y. Zhou, R. W. Field, C. C. Cummins, *J. Am. Chem. Soc.* **2014**, *136*, 13586–13589, c) D. Rottschäfer, B. Neumann, H.-G. Stammler, R. Kishi, M. Nakano, R. S. Ghadwal, *Chem. Eur. J.* **2019**, *25*, 3244–3247, d) G. Hierlmeier, A. Hinz, R. Wolf, J. M. Goicoechea, *Angew. Chem. Int. Ed.* **2018**, *57*, 431–436.

[23] M. D. Curtis, R. J. Klingler, *J. Organomet. Chem.* **1978**, *161*, 23.

[24] J. J. Schneider, D. Wolf, C. Janiak, O. Heinemann, J. Rust, C. Krüger, *Chem. Eur. J.* **1998**, *4*, 1982–1991.

[25] [$CpMo(CO)_2$}(η^3-P_3)] is observed as a side product, which is attributed to the follow-up reaction between **6** and an excess of P_2; see SI.

[26] *https://omics.pnl.gov/software/molecular-weight-calculator (15.11.2022)*.

[27] M. Gonsior, I. Krossing, N. Mitzel, *Z. anorg. allg. Chem.* **2002**, *628*, 1821-1830.

[28] W. Steinkopf, H. Dudek, S. Schmidt, *Ber. dtsch. Chem. Ges. A/B* **1928**, *61*, 1911–1918.

[29] R. P. Hughes, D. C. Lindner, A. L. Rheingold, G. P. A. Yap, *Inorg. Chem.* **1997**, *36*, 1726–1727.

[30] O. J. Scherer, R. Winter, G. Wolmershäuser, *Z. anorg. allg. Chem.* **1993**, *619*, 827–835.

[31] Agilent Technologies Ltd, *CrysAlis PRO*, Yarnton, Oxfordshire, England, **2014**.

[32] O. V. Dolomanov, L. J. Bourhis, R. J. Gildea, J. A. K. Howard and H. Puschmann, *J. Appl. Crystallogr.* **2009**, *42*, 339–341.

[33] G. M. Sheldrick, *Acta Cryst. A* **2015**, *71*, 3–8.

[34] a) G. M. Sheldrick, *Acta Cryst. A* **2008**, *64*, 112–122; b) G. M. Sheldrick, *Acta Cryst. C* **2015**, *71*, 3–8.

[35] O. J. Scherer, R. Winter, G. Wolmershäuser, *Chem. Commun.* **1993**, *3*, 313–314.

[36] a) F. Neese, F. Wennmohs, U. Becker, C. Rieplinger, *J. Chem. Phys.* **2020**, *152*, 224108; b) F. Neese, *WIREs Comput. Mol. Sci.* **2022**, *12*, 1606.

[37] A. D. Becke, *Phys. Rev. A* **1988**, *38*, 3098–3100.

[38] F. Weigend, R. Ahlrichs, *Phys. Chem. Chem. Phys.* **2005**, *7*, 3297–3305.

[39] J. Tomasi, B. Mennucci, R. Cammi, *Chem. Rev.* **2005**, *105*, 2999–3093.

[40] NBO 7.0. E. D. Glendening, J. K. Badenhoop, A. E. Reed, J. E. Carpenter, J. A. Bohmann, C. M. Morales, P. Karafiloglou, C. R. Landis, and F. Weinhold, Theoretical Chemistry Institute, University of Wisconsin, Madison, WI (**2018**).

9. Redox Chemistry of an End-Deck *cyclo*-As_3 Nickel Complex

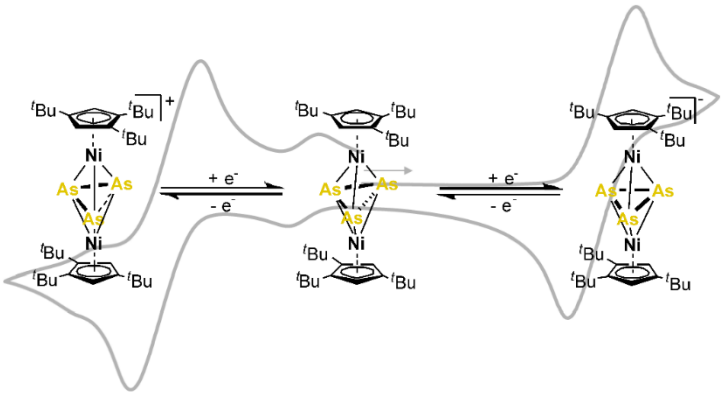

Preface

The following chapter has already been published. The article is reprinted with permission from

"Redox Chemistry of an End-Deck cyclo-As_3 Nickel Complex"

Organometallics **2023**, *42*, 2065–2069.

Authors

Christoph Riesinger,† Lisa Zimmermann† and Manfred Scheer

Author Contributions

Christoph Riesinger – Conceptualization, Synthesis of **1**, **2**, **3** and **5**, Interpretation of crystallographic data, Interpretation of computational data, Writing of original draft.
Lisa Zimmermann – Synthesis of **4**, Mechanistic Investigations, Writing of original draft.
Manfred Scheer – Project administration, Funding acquisition, Co-writing final manuscript.

† These authors contributed equally.

Acknowledgements

This work was supported by the Deutsche Forschungsgemeinschaft (DFG) within the project Sche 384/36-2 and Sche 384/32-2. C. R. is grateful to the Studienstiftung des Deutschen Volkes for a PhD fellowship. We thank Robert Szlosek for his assistance with electrochemical studies.

9.1. Abstract

*The redox chemistry of [Cp'''Ni(η^3-As$_3$)] (**A**), an end-deck cyclo-As$_3$ complex, is explored in terms of systematically accessing a series of Ni$_2$As$_3$ triple-decker compounds. While oxidation of **A** affords the cationic complex [{Cp'''Ni}$_2$(μ,$\eta^{3:3}$-As$_3$)][FAl] (**1**, [FAl]$^-$ = [FAl{O(1-C$_6$F$_5$)C$_6$F$_{10}$}$_3$]$^-$), reduction of **A** yields the anionic [K@crypt][{Cp'''Ni}$_2$(μ,$\eta^{3:3}$-As$_3$)] (**2**, crypt = [2.2.2]-cryptand). One-electron reduction of **1** as well as one-electron oxidation of **2** yield the neutral compound [{Cp'''Ni}$_2$(μ,$\eta^{3:3}$-As$_3$)] (**3**), representing the missing link between **1** and **2**, which is corroborated electrochemically. The cyclo-As$_3$ ligand in **2** undergoes bond weakening and finally splitting of one As-As bond upon stepwise oxidation to **3** and **1**, finally displaying an allylic As$_3$ ligand. In-depth experimental studies shed light onto the reaction pathway of the oxidation of **A** and additional DFT computations give insight into the electronic structure of the obtained complexes.*

9.2. Introduction

Transition metal polypnictogen (E$_n$) complexes are an important class of compounds as they enable the synthesis and investigation of highly reactive and otherwise unstable group 15 species.[1] Tremendous attention has been paid to polyphosphorus ligand complexes, mainly in the context of (transition) metal-mediated activation and conversion of white phosphorus (P$_4$).[2] In contrast, representatives of E$_n$ complexes of the heavier homologs As, Sb and Bi are far less known, which is commonly attributed to the lower homoatomic E-E bond energies.[3] Nevertheless, especially As$_n$ complexes raised considerable interest from very early on, as indeed the first reported E$_n$ ligand complexes contain an As$_2$ and a *cyclo*-As$_3$ ligand, respectively.[4] Since then, *cyclo*-As$_n$ ligand complexes bearing *cyclo*-As$_3$,[4a,5] *cyclo*-As$_4$,[6] *cyclo*-As$_5$,[7] *cyclo*-As$_6$[8] and even *cyclo*-As$_8$[9] ligands, which are related to the respective hydrocarbons via the isolobal principle,[10] have been isolated, often by using yellow arsenic (As$_4$).[11] Other representatives include transition metal polyarsenides, such as the recently

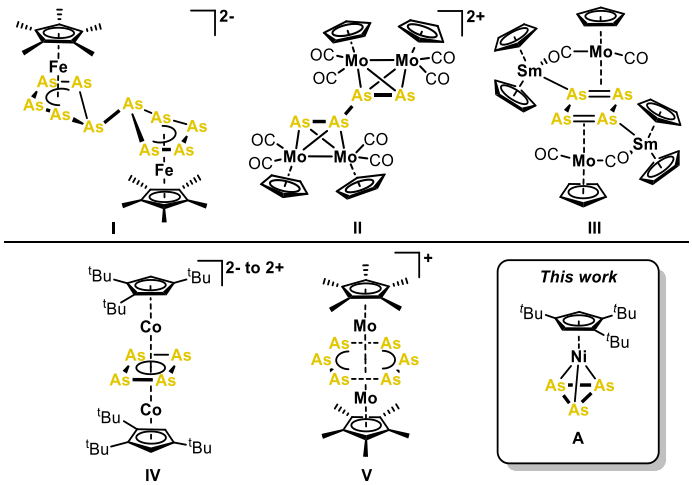

*Scheme 1: Selected examples of transition metal poly-arsenides (**I** - **V**) arising from the oxidation or reduction of As$_n$ ligand complexes and the starting material **A**.*

isolated binary Fe/As Zintl cluster[12] $[Fe_3(As_3)_3As_4]^{3-}$ or organometallic polyarsenides, as e. g. $[\{Cp^*Co\}_3(\mu_3,\eta^{4:4:4}\text{-}As_6)]^{0/+/2+}$ ($Cp^* = C_5Me_5$).[13] One field of particular interest is the redox chemistry of such E_n ligand complexes, as, on the one hand, it allows to study the redox properties of these species which are otherwise inaccessible and, on the other hand, grants access to completely unprecedented E_n structural motifs. Thus, one-electron oxidation of the prominent ferrocene analog $[Cp^*Fe(\eta^5\text{-}P_5)]$ affords a bicyclic P_{10} ligand, while its stepwise reduction first yields a bicyclic P_{10} motif as well, which can then be further reduced to the extremely reactive $[Cp^*Fe(\eta^4\text{-}P_5)]^{2-}$.[14] In contrast, the reduction of the heavier $[Cp^*Fe(\eta^5\text{-}As_5)]$ leads to a myriad of aggregated Fe polyarsenides, with $[\{Cp^*Fe\}_2(\mu,\eta^{4:4}\text{-}As_{10})]^{2-}$ (**I**) as one example (Scheme 1).[15] The smaller $[\{CpMo(CO)_2\}_2(\mu,\eta^2\text{-}As_2)]$ dimerizes upon oxidation to form a dicationic As_4 chain (**II**),[16] while its reduction leads to Mo-Mo bond cleavage or the formation of a *cyclo*-As_4 ligand (**III**). The latter reduction is highly dependent on the Cp^R ligand employed at the Mo centers.[17] The triple-decker complex $[\{Cp'''Co\}_2(\mu,\eta^{4:4}\text{-}As_4)]$ can be stepwisely oxidized as well as reduced by two electrons, each, in both cases surprisingly leading to sequential As-As bond formation within the As_4 ligand (**IV**, Scheme 1).[6d] Similarly, oxidation and reduction of the prismane complex $[\{Cp^*Fe\}_3(\mu_3,\eta^{4:4:4}\text{-}As_6)]$ only lead to minor distortion within the As_6 ligand.[18] Finally, the oxidation of the hexaarsa-benzene complex $[\{Cp^*Mo\}_2(\mu,\eta^{6:6}\text{-}As_6)]$ leads to the bis-allylic distortion of the *cyclo*-As_6 ligand (**V**).[19] In comparison, little is known about the redox chemistry of *cyclo*-As_3 ligand complexes. While the reduction of $[\{(nacnac)M\}_2(\mu,\eta^{3:3}\text{-}As_3)]^{2+}$ (M = Co, Ni, nacnac = $[\{N(2,6\text{-}^iPr_2C_6H_3)C(Me)\}_2CH]^-$) has no significant structural influences on the M_2As_3 core,[20] the redox properties of end-deck *cyclo*-As_3 ligand complexes are completely unexplored. Herein, we report on the oxidation as well as the reduction of $[Cp'''Ni(\eta^3\text{-}As_3)]$ (**A**, Scheme 1),[21] a complex with an end-deck *cyclo*-As_3 ligand, which leads to a series of triple-decker complexes bearing an Ni_2As_3 core. Additionally, light is shed onto the intriguing reaction pathway, which follows upon the initial one electron oxidation of **A**.

9.3. Results and Discussion

While the oxidation of $[Cp'''Ni(\eta^3\text{-}As_3)]$ (**A**) with an equimolar amount of oxidizing agent (e. g. [Thia][FAl], [Fc][FAl] or $[Fc^{Diac}][FAl]$; Thia = $C_{12}H_8S_2$, Fc = Cp_2Fe, Fc^{Diac} = $\{CpC(O)CH_3\}_2Fe$, $[FAl]^-$ = $[FAl\{O(1\text{-}C_6F_5)C_6F_{10}\}_3]^-$) results in a mixture of several products (see SI), the careful addition of 0.5 equivalents of $[Fc^{Diac}][FAl]$ (Fc^{Diac} = $\{CpC(O)CH_3\}_2Fe$, $[FAl]^-$ = $[FAl\{O(1\text{-}C_6F_5)C_6F_{10}\}_3]^-$) to a solution of **A** affords the triple-decker cation $[\{Cp'''Ni\}_2(\mu,\eta^{3:3}\text{-}As_3)][FAl]$ (**1**) in 49% yield, as well as three equivalents of grey arsenic (Scheme 2).[21] Similarly, the reduction of **A** with KC_8 leads to the extrusion of (grey) arsenic and the formation of the triple-decker anion $[K@crypt][\{Cp'''Ni\}_2(\mu,\eta^{3:3}\text{-}As_3)]$ (**2**) (Scheme 2). **2** can be isolated as a dark deep blue crystalline solid in 50% yield. Logically, a neutral As_3 triple-decker complex $[\{Cp'''Ni\}_2(\mu,\eta^{3:3}\text{-}As_3)]$ (**3**) was hypothesized to link both ionic species electrochemically. Indeed, the cyclic voltammogram of **1** in *o*-DFB reveals two reversible reduction processes at -0.07 V and -1.30 V (vs. Fc/Fc^+, see SI), reminiscent of the stepwise reduction of **1** to **2**. Chemical reduction of **1**

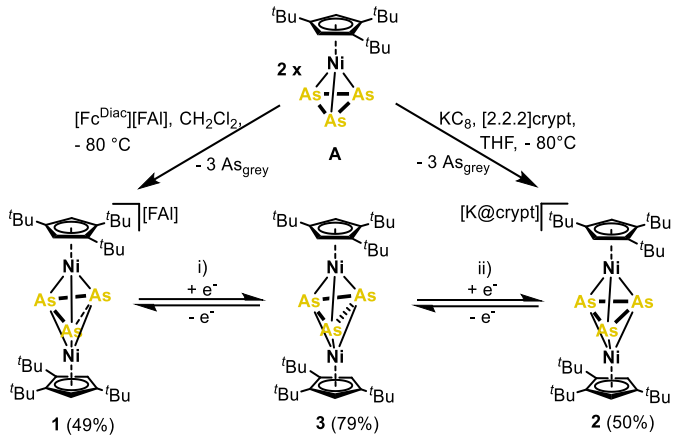

*Scheme 2: Oxidation and reduction of **A** to the ionic triple-decker species **1** and **2**, as well as the reduction of **1** to **3**; i) Cp_2Co, o-DFB, r. t., 2 h; isolated yields are given in parentheses; ii) [Fc][PF_6], THF, -80 °C, 2 h.*

with one equivalent of Cp_2Co affords a dark, intensely red colored solution of **3**. After workup, the neutral triple-decker species **3** can be isolated in good crystalline yields of 79% (Scheme 2). Likewise, **3** is accessible via the oxidation of **2** with [Fc][PF_6], with **3** being obtained in slightly lower yields of 62 % (see SI).

The core structural motifs of **1** - **3** are assembled from two {Cp'''Ni} moieties bridged by a central As_3 ligand (Figure 1). While the anion in **2** features very similar As-As bond lengths of *d*(As-As) = 2.438(4) - 2.505(6) Å, one of these bonds undergoes stepwise elongation via the neutral **3** (*d*(As1-As3) = 2.693(1) Å) to the cationic **1** (*d*(As1-As3) = 2.873(1) Å, Figure 1). This deformation of the *cyclo*-As_3 ligand in **2** to the allylic As_3 ligand in **1** is accompanied by a shift of the Ni atoms above the As1-As3 vector and significant tilting of the Cp''' against each other (**2**: 4.7(1)°, **3**: 18.6(1)°, **1**: 28.9(1)°). This behavior is consistent with the stepwise depopulation of the bonding As1-As3 interaction in **2** (*vide infra*). Notably, a similar structural trend has been observed for a series of lighter homologous P_3 triple-decker complexes.[22] Compounds **1** and **2** display diamagnetic character in their ^{1}H NMR spectra which agrees with their even electron count of 32 and 34 valence electrons (VE), respectively. In contrast, the neutral compound **3** shows highly broadened signals in its ^{1}H NMR spectrum, hinting towards its paramagnetic nature. Indeed, the X-band EPR spectrum of **3** in frozen *n*-pentane recorded at 77 K reveals

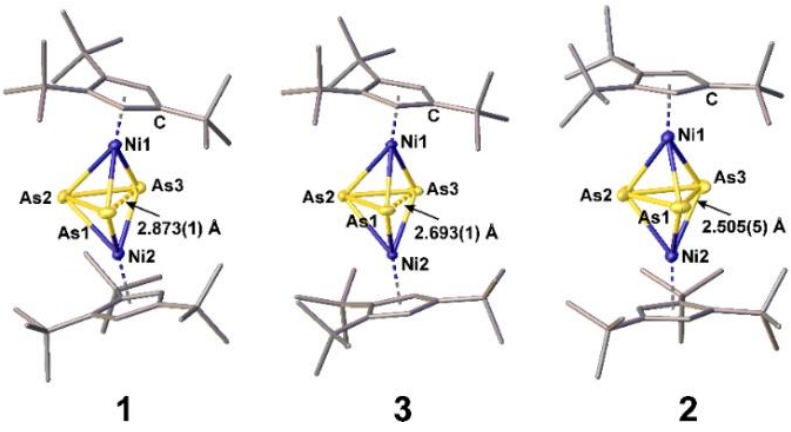

*Figure 1: Solid state structures of the triple-decker species **1** – **3**; the As1-As3 bond lengths are given as an insert and ellipsoids are drawn at the 50% probability level.*

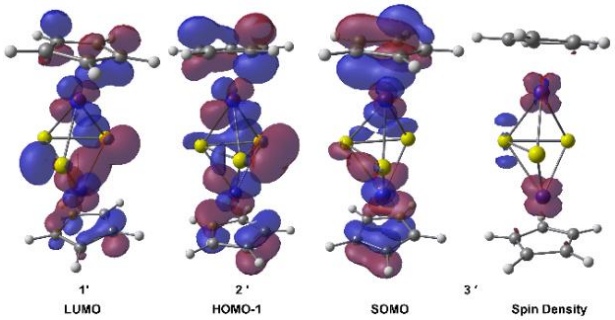

*Figure 2: Selected molecular orbitals of optimized (@ωB97-D3/def2-TZVP) model systems of **1'** – **3'** and overall spin density of **3´**; isosurface cut-off at 0.04 a. u. for MOs and 0.01 a. u. for the spin density.*

an axial signal with $g_{\parallel}$ = 2.15 and $g_{\perp}$ = 2.02 corroborating its paramagnetic character (see SI). This is in line with its odd 33 VE. Furthermore this axial signal is in line with the spin density being mostly metal centered (*vide infra*). To gain deeper insight into the electronic structure of these triple-decker compounds, DFT calculations were performed at the ωB97X-D3/def2-TZVP level of theory with the bulky Cp''' being replaced with Cp ligands to save computational resources. Looking at the LUMO of the oxidation product **1'** clearly reveals the contribution of p-orbitals of As1 and As3 (Figure 2). Populating this orbital with two electrons, as in the HOMO-1 of **2'**, leads to bonding interaction and, thus, the shortening of the As1-As3 distance observed experimentally. In contrast, the SOMO of compound **3'** shows only minor contribution of the As atoms and localization of the spin primarily at the Ni atoms. However, close inspection of the overall spin density distribution in **3´** reveals a small contribution of the As2 atom, besides those of the Ni atoms. This agrees with the experimental finding of small, yet unresolved ^{75}As coupling observed in the EPR spectrum of **3**.

Initial experiments on the oxidation of **A** in a 1:1 stoichiometry resulted in a product mixture (*vide supra*), from which a second product, namely [{Cp'''Ni}$_2$(μ,$\eta^{2:2:1:1:1}$-As$_5$)][FAl] (**4**), could be identified. Thus, the oxidative fragmentation of **A** was further studied to obtain a deeper understanding of the reaction pathway (Figure 3a). **A** reacts with the relatively strong oxidizing agent [Thia][FAl] (0.860 V vs. Fc/Fc$^+$)[23] by releasing the complete *cyclo*-As$_3$ ring to form [Cp'''Ni($\eta^{1:1}$-thia)][FAl] (**5**) in 16 % isolated crystalline yield (Figure 3). Even if **1** was not obtained, this reaction nonetheless indicates the formation of a {Cp'''Ni}$^+$ fragment which could be trapped with thianthrene. Notably, **5** can be accessed in even higher yields via a salt metathesis approach starting from [{Cp'''Ni}(μ-Br)]$_2$ (see SI). On the one hand, the one-electron oxidation of **A** to form the radical cation [Cp'''Ni(η^3-As$_3$)]$^{\cdot+}$, followed by the dissociation of the As$_3$ ligand (in form of As$_{grey}$) and further reaction with another molecule **A**, is anticipated to be responsible for the formation of **1** (see SI). On the other hand, the formation of **4** should be favored by a constant high local concentration of [**A**]$^+$ to increase the probability for two [Cp'''Ni(η^3-As$_3$)]$^{\cdot+}$ to encounter each other and simultaneously prevent formation of **1**. This was achieved by changing the order of addition. When first charging the Schlenk flask with both solids, **A** and [Fc^{Diac}][TEF^{Cl}] ([TEF^{Cl}]$^-$ = [Al{OC(CF$_3$)$_2$(CCl$_3$)}$_4$]$^-$), followed by the addition of cold (-80 °C) CD_2Cl_2, yielded a ratio of 0.35:1 (**4**:**1**) of the products. When **A** was added slowly (2 min) at -80 °C to an equimolar amount of [Fc^{Diac}][TEF^{Cl}], a ratio of 0.42:1 (**4**:**1**) was obtained.

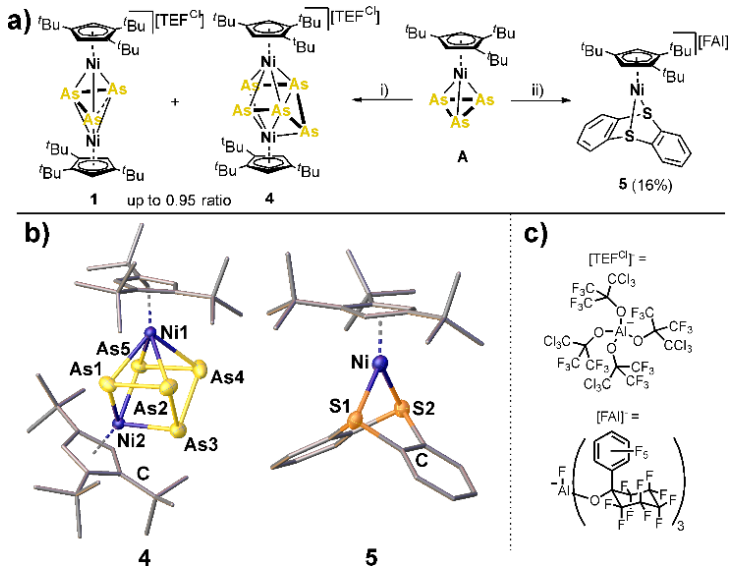

*Figure 3: a) Synthesis of **4** and **5**, i) [Fc^{Diac}][TEF^{Cl}], CD_2Cl_2, -80 °C, 10 min, ii) [Thia][FAl], o-DFB, r.t., 4h; b) Solid state structures of **4** and **5**, ellipsoids are drawn at the 50% probability level; c) schematic representation of the anions [TEF^{Cl}]$^-$ and [FAl]$^-$.*

Prolonging the addition time to 10 min, further increased the ratio up to 0.95:1 (**4**:**1**, for details see SI). A concentrated solution of **1** + **4** in CH_2Cl_2 layered with *n*-pentane afforded crystals in which **1** and **4** are co-crystallized (see SI), enabling the structural elucidation of the latter compound. In **4**, two {Cp'''Ni} fragments are bridged by a chain-type, strongly bent As_5 ligand (Figure 3b). The As-As bond lengths (2.402(7) – 2.431(7) Å) are in the range of single bonds,[24] while the As1-As5 (2.831(6) Å) and the As2-As4 (2.796(6) Å) distances indicate the chain character of the As_5 ligand. The As3 atom is strongly bent out of the plane of the other As atoms by 79.9(2)°. Notably, **4** displays the first species featuring such a bent As_5 ligand in the coordination sphere of two Ni atoms.

9.4. Conclusion

In summary, the redox reactivity of the end-deck *cyclo*-As_3 complex [Cp'''Ni($\eta^{3:3}$-As_3)] (**A**) undergoes fragmentation upon both oxidation, and reduction. While oxidation affords the cationic triple-decker [{Cp'''Ni}$_2$(μ,$\eta^{3:3}$-As_3)][FAl] (**1**), reduction yields the corresponding anionic complex [K@crypt][{Cp'''Ni}$_2$(μ,η^3-As_3)] (**2**). Interestingly, these compounds are electrochemically linked via the neutral paramagnetic [{Cp'''Ni}$_2$(μ,$\eta^{3:3}$-As_3)] (**3**), which is accessible from both **1** and **2** and confirmed by cyclic voltammetry. The variation of the reaction conditions during the oxidation of **A** gives insight into the reaction pathway, which presumably involves the cleavage of the As_3 ligand from the initial oxidation product followed by the trapping of the highly reactive {Cp'''Ni}$^+$ with either another equivalent of **A** or e.g. with thianthrene to afford the As-rich complex [{Cp'''Ni}$_2$(μ,$\eta^{2:2:1:1:1}$-As_5)][FAl] (**4**) or the product [Cp'''Ni($\eta^{1:1}$-thia)][FAl] (**5**), which does not contain As. Our findings are supported by detailed computational studies providing insight into the electronic structure of the triple-decker series **1** - **3**.

9.5. Supporting Information

9.5.1. Experimental Procedures

General Considerations

All manipulations were carried out using standard Schlenk techniques at a Stock apparatus under N_2 as an inert gas or in a glovebox with Ar atmosphere. The nitrogen inert gas was led over a BASF R 3-1 ($CuO/MgSiO_3$) catalyst to remove traces of oxygen. By flowing the nitrogen inert gas through concentrated sulfuric acid, orange gel and SICAPENT® traces of moisture were eliminated. All glassware was dried with a heatgun (600 °C) for at least 30 min prior to use. *o*-DFB and CD_2Cl_2 were distilled from CaH_2 and other solvents were directly taken from an MBraun SPS-800 solvent purification system and degassed at room temperature prior to use. Solution ^{1}H (400.130 MHz), ^{11}B (128.379 MHz) and ^{19}F (376.498 MHz) NMR spectra were recorded on a Bruker Avance400 spectrometer using $(H_3C)_4Si$ (^{1}H), $BF_3{\cdot}Et_2O$ (^{11}B) or $CFCl_3$ (^{19}F), respectively, as external standards. Chemical shifts (δ) are provided in parts per million (ppm) and coupling constants (*J*) are reported in Hertz (Hz). The following abbreviations are used: s = singlet, d = doublet, dd = doublet of doublets, t = triplet, br = broad and m = multiplet. Elemental analysis of the products was conducted by the elemental analysis department at the University of Regensburg using an Elementar Vario EL. ESI mass spectra were either recorded at the internal mass spectrometry department using a ThermoQuest Finnigan TSQ 7000 mass spectrometer or in our own group using a Micro mass spectrometer. The peak assignment was performed using the molecular weight calculator 6.50.[25] IR spectra were recorded as solids using a ThermoFisher Nicolet iS5 FT-IR spectrometer with an iD7 ATR module and an ITX Germanium or ITX Diamond crystal. The starting materials [Cp'''Ni(η^3-As_3)][21], [Cp'''Ni(μ-CO)]$_2$,[26] [Thia][FAl][16] and KC_8[27] were synthesized following literature procedures. [Fc^{Diac}][X] ([X]$^-$ = [FAl]$^-$, [TEF^{Cl}]$^-$) were synthesized according to the literature procedure for [Fc^{Diac}][TEF].[28] All other chemicals were purchased from commercial vendors.

Yellow arsenic and arsenic compounds are extremely hazardous. Their handling has to be performed with great care and contact (skin, breathing, swallowing) must be avoided at all costs. The arsenic compounds used during this work were handled and disposed according to the regulation (EG) Nr. 1272/2008 of the European union (Appendix VI, Table 3.1, 033-002-00-X and 033-002-00-5, arsenic and arsenic compounds, with the exception of those specified elsewhere in this annex). The following GHS hazard statements need to be considered before using these compounds: H301, H331, H400, H410. Due to their high toxicity, these compounds need to be handled extremely carefully, the respective solids or solutions were disposed in special collecting tanks for Hg-, Tl-, As-, Se-, Be-containing waste.

*[(Cp'''Ni)$_2$($\mu,\eta^{3:3}$-As$_3$)][FAl] (**1**)*

Compound **1** was prepared according to literature procedures. Nevertheless, compound **1** was fully characterized due to reasons of completeness.[21]

A solution of [Fc^{Diac}][FAl] (83 mg, 0.05 mmol, 1 eq.) in CH_2Cl_2 (3 mL) was added at -80 °C to a solution of [Cp'''Ni(η^3-As$_3$)] (**A**) (52 mg, 0.1 mmol, 2 eq.) in CH_2Cl_2. The colour of the reaction mixture changed from red to dark brown immediately. After the reaction mixture was stirred for 2 h at room temperature, *n*-pentane (30 mL) was added to precipitate a brown powder which was washed with *n*-pentane (2 x10 mL) and with toluene (10 mL). After drying under reduced pressure (10^{-3} mbar), the residue was dissolved with CH_2Cl_2 (3 mL) and layered with *n*-pentane (15 mL). After one day room temperature, dark orange blocks of [(Cp'''Ni)$_2$($\mu,\eta^{3:3}$-As$_3$)][FAl] (**1**) suitable for single crystals X-ray analysis were obtained.

Yield:	55 mg (0.0247 mmol, 49%).
Elemental analysis:	calc. (%) for $C_{70}H_{58}O_3F_{46}Ni_2As_3Al$: C: 38.39, H: 2.67.
	found (%): C: 38.65, H: 2.65.
ESI(+) MS (*o*-DFB):	calc. (g/mol) for $[C_{34}H_{58}Ni_2As_3]^+$: *m/z* = 807.0831 $[M]^+$.
	found: *m/z* (%) = 807.1 (10%) [(Cp'''Ni)$_2$($\mu,\eta^{3:3}$-As$_3$)]$^+$ (M^+), 332.2 (100%) [Cp'''Ni(MeCN)]$^+$, 373.2 (25%) [Cp'''Ni(MeCN)$_2$]$^+$, 668.1 (10%) (unidentified) 1175.2 (10%) [(Cp'''Ni)$_3$As$_4$]$^+$.
NMR (CD_2Cl_2, r.t.):	**^{1}H**: *δ*/ppm = 0.95 (s, 18 H, $C_5H_2\underline{^tBu_3}$), 1.35 (s, 36 H, $C_5H_2\underline{^tBu_3}$), 5.09 (s, 4 H, $C_5\underline{H_2}{}^tBu_3$).
	^{19}F{^{1}H}: *δ*/ppm = -172.0 (s, 1 F, AlF), -165.1 (t, $J_{F\text{-}F}$ = 20 Hz, 6F, *m*-C_6F_5), -154.5 (t, $^3J_{F\text{-}F}$ = 20 Hz, 3F, *p*-C_6F_5), -141.4 (d, $J_{F\text{-}F}$=272 Hz, 3F), -137.7 (d, $J_{F\text{-}F}$=274 Hz, 6F), -130.6 (d, $J_{F\text{-}F}$=288 Hz, 6F), -127.9 (s, 6F), -121.8 (d, $J_{F\text{-}F}$=270 Hz, 3F), -117.1 (d, $J_{F\text{-}F}$=280 Hz, 6F), -112.6 (d, $J_{F\text{-}F}$=280 Hz, 6F).

*[(Cp'''Ni)$_2$(μ,$\eta^{3:3}$-As$_3$)][TEF^{Cl}] (**1**) and [(Cp'''Ni)$_2$(μ,$\eta^{2:2:1:1:1}$-As$_5$)][TEF^{Cl}] (**4**)*

A solution of [Cp'''Ni(η^3-As$_3$)] (26 mg, 0.05 mmol, 1 eq.) in CH_2Cl_2 (0.5 mL) was added at -80 °C to a solution of [Fc^{Diac}][TEF^{Cl}] (72 mg, 0.05 mmol, 1 eq.) in CH_2Cl_2 (0.5 mL) over a period of 10 min. The colour of the reaction mixture changed from red to dark reddish-brown immediately. After the reaction mixture was allowed to warm to room temperature, the NMR sample was submitted. An integral ratio of **1**:**4** of 1:0.95 was found in the ^{1}H NMR spectrum.

ESI(+) MS (*o*-DFB): calc. (g/mol) for $[C_{34}H_{58}Ni_2As_3]^+$: *m/z* = 807.0831 $[M_1]^+$, calc. (g/mol) for $[C_{34}H_{58}Ni_2As_5]^+$: *m/z* = 956.9325 $[M_4]^+$.

found: *m/z* (%) = 807.1 (100%) [(Cp'''Ni)$_2$(μ,$\eta^{3:3}$-As$_3$)]$^+$ (M_1^+), 956.9 (50%) [(Cp'''Ni)$_2$(μ,$\eta^{2:2:1:1:1}$-As$_5$)]$^+$ (M_4^+), 332.2 (90%) [Cp'''Ni(MeCN)]$^+$, 271.0 (95%) (unidentified), 373.2 (25%) [Cp'''Ni(MeCN)$_2$]$^+$, 638 (40%) (unidentified).

NMR (CD_2Cl_2, r.t.): **^{1}H**: δ/ppm = 0.96 (s, 18 H, $C_5H_2{}^t\underline{Bu_3}$ of **1**), 1.32 (s, 18 H, $C_5H_2{}^t\underline{Bu_3}$ of **4**), 1.35 (s, 36 H, $C_5H_2{}^t\underline{Bu_3}$ of **1**), 1.45 (s, 36 H, $C_5H_2{}^t\underline{Bu_3}$ of **4**), 5.10 (s, 4 H, $C_5\underline{H_2}{}^tBu_3$ of **1**), 5.52 (s, 4 H, $C_5\underline{H_2}{}^tBu_3$ of **4**).

*[K@crypt][(Cp'''Ni)$_2$(μ,$\eta^{3:3}$-As$_3$)] (**2**)*

THF (8 mL) was condensed into a Schlenk flask containing [Cp'''Ni(η^3-As$_3$)] (**A**) (207 mg, 0.4 mmol, 2.0 eq.), KC_8 (30 mg, 0.22 mmol, 1.1 eq) and [2.2.2]cryptant (75 mg, 0.2 mmol, 0.5 eq.) The reaction mixture was stirred for 3 h at -80 °C, allowed to warm to room temperature and further stirred for 1 h. The colour of the reaction mixture changed from red to black immediately. The solvent was removed *in vacuo* and the black residue washed with *n*-hexane (3 x 10 mL). After drying under reduced pressure (10^{-3} mbar), the residue was dissolved with THF (5 mL) and filtered through a glass fibre filter paper. The black solution was layered with *n*-hexane. After five days at room temperature, black crystals of [K@crypt][(Cp'''Ni)$_2$(μ,$\eta^{3:3}$-As$_3$)] (**2**) suitable for single crystal X-ray analysis were obtained. The solvent was removed by decanting and the crystals dried in vacuum for 3 h.

Yield:	122 mg (0.10 mmol, 50%).
Elemental analysis*:	calc. (%) for $C_{52}H_{94}N_2O_6KNi_2As_3$: C: 51.00, H: 7.74, N: 2.29.
	found (%): C: 50.18, H: 7.38., N: 2.12.
ESI(-) MS (THF):	calc. (g/mol) for $[C_{34}H_{58}Ni_2As_3]$: *m/z* = 807.0831 $[M]^+$.
	found: *m/z* (%) = no signal due to decomposition during the ionization process.
NMR (THF-d^8, r.t.):	**^{1}H**: δ/ppm = 1.19 (s, 18 H, $C_5H_2\underline{^tBu_3}$), 1.36 (s, 36 H, $C_5H_2\underline{^tBu_3}$), 2.61 (t, $^3J_{H\text{-}H}$ = 4.6 Hz, 12H, 2.2.2-crypt), 3.59 (t, $^3J_{H\text{-}H}$ = 4.6 Hz, 12H, 2.2.2-crypt overlapping with THF-d^8 signal), 3.64 (s, 12H, 2.2.2-crypt), 4.54 (s, 4 H, $C_5\underline{H_2}^tBu_3$).

* Compound **2** is extremely sensitive and rapidly decomposes to form grey arsenic, contaminating samples for elemental analysis.

[(Cp'''Ni)$_2$($\mu,\eta^{3:3}$-As$_3$)] (***3***)

Method A:

A solution of [Cp_2Co] (45 mg, 0.24 mmol, 0.96 eq.) in *o*-DFB (3 mL) was added slowly to a solution of [(Cp'''Ni)$_2$($\mu,\eta^{3:3}$-As$_3$)][PF_6] (237 mg, 0.25 mmol, 1.0 eq.) in *o*-DFB (3 mL). The colour of the reaction mixture changed immediately to intense red. The reaction mixture was stirred for 1 h at room temperature, the solvent was removed *in vacuo* and the dark residue was extracted with *n*-hexane (5 mL) and filtered through a glass fibre filter paper. The solvent was removed and the residue dissolved in 1 mL *n*-pentane. Red crystals suitable for single crystal X-ray analysis were obtained by slow diffusion of *n*-pentane into toluene. The solvent was removed by decanting and the crystals dried in vacuum for 3 h.

Method B:

A solution of [Fc][PF_6] (53 mg, 0.16 mmol, 1 eq.) in THF (3 mL) was added at -80 °C slowly to a solution of [K@crypt][(Cp'''Ni)$_2$($\mu,\eta^{3:3}$-As$_3$)] (**2**) (204 mg, 0.16 mmol, 1.0 eq.) in THF (3 mL). The colour of the reaction mixture changed immediately to intense red. The reaction mixture was allowed to warm to room temperature and stirred for 2 h at room temperature. The solvent was removed *in vacuo* and the dark residue was extracted with *n*-hexane (10 mL) and filtered through a glass fibre filter paper. A dark powder was obtained by removing the solvent under reduced pressure (10^{-3} mbar) and subsequent drying in vacuum for 3 h.

Yield:	Method A: 153 mg (0.19 mmol, 79 %).
	Method B: 83 mg (0.10 mmol, 62 %).
Elemental analysis:	calc. (%) for $C_{34}H_{58}Ni_2As_3$: C: 50.48, H: 7.23.
	found (%): C: 50.61, H: 7.34.
LIFDI MS (toluene):	calc. (g/mol) for $[C_{34}H_{58}Ni_2As_3]^+$: *m/z* = 807.0831 $[M]^+$.
	found: *m/z* (%) = no signal of **3** due to decomposition during the ionization process.
NMR (C_6D_6, r.t.):	**^{1}H**: *δ*/ppm = 3.24 (s(*br*), 36 H, $C_5H_2{}^t\underline{Bu_3}$), 4.15 (s(*br*), 18 H, $C_5H_2{}^t\underline{Bu_3}$).

*[Cp'''Ni($\eta^{1:1}$-thia)][FAl] (**5**)*

A solution of [Thia][FAl] (159 mg, 0.1 mmol, 1 eq.) in *o*-DFB (10 mL) was added at room temperature to a solution of [Cp'''Ni(η^3-As_3)] (**A**) (52 mg, 0.1 mmol, 1 eq.) in *o*-DFB. The colour of the reaction mixture changed from red to dark brown-red immediately. After the reaction mixture was stirred for 4 h at room temperature, *n*-pentane (40 mL) was added to precipitate a brown powder which was dried under reduced pressure (10^{-3} mbar). The residue was dissolved with *o*-DFB (12 mL) and layered with *n*-pentane (40 mL). After five days at room temperature, red blocks of [Cp'''Ni($\eta^{1:1}$-thia)][FAl] (**5**) suitable for single crystal X-ray analysis were obtained. The solvent was decanted, and the crystals were dried in vacuum for 3 h.

Alternatively, **5** can be synthesized via halide substitution of [Cp'''Ni(μ-Br)]$_2$:

[Cp'''Ni(μ-Br)]$_2$ (37 mg, 0.05 mmol, 0.5 eq.), Ag[FAl]•CH_2Cl_2 (157 mg, 0.1 mmol, 1 eq.) and thianthrene (22 mg, 0.1 mmol, 1 eq.) were dissolved in 4 mL of *o*-DFB rapidly affording a dark red suspension and white solid. After completing the reaction by stirring at room temperature for 16 h, the solution was filtered, and 60 mL of *n*-hexane were added to precipitate **5** as a light red powder. Drying under reduced pressure (10^{-3} mbar) afforded **5** as analytically pure compound in 90% yield.

Yield:	30 mg (0.016 mmol, 16%).
Elemental analysis:	calc. (%) for $C_{65}H_{37}O_3F_{46}AlS_2Ni$•(o-DFB)$_{0.6}$: C: 42.08, H: 2.03, S: 3.28.
	found (%): C: 42.16, H: 2.15, S: 3.52.
ESI(+) MS (*o*-DFB):	calc. (g/mol) for $[C_{29}H_{37}NiS_2]^+$: *m/z* = 507.1690 $[M]^+$.
	found: *m/z* (%) = 507.2 (1%) [Cp'''Ni($\eta^{1:1}$-thia)]$^+$ (M^+), 332.2 (100%) [Cp'''Ni(MeCN)]$^+$, 373.2 (30%) [Cp'''Ni(MeCN)$_2$]$^+$.
NMR (CD_2Cl_2, r.t.):	**^{1}H**: *δ*/ppm = 0.99 (s, 9 H, $C_5H_2{}^t\underline{Bu_3}$), 1.18 (s, 18 H, $C_5H_2{}^t\underline{Bu_3}$), 4.74 (s, 2 H, $C_5\underline{H_2}{}^tBu_3$), 7.47 (m, 4 H, thianthrene), 7.91 (m, 4 H, thianthrene).

9.5.2. Mechanistic Investigations on the Oxidation of A

First attempts on the oxidation of **A** with [Fc^{Diac}][FAl] afforded compounds **1** and **4** in a 9:1 ratio according to X-ray crystallography and ^{1}H NMR spectroscopy. Hence, we aimed to direct the reaction towards **1** and **4** respectively by variation of reaction parameters (oxidation agent, temperature, time/order of addition, solvent). Since **A** reacts with the relatively strong oxidation agent [thia][FAl] to form [Cp'''Ni($\eta^{1:1}$-thia)][FAl] (**5**), it indicates the formation of a {Cp'''Ni}$^{+}$ fragment which is formed during the reaction and could be trapped with thianthrene. We obtained **1** selectively by addition of 0.5 eq. [Fc^{Diac}][FAl] to **A** in CH_2Cl_2 at -80 °C. We anticipate the mechanism to occur via the middle path of Scheme 1. One-electron oxidation of **A** leads to the formation of the radical cation [Cp'''NiAs$_3$]$^{\cdot+}$, dissociation of the As$_3$ ligand (in form of gray arsenic) and further reaction with another molecule of **A** should give **1**.

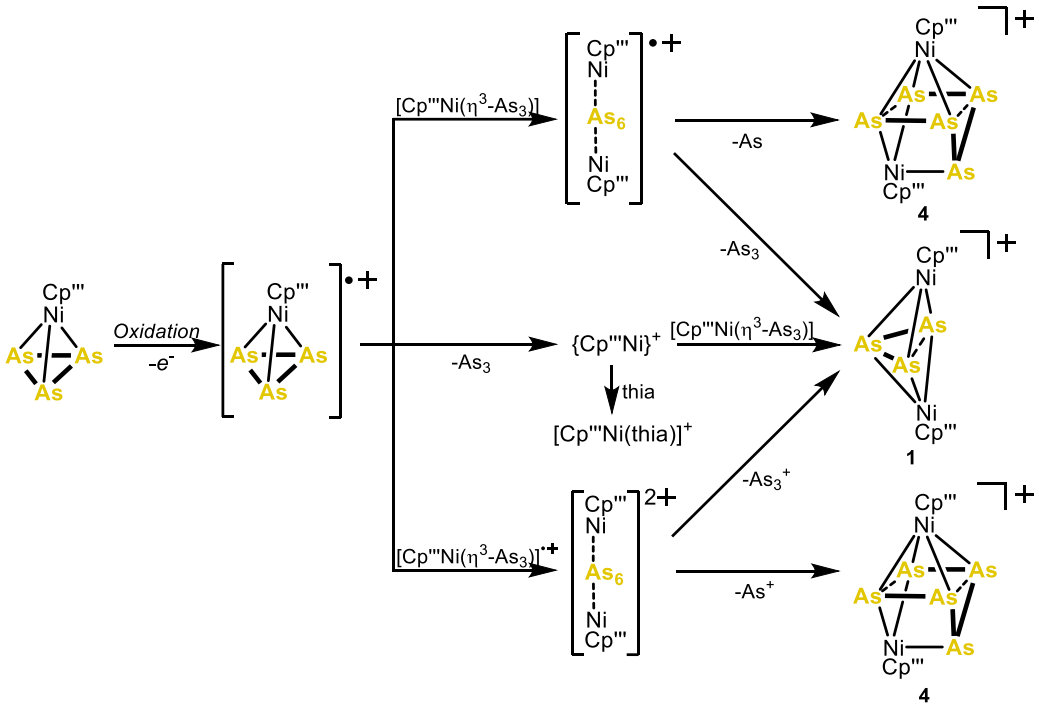

*Scheme S 1: Possible reaction pathways for the oxidation of **A**.*

As oxidation agent, solvent and temperature seemed not to play a significant role in the product ratio, we expected presence of the {Cp'''Ni}$^{+}$ fragment favors formation of **1**. First, we decided to use concentrated solutions of **A**, in order to ensure a high local concentration of [**A**]$^{+}$. By this, we hoped to favor the formation of [(Cp'''Ni)$_2$As$_6$]$^{+}$ or [(Cp'''Ni)$_2$As$_6$]$^{2+}$ (upper and lower part of Scheme 1). Nevertheless, we almost only saw formation of **1**, thus As$_3$ elimination has to be much faster than As elimination. Next, we changed the order of addition. By adding **A** to the oxidation agent, a constant excess of oxidation agent would increase the probability for two [Cp'''NiAs$_3$]$^{+}$ to meet each other (Scheme S1, bottom part) and favor formation of **4**. Indeed,

charging the Schlenk flask with **A** and [Fc^{Diac}][TEF^{Cl}] increased the ratio of **1**:**4** to 1:0.35. Next we added a concentrated solution of **A** to [Fc^{Diac}][TEF^{Cl}] at -80 °C over a period of 2 min, with a ratio of **1**:**4** of 1:0.42. Elongating the reaction time from 2 min to 10 min did further increase the preferred formation of **4**, and a ratio of **1**:**4** of 1:0.95 was observed.

In summary, formation of **1** could not be circumvented, however we were able to find conditions for increasing its ratio significantly. Presumably, the middle path of Scheme S1 is kinetically most favored. Maximum excess of the oxidation agent ensures the possibility for two $[Cp'''NiAs_3]^+$ to meet each other and to follow the bottom part of Scheme S1.

*Table S 1: Optimization for the syntheses of **1** and **4**, respectively. Procedure: Solution 2 was added to solution 1 under the given conditions.*

Entry	***Solution 1***	***Solution 2***	***Conditions***	***Ratio 1:4***
1	***A** (0.1 mmol) in CH_2Cl_2 (1.0 mL)*	*[Fc^{Diac}][FAl] (0.025 mmol) in CH_2Cl_2 (1.0 mL)*	*addition time: 1 min, addition temp. -80 °C*	*1:0.03*
2	***A** (0.1 mmol) in CH_2Cl_2 (0.5 mL)*	*[Fc][FAl] (0.05 mmol) in CH_2Cl_2 (1.0 mL)*	*addition time: 1 min, addition temp. r.t.*	*1:0.08*
3	***A** (0.1 mmol) in o-DFB (1.0 mL)*	*[Fc][FAl] (0.05 mmol) in o-DFB (1.0 mL)*	*addition time: 1 min, addition temp. r.t.*	*1:0.26*
4	***A** (0.05 mmol) and [Fc^{Diac}][TEF^{Cl}] (0.5 mmol) were weight in together in CD_2Cl_2 (1.5 mL)*		*addition temp. -80 °C*	*1:0.35*
5	*[Fc^{Diac}][TEF^{Cl}] (0.05 mmol) in CH_2Cl_2 (0.5 mL)*	***A** (0.05 mmol) in CH_2Cl_2 (0.5 mL)*	*addition time: 2 min, addition temp. -80 °C*	*1:0.42*
6	*[Fc^{Diac}][TEF^{Cl}] (0.05 mmol) in CH_2Cl_2 (0.5 mL)*	***A** (0.05 mmol) in CH_2Cl_2 (0.5 mL)*	*addition time: 10 min, addition temp. -80 °C*	*1:0.95*

9.5.3. X-ray Crystalloraphic Data

General Considerations

The crystallographic data for all synthesized compounds was collected either on an Xcalibur Gemini with an AtlasS2 detector using Cu-K_α radiation (**1**) on a GV1000 diffractometer (AT) with a TitanS2 detector using Cu-K_α radiation (**5**) or Cu-K_β radiation (**1** + **4**) or on a XtaLAB Synergy R, DW system with HyPix-Arc 150 detector applying Cu-Kα radiation (**2**, **3**) from a rotating anode X-ray source. All measurements were performed at 123 K. Data collection, data reduction and absorption correction were performed with the CrysAlisPro[29] software package. Structure solution and refinement was conducted in Olex2[30] with ShelXT[31] and ShelXL[32] (full-matric least-squares method against F^2). All non-hydrogen atoms were refined with anisotropic displacement parameters and hydrogen atoms were treated as riding models with isotropic displacement parameters and fixed C-H bond lengths (sp^3: 0.96 (CH_3), 0.97 (CH_2), sp^2: 0.93 (CH)). Visualization of the crystal structures was performed with Olex2.[30]

CCDC-2064654 (**1**), CCDC-2263450 (**2**), CCDC-2263451 (**3**), CCDC-2263452 (**4**), and CCDC-2263453 (**5**), contain the supplementary crystallographic data for this paper. These data can be obtained free of charge at www.ccdc.cam.ac.uk/conts/retrieving.html (or from the Cambridge Crystallographic Data Centre, 12 Union Road, Cambridge CB2 1EZ, UK; Fax: + 44-1223-336-033; e-mail: deposit@ccdc.cam.ac.uk).

*Table S 2: X-ray crystallographic data of compounds **1**, **2** and **3**.*

Compound	1	2	3
Formula	$C_{70}H_{58}O_3F_{46}AlNi_2As_3$	$C_{52}H_{94}As_3KN_2Ni_2O_6$	$C_{34}H_{58}Ni_2As_3$
ρ_{calc}	1.850	1.378	1.493
μ/mm^{-1}	3.549	3.639	4.500
Formula Weight	2190.32	1224.57	808.98
Colour	clear dark orange	dark brown	dark red
Shape	block-shaped	block-shaped	stick-shaped
Size/mm^3	0.48×0.40×0.22	0.23×0.10×0.07	0.26×0.07×0.05
T/K	293(2)	123.01(10)	123.01(10)
Crystal System	triclinic	triclinic	triclinic
Space Group	$P\bar{1}$	$P\bar{1}$	$P\bar{1}$
a/Å	14.3245(4)	10.70200(10)	12.2871(3)
b/Å	17.2360(5)	13.29600(10)	12.8493(3)
c/Å	19.5299(5)	21.45380(10)	13.3497(2)
α/°	99.648(2)	99.2150(10)	67.261(2)
β/°	109.149(2)	101.4120(10)	71.784(2)
γ/°	113.282(3)	90.5780(10)	71.514(2)
V/Å^3	3931.0(2)	2951.01(4)	1799.50(8)
Z	2	2	2
Z'	1	1	1
Wavelength/Å	1.54184	1.54184	1.54184
Radiation type	Cu K$_a$	Cu K$_a$	Cu K$_a$
Θ_{min}/°	3.469	2.130	3.678
Θ_{max}/°	72.120	73.717	71.773
Measured Refl's.	31525	113148	47740
Indep't Refl's	14915	11611	6894
Refl's I≥2 s(I)	13757	10529	6644
R_{int}	0.0290	0.0358	0.0231
Parameters	1144	641	370
Restraints	0	0	0
Largest Peak	1.017	0.376	0.315
Deepest Hole	-0.642	-0.355	-0.490
GooF	1.045	1.038	1.087
ωR_2 (all data)	0.0881	0.0639	0.0536
ωR_2	0.0856	0.0624	0.0531
R_1 (all data)	0.0367	0.0292	0.0221
R_1	0.0336	0.0257	0.0211

*Table S 3: X-ray crystallographic data of compounds **1** + **4** and **5**.*

Compound	**1 + 4**	**5**
Formula	$C_{70}H_{57.2}AlAs_{3.18}F_{46}Ni_2O_3$	$C_{68.66}H_{39.44}AlF_{47.22}NiO_3S_2$
ρ_{calc}	1.858	1.767
μ/mm^{-1}	5.248	2.582
Formula Weight	2202.99	1959.35
Colour	clear dark green	clear red
Shape	prism-shaped	block-shaped
Size/mm^3	0.42×0.23×0.22	0.26×0.15×0.10
T/K	123.02(10)	123.00(10)
Crystal System	triclinic	monoclinic
Space Group	$P\bar{1}$	$P2_1/n$
a/Å	14.3364(3)	19.41090(10)
b/Å	17.2418(5)	19.44110(10)
c/Å	19.5270(5)	19.63140(10)
α/°	99.412(2)	90
β/°	109.126(2)	96.0460(10)
γ/°	113.382(2)	90
V/Å^3	3938.72(19)	7367.08(7)
Z	2	4
Z'	1	1
Wavelength/Å	1.39222	1.54184
Radiation type	Cu K$_b$	Cu K$_a$
Θ_{min}/°	2.679	3.385
Θ_{max}/°	74.091	74.297
Measured Refl's.	45249	74655
Indep't Refl's	21198	14866
Refl's I≥2 s(I)	18223	13092
R_{int}	0.0443	0.0267
Parameters	1227	1494
Restraints	54	200
Largest Peak	0.630	0.727
Deepest Hole	-1.023	-0.355
GooF	1.028	1.042
ωR_2 (all data)	0.1192	0.0943
ωR_2	0.1105	0.0886
R_1 (all data)	0.0519	0.0406
R_1	0.0441	0.0347

*[(Cp'''Ni)$_2$(μ,$\eta^{3:3}$-As$_3$)][FAl] (**1**)*

Compound [(Cp'''Ni)$_2$(μ,$\eta^{3:3}$-As$_3$)][FAl] (**1**) crystallizes from a concentrated solution in CH_2Cl_2 layered with *n*-pentane at room temperature in the triclinic space group $P\bar{1}$ as clear dark orange blocks. The asymmetric unit (Figure S1) contains one cation and one anion.

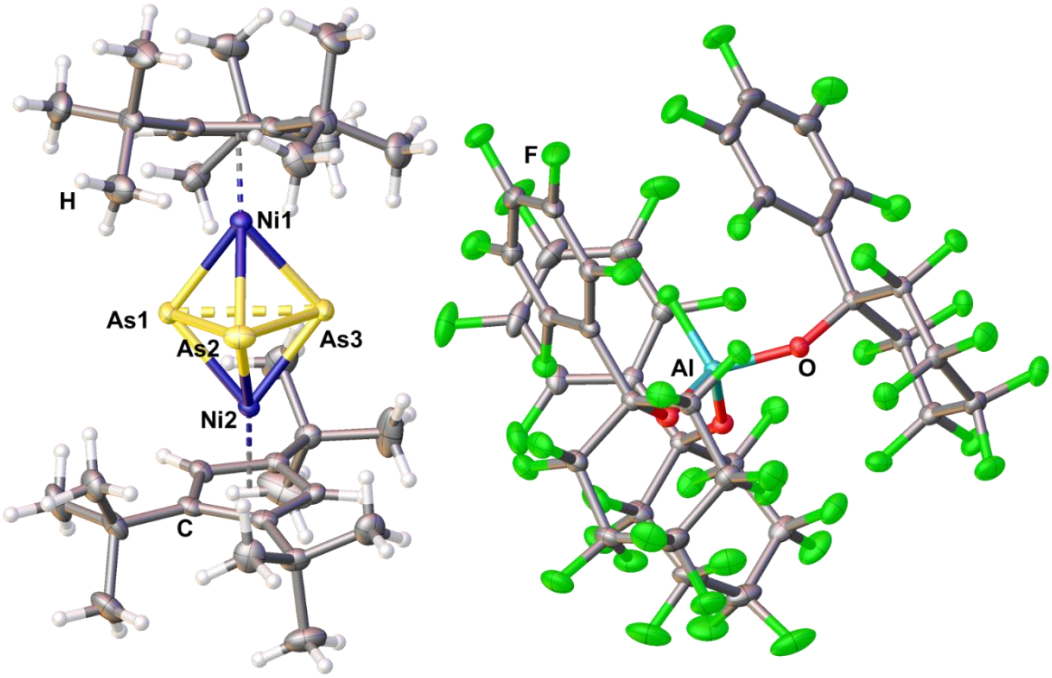

*Figure S 1: Solid state structure of **1**; Depicted is the asymmetric unit and ADPs (anisotropic displacement parameters) are drawn at 50 % probability.*

*[K@crypt][(Cp'''Ni)$_2$(μ,$\eta^{3:3}$-As$_3$)] (**2**)*

Compound [K@crypt][(Cp'''Ni)$_2$(μ,$\eta^{3:3}$-As$_3$)] (**2**) crystallizes from a concentrated solution in THF layered with *n*-hexane at room temperature in the triclinic space group $P\bar{1}$ as clear dark orange blocks. The asymmetric unit (Figure S2) contains one cation and one anion. Disorders within the cation were treated with adequate restraints.

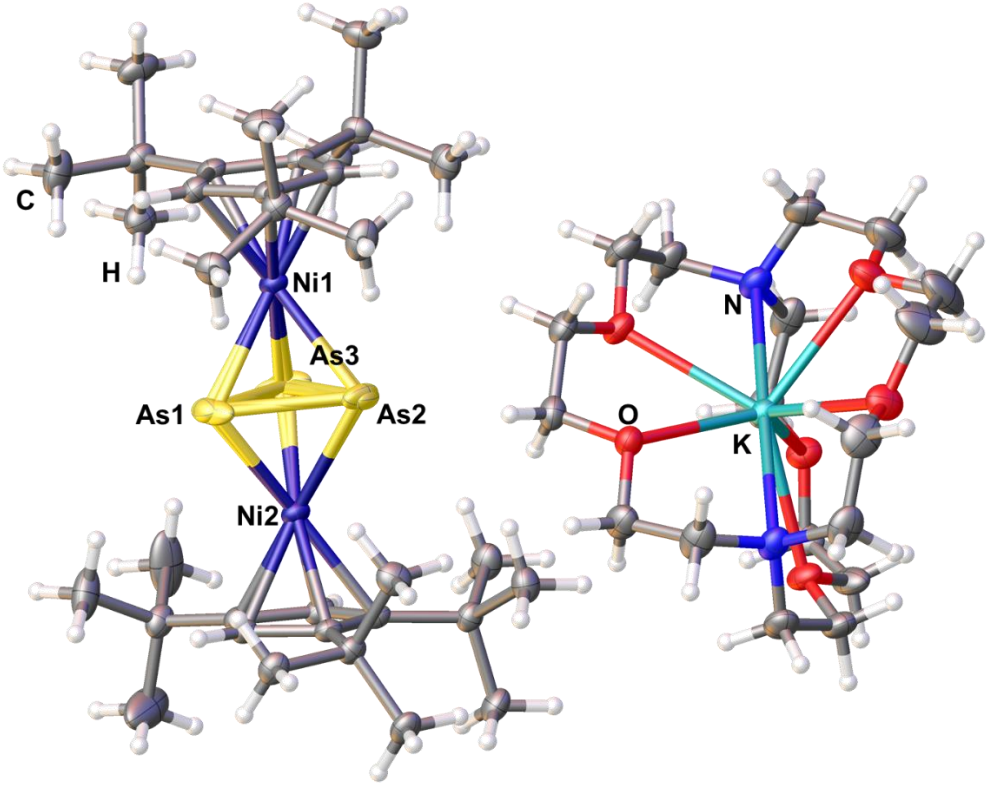

*Figure S 2: Solid state structure of **2**; Depicted is the asymmetric unit and ADPs (anisotropic displacement parameters) are drawn at 50 % probability.*

*[(Cp'''Ni)$_2$(μ,$\eta^{3:3}$-As$_3$)] (**3**)*

Compound [(Cp'''Ni)$_2$(μ,$\eta^{3:3}$-As$_3$)] (**3**) crystallizes by slow diffusion of a saturated solution of **3** in *n*-pentane into toluene at room temperature in the triclinic space group $P\bar{1}$ as dark red sticks. The asymmetric unit (Figure S3) contains one molecule **3**.

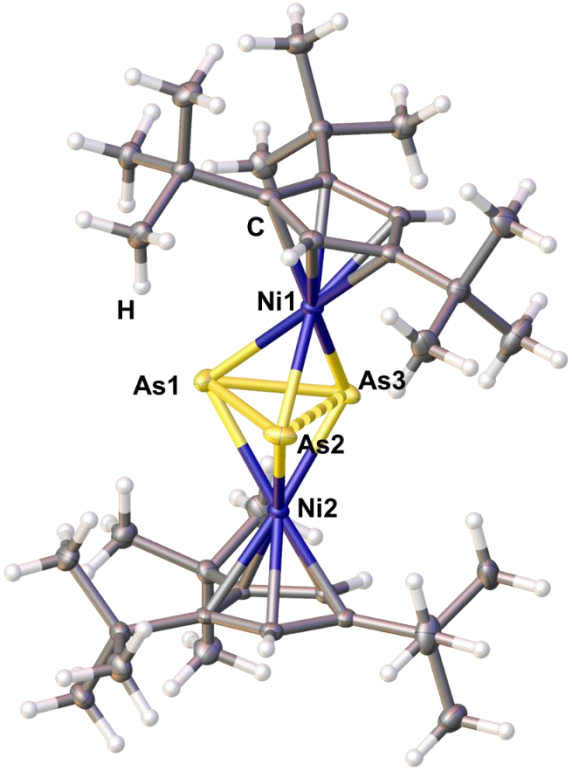

*Figure S 3: Solid state structure of **3**. Depicted is the asymmetric unit and ADPs (anisotropic displacement parameters) are drawn at 50 % probability.*

*[(Cp'''Ni)$_2$($\mu,\eta^{3:3}$-As$_3$)][FAl] (**1**) and [(Cp'''Ni)$_2$($\mu,\eta^{2:2:1:1:1}$-As$_5$)][FAl] (**4**)*

Compounds [(Cp'''Ni)$_2$($\mu,\eta^{3:3}$-As$_3$)][FAl] (**1**) and [(Cp'''Ni)$_2$($\mu,\eta^{2:2:1:1:1}$-As$_5$)][FAl] (**4**) crystallizes from a concentrated solution in CH_2Cl_2 layered with *n*-pentane at room temperature in the triclinic space group $P\bar{1}$ as clear dark orange blocks. The asymmetric unit (Figure S4) contains one cation and one anion. The cation shows a disorder. Part 1 includes [(Cp'''Ni)$_2$($\mu,\eta^{3:3}$-As$_3$)]$^+$ with an occupancy of 91.1 %, whereas part 2 includes [(Cp'''Ni)$_2$($\mu,\eta^{2:2:1:1:1}$-As$_5$)]$^+$ with an occupancy of 8.9 %.

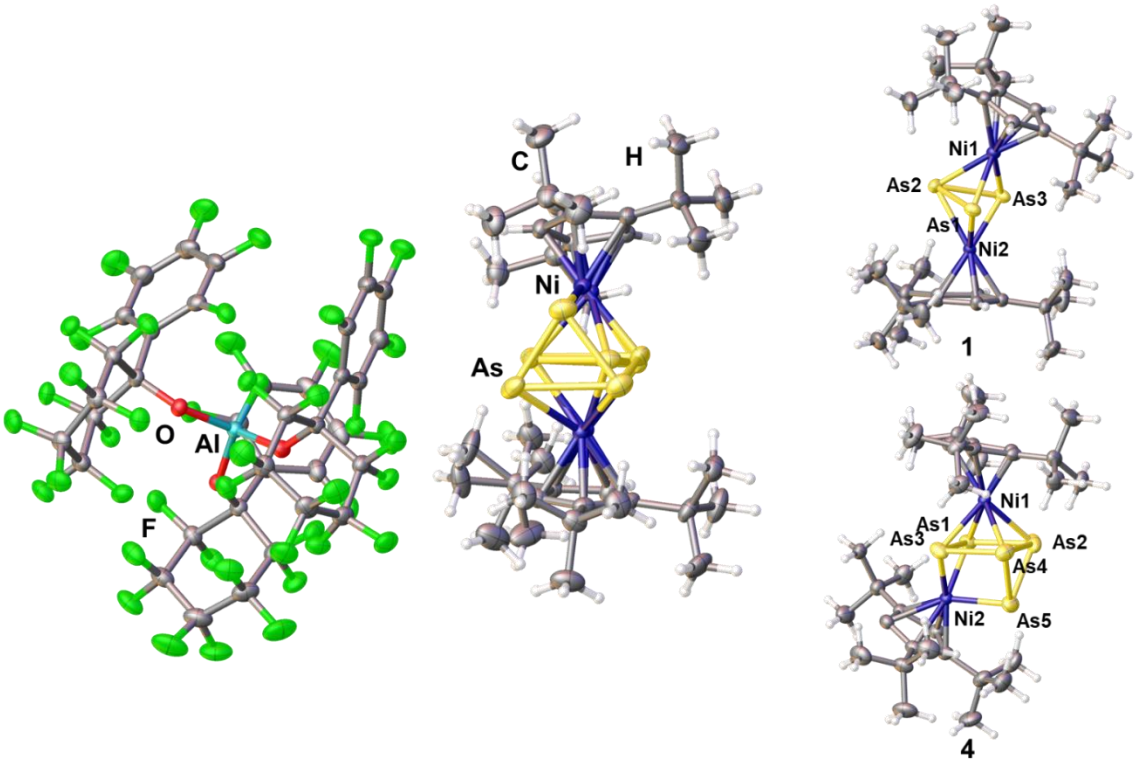

*Figure S 4: Solid state structures of a mixture of **1** and **4**; Depicted is the asymmetric unit (left) and the respective compounds **1** and **4** (right). ADPs (anisotropic displacement parameters) are drawn at 50 % probability.*

*[Cp'''Ni($\eta^{1:1}$-thia)][FAl] (**5**)*

Compound [Cp'''Ni($\eta^{1:1}$-thia)][FAl] (**5**) crystallizes from a concentrated solution in CH_2Cl_2 layered with *n*-pentane at room temperature in the monoclinic space group $P2_1/n$ as clear dark orange blocks. The asymmetric unit (Figure S5) contains one cation, one anion and one molecule *o*-DFB. Disorders within the cation and the *o*-DFB were treated with adequate restraints.

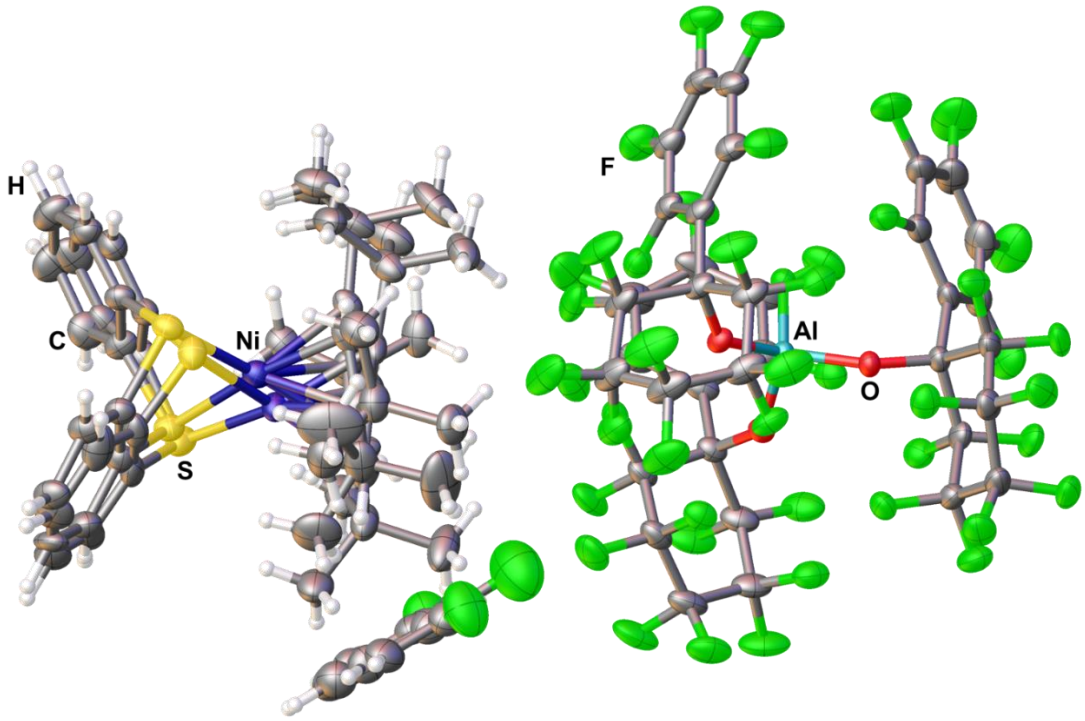

*Figure S 5: Solid state structure of **5**. Depicted is the asymmetric unit and ADPs (anisotropic displacement parameters) are drawn at 50 % probability.*

9.5.4. NMR Spectroscopic Investigations

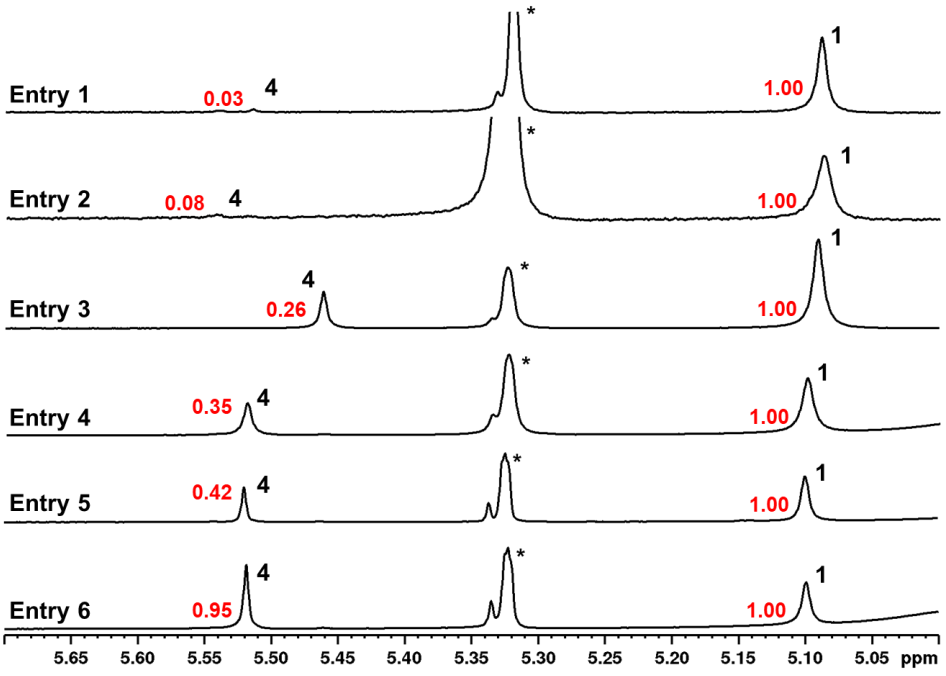

1

*Figure S 6: ^{1}H NMR spectra of the oxidation of **A** with different reaction conditions recorded in CD_2Cl_2. *: CD_2Cl_2; Integral ratio is given in red.*

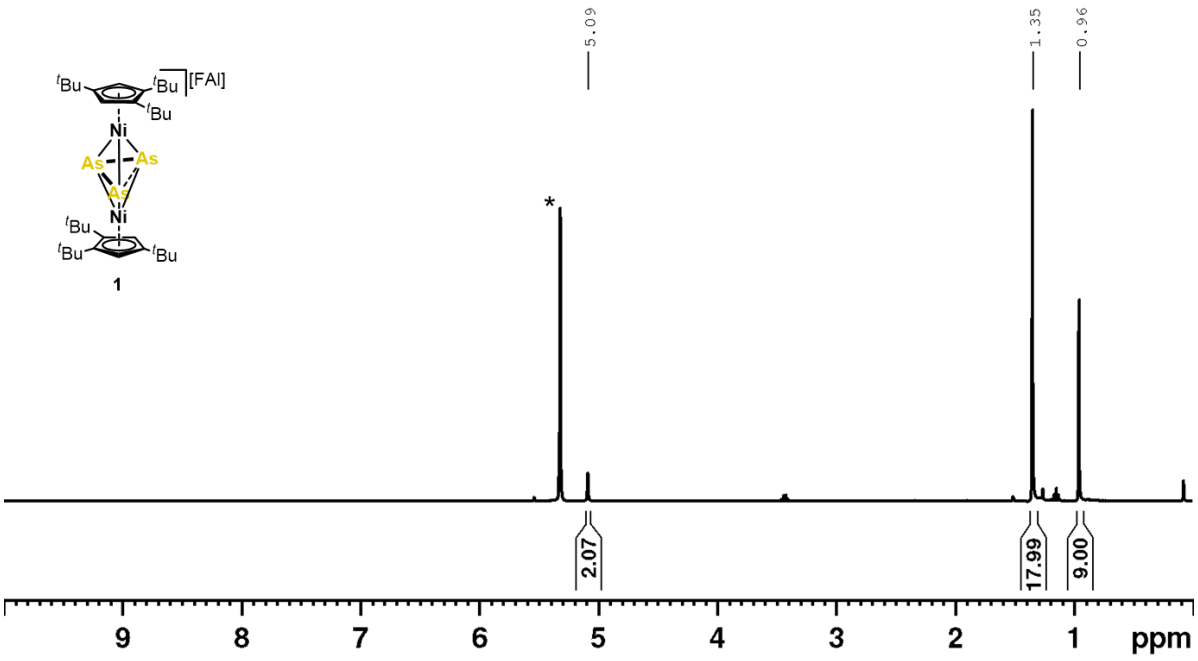

*Figure S 7: ^{1}H NMR spectrum of [(Cp'''Ni)$_2$(μ,$\eta^{3:3}$-As$_3$)][FAl] (**1**) in CD_2Cl_2 at room temperature; * = CD_2Cl_2.*

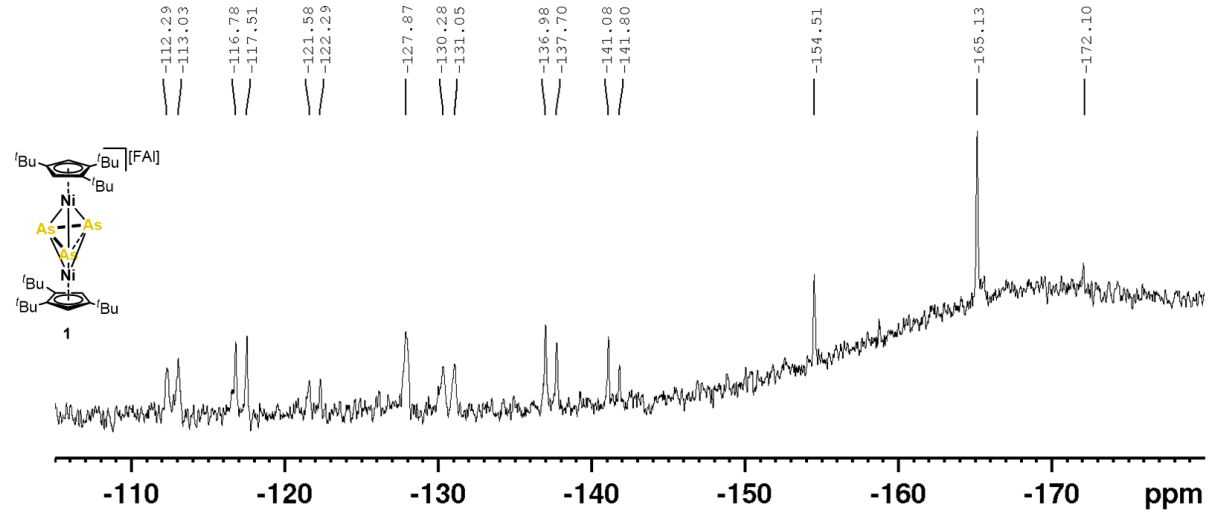

*Figure S 8: $^{19}F\{^{1}H\}$ NMR spectrum of $[(Cp'''Ni)_2(\mu,\eta^{3:3}\text{-}As_3)][FAl]$ (**1**) in CD_2Cl_2 at room temperature; low signal-to-noise ratio is caused due to low solubility of $[FAl]^-$ salts.*

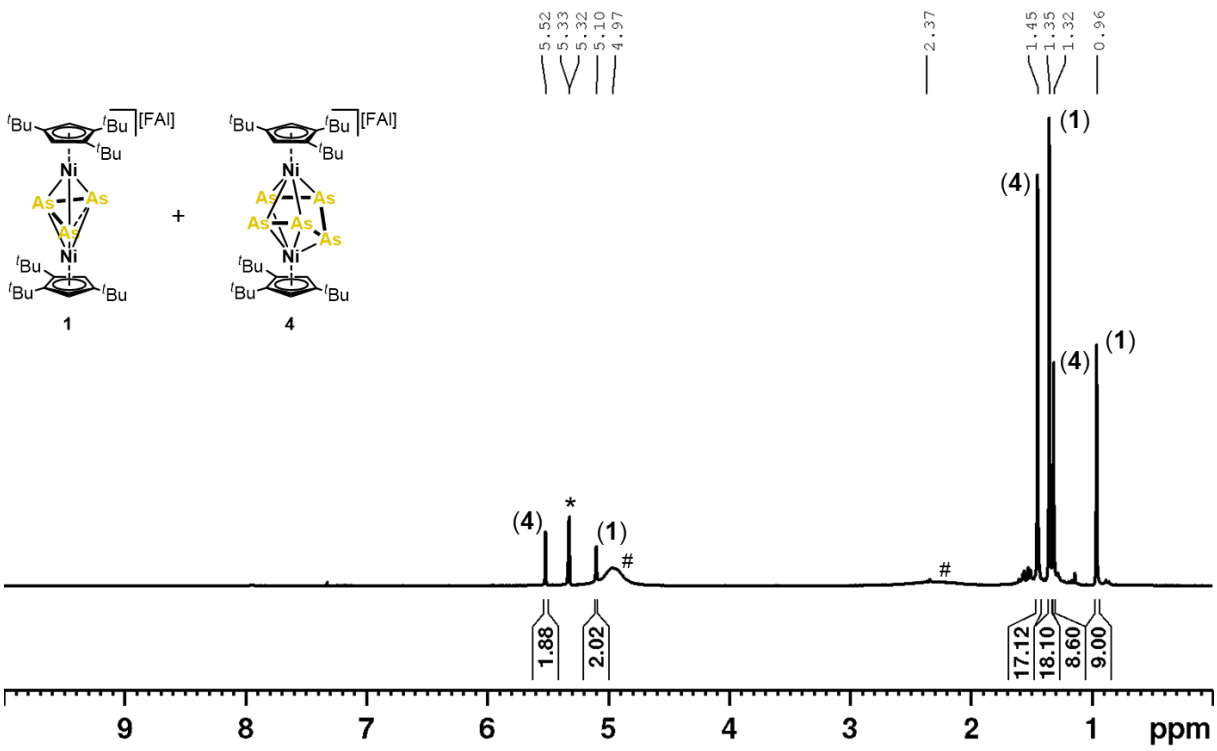

*Figure S 9: ^{1}H NMR spectrum of $[(Cp'''Ni)_2(\mu,\eta^{3:3}\text{-}As_3)][FAl]$ (**1**) and $[(Cp'''Ni)_2(\mu,\eta^{2:2:1:1:1}\text{-}As_5)][FAl]$ (**4**) in CD_2Cl_2 at room temperature; * = CD_2Cl_2; # = traces of $[Fc^{Diac}][FAl]$ since the reaction was carried out in a 1:1 stoichiometry.*

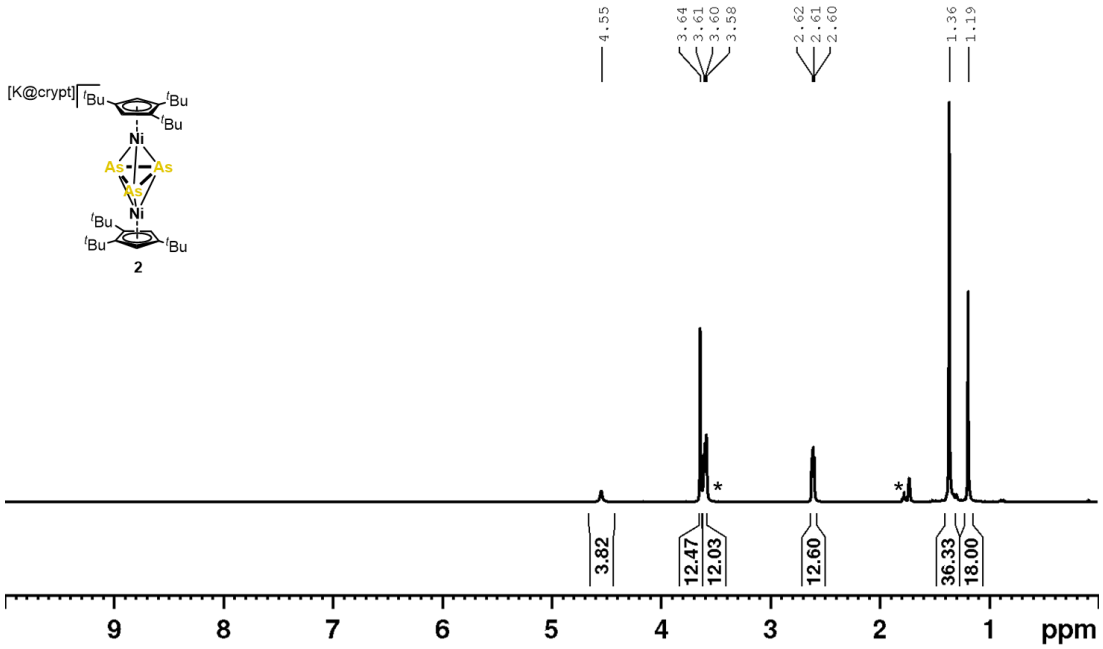

*Figure S 10: ^{1}H NMR spectrum of [K@crypt][(Cp'''Ni)$_2$(μ,$\eta^{3:3}$-As$_3$)] (**2**) in THF-d^8 at room temperature; * = THF-d^8.*

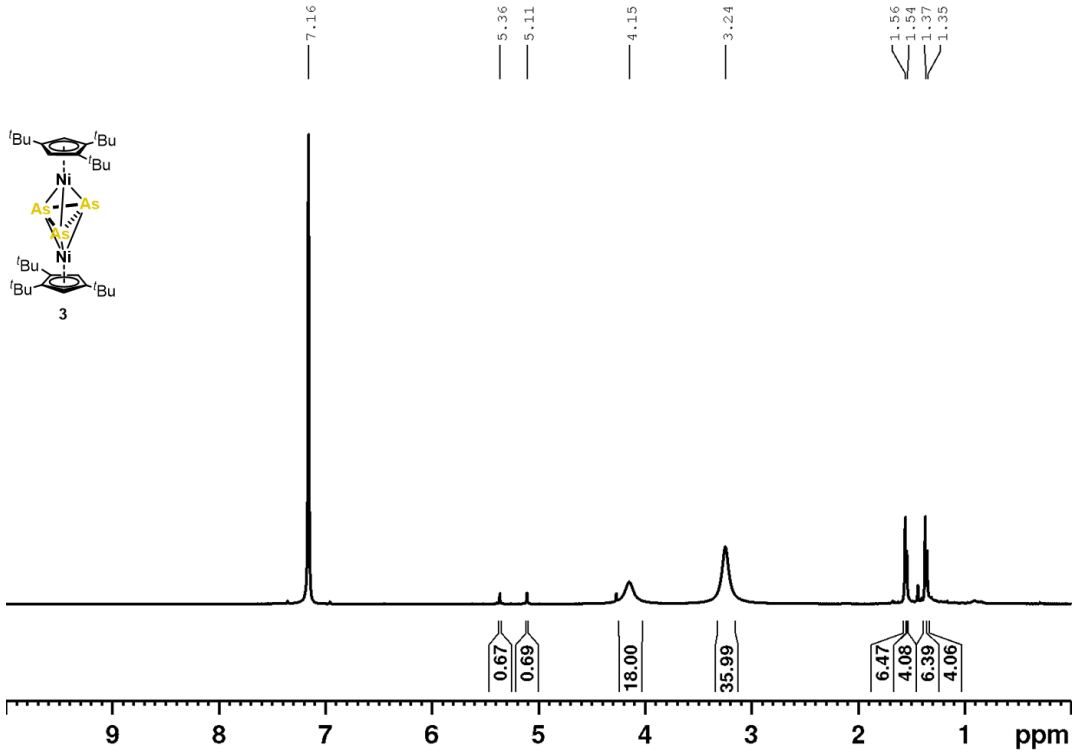

*Figure S 11: ^{1}H NMR spectrum of [(Cp'''Ni)$_2$(μ,$\eta^{3:3}$-As$_3$)] (**3**) in C$_6$D$_6$ at room temperature; * = C$_6$D$_6$.*

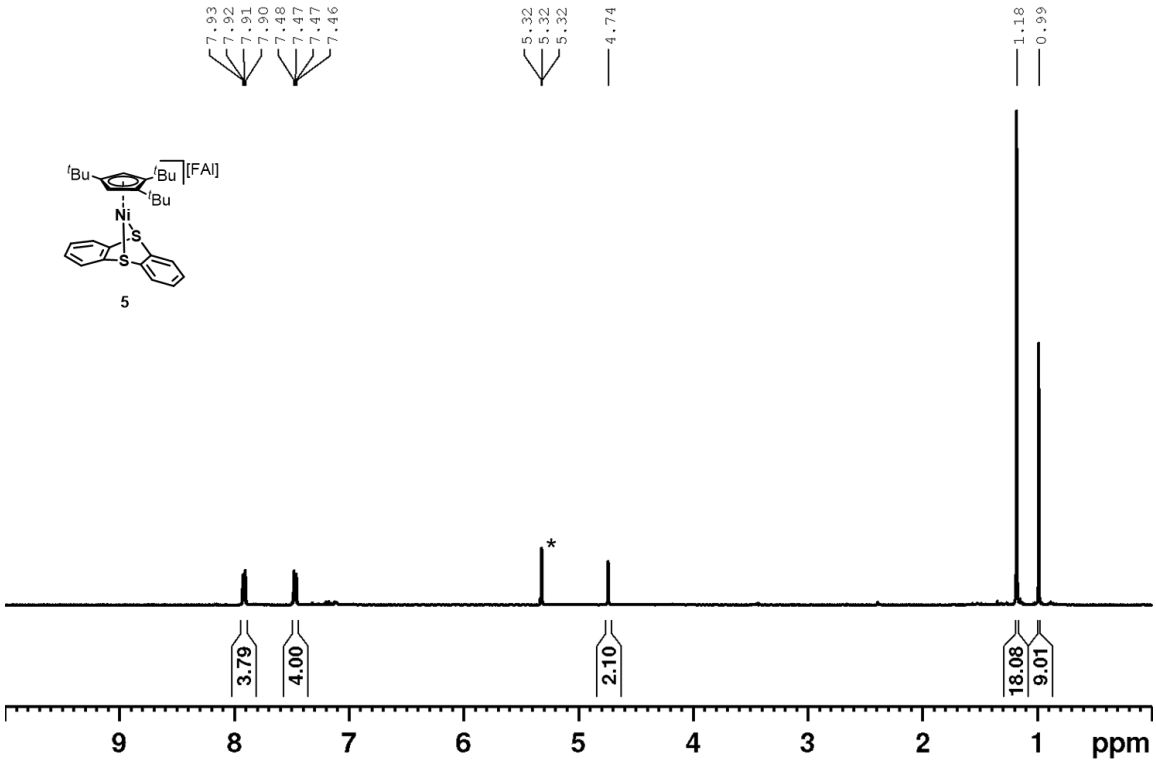

*Figure S 12: ^{1}H NMR spectrum of [(Cp'''Ni)$_2$($\mu,\eta^{1:1}$-thia)][FAl] (**5**) in CD_2Cl_2 at room temperature; * = CD_2Cl_2.*

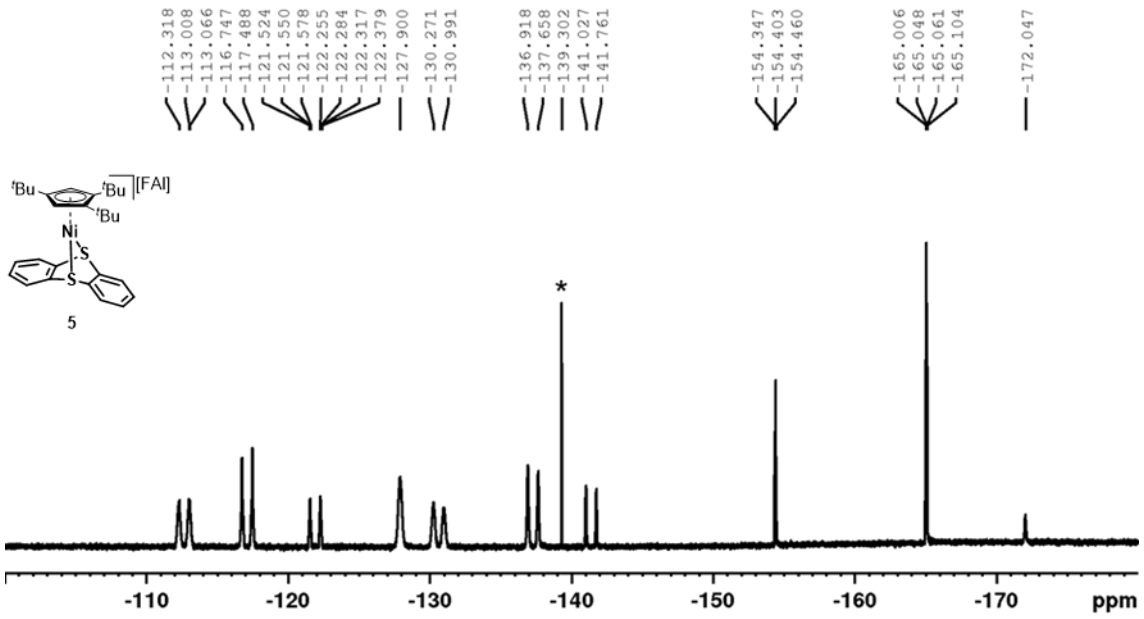

*Figure S 13: $^{19}F\{^{1}H\}$ NMR spectrum of [(Cp'''Ni)$_2$($\mu,\eta^{1:1}$-thia)][FAl] (**5**) in CD_2Cl_2 at room temperature; * marks the signal for residual o-DFB.*

9.5.5. Cyclovoltammetric Studies

To get an initial idea of the redox properties of **A**, we conducted cyclovolammetric studies in solution. Thus, 52 mg of **A** were dissolved in *o*-DFB (5 mL) and 750 mg [^{n}Bu$_4$N][PF$_6$] were added. The cyclovoltammogram (Figure S14) was then recorded.

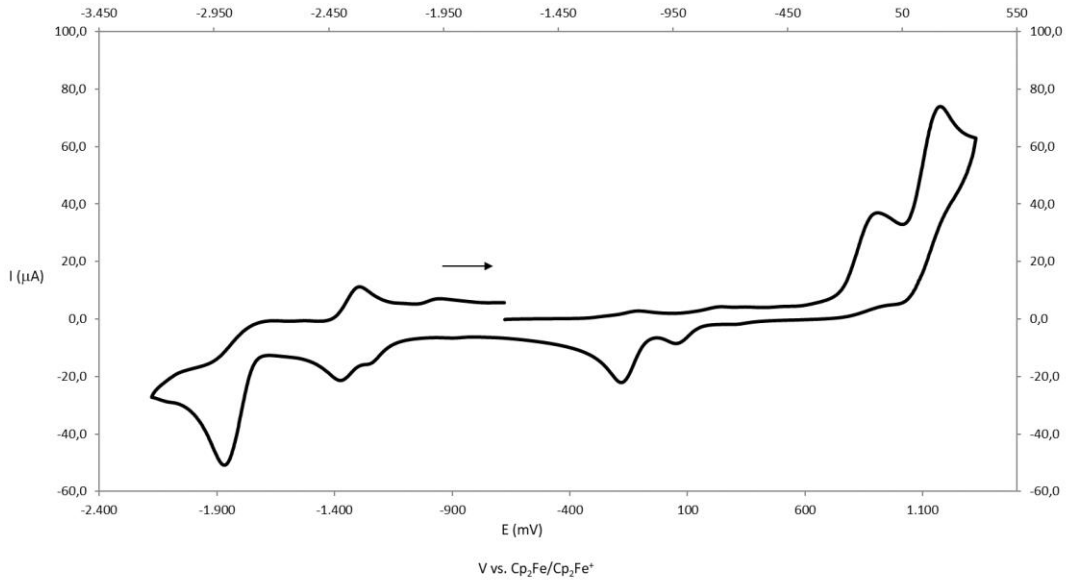

*Figure S 14: Cyclovoltammogram of **A** in o-DFB recorded at room temperature.*

Furthermore, we conducted cyclovoltammetric studies of **3** in solution. 50 mg of **3** were dissolved in *o*-DFB (5 mL) and 500 mg [^{n}Bu$_4$N][PF$_6$] were added. The cyclovoltammogram (Figure S15) was then recorded.

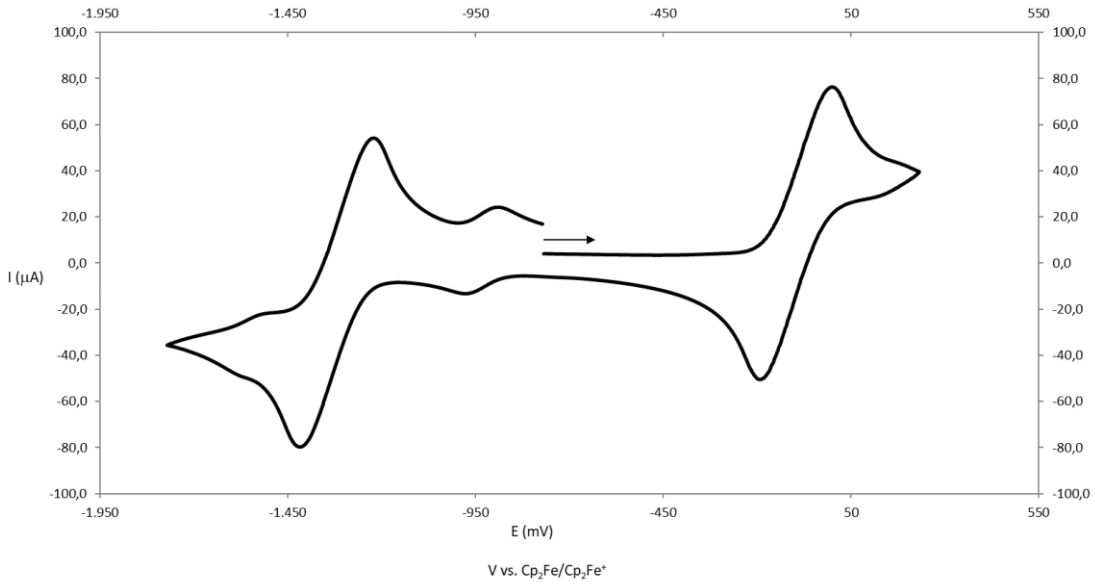

*Figure S 15: Cyclovoltammogram of **3** in o-DFB recorded at room temperature.*

9.5.6. EPR Studies on 3

As **3** has 33 VE and should thus be paramagnetic, we subjected a sample of it in *n*-pentane to EPR studies. While we could not observe a signal at room temperature, the frozen solution at 77 K reveals a signal with g_1 = 2.15 and g_2 = 2.02 and an additional hyperfine coupling to the arsenic nuclei (Figure S16), which however could not be resolved within the spectral simulation.

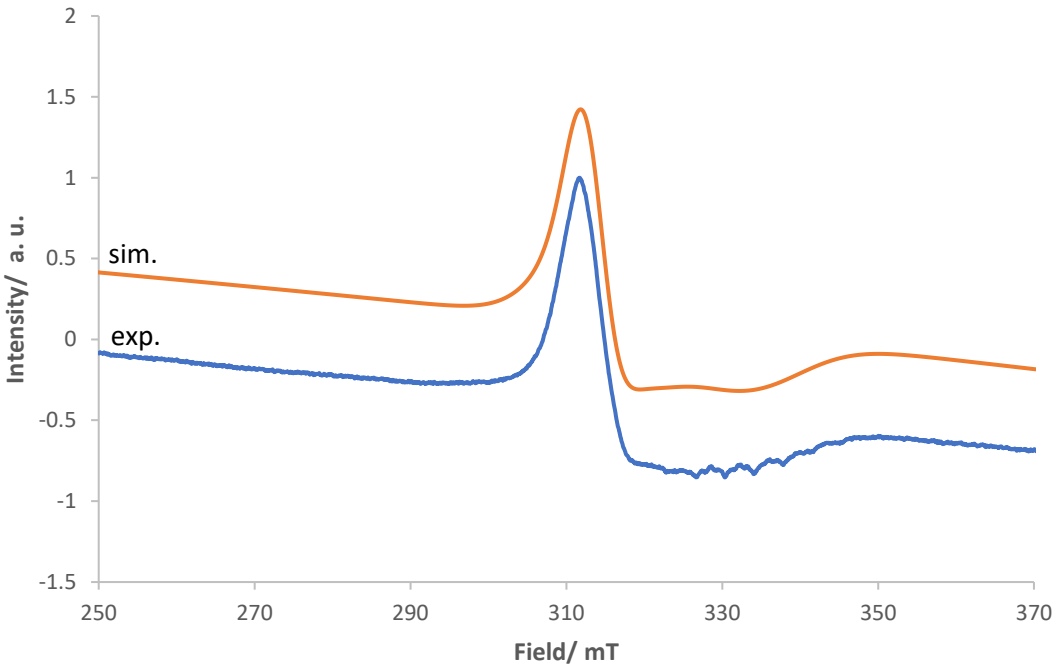

*Figure S 16: X-band EPR spectrum of **3** in frozen n-pentane solution at 77 K and its simulation.*

9.5.7. Computational Details

General Considerations

DFT calculations were performed using the Orca 5.0 software package.[33] The sterically demanding Cp''' ligands were replaced with unsubstituted Cp ligands to save computational resources. Geometry optimizations were performed at the ωB97X-D3[34]/def2-TZVP[35] level of theory with PCM solvent correction for either CH_2Cl_2 or THF.[36] Stationary points were verified by analytical frequency calculations (imaginary modes >-50cm^{-1} were neglected). Single point calculations were performed at the ωB97X-D3/def2-TZVP level of theory with solvent correction as described above.

*Molecular Orbitals and Spin Density of **3***

Molecular orbitals for compounds **1** – **3** were obtained from single point calculations on the optimized geometries of the respective species. Selected molecular orbitals, as well as the spin density within **3** are given in Figure S17. Notably, the former LUMO (in **1**) becomes a populated bonding orbital (HOMO-1 in **2**), upon the stepwise reduction. Furthermore, the spin density of **3** displays partial As contribution, explaining the hyperfine coupling observed in the experimental X-band EPR spectrum of **3**.

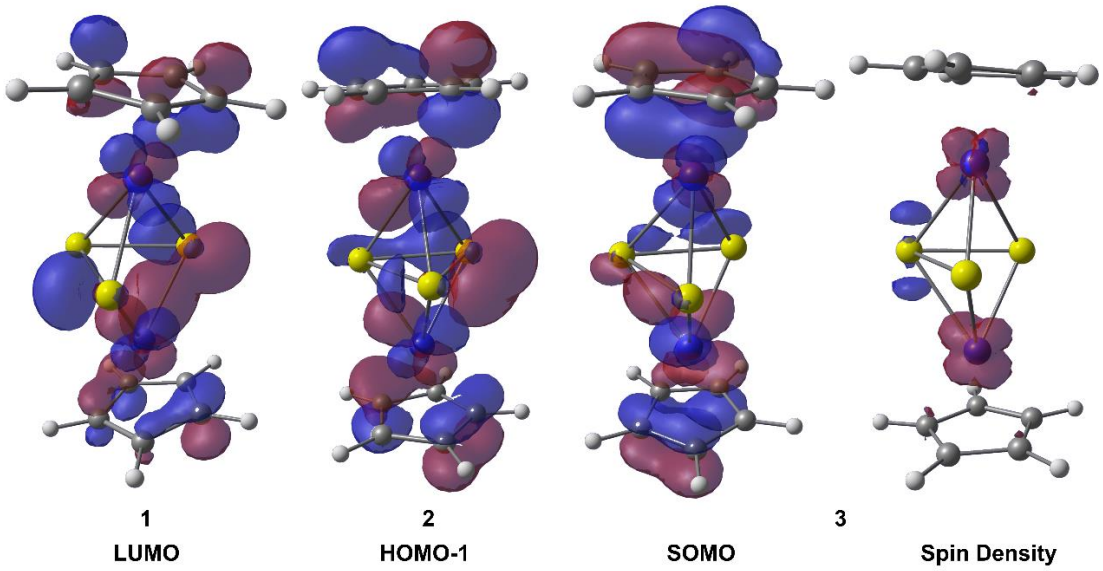

*Figure S 17: Selected molecular orbitals (MOs) of **1´** - **3´** and the spin density of **3´**; isosurfaces are drawn at 0.04 a. u. for MOs and 0.01 a. u. for the spin density.*

Optimized Geometries

*[(CpNi)$_2$(μ,$\eta^{3:3}$-As$_3$)]$^+$ (**1´**)*

ωB97XD/def2TZVP (CPCM (THF)): Energies/H = -10111.45850306, Enthalpies/H = -10111.45755885, Free Energies/H = -10111.51722937, ZPVE/ kcal/mol = 119.61

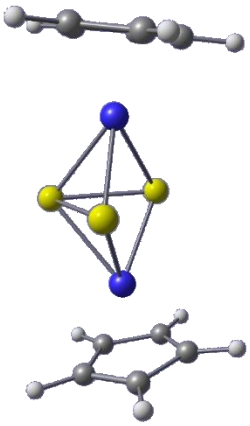

Symbol	X	Y	Z
As	-8.032890000	-1.388063000	6.064111000
As	-5.727193000	-0.007973000	5.984823000
As	-5.850060000	-2.379307000	6.421404000
Ni	-6.583601000	-1.307959000	4.312162000
Ni	-6.864048000	-0.627323000	7.862847000
C	-6.637908000	-0.233770000	2.572116000
C	-6.124197000	-0.719030000	9.815202000
C	-7.743541000	-1.160226000	2.602050000
H	-8.788035000	-0.889435000	2.586184000
C	-7.500932000	0.915779000	9.020869000
C	-5.788943000	-2.346173000	2.692595000
C	-8.314881000	-0.231544000	9.316635000
H	-9.380726000	-0.303918000	9.165547000
C	-6.155991000	0.621656000	9.393975000
H	-5.312204000	1.288621000	9.310477000
C	-5.435222000	-0.979279000	2.580666000
H	-4.433701000	-0.578945000	2.563091000
C	-7.464725000	-1.243023000	9.780770000
C	-7.215879000	-2.459438000	2.667378000
H	-6.723075000	0.840857000	2.520071000
H	-7.778224000	-3.378688000	2.721607000
H	-5.098209000	-3.171999000	2.777663000
H	-7.752169000	-2.247085000	10.053057000
H	-7.859082000	1.856617000	8.631481000
H	-5.246945000	-1.271425000	10.116949000

*$[(CpNi)_2(\mu,\eta^{3:3}\text{-}As_3)]^-$ (**2´**)*

ωB97XD/def2TZVP (CPCM (CH_2Cl_2)): Energies/H = -10111.75668011, Enthalpies/H = -10111.75573590, Free Energies/H = -10111.81585998, ZPVE/ kcal/mol = 117.18

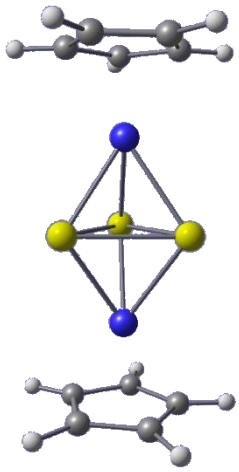

Symbol	X	Y	Z
As	-8.174482000	-0.647771000	5.911161000
As	-5.893030000	0.200934000	5.934589000
As	-6.312086000	-2.165873000	6.353149000
Ni	-6.634330000	-1.221445000	4.213589000
Ni	-6.954712000	-0.520548000	7.916919000
C	-6.625621000	-0.359519000	2.232399000
C	-6.080014000	-0.806189000	9.868792000
C	-7.678437000	-1.305400000	2.319612000
H	-8.730598000	-1.097001000	2.190487000
C	-7.499160000	0.939674000	9.409640000
C	-5.698041000	-2.414386000	2.673135000
C	-8.285143000	-0.230290000	9.590668000
H	-9.362541000	-0.285102000	9.532977000
C	-6.137023000	0.582644000	9.589158000
H	-5.291768000	1.252520000	9.525993000
C	-5.400051000	-1.047455000	2.448233000
H	-4.413814000	-0.607019000	2.428602000
C	-7.410173000	-1.308939000	9.873488000
C	-7.108615000	-2.574811000	2.599207000
H	-6.735052000	0.694187000	2.020900000
H	-7.649125000	-3.503444000	2.710405000
H	-4.978343000	-3.198769000	2.857331000
H	-7.702325000	-2.329462000	10.073662000
H	-7.873341000	1.929939000	9.194190000
H	-5.184556000	-1.377549000	10.065445000

*[(CpNi)$_2$(μ,$\eta^{3:3}$-As$_3$)] (**3´**)*

ωB97XD/def2TZVP (CPCM (CH_2Cl_2)): Energies/H = -10111.64813529, Enthalpies/H = -10111.64719108, Free Energies/H = -10111.70733936, ZPVE/ kcal/mol = 118.08

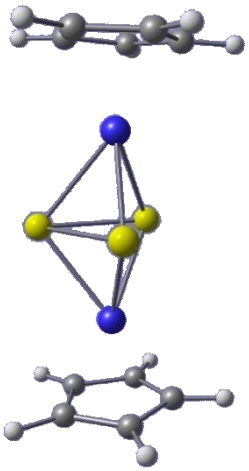

Symbol	X	Y	Z
As	-8.077512000	-1.067711000	6.009035000
As	-5.862975000	0.110686000	5.960479000
As	-6.017455000	-2.242083000	6.444089000
Ni	-6.621753000	-1.225782000	4.181075000
Ni	-6.902340000	-0.536631000	7.964048000
C	-6.637701000	-0.319359000	2.260608000
C	-6.113591000	-0.773908000	9.916152000
C	-7.707086000	-1.252324000	2.345639000
H	-8.757907000	-1.020899000	2.256542000
C	-7.497484000	0.953215000	9.327009000
C	-5.736598000	-2.394726000	2.627655000
C	-8.306120000	-0.201629000	9.529741000
H	-9.378585000	-0.252398000	9.417411000
C	-6.145423000	0.604083000	9.597283000
H	-5.295636000	1.267764000	9.546830000
C	-5.417760000	-1.028572000	2.422622000
H	-4.426037000	-0.602856000	2.398907000
C	-7.451244000	-1.271566000	9.879143000
C	-7.150983000	-2.535373000	2.575811000
H	-6.737087000	0.742667000	2.093394000
H	-7.700952000	-3.457332000	2.690331000
H	-5.028509000	-3.192440000	2.795990000
H	-7.753219000	-2.286869000	10.087978000
H	-7.855257000	1.932658000	9.046662000
H	-5.233164000	-1.349688000	10.159300000

9.6. References

[1] O. J. Scherer, *Angew. Chem. Int. Ed. Engl.* **1990**, *29*, 1104–1122.

[2] a) B. M. Cossairt, N. A. Piro, , C. C. Cummins, *Chem. Rev.* **2010**, *110*, 4164–4177; b) M. Caporali, L. Gonsalvi, A. Rossin, M. Peruzzini, *Chem. Rev.* **2010**, *110*, 4178–4235; c) M. Scheer, G. Balázs, A. Seitz, *Chem. Rev.* **2010**, *110*, 4236–4256; d) N. A. Giffin, J. D. Masuda, *Coord. Chem. Rev.* **2011**, *255*, 1342–1359, e) C. M. Hoidn, D. J. Scott, R. Wolf, *Chem. Eur. J.* **2021**, *27*, 1886–1902; f) L. Giusti, V. R. Landaeta, M. Vanni, J. A. Kelly, R. Wolf, M. Caporali, *Coord. Chem. Rev.* **2021**, *441*, 213927.

[3] S. W. Benson, *J. Chem. Educ.* **1965**, *42*, 502.

[4] a) A. S. Foust, M. S. Foster, L. F. Dahl, *J. Am. Chem. Soc.* **1969**, *91*, 5631–5633; b) A. S. Foust, M. S. Foster, L. F. Dahl, *J. Am. Chem. Soc.* **1969**, *91*, 5633–5635.

[5] a) I. Bernal, H. Brunner, W. Meier, H. Pfisterer, J. Wachter, M. L. Ziegler, *Angew. Chem. Int. Ed. Engl.* **1984**, *23*, 438–439; b) M. Gorzellik, H. Bock, L. Gang, B. Nuber, M. L. Ziegler, *J. Organomet. Chem.* **1991**, *412*, 95–120; c) O. J. Scherer, J. Braun, P. Walther, G. Wolmershäuser, *Chem. Ber.* **1992**, *125*, 2661–2665.

[6] a) O. J. Scherer, J. Vondung, G. Wolmershäuser, *J. Organomet. Chem.* **1989**, *376*, C35-C38; b) C. Schwarzmaier, A. Noor, G. Glatz, M. Zabel, A. Y. Timoshkin, B. M. Cossairt, C. C. Cummins, R. Kempe, M. Scheer, *Angew. Chem. Int. Ed.* **2011**, *50*, 7283–7286; c) M. Schmidt, A. E. Seitz, M. Eckhardt, G. Balázs, E. V. Peresypkina, A. V. Virovets,; F. Riedlberger, M. Bodensteiner, E. M. Zolnhofer, K. Meyer, M. Scheer, *J. Am. Chem. Soc.* **2017**, *139*, 13981–13984, d) M. Piesch, C. Graßl, M. Scheer, *Angew. Chem. Int. Ed.* **2020**, *59*, 7154–7160; e) M. Dietz, M. Arrowsmith, S. Reichl, L. I. Lugo-Fuentes, J. O. C. Jiménez-Halla, M. Scheer, H. Braunschweig, *Angew. Chem. Int. Ed.* **2022**, *61*, e202206840.

[7] a) A. L. Rheingold, M. J. Foley, P. J. Sullivan, *J. Am. Chem. Soc.* **1982**, *104*, 4727–4729; b) O. J. Scherer, W. Wiedemann, G. Wolmershäuser, *J. Organomet. Chem.* **1989**, *361*, C11–C14; c) O. J. Scherer, W. Wiedemann, G. Wolmershäuser, *Chem. Ber.* **1990**, *123*, 3–6; d) O. J. Scherer, C. Blath, G. Wolmershäuser, *J. Organomet. Chem.* **1990**, *387*, C21–C24.

[8] O. J. Scherer, H. Sitzmann, G. Wolmershäuser, *Angew. Chem. Int. Ed. Engl.* **1989**, *28*, 212–213.

[9] O. J. Scherer, R. Winter, G. Heckmann, G. Wolmershäuser, *Angew. Chem. Int. Ed. Engl.* **1991**, *30*, 850–852.

[10] R. Hoffmann, *Angew. Chem. Int. Ed. Engl.* **1982**, *21*, 711–724.

[11] M. Seidl, G. Balázs, M. Scheer, *Chem. Rev.* **2019**, *119* (14), 8406–8434.

[12] W.-Q. Zhang, Z.-S. Li, J. E. McGrady, Z.-M. Sun, *Angew. Chem. Int. Ed.* **2023**, *62*, e202217316.

[13] a) O. J. Scherer, K. Pfeiffer, G. Heckmann, G. Wolmershäuser, *J. Organomet. Chem.* **1992**, *425*, 141–149; b) C. von Hänisch, D. Fenske, F. Weigend, R. Ahlrichs, R. Ahlrichs, F. Weigend, *Chem. Eur. J.* **1997**, *3*, 1494–1498.

[14] M. V. Butovskiy, G. Balázs, M. Bodensteiner, E. V. Peresypkina, A. V. Virovets, J. Sutter, M. Scheer, *Angew. Chem. Int. Ed.* **2013**, *52*, 2972–2976.

[15] M. Schmidt, D. Konieczny, E. V. Peresypkina, A. V. Virovets, G. Balázs, M. Bodensteiner, F. Riedlberger, H. Krauss, M. Scheer, *Angew. Chem. Int. Ed.* **2017**, *56*, 7307–7311.

[16] L. Dütsch, M. Fleischmann, S. Welsch, G. Balázs, W. Kremer, M. Scheer, *Angew. Chem. Int. Ed.* **2018**, *57*, 3256–3261.

[17] N. Reinfandt, C. Schoo, L. Dütsch, R. Köppe, S. N. Konchenko, M. Scheer, P. W. Roesky, *Chem. Eur. J.* **2021**, *27*, 3974–3978.

[18] C. Riesinger, L. Dütsch, M. Scheer, *Z. Anorg Allg. Chem.* **2022**, *648*, e2022000102.

[19] M. Fleischmann, F. Dielmann, G. Balázs, M. Scheer, *Chem. Eur. J.* **2016**, *22*, 15248–15251.

[20] M. Haimerl, C. Graßl, M. Seidl, M. Piesch, M. Scheer, *Chem. Eur. J.* **2021**, *27*, 18129–18134.

[21] **1** was already obtained as a dismutation product of a heterobimetallic triple decker complex [{Cp'''Ni}{Cp'''Co} ($\mu,\eta^{3:3}$-As_3)][FAl] to the homobimetallic complexes and the solid state structure is deposited under CCDC2064654: M. Piesch, S. Reichl, C. Riesinger, M. Seidl,; G. Balazs, M. Scheer, *Chem. Eur. J.* **2021**, *27*, 9129–9140.

[22] a) E. Mädl, G. Balázs, E. V. Peresypkina, M. Scheer, *Angew. Chem. Int. Ed.* **2016**, *55*, 7702–7707; b) C. Riesinger, L. Dütsch, G. Balázs, M. Bodensteiner, M. Scheer, *Chem. Eur. J.* **2020**, *26*, 17165–17170.

[23] N. G. Conelly, W. E. Geiger, *Chem. Rev.* **1996**, *96*, 877–910.

[24] P. Pyykkö, *J. Phys. Chem. A* **2015**, *119*, 2326−2337.

[25] *omics.pnl.gov/software/molecular-weight-calculator* (16.12.2022).

[26] H. Sitzmann, G. Wolmershäuser, *Z. Naturforsch. B* **1995**, *50*, 750–756.

[27] J.-M. Lalancette, G. Rollin, P. Dumas, *Can. J. Chem.* **1972**, *50*, 3058–3062.

[28] A. Straube, P. Coburger, L. Dütsch, E. Hey-Hawkins, *Chem. Sci.* **2020**, *11*, 10657–10668.

[29] Agilent, CrysAlisPro **2014**, Agilent Technologies Ltd, Yarnton, Oxfordshire, England.

[30] O. V. Dolomanov, L. J. Bourhis, R. J. Gildea, J. A. K. Howard, H. Puschmann, J. Appl. Crystallogr. **2009**, 42, 339–341.

[31] G. M. Sheldrick, *Acta Cryst. A* **2015**, *71*, 3–8.

[32] G. M. Sheldrick, *Acta Cryst. A* **2008**, *64*, 112–122; b) G. M. Sheldrick, *Acta Cryst. C* **2015**, *71*, 3–8.

[33] a) F. Neese, *WIREs Comput. Mol. Sci.* **2022**, *12*, 1606–1621; b) F. Neese, F. Wennmohs, U. Becker, C. Riplinger, *J. Chem. Phys.* **2020**, *152*, 224108–224126;

[34] Y.-S. Lin, G.-D. Li, S.-P. Mao, J.-D. Chai, *J. Chem. Theory Comput.* **2013**, *9*, 263–272.

[35] F. Weigend, R. Ahlrichs, *Phys. Chem. Chem. Phys.* **2005**, *7*, 3297–3305.

[36] J. Tomasi, B. Mennucci, R. Cammi, *Chem. Rev.* **2005**, *105*, 2999–3093.

10. Synthesis and Redox Chemistry of a Homoleptic Iron Arsenic Prismane Cluster

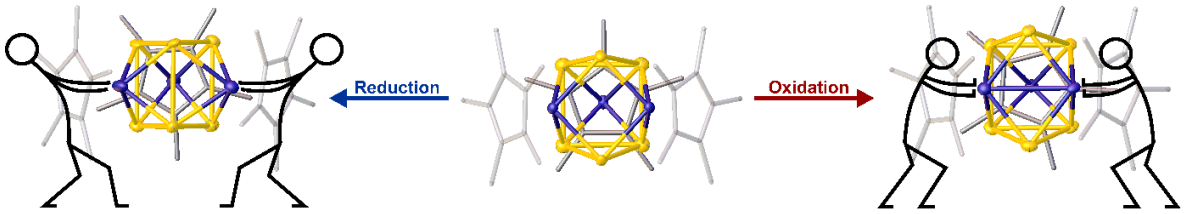

Redox Mediated Distortion of an Iron Arsenic Prismane Cluster

Preface

The following chapter has already been published. The article is reprinted with permission of Wiley-VCH. License Number: 5637020248485

"Synthesis and Redox Chemistry of a Homoleptic Iron Arsenic Prismane Cluster"

Z. Anorg. Allg. Chem. **2022**, *648*, e2022000102.

Parts of this chapter have already been described within the PhD thesis of Dr. Luis Dütsch.

Authors

Christoph Riesinger,† Luis Dütsch† and Manfred Scheer

Author Contributions

Christoph Riesinger – Conceptualization, Synthesis of **A**, [**2**][TEF]$_2$, [K@crypt][**3**], Interpretation of crystallographic data, Interpretation of computational investigations, Writing of original draft.
Luis Dütsch – Conceptualization, Synthesis of [**1**][TEF], [**1**][FAl], Electrochemical investigations, Writing of original draft.
Manfred Scheer – Project administration, Funding acquisition, Co-writing final manuscript.

† These authors contributed equally.

Acknowledgements

This work was supported by the Deutsche Forschungsgemeinschaft (DFG) within the project Sche 384/36-1. C. R. is grateful to the Studienstiftung des Deutschen Volkes for a PhD fellowship. Lisa Zimmermann is acknowledged for assistance in graphical design.

10.1. Abstract

*The redox chemistry of the homoleptic iron prismane cluster [{Cp*Fe}$_3$(μ_3,$\eta^{4:4:4}$-As$_6$)] (**A**, Cp* = C$_5$Me$_5$) is investigated both electrochemically and synthetically. While its first oxidation leads to the diamagnetic species [{Cp*Fe}$_3$(μ_3,$\eta^{4:4:4}$-As$_6$)][X] (**[1][TEF]**, **[1][FAl]**, [TEF]$^-$ = [Al{OC(CF$_3$)$_3$}$_4$]$^-$, [FAl]$^-$ = [FAl{O(1-C$_6$F$_5$)C$_6$F$_{10}$}$_3$]$^-$), the second oxidation yields the paramagnetic [{Cp*Fe}$_3$(μ_3,$\eta^{4:4:4}$-As$_6$)][TEF]$_2$ (**[2][TEF]$_2$**). The reduction of **A** leads to the monoanionic compound [K@[2.2.2]-cryptand][{Cp*Fe}$_3$(μ_3,$\eta^{4:4:4}$-As$_6$)] (**[K@crypt][3]**), while a second reduction could only be traced spectroscopically. All compounds were comprehensively characterized, revealing the structural changes accompanying the described redox processes. All findings are supported by spectroscopic as well as computational studies.*

10.2. Introduction

Molecular transition metal polyarsides (As$_n$ ligand complexes) are a continually growing class of compounds, owing their attraction to their multifaceted structural chemistry.[1] In general, the polyarsenic As$_n$ units adopt a size and hapticity necessary to fulfill the 18 valence electron (VE) rule at the utilized transition metal fragment(s), often resembling aromatic hydrocarbon ligands.[2] Thus, complexes featuring As$_2$ dumbbells,[3] As$_3$,[4] As$_4$,[5] As$_5$,[6] As$_6$[7] and As$_8$[8] rings have been described. Commonly, these species are obtained under thermolytic or photolytic conditions using transition metal carbonyl complexes and a suitable As source, such as yellow arsenic (As$_4$).[1c] One of these very prominent thermolysis reactions is the one between [Cp*Fe(CO)$_2$]$_2$ and yellow arsenic, which affords [Cp*Fe(η^5-As$_5$)], a pentaarsolide (*cyclo*-As$_5$) derivative of the prototypical ferrocene.[6b] However, we recently described two additional products arising from this reaction. The heteroleptic complex [{Cp*Fe}$_2$(μ_3,$\eta^{4:4:4}$-As$_6$)Fe(η^3-As$_3$)] could be obtained as an analytically pure compound, while the homoleptic

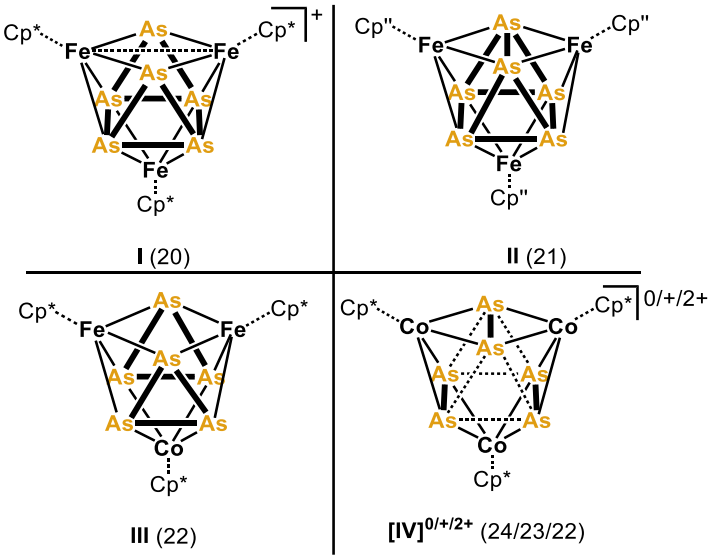

Scheme 1: Known arsenic prismane clusters and their respective skeletal electron counts in brackets; Cp = C$_5$Me$_5$, Cp'' = 1,3-^{t}Bu$_2$-C$_5$H$_3$.*

[{Cp*Fe}$_3$(μ_3,$\eta^{4:4:4}$-As$_6$)] (**A**) was hypothesized but could not be structurally validated yet.[9] Herein, we describe the isolation as well as surprising structural features of **A**, allowing to further study its reactivity. Amongst others, the group of Fenske succeeded in obtaining several hetero- and homometallic As$_6$ prismane clusters [{Cp^{R}M}$_3$(μ_3,$\eta^{4:4:4}$-As$_6$)]$^{+n}$ (**I** – **IV**; Cp^R = Cp*, Cp$^+$, Cp', Cp''; M = Fe, Co; n = 0, 1, 2, Scheme 1) as well as their lighter P-derivatives [{Cp*M}$_3$(μ_3,$\eta^{4:4:4}$-P$_6$)]$^{+n}$ (M = Fe, Co; n = 0, 1) from co-thermolysis as well as salt metathesis reactions.[10] However, studies on their reactivity are scarce and limited to "Aufbau"-reactions leading to extended heterotetranuclear clusters.[11] Yet, the redox chemistry of these compounds remains completely unstudied and no anionic arsenic prismane clusters could be isolated so far, which becomes even more of a target against the background of the wide range of skeletal electron numbers observed in the complexes mentioned above (Scheme 1).

10.3. Results and Discussion

A was synthesized by the co-thermolysis of [Cp*Fe(CO)$_2$]$_2$ with As$_4$ and could be isolated in an improved 39% yield by a more elaborate chromatographic workup involving toluene/hexane mixtures as eluents (see SI).[6b,9]

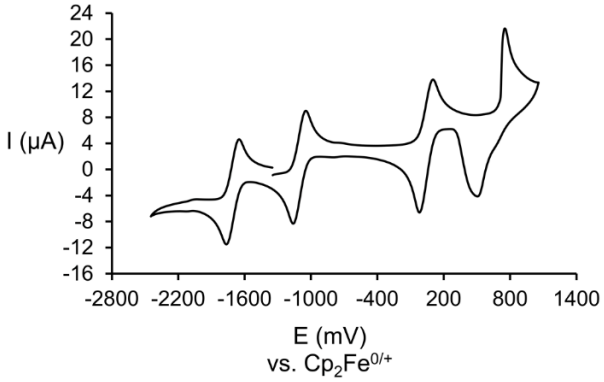

*Figure 1: Cyclic voltammogram of **A** in CH_2Cl_2 referenced to the Fc/Fc$^+$ couple with [^{n}Bu$_4$N][PF$_6$] as conducting salt.*

With **A** in hand, we investigated its electrochemical properties by means of cyclovoltammetric measurements that reveal four distinct and reversible redox processes at −1.76 V, −1.16 V, 0.10 V and 0.75 V versus the Fc/Fc$^+$ couple (**Fig. 1**, Fc = ferrocene). Accordingly, **A** should be doubly reducible as well as doubly oxidizable. Therefore, the thianthrenium radical cation [Thia]$^{+\bullet}$ should be a suitable oxidant for both oxidative processes.[12] When **A** is reacted with one equivalent of [Thia][X] ([X]$^-$ = [TEF]$^-$ or [FAl]$^-$, [TEF]$^-$ = [Al{OC(CF$_3$)$_3$}$_4$]$^-$, [FAl]$^-$ = [FAl{O(1-C$_6$F$_5$)C$_6$F$_{10}$}$_3$]$^-$)[13] in CH_2Cl_2 or *o*-DFB (*ortho*-difluorobenzene), a rapid reaction affords the respective diamagnetic monocationic species [{Cp*Fe}$_3$(μ_3,$\eta^{4:4:4}$-As$_6$)][X] (**[1][TEF]** (64%), **[1][FAl]** (82%), Scheme 2). The doubly oxidized species [{Cp*Fe}$_3$(μ_3,$\eta^{4:4:4}$-As$_6$)][TEF]$_2$ (**[2][TEF]$_2$**) is obtained in even better yields of 92% when two equivalents of [Thia][TEF] are employed. The paramagnetic dication **[2]$^{2+}$** is highly reactive, preventing the isolation of its salts with less innocent anions. Thus, samples of **[2][BAr^F]$_2$**, which we prepared to obtain better crystallographic data, are highly contaminated with a range of oxidized polyarsenic complexes. The reduction of **A** can be achieved by reacting it with one equivalent of KC$_8$ in

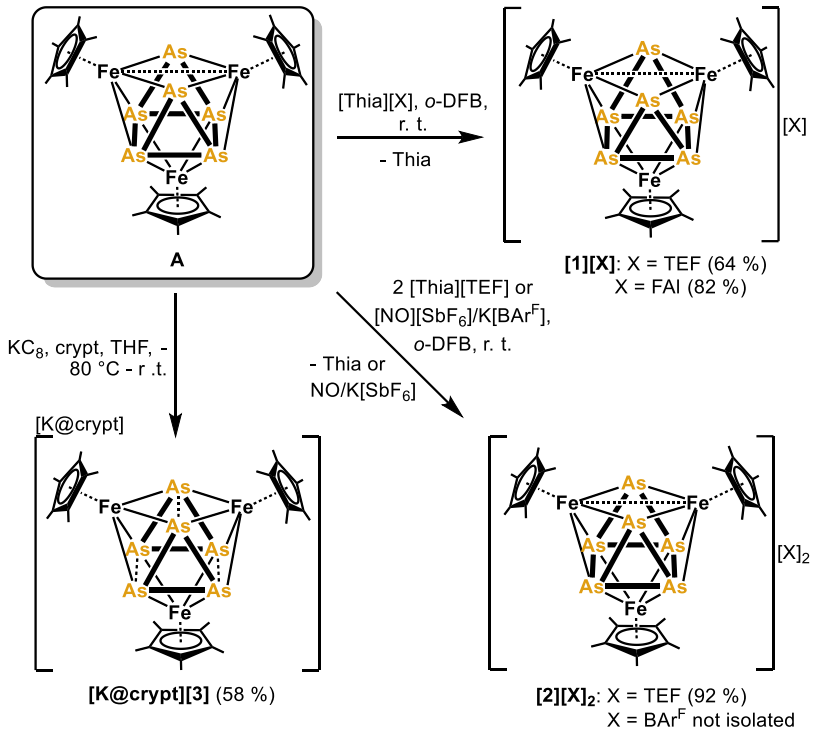

*Scheme 2: Synthesis of ionic iron-arsenic prismane clusters **1** – **3** starting from **A**. Isolated yields are given in parentheses. Thia = thianthrene ($C_{12}H_8S_2$), $[TEF]^-$ = $[Al\{OC(CF_3)_3\}_4]^-$, $[FAl]^-$ = $[FAl\{O(1\text{-}C_6F_5)C_6F_{10}\}_3]^-$, $[BArF]^-$ = $[B(C_6F_5)_4]^-$, crypt = [2.2.2]-cryptand ($C_{18}H_{36}O_6N_2$).*

THF. The product [K@crypt][{Cp*Fe}$_3$(μ_3,$\eta^{4:4:4}$-As$_6$)] (**[K@crypt][3]**, 58%, crypt = [2.2.2]-cryptand) was obtained after the addition of crypt to the reaction solution and careful workup. The second reduction of **A** could not be achieved, which we attribute to the high sensitivity of the proposed dianionic species [{Cp*Fe}$_3$(μ_3,$\eta^{4:4:4}$-As$_6$)]$^{2-}$, which appears to decompose upon workup. EPR spectroscopic data (see SI), however, points towards the presence of this paramagnetic compound in the reaction mixture.

Generally, the structural chemistry of the described iron arsenic prismane clusters is governed by the number of skeletal electrons.[10] Thus, it is even more surprising that, in contrast to its Cp'' analog, the As$_6$ core in **A** does not adopt a regular prismatic structure.[9] Instead, the As1-As2 edge is opened (3.5012(4) Å), which goes in hand with a shortening of the Fe1-Fe2 distance (3.2504(4) Å). The edges of the distorted prismane show As-As distances of 2.683(3)–2.706(7) Å, while those within the triangular faces are in between 2.512(2) Å and 2.636(8) Å and thus above the sum of the covalent radii.[14] Interestingly, the distortion of the prismane core is even more accentuated in the monocation, which was already reported.[10e] In the monocationic **[1][FAl]** synthesized here**,** the elongation of the As1-As2 distance (3.797(13) Å) increases (Fig. 2). Accordingly, the respective Fe1-Fe2 distance is even shorter (2.8956(9) Å) compared to **A**. The second oxidation, however, seems to have less structural influence on the As$_6$ core, as the As1-As2 (3.689(4) Å) as well as the Fe1-Fe2 distances (2.8993(6) Å) in **[2][BAr^F]$_2$** are similar to those in **[1][FAl]**. Furthermore, the prismane edges (2.698(4)–2.721(3) Å) as well as the As-As distances in the triangular faces (2.5047(7) – 2.6199(11) Å) remain similar to those found in **A**. The reduction of **A** to **[K@crypt][3]** is

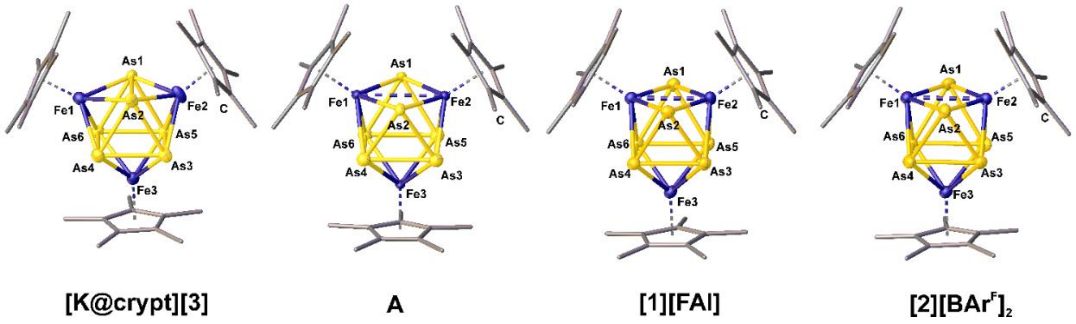

*Figure 2: Molecular structures of the [{Cp*Fe}$_3$(μ_3,$\eta^{4:4:4}$-As$_6$)]$^{-/0/+/2+}$ core within the compounds **A**, [**1**][FAl], [**2**][BArF]$_2$ and [K@crypt][**3**] in order of decreasing electron count for the central prismane cluster.*

accompanied by an equalization within the prismane core, as found in the Fe_2Co analog **III** (Scheme 1). The As-As distances along the edges amount to 2.795(10)–2.847(1) Å, while the triangular faces share As-As distances of 2.543(9)–2.5833(15) Å. Accordingly, the Fe-Fe distance is elongated to a nonbonding interaction of 3.7832(8) Å. Conclusively, the stepwise oxidation from **[3]**$^-$ to **[2]**$^{2+}$ primarily results in a gradual distortion of the central Fe_2As_2 square. While this is dominated by a closer As1-As2 distance in the reduced **[3]**$^-$, the oxidized **[2]**$^{2+}$ reveals a significantly closer Fe1-Fe2 and an elongated As1-As2 distance.

The diamagnetic species **[1][X]** ([X]$^-$ = [TEF]$^-$ or [FAl]$^-$) and **[K@crypt][3]** only show the expected signal for chemically equivalent Cp* ligands in their respective ^{1}H NMR spectra (see SI). In contrast, **A** in CD_2Cl_2 reveals a broad resonance at δ = 2.93 ppm with $\omega_{1/2}$ = 40 Hz indicating its paramagnetic character. The corresponding X-band EPR spectrum of **A** in frozen CH_2Cl_2 solution at 77 K shows a rhombic signal with g_1 = 2.20, g_2 = 2.13 and g_3 = 2.04 and additional hyperfine coupling to the arsenic nuclei. Similarly, a solution of the dicationic **[2][TEF]$_2$** in CD_2Cl_2 shows a broad signal at δ = –7.84 ppm with $\omega_{1/2}$ = 126 Hz in the ^{1}H NMR spectrum. The X-band EPR spectrum of **[2][TEF]$_2$** in frozen CH_2Cl_2 solution at 77 K again reveals a rhombic signal with g_1 = 2.42, g_2 = 2.00, g_3 = 1.96 and coupling to the arsenic nuclei (see SI).

To better understand the bonding and electronic situation within **A** and **1**–**3,** we conducted DFT computations at the B3LYP[15]/def2SVP[16] level of theory. As expected, the Wiberg bond indices (WBI) obtained from NBO analyses[17] for the central Fe_3As_6 core are all below 1 which is indicative of the cluster nature of these compounds. However, the WBIs for the As1-As2 interactions decrease from the reduced **[3]**$^-$ (0.283) to the neutral **A** (0.095) to the cationic **[1]**$^+$ and dicationic species **[2]**$^{2+}$ (0.078/0.080). Accordingly, the WBIs for the Fe1-Fe2 interaction increase from 0.089 ([**3**]$^-$) to 0.1 (**A**) to 0.207 (**[1]**$^+$)/0.219 (**[2]**$^{2+}$). This is in line with a decreased As1-As2 contribution and an increased Fe1–Fe2 contribution to the multi center bonding interaction within the Fe_2As_2 square upon oxidation. Furthermore, the spin density distribution was calculated for the neutral **A** and the dicationic **[2]**$^{2+}$(Figure 3). While the unpaired electron in **A** seems to be located mainly at the two iron atoms close to each other (Fe1 and Fe2), the spin density within **[2]**$^{2+}$ in a doublet ground state should solely be located at the Fe3 atom. In a hypothetical quartet ground state of **[2]**$^{2+}$, however, the spin density would be smeared out across all three iron atoms.

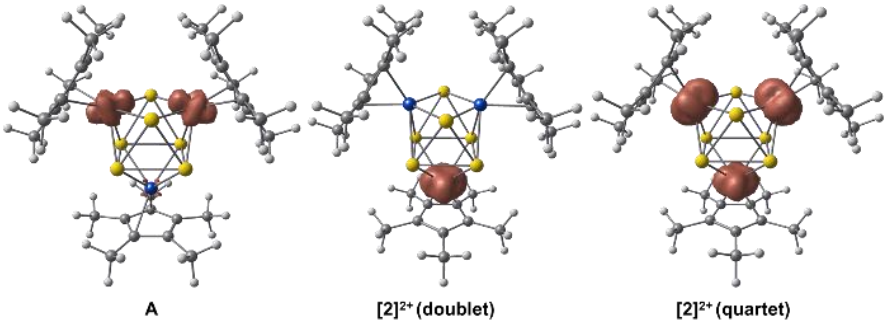

*Figure 3: Computed spin densities for **A** and [**2**]$^{2+}$ in a doublet and a hypothetical quartet ground state obtained at the B3LYP/def2SVP level of theory.*

10.4. Conclusion

In summary, we report the isolation and characterization of a side product that had long been unclarified, formed during the co-thermolysis of $[Cp^*Fe(CO)_2]_2$ and yellow arsenic (As_4), which is the prismatic cluster $[\{Cp^*Fe\}_3(\mu_3,\eta^{4:4:4}\text{-}As_6)]$ (**A**). For the first time, we shed light on the redox chemistry and the accompanying structural changes of arsenic prismane complexes, utilizing **A** as starting material. It was possible to oxidize **A** once to form **[1][X]** ($[X]^-$ = $[TEF]^-$ or $[FAl]^-$) and twice to give **[2][TEF]$_2$**. While **A** should be doubly reducible, we could only experimentally realize selectively its monoreduction to give **[K@crypt][3]** which represents the first anionic cluster of this type. Structural characterization of these compounds revealed Fe-Fe bond formation as well as As-As bond splitting upon oxidation. Reduction on the other hand leads to additional As-As interaction formation and Fe-Fe bond breaking. DFT calculations elucidated the electronic structures of **A** and **1**–**3**. These results display a starting point in the study of the electrochemical properties of polyarsenide prismane clusters and give insight into the influence of redox processes on As-As bond formation/splitting processes.

10.5. Supporting Information

10.5.1. Experimental Procedures

General Considerations

All manipulations were carried out using standard Schlenk techniques at a Stock apparatus under N_2 as an inert gas or in a glove box with Ar atmosphere. All glassware was dried with a heat gun (600 °C) for at least 30 min prior to use. *o*-DFB (1,2-difluorobenzene) was distilled from P_2O_5, CD_2Cl_2 was distilled from CaH_2, THF-d^8 and DME (1,2-Dimethoxyethane) were distilled from Na/K alloy and other solvents were directly taken from an MBraun SPS-800 solvent purification system and degassed at room temperature. Solution ^{1}H (400.130 MHz) and ^{19}F (376.498 MHz) NMR spectra were recorded at an Avance400 (Bruker) spectrometer using $(H_3C)_4Si$ (^{1}H) and $CFCl_3$ (^{19}F) as external standards. Chemical shifts (δ) are provided in parts per million (ppm) and coupling constants (J) are reported in Hertz (Hz). The following abbreviations are used: s = singlet, br = broad and m = multiplet. X-Band EPR spectra were recorded on a MiniScope MS400 device from Magnettech GmbH with a frequency of 9.5 GHz equipped with a rectangular resonator TE102. CV measurements were performed in *o*-DFB solution with $[NBu_4][PF_6]$ (0.1 M) as supporting electrolyte. The redox pair of ferrocene ($Fc^{0/+}$ = 0.000 V) was applied as reference. ESI mass spectra were recorded at the internal mass spectrometry department using a ThermoQuest Finnigan TSQ 7000 mass spectrometer or by the authors on a Waters Micromass LCT ESI-TOF mass-spectrometer and peak assignment was performed using the Molecular weight calculator 6.50.[19] Elemental analysis of the products was conducted by the elemental analysis department at the University of Regensburg using an Elementar Vario EL. The starting materials $[Cp^*Fe(CO)_2]_2$,[20] [Thia][X] ($[X]^-$ = $[TEF]^-$, $[FAl]^-$; $[TEF]^-$ = $[Al\{OC(CF_3)_3\}_4]^-$, $[FAl]^-$ = $[FAl\{O(1\text{-}C_6F_5)C_6F_{10}\}_3]^-$),[13] $K[B(C_6F_5)_4]$[21] and KC_8[22] were synthesized following literature procedures. All other chemicals were purchased from commercial vendors and used without further purification.

Reaction of $[Cp^*Fe(CO)_2]_2$ with As_4

This reaction has already been described previously, but with different workup.[6b] The following reaction steps were carried out under exclusion of light. Grey arsenic (~5 g) was heated to 550 °C and sublimed into 300 mL boiling decalin yielding a saturated solution of yellow As_4. This hot solution was transferred onto a orange brown solution of $[Cp^*Fe(CO)_2]_2$ (1.25 g, 2.53 mmol) in 15 mL decaline and refluxed for 90 minutes yielding a dark greenish brown solution, which is not light sensitive anymore. The solvent was condensed into another flask yielding a brown crude product. This procedure was conducted for a total of six times and the crude products were combined. The brown powder was redissolved in 20 mL of CH_2Cl_2, mixed with 20 g dried silica and the solvent removed under reduced pressure until a free-flowing powder was obtained. The powder was transferred onto a chromatographic column (silica, 3x15 cm). Elution with *n*-hexane yields a dark green fraction of $[Cp^*Fe(\eta^5\text{-}As_5)]$. Subsequently, by elution with *n*-hexane/toluene = 2:1 an additional brown fraction of $[(Cp^*Fe)_3As_6]$ (**A**) starts to arise, which can be separated by increasing the toluene percentage to 1:1. A last fraction, containing a mixture of **A** and $[(Cp^*Fe)_3As_6\{Fe(\eta^3\text{-}As_3)\}]$ (**IV**) was eluted but not isolated. From both, the green as well as the brown fraction, the solvent was removed and the powders redissolved in 10 mL ($[Cp^*Fe(\eta^5\text{-}As_5)]$) or 40 mL (**A**) of CH_2Cl_2, respectively, and stored at −30 °C yielding dark green ($[Cp^*Fe(\eta^5\text{-}As_5)]$) or brownish black (**A**) crystals. The latter were subjected to single crystal X-ray diffraction. The crystals were isolated and dried in vacuum for 3h. The solvents of the supernatant was removed under reduced pressure and the resulting powder again dried in vacuum for 3h.

$[(Cp^*Fe)_3As_6]$ (**A**):

Yield: 4.03 g (3.94 mmol = 39 % referred to $[Cp^*Fe(CO)_2]_2$).

Elemental analysis: calc. (%) for $[C_{30}H_{45}Fe_3As_6]$: C: 35.23 H: 4.43

found (%): C: 34.37 H: 4.53

The product may contain trace amounts of grey arsenic.

LIFDI MS (toluene): *m/z* (%) = (1022.63 (100), $[\mathbf{A}]^+$)

NMR (CD_2Cl_2, 298 K): ^{1}**H**: δ/ppm = 2.93 (br, $\omega_{1/2}$ = 40 Hz, Cp*)

EPR (77K, CH_2Cl_2) $g_1 = 2.20$, $g_2 = 2.13$ and $g_3 = 2.04$

*Synthesis of [(Cp*Fe)$_3$As$_6$][TEF] (**[1][TEF]**)*

A brown solution of [(Cp*Fe)$_3$As$_6$] (**A**; 91 mg, 0.09 mmol, 0.9 eq.) in 5 mL of CH_2Cl_2 was reacted with a dark purple solution of [Thia][TEF] (118 mg, 0.1 mmol, 1.0 eq.) in 5 mL of CH_2Cl_2 leading to an immediate colour change to orange brown. The solution was stirred for 60 minutes. Addition of 50 mL *n*-hexane led to precipitation of a dark brown powder. The supernatant was decanted, and the residue washed with 30 mL *n*-hexane and 30 mL toluene. The powder was dried in vacuum and recrystallization from CH_2Cl_2/*n*-hexane at room temperature yielded pure **[1][TEF]** as black needles suitable for single crystal X-ray diffraction. The solvent was removed by decanting and the crystals dried in vacuum for 3h.

Yield:	105 mg (0.058 mmol = 64 %)
Elemental Analysis:	calc. (%) for $[C_{30}H_{45}Fe_3As_6][AlO_4C_{16}F_{36}]$: C: 27.77 H: 2.28
	found: C: 27.90 H: 2.24
ESI (+) MS (CH_2Cl_2):	*m/z* (%) = 1022.69 (100) [**1**]$^+$
^{1}H NMR (CD_2Cl_2):	*δ*/ppm = 1.57 (s, Cp*)
^{19}F{^{1}H} NMR (CD_2Cl_2):	*δ*/ppm = –75.74 (s, [TEF]$^-$)

*Synthesis of [(Cp*Fe)$_3$As$_6$][FAl] (**[1][FAl]**)*

A brown solution of [(Cp*Fe)$_3$As$_6$] (**A**; 182 mg, 0.18 mmol, 1.0 eq.) in 15 mL of CH_2Cl_2 was reacted with a dark purple solution of [Thia][FAl] (118 mg, 0.18 mmol, 1.0 eq.) in 15 mL of CH_2Cl_2 leading to an immediate colour change to orange brown. The solution was stirred for 60 minutes. Addition of 80 mL *n*-hexane led to precipitation of a dark brown powder. The supernatant was decanted, and the residue washed with 30 mL *n*-hexane and 30 mL toluene. The powder was dried in vacuum and recrystallization from CH_2Cl_2/*n*-hexane at room temperature yielded pure **[1][FAl]** as black plates suitable for single crystal X-ray diffraction. The solvent was removed by decanting and the crystals dried in vacuum for 3h.

Yield:	355 mg (0.148 mmol = 82 %)
Elemental Analysis:	calc. (%) for $[C_{30}H_{45}Fe_3As_6][AlO_3C_{36}F_{46}]$: C: 33.00 H: 1.89
	found: C: 33.36 H: 1.88.
ESI (+) MS (CH_2Cl_2):	*m/z* (%) = 1022.71 (65) $[\mathbf{1}]^+$
^{1}H NMR (CD_2Cl_2):	*δ*/ppm = 1.57 (s, Cp*)

The $^{19}F\{^1H\}$ NMR spectrum of **1[FAl]** in CD_2Cl_2 shows signals characteristic for the presence of the $[FAl]^-$ anion.

*Synthesis of [(Cp*Fe)$_3$As$_6$][TEF]$_2$ (**[2][TEF]$_2$**)*

A brown solution of [(Cp*Fe)$_3$As$_6$] (**A**; 91 mg, 0.09 mmol, 1.0 eq.) in 15 mL of *o*-DFB was reacted with a dark purple solution of [Thia][TEF] (210 mg, 0.18 mmol, 2.0 eq.) in 5 mL of *o*-DFB leading to an immediate colour change to dark orange red. The solution was stirred for 60 minutes. Addition of 80 mL *n*-hexane led to precipitation of a black powder. The supernatant was decanted, and the residue washed with 50 mL toluene. The powder was dried in vacuum and recrystallization from *o*-DFB/*n*-hexane at room temperature yielded pure **[2][TEF]$_2$** as black stick shaped crystals. The solvent was removed by decanting and the crystals dried in vacuum for 3h.

Compound **[2][TEF]$_2$** can also be synthesized by analogous reaction in CH_2Cl_2, by reacting **[1][TEF]** with a further equivalent of [Thia][TEF]. To obtain appropriate crystallographic data for the dicationic species **[2]$^{2+}$**, we reacted **A** with two equivalents of [NO][SbF_6] in the presence of K[Bar^F] (2 equivalents) under the same conditions as for **[2][TEF]$_2$**. The ^{1}H NMR spectrum of **[2][BAr^F]$_2$** after crystallization however reveals the presence of several cationic iron arsenic clusters, which is why we could not isolate **[2][BAr^F]$_2$** as a clean compound.

Yield:	245 mg (0.083 mmol = 92 %).
Elemental Analysis:	calc. (%) for [$C_{30}H_{45}Fe_3As_6$][$AlO_4C_{16}F_{36}$]$_2$: C: 25.18 H: 1.53.
	found: C: 25.33 H: 1.46.
ESI (+) MS (*o*-DFB):	*m/z* (%) = 511.26 (100) [**2**]$^{2+}$, 1022.71 (100) [**1**]$^+$.
^{1}H NMR (CD_2Cl_2):	δ/ppm = –7.84 (br, $\omega_{1/2}$ = 126 Hz, Cp*)
^{19}F{^{1}H} NMR (CD_2Cl_2):	δ/ppm = –75.74 (s, [TEF]$^-$)
EPR (77K, CH_2Cl_2)	g_1 = 2.42, g_2 = 2.00, g_3 = 1.96

*Synthesis of [K@crypt][(Cp*Fe)$_3$As$_6$] (**[K@crypt][3]**)*

[(Cp*Fe)$_3$As$_6$] (**A**; 204 mg, 0.20 mmol, 1.0 eq.), KC_8 (27 mg, 0.20 mmol, 1.0 eq.) and [2.2.2.]cryptand ($N(CH_2CH_2OCH_2CH_2OCH_2CH_2)_3N$) (75 mg, 0.20 mmol, 1.0 eq.) were weighed in separate flasks and dissolved in 5 mL of THF, each. The KC_8 suspension was added to the solution of **A** at –80°C to afford an immediate colour change to dark reddish brown. After 5 minutes of stirring the solution of [2.2.2.]cryptand was added as well, the mixture was stirred for 2h and allowed to warm to room temperature. Filtration afforded a dark brownish red solution, which was layered with 80 mL *n*-pentane and storage at 4 °C yielded pure [K@crypt][(Cp*Fe)$_3$As$_6$] (**[K@crypt][3]**) as dark brown blocks suitable for single crystal diffraction. The solvent was removed by decanting and the crystals dried in vacuum for 3h.

Yield:	166 mg (0.115 mmol = 58 %)
Elemental Analysis:	calc. (%) for $[KC_{18}H_{36}N_2O_6][C_{30}H_{45}Fe_3As_6]\cdot(C_4H_8O)_{0.5}$: C: 40.73 H: 5.81 N: 1.90
	found: C: 40.82 H: 5.97 N: 1.90
ESI (–) MS (THF):	*m/z* (%) = 511.23 (100) $[\mathbf{3}]^{2-}$
^{1}H NMR (THF-d^8):	δ/ppm = 1.88 (s, 45 H, Cp*), 2.62 (s, 12 H, crypt), 3.61 (s (overlapping with THF-d^8 signal), 12 H, crypt), 3.65 (s (overlapping with THF-d^8 signal), 12 H, crypt)

10.5.2. X-ray Crystallographic Data

All crystal manipulations were performed under mineral oil. The diffraction experiments were performed at 123 K (if not stated otherwise) either on a Rigaku (former Agilent Technologies or Oxford Diffraction) Gemini Ultra with an AtlasS2 detector, on a GV50 diffractometer with a TitanS2 detector, on a Gemini Ultra with an AtlasS2 detector, or an XtaLAB Synergy R, DW System with a HyPix-Arc 150 detector using Cu-K_α, Cu-K_β or Mo-K_α radiation. Crystallographic data together with the details of the experiments are given in *Table S* . The cell determination, data reduction and absorption correction for all compounds were performed with the help of the CrysAlis PRO software.[23] All structures were solved by using the programs SHELXT[24] and Olex2.[25] The full-matrix least-squares refinement against F^2 was done using SHELXL[26] and Olex2.[25] If not stated otherwise, all atoms except hydrogen atoms were refined anisotropically. The H atoms were calculated geometrically, and a riding model was used during the refinement process.

CCDC reference numbers 2157447 (**A**), 2157448 (**[1][TEF]**), 2157449 (**[1][FAL]**), 2157450 (**[2][Bar^F]$_2$**), and 2157451 (**[K@crypt][3]**) contain the supplementary crystallographic data for this paper. These data can be obtained free of charge at www.ccdc.cam.ac.uk/conts/retreving.html (or from the Cambridge Crystallographic Data Center, 12 Union Road, Cambridge CB2 1EZ, UK; Fax: (internat.) + 44-1223-336-033; e-mail: deposit@ccdc.cam.ac.uk).

Table S 1: Crystallographic data for the described compounds.

Compound	A	1[TEF]	1[FAl]	2[Bar^F]$_2$	[K@crypt][3]
Empirical formula	$C_{30}H_{45}As_6Fe_3$	$C_{113}H_{114}Al_2As_{12}F_{72}Fe_6O_8$	$C_{66}H_{45}AlAs_6F_{46}Fe_3O_3$	$C_{78}H_{45}As_{6.1}2B_2F_{40}Fe_3$	$C_{48}H_{81}As_6Fe_3KN_2O_6$
Formula weight	1022.73	4256.14	2404.07	2389.82	1438.31
Temperature/K	293(2)	123.0(1)	123.00(10)	123.00(10)	123.01(10)
Crystal system	monoclinic	monoclinic	triclinic	triclinic	orthorhombic
Space group	$P2_1/m$	$P2_1/c$	$P\bar{1}$	$P\bar{1}$	*Pnma*
a/Å	8.2946(4)	40.3103(3)	15.9679(4)	12.86210(10)	20.36410(10)
b/Å	19.0247(6)	22.2643(2)	16.0682(4)	13.79760(10)	18.79330(10)
c/Å	11.2462(4)	16.3724(2)	17.5789(5)	24.4268(2)	16.04000(10)
α/°	90	90	70.388(2)	91.9560(10)	90
β/°	108.558(5)	101.0640(10)	67.422(2)	103.6610(10)	90
γ/°	90	90	73.953(2)	99.9570(10)	90
Volume/Å3	1682.40(12)	14420.8(2)	3866.17(19)	4136.10(6)	6138.65(6)
Z	2	4	2	2	4
ρcalcg/cm3	2.019	1.960	2.065	1.919	1.556
μ/mm-1	7.152	6.901	8.884	8.119	10.144
F(000)	1002.0	8328.0	2336.0	2326.0	2904.0
Crystal size/mm3	0.334 × 0.168 × 0.125	0.191 × 0.118 × 0.079	0.797 × 0.472 × 0.089	0.285 × 0.135 × 0.041	0.147 × 0.119 × 0.112
Radiation	Mo Kα (λ = 0.71073)	Cu Kβ (λ = 1.39222)	Cu Kα (λ = 1.54184)	Cu Kα (λ = 1.54184)	Cu Kα (λ = 1.54184)
2Θ range for data collection/°	6.722 to 64.398	5.396 to 145.118	7.044 to 145.744	6.524 to 150.526	7.016 to 148.278
Index ranges	-12 ≤ h ≤ 11, -26 ≤ k ≤ 28, -16 ≤ l ≤ 16	-55 ≤ h ≤ 52, -29 ≤ k ≤ 30, -21 ≤ l ≤ 21	-16 ≤ h ≤ 19, -19 ≤ k ≤ 19, -21 ≤ l ≤ 21	-15 ≤ h ≤ 15, -17 ≤ k ≤ 16, -30 ≤ l ≤ 30	-25 ≤ h ≤ 22, -23 ≤ k ≤ 21, -19 ≤ l ≤ 16
Reflections collected	15838	100762	30671	68603	30703
Independent reflections	5581 [Rint = 0.0260, Rsigma = 0.0334]	37344 [Rint = 0.0358, Rsigma = 0.0382]	14747 [Rint = 0.0524, Rsigma = 0.0640]	16532 [Rint = 0.0301, Rsigma = 0.0203]	6190 [Rint = 0.0395, Rsigma = 0.0255]
Data/restraints/ parameters	5581/6/261	37344/363/2437	14747/0/1141	16532/102/1233	6190/30/405
Goodness-of-fit on F2	1.034	1.037	1.055	1.045	1.049
Final R indexes [I>=2σ (I)]	R1 = 0.0257, wR2 = 0.0485	R1 = 0.0351, wR2 = 0.0771	R1 = 0.0490, wR2 = 0.1323	R1 = 0.0354, wR2 = 0.0930	R1 = 0.0328, wR2 = 0.0845
Final R indexes [all data]	R1 = 0.0377, wR2 = 0.0520	R1 = 0.0477, wR2 = 0.0834	R1 = 0.0543, wR2 = 0.1399	R1 = 0.0375, wR2 = 0.0942	R1 = 0.0368, wR2 = 0.0866
Largest diff. peak/hole / e Å-3	0.64/-0.50	0.71/-0.53	1.56/-1.35	1.84/-0.61	0.40/-0.59

A

Compound **A** crystallizes in the monoclinic space group *P*2/*m* with half a molecule in the asymmetric unit (Figure S1) exhibiting a distorted As_6 prism with an open As–As bond. The square sides of the prism are coordinated by {Cp*Fe} fragments. Rotational disorder of one of the Cp* ligands was refined using adequate restraints.

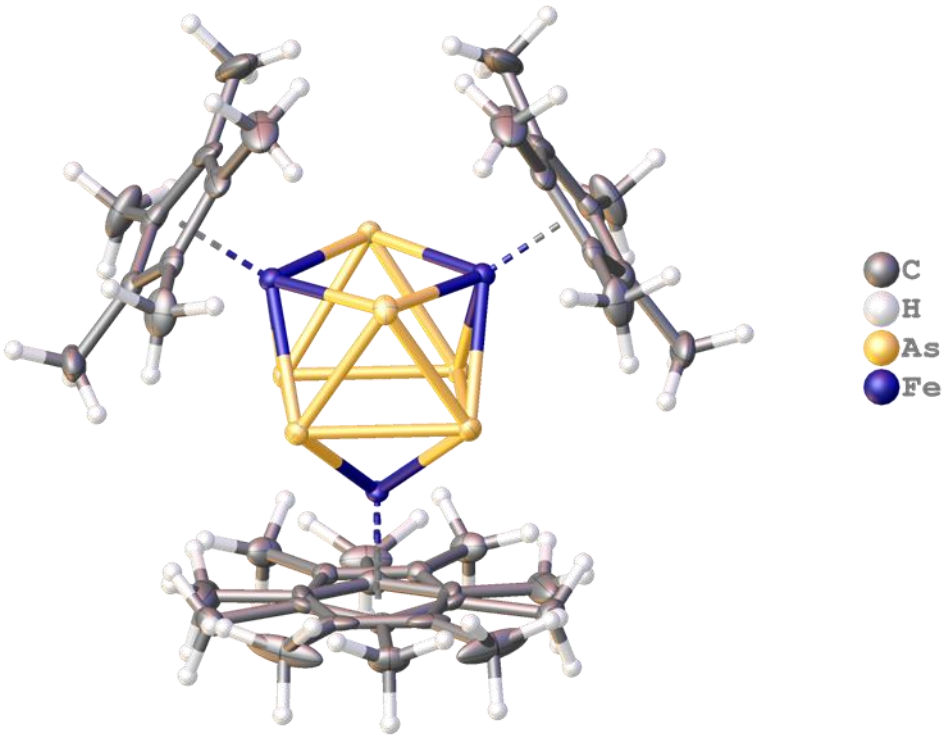

*Figure S 1: Molecular structure of **A**; The grown structure of the asymmetric unit is shown, which contains one half molecule of **A**.*

[1][TEF]

Compound **[1][TEF]** crystallizes in the monoclinic space group $P2_1/c$ with two cations, two $[TEF]^-$ anions and two toluene molecules in the asymmetric unit (Figure S2). One $[TEF]^-$ anion (including Al1) shows rotational disorder of three $OC(CF_3)_3$ groups in a ratio of 69:31, 63:37 and 56:44. Adequate restraints were used during the refinement of the disordered $[TEF]^-$ anion.

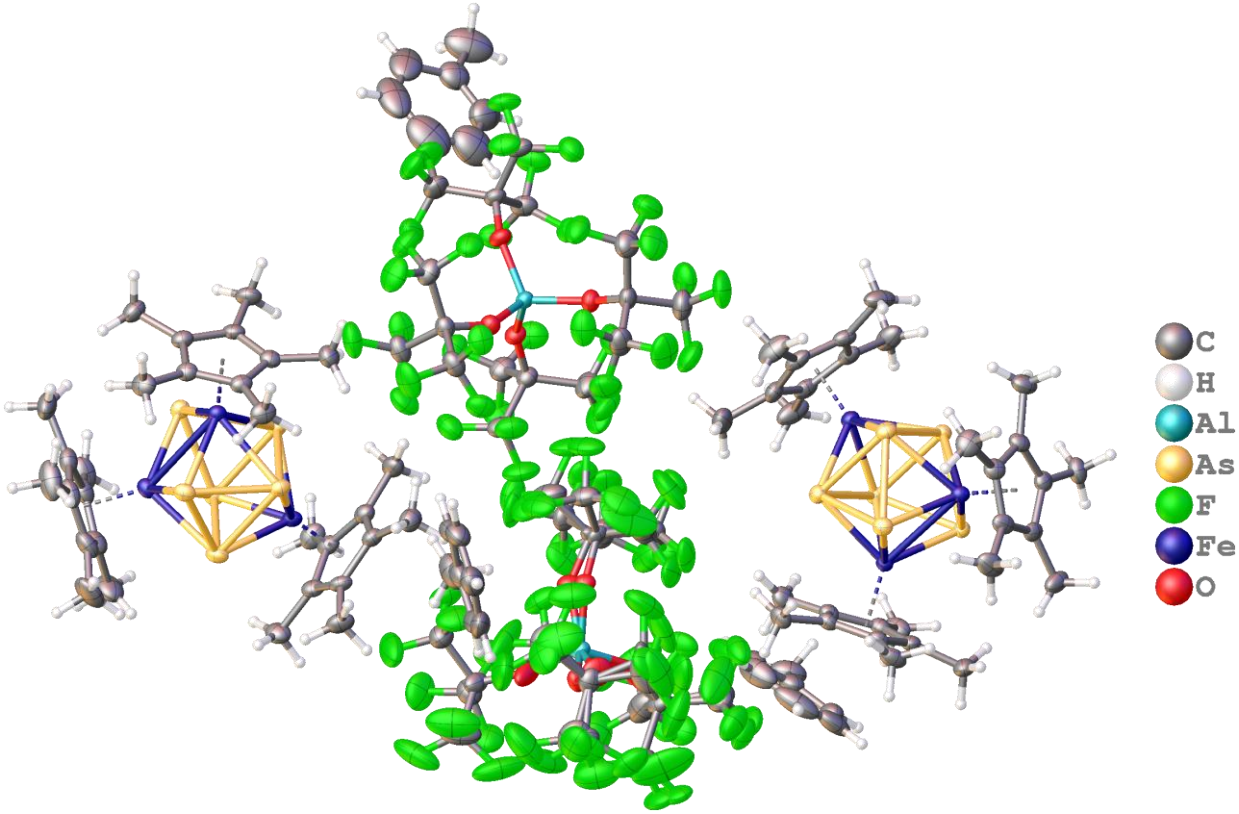

*Figure S 2: Molecular structure of **[1][TEF]**; The asymmetric unit is shown containing two cations, two $[TEF]^-$ anions and two toluene molecules.*

[1][FAl]

Compound **[1][FAl]** crystallizes in the triclinic space group $P\bar{1}$ with one cation and one $[FAl]^-$ anion in the asymmetric unit (Figure S3).

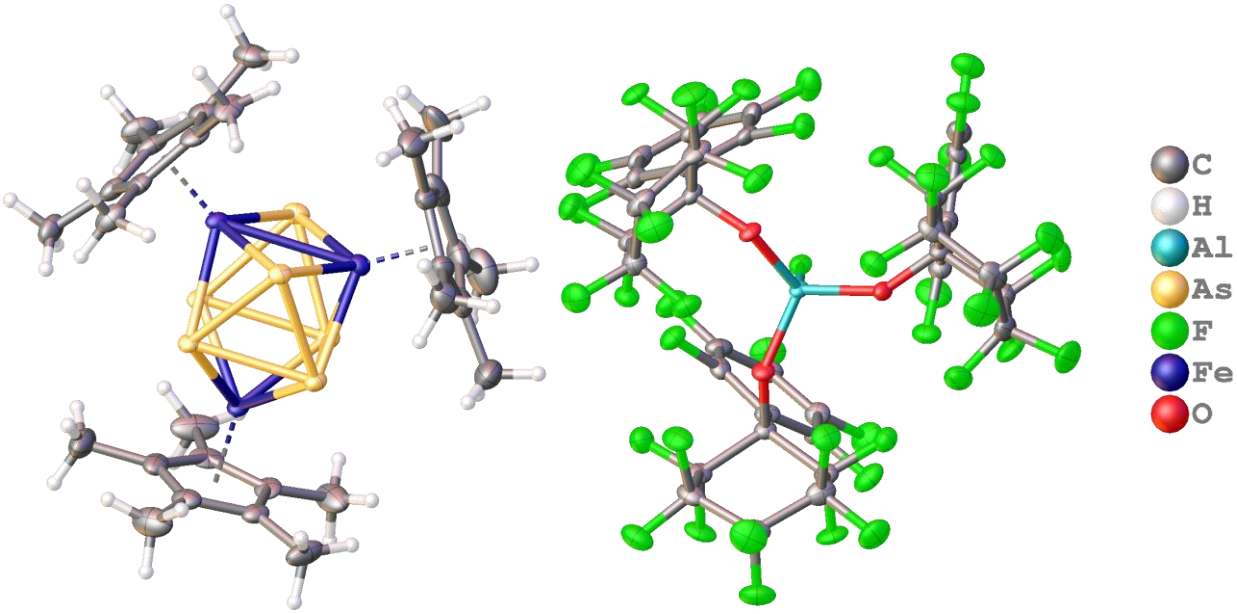

*Figure S 3: Molecular structure of **[1][FAl]**; The asymmetric unit is shown containing one cation and one $[FAl]^-$ anion.*

[2][BAr^F]$_2$

Compound **[2][Bar^F]$_2$** crystallizes in the triclinic space group $P\bar{1}$ with one cation, two [Bar^F]$^-$ anions and half a *o*-DFB molecule in the asymmetric unit (Figure S4). Residual electron density at the As_6 core indicates that **[2][Bar^F]$_2$** cocrystallizes with traces of another dicationic species, which could however not be fully resolved.

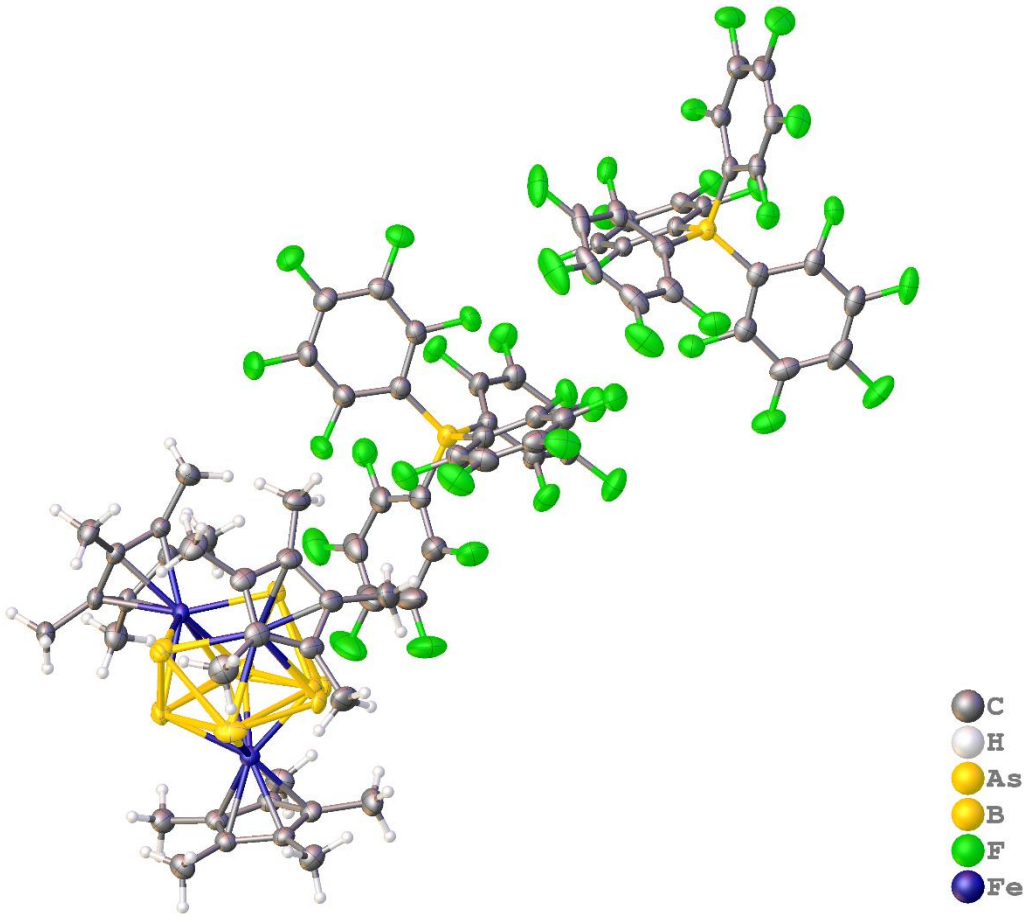

*Figure S 4: Molecular structure of **[2][Bar^F]$_2$**; The asymmetric unit contains one cation, two [BAr^F]$^-$ anions and half a o-DFB molecule.*

[K@crypt][3]

Compound **[K@crypt][3]** crystallizes in the orthorhombic space group *Pnma* with half an anion, half a cation and half of a THF molecule in the asymmetric unit (Figure S5). Adequate restraints were used during the refinement of both, the anion and the cation.

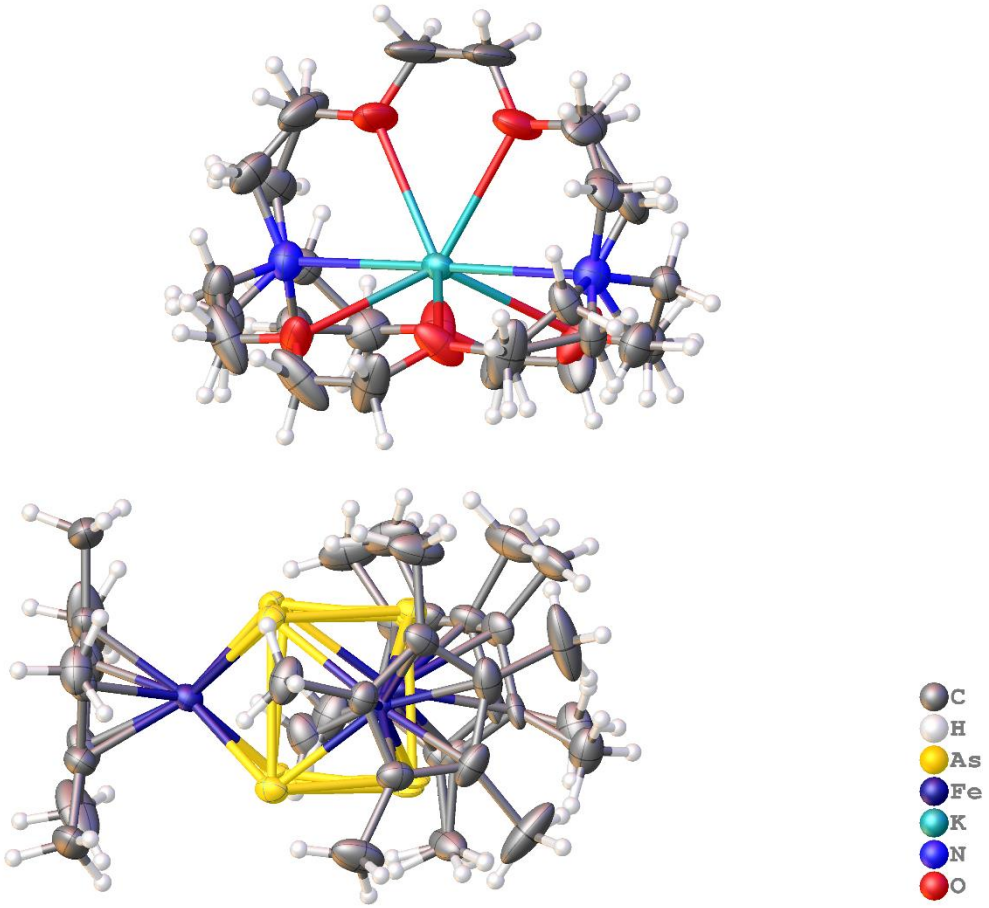

*Figure S 5: Molecular structure of **[K@crypt][3]**; The asymmetric unit contains only half of the cation and the anion and an additional half of a THF molecule.*

10.5.3. NMR Spectroscopic Investigations

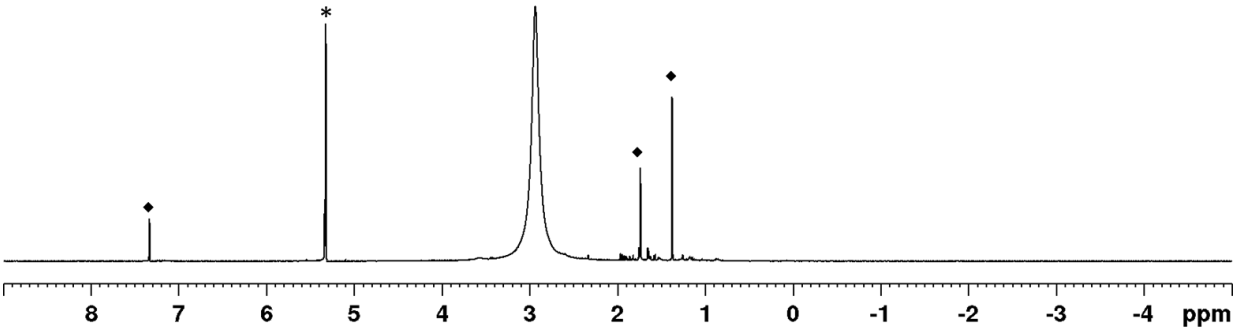

*Figure S 6: ^{1}H NMR spectrum of $[(Cp^*Fe)_3As_6]$ (**A**) in CD_2Cl_2; * = solvent residual signal, ◆ = unidentified trace impurities.*

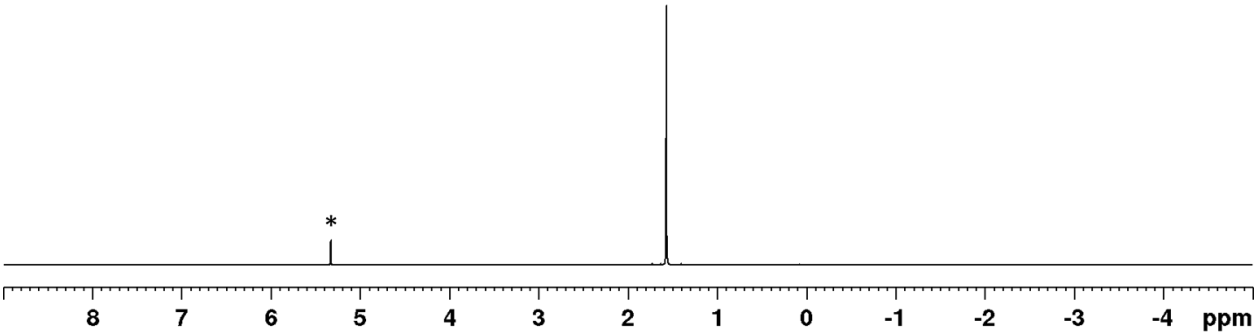

*Figure S 7: ^{1}H NMR spectrum of $[(Cp^*Fe)_3As_6][TEF]$ (**[1][TEF]**) in CD_2Cl_2; * = solvent residual signal.*

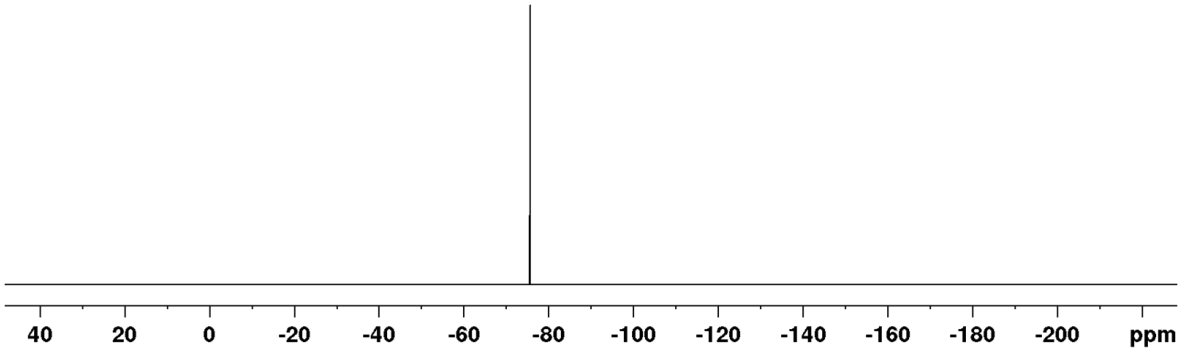

*Figure S 8: $^{19}F\{^{1}H\}$ NMR spectrum of $[(Cp^*Fe)_3As_6][TEF]$ (**[1][TEF]**) in CD_2Cl_2.*

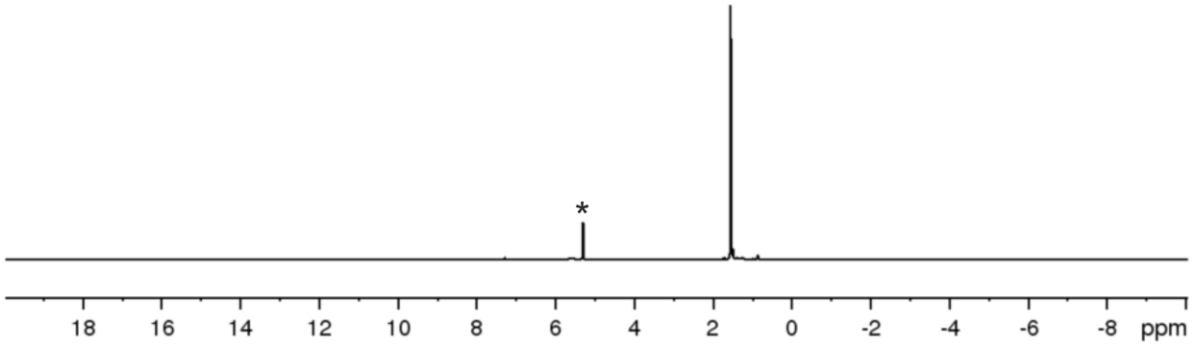

*Figure S 9: ^{1}H NMR spectrum of $[(Cp^*Fe)_3As_6][FAl]$ (**[1][FAl]**) in CD_2Cl_2; * = solvent residual signal.*

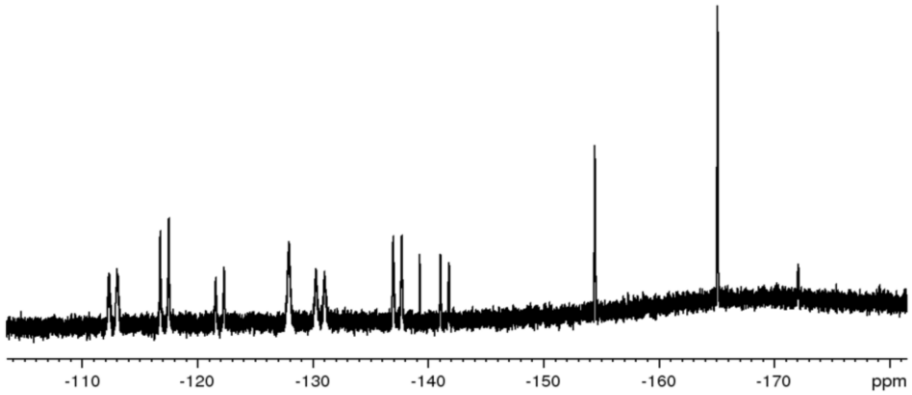

*Figure S 10: $^{19}F\{^{1}H\}$ NMR spectrum of $[(Cp^*Fe)_3As_6][FAl]$ (**[1][FAl]**) in CD_2Cl_2.*

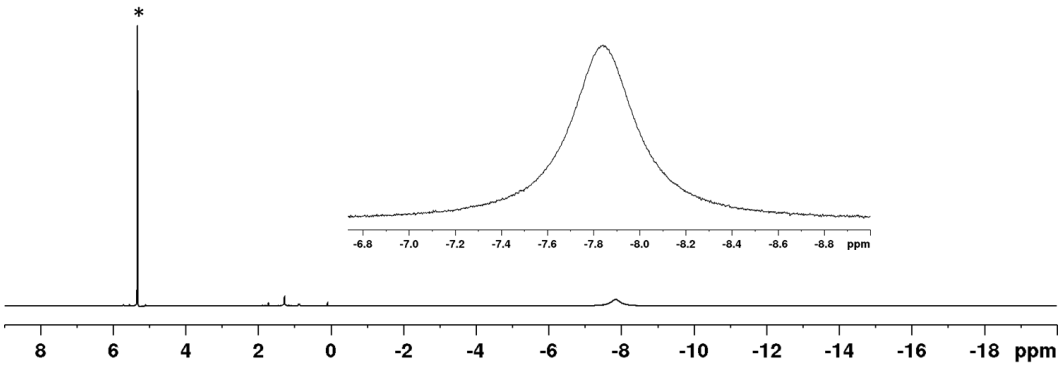

*Figure S 11: ^{1}H NMR spectrum of $[(Cp^*Fe)_3As_6][TEF]_2$ (**[2][TEF]$_2$**) in CD_2Cl_2; * = solvent residual signal.*

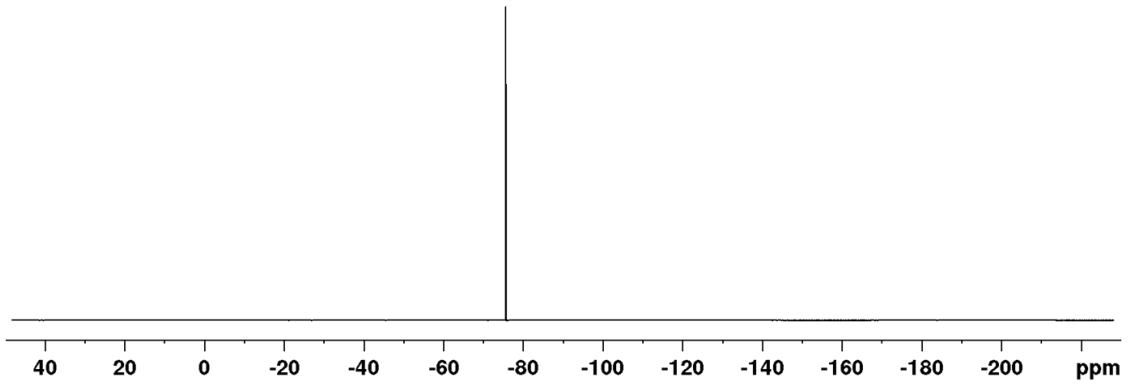

*Figure S 12: $^{19}F\{^{1}H\}$ NMR spectrum of $[(Cp^*Fe)_3As_6][TEF]_2$ (**[2][TEF]$_2$**) in CD_2Cl_2.*

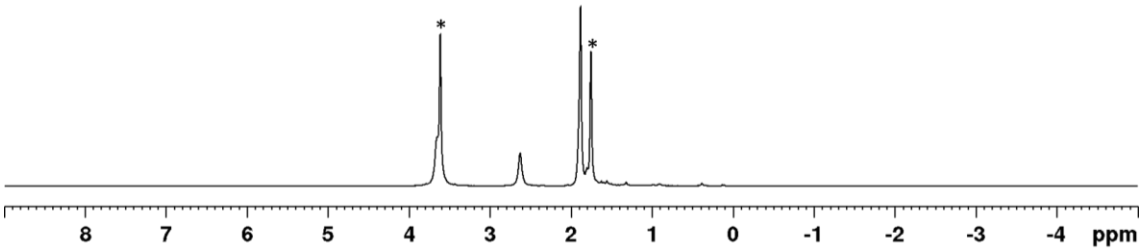

*Figure S 13: ^{1}H NMR spectrum of $[K@crypt][(Cp^*Fe)_3As_6]$ (**[K@crypt][3]**) in THF-d^8; * = solvent residual signal.*

10.5.4. Cyclovoltammetric Study of A

To get an initial idea of the redox properties of **A** we conducted cyclovoltammetric studies in solution. Thus, 50 mg of **A** were dissolved in 5 mL of CH_2Cl_2 and 750 mg of $[^nBu_4N][PF_6]$ were added. The cyclovoltammogram (Figure S14) was then recorded.

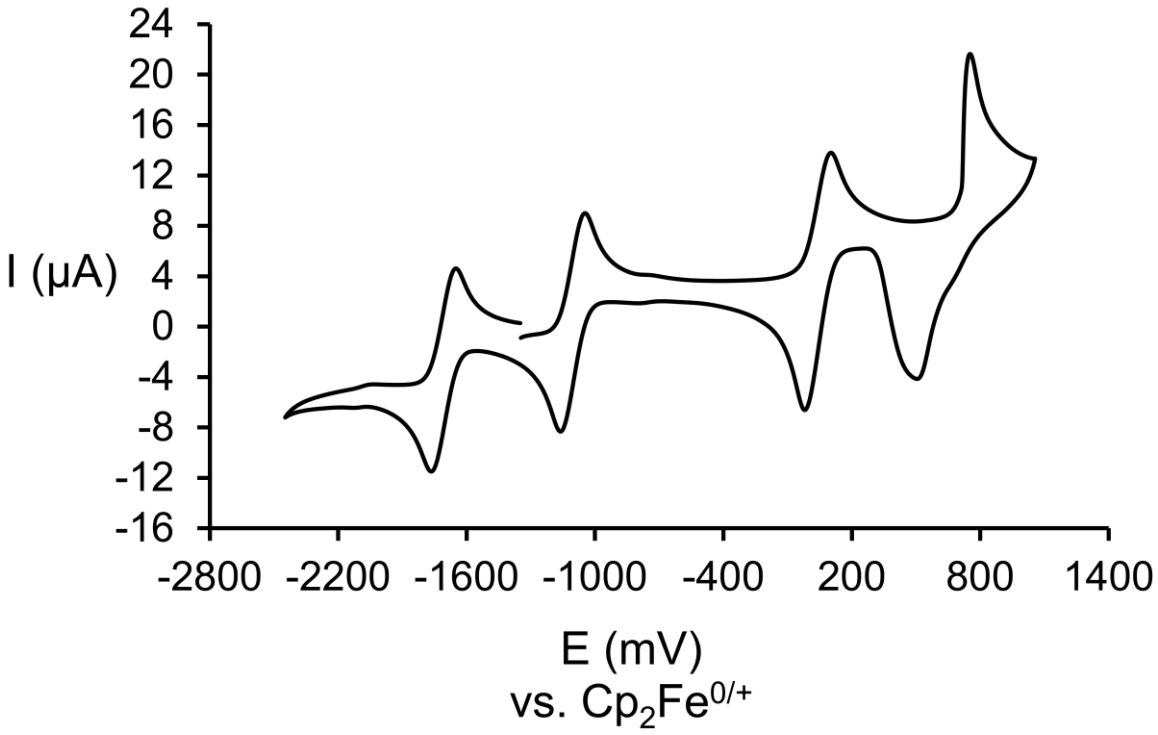

*Figure S 14: Cyclovoltammogram of **A** in CH_2Cl_2 recorded at room temperature.*

10.5.5. EPR Studies

As **A** itself is already paramagnetic, we subjected a sample of it in CH_2Cl_2 to EPR studies. While we could not observe a signal at room temperature, the frozen solution at 77 K reveals a rhombic signal (Figure S15) with $g_1 = 2.20$, $g_2 = 2.13$and $g_3 = 2.04$ and additional hyperfine coupling to the arsenic nuclei, which however is not resolved.

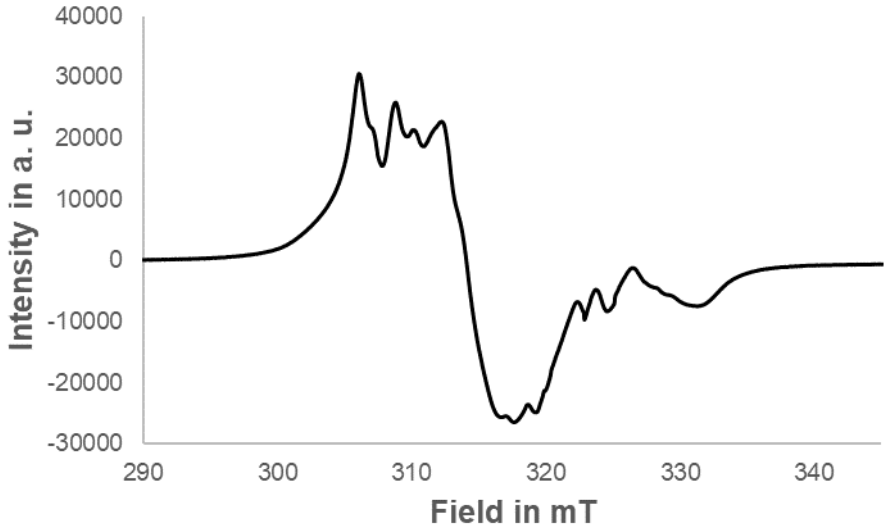

*Figure S 15: X-band EPR spectrum of **A** in frozen CH_2Cl_2 solution at 77 K.*

While **2[TEF]$_2$** bearing the paramagnetic $[(Cp^*Fe)_3As_6]^{2+}$ dication already shows an EPR signal in CH_2Cl_2 at room temperature, we also studied its X-band EPR spectrum at 77 K in frozen solution. Again, a rhombic signal (Figure S16, $g_1 = 2.42$, $g_2 = 2.00$, $g_3 = 1.96$) with additional hyperfine coupling to As nuclei is observed which could not be resolved.

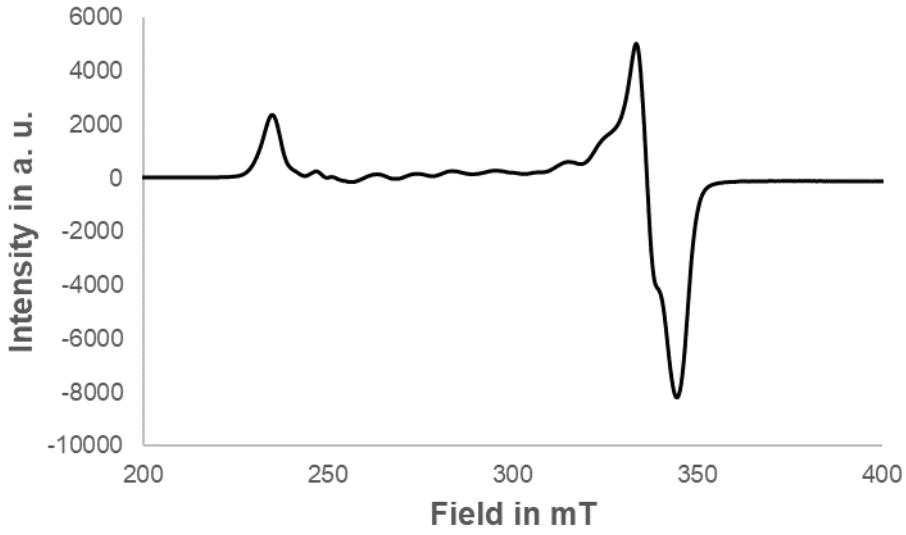

*Figure S 16: X-band EPR spectrum of **2[TEF]$_2$** in frozen CH_2Cl_2 solution at 77 K.*

While we were not able to realize the second reduction of **A** on a synthetic scale, EPR spectroscopic investigations (Figure S17) on reaction solutions of **A** and two equivalents of KC_8 reveal a weak rhombic signal with $g_1 = 2.07$, $g_2 = 2.03$ and $g_3 = 1.93$ in agreement with the presence of the doubly reduced $[\{Cp^*Fe\}_3As_6]^{2-}$.

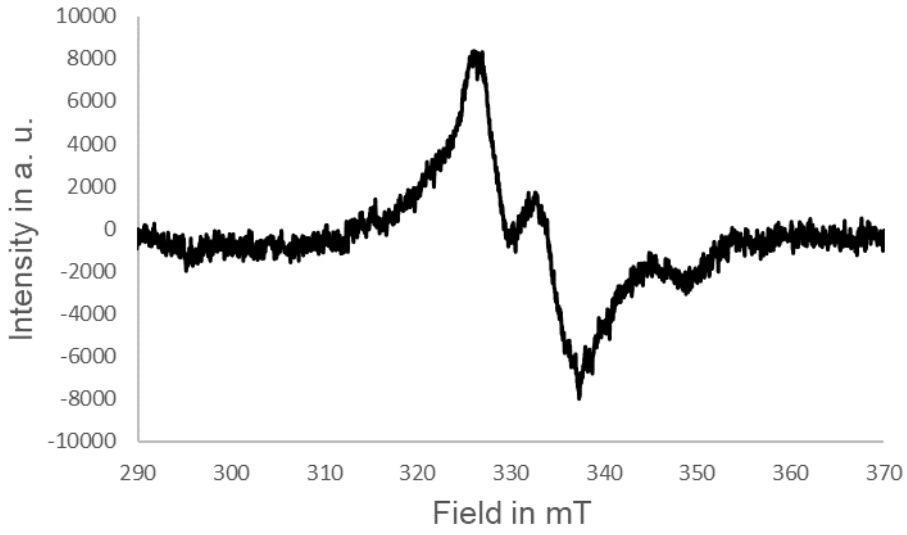

*Figure S 17: X-band EPR spectrum of a filtered mixture of **A** with two equivalents of KC_8 in frozen DME solution at 77 K.*

10.5.6. Computational Details

DFT calculations were performed using the Gaussian09 software package.[27] Geometry optimizations, frequency computations and population analyses were performed at the B3LYP[15]/def2-svp[16] level of theory. The NBO7[17] software package was used for population analyses and determination of Wiberg bond indices (WBI). The optimized structures are provided in the following.

*Table S 2: Wiberg Bond Indices for the Fe_3As_6 core structural motif in **A** and **1** – **3** obtained at the B3LYP/def2svp level of theory.*

	[3]$^-$	**A**	**[1]$^+$**	**[2]$^{2+}$ (doublet)**	**[2]$^{2+}$ (quartet)**
As1-As2	0.283	0.095	0.078	0.080	0.095
As3-As5	0.338	0.495	0.523	0.545	0.621
As4-As6	0.338	0.495	0.523	0.545	0.621
As1-As5	0.685	0.731	0.713	0.694	0.773
As1-As6	0.685	0.731	0.713	0.694	0.773
As5-As6	0.639	0.592	0.695	0.707	0.463
As2-As3	0.675	0.733	0.713	0.693	0.767
As2-As4	0.675	0.733	0.713	0.693	0.767
As3-As4	0.656	0.593	0.693	0.715	0.481
Fe1-As1	0.475	0.487	0.510	0.516	0.408
Fe1-As2	0.483	0.487	0.510	0.516	0.411
Fe1-As4	0.478	0.405	0.374	0.373	0.353
Fe1-As6	0.481	0.406	0.373	0.371	0.352
Fe2-As1	0.475	0.487	0.510	0.516	0.408
Fe2-As2	0.483	0.487	0.510	0.516	0.411
Fe2-As3	0.481	0.405	0.374	0.373	0.353
Fe2-As5	0.478	0.406	0.394	0.371	0.352
Fe3-As3	0.477	0.436	0.396	0.337	0.382
Fe3-As4	0.473	0.436	0.394	0.344	0.382
Fe3-As5	0.473	0.434	0.396	0.337	0.394
Fe3-As6	0.477	0.434	0.394	0.344	0.394
Fe1-Fe2	0.089	0.100	0.207	0.219	0.042

Optimized Geometries

[A]

B3LYP/def2SVP (doublet ground state): Energies/H = -18373.623680, Enthalpies/H = -18373.622735, Free Energies/H = -18373.768901, ZPVE/ kJ/mol = 1766.450

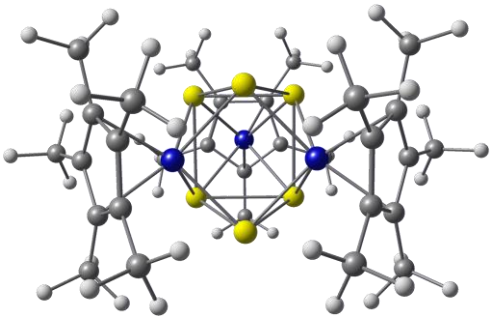

Symbol	X	Y	Z
As	-0.841105000	-1.319840000	-1.369219000
As	-0.851189000	-1.322243000	1.365459000
As	-0.841105000	1.319841000	-1.369219000
As	1.281072000	0.000000000	-1.738331000
As	-0.851188000	1.322244000	1.365458000
As	1.268436000	0.000000000	1.744280000
Fe	1.220664000	1.697878000	0.002875000
Fe	-2.349459000	0.000000000	-0.006512000
Fe	1.220664000	-1.697879000	0.002875000
C	1.179726000	-3.855532000	0.009192000
C	1.874024000	-3.375404000	-1.150933000
C	1.874664000	-3.368693000	1.166083000
C	3.015565000	-2.618763000	-0.710574000
C	-4.058808000	1.162370000	-0.390034000
C	3.015884000	-2.614501000	0.720801000
C	1.556162000	-3.722740000	-2.575859000
H	0.484126000	-3.918136000	-2.720520000
H	2.105396000	-4.629433000	-2.887026000
H	1.835169000	-2.912739000	-3.265588000
C	0.013674000	-4.801388000	0.012570000
H	-0.621455000	-4.665182000	0.899971000
H	0.361970000	-5.850316000	0.015818000
H	-0.622719000	-4.670752000	-0.874688000
C	1.557081000	-3.707987000	2.593003000
H	1.844892000	-2.897961000	3.279012000
H	2.098959000	-4.618406000	2.906169000
H	0.483648000	-3.893235000	2.740965000
C	-4.098049000	0.716020000	0.974965000
C	4.109282000	-2.091470000	-1.593052000
H	3.732142000	-1.779473000	-2.577421000
H	4.877192000	-2.867725000	-1.763025000
H	4.615105000	-1.224375000	-1.144203000
C	4.109974000	-2.081924000	1.599583000
H	4.617299000	-1.219288000	1.144008000
H	4.876613000	-2.857960000	1.776122000
H	3.732861000	-1.761502000	2.581273000
C	-4.175362000	2.586171000	-0.852368000
H	-3.729231000	3.288757000	-0.132805000
H	-5.235609000	2.872508000	-0.975457000
H	-3.678006000	2.745293000	-1.820232000
C	-4.248257000	1.588009000	2.187164000
H	-5.315535000	1.719176000	2.441908000
H	-3.822028000	2.589344000	2.030555000
H	-3.750221000	1.156910000	3.068217000
H	-3.624841000	0.885702000	-3.169683000
C	1.179728000	3.855531000	0.009198000
C	1.874020000	3.375407000	-1.150932000
C	1.874670000	3.368688000	1.166085000
C	3.015563000	2.618763000	-0.710580000
C	-4.058811000	-1.162362000	-0.390055000

C	3.015888000	2.614497000	0.720796000
C	-4.038442000	0.000012000	-1.236921000
C	1.556153000	3.722746000	-2.575855000
H	0.484118000	3.918149000	-2.720510000
H	2.105390000	4.629437000	-2.887024000
H	1.835152000	2.912745000	-3.265587000
C	0.013677000	4.801388000	0.012584000
H	-0.621450000	4.665177000	0.899986000
H	0.361973000	5.850316000	0.015838000
H	-0.622719000	4.670758000	-0.874673000
C	1.557093000	3.707979000	2.593006000
H	1.844912000	2.897952000	3.279013000
H	2.098968000	4.618399000	2.906172000
H	0.483660000	3.893221000	2.740975000
C	-4.098051000	-0.716036000	0.974953000
C	4.109276000	2.091473000	-1.593063000
H	3.732132000	1.779483000	-2.577434000
H	4.877188000	2.867726000	-1.763033000
H	4.615097000	1.224373000	-1.144221000
C	4.109981000	2.081916000	1.599571000
H	4.617302000	1.219280000	1.143990000
H	4.876622000	2.857950000	1.776109000
H	3.732872000	1.761491000	2.581262000
C	-4.112608000	0.000024000	-2.736516000
H	-5.162854000	0.000029000	-3.079949000
C	-4.175369000	-2.586153000	-0.852415000
H	-3.729253000	-3.288755000	-0.132858000
H	-5.235616000	-2.872481000	-0.975524000
H	-3.678000000	-2.745263000	-1.820275000
C	-4.248260000	-1.588045000	2.187136000
H	-5.315538000	-1.719217000	2.441877000
H	-3.822032000	-2.589379000	2.030510000
H	-3.750224000	-1.156962000	3.068196000
H	-3.624834000	-0.885664000	-3.169706000

[1]$^{+}$

B3LYP/def2SVP: Energies/H = -18373.438305, Enthalpies/H = -18373.437361, Free Energies/H = -18373.581314, ZPVE/ kJ/mol = 1773.109

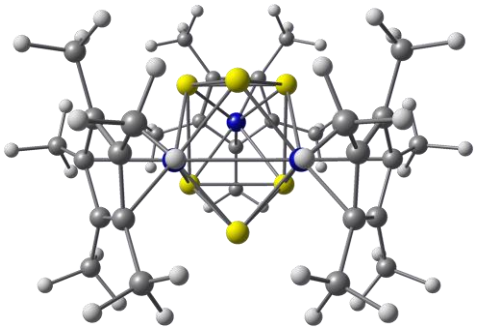

Symbol	X	Y	Z
As	-0.884006000	-1.293572000	-1.375619000
As	-0.893987000	-1.295597000	1.370497000
As	-0.884006000	1.293572000	-1.375619000
As	1.222805000	0.000000000	-1.857561000
As	-0.893987000	1.295597000	1.370497000
As	1.210017000	0.000000000	1.862534000
Fe	1.285147000	1.483954000	0.002792000
Fe	-2.410397000	0.000000000	-0.007221000
Fe	1.285147000	-1.483954000	0.002793000
C	1.242854000	-3.616400000	0.006114000
C	1.953627000	-3.160239000	-1.153739000
C	1.950874000	-3.156678000	1.166283000
C	3.093272000	-2.407012000	-0.709961000
C	-4.115903000	1.161334000	-0.387781000
C	3.091556000	-2.404850000	0.722961000
C	1.652509000	-3.545486000	-2.571061000
H	0.572667000	-3.635210000	-2.757910000
H	2.106433000	-4.526451000	-2.795486000
H	2.057047000	-2.822410000	-3.292883000
C	0.078960000	-4.563826000	0.006429000
H	-0.555294000	-4.441067000	0.896198000
H	0.441951000	-5.606510000	0.007765000
H	-0.555026000	-4.442994000	-0.883752000
C	1.646352000	-3.538041000	2.583940000
H	2.055393000	-2.816717000	3.304936000
H	2.093512000	-4.521750000	2.809894000
H	0.565811000	-3.620247000	2.770423000
C	-4.151414000	0.715549000	0.979394000
C	4.200201000	-1.912209000	-1.592510000
H	3.831813000	-1.525680000	-2.553547000
H	4.894647000	-2.739788000	-1.819280000
H	4.787133000	-1.118765000	-1.111952000
C	4.196283000	-1.907387000	1.606727000
H	4.786750000	-1.118145000	1.123666000
H	4.887986000	-2.735194000	1.840908000
H	3.825219000	-1.514417000	2.564123000
C	-4.236895000	2.584538000	-0.848069000
H	-3.781068000	3.289630000	-0.137996000
H	-5.300921000	2.862802000	-0.945326000
H	-3.768218000	2.743507000	-1.829596000
C	-4.302826000	1.589312000	2.189402000
H	-5.372382000	1.717988000	2.431315000
H	-3.881079000	2.592194000	2.033754000
H	-3.818016000	1.157219000	3.076854000
H	-3.716468000	0.887598000	-3.176204000
C	1.242854000	3.616400000	0.006121000
C	1.953622000	3.160243000	-1.153737000
C	1.950879000	3.156674000	1.166285000
C	3.093268000	2.407015000	-0.709967000
C	-4.115904000	-1.161327000	-0.387800000
C	3.091559000	2.404847000	0.722955000
C	-4.100967000	0.000010000	-1.235617000
C	1.652496000	3.545494000	-2.571056000

H	0.572654000	3.635223000	-2.757899000
H	2.106423000	4.526458000	-2.795481000
H	2.057028000	2.822418000	-3.292882000
C	0.078960000	4.563826000	0.006444000
H	-0.555289000	4.441066000	0.896217000
H	0.441951000	5.606510000	0.007780000
H	-0.555032000	4.442995000	-0.883732000
C	1.646364000	3.538033000	2.583945000
H	2.055411000	2.816708000	3.304937000
H	2.093522000	4.521743000	2.809899000
H	0.565823000	3.620235000	2.770434000
C	-4.151415000	-0.715565000	0.979382000
C	4.200194000	1.912215000	-1.592522000
H	3.831802000	1.525695000	-2.553561000
H	4.894642000	2.739793000	-1.819287000
H	4.787124000	1.118764000	-1.111973000
C	4.196290000	1.907381000	1.606714000
H	4.786756000	1.118142000	1.123646000
H	4.887993000	2.735187000	1.840897000
H	3.825230000	1.514405000	2.564110000
C	-4.191445000	0.000022000	-2.733859000
H	-5.247529000	0.000026000	-3.055150000
C	-4.236899000	-2.584524000	-0.848113000
H	-3.781083000	-3.289629000	-0.138047000
H	-5.300925000	-2.862780000	-0.945386000
H	-3.768213000	-2.743479000	-1.829638000
C	-4.302828000	-1.589348000	2.189375000
H	-5.372384000	-1.718028000	2.431286000
H	-3.881080000	-2.592227000	2.033711000
H	-3.818019000	-1.157269000	3.076834000
H	-3.716463000	-0.887557000	-3.176223000

[2]$^{2+}$

B3LYP/def2SVP (quartet ground state): Energies/H = -18373.156681, Enthalpies/H = -18373.155737, Free Energies/H = -18373.301525, ZPVE/ kJ/mol = 1769.063

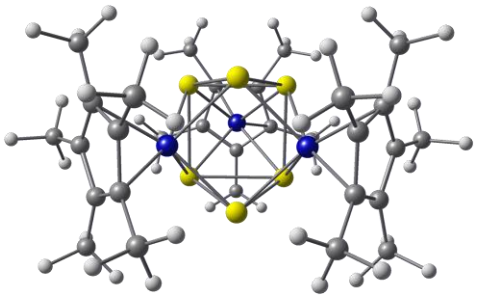

Symbol	X	Y	Z
As	-0.841654000	-1.375077000	-1.334794000
As	-0.837724000	-1.384523000	1.344062000
As	-0.841655000	1.375078000	-1.334793000
As	1.244446000	0.000000000	-1.746899000
As	-0.837725000	1.384524000	1.344061000
As	1.242183000	0.000001000	1.745440000
Fe	1.230591000	1.783524000	-0.002315000
Fe	-2.383554000	-0.000002000	0.018924000
Fe	1.230593000	-1.783524000	-0.002315000
C	1.275288000	-3.998382000	0.001029000
C	1.936626000	-3.481175000	-1.163209000
C	1.942289000	-3.478328000	1.160720000
C	3.041708000	-2.666216000	-0.724974000
C	-4.172578000	1.163363000	-0.387069000
C	3.044949000	-2.664173000	0.715076000
C	1.634648000	-3.848758000	-2.583307000
H	0.578570000	-4.113383000	-2.730244000
H	2.234784000	-4.729115000	-2.872826000
H	1.885832000	-3.040643000	-3.284545000
C	0.158786000	-4.996427000	0.004632000
H	-0.472106000	-4.914112000	0.900170000
H	0.583247000	-6.016007000	0.000527000
H	-0.481255000	-4.910687000	-0.884090000
C	1.647418000	-3.841996000	2.583291000
H	1.899408000	-3.030842000	3.280745000
H	2.251246000	-4.719708000	2.873140000
H	0.592708000	-4.108846000	2.735757000
C	-4.153712000	0.721275000	0.982328000
C	4.121285000	-2.116719000	-1.607744000
H	3.749022000	-1.838941000	-2.603443000
H	4.900614000	-2.884817000	-1.754894000
H	4.612873000	-1.239370000	-1.165815000
C	4.128149000	-2.111620000	1.591416000
H	4.616187000	-1.234271000	1.145622000
H	4.909383000	-2.878282000	1.735919000
H	3.760369000	-1.832686000	2.588447000
C	-4.309175000	2.581509000	-0.850740000
H	-3.866714000	3.295330000	-0.142019000
H	-5.378964000	2.838730000	-0.942100000
H	-3.853639000	2.744129000	-1.837623000
C	-4.308929000	1.592709000	2.191954000
H	-5.381291000	1.706445000	2.428543000
H	-3.903020000	2.601717000	2.036319000
H	-3.824994000	1.163315000	3.080286000
H	-3.836521000	0.890694000	-3.174861000
C	1.275285000	3.998382000	0.001030000
C	1.936623000	3.481176000	-1.163209000
C	1.942288000	3.478328000	1.160720000
C	3.041705000	2.666217000	-0.724976000
C	-4.172575000	-1.163358000	-0.387091000
C	3.044949000	2.664174000	0.715074000
C	-4.184303000	0.000010000	-1.228885000
C	1.634644000	3.848760000	-2.583307000

H	0.578566000	4.113385000	-2.730243000
H	2.234780000	4.729117000	-2.872826000
H	1.885828000	3.040646000	-3.284545000
C	0.158782000	4.996426000	0.004636000
H	-0.472114000	4.914101000	0.900170000
H	0.583243000	6.016007000	0.000542000
H	-0.481253000	4.910693000	-0.884091000
C	1.647419000	3.841995000	2.583292000
H	1.899410000	3.030841000	3.280745000
H	2.251247000	4.719708000	2.873139000
H	0.592709000	4.108845000	2.735758000
C	-4.153711000	-0.721295000	0.982315000
C	4.121282000	2.116723000	-1.607748000
H	3.749014000	1.838930000	-2.603442000
H	4.900602000	2.884827000	-1.754913000
H	4.612883000	1.239384000	-1.165814000
C	4.128150000	2.111620000	1.591413000
H	4.616186000	1.234271000	1.145619000
H	4.909384000	2.878282000	1.735913000
H	3.760371000	1.832688000	2.588445000
C	-4.294174000	0.000023000	-2.722562000
H	-5.359701000	0.000026000	-3.012344000
C	-4.309173000	-2.581494000	-0.850790000
H	-3.866738000	-3.295332000	-0.142070000
H	-5.378961000	-2.838704000	-0.942185000
H	-3.853611000	-2.744102000	-1.837663000
C	-4.308928000	-1.592751000	2.191925000
H	-5.381290000	-1.706494000	2.428510000
H	-3.903016000	-2.601755000	2.036273000
H	-3.824995000	-1.163372000	3.080265000
H	-3.836513000	-0.890654000	-3.174883000

[2]$^{2+}$

B3LYP/def2SVP (doublet ground state): Energies/H = -18373.145030, Enthalpies/H = -18373.144086, Free Energies/H = -18373.279055, ZPVE/ kJ/mol = 1771.863

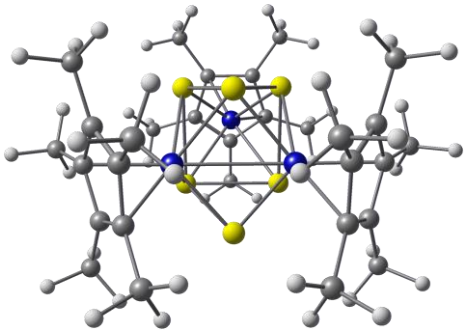

Symbol	X	Y	Z
As	-0.851903000	-1.299877000	-1.370948000
As	-0.845670000	-1.303712000	1.383781000
As	-0.851907000	1.299872000	-1.370951000
As	1.264459000	0.000001000	-1.851932000
As	-0.845673000	1.303707000	1.383785000
As	1.272463000	0.000001000	1.845883000
Fe	1.285602000	1.481847000	-0.002454000
Fe	-2.454814000	-0.000003000	0.017036000
Fe	1.285609000	-1.481843000	-0.002454000
C	1.242603000	-3.626491000	0.000635000
C	1.948175000	-3.170573000	-1.163413000
C	1.957216000	-3.167922000	1.158164000
C	3.089779000	-2.414460000	-0.725133000
C	-4.242518000	1.161371000	-0.385716000
C	3.095345000	-2.412883000	0.709359000
C	1.650092000	-3.565284000	-2.577770000
H	0.575533000	-3.711370000	-2.757176000
H	2.147436000	-4.525588000	-2.799476000
H	2.020686000	-2.831350000	-3.306638000
C	0.085109000	-4.580620000	0.006123000
H	-0.543692000	-4.471174000	0.901272000
H	0.462325000	-5.617982000	0.003884000
H	-0.553093000	-4.470497000	-0.882248000
C	1.670517000	-3.559422000	2.575748000
H	2.046086000	-2.823348000	3.299904000
H	2.170623000	-4.518662000	2.795857000
H	0.597572000	-3.706129000	2.764044000
C	-4.219528000	0.719270000	0.987906000
C	4.199157000	-1.931176000	-1.609584000
H	3.842030000	-1.584229000	-2.589566000
H	4.901244000	-2.761526000	-1.799408000
H	4.776728000	-1.121088000	-1.146374000
C	4.211316000	-1.927606000	1.584331000
H	4.787367000	-1.120804000	1.113617000
H	4.913052000	-2.758407000	1.773475000
H	3.861209000	-1.575506000	2.565024000
C	-4.375075000	2.579788000	-0.846972000
H	-3.922205000	3.291172000	-0.142860000
H	-5.445450000	2.839863000	-0.925698000
H	-3.930723000	2.739827000	-1.839050000
C	-4.359667000	1.593381000	2.196656000
H	-5.429245000	1.709284000	2.444920000
H	-3.953563000	2.600986000	2.033899000
H	-3.867274000	1.164340000	3.080590000
H	-3.911055000	0.890868000	-3.172840000
C	1.242587000	3.626494000	0.000639000
C	1.948157000	3.170582000	-1.163412000
C	1.957206000	3.167925000	1.158165000
C	3.089766000	2.414473000	-0.725138000
C	-4.242513000	-1.161373000	-0.385739000
C	3.095336000	2.412893000	0.709354000
C	-4.262005000	0.000007000	-1.228428000
C	1.650069000	3.565295000	-2.577767000

H	0.575508000	3.711378000	-2.757169000
H	2.147410000	4.525600000	-2.799474000
H	2.020661000	2.831362000	-3.306638000
C	0.085089000	4.580619000	0.006134000
H	-0.543714000	4.471161000	0.901280000
H	0.462302000	5.617983000	0.003909000
H	-0.553109000	4.470504000	-0.882241000
C	1.670511000	3.559422000	2.575751000
H	2.046085000	2.823349000	3.299904000
H	2.170612000	4.518664000	2.795859000
H	0.597565000	3.706124000	2.764050000
C	-4.219525000	-0.719299000	0.987892000
C	4.199142000	1.931195000	-1.609593000
H	3.842015000	1.584255000	-2.589577000
H	4.901230000	2.761546000	-1.799412000
H	4.776714000	1.121104000	-1.146389000
C	4.211313000	1.927618000	1.584322000
H	4.787367000	1.120821000	1.113603000
H	4.913045000	2.758422000	1.773466000
H	3.861210000	1.575513000	2.565015000
C	-4.369797000	0.000021000	-2.721787000
H	-5.434443000	0.000023000	-3.014709000
C	-4.375068000	-2.579780000	-0.847025000
H	-3.922221000	-3.291181000	-0.142915000
H	-5.445443000	-2.839847000	-0.925784000
H	-3.930691000	-2.739804000	-1.839095000
C	-4.359662000	-1.593433000	2.196626000
H	-5.429240000	-1.709346000	2.444886000
H	-3.953553000	-2.601033000	2.033850000
H	-3.867272000	-1.164407000	3.080568000
H	-3.911053000	-0.890817000	-3.172856000

[3]$^{-}$

B3LYP/def2SVP: Energies/H = -18373.685536, Enthalpies/H = -18373.684592, Free Energies/H = -18373.831185, ZPVE/ kJ/mol = 1761.759

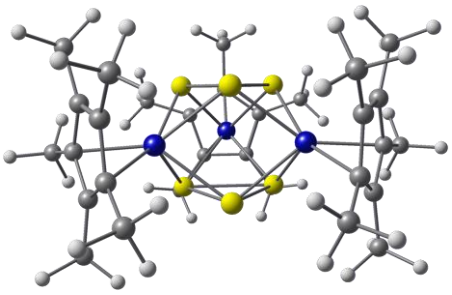

Symbol	X	Y	Z
As	0.747003000	-1.295302000	1.432136000
As	0.760223000	-1.291789000	-1.432981000
As	0.746987000	1.295312000	1.432134000
As	-1.467853000	-0.000009000	1.474679000
As	0.760207000	1.291798000	-1.432981000
As	-1.460859000	-0.000009000	-1.472705000
Fe	-1.123909000	1.926134000	-0.005816000
Fe	2.250714000	0.000013000	0.011176000
Fe	-1.123885000	-1.926147000	-0.005815000
C	-0.940183000	-3.999946000	-0.147178000
C	-1.576860000	-3.672082000	1.101113000
C	-1.779489000	-3.511235000	-1.210185000
C	-2.796697000	-2.978262000	0.808910000
C	3.957680000	1.163690000	0.401982000
C	-2.922790000	-2.875751000	-0.615927000
C	-1.122455000	-4.082179000	2.471967000
H	-0.043149000	-4.289792000	2.498938000
H	-1.647978000	-4.995089000	2.811704000
H	-1.312121000	-3.293028000	3.215775000
C	0.296393000	-4.836590000	-0.313090000
H	0.844793000	-4.570424000	-1.229213000
H	0.051639000	-5.914553000	-0.374275000
H	0.990835000	-4.704594000	0.530333000
C	-1.568315000	-3.720224000	-2.682002000
H	-1.901223000	-2.847960000	-3.265474000
H	-2.128041000	-4.601723000	-3.048616000
H	-0.506485000	-3.875689000	-2.921713000
C	4.008537000	0.715933000	-0.962314000
C	-3.824372000	-2.561545000	1.820750000
H	-3.360307000	-2.223947000	2.759331000
H	-4.504290000	-3.400277000	2.065084000
H	-4.445274000	-1.730361000	1.454265000
C	-4.112149000	-2.340186000	-1.359722000
H	-4.627737000	-1.551778000	-0.790496000
H	-4.851576000	-3.139496000	-1.559676000
H	-3.824596000	-1.903144000	-2.327320000
C	4.070212000	2.587847000	0.865738000
H	3.630285000	3.287679000	0.139018000
H	5.127571000	2.882901000	1.009122000
H	3.549995000	2.745289000	1.822298000
C	4.164737000	1.582335000	-2.178150000
H	5.228882000	1.672302000	-2.469252000
H	3.780802000	2.598845000	-2.008138000
H	3.616540000	1.176289000	-3.041774000
H	3.482086000	0.883294000	3.169848000
C	-0.940235000	3.999934000	-0.147194000
C	-1.576896000	3.672071000	1.101105000
C	-1.779544000	3.511204000	-1.210190000
C	-2.796726000	2.978233000	0.808920000
C	3.957696000	-1.163637000	0.401998000
C	-2.922832000	2.875709000	-0.615915000
C	3.934083000	0.000032000	1.248113000
C	-1.122482000	4.082185000	2.471951000

H	-0.043179000	4.289811000	2.498911000
H	-1.648013000	4.995092000	2.811686000
H	-1.312133000	3.293037000	3.215768000
C	0.296328000	4.836594000	-0.313124000
H	0.844724000	4.570427000	-1.229250000
H	0.051560000	5.914553000	-0.374316000
H	0.990780000	4.704613000	0.530293000
C	-1.568388000	3.720185000	-2.682010000
H	-1.901291000	2.847913000	-3.265472000
H	-2.128126000	4.601676000	-3.048624000
H	-0.506561000	3.875660000	-2.921732000
C	4.008547000	-0.715898000	-0.962304000
C	-3.824386000	2.561510000	1.820773000
H	-3.360307000	2.223922000	2.759351000
H	-4.504310000	3.400236000	2.065109000
H	-4.445282000	1.730317000	1.454300000
C	-4.112191000	2.340124000	-1.359694000
H	-4.627762000	1.551712000	-0.790458000
H	-4.851632000	3.139423000	-1.559646000
H	-3.824643000	1.903080000	-2.327293000
C	3.985490000	0.000044000	2.748738000
H	5.028561000	0.000077000	3.118547000
C	4.070248000	-2.587786000	0.865772000
H	3.630327000	-3.287632000	0.139063000
H	5.127611000	-2.882826000	1.009156000
H	3.550035000	-2.745222000	1.822336000
C	4.164759000	-1.582315000	-2.178128000
H	5.228906000	-1.672276000	-2.469225000
H	3.780833000	-2.598826000	-2.008103000
H	3.616562000	-1.176285000	-3.041759000
H	3.482136000	-0.883228000	3.169861000

10.6. References

[1] a) O. J. Scherer, Angew*. Chem. Int. Ed. Engl.* **1985**, *24*, 924–943; b) O. J. Scherer, *Acc. Chem. Res.* **1999**, *32*, 751-762; c) M. Seidl, G. Balázs, M. Scheer, *Chem. Rev.* **2019**, *119*, 8406–8434.

[2] R. Hoffmann, *Angew. Chem. Int. Ed. Engl.* **1982**, *21*, 711–724.

[3] a) A. S. Foust, M. S. Foster, L. F. Dahl, *J. Am. Chem. Soc.* **1969**, *91*, 5633-5635; b) O. J. Scherer, H. Sitzmann, G. Wolmershäuser, *J. Organomet. Chem.* **1984**, *268*, C9–C12.

[4] a) A. S. Foust, M. S. Foster, L. F. Dahl, *J. Am. Chem. Soc.* **1969**, *91*, 5631-5633; b) O. J. Scherer, W. Wiedemann, G. Wolmershäuser, *Chem. Ber.* **1990**, *123*, 3-6.

[5] O. J. Scherer, J. Vondung, G. Wolmershäuser, *J. Organomet. Chem.* **1989**, *376*, C35-C38.

[6] a) A. L. Rheingold, M. J. Foley, P. J. Sullivan, *J. Am. Chem. Soc.* **1982**, *104*, 4727–4729; b) O. J. Scherer, C. Blath, G. Wolmershäuser, *J. Organomet. Chem.* **1990**, *387*, C21-C24.

[7] O. J. Scherer, H. Sitzmann, G. Wolmershäuser, *Angew. Chem. Int. Ed. Engl.* **1989**, *28*, 212–213.

[8] O. J. Scherer, R. Winter, G. Heckmann, G. Wolmershäuser*, Angew. Chem. Int. Ed. Engl.* **1991**, *30*, 850–852.

[9] H. Krauss, G. Balázs, M. Seidl, M. Scheer, *Mendeleev Commun.* **2022**, *32*, 42–45.

[10] a) O. J. Scherer, K. Pfeiffer, G. Heckmann, G. Wolmershäuser, *J. Organomet. Chem.* **1992**, *425*, 141–149; b) R. Ahlrichs, D. Fenske, K. Fromm, H. Krautscheid, U. Krautscheid, O. Treutler, *Chem. Eur. J.* **1996**, *2*, 238–244; c) G. Friedrich, O. J. Scherer, G. Wolmerrshäuser, *Z. Anorg. Allg. Chem.* **1996**, *622*, 1478–1486; d) C. v. Hänisch, D. Fenske, F. Weigend, R. Ahlrichs, *Chem. Eur. J.* **1997**, *3*, 1494–1498; e) C. v. Hänisch, D. Fenske, *Z. Anorg. Allg. Chem.* **1999**, *624*, 367–369.

[11] M. Detzel, K. Pfeiffer, O. J. Scherer, G. Wolmershäuser, *Angew. Chem. Int. Ed. Engl.* **1993**, *32*, 914–916.

[12] N. G. Connelly, W. E. Geiger, *Chem. Rev.* **1996**, *96*, 877–910.

[13] L. Dütsch, M. Fleischmann, S. Welsch, G. Balázs, W. Kremer, M. Scheer, *Angew. Chem. Int. Ed.* **2018**, *57*, 3256–3261.

[14] a) P. Pyykkö, M. Atsumi, *Chem. Eur. J.* **2008**, *15*, 186–197; b) P. Pyykkö, M. Atsumi, *Chem. Eur. J.* **2009**, *15*, 12770–12779; c) P. Pyykkö, *J. Phys. Chem. A* **2015**, *119*, 2326–2337.

[15] a) P. A. M. Dirac, *Proc. Roy. Soc. Lond. A* **1929**, *123*, 714–733; b) J. C. Slater, *Phys. Rev.* **1951**, *81*, 385–390; c) S. H. Vosko, L. Wilk, M. Nusair, *Can. J. Phys.* **1980**, *58*, 1200–1211; d) C. Lee, W. Yang, R. G. Parr, *Phys. Rev. B* **1988**, *37*, 785–789; e) A. D. Becke, *Phys. Rev. A* **1988**, *38*, 3098–3100; f) A. D. Becke, *J. Chem. Phys.* **1993**, *98*, 5648–5652.

[16] a) F. Weigend, R. Ahlrichs, *Phys. Chem. Chem. Phys.* **2005**, *7*, 3297–3305; b) F. Weigend, *Phys. Chem. Chem. Phys.* **2006**, *8*, 1057–1065.

[17] a) E. D. Glendening, C. R. Landis, F. Weinhold, *J. Comput. Chem.* **2013**, *34*, 1363–1374; b) E. D. Glendening, C. R. Landis, F. Weinhold, *J. Comput. Chem.* **2013**, *34*, 2134.

[18] Supplementary crystallographic information on compounds **A**, **[1][TEF]**, **[1][FAl]**, **[2][BAr^F]$_2$** and **[K@crypt][3]** is available from the Cambridge Crystallographic Data Center under the reference numbers 2157447-2157451.

[19] *https://omics.pnl.gov/software/molecular-weight-calculator*, (30.01.2022).

[20] D. Catheline, D. Astruc, *Organometallics* **1984**, *3*, 1094–1100.

[21] V. D. Makhaev, A. N. Galiullin, E. E. Faingol´d, N. M. Bravaya, L. A. Petrova, *Russ. Chem. Bull.* **2014**, *63*, 651–656.#

[22] J.-M. Lalancette, G. Rollin, P. Dumas, *Can. J. Chem.* **1972**, *50*, 3058–3062.

[23] Agilent Technologies Ltd, *CrysAlis PRO*, Yarnton, Oxfordshire, England, **2014**.

[24] G. M. Sheldrick, *Acta Cryst. A* **2015**, *71*, 3–8.

[25] O. V. Dolomanov, L. J. Bourhis, R. J. Gildea, J. A. K. Howard and H. Puschmann, *J. Appl. Crystallogr.*, **2009**, *42*, 339–341.

[26] a) G. M. Sheldrick, *Acta Cryst. A* **2008**, *64*, 112–122; b) G. M. Sheldrick, *Acta Cryst. C*, **2015**, *71*, 3–8.

[27] M. J. Frisch, G. W. Trucks, H. B. Schlegel, G. E. Scuseria, M. A. Robb, J. R. Cheeseman, G. Scalmani, V. Barone, B. Mennucci, G. A. Petersson, H. Nakatsuji, M. Caricato, X. Li, H. P. Hratchian, A. F. Izmaylov, J. Bloino, G. Zheng, J. L. Sonnenberg, M. Hada, M. Ehara, K. Toyota, R. Fukuda, J. Hasegawa, M. Ishida, T. Nakajima, Y. Honda, O. Kitao, H. Nakai, T. Vreven, J. A. Montgomery Jr., J. E. Peralta, F. Ogliaro, M. Bearpark, J. J. Heyd, E. Brothers, K. N. Kudin, V. N. Staroverov, T. Keith, R. Kobayashi, J. Normand, K. Raghavachari, A. Rendell, J. C. Burant, S. S. Iyengar, J. Tomasi, M. Cossi, N. Rega, J. M. Millam, M. Klene, J. E. Knox, J. B. Cross, V. Bakken, C. Adamo, J. Jaramillo, R. Gomperts, R. E. Stratmann, O. Yazyev, A. J. Austin, R. Cammi, C. Pomelli, J. W. Ochterski, R. L. Martin, K. Morokuma, V. G. Zakrzewski, G. A. Voth, P. Salvador, J. J. Dannenberg, S. Dapprich, A. D. Daniels, O. Farkas, J. B. Foresman, J. V. Ortiz, J. Cioslowski and D. J. Fox, “Gaussian 09”, Revision E.01, *Gaussian Inc.*, Wallingford CT, **2013**.

11. Functionalization of Pentaphosphole Complexes: Enhancing the reactivity of [Cp*Fe(η^5-P_5)] via Electrophilic Activation

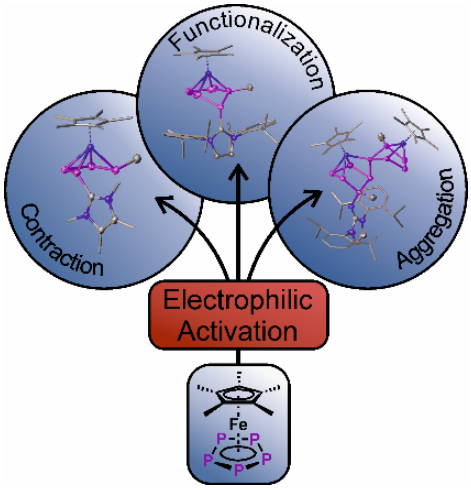

Preface

This chapter has not been published until the end of this thesis. It should give insight into the unprecedented reactivity of cationic pentaphosphole complexes towards carbenes and their analoga. While many of the described compounds are fully characterized, some of the results especially on the expanded compounds **7** and **8** are of preliminary nature, so far. Further characterization and additional synthetic as well as computational investigations are needed and should be a topic of future research. Some of the presented results have already been part of the BSc thesis of Philip Blank.

Authors

Christoph Riesinger, Philip M. Blank and Manfred Scheer

Author Contributions

Christoph Riesinger – Synthesis of compounds **1**, **4**, **6** ,**7** and **8**, Interpretation of crystallographic data, Interpretation of computational data, Writing of original draft.
Philip Blank – Synthesis of **2**, **3** and $\mathbf{4}_{INT2}$.
Manfred Scheer – Project administration, Funding acquisition, Co-writing final manuscript.

Acknowledgements

This work was supported by the Deutsche Forschungsgemeinschaft (DFG) within the project Sche 384/36-2. C. R. is grateful to the Studienstiftung des Deutschen Volkes for a PhD fellowship. P. M. B. is grateful to the Studienstiftung des Deutschen Volkes and the Max Weber-Programm for Bachelor and Master degree fellowships.

11.1. Abstract

*Electrophilic activation of the neutral cyclo-P_5 complex [Cp*Fe(η^5-P_5)] is demonstrated to drastically enhance its reactivity towards carbenes and their analoga. This is utilized within [Cp*Fe(η^5-P_5Me)][OTf] (**A**) to access unprecedented functionalized, shrunk, as well as complexly aggregated polyphosphorus compounds, highlighting the great potential of this almost unexplored mode of activation. Addition of carbenes to **A** affords the novel 1,2- or 1,1-difunctionalized cyclo-P_5 complexes [Cp*Fe(η^4-P_5(1-L)(2-Me)][OTf] (L = IDipp (**1**), ^{Et}CAAC (**2**), I^iPr (**3b**)) and [Cp*Fe(η^4-P_5(1-I^iPr)(1-Me)][OTf] (**3a**) based on the steric demand of the respective carbene. The even smaller IMe_4 for the first time gives rise to a complex with a contracted P_4 ligand [Cp*Fe(η^4-P_4(1-IMe)(4-Me)] (**4**) starting from cyclo-P_5. While DFT calculations shed light into the delicate mechanism of this reaction, additional invaluable insight could be gained by spectroscopic observation and even isolation of key intermediates ([Cp*Fe(η^4-P_5(1-IMe_4)(1-Me)][OTf] (**4$_{INT1}$**)). Furthermore, even the comparably weak nucleophile $IDippCH_2$ could be added on the cyclo-P_5 ligand in [Cp*Fe(η^4-P_5(1-$IDippCH_2$)(1/2-Me)][OTf] (**6a**/**b**), highlighting the explicitly more reactive nature of **A**. Lastly, **A** was found to react with IDippEH (E = N, P) in a complicated aggregation reaction affording [{Cp*Fe}$_2${μ_2,$\eta^{4:3:1}$-$P_{10}Me_2$(IDippN)}][OTf] (**7**) and [{Cp*Fe}$_2${μ_2,$\eta^{4:1:1:1}$-$P_{11}Me_2$(IDipp)}][OTf] (**8**), respectively. The unique substituted P_{10} and P_{11} ligands in these products are among the most complex polyphosphorus architectures known to date.*

11.2. Introduction

The functionalization and transformation of polyphosphorus compounds has been growing over the past decades and has been developed into a key area of fundamental chemical research. While this fundamental interest is based on the close relationship of phosphorus and carbon (diagonal relationship and isolobality of e. g., P and CH),[1] the field gained renewed attention in the context of the more sustainable conversion of P_4 to useful (organo)phosphorus compounds (e. g., phosphines).[2] Latest developments focus on the oxidative,[3] photocatalytic,[4] or main group mediated[5] conversion of the P_4 tetrahedron on the way to the desired phosphines. Transition metal mediated conversion of P_4 bears similarly high potential and additionally provides access to exotic polyphosphorus structural motifs.[2a–d,6] These often display highly reactive intermediates requiring the stabilization by the transition metal, as e. g., demonstrated by the recent side-on stabilization of P_2[7] or the trapping of its lighter homolog NP.[8] However, these species in turn give rise to more elaborate molecular polyphosphorus architectures, thus paving the way towards a structural prosperity, nearly comparable to organic (carbon based) chemistry.

From the early days of polyphosphorus chemistry on, great effort was put onto the nucleophilic and reductive functionalization of polyphosphorus species e. g., by the work of *Baudler et al*.[9] In contrast, the electrophilic[10] as well as oxidative[11] transformation of such compounds

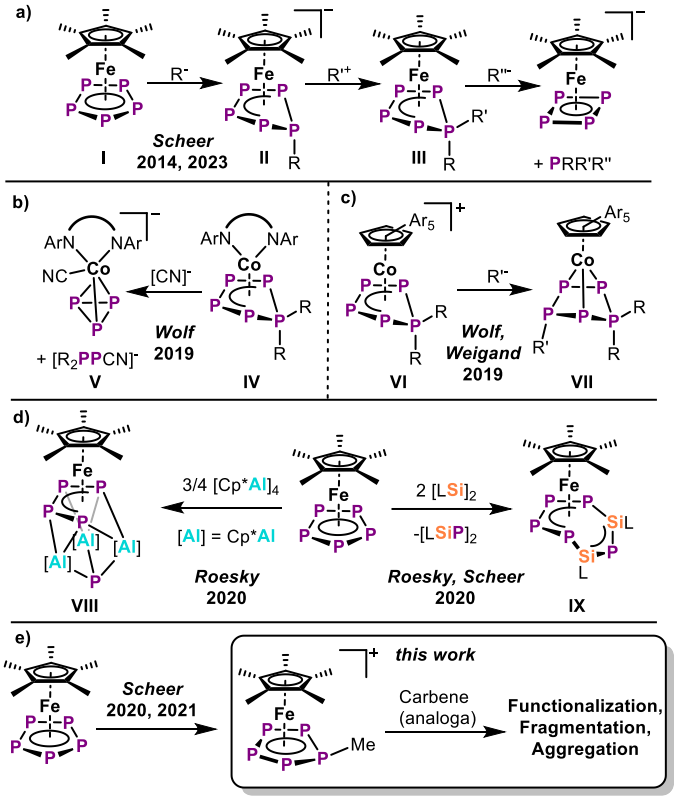

Scheme 1: Functionalization reactions of coordinated cyclo-P_5 ligands in selected complexes; a) R = alkyl/aryl, R' = alkyl, R'' = Bn; b) ArN^NAr = bis(2,6-diisopropylphenyl)phenanthrene-9,10-diimine, R = alkyl/aryl; c) R = alkyl, R'' = Cl, CN, Cy; d) L = PhC(N^{t}Bu)$_2$.

started to flourish only within the past two decades. Unsurprisingly, the reactivity of the resulting cationic polyphosphorus compounds is far less explored than for their anionic counterparts. Rare examples for such reactivity studies include the addition of cyclotriphosphines to (iso)nitriles,[12] the fragmentation of cage-type $[P_5RCl]^+$ cations by N-heterocyclic carbenes (NHCs)[13] or the utilization of cationic phosphinidene precursors to access phospha-olefins.[14]

This discrepancy is even more expressed for transition metal stabilized polyphosphorus compounds. The synthesis of anionic polyphosphorus complexes by means of nucleophilic functionalization[15] or reduction[16] is an established field, which also lead to numerous studies on the reactivity of these complexes.[17] In contrast, transition metal stabilized polyphosphorus cations became more available only from the early 2000s on,[18] with occasional studies having been reported before that.[19] Accordingly, this left the investigation of their reactivity comparably underexplored. Besides others, our group has undertaken significant effort to synthesize and characterize transition metal stabilized polyphosphorus cations ranging from P_2- up to P_{16}-complexes.[16f,16i,20] Thus, one of our key interests is to investigate the reactivity of these novel compounds and explore their utility in the preparation of complex functionalized polyphosphorus frameworks. For this purpose the class of *cyclo*-P_5 complexes is one of the most investigated classes of polyphosphorus ligand complexes to date, with the unsubstituted *cyclo*-P_5 ligand being found in organometallic sandwich compounds,[16d,21] purely inorganic

sandwich complexes,[22] and even triple- as well as quadruple-deckers.[23] Yet, studies on the nucleophilic functionalization of the fundamental [Cp*Fe(η^5-P_5)] (**I**, Scheme 1a)[21] revealed the robustness of the *cyclo*-P_5 ligand and primarily delivered complexes bearing functionalized *cyclo*-P_5R ligands (**II**)[15a] even when strong nucleophiles, such as NHCs were used.[15d] While further functionalization (**III**) and finally release of asymmetric phosphines could be achieved, this still requires extremely harsh nucleophiles (e. g. BnK).[17f] In contrast, the cobalt complex **IV** (Scheme 1b) already undergoes fragmentation with weak nucleophiles, such as $[CN]^-$, which may, however, partly be attributed to its beneficial ligand properties yielding the *cyclo*-P_3 complex **V**.[24] Furthermore, the *cyclo*-P_5R_2 ligand in **VI** (Scheme 1c) again demonstrates the robustness of this ligand class, by undergoing simple functionalization reactions (**VII**) even with strong nucleophiles.[25] Only when **I** is exposed to extremely reactive reagents, such as Al(I) species (**VIII**),[26] disilylenes (**IX**)[27] or iodine[28] under partly forcing conditions, direct transformation to more complex structural motifs could be observed (Scheme 1d). The recently reported functionalization of **I** with electrophiles from across the p-block (Scheme 1e)[20d,20f] was envisioned to greatly enhance the reactivity of the *cyclo*-P_5 ligand towards nucleophiles, such as ubiquitous carbenes and their analoga. The ligand system in **I** is chosen intentionally as its robustness usually prevents it to undergo complex rearrangement or fragmentation reactions under mild conditions (*vide supra*). Thus, demonstrating this concept on this challenging platform should allow for its simple transfer to a broad variety of polyphosphorus ligand complexes.

Within this study we demonstrate the drastic reactivity enhancement of **I** via its electrophilic activation. The observed reactivity ranges from novel functionalization patterns over the fragmentation of **I** to unprecedented aggregation reactions and should thus open a new and rational avenue towards complex polyphosphorus architectures.

11.3. Results and Discussion

To initially probe the reactivity enhancement of **I** by electrophilic activation, the methylated derivative [Cp*Fe(η^5-P_5Me)][OTf] (**A**) was chosen as a benchmark for its comparably high stability as well as its simple preparation (see SI).[21] Furthermore, stable singlet carbenes, such as NHCs or CAACs (Cyclic Alkyl Amino Carbenes) have been shown to only form labile adducts with **I**, which is attributed to the robustness of its *cyclo*-P_5 ligand.[15d] Thus, **A** was reacted with one equivalent of the sterically demanding NHC IDipp (IDipp=1,3-bis(2,6-diisopropyl-phenyl)imidazol-2-ylidene) as well as ^{Et}CAAC (^{Et}CAAC = (2,6-diisopropylphenyl)-4,4-diethyl-2,2-dimethyl-pyrrolidin-5-ylidene). Interestingly, both reactions proceed smoothly affording [Cp*Fe{η^4-P_5(1-L)(2-Me)}][OTf] (**1**: L = IDipp, **2**: L = ^{Et}CAAC) in good isolated yields of 98% and 63%, respectively (Figure 1). In both complexes, the carbene substituent is strongly bound to the *cyclo*-P_5 ligand without any signs of dynamic behaviour at room temperature, contrasting the reactivity towards **I**.[15d] Surprisingly, both products feature an η^4 bound 1,2-difunctionalized *cyclo*-P_5R_2 ligand instead of the expected and well established 1,1-regioisomer. Notably, synthetic access to 1,2-disubstituted *cyclo*-P_5 ligands is extremely

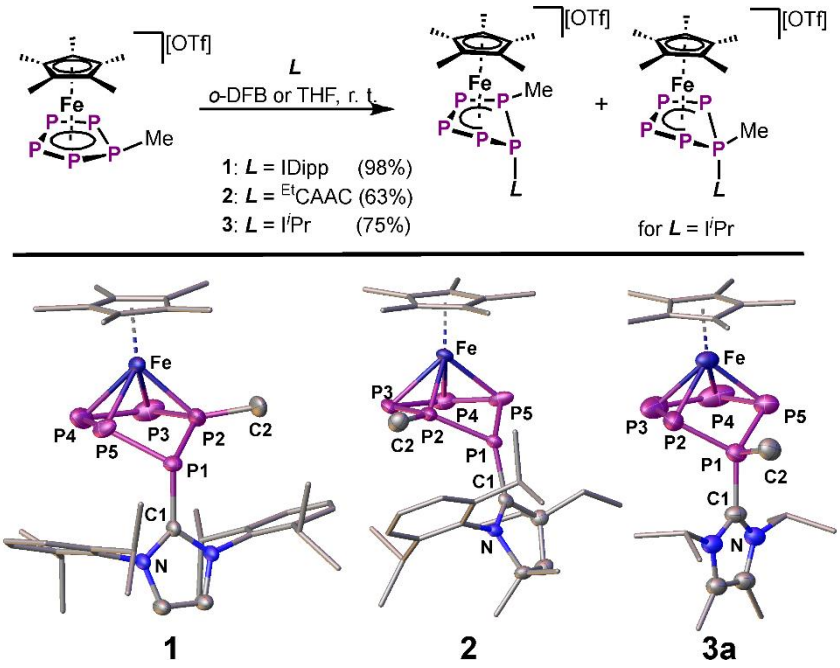

*Figure 1: Synthesis of **1** – **3** via functionalization of A with the corresponding carbene (top) and the corresponding molecular structures of **1**, **2** and **3a** in the solid state (bottom); H atoms and anions are omitted for clarity and ellipsoids are drawn at the 50% probability level.*

limited,[29] and **1** and **2** constitute the first complexes in which this structural motif could be realized via a selective addition reaction. When **A** is exposed to the smaller I^{i}Pr (I^{i}Pr = 1,4-diisopropyl-2,3-dimethylimidazol-5-ylidene) the product, obtained in 75% yield, is a mixture of both, the 1,1-regioisomer [Cp*Fe{η^4-P$_5$(1-I^{i}Pr)(1-Me)}][OTf] (**3a**) and the 1,2-regioisomer [Cp*Fe{η^4-P$_5$(1-I^{i}Pr)(2-Me)}][OTf] (**3b**). While the initial isomeric ratio (1,1 to 1,2 isomer) can be as high as 2:1, when the reaction is conducted at –80 °C, both isomers slowly equilibrate to a final ratio of 0.17:1 when kept in solution for prolonged times (cf. SI). Overall, this points towards the steric demand of the introduced carbene to govern the regioselectivity of the addition reaction to **A**. Moreover, potential dispersive interaction between the aryl side arms of the imidazolyl substituents and the Me group in **1** and **2** may reinforce this selectivity (*vide infra*).

Spectroscopically, **1** and **2** reveal their 1,2-difunctionalization as they show ABMQX and AMNQX spin systems in the respective ^{31}P NMR spectra (see SI). While solutions of **3** always contain both isomers **3a** and **3b**, the respective AMM´XX´ spin system of **3a** is indicative of its 1,1-disubstitution and allowed the assignment of signals to both compounds **3a** and **3b**. Structurally, the most striking feature of these complexes is the rare 1,2-difunctionalized cyclo-P$_5$ ligand in **1**, **2** and **3b** carrying an imidazolyl substituent at the bent P1 atom and an additional Me group at P2. While the P–P bond lengths (**1**: 2.112(3) – 2.155(1) Å, **2**: 2.049(1) – 2.252(1) Å, **3b**: 2.057(9) – 2.223(9) Å) and angles are similar to those observed in other complexes featuring envelope shaped *cyclo*-P$_5$ ligands,[15a,17f] the P1–C1 (**1**: 1.836(4) Å, **2**: 1.827(3) Å, **3b**: 1.834(5) Å) as well as the P2–C2 (**1**: 1.737(7) Å, **2**: 1.643(7)/1.743(1) Å, **3b**: 1.785(18)/1.890(30) Å) bond lengths are in agreement with their formulation as single bonds.[30]

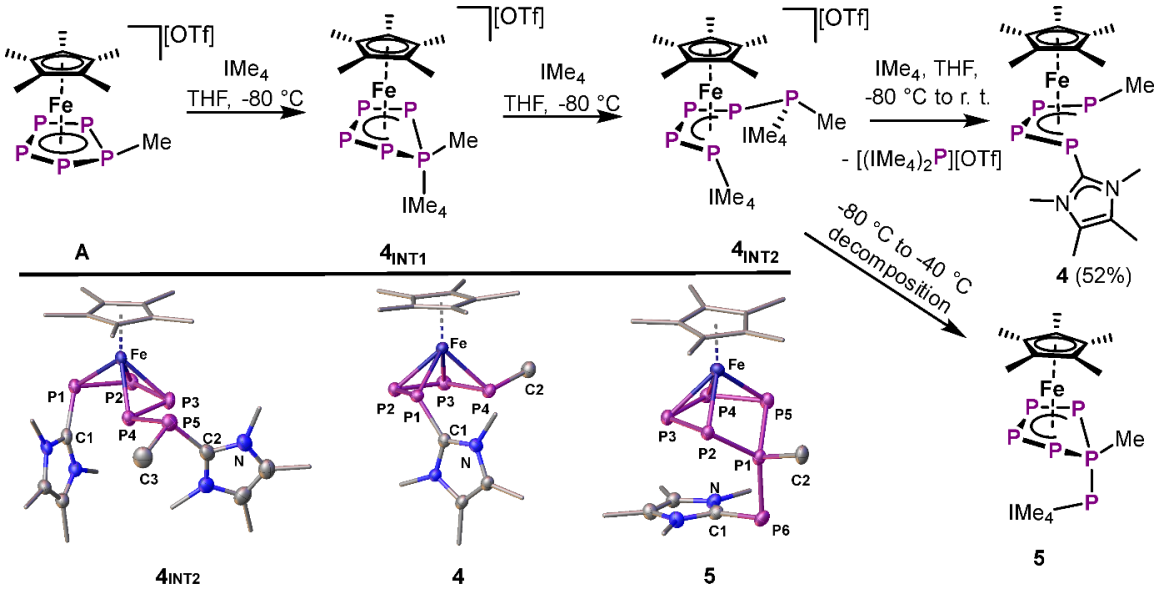

*Figure 2: Synthetic pathway towards **4** including both experimentally observed intermediates **4**$_{INT1}$ and **4**$_{INT2}$ as well as the decomposition product **5** (top) and the corresponding molecular structures of **4**$_{INT2}$, **4** and **5** in the solid state (bottom); H atoms and anions are omitted for clarity and ellipsoids are drawn at the 50% probability level.*

Notably, the imidazolyl substituent in **3b** is rotated perpendicular to the position it occupies in **1** and **2**. This may be a result of the smaller steric demand of I^{i}Pr but also prohibits any dispersive interaction of the ^{i}Pr groups with the Me substituent. Thus, the latter dispersive interactions may be responsible for the high regioselectivity in which **1** and **2** are formed. In contrast, the solid state structure of **3a** reveals a more common 1,1-disubstituted *cyclo*-P$_5$ ligand. Again, the P–P bond lengths (2.114(3) – 2.159(2) Å) and angles in **3a** are similar to reported derivatives with both P1–C bond lengths (1.811(7)/1.867(5) Å) in the range of single bonds.[30]

While the even smaller IMe$_4$ (IMe$_4$ = 1,2,3,4-tetramethylimidazol-5-ylidene) leads to ring contraction reactions with the majority of polyphosphorus ligands,[15c] it only affords labile adducts in combination with **I**.[15d] In contrast, exposing the electrophilically activated **A** to three equivalents of IMe$_4$ yields the contracted complex [Cp*Fe(η^4-P$_4$(1-IMe$_4$)(4-Me)] (**4**, 52%, Figure 2). Accordingly, extrusion of the [(IMe$_4$)$_2$P]$^+$[31] cation can easily be observed spectroscopically (see SI). While carbene induced fragmentation/rearrangement reactions are known for polyphosphorus compounds, mechanistic understanding is usually hard to obtain. Thus, experimental insight into the underlaying mechanism of these transformations has been reported in only a few cases.[32] When **A** is reacted with equimolar amounts or two fold excess of IMe$_4$, respectively, complicated product mixtures are obtained, which is attributed to the instability of the corresponding intermediates formed in these reactions. However, subjecting a 1:1 mixture of **A** and IMe$_4$ to ^{31}P{^{1}H} NMR spectroscopy at -80 °C reveals immediate formation of the anticipated first intermediate [Cp*Fe(η^4-P$_5$(1-IMe$_4$)(1-Me)][OTf] (**4**$_{INT1}$). Interestingly, no trace of the respective 1,2-difunctionalized regioisomer is observed, which agrees with the higher stability of the 1,1-isomer bearing the IMe$_4$ substituent (see SI). Exposing **A** to two equivalents of IMe$_4$ under the same conditions shows more complicated ^{31}P

NMR spectra (see SI). However, a second intermediate, formed already at -80 °C, can be identified from these spectra and assigned to [Cp*Fe{η^4-P_5(1-IMe_4)(1-Me)(5-IMe_4)}][OTf] (**4_{INT2}**), featuring an opened *catena*-P_5 ligand. More importantly, it was even possible to grow a single crystal of this key intermediate from the reaction mixture, corroborating the structural assignment of **4_{INT2}** (Figure 2). **4_{INT2}** decomposes rapidly upon warming to room temperature, leading to the surprisingly selective formation of [Cp*(η^4-P_5(1-PIMe_4)(1-Me)] (**5**, 45% based on Fe), possessing a phosphinidenido substituent. While this decomposition could not be further spectroscopically traced, it highlights the delicate reaction pathway during the formation of **4**. Finally, adding three or more equivalents of IMe_4 to **A** results in the formation of **4** and unreacted IMe_4, respectively.

Obtaining structural information on the highly reactive intermediates involved in the formation of **4** was key to elucidating the underlaying mechanism of its formation. While the molecular structure of **4_{INT1}** is consolidated by its spectroscopic data and the structural information obtained on the derivatives **1** – **3**, elucidating the structure of **4_{INT2}** was a far more complicated matter. This is due to its extreme sensitivity, complex spectroscopic features as well as lack of comparable data. However, it was possible to obtain single crystals of this key intermediate by performing the crystallization at low temperatures. The solid state structure of **4_{INT2}** reveals an opened *catena*-P_5 ligand attached to the Fe center in η^4 binding mode (Figure 2). Additionally, the *catena*-P_5 ligand bears an IMe_4 and a Me group at the uncoordinated P5 atom as well as another IMe_4 substituent at P1. This structural motif arises from the nucleophilic attack of the second IMe_4 at the P2 atom (in **4_{INT1}**), which is followed by cleavage of the P1–P5 bond and formation of the *catena*-P_5 ligand observed in **4_{INT2}**. While the P4–P5 bond length (2.234(1) Å) agrees with a single bond, the residual P–P bonds coordinated to Fe are slightly shortened (2.131(1) – 2.160(1) Å) and point towards delocalized double bond character.[30] Furthermore, the P1–C1 (1.835(3) Å) bond length as well as the P5–C2/3 distances (1.832(3)/1.845(4) Å) are in the range of single bonds.[30] Interestingly, the final product **4** shows a similar structural core compared to **4_{INT2}**, with only the phosphino group in the latter being replaced by the Me group. Accordingly, the P–P bond lengths (2.134(1) – 2.157(1) Å) in **4** are similar to those in **4_{INT2}** and agree with delocalized double bond character. Again, the P1–C1 (1.841(3) Å) and the P4–C2 (1.876(3) Å) bond lengths are best described as single bonds. In contrast, the decomposition product **5** shows a 1,1-disubstituted *cyclo*-P_5 ligand bearing an IMe_4 stabilized phosphinidenido and a Me group. Thus, the P_6 ligand in **5** displays the rare product of a formal expansion of the former *cyclo*-P_5 ligand. The overall envelope structure of the P_5 ring and the associated P–P bond lengths (2.134(1) – 2.187(1) Å) are similar to those observed in simple alkyl substituted derivatives **III**.[17f] The new P1–P6 bond (2.124(1) Å) is slightly shorter than the sum of the covalent single bond radii. While the P1–C2 (1.822(2) Å) bond as well as the P6–C1 (1.822(2) Å) bond are best described as single bonds, the IMe_4 substituent is located directly below the plane of the Fe-coordinated P atoms. This may allow for additional stabilization through π–π interactions.

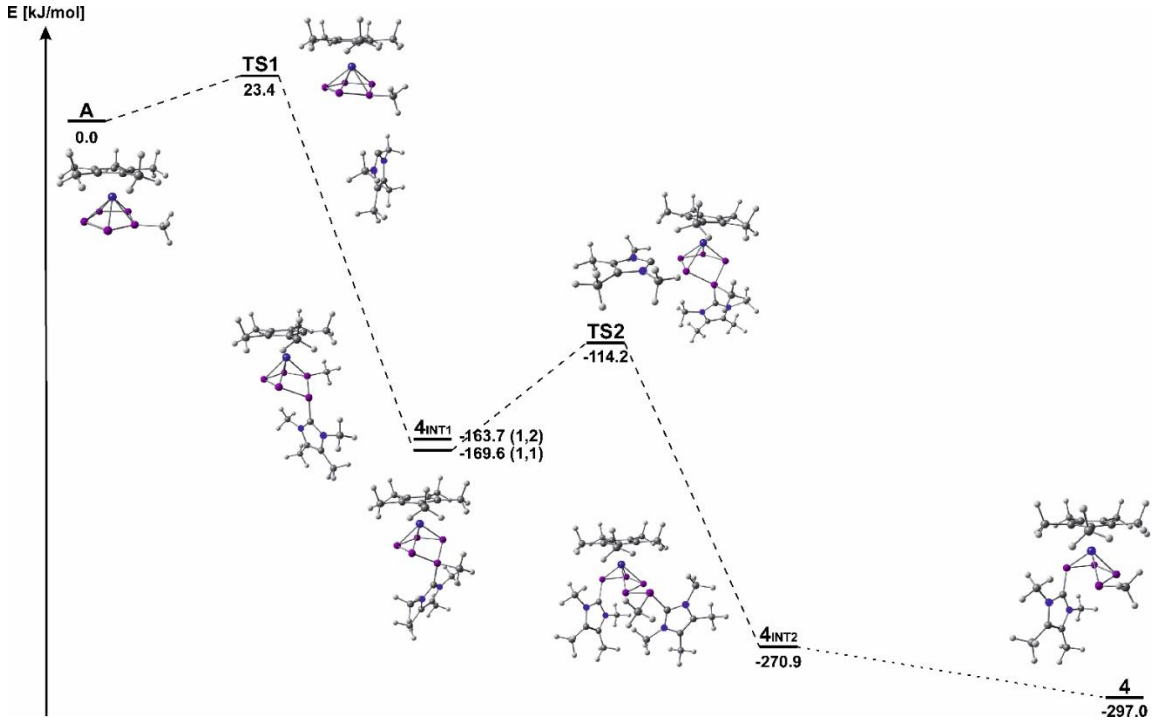

*Figure 3: Stepwise reaction of **A** with three equivalents of IMe_4 computed at the ωB97X-D4/def2-TZVPPD level of theory and PCM solvent correction for THF.*

To gain even deeper insight into the mechanistic key steps of the contraction reaction leading to **4**, DFT calculations (@ωB97X-D4/def2-TZVPPD, Figure 3) were carried out. The overall reaction of **A** with three equivalents of IMe_4 to **4** and $[(IMe_4)_2P]^+$ is strongly exergonic by 297 kJ/mol. However, the first steps of this reaction and especially the ring opening of the *cyclo*-P_5 ligand were of utmost interest, as this reactivity is unprecedented for **I**. Thus, the addition of the first equivalent of IMe_4 in **TS1** occurs at P1 with an energy barrier of 23.4 kJ/mol and follow-up formation of $\mathbf{4_{INT1}}$ is exergonic by 169.6 kJ/mol. Interestingly, the structural core of **A** is nearly undeformed within **TS1** and the carbene center is at 4.0 Å to P1. The corresponding 1,2-isomer of $\mathbf{4_{INT1}}$ is 5.9 kJ/mol higher in energy, which agrees with the exclusive experimental observation of the 1,1-isomer ($\mathbf{4_{INT1}}$) in solution (*vide supra*). Addition of the second equivalent of IMe_4 then proceeds via approach to the neighboring P2 in **TS2** which has an energetic barrier of 55.4 kJ/mol. Although, P1 shows a Mulliken charge of 0.9 addition of the second IMe_4 unit to P1, as discussed for the reaction of neutral *cyclo*-P_5R_2 ligands with anionic nucleophiles,[17f] can be discarded on steric arguments. While the carbene center in **TS2** is located only at 2.6 Å from P2 (as labelled in $\mathbf{4_{INT1}}$) the respective P1–P2 bond is at 2.4 Å and thus significantly elongated compared to $\mathbf{4_{INT1}}$. Next, the P1–P2 bond is cleaved in $\mathbf{4_{INT2}}$ and its computed molecular structure is in good agreement with the parameters observed experimentally in its solid state structure (*vide supra*). Finally, the addition of the last equivalent of IMe_4 to $\mathbf{4_{INT2}}$ leads to extrusion of $[(IMe_4)_2P]^+$ and accordingly to formation **4**, which is exergonic by 26.1 kJ/mol. However, we were unable to determine a suitable transition state for this last reaction step with sufficient certainty, as numerous points of nucleophilic attack at $\mathbf{4_{INT2}}$ are feasible.

To test the boundaries of the electrophilic reactivity enhancement of **1**, **A** was reacted with the weakly nucleophilic IDippCH$_2$ (N-heterocyclic olefin, NHO). Surprisingly, even this comparably weak nucleophile rapidly undergoes an addition to the *cyclo*-P$_5$ ligand of **A** affording the functionalized complex [Cp*Fe{η^4-P$_5$(1-NHO)(1/2-Me)}][OTf] (**6a/b**, Figure 4) in good yields of 74%. The formation of both the 1,1- as well as the 1,2-regioisomer is attributed to the diminished steric control invoked by the IDipp substituent due to the integration of the methylene moiety in **6**. Both isomers **6a** and **6b** co-crystallize and reveal 1,1- and 1,2-disubstituted *cyclo*-P$_5$ ligands, respectively (Figure 4). While the P–P bonds (2.040(14) – 2.224(19) Å) are close to those observed in simple alkyl substituted derivatives **III**,[17f] the P1–C1 bond in **6a** (1.786(9) Å) is shorter than in **6b** (1.914(4) Å). Similarly the P1–C2 bond in **6a** (1.70(4) Å) is shorter than the P2–C2 bond in **6b** (1.833(6) Å). The C=C bond (1.465(5) Å) in the IDippCH$_2$ substituent remains in the range of a double bond.[30]

Finally, **A** was reacted with the carbene stabilized parent phosphinidene IDippPH as well as its lighter homolog IDippNH (Figure 5). Interestingly, both reactions lead to highly complex products [{Cp*Fe}$_2${μ$_2$,η$^{4:3:1}$-P$_{10}$Me$_2$(IDippN)}][OTf] (**7**) and [{Cp*Fe}$_2${μ$_2$,η$^{4:1:1:1}$-P$_{11}$Me$_2$(IDipp)}][OTf] (**8**), respectively. Comparably large cationic polyphosphorus species of such complex substitution and coordination pattern are entirely unprecedented. Formally, both compounds arise from the addition of IDippXH (X = N, P) to **A** followed by deprotonation, insertion of a second equivalent of **A** and the loss of one equivalent of [IDippXH$_2$]$^+$ (X = N, P). The latter is easily confirmed as [IDippPH$_2$]$^+$ is observed in the ^{31}P NMR spectra of the crude reaction mixture of **8** (cf SI). While the initial 1:1 stoichiometry of **A** to IDippXH is necessary for the formation of **7** and **8**, it also leads to formation of the inseparable [IDippXH$_2$][OTf] as byproduct. Until the end of this thesis, this issue could not be resolved satisfactorily. Thus, both **7** and **8** could only be obtained in amounts of few single crystals, allowing solely for their Xray crystallographic structure determination. A possible way to prepare both species analytically pure would be to isolate potential intermediates. Surprisingly, reacting **A** with two equivalents of IDippNH lead to rapid formation of [Cp*Fe{η^4-P$_5$(1-NIDipp)(1-Me)}] (**7$_{INT}$**) as well as [IDippNH$_2$]$^+$. However, the latter can now easily be removed via filtration, allowing the isolation of **7$_{INT}$** in yields of up to 75%. Indeed, **7$_{INT}$** may display the key intermediate in the formation of **7**, where the deprotonated IDippN- substituent is already assembled at the *cyclo*-P$_5$ ligand but the second equivalent of **A** has not yet inserted. However, this needs to be further corroborated

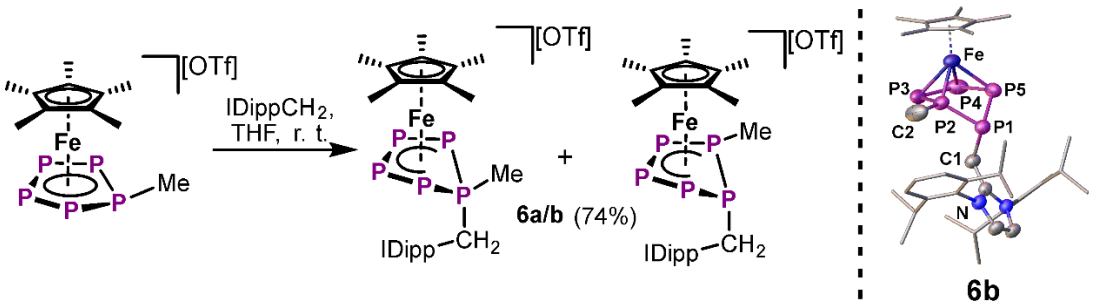

*Figure 4: Synthesis of **6a** and **6b** via addition of IDippCH$_2$ to **A** (left) and the molecular structure of **6b** in the solid state (right); H atoms and the anion are omitted for clarity and ellipsoids are drawn at the 50% probability level.*

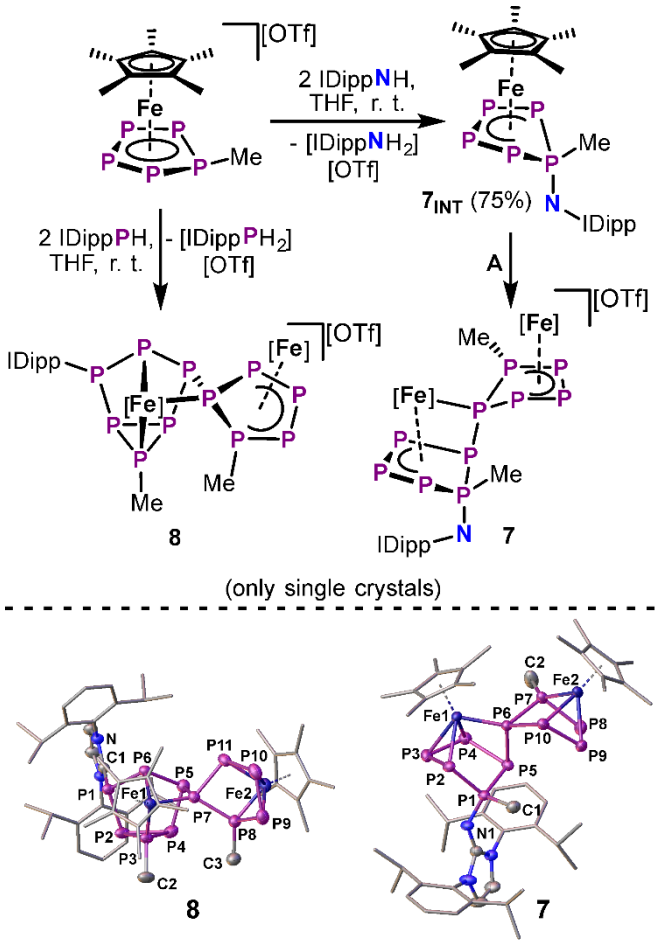

*Figure 5: Synthesis of **7** and **8** including formation of **7**$_{INT}$ (top) as well as the molecular structures of **7** and **8** in the solid state (bottom); H atoms and anions are omitted for clarity and ellipsoids are drawn at the 50% probability level.*

in future studies. Notably, this approach cannot be transferred to **8**, as the respective key intermediate **8**$_{INT}$ is inaccessible *via* this way. This is attributed to the strongly decreased basicity of IDippPH compared to the lighter IDippNH, preventing the *in situ* deprotonation of the former prior to the nucleophilic attack at **A**.

Both the solid state structures of **7** and **8** reveal extremely complex polyphosphorus ligands (Figure 5). While the former *cyclo*-P_5 ligands can still be recognized within the bicyclic P_{10} ligand of **7**, the P_{11} ligand in **8** has partly rearranged to a nortricyclan type scaffold with an inserted *cyclo*-P_5Me moiety. The P_{10} ligand in **7** is derived from the molecular structure of **7**$_{INT}$ which underwent insertion of another equivalent of **A** into the former P2–Fe bond. Notably, this insertion takes place via the P2 atom in **A** and results in a strong bend of the *cyclo*-P_5 ligand. As the steric demand of the Me substituents is comparably small, this insertion can occur with both Me groups pointing into the same or the opposing direction and thus affords two distinct isomers (cf SI) of which it was possible to crystallize the respective *trans* derivative. Furthermore, the formation of isomers of **7** as well as **8** is confirmed by inspection of the ^{31}P NMR spectra of the respective reaction mixtures. However, this issue could not be circumvented due to the low steric demand of the Me substituent in **A**, which does not afford enough steric discrimination between the potential isomers. The bond lengths between the Fe

coordinated P atoms in **7** (2.131(3) – 2.149(2) Å) agree with partial multiple bond character in the respective allylic (P2 – P4) and butadiene like (P7 – P10) fragments. The P1–P2/5 bonds (2.174(2)/2.191(2) Å) are also comparably short, which is attributed to the phosphonium character of P1, while the residual P4–P5, P5–P6 and P6–P7/10 bond lengths (2.201(2) – 2.262(2) Å) are in the range of single bonds.[30] The P1–C1 (1.814(7) Å) and the P7–C2 (1.825(8) Å) bonds are best described as single bonds as well. In contrast, the P1–N1 bond length (1.593(5) Å) as well as the corresponding N1–C distance (1.318(8) Å) are comparably short. On the other hand, the nortricyclan cage in **8** formally arises from the addition of an IDippP- moiety to **A**. While the Me group is bound to one of the basal P atoms (P3), the {Cp*Fe} fragment occupies one of the upper corner positions with the IDipp substituent bound to the adjacent P1 atom. The second equivalent of **A** can then be imagined inserting between the latter {Cp*Fe} fragment and the other adjacent P5 via the former P2 atom (in **A**). Again, formation of *cis*- and *trans*-Me isomers is possible due to the small steric demand of the Me group and can now even be observed in the solid state as positional disorder of C3. The P–P bond lengths in the nortricyclan part of **8** are best described as single bonds (2.201(1) – 2.257(1) Å) except for the P1–P6 bond (2.191(1) Å), which is slightly shortened. Similarly, the intact *cyclo*-P_5 moiety within **8** also displays shortened P–P bonds (2.128(1) – 2.191(1) Å) and only the P7–P11 bond (2.216(1) Å) is in the range of a single bond.[30] Again, the P1–C1 (1.843(3) Å), P3–C2 (1.831(4) Å) as well as the P8–C3 (1.822(4) Å) bond lengths are within the range of single bonds. While it was also possible to crystallize $\mathbf{7_{INT}}$, its solid state structure is incommensurately modulated, prohibiting satisfactory structural refinement. Yet, it was possible to derive a preliminary structural model for $\mathbf{7_{INT}}$ from these data, which confirms it to bear a 1,1-disubstituted *cyclo*-P_5 ligand with an envelope type structure (cf. SI). The molecular geometry of $\mathbf{7_{INT}}$ is well reproduced by DFT calculations and agrees with its spectroscopic data. Thus, the highly indicative AMM´XX´ spin system in the ^{31}P NMR spectrum agrees with the 1,1-disubstituted *cyclo*-P_5RR' ligand. Notably, the molecular geometry of $\mathbf{7_{INT}}$ reveals short P1–N1 (1.64 Å) as well as N1–C2 (1.31 Å) distances and a widened P1–N1–C2 angle (147.7°). While this points towards the double bond character of these bonds, the Wiberg Bond Index (WBI) of only the N1–C2 bond (1.40) allows for this formulation. In contrast, the WBI of the P1–N1 bond (0.91) indicates it to be a single bond, which is in line with the observation of highly localized NBOs and no π-type orbitals. Thus, the formulation of $\mathbf{7_{INT}}$ with separated charges and no P1–N1 double bond (see Scheme S3) seems to be most appropriate. This intriguing feature of the electronic structure of $\mathbf{7_{INT}}$ may be the reason for its unprecedented reactivity towards **A**, especially when compared to simple alkyl substituted derivatives **III**.[17f]

11.4. Conclusion

In conclusion, the reactivity enhancement of the robust *cyclo*-P_5 ligand in **I** by electrophilic activation to **A** has been demonstrated. Initial studies on the reactivity of **A** towards carbenes not only showed an increase in reactivity (strong covalent vs. labile bonding) but furthermore pave a rational/selective pathway towards 1,2-disubstituted *cyclo*-P_5 moieties in **1**, **2** and **3b**.

Notably, this regioselectivity can even be tuned via the variation of the steric bulk employed at the carbene. When the small IMe_4 is employed, the enhanced reactivity of **A** culminates in a contraction reaction affording the *catena*-P_4 complex **4**. DFT calculations provided valuable insight on the underlaying reaction mechanism, which was corroborated by low temperature NMR spectroscopic and even crystallographic studies on the isolated key intermediates $\mathbf{4_{INT1}}$ and $\mathbf{4_{INT2}}$, respectively. Lastly, **A** was exposed to IDippX (X = CH_2, NH, PH) and found to even react with these comparably weak nucleophiles. While the reaction with $IDippCH_2$ leads to functionalization at the *cyclo*-P_5 ligand in **6**, its group 15 analogs afford the more complex compounds **7** and **8**, bearing unprecedented functionalized P_{10} and P_{11} ligands, respectively. The isolation of the key intermediate $\mathbf{7_{INT}}$ gave insight into the reaction pathway of these complicated aggregation reactions and provides a stepping point for future investigations. The latter may involve fine-tuning of the stereoselectivity of the above aggregation reactions and the exploration of various substitution patterns at **A**. Thus, electrophilic reactivity enhancement of **A** was demonstrated as a powerful tool to access unprecedented, complex, and functionalized polyphosphorus architectures. This concept is expected to be easily expanded to various other polyphosphorus compounds and should thus aid in shaping phosphorus chemistry to novel complexity.

11.5. Supporting Information

11.5.1. Experimental Procedures

General Considerations

All manipulations were carried out using standard Schlenk techniques at a Stock apparatus under N_2 as an inert gas or in a glove box with Ar atmosphere. All glassware was dried with a heat gun (600 °C) for at least 30 min prior to use. *o*-DFB (1,2-difluorobenzene) was distilled from P_2O_5, CD_2Cl_2 was distilled from CaH_2 and other solvents were directly taken from an MBraun SPS-800 solvent purification system and degassed at room temperature. Solution ^{1}H (400.130 MHz), ^{13}C (100.627 MHz), ^{19}F (376.498 MHz) and ^{31}P (161.976 MHz) NMR spectra were recorded at an Avance400 (Bruker) spectrometer using $(H_3C)_4Si$ (^{1}H), $CFCl_3$ (^{19}F) or 85% phosphoric acid (^{31}P), respectively, as external standards. Chemical shifts (δ) are provided in parts per million (ppm) and coupling constants (*J*) are reported in Hertz (Hz). Chemical shifts and coupling constants for all $^{31}P\{^{1}H\}$ and ^{31}P NMR spectra were derived from spectral simulation using the built-in simulation package of TopSpin3.2. The following abbreviations are used: s = singlet, d = doublet, dd = doublet of doublets, dt = doublet of triplets, t = triplet, td = triplet of doublets br = broad and m = multiplet. ESI mass spectra were recorded at the internal mass spectrometry department using a ThermoQuest Finnigan TSQ 7000 mass spectrometer or by the first author on a Waters Micromass LCT ESI-TOF mass-spectrometer and peak assignment was performed using the Molecular weight calculator 6.50.[33] Elemental analysis of the products was conducted by the elemental analysis department at the University of Regensburg using an Elementar Vario EL. The starting materials [Cp*Fe(η^5-P_5)],[21] IDipp,[34] ^{Et}CAAC,[35] I^{i}Pr,[36] IMe_4,[36] $IDippCH_2$,[37] IDippNH[38] and IDippPH[39] were synthesized following literature procedures. All other chemicals were purchased from commercial vendors and used without further purification.

*[Cp*Fe(η^5-P_5Me)][OTf] (**A**)*

[Cp*Fe(η^5-P_5)] (1.00 g, 2.89 mmol, 1 eq.) was dissolved in 50 mL of *o*-DFB and MeOTf (0.595 g, 0.397 mL, 3.63 mmol, 1.3 eq.) was added to the green solution. Heating the mixture to reflux for three hours lead to a gradual color change to brownish red. The solution was concentrated to 10 mL under reduced pressure and addition of 50 mL of *n*-pentane were added to precipitate [Cp*Fe(η^5-P_5Me)][OTf] (**A**) as brownish red powder. After washing two times with 20 mL of *n*-pentane, each, **A** was dried under reduced pressure (10^{-3} mbar), redissolved in 20 mL of *o*-DFB and layered with 40 mL of *n*-pentane. Storage at room temperature for one day afforded stick shaped crystals of A in X-ray quality and nearly quantitative yield.

Derivatives of **A** have already been reported with different counterions[20d] and thus it is only characterized spectroscopically.

Yield: 1.45 g (2.84 mmol, 98%)

ESI(+) MS (*o*-DFB): *m/z* (%) = 360.94 ([Cp*Fe(η^5-P_5CH_3)]$^+$)

NMR (CD_2Cl_2, 298 K):**^{1}H**: δ/ppm = 1.69 (s, 15 H, Cp*), 2.78 (m (unresolved), 3 H, $P_5C\underline{H_3}$)

^{31}P{^{1}H}: δ/ppm = 114.4 (m, $^1J_{PA\text{-}PX/X'}$ = 609/608 Hz, $^2J_{PA\text{-}PB/B'}$ = 11/6 Hz, 1 P, P^A), 113.0 (m, $^1J_{PB/B'\text{-}PX/X'}$ = 458/456 Hz, $^1J_{PB\text{-}PB'}$ = 402 Hz, $^2J_{PB/B'\text{-}PX'/X}$ = –51/–58 Hz, $^2J_{PB/B'\text{-}PA}$ = 11/6 Hz, 2 P, $P^{B/B'}$), 77.9 (m, $^1J_{PX/X'\text{-}PA}$ = 609/608 Hz, $^1J_{PX/X'\text{-}PB/B'}$ = 458/456 Hz, $^2J_{PX/X'\text{-}PB'/B}$ = -51/-58 Hz $^2J_{PX\text{-}PX'}$ = 40 Hz, 2 P, $P^{X/X'}$)

^{31}P: δ/ppm = 114.4 (m, $^1J_{PA\text{-}PX/X'}$ = 609/608 Hz, $^2J_{PA\text{-}PB/B'}$ = 11/6 Hz, $^2J_{PA\text{-}H}$ = 14 Hz, 1 P, P^A), 113.0 (m, $^1J_{PB/B'\text{-}PX/X'}$ = 458/456 Hz, $^1J_{PB\text{-}PB'}$ = 402 Hz, $^2J_{PB/B'\text{-}PX'/X}$ = -51/-58 Hz, $^2J_{PB/B'\text{-}PA}$ = 11/6 Hz, 2 P, $P^{B/B'}$), 77.9 (m, $^1J_{PX/X'\text{-}PA}$ = 609/608 Hz, $^1J_{PX/X'\text{-}PB/B'}$ = 458/456 Hz, $^2J_{PX/X'\text{-}PB'/B}$ = –51/–58 Hz $^2J_{PX\text{-}PX'}$ = 40 Hz, 2 P, $P^{X/X'}$)

^{19}F{^{1}H}: δ/ppm = –78.3 (s, $[SO_3C\underline{F_3}]^-$)

*[Cp*Fe{η^4-P_5(1-IDipp)(2-Me)}][OTf] (**1**)*

A (102 mg, 0.2 mmol, 1 eq.) was dissolved in 2 mL of *o*-DFB and IDipp (80 mg, 0.2 mmol, 1 eq.), dissolved in 2 mL of *o*-DFB, was added at room temperature to afford a color change from brownish red to dark brown. The mixture was stirred for 1 h and then directly layered with 20 mL of *n*-pentane. Storage for one day at room temperature afforded dark brown rod shaped crystals of [Cp*Fe{η^4-P_5(1-IDipp)(2-Me)}][OTf] (**1**), which were isolated by decanting the supernatant and drying under reduced pressure (10^{-3} mbar).

Yield: 175 mg (0.195 mmol, 98%)

Elemental analysis: calc. (%) for: $[C_{39}H_{54}N_2O_3F_3P_5SFe]\cdot(C_6H_4F_2)_{0.3}$):

C: 52.53 H: 5.96 N: 3.00 S: 3.44

found (%): C: 53.03 H: 6.11 N: 2.86 S: 3.48

ESI(+) MS (*o*-DFB): *m/z* (%) = 749.2 (100, $[Cp^*Fe(\eta^4\text{-}P_5CH_3IDipp)]^+$)

NMR (CD_2Cl_2, 298 K): **^{1}H**: δ/ppm = 1.12 (d, $^3J_{H\text{-}H}$ = 7 Hz, 6 H, -CH(C$\underline{H}_3$)$_2$), 1.13 (d, $^3J_{H\text{-}H}$ = 7 Hz, 6 H, -CH(C$\underline{H}_3$)$_2$), 1.16 (m (overlapping), 3 H, $P_5C\underline{H}_3$), 1.52 (s, 15 H, Cp*), 1.54 (d (br), $^3J_{H\text{-}H}$ = 7 Hz, 12 H, -CH(C$\underline{H}_3$)$_2$), 2.22 (s, $^3J_{H\text{-}H}$ = 7 Hz, 4 H, -C$\underline{H}$(CH$_3$)$_2$), 7.38 (s, 2 H, C(N(Dipp)C$\underline{H}$)$_2$, 7.48 (d, $^3J_{H\text{-}H}$ = 8 Hz, 4 H, 1,3-^{i}Pr$_2$-C$_6\underline{H}_3$(meta)), 7.69 (t, $^3J_{H\text{-}H}$ = 8 Hz, 2 H, 1,3-^{i}Pr$_2$-C$_6\underline{H}_3$(para))

^{31}P{^{1}H}: δ/ppm = 42.7 (m, $^1J_{PA\text{-}PQ}$ = 494 Hz, $^1J_{PA\text{-}PX}$ = 494 Hz, $^2J_{PA\text{-}PM}$ = 48 Hz, $^2J_{PA\text{-}PN}$ = 6 Hz, 1 P, P^A), 23.7 (m, $^1J_{PM\text{-}PQ}$ = 361 Hz, $^1J_{PM\text{-}PN}$ = 343 Hz, $^2J_{PM\text{-}PA}$ = 48 Hz, $^2J_{PM\text{-}PX}$ = 37 Hz, 1 P, P^M), 16.8 (m, $^1J_{PN\text{-}PX}$ = 448 Hz, $^1J_{PN\text{-}PM}$ = 343 Hz, $^2J_{PN\text{-}PQ}$ = 64 Hz, $^2J_{PN\text{-}PA}$ = 6 Hz, 1 P, P^N), 2.0 (m, $^1J_{PQ\text{-}PA}$ = 494 Hz, $^1J_{PQ\text{-}PM}$ = 361 Hz, $^2J_{PQ\text{-}PN}$ = 64 Hz, $^2J_{PQ\text{-}PX}$ = 13 Hz, 1 P, P^Q), –106.4 (m, $^1J_{PX\text{-}PA}$ = 494 Hz, $^1J_{PX\text{-}PN}$ = 448 Hz, $^2J_{PX\text{-}PM}$ = 37 Hz, $^2J_{PX\text{-}PQ}$ = 13 Hz, 1 P, P^X)

^{31}P: δ/ppm = 42.7 (m, $^1J_{PA\text{-}PQ}$ = 492 Hz, $^1J_{PA\text{-}PX}$ = 492 Hz, $^2J_{PA\text{-}PM}$ = 47 Hz, $^2J_{PA\text{-}PN}$ = 6 Hz, $^2J_{PA\text{-}H}$ = 11 Hz, 1 P, P^A), 23.7 (m, $^1J_{PM\text{-}PQ}$ = 359 Hz, $^1J_{PM\text{-}PN}$ = 344 Hz, $^2J_{PM\text{-}PA}$ = 47 Hz, $^2J_{PM\text{-}PX}$ = 40 Hz, 1 P, P^M), 16.8 (m, $^1J_{PN\text{-}PX}$ = 446 Hz, $^1J_{PN\text{-}PM}$ = 344 Hz, $^2J_{PN\text{-}PQ}$ = 64 Hz, $^2J_{PN\text{-}PA}$ = 6 Hz, 1 P, P^N), 2.0 (m, $^1J_{PQ\text{-}PA}$ = 492 Hz, $^1J_{PQ\text{-}PM}$ = 359 Hz, $^2J_{PQ\text{-}PN}$ = 64 Hz, $^2J_{PQ\text{-}PX}$ = 16 Hz, $^3J_{PQ\text{-}H}$ = 7 Hz, 1 P, P^Q), –106.4 (m, $^1J_{PX\text{-}PA}$ = 492 Hz, $^1J_{PX\text{-}PN}$ = 446 Hz, $^2J_{PX\text{-}PM}$ = 40 Hz, $^2J_{PX\text{-}PQ}$ = 16 Hz, 1 P, P^X)

^{19}F{^{1}H}: δ/ppm = –78.9 (s, $[SO_3C\underline{F}_3]^-$)

*[Cp*Fe{η^4-P_5(1-^{Et}CAAC)(2-Me)}][OTf] (**2**)*

A (51 mg, 0.1 mmol, 1 eq.) was dissolved in 2 mL of *o*-DFB and ^{Et}CAAC (31 mg, 0.1 mmol, 1 eq.), dissolved in 2 mL of *o*-DFB, was added at room temperature to afford a color change from brownish red to dark brown. The mixture was stirred for 1 h and then directly layered with 20 mL of *n*-pentane. Storage for one day at room temperature afforded dark brown plate shaped crystals of [Cp*Fe{η^4-P_5(1-^{Et}CAAC)(2-Me)}][OTf] (**2**), which were isolated after decanting the supernatant and drying under reduced pressure (10^{-3} mbar).

Yield: 57 mg (0.063 mmol, 63%)

ESI(+) MS (*o*-DFB): *m/z* (%) = 674.2 (100, [Cp*Fe(η^4-$P_5CH_3CAAC^{Et}$)]$^+$)

NMR (CD_2Cl_2, 298 K): **^{1}H**: δ/ppm = 0.72 (t, $^3J_{H-H}$ = 7.5 Hz, 3 H, -$CH_2C\underline{H}_3$), 1.00 (t, $^3J_{H-H}$ = 7.4 Hz, 3 H, $CH_2C\underline{H}_3$), 1.30 (d, $^3J_{H-H}$ = 6.6 Hz, 3 H, -$CH(C\underline{H}_3)_2$), 1.33 (d, $^3J_{H-H}$ = 6.6 Hz, 3 H, -$CH(C\underline{H}_3)_2$),1.37 (s (overlapping), 3 H, -$C\underline{H}_3$) , 1.38 (s (overlapping), 3 H, -$C\underline{H}_3$), 1.42 (d, $^3J_{H-H}$ = 6.6 Hz, 3 H, -$CH(C\underline{H}_3)_2$), 1.46 (m, $^2J_{H-P}$ = 10.5 Hz, $^3J_{H-P}$ = 6.7 Hz, $^3J_{H-P}$ = 3.2 Hz, 3 H, $P_5C\underline{H}_3$), 1.62 (s (overlapping), 15 H, Cp*), 1.63 (d (overlapping), 3 H, -$CH(C\underline{H}_3)_2$), 1.68 (m (overlapping), 1 H, $C\underline{H}_2CH_3$), 2.00 (m (overlapping), 1 H, $C\underline{H}_2CH_3$), 2.00 (d (overlapping, $^2J_{H-H}$ = 14 Hz, 1 H, $C\underline{H}_2$ (CAAC-backbone)), 2.13 (d, $^2J_{H-H}$ = 14 Hz, 1 H, $C\underline{H}_2$ (CAAC-backbone)), 2.21 (m (overlapping), 1 H, $C\underline{H}_2CH_3$), 2.28 (m (overlapping), 1 H, $C\underline{H}_2CH_3$), 2.46 (h, $^3J_{H-H}$ = 6.6 Hz, 1 H, -$C\underline{H}(CH_3)_2$), 2.57 (h, $^3J_{H-H}$ = 6.6 Hz, 1 H, -$C\underline{H}(CH_3)_2$), 7.49 (m, 2 H, -2,6-(^{i}Pr)-$C_6\underline{H}_3$(m)), 7.49 (m, 1 H, -2,6-(^{i}Pr)-$C_6\underline{H}_3$(p))

^{31}P{^{1}H}: δ/ppm = 61.0 (m, $^1J_{PA-PM}$ = 578 Hz, $^1J_{PA-PX}$ = 491 Hz, $^2J_{PA-PB}$ = 35 Hz, $^2J_{PA-PQ}$ = 10 Hz, 1 P, P^A), 53.5 (m, $^1J_{PB-PM}$ = 401 Hz, $^1J_{PB-PQ}$ = 348 Hz, $^2J_{PB-PA}$ = 35 Hz, $^2J_{PB-PX}$ = 34 Hz, 1 P, P^B), 27.5 (m, $^1J_{PM-PA}$ = 578 Hz, $^1J_{PM-PB}$ = 401 Hz, $^2J_{PM-PQ}$ = 59 Hz, $^2J_{PM-PX}$ = 10 Hz 1 P, P^M), 9.9 (m, $^1J_{PQ-PX}$ = 444 Hz, $^1J_{PQ-PB}$ = 348 Hz, $^2J_{PQ-PM}$ = 59 Hz, $^2J_{PQ-PA}$ = 10 Hz 1 P, P^Q), –106.5 (m, $^1J_{PX-PA}$ = 491 Hz, $^1J_{PX-PQ}$ = 444 Hz, $^2J_{PX-PB}$ = 35 Hz, $^2J_{PX-PM}$ = 10 Hz 1 P, P^X)

^{31}P: δ/ppm = 61.0 (m, $^1J_{PA-PM}$ = 577 Hz, $^1J_{PA-PX}$ = 491 Hz, $^2J_{PA-PB}$ = 36 Hz, $^2J_{PA-PQ}$ = 9 Hz, $^2J_{PA-H}$ = 11 Hz, 1 P, P^A), 53.5 (m, $^1J_{PB-PM}$ = 401 Hz, $^1J_{PB-PQ}$ = 348 Hz, $^2J_{PB-PA}$ = 35 Hz, $^2J_{PB-PX}$ = 34 Hz, 1 P, P^B), 27.5 (m, $^1J_{PM-PA}$ = 577 Hz, $^1J_{PM-PB}$ = 401 Hz, $^2J_{PM-PQ}$ = 59 Hz, $^2J_{PM-PX}$ = 9 Hz 1 P, P^M), 9.9 (m, $^1J_{PQ-PX}$ = 444 Hz, $^1J_{PQ-PB}$ = 348 Hz, $^2J_{PQ-PM}$ = 59 Hz, $^2J_{PQ-PA}$ = 9 Hz 1 P, P^Q), –106.5 (m, $^1J_{PX-PA}$ = 491 Hz, $^1J_{PX-PQ}$ = 444 Hz, $^2J_{PX-PB}$ = 36 Hz, $^2J_{PX-PM}$ = 9 Hz 1 P, P^X)

^{19}F{^{1}H}: δ/ppm = –78.8 (s, $[SO_3C\underline{F}_3]^-$)

*[Cp*Fe{η⁴-P₅(1- I^{i}Pr)(1-Me)}][OTf] (**3a**) and [Cp*Fe{η⁴-P₅(1- I^{i}Pr)(2-Me)}][OTf] (**3b**)*

A (102 mg, 0.2 mmol, 1 eq.) was dissolved in 2 mL of THF and I^{i}Pr (36 mg, 0.2 mmol, 1 eq.), dissolved in 2 mL of THF, was added at – 80 °C to afford a color change from brownish red to dark brown. The mixture was stirred and allowed to slowly warm up to room temperature over the course of 2 h. The resulting dark brown solution was concentrated to 2 mL and directly layered with 20 mL of *n*-pentane. Storage for one day afforded brown crystals of both isomers [Cp*Fe{η^4-P$_5$(1- I^{i}Pr)(1-Me)}][OTf] (**3a**) and [Cp*Fe{η^4-P$_5$(1- I^{i}Pr)(2-Me)}][OTf] (**3b**) in X-ray quality. Attempts to selectively prepare either one of these isomers however failed due to equilibration in solution.

Yield: 104 mg (0.15 mmol, 75%)

Elemental analysis: calc. (%) for: $[C_{23}H_{38}N_2O_3F_3P_5SFe]\cdot(C_4H_8O)_{0.8}$:

C: 42.07 H: 5.98 N: 3.75 S: 4.29

found (%): C: 42.54 H: 5.84 N: 3.85 S: 4.33

ESI(+) MS (*o*-DFB): *m/z* (%) = 541.10 (100, [Cp*Fe(η^5-P$_5$CH$_3$ I^{i}Pr)]$^+$)

NMR: **3a** (CD_2Cl_2, 298 K): **^{1}H**: δ/ppm = 1.51 (d, $^3J_{H\text{-}H}$ = 7 Hz, 12 H, -CH(C$\underline{H}_3$)$_2$), 1.66 (s, 15 H, Cp*), 2.20 (s, 6 H, C(N(^{i}Pr)C(C$\underline{H}_3$))$_2$), 2.78 (dt, $^2J_{H\text{-}P}$ = 9 Hz, $^3J_{H\text{-}P}$ = 5 Hz, 3 H, P$_5$C$\underline{H}_3$), 5.27 (m, $^3J_{H\text{-}H}$ = 7 Hz, $^4J_{H\text{-}P}$ = 1 Hz, 2 H, -C$\underline{H}$(CH$_3$)$_2$)

^{31}P{^{1}H}: δ/ppm = 74.7 (m, $^1J_{PA\text{-}PX/X'}$ = 441 Hz, $^2J_{PA\text{-}PM/M'}$ = 14/8 Hz, 1 P, P^A), 38.2 (m, $^1J_{PM/M'\text{-}PX/X'}$ = 399 Hz, $^1J_{PM\text{-}PM'}$ = 398 Hz, $^2J_{PM/M'\text{-}PX'/X}$ = 50/44 Hz, $^2J_{PM/M'\text{-}PA}$ = 14/8 Hz, 2 P, P$^{M/M'}$), -34.4 (m, $^1J_{PX/X'\text{-}PA}$ = 441 Hz, $^1J_{PX/X'\text{-}PM/M'}$ = 399 Hz, $^2J_{PX/X'\text{-}PM/M'}$ = 50/44 Hz, $^2J_{PX/X'}$ = 10 Hz, 2 P, P$^{X/X'}$)

^{31}P: δ/ppm = 74.7 (m, $^1J_{PA\text{-}PX/X'}$ = 442/439 Hz, $^2J_{PA\text{-}PM/M'}$ = 11/10 Hz, $^2J_{PA\text{-}H}$ = 8 Hz, 1 P, P^A), 38.2 (m, $^1J_{PM/M'\text{-}PX/X'}$ = 397/394 Hz, $^1J_{PM\text{-}PM'}$ = 391 Hz, $^2J_{PM/M'\text{-}PX'/X}$ = 45/41 Hz, $^2J_{PM/M'\text{-}PA}$ = 11/10 Hz, 2 P, P$^{M/M'}$), -34.5 (m, $^1J_{PX/X'\text{-}PA}$ = 442/439 Hz, $^1J_{PX/X'\text{-}PM/M'}$ = 397/394 Hz, $^2J_{PX/X'\text{-}PM/M'}$ = 45/41 Hz, $^2J_{PX/X'}$ = 1 Hz, 2 P, P$^{X/X'}$)

^{19}F{^{1}H}: δ/ppm = –78.81 (s, [SO$_3$C$\underline{F}_3$]$^-$)

3b (CD_2Cl_2, 298 K): **^{1}H**: δ/ppm = 1.29 (d, $^3J_{H\text{-}H}$ = 7 Hz, 12 H, -CH(CH$_3$)$_2$), 1.72 (s, 15 H, Cp*), 2.19 (s, 6 H, C(N(^{i}Pr)C(C$\underline{H}_3$))$_2$), 2.36 (m, $^2J_{H\text{-}P}$ = 10 Hz, $^3J_{H\text{-}P}$ = 7 Hz, $^3J_{H\text{-}P}$ = 4 Hz, 3 H, P$_5$C$\underline{H}_3$), 4.57 (br, 2 H, -C$\underline{H}$(CH$_3$)$_2$)

$^{31}P\{^{1}H\}$: δ/ppm = 63.6 (br, 1 P, P^A), 61.0 (br, 1 P, P^B), 17.1 (m, 1 P, P^M), –28.3 (br, 1 P, P^Q), –101.2 (t (br), 1 P, P^X)

^{31}P: δ/ppm = 63.6 (br, 1 P, P^A), 61.0 (br, 1 P, P^B), 17.1 (m, 1 P, P^M), –28.3 (br, 1 P, P^Q), –101.2 (t (br), 1 P, P^X)

$^{19}F\{^{1}H\}$: δ/ppm = –78.81 (s, $[SO_3C\underline{F}_3]^-$)

(CD_2Cl_2, 193 K): **^{1}H**: δ/ppm = 1.42 (br, 12 H, -CH(CH_3)$_2$), 1.63 (s, 15 H, Cp*), 2.13 (s, 6 H, C(N(^{i}Pr)C($C\underline{H}_3$))$_2$), 2.28 (t(br), $^2J_{H\text{-}P}$ = 10 Hz, 3 H, $P_5C\underline{H}_3$), 4.53 (m, $^3J_{H\text{-}H}$ = 7 Hz, 2 H, -C$\underline{H}$(CH_3)$_2$)

$^{31}P\{^{1}H\}$: δ/ppm = 62.4 (m, $^1J_{PA\text{-}PX}$ = 492 Hz, $^1J_{PA\text{-}PQ}$ = 482 Hz, $^2J_{PA\text{-}PB}$ = 53 Hz, $^2J_{PA\text{-}PM}$ = 10 Hz, $^2J_{PA\text{-}H}$ = 11 Hz, 1 P, P^A), 58.0 (m, $^1J_{PB\text{-}PQ}$ = 372 Hz, $^1J_{PB\text{-}PM}$ = 347 Hz, $^2J_{PB\text{-}PA}$ = 53 Hz, $^2J_{PB\text{-}PX}$ = 32 Hz, 1 P, P^B), 11.6 (m, $^1J_{PM\text{-}PX}$ = 442 Hz, $^1J_{PM\text{-}PB}$ = 347 Hz, $^2J_{PM\text{-}PQ}$ = 77 Hz, $^2J_{PM\text{-}PA}$ = 10 Hz, 1 P, P^M), –35.8 (m, $^1J_{PQ\text{-}PA}$ = 482 Hz, $^1J_{PQ\text{-}PB}$ = 372 Hz, $^2J_{PQ\text{-}PM}$ = 77 Hz, $^2J_{PQ\text{-}PX}$ = 2 Hz, 1 P, P^Q), –106.4 (m, $^1J_{PX\text{-}PA}$ = 492 Hz, $^1J_{PX\text{-}PM}$ = 442 Hz, $^2J_{PX\text{-}PB}$ = 32 Hz, $^2J_{PX\text{-}PQ}$ = 2 Hz, 1 P, P^X)

^{31}P: δ/ppm = 62.5 (m, $^1J_{PA\text{-}PX}$ = 490 Hz, $^1J_{PA\text{-}PQ}$ = 484 Hz, $^2J_{PA\text{-}PB}$ = 52 Hz, $^2J_{PA\text{-}PM}$ = 12 Hz, $^2J_{PA\text{-}H}$ = 11 Hz, 1 P, P^A), 58.0 (m, $^1J_{PB\text{-}PQ}$ = 368 Hz, $^1J_{PB\text{-}PM}$ = 348 Hz, $^2J_{PB\text{-}PA}$ = 52 Hz, $^2J_{PB\text{-}PX}$ = 32 Hz, 1 P, P^B), 11.6 (m, $^1J_{PM\text{-}PX}$ = 441 Hz, $^1J_{PM\text{-}PB}$ = 348 Hz, $^2J_{PM\text{-}PQ}$ = 76 Hz, $^2J_{PM\text{-}PA}$ = 12 Hz, 1 P, P^M), –35.9 (m, $^1J_{PQ\text{-}PA}$ = 484 Hz, $^1J_{PQ\text{-}PB}$ = 368 Hz, $^2J_{PQ\text{-}PM}$ = 76 Hz, $^2J_{PQ\text{-}PX}$ = 4 Hz, 1 P, P^Q), –106.4 (m, $^1J_{PX\text{-}PA}$ = 490 Hz, $^1J_{PX\text{-}PM}$ = 441 Hz, $^2J_{PX\text{-}PB}$ = 32 Hz, $^2J_{PX\text{-}PQ}$ = 4 Hz, 1 P, P^X)

*[Cp*Fe{η^4-P_4(1-IMe_4)(4-Me)}][OTf] (**4**)*

A (306 mg, 0.6 mmol, 1 eq.) was dissolved in 10 mL of THF and IMe_4 (224 mg, 1.8 mmol, 3 eq.), dissolved in 20 mL of THF, was added very slowly at – 80 °C to afford a color change from brownish red to dark brown. The solution was stirred and allowed to slowly reach room temperature over the course of 2 h upon which the solvent was removed *in vacuo*. The resulting dark brown oily solid containing [Cp*Fe{η^4-P_4(1-IMe_4)(4-Me)}][OTf] (**4**) was redissolved in 15 mL of MeCN, stirred for 5 min and extracted with *n*-hexane (5x50 mL). The dark brown *n*-hexane fractions were combined, and the solvent removed to provide crude **4** as brown powder. Recrystallization from a concentrated *n*-hexane solution at –30 °C gave **4** as analytically pure microcrystalline substance. Crystals of **4** suitable for single crystal X-ray analysis could be obtained by slowly evaporating solvent from concentrated benzene solutions.

Yield: crude: 142 mg (0.31 mmol, 52%)

crystalline: 45 mg (0.1 mmol, 17%)

LIFDI MS (toluene): *m/z* (%) = 125.11 (100, $[IMe_4H]^+$), complete decomposition under mass spectrometric conditions.

NMR (C_6D_6, 298 K): **^{1}H**: δ/ppm = 0.85 (s, 3 H, C(N(CH_3)C($C\underline{H}_3$))$_2$), 1.11 (s, 3 H, C(N(CH_3)C($C\underline{H}_3$))$_2$), 1.53 (dd, $^2J_{H\text{-}PM}$ = 7 Hz, $^3J_{H\text{-}PA}$ = 13 Hz, 3 H, P-$C\underline{H}_3$), 1.97 (s, 15 H, Cp*), 2.94 (s, 3 H, C(N($C\underline{H}_3$)C(CH_3))$_2$), 3.18 (s, 3 H, C(N($C\underline{H}_3$)C(CH_3))$_2$)

^{31}P{^{1}H}: δ/ppm = 106.5 (ddd, $^1J_{PA\text{-}PX}$ = 410 Hz, $^1J_{PA\text{-}PM}$ = 388 Hz, $^2J_{PA\text{-}PQ}$ = 44 Hz, 1 P, P^A), 32.7 (ddd, $^1J_{PM\text{-}PA}$ = 388 Hz, $^2J_{PM\text{-}PX}$ = 18 Hz, $^3J_{PM\text{-}PQ}$ = 41 Hz, 1 P, P^M), 0.1 (dt, $^1J_{PQ\text{-}PX}$ = 436 Hz, $^2J_{PQ\text{-}PA}$ = 44 Hz, $^3J_{PQ\text{-}PM}$ = 41 Hz, 1 P, P^Q), –77.7 (ddd, $^1J_{PX\text{-}PQ}$ = 436 Hz, $^1J_{PX\text{-}PA}$ = 410 Hz, $^2J_{PX\text{-}PM}$ = 18 Hz, 1 P, P^X)

^{31}P: δ/ppm = 106.5 (m, $^1J_{PA\text{-}PX}$ = 410 Hz, $^1J_{PA\text{-}PM}$ = 388 Hz, $^2J_{PA\text{-}PQ}$ = 44 Hz, $^3J_{PA\text{-}H}$ = 13 Hz, 1 P, P^A), 32.7 (m, $^1J_{PM\text{-}PA}$ = 388 Hz, $^2J_{PM\text{-}PX}$ = 18 Hz, $^3J_{PM\text{-}PQ}$ = 41 Hz, $^2J_{PM\text{-}H}$ = 7 Hz, 1 P, P^M), 0.1 (dt, $^1J_{PQ\text{-}PX}$ = 436 Hz, $^2J_{PQ\text{-}PA}$ = 44 Hz, $^3J_{PQ\text{-}PM}$ = 41 Hz, 1 P, P^Q), –77.7 (ddd, $^1J_{PX\text{-}PQ}$ = 436 Hz, $^1J_{PX\text{-}PA}$ = 410 Hz, $^2J_{PX\text{-}PM}$ = 18 Hz, 1 P, P^X)

*[Cp*Fe{η⁴-P₅(1-IMe₄P)(1-Me)}][OTf] (**5**)*

A (102 mg, 0.2 mmol, 1 eq.) was dissolved in 6 mL of THF and IMe_4 (50 mg, 0.4 mmol, 2 eq.), dissolved in 15 mL of THF, was added very slowly at – 80 °C to afford a color change from brownish red to dark brown. The solution was stirred for 1 h, left to warm up to room temperature, and then concentrated to a volume of 2 mL. Addition of 10 mL of *n*-hexane afforded precipitation of colorless and brown solids. The supernatant, containing [Cp*Fe{η^4-P_5(1-IMe_4P)(1-Me)}][OTf] (**5**), was filtered and the solvent removed *in vacuo*. Dark green crystals of **5** could be obtained by storing a concentrated solution (toluene/*n*-hexane, 2:1) at -30 °C for one week.

Yield: 46 mg

LIFDI MS (toluene): *m/z* (%) = 516.06 (15, $[Cp^*Fe(\eta^4\text{-}P_5MePIMe_4)]^+$), 125 (100, $[IMe_4H]^+$)

NMR (C_6D_6, 298 K):

^{1}H: δ/ppm = 1.54 (s, 6 H, $C(N(CH_3)C(C\underline{H}_3))_2$), 1.69 (s, 15 H, Cp*), 2.35 (m, $^2J_{H\text{-}P}$ = 7 Hz, $^3J_{H\text{-}P}$ = 10 Hz, $^3J_{H\text{-}P}$ = 5 Hz, 3 H, $P_5C\underline{H}_3$), 3.30 (s, 6 H, $C(N(C\underline{H}_3)C(CH_3))_2$)

^{31}P{^{1}H}: δ/ppm = 140.4 (m, $^1J_{PA\text{-}PN}$ = 448 Hz, $^1J_{PA\text{-}PX/X'}$ = 342/339 Hz, $^2J_{PA\text{-}PM/M'}$ = 14/14 Hz, 1 P, P^A), 18.6 ($^1J_{PM/M'\text{-}PX/X'}$ = 417/414 Hz, $^1J_{PM\text{-}M'}$ = 373 Hz, $^2J_{PM/M'\text{-}X'/X}$ = 24/22 Hz, $^2J_{PM/M'\text{-}PA}$ = 14/14 Hz, 2 P, $P^{M/M'}$), 14.7 ($^1J_{PN\text{-}PA}$ = 448 Hz, $^2J_{PN\text{-}PX/X'}$ = 36/35 Hz, 1 P, P^N), -25.3 ($^1J_{PX/X'\text{-}PM/M'}$ = 417/414 Hz, $^1J_{PX/X'\text{-}PA}$ = 342/339 Hz, $^2J_{PX/X'\text{-}PN}$ = 36/35 Hz, $^2J_{PX/X'\text{-}PM'/M}$ = 24/22 Hz, 2 P, $P^{X/X'}$)

^{31}P: δ/ppm = 140.5 (m, $^1J_{PA\text{-}PN}$ = 448 Hz, $^1J_{PA\text{-}PX/X'}$ = 341/339 Hz, $^2J_{PA\text{-}PM/M'}$ = 15/8 Hz, $^2J_{PA\text{-}H}$ = 7 Hz, 1 P, P^A), 18.6 ($^1J_{PM/M'\text{-}PX/X'}$ = 419/412 Hz, $^1J_{PM\text{-}M'}$ = 373 Hz, $^2J_{PM/M'\text{-}X'/X}$ = 25/20 Hz, $^2J_{PM/M'\text{-}PA}$ = 15/8 Hz, 2 P, $P^{M/M'}$), 14.7 ($^1J_{PN\text{-}PA}$ = 448 Hz, $^2J_{PN\text{-}PX/X'}$ = 37/35 Hz, $^3J_{PN\text{-}H}$ = 10 Hz, 1 P, P^N), -25.3 ($^1J_{PX/X'\text{-}PM/M'}$ = 419/412 Hz, $^1J_{PX/X'\text{-}PA}$ = 341/339 Hz, $^2J_{PX/X'\text{-}PN}$ = 37/35 Hz, $^2J_{PX/X'\text{-}PM'/M}$ = 25/20 Hz, $^3J_{PM/M'\text{-}H}$ = 5 Hz, 2 P, $P^{X/X'}$)

*[Cp*Fe{η^4-P_5(1-NHO)(1-Me)}][OTf] (**6a**) and [Cp*Fe{η^4-P_5(1-NHO)(2-Me)}][OTf] (**6b**)*

A (102 mg, 0.2 mmol, 1 eq.) was dissolved in 4 mL of *o*-DFB and $IDippCH_2$ (81 mg, 0.2 mmol, 1 eq.), dissolved in 4 mL of o-DFB, was added at room temperature to afford a color change from brownish red to a greenish brown. The resulting solution was concentrated to 4 mL and directly layered with 40 mL of *n*-pentane. Storage at -30 °C for several days afforded brown crystals of both co-crystallized isomers [Cp*Fe{η^4-P_5(1-NHO)(1-Me)}][OTf] (**6a**) and [Cp*Fe{η^4-P_5(1-NHO)(2-Me)}][OTf] (**6b**) in X-ray quality. Attempts to selectively prepare either one of these isomers however failed due to equilibration in solution.

Yield:	135 mg (0.148 mmol, 74%)
Elemental analysis:	calc. (%) for $[C_{40}H_{56}N_2O_3F_3P_5SFe]\cdot(C_6H_4F_2)_{1.7}$: C: 54.48 H: 5.72 N: 2.53 S: 2.90
	found (%): C: 54.91 H: 6.15 N: 2.74 S: 3.23
ESI(+) MS (*o*-DFB):	*m/z* (%) = 763.1 (80, $[Cp^*Fe(\eta^4\text{-}P_5CH_3NHO)]^+$), 403.3 (100, $[IDippCH_3]^+$)
NMR (CD_2Cl_2, 298 K):	**^{1}H**: δ/ppm = 1.15 – 1.44 (several overlapping multiplets, -CH($C\underline{H}_3$)$_2$), 1.49 (s, 15 H, Cp*(**6a**), 1.60 (s, 15 H, Cp*(**6b**)), 2.05 – 2.40 (several overlapping multiplets, IDippC$\underline{H}_2$, $P_5C\underline{H}_3$), 7.4 – 7.84 (several overlapping multiplets, C(N(Dipp)C$\underline{H}$)$_2$, -2,6-(^{i}Pr)-$C_6\underline{H}_3$)
	^{31}P{^{1}H}: δ/ppm = 88.8 (m, 1 P, P^A (**6a**)), 36.4 (m, 2 P, $P^{M/M'}$ (**6a**)), 35.0 – 27.0 (complex multiplet, 3 P, $P^{A/B/C}$ (**6b**)), 7.2 (m, 1 P, P^M (**6b**)), –93.9 (m, 2 P, $P^{X/X'}$ (**6a**)), –110.5 (m, 1 P, P^X (**6b**)
	^{31}P: δ/ppm = 88.8 (m, 1 P, P^A (**6a**)), 36.4 (m, 2 P, $P^{M/M'}$ (**6a**)), 35.0 – 27.0 (complex multiplet (broadening due to unresolved $^nJ_{P\text{-}H}$ coupling), 3 P, $P^{A/B/C}$ (**6b**)), 7.2 (m, 1 P, P^M (**6b**)), –93.9 (m, 2 P, $P^{X/X'}$ (**6a**)), –110.5 (m, 1 P, P^X (**6b**)
	^{19}F{^{1}H}: δ/ppm = –78.7 (s, $[SO_3C\underline{F}_3]^-$)

Simulation of the $^{31}P\{^1H\}$ as well as the ^{31}P NMR spectrum of the mixture of **6a**/**b** could not be obtained satisfactorily due to the overlap of four signals in the range of 27 – 38 ppm (vide infra).

*[{Cp*Fe}$_2${μ_2,$\eta^{4:3:1}$-$P_{10}Me_2$(IDippN)}][OTf] (**7**)*

IDippNH (81 mg, 0.2 mmol, 1 eq.) dissolved in 2 mL of *o*-DFB was added to **A** (102 mg, 0.2 mmol, 1 eq.) dissolved in 2 mL of o-DFB at room temperature affording a color change to red. The solution was stirred for 1 h. The solvent was then removed and the resulting brown solid dissolved in 1 mL of CH_2Cl_2. Addition of 20 mL of *n*-pentane afforded precipitation of a dark solid. The supernatant was decanted, the solid washed with 10 mL of *n*-pentane and the solid then dried under reduced pressure. After dissolving it in 3 mL of *o*-DFB it was layered with 40 mL of *n*-pentane and stored at room temperature for several days. A few single crystals of the product [{Cp*Fe}$_2${μ_2,$\eta^{4:3:1}$-$P_{10}Me_2$(IDippN)}][OTf] (**7**) could be obtained from this mixture, but isolation of bulk **7** as analytically pure product was not possible within the time frame of this thesis.

*[Cp*Fe{η^4-P_5(1-NIDipp)(1-Me)}] (**7**$_{INT}$)*

A (102 mg, 0.2 mmol, 1 eq.) was dissolved in 4 mL of *o*-DFB and added to IDippNH (161 mg, 0.4 mmol, 2 eq.) dissolved in 4 mL of *o*-DFB at –30 °C. After a rapid color change to greenish brown the solution was stirred for 1 h and left to warm up to room temperature. The solvent was removed under reduced pressure and the residue extracted with 6 mL of *n*-hexane. After filtration (a colorless solid remained) the dark greenish brown solution was concentrated to 2 mL and stored at –30 °C over night affording [Cp*Fe{η^4-P_5(1-NIDipp)(1-Me)}] (**7**$_{INT}$) as brown plate shaped crystals of X-ray quality. After decanting the solvent and drying under reduced pressure, **7**$_{INT}$ could isolated as analytically pure compound.

Yield:	116 mg (0.15 mmol, 75%)
Elemental analysis:	calc. (%) for [$C_{38}H_{54}N_3P_5Fe$]: C: 59.77 H: 7.13 N: 5.50
	found (%): C: 60.04 H: 7.44 N: 5.38
LIFDI MS (tol):	*m/z* (%) = 763.2 (100, [Cp*Fe(η^4-P_5CH_3NIDipp)]$^+$)
NMR (C_6D_6, 298 K):	**^{1}H**: δ/ppm = 0.97 (d, $^3J_{H-H}$ = 7 Hz, 12 H, -CH(C<u>H</u>$_3$)$_2$) , 1.47 (d, $^3J_{H-H}$ = 7 Hz, 12 H, -CH(C<u>H</u>$_3$)$_2$), 1.55 (s, 15 H, Cp*), 1.79 (dt, $^2J_{H-P}$ = 9 Hz, $^3J_{H-P}$ = 6 Hz, 3 H, P_5CH_3), 2.63 (sept, $^3J_{H-H}$ = 7 Hz, 4 H, -C<u>H</u>(CH$_3$)$_2$), 5.76 (s, 2 H, C(N(Dipp)C<u>H</u>)$_2$), 7.13 (m, 4 H, -2,6-(^{i}Pr)-C$_6$<u>H</u>$_3$(m), 7.26 (m, 2 H, -2,6-(^{i}Pr)-C$_6$<u>H</u>$_3$(p)
	^{31}P{^{1}H}: δ/ppm = 89.7 (m, $^1J_{PA-PX/X'}$ = 404/402 Hz, $^2J_{PA-PM/M'}$ = 19/14 Hz, 1 P, P^A), 29.8 (m, $^1J_{PM/M'-PX/X'}$ = 431/429 Hz, $^1J_{PM-PM'}$ = 381 Hz, $^2J_{PM/M'-PX'/X}$ = –32/–30 Hz, $^2J_{PM/M'-PA}$ = 19/14 Hz, 2 P, $P^{M/M'}$), -20.5 (m, $^1J_{PX/X'-PM/M'}$ = 431/429 Hz, $^1J_{PX/X'-PA}$ = 404/402 Hz, $^2J_{PX/X'-PM'/M}$ = –32/–30 Hz $^2J_{PX-PX'}$ = 12 Hz, 2 P, $P^{X/X'}$)
	^{31}P: δ/ppm = 89.7 (m, $^1J_{PA-PX/X'}$ = 404/402 Hz, $^2J_{PA-PM/M'}$ = 19/14 Hz, $^2J_{PA-H}$ = 9 Hz, 1 P, P^A), 29.8 (m, $^1J_{PM/M'-PX/X'}$ = 431/429 Hz, $^1J_{PM-PM'}$ = 381 Hz, $^2J_{PM/M'-PX'/X}$ = –32/–30 Hz, $^2J_{PM/M'-PA}$ = 19/14 Hz, 2 P, $P^{M/M'}$), -20.5 (m, $^1J_{PX/X'-PM/M'}$ = 431/429 Hz, $^1J_{PX/X'-PA}$ = 404/402 Hz, $^2J_{PX/X'-PM'/M}$ = –32/–30 Hz $^2J_{PX-PX'}$ = 12 Hz, $^3J_{PA-H}$ = 6 Hz, 2 P, $P^{X/X'}$)

*[{Cp*Fe}$_2${μ_2,$\eta^{4:1:1:1}$-$P_{11}Me_2$(IDipp)}][OTf] (**8**)*

IDippPH (84 mg, 0.2 mmol, 1 eq.) dissolved in 3 mL of *o*-DFB was added to **A** (102 mg, 0.2 mmol, 1 eq.) dissolved in 3 mL of *o*-DFB at room temperature affording a color change to dark brown. The solution was stirred for 3 h and allowed to reach room temperature. The solvent was then removed and the resulting brown solid washed with toluene (5 mL) once. After drying the solid, CH_2Cl_2 (4 mL) was added, layered with 40 mL of *n*-hexane and stored at –30 °C for eleven days. A few single crystals of the product [{Cp*Fe}$_2${μ_2,$\eta^{4:1:1:1}$-$P_{11}Me_2$(IDipp)}][OTf] (**8**) could be obtained from this mixture, but isolation of bulk **8** as analytically pure product was not possible within the time frame of this thesis.

11.5.2. X-ray Crystallographic Data

General Considerations

The crystallographic data for all synthesised compounds was collected on an XtaLAB Synergy R, DW System (Rigaku) with a HyPix-Arc 150 detector using Cu-K_α radiation from a rotating anode (**3a**, **4**, **6a**/**b**, **7**, **7$_{INT}$**, **8**), on a SuperNova diffractometer (Rigaku) with a Titan^{S2} detector using a standard Cu–K_α (**A**, **2**, **3b**, **4$_{INT2}$,**) sealed tube microfocus source, or an Xcalibur Gemini Ultra diffractometer with a Titan^{S2} detector using a standard Cu-K_α sealed tube (**1**). Data reduction and absorption correction were performed with the CrysAlisPro software package.[40] Structure solution and refinement was conducted in Olex2 (1.5-alpha)[41] with ShelXT[42] (solution) and ShelXL-2014[43] (least squares refinement (F^2)). All non-H atoms were refined with anisotropic displacement parameters and H atoms were treated as riding models with isotropic displacement parameters and fixed C–H bond lengths (sp^3: 0.96 (CH_3), 0.97 (CH_2); sp^2: 0.93 (CH)). Visualisation of the crystal structures was performed with Olex2 (1.5-alpha).[41]

*Table S 1: X-ray crystallographic data on **A**, **1**, **2** and **3a**.*

Compound	A	1	2	3a
Empirical formula	$C_{12}H_{18}O_3F_3P_5SFe$	$C_{39}H_{54}N_2O_3F_3P_5SFe$	$C_{37}H_{55}NO_3F_4P_5SFe$	$C_{27}H_{46}N_2O_4F_3P_5SFe$
Formula weight	510.02	898.60	880.58	762.42
Temperature/K	122.97(13)	123.01(10)	122.95(14)	100.01(10)
Crystal system	monoclinic	orthorhombic	triclinic	triclinic
Space group	$P2_1/n$	$Pnma$	$P\bar{1}$	$P\bar{1}$
a/Å	9.1509(2)	25.9001(17)	10.1565(4)	8.3380(2)
b/Å	17.0741(3)	16.7754(10)	13.5001(4)	12.3540(3)
c/Å	12.5903(2)	10.2972(7)	17.0838(6)	18.5372(7)
α/°	90	90	67.137(3)	108.186(3)
β/°	90.771(2)	90	73.999(3)	94.641(3)
γ/°	90	90	83.156(3)	100.417(2)
Volume/Å3	1966.97(6)	4474.0(5)	2074.58(14)	1764.81(10)
Z	4	4	2	2
ρcalcg/cm3	1.722	1.334	1.410	1.435
μ/mm-1	11.361	5.245	5.670	6.560
F(000)	1032.0	1880.0	922.0	796.0
Crystal size/mm3	0.34 × 0.17 × 0.13	0.34 × 0.09 × 0.05	0.53 × 0.24 × 0.09	0.237 × 0.104 × 0.03
Radiation	Cu Kα (λ = 1.54184)	Cu Kα (λ = 1.54184)	Cu Kα (λ = 1.54184)	Cu Kα (λ = 1.54184)
2Θ range for data collection/°	8.726 to 142.854	8.626 to 134.19	7.31 to 133.648	5.072 to 145.484
Index ranges	-10 ≤ h ≤ 10, -19 ≤ k ≤ 20, -14 ≤ l ≤ 15	-30 ≤ h ≤ 30, -19 ≤ k ≤ 8, -12 ≤ l ≤ 12	-12 ≤ h ≤ 12, -13 ≤ k ≤ 16, -20 ≤ l ≤ 20	-10 ≤ h ≤ 10, -11 ≤ k ≤ 15, -22 ≤ l ≤ 22
Reflections collected	26114	25571	32114	23229
Independent reflections	3510 [Rint = 0.1523, Rsigma = 0.0570]	4117 [Rint = 0.0760, Rsigma = 0.0423]	7312 [Rint = 0.0637, Rsigma = 0.0409]	6634 [Rint = 0.0445, Rsigma = 0.0339]
Data/restraints/parameters	3510/0/233	4117/60/314	7312/143/522	6634/231/569
Goodness-of-fit on F2	1.080	1.075	1.024	1.053
Final R indexes [I>=2σ (I)]	R1 = 0.0551, wR2 = 0.1437	R1 = 0.0575, wR2 = 0.1528	R1 = 0.0463, wR2 = 0.1159	R1 = 0.0783, wR2 = 0.2074
Final R indexes [all data]	R1 = 0.0624, wR2 = 0.1611	R1 = 0.0679, wR2 = 0.1618	R1 = 0.0509, wR2 = 0.1203	R1 = 0.0901, wR2 = 0.2143
Largest diff. peak/hole / e Å-3	0.88/-0.98	0.61/-0.57	0.52/-0.44	1.00/-0.75

*Table S 2: X-ray crystallographic data on **3b**, **4**, **4$_{INT2}$** and **5**.*

Compound	3b	4	4_{INT2}	5
Empirical formula	$C_{23}H_{38}N_2O_3F_3P_5SFe$	$C_{18}H_{30}N_2P_4Fe$	$C_{26}H_{42}N_4O_3F_3P_5SFe$	$C_{25}H_{38}N_2P_6Fe$
Formula weight	690.31	454.17	758.39	608.24
Temperature/K	122.96(16)	122.99(10)	122.96(14)	100.01(10)
Crystal system	monoclinic	monoclinic	triclinic	monoclinic
Space group	$P2_1$	$P2_1/c$	$P\bar{1}$	$P2_1/c$
a/Å	13.2702(3)	16.5964(3)	8.7342(2)	14.46230(10)
b/Å	8.4823(2)	8.1636(2)	11.9121(3)	15.12650(10)
c/Å	14.8511(4)	16.0457(3)	17.9581(8)	13.58670(10)
α/°	90	90	80.410(3)	90
β/°	110.969(3)	92.071(2)	77.321(3)	92.5620(10)
γ/°	90	90	77.526(2)	90
Volume/Å3	1560.96(7)	2172.55(8)	1765.83(10)	2969.31(4)
Z	2	4	2	4
ρcalcg/cm3	1.469	1.389	1.426	1.361
μ/mm-1	7.331	8.378	6.550	7.261
F(000)	716.0	952.0	788.0	1272.0
Crystal size/mm3	0.13 × 0.1 × 0.06	0.1 × 0.05 × 0.04	0.319 × 0.121 × 0.029	0.169 × 0.116 × 0.032
Radiation	Cu Kα (λ = 1.54184)	Cu Kα (λ = 1.54184)	Cu Kα (λ = 1.54184)	Cu Kα (λ = 1.54184)
2Θ range for data collection/°	7.134 to 133.184	5.328 to 149.67	7.662 to 132.978	6.118 to 149.676
Index ranges	-15 ≤ h ≤ 15, -10 ≤ k ≤ 8, -17 ≤ l ≤ 17	-20 ≤ h ≤ 19, -9 ≤ k ≤ 10, -15 ≤ l ≤ 19	-8 ≤ h ≤ 10, -14 ≤ k ≤ 14, -21 ≤ l ≤ 21	-17 ≤ h ≤ 18, -18 ≤ k ≤ 13, -15 ≤ l ≤ 16
Reflections collected	18606	14586	25241	19803
Independent reflections	4354 [Rint = 0.0389, Rsigma = 0.0271]	4349 [Rint = 0.0405, Rsigma = 0.0327]	6217 [Rint = 0.0425, Rsigma = 0.0343]	5942 [Rint = 0.0257, Rsigma = 0.0258]
Data/restraints/parameters	4354/359/533	4349/0/236	6217/41/449	5942/0/254
Goodness-of-fit on F2	1.042	1.040	1.034	1.093
Final R indexes [I>=2σ (I)]	R1 = 0.0492, wR2 = 0.1301	R1 = 0.0462, wR2 = 0.1231	R1 = 0.0412, wR2 = 0.1030	R1 = 0.0328, wR2 = 0.0908
Final R indexes [all data]	R1 = 0.0557, wR2 = 0.1377	R1 = 0.0509, wR2 = 0.1267	R1 = 0.0464, wR2 = 0.1078	R1 = 0.0368, wR2 = 0.0929
Largest diff. peak/hole / e Å-3	0.59/-0.47	1.19/-0.70	0.60/-0.44	0.36/-0.30
Flack parameter	0.521(18)	/	/	/

*Table S 3: X-ray crystallographic data on **6**, **7**, **8** and **7$_{INT}$**.*

Compound	**6**	**7**	**8**	**7$_{INT}$ (preliminary)**
Empirical formula	$C_{46}H_{60}F_5N_2O_3P_5SFe$	$C_{50}H_{72}F_3N_3O_3P_{10}SFe_2$	$C_{50.9}H_{73.7}N_2O_3F_3P_{11}SCl_{1.7}Fe_2$	$C_{38}H_{54}N_3P_5Fe$
Formula weight	1026.72	1273.56	1363.56	762.85
Temperature/K	123.00(10)	123.00(10)	123.00(10)	123.00(10)
Crystal system	triclinic	monoclinic	monoclinic	monoclinic
Space group	$P\bar{1}$	Pc	$P2_1/c$	$P2_1/c$
a/Å	11.8365(3)	16.71360(10)	16.9970(2)	29.2310(2)
b/Å	13.3304(5)	9.22940(10)	13.06670(10)	15.74720(10)
c/Å	17.3232(5)	21.34890(10)	29.9768(3)	35.6574(4)
α/°	80.796(3)	90	90	90
β/°	75.088(2)	110.0120(10)	104.4870(10)	92.0620(10)
γ/°	82.345(3)	90	90	90
Volume/Å3	2595.12(14)	3094.37(4)	6446.00(11)	16402.7(2)
Z	2	2	4	16
ρcalcg/cm3	1.314	1.367	1.405	1.236
μ/mm-1	4.647	6.931	7.555	5.005
F(000)	1072.0	1324.0	2824.0	6458.0
Crystal size/mm3	0.155 × 0.067 × 0.02	0.157 × 0.091 × 0.021	0.208 × 0.163 × 0.063	0.36 × 0.21 × 0.06
Radiation	Cu Kα (λ = 1.54184)	Cu Kα (λ = 1.54184)	Cu Kα (λ = 1.54184)	Cu Kα (λ = 1.54184)
2Θ range for data collection/°	5.326 to 150.712	5.628 to 149.2	5.37 to 148.022	4.96 to 145.152
Index ranges	-14 ≤ h ≤ 14, -16 ≤ k ≤ 16, -20 ≤ l ≤ 21	-20 ≤ h ≤ 20, -11 ≤ k ≤ 11, -25 ≤ l ≤ 18	-20 ≤ h ≤ 21, -8 ≤ k ≤ 15, -36 ≤ l ≤ 37	-35 ≤ h ≤ 25, -19 ≤ k ≤ 18, -43 ≤ l ≤ 43
Reflections collected	39422	64732	79034	158930
Independent reflections	10185 [Rint = 0.0500, Rsigma = 0.0401]	10535 [Rint = 0.0555, Rsigma = 0.0322]	12758 [Rint = 0.0494, Rsigma = 0.0311]	31189 [Rint = 0.0569, Rsigma = 0.0447]
Data/restraints/parameters	10185/36/638	10535/198/742	12758/97/807	31189/2067/2174
Goodness-of-fit on F2	1.093	1.173	1.043	1.046
Final R indexes [I>=2σ (I)]	R1 = 0.0777, wR2 = 0.2205	R1 = 0.0413, wR2 = 0.1192	R1 = 0.0440, wR2 = 0.1148	R1 = 0.1089, wR2 = 0.2894
Final R indexes [all data]	R1 = 0.0932, wR2 = 0.2335	R1 = 0.0429, wR2 = 0.1206	R1 = 0.0541, wR2 = 0.1199	R1 = 0.1381, wR2 = 0.3115
Largest diff. peak/hole / e Å-3	0.85/-1.01	0.37/-0.43	0.54/-0.45	1.29/-0.85
Flack parameter	/	-0.022(4)	/	/

*[Cp*Fe(η^5-P_5Me)][OTf] (**A**)*

Layering a concentrated solution of **A** in *o*-DFB with *n*-pentane leads to formation of red stick shaped crystals after one day of storage at room temperature. **A** crystallizes in the monoclinic space group $P2_1/n$ with one anion and one cation in the asymmetric unit, which is depicted in Figure S1.

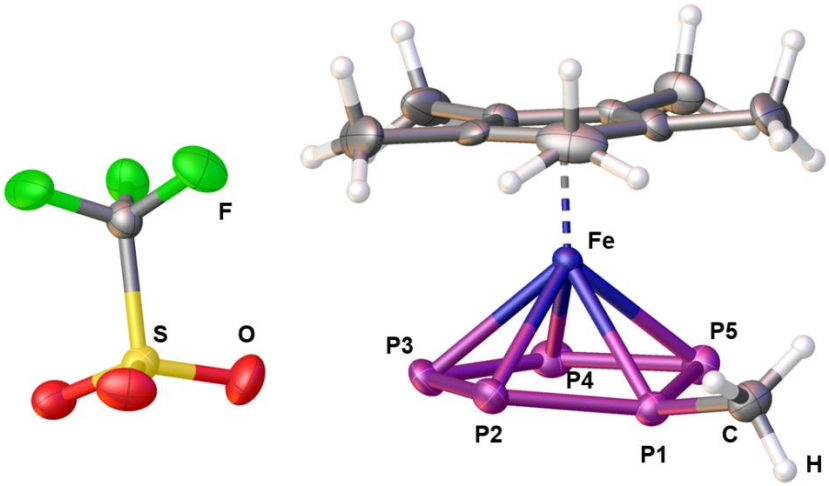

*Figure S 1: Solid state structure of **A**; Depicted is the asymmetric unit and ADPs (anisotropic displacement parameters) are drawn at the 50% probability level.*

*[Cp*Fe{η⁴-P₅(1-IDipp)(2-Me)}][OTf] (**1**)*

Layering a concentrated solution of **1** in *o*-DFB with *n*-pentane leads to formation of dark brown rod shaped crystals after one day of storage at room temperature. **1** crystallizes in the orthorhombic space group *P*nma with half an anion and half a cation in the asymmetric unit. The grown structure is depicted in Figure S2 and disorder has been treated with adequate restraints.

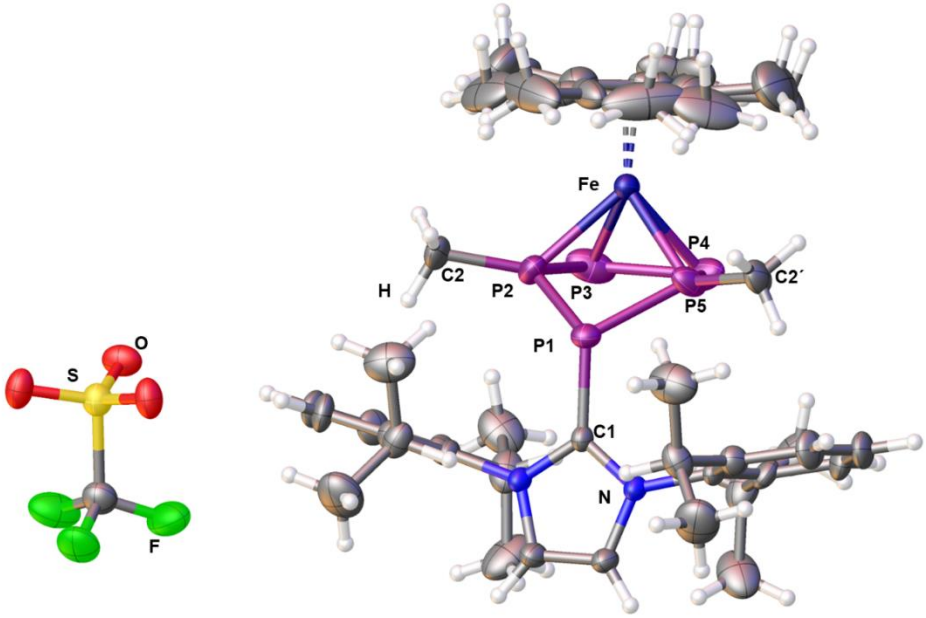

*Figure S 2: Solid state structure of **1**; Depicted are two asymmetric units and ADPs (anisotropic displacement parameters) are drawn at the 50% probability level.*

*[Cp*Fe{η⁴-P₅(1-^{Et}CAAC)(2-Me)}][OTf] (**2**)*

Layering a concentrated solution of **2** in *o*-DFB with *n*-pentane leads to formation of brown plate shaped crystals after one day of storage at room temperature. **2** crystallizes in the triclinic space group $P\bar{1}$ with one anion and one cation in the asymmetric unit, which is depicted in Figure S3. Disorder has been treated with adequate restraints.

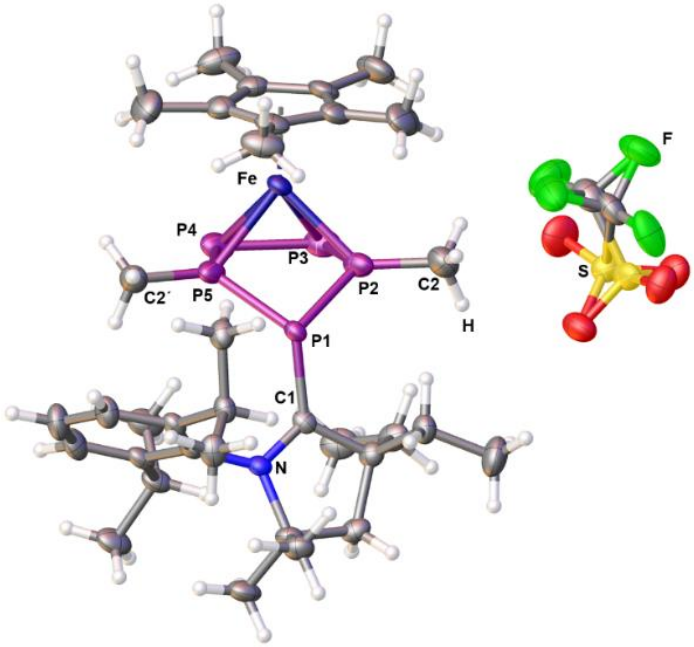

*Figure S 3: Solid state structure of **2**; Depicted is the asymmetric unit and ADPs (anisotropic displacement parameters) are drawn at the 50% probability level.*

*[Cp*Fe{η⁴-P₅(1- IⁱPr)(1-Me)}][OTf] (**3a**) and [Cp*Fe{η⁴-P₅(1- IⁱPr)(2-Me)}][OTf] (**3b**)*

Layering a concentrated solution of **3** in THF with *n*-pentane leads to formation of brown plate (**3a**) and block (**3b**) shaped crystals after one day of storage at room temperature. **3a** crystallizes in the triclinic space group $P\bar{1}$ with one anion and one cation as well as one THF molecule in the asymmetric unit, which is depicted in Figure S 4 (left). **3b** crystallizes in the monoclinic space group $P2_1$ with one cation and one anion in the asymmetric unit, which is depicted in Figure S4 (right). Notably, both compounds crystallize alongside each other and can only be separated by visual distinction. Disorder within both structures has been treated with adequate restraints.

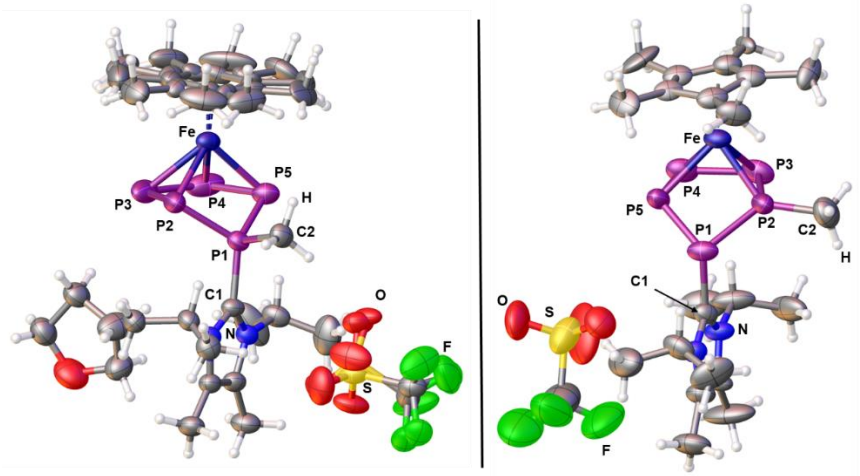

*Figure S 4: Solid state structure of **3a** (left) and **3b** (right); Depicted is the asymmetric unit of each compound and ADPs (anisotropic displacement parameters) are drawn at the 50% probability level.*

*[Cp*Fe{η⁴-P₄(1-IMe₄)(4-Me)}] (**4**)*

Small brownish red block shaped crystals of **4** can be obtained by slowly evaporating benzene from a concentrated solution. **4** crystallizes in the monoclinic space group $P2_1/c$ with one molecule in the asymmetric unit, which is shown in Figure S5.

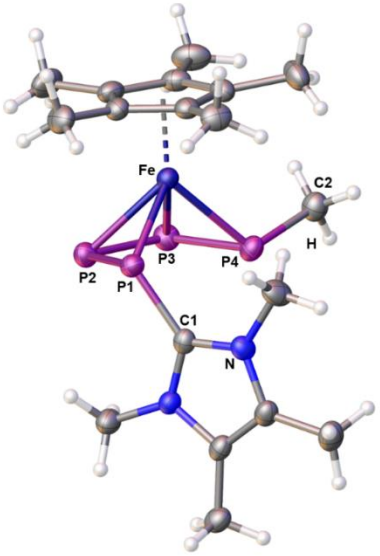

*Figure S 5: Solid state structure of **4**; Depicted is the asymmetric unit and ADPs (anisotropic displacement parameters) are drawn at the 50% probability level.*

*[Cp*Fe{η⁴-P₅(1-IMe₄)(1-Me)(5-IMe₄)}][OTf] (**4**$_{INT2}$)*

Few single crystals of **4**$_{INT2}$ formed upon layering a concentrated solution in THF with *n*-pentane at –30 °C and storage for one day. **4**$_{INT2}$ crystallizes in the triclinic space group $P\bar{1}$ with one cation and one anion in the asymmetric unit, which is shown in Figure S6. Disorder within the anion has been treated with adequate restraints.

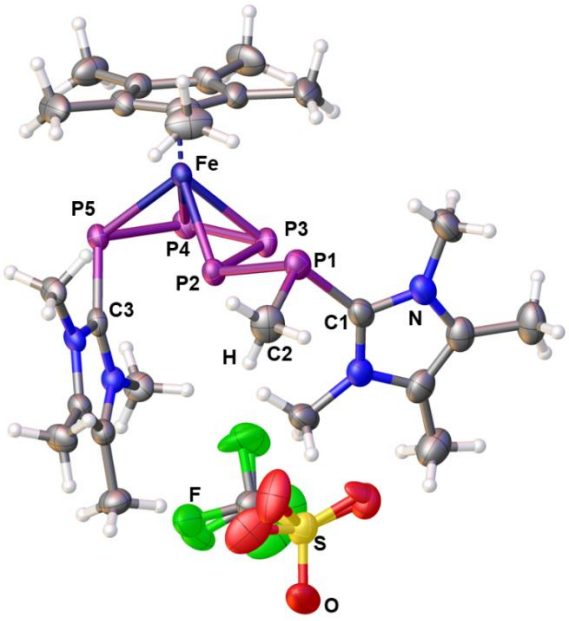

*Figure S 6: Solid state structure of **4**$_{INT2}$; Depicted is the asymmetric unit and ADPs (anisotropic displacement parameters) are drawn at the 50% probability level.*

*[Cp*Fe{η⁴-P₅(1-IMe₄P)(1-Me)}] (**5**)*

5 could be obtained as dark green plate shaped crystals by storing a concentrated solution (toluene/*n*-hexane, 2:1) at –30 °C for one week. **5** crystallizes in the monoclinic space group $P2_1/c$ with one molecule and one toluene in the asymmetric unit, which is displayed in Figure S7. The toluene molecule has been treated with a solvent mask.

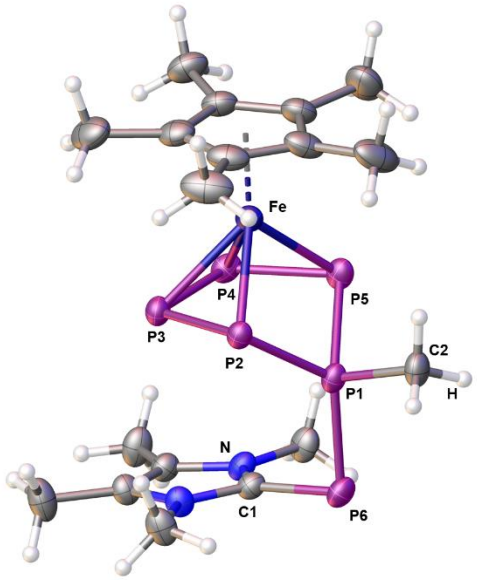

*Figure S 7: Solid state structure of **5**; Depicted is the asymmetric unit and ADPs (anisotropic displacement parameters) are drawn at the 50% probability level.*

*[Cp*Fe{η⁴-P₅(1-NHO)(1-Me)}][OTf] (**6a**) and [Cp*Fe{η⁴-P₅(1-NHO)(2-Me)}][OTf] (**6b**)*

Layering a concentrated solution of **6** in *o*-DFB with *n*-pentane leads to formation of brown plate shaped crystals after several days of storage at room temperature. **6a** and **6b** co-crystallize in the triclinic space group $P\bar{1}$ with one anion and one cation as well as one molecule of *o*-DFB in the asymmetric unit, which is depicted in Figure S8. Disorder has been treated with adequate restraints.

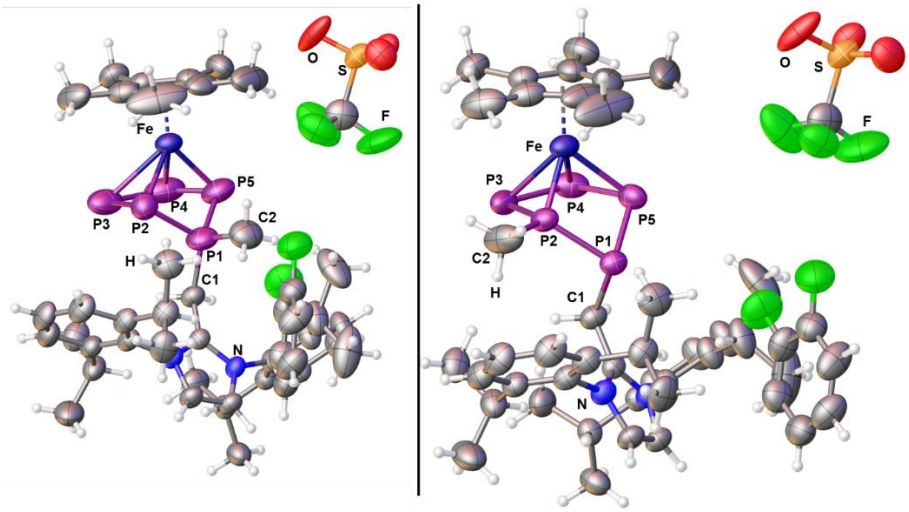

*Figure S 8: Solid state structure of **6a** (left) and **6b** (right); Depicted is the asymmetric unit in which both compounds appear as positionally disordered and ADPs (anisotropic displacement parameters) are drawn at the 50% probability level.*

*[{Cp*Fe}$_2${μ_2,$\eta^{4:3:1}$-$P_{10}Me_2$(IDippN)}][OTf] (**7**)*

Layering a concentrated solution of **7** in CH_2Cl_2 with *n*-pentane leads to formation of brown plate shaped crystals after several days of storage at room temperature. **7** crystallizes in the monoclinic space group *Pc* with one cation and one anion in the asymmetric unit, which is shown in Figure S9. Disorder has been treated with adequate restraints.

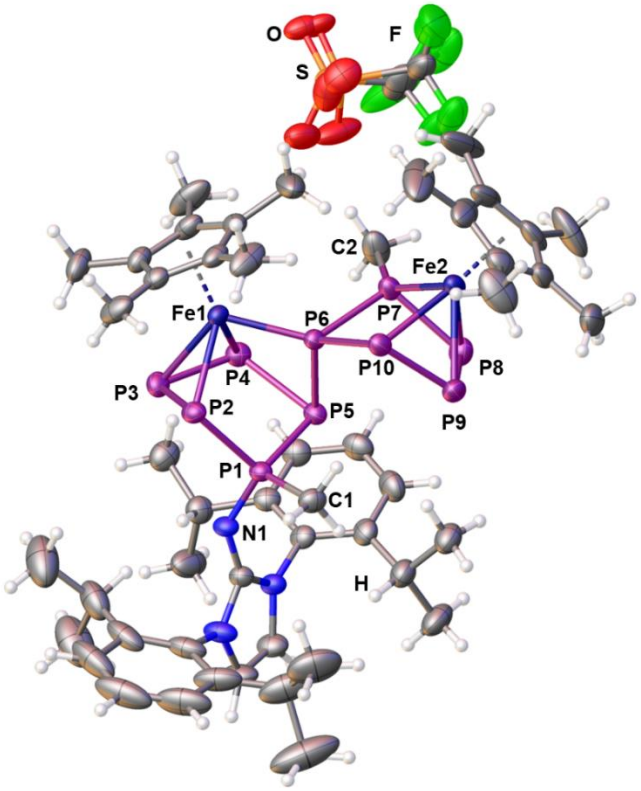

*Figure S 9: Solid state structure of **7**; Depicted is the asymmetric unit and ADPs (anisotropic displacement parameters) are drawn at the 50% probability level.*

*[Cp*Fe{η⁴-P₅(1-IDippN)(1-Me)}] (**7**$_{INT}$)*

7$_{INT}$ crystallizes upon slowly evaporating *n*-hexane from its concentrated solutions and forms dark brownish green plate shaped crystals. While these crystals visually appear as of sufficient quality for X-ray diffraction analysis, the crystal structure of **7**$_{INT}$ ($P2_1/c$) turns out to be incommensurably modulated in nature. In addition, all four molecules within the asymmetric unit are highly disordered, further impeding proper structural refinement. Thus, we herein only provide only a preliminary structure of **7**$_{INT}$, which reveals a 1,1-disubstituted *cyclo*-P_5(IDippN)(Me) ligand coordinated to the {Cp*Fe} moiety in η^4 fashion (Figure S10). The P1–N1 (1.594(5) Å) as well as the N1–C (1.286(7) Å) bond lengths are remarkable, as they may indicate double bond character for these bonds. In agreement, the P1–N1–C angle is enlarged drastically to 151.9(5)° from the expected ~120°. However, these values (from the non-disordered molecule in the asymmetric unit) must be considered carefully due to the preliminary nature of this solid state structure.

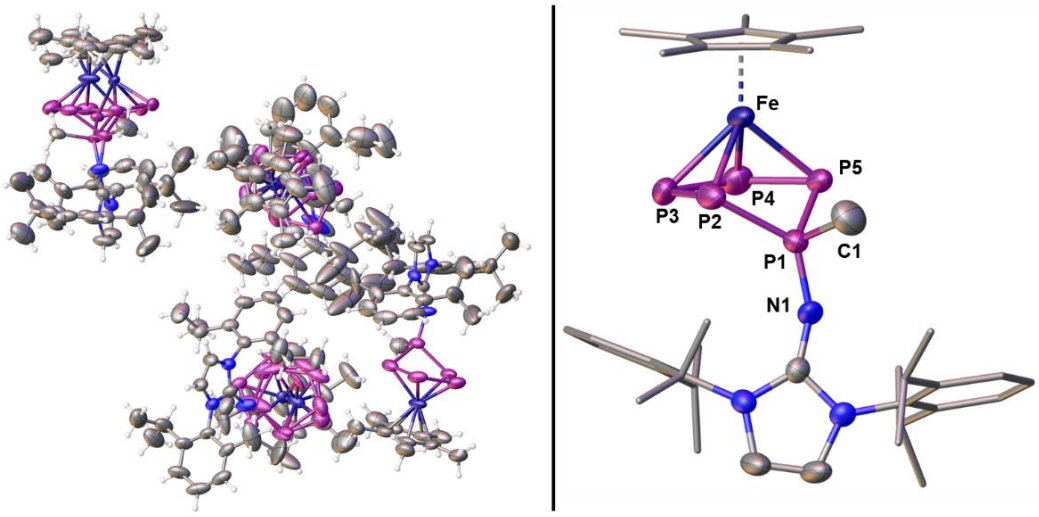

*Figure S 10: Solid state structure of **7**$_{INT}$; Depicted is the asymmetric unit (left) as well as the one non-disordered molecule within (right); ADPs (anisotropic displacement parameters) are drawn at the 50% probability level.*

*[{Cp*Fe}$_2${$\mu_2,\eta^{4:1:1:1}$-$P_{11}Me_2$(IDipp)}][OTf]* (***8***)

Layering a concentrated solution of **8** in CH_2Cl_2 with *n*-hexane leads to formation of brown plate shaped crystals after eleven days of storage at –30 °C. **8** crystallizes in the monoclinic space group $P2_1/c$ with one cation and one anion as well as a not fully occupied CH_2Cl_2 molecule in the asymmetric unit, which is shown in Figure S11. Disorder has been treated with adequate restraints.

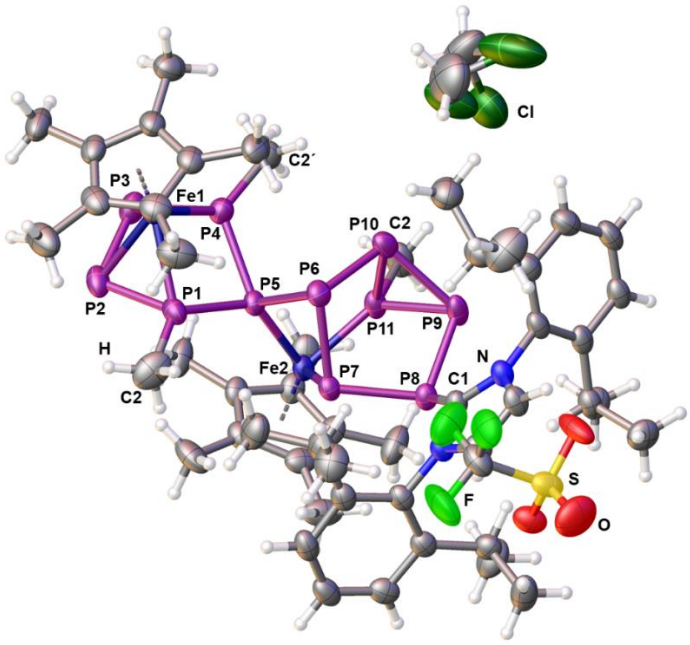

*Figure S 11: Solid state structure of **8**; Depicted is the asymmetric unit and ADPs (anisotropic displacement parameters) are drawn at the 50% probability level.*

11.5.3. NMR Spectroscopic Investigations

*[Cp*Fe(η^5-P_5Me)][OTf] (**A**)*

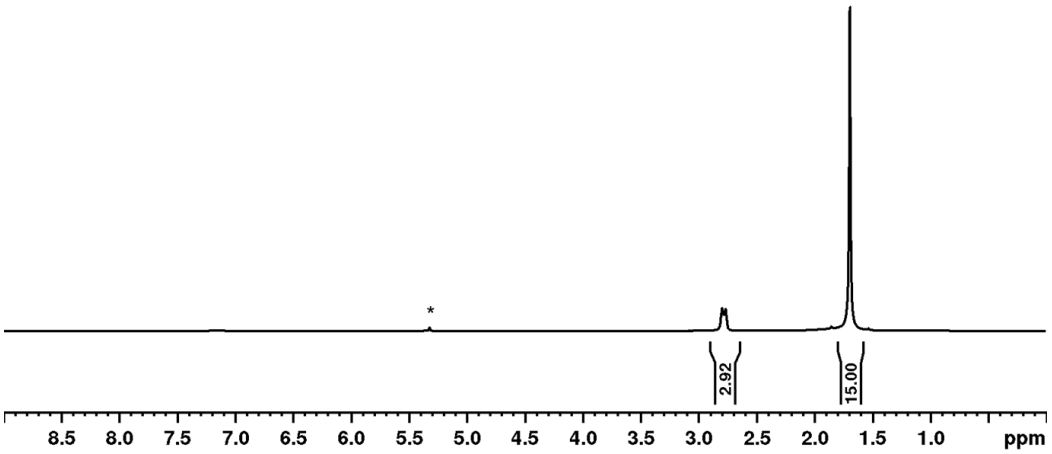

*Figure S 12: ^{1}H NMR spectrum of **A** in CD_2Cl_2 recorded at room temperature; * marks the signal of residual protonated solvent.*

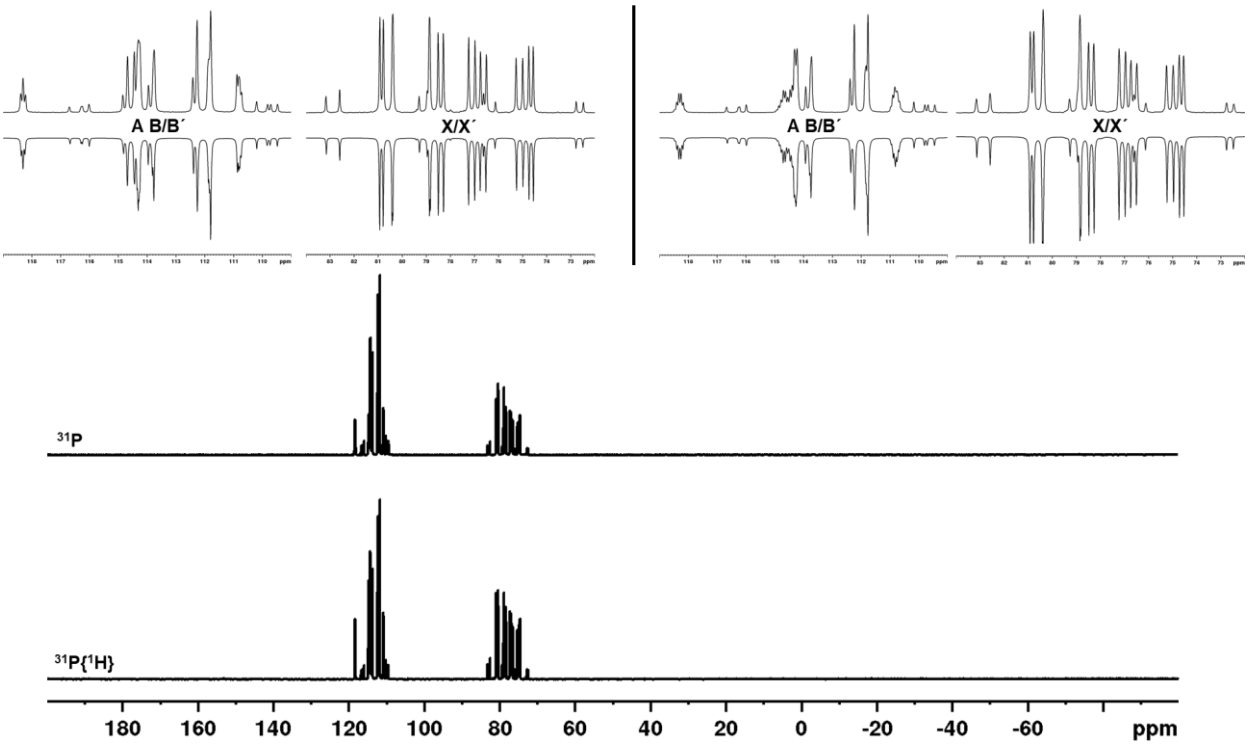

*Figure S 13: $^{31}P\{^1H\}$ (bottom) and ^{31}P (middle) NMR spectra of **A** in CD_2Cl_2 recorded at room temperature and the corresponding simulated $^{31}P\{^1H\}$ (left) and ^{31}P (right) NMR spectra (inverted).*

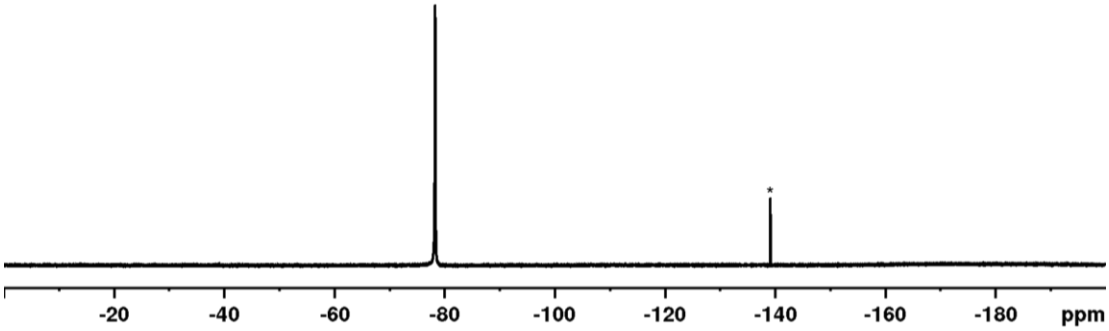

*Figure S 14: $^{19}F\{^{1}H\}$ NMR spectrum of **A** in CD_2Cl_2 recorded at room temperature; * marks the signal for residual traces of o-DFB.*

*[Cp*Fe{η⁴-P₅(1-IDipp)(2-Me)}][OTf] (**1**)*

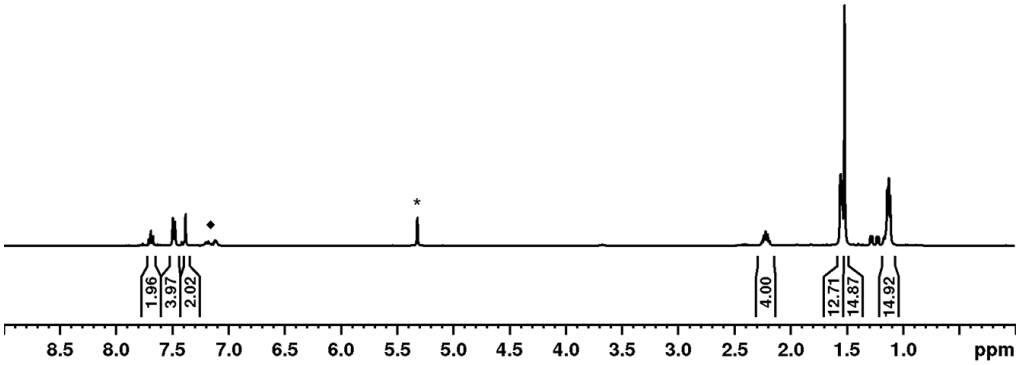

*Figure S 15: ^{1}H NMR spectrum of **1** in CD_2Cl_2 recorded at room temperature; * marks the signal for residual protonated solvent and ◆ indicates trace amounts of o-DFB.*

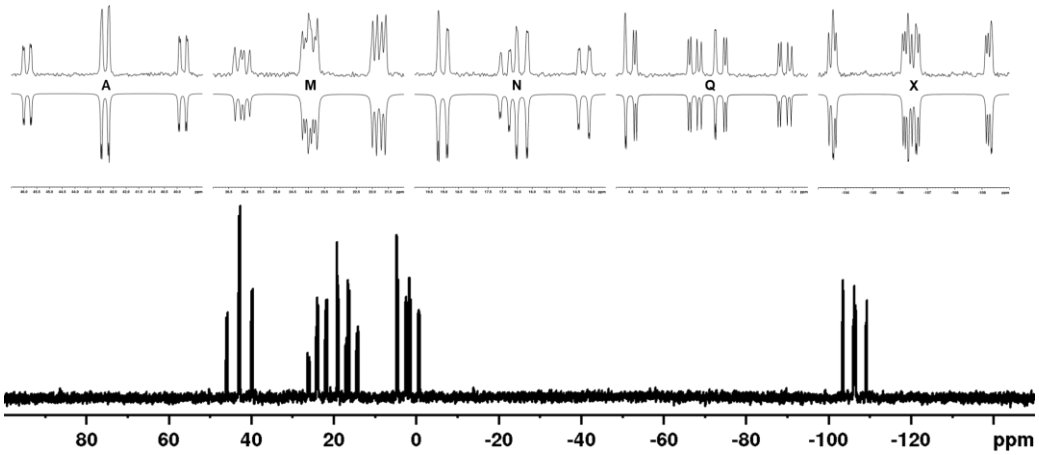

*Figure S 16: Experimental (top) and simulated (inverted) $^{31}P\{^{1}H\}$ NMR spectrum of **1** in CD_2Cl_2 recorded at room temperature.*

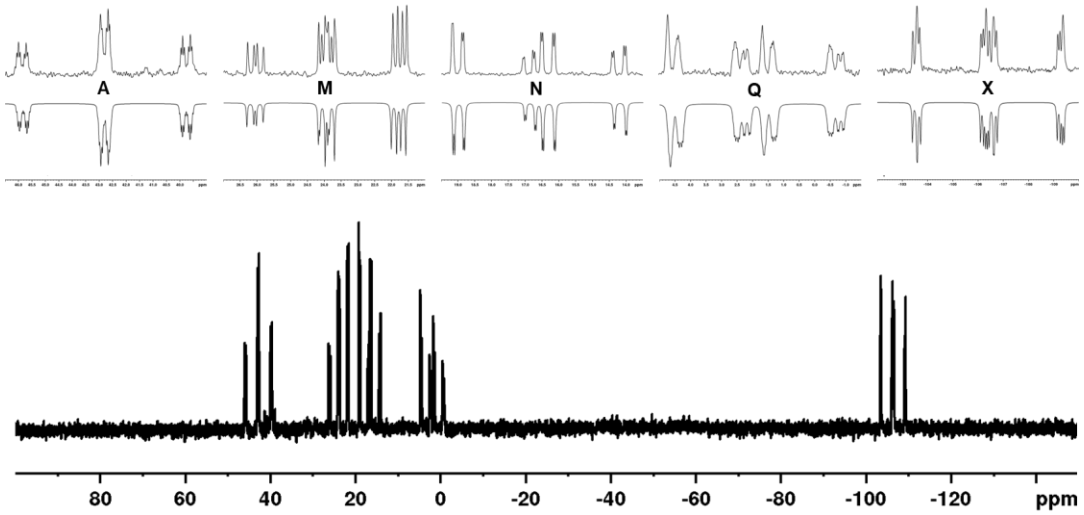

*Figure S 17: Experimental (top) and simulated (inverted) ^{31}P NMR spectrum of **1** in CD_2Cl_2 recorded at room temperature.*

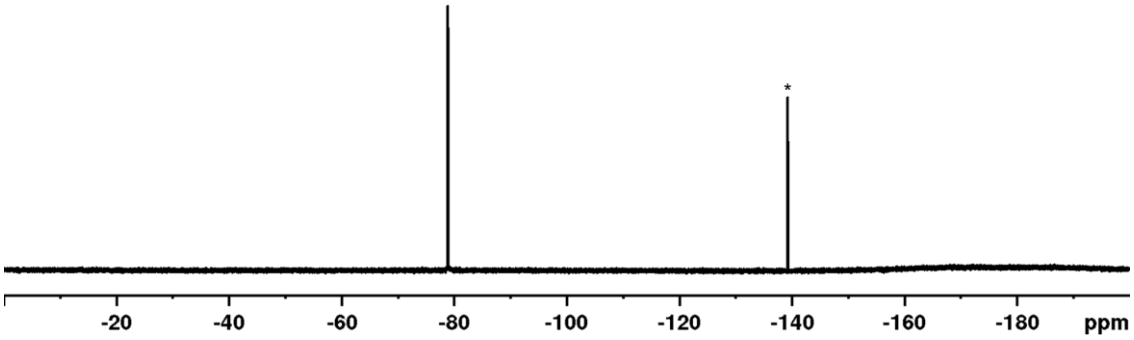

*Figure S 18: $^{19}F\{^{1}H\}$ NMR spectrum of **1** in CD_2Cl_2 recorded at room temperature; * marks the signal for trace amounts of o-DFB.*

*[Cp*Fe{η⁴-P₅(1-^{Et}CAAC)(2-Me)}][OTf] (**2**)*

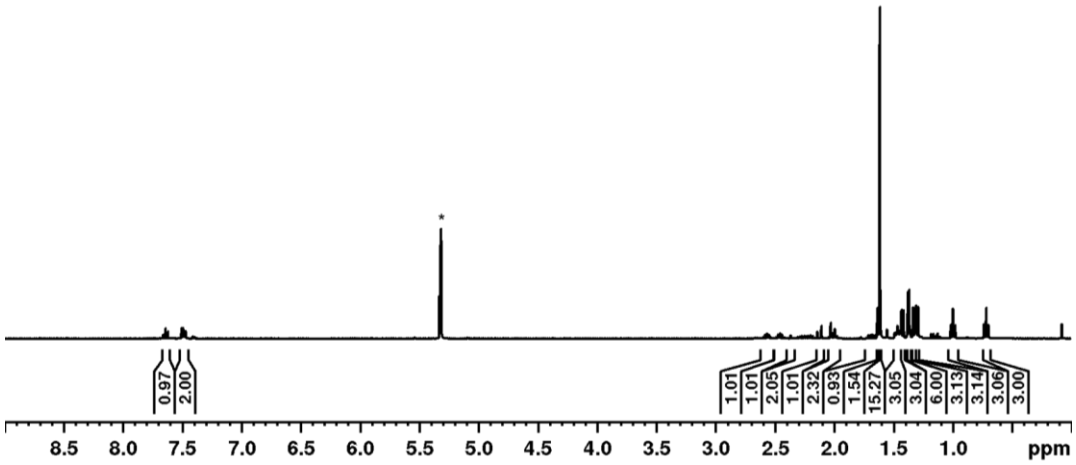

*Figure S 19: ^{1}H NMR spectrum of **2** in CD_2Cl_2 recorded at room temperature; * marks the signal of residual protonated solvent.*

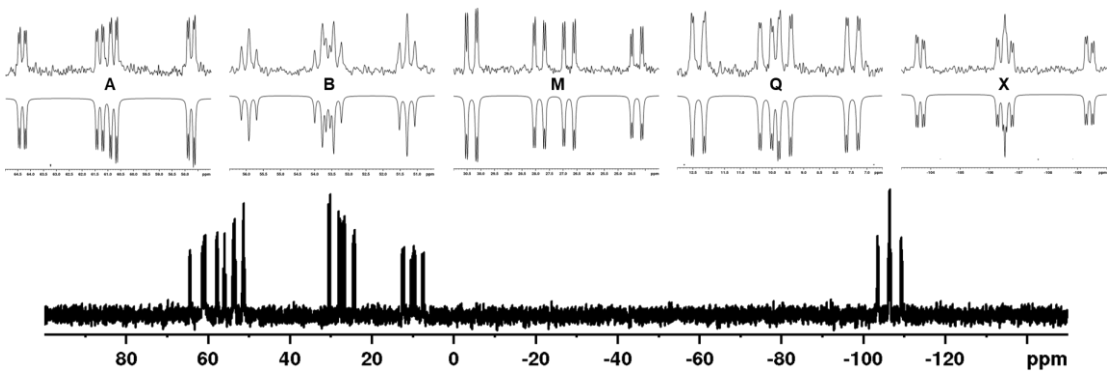

*Figure S 20: Experimental (top) and simulated (inverted) $^{31}P\{^{1}H\}$ NMR spectrum of **2** in CD_2Cl_2 recorded at room temperature.*

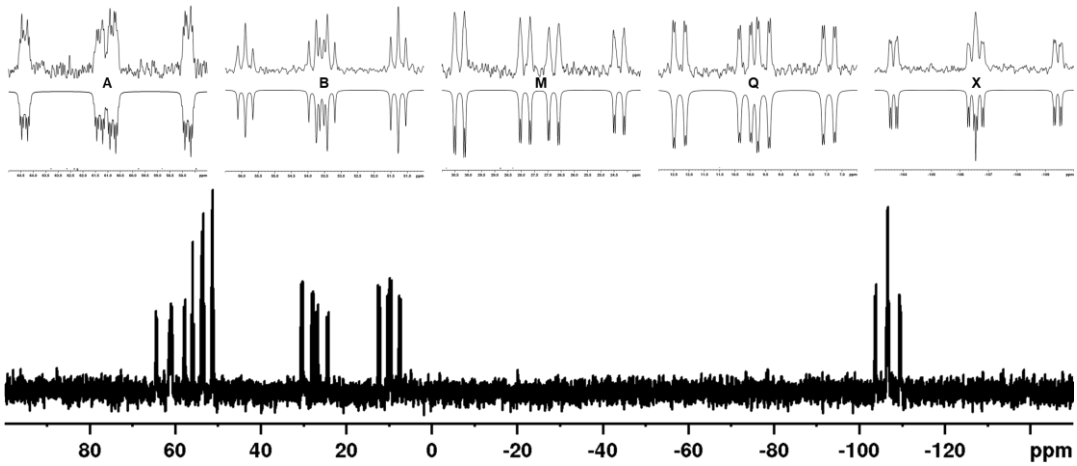

*Figure S 21: Experimental (top) and simulated (inverted) $^{31}P\{^{1}H\}$ NMR spectrum of **2** in CD_2Cl_2 recorded at room temperature.*

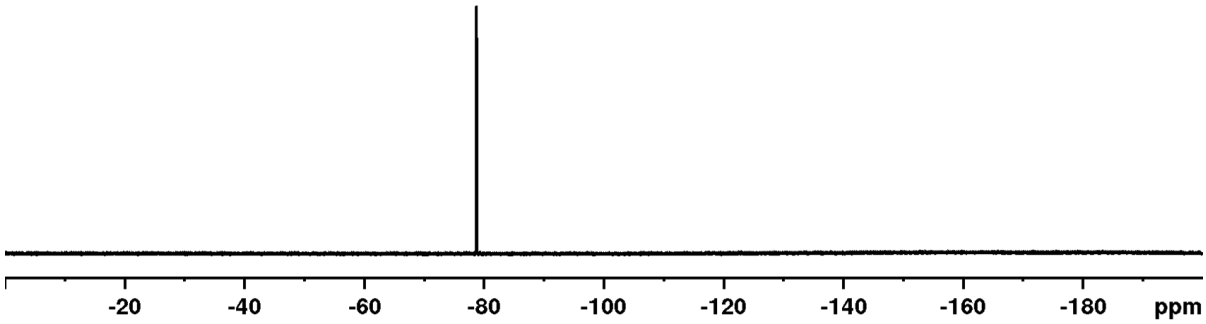

*Figure S 22: $^{19}F\{^{1}H\}$ NMR spectrum of **2** in CD_2Cl_2 recorded at room temperature.*

*[Cp*Fe{η⁴-P₅(I^{i}Pr)(Me)}][OTf] (**3**)*

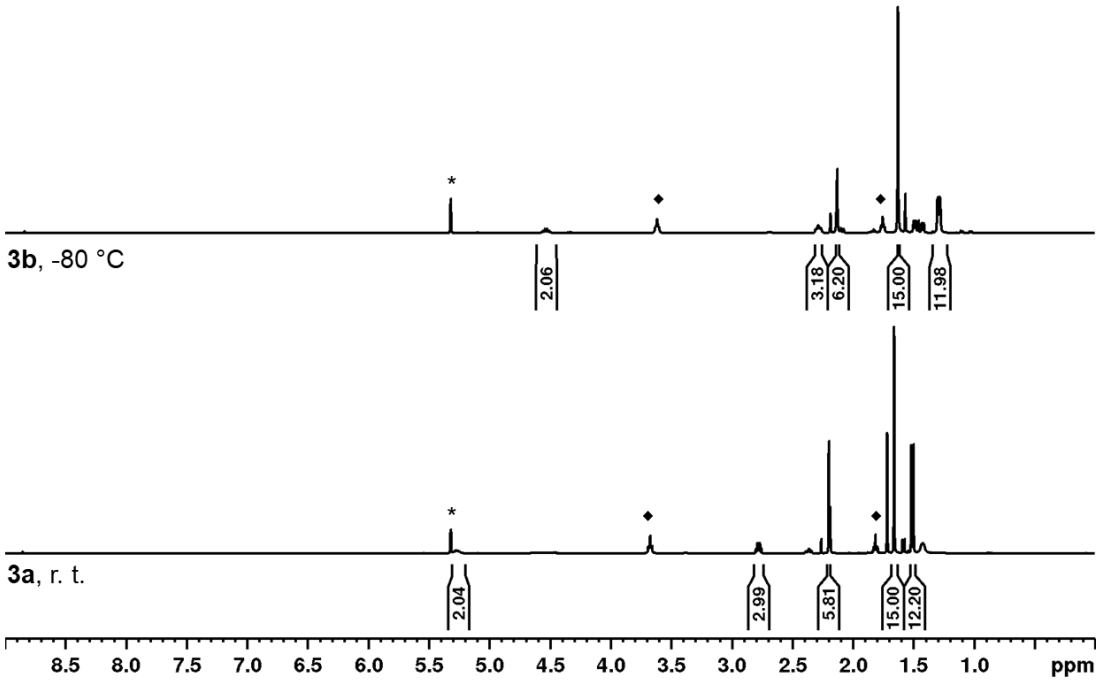

*Figure S 23: ^{1}H NMR spectra of freshly dissolved crystalline **3a** (bottom) and **3b** (top) in CD_2Cl_2 recorded at indicated temperatures; * marks the signal of residual protonated solvent and ◆ indicates trace amounts of THF.*

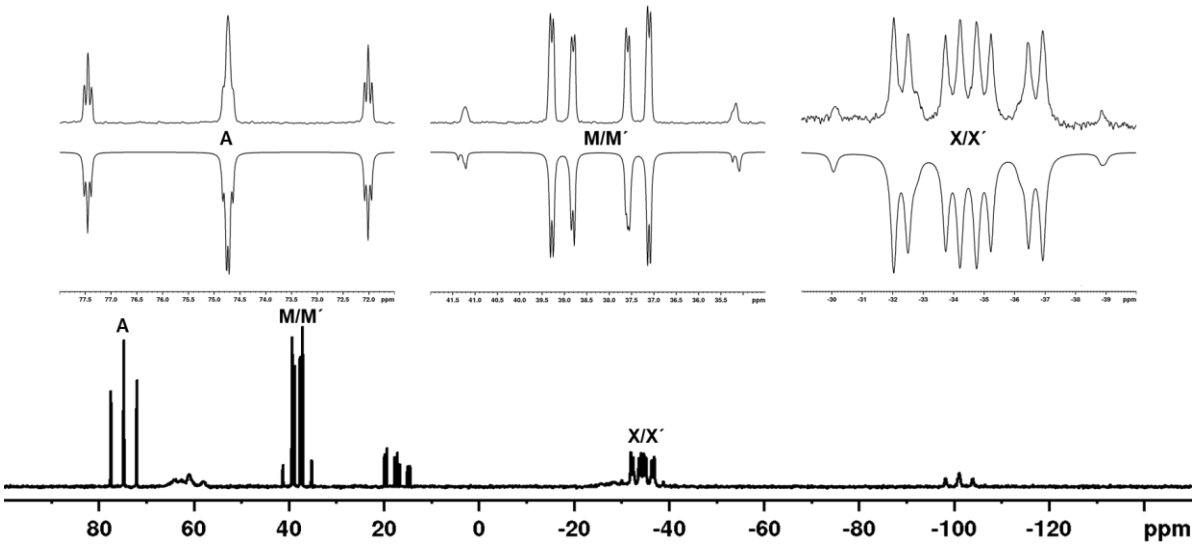

*Figure S 24 Experimental (top) and simulated (inverted) $^{31}P\{^1H\}$ NMR spectrum of freshly dissolved **3a** in CD_2Cl_2 recorded at room temperature; traces of **3b** are already observable even after short amounts of time.*

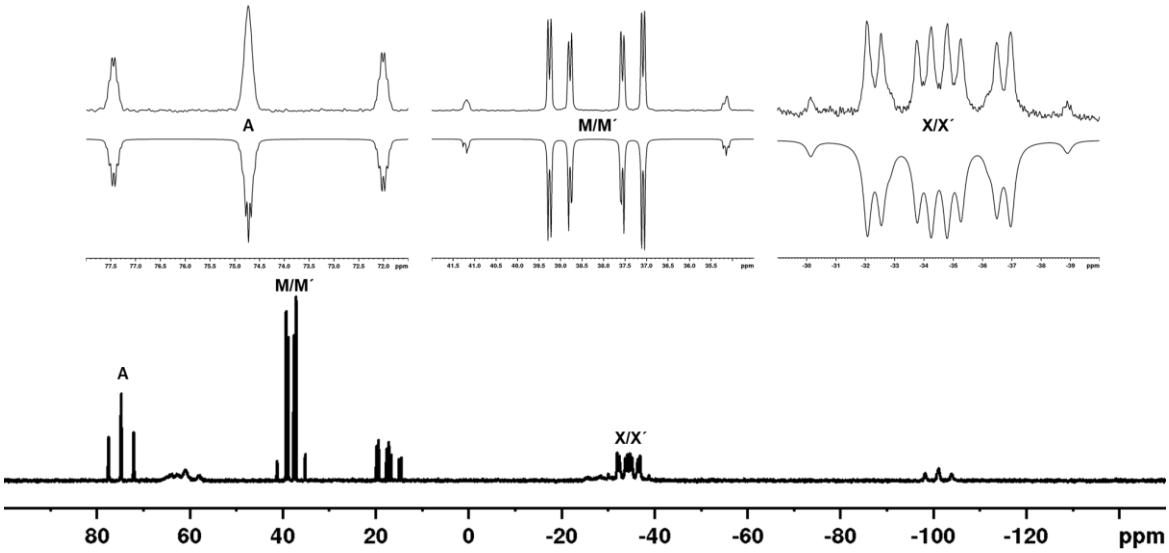

*Figure S 25: Experimental (top) and simulated (inverted) ^{31}P NMR spectrum of freshly dissolved **3a** in CD_2Cl_2 recorded at room temperature; traces of **3b** are already observable even after short amounts of time.*

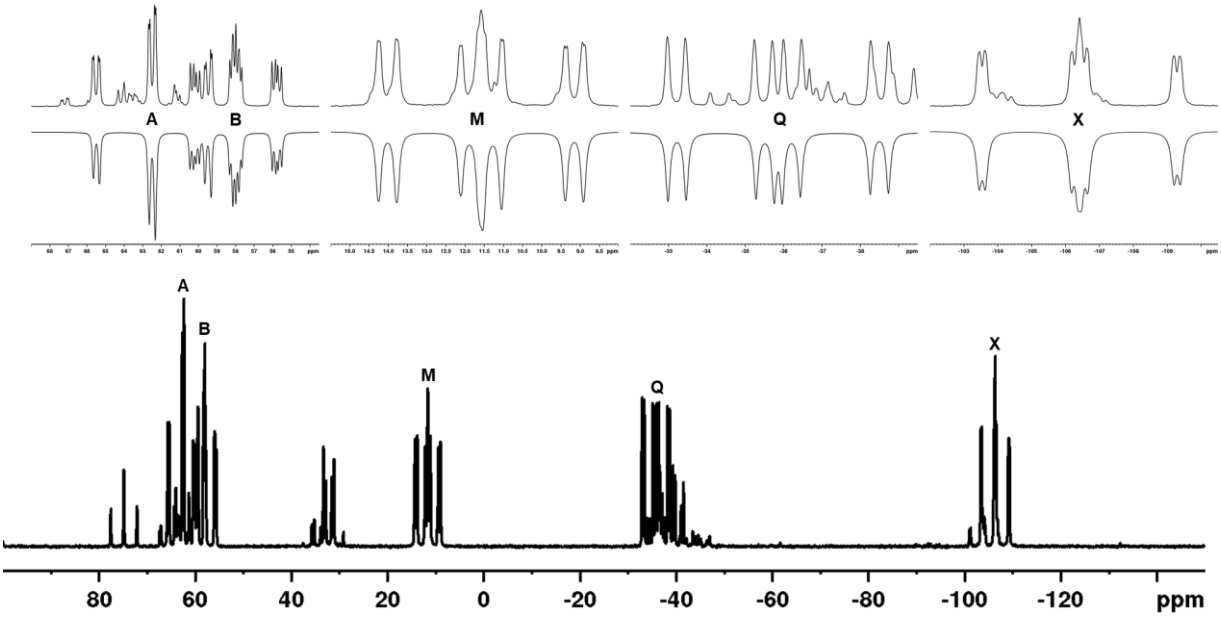

*Figure S 26: Experimental (top) and simulated (inverted) $^{31}P\{^1H\}$ NMR spectrum of freshly dissolved **3b** in CD_2Cl_2 recorded at –80 °C; formation of **3a** is observable even after short amounts of time.*

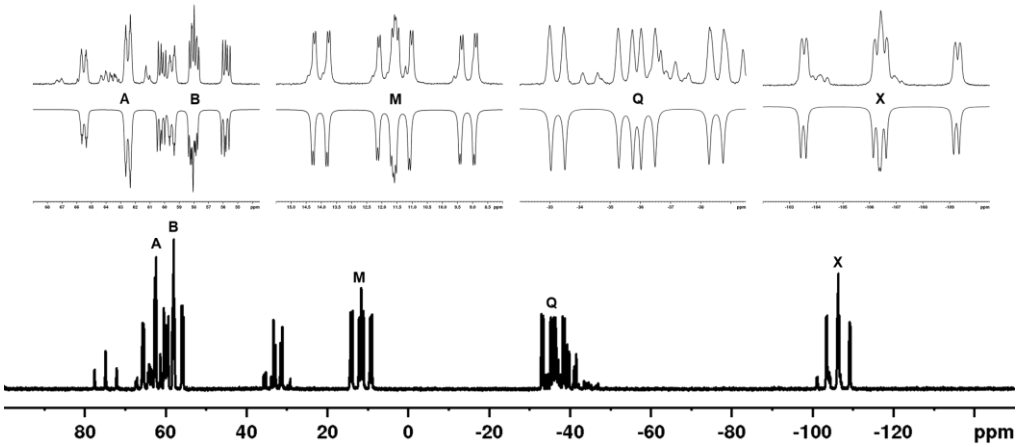

*Figure S 27: Experimental (top) and simulated (inverted) ^{31}P NMR spectrum of freshly dissolved **3b** in CD_2Cl_2 recorded at –80 °C; formation of **3a** is observable even after short amounts of time.*

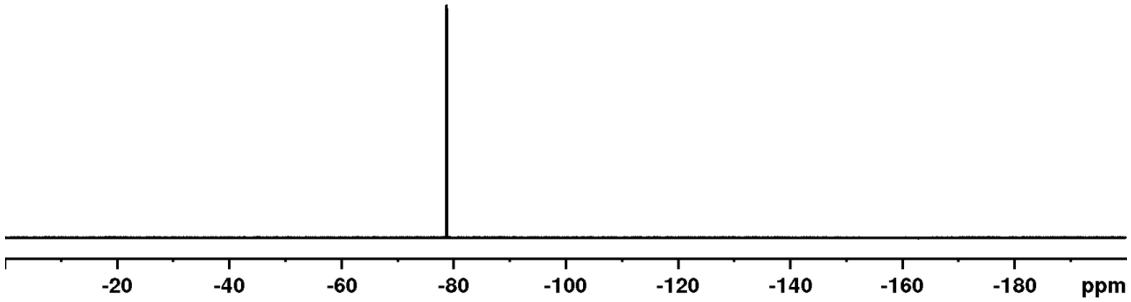

*Figure S 28: $^{19}F\{^1H\}$ NMR spectrum of **3** in CD_2Cl_2 recorded at room temperature.*

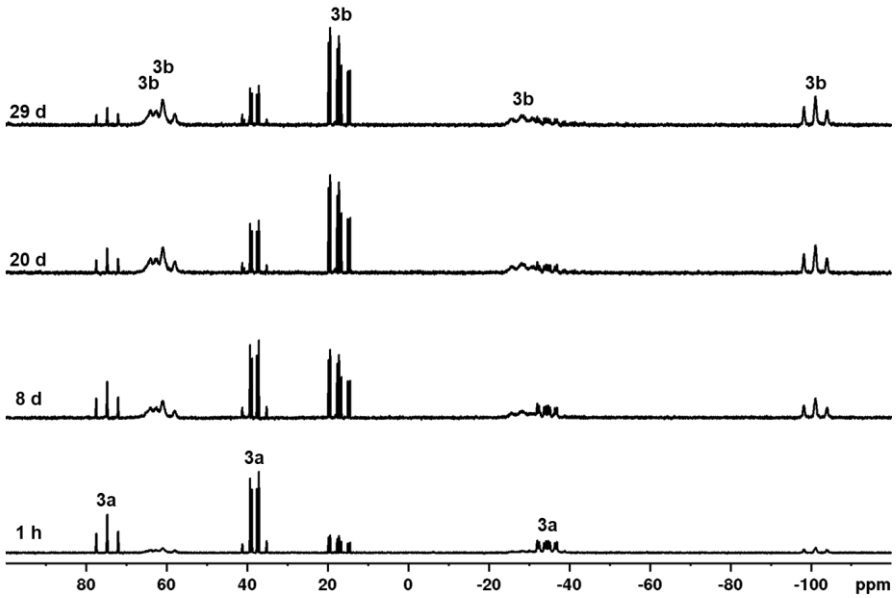

*Figure S 29: ^{31}P NMR spectra of **3** in CD_2Cl_2 recorded at room temperature over the period of 29 days; equilibration of both isomers is initially fast and finally approaches a ratio of 0.17:1 (**3a**/**3b**).*

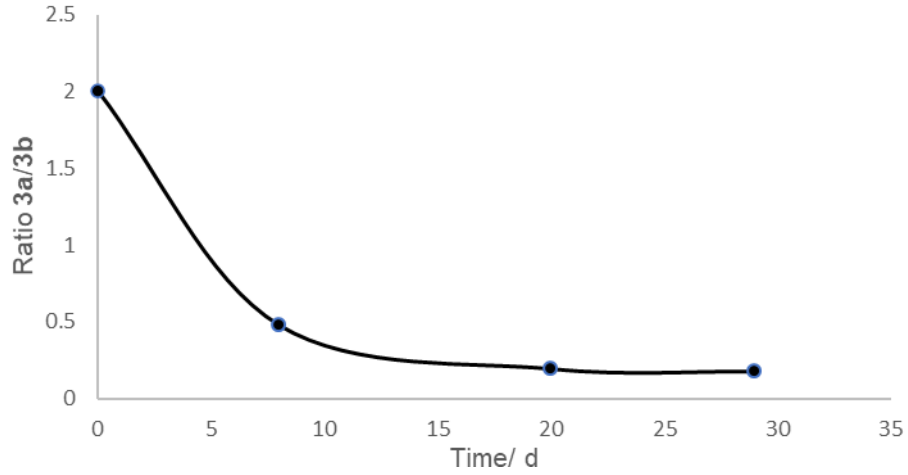

*Figure S 30: Ratio (**3a**/**3b**) obtained by integration of the ^{31}P NMR spectra in Figure S 29 against the time which the isomeric mixture of **3** was kept in solution.*

*[Cp*Fe{η⁴-P₄(1-IMe4)(4-Me)}] (**4**)*

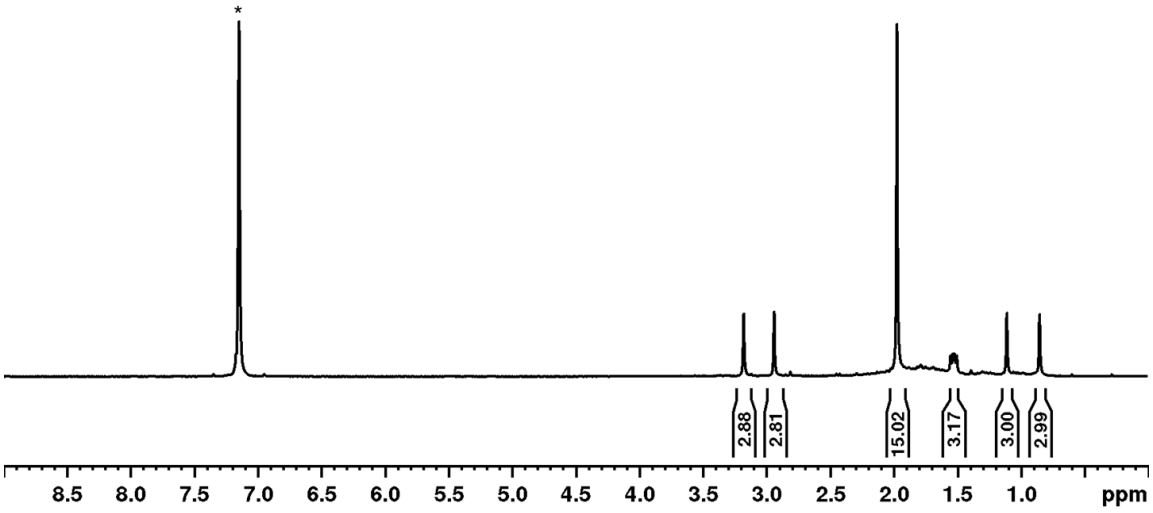

*Figure S 31: ^{1}H NMR spectrum of **4** in C_6D_6 recorded at room temperature; * marks the signal for residual protonated solvent.*

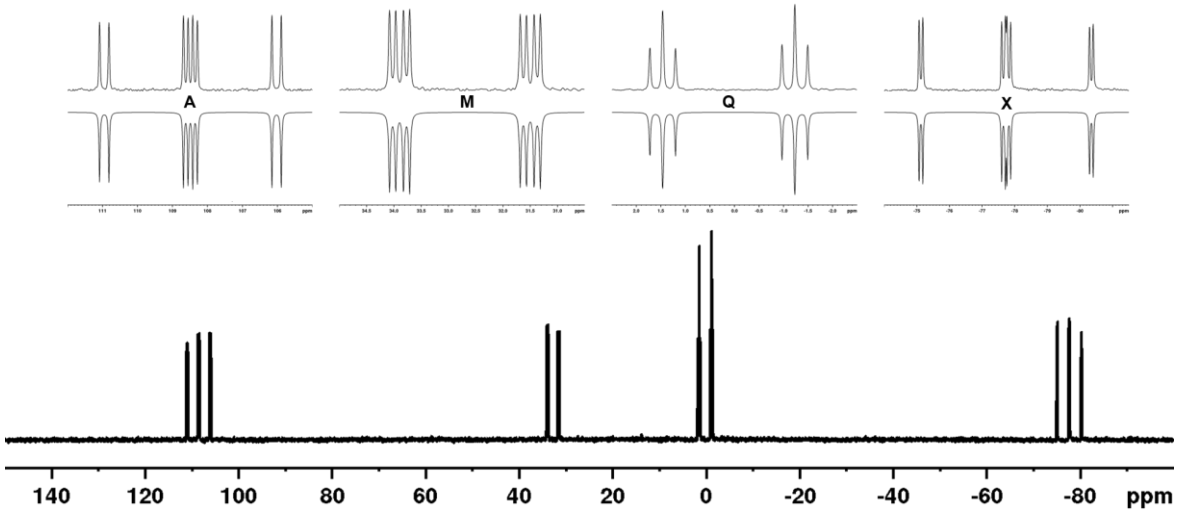

*Figure S 32: Experimental (top) and simulated (inverted) $^{31}P\{^{1}H\}$ NMR spectrum of **4** in C_6D_6 recorded at room temperature.*

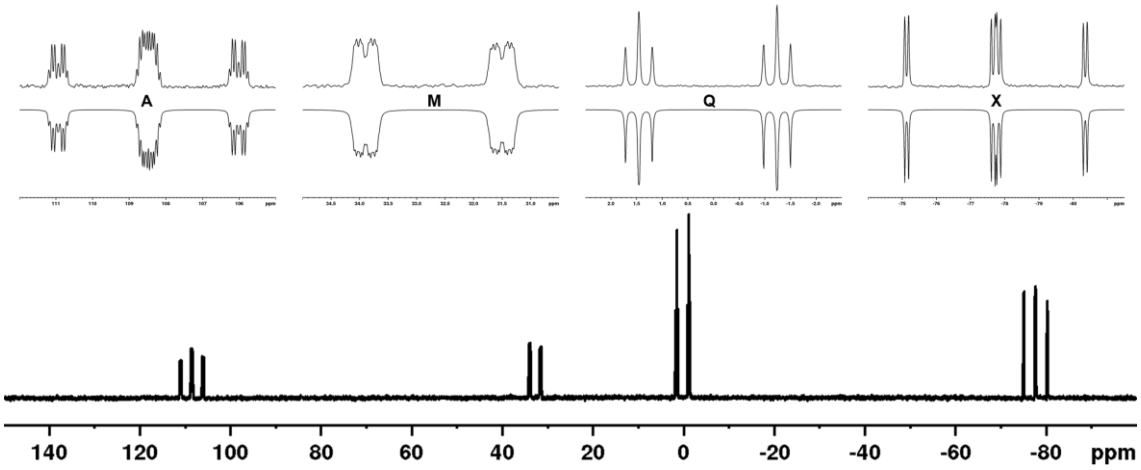

*Figure S 33: Experimental (top) and simulated (inverted) ^{31}P NMR spectrum of **4** in C_6D_6 recorded at room temperature.*

The crude product of **4** contains impurities of several side products (due to the extremely delicate reaction pathway) which necessitates the purification via liquid/liquid extraction (*vide supra*). However, the $^{31}P\{^1H\}$ NMR spectrum of the crude reaction product (Figure S34) clearly shows the presence of $[(IMe_4)_2P]^+$ further corroborating the outlined reaction pathway.

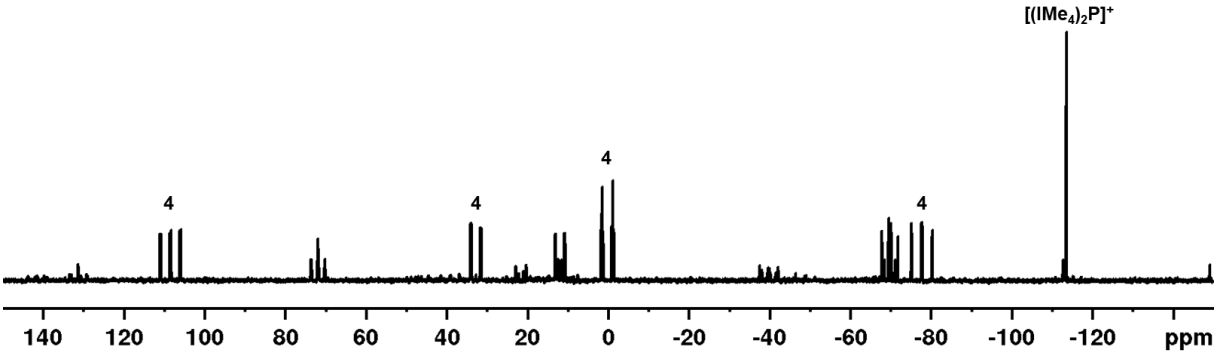

*Figure S 34: Experimental $^{31}P\{^1H\}$ NMR spectrum of the crude product mixture of **4**; unassigned signals correspond to unidentified side products.*

To probe the pathway leading to the formation of **4**, several (sub)stoichiometric reactivity studies were carried out. Note that the formation of **4** requires three equivalents of IMe_4, as two equivalents abstract a P atom resulting in $(IMe_4)_2P^+$ and the third equivalent is needed to stabilize **4** itself. While reacting **A** with equimolar amounts of IMe_4 results in an untraceable mixture of products, it was hypothesized that the smallest of the NHCs used within this study should exclusively form the 1,1-disubstituted species $\mathbf{4_{INT1}}$. The instability of this compound may be attributed to the strongly nucleophilic character of IMe_4 in combination with minimal steric protection, which allows for a myriad of possible side reactions, such as e. g. deprotonation. Thus, $\mathbf{4_{INT1}}$ may only be formed and stable at low temperatures, preventing its isolation and structural study. However, it could be possible to spectroscopically observe this key intermediate on track to **4** via spectroscopic methods. Accordingly, when dissolving

equimolar amounts of **A** and IMe_4 in cold (–80 °C) THF and subjecting the mixture to $^{31}P\{^1H\}$ NMR spectroscopy, the selective formation of $\mathbf{4_{INT1}}$ can be observed as displayed in Figure S35. Indeed, the exclusive formation of the hypothesized 1,1-disubstituted isomer is revealed by the indicative (broadened) AMM'XX' spin system.

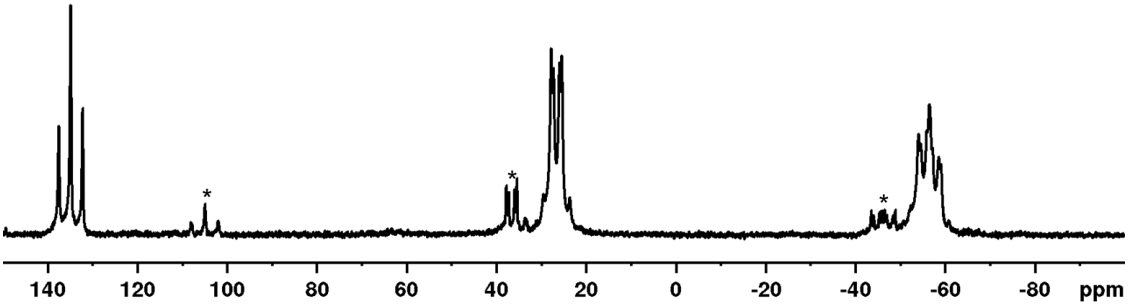

*Figure S 35: Experimental $^{31}P\{^1H\}$ NMR spectrum of mixture of **A** and one equivalent of IMe_4 in THF recorded at –80 °C; The spectrum clearly indicates the formation of $\mathbf{4_{INT1}}$ as the 1,1-substituted isomer exclusively and * marks the signals associated with traces of an unidentified side product.*

To further probe the mechanism leading to the formation of **4**, it was exposed to two equivalents of IMe_4. While this reaction ultimately affords the scrambling product **5** (*vide infra*) it was hypothesized that the potential intermediate formed upon addition of two units of IMe_4 to **A** would be highly sensitive and susceptible to decomposition. Again, low temperature $^{31}P\{^1H\}$ NMR spectroscopy was employed to identify this second key intermediate on the way towards **4**. Dissolving a mixture of **A** and two equivalent of IMe_4 in cold (–80 °C) THF affords a highly complex $^{31}P\{^1H\}$ NMR spectrum (Figure S36) in which several species can be identified. However, the primary product of this reaction reveals five distinct multiplets, which is in line with a chain type P_5 ligand in $\mathbf{4_{INT2}}$ This indicates the cleavage of one P–P bond upon addition of the second equivalent of IMe_4 to $\mathbf{4_{INT1}}$. The presence of several other compounds in this mixture highlights the sensitivity of $\mathbf{4_{INT2}}$. The formation of **5** is directly attributed to the degradation of this intermediate, as shown by its isolation (at room temperature) from mixtures of **A** with two equivalents of IMe_4. Additionally, the presence of 4_{INT1} as well as $[(IMe_4)_2P]^+$ points towards a relatively unselective reaction under the given conditions. This is however expected, as both reagents were dissolved simultaneously. Finally, the formation of both **4** and **5** is observed upon warming the reaction mixture to 0 °C, which is in line with these species being the only ones within this system stable at room temperature. Identification of other species within this complex mixture (especially at low temperatures) was hampered due to signal broadening and overlap. However, most of the observed species are formed in small amounts and their formation is largely attributed to the non-ideal reaction conditions an NMR study provides (e. g. mixing, homogeneity). To our surprise it was however possible to grow a

single crystal of the key intermediate **4$_{INT2}$** at low temperatures (*vide supra*) manifesting its constitution and providing essential structural insight into the reaction pathway towards **4**.

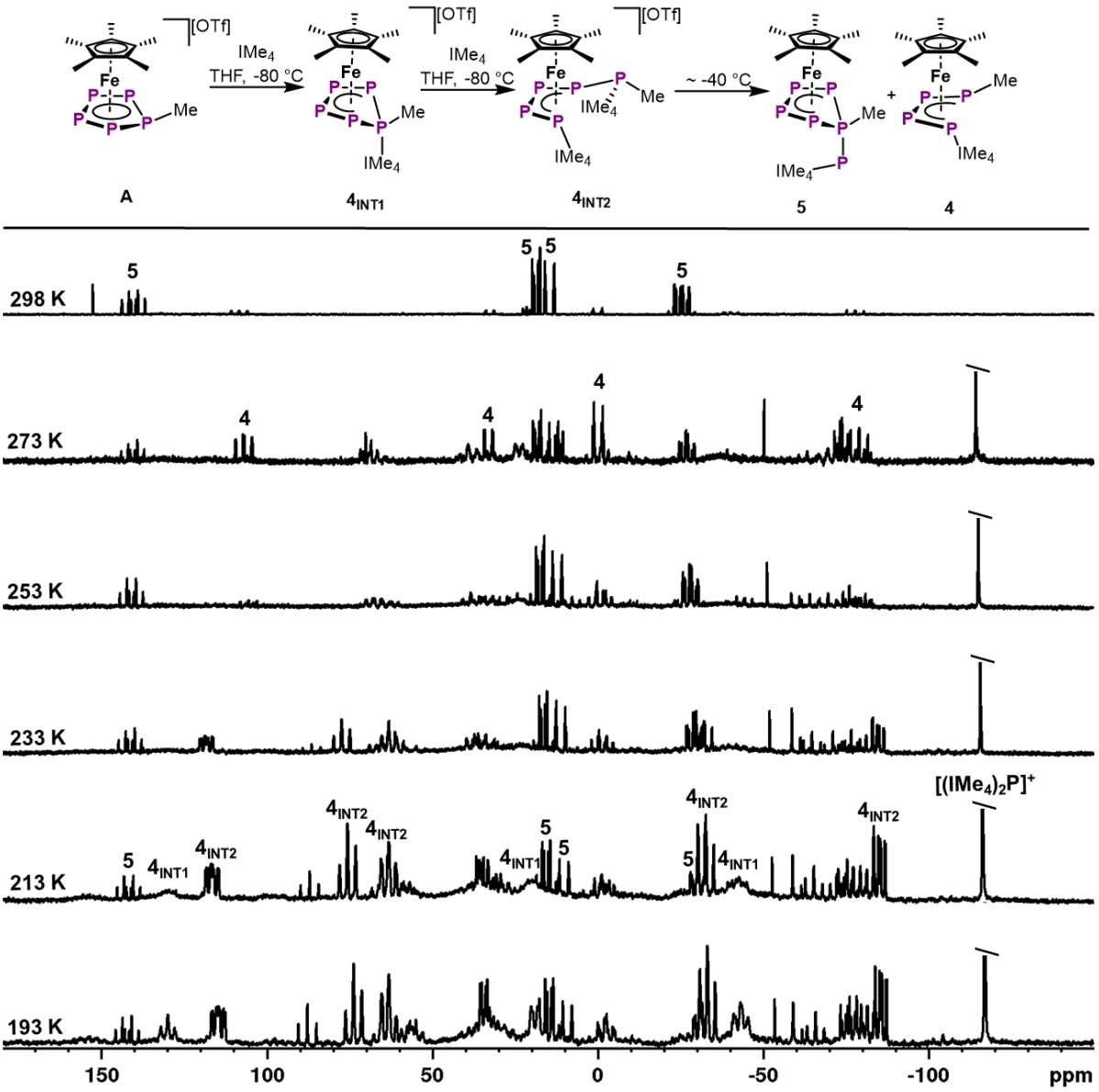

*Figure S 36: Experimental $^{31}P\{^{1}H\}$ NMR spectra of a mixture of **A** with two equivalents of IMe$_4$ in THF recorded at given temperatures; The top spectrum corresponds to the spectrum of isolated **5** and is provided as reference and inserts provide assignment of the signals to the corresponding species in the reaction solution.*

*[Cp*Fe{η⁴-P₅(1-IMe₄P)(1-Me)}] (**5**)*

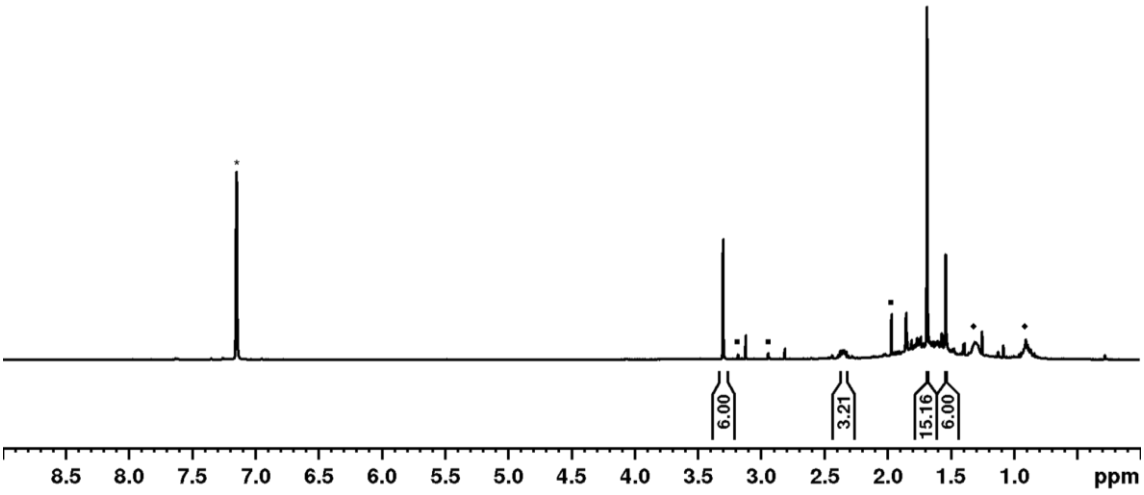

*Figure S 37: ^{1}H NMR spectrum of **5** in C_6D_6 recorded at room temperature; * marks the signal for residual protonated solvent, ⬩ indicates residual n-hexane and ▪ marks the signals associated with traces of **4** which are obtained as a side product in this reaction and cannot be fully separated due to nearly equivalent solubility.*

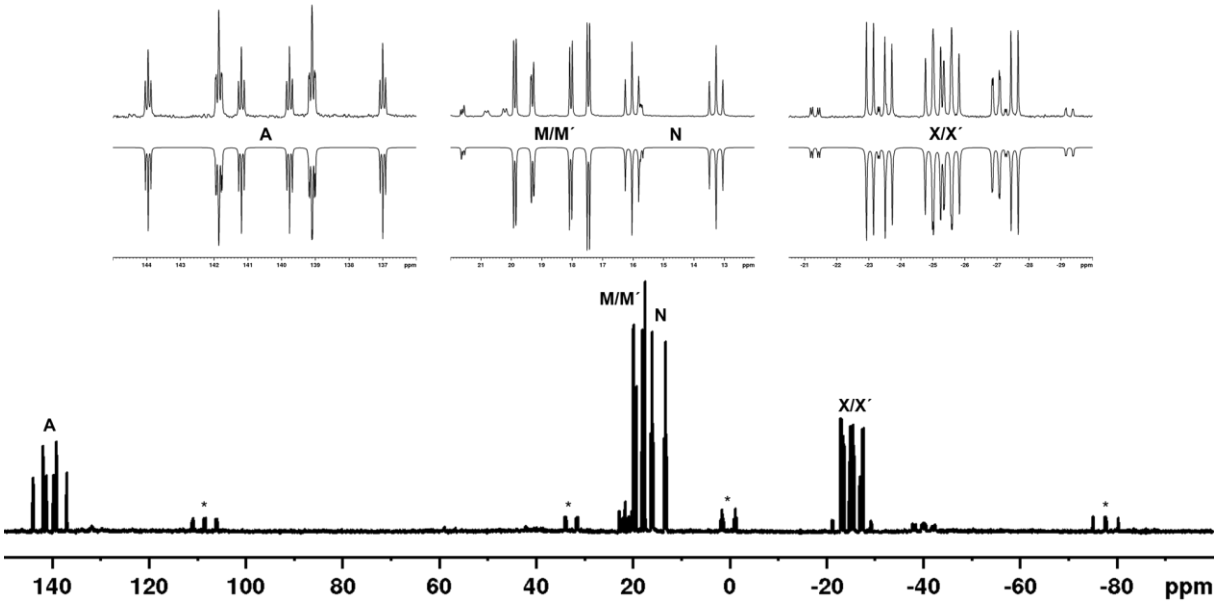

*Figure S 38: Experimental (top) and simulated (inverted) $^{31}P\{^{1}H\}$ NMR spectrum of **5** in C_6D_6 recorded at room temperature; * marks the signals of trace amounts of **4** which could not be separated due to similar solubility.*

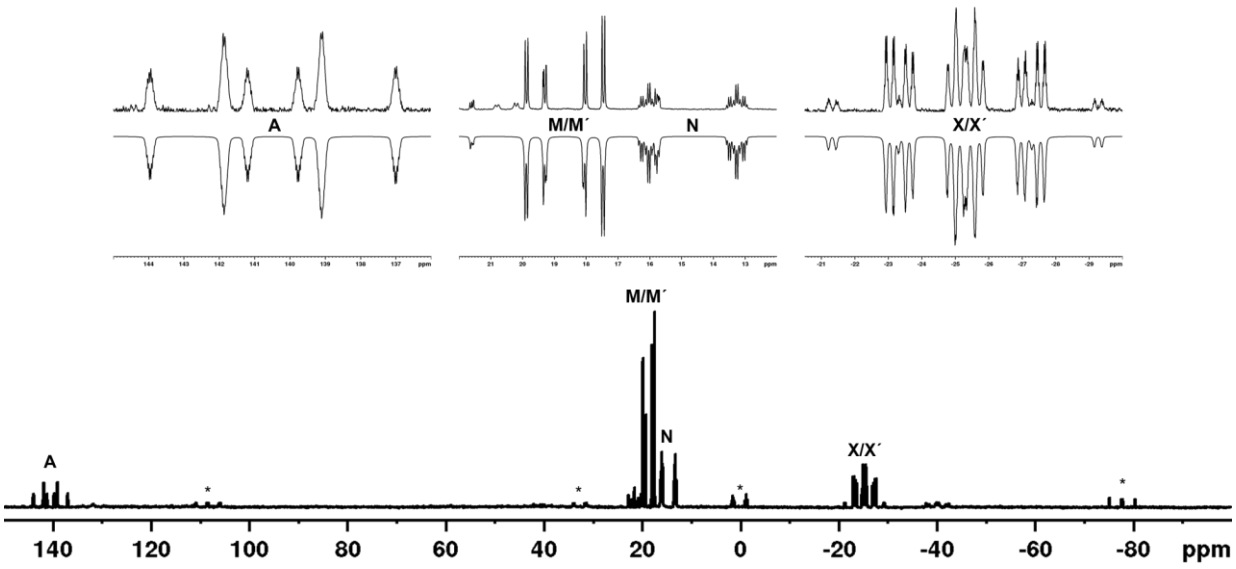

*Figure S 39: Experimental (top) and simulated (inverted) ^{31}P NMR spectrum of **5** in C_6D_6 recorded at room temperature; * marks the signals of trace amounts of **4** which could not be separated due to similar solubility.*

*[Cp*Fe{η⁴-P₅(NHO)(Me)}][OTf] (**6**)*

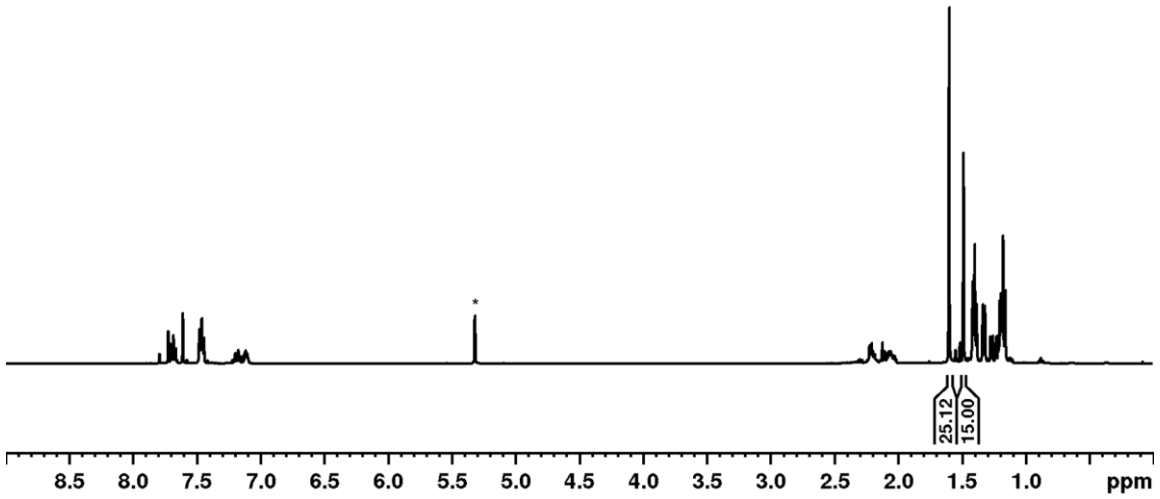

*Figure S 40: ^{1}H NMR spectrum of **6** in CD_2Cl_2 recorded at room temperature; * marks the signal for residual protonated solvent; only the Cp* signals are integrated to obtain a relative ratio of both isomers, while all other signals are strongly overlapping.*

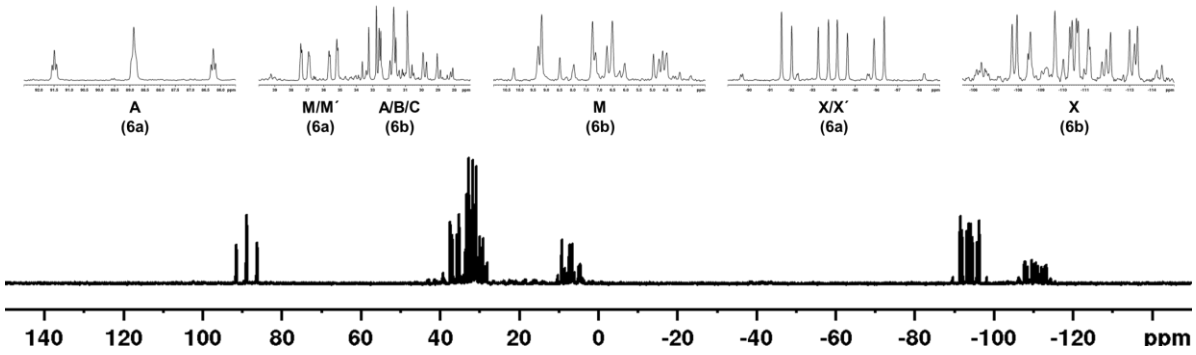

*Figure S 41: Experimental $^{31}P\{^{1}H\}$ NMR spectrum of **6** in CD_2Cl_2 recorded at room temperature and signal assignment for both isomers.*

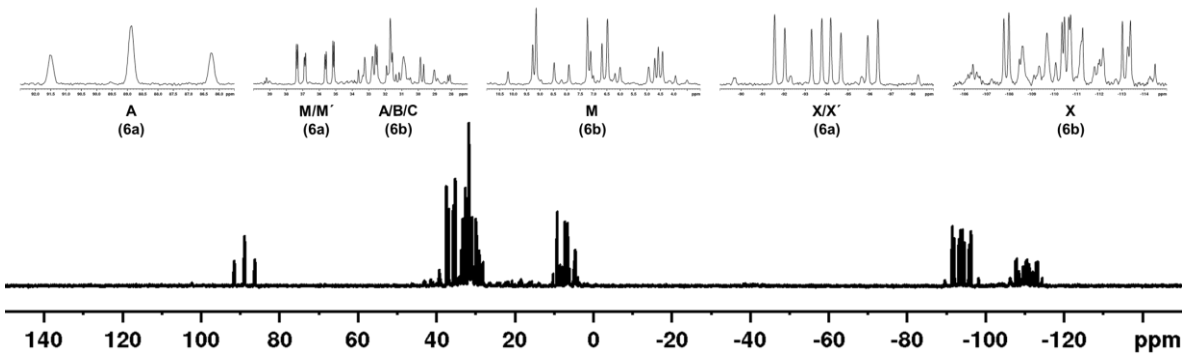

*Figure S 42: Experimental ^{31}P NMR spectrum of **6** in CD_2Cl_2 recorded at room temperature and signal assignment for both isomers.*

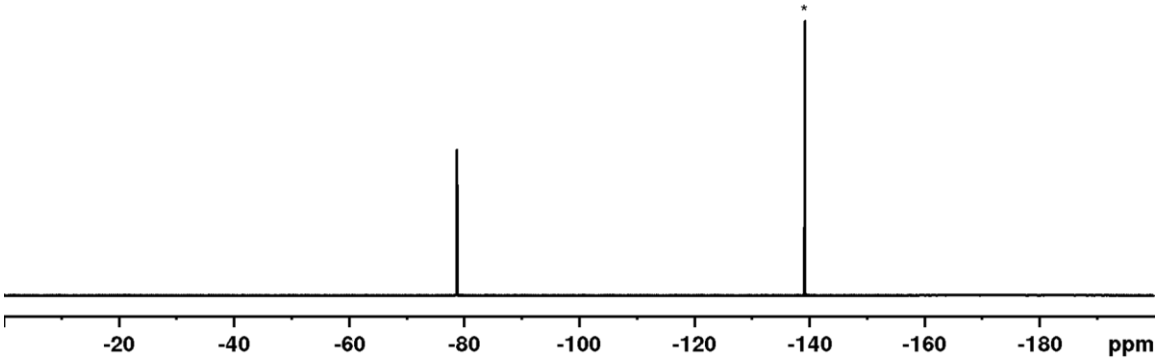

*Figure S 43: $^{19}F\{^{1}H\}$ NMR spectrum of **6** in CD_2Cl_2 recorded at room temperature; * marks the signal for o-DFB, which is also found in the crystal lattice of this compound.*

*[{Cp*Fe}2{$\mu_2,\eta^{4:3:1}$-$P_{10}Me_2$(IDippN)}][OTf] (**7**)*

NMR spectra of **7** could not yet be obtained within the time frame of this thesis, due to the complicated separation of this compound from side products. Furthermore, the potential for formation of isomers of **7** (Scheme S1) may further complicate the issue of obtaining interpretable NMR spectra.

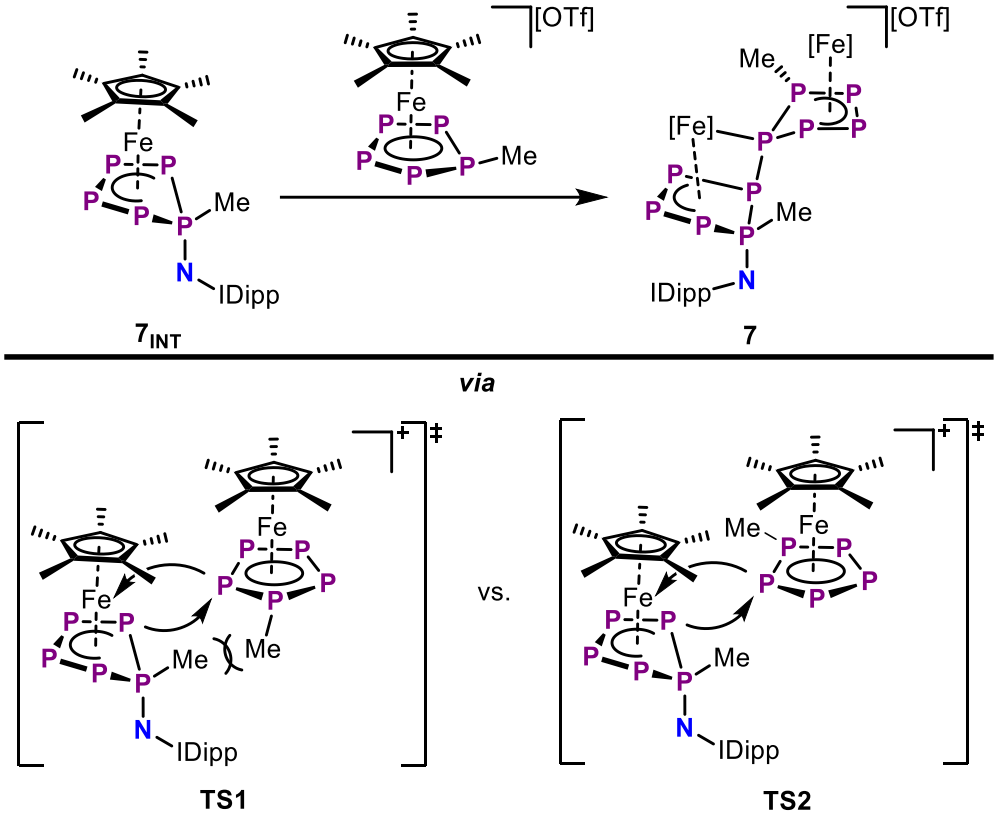

*Scheme S 1: Potential pathways for the formation of isomers of **7**.*

*[Cp*Fe{η⁴-P₅(1-IDippN)(1-Me)}] (**7**$_{INT}$)*

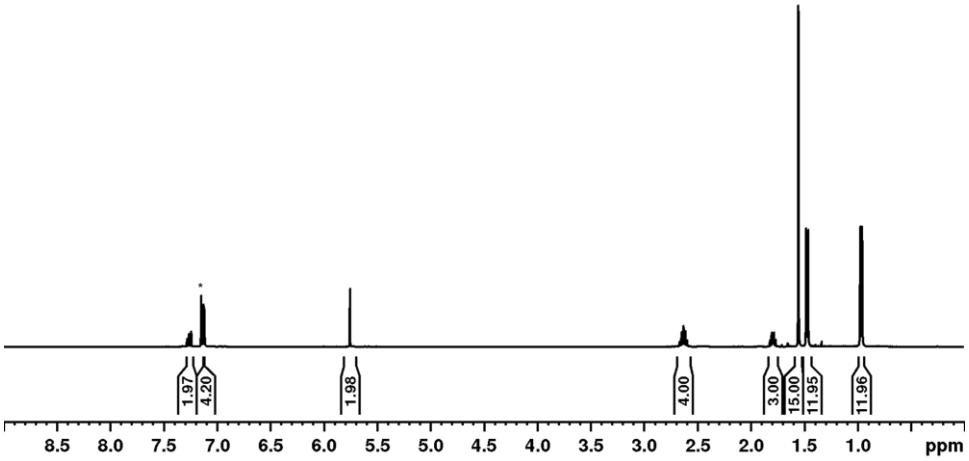

*Figure S 44: ^{1}H NMR spectrum of **7**$_{INT}$ in C_6D_6 recorded at room temperature; * marks the signal of residual protonated solvent.*

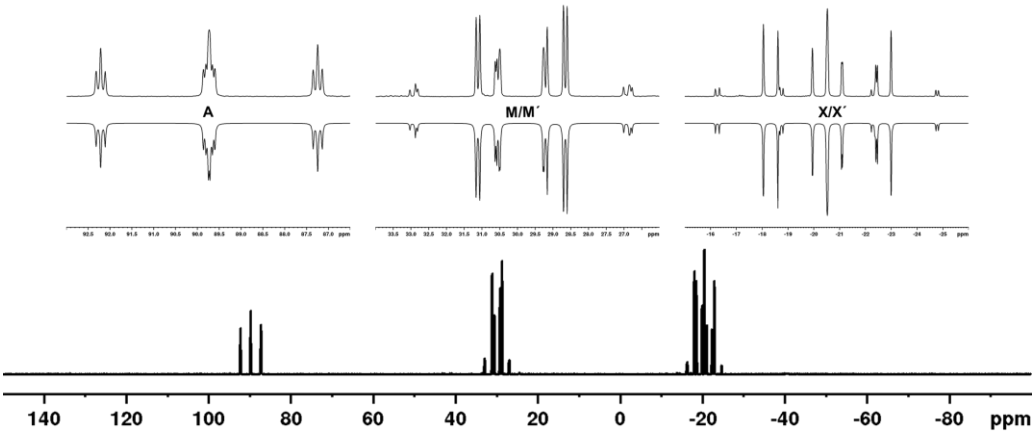

*Figure S 45: Experimental (top) and simulated (inverted) $^{31}P\{^{1}H\}$ NMR spectrum of **7**$_{INT}$ in C_6D_6 recorded at room temperature.*

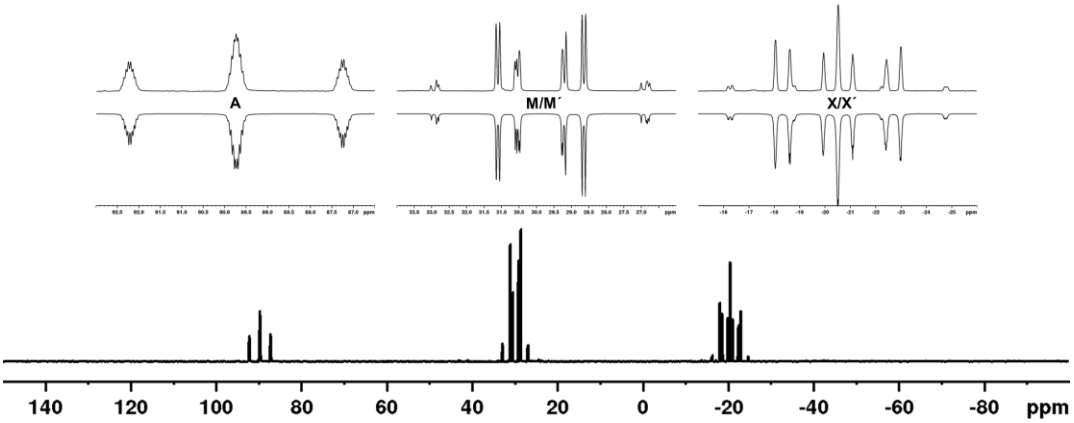

*Figure S 46: Experimental (top) and simulated (inverted) ^{31}P NMR spectrum of **7**$_{INT}$ in C_6D_6 recorded at room temperature.*

*[{Cp*Fe}2{$\mu_2,\eta^{4:1:1:1}$-$P_{11}Me_2$(IDipp)}][OTf] (**8**)*

NMR spectra of **8** could not yet be obtained in sufficient quality within the time frame of this thesis. As the solid state structure of this compound (Figure S 11) already indicates the positional disorder of one of the Me groups, the presence of two isomers of **8** may further complicate this issue. The selective syntheses of either one of these isomers or their separation are however not possible due to the comparably small steric demand of the Me substituent. Scheme S2 shows two possible transition states which would be accountable for the formation of the respective isomers.

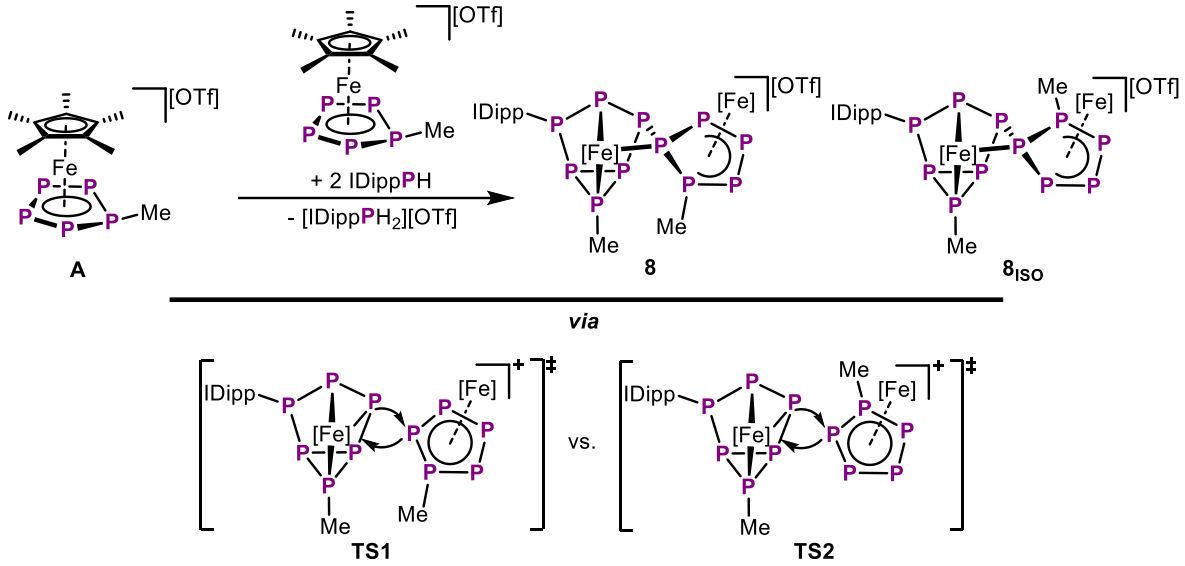

*Scheme S 2: Synthesis of **8** (top) and two possible transition states leading to the observed formation of two isomers (bottom).*

11.5.4. Computational Details

General Considerations

DFT calculations were performed using the Orca 5.0 software package.[44] Geometry optimizations were performed at the BP86[45]/def2-SVP[46] and single point calculations were performed at the ωB97X-D4[47]/def2-TZVPPD[46] or ωB97X-D4/def2-TZVP[46] (**7**$_{INT}$) level of theory with PCM solvent correction for THF.[48] Stationary points were verified by analytical frequency calculations.

NBO Analysis of ***7***$_{INT}$

To gain deeper insight into the electronic structure of the key intermediate **7**$_{INT}$, NBO analysis was performed using the NBO 7.0 software package.[49] Selected NBOs as well as NLMOs are depicted in Figure S 56. Although the P1–N1 (1.64 Å) and the N1–C2 (1.31 Å) distances are below the sum of the covalent single bond radii,[50] the Wiberg bond indices of 1.40 (N1–C2) and 0.91 (P1–N1) indicate only weak or even no multiple bonding, respectively. In agreement, the NBOs in Figure S 56 show clear P1–N1 (NBO 94) and N1–C2 (NBO 116) σ bonds but no clear π type interaction between these atoms. Instead, two occupied p-type orbitals are strongly located at the N1 center (NBO 85/86). The corresponding NLMOs (Figure S81, bottom) only show minor delocalization of these orbitals. Thus, the mesomeric formulations **B** and **C** (Scheme S3) of **7**$_{INT}$ should have the most significant statistical weight for the electronic structure of this intriguing compound. The potential π donor capability of the IDippN- substituent in **7**$_{INT}$ may cause the interesting insertion reactivity observed o the way towards the complex P_{10} species **7**.

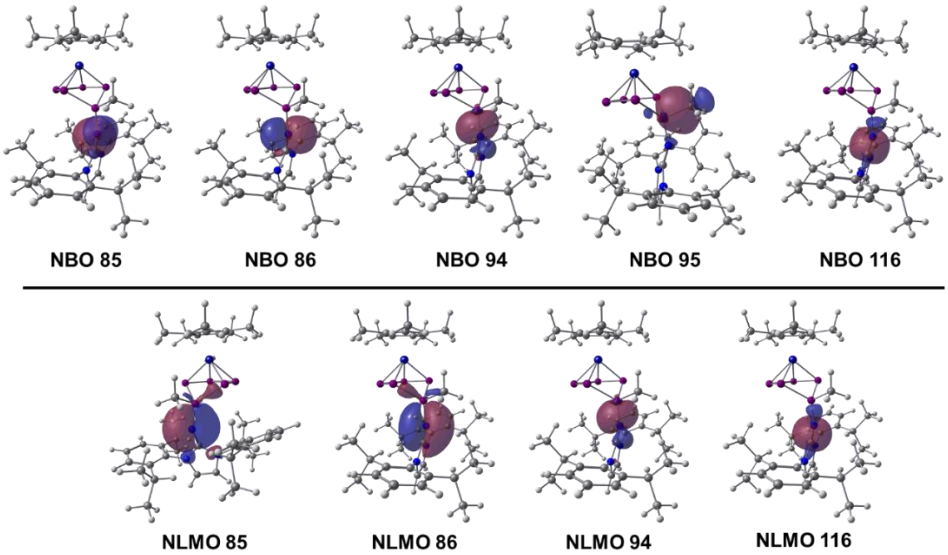

Figure S 47: Selected NBOs (top) and NLMOs (bottom) of ***7***$_{INT}$*; cutoff: 0.03 a. u.*

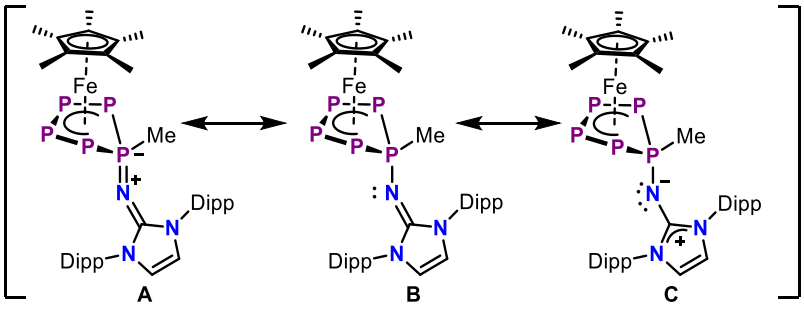

Scheme S 3: Potential mesomeric forms of ***7***$_{INT}$.

Optimized Geometries

A

ωB97XD/def2-TZVPPD (CPCM (THF)): Energies/H = -3401.01259, Free Energies/H = -3400.71573, ZPVE/ kcal/mol (ωB97XD/def2-TZVP) = 186.28

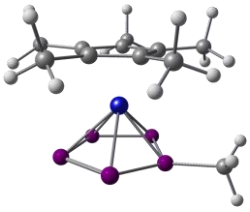

Symbol	X	Y	Z
Fe	0.10559879035376	-0.07838594303334	0.00013385472559
P	-2.13074740294512	0.23834037929977	0.00060779474583
P	-1.39593109571540	-0.53002028505533	1.77495454788850
P	-1.39804576401621	-0.52126357669397	-1.77765618689648
P	-0.30610604294046	-2.15304903979102	1.04262455140255
P	-0.30560379392813	-2.14651113484533	-1.05698875950531
C	1.78624923693764	0.41207757083728	1.09026980688740
C	2.16513062652332	-0.14088074086072	-0.16885053426497
C	1.60613267386901	0.67834584567843	-1.19385388187218
C	0.88626856262668	1.74189705609722	-0.56831132358961
C	0.99978278272364	1.57864949471843	0.84394512549700
C	3.03527268068476	-1.33775192673872	-0.37598175035370
C	1.79391614771410	0.49300637042774	-2.66475138131433
C	0.20411250008174	2.86364909964220	-1.28382315096007
C	2.19301368572275	-0.09904326042590	2.43425175959207
C	0.46474184491882	2.50024820297416	1.89198127679982
H	2.89382666641571	-2.07682370838336	0.41335300869949
H	2.83138730756512	-1.81692988762490	-1.33354253581037
H	1.85461033769440	-0.56308286147105	-2.93062039670351
H	1.42908171373092	0.10103048458386	3.18678962122055
H	-0.31814829754466	2.51309196125301	-2.17557563143590
H	2.37869250627554	-1.17290662782555	2.41297449134681
H	4.08548956093968	-1.03090035194199	-0.36730008479706
H	0.20607567152384	1.96141225600621	2.80378843573777
H	3.11488935367410	0.39817189426552	2.75066428581167
H	2.72589401590978	0.97326752557912	-2.97755551128091
H	-0.41895599504437	3.03652735794307	1.54678321545062
H	0.97778932034024	0.94316218331104	-3.23054872662211
H	1.22749560140222	3.24251830976674	2.14579158279333
H	-0.51323876701109	3.37219347974340	-0.64066994912754
H	0.94805599565381	3.59993104556189	-1.60173238213048
C	-3.00236912091963	1.81826978848997	-0.00155785639633
H	-4.07238241811760	1.61920144308499	0.06617407020871
H	-2.67850321287093	2.40948295680447	0.85454271388161
H	-2.78063445922799	2.34262664262266	-0.93068556962845

IMe₄

ωB97XD/def2-TZVPPD (CPCM (THF)): Energies/H = -383.77637, Free Energies/H = -383.58229, ZPVE/ kcal/mol (ωB97XD/def2-TZVP) = 121.79

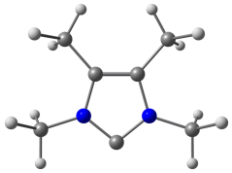

Symbol	X	Y	Z
N	-1.05762745562582	-0.71130274814583	-0.00012057868859
N	1.05766714875597	-0.71125343615683	0.00006033206527
C	0.00003955544504	-1.56049968428159	-0.00008246622139
C	0.67677967058418	0.62870132743418	0.00003571540730
C	-0.67680135678220	0.62866875708230	-0.00001644103067
C	-2.44034029601476	-1.15143383198125	0.00007360325640
H	-2.44628794704463	-2.23958963703951	-0.00154713946175
C	2.44039921488199	-1.15132000487459	-0.00013606731078
H	2.44639614387805	-2.23947620775481	0.00097856226099
H	-2.96263468894549	-0.78659617636396	-0.88742719840021
C	-1.66257009018030	1.74660067459461	-0.00013565924442
H	-2.30673887551936	1.71008944699996	-0.88362631032513
H	-1.14385986791616	2.70570240821819	0.00101875799136
H	-2.30834357656884	1.70884951746393	0.88212326490619
H	2.96178012352303	-0.78869896145256	-0.88909355042677
C	1.66250003834455	1.74667616504014	0.00019643904878
H	2.30696483023733	1.70988245769978	0.88345821244922
H	1.14375096132948	2.70575710822032	-0.00045499812346
H	2.30798078526098	1.70926015390318	-0.88229212243486
H	2.96256418034475	-0.78687373599488	0.88760391180053
H	-2.96162449798778	-0.78925059261077	0.88926773248199

[(IMe$_4$)$_2$P]$^+$

ωB97XD/def2-TZVPPD (CPCM (THF)): Energies/H = -1108.87590, Free Energies/H = -1108.47760, ZPVE/ kcal/mol (ωB97XD/def2-TZVP) = 249.95

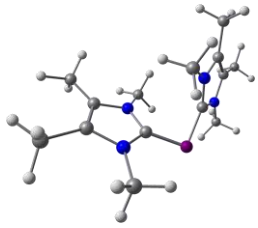

Symbol	X	Y	Z
N	-2.53326561471294	0.83634976132142	-0.44403498043662
N	-1.38499863309345	-0.36077555689940	0.92902965145354
C	-2.61836545950980	-0.98641850957086	0.78683191094077
C	-3.34687443592624	-0.22240694696071	-0.06323645935661
C	-2.92698174640079	1.89184321672068	-1.36348033078828
H	-2.02496627676761	2.32975764287271	-1.78855785006555
C	-0.33503957303628	-0.80240227642149	1.83338006418670
H	0.20806526298230	0.07221823311532	2.18856403167754
H	-3.49235944375984	2.66334815798295	-0.83844040048810
C	-4.73788592366522	-0.37962543566642	-0.57074643469873
H	-5.33656925000164	0.50874815670947	-0.35393256423607
H	-5.21159159999948	-1.23548582292170	-0.09147293618499
H	-4.75163423945651	-0.54090922205589	-1.65191408319285
H	-0.78982931357939	-1.31183952284668	2.68024965940118
C	-2.95547084249849	-2.25823061490007	1.48354891457679
H	-2.22655276821393	-3.03797405026550	1.24753225822531
H	-3.93855989385186	-2.60339787722591	1.16571931255400
H	-2.97447889707068	-2.12864201782722	2.56894159254120
H	0.35387720528588	-1.48373874718319	1.33153235462754
H	-3.53920317929597	1.46693548381118	-2.15719250347839
C	-1.33533980895548	0.74544242266372	0.16088179141910
P	0.00048383462415	1.94868999847237	-0.00174459975131
C	2.61790958581657	-0.98889156842684	-0.78600820038885
C	3.34670495837269	-0.22402708874238	0.06304092610256
C	0.33494631401735	-0.80512618701928	-1.83334621112829
H	-0.35440663747990	-1.48553153570553	-1.33083435274463
H	-0.20764150535653	0.06929879909005	-2.18980531968434
H	0.78973545365952	-1.31582794329962	-2.67945338313306
C	2.95446717516214	-2.26193596219388	-1.48072492695297
H	2.22510118814155	-3.04093399629730	-1.24363120921472
H	2.97373641669735	-2.13403567822903	-2.56631259145924
H	3.93731187856996	-2.60713322162468	-1.16217581557087
C	4.73760117719893	-0.38126534386756	0.57087341446419
H	4.75121590790906	-0.54111432203188	1.65225720342796
H	5.21089666663839	-1.23800697806440	0.09277055606421
H	5.33675831847022	0.50650523562820	0.35290035951943
C	2.92767375129988	1.89242864312281	1.36005598022049
H	3.49287558063806	2.66321815211870	0.83377509304529
H	2.02582692529074	2.33093885166844	1.78488471632905
H	3.54016621090334	1.46857220340788	2.15411626587529
C	1.33567904697763	0.74451973521739	-0.16274537048228
N	1.38488002021363	-0.36282347264989	-0.92929959799357
N	2.53358616376272	0.83570720497403	0.44217106477818

***4$_{INT1}$** (1,1-isomer)*

ωB97XD/def2-TZVPPD (CPCM (THF)): Energies/H = -3784.85850, Free Energies/H = -3784.36260, ZPVE/ kcal/mol (ωB97XD/def2-TZVP) = 311.15

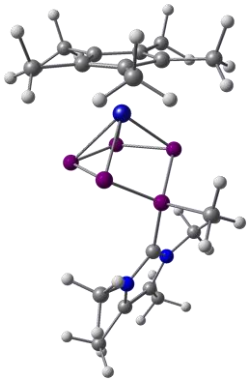

Symbol	X	Y	Z
Fe	1.66914085650634	0.05213711463635	-0.07166947937175
P	-1.05233972627025	0.16036862224655	1.11539912738271
P	0.16132852231626	-1.51510743548857	0.70027938960214
P	0.08659846135468	1.70730129846019	0.23758117917827
P	0.30034078428644	-1.23899345479225	-1.40156392503291
P	0.24484663300754	0.85234995795445	-1.70160979406026
N	-3.53925912300521	1.08404315060810	0.11109268860047
N	-3.48489102664910	-1.06196501419688	0.30439477676397
C	-2.79779212283869	0.05945222131660	0.54697612438958
C	-4.67539201136488	-0.75052386695519	-0.31993493144395
C	-3.20326249492920	2.50433855977710	0.20148829457113
H	-2.54074092718636	2.67334297921022	1.04486426116653
C	-4.71027086717369	0.60697792748670	-0.44120737067018
H	-4.12249195178375	3.06312696156494	0.36170498468313
C	-5.74615134104824	1.50638490575251	-1.01805863924021
H	-6.19333643939979	2.13699354776778	-0.24517993575921
H	-6.53730350794976	0.91307158379256	-1.47345690767899
H	-5.31720547800488	2.15551991223276	-1.78465578808634
H	-2.72145014168172	2.83158258192486	-0.71924506405148
C	-1.15124360522510	0.39464193583557	2.90338385249698
H	-1.69612985923624	1.31221677787758	3.13062011327774
H	-0.13065930015136	0.46502433906596	3.28456204381746
H	-1.65681289603353	-0.45996615691707	3.35561398687613
C	-5.65545205032282	-1.78999479442699	-0.73666285133025
H	-5.18034984952338	-2.53765225373227	-1.37579157449442
H	-6.46812462377251	-1.32778532671761	-1.29475859969652
H	-6.08369801184602	-2.30009391065436	0.12986928748495
C	-3.08241817231011	-2.42190926252547	0.66037455721222
H	-2.45050915763588	-2.39553992186312	1.54339577545464
H	-3.97876352611141	-2.99429009434188	0.88746436113800
H	-2.54531771114686	-2.88089742734933	-0.16881229880277
C	3.18003712067691	1.02629113487497	0.95420539412119
C	3.17877126162712	-0.36001364719334	1.27015911502088
C	3.35608631403872	1.16209159283889	-0.45670414844261
C	3.36140032858140	-1.09159505600285	0.05406555427938
C	3.47215704801945	-0.14803952590381	-1.01207989464580
C	3.07747328837159	2.14628333373695	1.94073463020741
H	2.44264928747952	1.87468372376777	2.78564314309161
H	2.66500833939912	3.04488124002581	1.48089010919445
H	4.07022368601305	2.39276460343165	2.33156674026278
C	3.45426849169021	2.45344568142386	-1.20631260858214
H	2.79336951369117	3.21124789704796	-0.78095065261276
H	3.18485619074071	2.32224434567699	-2.25477600524786
H	4.47698224789692	2.84182129144738	-1.16572697539561
C	3.06819392994751	-0.94097916650100	2.64528699188425
H	4.05069677497785	-0.95756498418850	3.12828200360979
H	2.69080740416077	-1.96354239390665	2.61540470613049
H	2.39711392849888	-0.35124557571762	3.27206699065106
C	3.69851892649301	-0.46544088211668	-2.45639525820012
H	3.19451576550385	0.25547161693483	-3.10170159273928
H	3.32463706778910	-1.45872396683179	-2.70667304259323
H	4.76779175587444	-0.43649557863144	-2.68875229420138
C	3.45956702187134	-2.58045618424552	-0.06275381333250
H	4.48734901645024	-2.91187507385450	0.11556767027401

H	3.16308570250773	-2.92067122311806	-1.05590044544340
H	2.81951125282885	-3.07838466054511	0.66807303833257

***4**INT1* (1,2-isomer)*

ωB97XD/def2-TZVPPD (CPCM (THF)): Energies/H = -3784.85600, Free Energies/H = -3784.36040, ZPVE/ kcal/mol (ωB97XD/def2-TZVP) = 311.00

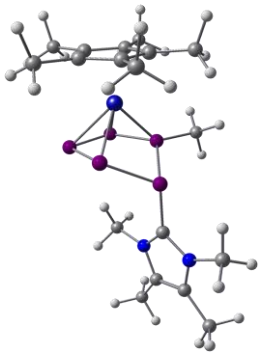

Symbol	X	Y	Z
Fe	1.77958732983334	-0.05228277383639	-0.07869776622866
P	-1.23298500626667	0.92824820852197	-0.17467920548550
P	0.08688475272585	0.06711565090478	-1.66105859527223
P	0.06487662670946	0.08815811089271	1.25284810115797
P	0.77430433575427	-1.88002375156030	1.01170039702401
P	0.79773234221674	-1.86546359171438	-1.08786967725916
N	-4.00823808053758	1.18496046937087	-0.18882675157851
N	-3.48975913613647	-0.89843571314022	-0.04135079364282
C	-2.96913104233319	0.33253368408174	-0.13405715825522
C	-4.86523024134505	-0.83254037896025	-0.03091109651099
C	-5.19412174900064	0.48743284276886	-0.13091158854936
C	-3.94451438741232	2.64009792017321	-0.30304787790407
H	-2.90721652009196	2.95856237782460	-0.26169215887592
C	-2.73346315191999	-2.13812316944215	0.06947601417819
H	-1.74596699783461	-1.98247979115771	-0.34755389002118
H	-4.49742157971434	3.08606600979827	0.52284850967516
C	-6.51967242582756	1.16173427809430	-0.18134215163989
H	-6.64831396008040	1.83829227944642	0.66728582338725
H	-7.31545315110129	0.41916176366730	-0.15232828469502
H	-6.62604320656652	1.74392340556691	-1.09994406416313
H	-2.65082952440408	-2.43122162492440	1.11656673705686
C	-5.72163399559765	-2.04457891632333	0.07959092496334
H	-5.57803497583026	-2.70735332607338	-0.77734459390414
H	-6.77052468220321	-1.75477573827972	0.11684007482001
H	-5.48720008626550	-2.60586156809315	0.98747059634811
H	-3.24551881640102	-2.91551068649771	-0.49373373445859
H	-4.38556592339715	2.94619555427950	-1.25137392732631
C	-0.13602189322443	0.62795396161937	2.96880659334765
H	-1.09808056010312	0.29268517493346	3.35723241778248
H	-0.07758918524545	1.71607666706430	3.01127564258672
H	0.67048643652611	0.19764189920417	3.56402858944038
C	3.76748661690728	-0.55146019711537	-0.19592472223521
C	3.39665915787558	0.26454400959091	-1.30520152830148
C	2.91034320995070	1.51049612181292	-0.79388855146294
C	2.98561609025383	1.46070087079785	0.62654676519978
C	3.51102310602500	0.18484234922590	1.00070408805218
C	3.80235185363679	-0.27888219037236	2.39347038593005
H	3.13174699505221	0.18574662895397	3.11744084993786
H	4.82798240070726	-0.01834678098411	2.67385460193662
H	3.69502348909557	-1.36063772686056	2.47982667502269
C	2.62661691778345	2.58149415180732	1.55178529355744
H	1.75556588879177	3.13077114849679	1.19076725276795
H	3.46039460806675	3.28700423840308	1.62563693156221
H	2.40840804238144	2.21770440030447	2.55616323971514
C	2.46533997630662	2.68964131558302	-1.60059263468794
H	2.09643597921181	2.38489545092555	-2.58024886647117
H	3.30169282663584	3.37990895112740	-1.75220167921955
H	1.66761708278225	3.23566388657740	-1.09438541749446
C	3.53154925571775	-0.09710221398398	-2.75064193621182
H	3.48903033659267	-1.17743359662720	-2.89391213156549
H	4.48976517901573	0.25739843752141	-3.14305229186238

H	2.73736719223598	0.35454567469710	-3.34748335118309
C	4.34399434500425	-1.93014554935402	-0.26737202529846
H	4.05814070626846	-2.52278730832183	0.60280110893033
H	5.43712606097526	-1.88403551151741	-0.29875799677512
H	4.00290813780045	-2.45578178889796	-1.15971016584061

4INT2

ωB97XD/def2-TZVPPD (CPCM (THF)): Energies/H = -4168.67790, Free Energies/H = -4167.98350, ZPVE/ kcal/mol (ωB97XD/def2-TZVP) = 435.71

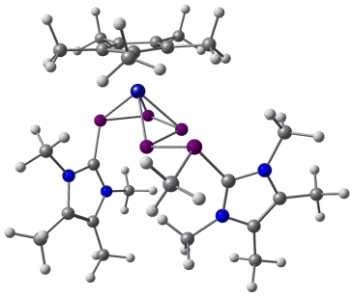

Symbol	X	Y	Z
Fe	1.85413110177616	-0.48326043181342	-0.21967878325519
P	2.07229195757262	1.64640590960001	-1.01490195895688
P	-0.15629853021065	0.26364921365242	0.59126620270332
P	1.29085124497069	0.19300212939549	-2.35737650155721
P	-0.17801671546802	-0.82338937805941	-1.22001607220051
P	-1.24577684686785	-1.31964296080929	1.68547729714853
N	0.70958151500524	3.32478987269613	0.72907155025480
N	-0.39391876412099	3.17202346118202	-1.10992688029974
N	-3.65401657445307	-0.47652790160675	0.30196332810636
N	-3.19049004644605	-2.56822581749126	0.12117979650036
C	3.54831078212917	-0.55755698960756	0.95799863321577
C	0.70145191214819	2.73239829542335	-0.47509475947924
C	3.05790736192406	-2.07714712452714	-0.70779768876312
C	3.84696432508260	-0.93313515735546	-0.38895538016902
C	-1.12560762484112	4.00122645444666	-0.26841495338642
C	-0.42945981903643	4.09463126319881	0.89217261616765
C	2.57760288861385	-1.46749509567258	1.46364388550587
C	1.70413243268387	3.05166401385605	1.75092062462060
H	1.56609271017583	2.03671345517852	2.12868500715455
H	1.59171910620047	3.76876890487592	2.55999808888416
H	2.70182716517754	3.14629239131411	1.32464828490827
C	2.27543957247640	-2.41150548583867	0.43431994949079
C	-0.79591695966934	2.83937405708917	-2.46830835119822
H	0.09076061076679	2.67241158229666	-3.07347574452808
H	-1.35777375220510	3.67583915465431	-2.87900626286055
H	-1.41289408316764	1.94030715962620	-2.47332280867626
C	-4.63945670232543	-1.03507199096011	-0.49234385719842
C	-2.77564184667649	-1.41864453087444	0.67541143059159
C	-0.72187424691204	4.84151304240803	2.14640772877942
H	-0.79278339728550	4.16452790354978	3.00170041558794
H	-1.66974143379775	5.36941467653914	2.04959962408498
H	0.05663961006926	5.57846914912251	2.36044193612632
C	-4.34013164386724	-2.35547524019198	-0.61493743619574
C	-2.41659650984852	4.61909005043758	-0.67840437456516
H	-2.27977357629827	5.32427066494893	-1.50257167356569
H	-2.84882048778809	5.16077194807117	0.16204319606334
H	-3.13301745510474	3.85826429998900	-0.99841150388444
C	3.07292905785926	-2.83551604574985	-1.99721431546659
H	2.07727211674783	-3.20731552815644	-2.24673447248961
H	3.74525089817197	-3.69693515805925	-1.92461272926880
H	3.41404587035540	-2.20836990330988	-2.82114551506875
C	4.22268887094969	0.53045636304270	1.73242208544472
H	4.44596453728243	1.39107447515316	1.10037520144132
H	5.16792221648130	0.16644947874614	2.14942362013828
H	3.60441063780419	0.86918458394856	2.56431222894555
C	4.86337227791829	-0.28605491917472	-1.27594980152086
H	4.57119603691006	-0.34718025007135	-2.32586915897073
H	5.83483888643933	-0.77924412669528	-1.16710338743656
H	4.99330774786091	0.76742185986362	-1.02485610429082
C	2.06145460813790	-1.48320430817180	2.86942628010080
H	1.87482701859892	-0.47275953796418	3.23825744805519
H	2.79423169240303	-1.95162750778498	3.53496480864482

H	1.13427039249116	-2.05083338120900	2.94831577771531
C	-3.61363856054258	0.93784711214498	0.65561955992778
H	-3.97510971366695	1.51730953660099	-0.19155502880239
H	-2.58719464863994	1.22789754015447	0.85917349311898
H	-4.24580508327768	1.12654363542438	1.52405259370406
C	1.39213038117909	-3.61446762135325	0.54554380454190
H	0.67918069375861	-3.51296269074611	1.36235752487020
H	1.99705820330107	-4.50879232682181	0.73002953681191
H	0.82760306512905	-3.77760820276095	-0.37435032928435
C	-1.82632924325019	-0.36448825498620	3.14980806140975
H	-0.97668373697870	-0.31153047800442	3.83536489012525
H	-2.62944322854203	-0.91154758412897	3.64828786925918
H	-2.15271236857216	0.65110643527896	2.92929268323233
C	-2.52213683941813	-3.86280687109061	0.20215542364890
H	-2.03349256751062	-4.08034198660923	-0.74817944500603
H	-3.26191683339769	-4.63083472480570	0.42200347143557
H	-1.77971523069614	-3.82896458778847	0.99381269349635
C	-5.77332805154121	-0.24061416085616	-1.03912094301369
H	-6.32681723036739	0.25409597358759	-0.23730224099027
H	-6.45922788002469	-0.89628622754889	-1.57353707277991
H	-5.42268843296078	0.52654051794689	-1.73429352782325
C	-5.02693528665985	-3.45120517418965	-1.35194908981615
H	-4.34792362227012	-3.92943700185363	-2.06219860058710
H	-5.87477585525920	-3.05113308512174	-1.90601450817395
H	-5.39557007658582	-4.21788881562383	-0.66562239043313

4

ωB97XD/def2-TZVPPD (CPCM (THF)): Energies/H = -3443.58910, Free Energies/H = -3443.09810, ZPVE/ kcal/mol (ωB97XD/def2-TZVP) = 308.12

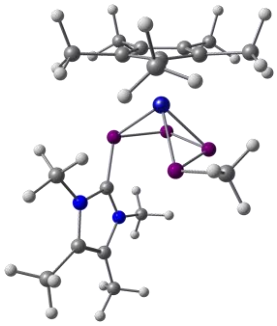

Symbol	X	Y	Z
Fe	-1.21664443712960	0.10721989249554	-0.05035129430529
P	0.49480548668823	0.41070218954995	-1.53031960490659
P	0.43410185302360	-0.18236442739119	1.54065315959440
P	-0.35795708168408	2.15976165287112	-0.66317631701583
P	-0.45993278846604	1.72074156040353	1.40471210459406
C	-0.22893905267367	-0.62635535409840	3.22575432176227
N	2.64800985535503	-1.10057189238917	-0.65194559574576
N	3.08767822030794	0.98549441495350	-0.37861778709140
C	-2.15144064628840	-1.44416609615998	-1.04325522311063
C	2.13601703140921	0.13232890691349	-0.78131290031784
C	-3.21831820085316	0.47545027997247	-0.33681540239688
C	-2.66356091242631	-0.18147112007754	-1.47461617008488
C	4.19844219414998	0.27751500407814	0.06694707112238
C	3.91923538988941	-1.03829723234030	-0.10508898072483
C	-2.38356924584541	-1.56169255647173	0.35602112404214
C	1.88802686348238	-2.30683047154470	-0.92160568849272
H	1.04692863282210	-2.35927017122480	-0.22732915843635
H	2.53317060167271	-3.17226439463651	-0.79465327267028
H	1.51039533716328	-2.28506452205002	-1.94367740259571
C	-3.05417586865924	-0.37631403611621	0.79205806457772
C	2.99960262042355	2.43775570580651	-0.38837417425051
H	2.37633487075895	2.75304529841449	-1.22050114192408
H	4.00054720768414	2.84577784929962	-0.51425298139807
H	2.56624351293391	2.79916583094841	0.54453974178611
C	4.72902377504311	-2.25339129007484	0.18680330566257
H	4.23008585580676	-2.89548957610167	0.91732513358111
H	5.69720992900888	-1.96351565787420	0.59310056719560
H	4.90249276312131	-2.84022023422341	-0.71903036306420
C	5.41123979260966	0.95189722300091	0.60686444716686
H	5.90590886751132	1.55894202307755	-0.15620563430542
H	6.12214595382582	0.20530768105485	0.95912301635693
H	5.15717742253574	1.60407179240455	1.44613578019775
C	-3.90050265930937	1.80714049966404	-0.32126883224208
H	-3.71417359616827	2.33096757769906	0.61845742977380
H	-4.98383174688758	1.68674527108828	-0.42984593629838
H	-3.54855838478886	2.44311763556276	-1.13415320928251
C	-1.57330967302998	-2.50053233412724	-1.93116103862669
H	-0.98455762952138	-2.06498840305826	-2.73977746329403
H	-2.37568540068586	-3.09485812497372	-2.38225363221264
H	-0.93154749527865	-3.18229338614002	-1.37223867691771
C	-2.68101468698349	0.32215195937181	-2.88387969544614
H	-2.65933140072564	1.41295826407085	-2.91465959939541
H	-3.58671039058894	-0.01137361331433	-3.40136292039083
H	-1.82091319589203	-0.04534007336788	-3.44585996864561
C	-2.08161168836276	-2.77526495125254	1.17981588362901
H	-1.09617798377947	-3.18113043667138	0.94366854523322
H	-2.82184238530905	-3.55960650145883	0.98830492174966
H	-2.10509290173271	-2.55097596652060	2.24519988342662
C	-3.62101957390651	-0.10651336531194	2.15188330954144
H	-3.24050240073723	-0.80615561784068	2.89523866464235
H	-4.71098388908269	-0.21188815246101	2.12944450435038

H	-3.39179284964669	0.90602187124470	2.49004535958689
H	-0.26015277420172	-1.71510140433468	3.31158587601467
H	-1.22031794925385	-0.22907349660438	3.43747806452316
H	0.46838585267162	-0.25852252373395	3.98316878547820

TS1

ωB97XD/def2-TZVPPD (CPCM (THF)): Energies/H = -3784.77470, Free Energies/H = -3784.28910, ZPVE/ kcal/mol (ωB97XD/def2-TZVP) = 304.73

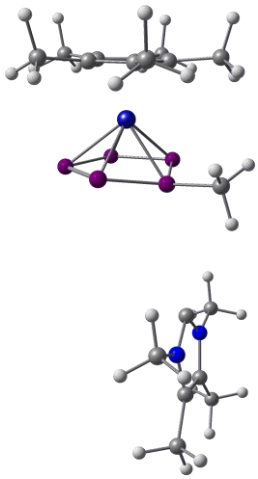

Symbol	X	Y	Z
Fe	2.09192025853514	1.33155786312571	1.27310103561102
P	0.18569271528306	0.50254807968120	0.18875161871209
P	-0.04171645318865	2.36811621065928	1.21792359817165
P	1.45736922333618	-0.94802837597472	1.11942900669284
P	0.68873959581734	1.83161097713334	3.16953237237674
P	1.57584953916043	-0.14439884112540	3.11266322126092
N	-4.61042509902651	-0.96926517651733	0.40861587025088
N	-3.58929552977392	-2.74227104783762	-0.22578330506001
C	-3.35702081972621	-1.42072386195624	0.07562588152198
C	-4.93819862941782	-3.10837109603854	-0.08919767132470
C	-4.88634748085056	0.40037124252751	0.82103668403866
H	-3.93447475767899	0.96043207251285	0.81114342919781
C	-5.59662700933577	-1.96504850557427	0.31933023202589
H	-5.31333608543438	0.42965751158672	1.84505712850450
C	-7.03885634417822	-1.72371357366956	0.62805580289049
H	-7.19110699092116	-1.39198199800798	1.67737001120442
H	-7.62542300731884	-2.65102762975204	0.48221236981004
H	-7.47853431667044	-0.94162265242913	-0.02744526029979
H	-5.60242307043823	0.89046233578743	0.12962388979167
C	-0.02535707763415	0.47386264551475	-1.63492417629774
H	0.81299022760831	-0.07983189731694	-2.09722927203677
H	-0.06007059157308	1.51396376770270	-2.01057036196226
H	-0.98518349918218	-0.03547266145837	-1.83345026306040
C	-5.44512386817935	-4.48851165977528	-0.35806644126895
H	-5.25970533267860	-4.80222863504079	-1.40719472851542
H	-6.53630400026378	-4.54173166874940	-0.17958566674617
H	-4.96061323228207	-5.24319526264567	0.29793794332277
C	-2.54636168253311	-3.66873879922169	-0.64469017568205
H	-1.58232639189226	-3.12077930136326	-0.62364459564397
H	-2.48681619303964	-4.53845783534123	0.04126801225028
H	-2.73145873787570	-4.05313719452733	-1.67246923346640
C	3.70981278107976	1.23304023172995	-0.06751240982957
C	3.09265256963777	2.54000259763213	-0.12628569482353
C	4.17566999637379	1.02069688801695	1.28779126309638
C	3.17998545293432	3.13379569646459	1.19173213007958
C	3.84996595054257	2.19579458996161	2.06588194296490
C	3.96420929009685	0.31768726134550	-1.22604483506836
H	3.24928332406460	0.48427603075283	-2.05365749364263
H	3.91778118545691	-0.74862813515057	-0.93139863203646
H	4.98428782981004	0.50610338435627	-1.62601780483715
C	4.96858077417299	-0.15656579951759	1.76538583893559
H	4.71235441341195	-1.08093245146888	1.21223011882168
H	4.82119882310925	-0.34550264787316	2.84608265458422
H	6.05116851873811	0.03861838180690	1.60327571925510
C	2.58263495741869	3.22794637467802	-1.35558384721558
H	3.37747132436002	3.88775836336722	-1.76655324906671
H	1.70399624922630	3.86678090941707	-1.14011827532052
H	2.30831165145278	2.50855506482681	-2.14956526540136
C	4.24967037943584	2.45046495676519	3.48599287940125
H	4.32657106901074	1.51430452539302	4.07178935003479
H	3.54050664777102	3.12610326973043	4.00207346020040

H	5.24889935329853	2.93828427975648	3.50328807258429
C	2.76500347185896	4.52684808755485	1.55308175175374
H	3.61777945871794	5.21976354048996	1.38215598294246
H	2.47536016300438	4.61201966996079	2.61807669044528
H	1.92012081636910	4.88165924609492	0.93172058387217

TS2

ωB97XD/def2-TZVPPD (CPCM (THF)): Energies/H = -4168.60990, Free Energies/H = -4167.92380, ZPVE/ kcal/mol (ωB97XD/def2-TZVP) = 430.50

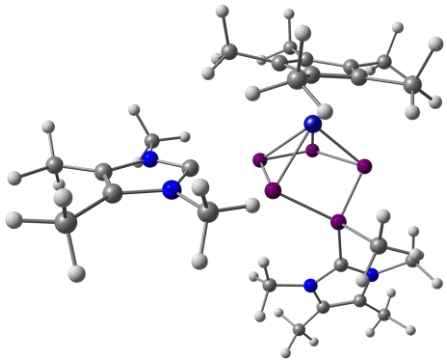

Symbol	X	Y	Z
Fe	-0.455054000	1.759314000	-0.174854000
P	-0.402909000	-0.668228000	0.311778000
P	1.875029000	-0.136962000	0.773942000
P	1.903049000	1.917250000	0.089581000
P	1.132275000	1.572599000	-1.927473000
P	-0.369702000	0.020164000	-1.764346000
C	-2.756851000	-1.644220000	0.053551000
N	3.442624000	-2.296686000	-0.315042000
N	4.710861000	-0.699010000	0.424276000
C	3.421989000	-1.096356000	0.306482000
C	5.555999000	-1.658906000	-0.115889000
C	2.288708000	-3.126903000	-0.658066000
H	1.364191000	-2.598963000	-0.400327000
C	4.751166000	-2.671462000	-0.584672000
H	2.336795000	-4.074592000	-0.104321000
C	5.093733000	-3.955990000	-1.258061000
H	4.727277000	-4.823077000	-0.685277000
H	6.181708000	-4.053536000	-1.358397000
H	4.655104000	-4.013326000	-2.267122000
H	2.294522000	-3.335595000	-1.736171000
C	1.992815000	-0.148625000	2.615776000
H	1.911788000	-1.184276000	2.977830000
H	1.144367000	0.434825000	3.000830000
H	2.930010000	0.293385000	2.981167000
C	7.039527000	-1.513453000	-0.131173000
H	7.356332000	-0.650488000	-0.739256000
H	7.503014000	-2.411157000	-0.559338000
H	7.444423000	-1.375280000	0.883919000
C	5.184776000	0.531556000	1.054488000
H	4.367803000	1.259689000	1.102251000
H	5.561984000	0.321417000	2.065687000
H	5.992708000	0.960867000	0.449704000
C	-2.080047000	2.298918000	1.096864000
C	-0.979923000	3.197888000	1.270557000
C	-2.498723000	2.358505000	-0.275620000
C	-0.715067000	3.821083000	-0.002370000
C	-1.651141000	3.294401000	-0.955393000
C	-2.776842000	1.547286000	2.191272000
H	-2.081697000	1.228175000	2.981143000
H	-3.286099000	0.654995000	1.804969000
H	-3.540120000	2.189312000	2.666752000
C	-3.712873000	1.697888000	-0.855023000
H	-3.897029000	0.716692000	-0.398015000
H	-3.618421000	1.551816000	-1.940163000
H	-4.606548000	2.324563000	-0.683266000
C	-0.322059000	3.540627000	2.575031000
H	-0.849093000	4.378655000	3.065703000
H	0.725583000	3.844514000	2.439083000
H	-0.337156000	2.693434000	3.276434000
C	-1.802521000	3.732776000	-2.381963000
H	-2.127904000	2.905905000	-3.029948000

H	-0.859650000	4.121803000	-2.790891000
H	-2.558307000	4.534144000	-2.462608000
C	0.267908000	4.926619000	-0.253447000
H	-0.205377000	5.909777000	-0.082900000
H	0.641632000	4.915295000	-1.287818000
H	1.138464000	4.861190000	0.415111000
C	-4.163288000	-3.265443000	0.855942000
C	-4.403448000	-3.142436000	-0.485076000
N	-3.530743000	-2.149792000	-0.944737000
N	-3.155046000	-2.342851000	1.152640000
C	-3.500055000	-1.714634000	-2.332164000
H	-2.724039000	-0.950710000	-2.446412000
H	-3.267377000	-2.559317000	-2.998243000
H	-4.472318000	-1.292107000	-2.628438000
C	-5.365321000	-3.854001000	-1.376848000
H	-5.953548000	-4.582808000	-0.803083000
H	-6.072815000	-3.157407000	-1.856814000
H	-4.849547000	-4.401650000	-2.183401000
C	-4.784770000	-4.147610000	1.886393000
H	-5.556222000	-4.783518000	1.431921000
H	-4.043355000	-4.810776000	2.362682000
H	-5.264043000	-3.563567000	2.689963000
C	-2.616484000	-2.172873000	2.493115000
H	-2.215055000	-3.125056000	2.872250000
H	-1.808036000	-1.435941000	2.460408000
H	-3.395779000	-1.821256000	3.186158000

7INT

ωB97XD/def2-TZVP (CPCM (THF)): Energies/H = -4614.02923, Free Energies/H = -4613.29140008, ZPVE/ kcal/mol = 548.87

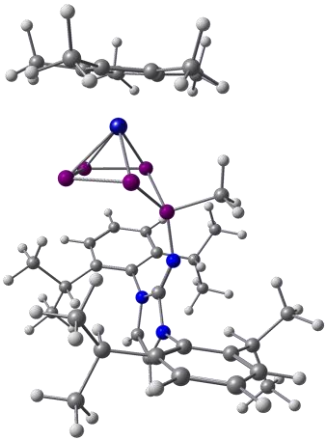

Symbol	X	Y	Z
Fe	1.50564876349966	9.06891562540117	5.20867796192496
P	0.28359569210542	7.09086813988539	5.31740518455039
P	1.17886013213032	9.10773000358900	2.91023695663565
P	-0.25287020853547	7.42891637717046	3.18207046846872
P	3.04550604889105	8.24835058033417	3.61111287211562
P	2.44212725471066	6.90770202759770	5.24747250280622
N	-0.35522769164548	5.14636545866085	-0.04684756059876
N	0.07611514493630	3.99614542848258	1.79454789643054
C	-0.10662483783431	3.82687408988582	-0.42955234263490
C	0.77523702307318	11.01691242836616	5.56980476537142
C	0.36027331593836	10.12908129213503	6.62819683742929
C	0.36235089944765	3.59746193216725	3.15160777179421
C	-0.26549496483240	5.27255857192678	1.34017523497807
C	-1.04557080279483	9.93628262396115	7.12043447761745
C	2.22156176867008	10.99648636340568	5.50531472066149
C	0.15796928549710	3.11673813968696	0.70498716542592
C	2.70421433495668	10.08352922027464	6.52505328681391
C	1.70161718182654	3.25726328389165	3.49086879815071
C	-0.71758874047240	6.21508943160346	-0.94295746837257
C	-0.12437016361067	11.90401490015668	4.75753283074967
N	-0.60105076641242	6.35896213336624	1.98278570889632
C	1.54817453267217	9.55286976780284	7.22384369123935
C	1.56882772279695	8.64735312071512	8.42202701423401
C	0.31522916792384	6.99439308051694	-1.53025882525012
C	-3.03328389823244	4.30658024816140	4.80391846830798
C	-3.19879504878704	5.56840343827317	-0.62235961355276
C	4.14218406165514	9.84999239350640	6.89053699280118
C	-0.40249675720935	3.04882432572340	5.38305682311769
C	-0.71090319351596	3.48710352025002	4.07971398327410
C	3.06622088706705	11.85052889162995	4.60379445611450
C	-1.87530289469155	8.30124277464473	3.33210818548169
C	-4.24786031798246	6.41403483179579	0.12756700045537
C	2.85571841776864	3.30715911245962	2.48645562733290
C	-2.15967256658923	3.75101854894094	3.66517838099735
C	-3.86110735020259	4.68090362862646	-1.69855588665392
C	1.79395477634676	6.72597952149922	-1.25320896029393
C	-2.09235057113139	6.43023576002101	-1.22929122507761
C	-0.06720862705012	8.01253233749369	-2.42847515387833
C	3.30820427959491	1.88200613405174	2.09638362705593
C	1.94623944629215	2.81284447855325	4.80799106396087
C	-2.78724218726763	2.47072792575736	3.06676774708765
C	0.91084453388450	2.71492468755037	5.74594342913947
C	-2.41732614872953	7.46428740373843	-2.13186205658421
C	-1.41746763761993	8.24786163128971	-2.72559911346357
C	2.44634010162248	5.99105396134622	-2.44530879594442
C	2.57245397977229	8.00666825723987	-0.89586396435086
C	4.05387091678113	4.13270728090818	2.99445913136241
H	-0.14933305413655	3.51534774388418	-1.47713941045466
H	-1.79346731039483	10.12326718583742	6.32488982125985
H	-1.21097795703387	8.91139445272647	7.50712304642592
H	-1.26574091511050	10.64432283479685	7.95045370851645

H	0.39226211451613	2.05809696624154	0.84579629600645
H	0.29072199409570	12.09701854952278	3.74878928998892
H	-1.13343062718928	11.46512238625267	4.62971026583369
H	-0.25389197630663	12.88950530892308	5.25819574427766
H	0.71182422894215	7.94355309592957	8.41695608287687
H	2.49662254784295	8.04349459452809	8.46340744697407
H	1.50837144993701	9.23494028606271	9.36517233722876
H	-4.02743433284276	4.59933740584993	4.40863518039486
H	-3.20957270085151	3.55446302064138	5.60107059611154
H	-2.57207169564913	5.20013504742978	5.27280421602064
H	-2.72800218678530	4.89194799393746	0.11980019086516
H	4.80816290629931	9.95131301570189	6.01069391136202
H	4.48342398795653	10.58457084424226	7.65355571852402
H	4.29823393753884	8.83661266458041	7.31084155039381
H	-1.20738947920198	2.95662720861292	6.12684040679250
H	3.22378512511199	12.85992199500846	5.04517541663902
H	4.06445931049740	11.40193397195650	4.43236100916339
H	2.59037696879078	11.99576533343552	3.61275116205812
H	-2.64848883409472	7.56439120758620	3.62508514302157
H	-1.80577336056956	9.10123935947088	4.09154428845823
H	-2.13680681029522	8.72963715099499	2.34515042988164
H	-4.78825782952150	7.09912684816649	-0.55852894735732
H	-5.00379470767371	5.75515946393997	0.60266732374756
H	-3.77748598503144	7.02595850059681	0.92311381719239
H	2.48480836256618	3.80586811766055	1.56777779672689
H	-2.14185992890612	4.52301633773763	2.86920183634159
H	-4.62962430458605	4.02404779220552	-1.24066643118398
H	-4.36202992967750	5.29741922327307	-2.47434369603484
H	-3.11721608753780	4.03450790403669	-2.20768542344485
H	1.85235509745591	6.04975987496879	-0.37524812789465
H	0.70788731975282	8.63232184062211	-2.90504658379001
H	4.10294317706703	1.92625123298936	1.32293968290210
H	3.72218089655223	1.34308893723333	2.97450336486270
H	2.47341203135551	1.27335672613235	1.69376874119389
H	2.97172466825863	2.54081321351581	5.10195004684628
H	-2.83622666206947	1.66376831332076	3.82808699529880
H	-3.82055981869708	2.67163738598562	2.71484125944120
H	-2.20204759582614	2.08921462042418	2.20577427856089
H	1.12693857041449	2.37154951807075	6.76979136795681
H	-3.47391416136301	7.65547313843336	-2.37661784472954
H	-1.69295014879465	9.04945683519743	-3.42892187761899
H	2.42663257488415	6.62072692803777	-3.35990083154475
H	3.50659599465428	5.75149754493998	-2.22097741274068
H	1.92231156181880	5.04131704850301	-2.67697296508888
H	3.61996386904089	7.75448490969078	-0.63129465654064
H	2.60895253145210	8.71855185273304	-1.74663894976549
H	2.11888764179436	8.52713684424649	-0.02736687652079
H	4.52649492984665	3.66982743876890	3.88600763215842
H	4.83150991846932	4.19831835817111	2.20539224572103
H	3.74968038852008	5.16319851179555	3.26644029055571

11.6. References

[1] R. Hoffmann, *Angew. Chem. Int. Ed. Engl.* **1982**, *21*, 711–724.

[2] a) B. M. Cossairt, N. A. Piro, C. C. Cummins, *Chem. Rev.* **2010**, *110*, 4164–4177; b) M. Caporali, L. Gonsalvi, A. Rossin, M. Peruzzini, *Chem. Rev.* **2010**, *110*, 4178–4235; c) M. Scheer, G. Balázs, A. Seitz, *Chem. Rev.* **2010**, *110*, 4236–4256; d) L. Giusti, V. R. Landaeta, M. Vanni, J. A. Kelly, R. Wolf, M. Caporali, *Coord. Chem. Rev.* **2021**, *441*, 213927; e) C. M. Hoidn, D. J. Scott, R. Wolf, *Chem. Eur. J.* **2021**, *27*, 1886–1902.

[3] M. Donath, K. Schwedtmann, T. Schneider, F. Hennersdorf, A. Bauzá, A. Frontera, J. J. Weigand, *Nat. Chem.* **2022**, *14*, 384–391.

[4] a) U. Lennert, P. B. Arockiam, V. Streitferdt, D. J. Scott, C. Rödl, R. M. Gschwind, R. Wolf, *Nat. Cat.* **2019**, *2*, 1101–1106; b) R. Rothfelder, V. Streitferdt, U. Lennert, J. Cammarata, D. J. Scott, K. Zeitler, R. M. Gschwind, R. Wolf, *Angew. Chem. Int. Ed.* **2021**, *60*, 24650–24658.

[5] D. J. Scott, J. Cammarata, M. Schimpf, R. Wolf, *Nat. Chem.* **2021**, *13*, 458–464.

[6] O. J. Scherer, *Angew. Chem. Int. Ed. Engl.* **1990**, *29*, 1104–1122.

[7] S. Wang, J. D. Sears, C. E. Moore, A. L. Rheingold, M. L. Neidig, J. S. Figueroa, *Science* **2022**, *375*, 1393–1397.

[8] A. K. Eckhardt, M.-L. Y. Riu, M. Ye, P. Müller, G. Bistoni, C. C. Cummins, *Nat. Chem.* **2022**, *14*, 928–934.

[9] a) M. Baudler, *Angew. Chem. Int. Ed. Engl.* **1982**, *21*, 492–512; b) M. Baudler, *Angew. Chem. Int. Ed. Engl.* **1987**, *26*, 419–441; c) M. Baudler, K. Glinka, *Chem. Rev.* **1993**, *93*, 1623–1667.

[10] a) N. Burford, T. S. Cameron, P. J. Ragogna, E. Ocando-Mavarez, M. Gee, R. McDonald, R. E. Wasylishen, *J. Am. Chem. Soc.* **2001**, *123*, 7947–7948; b) M. Gonsior, I. Krossing, L. Müller, I. Raabe, M. Jansen, L. van Wüllen, *Chem. Eur. J.* **2002**, *8*, 4475–4492; c) J. J. Weigand, N. Burford, M. D. Lumsden, A. Decken, *Angew. Chem. Int. Ed.* **2006**, *45*, 6733–6737; d) J. J. Weigand, M. Holthausen, R. Fröhlich, *Angew. Chem. Int. Ed.* **2009**, 48, 295–298; e) M. H. Holthausen, J. J. Weigand, *Chem. Soc. Rev.* **2014**, *43*, 6639–6657; f) A. Wiesner, S. Steinhauer, H. Beckers, C. Müller, S. Riedel, *Chem. Sci.* **2018**, *9*, 7169–7173; g) C. Taube, K. Schwedtmann, M. Noikham, E. Somsook, F. Hennersdorf, R. Wolf, J. J. Weigand, *Angew. Chem. Int. Ed.* **2020**, *59*, 3585–3591.

[11] a) O. Back, B. Donnadieu, P. Parameswaran, G. Frenking, G. Bertrand, *Nat. Chem.* **2010**, *2*, 369–373; b) T. Köchner, T. A. Engesser, H. Scherer, D. A. Plattner, A. Steffani, I. Krossing, *Angew. Chem. Int. Ed.* **2012**, *51*, 6529–6531; c) J. Frötschel-Rittmeyer, M. Holthausen, C. Friedmann, D. Röhner, I. Krossing, J. J. Weigand, *Sci. Adv.* **2022**, *8*, eabq8613.

[12] a) S. S. Chitnis, H. A. Sparkes, V. T. Annibale, N. E. Pridmore, A. M. Oliver, I. Manners, *Angew. Chem. Int. Ed.* **2017**, *56*, 9536–9540; b) S. S. Chitnis, R. A. Musgrave, H. A. Sparkes, N. E. Pridmore, V. T. Annibale, I. Manners, *Inorg. Chem.* **2017**, *56*, 4522–4538.

[13] M. H. Holthausen, S. K. Surmiak, P. Jerabek, G. Frenking, J. J. Weigand, *Angew. Chem. Int. Ed.* **2013**, *52*, 11078–11082.

[14] P. Royla, K. Schwedtmann, Z. Han, J. Fidelius, D. P. Gates, R. M. Gomila, A. Frontera, J. J. Weigand, *J. Am. Chem. Soc.* **2023**, *145*, 10364–10375.

[15] a) E. Mädl, M. V. Butovskii, G. Balázs, E. V. Peresypkina, A. V. Virovets, M. Seidl, M. Scheer, *Angew. Chem. Int. Ed.* **2014**, *53*, 7643–7646; b) E. Mädl, G. Balázs, E. V. Peresypkina, M. Scheer, *Angew. Chem. Int. Ed.* **2016**, *55*, 7702–7707; c) M. Piesch, S. Reichl, M. Seidl, G. Balázs, M. Scheer, *Angew. Chem. Int. Ed.* **2019**, *58*, 16563–16568; d) F. Riedlberger, S. Todisco, P. Mastrorilli, A. Y. Timoshkin, M. Seidl, M. Scheer, *Chem. Eur. J.* **2020**, *26*, 16251–16255; e) F. Riedlberger, M. Seidl, M. Scheer, *Chem. Commun.* **2020**, *56*, 13836–13839; f) M. Piesch, M. Seidl, M. Scheer, *Chem. Sci.* **2020**, 11, 6745–6751; g) V. Heinl, M. Seidl, G. Balázs, M. Scheer, *Chem. Eur. J.* **2023**, *29*, e202301016.

[16] a) B. M. Cossairt, C. C. Cummins, *Angew. Chem. Int. Ed.* **2008**, *47*, 169–172; b) D. Tofan, B. M. Cossairt, C. C. Cummins, *Inorg. Chem.* **2011**, *50*, 12349–12358; c) T. Li, J. Wiecko, N. A. Pushkarevsky, M. T. Gamer, R. Köppe, S. N. Konchenko, M. Scheer, P. W. Roesky, *Angew. Chem. Int. Ed.* **2011**, *50*, 9491–9495; d) C. M. Knapp, B. H. Westcott, M. A. C. Raybould, J. E. McGrady, J. M. Goicoechea, *Angew. Chem. Int. Ed.* **2012**, *51*, 9097–9100; e) A. Velian, C. C. Cummins, *Chem. Sci.* **2012**, *3*, 1003; f) T. Li, M. T. Gamer, M. Scheer, S. N. Konchenko, P. W. Roesky, *Chem. Commun.* **2013**, *49*, 2183–2185; g) M. V. Butovskiy, G. Balázs, M. Bodensteiner, E. V. Peresypkina, A. V. Virovets, J. Sutter, M. Scheer, *Angew. Chem. Int. Ed.* **2013**, *52*, 2972–2976; h) S. Pelties, A. W. Ehlers, R. Wolf, *Chem. Commun.* **2016**, 52, 6601–6604; i) S. Pelties, T. Maier, D. Herrmann, B. de Bruin, C. Rebreyend, S. Gärtner, I. G. Shenderovich, R. Wolf, *Chem. Eur. J.* **2017**, *23*, 6094–6102; j) M. Piesch, C. Graßl, M. Scheer, *Angew. Chem. Int. Ed.* **2020**, *59*, 7154–7160; k) R. Yadav, M. Weber, A. K. Singh, L. Münzfeld, J. Gramüller, R. M. Gschwind, M. Scheer, P. W. Roesky, *Chem. Eur. J.* **2021**, *27*, 14128–14137; l) P. Coburger, J. Leitl, D. J. Scott, G. Hierlmeier, I. G. Shenderovich, E. Hey-Hawkins, R. Wolf, *Chem. Sci.* **2021**, *12*, 11225–11235.

[17] a) B. M. Cossairt, M.-C. Diawara, C. C. Cummins, *Science* **2009**, *323*, 602; b) B. M. Cossairt, C. C. Cummins, *Angew. Chem. Int. Ed.* **2010**, *49*, 1595–1598; c) U. Chakraborty, J. Leitl, B. Mühldorf, M. Bodensteiner, S. Pelties, R. Wolf, *Dalton Trans.* **2018**, *47*, 3693–3697; d) E. Mädl, E. Peresypkina, A. Y. Timoshkin, M. Scheer, *Chem. Commun.* **2016**, *52*, 12298–12301; e) M. Piesch, S. Reichl, M. Seidl, G. Balázs, M. Scheer, *Angew. Chem. Int. Ed.* **2021**, *60*, 15101–15108; f) S. Reichl, E. Mädl, F. Riedlberger, M. Piesch, G. Balázs, M. Seidl, M. Scheer, *Nat. Commun.* **2021**, *12*, 5774; g) J. A. Kelly, V. Streitferdt, M. Dimitrova, F. F. Westermair, R. M. Gschwind, R. J. F. Berger, R. Wolf, *J. Am. Chem. Soc.* **2022**, *144*, 20434–20441; h) S. B. Dinauer, M. Piesch, R. Szlosek, M. Seidl, G. Balázs, M. Scheer, *Chem. Eur. J.* **2023**, *29*, e202300459.

[18] a) I. de los Rios, J.-R. Hamon, P. Hamon, C. Lapinte, L. Toupet, A. Romerosa, M. Peruzzini, *Angew. Chem. Int. Ed.* **2001**, *40*, 3910–3912; b) I. Krossing, *J. Am. Chem. Soc.* **2001**, 123, 4603–4604; c) P. Barbaro, A. Ienco, C. Mealli, M. Peruzzini, O. J. Scherer, G. Schmitt, F. Vizza, G. Wolmershäuser, *Chem. Eur. J.* **2003**, *9*, 5196–5210; d) M. Peruzzini, R. R. Abdreimova, Y. Budnikova, A. Romerosa, O. J. Scherer, H. Sitzmann, *J. Organomet. Chem.* **2004**, *689*, 4319–4331; e) P. Barbaro, C. Bazzicalupi, M. Peruzzini, S. Seniori Costantini, P. Stoppioni, *Angew. Chem. Int. Ed.* **2012**, *51*, 8628–8631; f) I. M. Riddlestone, P. Weis, A. Martens, M. Schorpp, H. Scherer, I. Krossing, *Chem. Eur. J.* **2019**, *25*, 10546–10551; g) J. Sun, H. Verplancke, J. I. Schweizer, M. Diefenbach, C. Würtele, M. Otte, I. Tkach, C. Herwig, C. Limberg, S. Demeshko, M. C. Holthausen, S. Schneider, *Chem* **2021**, *7*, 1952–1962.

[19] a) G. Capozzi, L. Chiti, M. Di Vaira, M. Peruzzini, P. Stoppioni, *Chem. Commun.* **1986**, 1799–1800; b) A. Barth, G. Huttner, M. Fritz, L. Zsolnai, *Angew. Chem. Int. Ed. Engl.* **1990**, *29*, 929–931.

[20] a) M. Fleischmann, F. Dielmann, L. J. Gregoriades, E. V. Peresypkina, A. V. Virovets, S. Huber, A. Y. Timoshkin, G. Balázs, M. Scheer, *Angew. Chem. Int. Ed.* **2015**, *54*, 13110–13115; b) L. Dütsch, M. Fleischmann, S. Welsch, G. Balázs, W. Kremer, M. Scheer, *Angew. Chem. Int. Ed.* **2018**, *57*, 3256–3261; c) C. Riesinger, L. Dütsch, G. Balázs, M. Bodensteiner, M. Scheer, *Chem. Eur. J.* **2020**, *26*, 17165–17170; d) C. Riesinger, G. Balázs, M. Bodensteiner, M. Scheer, *Angew. Chem. Int. Ed.* **2020**, *59*, 23879–23884; e) M. Piesch, S. Reichl, C. Riesinger, M. Seidl, G. Balazs, M. Scheer, *Chem. Eur. J.* **2021**, *27*, 9129–9140; f) C. Riesinger, G. Balázs, M. Seidl, M. Scheer, *Chem. Sci.* **2021**, *12*, 13037–13044; g) M. Piesch, A. Nicolay, M. Haimerl, M. Seidl, G. Balázs, T. Don Tilley, M. Scheer, *Chem. Eur. J.* **2022**, *28*, e202201144; h) C. Riesinger, F. Dielmann, R. Szlosek, A. V. Virovets, M. Scheer, *Angew. Chem. Int. Ed.* **2023**, *62*, e202218828; i) L. Zimmermann, C. Riesinger, G. Balázs, M. Scheer, *Chem. Eur. J.* **2023**, e202301974.

[21] O. J. Scherer, T. Brück, *Angew. Chem. Int. Ed. Engl.* **1987**, *26*, 59.

[22] E. Urnius, W. W. Brennessel, C. J. Cramer, J. E. Ellis, P. v. R. Schleyer, *Science* **2002**, *295*, 832–834.

[23] a) O. J. Scherer, J. Schwalb, G. Wolmershäuser, W. Kaim, R. Gross, *Angew. Chem. Int. Ed. Engl.* **1986**, *25*, 363–364; b) C. Riesinger, D. Röhner, I. Krossing, M. Scheer, *Chem. Commun.* **2023**, *59*, 4495–4498.

[24] C. M. Hoidn, T. M. Maier, K. Trabitsch, J. J. Weigand, R. Wolf, *Angew. Chem. Int. Ed.* **2019**, *58*, 18931–18936.

[25] A. K. Adhikari, C. G. P. Ziegler, K. Schwedtmann, C. Taube, J. J. Weigand, R. Wolf, *Angew. Chem. Int. Ed.* **2019**, *58*, 18584–18590.

[26] R. Yadav, T. Simler, B. Goswami, C. Schoo, R. Köppe, S. Dey, P. W. Roesky, *Angew. Chem. Int. Ed.* **2020**, *59*, 9443–9447.

[27] R. Yadav, T. Simler, S. Reichl, B. Goswami, C. Schoo, R. Köppe, M. Scheer, P. W. Roesky, *J. Am. Chem. Soc.* **2020**, *142*, 1190–1195.

[28] H. Brake, E. Peresypkina, A. V. Virovets, M. Piesch, W. Kremer, L. Zimmermann, C. Klimas, M. Scheer, *Angew. Chem. Int. Ed.* **2020**, *59*, 16241–16246.

[29] a) C. G. P. Ziegler, T. M. Maier, S. Pelties, C. Taube, F. Hennersdorf, A. W. Ehlers, J. J. Weigand, R. Wolf, *Chem. Sci.* **2019**, *10*, 1302–1308; b) C. M. Hoidn, K. Trabitsch, K. Schwedtmann, C. Taube, J. J. Weigand, R. Wolf, *Chem. Eur. J.* **2023**, e202301930.

[30] P. Pyykkö, *J. Phys. Chem. A* **2015**, *119*, 2326–2337.

[31] C. B. Macdonald, J. F. Binder, A. Swidan, J. H. Nguyen, S. C. Kosnik, B. D. Ellis, *Inorg. Chem.* **2016**, *55*, 7152–7166.

[32] a) J. D. Masuda, W. W. Schoeller, B. Donnadieu, G. Bertrand, *J. Am. Chem. Soc.* **2007**, *129*, 14180–14181; b) J. D. Masuda, W. W. Schoeller, B. Donnadieu, G. Bertrand, *Angew. Chem. Int. Ed.* **2007**, *46*, 7052–7055; c) C. D. Martin, C. M. Weinstein, C. E. Moore, A. L. Rheingold, G. Bertrand, *Chem. Commun.* **2013**, *49*, 4486–4488.

[33] *https://omics.pnl.gov/software/molecular-weight-calculator*, (07.08.2023).

[34] A. J. Arduengo, R. Krafczyk, R. Schmutzler, H. A. Craig, J. R. Goerlich, W. J. Marshall, M. Unverzagt, *Tetrahedron* **1999**, *55*, 14523-14534.

[35] V. Lavallo, Y. Canac, C. Präsang, B. Donnadieu, G. Bertrand, *Angew. Chem. Int. Ed.* **2005**, *44*, 5705-5709.

[36] N. Kuhn, T. Kratz, *Synth.* **1993**, *6*, 561-562.

[37] S. M. I. Al-Rafia, A. C. Malcolm, S. K. Liew, M. J. Ferguson, R. McDonald, E. Rivard, *Chem. Commun.* **2011**, *47*, 6987-6989.

[38] M. Tamm, D. Petrovic, S. Randoll, S. Beer, T. Bannenberg, P. G. Jonesa, J. Grunenberg, *Org. Biomol. Chem.* **2007**, *5*, 523-530.

[39] A.M. Tondreau, Z. Benkö, J. R. Harmer, H. Grützmacher, *Chem. Sci.* **2014**, *5*, 1545-1554.

[40] Agilent (**2014**). CrysAlis PRO. Agilent Technologies Ltd, Yarnton, Oxfordshire, England.

[41] O. V. Dolomanov, L. J. Bourhis, R. J. Gildea, J. A. K. Howard, H. Puschmann, *J. Appl. Crystallogr.* **2009**, *42*, 339-341

[42] G. M. Sheldrick, *Acta Crystallogr. A* **2015**, *71*, 3–8.

[43] a) G. M. Sheldrick, *Acta Crystallogr. C* **2015**, *71*, 3-8; b) G. M. Sheldrick, *Acta Crystallogr. A* 2008, *64*, 112-122.

[44] a) F. Neese, F. Wennmohs, U. Becker, C. Rieplinger, *J. Chem. Phys.* **2020**, *152*, 224108–224125; b) F. Neese, *WIREs Comput. Mol. Sci.* **2022**, *12*, 1606-1620.

[45] A. D. Becke, *Phys. Rev. A* **1988**, *38*, 3098-3100.

[46] a) F. Weigend, R. Ahlrichs, *Phys. Chem. Chem. Phys.* **2005**, *7*, 3297-3305; b) D. Rappoport, F. Furche, *J. Chem. Phys.* **2010**, *133*, 134105-134116.

[47] a) J.-D. Chai, M. Head-Gordon, *Phys. Chem. Chem. Phys.* **2008**, *10*, 6615–6620; b) J.-D. Chai, M. Head-Gordon, *J. Chem. Phys.* **2008**, *128*, 84106; c) Y.-S. Lin, G.-D. Li, S.-

P. Mao, J. D. Chai, *J. Chem. Theory Comput.* **2013**, *9*, 263-272; d) E. Caldeweyher, S. Ehlert, A. Hansen, H. Neugebauer, S. Spicher, C. Bannwarth, S. Grimme, *J. Chem. Phys.* **2019**, *150*, 154122-154140.

[48] J. Tomasi, B. Mennucci, R. Cammi, *Chem. Rev.* **2005**, *105*, 2999-3093.

[49] NBO 7.0. E. D. Glendening, J. K. Badenhoop, A. E. Reed, J. E. Carpenter, J. A. Bohmann, C. M. Morales, P. Karafiloglou, C. R. Landis, F. Weinhold, Theoretical Chemistry Institute, University of Wisconsin, Madison, WI (**2018**).

[50] P. Pyykkö, *J. Phys. Chem.* A **2015**, *119*, 2326–2337.

12. The Metal Matters: Transition Metal Dependent Functionalization of Cationic Polyphosphorus Ligand Complexes

Preface

This chapter has not been published until the end of this thesis. It should give a first insight into the drastically differing functionalization reactivity of two isovalence electronic transition metal complexes featuring *cyclo*-P_4R_2 ligands. While most Nickel based compounds are fully characterized, some of the results on the Molybdenum based species are of preliminary nature, so far. Further characterization and additional synthetic as well as computational investigations are needed and should be a topic of future research. Some of the presented results have already been part of the PhD thesis of Dr. Luis Dütsch and the BSc theses of Jan Wieneke and Lisa Orel.

Authors

Christoph Riesinger, Lisa Zimmermann, Jan Thomas Wieneke, Lisa Orel, Luis Dütsch and Manfred Scheer

Author Contributions

Christoph Riesinger – Conceptualization, Synthesis of **A1**, **A2**, **1a – d**, **3**, **4**, **5**, **7** and **8**, Interpretation of crystallographic data, Writing of original draft.
Lisa Zimmermann – Synthesis of **B1**, **B2**, **2a – d**, **6**, Writing of original draft.
Jan Thomas Wieneke – Synthetic assistance for compounds **A1**, **A2**, **1a – d**, **3**, **4**, **5**, **7** and **8**.
Lisa Orel – Synthetic assistance for compounds **B1**, **B2**, **2a – d**, **6**.
Luis Dütsch – Initial reactivity studies of **B** towards phosphenium cations.
Manfred Scheer – Project administration, Funding acquisition, Writing of original draft.

Acknowledgements

This work was supported by the Deutsche Forschungsgemeinschaft (DFG) within the project Sche 384/36-2. C. R. is grateful to the Studienstiftung des Deutschen Volkes for a PhD fellowship.

12.1. Abstract

*Reaction of the isostructural complexes [{L_nM}(η^3-P_4R_2)] ({L_nM} = Cp'''Ni (**A**), $CpMo(CO)_2$ (**B**), R = Ph, ^{i}Pr) with NHCs results in functionalization of the cyclo-P_4R_2 ligand. Concomitantly, the ligand either rearranges or is opened solely depending on the transition metal present. Further reaction with the anionic nucleophiles $[CN]^-$, $[EtO]^-$ and $[ECO]^-$ (E = P, As) furnishes fragmentation, functionalization or expansion of the respective P_4 ligand. The products reveal novel substituted polyphosphorus ligands featuring highly complex functionalization patterns. Furthermore, the comparison between the Ni and the corresponding Mo complexes for the first time provides insight into the tremendous influence the transition metal has on the reactivity of coordinated polyphosphorus cations.*

12.2. Introduction

The structural complexity and abundance of reactivity patterns within organic chemistry and specifically of the element carbon is unmatched within the periodic table. This is commonly attributed to the inherent stability of C–C single as well as multiple bonds and further substantiated by carbons capability to engage in four bonds.[1] While no other element comes even close to the structural richness of carbon-based compounds, its arguably closest neighbor, phosphorus, is popularly regarded as a carbon copy.[2] Indeed, phosphorus is closely related to carbon, as they share a diagonal relationship in the periodic table. Furthermore, several hydrocarbon fragments are isolobal to P based ones, as e. g. P and CH,[3] commonly found in organic aromatic compounds. Besides this fundamental interest, recently the (catalytic) conversion of white phosphorus (P_4) to value added phosphines has reinforced the scientific endeavors in phosphorus chemistry.[4] Novel approaches focus on the transition metal,[5] main group,[6] oxidative[7] and even photocatalytic[8] transformation of P_4 to organophosphorus species, thereby avoiding hazards (e. g. poisonous, corrosive and flammable intermediates, stoichiometric amounts of waste) commonly attributed to the synthesis of these highly demanded products.[9] Yet, most of these routes are highly specific and often limited to products of comparably low complexity. Recently our group demonstrated an Fe mediated cyclic conversion of P_4 to asymmetric mono-phosphines in a more general approach.[10] However, transition metal mediated functionalization of polyphosphorus species bears even greater potential, as it may allow the stabilization of otherwise unstable intermediates. Thus, it paves the way towards polyphosphorus species of yet unprecedented complexity, bordering that of carbon based organic compounds. While several prominent representatives of polyphosphorus ligand complexes, such as the side on P_2 complex $[(RNC)_4Fe(\eta^2\text{-}P_2)]$ (R = 2,6-(2,6(^{i}Pr)$_2$C$_6$H$_3$)$_2$C$_6$H$_3$),[11] the all-P sandwich $[Ti(cyclo\text{-}P_5)_2]^{2-}$[12] or a *cyclo*-$P_8$ ligand complex[13] are of more recent nature, the synthesis of such compounds played an essential role for several decades already.[14] However, studies on the targeted functionalization of such complexes have only been a topic of recent years. It was shown that P_2[15] as well as end-deck *cyclo*-P_n (n = 3,[16] 4[15a,17] and 5[18]) complexes can readily be

functionalized with both nucleophiles and electrophiles. Comparably, studies on the functionalization of P_n ligands in triple decker complexes are much rarer.[13,19] Strikingly however, most of these studies focus on the initial one or two functionalization steps,[19b,20] while the opportunity to access much more complex functional and structural motifs has largely been overlooked. Regardless of the variety of different transition metals used in these complexes the structural motifs observed for the coordinated polyphosphorus ligands are often similar and usually base on the fulfillment of the 18 valence electron rule for the transition metal center. Thus, the nucleophilically functionalized $[Cp'''Co(\eta^3\text{-}P_4R)]^-$ (**I**)[17c] and $[Cp''Ta(CO)_2(\eta^3\text{-}P_4R)]^-$ (**II**)[15a] possess isostructural *cyclo*-P_4R ligands (Scheme 1). Moreover, the *cyclo*-P_5R_2 ligands in $[Cp^*Fe(\eta^4\text{-}P_5R_2)]$ (**III**),[10a] $[Cp^{Ar}Co(\eta^4\text{-}P_5R_2)]^+$ (**IV**),[20b] as well as $[Cp'''Ta(CO)_2(\eta^4\text{-}P_5R_2)]^+$ (**V**)[17d] are isostructural despite the presence of a 3d or a 5d metal and even the introduction of a positive charge. Although the introduction of electronically more complex ligands, such as BIAN (bis(arylimino)acenaphthene diamine) results in neutral complexes, the respective *cyclo*-P_5R_2 ligand remains isostructural to the above ones.[17a,17b] Yet, the details of the influence of the coordinated transition metal onto the structure, bonding and reactivity of coordinated polyphosphorus ligands remain substantially underexplored to the best of our knowledge. Herein, this challenge is tackled and the reactivity of three isostructural *cyclo*-P_4R_2 complexes, namely $[\{L_nM\}(\eta^3\text{-}P_4R_2)]^{n+}$ ($\{L_nM\}$ = {Cp‴Ni} (**A**, n = 1),[16c] {$CpMo(CO)_2$} (**B**, n = 1),[21] {Cp‴Co} (**C**, n = 0)[16e]) towards nucleophiles is comparred, which leads to drastically different products dependent on the employed transition metal. Furthermore, the multi-step functionalization of these compounds is explored, utilizing the above metal induced distinction, and providing a series of substituted polyphosphorus ligands of unprecedented complexity.

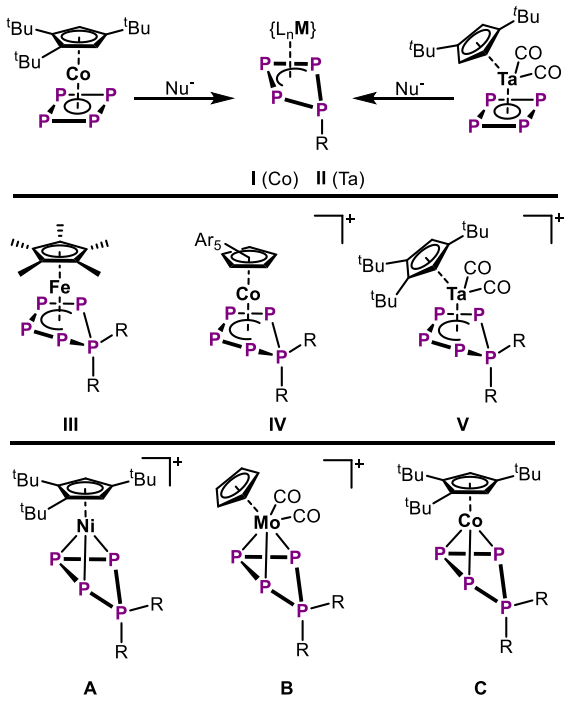

Scheme 1: Selected examples of isostructural polyphosphorus ligand complexes; Ar = 4-EtC_6H_4, R = alkyl, aryl.

12.3. Results and Discussion

To further extend the series of the isoelectronic complexes of the type [{L_nM}(η^3-P_4R_2)]$^{n+}$,[16d,16e] the *cyclo*-P_3 complex [CpMo(CO)$_2$(η^3-P_3)][21] was successfully reacted with a variety of phosphenium cations (see ESI). Notably, the derivatives [{L_nM}(η^3-P_4R_2)][WCA] (L_nM = Cp‴Ni, [WCA]$^-$ = [PF_6]$^-$, R = Ph (**A1**), ^{i}Pr (**A2**); L_nM = CpMo(CO)$_2$, [WCA]$^-$ = [OTf]$^-$ or [TEF]$^-$, R = Ph (**B1**), ^{i}Pr (**B2**); [OTf]$^-$ = [SO_3CF_3]$^-$, [TEF]$^-$ = [Al{$OC(CF_3)_3$}$_4$]$^-$) could be prepared on multi-gram scale enabling the desired investigation of their reactivity towards nucleophiles (see ESI). Interestingly, reacting **A1**/**2** with IDipp (1,3-bis(2,4,6-trimethyl-phenyl)imidazol-2-ylidene) or I^{i}Pr$_2$Me$_2$ (1,4-Diisopropyl-2,3-dimethylimidazol-5-ylidene) leads to selective addition of the carbene to the P_4R_2 ligand (Figure 1a, left). In turn the ligand rearranges to form a carbene substituted *cyclo*-P_3 moiety with an exocyclic phosphino group in the products [Cp‴Ni($\eta^{1:1}$-P_4R_2NHC)][PF_6] (**1a**: 90%, **1b**: 91%, **1c**: 91%, **1d**: 81%). On the other hand, performing the same reactions with the Mo derivatives **B1**/**2** leads to ring opening of the *cyclo*-P_4R_2 ligand and results in a substituted P_4 chain within [CpMo(CO)$_2$(η^3-P_4R_2NHC)][WCA] (**2a**: 89%, **2b**: 92%, **2c**: 90%, **2d**: 91%, Figure 1a, right). This difference highlights the tremendous influence of the transition metal on the polyphosphorus unit bound to it, even though the number of VE is the same. While the softer Ni prefers bonding which is best described as dative/polar, the harder Mo engages is more covalent Mo–P interactions. In contrast to the former reactions, the isoelectronic but neutral [Cp‴Co(η^3-P_4Ph_2)] (**C**)[16e] does not show reactivity towards NHCs, which is rationalized by the drastically decreased electrophilicity of this compound due to the lack of positive charge (see ESI).

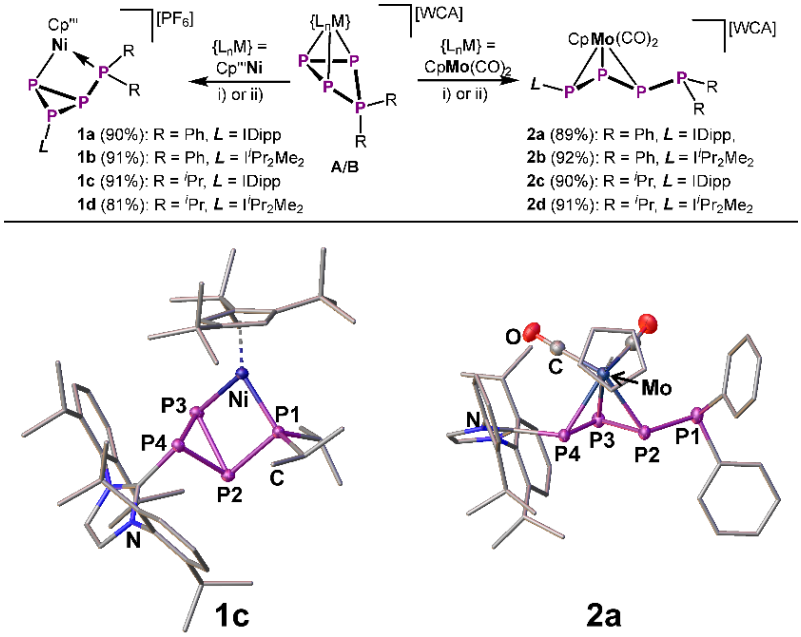

*Figure 1: Synthesis of **1** and **2** via nucleophilic functionalization of **A**/**B** with NHCs (i) + IDipp, o-DFB, r. t., 2 – 16 h; ii) + I^{i}Pr$_2$Me$_2$, THF, -80 °C to r. t., 3 – 16 h; [WCA]$^-$ = [OTf]$^-$ (**2a**, **2b**), [TEF]$^-$ (**2c**, **2d**); top) and the corresponding molecular structures of two of the derivatives in the solid state (bottom); yields are given in parentheses and ellipsoids are drawn at the 50% probability level.*

Compounds **1a** – **d** are isostructural revealing a *cyclo*-P_3PR_2 ligand bearing an NHC substituent at P3 and being coordinated to the {Cp‴Ni} moiety in an $\eta^{1:1}$ fashion (Figure 1). In other words, the molecular structure of **1a** – **d** can be described as a housane-type, where the {Cp‴Ni} fragment occupies one of the basal positions, while the capping position is taken by the (NHC)P moiety. The P–P bonds within **1a** – **d** (2.184(1) – 2.248(1) Å) are in the range of single bonds,[22] while the angle between the two planes of the housane scaffold is in all cases close to 90°. Contrastingly, the molecular structures of **2a**/**c** (**2b**/**d** could not be obtained in sufficient crystal quality within the time frame of this thesis) show a chain type P_4R_2 ligand bearing the NHC substituent at P4 and being coordinated to the {$CpMo(CO)_2$} moiety via P2 – P4 in η^3 fashion. Interestingly, the phosphino group in **2a**/**c** remains uncoordinated within these compounds. Accordingly, the P2–P3 bond is slightly shortened (2.139(13)/2.142(1) Å) and close to the expected value for a P–P double bond,[22] reminiscent of the allylic character of the (NHC)P_4R_2 ligand in **2a**/**c**. The P1–P2 bond is within the range of the P–P single bond (2.202(11)/2.225(1) Å) in both compounds and the P3–P4 bond (2.110(9)/2.148(1) Å) again shows slight shortening due to the delocalization within the P_4 chain.

Spectroscopically, **1a** – **d** show behavior consistent with their integrity in solution, which can be seen e. g. in the $^{31}P\{^1H\}$ NMR spectra revealing comparably small $^1J_{P–P}$ coupling constants (see SI), which are indicative for the *cyclo*-P_3 structural motif. Furthermore, pronounced $^nJ_{P–H}$ coupling in the ^1H and $^{31}P\{^1H\}$ spectra allow the assignment of the phosphino group and thus the whole AMQX spin systems, which are found for these compounds (see SI). Similarly, the $^{31}P\{^1H\}$ NMR spectra of **2a** – **2d** are in line with the chain type P_4 ligand being retained in solution, indicated by comparably larger $^1J_{P–P}$ coupling constants. Again, $^nJ_{P–H}$ coupling allows the assignment of the phosphino residue and thus the whole spin system. Interestingly, **2a** – **d** express high $^2J_{P–P}$ coupling constants for the coupling of the PR_2 group (P1 in the solid state structure) with the respective P3 atom (**2a**: 366 Hz, **2b**: 361 Hz, **2c**: 350 Hz, **2d**: 358 Hz). This is attributed to geometrically enforced orbital interaction between these two P atoms (see solid state structures).

To gain deeper insight into the electronic structure, spectroscopic data and ultimately the reactivity of **1a** – **d** and **2a** – **d** DFT calculations are needed, which however could not be obtained within the time frame of this thesis.

While the structural and spectroscopic distinctions between **1a** – **d** and **2a** – **d** are remarkable, their reactivity was envisioned to differ even further allowing the access to a broad manifold of polyphosphorus architectures. As cyanolysis is an established reaction in this field,[20a] **1** was reacted with one equivalent of $[Et_4N][CN]$, each. The reaction proceeds rapidly affording [{Cp‴Ni}(μ,$\eta^{1:1:1:1}$-$P_4(PR_2)_2$)] (**3a**: R = Ph; **3b**: R = ^{i}Pr), which could be isolated after chromatographic workup in good yields of 60% and 53%, respectively (Figure 2). The crude reaction mixture reveals the formation of (NHC)PCN,[23] corroborating the fragmentation of the initial P_4R_2 ligand in **1** by $[CN]^-$. Additionally, small amounts of a second fragmentation product, namely [{Cp‴Ni}(μ,$\eta^{2:2}$-$P_2(P^iPr_2)_2$)] (**4**, 20%), were obtained for the less sterically protected ^{i}Pr substituted derivatives.

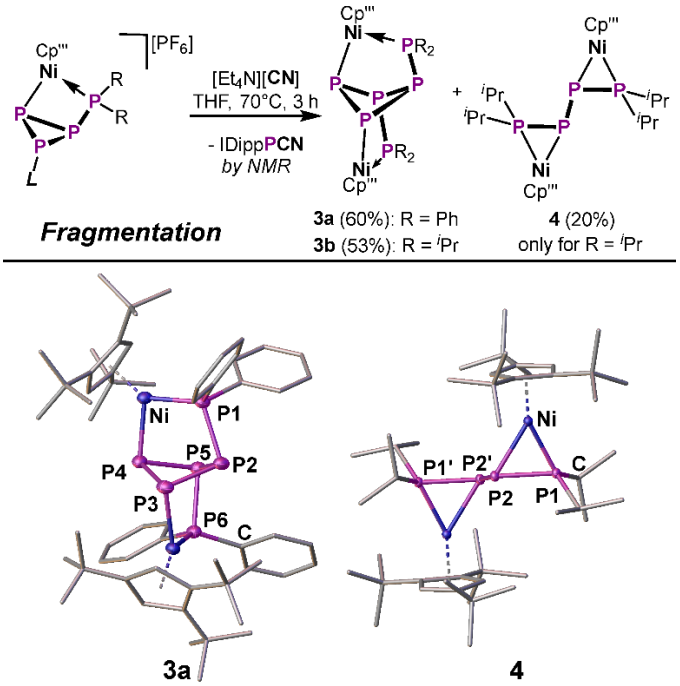

*Figure 2: Synthesis of **3** and **4** via cyanolysis of **1** (top) and the solid state structures of **3a** and **4** (bottom yields are given in parentheses and ellipsoids are drawn at the 50% probability level.*

While the cyanolysis of derivatives of **2** was attempted, the isolation of potential products of this reaction could not yet be achieved and should be a target of future investigations. Structurally, **3a** and **3b** can be derived from **1** via extrusion of the (NHC)PCN fragment, leading to a formally P=P double bonded species, which could then dimerize to the title compounds. While **3b** could not be obtained as crystals of sufficient quality, the rare cis-*cyclo*-$P_4(PR_2)_2$ ligand in **3a** shows bonds lengths (2.215(2) – 2.245(1) Å) in the range of P–P single bonds[22] and bridges two {Cp‴Ni} fragments in $\mu,\eta^{1:1:1:1}$ fashion. Notably, this ligand can be described as an exotic 1,2-disubstituted butterfly-type structural motif. In contrast, the chain type $P_2(P^iPr_2)_2$ ligand in **4** features shortened P1/P1′–P2/P2′ bonds (2.128(1) Å) in agreement with partial double bond character of these bonds, while the P2–P2′ bond length (2.244(1) Å) is in line with a P–P single bond.[22] The two {Cp‴Ni} fragments are thus bridged by this ligand in a $\mu,\eta^{2:2}$ fashion.

The $^{31}P\{^1H\}$ NMR spectra of **3a** and **3b** show similar but extremely complex AA′MM′XX′ spin systems indicating the preservation of their C_2 symmetry in solution. Moreover, all three signals for **3a**/**b** are significantly low field shifted compared to **1**, which further agrees with the butterfly type structure and thus expanded P_4 cycle, found for these compounds. In contrast, compound **4** only shows two signals consistent with its AA′XX′ spin system and again the preservation of its C_2 symmetry in solution. Interestingly, the comparably high $^1J_{PA/A'–PX/X'}$ coupling constant (482/481 Hz) is in line with the partial double bond character for the P1/P1′–P2/P2′ bonds. Interestingly, this disagrees with the expected butene-like character for the $R_2PP{=}PPR_2$ ligand written in its Lewis formula, where the formal double bond character is denoted to the central $P^X–P^{X'}$ bond. The respective coupling constant ($^1J_{PX\text{-}X'}$ = 324 Hz) however further stresses the

presence of single bond character for the central P–P bond, while double bond character is observed for the outer two (in agreement with the solid state structure). This effect is attributed to the coordination to the {Cp‴Ni} moieties and its dramatic effect on the electronic structure of the ligand, which needs to be corroborated by future DFT calculations.

In contrast to $[CN]^-$, the weakly nucleophilic character of EtO^- should preserve the integrity of the P_4 ligand, while the formation of a new P–O bond should provide the driving force and lead to comparably stable products. Interestingly, addition of KOEt to the IDipp substituted **1a**/**c** at cold temperatures affords dark green/turquoise solutions, which however rapidly turn to a reddish brown upon warming to room temperature. Investigating this behavior by means of low temperature ^{31}P NMR spectroscopy revealed the formation of an intermediate [Cp‴Ni($\eta^{1:1}$-IDippPPP(OEt)PR_2)] (**5a$_{INT}$**: R = ^{i}Pr, **5b$_{INT}$**: R = Ph), which however rearranged upon warming beyond -20 °C (**5a$_{INT}$**) or -40 °C (**5b$_{INT}$**), respectively (Figure 3). In an attempt to structurally consolidate this intermediate, single crystals of **5a$_{INT}$** could be obtained at -30 °C revealing a chain type P_4 ligand bearing the EtO^- substituent at P2 (Figure 3, see SI). However, the temperature sensitivity of these compounds prevented their isolation as pure compounds. Above -20 °C **5a$_{INT}$** rearranges to give [Cp‴Ni(η^2-IDippPP(OEt)P^{i}Pr$_2$)] (**5a**, 67%) as an isolable product. Interestingly, the isostructural [Cp‴Ni(η^2-IDippPP(OEt)PPh_2)] could not be isolated as it further rearranges to a yet unidentified final product (see SI). Thus, the addition of EtO^- to the P_4 ligand in **1** appears to initially take place at P2, which is accompanied by opening of the *cyclo*-P_3 moiety and formation of the IDippPPP(OEt)P^{i}Pr$_2$ ligand found in **5a$_{INT}$**. Afterwards, the EtO^- substituent shifts to P3 to give the IDippPP(OEt)P^{i}Pr$_2$ ligand, which is accompanied by the {Cp‴Ni} fragment switching from $\eta^{1:1}$ into η^2 coordination mode. While this arrangement could only be stabilized within **5a**, it appears to further rearrange upon introducing different substituents at the P_4 chain (see SI). In contrast to this complicated reactivity observed for the Ni complexes **1a** – **d**, the corresponding Mo complex **2b** reacted with KOEt in a much

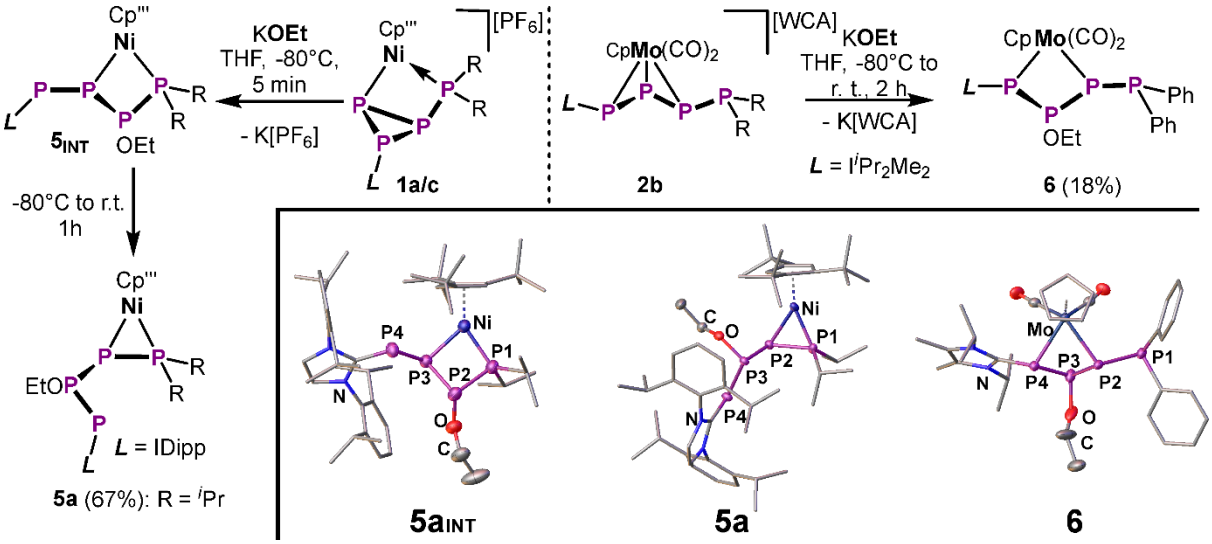

*Figure 3: Reactivity of **1a/c** and **2b** towards $[EtO]^-$ (top) and the solid state structures of **5a$_{INT}$**, **5a** and **6** (bottom); yields are given in parentheses and ellipsoids are drawn at the 50% probability level.*

simpler addition reaction. As the P_4 ligand in **2b** is already a chain, the EtO^- easily adds to P3 affording $[CpMo(CO)_2(\eta^{1:1}$-IDippPP(OEt)PR_2 (**6**, 18%, Figure 3). However, in contrast to **5a**, which features the same ligand bound to Ni in an η^2 mode, the $\{CpMo(CO)_2\}$ fragment in **6** is coordinated to it in an $\eta^{1:1}$ fashion via P2 and P4. This again highlights the preference of Mo for more covalent (X-type) interactions with polyphosphorus ligands compared to the preferential coordination of Ni via dative interaction (L-type).

Structurally, the complexes $\mathbf{5a_{INT}}$, **5a** and **6** all feature constitutional isomers of a P_4 ligand bearing two hydrocarbon residues at P1 and an NHC substituent at P4. While the EtO^- substituent is attached to P2 in $\mathbf{5a_{INT}}$ it is shifted to P3 in both **5a** and **6**. However, the latter compounds are easily distinguished, as the Ni atom in **5a** coordinates to the P_4 ligand via P1 and P2 in η^2 mode, while the Mo atom in **6** is bound in $\eta^{1:1}$ fashion via P2 and P4. The coordination mode of Ni in **5a** goes in hand with a decrease in bond length for the P1–P2 bond (2.123(1) Å), which is closer to the value expected for a P=P double bond. This is also in line with the decreased pyramidalization (ca. 333.2°) found for P1 in **5a**. The residual P–P bonds in $\mathbf{5a_{INT}}$ (2.180(1) – 2.202(1) Å), **5a** (2.183(1) Å) and **6** (2.176(1) – 2.234(1) Å) are best described as P–P single bonds.[22]

The NMR spectra of the deep turquoise/green reaction mixture of **1a**/**c** with KOEt indicates immediate formation of the intermediates $\mathbf{5a_{INT}}$ or $\mathbf{5b_{INT}}$, respectively. In the $^{31}P\{^1H\}$ NMR spectrum $\mathbf{5a_{INT}}$ shows an AMXY spin system reminiscent of the transformation to a *catena*-P_4 ligand. Upon warming to room temperature $\mathbf{5a_{INT}}$ rearranges rapidly to **5a**, simplifying the observed spectrum to an AMQX spin system. In the ^{31}P spectrum, the P^M signal of **5a** significantly broadens, corroborating it as the $^{i}Pr_2P$-moiety. Furthermore, the comparably large $^1J_{PM\text{-}PX}$ coupling constant (472 Hz) is in a similar range to that observed for **3a**/**b** and thus hints towards the double bond character of this bond. Similar spectra are observed in the case of $\mathbf{5b_{INT}}$, however at far lower temperatures (see SI). At above -20 °C another rearrangement to the final, yet unidentified, product is indicated by the respective $^{31}P\{^1H\}$ NMR spectrum now revealing an AXYZ spin system. However, this compound could not be isolated so far, nor could it be structurally validated within the time frame of this thesis. **6** again shows a comparably simple $^{31}P\{^1H\}$ NMR spectrum in agreement with an AMXY spin system and thus corroborating the structural integrity of the *catena*-P_4 ligand in solution (see SI).

To complete this reactivity survey, the "E-" surrogates $[ECO]^-$ (E = N, P,[24] As[25]) were reacted with both **1** and **2**, respectively. However, while neither **1** or **2** react with $[NCO]^-$ or even N_3^- salts, the latter rapidly decompose upon exposure to Na[OCP][24] or K[AsCO].[25] In contrast, **1a** reacts with both of these salts to afford the pnictogen expanded species [Cp'''Ni($\eta^{1:1}$-EP_4Ph_2IDipp)] (**7**: E = P, **8**: E = As (73%), Figure 4). Notably, the other derivatives **1b** – **d** react similarly with $[ECO]^-$ (E = P, As) salts, but do so in a much less selective fashion, labelling the isolation of the respective products unfeasible. This is attributed to the high degree of stabilization invoked by the substitution pattern in **1a** and thus **7** and **8**, respectively. Yet, the formation of **7** is accompanied by formation of a side product hampering its isolation as a pure compound within the time frame of this thesis (see SI). Nevertheless, it was possible to obtain

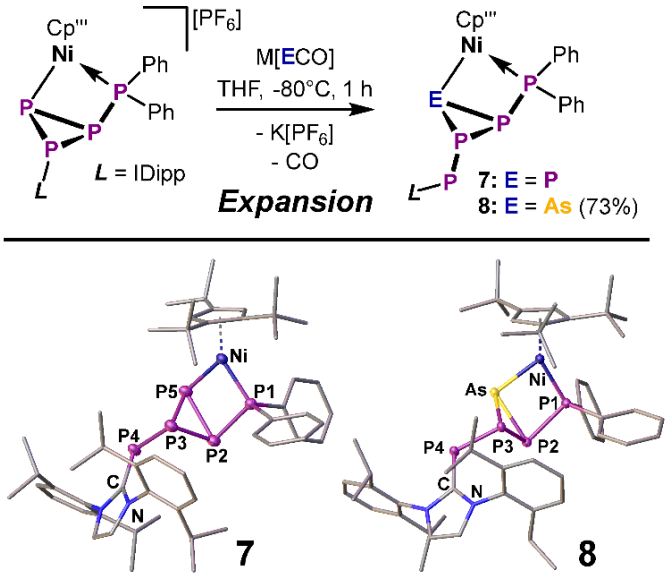

*Figure 4: Expansion reactions of **1a** with $[ECO]^-$ (E = P, As; top) and molecular structures of **7** and **8** (bottom); yields are given in parentheses and ellipsoids are drawn at the 50% probability level.*

a few single crystals of **7** via slow evaporation of solvent from a concentrated *n*-hexane solution. Both, **7** and **8** are isostructural and show the expansion of the initial P_4 ligand by another pnictogen atom (Figure 4). Interestingly, the As atom in **8** occupies the unsubstituted P5 (in **7**) position to 87% and is barely disordered within the three membered ring (13%). Thus, the housane-type structural motif is retained, with the introduced pnictogen atom adding to the P2–P3 bond (in **1a**). Accordingly, P4 is kicked out of the P_3 ring and now serves as the capping IDippP-substituent of the housane scaffold in **7** and **8**. The P–P (**7**: 2.210(1) – 2.266(1) Å) and P–P/As (**8**:2.184(6) – 2.219(6)/2.306(5) – 2.361(7) Å) bond lengths in both compounds are similar to those in the starting material **1a** and thus best described as single bonds.[22] **7** features a distinct AMQXY spin system in its $^{31}P\{^1H\}$ NMR spectrum (see SI), agreeing with its five chemically inequivalent P atoms. The broadening of the P^A signal corroborates the presence of the Ph_2P-moiety and additionally allows for the assignment of the whole spin systems. Notably, the $^{31}P\{^1H\}$ NMR spectrum of **8** is highly similar to that of **7** (see SI) with only the P^Q signal missing and thus leading to an AMXY spin system. Again, the P^A signal is significantly broadened in the ^{31}P NMR spectrum, indicating the Ph_2P-moiety and thus allowing the assignment of the whole spin system.

12.4. Conclusion

In conclusion, the reaction of the isostructural *cyclo*-P_4R_2 complexes **A** and **B** with NHCs affords the structurally distinct products **1a** – **d**, as well as **2a** – **d**, based on the employed transition metal fragment. While rearrangement and formation of a *cyclo*-P_3 ligand with an exocyclic phosphino group is observed in the Ni system **1**, the Mo system **2** reveals opening of the P_4 cycle to afford a trisubstituted *catene*-P_4 ligand. To explore the complex reactivity of these species, both **1** and **2** were further reacted with $[CN]^-$. Again, the influence of the present

transition metal fragment is stressed, as **1** undergoes a rapid fragmentation process to yield **3** and **4**, while the reactivity of **2** towards $[CN]^-$ could not finally be disclosed but appears to take a different course. Functionalization of **1** and **2** with $[EtO]^-$ gives rise to several regioisomers of a complexly tetra-substituted *catena*-P_4 ligand (in $\mathbf{5a_{INT}}$, **5a** and **6**) based on reaction conditions and importantly the coordinated transition metal. To complete this reactivity survey, the Ni species **1a** was shown to be expandable by one pnictogen atom via the reaction with $[ECO]^-$ salts. While similar reactivity could not be observed for the Mo system, the products **7** and **8** feature unprecedented phosphino-phosphinideno-*cyclo*-P_3 and -*cyclo*-P_2As ligands, respectively. Notably, the As atom in **8** is selectively (87%) introduced at the former P5 (in **7**) position providing valuable information about the reaction pathway of this expansion reaction. These experimental findings need to be further substantiated by future computational studies, giving insight into the electronic structure of the discussed compounds. Most notably, they may focus on the tremendous influence of the different, yet iso-valence electronic transition metal centers on the reactivity of the coordinated polyphosphorus ligand. Careful choice of the latter enables distinct reactivity and thus grants access to polyphosphorus species with functionalization patterns of unprecedented complexity. While this study focused on the Ni/Mo systems **1** and **2**, its implications are expected to be generalizable and promote the design and synthesis of novel (poly-)phosphorus species for future applications.

12.5. Supporting Information

12.5.1. Experimental Procedures

General Considerations

All manipulations were carried out using standard Schlenk techniques at a Stock apparatus under N_2 as an inert gas or in a glove box with Ar atmosphere. All glassware was dried with a heat gun (600 °C) for at least 30 min prior to use. *o*-DFB (1,2-difluorobenzene) was distilled from P_2O_5, CD_2Cl_2 was distilled from CaH_2 and other solvents were directly taken from an MBraun SPS-800 solvent purification system, degassed at room temperature and stored over molecular sieves. Solution ^{1}H (400.130 MHz), ^{19}F (376.498 MHz), ^{31}P (161.976 MHz) and spectra were recorded at an Avance400 (Bruker) spectrometer using $(H_3C)_4Si$ (^{1}H, ^{13}C), $CFCl_3$ (^{19}F) or 85% phosphoric acid (^{31}P), respectively, as external standards. Chemical shifts (δ) are provided in parts per million (ppm) and coupling constants (J) are reported in Hertz (Hz). Chemical shifts and coupling constants for $^{31}P\{^{1}H\}$ and ^{31}P NMR spectra were partly derived from spectral simulation using the built-in simulation package of TopSpin3.2. The following abbreviations are used: s = singlet, d = doublet, dd = doublet of doublets, dt = doublet of triplets, t = triplet, td = triplet of doublets br = broad and m = multiplet. Mass spectra were recorded at the internal mass spectrometry department using a ThermoQuest Finnigan TSQ 7000 (ESI), Finnigan MAT 95 (LIFDI) mass spectrometer or by the first author on a Waters Micromass LCT ESI-TOF mass-spectrometer and peak assignment was performed using the Molecular weight calculator 6.50.[1] IR spectra were recorded as solids using a ThermoFisher Nicolet iS5 FT-IR spectrometer with an iD7 ATR module and an ITX Germanium or ITX Diamond crystal. Elemental analysis of the products was conducted by the elemental analysis department at the University of Regensburg using an Elementar Vario EL. The starting materials [Cp'''Ni(η^3-P_3)],[16c] [CpMo(CO)$_2$(η^3-P_3)],[21] IDipp,[27] I^{i}Pr$_2$Me$_2$,[28] NaOCP•diox,[24] KAsCO (adapted from literature procedures)[25] and Tl[TEF][29] were synthesized according to literature procedures. The synthesis of [Cp'''Ni(η^3-P_4R_2)][PF_6] (R = Ph, ^{i}Pr) is adapted from literature procedures.[16d] All other chemicals were purchased from commercial vendors and used without further purification.

*Synthesis of [Cp'''Ni(η^3-P_4Ph_2)][PF_6] (**A1**)*

[Cp'''Ni(η^3-P_3)] (154 mg, 0.4 mmol, 1 eq.) and Tl[PF_6] (140 mg, 0.4 mmol, 1 eq.) were mixed and dissolved in 6 mL of *o*-DFB. Ph_2PCl (88mg, 73 µL, 0.4 mmol, 1 eq.) dissolved in 2 mL of toluene was added leading to a slow change of color to intense red and the precipitation of colorless solid. The mixture was stirred for 21 h and then left for the precipitate to settle. Afterwards, the solution was decanted and directly layered below 25 mL of *n*-hexane. Storage of this mixture for three days afforded **A1** as dark red crystalline blocks of X-ray quality.

Notably, **A1** has been prepared with several other counter anions.[16d] The procedure described here can be expanded to multigram scale.

Yield:	215 mg (75%)
Elemental analysis:	Calculated (%) for $C_{29}H_{39}F_6P_5Ni$: C: 48.70, H: 5.50; found: C:48.80, H: 5.19.
^{1}H-NMR (CD_2Cl_2, 300 K):	δ/ ppm = 1.20 (s, 9 H, $C_5H_2{}^t\underline{Bu_3}$), 1.31 (s, 18 H, $C_5H_2{}^t\underline{Bu_3}$), 5.92 (s, 2 H, $C_5\underline{H_2}{}^tBu_3$), 7.5 – 7.9 (several multiplets, 10 H, Ph)
^{31}P{^{1}H}-NMR (CD_2Cl_2, 300 K):	δ/ ppm = 73.5 (m, $^1J_{PA\text{-}PM/M'}$ = 293/281 Hz, $^2J_{PA\text{-}PX}$ = 14 Hz, 1 P, P^A), 57.7 (m, $^1J_{PM/M'\text{-}PA}$ = 293/281 Hz, $^1J_{PM/M'\text{-}PX}$ = 271/270 Hz, $^2J_{PM\text{-}PM'}$ = 2 Hz, 2 P, $P^{M/M'}$), 12.3 (m, $^1J_{PX\text{-}PM/M'}$ = 271/270 Hz, $^2J_{PX\text{-}PA}$ = 14 Hz, 1 P, P^X), -143.9 (sept, $^1J_{P\text{-}F}$ = 710 Hz, $[PF_6]^-$)
^{31}P-NMR (CD_2Cl_2, 300 K):	δ/ ppm = 73.5 (m, $^1J_{PA\text{-}PM/M'}$ = 293/281 Hz, $^2J_{PA\text{-}PX}$ = 14 Hz, 1 P, P^A), 57.7 (m, $^1J_{PM/M'\text{-}PA}$ = 293/281 Hz, $^1J_{PM/M'\text{-}PX}$ = 271/270 Hz, $^2J_{PM\text{-}PM'}$ = 2 Hz, 2 P, $P^{M/M'}$), 12.3 (m (br), significant broadening due to unresolved $^nJ_{P\text{-}H}$ coupling, 1 P, P^X), -143.9 (sept, $^1J_{P\text{-}F}$ = 710 Hz, $[PF_6]^-$)
^{19}F{^{1}H}-NMR (CD_2Cl_2, 300 K):	δ/ ppm = -73.1 (d, $^1J_{F\text{-}P}$ = 710 Hz, $[PF_6]^-$)

*Synthesis of [Cp'''Ni(η^3-$P_4{}^iPr_2$)][PF_6] (**A2**)*

[Cp'''Ni(η^3-P_3)] (154 mg, 0.4 mmol, 1 eq.) and Tl[PF_6] (140 mg, 0.4 mmol, 1 eq.) were mixed and dissolved in 10 mL of *o*-DFB. $^iPr_2PCl$ (61mg, 63 µL, 0.4 mmol, 1 eq.) dissolved in 2 mL of *o*-DFB was added leading to a slow change of color to red and the precipitation of colorless solid. The mixture was stirred for 3 d and then 30 mL of *n*-hexane were added to precipitate a red solid. The supernatant was decanted, the solid dried and then 4 mL *o*-DFB were added. The red solution was filtered and then layered with 50 mL of *n*-hexane. This mixture was stored for 5 d at room temperature to afford **A2** as dark red crystals in X-ray quality. The procedure described here can be expanded to multigram scale.

Yield:	225 mg (88%)
ESI(+)-MS (*o*-DFB):	*m/z* (%) = 501.2 (100, [**A2**]$^+$)
Elemental analysis:	Calculated (%) for $C_{23}H_{43}F_6P_5Ni$: C: 42.69, H: 6.70; found: C: 43.14, H: 6.80.
^{1}H-NMR (CD_2Cl_2, 300 K):	δ/ ppm = 1.25 (d, 3 H, CH$\underline{Me_2}$), 1.27 (s, 9 H, $C_5H_2{}^t\underline{Bu_3}$), 1.30 (d, 3 H, CH$\underline{Me_2}$), 1.39 (d, 3 H, CH$\underline{Me_2}$), 1.43 (s, 18 H, $C_5H_2{}^t\underline{Bu_3}$), 1.44 (d, 3 H, CH$\underline{Me_2}$), 2.74 (m (overlapping), 2 H, 2x C$\underline{H}Me_2$), 5.97 (s, 2 H, $C_5\underline{H_2}{}^tBu_3$)
^{31}P{^{1}H}-NMR (CD_2Cl_2, 300 K):	δ/ ppm = 81.0 (m, $^1J_{PA\text{-}PX/X'}$ = 293/286 Hz, $^2J_{PA\text{-}PM}$ = 16 Hz, 1 P, P^A), 58.6 (m, $^1J_{PM\text{-}PX/X'}$ = 264/262 Hz, $^2J_{PM\text{-}PA}$ = 16 Hz, 1 P, P^M), 34.5 (m, $^1J_{PX\text{-}PA}$ = 293/286 Hz, $^1J_{PX\text{-}PM}$ = 264/262 Hz, $^2J_{PX\text{-}PX'}$ = 3 Hz, 2 P, $P^{X/X'}$), -143.9 (sept, $^1J_{P\text{-}F}$ = 710 Hz, $[PF_6]^-$)
^{31}P-NMR (CD_2Cl_2, 300 K):	δ/ ppm = 81.0 (m, $^1J_{PA\text{-}PX/X'}$ = 293/286 Hz, $^2J_{PA\text{-}PM}$ = 16 Hz, 1 P, P^A), 58.6 (m (br), significant broadening due to unresolved $^nJ_{P\text{-}H}$ coupling, 1 P, P^M), 34.5 (m, $^1J_{PA\text{-}PX/X'}$ = 293/286 Hz, $^2J_{PX\text{-}PX'}$ = 3 Hz, 2 P, $P^{X/X'}$), -143.9 (sept, $^1J_{P\text{-}F}$ = 710 Hz, $[PF_6]^-$)
^{19}F{^{1}H}-NMR (CD_2Cl_2, 300 K):	δ/ ppm = -73.1 (d, $^1J_{F\text{-}P}$ = 710 Hz, $[PF_6]^-$)

*Synthesis of [CpMo(CO)$_2$(η^3-P$_4$Ph$_2$)][OTf] (**B1**)*

[CpMo(CO)$_2$(η^3-P$_3$)] (1.00 g, 3.23 mmol, 1 eq.) and Tl[OTf] (1.14 g, 3.23 mmol, 1 eq.) were mixed and dissolved in 15 mL of *o*-DFB. Ph$_2$PCl (0.58 mL, 3.23 mmol, 1 eq.) was added slowly leading to a slow change of color to yellow and the precipitation of colorless solid. The mixture was stirred for 18 h at room temperature, concentrated and precipitated by addition of *n*-hexane (50 mL). The yellow precipitate was washed with *n*-hexane (5 mL) and dried under reduced pressure (10^{-3} mbar). Afterwards, the solid was dissolved in 50 mL of *o*-DFB, filtered through a glass fiber filter paper and dried under reduced pressure (10^{-3} mbar). Crystals of **B1** suitable for single crystal X-ray measurements were obtained by layering a concentrated solution of **B1** in *o*-DFB with *n*-hexane (30 mL).

Yield:	1.48 g (2.24 mmol, 69%)
ESI(+)-MS (*o*-DFB):	*m/z* (%) = 496.9 (100, [**B1**]$^+$), 468.9 (50, [**B1**-CO]$^+$), 440.9 (5, [**B1**-2CO]$^+$)
Elemental analysis:	Calculated (%) for $C_{20}H_{15}F_3P_4SMo$: C: 37.29, H: 2.35, S: 4.98; found: C: 37.67, H:2.52, S: 5.17.
^{1}H-NMR (CD_2Cl_2, 300 K):	δ/ ppm = 5.82 (s, 5 H, $C_5\underline{H}_5$), 7.42 – 7.99 (several multiplets, 10 H, Ph)
^{31}P{^{1}H}-NMR (CD_2Cl_2, 300 K):	δ/ ppm = 63.7 (m, $^1J_{PA\text{-}PM/M'}$ = 275/276 Hz, $^2J_{PA\text{-}PX}$ = 16 Hz, 1 P, P^A), 1.9 (m, $^1J_{PM/M'\text{-}PA}$ = 275/276 Hz, $^1J_{PM/M'\text{-}PX}$ = 265/266 Hz, $^2J_{PM\text{-}PM'}$ = -2 Hz, 2 P, P$^{M/M'}$), -70.6 (m, $^1J_{PX\text{-}PM/M'}$ = 265/266 Hz, $^2J_{PX\text{-}PA}$ = 16 Hz, 1 P, P^X)
^{31}P-NMR (CD_2Cl_2, 300 K):	δ/ ppm = 63.7 (m (br), significant broadening due to unresolved $^nJ_{P\text{-}H}$ coupling, 1 P, P^A), 1.9 (m, $^1J_{PM/M'\text{-}PA}$ = 275/276 Hz, $^1J_{PM/M'\text{-}PX}$ = 265/266 Hz, $^2J_{PM\text{-}PM'}$ = -2 Hz, 2 P, P$^{M/M'}$), -70.6 (m, $^1J_{PX\text{-}PM/M'}$ = 265/266 Hz, $^2J_{PX\text{-}PA}$ = 16 Hz, 1 P, P^X)
^{19}F{^{1}H}-NMR (CD_2Cl_2, 300 K):	δ/ ppm = -78.6 (s, 1F, [OTf]$^-$)
IR:	$\tilde{\nu}$(CO)/cm^{-1} = 2042 (m), 2000 (m)

*Synthesis of [CpMo(CO)$_2$(η^3-P$_4$^{i}Pr$_2$)][OTf] (**B2**)*

[CpMo(CO)$_2$(η^3-P$_3$)] (1.00 g, 3.23 mmol, 1 eq.) and Tl[TEF] (3.78 g, 3.23 mmol, 1 eq.) were mixed and dissolved in 10 mL of *o*-DFB. ^{i}Pr$_2$PCl (0.52 mL, 3.23 mmol, 1 eq.) was added slowly leading to a slow change of color to yellow and the precipitation of colorless solid. The mixture was stirred for 3 h at room temperature, concentrated and precipitated by addition of *n*-hexane (50 mL). The yellow precipitate was washed with *n*-hexane (5 mL) and dried under reduced pressure (10^{-3} mbar). Afterwards, the solid was dissolved in 20 mL of *o*-DFB, filtered through a glass fiber filter paper and precipitated again by addition of *n*-hexane (30 mL). The solvent was decanted and the yellow powder was dried under reduced pressure (10^{-3} mbar). Crystals of **B2** suitable for single crystal X-ray measurements were obtained by layering a concentrated solution of **B2** in CH_2Cl_2 with *n*-hexane (30 mL).

Yield:	3.95 g (2.83 mmol, 87%)
ESI(+)-MS (*o*-DFB):	*m/z* (%) = 428.9 (100, [**B2**]$^+$), 400.9 (60, [**B2**-CO]$^+$)
Elemental analysis:	Calculated (%) for $C_{29}H_{19}O_6F_{36}P_4AlMo$: C: 24.98, H: 1.37; found: C: 25.07, H: 1.71.
^{1}H-NMR (CD_2Cl_2, 300 K):	δ/ ppm = 1.10 (d, 3 H, CH$\underline{Me_2}$), 1.15 (d, 3 H, CH$\underline{Me_2}$), 1.65 (d, 3 H, CH$\underline{Me_2}$), 1.70 (d, 3 H, CH$\underline{Me_2}$), 2.74 (m (overlapping), 2 H, C$\underline{H}$Me$_2$), 5.82 (s, 5 H, C$_5\underline{H_5}$)
^{31}P{^{1}H}-NMR (CD_2Cl_2, 300 K):	δ/ ppm = 109.3 (m, $^1J_{PA\text{-}PM/M'}$ = 267/268 Hz, $^2J_{PA\text{-}PX}$ = 16 Hz, 1 P, P^A), -20.5 (m, $^1J_{PM/M'\text{-}PA}$ = 267/268 Hz, $^1J_{PM/M'\text{-}PX}$ = 266/271 Hz, $^2J_{PM\text{-}PM'}$ = 4 Hz, 2 P, P$^{M/M'}$), -71.2 (m, $^1J_{PX\text{-}PM/M'}$ = 266/271 Hz, $^2J_{PX\text{-}PA}$ = 16 Hz, 1 P, P^X)
^{31}P-NMR (CD_2Cl_2, 300 K):	δ/ ppm = 109.3 (m (br), significant broadening due to unresolved $^nJ_{P\text{-}H}$ coupling, 1 P, P^A), -20.5 (m, $^1J_{PM/M'\text{-}PA}$ = 267/268 Hz, $^1J_{PM/M'\text{-}PX}$ = 266/271 Hz, $^2J_{PM\text{-}PM'}$ = 4 Hz, 2 P, P$^{M/M'}$), -71.2 (m, $^1J_{PX\text{-}PM/M'}$ = 266/271 Hz, $^2J_{PX\text{-}PA}$ = 16 Hz, 1 P, P^X)
^{19}F{^{1}H}-NMR (CD_2Cl_2, 300 K):	δ/ ppm = -75.6 (s, 36F, [TEF]$^-$)
IR:	$\tilde{\nu}$(CO)/cm^{-1} = 2058 (m), 2018 (m)

*Synthesis of [Cp'''Ni($\eta^{1:1}$-P_4Ph_2IDipp)][PF_6] (**1a**)*

A1 (1 g, 1.4 mmol, 1 eq.) was dissolved in 4 mL of *o*-DFB and IDipp (544 mg, 1.4 mmol, 1 eq.) dissolved in 4 mL of *o*-DFB was added at -30 °C to afford an immediate change of color from dark red to yellowish brown. The solution was allowed to reach room temperature and stirred for additional 2 h. Afterwards, the solution was constrained to 3 mL and 50 mL of *n*-hexane were added to precipitate [Cp'''Ni($\eta^{1:1}$-P_4Ph_2IDipp)][PF_6] (**1a**) as an olive green powder. The supernatant was decanted and the solid washed three times with 15 mL of *n*-hexane, each. Drying under reduced pressure afforded **1a** as an olive green solid, which could be recrystallized from concentrated THF solutions layered with *n*-hexane and storage at room temperature.

Yield:	1.39 g (90%)
Elemental analysis:	Calculated (%) for $C_{56}H_{75}NiP_5F_6N_2$: C:60.94, H:6.85, N: 2.54; found: C: 61.39, H:7.03, N: 2.37
^{1}H-NMR (CD_2Cl_2, 300 K):	δ/ ppm = 0.90 (s, 9 H, $C_5H_2{}^t\underline{Bu_3}$), 0.97 (s, 9 H, $C_5H_2{}^t\underline{Bu_3}$), 1.13 (d, 6 H, CH$\underline{Me_2}$), 1.17 (d, 6 H, CH$\underline{Me_2}$), 1.20 (s, 9 H, $C_5H_2{}^t\underline{Bu_3}$), 1.34 (d, 6 H, CH$\underline{Me_2}$), 1.44 (d, 6 H, CH$\underline{Me_2}$), 2.20 (m, 2 H, C$\underline{H}Me_2$), 2.28 (m, 2 H, C$\underline{H}Me_2$), 4.47 (s, 1 H, $C_5\underline{H_2}{}^tBu_3$), 4.68 (s, 1 H, $C_5\underline{H_2}{}^tBu_3$), 6.95 (m, 2 H, Ph), 7.22 (m, 2 H, Ph), 7.35 – 7.75 (several overlapping multiplets, 12 H, Ph and Dipp groups), 7.43 (s, 2 H, ($\underline{H}$CN(Dipp))$_2$C)
^{31}P{^{1}H}-NMR (CD_2Cl_2, 300 K):	δ/ ppm = -43.3 (ddd, $^1J_{PA\text{-}PM}$ = 167 Hz, $^2J_{PA\text{-}PX}$ = 99 Hz, $^2J_{PA\text{-}PQ}$ = 34 Hz, 1 P, P^A), -118.7 (ddd, $^1J_{PM\text{-}PA}$ = 167 Hz, $^1J_{PM\text{-}PX}$ = 155 Hz, $^1J_{PM\text{-}PQ}$ = 78 Hz, 1 P, P^M), -143.9 (sept, $^1J_{P\text{-}F}$ = 710 Hz, $[PF_6]^-$), -162.2 (ddd, $^1J_{PQ\text{-}PX}$ = 263 Hz, $^1J_{PQ\text{-}PM}$ = 78 Hz, $^2J_{PQ\text{-}PA}$ = 34 Hz, 1 P, P^Q), -175.0 (ddd, $^1J_{PX\text{-}PQ}$ = 263 Hz, $^1J_{PX\text{-}PM}$ = 155 Hz, $^2J_{PX\text{-}PA}$ = 99 Hz, 1 P, P^X)
^{31}P-NMR (CD_2Cl_2, 300 K):	δ/ ppm = -43.3 (m (br), significant broadening due to unresolved $^nJ_{P\text{-}H}$ coupling, 1 P, P^A), -118.7 (ddd, $^1J_{PM\text{-}PA}$ = 167 Hz, $^1J_{PM\text{-}PX}$ = 155 Hz, $^1J_{PM\text{-}PQ}$ = 78 Hz, 1 P, P^M), -143.9 (sept, $^1J_{P\text{-}F}$ = 710 Hz, $[PF_6]^-$), -162.2 (ddd, $^1J_{PQ\text{-}PX}$ = 263 Hz, $^1J_{PQ\text{-}PM}$ = 78 Hz, $^2J_{PQ\text{-}PA}$ = 34 Hz, 1 P, P^Q), -175.0 (ddd, $^1J_{PX\text{-}PQ}$ = 263 Hz, $^1J_{PX\text{-}PM}$ = 155 Hz, $^1J_{PX\text{-}PA}$ = 99 Hz, 1 P, P^X)
^{19}F{^{1}H}-NMR (CD_2Cl_2, 300 K):	δ/ ppm = -73.1 (d, $^1J_{F\text{-}P}$ = 710 Hz, $[PF_6]^-$)

*Synthesis of [Cp'''Ni($\eta^{1:1}$-$P_4Ph_2I^iPr_2Me_2$)][PF_6] (**1b**)*

A1 (1.43 g, 2 mmol, 1 eq.) was dissolved in 8 mL of THF and $I^iPr_2Me_2$ (380 mg, 2.1 mmol, 1.05 eq.) dissolved in 10 mL of THF was added at -80 °C to afford an immediate change of color from dark red to brownish red. The solution was allowed to reach room temperature and stirred for additional 16 h. Afterwards, the solvent was removed *in vacuo* and the solid washed two times with 20 mL of *n*-hexane, each. Drying under reduced pressure afforded [Cp'''Ni($\eta^{1:1}$-$P_4Ph_2I^iPr_2Me_2$)][PF_6] (**1b**) as a dark red solid, which could be recrystallized from concentrated THF solutions layered with *n*-hexane and storage at room temperature.

Yield:	1.62 g (91%)
ESI(+)-MS (*o*-DFB):	*m/z* (%) = 749.3 (100, [**1b**]$^+$), 181.2 (80, [$I^iPr_2Me_2H]^+$)
Elemental analysis:	Calculated (%) for $C_{40}H_{59}N_2F_6P_5Ni•(C_6H_{14})_{0.5}$: C: 55.03, H: 7.09, N: 2.98; found: C: 55.12, H: 6.77, N: 3.02
^{1}H-NMR (CD_2Cl_2, 300 K):	δ/ ppm = 0.99 (s, 9 H, $C_5H_2{}^t\underline{Bu_3}$), 1.29 (s, 9 H, $C_5H_2{}^t\underline{Bu_3}$), 1.44 (d, 6 H, CH$\underline{Me_2}$), 1.46 (s, 9 H, $C_5H_2{}^t\underline{Bu_3}$), 1.48 (d, 6 H, CH$\underline{Me_2}$), 2.23 (s, 6 H, ($\underline{Me}$CN(^{i}Pr))$_2$C), 4.96 (s, 1 H, $C_5\underline{H_2}{}^tBu_3$), 5.05 (s, 1 H, $C_5\underline{H_2}{}^tBu_3$), 5.58 (m, 2 H, C$\underline{H}Me_2$), 7.4 – 7.8 (several overlapping multiplets, 10 H, Ph)
^{31}P{^{1}H}-NMR (CD_2Cl_2, 300 K):	δ/ ppm = -48.1(ddd, $^1J_{PA-PM}$ = 156 Hz, $^2J_{PA-PX}$ = 114 Hz, $^2J_{PA-PQ}$ = 35 Hz, 1 P, P^A), -93.4 (td, $^1J_{PM-PA/X}$ = 156 Hz, $^1J_{PM-PQ}$ = 94 Hz, 1 P, P^M), -138.8 (ddd, $^1J_{PQ-PX}$ = 247 Hz, $^2J_{PQ-PM}$ = 94 Hz, $^2J_{PQ-PA}$ = 35 Hz, 1 P, P^Q), -143.9 (sept, $^1J_{P-F}$ = 710 Hz, $[PF_6]^-$), -181.3 (ddd, $^1J_{PX-PQ}$ = 247 Hz, $^1J_{PX-PM}$ = 156 Hz, $^2J_{PX-PA}$ = 114 Hz, 1 P, P^X)
^{31}P-NMR (CD_2Cl_2, 300 K):	δ/ ppm = -48.1(m (br), significant broadening due to unresolved $^nJ_{P-H}$ coupling, 1 P, P^A), -93.4 (td, $^1J_{PM-PA/X}$ = 156 Hz, $^1J_{PM-PQ}$ = 94 Hz, 1 P, P^M), -138.8 (ddd, $^1J_{PQ-PX}$ = 247 Hz, $^2J_{PQ-PM}$ = 94 Hz, $^2J_{PQ-PA}$ = 35 Hz, 1 P, P^Q), -143.9 (sept, $^1J_{P-F}$ = 710 Hz, $[PF_6]^-$), -181.3 (ddd, $^1J_{PX-PQ}$ = 247 Hz, $^1J_{PX-PM}$ = 156 Hz, $^2J_{PX-PA}$ = 114 Hz, 1 P, P^X)
^{19}F{^{1}H}-NMR (CD_2Cl_2, 300 K):	δ/ ppm = -73.1 (d, $^1J_{F-P}$ = 710 Hz, $[PF_6]^-$)

*Synthesis of [Cp'''Ni($\eta^{1:1}$-$P_4{}^{i}Pr_2$IDipp)][PF_6] (**1c**)*

A2 (1.04 g, 1.6 mmol, 1 eq.) was dissolved in 8 mL of THF and IDipp (652 mg, 1.68 mmol, 1.05 eq.) dissolved in 10 mL of THF was added at -80 °C to afford an immediate change of color from dark red to brownish red. The solution was allowed to reach room temperature, leading to a change of color too yellowish brown, and stirred for additional 16 h. Afterwards, the solvent was removed *in vacuo* and the solid washed two times with 15 mL of *n*-hexane, each. Drying under reduced pressure afforded [Cp'''Ni($\eta^{1:1}$-$P_4{}^{i}Pr_2$IDipp)][PF_6] (**1c**) as a dark yellowish brown solid, which could be recrystallized from concentrated *o*-DFB solutions layered with *n*-hexane and storage at room temperature.

Yield:	1.62 g (91%)
ESI(+)-MS (*o*-DFB):	*m/z* (%) = 889.5 (100, [**1c**]$^+$), 389.3 (40, [IDippH]$^+$)
Elemental analysis:	Calculated (%) for $C_{50}H_{79}N_2F_6P_5Ni•(C_6H_{14})_{0.5}$: C: 59.01, H: 8.04, N: 2.60; found: C: 59.46, H: 8.38, N: 2.60
^{1}H-NMR (CD_2Cl_2, 300 K):	δ/ ppm = 0.66 (dd, 6 H, CH$\underline{Me_2}$), 1.05 – 1.23 (several overlapping doublets, 15 H, CH$\underline{Me_2}$), 1.11 (s, 9 H, $C_5H_2{}^{t}\underline{Bu_3}$), 1.17 (s, 9 H, $C_5H_2{}^{t}\underline{Bu_3}$), 1.21 (s, 9 H, $C_5H_2{}^{t}\underline{Bu_3}$), 1.47 (dd, 6 H, CH$\underline{Me_2}$), 1.58 (dd, 3 H, CH$\underline{Me_2}$), 1.65 (m, 1 H, C$\underline{H}Me_2$), 2.21 (m, 3 H, C$\underline{H}Me_2$), 2.32 (m, 2 H, C$\underline{H}Me_2$), 4.41 (s, 1 H, $C_5\underline{H_2}{}^{t}Bu_3$), 4.46 (s, 1 H, $C_5\underline{H_2}{}^{t}Bu_3$), 7.39 (m, 4 H, Dipp), 7.50 (s, 2 H, ($\underline{H}$CN(Dipp))$_2$C), 7.61 (m, 2 H, Dipp)
^{31}P{^{1}H}-NMR (CD_2Cl_2, 300 K):	δ/ ppm = -12.8 (ddd, $^1J_{PA-PM}$ = 173 Hz, $^2J_{PA-PX}$ = 80 Hz, $^2J_{PA-PQ}$ 29 Hz, 1 P, P^A), -143.9 (sept, $^1J_{P-F}$ = 710 Hz, $[PF_6]^-$), -151.3 (ddd, $^1J_{PM-PA}$ = 173 Hz, $^1J_{PM-PX}$ = 154 Hz, $^1J_{PM-PQ}$ = 82 Hz, 1 P, P^M), -157.8 (ddd, $^1J_{PQ-PX}$ = 262 Hz, $^1J_{PQ-PM}$ = 82 Hz, $^2J_{PQ-PA}$ = 29 Hz, 1 P, P^Q), -181.8 (ddd, $^1J_{PX-PQ}$ = 262 Hz, $^1J_{PX-PM}$ = 154 Hz, $^2J_{PX-PA}$ = 80 Hz, 1 P, P^X)
^{31}P-NMR (CD_2Cl_2, 300 K):	δ/ ppm = -12.8 (m (br), significant broadening due to unresolved $^nJ_{P-H}$ coupling, 1 P, P^A), -143.9 (sept, $^1J_{P-F}$ = 710 Hz, $[PF_6]^-$), -151.3 (ddd, $^1J_{PM-PA}$ = 173 Hz, $^1J_{PM-PX}$ = 154 Hz, $^1J_{PM-PQ}$ = 82 Hz, 1 P, P^M), -157.8 (ddd, $^1J_{PQ-PX}$ = 262 Hz, $^1J_{PQ-PM}$ = 82 Hz, $^2J_{PQ-PA}$ = 29 Hz, 1 P, P^Q), -181.8 (ddd, $^1J_{PX-PQ}$ = 262 Hz, $^1J_{PX-PM}$ = 154 Hz, $^2J_{PX-PA}$ = 80 Hz, 1 P, P^X)
^{19}F{^{1}H}-NMR (CD_2Cl_2, 300 K):	δ/ ppm = -73.1 (d, $^1J_{F-P}$ = 710 Hz, $[PF_6]^-$)

*Synthesis of [Cp'''Ni($\eta^{1:1}$-$P_4{}^iPr_2I^iPr_2Me_2$)][PF_6] (**1d**)*

A2 (1.04 g, 1.6 mmol, 1 eq.) was dissolved in 8 mL of THF and $I^iPr_2Me_2$ (302 mg, 1.68 mmol, 1.05 eq.) dissolved in 10 mL of THF was added at -80 °C to afford an immediate change of color from dark red to brownish red. The solution was allowed to reach room temperature, leading to a change of color too yellowish brown, and stirred for additional 16 h. Afterwards, the solvent was removed *in vacuo* and the solid washed three times with 15 mL of *n*-hexane, each. Drying under reduced pressure afforded [Cp'''Ni($\eta^{1:1}$-$P_4{}^iPr_2I^iPr_2Me_2$)][PF_6] (**1d**) as a dark brown solid, which could be recrystallized from concentrated *o*-DFB solutions layered with *n*-hexane and storage at room temperature.

Yield:	1.08 g (81%)
ESI(+)-MS (*o*-DFB):	*m/z* (%) = 681.3 (100, [**1d**]$^+$), 181.2 (10, [$I^iPr_2Me_2H$]$^+$)
Elemental analysis:	Calculated (%) for $C_{34}H_{63}N_2F_6P_5Ni$: C: 49.35, H:7.67, N: 3.39; found: C: 49.07, H: 7.67, N: 4.00
^{1}H-NMR (CD_2Cl_2, 300 K):	δ/ ppm = 1.2 – 1.7 (several overlapping multiplets, 24 H, CH<u>Me$_2$</u>), 1.27 (s, 9 H, $C_5H_2{}^t$<u>Bu$_3$</u>), 1.40 (s, 9 H, $C_5H_2{}^t$<u>Bu$_3$</u>), 1.45 (s, 9 H, $C_5H_2{}^t$<u>Bu$_3$</u>), 2.20 (m, 1 H, P(C<u>H</u>Me$_2$)$_2$), 2.27 (s, 6 H, (<u>Me</u>CN(^{i}Pr))$_2$C), 2.30 (m, 1 H, P(C<u>H</u>Me$_2$)$_2$), 4.80 (s, 1 H, C_5<u>H$_2$</u>^{t}Bu$_3$), 4.92 (s, 1 H, C_5<u>H$_2$</u>^{t}Bu$_3$), 5.77 (m, 2 H, C<u>H</u>Me$_2$), trace amounts of [$I^iPr_2Me_2$]$^+$ overlapping
^{31}P{^{1}H}-NMR (CD_2Cl_2, 300 K):	δ/ ppm = -11.9 (ddd, $^1J_{PA-PQ}$ = 163 Hz, $^2J_{PA-PX}$ = 79 Hz, $^2J_{PA-PM}$ = 30 Hz, 1 P, P^A), -130.7 (ddd, $^1J_{PM-PX}$ = 238 Hz, $^1J_{PM-PQ}$ = 97 Hz, $^2J_{PM-PA}$ = 30 Hz, 1 P, P^M), -135.8 (td, $^1J_{PQ-PA/X}$ = 163 Hz, $^1J_{PQ-PM}$ = 97 Hz, 1 P, P^Q), -186.0 (ddd, $^1J_{PX-PM}$ = 238 Hz, $^1J_{PX-PQ}$ = 163 Hz, $^2J_{PX-PA}$ = 79 Hz, 1 P, P^X)
^{31}P-NMR (CD_2Cl_2, 300 K):	δ/ ppm = -11.9 (m (br), significant broadening due to unresolved $^nJ_{P-H}$ coupling, 1 P, P^A), -130.7 (ddd, $^1J_{PM-PX}$ = 238 Hz, $^1J_{PM-PQ}$ = 97 Hz, $^2J_{PM-PA}$ = 30 Hz, 1 P, P^M), -135.8 (td, $^1J_{PN-PA/X}$ = 163 Hz, $^1J_{PQ-PM}$ = 97 Hz, 1 P, P^Q), -186.0 (ddd, $^1J_{PX-PM}$ = 238 Hz, $^1J_{PX-PQ}$ = 163 Hz, $^2J_{PX-PA}$ = 79 Hz, 1 P, P^X)
^{19}F{^{1}H}-NMR (CD_2Cl_2, 300 K):	δ/ ppm = -73.1 (d, $^1J_{F-P}$ = 710 Hz, $[PF_6]^-$)

*Synthesis of [CpMo(CO)$_2$(η^3-P$_4$Ph$_2$IDipp)][OTf] (**2a**)*

B1 (570 mg, 0.88 mmol, 1 eq.) was dissolved in 15 mL of *o*-DFB and IDipp (341 mg, 0.88 mmol, 1 eq.) dissolved in 5 mL of *o*-DFB was added at room temperature to afford an immediate change of color from yellow to orange. The solution was stirred for 16 h. Afterwards, the solution was constrained to 3 mL and 50 mL of *n*-pentane were added to precipitate [CpMo(CO)$_2$(η^3-P$_4$Ph$_2$IDipp)][OTf] (**2a**) as an orange powder. The supernatant was decanted and the solid washed with 15 mL of *n*-pentane, each. Drying under reduced pressure afforded **2a** as an orange solid, which could be recrystallized from concentrated *o*-DFB solutions layered with *n*-hexane and storage at room temperature.

Yield:	0.81 g (0.78 mmol, 89%)
ESI(+)-MS (*o*-DFB):	*m/z* (%) = 883.2 (100, [**2a**]$^+$), 855.2 (5, [**2a**-CO]$^+$), 389.3 (80, [IDippH]$^+$)
Elemental analysis:	Calculated (%) for $C_{47}H_{51}MoP_4F_3N_2O_5S\cdot(C_6H_4F_2)$: C:55.50, H:4.83, N: 2.44, S: 2.80; found: C: 55.78, H:4.82, N: 2.84, S: 3.20
^{1}H-NMR (CD_2Cl_2, 300 K):	δ/ ppm = 1.23 (d, 6 H, CH$\underline{Me_2}$), 1.29 (d, 6 H, CH$\underline{Me_2}$), 1.37 (d, 6 H, CH$\underline{Me_2}$), 1.44 (d, 6 H, CH$\underline{Me_2}$), 2.56 (m (*br*), 4 H, C$\underline{H}$Me$_2$), 4.56 (s, 5 H, $C_5\underline{H_5}$), 7.28 – 7.63 (several overlapping multiplets, 16 H, Ph and Dipp groups), 7.65 (s, 2 H, ($\underline{H}$CN(Dipp))$_2$C)
^{31}P{^{1}H}-NMR (CD_2Cl_2, 300 K):	δ/ ppm = 1.3 (ddd, $^2J_{PA\text{-}PM}$ = 145 Hz, $^1J_{PA\text{-}PQ}$ = 188 Hz, $^3J_{PA\text{-}PX}$ = 40 Hz, 1 P, P^A), -36.4 (td, $^2J_{PM\text{-}PA}$ = 145 Hz, $^1J_{PM\text{-}PQ/X}$ = 324 Hz, 1 P, P^M), -67.5 (ddd, $^1J_{PQ\text{-}PM}$ = 324 Hz, $^1J_{PQ\text{-}PA}$ = 188 Hz, $^2J_{PQ\text{-}PX}$ = 366 Hz, 1 P, P^Q), -101.7 (ddd, $^1J_{PX\text{-}PM}$ = 324 Hz, $^2J_{PX\text{-}PQ}$ = 366 Hz, $^3J_{PX\text{-}PA}$ = 39 Hz, 1 P, P^X)
^{31}P-NMR (CD_2Cl_2, 300 K):	δ/ ppm = 1.3 (m (br), significant broadening due to unresolved $^nJ_{P\text{-}H}$ coupling, 1 P, P^A), -36.4 (td, $^2J_{PM\text{-}PA}$ = 145 Hz, $^1J_{PG\text{-}PQ/X}$ = 324 Hz, 1 P, P^M), -67.5 (ddd, $^1J_{PQ\text{-}PM}$ = 324 Hz, $^1J_{PQ\text{-}PA}$ = 188 Hz, $^2J_{PQ\text{-}PX}$ = 366 Hz, 1 P, P^Q), -101.7 (ddd, $^1J_{PX\text{-}PM}$ = 324 Hz, $^2J_{PX\text{-}PQ}$ = 366 Hz, $^3J_{PX\text{-}PA}$ = 40 Hz, 1 P, P^X)
^{19}F{^{1}H}-NMR (CD_2Cl_2, 300 K):	δ/ ppm = -78.8 (s, [OTf]$^-$)
IR:	$\tilde{\nu}$(CO)/cm^{-1} = 2016 (m), 1966 (m)

*Synthesis of [CpMo(CO)$_2$(η^3-P$_4$Ph$_2$I^{i}Pr$_2$Me$_2$)][OTf] (**2b**)*

B1 (644 mg, 1.0 mmol, 1 eq.) was dissolved in 20 mL of THF and I^{i}Pr$_2$Me$_2$ (180 mg, 1.0 mmol, 1.0 eq.) dissolved in 5 mL of THF was added at -80 °C to afford an immediate change of color from yellow to red. The solution was allowed to reach room temperature and stirred for additional 16 h. Afterwards, the solvent was reduced *in vacuo* to 5 mL and *n*-pentane was added to precipitate an orange powder [CpMo(CO)$_2$(η^3-P$_4$Ph$_2$I^{i}Pr$_2$Me$_2$)][OTf] (**2b**) which was washed with 20 mL of *n*-pentane. Drying under reduced pressure afforded (**2b**) as an orange solid, which could be recrystallized from concentrated THF solutions layered with *n*-hexane and storage at room temperature.

Yield:	0.76 g (0.92 mmol, 92%)
ESI(+)-MS (*o*-DFB):	*m/z* (%) = 675.1 (100, [**2b**]$^+$), 647.1 (5, [**2b**-CO]$^+$), 181.2 (20, [I^{i}Pr$_2$Me$_2$H]$^+$)
Elemental analysis:	Calculated (%) for $C_{31}H_{35}O_5N_2F_3P_4Mo\bullet(C_4H_8O)_{0.5}$: C: 46.06, H: 4.57, N: 3.25, S: 3.72; found: C: 46.18, H: 4.55, N: 3.38, S: 4.03
^{1}H-NMR (CD_2Cl_2, 300 K):	δ/ ppm = 1.67 (d, 6 H, CH<u>Me$_2$</u>), 1.75 (d, 6 H, CH<u>Me$_2$</u>), 2.42 (s, 6 H, (<u>Me</u>CN(^{i}Pr))$_2$C), 5.32 (s, 5 H, C$_5$<u>H$_5$</u>), 5.55 (m, 2 H, C<u>H</u>Me$_2$), 7.39 – 7.78 (several overlapping multiplets, 10 H, Ph)
^{31}P{^{1}H}-NMR (CD_2Cl_2, 300 K):	δ/ ppm = 2.0 (ddd, $^2J_{PA\text{-}PM}$ = 158 Hz, $^1J_{PA\text{-}PQ}$ = 189 Hz, $^3J_{PA\text{-}PX}$ = 39 Hz, 1 P, P^A), -25.5 (td, $^2J_{PM\text{-}PA}$ = 158 Hz, $^1J_{PM\text{-}PQ/X}$ = 327 Hz, 1 P, P^M), -87.6 (ddd, $^1J_{PQ\text{-}PM}$ = 327 Hz, $^1J_{PQ\text{-}PA}$ = 189 Hz, $^2J_{PQ\text{-}PX}$ = 361 Hz, 1 P, P^Q), -126.0 (ddd, $^1J_{PX\text{-}PM}$ = 327 Hz, $^2J_{PX\text{-}PQ}$ = 362 Hz, $^3J_{PX\text{-}PA}$ = 39 Hz, 1 P, P^X)
^{31}P-NMR (CD_2Cl_2, 300 K):	δ/ ppm = 2.0 (m (br), significant broadening due to unresolved $^nJ_{P\text{-}H}$ coupling, 1 P, P^A), -25.5 (td, $^2J_{PM\text{-}PA}$ = 158 Hz, $^1J_{PM\text{-}PQ/X}$ = 327 Hz, 1 P, P^M), -87.6 (ddd, $^1J_{PQ\text{-}PM}$ = 327 Hz, $^1J_{PQ\text{-}PA}$ = 189 Hz, $^2J_{PQ\text{-}PX}$ = 361 Hz, 1 P, P^Q), -126.0 (ddd, $^1J_{PX\text{-}PM}$ = 327 Hz, $^2J_{PX\text{-}PQ}$ = 362 Hz, $^3J_{PX\text{-}PA}$ = 39 Hz, 1 P, P^X)
^{19}F{^{1}H}-NMR (CD_2Cl_2, 300 K):	δ/ ppm = -78.7 (s, [OTf]$^-$)
IR:	$\tilde{\nu}$(CO)/cm^{-1} = 2007 (m), 1965 (m)

*Synthesis of [CpMo(CO)$_2$(η^3-P$_4$^{i}Pr$_2$IDipp)][TEF] (**2c**)*

B2 (1.39 g, 1.0 mmol, 1 eq.) was dissolved in 15 mL of *o*-DFB and IDipp (390 mg, 1.0 mmol, 1 eq.) dissolved in 5 mL of *o*-DFB was added at room temperature to afford an immediate change of color from yellow to red. The solution was stirred for 3 h. Afterwards, the solution was concentrated to 3 mL and 50 mL of *n*-hexane were added to precipitate [CpMo(CO)$_2$(η^3-P$_4$^{i}Pr$_2$IDipp)][TEF] (**2c**) as an orange powder. The supernatant was decanted and the solid washed with 15 mL of *n*-hexane, each. Drying under reduced pressure afforded **2c** as an orange solid, which could be recrystallized from concentrated *o*-DFB solutions layered with *n*-hexane and storage at room temperature.

Yield:	1.61 g (0.90 mmol, 90%)
ESI(+)-MS (*o*-DFB):	*m/z* (%) = 815.2 (95, [**2c**]$^+$), 787.2 (5, [**2c**-CO]$^+$), 389.3 (100, [IDippH]$^+$)
^{1}H-NMR (CD_2Cl_2, 300 K):	δ/ ppm = 1.00 – 1.11 (several overlapping doublets, 15 H, CH<u>Me$_2$</u>), 1.22 (d, 6 H, CH<u>Me$_2$</u>), 1.31 (d, 3 H, CH<u>Me$_2$</u>), 1.38 (d, 6 H, CH<u>Me$_2$</u>), 1.44 (d, 6 H, CH<u>Me$_2$</u>), 1.83 (m, 1 H, C<u>H</u>Me$_2$), 1.90 (m, 1 H, C<u>H</u>Me$_2$), 2.58 (m, 4 H, C<u>H</u>Me$_2$), 4.99 (s, 5 H, C_5H_5), 7.43 (s, 2 H, (<u>H</u>CN(Dipp))$_2$C), 7.45-7.56 (m, 4 H, Dipp), 7.71 (m, 2 H, Dipp)
^{31}P{^{1}H}-NMR (CD_2Cl_2, 300 K):	δ/ ppm = 35.6 (ddd, $^2J_{PA-PM}$ = 129 Hz, $^1J_{PA-PQ}$ = 204 Hz, $^3J_{PA-PX}$ = 20 Hz, 1 P, P^A), -22.0 (td, $^2J_{PM-PA}$ = 129 Hz, $^1J_{PM-PQ/X}$ = 329 Hz, 1 P, P^M), -83.6 (ddd, $^1J_{PQ-PM}$ = 329 Hz, $^1J_{PQ-PA}$ = 204 Hz, $^2J_{PQ-PX}$ = 350 Hz, 1 P, P^Q), -95.5 (ddd, $^1J_{PX-PM}$ = 329 Hz, $^2J_{PX-PQ}$ = 350 Hz, $^3J_{PX-PA}$ = 20 Hz, 1 P, P^X)
^{31}P-NMR (CD_2Cl_2, 300 K):	δ/ ppm = 35.6 (m (br), significant broadening due to unresolved $^nJ_{P-H}$ coupling, 1 P, P^A), -22.0 (td, $^2J_{PM-PA}$ = 129 Hz, $^1J_{PM-PQ/X}$ = 329 Hz, 1 P, P^M), -83.6 (ddd, $^1J_{PQ-PM}$ = 329 Hz, $^1J_{PQ-PA}$ = 204 Hz, $^2J_{PQ-PX}$ = 350 Hz, 1 P, P^Q), -95.5 (ddd, $^1J_{PX-PM}$ = 329 Hz, $^2J_{PX-PQ}$ = 350 Hz, $^3J_{PX-PA}$ = 20 Hz, 1 P, P^X)
^{19}F{^{1}H}-NMR (CD_2Cl_2, 300 K):	δ/ ppm = -75.6 (s, [TEF]$^-$)
IR:	$\tilde{\nu}$(CO)/cm^{-1} = 2022 (m), 1979 (m)

*Synthesis of [CpMo(CO)$_2$(η^3-P$_4$^{i}Pr$_2$I^{i}Pr$_2$Me$_2$)][TEF] (**2d**)*

B2 (1.39 g, 1.0 mmol, 1 eq.) was dissolved in 20 mL of THF and I^{i}Pr$_2$Me$_2$ (180 mg, 1.0 mmol, 1.0 eq.) dissolved in 5 mL of THF was added at -80 °C to afford an immediate change of color from yellow to red. The solution was allowed to reach room temperature and stirred for additional 3 h. Afterwards, the solvent was removed *in vacuo.* 5 mL of *o*-DFB were added and then *n*-pentane was added to precipitate an orange powder [CpMo(CO)$_2$(η^3-P$_4$^{i}Pr$_2$I^{i}Pr$_2$Me$_2$)][TEF] (**2d**) which was washed with 20 mL of *n*-hexane. Drying under reduced pressure afforded **2d** as an orange solid, which could be recrystallized from concentrated THF solutions layered with *n*-hexane and storage at room temperature.

Yield:	1.44 g (0.91 mmol, 91%)
ESI(+)-MS (*o*-DFB):	*m/z* (%) = 607.1 (100, [**2d**]$^+$), 679.1 (10, [**2d**-CO]$^+$), 428.9 (10, [**B2**]$^+$) 181.2 (40, [I^{i}Pr$_2$Me$_2$H]$^+$)
^{1}H-NMR (CD_2Cl_2, 300 K):	δ/ ppm = 1.1 – 1.5 (several overlapping multiplets, 24 H, CH<u>Me$_2$</u>) 1.56 (d, 6 H, NCH<u>Me$_2$</u>), 1.64 (d, 6 H, NCH<u>Me$_2$</u>), 1.97 (m, 1 H, P(C<u>H</u>Me$_2$)$_2$), 2.15 (m, 1 H, P(C<u>H</u>Me$_2$)$_2$), 2.31 (s, 6 H, (<u>Me$_2$</u>CN(^{i}Pr))$_2$C),5.48 (m, 2 H, C<u>H</u>Me$_2$), 5.65 (s, 5 H, C$_5$<u>H$_5$</u>)
^{31}P{^{1}H}-NMR (CD_2Cl_2, 300 K):	δ/ ppm = 35.0 (ddd, $^2J_{PA-PM}$ = 117 Hz, $^1J_{PA-PQ}$ = 208 Hz, $^3J_{PA-PX}$ = 17 Hz, 1 P, P^A), -14.6 (td, $^2J_{PM-PA}$ = 117 Hz, $^1J_{PM-PQ/X}$ = 333 Hz, 1 P, P^M), -96.0 (ddd, $^1J_{PQ-PM}$ = 333 Hz, $^1J_{PQ-PA}$ = 208 Hz, $^2J_{PQ-PX}$ = 358 Hz, 1 P, P^Q), -120.1 (ddd, $^1J_{PX-PM}$ = 333 Hz, $^2J_{PX-PQ}$ = 358 Hz, $^3J_{PX-PA}$ = 17 Hz, 1 P, P^X)
^{31}P-NMR (CD_2Cl_2, 300 K):	δ/ ppm = 35.0 (m (br), significant broadening due to unresolved $^nJ_{P-H}$ coupling, 1 P, P^A), -14.6 (td, $^2J_{PM-PA}$ = 117 Hz, $^1J_{PM-PQ/X}$ = 333 Hz, 1 P, P^M), -96.0 (ddd, $^1J_{PQ-PM}$ = 333 Hz, $^1J_{PQ-PA}$ = 208 Hz, $^2J_{PQ-PX}$ = 358 Hz, 1 P, P^Q), -120.1 (ddd, $^1J_{PX-PM}$ = 333 Hz, $^2J_{PX-PQ}$ = 358 Hz, $^3J_{PX-PA}$ = 17 Hz, 1 P, P^X)
^{19}F{^{1}H}-NMR (CD_2Cl_2, 300 K):	δ/ ppm = -75.6 (s, [TEF]$^-$)
IR:	$\tilde{\nu}$(CO)/cm^{-1} = 2028 (m), 1979 (m)

Cyanolysis of [Cp'''Ni($\eta^{1:1}$-P_4R_2IDipp)][PF_6] (R = Ph, ^{i}Pr)

1a/**1c** (663 mg (**1a**) or 621 mg (**1c**), 0.6 mmol, 1 eq.) and [Et_4N][CN] (94 mg, 0.6 mmol, 1 eq.) were mixed and dissolved in 10 mL of THF, resulting in a slow change of color towards reddish brown. The mixture was stirred at 70 °C for 3 h and then the solvent was removed *in vacuo*. The residue was dissolved in CH_2Cl_2 and SiO_2 (ca. 10 g) were added. The solvent was removed again, and the resulting free flowing solid was transferred onto a column (SiO_2/*n*-hexane, 2/20cm). Eluting with pure *n*-hexane yields a pale yellow and of [Cp'''Ni(η^3-P_3)] which was discarded. In case of **1c** (R = ^{i}Pr), increasing the polarity to *n*-hexane/toluene (10:1) affords an additional small red band of the decomposition product [{Cp'''Ni}$_2$(μ,$\eta^{2:2}$-(PP^iPr_2)$_2$)] (**4**). Finally, a mixture of *n*-hexane/toluene (5:1) elutes the main products [{Cp'''Ni}$_2$(μ,$\eta^{1:1:1:1}$-*cyclo*-$P_4(PR_2)_2$)] (**3a**: R = Ph, **3b**: R = ^{i}Pr) as dark brownish red bands. Simple removing the solvent *in vacuo* affords the respective crude product. While **4** can be obtained as a pure compound by recrystallization from concentrated *n*-hexane solutions at 4 °C, **3a**/**b** were further purified by layering concentrated solutions in toluene with acetonitrile and storage at 4 °C. Notably, the proposed byproduct of this reaction, namely IDippPCN, has not been described in the literature before. However, the $^{31}P\{^1H\}$ NMR spectrum of crude **3a** (Figure S 55) reveals a sharp singlet (δ = -122.4 ppm) in nearly perfect agreement with previously reported carbene supported cyano-phosphinidene species,[23] such as I^iPr_2Me_2PCN, which is formed during the preparation of **3b**.

3a:

Yield:	194 mg (60%, crude)/50 mg (23%, crystalline)
ESI(+)-MS (*o*-DFB):	*m/z* (%) = 1076.6 (100, [**3a**]$^+$)
Elemental analysis:	Calculated (%) for $C_{58}H_{78}P_6Ni_2$•$(C_7H_8)_{0.5}$: C:65.69, H: 7.35; found: C: 65.92, H: 7.52
^{1}H-NMR (C_6D_6, 300 K):	δ/ ppm = 1.21 (s, 9 H, $C_5H_2{}^t\underline{Bu_3}$), 1.35 (s, 9 H, $C_5H_2{}^t\underline{Bu_3}$), 1.44 (s, 9 H, $C_5H_2{}^t\underline{Bu_3}$), 5.35 (m, 1 H, $C_5\underline{H_2}{}^tBu_3$), 5.42 (m, 1 H, $C_5\underline{H_2}{}^tBu_3$), 6.90 – 7.15 (several multiplets overlapping with residual solvent signal (C_6D_6), 6 H, Ph), 8.11 (m, 2 H, Ph), 8.24 (m, 2 H, Ph)
^{31}P{^{1}H}-NMR (C_6D_6, 300 K):	δ/ ppm = 210.8 (m, 2 P, $P^{A/A'}$), 121.0 (m, 2 P, $P^{M/M'}$), 89.6 (m, 2 P, $P^{X/X'}$)
^{31}P-NMR (C_6D_6, 300 K):	δ/ ppm = 210.8 (m, 2 P, $P^{A/A'}$), 121.0 (m, 2 P, $P^{M/M'}$), 89.6 (m (broadening due to unresolved $^nJ_{P-H}$ coupling), 2 P, $P^{X/X'}$)

The resolution of these ^{31}P NMR spectra is not sufficient to reliably simulate the extremely complex spin system of compound **3a**, which is why the provision of coupling constants is neglected.

3b:

Yield: 151 mg (53%, crude)/44 mg (24%, crystalline)

ESI(+)-MS (*o*-DFB): *m/z* (%) = 940.6 (100, [**3b**]$^+$)

Elemental analysis: Calculated (%) for $C_{46}H_{86}Ni_2P_6$: C: 58.63, H: 9.20; found: C: 59.22, H: 9.61

^{1}H-NMR (C_6D_6, 300 K): δ/ ppm = 1.32 – 1.55 (several overlapping doublets/multiplets, 12 H, CH$\underline{Me_2}$), 1.38 (s, 9 H, $C_5H_2{}^t\underline{Bu_3}$), 1.51 (d, 18 H, $C_5H_2{}^t\underline{Bu_3}$), 2.74 (m, 1 H, C$\underline{H}Me_2$), 3.06 (m, 1 H, C$\underline{H}Me_2$), 5.28 (m, 1 H, $C_5\underline{H_2}{}^tBu_3$), 5.40 (m, 1 H, $C_5\underline{H_2}{}^tBu_3$)

^{31}P{^{1}H}-NMR (C_6D_6, 300 K): δ/ ppm = 201.3 (m, 2 P, $P^{A/A'}$), 126.5 (m, 2 P, $P^{M/M'}$), 80.7 (m, 2 P, $P^{X/X'}$)

^{31}P-NMR (C_6D_6, 300 K): δ/ ppm = 201.3 (m, 2 P, $P^{A/A'}$), 126.5 (m (broadening due to unresolved $^nJ_{P\text{-}H}$ coupling), 2 P, $P^{M/M'}$), 80.7 (m, 2 P, $P^{X/X'}$)

The resolution of these ^{31}P NMR spectra is not sufficient to reliably simulate the extremely complex spin system of compound **3b**, which is why the provision of coupling constants is neglected.

4:

Yield: 55 mg (20%)

LIFDI-MS (toluene): *m/z* (%) = 894.6 (100, [**4**+O]$^+$)

Elemental analysis: Calculated (%) for $C_{46}H_{86}P_4Ni_2$: C: 62.75, H: 9.85; found: C: 62.96, H: 10.25

^{1}H-NMR (C_6D_6, 300 K): δ/ ppm = 1.04 (dd, 3 H, CH$\underline{Me_2}$), 1.20 (dd, 3 H, CH$\underline{Me_2}$), 1.38 (s, 9 H, $C_5H_2{}^t\underline{Bu_3}$), 1.53 (s, 9 H, $C_5H_2{}^t\underline{Bu_3}$), 1.54 (s, 9 H, $C_5H_2{}^t\underline{Bu_3}$), 1.56 – 1.64 (overlapping doublets, 6 H, CH$\underline{Me_2}$), 2.37 (m, 1 H, C$\underline{H}$Me$_2$), 2.96 (m, 1 H, C$\underline{H}$Me$_2$), 5.14 (d, 1 H, $C_5\underline{H_2}{}^tBu_3$), 5.28 (d, 1 H, $C_5\underline{H_2}{}^tBu_3$)

$^{31}P\{^{1}H\}$-NMR (C_6D_6, 300 K): δ/ ppm = 52.8 (m, $^{1}J_{PA/A'-PX/X'}$ = 482/481 Hz, $^{2}J_{PA/A'-PX'/X}$ = 21/22 Hz, $^{3}J_{PA-PA'}$ = 26 Hz, 2 P, $P^{A/A'}$), -101.3 (m, $^{1}J_{PX/X'-PA/A'}$ = 482/481 Hz, $^{1}J_{PX-PX'}$ = 324 Hz, $^{2}J_{PX/X'-PA'/A}$ = 21/22 Hz, 2 P, $P^{X/X'}$)

^{31}P-NMR (C_6D_6, 300 K): δ/ ppm = 52.8 (m (br), significant broadening due to unresolved $^{n}J_{P-H}$ coupling, 2 P, $P^{A/A'}$), -101.3 (m, 2 P, $P^{X/X'}$)

*Reactivity of **1c** towards KOEt*

1c (207 mg, 0.2 mmol, 1eq.) was dissolved in 3 mL of THF and KOEt (18 mg, 0.2 mmol, 1 eq.) dissolved in 3 mL of THF was added at -80 °C affording an immediate change of color to an intense turquoise. Upon letting the solution reach room temperature it changes in color via greenish brown to a brownish red. After stirring the solution at room temperature for 1 h the solvent was removed *in vacuo*. 20 mL of *n*-hexane were added to the solid to afford a brownish red solution (and a colorless solid), which was filtered and then constrained to 0.1 mL upon which [Cp'''Ni(η^2-IDippPP(OEt)PP^{i}Pr$_2$)] (**5a**) started to precipitate. The mixture was dissolved in 4 mL of toluene, layered with 30 mL of acetonitrile and stored at 4 °C to afford **5a** as a crystalline material suitable for X-ray analysis. The crude product of **5a** can be obtained by completely removing the *n*-hexane after filtration and not performing the recrystallization.

Notably, the intermediate **5a$_{INT}$** could not be isolated as a pure compound due to its rapid degradation above -10 °C. However, it was possible to study this highly sensitive species by means of low temperature NMR spectroscopy (*vide infra*). Furthermore, gas phase diffusion at -30 °C even allowed for the growth of a single crystal of **5a$_{INT}$** and thus its crystallographic study.

5a

Yield:	125 mg (67%)
LIFDI-MS (toluene):	*m/z* (%) = 879.4 (15, unassigned fragmentation product), 389.4 (100, [IDipp]$^+$)
Elemental analysis:	Calculated (%) for $C_{52}H_{84}N_2OP_4Ni•(C_2H_3N)_{0.2}•(C_6H_{14})_{0.4}$: C: 67.26, H: 9.29, N: 3.15; found: C: 67.74, H: 9.70, N: 3.49
^{1}H-NMR (C_6D_6, 300 K):	δ/ ppm = 1.05 – 1.13 (overlapping doublets, 18 H, CH<u>Me$_2$</u>), 1.16 (t, 3 H, OCH$_2$<u>Me</u>), 1.37 (s, 9 H, C$_5$H$_2$^{t}<u>Bu$_3$</u>), 1.40 – 1.48 (overlapping doublets, 18 H, CH<u>Me$_2$</u>), 1.55 (s, 9 H, C$_5$H$_2$^{t}<u>Bu$_3$</u>), 1.56 (s, 9 H, C$_5$H$_2$^{t}<u>Bu$_3$</u>), 2.15 (m, 1 H, P(C<u>H</u>Me$_2$)$_2$), 2.54 (m, 1 H, P(C<u>H</u>Me$_2$)$_2$), 2.92 (m, 2 H, C<u>H</u>Me$_2$), 3.05 (m, 2 H, C<u>H</u>Me$_2$), 3.94 (br, 1 H, OC<u>H$_2$</u>Me), 4.08 (br, 1 H, OC<u>H$_2$</u>Me), 5.20 (m, 2 H, C$_5$<u>H$_2$</u>^{t}Bu$_3$), 6.18 (s, 2 H, (<u>H</u>CN(Dipp))$_2$C), 7.11 (m, 4 H, Dipp), 7.25 (m, 2 H, Dipp), integrals are slightly off due to the presence of isomers
^{31}P{^{1}H}-NMR (C_6D_6, 300 K):	δ/ ppm = 123.7 (ddd, $^1J_{PA-PQ}$ = 335 Hz, $^1J_{PA-PX}$ = 239 Hz, $^2J_{PA-PM}$ = 30 Hz, 1 H, P^A), 50.7 (dd, $^1J_{PM-PX}$ = 472 Hz, $^2J_{PM-}$

$_{PA}$ = 30 Hz, 1 H, P^M), -47.6 (dd, $^1J_{PQ-PA}$ = 335 Hz, $^2J_{PQ-PX}$ = 272 Hz, 1 H, P^Q), -121.2 (ddd, $^1J_{PX-PM}$ = 472 Hz, $^2J_{PX-PQ}$=272 Hz, $^1J_{PX-PA}$ = 239 Hz, 1 H, P^X)

^{31}P-NMR (C_6D_6, 300 K): δ/ ppm = 123.7 (ddd, $^1J_{PA-PQ}$ = 335 Hz, $^1J_{PA-PX}$ = 239 Hz, $^2J_{PA-PM}$ = 30 Hz, 1 H, P^A), 50.7 (d (br), significant broadening due to $^nJ_{P-H}$ coupling,1 P, P^M), -47.6 (dd, $^1J_{PQ-PA}$ = 335 Hz, $^2J_{PQ-PX}$ = 272 Hz, 1 H, P^Q), -121.2 (ddd, $^1J_{PX-PM}$ = 472 Hz, $^2J_{PX-PQ}$=272 Hz, $^1J_{PX-PA}$ = 239 Hz, 1 H, P^X)

Spectroscopic Data for **5a$_{INT}$**

^{31}P{^{1}H}-NMR (C_6D_6, 300 K): δ/ ppm = 84.1 (ddd, $^1J_{PA-PM}$ = 249 Hz, $^1J_{PA-PX}$ = 233 Hz, $^2J_{PA-PY}$ = 94 Hz, 1 P, P^A), 23.8 (ddd, $^1J_{PM-PA}$ = 249 Hz, $^2J_{PM-PY}$ = 57 Hz, $^2J_{PM-PX}$ = 41 Hz, 1 P, P^M), -34.0 (ddd, $^1J_{PX-PY}$ = 339 Hz, $^1J_{PX-PA}$ = 233 Hz, $^2J_{PX-PM}$ = 41 Hz, 1 P, P^X), -40.1 (ddd, $^1J_{PY-PX}$ = 339 Hz, $^2J_{PY-PA}$ = 94 Hz, $^2J_{PY-PM}$ = 57 Hz, 1 P , P^Y)

^{31}P-NMR (C_6D_6, 300 K): δ/ ppm = 84.1 (ddd, $^1J_{PA-PM}$ = 249 Hz, $^1J_{PA-PX}$ = 233 Hz, $^2J_{PA-PY}$ = 94 Hz, 1 P, P^A), 23.8 (br, significant broadening due to $^nJ_{P-H}$ coupling, 1 P, P^M), -34.0 (ddd, $^1J_{PX-PY}$ = 339 Hz, $^1J_{PX-PA}$ = 233 Hz, $^2J_{PX-PM}$ = 41 Hz, 1 P, P^X), -40.1 (ddd, $^1J_{PY-PX}$ = 339 Hz, $^2J_{PY-PA}$ = 94 Hz, $^2J_{PY-PM}$ = 57 Hz, 1 P , P^Y)

*Reactivity of **2b** towards KOEt*

2b (82 mg, 0.1 mmol, 1eq.) was dissolved in 5 mL of THF and KOEt (9 mg, 0.1 mmol, 1 eq.) dissolved in 3 mL of THF was added at -80 °C affording an immediate change of color from yellow to light red. Upon letting the solution reach room temperature it changes in color to an intense red. After stirring the solution at room temperature for 1 h the solvent was removed *in vacuo*. The solid was washed with 20 mL of *n*-hexane and subsequently dried under reduced pressure (10^{-3} mbar). The solid was dissolved in 7 mL of toluene, filtered through a glass fiber filter paper, concentrated to 3 mL and stored at -30 °C to afford [$CpMo(CO)_2(\eta^{1:1}$-$I^iPr_2Me_2PPP(OEt)PPh_2$)] (**6**) as a crystalline material suitable for X-ray analysis.

Yield:	13 mg (0.018 mmol, 18%)
LIFDI-MS (toluene/THF):	*m/z* (%) = 722.1 (10, [**6**]$^+$), 675.1 (10, [**6**-OEt]$^+$), 181.2 (100, [$I^iPr_2Me_2H$]$^+$)
Elemental analysis:	Calculated (%) for $C_{32}H_{40}MoP_4N_2O_3\cdot(C_7H_8)$: C:57.64, H:5.95, N: 3.45; found: C: 57.90, H:6.05, N: 3.72
$^{31}P\{^1H\}$-NMR (C_6D_6/THF, 300 K):	δ/ ppm = 78.0 (ddd, $^2J_{PA-PM}$ = 177 Hz, $^1J_{PA-PY}$ = 261 Hz, $^1J_{PA-PX}$ = 232 Hz, 1 P, P^A), 0.2 (ddd, $^3J_{PM-PY}$ = 44 Hz, $^2J_{PM-PA}$ = 177 Hz, $^1J_{PM-PX}$ = 191 Hz, 1 P, P^M), -70.7 (ddd, $^1J_{PX-PM}$ = 191 Hz, $^1J_{PX-PA}$ = 232 Hz, $^2J_{PX-PY}$ = 277 Hz, 1 P, P^X), -74.7 (ddd, $^1J_{PY-PA}$ = 261 Hz, $^2J_{PY-PX}$ = 277 Hz, $^3J_{PY-PM}$ = 44 Hz, 1 P, P^Y)
^{31}P-NMR (C_6D_6/THF, 300 K):	δ/ ppm = 78.0 (ddd, $^2J_{PA-PM}$ = 177 Hz, $^1J_{PA-PY}$ = 261 Hz, $^1J_{PA-PX}$ = 232 Hz, 1 P, P^A), 0.2 (m (br), significant broadening due to unresolved $^nJ_{P-H}$ coupling, 1 P, P^M), -70.7 (ddd, $^1J_{PX-PM}$ = 191 Hz, $^1J_{PX-PA}$ = 232 Hz, $^2J_{PX-PY}$ = 277 Hz, 1 P, P^X), -74.7 (ddd, $^1J_{PY-PA}$ = 261 Hz, $^2J_{PY-PX}$ = 277 Hz, $^3J_{PY-PM}$ = 44 Hz, 1 P, P^Y)
IR:	$\tilde{\nu}$(CO)/cm^{-1} = 1899 (s), 1824 (s)

*Reactivity of **1a** towards [ECO]⁻ salts (E = P, As)*

1a (234 mg, 0.2 mmol, 1 eq.) was dissolved in 4 mL of THF and NaOCP•diox (34 mg, 0.2 mmol, 1 eq.) or KAsCO (28 mg, 0.2 mmol, 1 eq.) in 6 mL of THF was added at -80 °C affording a rapid change of color to intense red or dark brownish red, respectively. The solution was allowed to reach room temperature and stirred for 2 h. The solvent was removed *in vacuo* and 30 mL of *n*-hexane added to the solid residue. The dark red solution was filtered, and the solvent removed afterwards affording [Cp'''Ni($\eta^{1:1}$-EP_4Ph_2IDipp)] (**7**: E = P, **8**: E = As) as dark red powders. Crystals of **7** could be obtained by gas phase diffusion of a saturated *n*-pentane solution into toluene at room temperature. In contrast, **8** can simply be recrystallized by layering a concentrated solution in Et_2O upon acetonitrile and storing the mixture at -30 °C yielding the compound as dark red needles suitable for X-ray analysis.

7:

Compound **7** could so far only be obtained in amounts of few single crystals by the method described above. Separation of bulk **7** from side products is hampered by the low stability of this compound and a matter of future investigations.

8:

Yield:	150 mg (73%)
ESI(+)-MS (*o*-DFB):	*m/z* (%) = 950.6 (5, [**8**-Me]⁺), 889.6 (4, unassigned fragmentation), 858.6 (4, unassigned fragmentation), 389.4 (100, [IDipp]⁺)
Elemental analysis:	Calculated (%) for $C_{56}H_{75}N_2P_4NiAs$: C: 65.07, H: 7.31, N: 2.71; found: C: 64.85, H: 7.50, N: 2.97
^{1}H-NMR (C_6D_6, 300 K):	δ/ ppm = 1.07 – 1.16 (overlapping doublets, 12 H, CH$\underline{Me_2}$), 1.13 (s, 9 H, $C_5H_2{}^t\underline{Bu_3}$), 1.28 (s, 9 H, $C_5H_2{}^t\underline{Bu_3}$), 1.38 (s, 9 H, $C_5H_2{}^t\underline{Bu_3}$), 1.39 (d, 6 H, CH$\underline{Me_2}$), 1.58 (d, 6 H, CH$\underline{Me_2}$), 2.93 (m, 2 H, C$\underline{H}Me_2$), 3.05(m, 2 H, C$\underline{H}Me_2$), 4.87 (m, 2 H, $C_5\underline{H_2}{}^tBu_3$), 6.13 (s, 2 H, ($\underline{H}$CN(Dipp))$_2$C), 7.00 (overlapping multiplets, 5 H, Ph and Dipp), 7.16 (overlapping multiplets, 5 H, Ph and Dipp), 7.54 (m, 2 H, Ph), 7.94 (m, 2 H, Ph), integrals are slightly off due to the presence of isomers.
^{31}P{^{1}H}-NMR (C_6D_6, 300 K):	δ/ ppm = -31.3 (m, $^1J_{PA-PY}$ = 207 Hz, $^2J_{PA-PX}$ = 62 Hz, $^3J_{PA-PM}$ = 27Hz, 1 P, P^A), -67.5 (m, $^1J_{PM-PX}$ = 261 Hz, $^2J_{PM-PY}$ = 104 Hz, $^3J_{PM-PA}$ = 27 Hz, 1 P, P^M), -148.4 (m, $^1J_{PX-PM}$ = 261

Hz, $^{1}J_{PX\text{-}PY}$ = 220 Hz, $^{2}J_{PX\text{-}PA}$ = 62 Hz, 1 P, P^{X}), -151.6 (m, $^{1}J_{PY\text{-}PX}$ = 220 Hz, $^{1}J_{PY\text{-}PA}$ = 207 Hz, $^{2}J_{PY\text{-}PM}$ = 104 Hz, 1 P, P^{Y})

^{31}P-NMR (C_6D_6, 300 K): δ ppm = -31.3 (m (br), significant broadening due to $^{n}J_{P\text{-}H}$ coupling, 1 P, P^{A}), -67.5 (m, $^{1}J_{PM\text{-}PX}$ = 261 Hz, $^{2}J_{PM\text{-}PY}$ = 104 Hz, $^{3}J_{PM\text{-}PA}$ = 27 Hz, 1 P, P^{M}), -148.4 (m, $^{1}J_{PX\text{-}PM}$ = 261 Hz, $^{1}J_{PX\text{-}PY}$ = 220 Hz, $^{2}J_{PX\text{-}PA}$ = 62 Hz, 1 P, P^{X}), -151.6 (m, $^{1}J_{PY\text{-}PX}$ = 220 Hz, $^{1}J_{PY\text{-}PA}$ = 207 Hz, $^{2}J_{PY\text{-}PM}$ = 104 Hz, 1 P, P^{Y})

12.5.2. X-ray Crystallographic Data

General Considerations

The crystallographic data for all synthesized compounds was collected either on an Xcalibur Gemini with an AtlasS2 detector using Cu-K_α radiation (**A1**) on a GV1000 diffractometer (AT) with a TitanS2 detector using Cu-K_α radiation (**B1**, **3a**, **5a**, **6**, **8**) or on a XtaLAB Synergy R, DW system with HyPix-Arc 150 detector applying Cu-Kα radiation (**A2**, **1a**, **1b**, **1c**, **1d**, **2a**, **2c**, **4**, **5a$_{INT}$**, **7**) from a rotating anode X-ray source. All measurements were performed at 123 K. Data collection, data reduction and absorption correction were performed with the CrysAlisPro software package.[30] Structure solution and refinement was conducted in Olex2 (1.5 alpha)[31] with ShelXT (solution)[32] and ShelXL (refinement)[33] (full-matric least-squares method against F^2). All non-hydrogen atoms were refined with anisotropic displacement parameters and hydrogen atoms were treated as riding models with isotropic displacement parameters and fixed C-H bond lengths (sp^3: 0.96 (CH_3), 0.97 (CH_2), sp^2: 0.93 (CH)). Visualization of the crystal structures was performed with Olex2.[31]

*Table S 1: Crystallographic and refinement data for compounds **A1**, **A2**, **B1** and **1a**.*

Compound	A1	A2	B1	1a
Empirical formula	$C_{29}H_{39}F_6P_5Ni$	$C_{23}H_{43}F_6NiP_5$	$C_{40}H_{30}F_6Mo_2O_{10}P_8S_2$	$C_{112}H_{150}F_{12}N_4Ni_2P_{10}$
Formula weight	715.16	647.13	1288.40	2207.47
Temperature/K	293(2)	100.00(10)	123.15	210(120)
Crystal system	monoclinic	monoclinic	triclinic	triclinic
Space group	$P2_1/n$	$P2_1/c$	$P\bar{1}$	$P\bar{1}$
a/Å	10.4531(5)	15.5378(2)	10.3127(2)	17.5318(2)
b/Å	24.9776(9)	13.9119(2)	10.7357(2)	17.6671(2)
c/Å	13.0061(6)	14.4028(2)	24.2951(4)	19.0793(3)
α/°	90	90	88.244(2)	81.9830(10)
β/°	108.778(5)	104.226(2)	84.235(2)	86.0820(10)
γ/°	90	90	64.221(2)	85.5260(10)
Volume/Å^3	3215.1(3)	3017.84(8)	2409.61(8)	5824.07(13)
Z	4	4	2	2
ρ_{calc}g/cm^3	1.477	1.424	1.776	1.259
μ/mm^{-1}	0.907	3.876	8.285	2.237
F(000)	1480.0	1352.0	1280.0	2328.0
Crystal size/mm^3	1.027 × 0.157 × 0.118	0.35 × 0.29 × 0.12	0.2 × 0.14 × 0.12	0.49 × 0.16 × 0.11
Radiation	Mo Kα (λ = 0.71073)	Cu Kα (λ = 1.54184)	Cu Kα (λ = 1.54184)	Cu Kα (λ = 1.54184)
2Θ range for data collection/°	6.564 to 64.9	5.868 to 143.734	7.316 to 133.542	5.064 to 148.204
Index ranges	-9 ≤ h ≤ 15, -37 ≤ k ≤ 35, -19 ≤ l ≤ 18	-18 ≤ h ≤ 18, -16 ≤ k ≤ 16, -17 ≤ l ≤ 16	-12 ≤ h ≤ 12, -12 ≤ k ≤ 12, -19 ≤ l ≤ 28	-19 ≤ h ≤ 21, -22 ≤ k ≤ 21, -23 ≤ l ≤ 23
Reflections collected	18134	41024	40387	65155
Independent reflections	10126 [R_{int} = 0.0222, R_{sigma} = 0.0466]	5810 [R_{int} = 0.0580, R_{sigma} = 0.0286]	8493 [R_{int} = 0.0813, R_{sigma} = 0.0462]	22252 [R_{int} = 0.0184, R_{sigma} = 0.0171]
Data/restraints/parameters	10126/0/376	5810/54/536	8493/605/844	22252/833/1942
Goodness-of-fit on F^2	1.037	1.051	1.026	1.179
Final R indexes [I>=2σ (I)]	R_1 = 0.0386, wR_2 = 0.0760	R_1 = 0.0517, wR_2 = 0.1162	R_1 = 0.0573, wR_2 = 0.1523	R_1 = 0.0434, wR_2 = 0.1001
Final R indexes [all data]	R_1 = 0.0585, wR_2 = 0.0842	R_1 = 0.0586, wR_2 = 0.1195	R_1 = 0.0626, wR_2 = 0.1602	R_1 = 0.0455, wR_2 = 0.1011
Largest diff. peak/hole / e Å^{-3}	0.66/-0.33	0.56/-0.69	0.91/-1.37	0.38/-0.28

*Table S 2: Crystallographic and refinement data for compounds **1b**, **1c**, **1d** and **2a**.*

Compound	**1b**[OTf]	**1c**	**1d**	**2a**
Empirical formula	$C_{41}H_{59}N_2O_3F_3P_4SNi$	$C_{53}H_{86}F_6N_2NiP_5$	$C_{34}H_{63}N_2F_6P_5Ni$	$C_{59}H_{59}F_7MoN_2O_5P_4S$
Formula weight	899.55	1078.79	827.42	1260.96
Temperature/K	123.00(10)	123.00(10)	123.01(10)	123.15
Crystal system	orthorhombic	monoclinic	orthorhombic	triclinic
Space group	*Pbca*	$P2_1/n$	$Pna2_1$	$P\bar{1}$
a/Å	15.77900(10)	14.48490(10)	22.7672(2)	13.2210(2)
b/Å	16.73710(10)	17.85970(10)	15.11330(10)	14.2245(2)
c/Å	34.2446(2)	23.26710(10)	26.6638(2)	18.6479(3)
α/°	90	90	90	102.0130(10)
β/°	90	105.0590(10)	90	96.9240(10)
γ/°	90	90	90	112.378(2)
Volume/Å^3	9043.82(9)	5812.40(6)	9174.68(12)	3093.49(9)
Z	8	4	11	2
ρ_{calc}g/cm^3	1.321	1.233	1.647	1.354
μ/mm^{-1}	2.806	2.224	3.668	3.607
F(000)	3792.0	2300.0	4818.0	1296.0
Crystal size/mm^3	0.263 × 0.069 × 0.033	0.42 × 0.3 × 0.11	0.37 × 0.3 × 0.14	0.16 × 0.13 × 0.09
Radiation	Cu Kα (λ = 1.54184)	Cu Kα (λ = 1.54184)	Cu Kα (λ = 1.54184)	Cu Kα (λ = 1.54184)
2Θ range for data collection/°	5.162 to 147.328	6.322 to 143.24	6.63 to 146.216	4.968 to 143.27
Index ranges	-19 ≤ h ≤ 14, -20 ≤ k ≤ 20, -42 ≤ l ≤ 41	-17 ≤ h ≤ 17, -20 ≤ k ≤ 21, -27 ≤ l ≤ 28	-21 ≤ h ≤ 27, -18 ≤ k ≤ 17, -26 ≤ l ≤ 32	-16 ≤ h ≤ 16, -17 ≤ k ≤ 16, -22 ≤ l ≤ 22
Reflections collected	146284	45552	44608	47984
Independent reflections	9105 [R_{int} = 0.0281, R_{sigma} = 0.0123]	10976 [R_{int} = 0.0224, R_{sigma} = 0.0171]	14134 [R_{int} = 0.0249, R_{sigma} = 0.0233]	11777 [R_{int} = 0.0300, R_{sigma} = 0.0294]
Data/restraints/parameters	9105/0/511	10976/0/598	14134/216/1031	11777/589/847
Goodness-of-fit on F^2	1.042	1.032	1.050	1.065
Final R indexes [I>=2σ (I)]	R_1 = 0.0313, wR_2 = 0.0809	R_1 = 0.0334, wR_2 = 0.0885	R_1 = 0.0370, wR_2 = 0.1013	R_1 = 0.0433, wR_2 = 0.1314
Final R indexes [all data]	R_1 = 0.0342, wR_2 = 0.0826	R_1 = 0.0354, wR_2 = 0.0897	R_1 = 0.0394, wR_2 = 0.1030	R1 = 0.0521, wR2 = 0.1374
Largest diff. peak/hole / e Å^{-3}	0.87/-0.31	0.69/-0.42	0.50/-0.40	0.56/-0.53

*Table S 3: Crystallographic and refinement data for compounds **2c**, **3a**, **4** and **5a**.*

Compound	2c	3a	4	5a
Empirical formula	$C_{56}H_{55}AlF_{36}MoN_2O_6P_4$	$C_{61.5}H_{82}Ni_2P_6$	$C_{46}H_{86}Ni_2P_4$	$C_{57}H_{94}N_3NiOP_4$
Formula weight	1782.82	1078.44	880.44	1019.94
Temperature/K	123.15	123.15	293(2)	123.00(10)
Crystal system	monoclinic	monoclinic	triclinic	monoclinic
Space group	$P2_1/c$	I2/a	$P\bar{1}$	$P2_1/c$
a/Å	11.26790(10)	20.3249(6)	9.19120(10)	15.2032(2)
b/Å	17.93300(10)	10.6940(3)	10.7346(2)	38.7912(4)
c/Å	36.1886(3)	54.5604(15)	14.0769(2)	10.37670(10)
α/°	90	90	99.3150(10)	90
β/°	94.4380(10)	93.485(2)	104.2670(10)	107.8070(10)
γ/°	90	90	110.4560(10)	90
Volume/Å^3	7290.60(10)	11837.0(6)	1213.22(3)	5826.48(12)
Z	4	8	1	4
ρ_{calc}g/cm^3	1.624	1.210	1.205	1.163
μ/mm^{-1}	3.704	2.573	2.409	1.805
F(000)	3568.0	4576.0	478.0	2212.0
Crystal size/mm^3	0.16 × 0.1 × 0.08	0.132 × 0.055 × 0.038	0.3 × 0.08 × 0.06	0.61 × 0.22 × 0.11
Radiation	Cu Kα (λ = 1.54184)	CuKα (λ = 1.54184)	Cu Kα (λ = 1.54184)	Cu Kα (λ = 1.54184)
2Θ range for data collection/°	4.898 to 143.232	8.426 to 134.168	6.736 to 143.152	7.62 to 133.878
Index ranges	-13 ≤ h ≤ 13, -20 ≤ k ≤ 22, -43 ≤ l ≤ 44	-24 ≤ h ≤ 24, -12 ≤ k ≤ 12, -63 ≤ l ≤ 65	-10 ≤ h ≤ 11, -13 ≤ k ≤ 12, -16 ≤ l ≤ 17	-18 ≤ h ≤ 17, -46 ≤ k ≤ 45, -10 ≤ l ≤ 12
Reflections collected	46128	115687	14164	57284
Independent reflections	13843 [R_{int} = 0.0279, R_{sigma} = 0.0304]	10497 [R_{int} = 0.1583, R_{sigma} = 0.0699]	4540 [R_{int} = 0.0191, R_{sigma} = 0.0175]	10321 [R_{int} = 0.0518, R_{sigma} = 0.0263]
Data/restraints/parameters	13843/739/1194	10497/78/675	4540/0/248	10321/0/621
Goodness-of-fit on F^2	1.033	1.017	1.051	1.040
Final R indexes [I>=2σ (I)]	R_1 = 0.0399, wR_2 = 0.1021	R_1 = 0.0489, wR_2 = 0.1108	R_1 = 0.0234, wR_2 = 0.0609	R_1 = 0.0352, wR_2 = 0.0940
Final R indexes [all data]	R_1 = 0.0485, wR_2 = 0.1068	R_1 = 0.0784, wR_2 = 0.1252	R_1 = 0.0242, wR_2 = 0.0613	R_1 = 0.0374, wR_2 = 0.0959
Largest diff. peak/hole / e Å^{-3}	0.46/-0.34	0.40/-0.28	0.30/-0.23	0.51/-0.36

*Table S 4: Crystallographic and refinement data for compounds **5a$_{INT}$**, **6**, **7** and **8**.*

Compound	5a$_{INT}$	6	7	8
Empirical formula	$C_{113}H_{189}N_4Ni_2O_2P_8$	$C_{37.6}H_{46.4}MoN_2O_3P_4$	$C_{56}H_{75}N_2P_5Ni$	$C_{60.5}H_{84}AsN_3NiP_4$
Formula weight	2000.85	794.18	989.74	1110.81
Temperature/K	123.00(10)	159.15	123.01(10)	122.97(10)
Crystal system	triclinic	triclinic	monoclinic	monoclinic
Space group	$P\bar{1}$	$P\bar{1}$	$P2_1/c$	$C2/c$
a/Å	13.8094(2)	12.1481(2)	22.6390(5)	25.2732(3)
b/Å	20.4395(3)	12.4558(2)	10.4198(2)	10.53900(10)
c/Å	21.9281(4)	14.9933(2)	24.9039(5)	45.1650(5)
α/°	96.889(2)	86.9260(10)	90	90
β/°	95.901(2)	81.9380(10)	111.938(2)	104.2430(10)
γ/°	105.303(2)	61.533(2)	90	90
Volume/Å^3	5868.08(17)	1974.46(6)	5449.3(2)	11660.1(2)
Z	2	2	4	8
ρ_{calc}g/cm^3	1.132	1.336	1.206	1.266
μ/mm^{-1}	1.777	4.537	2.172	2.441
F(000)	2174.0	824.0	2112.0	4712.0
Crystal size/mm^3	0.11 × 0.04 × 0.02	0.22 × 0.18 × 0.12	0.17 × 0.03 × 0.03	0.39 × 0.12 × 0.05
Radiation	Cu Kα (λ = 1.54184)	Cu Kα (λ = 1.54184)	Cu Kα (λ = 1.54184)	Cu Kα (λ = 1.54184)
2Θ range for data collection/°	4.536 to 143.37	8.076 to 133.39	7.226 to 148.582	7.352 to 134.156
Index ranges	-16 ≤ h ≤ 16, -21 ≤ k ≤ 24, -27 ≤ l ≤ 26	-13 ≤ h ≤ 14, -14 ≤ k ≤ 14, -17 ≤ l ≤ 16	-27 ≤ h ≤ 25, -12 ≤ k ≤ 12, -29 ≤ l ≤ 30	-30 ≤ h ≤ 29, -12 ≤ k ≤ 11, -53 ≤ l ≤ 53
Reflections collected	71952	34276	33659	49384
Independent reflections	22138 [R_{int} = 0.0504, R_{sigma} = 0.0762]	6945 [R_{int} = 0.0478, R_{sigma} = 0.0253]	10310 [R_{int} = 0.0515, R_{sigma} = 0.0538]	10287 [R_{int} = 0.0486, R_{sigma} = 0.0267]
Data/restraints/parameters	22138/114/1185	6945/0/397	10310/0/594	10287/271/709
Goodness-of-fit on F^2	1.028	1.058	1.067	1.043
Final R indexes [I>=2σ (I)]	R_1 = 0.0588, wR_2 = 0.1394	R1 = 0.0303, wR2 = 0.0842	R_1 = 0.0609, wR_2 = 0.1677	R_1 = 0.0346, wR_2 = 0.0922
Final R indexes [all data]	R_1 = 0.1087, wR_2 = 0.1589	R_1 = 0.0309, wR_2 = 0.0847	R_1 = 0.0789, wR_2 = 0.1813	R_1 = 0.0367, wR_2 = 0.0939
Largest diff. peak/hole / e Å^{-3}	0.65/-0.56	0.46/-0.80	1.26/-0.78	0.46/-0.41

*[Cp'''Ni(η^3-P_4Ph_2)][PF_6] (**A1**)*

A1 crystallizes as red blocks from concentrated solutions in *o*-DFB layered with *n*-hexane and upon storage at room temperature for several days (Figure S1). **A1** crystallizes in the monoclinic space group $P2_1/n$ with one anion and one cation in the asymmetric unit.

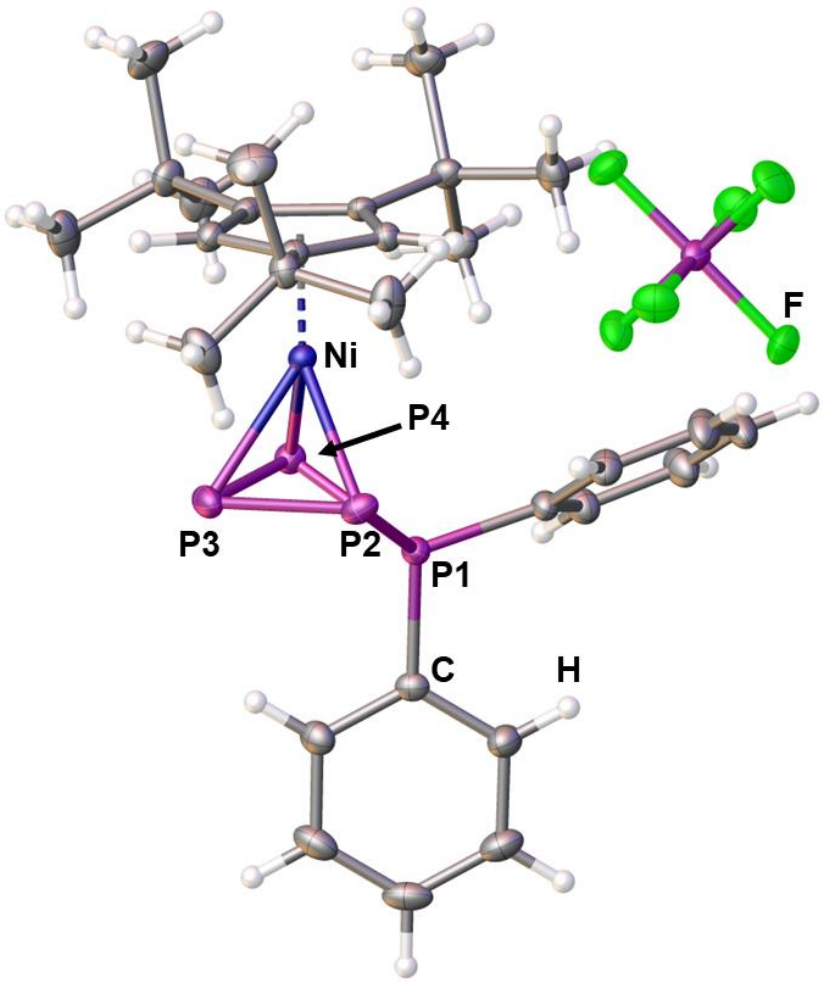

*Figure S 1: Solid state structure of **A1**. Depicted is the asymmetric unit and ADPs (anisotropic displacement parameters) are drawn at 50 % probability.*

*[Cp'''Ni(η^3-$P_4{}^iPr_2$)][PF_6] (**A2**)*

A2 crystallizes as dark red plates from concentrated solutions in *o*-DFB layered with *n*-hexane and upon storage at room temperature for several days (Figure S2). **A2** crystallizes in the monoclinic space group $P2_1/n$ with one anion and one cation in the asymmetric unit. Disorder was treated with adequate restraints.

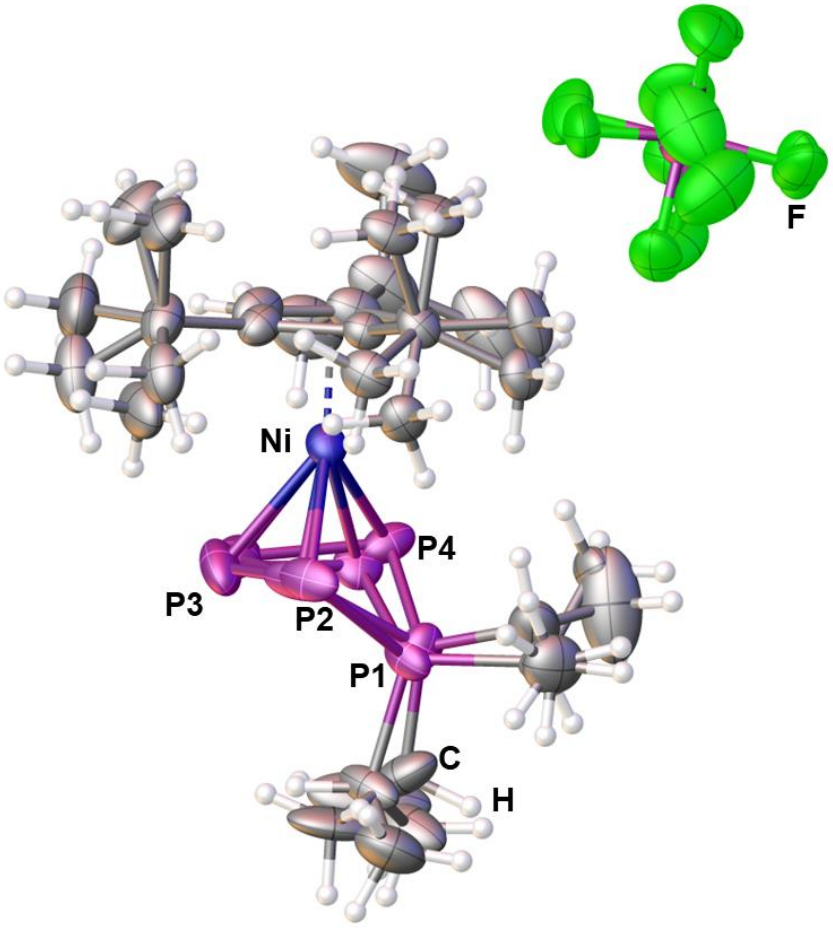

*Figure S 2: Solid state structure of **A2**. Depicted is the asymmetric unit and ADPs (anisotropic displacement parameters) are drawn at 50 % probability.*

*[CpMo(CO)$_2$(η^3-P$_4$Ph$_2$)][OTf] (**B1**)*

B1 crystallizes as light yellow blocks from concentrated solutions in *o*-DFB layered with *n*-hexane and upon storage at room temperature for several days (Figure S3). **B1** crystallizes in the triclinic space group $P\bar{1}$ with two anions and two cations in the asymmetric unit. Disorders within the anions and the C_6H_5 group of the cation were treated with adequate restraints.

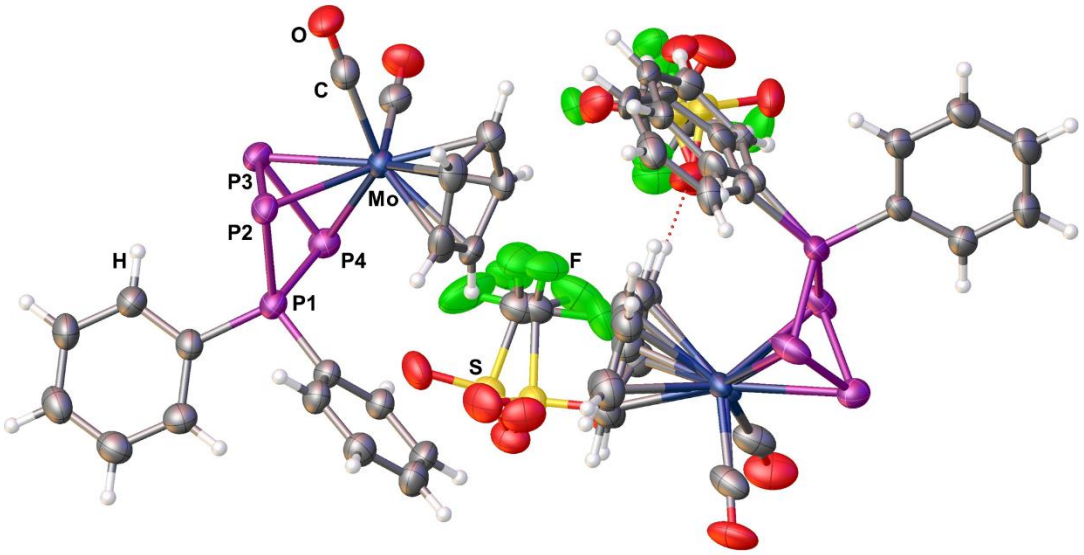

*Figure S 3: Solid state structure of **B1**. Depicted is the asymmetric unit and ADPs (anisotropic displacement parameters) are drawn at 50 % probability.*

*[Cp'''Ni($\eta^{1:1}$-P_4Ph_2IDipp)][PF_6] (**1a**)*

1a crystallizes as dark greenish brown sticks from concentrated solutions in THF layered with *n*-hexane and upon storage at room temperature for several days (Figure S4). **1a** crystallizes in the monoclinic space group $P2_1/n$ with one anion and one cation in the asymmetric unit. Disorder was treated with adequate restraints.

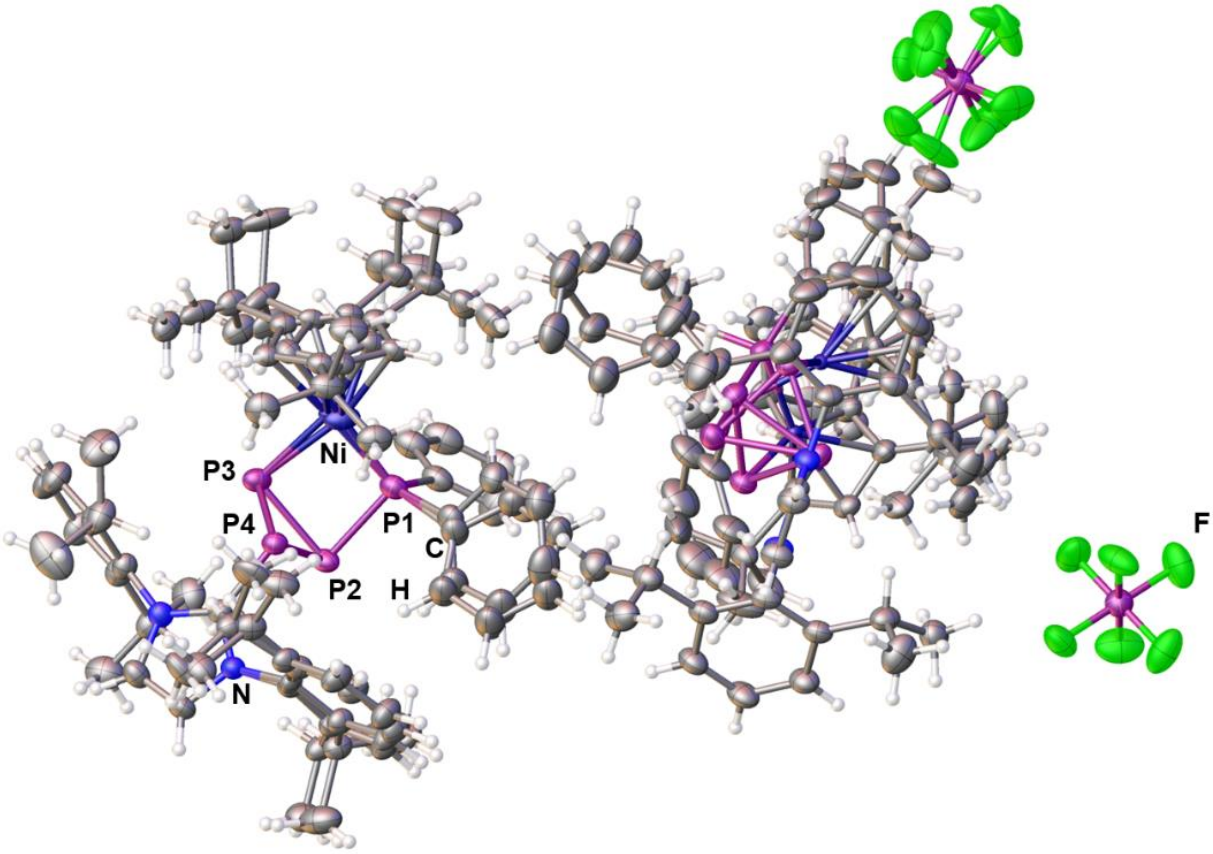

*Figure S 4: Solid state structure of **1a**. Depicted is the asymmetric unit and ADPs (anisotropic displacement parameters) are drawn at 50 % probability.*

*[Cp'''Ni($\eta^{1:1}$-$P_4Ph_2{}^iPr_2Me_2$)][OTf] (**1b**[OTf])*

1b crystallizes from concentrated solutions in THF layered with *n*-hexane and upon storage at room temperature for several days. **1b** crystallizes in the orthorhombic space group *Pbcn* with one anion, one cation and one molecule of *n*-hexane in the asymmetric unit. However, the crystal quality of **1b** could not be improved to a satisfactory limit. Thus, the $[PF_6]^-$ anion was exchanged for $[OTf]^-$. **1b**[OTf] also crystallizes from concentrated THF solutions layered with *n*-hexane and storage at room temperature forming brownish sticks (Figure S5). However, it crystallizes in the orthorhombic space group *Pbca* with only an anion and a cation being present in the asymmetric unit.

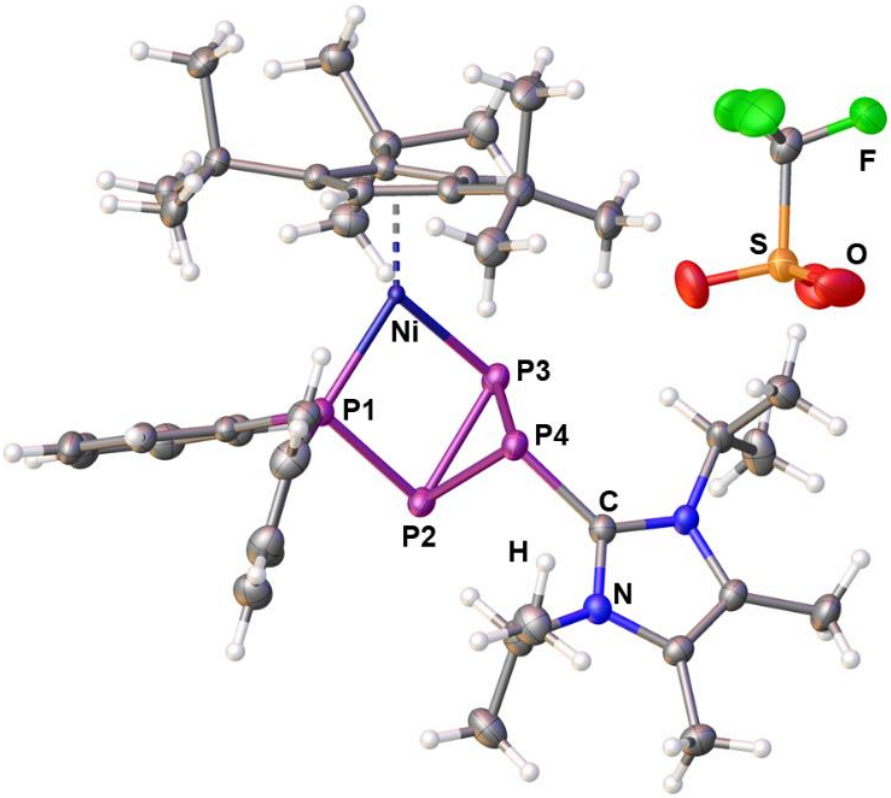

*Figure S 5: Solid state structure of **1b**. Depicted is the asymmetric unit and ADPs (anisotropic displacement parameters) are drawn at 50 % probability.*

*[Cp'''Ni($\eta^{1:1}$-$P_4{}^{i}Pr_2$IDipp)][PF_6] (**1c**)*

1c crystallizes as greenish plates from concentrated solutions in *o*-DFB layered with *n*-hexane and upon storage at room temperature for several days (Figure S6). **1c** crystallizes in the monoclinic space group $P2_1/n$ with one anion and one cation in the asymmetric unit.

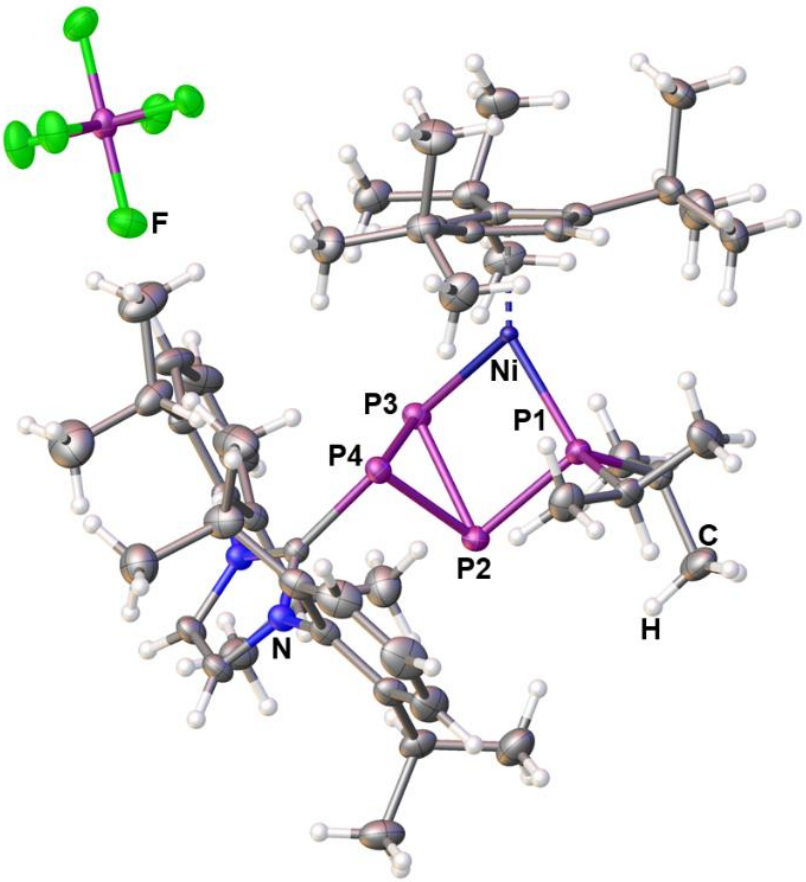

*Figure S 6: Solid state structure of **1c**. Depicted is the asymmetric unit and ADPs (anisotropic displacement parameters) are drawn at 50 % probability.*

*[Cp'''Ni($\eta^{1:1}$-$P_4{}^iPr_2{}^iPr_2Me_2$)][PF_6] (**1d**)*

1d crystallizes as greenish brown plates from concentrated solutions in *o*-DFB layered with *n*-hexane and upon storage at room temperature for several days (Figure S7). **1d** crystallizes in the orthorhombic space group *Pna*2_1 with two anions, two cations and one molecule of *n*-hexane in the asymmetric unit. Disorder was treated with adequate restraints and the *n*-hexane was treated with a solvent mask.

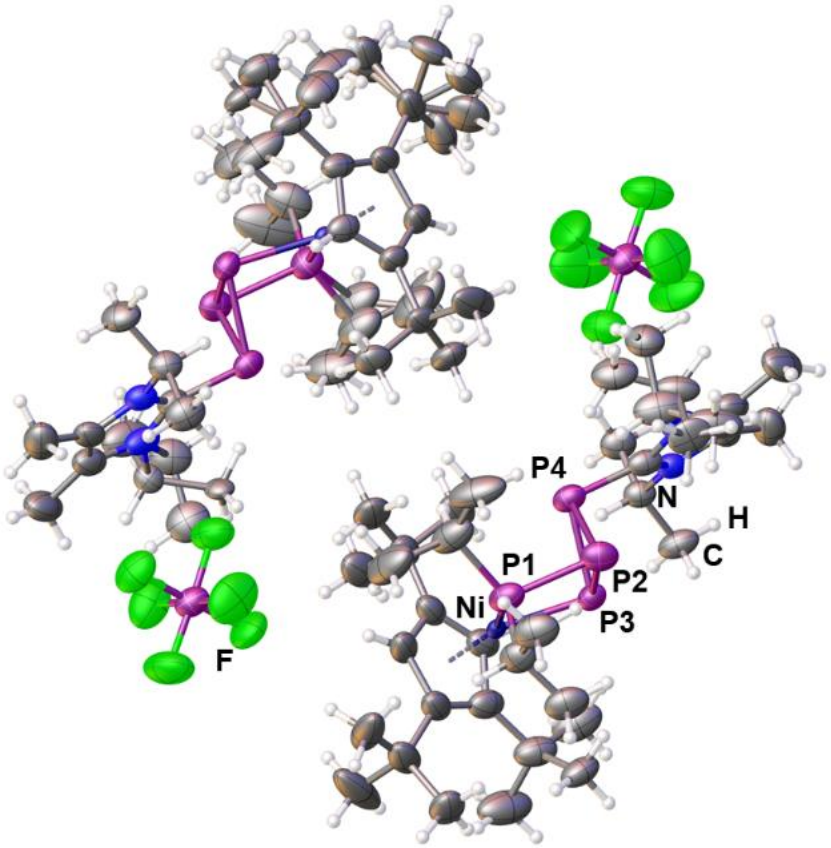

*Figure S 7: Solid state structure of **1d**. Depicted is the asymmetric unit and ADPs (anisotropic displacement parameters) are drawn at 50 % probability.*

*[CpMo(CO)$_2$(η^3-P$_4$Ph$_2$IDipp)][OTf] (**2a**)*

2a crystallizes as light yellow plates from concentrated solutions in *o*-DFB layered with *n*-hexane and upon storage at room temperature for several days (Figure S8). **2a** crystallizes in the triclinic space group $P\bar{1}$ with one anion, one cation and two molecules *o*-DFB in the asymmetric unit. Disorder was treated with adequate restraints. The *o*-DFB was treated with a solvent mask.

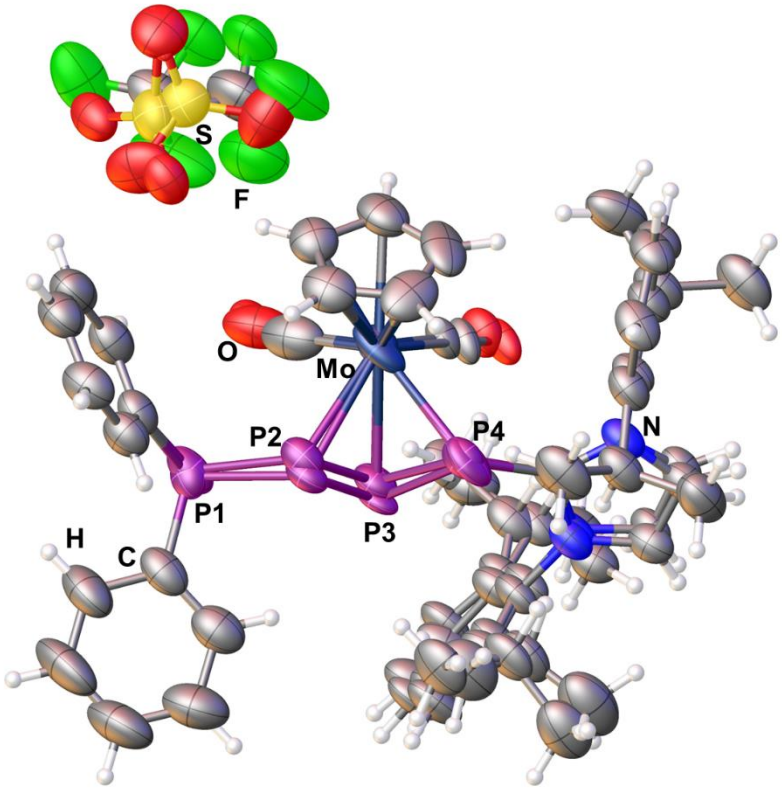

*Figure S 8 Solid state structure of **2a**. Depicted is the asymmetric unit and ADPs (anisotropic displacement parameters) are drawn at 50 % probability.*

*[CpMo(CO)$_2$(η^3-P$_4$^{i}Pr$_2$IDipp)][TEF] (**2c**)*

2c crystallizes as light yellow plates from concentrated solutions in *o*-DFB layered with *n*-hexane and upon storage at room temperature for several days (Figure S9). **2c** crystallizes in the monoclinic space group $P2_1/c$ with one anion and one cation in the asymmetric unit. Disorder was treated with adequate restraints.

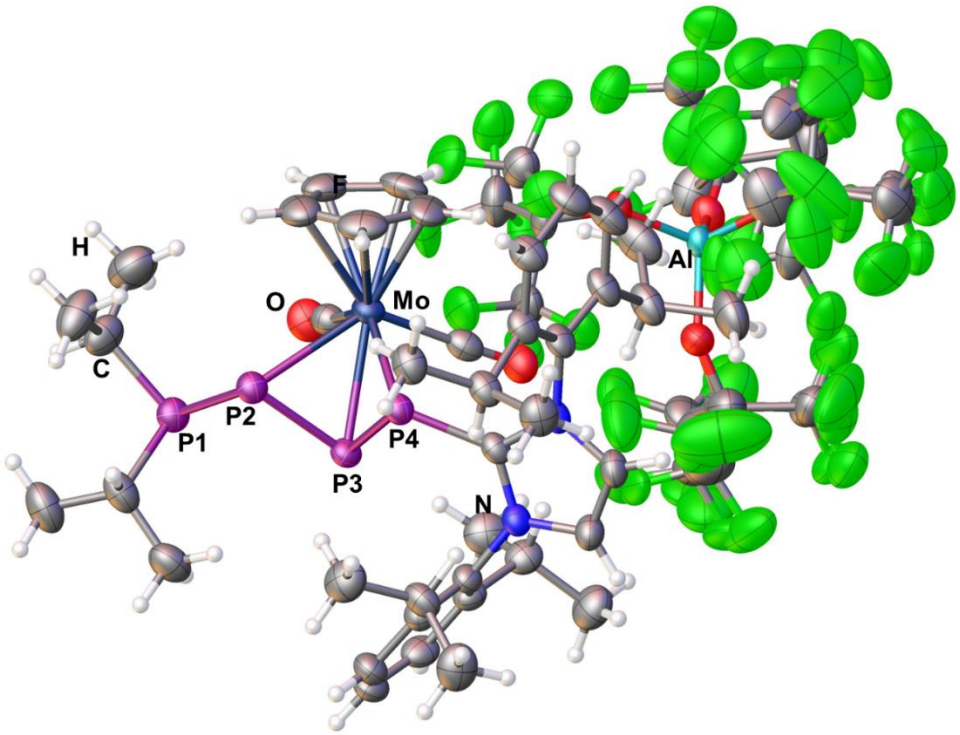

*Figure S 9: Solid state structure of **2c**. Depicted is the asymmetric unit and ADPs (anisotropic displacement parameters) are drawn at 50 % probability.*

[{Cp'''Ni}$_2$(μ,$\eta^{1:1:1:1}$-cyclo-P$_4$(PPh$_2$)$_2$)] (***3a***)

3a crystallizes as dark brownish red sticks from concentrated toluene solutions layered with acetonitrile and storage at 4 °C for several days (Figure S10). **3a** crystallizes in the monoclinic space group *I*2/*a* with one molecule in the asymmetric unit. Disorder was treated with adequate restraints.

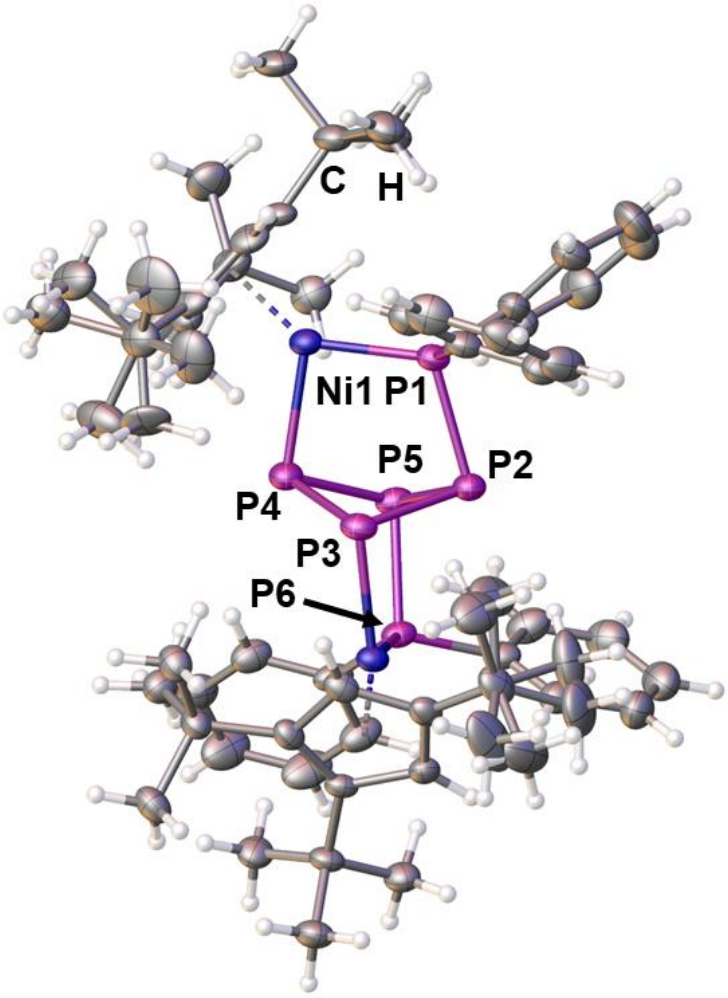

Figure S 10: Solid state structure of ***3a****. Depicted is the asymmetric unit and ADPs (anisotropic displacement parameters) are drawn at 50 % probability.*

[{Cp'''Ni}$_2$($\mu,\eta^{2:2}$-(PP^{i}Pr$_2$)$_2$)] (***4***)

4 crystallizes as clear red sticks by storing a concentrated solution in *n*-hexane at 4°C for 2 days (Figure S11). It crystallizes in the triclinic space group $P\bar{1}$ with half of a molecule in the asymmetric unit.

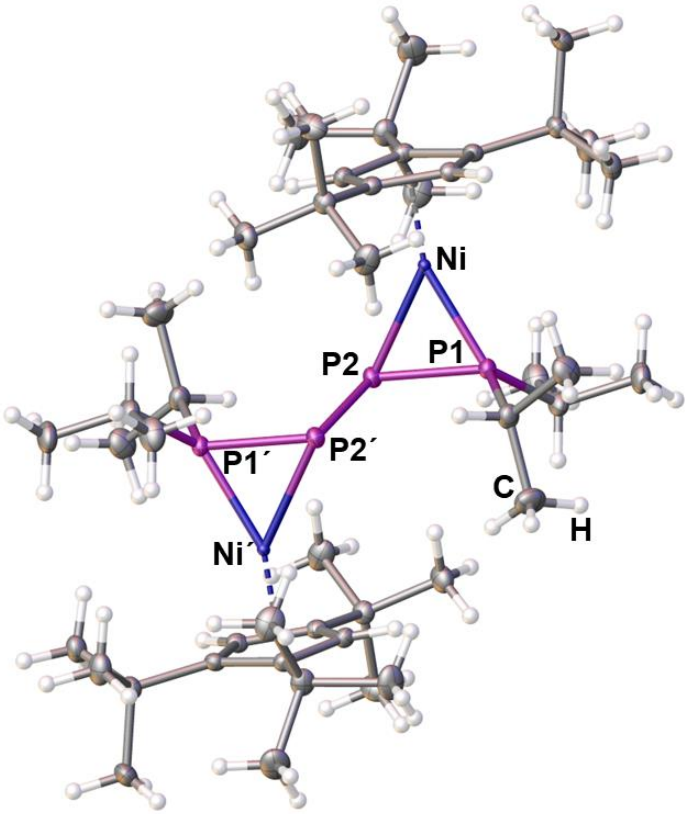

*Figure S 11: Solid state structure of **4** Depicted is the asymmetric unit and its symmetry equivalent, and ADPs (anisotropic displacement parameters) are drawn at 50 % probability.*

*[Cp'''Ni(η^2-IDippPP(OEt)PP^{i}Pr$_2$)] (**5a**)*

5a crystallizes as dark yellowish brown sticks from concentrated toluene solutions layered with acetonitrile and storage at 4 °C for several days (Figure S12). **5a** crystallizes in the monoclinic space group $P2_1/c$ with one molecule, one acetonitrile and half of a molecule of *n*-hexane in the asymmetric unit. Disorder was treated with adequate restraints and the *n*-hexane was treated with a solvent mask.

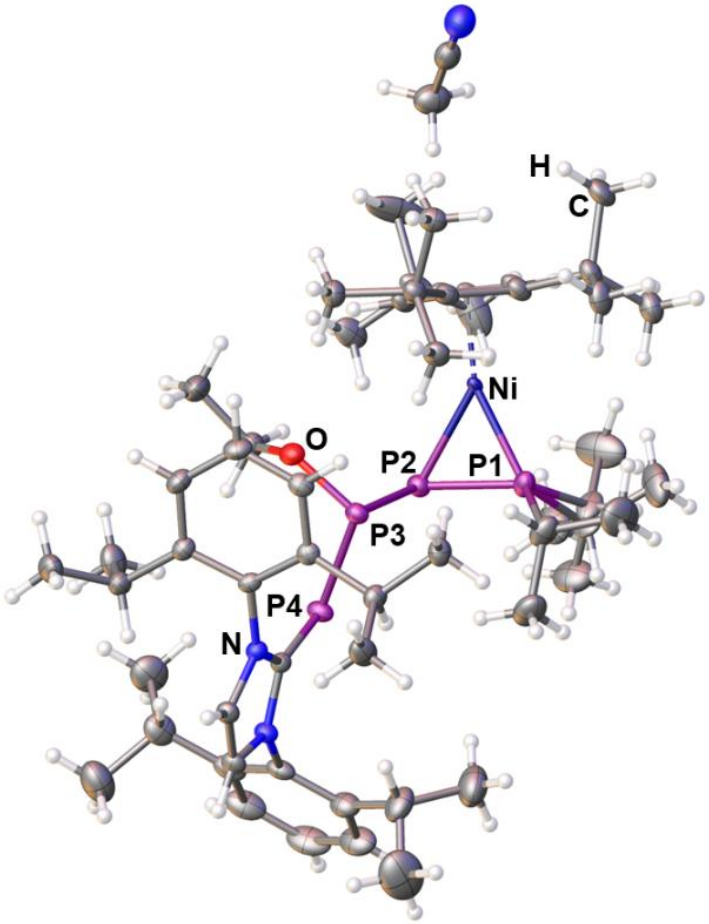

*Figure S 12: Solid state structure of **5a**. Depicted is the asymmetric unit and ADPs (anisotropic displacement parameters) are drawn at 50 % probability.*

*[Cp'''Ni($\eta^{1:1}$-IDippPPP(OEt)P^{i}Pr$_2$)] (**5a$_{INT}$**)*

5a$_{INT}$ must be handled with great care as it decomposes at temperatures higher than -10 °C. **5a$_{INT}$** crystallizes as dark turquoise platelets via inverse gas diffusion from a concentrated *n*-hexane solution into toluene at -30 °C (Figure S13). It crystallizes in the triclinic space group $P\bar{1}$ with two molecules and 1.5 *n*-hexane molecules in the asymmetric unit. Disorder was treated with adequate restraints and the *n*-hexane was treated with a solvent mask.

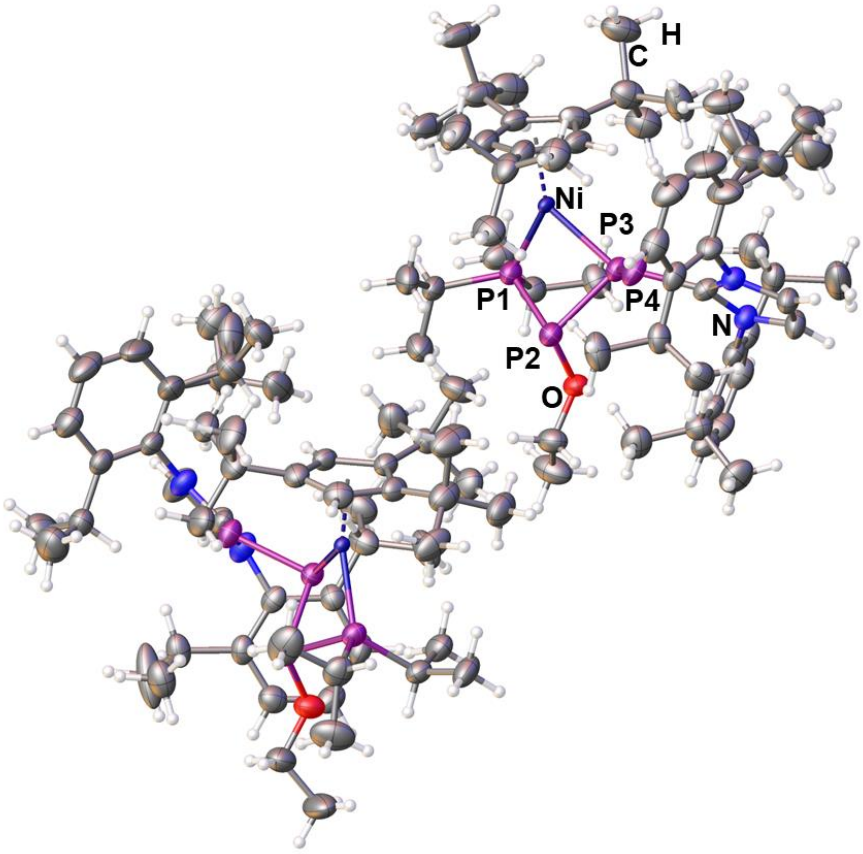

*Figure S 13: Solid state structure of **5a$_{INT}$**. Depicted is the asymmetric unit and ADPs (anisotropic displacement parameters) are drawn at 50 % probability.*

[CpMo(CO)$_2$($\eta^{1:1}$-l^{i}Pr$_2$Me$_2$PPP(OEt)PPh$_2$)] (**6**)

6 crystallizes as intense orange blocks from concentrated toluene solutions and storage at 4 °C for several days (Figure S14). **6** crystallizes in the triclinic space group $P\bar{1}$ with one molecule and 0.8 molecules of toluene in the asymmetric unit. The toluene was treated with a solvent mask. Disorders within the OEt group was treated with adequate restraints.

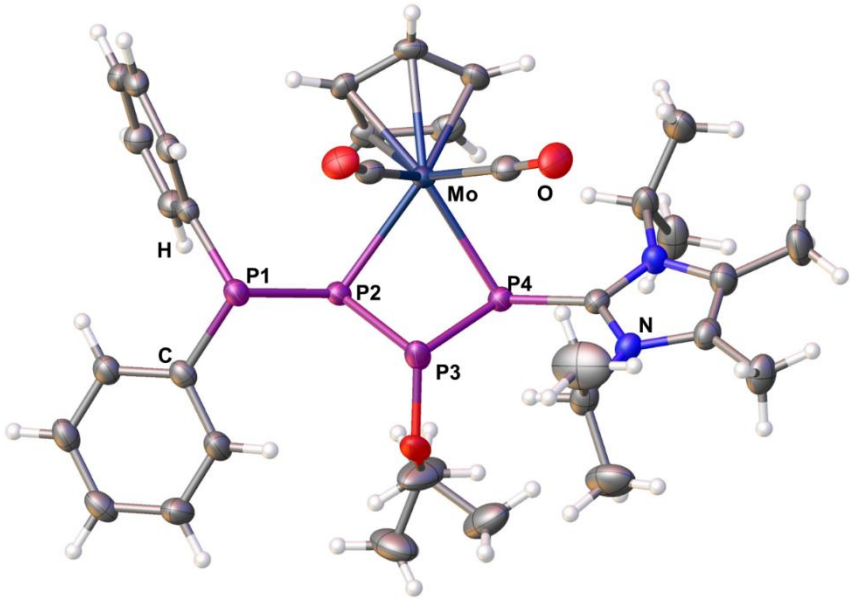

*Figure S 14: Solid state structure of **6**. Depicted is the asymmetric unit and ADPs (anisotropic displacement parameters) are drawn at 50 % probability.*

*[Cp'''Ni($\eta^{1:1}$-P_5Ph_2IDipp)] (**7**)*

7 crystallizes as yellow needles via inverse gas diffusion from a concentrated *n*-hexane solution into toluene at room temperature (Figure S15). It crystallizes in the monoclinic space group $P2_1/c$ with one molecule in the asymmetric unit.

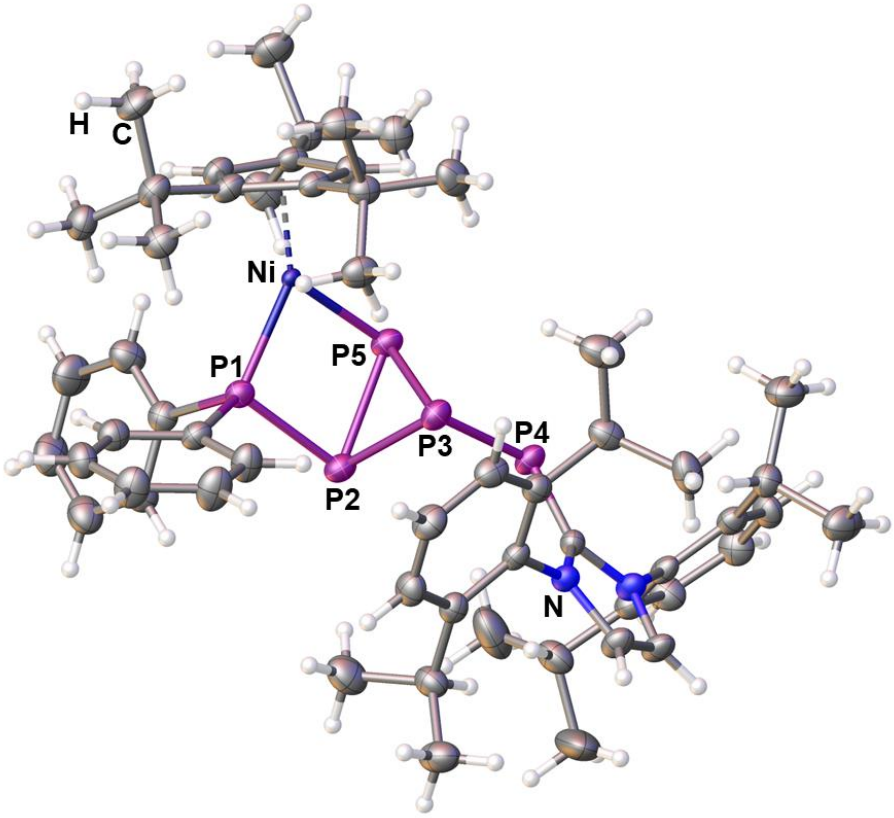

*Figure S 15: Solid state structure of **7**. Depicted is the asymmetric unit and ADPs (anisotropic displacement parameters) are drawn at 50 % probability.*

[Cp'''Ni($\eta^{1:1}$-AsP_4Ph_2IDipp)] (***8***)

8 crystallizes as dark red needles from concentrated Et_2O solutions layered with acetonitrile and storage at -30 °C for several days (Figure S16). **8** crystallizes in the monoclinic space group *C*2/*c* with one molecule, half of a molecule of *n*-hexane and one acetonitrile molecule in the asymmetric unit. Disorder was treated with adequate restraints. Notably, the As atom is disordered across all three positions within the three membered ring. However, it occupies the unsubstituted position to 87%, while the others are equally occupied to 6/7%, each.

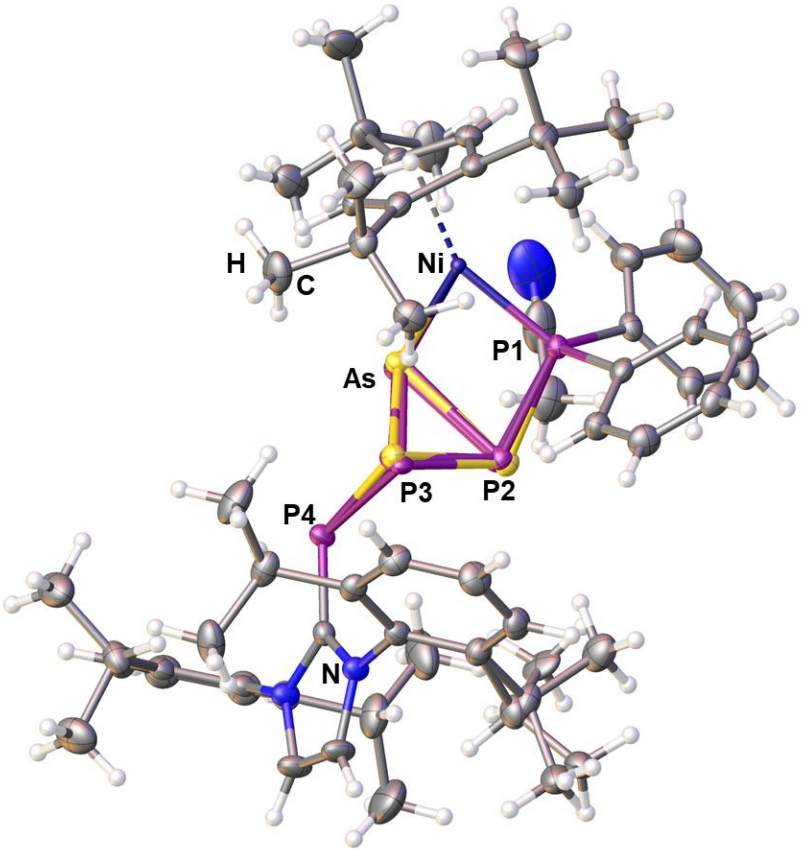

*Figure S 16: Solid state structure of **8**. Depicted is the asymmetric unit and ADPs (anisotropic displacement parameters) are drawn at 50 % probability.*

12.5.3. NMR Spectroscopic Investigations

*[Cp'''Ni(η^3-P_4Ph_2)][PF_6] (**A1**)*

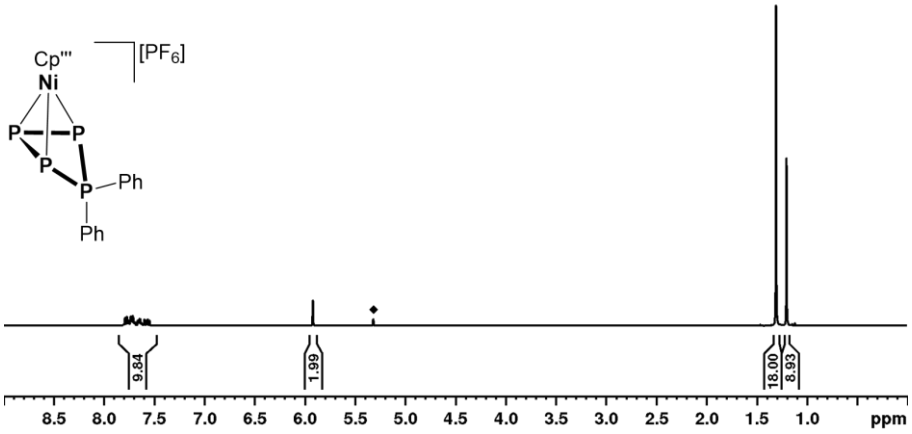

*Figure S 17: ^1H NMR spectrum of **A1** in CD_2Cl_2 recorded at room temperature; ◆ = residual solvent signal of CD_2Cl_2.*

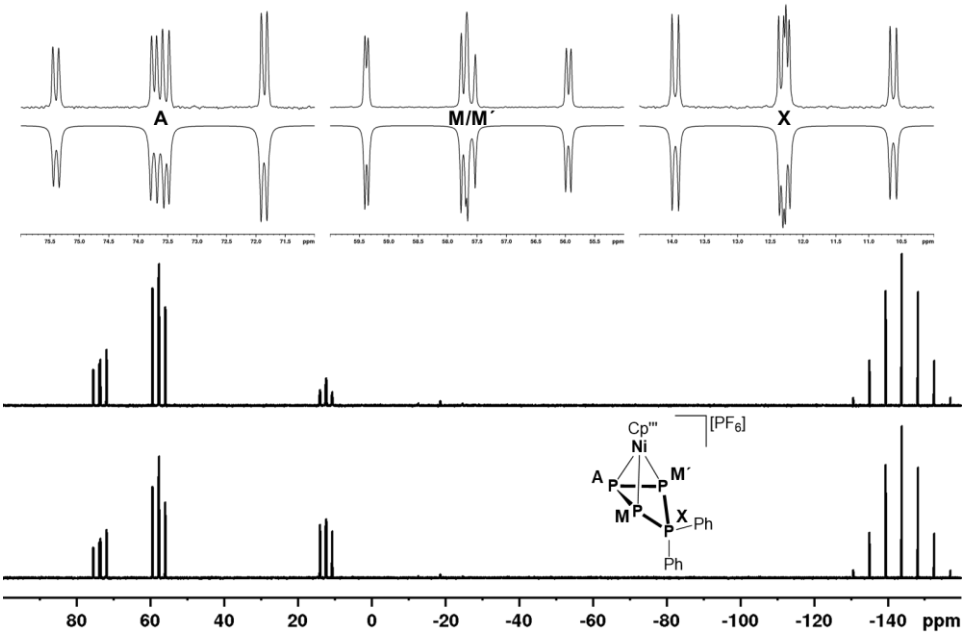

*Figure S 18: $^{31}P\{^1H\}$ (bottom) and ^{31}P (middle) NMR spectrum of **A1** in CD_2Cl_2 recorded at room temperature as well as enlarged signals within the measured (top) and simulated (inverted) $^{31}P\{^1H\}$ NMR spectrum.*

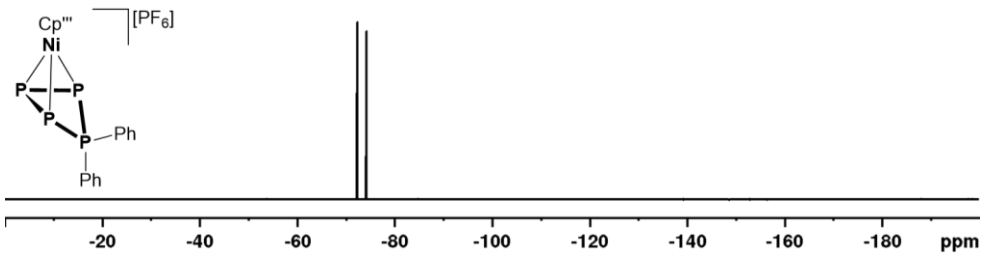

*Figure S 19: $^{19}F\{^1H\}$ NMR spectrum of **A1** in CD_2Cl_2 recorded at room temperature.*

*[Cp'''Ni(η^3-$P_4{}^iPr_2$)][PF_6] (**A2**)*

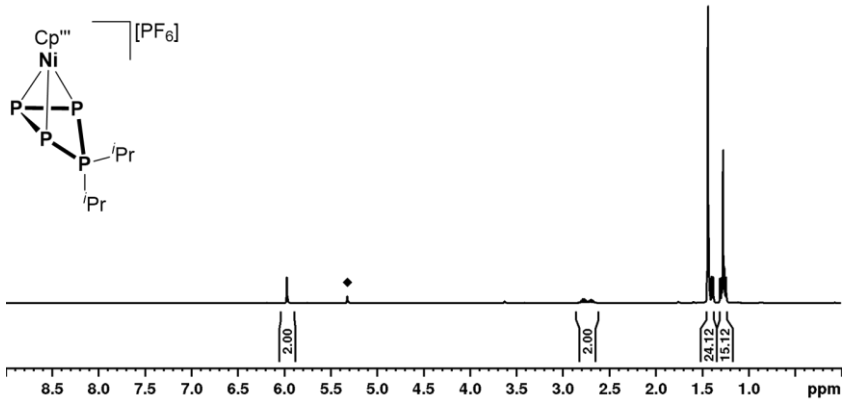

*Figure S 20: ^{1}H NMR spectrum of **A2** in CD_2Cl_2 recorded at room temperature; ◆ = residual solvent signal of CD_2Cl_2.*

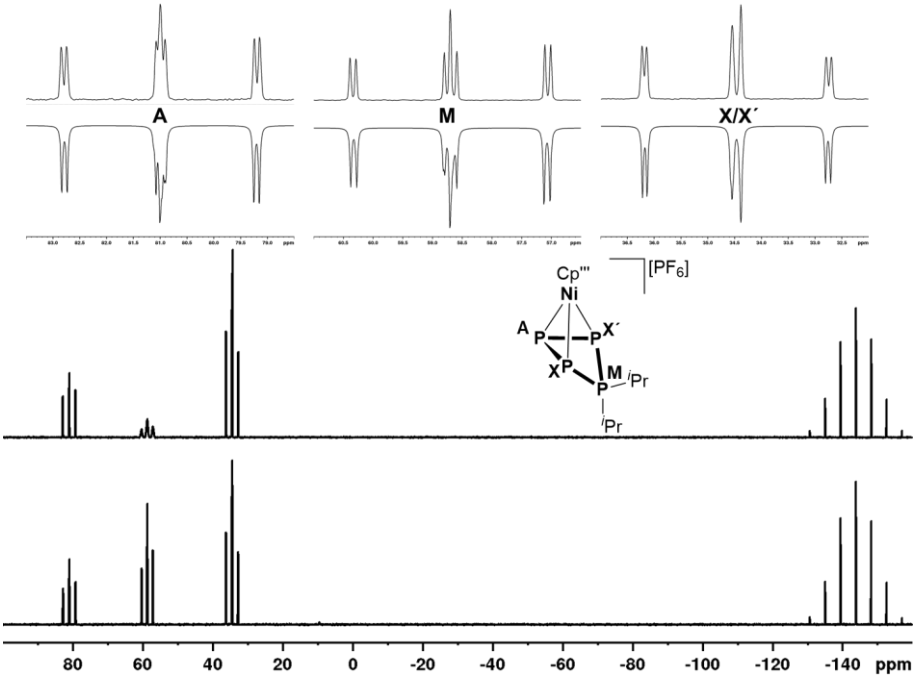

*Figure S 21: $^{31}P\{^1H\}$ (bottom) and ^{31}P (middle) NMR spectrum of **A2** in CD_2Cl_2 recorded at room temperature as well as enlarged signals within the measured (top) and simulated (inverted) $^{31}P\{^1H\}$ NMR spectrum.*

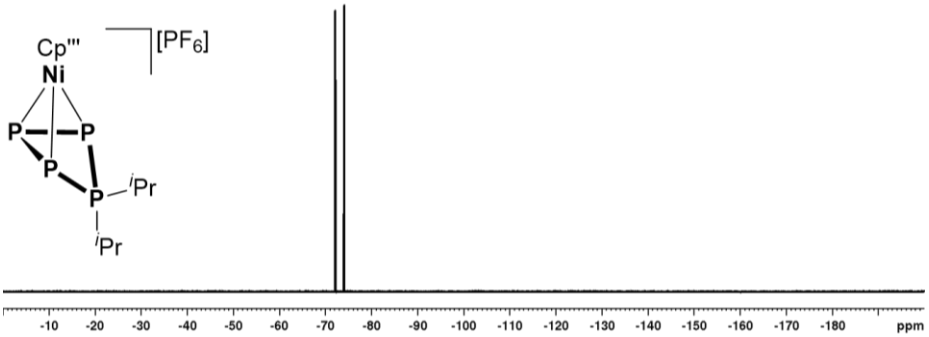

*Figure S 22: $^{19}F\{^1H\}$ NMR spectrum of **A2** in CD_2Cl_2 recorded at room temperature.*

*[CpMo(CO)$_2$(η^3-P$_4$Ph$_2$)][OTf] (**B1**)*

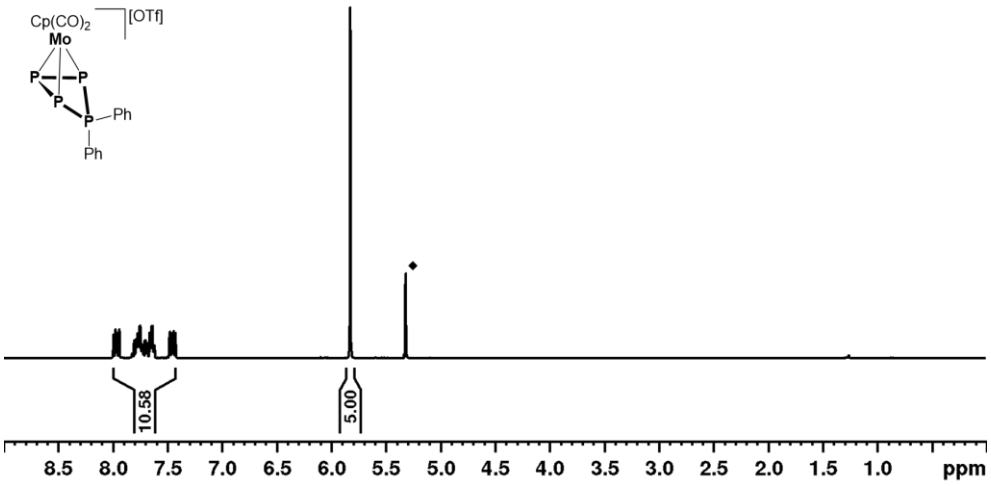

*Figure S 23: ^{1}H NMR spectrum of **B1** in CD_2Cl_2 recorded at room temperature; ◆ = residual solvent signal of CD_2Cl_2.*

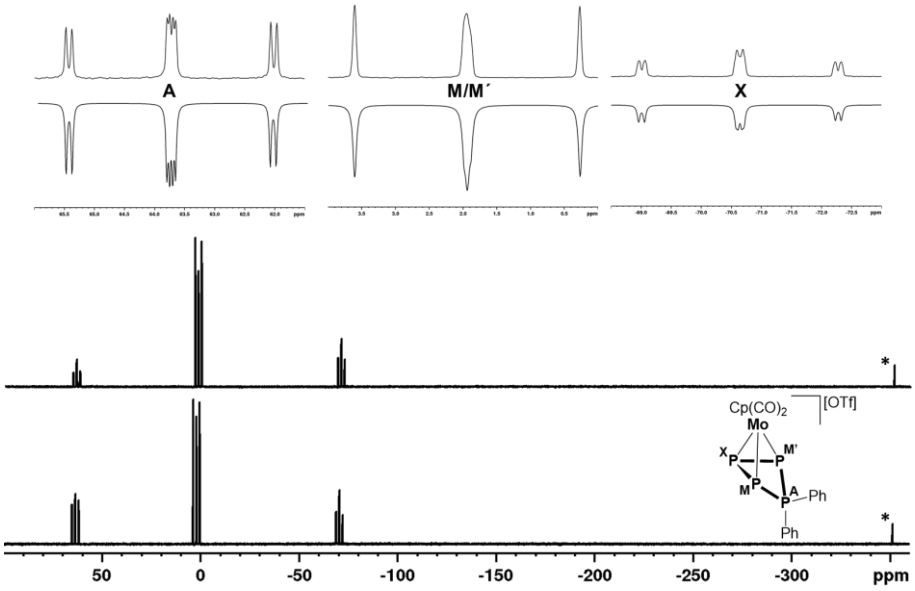

*Figure S 24: $^{31}P\{^1H\}$ (bottom) and ^{31}P (middle) NMR spectrum of **B1** in CD_2Cl_2 recorded at room temperature as well as enlarged signals within the measured (top) and simulated (inverted) $^{31}P\{^1H\}$ NMR spectrum. * = residual [CpMo(CO)$_2$(η^3-P$_3$)] (3 %).*

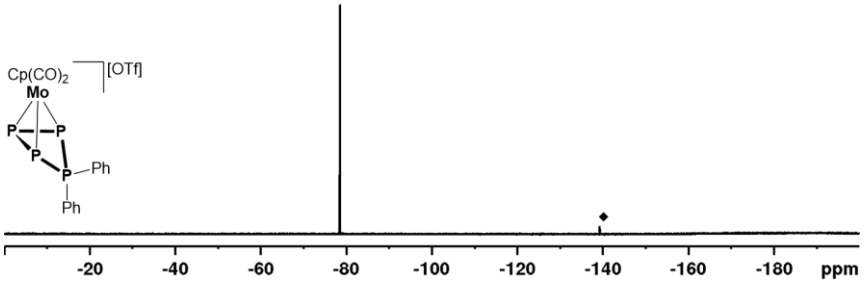

*Figure S 25: $^{19}F\{^1H\}$ NMR spectrum of **B1** in CD_2Cl_2 recorded at room temperature. ◆: residual o-DFB.*

*[CpMo(CO)$_2$(η^3-P$_4$^{i}Pr$_2$)][TEF] (**B2**)*

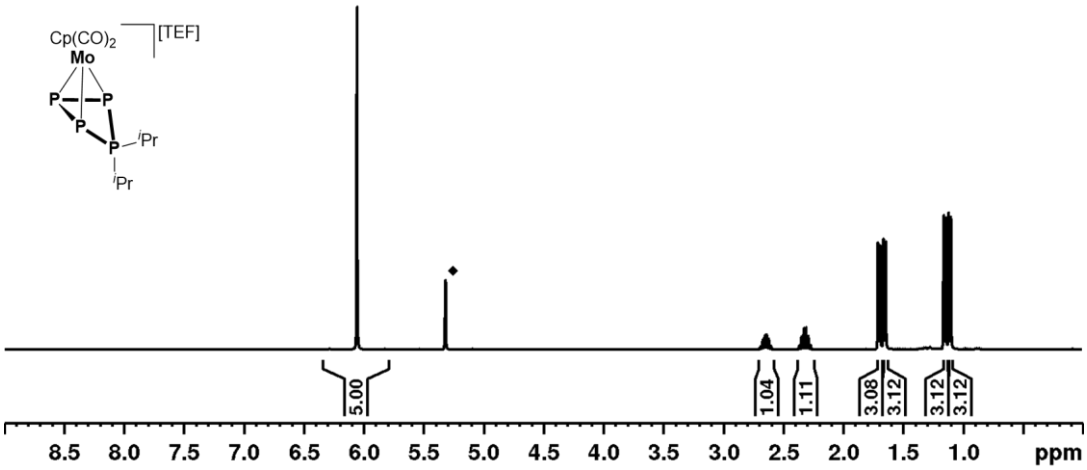

*Figure S 26: ^{1}H NMR spectrum of **B2** in CD_2Cl_2 recorded at room temperature; ◆ = residual solvent signal of CD_2Cl_2.*

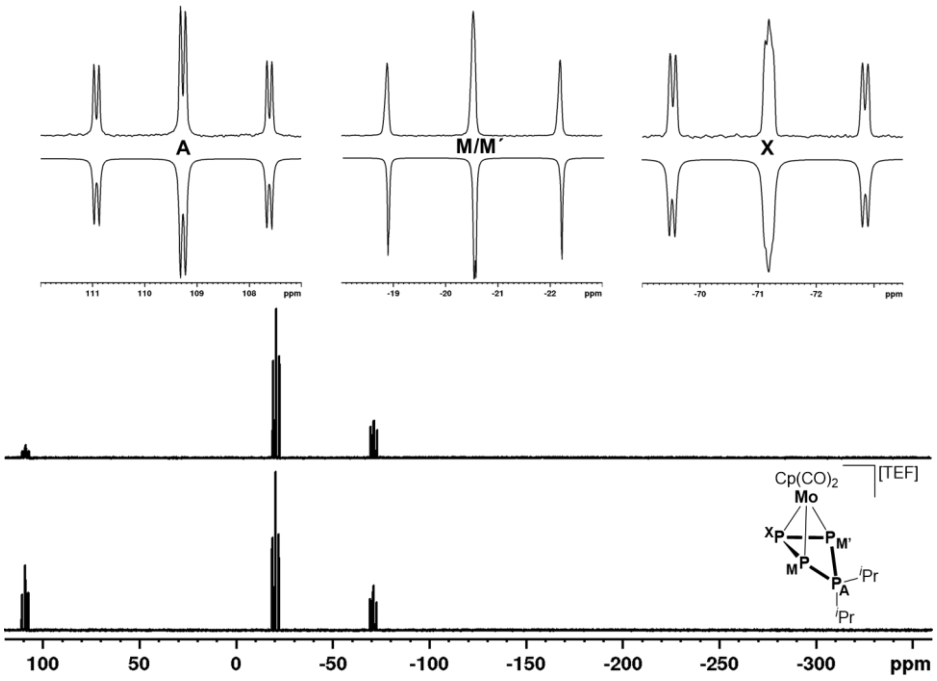

*Figure S 27: $^{31}P\{^1H\}$ (bottom) and ^{31}P (middle) NMR spectrum of **B2** in CD_2Cl_2 recorded at room temperature as well as enlarged signals within the measured (top) and simulated (inverted) $^{31}P\{^1H\}$ NMR spectrum.*

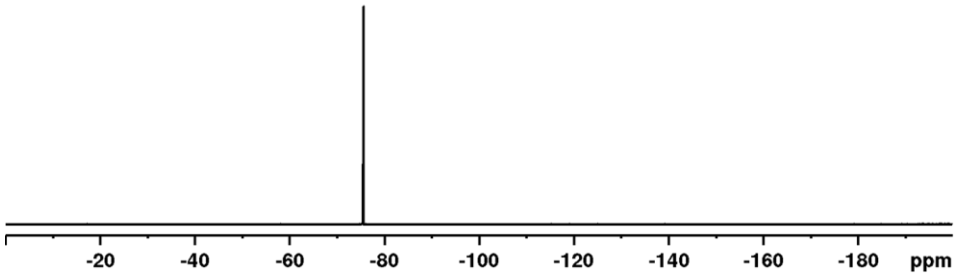

*Figure S 28: $^{19}F\{^1H\}$ NMR spectrum of **B2** in CD_2Cl_2 recorded at room temperature.*

*[Cp'''Ni($\eta^{1:1}$-P_4Ph_2IDipp)][PF_6] (**1a**)*

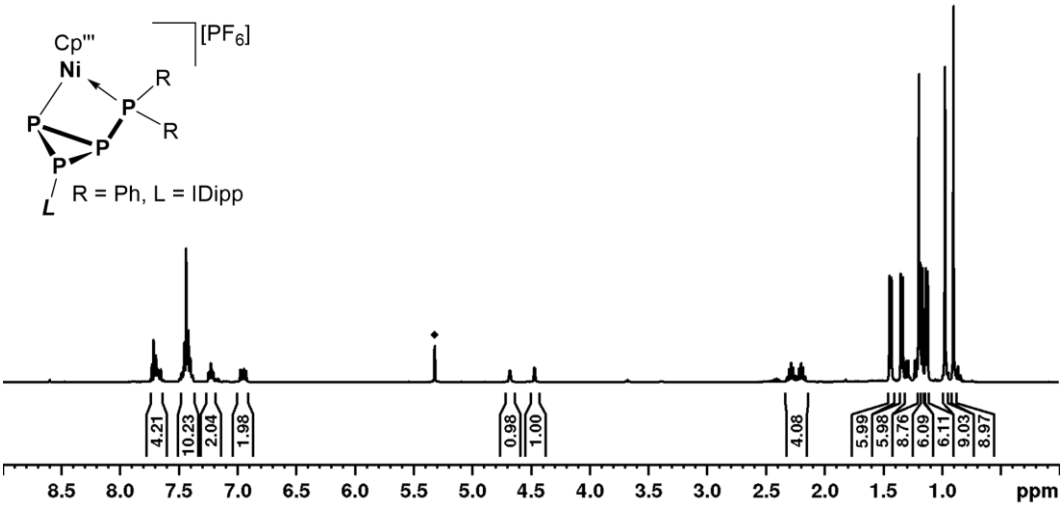

*Figure S 29: ^{1}H NMR spectrum of **1a** in CD_2Cl_2 recorded at room temperature; ◆ = residual solvent signal of CD_2Cl_2.*

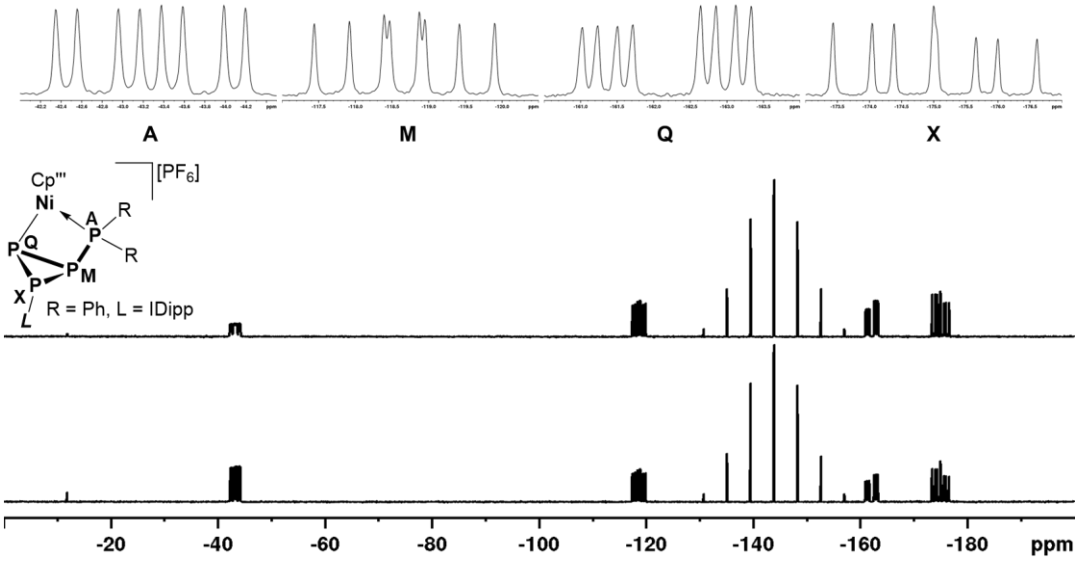

*Figure S 30: $^{31}P\{^{1}H\}$ (bottom) and ^{31}P NMR spectrum of **1a** in CD_2Cl_2 recorded at room temperature as well as enlarged signals within the measured $^{31}P\{^{1}H\}$ NMR spectrum.*

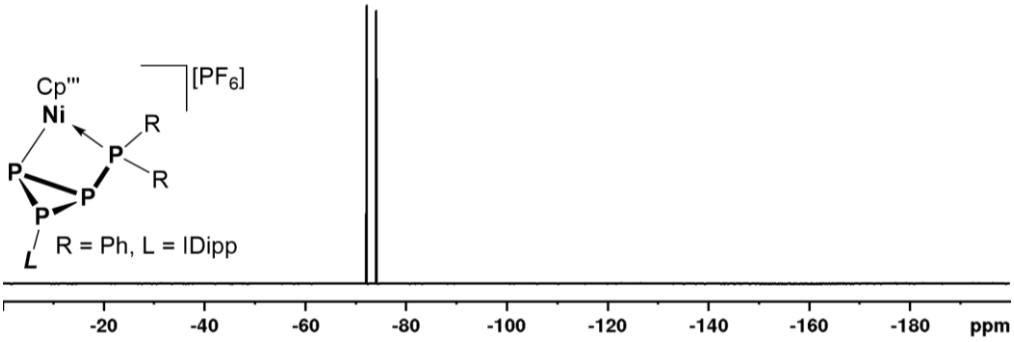

*Figure S 31: $^{19}F\{^{1}H\}$ NMR spectrum of **1a** in CD_2Cl_2 recorded at room temperature.*

*[Cp'''Ni($\eta^{1:1}$-$P_4Ph_2I^iPr_2Me_2$)][PF_6] (**1b**)*

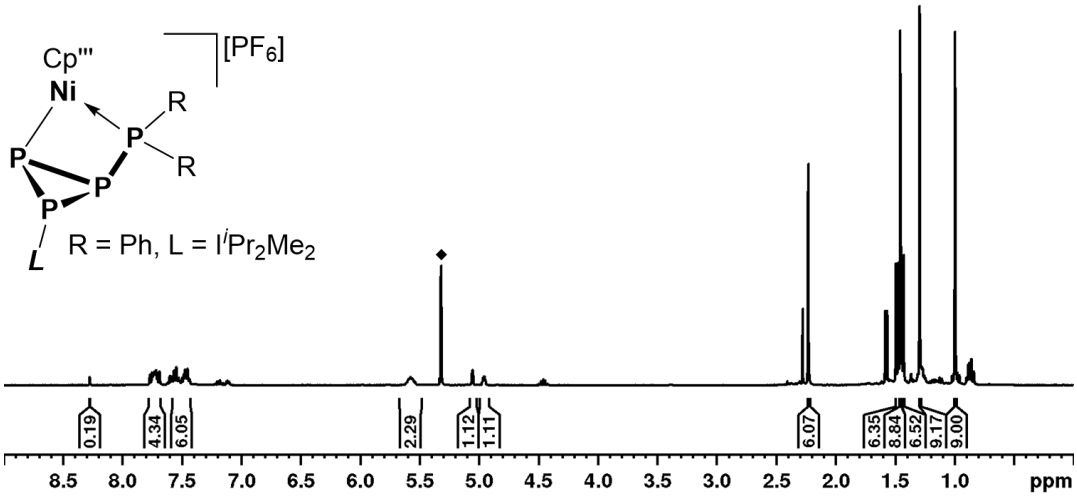

*Figure S 32: ^{1}H NMR spectrum of **1b** in CD_2Cl_2 recorded at room temperature; ◆ = residual solvent signal of CD_2Cl_2, several small unassigned signals mark trace impurities of $[I^iPr_2Me_2H]^+$.*

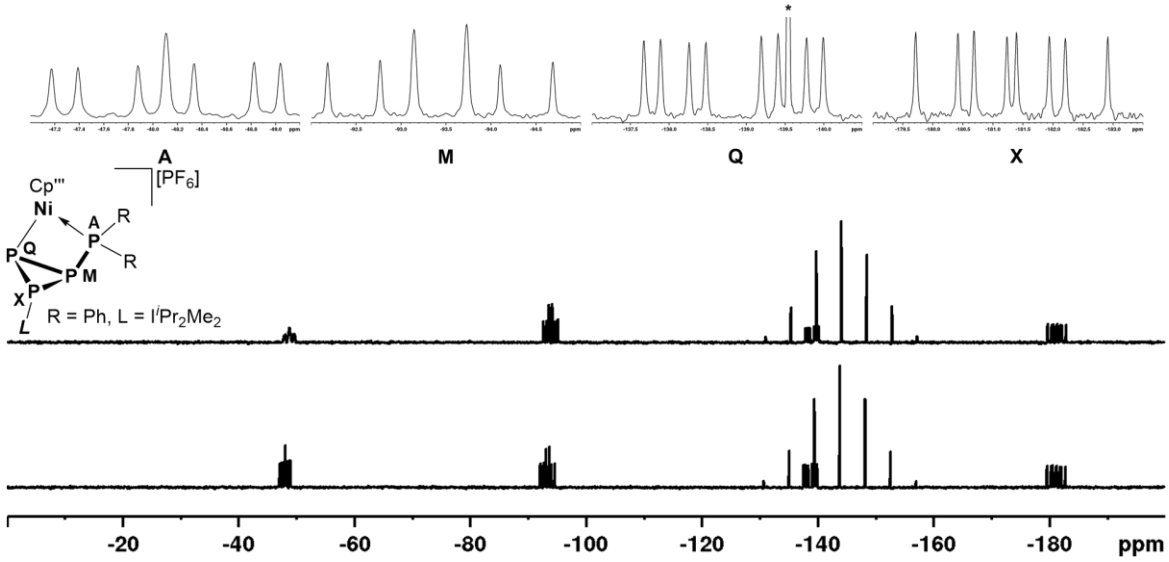

*Figure S 33: $^{31}P\{^1H\}$ (bottom) and ^{31}P NMR spectrum of **1b** in CD_2Cl_2 recorded at room temperature as well as enlarged signals within the measured $^{31}P\{^1H\}$ NMR spectrum; * marks one of the lines of the $[PF_6]^-$ signal.*

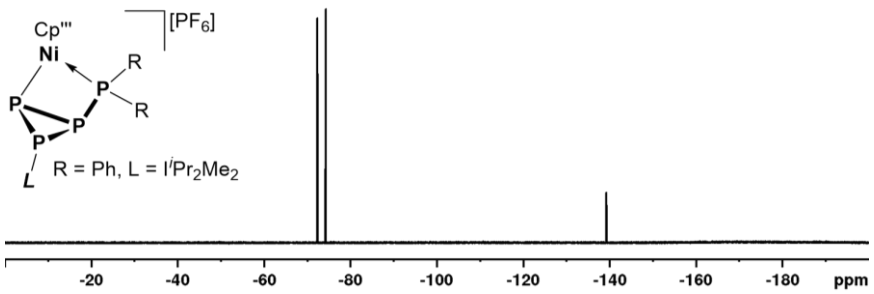

*Figure S 34: $^{19}F\{^1H\}$ NMR spectrum of **1b** in CD_2Cl_2 recorded at room temperature.*

*[Cp'''Ni($\eta^{1:1}$-$P_4{}^iPr_2IDipp$)][PF_6] (**1c**)*

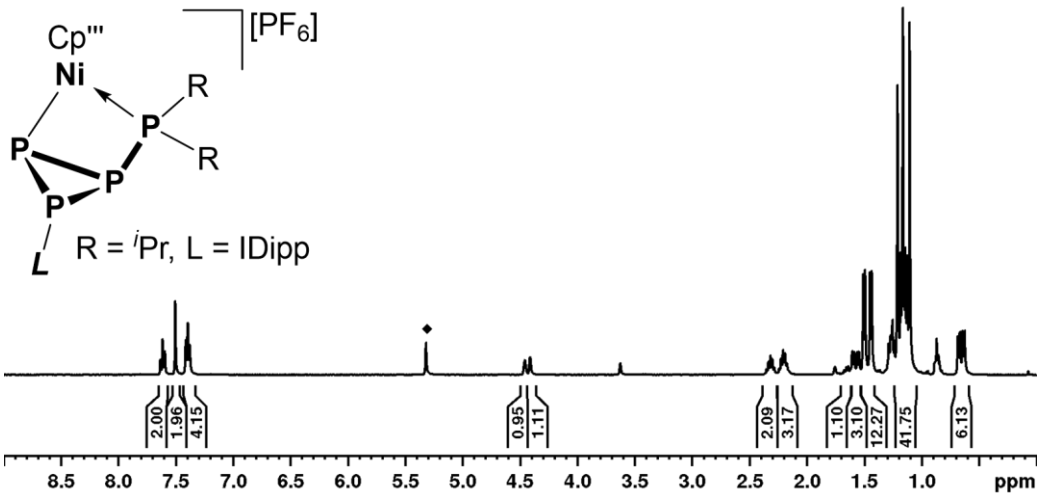

*Figure S 35: ^1H NMR spectrum of **1c** in CD_2Cl_2 recorded at room temperature; ◆ = residual solvent signal of CD_2Cl_2.*

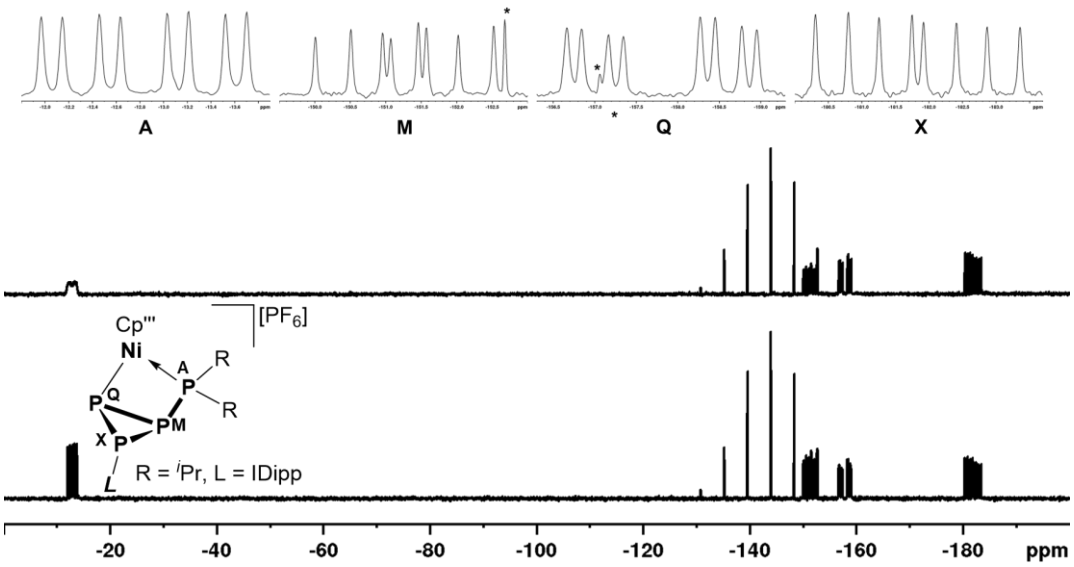

*Figure S 36: $^{31}P\{^1H\}$ (bottom) and ^{31}P NMR spectrum of **1c** in CD_2Cl_2 recorded at room temperature as well as enlarged signals within the measured $^{31}P\{^1H\}$ NMR spectrum; * marks lines of the $[PF_6]^-$ signal.*

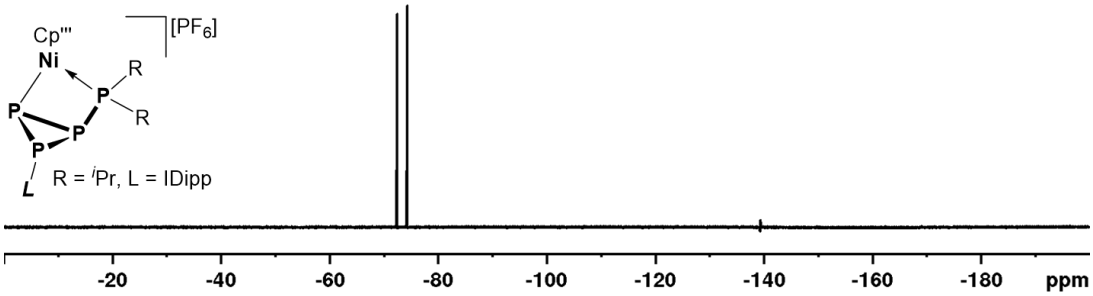

*Figure S 37: $^{19}F\{^1H\}$ NMR spectrum of **1c** in CD_2Cl_2 recorded at room temperature.*

*[Cp'''Ni($\eta^{1:1}$-$P_4{}^iPr_2{}^iPr_2Me_2$)][PF_6] (**1d**)*

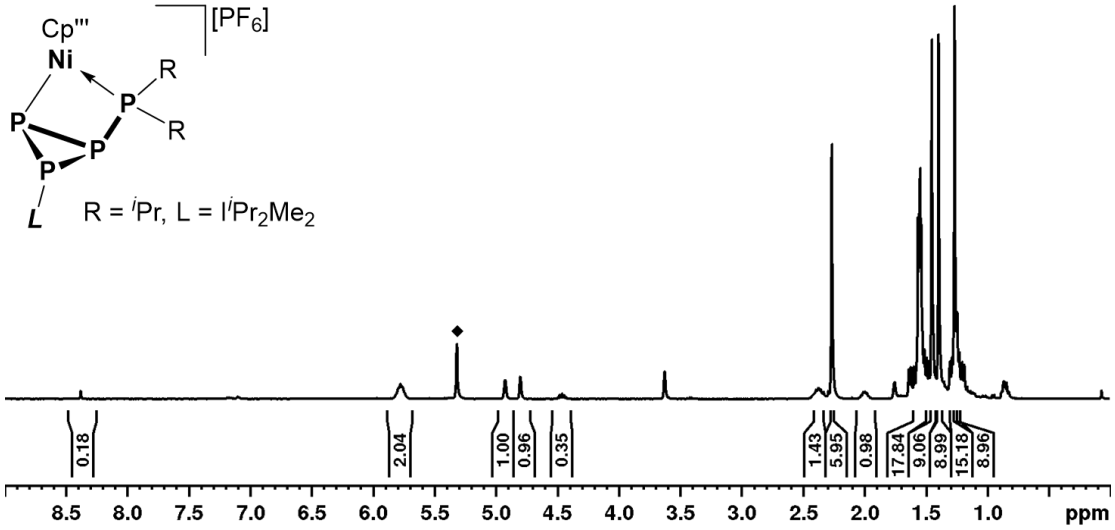

*Figure S 38: ^1H NMR spectrum of **1d** in CD_2Cl_2 recorded at room temperature; ◆ = residual solvent signal of CD_2Cl_2, several small unassigned signals mark trace impurities of $I^iPr_2Me_2H^+$.*

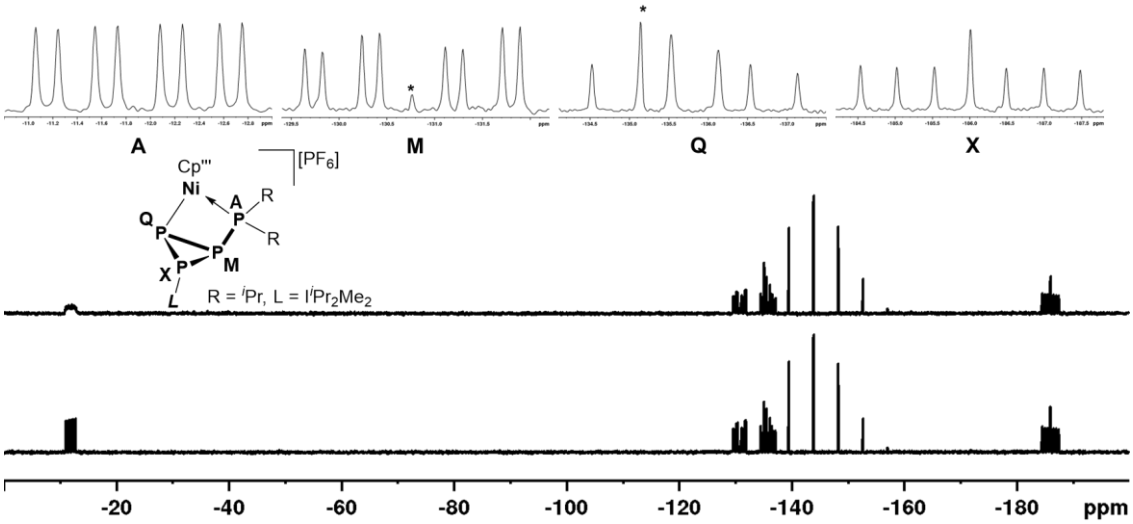

*Figure S 39: $^{31}P\{^1H\}$ (bottom) and ^{31}P NMR spectrum of **1d** in CD_2Cl_2 recorded at room temperature as well as enlarged signals within the measured $^{31}P\{^1H\}$ NMR spectrum; * marks lines of the $[PF_6]^-$ signal.*

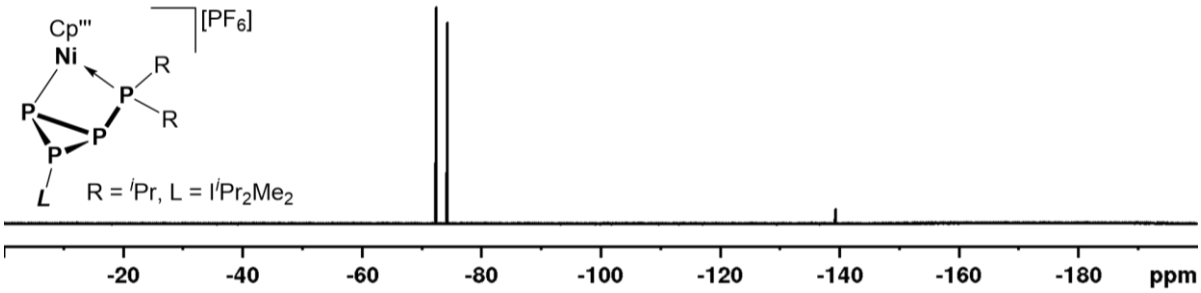

*Figure S 40: $^{19}F\{^1H\}$ NMR spectrum of **1d** in CD_2Cl_2 recorded at room temperature.*

*[CpMo(CO)$_2$(η^3-P$_4$Ph$_2$IDipp)][OTf] (**2a**)*

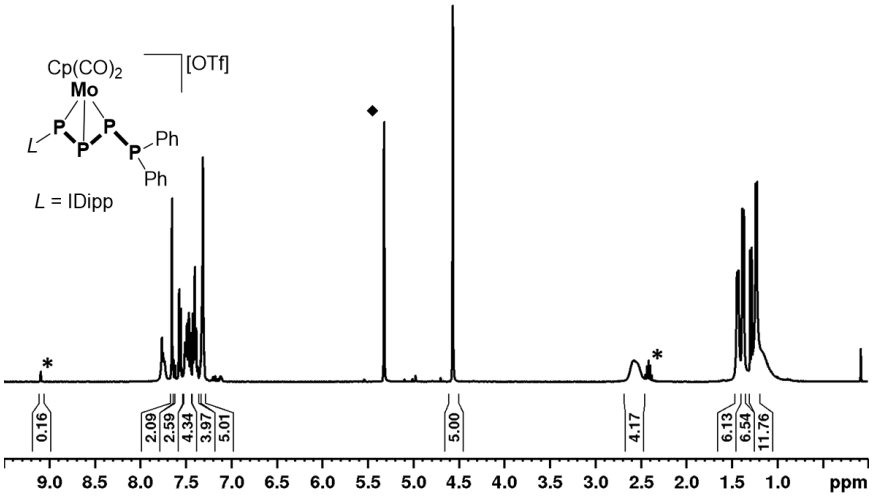

*Figure S 41: ^{1}H NMR spectrum of **2a** in CD_2Cl_2 recorded at room temperature; ◆ = residual solvent signal of CD_2Cl_2. * = trace impurities of $[IDippH]^+$.*

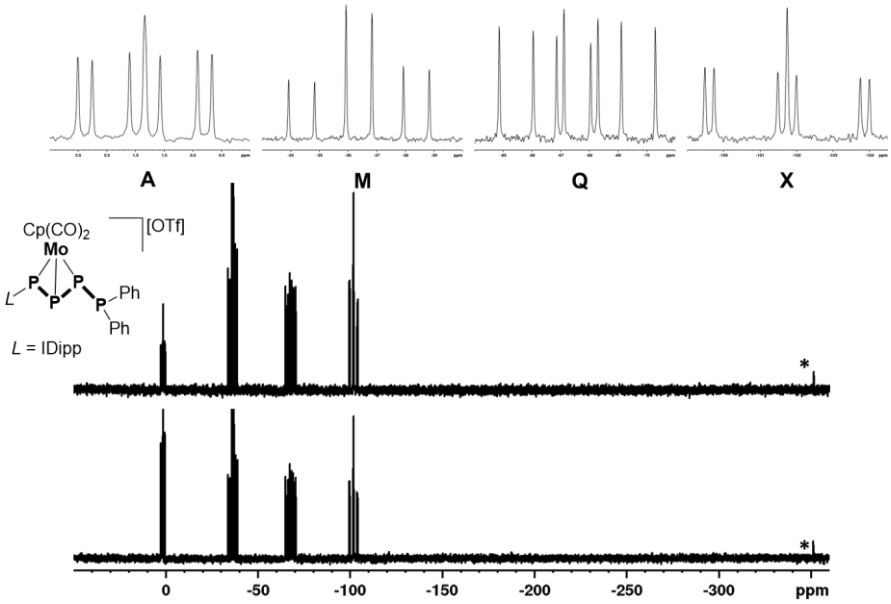

*Figure S 42: $^{31}P\{^1H\}$ (bottom) and ^{31}P NMR spectrum of **2a** in CD_2Cl_2 recorded at room temperature as well as enlarged signals within the measured $^{31}P\{^1H\}$ NMR spectrum. * = residual [CpMo(CO)$_2$(η^3-P$_3$)] (<1 %).*

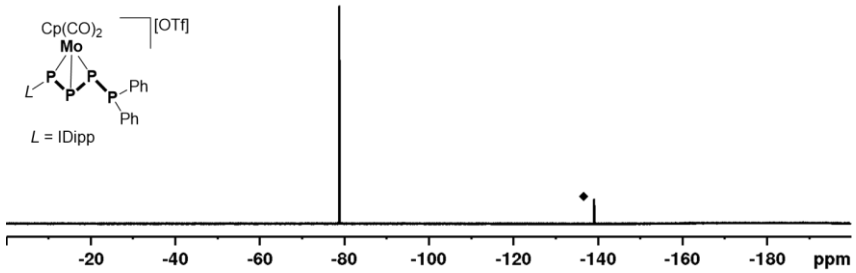

*Figure S 43: $^{19}F\{^1H\}$ NMR spectrum of **2a** in CD_2Cl_2 recorded at room temperature. ◆ = residual o-DFB.*

*[CpMo(CO)$_2$(η^3-P$_4$Ph$_2$l^{i}Pr$_2$Me$_2$)][OTf] (**2b**)*

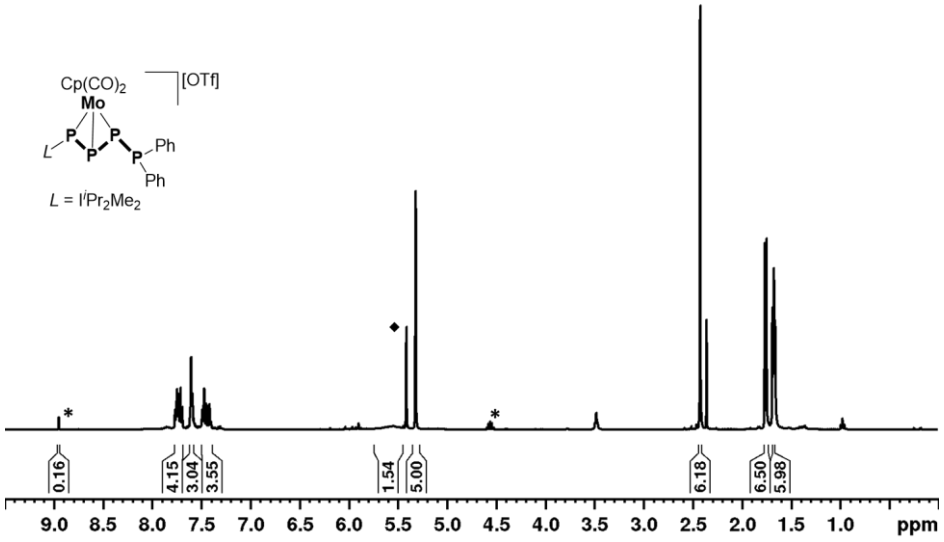

*Figure S 44: ^{1}H NMR spectrum of **2b** in CD_2Cl_2 recorded at room temperature; ◆ = residual solvent signal of CD_2Cl_2. * = trace impurities of [l^{i}Pr$_2$Me$_2$H]$^+$.*

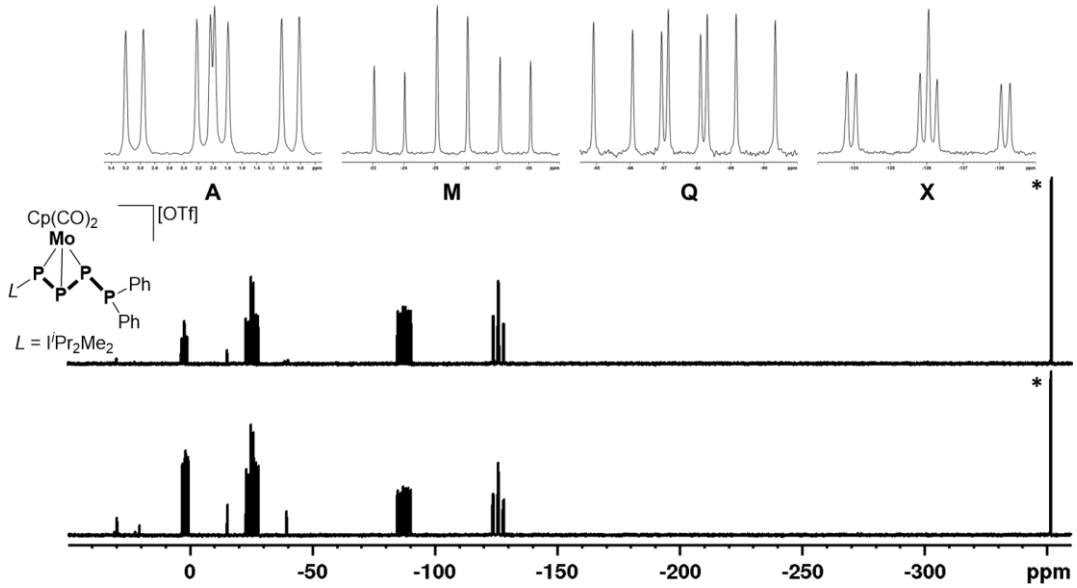

*Figure S 45: $^{31}P\{^1H\}$ (bottom) and ^{31}P NMR spectrum of **2b** in CD_2Cl_2 recorded at room temperature as well as enlarged signals within the measured $^{31}P\{^1H\}$ NMR spectrum. * = residual [CpMo(CO)$_2$(η^3-P$_3$)] (<1 %).*

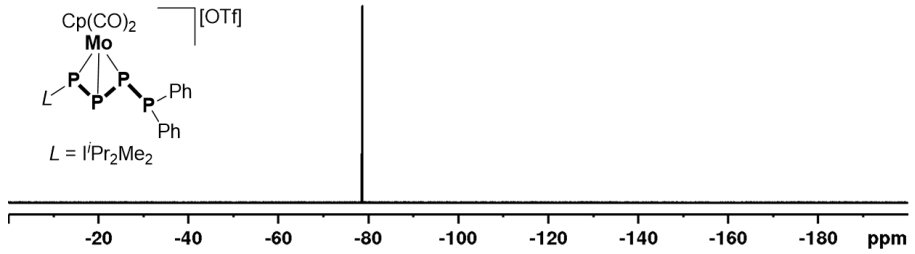

*Figure S 46: $^{19}F\{^1H\}$ NMR spectrum of **2b** in CD_2Cl_2 recorded at room temperature.*

*[CpMo(CO)$_2$(η^3-P$_4$^{i}Pr$_2$IDipp)][TEF] (**2c**)*

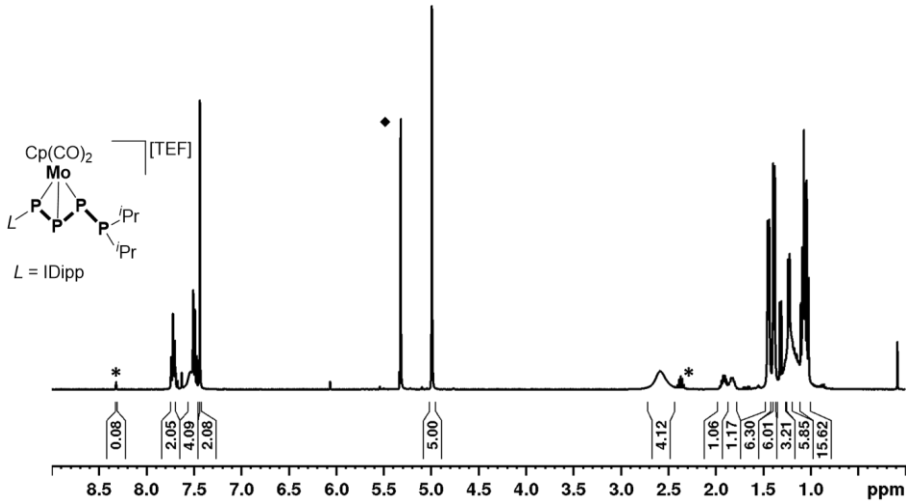

*Figure S 47: ^{1}H NMR spectrum of **2c** in CD_2Cl_2 recorded at room temperature; ◆ = residual solvent signal of CD_2Cl_2. * = trace impurities of $[IDippH]^+$.*

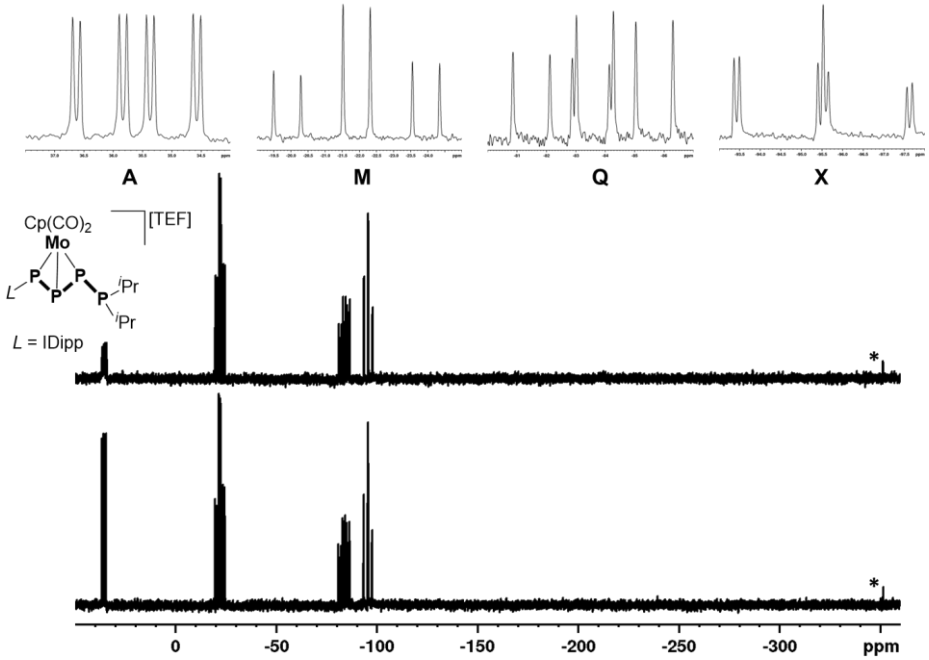

*Figure S 48: $^{31}P\{^1H\}$ (bottom) and ^{31}P NMR spectrum of **2c** in CD_2Cl_2 recorded at room temperature as well as enlarged signals within the measured $^{31}P\{^1H\}$ NMR spectrum. * = residual [CpMo(CO)$_2$(η^3-P$_3$)] (<1 %).*

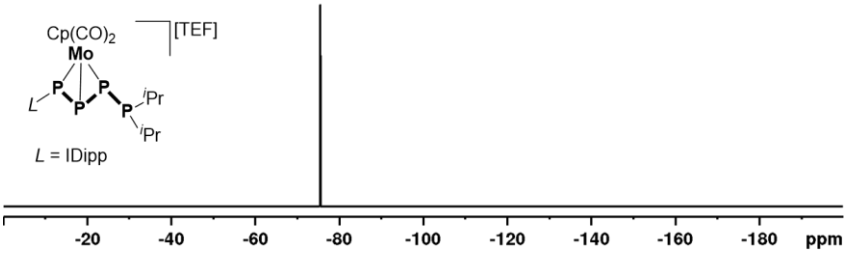

*Figure S 49: $^{19}F\{^1H\}$ NMR spectrum of **2c** in CD_2Cl_2 recorded at room temperature.*

*[CpMo(CO)$_2$(η^3-P$_4$^{i}Pr$_2$l^{i}Pr$_2$Me$_2$)][TEF] (**2d**)*

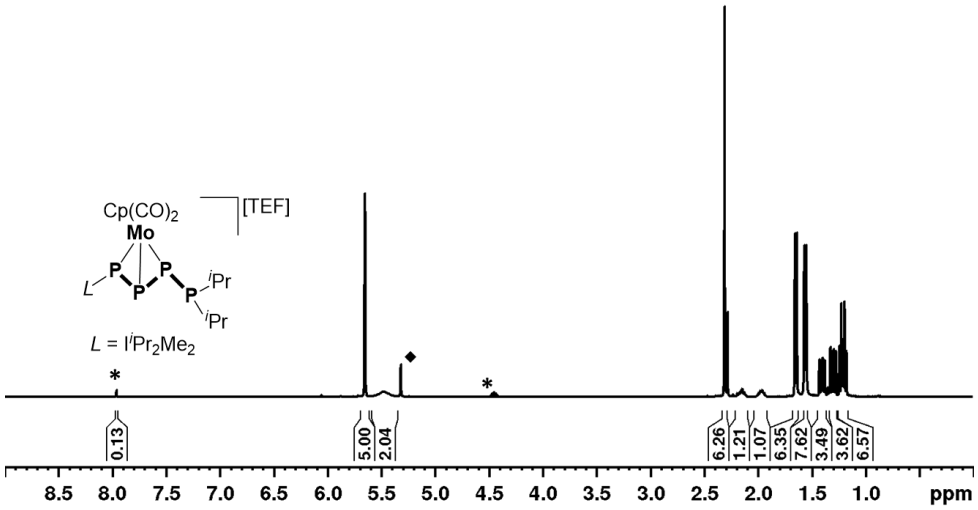

*Figure S 50: ^{1}H NMR spectrum of **2d** in CD_2Cl_2 recorded at room temperature; ◆ = residual solvent signal of CD_2Cl_2. * = trace impurities of $[^iPr_2Me_2H]^+$.*

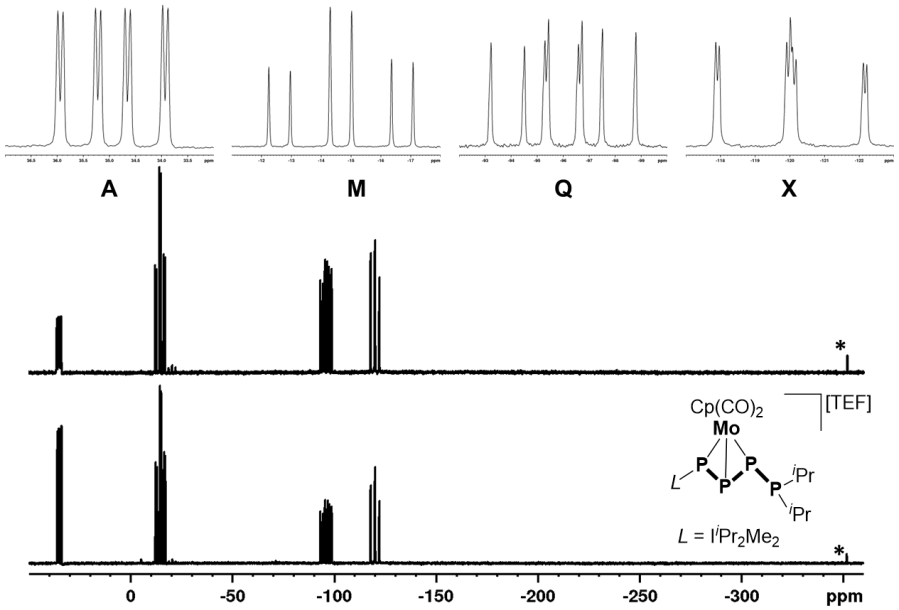

*Figure S 51: $^{31}P\{^1H\}$ (bottom) and ^{31}P NMR spectrum of **2d** in CD_2Cl_2 recorded at room temperature as well as enlarged signals within the measured $^{31}P\{^1H\}$ NMR spectrum. * = residual [CpMo(CO)$_2$(η^3-P$_3$)] (<1 %).*

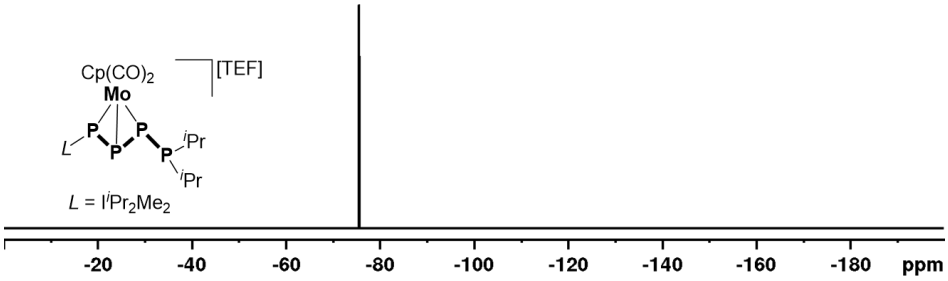

*Figure S 52: $^{19}F\{^1H\}$ NMR spectrum of **2d** in CD_2Cl_2 recorded at room temperature.*

*[{Cp'''Ni}$_2$(μ,$\eta^{1:1:1:1}$-cyclo-P$_4$(PPh$_2$)$_2$)] (**3a**)*

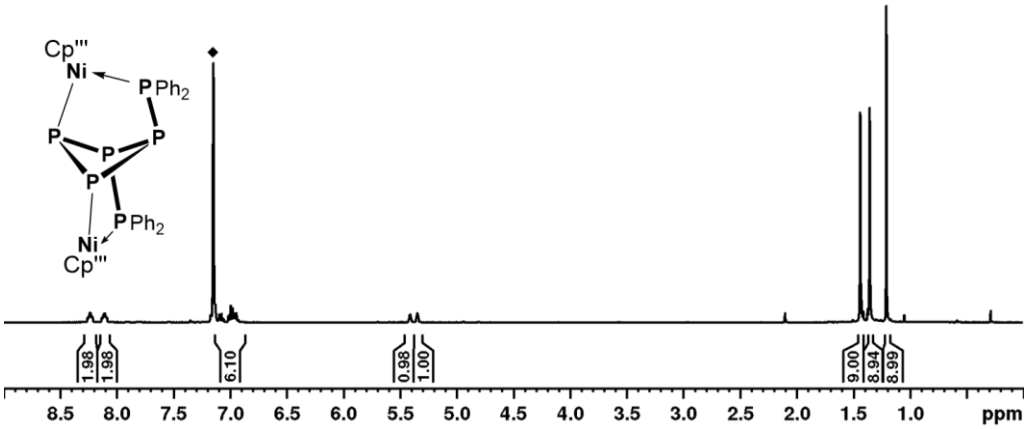

*Figure S 53: ^{1}H NMR spectrum of **3a** in C$_6$D$_6$ recorded at room temperature; ◆ = residual solvent signal of C$_6$D$_6$.*

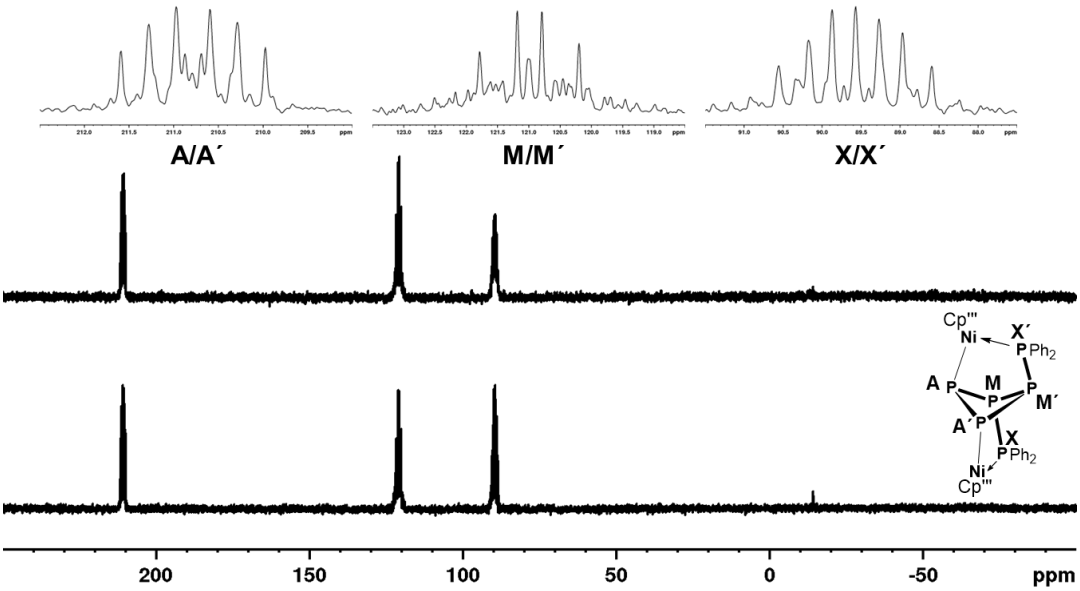

*Figure S 54: ^{31}P{^{1}H} (bottom) and ^{31}P (middle) NMR spectra of **3a** in C$_6$D$_6$ recorded at room temperature as well as enlarged signals within the measured (top) and simulated (inverted) ^{31}P{^{1}H} NMR spectrum.*

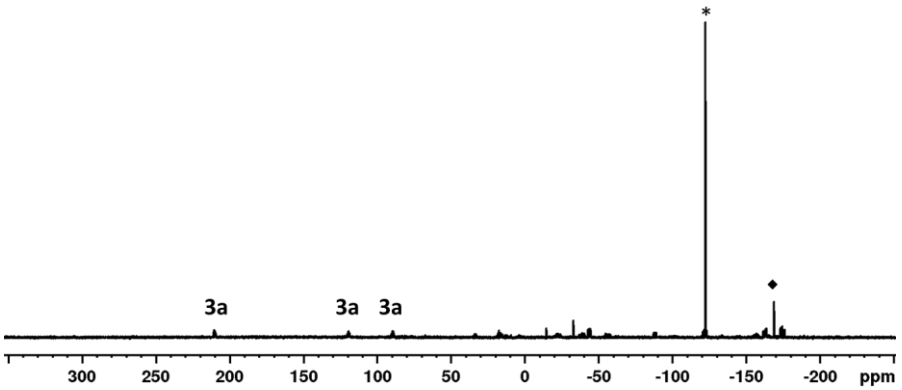

*Figure S 55: ^{31}P{^{1}H} NMR spectrum of the crude reaction mixture of 3a; The signal marked with * corresponds to proposed IDippPCN and ◆ marks the signal of [Cp'''Ni(η^3-P$_3$)].*

[{Cp'''Ni}$_2$($\mu,\eta^{1:1:1:1}$-cyclo-P$_4$(P^{i}Pr$_2$)$_2$)] (***3b***)

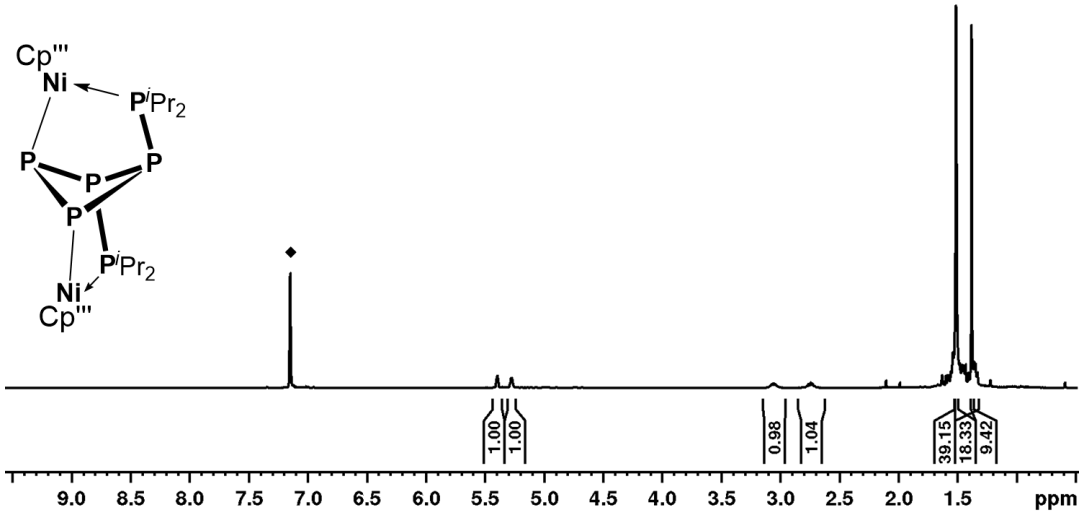

*Figure S 56: ^{1}H NMR spectrum of **3b** in C_6D_6 recorded at room temperature; ◆ = residual solvent signal of C_6D_6.*

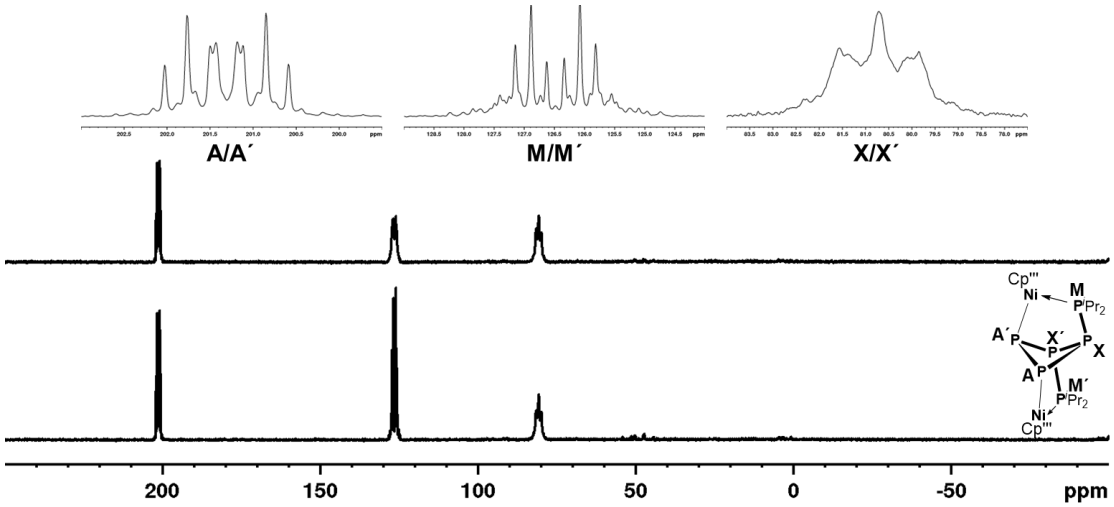

*Figure S 57: ^{31}P{^{1}H} (bottom) and ^{31}P (middle) NMR spectra of **3b** in C_6D_6 recorded at room temperature as well as enlarged signals within the measured (top) and simulated (inverted) ^{31}P{^{1}H} NMR spectrum.*

[{Cp'''Ni}$_2$(μ,$\eta^{2:2}$-(PP^{i}Pr$_2$)$_2$)] (***4***)

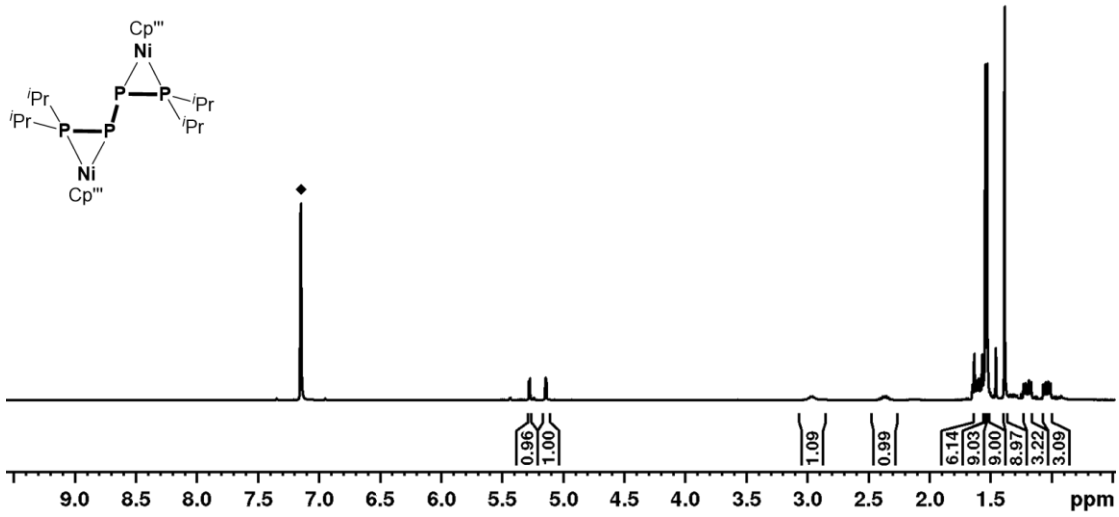

*Figure S 58: ^{1}H NMR spectrum of **4** in C_6D_6 recorded at room temperature; ◆ = residual solvent signal of C_6D_6.*

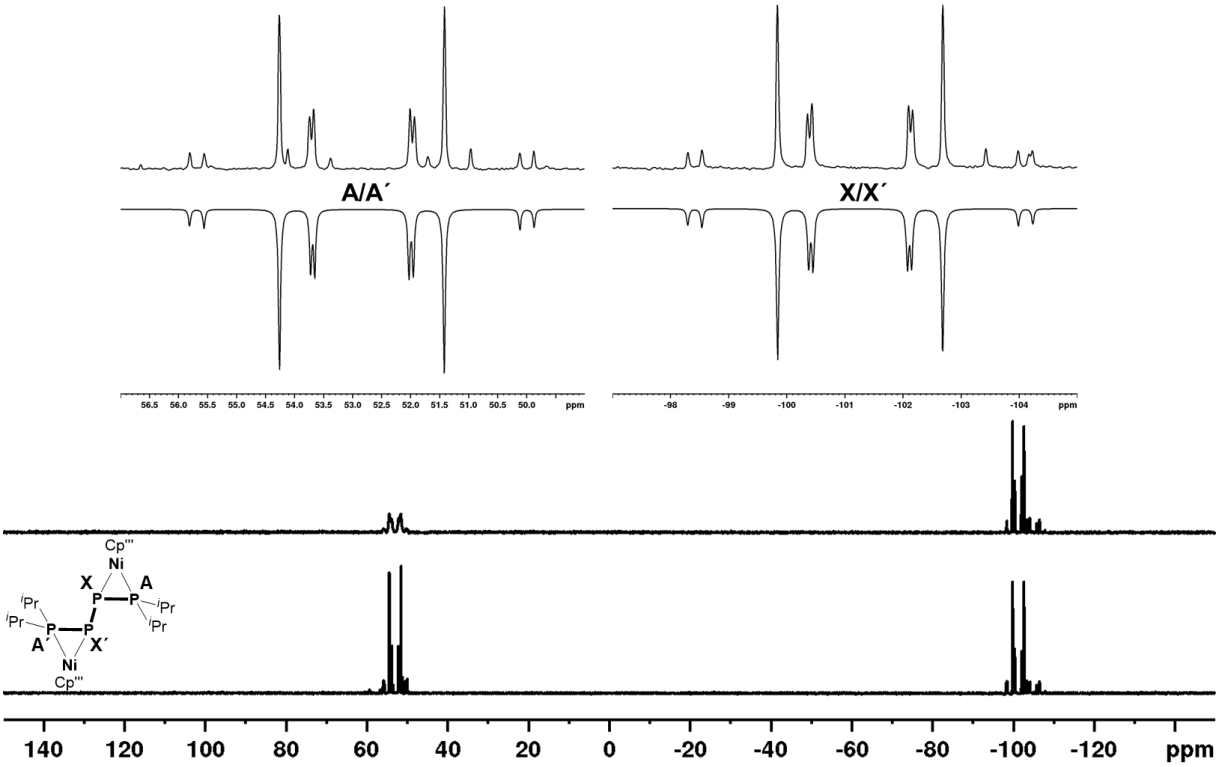

*Figure S 59: $^{31}P\{^1H\}$ (bottom) and ^{31}P (middle) NMR spectra of **4** in C_6D_6 recorded at room temperature as well as enlarged signals within the measured (top) and simulated (inverted) $^{31}P\{^1H\}$ NMR spectrum.*

*[Cp'''Ni(η²-IDippPP(OEt)PP^{i}Pr$_2$)] (**5a**)*

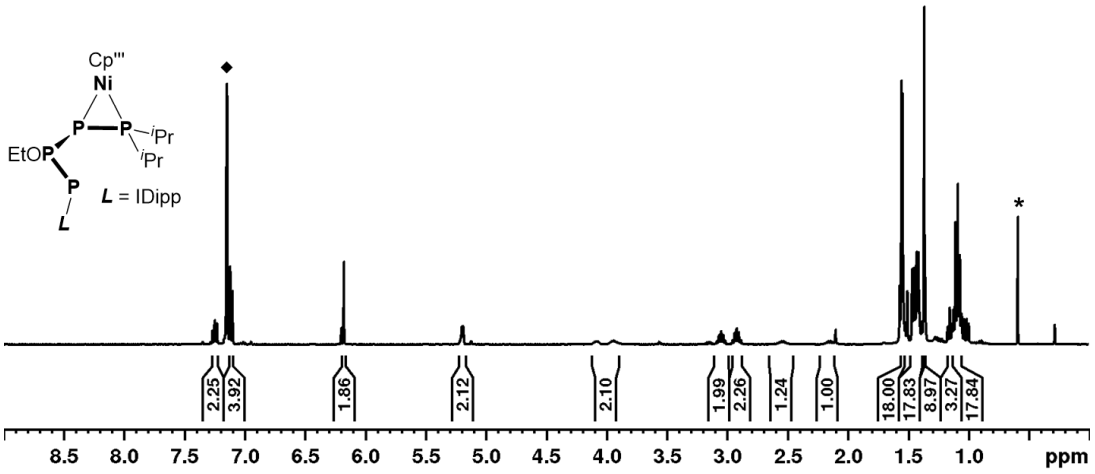

*Figure S 60: ^{1}H NMR spectrum of **5a** in C_6D_6 recorded at room temperature; ◆ = residual solvent signal of C_6D_6, * = residual MeCN from the dissolved crystals.*

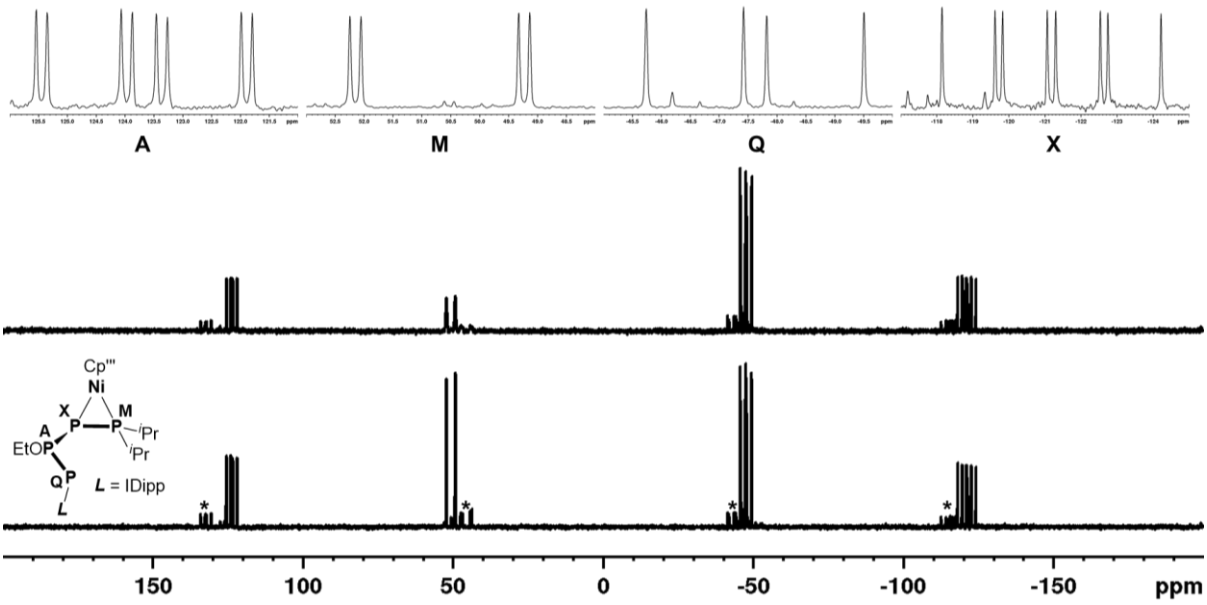

*Figure S 61: $^{31}P\{^1H\}$ (bottom) and ^{31}P (middle) NMR spectra of **5a** in C_6D_6 recorded at room temperature as well as enlarged signals within the measured (top) $^{31}P\{^1H\}$ NMR spectrum; * = rotational isomer of **5a**.*

As to get further insight into the intriguing color change during the synthesis of **5a**, variable temperature ^{31}P NMR spectroscopy was employed. Dissolving **1c** (52 mg, 0.05 mmol) and KOEt (5 mg, 0.05 mmol) in 0.6 mL of THF-d^8 affords a dark turquoise solution of **5a$_{INT}$** which was then subjected to NMR spectroscopy (Figure S62). As complete dissolution of KOEt was not possible under the given conditions (the NMR tube was shaken several times outside the cold bath to guarantee it not warming up beyond -80 °C), some staring material **1c** is still present within the mixture. The formation of **5a$_{INT}$** appears to be immediate as indicated by its

sole presence in the ^{31}P NMR spectra at -80 °C. Furthermore **5a$_{INT}$** appears to be temperature stable up to -20 °C at which it slowly starts to rearrange to **5a**. This rearrangement process drastically speeds up upon further warming the sample to 0 °C and then room temperature, at which there is only product **5a** left in solution.

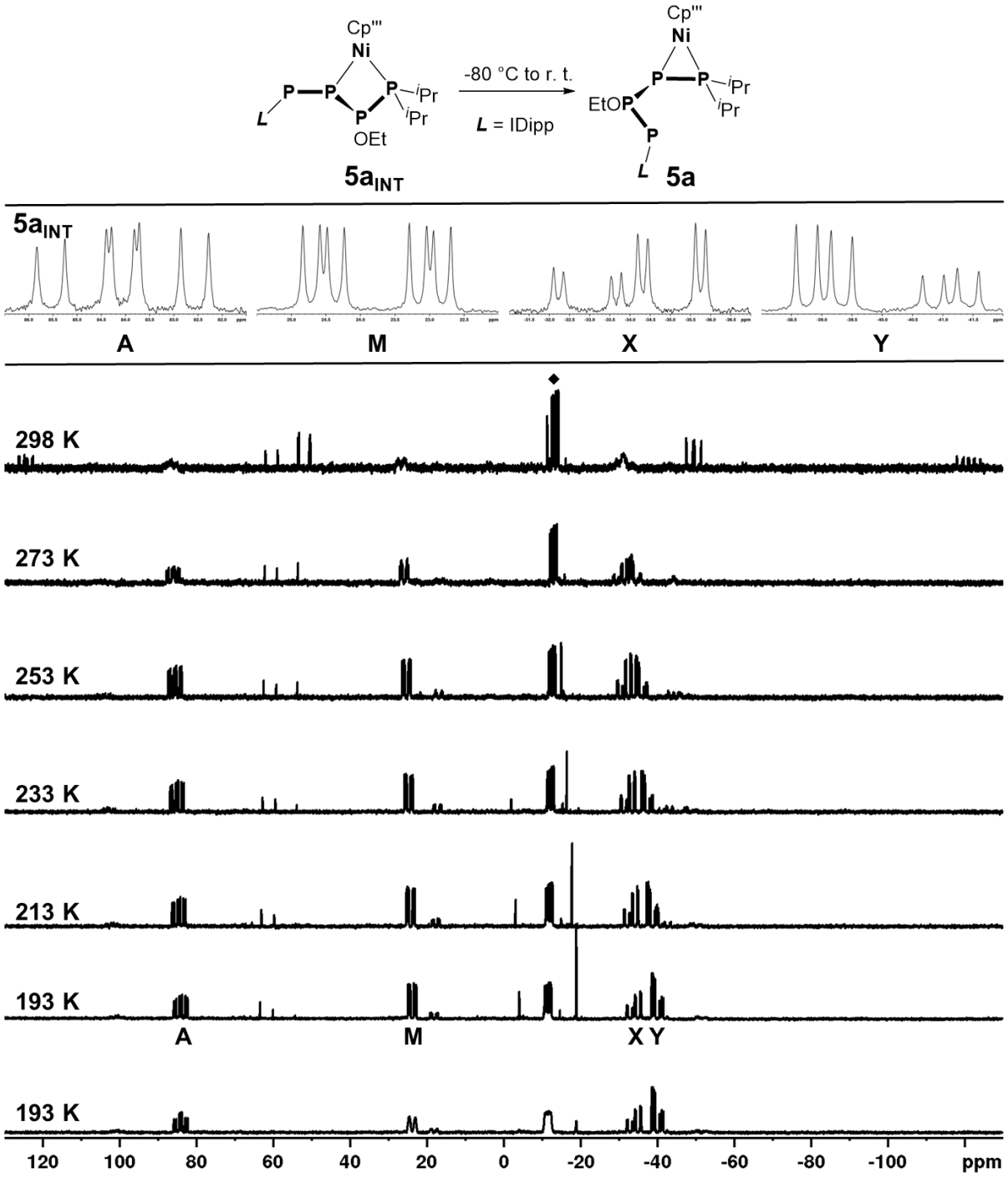

*Figure S 62: ^{31}P (bottom) and $^{31}P\{^{1}H\}$ NMR spectra of the reaction of **1c** (52 mg, 0.05 mmol) with KOEt (5 mg, 0.05 mmol) intermediately forming **5a$_{INT}$**, which rapidly rearranges at around -10 °C to afford **5a**; Enlarged signals of **5a$_{INT}$** at -80 °C (top); ◆ marks residual starting material **1c**.*

*Reactivity studies of **1a** towards KOEt*

Similar to the synthesis of **5a** the addition of one equivalent of KOEt to a THF solution of 1a at -80 °C results in a color change to dark green. Variable temperature ^{31}P NMR spectroscopy was employed to elucidate the nature of this color change. Dissolving **1a** (59 mg, 0.05 mmol) and KOEt (5 mg, 0.05 mmol) in 0.6 mL of THF-d_8 affords a dark intense green solution of **5b$_{INT}$** which was then subjected to NMR spectroscopy (Figure S63). Interestingly, the ^{31}P NMR spectrum of this solution reveals two sets of signals, whose spin systems are however extremely similar. Thus, and in comparison to the ^{31}P NMR spectrum of **5a$_{INT}$** both spin systems are attributed to isostructural (to **5a$_{INT}$**) species **5b$_{INT}$**. However, **5b$_{INT}$** appears to form two distinct isomers, **5b$_{INT1}$** and **5b$_{INT2}$**, which are most probably related by either rotation around a P–P bond or are diastereomers arising from the stereochemistry at the P_4 chain. Nevertheless, both isomers are only stable up to a temperature of ca. -40 °C. Warming the solution beyond this temperature leads to rapid rearrangement resulting in the formation of **5b** at -20 °C, which is completed already at 0 °C. While this reaction appears to be reasonably selective, isolation and thus characterization of **5b** could not be achieved within the time frame of this thesis. However, small signals, which may be attributed to a compound isostructural to **5a**, namely **5b$_{INT3}$**, can be found in the ^{31}P NMR spectra between -60 °C and -40 °C. This suggests further rearrangement of the *catena*-P_4 ligand (found in **5a**) to the yet unidentified final product **5b**.

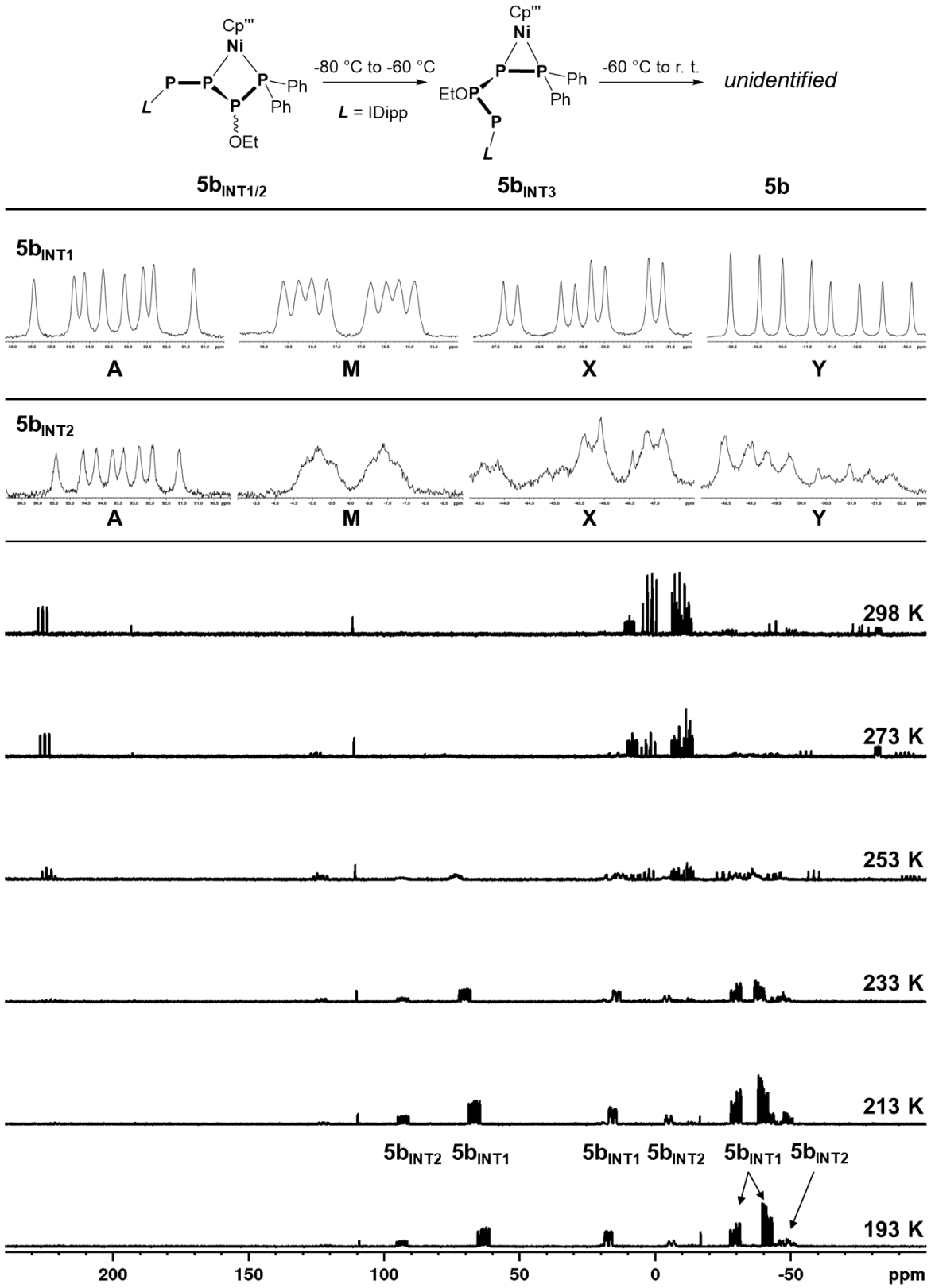

*Figure S 63: ^{31}P NMR spectra of the reaction of **1a** (59 mg, 0.05 mmol) with KOEt (5 mg, 0.05 mmol) intermediately forming two isomers of **5b$_{INT}$**, which rapidly rearrange at around -40 °C to finally afford **5b** at room temperature; Enlarged signals of both isomers **5b$_{INT1}$** and **5b$_{INT2}$** at -80 °C (top); * marks the signals associated with **5b$_{IN3}$**.*

*[CpMo(CO)$_2$($\eta^{1:1}$-^{i}Pr$_2$Me$_2$PPP(OEt)PPh$_2$)] (**6**)*

6 could so far only be isolated in poor yields prohibiting its complete spectroscopic characterization. NMR spectra of the crude reaction mixture allowed the assignment of **6** but spectra (*vide supra*) of reasonable quality could not yet be obtained.

*[Cp'''Ni($\eta^{1:1}$-P$_5$Ph$_2$IDipp)] (**7**)*

While single crystals of **7** could be obtained (*vide supra*), separation of **7** as a bulk material from side products could not be achieved within the time frame of this thesis. Thus, spectroscopic data of reasonable quality cannot be provided so far.

*[Cp'''Ni($\eta^{1:1}$-AsP$_4$Ph$_2$IDipp)] (**8**)*

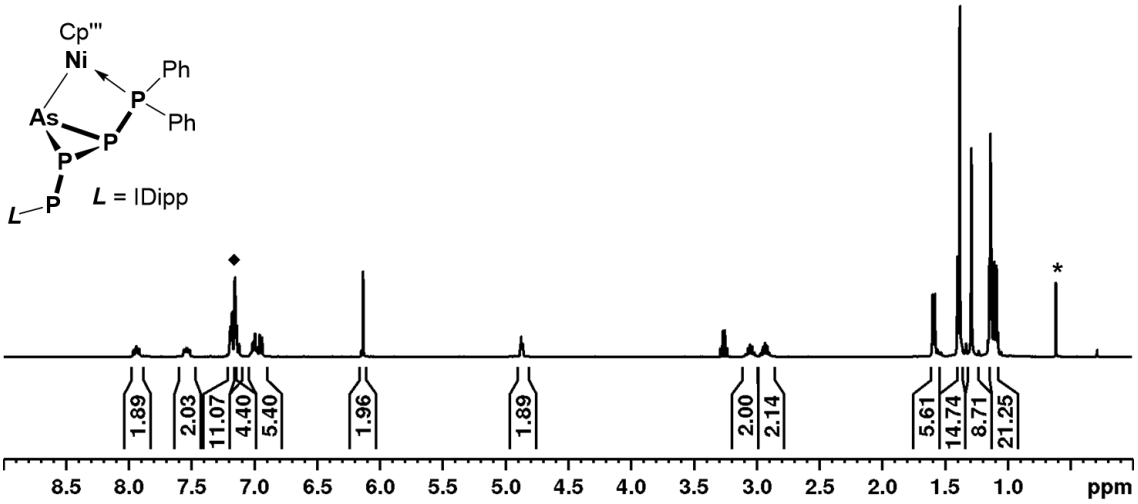

*Figure S 64: ^{1}H NMR spectrum of **10** in C_6D_6 recorded at room temperature; ◆ = residual solvent signal of C_6D_6, * = residual MeCN from the dissolved crystals.*

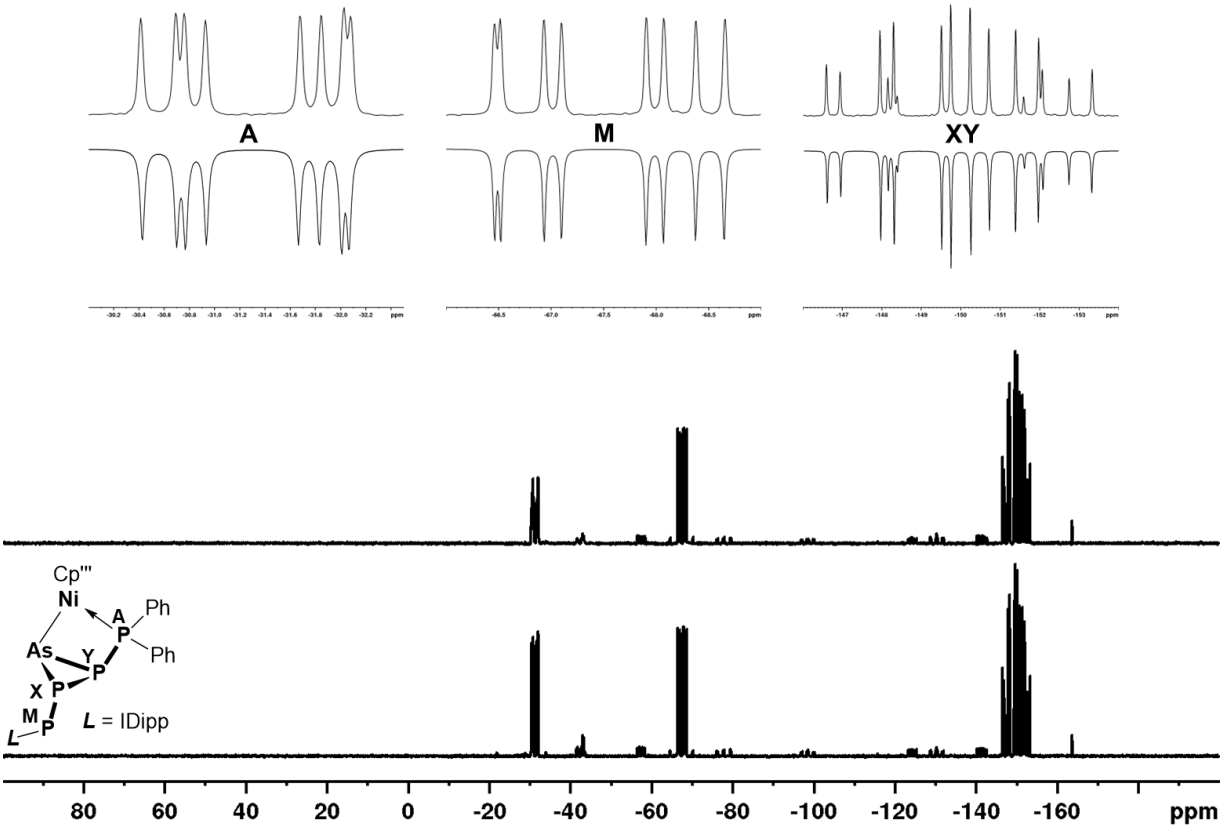

*Figure S 65: ^{31}P{^{1}H} (bottom) and ^{31}P (middle) NMR spectra of **10** in C_6D_6 recorded at room temperature as well as enlarged signals within the measured (top) and simulated (inverted) ^{31}P{^{1}H} NMR spectrum.*

12.6. References

[1] A. F. Holleman, N. Wiberg, *Lehrbuch der anorganischen Chemie*, De Gruyter, Berlin (DE), **2007**, 143.

[2] a) F. Mathey, *Angew. Chem. Int. Ed.* **2003**, *42*, 1578–1604; b) K. B. Dillon, F. Mathey, J. F. Nixon, *Phosphorus*. *The carbon copy: from organophosphorus to phospha-organic chemistry*, John Wiley & Sons, Chichester, New York, Weinheim, Brisbane, Singapore, Toronto, **2022**.

[3] R. Hoffmann, *Angew. Chem. Int. Ed. Engl.* **1982**, *21*, 711–724.

[4] D. J. Scott, *Angew. Chem. Int. Ed.* **2022**, *61*, e202205019.

[5] a) B. M. Cossairt, N. A. Piro, C. C. Cummins, *Chem. Rev.* **2010**, *110*, 4164–4177; b) M. Caporali, L. Gonsalvi, A. Rossin, M. Peruzzini, *Chem. Rev.* **2010**, *110*, 4178–4235; c) L. Giusti, V. R. Landaeta, M. Vanni, J. A. Kelly, R. Wolf, M. Caporali, *Coord. Chem. Rev.* **2021**, *441*, 213927–214019; d) C. M. Hoidn, D. J. Scott, R. Wolf, *Chem. Eur. J.* **2021**, *27*, 1886–1902.

[6] a) M. Scheer, G. Balázs, A. Seitz, *Chem. Rev.* **2010**, *110*, 4236–4256; b) D. J. Scott, J. Cammarata, M. Schimpf, R. Wolf, *Nat. Chem.* **2021**, *13*, 458–464.

[7] M. Donath, K. Schwedtmann, T. Schneider, F. Hennersdorf, A. Bauzá, A. Frontera, J. J. Weigand, *Nat. Chem.* **2022**, *14*, 384–391.

[8] U. Lennert, P. B. Arockiam, V. Streitferdt, D. J. Scott, C. Rödl, R. M. Gschwind, R. Wolf, *Nat. Cat.* **2019**, *2*, 1101–1106.

[9] a) J. Svara, N. Weferling, T. Hofmann in *Ullmann's Encyclopedia of Industrial Chemistry*, Wiley, **2003**; b) G. Bettermann, W. Krause, G. Riess, T. Hofmann in *Ullmann's Encyclopedia of Industrial Chemistry*, Wiley, **2003**.

[10] a) S. Reichl, E. Mädl, F. Riedlberger, M. Piesch, G. Balázs, M. Seidl, M. Scheer, *Nat. Commun.* **2021**, *12*, 5774; b) S. Reichl, G. Balázs, M. Scheer, *Chem. Sci.* **2023**, *14*, 3834–3838; c) S. Reichl, F. Riedlberger, M. Piesch, G. Balázs, M. Seidl, M. Scheer, *Chem. Sci.* **2023**, *14*, 7285–7290.

[11] S. Wang, J. D. Sears, C. E. Moore, A. L. Rheingold, M. L. Neidig, J. S. Figueroa, *Science* **2022**, *375*, 1393–1397.

[12] E. Urnius, W. W. Brennessel, C. J. Cramer, J. E. Ellis, P. v. R. Schleyer, *Science* **2002**, *295*, 832–834.

[13] C. Riesinger, F. Dielmann, R. Szlosek, A. V. Virovets, M. Scheer, *Angew. Chem. Int. Ed.* **2023**, *62*, e202218828.

[14] a) O. J. Scherer, *Angew. Chem. Int. Ed. Engl.* **1990**, *29*, 1104–1122; b) O. J. Scherer, *Acc. Chem. Res.* **1999**, *32*, 751–762.

[15] a) F. Riedlberger, M. Seidl, M. Scheer, *Chem. Commun.* **2020**, *56*, 13836–13839; b) L. Zimmermann, C. Riesinger, G. Balazs, M. Scheer, *Chem. Eur. J.* **2023**, e202301974.

[16] a) G. Capozzi, L. Chiti, M. Di Vaira, M. Peruzzini, P. Stoppioni, *J. Chem. Soc., Chem. Commun.* **1986**, 1799–1800; b) M. Di Vaira, P. Stoppioni, S. Midollini, F. Laschi, P. Zanello, *Polyhedron* **1991**, *10*, 2123–2129; c) E. Mädl, G. Balázs, E. V. Peresypkina, M. Scheer, *Angew. Chem. Int. Ed.* **2016**, *55*, 7702–7707; d) C. Riesinger, L. Dütsch, G. Balázs, M.

Bodensteiner, M. Scheer, *Chem. Eur. J.* **2020**, *26*, 17165–17170; e) M. Piesch, S. Reichl, M. Seidl, G. Balázs, M. Scheer, *Angew. Chem. Int. Ed.* **2021**, *60*, 15101–15108.

[17] a) C. G. P. Ziegler, T. M. Maier, S. Pelties, C. Taube, F. Hennersdorf, A. W. Ehlers, J. J. Weigand, R. Wolf, *Chem. Sci.* **2019**, *10*, 1302–1308; b) C. G. P. Ziegler, F. Hennersdorf, J. J. Weigand, R. Wolf, *Z. Anorg. Allg. Chem.* **2020**, *646*, 552–557; c) M. Piesch, M. Seidl, M. Scheer, *Chem. Sci.* **2020**, *11*, 6745–6751; d) C. Riesinger, A. Erhard, M. Scheer, *Chem. Commun.* **2023**, *59*, 10117–10120; e) C. M. Hoidn, K. Trabitsch, K. Schwedtmann, C. Taube, J. J. Weigand, R. Wolf, *Chem. Eur. J.* **2023**, e202301930.

[18] a) E. Mädl, M. V. Butovskii, G. Balázs, E. V. Peresypkina, A. V. Virovets, M. Seidl, M. Scheer, *Angew. Chem. Int. Ed.* **2014**, *53*, 7643–7646; b) F. Riedlberger, S. Todisco, P. Mastrorilli, A. Y. Timoshkin, M. Seidl, M. Scheer, *Chem. Eur. J.* **2020**, *26*, 16251–16255; c) C. Riesinger, G. Balázs, M. Bodensteiner, M. Scheer, *Angew. Chem. Int. Ed.* **2020**, *59*, 23879–23884; d) C. Riesinger, G. Balázs, M. Seidl, M. Scheer, *Chem. Sci.* **2021**, *12*, 13037–13044.

[19] a) U. Chakraborty, J. Leitl, B. Mühldorf, M. Bodensteiner, S. Pelties, R. Wolf, *Dalton Trans.* **2018**, *47*, 3693–3697; b) S. B. Dinauer, M. Piesch, R. Szlosek, M. Seidl, G. Balázs, M. Scheer, *Chem. Eur. J.* **2023**, *29*, e202300459.

[20] a) C. M. Hoidn, T. M. Maier, K. Trabitsch, J. J. Weigand, R. Wolf, *Angew. Chem. Int. Ed.* **2019**, *58*, 18931–18936; b) A. K. Adhikari, C. G. P. Ziegler, K. Schwedtmann, C. Taube, J. J. Weigand, R. Wolf, *Angew. Chem. Int. Ed.* **2019**, *58*, 18584–18590.

[21] O. J. Scherer, H. Sitzmann, G. Wolmershäuser, *J. Organomet. Chem.* **1984**, *268*, C9-C12.

[22] P. Pyykkö, *J. Phys. Chem A* **2015**, *119*, 2326–2337.

[23] Y. Mei, Z. Yan, L. L. Liu, *J. Am. Chem. Soc.* **2022**, *144*, 1517–1522.

[24] a) F. F. Puschmann, D. Stein, D. Heift, C. Hendriksen, Z. A. Gal, H.-F. Grützmacher, H. Grützmacher, *Angew. Chem. Int. Ed.* **2011**, *50*, 8420–8423; b) A. R. Jupp, J. M. Goicoechea, *Angew. Chem. Int. Ed.* **2013**, *52*, 10248-10251.

[25] a) A. Hinz, J. M. Goicoechea, *Angew. Chem. Int. Ed.* **2016**, *55*, 15515–15519; b) S. Yao, Y. Grossheim, A. Kostenko, E. Ballestero-Martínez, S. Schutte, M. Bispinghoff, H. Grützmacher, M. Driess, *Angew. Chem. Int. Ed.* **2017**, *56*, 7465–7469.

[26] *https://omics.pnl.gov/software/molecular-weight-calculator*, (07.08.2023).

[27] A. J. Arduengo, R. Krafczyk, R. Schmutzler, H. A. Craig, J. R. Goerlich, W. J. Marshall, M. Unverzagt, *Tetrahedron* **1999**, *55*, 14523-14534.

[28] N. Kuhn, T. Kratz, *Synth.* **1993**, *6*, 561-562.

[29] M. Gonsior, I. Krossing and N. Mitzel, *Z. anorg. allg. Chem.*, **2002**, *628*, 1821–1830.

[30] Agilent (**2014**). CrysAlis PRO. Agilent Technologies Ltd, Yarnton, Oxfordshire, England.

[31] O. V. Dolomanov, L. J. Bourhis, R. J. Gildea, J. A. K. Howard, H. Puschmann, *J. Appl. Crystallogr.* **2009**, *42*, 339-341.

[32] G. M. Sheldrick, *Acta Crystallogr. A* **2015**, *71*, 3–8.

[33] a) G. M. Sheldrick, *Acta Crystallogr. C* **2015**, *71*, 3-8; b) G. M. Sheldrick, *Acta Crystallogr. A* **2008**, *64*, 112-122.

13. Conclusion

In conclusion, this thesis tackles the challenge of expanding the chemistry of polypnictogen cations within three distinct categories. Chapters 3 – 8 systematically established the functionalization of neutral *cyclo*-P_n (n = 3, 4, 5, 8) ligand complexes with cationic electrophiles as one of the most versatile synthetic entries into cationic polyphosphorus chemistry. Without nearly any exceptions,[1] this approach has previously been overlooked. Chapters 9 and 10 expanded the redox chemistry of As_n ligand complexes. While the oxidation of Pn_n ligand complexes has already been employed to access polypnictogen cations,[2] most of the earlier results were obtained for P_n ligand systems. Lastly, chapters 11 and 12 targeted the reactivity of the most accessible of the above cationic species towards nucleophiles. Again, this reactivity has barely been explored previously,[3] but demonstrated itself as a useful tool to access highly complex polyphosphorus architectures within this thesis.

The *cyclo*-P_3 complex [Cp'''Ni(η^3-P_3)],[4] which is isolobal to P_4,[5] reacted with phosphenium cations $[R_2P]^+$ (R = alkyl, aryl, halide) under ring expansion and formation of *cyclo*-P_4R_2 units (Scheme 1). Notably, similar reactivity was observed for an isoelectronic molybdenum complex. However, reacting these complexes with strong neutral nucleophiles, such as NHCs, resulted in completely different products. While the P_4R_2 structural motif in the Ni system rearranged to a substituted *cyclo*-P_3 unit with an exocyclic phosphino residue, the one in the Mo system underwent ring opening and formation of a *catena*-P_4 ligand. The respective products were then investigated with regard to their further nucleophilic functionalization. However, only the Ni system provided a variety of complexly functionalized neutral polyphosphorus species, so far. Yet, initial results on the Mo system again hint towards the drastic influence of the transition metal on the product formed.

The insertion reactivity of phosphenium cations developed for the *cyclo*-P_3 ligands above was then transferred to the *cyclo*-P_4 compounds [$Cp^RTa(CO)_2(\eta^4$-$P_4)$] (Cp^R = Cp'',[6] Cp''',[7] Scheme 2). Again ring expansion and thus the formation of *cyclo*-P_5R_2 ligands could be observed. However, when the heavier congeners, namely arsenium and stibenium cations, were used, the products displayed substitution reactivity and lead to functionalized *cyclo*-P_4 ligands. In case of the arsenium species, an intriguing equilibrium between solid state structure and spectroscopic behavior in solution could be observed.

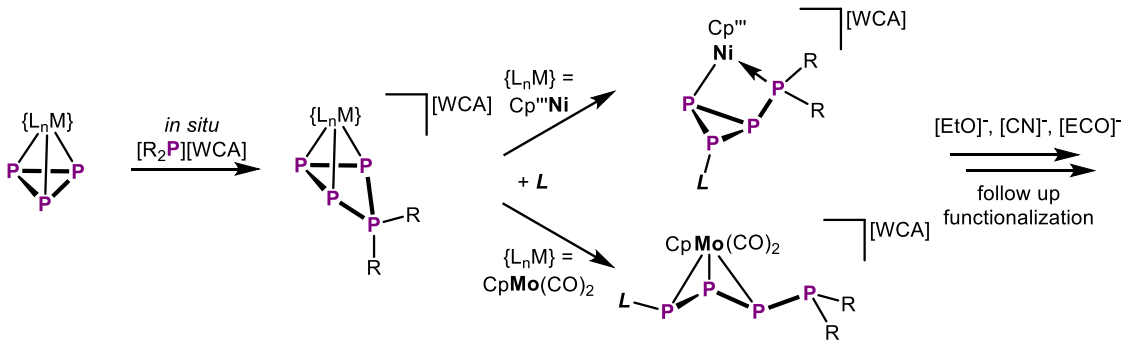

Scheme 1: Reactivity of [Cp'''Ni(η^3-P_3)] and an isostructural Mo complex towards phosphenium cations and the reactivity of the resulting products towards carbenes and anionic nucleophiles.

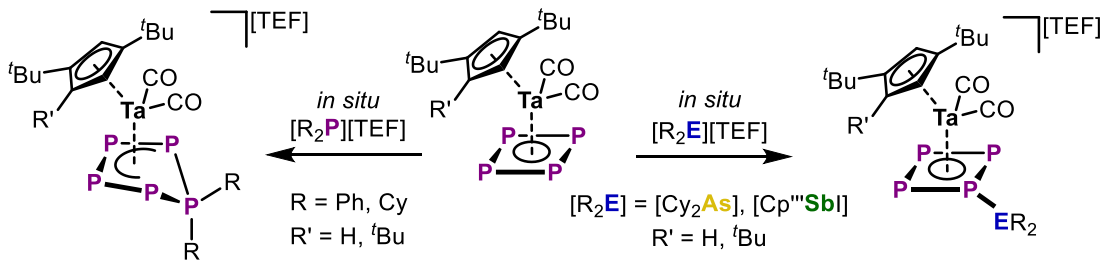

Scheme 2: Reactivity of a cyclo-P_4 complex towards phosphenium cations and their heavier analogs, arsenium and stibenium cations.

Further increasing the ring size to *cyclo*-P_5 ligands completely shut down the insertion reactivity of phosphenium cations observed beforehand (see chapter 6). Instead, the functionalization of [Cp*Fe(η^5-P_5)][8] with p-block electrophiles yielded a plethora of substituted pentaphosphole ligand complexes (Scheme 3). While these species have previously been synthetically inaccessible the stabilization invoked by the coordination to the {Cp*Fe}$^+$ fragment even allowed the preparation of the parent pentaphosphole compound bearing a proton substituent (*cyclo*-P_5H). Investigating the reactivity of the simpler carbon substituted derivative [Cp*Fe(η^5-P_5Me)][OTf] towards carbenes and their analogs showcased the unprecedented reactivity potential of these compounds in polyphosphorus chemistry. It provided easy access to further substituted and contracted P_5R_2 and P_4R_2 species, respectively. However, an expansion reaction leading to elaborate P_{10} as well as P_{11} scaffolds could also be identified. Lastly, the reactivity of the neutral [Cp*Fe(η^5-P_5)] towards cationic transition metal compounds was also explored. This not only allowed the preparation of a serious of triple-decker complexes but even granted access to novel *cyclo*-P_5 bearing quadruple-decker compounds.

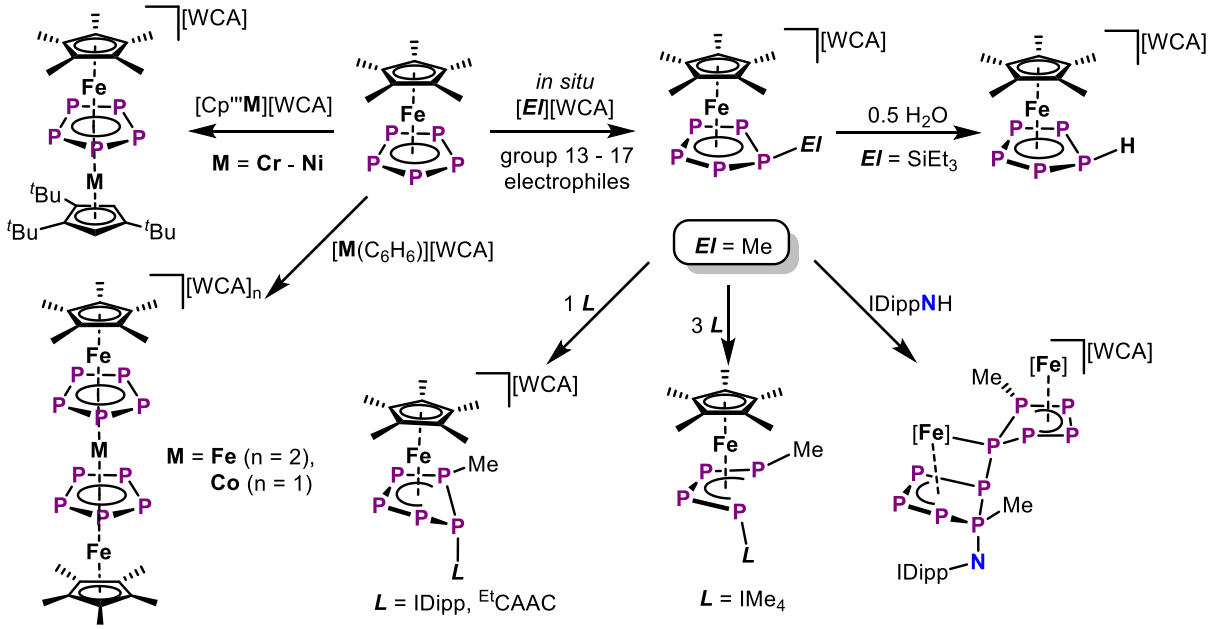

*Scheme 3: Synthesis of pentaphosphole complexes from [Cp*Fe(η^5-P_5)] even including the parent compound (top right), reactivity of these pentaphosphole complexes towards carbenes ad their analoga (bottom right) and synthesis of novel triple-decker as well as quadruple-decker complexes (left).*

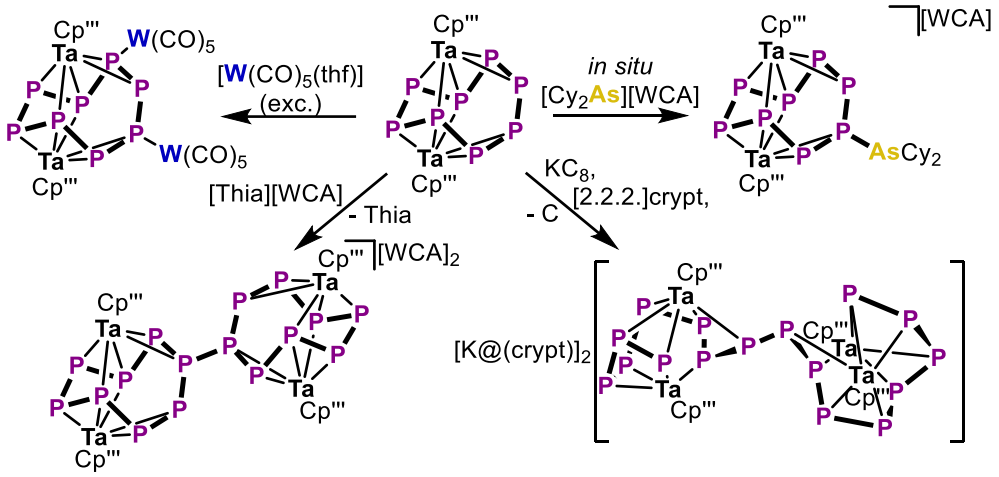

Scheme 4: Reactivity of a cyclo-P_8 complex upon coordination, arsenium functionalization, oxidation, and reduction.

The *cyclo*-P_8 ligand in [{Cp'''Ta}$_2$(μ,$\eta^{2:2:2:2:1:1}$-P_8)] is, to the best of our knowledge, the largest monocyclic polyphosphorus species reported to date. Its´ preparation also allowed the assessment of its basic modes of reactivity (Scheme 4). Thus, it was shown to readily coordinate to {W(CO)$_5$} fragments and easily be functionalized with an arsenium cation. Furthermore, exploring the redox reactivity of this unprecedented compound gave rise to a cationic complex bearing a P_{16} ligand, which represents the largest cationic polyphosphorus species known to date. Similarly, reduction also leads to dimerization but concomitant P–P bond cleavage, thus resulting in a complex bearing a *catena*-P_{16} ligand.

In contrast, the redox reactivity of the *cyclo*-As_3 complex [Cp'''Ni(η^3-As_3)][9] results in fragmentation reactions. This provided access to a series of As_3 triple-decker complexes in three different redox states (Scheme 5). Interestingly, one of the As–As bonds in the respective anion undergoes stepwise cleavage upon oxidation. A similar trend has previously been observed for the isostructural P_3 complex.[4]

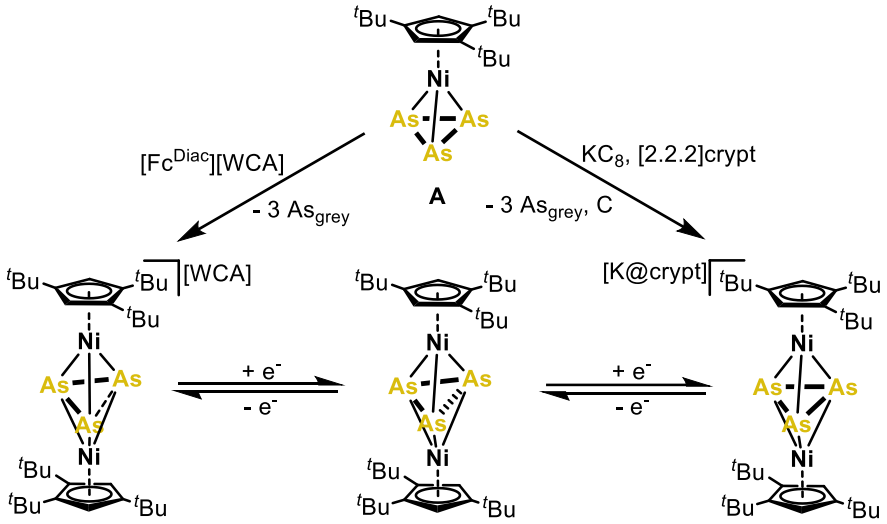

Scheme 5: Redox reactivity of an end-deck cyclo-As_3 complex yielding ionic triple-decker complexes upon fragmentation and synthesis of the neutral derivative via oxidation of the anion or reduction of the cation.

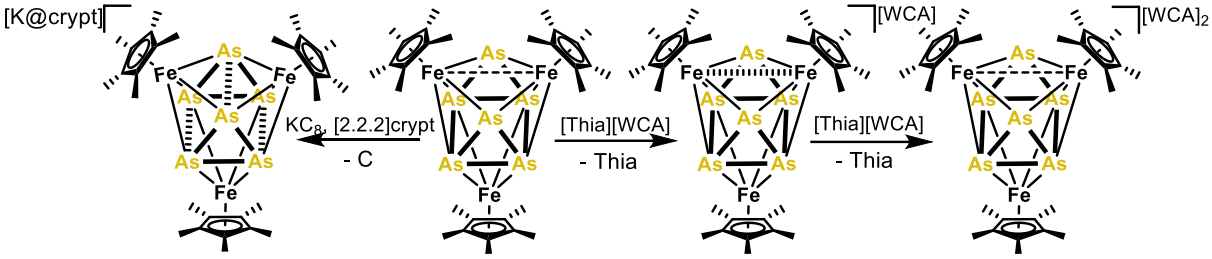

*Scheme 6: Redox reactivity of a {Cp*Fe} stabilized As_6 prismane complex.*

Lastly, the redox reactivity of an As_6 prismane complex with three {Cp*Fe} units was explored. While the different redox states only lead to minor structural changes, the compound showed electrochemical stability over five distinct redox states, of which four could even be realized and isolated synthetically (Scheme 6).

With the above results in mind, future research on polypnictogen cations should focus on several key aspects. While P_n ligand complexes with n = 3 – 5 and 8 could successfully be functionalized with cationic electrophiles simple P_2 as well as *cyclo*-P_6 ligand in hexaphosphabenzene complexes have not been part of this thesis. While the former of these two could recently be realized,[10] the latter still needs to be explored. On the other hand, the oxidation of neutral polypnictogen complexes continues to prove itself as a valuable tool to access polypnictogen cations. Further exploration of this synthetic avenue may involve other As_n as well as larger Sb_n ligand complexes, such as [Cp*Fe(η^5-As_5)][11] or [{Cp'''Mo}$_2$(μ,$\eta^{5:5}$-Sb_5)].[12] Finally, the availability of more and more transition metal stabilized polypnictogen cations provides the basis for studies towards their nucleophilic functionalization. The two distinct studies within this thesis highlight the extraordinary potential of this pathway towards polyphosphorus species revealing yet unprecedented molecular and electronic structures. Future work could focus on the reactivity of larger polyphosphorus cations and especially polyarsenic and -antimony species.

References

[1] a) G. Capozzi, L. Chiti, M. Di Vaira, M. Peruzzini, P. Stoppioni, *J. Chem. Soc., Chem. Commun.* **1986**, 1799–1800; b) M. Di Vaira, P. Stoppioni, S. Midollini, F. Laschi, P. Zanello, *Polyhedron* **1991**, *10*, 2123–2129; c) M. Weber, G. Balázs, A. V. Virovets, E. Peresypkina, M. Scheer, *Molecules* **2021**, *26*, 3920–3933.

[2] a) M. V. Butovskiy, G. Balázs, M. Bodensteiner, E. V. Peresypkina, A. V. Virovets, J. Sutter, M. Scheer, *Angew. Chem. Int. Ed.* **2013**, *52*, 2972–2976; b) M. Fleischmann, F. Dielmann, L. J. Gregoriades, E. V. Peresypkina, A. V. Virovets, S. Huber, A. Y. Timoshkin, G. Balázs, M. Scheer, *Angew. Chem. Int. Ed.* **2015**, *54*, 13110–13115; c) M. Fleischmann, F. Dielmann, G. Balázs, M. Scheer, *Chem. Eur. J.* **2016**, *22*, 15248–15251; d) L. Dütsch, M. Fleischmann, S. Welsch, G. Balázs, W. Kremer, M. Scheer, *Angew. Chem. Int. Ed.* **2018**, *57*, 3256–3261; e) L. Dütsch, C. Riesinger, G. Balázs, M. Seidl, M. Scheer, *Chem. Sci.* **2021**, *12*, 14531–14539.

[3] A. K. Adhikari, C. G. P. Ziegler, K. Schwedtmann, C. Taube, J. J. Weigand, R. Wolf, *Angew. Chem. Int. Ed.* **2019**, *58*, 18584–18590.

[4] E. Mädl, G. Balázs, E. V. Peresypkina, M. Scheer, *Angew. Chem. Int. Ed.* **2016**, *55*, 7702–7707.

[5] R. Hoffmann, *Angew. Chem. Int. Ed. Engl.* **1982**, *21*, 711–724.

[6] O. J. Scherer, R. Winter, G. Wolmershäuser, *Z. Anorg. Allg. Chem.* **1993**, *619*, 827–835.

[7] F. Dielmann, E. V. Peresypkina, B. Krämer, F. Hastreiter, B. P. Johnson, M. Zabel, C. Heindl, M. Scheer, *Angew. Chem. Int. Ed.* **2016**, *55*, 14833–14837.

[8] O. J. Scherer, T. Brück, *Angew. Chem. Int. Ed. Engl.* **1987**, *26*, 59.

[9] M. Piesch, S. Reichl, C. Riesinger, M. Seidl, G. Balazs, M. Scheer, *Chem. Eur. J.* **2021**, *27*, 9129–9140.

[10] L. Zimmermann, C. Riesinger, G. Balazs, M. Scheer, *Chem. Eur. J.* **2023**, e202301974.

[11] O. J. Scherer, C. Blath, G. Wolmershäuser, *J. Organomet. Chem.* **1990**, *387*, C21-C24.

[12] H. J. Breunig, N. Burford, R. Rösler, *Angew. Chem. Int. Ed.* **2000**, *39*, 4148–4150.

14. Appendices

14.1. Abbreviations

Å	Angstroem, 1 Å = $1 \cdot 10^{-10}$ m
ADP	anisotropic displacement parameters
ATP	adenosine triphosphate
br (NMR)	broad
°C	degree Celsius
Cp	cyclopentadienyl, $C_5H_5^-$
Cp*	pentamethylcyclopentadienyl, $C_5Me_5^-$
Cp'	methylcyclopentadienyl, $C_5H_4Me^-$
Cp''	1,3-di-*tert*-butylcyclopentadienyl, $C_5H_3{}^tBu_2^-$
Cp'''	1,2,4-tris-*tert*-butylcyclopentadienyl, $C_5H_2{}^tBu_3^-$
CV	cyclic voltammetry
d (NMR)	doublet
δ	chemical shift (NMR)
DFT	density functional theory
Dipp	2,6-di-isopropylphenyl
DME	dimethoxyethane
DNA	deoxyribonucleic acid
e^-	electron, elemental charge
EA	elemental analyses
EPR	electron paramagnetic resonance
eq.	equivalent(s)
ESI	electro spray ionization
Et	ethyl, $-C_2H_5$
$[FAl]^-$	falanate, $[FAl\{OC(C_5H_{10})(C_6F_5)\}_3]^-$
Fc	ferrocene, Cp_2Fe
Fc^{Diac}	diacetylferrocene, $(C_5H_4COMe)_2Fe$
FD	field desorption
g	gram
gr.	ancient greek
h	hour(s)
Hal, X	halide
HOMO	highest occupied molecular orbital
Hz	Hertz
^{i}Pr	*iso*-Propyl, $-C_3H_7$
IR	infrared spectroscopy
J	coupling constant
K	Kelvin

kcal	kilCalory
kg	kilgram
kJ	kiloJoule
L	ligand (specified in text)
LIFDI	liquid injection field desorption ionization
LUMO	lowest unoccupied molecular orbital
m (NMR)	multiplet
M	metal (specified in text)
$[M]^+$	molecular ion peak (MS)
Me	methyl, $-CH_3$
Mes	mesityl, 2,4,6-trimethylphenyl
mg	milligram
µg	mikrogram
min	minute(s)
mL	milliliter
µL	mikroliter
MS	mass spectrometry
m/z	mass to charge ratio
NICS	nuclear independent chemical shift
nm	nanometre
NMR	nuclear magnetic resonance (spectroscopy)
ν	freqency/wavenumber
o-DFB	*ortho*-difluorobenzene, $C_6H_4F_2$
Ph	phenyl, $-C_6H_5$
P_n	polyphosphorus
Pn	pnictogen
Pn_n /E_n	polypnictogen
ppm	parts per million
q (NMR)	quartet
R	(organic) substituent
r.t.	room temperature
s (NMR)	singlet
SI (or ESI)	supporting information
SOMO	singly occupied molecular orbital
T	metric ton
t (NMR)	triplet
^{t}Bu	*tert*-butyl, $-C_4H_9$
$[TEF]^-$	teflonate, $[Al\{OC(CF_3)_3\}_4]^-$
$[TEF^{Cl}]^-$	teflonate, $[Al\{OC(CF_3)_2(CCl_3)\}_4]^-$
THF	tetrahydrofurane, C_4H_8O

Thia	thianthrene, $C_{12}H_8S_2$
V	volume
vdW	van-der-Waals
VE	valence electron
VT	various temperature
$\omega_{1/2}$	half width
WBI	wiberg bond indices
WCA	weakly coordinating anion
4FB	1,2,3,4-tetrafluorobenzene

14.2. Acknowledgements

Finally, I want to thank:

- Prof. Dr. Manfred Scheer, for providing me the opportunity to work on this fascinating topic, a positive and thriving research environment in his group, his scientific mentorship and the possibility to perform international research stays as well as attend national and international conferences.

- Prof. Dr. Nikolaus Korber (Zweitgutachter), Prof. Dr. Frank-Michael Matysik (Drittprüfer) and Apl. Prof. Dr. Rainer Müller (Vorsitz) for chairing the examination committee.

- Prof. Dr. Neil Burford at the University of Victoria (BC, Canada) for accepting me into his group for a research stay during my Msc studies. The experience I gained from this stay invaluably benefited my later research and personal development.

- Prof. Dr. T. Don Tilley at the University of California, Berkeley for accepting me into his group for a research stay during the summer in 2023. I learned so much about chemistry and beyond in these short three months. Thanks also to the whole Tilley group and especially my lab mates Matt See and Jose Martinez Fernandez who kindly introduced me into their chemistry as well as the city of Berkeley and its surroundings.

- Dr. Gábor Balázs for all the discussions about chemistry (accompanied by nice coffee or a cold beer), your help with spectroscopic data and your assistance with any other problems beyond that. I especially want to thank you for the countless hours you invested in helping me to learn useful DFT methods.

- Dr. Michael Bodensteiner for all the time you spent on helping and training me on X-ray crystallographic problems. Without your help I would have never been able to conduct the research in this thesis.

- My lab mate and former lab supervisor Dr. Luis Dütsch, who trained me during my BSc and MSc theses and taught me all the necessary synthetic skills for conducting research on highly sensitive compounds. Thank you for all the discussions and advice on chemistry, life in general and especially for simply all the good times we had in- and outside the lab.

- My former MSc student and now lab mate Lisa Zimmermann for the great vibe in the lab, numerous discussions on chemistry and all your valuable input when it comes to graphical design. However, I especially want to thank you for all the great time beyond the lab, be it high up in the alps or just climbing the local rocks in close-by Schönhofen.

You are the greatest climbing partner I could imagine and the memories of our adventures are some of the best I have.

- My former MSc student and now lab mate Maximilian Widmann for even more great vibe in our “cations” lab. Thanks for all your input, your help in the lab and especially all the Bavarian sayings you do not hesitate to recite. They often really made my day and helped to keep a good mood around the lab even when the chemistry did not work out as planned.

- My BSc students Alexander Erhard, Philip Blank, Adrian Stadler and Jan Wieneke for all your commitment and great ideas. Without your hard work most of the projects in this thesis would not have been possible.

- Dr. Michael Seidl for your assistance with X-ray crystallographic data, when I was at my wits end.

- Prof. Dr. Ingo Krossing and Prof. Dr. Fabian Dielmann for two fruitful collaborations (chapters 7 and 8, respectively).

- All past and present members of the Scheer group for the great working environment and enriching scietific exchange, including Bijan, Felix, Helena, Kevin, Julian, Lena, Lisa, Luis, Lukas, Maria, Martin, Martin, Matthias, Maximilian, Mehdi, Michael Robert, Sabrina, Sarah, Sophie, Stephan, Tania, Thach and Veronika.
  A special thanks goes to the technicians Martina, Petra, Lukas and Sophie for all your help on preparing even the most complicated starting materials and secretary Mina Pesé for always helping me with any kind of bureaucratic challenges.

- All staff members at the analytical facilities including Dr. Michael Bodensteiner, Dr. Stefanie Gärtner, Birgit Hischa, Sabine Stempfhuber, Florian Meurer, Charmaine Berner and Angelika Hinterberger (X-ray crystallography), Dr. Ilya Shenderovich, Fritz Kastner, Tuan Anh Nguyen and Annette Schramm (NMR spectroscopy), Dr. Thomas Herl, Josef Kiermaier and Wolfgang Söllner (mass spectrometry), and Helmut Schüller and Barbara Baumann (elemental analysis), as well as the members of the glass blowing workshop at the University of Regensburg.

- The Studienstiftung des deutschen Volkes e. V. for financial as well as ideational support throughout the time frame of this thesis.

- All of my friends for the great time we had and the memories we made. Without any of you it would not have been the same. Thanks for all your support even in when times were not the most joyful (especially during COVID-19).

- Kati, a friend I thought I lost. Thank you for returning into my life. You make every single day of it a special one to me.

- My family for always having my back, for your endless support and enabling me to pursue the path I am on. You are the best!